GUIDE TO STABILITY DESIGN CRITERIA FOR METAL STRUCTURES

Fifth Edition

Edited by
THEODORE V. GALAMBOS

JOHN WILEY & SONS, INC.
New York - Chichester - Weinheim - Brisbane - Singapore - Toronto

This book is printed on acid-free paper.

Published simultaneously in Canada.

Library of Congress Cataloging-in-Publication Data:

Guide to stability design criteria for metal structures. –5th ed./
edited by Theodore V. Galambos.
p. cm.
Includes bibliographical references and indexes.
ISBN 0-471-12742-6 (alk. paper)
1. Columns. 2. Girders. I. Galambos, T. V. (Theodore V.)
TA660.C6G85 1998
624.1′821–dc21 97-3240

Printed in the United States of America.

10 9 8 7 6 5 4 3 2 1

CONTENTS

FOREWORD

Since its founding in 1944, the principal objectives of the Structural Stability Research Council (formerly the Column Research Council) have been to foster research on the behavior of compressive components of metal structures and of structural systems, and to assist in the development of improved design procedures. The Council provides guidance to practicing engineers and writers of design specifications, codes, and standards in offering both simplified and refined procedures applicable to design and assessing their limitations.

The initial outline of the guide was prepared in 1956 by Lynn S. Beedle and Jonathan Jones. The first edition, published in 1960, was dedicated to the Council's first chairman with these words: "As first Chairman of Column Research Council, Shortridge Hardesty gave freely for twelve years his time, devotion, and material assistance. His mind grasped both the practical problems of engineering application and the fundamental knowledge necessary to research. His influence was a personal inspiration to all who worked in Column Research Council."

This is the fifth edition of the guide. It is essentially an evolutionary extension of the previous editions, which were published about every decade since the first edition in 1960. This fifth edition has the same number of chapters as the fourth edition. However, a number of new chapters have replaced previous chapters, and most of the chapters which were retained under the same title have been extensively revised or entirely rewritten so that new research results could be presented and evaluated. The entirely new chapters are: *Horizontally Curved Steel I-Girders* (Chapter 9), *Composite Columns and Structural Systems* (Chapter 10), *Stability of Angle Members* (Chapter 11), *Bracing* (Chapter 12), *Frame Stability* (Chapter 16), *Doubly Curved Shells and Shell-like Structures* (Chapter 18), *Stability Under Seismic Loading* (Chapter 20), and *Stability Analysis by Finite-Element Method* (Chapter 21). In additon, three new Technical Memoranda were added to this new edition.

The Council was fortunate in having Bruce G. Johnston as editor of the first three editions of the guide and is indebted to him for the time and effort he has devoted to this work. As a result of Dr. Johnston's guidance, inspiration, and example, the Task Groups of the SSRC have produced the world's foremost collection of ideas and information on the subject of the stability of metal structures in the first three editions of the guide. The fourth and fifth editions were shepherded through the publication process by the current editor.

The concept that the Task Groups of the SSRC would have the responsibility for most individual chapters was retained also in the fifth edition. Additional substantial contributions were provided by others, who wrote drafts of chapters or who reviewed manuscripts at various stages of completion

of the guide. I sincerely thank all those who had a hand in this effort. (See the end of Chapter 1 for a list of those primarily responsible for each chapter.) Special thanks go to Dr. Bruce G. Johnston for preparing the index for the fourth edition.

The first edition of the guide received special financial support from the Engineering Foundation and the Association of American Railroads. Costs in preparing the second edition were borne jointly by the American Institute of Steel Construction and the Column Research Council. Preparation of the third edition was supported by the National Science Foundation and the American Institute of Steel Construction. The preparation of both the fourth and fifth editions was supported by a grant from the National Science Foundation. The Council further enjoys the financial support of many organizations, listed in Appendix C, which provide for its continuity and make it possible to sponsor publication of the guide. Through the members of these organizations we also maintain the vital creative interaction between structural engineering practice and research.

The Structural Stability Research Council and the editor deeply thank all those who have provided intellectual and financial support for this edition of the Guide. Special gratitude is to the National Science Foundation for encouraging the dissemination of research results on the stability of metal structures to the professional and research community.

T. V. Galambos, Editor

Minneapolis
February 1998

NOTATION

A	a coefficient; area of cross section; flexural stiffness of arch cross section about x-axis; arc length in a shell
A_1	internal area of cylindrical tube
A_2	external area of cylindrical tube
A_b	area of all battens within one batten spacing
A_c	area of compression flange; are of longitudinal in laced or battened member
A_d	area of diagonal in a laced member
A_e	area of cross section remaining elastic; required area of plate-girder end plate
A_{eff}	effective area in a thin-walled section such that $P = \sigma_y A_{\text{eff}}$
A_f	area of flange
A_g	gross area of composite column
A_S	area of large stiffener plus total area of shell between small stiffeners
A_s	area of steel in a composite column; area of stiffener cross section; area of small stiffener plus total shell area between stiffeners
A_{st}	area of intermediate stiffener
A_t	area of tension flange
A_u	area of plate-girder bearing stiffener
A_w	area of web
a	length of side of stiffened plate; length of perforation in a perforated plate; torsion bending constant for an I-section; coefficient defining stable region under dynamic load; distance between plate-girder stiffeners
B	a coefficient; coefficient in postbuckling plate formula; coefficient to correct for a one-sided stiffener; flexural stiffness of an arch about y-axis
$\bar{B}$	coefficient in postbuckling plate formula
B_c	coefficient in design formula for aluminum columns
B_p	coefficient in design formula for aluminum-alloy plates
$B_x(B_y)$	distributed bending stiffness in a stiffened plate about $x(y)$-axis
b	width of rectangular cross section; width of plate; width of pony-truss bridge, center-to-center of trusses; length of short side of a box section, center-to-center of long sides; length of side of stiffened plate; transverse distance from edge of a perforation to nearest line of longitudinal fasteners; coefficient defining stable region under dynamic load
b_c	width of compression flange
b_e	width of flange of a W shape

b_t width of tension flange
b_w width between centers of flanges in a wide-flange column

C a coefficient; transverse pony-truss bridge frame spring constant, particularly the least one; torsional rigidity; coefficient in formula for design of one-sided stiffeners;
C_1, C_2 C_3, C_4 coefficients for lateral-torsional buckling of a beam
C_{AA}, C_{BB}, C_{AB} coefficients in generalized slope-deflection equations
C_a membrane stiffness of a stiffened cylinder
C_b coefficient for a laterally unsupported bent beam; bending stiffness of a stiffened cylinder
C_{by} coefficient for a tapered beam
C_c column formula coefficient
C_m coefficient to determine equivalent uniform moment in a beam-column
C_{req} required transverse pony-truss bridge frame spring constant
C_w torsional warping constant
c distance to extreme fiber of beam or column section in bending; distance center-to-center of perforations in a perforated plate; distance from middle plane of channel web to centroid of section; distance from stiffener to assumed location of plastic hinge in plate-girder flange

D flexural rigidity of a plate per unit width; mean diameter of a cylindrical tube
D_c coefficient in design formula for aluminum columns
D_p coefficient in design formula for aluminum plates
d depth of a section; diameter of circular cross section; long side of box section, center-to-center of short sides, transverse distance between lines of longitudinal fasteners in a peforated plate; stiffener spacing for a stiffened plate
d_e diameter of elastic portion of a circular cross section
d_z depth of tapered member at z

E modulus of elasticity
E_r reduced modulus
E_s secant modulus
E_{st} strain-hardening modulus (initial)
E_t tangent modulus
e distance from centroid of girder cross section to shear center (positive if shear center lies between centroid and compression flange, otherwise negative); distance from shear center to the middle plane of a channel web; width of end post in a plate girder; eccentricity of end load in a beam-column. Initial out-of-roundness of an unstiffened shell
e_0 assumed equivalent eccentricity (representing defects, etc.)

F_a allowable average compressive stress in axially loaded members
F_{a0} allowable stress for a column having zero slenderness ratio
F_b allowable compressive bending stress
F_c maximum allowable compressive stress on unstiffened element (AISI)
F_{cr} critical thrust load applied at ends of an arch
F_s allowable stress for steel in a composite column; axial force in a transverse plate-girder stiffener
F_y yield point of structural steel
FS factor of safety
f_a average compressive stress due to axial load
f_b compressive stress due to bending moment
f_v average shear stress in a beam web
f_c' compressive strength of concrete
f_c'' average compressive strength of concrete at ultimate load

G elastic shear modulus
G, G_A, G_B joint bending stiffness ratio (subscripts apply to respective ends of the column)
G_{eff} effective shear modulus of diaphragm
G_{st} shearing strain-hardening modulus (initial)
g distance from shear center of girder to point of application of transverse load (positive when load is below shear center, otherwise negative); equivalent-length factor in a tapered beam; end-panel length of a plate girder

H horizontal component of arch thrust; distributed torsional stiffness in a stiffened plate; horizontal force at a multi-story frame floor level
H_i' sway force in multistory frame due to vertical loads
h depth of a rectangular cross section; clear depth of plate girder or beam web between flanges; depth of pony truss at truss vertical, measured from center of floorbeam to center of top chord; long side of box section, center-to-center of short sides; distance between beam- or girder-flange centroids; rise of arch axis; effective-length factor in a tapered beam
h_e distance to compression-flange centroid from centroid of section
h_f distance between flange centroids
h_i height of story i in building frame
h_s, h_w effective-length factors in tapered beams
h_t distance to tension-flange centroid from centroid of section
h_w depth of web

I moment of inertia of cross section
I_b moment of inertia of floorbeam in a pony truss
I_c moment of inertia of column cross section; moment of inertia of compression flange about the y-axis; moment of inertia of truss vertical in a pony truss; moment of inertia of longitudinal component of spaced column; moment of inertia at crown of an arch
I_E moment of inertia of large stiffener plus effective width of shell L_e
I_e moment of inertia of cross section remaining elastic
I_{eq} equivalent uniform moment of inertia for buckling of a nonuniform arch
I_{FE} value of I_E that makes the large ring stiffener in a shell equivalent to a bulkhead
I_g moment of inertia of girder cross section
I_0 polar moment of inertia about shear center; moment of inertia of a segment of a stiffened plate; moment of inertia at smaller end of a tapered beam
I_p polar moment of inertia of cross section about centroid
I_s moment of inertia of transverse stiffener
I_t moment of inertia of tension flange about y-axis
I_x, I_y moment of inertia of cross section, x and y denoting the coordinate axes
$(I_y)_{\text{eff}}$ effective moment of inertia about y-axis
I_{yc}, I_{yt} moment of inertia of compression and tension portions of section about axis parallel to the web, respectively

J torsion constant; coefficient in AASHTO formula for transverse stiffener design
$J_{DX}(J_{DY})$ torsion constant of stiffeners in $X(Y)$ direction
j lateral-torsional buckling constant; number of panels in a stiffened plate

K effective- or equivalent-length factor; spring constant; coefficient in edge-loading analysis of a plate-girder web
K' modified effective-length factor
$K_{11}, K_{22}, K_{33}, K_{23}$ coefficients in flexural-torsional buckling
K_γ effective-length factor in a tapered beam
K_m average effective-length factor of all panel length compression chords in a pony truss
K_s elastic support restraint coefficient for a shallow arch; horizontal elastic support coefficient for an arch
k coefficient of proportionality; coefficient applied in plate buckling; elastic foundation modulus, $\sqrt{P/EI}$
k_1, k_2, k_3 coefficients in design formulas for aluminum-alloy plates
k_h local buckling parameter for box columns
k_s buckling coefficient for a plate in pure shear

k_w local buckling parameter for wide-flange columns

L span of an arch
L, l length of member, particularly a laterally unbraced length
L_b length of shell between bulkheads
L_c unbraced length of a column
L_e effective width of shell acting as part of a stiffener
L_F center-to-center spacing of large shell stiffeners
L_f center-to-center spacing of stiffener rings
L_g unbraced length of a girder
LF load factor
l panel length in a pony-truss bridge

M bending moment
M', M'' rotational stiffness of near end of member with far end fixed or hinged, respectively, but with no end translation
$\bar{M}', \bar{M}''$ rotational stiffness of near end of member with far end fixed or hinged, respectively, but with near end translationally restrained by a linear spring
M_{AB} moment at $A(B)$ acting on member AB
M_a, M_b end moments acting on a beam-column at ends a and b, respectively
M_c critical-bending moment
M_e end moment for a framed column
M_{eq} equivalent uniform moment in a beam column
M_{exp} resisting moment by test of plate girder
M_f plate-girder moment contributed by flanges
M_{max} maximum-bending moment
M_0 applied-end moment
M_0, M_{0x}, M_{0y} moment in a beam-column without regard to moment caused by deflection
M_p plastic-bending moment
M_{pc}, M_{pcx}, M_{pcy} plastic bending moment modified by axial force
M_{px}, M_{py} plastic-resisting moment about indicated axis
M_{th} theoretical plate-girder resisting moment
M_u, M_{ux}, M_{uy} ultimate bending moment of a plate girder; ultimate bending moment in the absence of axial load in a laterally unsupported beam-column
M_{ucx}, M_{ucy} maximum moments resisted by a biaxially loaded beam-column in the presence of axial load
M_w warping torsional moment
M_x, M_y, M_z moment about coordinate axes x, y, and z, respectively
M_y yield moment
m width of a perforation in a perforated plate; mass per unit length of column; buckling coefficient in an arch; coefficient in tapered

	beam analysis; number of panels in transversely stiffened plate; coefficient in out-of-plane arch buckling
m_{pb}, m_{pt}	plastic resisting moment of bottom and top flanges of a plate girder
m	plastic moment of web
N	nominal axial load; number of panels in a stiffened plate
N, n	a factor of safety
$N_x(N_y)$	force per unit length in $x(y)$ direction
n	number of perforated plates used in a column; number of parallel planes of battens in a battened column; number of panels in a pony truss; number denoting an individual compression member as one of several meeting at a common joint; coefficient in tapered beam analysis; number of circumferential lobes in a shell at collapse
P	column axial load; concentrated load on a plate-girder web
$P(t)$	variable axial force
P_1, P_2	axial compression force in truss member (subscripts refer to first and second member, respectively)
$P_{\phi e}$	critical load for pure torsional buckling
P_a	permissible axial load on composite column
P_c	chord stress in a truss at maximum load
P_{cr}	critical load
P_e, P_{ex}, P_{ey}	Euler buckling load; critical thrust at quarter points for a uniform arch
P_F	probability of failure
P_f	conservative estimate of failure load in torsional-flexural buckling
P_k	critical load in kth mode
$P_{\max}$	maximum column load
P_n	axial compressive force of nth member
P_0	static component of dynamic load
P_p	column load at proportional limit
P_r	reduced-modulus column load
P_S	probability of survival
P_{TF}	critical load in combined flexural-torsional buckling
P_t	tangent-modulus column load
P_u	ultimate load of axially loaded column; ultimate patch load on plate-girder web
P_{ue}	ultimate eccentric load
$P_{uex}(P_{uey})$	failure loads for bending about $x(y)$-axis for long column
P_{ux}	failure load of long column under axial load constrained to permit bending only major axis
P_y	column axial load at full-yield condition
p	difference between uniform loads on two halves of an arch
p_1	internal pressure in a cylindrical tube
p_2	external pressure on a cylindrical tube

p_B	critical pressure of small stiffener plus total area of shell between stiffeners
p_c	critical external pressure to cause buckling between stiffeners
p_{crE}	critical pressure for elastic buckling of a spherical shell-like structure
p_{crP}	critical pressure for plastic buckling of a spherical shell-like structure
p_e	elastic buckling pressure on a shell
p_F	critical pressure in shell buckling
p_i	inelastic buckling pressure on a shell
p_y	hydrostatic pressure at initial yield in unstiffened shell with initial out-of-roundness
Q	transverse shear in centrally loaded column; form factor for thin-walled section; shear rigidity of diaphragm; unit radial load on a shell stiffener ring
Q_a	area factor to modify members composed entirely of stiffened elements
Q_s	stress factor to modify members composed entirely of unstiffened elements
R	mean radius of cylindrical tube; resistance, or load capacity. Radius of a circular arch; spherical radius of a shell
R_1	a specific low value of resistance strength chosen to ensure a safe design
R_c	radius to centroidal axis of combined stiffener and effective shell ring
$R_c(R_s)$	ratio of critical compressive (shear) stress in combined shear and direct stress to critical compressive (shear) stress in pure compression (shear)
R_d	radius to centroidal axis of large stiffener plus effective width of shell
R_m	mean value of resistance strength
R_n	nominal value of resistance strength
R_0	outside radius of shell
r	radius of gyration of member
r_c	radius of gyration of concrete core
r_e	radius of gyration of a stiffener-panel combination
r_f	radius of gyration of column flange
r_0	polar radius of gyration of the cross section about its shear center, radius of gyration of one chord in a battened column
r_s	radius of gyration of steel tube
r_x	radius of gyration about the centroidal axis x-x (strong axis)
r_y	radius of gyration about the centroidal axis y-y (weak axis)

S load, in a generalized sense; circumferential half length of an arch axis from springline to centerline
S_1 specific high value of load chosen to provide a safe design
S_c section modulus for compression
S_{eff} effective section modulus
S_L section modulus of longitudinal stiffener
S_T section modulus of transverse stiffener in a plate girder
S_t section modulus for tension
S_x section modulus about x-x axis
S_{xc} section modulus for compression stress about x-x axis
SF_x safety factor applied to longitudinal stress
$s_x(s_y)$ spacing of stiffeners in $x(y)$ direction

T tensile residual stress designation
T1,T2, T3, T4 heat treatment designations for aluminum alloys
t thickness of plate or tubular wall
t_B effective-bending thickness of a shell-like structure
t_b thickness of side b of box-section column
t_c thickness of compression flange
t_h thickness of side h of box-section column
t_m effective-membrane thickness of a shell-like structure
t_t thickness of tension flange
t_w thickness of web plates of box-section beam; thickness of web

U cube strength of concrete
u displacement in the x direction

V transverse shear force in plate girder
V_i' additional shear at ith floor due to sway forces
V_σ shear strength of plate girder due to tension-field action
V_τ shear strength of plate girder due to beam action
V_{ex} experimental value of plate-girder shear strength
V_p plastic shear strength of plate girder
V_{th} theoretical value of plate-girder shear-strength
V_u ultimate shear strength of plate girder
V_w shear strength of plate-girder web
v displacement in the y direction

W uniformly distributed total lateral load in a beam-column
W wide-flange shape symbol
WW welded wide-flange shape
W_{ar}, W_{bm} relative magnitudes of total load carried by arch and beam action respectively, in a shallow arch
W_{cr} concentrated critical load at a node in a shell-like structure

w uniform load intensity; displacement in the z direction; unit weight of concrete in a composite column; distributed radial load on arch
w_c critical radial load at arch or ring buckling; critical load for out-of-plane arch buckling
$(w_c)_s$ sinusoidal load for symmetrical buckling of a shallow arch
$(w_c)_u$ sinusoidal load for unsymmetrical buckling of a shallow arch
w_e critical uniform buckling load for an arch
$(w_u)_c$ unsymmetrical buckling of an arch under uniform load
$(w_u)_{cs}$, $(w_u)_{cu}$ uniform load for symmetrical and unsymmetrical buckling, respectively, for a shallow arch

X_e width of rectangular cross section remaining elastic
X-X,x-x coordinate axis
x coordinate axis, particularly a principal axis; a distance;
x_0 distance between the shear center and the centroid in the direction of the x-axis

Y_e depth of rectangular cross section remaining elastic
Y-Y, y-y coordinate axis
y coordinate axis, particularly a principal axis
y_c distance from centroidal axis x-x to face of tee flange; height of loaded arch axis at midspan; distance from neutral axis to compression edge web
$(y_c)_s$ height of arch axis at midspan at symmetrical buckling
$(y_c)_u$ height of arch axis at midspan at unsymmetrical buckling
y_0 distance between the shear center and the centroid in the direction of the y-axis; portion of plate-girder web in compression
y_s distance from neutral axis to longitudinal stiffener
y_t distance from neutral axis to tension edge of web

Z plastic modulus
z coordinate axis; distance along the z-axis

α aspect ratio a/b or a/h for stiffened plates; load ratio P/P_e; ratio of moments of inertia of adjacent framed columns; buckling coefficient for uniform arch; angle sub-tended by whole span of a circular arch
α_1 buckling coefficient for a nonuniform arch
β constant for stiffened plates; angle of twist of cross section; buckling parameter in a stiffened arch; buckling parameter for a shallow arch; equivalent-length modification factor for unsymmetrical framed columns
β_2 coefficient in torsional-flexural buckling
γ buckling parameter for a stiffened plate; uncertainty factor in nominal load; taper coefficient in tapered beam analysis
Δ a deflection

Δ_ϵ an increment of strain
Δ_σ an increment of stress
Δ_{AB} deflection of point A relative to point B
δ column deflection caused by bending moment due to an axial load P; buckling parameter for a stiffened plate; amplification factor in a beam-column
δ_0 maximum initial out-of-straightness of a column; deflection without regard to moment induced by axial load
ϵ strain; coefficient in plate-buckling equation
ϵ_m maximum strain
ϵ_{st} strain at initial strain hardening
ϵ_y elastic strain at yield stress
ζ first mode damping ratio for an unloaded rod; coefficient in tapered beam analysis; exponent in formula for biaxially loaded short beam-column
η ratio of tangent modulus to elastic modulus, E_t/E; plasticity reduction factor for shell buckling; exponent in formula for biaxially loaded beam-column; coefficient in stiffened plate buckling formula; eccentricity parameter for a composite column
η_b, η_c shear shape factors for longitudinal and batten elements
Θ an angle
θ angle of tension-field yield band; a shell geometry parameter; subtending angle of half-span of a circular arch
$\theta_{AB}(\theta_{BA})$ rotation of tangent to elastic curve at $A(B)$ with respect to the line $AB(BA)$
θ_d angle of panel diagonal with flange
κ moment coefficient for lateral-torsional buckling
λ slenderness function $\sqrt{\sigma_y/\sigma_c}$, $\sqrt{\sigma_y/\sigma_c}$; length parameter in a stiffened shell; load ratio between adjacent framed columns
λ_e equivalent slenderness function
μ shear flexibility parameter in a laced or battened member; coefficient in tapered beam analysis
ν Poisson's ratio
ξ coefficient for buckling for a stiffened plate
ξ_a, ξ_b coefficients in laced and battened columns
ρ ratio of tension bands in a plate-girder web
σ normal stress
σ_1, σ_2 normal stress at edges of a plate under nonuniform edge loading
σ_ϕ circumferential stress in a shell
σ_a, σ_{av} average normal stress
σ_c critical stress
σ_c^* critical stress for a plate under normal compression alone, as used in an interaction formula for critical stress under mixed boundary stresses

σ_{cb} maximum nonuniform "pure bending" component of normal stress in a plate at critical load
σ_{cb}^* value of σ_{cb} as used in an interaction formula for combined normal stress and shear stress
$\sigma_{c(v)}$ critical stress for a variable cross section
σ_{cy} compressive yield strength, 0.2% offset
σ_e average stress at Euler buckling load; edge stress in a buckled plate
σ_{eb} elastic buckling stress for a beam
σ_f normal stress in a plate-girder flange
σ_i normal stress in the inelastic range (in a shell)
σ_m maximum stress at mid-length of column by the secant formula
$\sigma_{\max}$ maximum combined stress due to column load and bending moment
σ_n transverse normal stress in a plate-girder web
σ_p proportional limit stress
σ_r local residual stress; residual tension stress in plate-girder web; radial stress in a shell
σ_{rc} maximum residual compressive stress
σ_t tension-field stress in plate girder
σ_u average stress at failure in thin plate; ultimate unit strength of a column
σ_{uy} upper yield-point stress
σ_w warping normal stress
σ_x longitudinal stress in a compressed shell
σ_y yield-stress level; yield strength
σ_{yf} yield-stress in girder flange
σ_{ym} empirical stress level at which flange buckling is likely to occur
σ_{yr} reduced effective hoop yield stress in a shell
σ_{yw} yield stress in plate-girder web
τ shear stress; time parameter in modal response
τ_c, τ_{cr} critical shear stress in a plate
τ_c^* critical stress in pure shear as used in an interaction formula for critical plate stress under combined shear and normal stress
τ_{cri} inelastic critical buckling stress in web
τ_u shear stress at optimum tension-field angle
τ_w warping shear stress
τ_y shear stress at tension yield in plate girder
τ_{yw} shear yield stress in plate-girder web
ϕ angle of rotation; uncertainty factor of nominal resistance; angle of slope of arch axis
ψ parameter used in beam-column formulas; parameter to convert R_m to R_1
Ω arch buckling reduction factor for unsymmetrical loads
ω_k kth natural frequency of unloaded column

Abbreviations

AA	Aluminum Association
AASHTO	American Association of State Highway and Transportation Officials
AISC	American Institute of Steel Construction
AISE	Association of Iron and Steel Engineers
AISI	American Iron and Steel Institute
AREA	American Railway Engineering Association
ASCE	American Society of Civil Engineers
ASME	American Society of Mechanical Engineers
ASTM	American Society for Testing and Materials
CISC	Canadian Institute of Steel Construction
CRC	Column Research Council
CSA	Canadian Standards Association
ECCS	European Convention for Construction Steelwork
NACA	National Advisory Committee for Aeronautics
SSRC	Structural Stability Research Council
WRC	Welding Research Council

CHAPTER ONE

INTRODUCTION

1.1 THE METAL COLUMN

Whether a structure is man-made or created by nature, the column is the key element in resisting collapse under gravity loads, in buildings and bridges, and in trees and plants. This guide is a summary of modern knowledge on the behavior under load of metal columns. Development of the metal structural column has involved the interrelated development of theory, materials, testing machines, test instruments, design procedures, and design standardization. The history of column theory goes back to the work of the Swiss mathematician Leonard Euler, who in 1744 published his famous column formula. The theoretical developments since then represent some of the finest achievements in the discipline of applied mechanics. Bruce G. Johnston, editor of the first three editions of this guide, has given a clear review of this history in the paper "Column Buckling Theory: Historic Highlights" (Johnston, 1983).

Since 1944, when the Column Research Council (CRC) was founded, much of the theoretical and practical work related to metal column design was performed under the auspices of the council. In 1976 the name of the council was changed to Structural Stability Research Council (SSRC) to reflect the broadened scope of the research. The history of the CRC–SSRC—its accomplishments and the personalities involved—has been recounted by Bruce G. Johnston (1981) from the firsthand point of view of an active and creative initial and continuous participant.

Ever since the inception of the council it has played a leading role in developing rational design criteria based on research not only for metal columns but

also for all types of structures and structural elements where stability is a controlling feature of behavior under load. This accumulated knowledge has been disseminated by the SSRC in many forms, but the chief vehicles for presenting the sum of it have been the four previous editions of this guide (1960, 93 pages; 1966, 217 pages; 1975, 616 pages; 1988, 786 pages). The present fifth edition aims to continue the tradition.

1.2 SCOPE AND SUMMARY OF THE GUIDE

The continued importance and vitality of the research on stability problems is due to technical and economic developments that demand the use of ever-stronger and ever-lighter structures in an increasingly wider range of applications. Such an expansion of use is made possible by developments in (1) manufacturing, such as metallurgy, cold forming, extruding, and welding; (2) theory and understanding of behavior under load; (3) fabrication technology, such as the automated assembly of structural members; (4) computer-aided design; (5) economic competition from nonmetallic materials; and (6) construction efficiency. These developments continually not only change the way in which traditional structures are designed and built, but they also make possible the economical use of material in other areas of application, such as offshore structures, transportation vehicles, and outer-space structures. In all these applications the demands of higher strength and lighter weight inexorably lead to structures in which a consideration of stability must play a crucial role in design. Increased strength and increased slenderness invariably spell more problems with instability.

The third edition of this guide (published in 1975) was a substantial expansion over the second edition (published in 1966), introducing a number of new chapters that reflected the expanded scope of the Council. The fourth edition (published in 1988) added three new chapters, two on the fundamental topics of stability theory and finite element analysis of stability problems and one on box girders which dealt with the special stability problems of these structures having very slender plate elements.

The coverage of this fifth edition is compared with the contents of the fourth edition in Table 1.1. Some of the chapters, which deal with topics that did not receive a great amount of research interest from the task groups of the SSRC, were left relatively unchanged except for some updating of the literature and introducing one or two new topics. For example, in Chapter 14, on circular tubes and shells, the newly significant topic of the strength of damaged and repaired circular tubes in offshore platforms was added. Several chapters were eliminated in the new edition: structural safety is a mature topic of its own and is covered amply in the Commentaries of our major design specifications. The material from the chapters in the fourth edition on tapered structural members, columns with lacing, battens, or perforated cover plates, and mill building

TABLE 1.1 Comparison of the Fourth and Fifth Editions

Fourth Edition	Fifth Edition
1. Introduction	1. Introduction[a]
2. Stability Theory	2. Stability Theory[a]
3. Centrally Loaded Columns	3. Centrally Loaded Columns[b]
4. Plates	4. Plates[a]
5. Laterally Unsupported Beams	5. Beams[b]
6. Plate Girders	6. Plate Girders[b]
7. Box Girders	7. Box Girders[a]
8. Beam-Columns	8. Beam-Columns[b]
9. Tapered Structural Members	Absorbed into Chapters 3 and 5 in abridged form
10. Composite Columns	10. Composite Columns and Structural Systems[c]
11. Columns with Lacing, Battens, or Perforated Cover Plates	Absorbed into Chapter 3 in abridged form
12. Mill Building Columns	Absorbed into Chapter 3 in abridged form
13. Thin-Walled Metal Construction	13. Thin-Walled Metal Construction[b]
14. Circular Tubes and Shells	14. Circular Tubes and Shells[a]
15. Members with Elastic Lateral Restraints	15. Members with Elastic Lateral Restraints[b]
16. Frame Stability	16. Frame Stability[c]
17. Arches	17. Arches[b]
18. Doubly Curved Shells and Shell-like Structures	18. Doubly Curved Shells and Shell-like Structures[c]
19. Selected Topics in Dynamic Stability	19. Selected Topics in Dynamic Stability[a]
20. Structural Safety	Chapter was eliminated.
21. Finite Element Analysis of Stability Problems	21. Stability Analysis by Finite-Element Method[c]
	9. Horizontally Curved Steel I-Girders[c]
	11. Stability of Angle Members[c]
	12. Bracing[c]
	20. Stability Under Seismic Loading[c]
Appendix B Technical memoranda (seven)	Appendix B Technical memoranda (ten)

[a]Essentially the same as in the fourth edition, with minor editing.
[b]Substantially revised and new material added.
[c]Completely new chapter.

columns was absorbed into other chapters, such as those on centrally loaded columns and laterally unsupported beams.

Some topics that were part of other chapters in the fourth edition became important enough to deserve a completely new chapter of their own in the fifth edition. These are the chapters on stability of horizontally curved beams, stability of angle members, bracing, and stability under seismic loading. While

still carrying essentially the same name as in the fourth edition, several chapters are completely new and reflect modern developments in these areas of research. These are the chapters on composite columns, frame stability, doubly curved shells and shell-like structures, and stability analysis by finite element method. The remaining chapters include substantial new material.

The Technical Memoranda in Appendix B are of special interest to experimental researchers. Three new TMs are added in this edition: "Standard Methods and Definitions for Tests for Static Yield Stress," "Flexural Testing," and "Statistical Evaluation of Test Data for Limit States Design."

1.3 MECHANICAL PROPERTIES OF STRUCTURAL METALS

A knowledge of the stress-strain relationship during the elastic and initial inelastic ranges of behavior is an essential requisite to compression-member analysis. In the elastic range there are accepted average values of the modulus of elasticity, and test values vary within reasonably small limits. Specified values of the yield point or yield strength (depending on whether the initiation of yielding is a sudden or gradual process) are provided by the various specifications of the American Society for Testing and Materials (ASTM) and by product information from manufacturers. In this guide the term *yield stress* generally is used to denote either the yield point or yield strength, whichever is applicable.

Stress-Strain Relationships. The initial portions of the typical stress-strain curves for structural steels in compression or tension are shown in Fig. 1.1. The strengths of beams and columns are determined largely by stress-strain characteristics in the range shown. (The complete curves plotted to the same scale as Fig. 1.1 would take up a horizontal space between 20 and 30 times that available on the drawing.)

The structurally significant aspects of a stress-strain curve for carbon or high-strength low-alloy structural steels can be characterized by the following five properties (see Fig. 1.1):

E = modulus of elasticity = slope of stress-strain curve in the elastic range
σ_{uy} = upper yield point (maximum stress prior to yield stress level)
σ_y = yield-stress level (stress at a constant strain rate in the flat portion of the stress-strain curve after initial yield)
ϵ_{st} = strain at initial strain hardening
$E_{st} = (d\sigma/d\epsilon)_{\epsilon=\epsilon_{st}}$ = strain-hardening modulus (initial)

These properies are generally sufficient for calculation of the inelastic strength and plastic deformation of structural steel members.

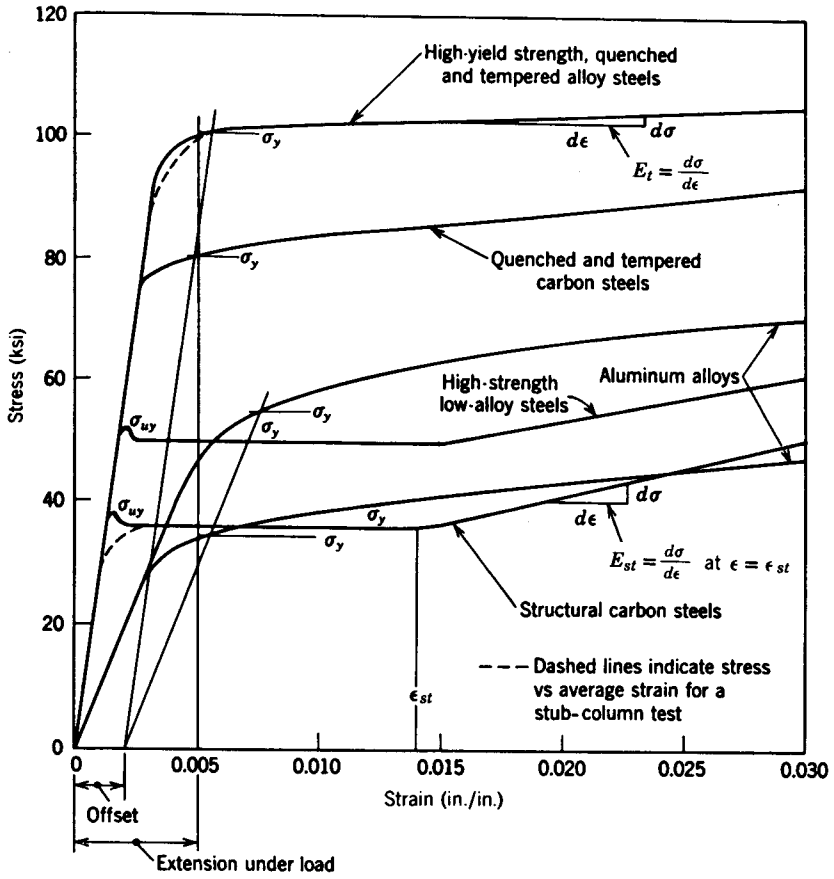

Fig. 1.1 Initial stress-strain relationships for structural steels in compression or tension.

Structurally significant properties of the aluminum alloys, quenched and tempered steels, cold-worked steels, and stainless steels include the modulus of elasticity, E; the yield strength, preferably determined by the offset method (ASTM Designation A370); and the tangent modulus, $E_t = d\sigma/d\epsilon$, which varies with stress for strains greater than the elastic limit. For all steels and aluminum alloys the maximum tensile (ultimate) strength, based on original area, is also a part of the mill test report, although of no direct relevance to compression-member behavior.

The yield stress of both steel and aluminum alloy varies with temperature, rate of strain, and the surface characteristics of the test specimen, as well as with the testing machine and test method. The yield stress is a function of the rate of strain, becoming lower as the testing speed is lowered. *Zero strain rate*

defines a lower limit of the testing speed corresponding to the lowest yield-stress level for structural steels. ASTM specifications establish a maximum allowable strain rate. Tests made according to these specifications may be suitable for quality control but indicate yield-stress values as much as 15% greater than those from tests at low rates of strain. The influence of strain rate is less, percentagewise, for the higher-strength steels.

For as-rolled structural steels the yield-stress level in a tension or compression test can be regarded as the level of stress, after initial yield, that is sufficient at a given temperature and rate of strain to develop successively new planes of slip in the portions of the test specimen that remain in the elastic state. After initial yielding has proceeded discontinuously from point to point throughout the specimen, a general strain hardening begins, and the stress rises with further increase in strain. The sharp yield point may disappear with cold work or heat treatment.

The yield-stress level is structurally more significant than the upper yield point, and its existence for relatively large average strains with no appreciable change in stress is taken advantage of in plastic design and inelastic analyses by permitting the assumption that the stress is constant and equal to the yield stress across yielded portions of the cross section.

The plot of average stress versus strain as determined by a stub-column test is somewhat different from that resulting from the test of a small specimen. Residual stresses are one cause of these differences (indicated qualitatively in Fig. 1.1); other factors are the lack of uniformity of yield stress over the cross section and varying degrees of working during the rolling process. Similarly, strain hardening caused by the forming processes in cold-formed members may result in changes in yield stress which tend to shift the curve of average stress versus strain toward higher values of stress and more gradual yield development. Cold-forming effects are particularly pronounced for the stainless steels.

1.4 DEFINITIONS

The following list of terms defines their use in this guide. These terms are supplementary to the list of symbols provided in the notation and include primarily those for which variations in meaning are prevalent in the technical literature.

Beam: a straight or curved structural member, primarily supporting loads applied at right angles to the longitudinal axis. The internal stresses on a transverse cross section may be resolved into one or more of three resultant components: a transverse shear, a bending moment, and a torsional moment.

Beam-Column: a beam that also functions to transmit compressive axial force.

Bifurcation: a term relating to the load-deflection behavior of a perfectly straight and perfectly centred compression element at critical load. Bifurcation can occur in the inelastic range only if the pattern of postyield properties and/or residual stresses is symmetrically disposed so that no bending moment is developed at subcritical loads. At the critical load a member can be in equilibrium in either a straight or slightly deflected configuration, and a bifurcation results at a branch point in the plot of axial load versus lateral deflection from which two alternative load-deflection plots are valid.

Braced Frame: a frame in which the resistance to both lateral load and frame instability is provided by the combined action of floor diaphragms and a structural core, shear walls, and/or a diagonal, K brace, or other auxiliary system of bracing.

Buckle: to kink, wrinkle, bulge, or otherwise lose original shape as a result of elastic or inelastic strain.

Buckled: descriptive of the final shape after buckling.

Buckling Load: the load at which a compressed element, member, or frame collapses in service or buckles in a loading test.

Critical Load: the load at which bifurcation (*see* Bifurcation) occurs as determined by a theoretical stability analysis.

Effective Length: the equivalent or effective length (KL) which, in the buckling formula for a pin-ended column, results in the same elastic critical load as for the framed member or other compression element under consideration at its theoretical critical load. Use of the effective length concept in the inelastic range implies that the ratio between elastic and inelastic critical loads for an equivalent pin-ended column is the same as the ratio between elastic and inelastic critical loads in the beam, frame, plate, or other structural element for which buckling equivalence has been assumed.

Effective Width: a reduced width of plate, slab, or flat segment of a cross section which, assuming uniform stress distribution, leads to the same behavior of a structural member as the actual section of plate and the actual nonuniform stress distribution.

First yield: a limiting stress level above which a permanent set results upon removal of a load.

Initial Imperfection: an unavoidable deviation from perfect geometry: for example, initial crookedness of a member, initial out-of-plumb of a story, initial out-of-flatness of a plate, or initial denting or bulging of a shell, which is within the accepted practical tolerance of the particular applicable fabrication technology.

Instability: a condition reached during buckling under increasing load in a compressive member, element, or frame at which the capacity for resistance to additional load is exhausted and continued deformation results in a decrease in load-resisting capacity.

Proportional Limit: the load or stress beyond which there is a significant amount of deviation from a prior linear load-deformation or stress-strain relationship. The term is usually used in connection with a tensile or compressive test, and the sensitivity of the strain or deformation measuring device is a determining factor in the evaluation.

Residual Stress: the stresses that exist in an unloaded member after it has been formed into a finished product. Such stresses can be caused by cold bending, finishing, straightening, flame cambering, oxygen cutting, welding, cooling after rolling, or quenching during heat treatment.

Restraint: deviation from the ideal articulated boundary condition or unbraced condition of an element, a member, or a structure.

Stability: the capacity of a compression member or element to remain in position and support load, even if forced slightly out of line or position by an added lateral force. In the elastic range, removal of the added lateral force would result in a return to the prior loaded position, unless the disturbance causes yielding to commence.

Strain-Hardening Modulus: for structural steels that have a flat (plastic) region in the stress-strain relationship, the strain-hardening modulus is the initial slope of the stress-strain curve just beyond the terminus of the flat region. It depends on prior strain and thermal history and exhibits a much greater range of variation than does the elastic modulus of the material.

Stub Column: a short compression test specimen utilizing the complete cross section, sufficiently long to provide a valid measure of the stress-strain relationship as averaged over the cross section, but short enough so that it will not buckle as a column in the elastic or plastic range.

Tangent Modulus: the slope of the stress-strain curve of material in the inelastic range, at any given stress level, as determined by the compression test of a small specimen under controlled conditions. The *effective tangent modulus* (as determined by a stub-column test) is modified by nonhomogeneity of material properties and by residual stresses.

Tangent-Modulus Load: the critical column load obtained by substituting E_t, the tangent modulus, for E in the Euler formula.

Tension-Field Action: a description of the postbuckling behavior of a plate girder panel under shear force, during which diagonal compressive stresses cause the web to form diagonal waves. The tensile stresses, parallel to the wave troughs, induce compressive stresses in the transverse stiffeners.

Unbraced Frame: a frame in which the resistance to lateral load is provided primarily by the bending resistance of the frame members and their connections.

Yield Point: the maximum stress recorded in a tensile or compressive test of steel specimen prior to entering the plastic range.

Yield Strength: in a tension or compression test, the stress at which there is a specified amount of measured deviation from an extension of the initial linear stress-strain plot, commonly taken as the intersection of the stress-strain curve and a line parallel with the linear portion of the curve but offset by a strain of 0.002.

Yield Stress: a general term, denoting either yield strength, yield-stress level, or yield point, as defined herein.

Yield-Stress Level: for carbon- and low-alloy structural steels, the stress immediately beyond the elastic strain range, within which range the strain appears to increase without change in stress. It may be defined arbitrarily as the stress determined at a strain of 0.005.

1.5 POSTBUCKLING BEHAVIOR

Load-deflection relationships in the postbuckling range have an important bearing on the structural design significance of the critical load. For the idealized "perfect" compression element—one that is perfectly elastic, devoid of imperfection, and within which the load-induced stress is perfectly uniform—three different types of postbuckling behavior are typified by (1) the column, (2) the stiffened plate, and (3) the cylindrical shell. For each of these three cases Fig. 1.2 illustrates with light lines the load-deflection curves beyond the critical load for each "perfect" element, which for a given situation and given buckling mode are uniquely determinable by a theoretical analysis. The heavy lines in Fig. 1.2 indicate the theoretical behavior for the same elements when a given degree of imperfection is assumed. The heavy lines approach the light lines as a limit, as the degree of imperfection is assumed to diminish toward zero. The heavy lines are also indicative of what may be expected in a laboratory test.

In the elastic range of behavior of a slender column, (1) the critical load and the maximum load carried by an imperfect column are in reasonable agreement; thus the critical load provides a satisfactory basis for computing the design load. For the stiffened plate, (2), if the added postbuckling strength is achieved with acceptably small lateral deflections, a greater design load in relation to the critical load might be acceptable. But for the thin-walled cylinder, (3), the maximum load in the real situation is drastically reduced with respect to the critical load; it is to an uncertain degree dependent on the amount of imperfection. Thus the critical load in this case is not a suitable criterion on which to base an allowable design load.

Figure 1.2 depicts only elastic behavior; inelastic behavior of the material may alter the relationships in either of two ways: Buckling may be elastic, as indicated, but the added stress (1) due to bending may cause the combined stress to exceed the elastic stress range, or (2) due either to residual stress or inherent nonlinearity of the stress-strain relationship, the critical and buckling loads may occur in the inelastic range.

In the first case, when the yield point is reached after initial elastic behavior, the curves shown in Fig. 1.2 will simply branch into new paths below those

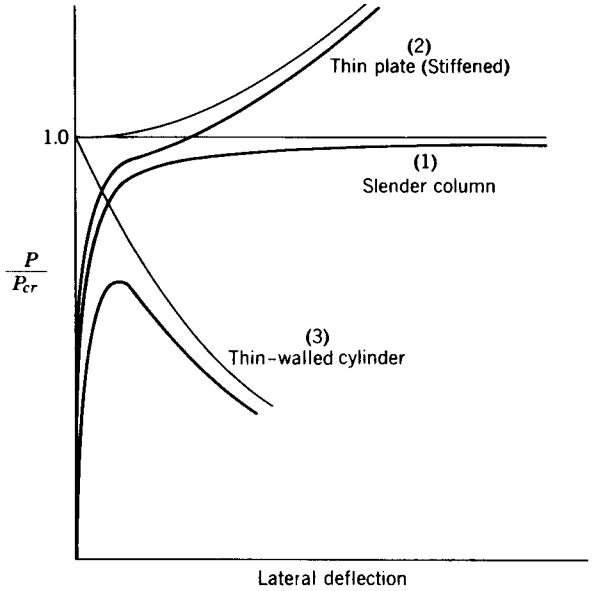

Fig. 1.2 Elastic postbuckling curves for compressed elements.

shown. In the second case, the light lines emanating from the critical load bifurcation point will each take on a different initial increment of slope. In the case of the column, the horizontal line indicative of Euler buckling will be replaced by a curved line, initially sloping upward and reaching a maximum (instability point) somewhat greater than the critical load. The column with very small imperfections tends to approach this behavior as the imperfections lessen in size, with the result that with small imperfections a column under test may reach or slightly exceed the critical (tangent modulus) load. Most important, the relevance of the critical load, or lack of relevance, is not altered from that pertinent to the completely elastic behavior, as discussed previously. Large initial imperfections, however, may cause the maximum buckling strength to be significantly lower than the critical load.

1.6 CREDITS FOR THE CHAPTERS IN THE FIFTH EDITION OF THE SSRC GUIDE

This book is the product of the many people who have given unstintingly of their time and talent. This effort is gratefully acknowledged. Following is a recognition of those individuals and groups who have made major contributions arranged by chapters:

Chapter 1, "Introduction," was revised by the editor of this volume of the guide.

Chapter 2, "Stability Theory," was originally written by Alex Chajes for the fourth edition and kept without many changes for this edition.

Chapter 3, "Centrally Loaded Columns," was revised extensively by the members of SSRC Task Group 1. The following persons provided substantial input: Reidar Bjorhovde, Wai-Fah Chen, Mo Elgaaly, Laurie Kennedy, LeRoy Lutz, Murty Madugula, Maurice Sharp, and the editor. The work was assembled and coordinated by Laurie Kennedy.

Chapter 4, "Plates," was originally written by Shien T. Wang and updated and revised by SSRC Task Group 13 under the guidance of Dymos Polyzois.

Chapter 5, "Beams," was revised by Sriramulu Vinnakota, who received advice from J. J. Cheng, Duane Ellifritt, Jindrich Melcher, and the other members of SSRC Task Group 15. The original text was written by the editor, with assistance from Sriramulu Vinnakota, Nicholas Trahair, Yuhsi Fukumoto, Joachim Lindner, David Nethercot, and Kit Kitipornchai.

Chapter 6, "Plate Girders," was revised and updated extensively by Mo Egaaly, chairman of Task Group 27.

Chapter 7, "Box Girders," was written by Patrick Dowling and his colleagues at Imperial College in London. It was changed only minimally for this edition by the editor.

Chapter 8, "Beam-Columns," originally written by David Nethercot, was revised and updated for this edition by the editor.

Chapter 9, "Horizontally Curved Steel I-Girders," was written by Abdul Zureick.

Chapter 10, "Composite Columns, and Structural Systems," was written by Roberto Leon.

Chapter 11, "Stability of Angle Members," was produced by SSRC Task Group 26, under the editorship of LeRoy Lutz and Mo Elgaaly, with substantial input from Murti Madugula and the editor of this edition of the guide.

Chapter 12, "Bracing," was written by Todd Hellwig and Joe Yura.

Chapter 13, "Thin-Walled Metal Construction," is the result of the work of SSRC Task Group 13. The revisions were coordinated by Roger LaBoube with the assistance of Sam Errera, Reinie Schuster, Greg Hancock, and Teoman Pekoz.

Chapter 14, "Circular Tubes and Shells," was originally written by Don Shermann, who also revised the chapter for this edition, with assistance from Peter Birkemoe, Jim Rickles, and the editor.

Chapter 15, "Members with Elastic Lateral Restraints," was originally written by Mo Elgaaly and Bruce Johnston and revised for this edition by Mo Elgaaly.

Chapter 16, "Frame Stability," was written by Greg Deierlein and Don White, with assistance from the members of Task Group 4.

Chapter 17, "Arches," was updated by Sriramulu Vinnakota, with assistance from S. Kuranishi, T. Yabuki, and T. Sakimoto.

Chapter 18, "Doubly Curved Shells and Shell-like Structures," was written by Nick Morris.

Chapter 19, "Selected Topics in Dynamic Stability,' was originally written by D. Krajcinovic, A. E. Sommers, R. Plaut, S. S. Chen, and G. J. Simitses. The chapter is identical in both the fourth and fifth editions.

Chapter 20, "Stability Under Seismic Loadings," was written by Subhash Goel and reviewed by the members of Task Group 24.

Chapter 21, "Stability Analysis by Finite Element Methods," was written by P. K. Basu.

REFERENCES

Johnston, B. G. (1981), "History of Structural Stability Research Council," *ASCE J. Struct. Div.*, Vol. 107, No. ST8, pp. 1529–1550.

Johnston, B. G. (1983), "Column Buckling Theory: Historic Highlights," *ASCE J. Struct. Eng.*, Vol. 109, No. 9, pp. 2086–2096.

CHAPTER TWO

STABILITY THEORY

2.1 INTRODUCTION

The principal subject matter of this guide is the stability of metal structures. This chapter introduces the various types of instability encountered in the other chapters by presenting the solutions to several simple illustrative problems.

Instability is a condition wherein a compression member loses the ability to resist increasing loads and exhibits instead a decrease in load-carrying capacity. In other words, instability occurs at the maximum point on the load-deflection curve.

Problems in instability of compression members can be subdivided into two categories: those associated with the phenomenon *bifurcation of equilibrium*, and those in which instability occurs when the system reaches a maximum, or limit, load without previous bifurcation. In the first case a perfect member, when subjected to increasing load, initially deforms in one mode and then, at a load referred to as the *critical load*, the deformation suddenly changes into a different pattern. Axially compressed columns, plates, and cylindrical shells experience this type of instability. By comparison, members belonging to the latter category deform in a single mode from the beginning of loading until the maximum load is reached. Shallow arches and spherical caps subjected to uniform external pressure are examples of the second type of instability.

2.2 BIFURCATION BUCKLING

2.2.1 Initially Perfect Systems

The critical load of a compression member, obtained from the linear analysis of an idealized perfect member, does not necessarily coincide with the load at which collapse of a real imperfect member occurs. To determine the failure load of an actual member it is necessary to take initial imperfections into account and to consider the entire nonlinear load-deflection curve of the member. Unfortunately, the process of obtaining such a curve is often too difficult and time consuming to be used in routine engineering design. Instead, the maximum load of a compression member is generally calculated by semiempirical means, that is, using curves fitted to numerically obtained maximum strength curves or combining test results with a qualitative understanding of the nonlinear load-deflection behavior of the imperfect member.

A general understanding of the basic characteristics of the elastic buckling and postbuckling behavior of members that become unstable as a result of bifurcation can be obtained by considering the simple model in Fig. 2.1. The model consists of two rigid bars hinged to one another and to the supports, and restrained laterally by a nonlinear elastic spring. A similar model has been used by many, including Budiansky and Hutchinson (1964) and Hoff (1966).

The restraining force F exerted by the spring on the bars is assumed to be related to the lateral displacement x by

$$F = k_1\epsilon - k_2\epsilon^2 + k_3\epsilon^3 \tag{2.1}$$

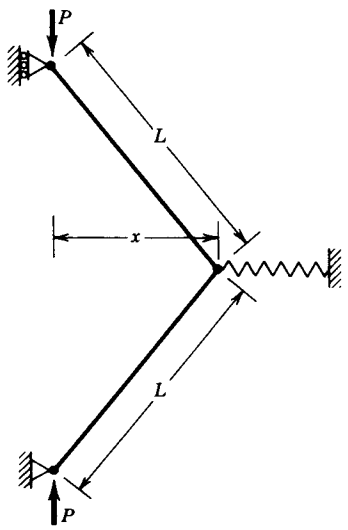

Fig. 2.1 Bifurcation-buckling model.

where $\epsilon = x/L$. If the model is initially straight, equilibrium in a deformed configuration requires that

$$P\epsilon = \frac{F}{2}(1-\epsilon^2)^{1/2} = \tfrac{1}{2}(k_1\epsilon - k_2\epsilon^2 + k_3\epsilon^3)(1-\epsilon^2)^{1/2} \tag{2.2}$$

Letting ϵ become infinitesimally small in Eq. 2.2, we obtain for the critical load

$$P_c = \frac{k_1}{2} \tag{2.3}$$

Based on the work of Koiter (1970), it has been demonstrated that the essential characteristics of the postbuckling behavior of a member can be determined by considering the initial stages of the postbuckling curve, in the vicinity of the critical load. Thus ϵ is assumed to be small but finite, which reduces Eq. 2.2 to

$$P\epsilon = \tfrac{1}{2}(k_1\epsilon - k_2\epsilon^2 + k_3\epsilon^3) \tag{2.4}$$

In view of Eq. 2.3, the foregoing expression can be rewritten in the form

$$P = P_c(1 - a\epsilon + b\epsilon^2) \tag{2.5}$$

where $a = k_2/k_1$ and $b = k_3/k_1$.

Certain structures behave in a symmetrical manner; that is, the buckling characteristics are the same regardless of whether the deformation is positive or negative. To simulate the behavior of such structures, we let $a = 0$. Equation 2.5 then reduces to

$$P = P_c(1 + b\epsilon^2) \tag{2.6}$$

The load-deflection curves corresponding to Eq. 2.6 are shown in Fig. 2.2. The type of behavior depicted by these curves is referred to as *bifurcation buckling*. The member initially deforms in one mode, the prebuckling deformation, and then at the critical load, due to a branch in the load-deflection curve, the deformation suddenly changes into a different pattern, the buckling mode. For example, axially loaded columns initially shorten due to axial compression. Then at the critical load the member suddenly begins to bend.

The curve in Fig. 2.2*a* results if $b > 0$, and the curve in Fig. 2.2*b* if $b < 0$. These two cases correspond to models whose springs become either stiffer or more flexible with increasing lateral deflection. In a similar manner the stiffness of an actual structure may either increase or decrease subsequent to the onset of buckling. In other words, the load required to keep the structure in a deformed configuration may either increase or decrease as the deformation increases in magnitude. If the load that the structure can support subsequent

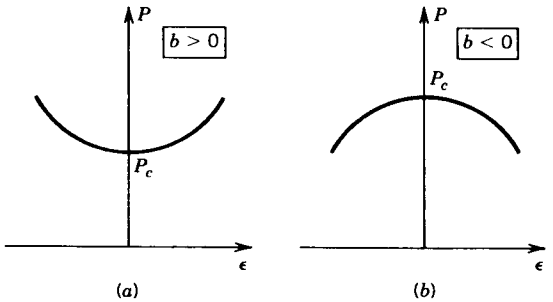

Fig. 2.2 Symmetric buckling of a bifurcation model: (*a*) stable postbuckling curve; (*b*) unstable postbuckling curve.

to the onset of buckling increases with increasing deformation, as shown in Fig. 2.2*a*, the structure is said to have a *stable postbuckling curve*. By comparison, if the load decreases, as indicated in Fig. 2.2*b*, the member has an *unstable postbuckling curve*.

An axially compressed plate is an example of a structure with a stable postbuckling curve. As the plate buckles, the buckling deformations give rise to tensile membrane stresses which increase the stiffness of the plate and give it the capacity to resist increases in the load. By comparison, the guyed tower in Fig. 2.3 has an unstable postbuckling curve. As the top of the tower deflects laterally, some of the cables are stretched, causing them to push down on the post. As a consequence, the external load required to maintain equilibrium decreases with the magnitude of the lateral deflection. The most notorious example of a structure with an unstable postbuckling curve is the axially compressed cylindrical shell. However, this system does not buckle in a symmetric manner and its behavior is therefore not fully described by Fig. 2.2*b*.

To simulate the behavior of structures that behave in an asymmetric manner, we let $b = 0$ in Eq. 2.5. Thus

$$P = P_c(1 - a\epsilon) \tag{2.7}$$

The load-deflection curve corresponding to Eq. 2.7 is shown in Fig. 2.4. Unlike the symmetric system, the unsymmetric one becomes stiffer if it deflects one way and more flexible if it deflects the opposite way.

The simple frame in Fig. 2.5*a* is an example of a structure that has an asymmetric postbuckling curve. If the frame buckles as shown in Fig. 2.5*b*, a secondary tension force V is induced in the vertical member. As a consequence the external load P that the structure can support increases with increasing deformations. By comparison, if the frame buckles as indicated in Fig. 2.5*c*, a secondary compression force is induced in the vertical member and the resistance of the system to applied loads decreases with increasing deformations.

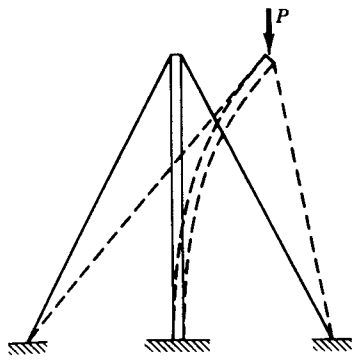

Fig. 2.3 Guyed tower.

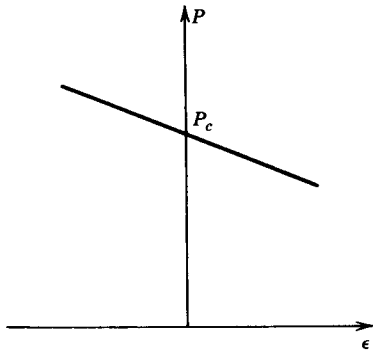

Fig. 2.4 Asymmetric buckling of a bifurcation model.

The foregoing analytically predicted behavior of the frame in Fig. 2.5 has been verified experimentally by Roorda (1965).

2.2.2 Initially Imperfect Systems

The postbuckling curve of an initially perfect system does not by itself give sufficient information to allow one to determine when failure takes place. To obtain that information, one must also consider the initial imperfections of shape and eccentricities of loading that are present in all real structures.

Assuming that our model has an initial deformation x_0, as indicated in Fig. 2.6, Eq. 2.4 takes the form

$$P(\epsilon + \epsilon_0) = \frac{1}{2}(k_1\epsilon - k_2\epsilon^2 + k_3\epsilon^3) \tag{2.8}$$

where $\epsilon_0 = x_0/L$. In view of Eq. 2.3, the relation above can be rewritten as

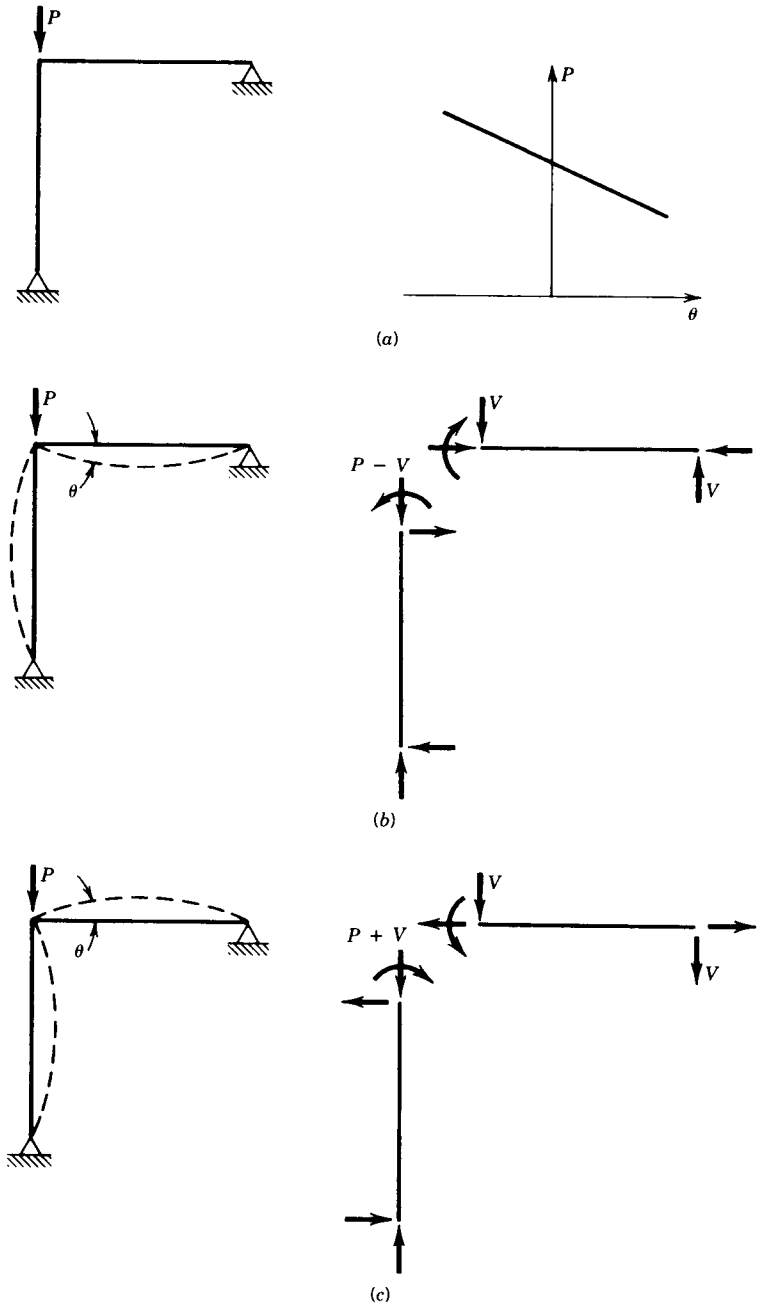

Fig. 2.5 Buckling of an L-shaped frame.

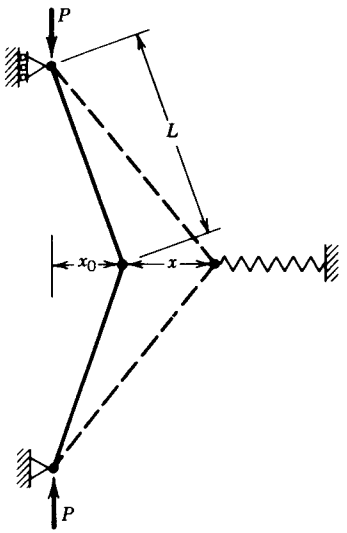

Fig. 2.6 Model of an initially imperfect system.

$$P = \frac{P_c(\epsilon - a\epsilon^2 + b\epsilon^3)}{\epsilon + \epsilon_0} \tag{2.9}$$

For symmetric behavior $a = 0$ and

$$P = \frac{P_c(\epsilon + b\epsilon^3)}{\epsilon + \epsilon_0} \tag{2.10}$$

and for asymmetric behavior $b = 0$ and

$$P = \frac{P_c(\epsilon - a\epsilon^2)}{\epsilon + \epsilon_0} \tag{2.11}$$

The load-deflection curves corresponding to Eqs. 2.10 and 2.11 are shown as dashed lines in Fig. 2.7. It is evident from these curves that small initial imperfections do not significantly affect the behavior of systems with stable postbuckling curves. These members can continue to resist increasing loads above the critical load, and failure takes place only after yielding of the material has occurred.

The amount of postbuckling strength that a system with a stable postbuckling curve possesses depends on two factors: the steepness of the postbuckling curve, and the relative magnitude of the critical load and the load at which yielding begins. For example, axially compressed plates possess a relatively steep postbuckling curve and as a consequence often exhibit sizable postbuckling strength. Failure loads three or four times as large as the critical load have

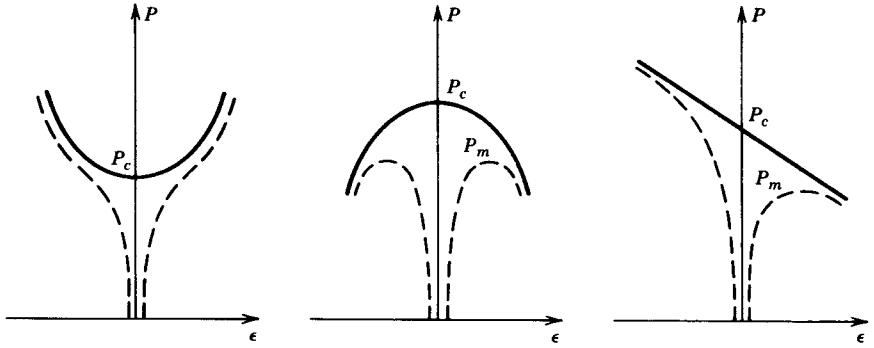

Fig. 2.7 Postbuckling curves of initially imperfect system.

been obtained (Gerard, 1957). By comparison, the slope of the postbuckling curve of an axially loaded column is extremely small and the failure load of such a member therefore coincides, very nearly, with the critical load.

In addition to possessing a relatively steep postbuckling curve, a system must have a yield load that is considerably in excess of its critical load if the system is to exhibit significant postbuckling strength. A very rough estimate of the postbuckling strength of an axially compressed plate is given by the expression

$$\frac{P_c}{P_f} = \left(\frac{P_c}{P_y}\right)^{1/2} \tag{2.12}$$

where P_c is the critical load, P_f the failure load, and P_y the load when yielding commences. According to Eq. 2.12, a plate possesses significant postbuckling strength when P_c/P_y is considerably smaller than unity. Hence only thin plates can be expected to display sizable postbuckling strength.

Whereas small initial imperfections have only a negligible effect on the behavior of systems with stable postbuckling curves, they have a very marked effect on systems with unstable postbuckling curves. As indicated by the curves in Fig. 2.7, the presence of small initial imperfections will cause systems with unstable postbuckling curves to fail at loads below the critical load. These structures are accordingly referred to as being *imperfection sensitive.*

By setting $dP/d\epsilon = 0$ for Eqs. 2.10 and 2.11, the following approximations of the maximum load P_m can be obtained. For the symmetric system with $b < 0$,

$$\frac{P_m}{P_c} = 1 - 3\left(-\frac{b}{4}\right)^{1/3} \epsilon_0^{2/3} \tag{2.13}$$

and for the asymmetric system,

$$\frac{P_m}{P_c} = 1 - 2(a\epsilon_0)^{1/2} \tag{2.14}$$

Equations 2.13 and 2.14 indicate that the larger the initial imperfection x_0, and the steeper the postbuckling curve (i.e., the larger a or b), the smaller will be the ratio of P_m to P_c. Axially compressed cylindrical shells that have a very steep postbuckling curve have been found to fail at loads significantly below the critical load (Brush and Almroth, 1975). Using both theory and tests it has been demonstrated that initial imperfections whose magnitude is only 10% of the shell thickness can result in maximum loads whose magnitude is 60% of the critical load (Hutchinson and Koiter, 1970). Conversely, by manufacturing and testing nearly perfect shell specimens, failure loads only slightly below the critical load have been obtained (Tennyson, 1964).

In conclusion, it is evident that the behavior of real imperfect members can be predicted from the shape of the postbuckling curve for perfect systems. Members with stable postbuckling curves will fail at loads equal to or above the critical load, whereas members with unstable postbuckling curves will fail at loads below the critical load.

2.3 LIMIT-LOAD BUCKLING

Buckling that is associated with a bifurcation of equilibrium is not the only form of instability that can occur. A second type of instability that can take place is illustrated by the model in Fig. 2.8. The model consists of a simple arch, formed by two elastic bars hinged to each other and to the supports. As the load P acting on the model increases, legs AB and BC shorten by an amount Δ, and point B moves down a distance d. The axial force F induced in the bars by the applied load P is equal to

$$F = \frac{P}{2\sin\phi} = \frac{PS}{2(h-d)} \tag{2.15}$$

and the axial shortening Δ of each bar is given by

$$\Delta = \frac{F}{K} = \frac{PS}{2K(h-d)} \tag{2.16}$$

in which $S = \sqrt{L^2 + d^2 - 2dh}$ is the length of the compressed bars and $K = AE/L$ is the stiffness of the bars. Substitution of $\Delta = L - S$ in Eq. 2.16 leads to

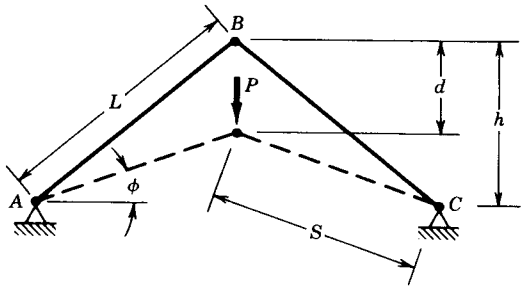

Fig. 2.8 Limit-load buckling model.

$$L - S = \frac{PS}{2K(h-d)}$$

or

$$L - \sqrt{L^2 + d^2 - 2dh} = P\frac{\sqrt{L^2 + d^2 - 2dh}}{2K(h-d)} \tag{2.17}$$

If the rise h of the arch is assumed to be small compared to L, Eq. 2.17 reduces to

$$P = \frac{Kh^3}{L^2}(2\delta - 3\delta^2 + \delta^3) \tag{2.18}$$

in which $\delta = d/h$.

The load-deflection relation corresponding to Eq. 2.18 is depicted by the solid curve in Fig. 2.9. It is evident that no bifurcation of equilibrium exists. Instead, the load and deformation increase simultaneously until a maximum or limit load is reached (point 1) beyond which the system becomes unstable.

If the rise h of the model is large enough compared to L, the axial forces in the legs may reach their critical loads, causing the legs to buckle as hinged–hinged columns before the entire system reaches its limit load at point 1. In that case buckling occurs as a result of a bifurcation of equilibrium at point 5 on the curve.

The behavior of arches and spherical shells subject to uniform external pressure is similar to that described by the curves in Fig. 2.9. Arches and spherical caps with a large rise-to-span ratio fail in an asymmetric mode as a result of bifurcation buckling, whereas shallow arches and spherical caps fail in a symmetric mode, due to limit-load buckling.

An extensive treatment of similar and more complex elastic stability phenomena is presented by Thompson and Hunt (1984).

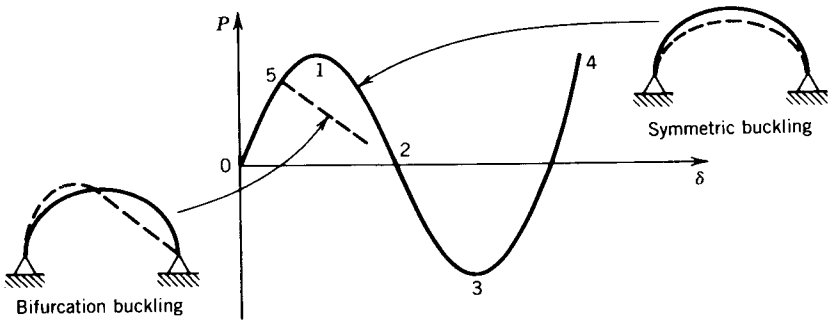

Fig. 2.9 Load-deflection curve of a limit-load model.

REFERENCES

Brush, D. O., and Almroth, B. O. (1975), *Buckling of Bars, Plates and Shells*, McGraw-Hill, New York.

Budiansky, B., and Hutchinson, J. W. (1964), "Dynamic Buckling of Imperfection-Sensitive Structures," *Proc. 11th Int. Congr. Appl. Mech.*, Munich, Germany.

Gerard, G. (1957), "Handbook of Structural Stability: Part IV. Failure of Plates and Composite Elements," *NACA Tech. Note No. 3784*, Aug.

Hoff, N. J. (1966), "The Perplexing Behavior of Thin Circular Cylindrical Shells in Axial Compression," *Isr. J. Technol.*, Vol. 4, No. 1.

Hutchinson, J. W., and Koiter, W. T. (1970), "Postbuckling Theory," *Appl. Mech. Rev.*, Vol. 23.

Koiter, W. T. (1970), "On the Stability of Elastic Equilibrium," *Tech. Rep. No. AFFDL-TR-70-25*, Air Force Flight Dynamics Laboratory, Wright Patterson Air Force Base, Ohio, Feb.

Roorda, J. (1965), "Stability of Structures with Small Imperfections," *ASCE J. Eng. Mech. Div.*, Vol. 91, No. EM1, pp. 87–106.

Tennyson, R. C. (1964), "An Experimental Investigation of the Buckling of Circular Cylindrical Shells in Axial Compression Using the Photoelastic Technique," *Rep. No. 102*, Institute of Aerospace Sciences, University of Toronto, Toronto, Ontario, Canada, Nov.

Thompson, J. M. T., and Hunt, G. W. (1984), *Elastic Instability Phenomena*, Wiley, New York.

CHAPTER THREE

CENTRALLY LOADED COLUMNS

3.1 INTRODUCTION

The cornerstone of column theory is the Euler column, a mathematically straight, prismatic, pin-ended, perfectly centrally loaded strut that is slender enough to buckle without the stress at any point in the cross section exceeding the proportional limit of the material. The *buckling load* or *critical load* or *bifurcation load* (see Chapter 2 for a discussion of the significance of these terms) is defined as

$$P_E = \frac{\pi^2 EI}{L^2} \tag{3.1}$$

where EI is the elastic stiffness and L is the length of the column. The Euler load P_E is the reference value to which the strength of actual columns is usually compared.

If end conditions other than perfectly frictionless pins can be defined mathematically, the critical load is expressed by

$$P_{EK} = \frac{\pi^2 EI}{(KL)^2} \tag{3.2}$$

where KL is an *effective length* defining the portion of the deflected shape between points of zero curvature. In other words, KL is the length of an equivalent pin-ended column buckling at the same load as the end-restrained column. For example, for columns in which one end of the member is prevented from translating with respect to the other end, K can take on values ranging from 0.5 to 1, depending on the end restraint.

The isolated column is a theoretical concept; it rarely exists in practice. Usually, a column forms part of a structural frame and its stability is interrelated with the stability of the entire structure. The structure imposes not only axial forces but also end restraints and flexural and torsional forces on the column. This interrelationship is treated elsewhere in many parts of this guide. This chapter treats only the isolated column because (1) many structural design situations are idealized such that elements can be thought of as centrally loaded columns (e.g., truss members), and (2) the centrally loaded column is a limiting point in the mathematical space defining the interaction between axial and flexural forces in a member in a structure. Thus an understanding of the strength of individual centrally loaded columns is essential to the development of design criteria for compression members in general.

Columns are made in a variety of cross sections and by several processes, depending on their size and shape. Most steel columns are prismatic (i.e., the cross section is the same from end to end). These are discussed in Section 3.2. Virtually all rolled shapes can be used as columns, although some are much more efficient than others because of such factors as the ratio of the governing moment of inertia to the weight per unit length; the ratio of the radii of gyration about perpendicular axes, double or single symmetry or asymmetry of the cross section; and the propensity toward torsional or torsional–flexural buckling.

Section 3.3 deals with tapered columns, generally fabricated by welding flange plates to a tapered web plate. These find much use in rigid moment-resisting steel frames, where they act, of course, as beam-columns. For frames with hinged bases, the cross-sectional depth increases from the base to the knee, where the bending moments are large.

Built-up columns, the subject of Section 3.4, now are likely to take the form of members with perforated cover plates. They find use in large bridges and mill buildings where either the loads are relatively large or special circumstances suggest their use. Section 3.5 covers the special problems of mill building columns.

3.2 PRISMATIC COLUMNS

3.2.1 Column Strength

Column strength is characterized by the maximum axial force that can be supported without excessive lateral deformations. Column strength has been studied extensively for several centuries, and many reviews of this rich and varied subject of structural mechanics exist in papers and textbooks. The previous editions of this guide provide an excellent introduction to those wishing

to learn more on the subject (see Chapter 1 for further references on the history of column formulas). Here only the concepts essential to developments in the later portions of this chapter are briefly explained.

Column strength can be approximated by considering theoretically either (1) a column with mathematically perfect geometry and perfect centroidal loading: *critical load theory*, and (2) a column in which the geometry and/or the loading deviate slightly from the perfect: *theory of imperfect columns*. The imperfections are practically unavoidable and they represent acceptable construction tolerances which are, as a general rule, not visible to the naked eye, nor can they be quantified precisely beforehand.

The reason for this dual representation (i.e., perfect and imperfect) is that for practical purposes some types of columns (e.g., cold-formed steel and aluminum columns) can be idealized as perfect, while for other columns (e.g., hot-rolled or welded built-up structural steel columns), it is necessary to consider the effects of the imperfections.

The following discussion focuses on columns failing by instability of the entire member. Columns made from thin plate elements can also fail by local plate or shell instability, and in some cases there is interaction between overall and local buckling. These topics are treated in greater detail in Chapters 4, 13, and 14.

Critical-Load Theory. The strength of a perfectly straight prismatic column with perfect central loading and well-defined end restraints is the Euler load, P_E (Eq. 3.2), as long as the material is still elastic when buckling occurs. When the axial load attains P_E, a stable equilibrium configuration is possible even in the presence of lateral deflection (Fig. 3.1*a*), while the load remains essentially constant (Fig. 3.1*b*, lines *OAB*). Even if an initial deflection, and/or an initial load eccentricity is present, the maximum load will approach the Euler load asymptotically as long as the material remains elastic (curve *C* in Fig. 3.1*b*).

Many practical columns are in a range of slenderness where at buckling portions of the columns are no longer elastic, and thus one of the key assumptions underlying Euler column theory is violated. Essentially, the stiffness of the column is reduced by yielding. This degradation of the stiffness may be the result of a nonlinearity in the material iteself (e.g., aluminum, which has a nonlinear stress-strain curve), or it may be due to partial yielding of the cross section at points of compressive residual stress (e.g., steel shapes).

The postbuckling behavior of such a column is radically different from the elastic column: Bifurcation buckling occurs at the tangent-modulus load (point *D* in Fig. 3.1*c*),

$$P_t = \frac{\pi^2 E_t I}{L^2} \tag{3.3}$$

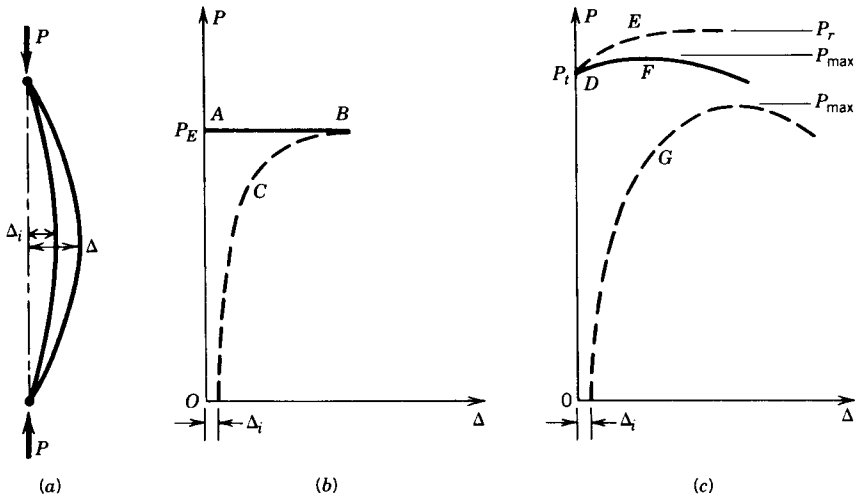

Fig. 3.1 Behavior of perfect and imperfect columns.

but further lateral deflection is possible only if the load increases. If there were no further changes in stiffness due to yielding, the load would asymptotically approach the *reduced-modulus load* (*E* in Fig. 3.1*c*),

$$P_r = \frac{\pi^2 E_r I}{L^2} \tag{3.4}$$

as the deflection tends to large values. The increase in load is due to the elastic unloading of some fibers in the cross section, which results in an increase in stiffness. The tangent modulus E_t is the slope of the stress-strain curve (Fig. 3.2) when the material is nonlinear, but E_r and E_t when residual stresses are present also depend on the shape of the cross section. Since increased loading beyond the tangent-modulus load results in further yielding, stiffness continues to be reduced and the load-deflection curve achieves a peak ($P_{\max}$, point *F* in Fig. 3.1*c*), beyond which it falls off.

The improved understanding of the postbuckling behavior of inelastic columns made possible by Shanley ((1947) represented the single most significant step in understanding column behavior since Euler's original development of elastic buckling theory in 1744. Thus a perfect inelastic column will begin to deflect laterally when $P = P_t$ and $P_t < P_{\max} < P_r$.

Imperfect Column Theory. Geometric imperfections, in the form of tolerable but unavoidable out-of-straightness of the column and/or eccentricity of the axial load, will introduce bending from the onset of loading, and curve *G* in Fig. 3.1*c* characterizes the performance of such a column. Lateral deflec-

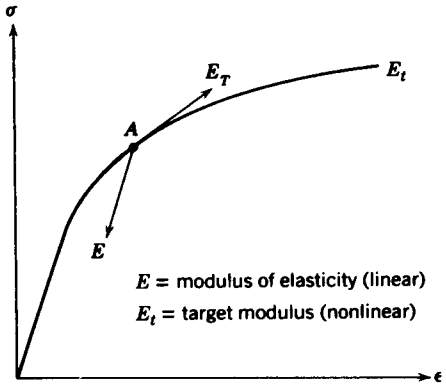

Fig. 3.2 General stress-strain relationship.

tion exists from the start of loading, and the maximum load is reached when the internal moment capacity at the critical section is equal to the external moment caused by the product of the load and the deflection. The maximum load is thus a function of the imperfection. For some types of columns the nature of the problem is such that the maximum capacity of the imperfect column is closely approximated by the tangent modulus load of the perfect column, but for many types of columns the imperfections must be included to give a realistic maximum load.

In general, the strength of columns must be determined by including both the imperfections and the material nonlinearity and/or the residual stress effects. The following parts of this chapter examine in detail how the maximum strength of metal columns can be determined and how this information is used in developing design methods.

Design of Metal Columns as Related to Strength Theories. The determination of the maximum strength of metal columns can be a complicated process, often involving numerical integration, especially when initial imperfections and material nonlinearities or residual stresses must be considered. The structural designers, having to proportion many columns in the course of their working day, cannot be concerned with such lengthy calculations. Simplified column formulas are usually provided for design office practice. These column formulas involve the major parameters of strength, such as the yield point, the length, and the cross-sectional properties, and factors of safety (or local factors) are prescribed to give designs of acceptable safety. Many column formulas have been used throughout the history of structural engineering, and the reader can consult many textbooks, including the third edition of this guide, to learn more about the subject.

While elastic columns can be designed on the basis of the Euler theory, inelastic columns, by necessity of having to account for geometric imperfections and material nonlinearities, are usually designed with empirical column formulas. There are essentially four basic ways by which column design formulas, curves, or charts have been developed:

1. *Empirical formulas based on the results of column tests.* Such formulas are applicable only to the material and the cross section for which the tests were performed. The earliest column formulas (from the 1840s) are of this type. However, some recent papers (e.g., Hall, 1981; Fukumoto et al., 1983) have utilized the availability of computerized data banks that contain a large proportion of all the column tests reported in the literature. It appears that such formulas may have some difficulty in gaining modern acceptance because they are based entirely on tests. Also, they cannot, in a rational way, account for end restraint.

2. *Formulas based on the yield limit state.* These formulas define the strength of a column as that axial load which will give an elastic stress for an initially imperfect column equal to the yield stress. Such column formulas have a long history, also dating back to the middle of the nineteenth century, and they continue to enjoy popularity to the present (e.g., the British use of the Perry–Robertson formula) (Trahair, 1988). Empirical factors can account for initial imperfections of geometry and loading, but the formulas do not consider the necessarily inelastic basis of column strength, nor can they rationally account for end restraint.

3. *Formulas based on the tangent-modulus theory.* Such formulas can rationally account for the bifurcation load (but not the maximum strength) of perfectly straight columns. If the effects of imperfections are such that they just reduce the maximum strength to the tangent-modulus strength, these formulas have empirical justification. On the other hand, if the perfect column can be thought of as an anchor point in an interaction surface, initial imperfections of geometry and loading can be represented as flexural effects in the interaction equation.

The "CRC—Column Strength Curve," named after the acronym of the former name of the Structural Stability Research Council (i.e., Column Research Council), is given by

$$\frac{\sigma_{cr}}{\sigma_y} = \begin{cases} 1 - \dfrac{\lambda^2}{4} & \text{for } \lambda \le \sqrt{2} \quad (3.5) \\ \dfrac{1}{\lambda^2} & \text{for } \lambda \ge \sqrt{2} \quad (3.6) \end{cases}$$

where

$$\lambda = \frac{KL}{r}\frac{1}{\pi}\sqrt{\frac{\sigma_y}{E}} \quad (3.7)$$

This curve was recommended in the first edition of this guide (1960) and has been used for many steel design specifications in North America and elsewhere (AISC, 1979). It is based on the average critical stress for small and medium-sized hot-rolled wide-flange sections of mild structural steel, with a symmetrical residual stress distribution typical of such members. The column curves based on the tangent-modulus theory can also accurately account for end restraints (Yura, 1971).

4. *Formulas based on maximum strength.* Modern trends in column design involve column formulas which are a numerical fit of curves obtained from maximum strength analysis of representative geometrically imperfect columns containing residual stresses. The third edition of this guide (1976) presented new column curves based on this principle. Following this, SSRC published Technical Memorandum No. 5, stating the principle that design of metal structures should be based on the maximum strength, including the effects of geometric imperfections. It was also suggested that the strength of columns might be represented better by more than one column curve, thus introducing the concept of multiple column curves. The SSRC curves 1, 2, and 3 are one set of such curves; another example is the set of curves in Eurocode 3 (ECS, 1994). The Canadian standard (CSA, 1994) contains two column curves.

3.2.2 Influence of Residual Stress

Structural steel shapes and plates contain residual stresses that result primarily from uneven cooling after rolling. Welded built-up members exhibit tensile residual stresses in the immediate vicinity of the welds, due to the cooling of the weld metal. These are equal to the yield point of the weld metal, which will normally be somewhat greater than the yield point of the parent metal (Tall, 1966; Alpsten and Tall, 1970; Bjorhovde et al., 1972). Flame cutting introduces intense heat in a thin region close to the flame-cut edge. As a result, the material in this region acquires properties that are significantly different from those of the base metal, and residual stresses develop that are often much higher than the yield point of the parent material (McFalls and Tall, 1970; Alpsten and Tall, 1970; Bjorhovde et al., 1972). Finally, cold forming and cold straightening introduce residual stresses, especially in regions with the most severe bending effects (e.g., corners) (Frey, 1969; Alpsten, 1972b; Sherman, 1976; Yu, 1992).

In 1908, in a discussion of the results of column tests at the Watertown Arsenal, residual stresses due to the cooling of hot-rolled steel columns were cited as the probable cause of reduced column strength in the intermediate slenderness range (Howard, 1908). The possible influence of residual stresses on the buckling strength of both rolled members and welded plates in girders was subsequently noted by others (Salmon, 1921; Madsen, 1941). Systematic research on the effect of residual stress on column strength was initiated in the late 1940s under the guidance of Research Committee A of the Column

Research Council (Osgood, 1951; Yang et al., 1952; Beedle and Tall, 1960). This work continued through extensive investigations, primarily at Lehigh University, through the early 1970s (Kishima et al., 1969; McFalls and Tall, 1970; Alpsten and Tall, 1970; Brozzetti et al., 1970a; Bjorhovde et al., 1972). Work in Europe and Canada on these effects must also be noted to appreciate fully the magnitude and complexity of the problem (Sfintesco, 1970; Beer and Schultz, 1970; Alpsten, 1972a; Chernenko and Kennedy, 1991).

At the time of the first edition of this guide (1960), the critical-load tangent-modulus curve, based on the effect of typical residual-stress distributions in hot-rolled steel shapes, seemed a proper basis for the determination of allowable column design stresses. Column strength theory could thus be unified, and the tangent-modulus concept, as modified for steel shapes with residual stress, could be extended to all metals. The CRC column strength curve, based on computed column curves for rolled steel H-shaped members, taken as an approximate average of the strong- and weak-axis buckling curves, served as a basis for the column design provisions of the AISC and CSA specifications. The second edition of this guide (1966) mentioned the increasing use of columns made of (1) high-strength steels with yield stresses up to 70 ksi, and (2) heat-treated steels with yield stresses up to 100 ksi or more. It noted the importance of initial imperfections as well as of residual stresses in determining the strengths of pin-ended columns made of higher-strength steels.

One of the possible ways of discriminating between different categories of column strength is through the use of the concept of multiple column curves, such as those that were developed through research work at Lehigh University (Bjorhovde and Tall, 1971; Bjorhovde, 1972) and those that have been provided by the studies in Europe (Beer and Schultz, 1970). In addition, large numbers of column tests have also been performed, in some cases on a systematic basis, to provide further assurance of the theoretical results obtained by computer studies. The single largest group of such column tests is probably the more than 1000 tests that were made at a number of European universities and laboratories, as well as a number of tests on heavy shapes at Lehigh University, under the auspices of the European Convention for Constructional Steelworks (Sfintesco, 1970). Over the years, a great many other tests have also been performed, and these have been summarized by Fukumoto et al. (1983).

Hot-Rolled Shapes. The magnitude and distribution of residual stresses in hot-rolled shapes depend on the type of cross section, rolling temperature, cooling conditions, straightening procedures, and metal properties (Beedle and Tall, 1960). Examples of residual-stress distributions resulting from cooling without straightening of wide-flange shapes are shown in Fig. 3.3 (Tall, 1964). For the heavier shapes, residual stresses vary significantly through the thickness. Figure 3.4 shows residual stresses measured (Brozzetti et al., 1970a) in one of the heaviest (W14 × 730) rolled shapes currently produced.

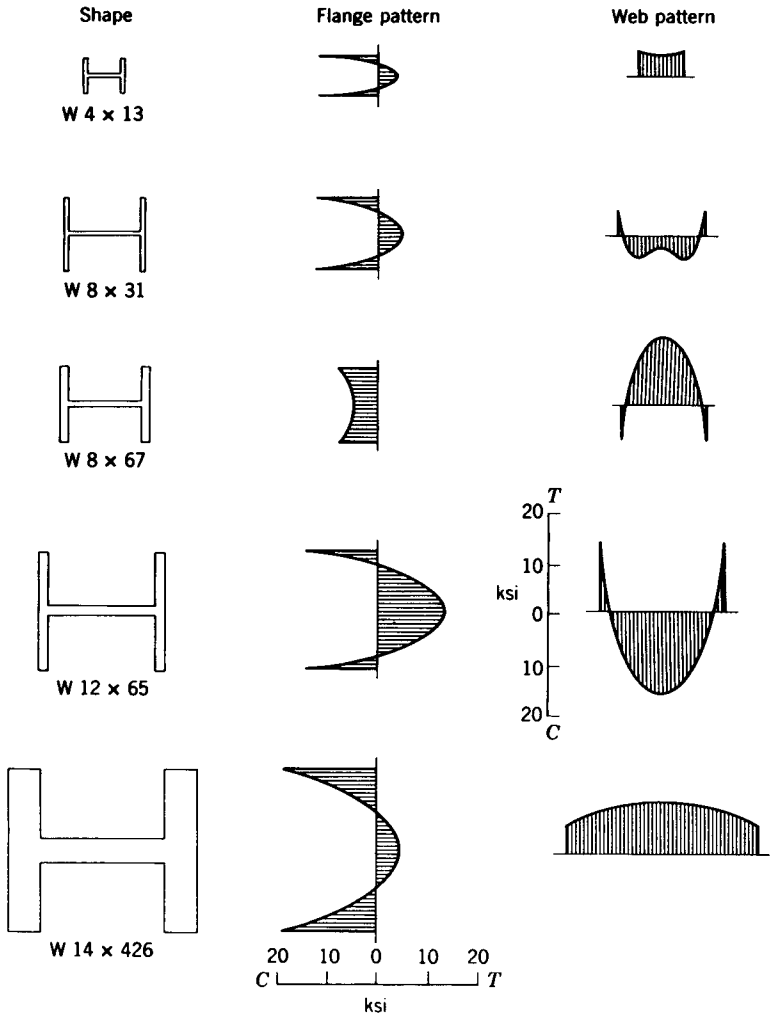

Fig. 3.3 Residual-stress distribution in rolled wide-flange shapes.

The effect of steel grade on the residual-stress distribution is not as great as the effect of geometry (Tall, 1964). Residual-stress measurements in the flanges of similar shapes made of different steel grades show that the distributions and magnitudes of the residual stress are similar and it is here—in the flanges—that residual stresses have a major effect on the column strength of H-shaped sections.

Calculated critical-load column curves based on the residual stresses found in the five particular shapes of Fig. 3.3 are plotted in Fig. 3.5 for buckling about the minor axis, along with maximum strength column curves determined

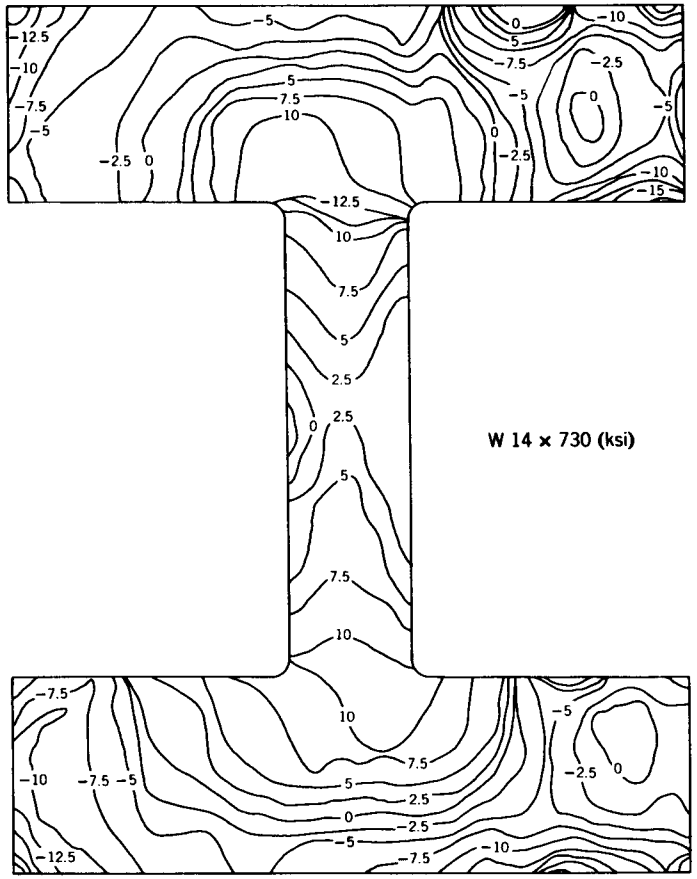

Fig. 3.4 Residual-stress distribution in W14 x 730 shape.

by computer analyses and based on a combination of the measured residual stresses and an initial curvature equal to the maximum tolerated by the ASTM A6 standard.

To interrelate the residual stress and initial curvature effects systematically, extensive column strength analyses were made at the University of Michigan (Batterman and Johnston, 1967). The studies included yield stresses of 36, 60, and 100 ksi (248, 414, and 689 MPa); maximum compressive residual stresses of 0, 10, and 20 ksi (0, 69, and 138 MPa); five curvatures corresponding to initial midlength out-of-straightness ranging from 0 to $0.004L$; and slenderness ratios ranging from 20 to 240. Emphasis was on buckling about the minor axis, and the results of this condition are presented graphically in the work by Batterman and Johnston (1967), permitting maximum-strength evaluation within the range of the parameters cited. On the basis of a maximum residual stress of

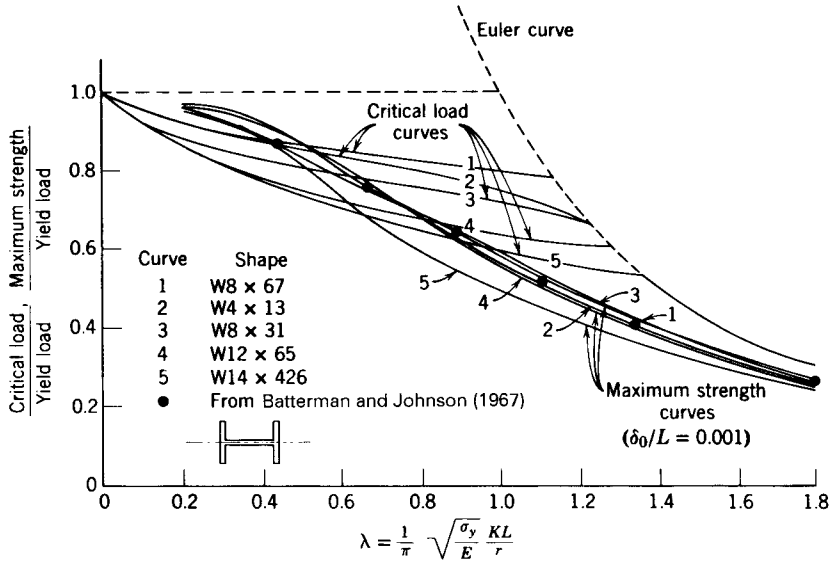

Fig. 3.5 Critical-load curves for straight columns compared with maximum-strength curves for initially curved rolled steel W-shapes.

13 ksi (90 MPa), which is the scaled average maximum for the five sections shown in Fig. 3.3, together with a yield stress of 36 ksi (248 MPa), the maximum column strength predicted by Batterman and Johnston is shown by the solid circles on Fig. 3.5. The solid curves are from an analysis neglecting the webs. Although the shapes and residual stress distributions are different, there is good correlation between the two independently developed analysis procedures. These findings are also corroborated by those of a wide-ranging investigation of column strength (Bjorhovde, 1972), which examined the behavior and strength of a large and diverse number of structural shapes. The computational procedure is very accurate but requires knowledge of the residual stresses and the out-of-straightness. In the study performed at Lehigh University (Bjorhovde, 1972), the full range of structural steel grades and shapes was examined, as well as a number of welded build-up box and H-shapes.

The results obtained by the studies of Batterman and Johnston (1967) and Bjorhovde (1972) show clearly that:

1. The separate effects of residual stress and initial curvature cannot be added to give a good approximation of the combined effect on the maximum column strength. Thus in some cases and for some slenderness ratios, the combined effect is less than the sum of the parts (intermediate slenderness ratios, low residual stresses). In other cases the combined effect is more than the sum of the parts. The latter applies to the intermediate slenderness ratio

range for heavy hot-rolled shapes in all steel grades and for welded built-up H-shapes. It is emphasized that the magnitudes of the maximum compressive residual stresses in a large number of these shapes were 50% or more of the yield stress of the steel itself.

2. Residual stress has little effect on the maximum strength of very slender columns, either straight or initially crooked, which have strengths approaching the Euler load. However, such columns made of the higher-strength steels can tolerate much greater lateral deflection before yield or before becoming unstable.

3. Strengths are slightly underestimated in a computer analysis when based on the assumption that an initial crookedness in the shape of a half-sine wave remains a half-sine wave during further loading.

4. Differences in column strength caused by variations in the shape of the residual stress pattern are smaller for initially crooked columns than for initially straight columns.

More recent data on the residual stresses of very heavy hot-rolled shapes confirmed the findings of Brozzetti et al. (1970a) and demonstrated further that the relative maximum column strength (i.e., computed maximum strength divided by the yield load) reaches a minimum for flange thicknesses around 3 to 4 in (75 to 100 mm). The relative strength increases as the flange thickness exceeds this magnitude (Bjorhovde, 1988; 1991).

Welded Built-Up Columns. Residual stresses resulting either from welding or from the manufacture of the component plates have a significant influence on the strength of welded H- or box-section columns. The maximum tensile residual stress at a weld or in a narrow zone adjacent to a flame-cut edge is equal to or greater than the yield stress of the plates (Alpsten and Tall, 1970; McFalls and Tall, 1970; Alpsten, 1972a; Brozzetti et al., 1970b; Bjorhovde et al., 1972). Welding modifies the prior residual stresses due either to flame cutting or cooling.

Figure 3.6 shows that the strengths of welded columns made of higher-strength steels appear to be influenced relatively less by residual stresses than are the strengths of similar columns made of lower-strength steels (Kishima et al., 1969; Bjorhovde, 1972). It is also evident that the differences in strengths of columns with the maximum permissible initial crookedness are less than the differences in critical loads of initially straight columns (see Fig. 3.5).

As shown in Fig. 3.7, plates with mill-rolled edges (universal mill plates) have compressive residual stresses at the plate edges, whereas flame-cut plates have tensile residual stresses at the edges. In built-up H-shapes made of universal mill plates, the welding will increase the compressive stress at the flange tips, enlarging the region of compressive residual stress and adversely affecting the column strength. Thus, as illustrated in Fig. 3.8, an H-shape column made from flame-cut plates will have favorable tensile residual stresses at the flange

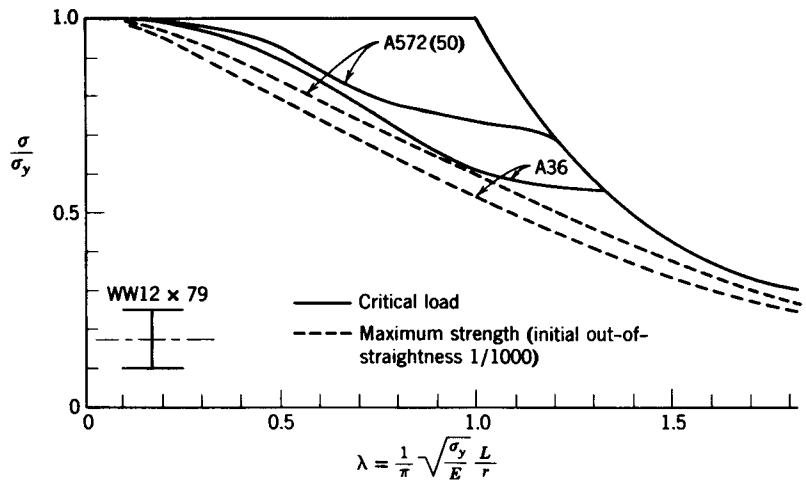

Fig. 3.6 Critical-load curves for welded WW12 × 79 of flame-cut plates compared with maximum-strength curves for initially curved members (Kishima et al., 1969; Bjorhovde, 1972).

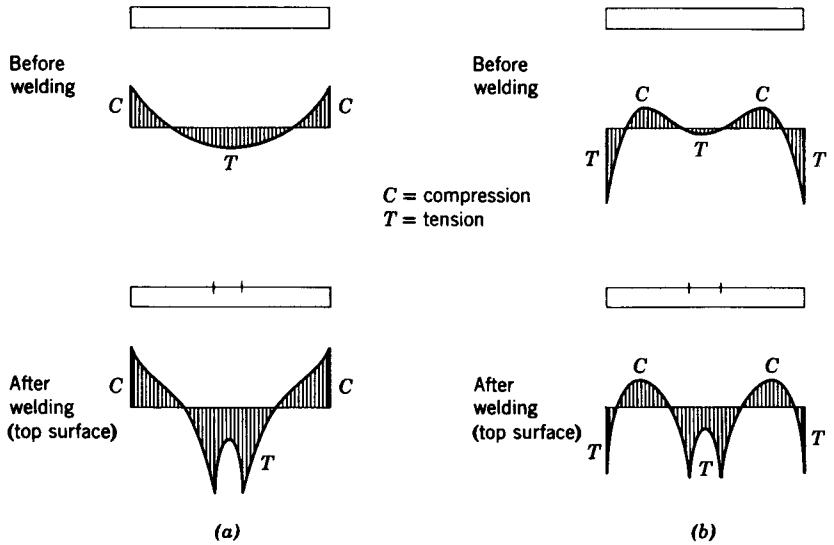

Fig. 3.7 Qualitative comparison of residual stresses in as-received and center-welded universal mill and oxygen-cut plates: (*a*) universal mill plate: (*b*) oxygen-cut plate.

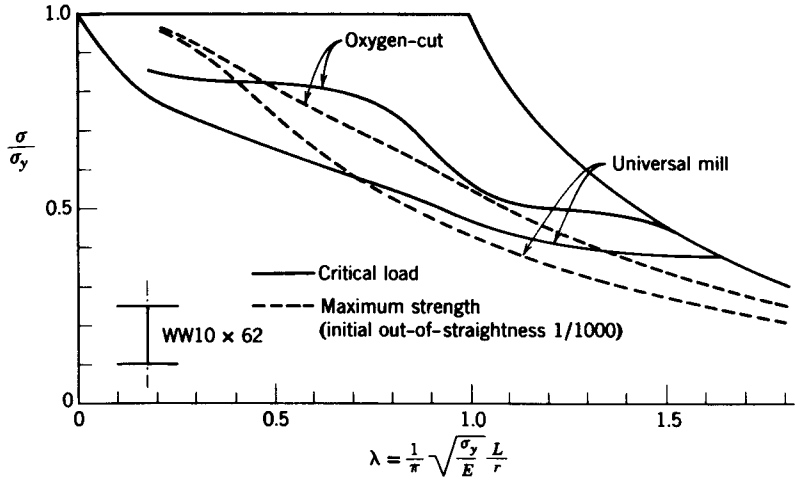

Fig. 3.8 Comparison of column curves for WW10 × 62 (A7 steel) with universal mill versus oxygen-cut plates (Bjorhovde, 1972).

tips. It therefore exhibits greater column strength than that of a column of the same section with flanges consisting of a universal mill plate in which both rolled edges are retained. It is also seen that for short welded columns, the maximum strength of an initially curved column may in some cases be greater than the critical load of a straight column. Obviously, the maximum strength of an initially straight column will always be greater than the critical load of the same column.

Strength differences between box section columns made of universal mill and flame-cut plates are relatively small, because the edge welds override the residual stresses in the component plates (Bjorhovde and Tall, 1971). The sequence of welding can be a significant factor for such columns, particularly for those with large welds (Beer and Tall, 1970).

Several investigations have considered the effects of column size. It has been shown (Kishima et al., 1969; Alpsten and Tall, 1970; Brozzetti et al., 1970b; Bjorhovde et al., 1972), that welding has a greater influence on the overall distribution of residual stress in small and medium-sized shapes than in the case of heavy shapes.

The distribution of residual stress in heavy plates and shapes is not uniform through the thickness (Brozzetti et al., 1970a; Alpsten and Tall, 1970). As thickness increases, the difference between surface and interior residual stresses may be as much as 10 ksi (69 MPa). As an example, Fig. 3.9 shows an isostress diagram for a heavy welded shape made from flame-cut plates. However, it has been found that calculated critical loads and maximum column strengths are only a few percent less when based on the complete residual-stress distribu-

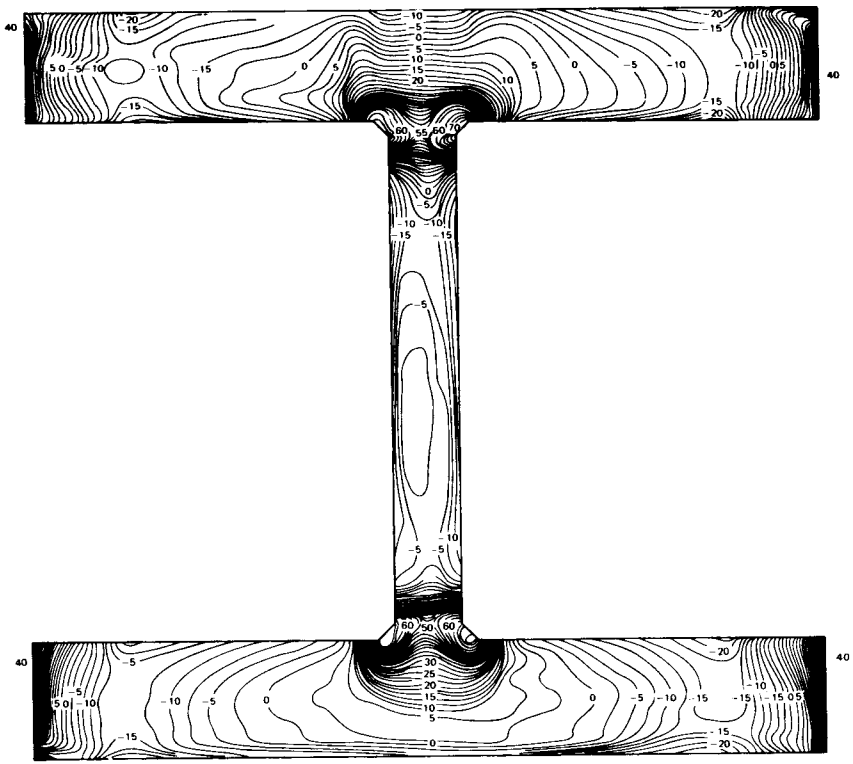

Fig. 3.9 Isostress diagram for WW23 × 681 welded built-up shape (stresses in kips per square inch) (Alpsten and Tall, 1970).

tions, as compared with analyses that assume the stress to be constant through the thickness and equal to the surface-measured residual stress.

In general, shapes made from flame-cut plates exhibit higher strength than shapes that are made from universal mill plates. This is demonstrated by the curves in Fig. 3.10. Similarly, flame-cut shapes tend to have strengths that are comparable with those of similar rolled shapes, whereas universal mill shapes tend to be comparatively weaker (Fig. 3.10).

Figure 3.11 compares the strengths of two typical welded columns with flame-cut flange plates, and one being distinctly heavier than the other. It is seen that the heavier shape tends to be relatively stronger than the lighter one. This is even more accentuated for shapes that are welded from universal mill plates; for these the strength of the lighter shape will be significantly lower than the heavy one (Bjorhovde and Tall, 1971; Bjorhovde, 1972). This is the reason the Canadian Standards Association in its limit-states design standard has since 1974 required that welded built-up shapes can only be made from flame-cut plates. In a major study, Chernenko and Kennedy (1991) examined

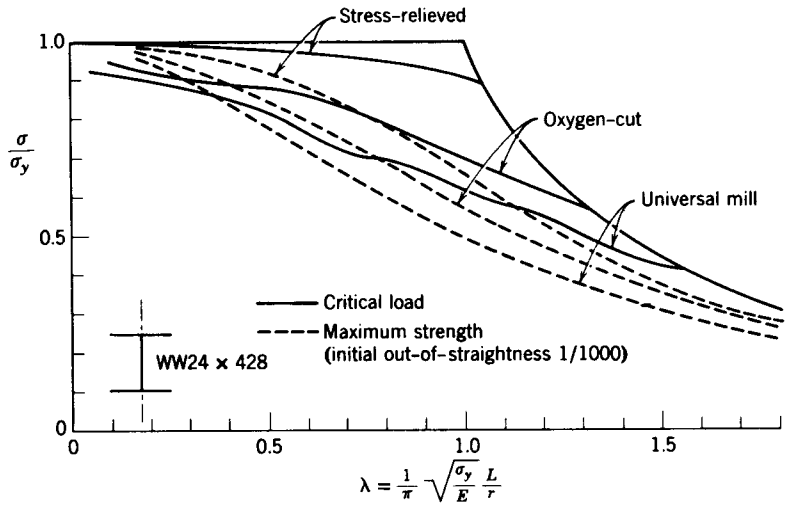

Fig. 3.10 Column curves for heavy and light welded wide-flange shapes (Bjorhovde, 1972).

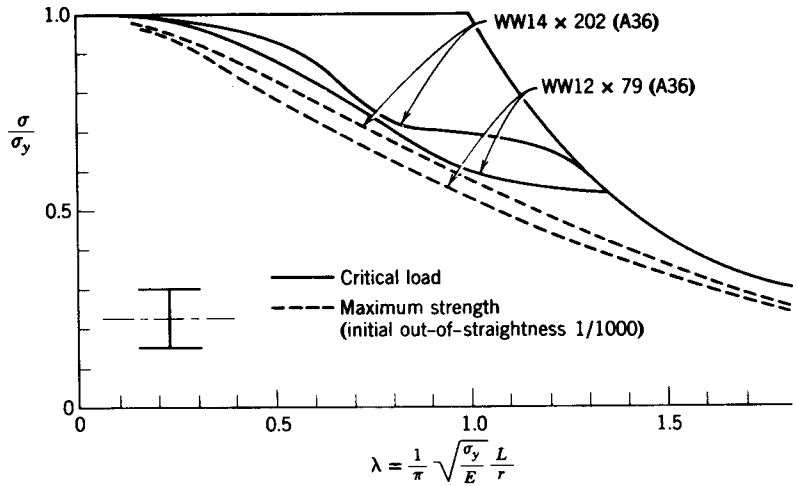

Fig. 3.11 Comparison of column curves for WW24 × 428 (A36 steel) with stress-relieved, oxygen-cut, and universal mill plates (Bjorhovde, 1972).

an extensive range of welded built-up wide-flange shapes. In addition to performing maximum-strength computations for columns with a variety of residual-stress distributions and out-of-straightnesses, the work also examined statistical data on material and other properties. Resistance factors for use with LRFD criteria for welded columns were developed. It is shown that

current approaches were conservative. As a consequence, these shapes were assigned to the higher of the two column curves in the 1994 edition of the CSA standard (CSA, 1994).

The sequence of welding and the number of welding passes are factors influencing the distribution of residual stresses. Other welding parameters, such as voltage, speed of welding, and temperature and areas of preheating, have less influence (Brozzetti et al., 1970b). Stress-relief annealing of the component plates prior to welding of the shape raises column strength very significantly by reducing the magnitude of the residual stresses, even though it lowers the yield stress of the steel. Figure 3.10 compares the column curves for shapes made from flame-cut and universal mill plates, along with curves for the same shapes made from stress-relieved plates.

Cold-Straightened Columns. Cold straightening of structural sections to meet tolerances for camber and sweep induces a redistribution and reduction of the residual stresses that were caused by earlier rolling and cooling. In current mill practice, either rolls or gag presses are used to straighten structural shapes (Brockenbrough, 1992). In *roller straightening* (also called *rotorizing*), the shape is passed through a train of rolls that bend the member back and forth with progressively diminishing deformation. In *gag straightening*, concentrated forces are applied locally along the length of the member to bend it to approximate straightness. The process is used on structural shapes of all sizes.

The roller-straightening process redistributes and reduces the initial residual stresses in the flanges, as shown in Fig. 3.12. In gag straightening, moments that approximate the full plastic value, M_p, are produced at the points where the forces are applied, and the cooling residual stresses are therefore redistributed only at or near points of loading. In the usual case of gag straightening, to remove sweep [curvature about the weak (y–y) axis of a wide-flange shape], change in residual stress from compression to tension takes place locally at the edges on the side of the flanges where the load is applied. Figure 3.13 shows the residual stresses measured in a W8 × 31 shape (Huber, 1956) after gag straightening about the weak axis.

The strength of a cold-straightened column is, in general, greater than that of the corresponding as-rolled member (Frey, 1969; Alpsten, 1970), because of the improved straightness and the redistribution of residual stress. Roller straightening produces a greater improvement than gag straightening and, according to theoretical analyses and experimental results, it may increase the column strength by as much as 20% when compared at the same slenderness ratio and initial out-of-straightness (Alpsten, 1970, 1972b).

The strength and behavior of cold-straightened columns still have not been documented satisfactorily, and research should be undertaken to detail all of the individual influences and effects. This is particularly important in view of the fact that almost all hot-rolled wide-flange shapes are straightened in the mill to meet straightness requirements.

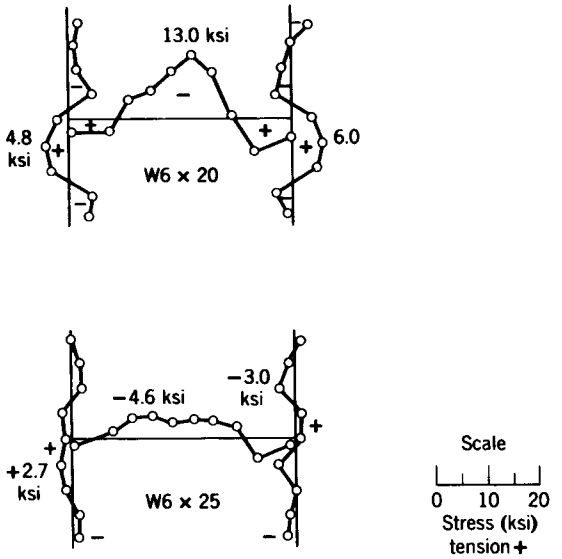

Fig. 3.12 Residual stresses in roller-straightened shapes.

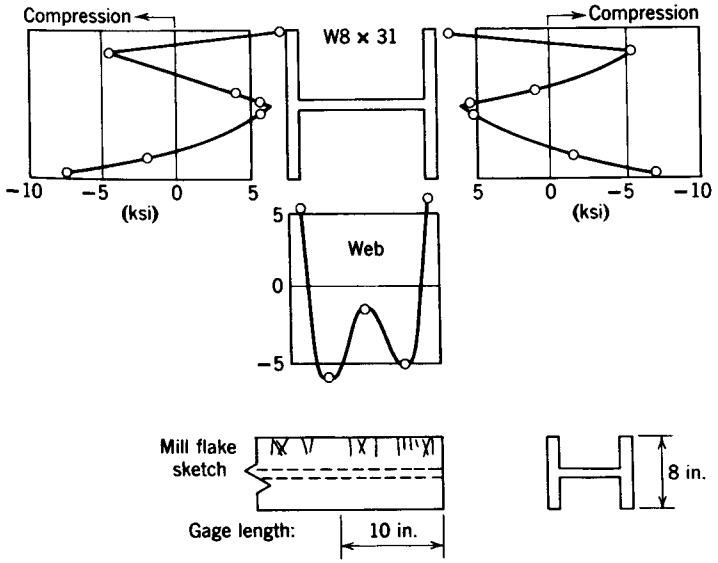

Fig. 3.13 Residual stresses in a gag-straightened shape, bent about the weak axis to remove sweep (Huber, 1956).

For tubular shapes the situation is somewhat different. The final mill process in most cases is cold forming or rolling, producing very small initial out-of-straightness, followed in some mills by partial stress relieving (Birkemoe 1977a; Bjorhovde and Birkemoe, 1979). This is also the case for welded built-up wide-flange columns (Chernenko and Kennedy, 1991).

3.2.3 Out-of-Straightness

Section 3.2.2 details the influence of the residual stresses, one of the primary column strength factors. Another factor is the *initial out-of-straightness* (also referred to as *initial crookedness* or *initial curvature*). The behavior of the initially crooked column has already been examined in the context of critical load theory; in brief, any geometric imperfection changes the stability problem from one of bifurcation to one of in-plane bending.

Some of the characteristics of the behavior and strength of inelastic, initially curved columns have already been discussed in the evaluation of residual-stress influences; the two parameters interact in many ways. Thus the explanation of the ranges of slenderness ratios and column types, for which the combined effect of residual stress and initial crookedness is more than the sum of the parts, emphasizes the complexity of the phenomenon.

The analyses that have been made of the strength of inelastic, initially curved columns have either made use of assumed values and shapes of the initial out-of-straightness, or have used actually measured data. The former is by far the most common, mostly because the measurements that are available for columns are scarce. This applies in particular to the magnitude of the maximum out-of-straightness, normally assumed to occur at midheight of the member, as well as the shape of the bent member. The latter is usually thought to be that of a half sine wave (Batterman and Johnston, 1967; Bjorhovde and Tall, 1971; Bjorhovde, 1972). The real configuration of the initial out-of-straightness of a column may be very complicated, often expressed as a simultaneous crookedness about both principal axes of the cross section. Systematic measurements have been made in some laboratories in conjunction with testing programs (Beer and Schultz, 1970; Bjorhovde, 1972, 1977; Bjorhovde and Birkemoe, 1979; Fukumoto, 1983, Essa and Kennedy, 1993), but very few data are available for columns in actual structures (Tomonaga, 1971; Lindner and Gietzelt, 1984). Chernenko and Kennedy (1991) measured the out-of-straightness of welded wide-flange shapes at the steel mill.

Magnitude and Limitations. The magnitude of the maximum initial out-of-straightness is limited by the structural steel delivery specifications (e.g., ASTM A6 in the United States; CSA G40.20 in Canada) and is normally expressed as a fraction of the length of the member. Hot-rolled wide-flange shapes are required to have a maximum initial crookedness of $L/960$ [measured as $\frac{1}{8}$ in. (3 mm) in 10 ft (3 m) of length], which is usually given as $L/1000$ for convenience. Tubular shapes are required to meet a straightness tolerance of $L/480$, commonly given as $L/500$. There are currently no requirements for welded built-up shapes.

The measurements that are available show that most hot-rolled W-shapes tend to have values toward the maximum permissible, with an average of approximately $L/1500$ (Bjorhovde, 1972), although Dux and Kitipornchai (1981) and Essa and Kennedy (1993) give a mean value the maximum initial deflection of 1/3300 and 1/2000, respectively, for wide-flange shapes of lengths of 6 to 10 m. Tubular members typically exhibit values significantly smaller than the specification limitations, with out-of-straightnesses on the order of $L/3000$ to $L/8000$, with an average of $L/6300$ (Bjorhovde, 1977; Bjorhovde and Birkemoe, 1979). The data for welded wide-flange shapes indicate small initial crookedness values, with a mean of approximately $L/3300$ (Chernenko and Kennedy, 1991). On the whole, therefore, it is rare to encounter columns with out-of-straightnesses larger than the maximum permitted. Such columns are straightened before shipment.

In the development of column strength criteria such as the SSRC curves (Bjorhovde, 1972) and the ECCS curves (Beer and Schultz, 1970), the maximum permissible values of the initial crookedness were utilized. This was done for several reasons, the primary one being that $L/1000$ constituted the upper limit of what is acceptable for actually delivered members and therefore could be regarded as a conservative measure. On the other hand, since mean characteristics were used for the other strength parameters, it can rationally be argued that the mean crookedness also should be utilized. This was done by Bjorhovde (1972) in parallel with his development of the original SSRC curves, using the mean of $L/1470$ that was determined through statistical evaluations. The resulting multiple column curves are shown in Fig. 3.14, where the curves labeled as 1P, 2P, and 3P have used $L/1470$. For comparison, the SSRC curves have been included in the figure; these have used an initial out-of-straightness of $L/1000$. The mathematical equations for both sets of curves are given in Section 3.2.7.

Variations in the magnitude of the initial crookedness were considered in the study by Bjorhovde (1972). The strength of the 112 columns that were included in the investigation was examined using maximum initial out-of-straightnesses of $L/500$, $L/2000$, and $L/10{,}000$; the results for the band of column strength curves are given in Fig. 3.15. (The curves that are shown include only the data for $L/500$ to $L/2000$.) The results of the studies on the maximum strength of columns emphasize the need for incorporation of the initial out-of-straightness into column strength models which form the basis for design criteria.

3.2.4 Influence of end restraint

Extensive studies on the influence of end restraint on the strength and behavior of columns have been conducted by Chen (1980), Jones et al. (1980, 1982), Razzaq and Chang (1981), Chapuis and Galambos (1982), Vinnakota (1982,

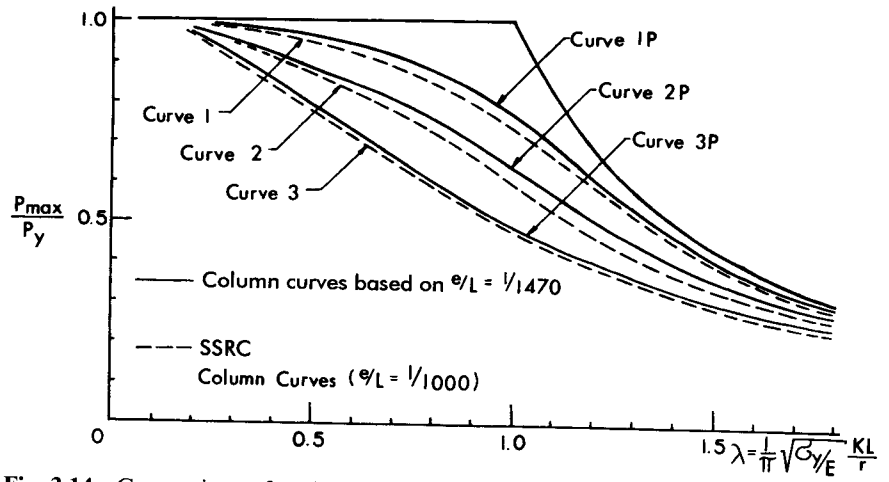

Fig. 3.14 Comparison of multiple column curves developed on the basis of mean out-of-straightness ($L/1470$) and maximum permissible out-of-straightness ($L/1000$) (Bjorhovde, 1972).

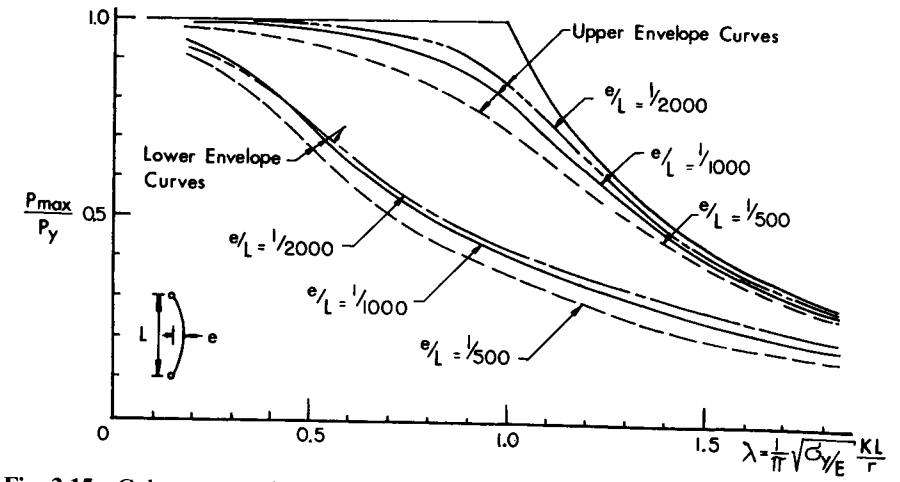

Fig. 3.15 Column curve bands for 112 columns, based on initial out-of-straightnesses of $L/500$, $L/1000$, and $L/2000$ (Bjorhovde, 1972).

1983, 1984), and Shen and Lu (1983), among others. In addition, the analysis of frames with semirigid connections has been dealt with in several studies (DeFalco and Marino, 1966; Romstad and Subramanian, 1970; Frye and Morris, 1975; Ackroyd, 1979; Lui and Chen, 1988; Nethercot and Chen, 1988; Goto et al, 1993; King and Chen, 1993, 1994; Kishi et al., 1993a and b. The column investigations have examined different aspects of restrained member behavior: specifically, determining the influence of:

1. Type of beam-to-column connection
2. Length of column
3. Magnitude and distribution of residual stress
4. Initial out-of-straightness

The frame analysis studies have focused on evaluations of the drift characteristics of frames with less than fully rigid connections, in part prompted by a study by Disque (1975). However, frame-related subjects of this kind are beyond the scope of this chapter. In fact, connection flexibility and member instability are closely related, and their interaction effects can have a significant influence on the overall performance of the frame.

As would be intuitively expected, the stiffness of the restraining connection is a major factor. One illustration of the influence is given by the M–ϕ curves in Fig. 3.16, another by the load-deflection curves for columns with different end restraint that are shown in Fig. 3.17 (Jones et al., 1982). A British wide-flange shape was used for the data generated for Fig. 3.17 incorporating an initial out-of-straightness of $L/1000$. The curves that are shown apply for a slenderness ratio of 120 ($\lambda = 1.31$), but similar data were developed for longer as well as shorter columns. Other investigators have provided additional load-deflection curves; the primary differences between the individual studies are found in the methods of column analysis and end-restraint modeling, but the resulting curves are very similar (Jones et al., 1980, 1982; Razzaq and Chang, 1981); (Sugimoto and Chen, 1982).

Figure 3.17 also includes the load-deflection curve for a pin-ended column. As is evident, the greater the connection restraint, the stiffer will be the initial response of the column, and the greater the maximum load that can be carried as compared to a pin-ended column. The same relative picture emerges for all slenderness ratios, although the magnitude of the increase becomes small for values of L/r 50 and less.

A further illustration of the influence of end restraint is given by the data in Fig. 3.18, which shows column strength curves for members with a variety of end conditions (Jones et al., 1982; Lui and Chen, 1983a). The effect of the connection type is again evident, as is the fact that the influence diminishes for shorter columns. Also included in the figure is the Euler curve, as well as SSRC curve 2 (Bjorhovde, 1972).

It is emphasized that the connections that were used to develop the column curves in Fig. 3.18 are all of the "simple" type. The potential for the structural economies that may be gained by incorporating the end restraint into the column design procedure is clear, although the realistic ranges for the values of λ must be borne in mind and the possible use of bracing to reduce frame drift in designing semirigid frames with flexible base joints must be considered. The ranges for λ have been delineated in Fig. 3.18 for steels with yield stresses of 36 and 50 ksi (248 and 345 MPa). Consequently, the very large column strength increases that have been reported by several researchers are real

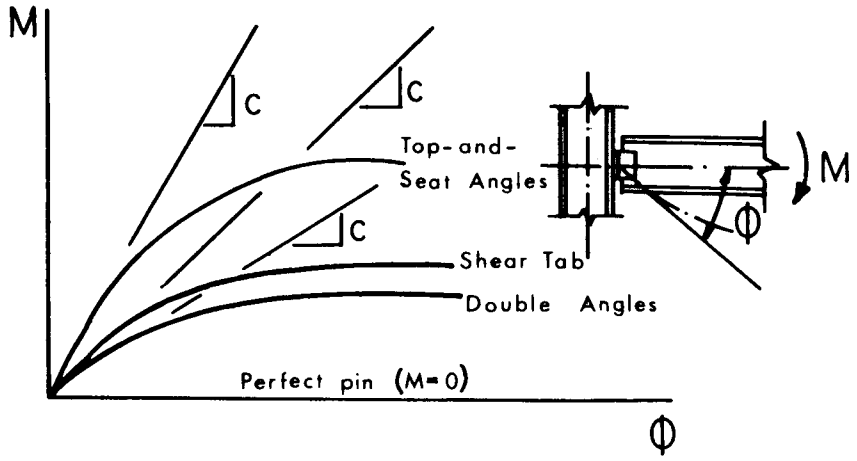

Fig. 3.16 Moment-rotation curves for some typical simple connections (schematic).

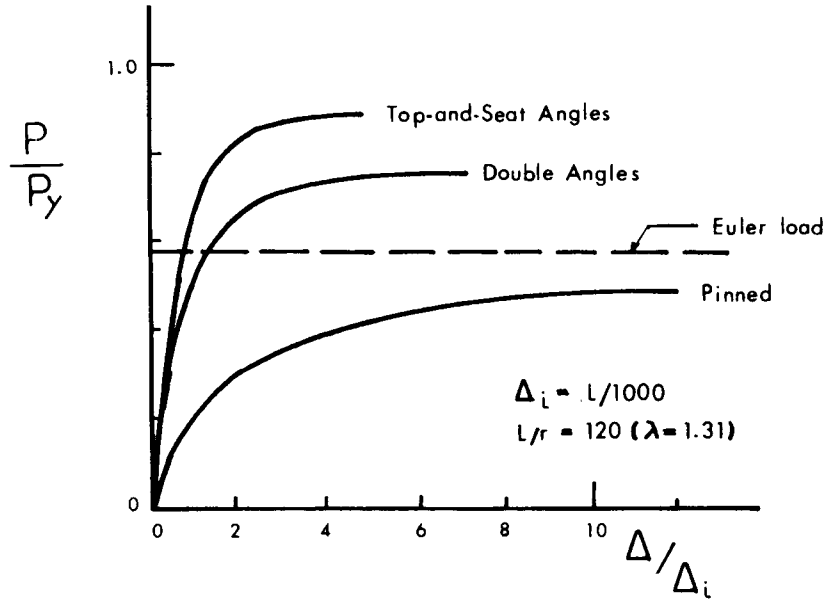

Fig. 3.17 Typical load-deflection curves for columns (Jones et al., 1982).

(Chen, 1980; Jones et al., 1980, 1982; Razzaq and Chang, 1981; Sugimoto and Chen, 1982; Lui and Chen, 1983b), but they occur for slenderness ratios that are in excess of practical values (Bjorhovde, 1981; Ackroyd and Bjorhovde, 1981). Overall, end restraint clearly increases strength.

Using the individual column strength studies as the basis, recent research demonstrates the application of end restraint to the design of columns in

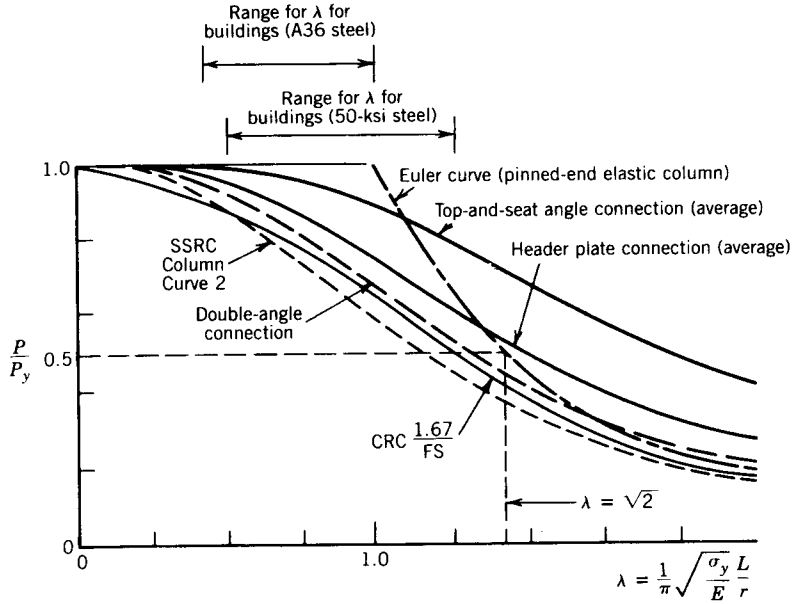

Fig. 3.18 Column curves for members with different types of end restraint.

frames (Bjorhovde, 1984; Chen and Lui, 1991; Chen and Sohal, 1995; Chen et al., 1996). Taking into account actual connection stiffness and the influence of beams, effective length factors for columns in frames have been developed. The method incorporates the use of the well-known alignment charts for the effective length of framed columns, and recognizes that buckling of a column in a frame is influenced by the end-restraint relative stiffness distribution factor, G_r, given as

$$G_r = \frac{\sum(EI/L)_{\text{columns}}}{C^*} \tag{3.8}$$

where C^* is the effective end restraint that is afforded to a column in a beam and column subassemblage, using connections whose initial stiffness is C = initial slope of the moment rotation curve. Barakat and Chen (1990) state that the initial connection stiffness should be used for the design of columns in braced frames, but a secant connection stiffness based on the beam-line concept be used for columns in unbraced frames.

The G_r procedure can incorporate detailed design suggestions as well as applications of inelastic K-factor principles, as developed by Yura (1971), expanded by Disque (1973), refined by Barakat and Chen (1990), and implemented in Chen and Lui (1991) and in Chen et al. (1996). Practical design examples illustrate the potential for significant structural economies.

However, it is emphasized that in all these methods of analysis the data for the actual end-restraint characteristics of the connection are required. Specifically, the C value must be known.

A large amount of research has been reported on methods of accounting for the connection flexibility in providing effective end restraint to framed columns. An extensive review of recent research on the behavior and modeling of connections is provided in Chen (1987, 1988), Chen and Lui (1991), Beedle (1993), and Chen et al. (1996). Based on the evaluation of different connection models available in the literature, a three-parameter connection power model proposed by Kishi and Chen (1990), together with its large database (Kishi and Chen, 1986; Chen and Kishi, 1989) and design aids (Kishi et al., 1993), can be recommended for general use.

3.2.5 Effective Length of Columns

The effective-length factor, K, was discussed briefly when introduced in Eq. 3.2. The coverage of effective column length in this chapter is limited to certain idealized cases and to certain special situations that occur in compression members of trusses. The effective-length concept has also been applied to members of nonuniform cross section, whereby they are converted to an equivalent pin-ended member with an effective moment of inertia that is referenced to a particular location of the nonuniform member.

Figure 3.19 gives theoretical K values for idealized conditions in which the rotational and/or translational restraints at the ends of the column are either full or are nonexistent. At the base, shown fixed for conditions a, b, c, and e in Fig. 3.19, the condition of full fixity is approached only when the column is anchored securely to a footing for which the rotation is negligible. Restraint conditions a, c, and f at the top are approached when the top of the column is framed integrally to a girder many times more rigid than itself. Column condition c is the same as a except that translational restraint is either absent or minimal at the top. Condition f is the same as c except that there is no rotational restraint at the bottom. The recommended design values of K are modifications of the ideal values, taking into account the fact that neither perfect fixity nor perfect flexibility is attained in practice.

The more general determination of K for a compression member as part of any framework requires the application of methods of indeterminate structural analysis, modified to take into account the effects of axial load and inelastic behavior on the rigidity of the members. Gusset-plate effects can be included; for this case extensive charts for modified slope-deflection equations, and for moment-distribution stiffness and carryover factors, respectively, have been developed (Goldberg, 1954; Michalos and Louw, 1957). These procedures are not directly applicable to routine design, but they can be used to determine end restraints and resultant modified effective lengths of the component members of a framework.

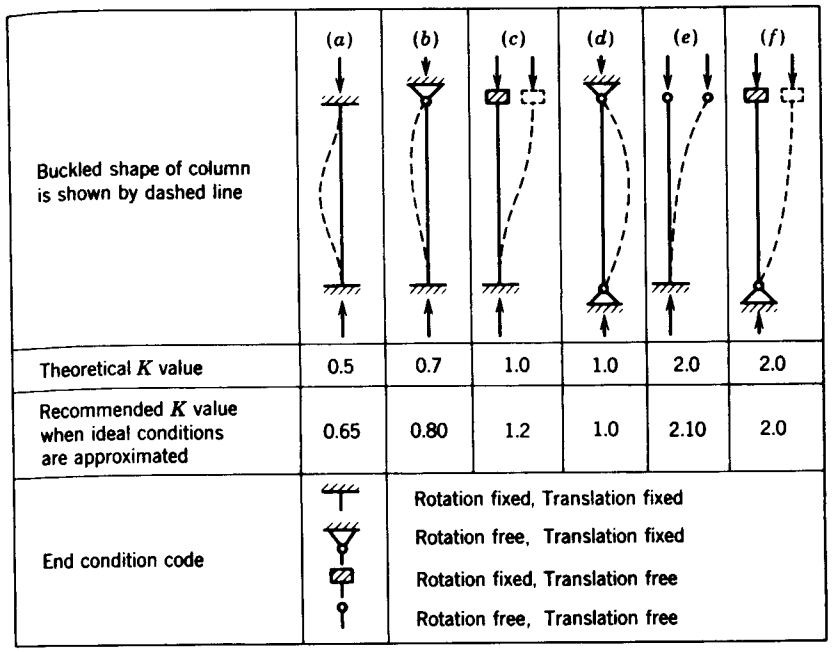

Fig. 3.19 Effective-length factors K for centrally loaded columns with various end conditions.

In triangulated frameworks (trusses), the loads are usually applied at the joints. Thus, if the joints are truly pinned, the members are axially loaded. Deflections of the joints and the truss as a whole are caused by the axial deformations of the members. The angles between members meeting at a joint also change because of these deformations. If the members are connected together at the joints by welds or bolts, the angle changes cause secondary bending stresses to be introduced. These have little effect on the buckling strength (and tensile strength) of the truss members. Because of local yielding of extreme fibers of the members near the joints, as the truss is loaded to ultimate the secondary moments gradually dissipate. They can therefore be neglected in the buckling analysis (Korol et al., 1986).

When a truss is designed and loaded under a particular loading condition such that all members reach their factored resistances simultaneously, no member restrains any other. Therefore the effective length factors for compression chord members and compression diagonals would be 1.0 for in-plane buckling. In a roof truss of constant or nearly constant depth, and where the compression chord has the same cross section for the full length of the truss, this does not occur, and K may be taken as 0.9. In a continuous truss, K may be taken as 0.85 for the compression chord connected to the joint where the force in the chord changes to compression.

When the magnitude of the force in the compression chord changes at a subpanel point that is not braced normal to the plane on the main truss (Fig. 3.20), the effective-length factor for chord buckling normal to the plane of the main truss can be approximated from the two compressive forces P_2 and P_1, as follows:

$$K = 0.75 + 0.25\left(\frac{P_1}{P_2}\right) \tag{3.9}$$

where $P_2 < P_1$.

Web members in trusses designed for moving live-load systems may be designed with $K = 0.85$. This is because the position of live load that produces maximum force in the web member being designed will result in less than the maximum forces in members framing into it, so that rotational restraints are developed.

The design of vertical web members, U_iL_i, of a K-braced truss (Fig. 3.21) should be based on the length KL. Web-member buckling occurs normal to the plane of the truss, and Eq. 3.9 again applies. Also, P_2 is negative in Eq. 3.9 since it is a tensile force. When P_1 and P_2 are numerically equal, Eq. 3.9 yields a value of $K = 0.5$

For buckling normal to the plane of a main truss, the web compression members should be designed for $K = 1$ unless detailed knowledge of the make-up of the cross frames (perpendicular to the truss) is available. For example, with cross frames of type 1 (Fig. 3.21), it is satisfactory to take $K = 0.8$, and for the type 2 it is satisfactory to use $K = 0.7$, provided that the top and bottom lateral bracing systems are adequate to prevent joint translation. When translation of the cross frames is possible, a more exact analysis of web-member stability should be undertaken.

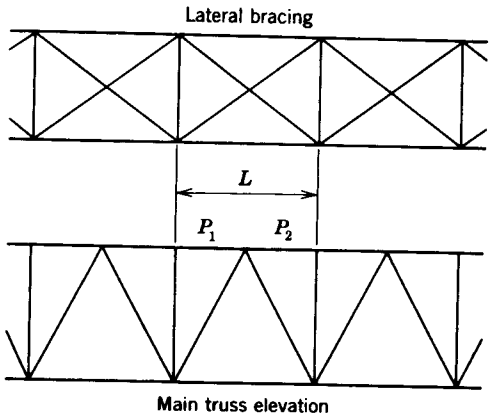

Fig. 3.20

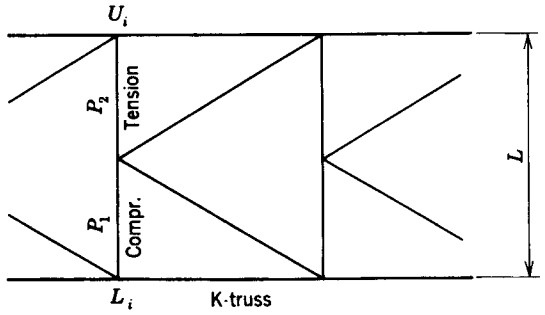

Fig. 3.21

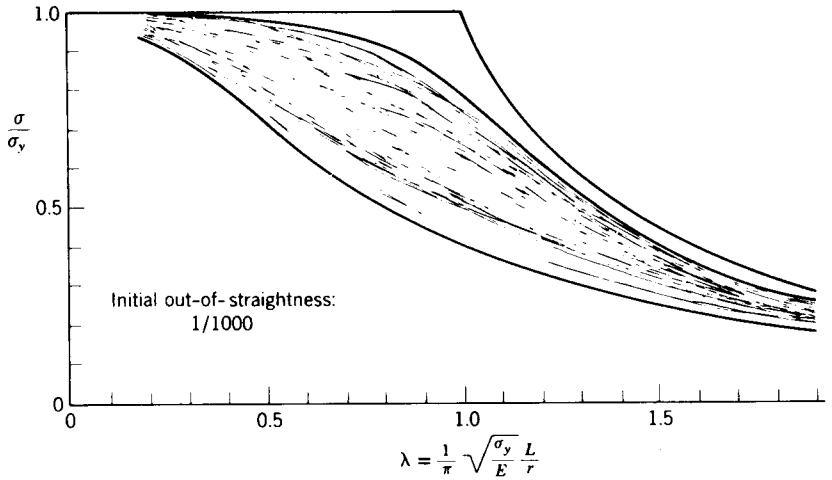

Fig. 3.22 Maximum-strength column curves for a number of different column types (Bjorhovde, 1972).

In the case of redundant trusses, there is a reserve strength above the load at initial buckling of any compression member. Masur (1954) has reviewed developments on this subject and established upper and lower bounds for the ultimate load of the buckled members of elastic redundant trusses.

3.2.6 Strength Criteria for Steel Columns

The position of the Structural Stability Research Council on the basis for the design of columns is stated in Technical Memorandum No. 5. The following quote from this memorandum summarizes this position: "Maximum strength, determined by the evaluation of those effects that influence significantly the

maximum load-resisting capacity of a frame, member, or element, is the proper basis for the establishment of strength design criteria." Thus the proper column strength model is one that incorporates both the residual stress and initial out-of-straightness.

Multiple Column Curves. In a major study Bjorhovde (1972) examined the deterministic and probabilistic characteristics of column strength in general and developed an extensive database for the maximum strengths of centrally loaded compression members. Covering the full practical range of shapes, steel grades, and manufacturing methods, the study demonstrated the wide variability of column strength. Figure 3.22 illustrates this variability through a collection of 112 maximum-strength column curves. Subsequent and parallel investigations of other researchers have added to and confirmed the band of column strength that is shown in Fig. 3.22 (Birkemoe, 1977a; Bjorhovde, 1988, 1991; Bjorhovde and Birkemoe, 1979; Fukumoto et al., 1983; Jacquet, 1970; Kato, 1977; Sherman, 1976).

The key problem in developing a rational, representative, and sufficiently reliable column strength criterion is how to take the large variability into account. This may be achieved by using a mean or other central curve of the band of strength variation of Fig. 3.22, or it may be done by subdividing the band into groups of curves with a mean or similar curve for each group. The latter defines the *multiple column curve concept* (Bjorhovde and Tall, 1971; Bjorhovde, 1972).

Research and development leading to the use of multiple column curves were actively pursued from the late 1950s to the early 1980s. In 1959 the German standard DIN 4114 introduced a special curve for tubes and another curve for all other shapes. Subsequently, the work under the auspices of the European Convention for Constructional Steelwork (ECCS) (Beer and Schultz, 1970; Jacquet, 1970; Sfintesco, 1970) resulted in recommended design application and code adoption in several countries (Sfintesco, 1976). The ECCS curves in somewhat modified form are now part of the column design criteria of Eurocode 3 (ECS, 1992). In 1984 the Canadian Standards Association (CSA) adopted SSRC curve 1 for use with heat-treated tubes; CSA had earlier (1974) adopted SSRC curve 2 as the basic column strength criterion, and in 1994 (CSA, 1994) assigned welded wide-flange columns made from flame-cut plate to SSRC Column Curve 1 (Chernenko and Kennedy, 1991).

Research basic to the development of multiple column curves in North America was conducted at Lehigh University starting in the 1960s (Bjorhovde and Tall, 1971; Bjorhovde, 1972, 1988), and elsewhere (Birkemoe, 1977a,b; Bjorhovde, 1977; Bjorhovde and Birkemoe 1979; Kato, 1977; Sherman, 1976).

The maximum strength of steel columns depends, in addition to the length and the cross-sectional properties and the material properties, F_y and E, on (1) the residual-stress magnitude and distribution, (2) the shape and magnitude of the initial out-of-straightness, and (3) the end restraint. The effects of these three variables were discussed in detail earlier in this chapter. Unless special procedures are utilized in the manufacture of steel columns, such as stress relieving or providing actual pins at each end, all three of these effects are present and should be accounted for. The present state of research is such that if the following information is known, accurate calculation of the maximum strength is possible (Bjorhovde, 1972, 1978; Chen and Lui, 1985):

1. *Material properties* (i.e., the yield stress F_y and the modulus of elasticity E); in some cases it is necessary to know the variation of the yield stress across the cross section (welded build-up shapes) or the entire stress-strain curve (cold-formed shapes).
2. *Cross-sectional dimensions*; in cases of columns with variable sections, the dimensions along the column length need also be known.
3. *Distribution of the residual stresses* in the cross section, including variations through the plate thickness if the shape is a tubular shape or if the plate elements are thick.
4. *The shape and the magnitude of the initial out-of-straightness.*
5. *The moment-rotation relationship of the end restraint.*

Maximum strength may be calculated by postulating suitable but realistic idealizations so that closed-form algebraic expressions may be derived, or one of many available numerical techniques may be used. In numerical calculations it is usually assumed that deformations are small and that plane sections remain plane. The literature on determining the maximum strength of columns is rich and diverse, but the major methods are described in textbooks (see, e.g., Chen and Atsuta, 1976; Chen and Han, 1985).

Residual stress, initial crookedness, and end restraint are random properties, and complete statistical information is lacking. In particular, data on end restraint in terms of beam-to-column moment-rotation curves are limited; this is a result of the great variety of connections that are used in steel construction practice. Techniques for evaluating end restraint effects have been given in Section 3.2.4, and much research has been conducted over the past 15 years (Ackroyd, 1979; Chen, 1980; Jones et al., 1980; 1982; Ackroyd and Bjorhovde, 1981; Bjorhovde, 1981, 1984; Chapuis and Galambos, 1982; Sugimoto and Chen, 1982; Lui and Chen, 1983a,b, Shen and Lu, 1983). At this time the procedures that have been developed are applicable to a range of problems, but additional work needs to be done to make the concept suitable for specification utilization.

The basic column element continues to be the pin-ended, centrally loaded column. The key research work focused on this issue, and the studies that were done for multiple column curves used the basic column. An answer to the problem of a suitable specification format was provided by Bjorhovde (1972), who proceeded as detailed in the following.

A computerized maximum strength analysis was performed first on basic data available from carefully constructed column tests performed at Lehigh University, and it was demonstrated that the method of numerical analysis gave an accurate prediction of the test strengths. Next, a set of 112 column curves was generated for members for which measured residual-stress distributions were available, assuming that the initial crookedness was of a sinuosoidal shape having a maximum amplitude of 1/1000 of the column length and that the end restraint was zero. These shapes encompassed the major shapes used for columns, including rolled and welded shapes from light to heavy dimensions. The column curves thus obtained represent essentially the whole spectrum of steel column behavior. The resulting curves are shown in Fig. 3.22.

Bjorhovde then observed that there were definite groupings among the curves, and from these three subgroups were identified, each giving a single "average" curve for the subgroup (Bjorhovde and Tall, 1971; Bjorhovde, 1972). The resulting three curves are known as *SSRC column strength curves 1, 2, and 3*, and they are reproduced in Figs. 3.23 through 3.25. These figures contain:

1. The number of column curves used as a basis for the statistical analysis and the width of their scatter band
2. The calculated $2\frac{1}{2}$ and $97\frac{1}{2}$ percentile lower and upper probability limits for the particular set of curves
3. The column types to which each of the three curves is related

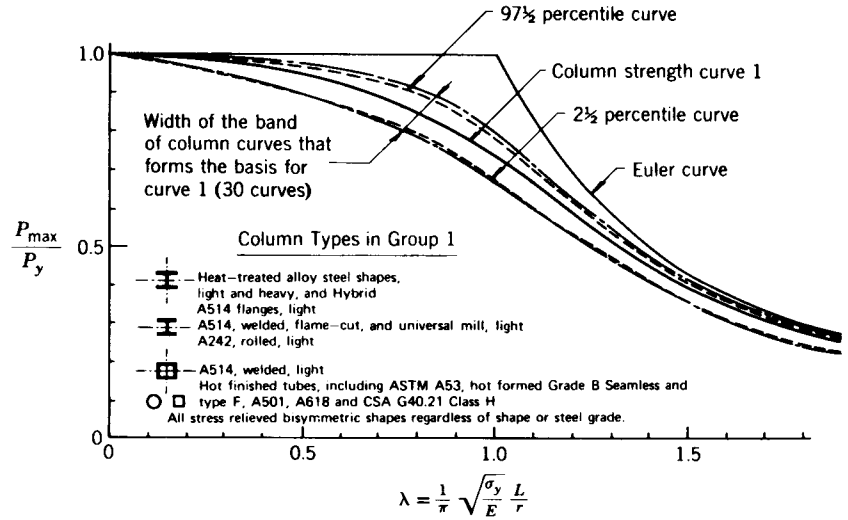

Fig. 3.23 SSRC column strength curve 1 for structural steel (Bjorhovde, 1972). (Based on maximum strength and initial out-of-straightness of $\delta_0 = 0.001L$.)

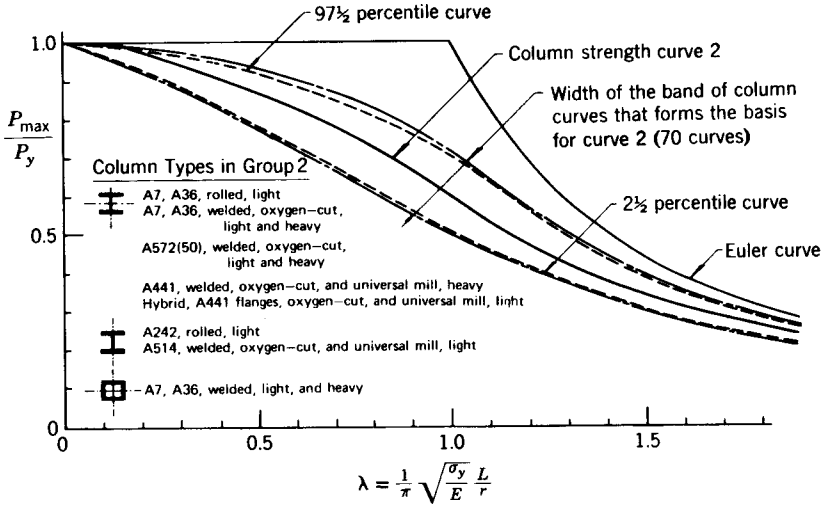

Fig. 3.24 SSRC column strength curve 2 for structural steel (Bjorhovde, 1972). (Based on maximum strength and initial out-of-straightness of $\delta_0 = 0.001L$.)

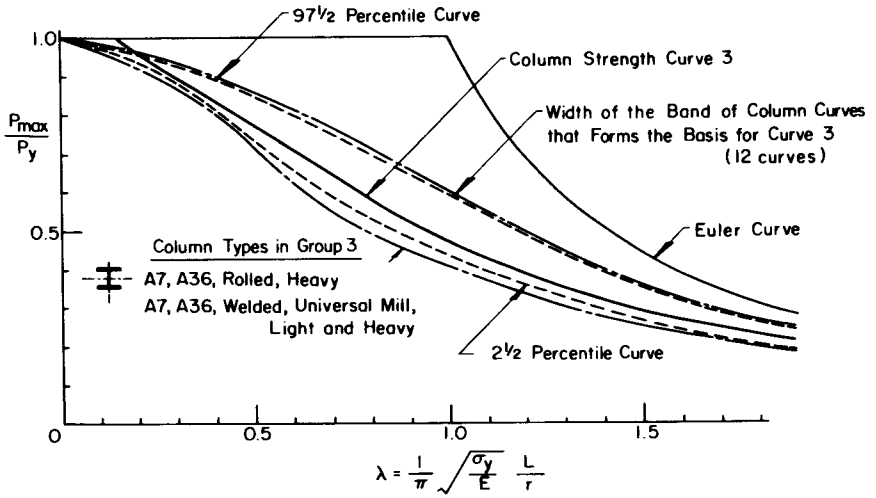

Fig. 3.25 Column strength curve 3 for structural steel (Bjorhovde, 1972). (Based on maximum strength and initial out-of-straightness of $\delta_0 = 0.001L$.)

Algebraic representations of the three column strength curves were obtained by curve fitting, and the resulting equations are as follows;

SSRC curve 1:

$$\left.\begin{array}{lll} 1. & \text{For } 0 \le \lambda \le 0.15 & \sigma_u = \sigma_y \\ 2. & \text{For } 0.15 \le \lambda \le 1.2 & \sigma_u = \sigma_y(0.990 + 0.122\lambda - 0.367\lambda^2) \\ 3. & \text{For } 1.2 \le \lambda \le 1.8 & \sigma_u = \sigma_y(0.051 + 0.801\lambda^{-2}) \\ 4. & \text{For } 1.8 \le \lambda \le 2.8 & \sigma_u = \sigma_y(0.008 + 0.942\lambda^{-2}) \\ 5. & \text{For } \lambda \ge 2.8 & \sigma_u = \sigma_y\lambda^{-2} \ (=\text{Euler curve}) \end{array}\right\} \quad (3.10)$$

SSRC curve 2:

$$\left.\begin{array}{lll} 1. & \text{For } 0 \le \lambda \le 0.15 & \sigma_u = \sigma_y \\ 2. & \text{For } 0.15 \le \lambda \le 1.0 & \sigma_u = \sigma_y(1.035 - 0.202\lambda - 0.222\lambda^2) \\ 3. & \text{For } 1.0 \le \lambda \le 2.0 & \sigma_u = \sigma_y(-0.111 + 0.636\lambda^{-1} + 0.087\lambda^{-2}) \\ 4. & \text{For } 2.0 \le \lambda \le 3.6 & \sigma_u = \sigma_y(0.009 + 0.877\lambda^{-2}) \\ 5. & \text{For } \lambda \ge 3.6 & \sigma_u = \sigma_y\lambda^{-2} \ (=\text{Euler curve}) \end{array}\right\} \quad (3.11)$$

SSRC curve 3:

$$\left.\begin{array}{lll} 1. & \text{For } 0 \le \lambda \le 0.15 & \sigma_u = \sigma_y \\ 2. & \text{For } 0.15 \le \lambda \le 0.8 & \sigma_u = \sigma_y(1.093 - 0.622\lambda) \\ 3. & \text{For } 0.8 \le \lambda \le 2.2 & \sigma_u = \sigma_y(-0.128 + 0.707\lambda^{-1} - 0.102\lambda^{-2}) \\ 4. & \text{For } 2.2 \le \lambda \le 5.0 & \sigma_u = \sigma_y(0.008 + 0.792\lambda^{-2}) \\ 5. & \text{For } \lambda \ge 5.0 & \sigma_u = \sigma_y\lambda^{-2} \ (=\text{ Euler curve}) \end{array}\right\} \quad (3.12)$$

These expressions can also be represented quite accurately (maximum deviations -2.1 to $+3.6\%$) by one equation (Rondal and Maquoi, 1979; Lui and Chen, 1984):

$$\sigma_u = \frac{\sigma_y}{2\lambda^2}(Q - \sqrt{Q^2 - 4\lambda^2}) \le \sigma_y \quad (3.13)$$

where

$$Q = 1 + \alpha(\lambda - 0.15) + \lambda^2 \quad (3.14)$$

and

$$\alpha = \begin{cases} 0.103 & \text{for curve 1} \\ 0.293 & \text{for curve 2} \\ 0.622 & \text{for curve 3} \end{cases}$$

Another expression using a single parameter n in a double exponential representation, as used in CSA Standard S16.1-94 (CSA, 1994; Loov, 1995), is

$$\sigma_u = F_y(1 + \lambda^{2n})^{\frac{-1}{n}} \quad (3.15)$$

where $n = 2.24$ for curve 1, 1.34 for curve 2, and 1.00 for curve 3 (the latter is not utilized in the CSA standard). These expressions give strengths generally within 1% of the polynomials of Eqs. 3.10 through 3.12, and are never more than 3% different.

Bjorhovde (1972) also developed multiple column curves where the initial out-of-straightness was equal to its mean value of 1/1470 of the column length (Fig. 3.14). The mathematical equations describing these curves are as follows:

SSRC curve IP:

$$\left.\begin{array}{lll} 1. & \text{For } 0 \le \lambda \le 0.15 & \sigma_u = \sigma_y \\ 2. & \text{For } 0.15 \le \lambda \le 1.2 & \sigma_u = \sigma_y(0.979 + 0.205\lambda - 0.423\lambda^2) \\ 3. & \text{For } 1.2 \le \lambda \le 1.8 & \sigma_u = \sigma_y(0.03 + 0.842\lambda^{-2}) \\ 4. & \text{For } 1.8 \le \lambda \le 2.6 & \sigma_u = \sigma_y(0.018 + 0.881\lambda^{-2}) \\ 5. & \text{For } \lambda \ge 2.6 & \sigma_u = \sigma_y\lambda^{-2} \ (=\text{Euler curve}) \end{array}\right\} \quad (3.16)$$

SSRC curve 2P:

$$\left.\begin{array}{lll} 1. & \text{For } 0 \le \lambda \le 0.15 & \sigma_u = \sigma_y \\ 2. & \text{For } 0.15 \le \lambda \le 1.0 & \sigma_u = \sigma_y(1.03 - 0.158\lambda - 0.206\lambda^2) \\ 3. & \text{For } 1.0 \le \lambda \le 1.8 & \sigma_u = \sigma_y(-0.193 + 0.803\lambda^{-1} + 0.056\lambda^{-2}) \\ 4. & \text{For } 1.8 \le \lambda \le 3.2 & \sigma_u = \sigma_y(0.018 + 0.815\lambda^{-2}) \\ 5. & \text{For } \lambda \ge 3.2 & \sigma_u = \sigma_y\lambda^{-2} \end{array}\right\} \quad (3.17)$$

SSRC curve 3P:

$$\left.\begin{array}{lll} 1. & \text{For } 0 \le \lambda \le 0.15 & \sigma_y = \sigma_y \\ 2. & \text{For } 0.15 \le \lambda \le 0.8 & \sigma_u = \sigma_y(1.091 - 0.608\lambda) \\ 3. & \text{For } 0.8 \le \lambda \le 2.0 & \sigma_u = \sigma_y(0.021 + 0.385\lambda^{-1} + 0.066\lambda^{-2}) \\ 4. & \text{For } 2.0 \le \lambda \ge 4.5 & \sigma_u = \sigma_y(0.005 + 0.9\lambda^{-2}) \\ 5. & \text{For } \lambda \ge 4.5 & \sigma_u = \sigma_y\lambda^{-2} \ (=\text{Euler curve}) \end{array}\right\} \quad (3.18)$$

A single expression for the SSRC-P curves has not been developed. However, this can be achieved relatively easily, using the approach of Rondal and Maquoi (1979), Loov (1996), or Rotter (1982). The single curve that is used in Chapter E of the AISC load and resistance factor design (LRFD) specification (AISC, 1993b) is identical to SSRC 2P (Tide, 1985). Two equations are used to describe this curve for two regions of slenderness, λ, as follows:

$$F_\alpha = \begin{cases} (0.658/\lambda^2)F_y & \text{for } 0 \le \lambda \le 1.5 \\ (0.877/\lambda^2)F_y & \text{for } \lambda \ge 1.5 \end{cases} \tag{3.19}$$

Design Procedure Alternatives. It was demonstrated in the preceding section that it is possible to develop multiple column curves into which column types can be grouped for convenience. In developing column design criteria, the following questions should be considered:

1. *What should be the shape and the amplitude of the initial out-of-straightness*? As to the shape, there is fairly general agreement that a sinusoidal shape with the maximum amplitude in the center is a conservative and reasonable assumption. The maximum amplitude is, however, a crucial quantity since changes affect the strength, especially in the intermediate slenderness range. Knowledge about initial out-of-straightness is available from measurements of laboratory specimens used for column tests, but there is a paucity of field data. Initial out-of-straightness is a function of the manufacturing process, and some column types, such as manufactured tubes, tend to be very straight. In the development of the SSRC and ECCS multiple column curves the position was taken that an initial amplitude of 1/1000 of the length, essentially the mill tolerance, is a reasonable and conservative value for the basis of developing column curves. One can argue that this conservative approach is justified because the initial out-of-straightness takes care of all other geometric imperfections, such as initial out-of-plumb and the unavoidable eccentricity of the axial load. The out-of-straightness thus may be used to represent the effects of other types of geometric imperfections.

In opposition, it can be argued that all geometric imperfections are small enough so that their effect can be relegated to be accounted for by the factors of safety or the resistance factors. This was the underlying philosophy of the use of the CRC column curve, which has its basis in the tangent-modulus theory, with a factor of safety that depends on the column slenderness ratio. This design approach was entirely sensible when it was initially formulated (in the 1950s), but a convincing mass of research has since shown that the maximum strength can be determined from a knowledge of initial imperfections, and that the economical and safe use of steel columns should take cognizance of the out-of-straightness.

A task force of SSRC (1985) took an intermediate position, recommending that the basis for the development of design curves for steel columns should be an initial out-of-straightness of 1/1500 of the length. This is close to the average measured in laboratory columns (Bjorhovde, 1972; Fukumoto et al., 1983) and reflects the current position of the SSRC in this matter. For all practical purposes, Eqs. 3.16 through 3.18 represent this condition. By its adoption of Eq. 3.19, AISC is effectively using $L/1500$ as the governing out-of-straightness criterion.

2. *Should column curves be based on the tangent-modulus theory for straight columns, and the geometric imperfection be accounted for by a specified eccentricity of the load which produces an end moment on the column*? Column design would then always be performed with an interaction equation. Such an approach is rational and it appears to be a consideration in the column design criteria for beam-columns as proposed in Europe, where, however, it seems that both initial crookedness and load eccentricity are used for beam-columns, but where intentionally axially loaded columns are designed with consideration of out-of-straightness only.

3. *Should design be based on the concept of multiple column curves, or should one composite column curve, or formula, be used for the design of all steel columns?* The European answer to this question has been to recommend multiple column curves (these are shown in Fig. 3.26). As a first step in North America, the Canadian Standards Association (CSA) adopted the use of SSRC curve 2 as the basic design curve. In 1984 the CSA also adopted SSRC curve 1 for hollow structural sections, cold formed to final shape and heat treated. This recommendation was based in part on research on such columns (Bjorhovde, 1977; Birkemoe, 1977b; Bjorhovde and Birkemoe, 1979; Kennedy and Gad Aly, 1980). The original reluctance to adopt multiple column curves for the U.S. structural steel design specifications was founded on the belief that the design criteria would become too complicated. Another reason was that it was felt necessary to complete certain additional studies, to ensure that all conceivable column types and materials would be properly assigned to one of the three strength categories (Bjorhovde, 1980). This work has now been concluded, and the results are summarized in the *column curve selection table (CCS Table)* shown in Fig. 3.27 (Bjorhovde and Tall, 1971; Bjorhovde, 1972, 1988). The CCS table will facilitate the column curve selection process and is also suited for a decision-table format for use with computer-based design.

4. *The final question to be asked is: What end restraint should be assumed for nominally pinned-end columns?* As shown in Section 3.2.4 any practical framing scheme or base condition will increase the column strength and thus there are really no truly pin-ended columns in existence. Methods have been developed to use this end restraint in determining the maximum strength of columns, but the question of how to use the available information in design is still unresolved. Should explicit restraint factors for different kinds of end conditions be

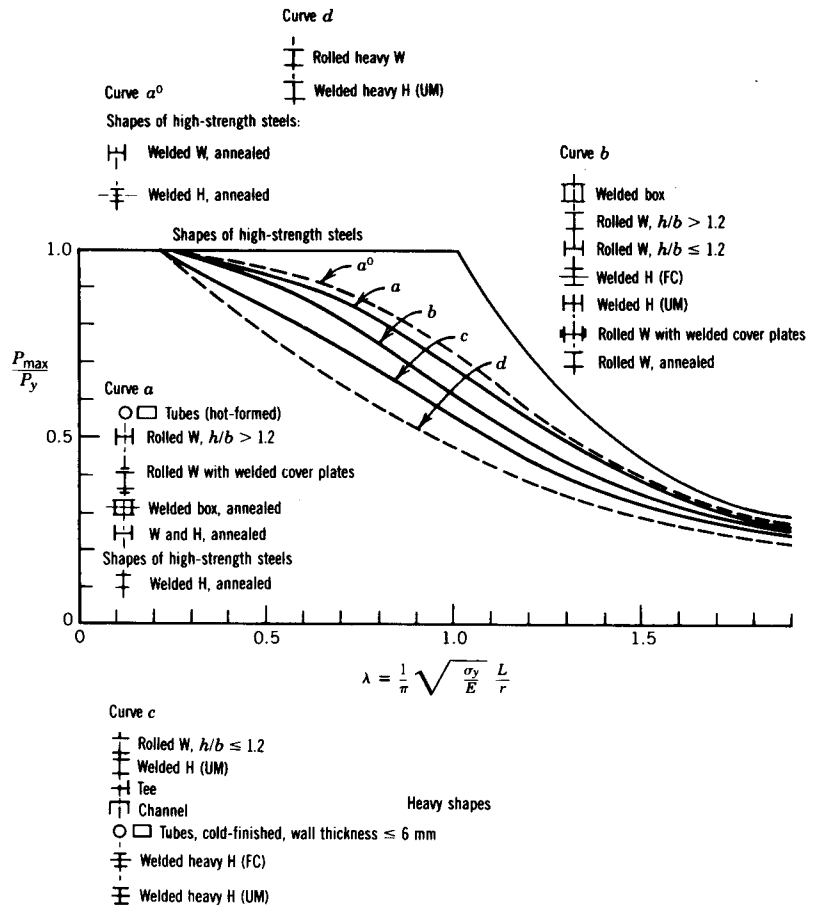

Fig. 3.26 European multiple column curves, recommended by the European Convention for Constructional Steelwork (ECCS 1978). (Based on initial out-of-straightness, $\delta_0 = 0.001L$.)

tabulated for use with effective-length-factor alignment charts, or should the design curves implicitly contain minimal end restraints? The latter approach was used in the development of the AISC–LRFD column curve, which is based on an implicit end restraint producing an elastic effective-length factor of 0.96 ($G = 10$), as well as an initial out-of-straightness of 1/1500 of the length.

Summary. In the previous discussion on the strength of steel columns a number of alternatives were presented. Specification writing groups need to make decisions to select the column curve satisfying their needs and wishes. The necessary theory is available to do so, and much information is on hand. It is the SSRC's firm opinion that design criteria for steel columns should be based on the initially crooked column with residual stresses. With

Column Curve Selection Table

Fabrication Details		Axis	Specified Minimum Yield Stress of Steel (ksi) ≤ 36	37 to 49	50 to 59	60 to 89	≥ 90
Hot-rolled W-shapes	Light and medium W-shapes	Major	2	2	1	1	1
		Minor	2	2	2	1	1
	Heavy W-shapes (flange over 2 in.)	Major	3	2	2	2	2
		Minor	3	3	2	2	2
Welded Built-up H-shapes	Flame-cut plates	Major	2	2	2	1	1
		Minor	2	2	2	2	1
	Universal mill plates	Major	3	3	2	2	2
		Minor	3	3	3	2	2
Welded Box Shapes	Flame-cut and universal mill plates	Major	2	2	2	1	1
		Minor	2	2	2	1	1
Square and Rectangular Tubes	Cold-formed	Major	N/A	2	2	2	2
		Minor	N/A	2	2	2	2
	Hot-formed and cold-formed heat-treated	Major	1	1	1	1	1
		Minor	1	1	1	1	1
Circular Tubes	Cold-formed	N/A	2	2	2	2	2
	Hot-formed	N/A	1	1	1	1	1
All stress-relieved Shapes		Major and Minor	1	1	1	1	1

Fig. 3.27 Column curve selection table (Bjorhovde, 1972, 1988).

this concept as a basis, intelligent choices for column design can be made, resulting in a rational method of design.

3.2.7 Aluminum columns

Material Properties. Alloying elements, heat treatment, and working have a great influence on all the essential properties of aluminum, with the exception of the elastic modulus, which falls within the range 9900 to 10,200 ksi (68 to 70 GPa) for other than aircraft alloys. In general engineering, a value of 10,000 ksi (68.3 GPa) is used.

Yield strength is more strongly influenced by heat treatment and working than is the ultimate strength. For heat-treated or strain-hardened alloys there is also an increased sharpness of the "knee" between the elastic and plastic ranges, which is significant for columns in the lower range of slenderness ratios. For this reason column formulas for aluminum alloys are divided into two groups, heat-treated and non-heat-treated, which reflect the differing ratio $\sigma_{0.2}/\sigma_{0.1}$. Alloys that are solution heat-treated but not artificially aged, seldom used in engineering, fall in the non-heat-treated group. Guaranteed values for the yield strength, defined by the 0.2% offset, and the ultimate strength are established at levels at which 99% of the material is expected to conform at a

0.95 confidence level. In practice, typical values are some 15% above the guaranteed value; thus the use of the guaranteed value in a design formula which has been formulated on the basis of measured values provides an additional factor to be considered when selecting resistance factors or factors of safety for columns with short and medium slenderness ratios. The yield strength, σ_y, is the value of the stress in the stress-strain curve at a specified offset from the initial elastic line, usually 0.2% ($\sigma_{0.2}$) and sometimes 0.1% ($\sigma_{0.1}$).

Imperfections. Deviations of real columns from the perfect elastic-plastic model are of two essential forms: nonlinearity of the stress-strain relationships, and geometric imperfections such as eccentricity and initial curvature. Non-linearity of the stress-strain relationship arises as a natural property of the material, as a consequence of the presence of residual stresses, or as a consequence of the local change in yield stress caused by welding. Residual stresses in aluminum extruded members are small because of the method of production and the straightening of the finished member by stretching. The fact that residual stress effects on column strength of aluminum extruded members are insignificant has been confirmed in European studies (Mazzolani and Frey, 1977). Nonlinearity in unwelded bars is thus attributable only to the material behavior and will vary with the type of alloy and heat treatment. The value of the yield strength does not vary significantly across a profile (Bernard et al., 1973).

Welding introduces residual tensile stresses in the weld bead on the order of the yield strength for the annealed material, and compressive stresses elsewhere. There is also a local reduction in mechanical properties effected by welding that is significant in heat-treated or work-hardened material.

Residual stresses created by cold forming are related to the yield strength in the same manner as in steel; however, longitudinal beads are considered to have little influence on column strength, as a result of either the residual stresses or of any strain hardening. Geometric imperfections fall into two groups: those that are length dependent, such as initial curvature, and those independent of length, such as eccentricity in the profile of the section itself and inaccuracies in the dimensioning of the assembly.

Commercial tolerances on initial curvature allow $L/500$ in some extruded structural members, but in reality $L/1000$ is rarely exceeded. If a bar with such an initial curvature forms two or more bays of the chord of a truss, the final out-of-straightness will be negligible in comparison to the inaccuracies in the assembly. Even in laboratory tests, the initial curvature of the bar as supplied has usually been less than the error in centering the specimen. End moments, due to frame action or eccentricities in joints, will in most cases dominate any moments due to initial curvature. For large assembled columns, such as latticed masts, an initial curvature of $L/1000$ has been found to be representative, and design as a beam-column using this value has been adopted.

Strength of Aluminum-Alloy Columns. Aluminum-alloy column strength has generally been based, in design application, on the tangent-modulus theory—justifiably so because of the generally good agreement with column test results. Evaluation of the maximum strength of both straight and initially curved columns is practicable with digital computers. A systematic study of the effects of important parameters that affect column strength has been made by Batterman and Johnston (1967) and Hariri (1967).

Initially Straight Columns. Such members were studied by Duberg and Wilder (1950), and Johnston (1963, 1964). In studying the behavior above the critical load, Batterman and Johnston (1967) assumed the stress-strain curve of the material to be represented by the average of a large number of tests of aluminum alloy 6061-T6. By considering both strong- and weak-axis buckling of an H-type section, the practical range of the shape effect was approximately covered. A section having a depth equal to the width was chosen, with flange thickness approximately one-tenth of the depth, and with a web having a thickness two-thirds that of the flange. The maximum increase in strength above the tangent-modulus load was found to be about 2% for weak-axis bending. This small difference further justifies the use of the tangent-modulus load as a reasonable basis for estimating the strength of initially straight aluminum-alloy columns.

Initially Curved Columns. The maximum strength of initially curved hinge-ended aluminum-alloy columns can be evaluated by use of the computer, as described previously (Batterman and Johnston, 1967). For a typical H shape of alloy 6061-T6 with buckling about the strong axis, Fig. 3.28 shows typical plots of load versus midheight lateral deflection for an L/r value of 40 and for initial midheight out-of-straightness ranging from zero up to $0.004L$. Figure 3.29 illustrates the strength-reduction factor, referenced to the critical load and plotted as a function of L/r for both strong- and weak-axis bending.

The effects of initial curvature are accentuated in unsymmetrical sections, such as the T, as illustrated by the computer-plotted curves in Fig. 3.30. An initial crookedness of $0.001L$ (with the flange on the convex side) reduced the ultimate strength in comparison with the tangent-modulus load by about 18% at $L/r = 40$, which is about twice the reduction shown in Fig. 3.29 for the doubly symmetric section. Buckling of axially loaded straight members (as confirmed by tests) will occur so as to put the flange of the T on the convex side of the column. The shaded lines at the top of Fig. 3.30 indicate the upper bounds of theoretical strength of a straight column, that is, the inelastic buckling gradients and the reduced-modulus strengths for buckling in either of the two possible directions (Johnston, 1964). Tests also indicated that the effect of end eccentricity was somewhat more deleterious than the effect of the same magnitude of initial out-of-straightness (Hariri, 1967).

The effect of end restraint on initially curved aluminum columns has been studied by Chapuis and Galambos (1982). They conclude: "It is conservative to

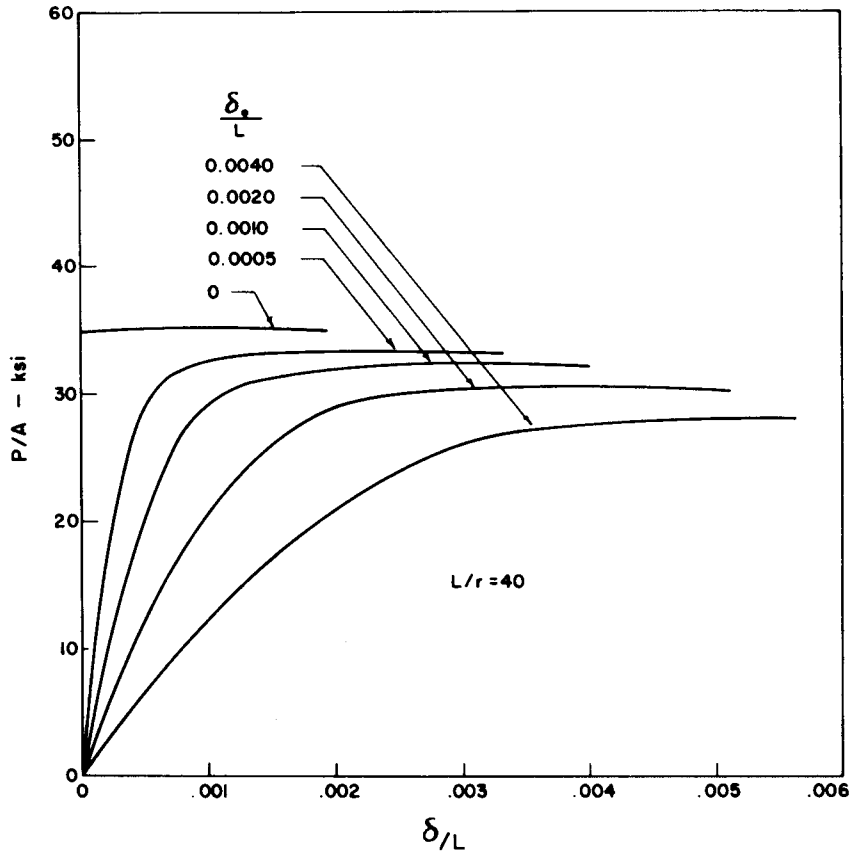

Fig. 3.28 Effect of initial curvature on load-deflection relationships of an aluminum-alloy column (Batterman and Johnston, 1967).

base a design on K_{el} (the effective length factor determined from elastic buckling analysis) and a column curve derived for pinned crooked columns."

Effects of Welding. For most alloys used in structural applications the heat of welding reduces the strength of the metal in a narrow zone around the weld, thereby diminishing the capacity of columns of low and intermediate slenderness ratios. Welding can also introduce residual stresses and crookedness in the column. Rectangular section columns with longitudinal and transverse welds have been tested by Brungraber and Clark (1962). Wide-flange and tubular box section columns with longitudinal welds were tested by Mazzolani (1985), and experiments of tubular box section columns with transverse welds were performed by Hong (1991). Lai and Nethercot (1992) provided analytical results for aluminum wide-flange columns with transverse welds.

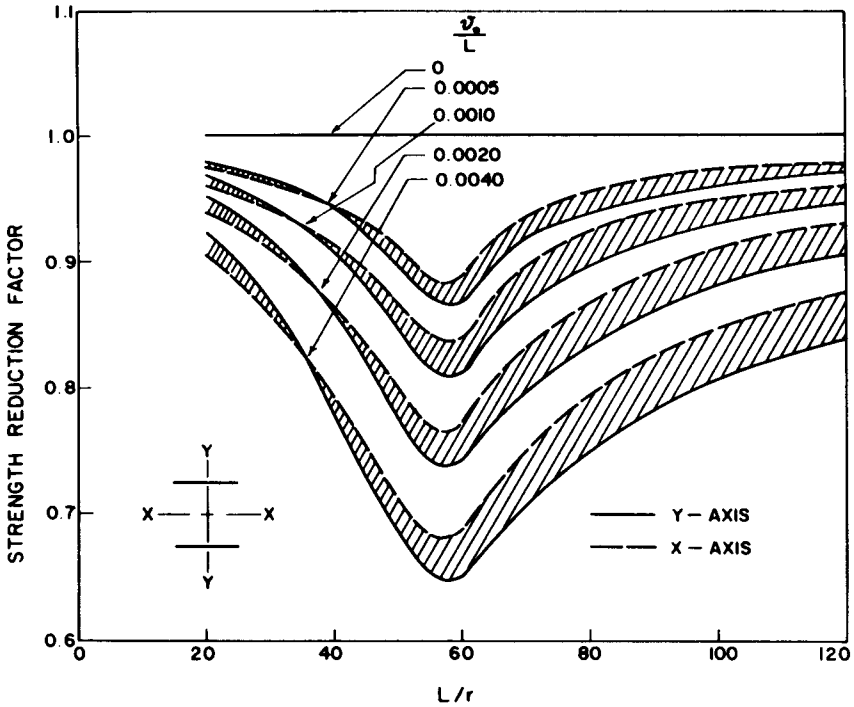

Fig. 3.29 (Maximum strength)/(tangent-modulus load) of aluminum-alloy columns for different amounts of initial curvature (Batterman and Johnston, 1967).

For columns with longitudinal welds or with transverse welds that affect only a portion of the cross section, the test values are reasonably predicted by the equation

$$\sigma_{pw} = \sigma_n - \frac{A_w}{A}(\sigma_n - \sigma_w) \tag{3.20}$$

where

σ_{pw} = critical stress for columns with part of the cross section affected by welding
σ_n = critical stress for the same column if there were no welds
σ_w = critical stress for the same column if the entire cross section were affected by welding
A_w = affected zone (designated by the symbol A_r in Figs. 3.31 and 3.32)
A = total area of cross section

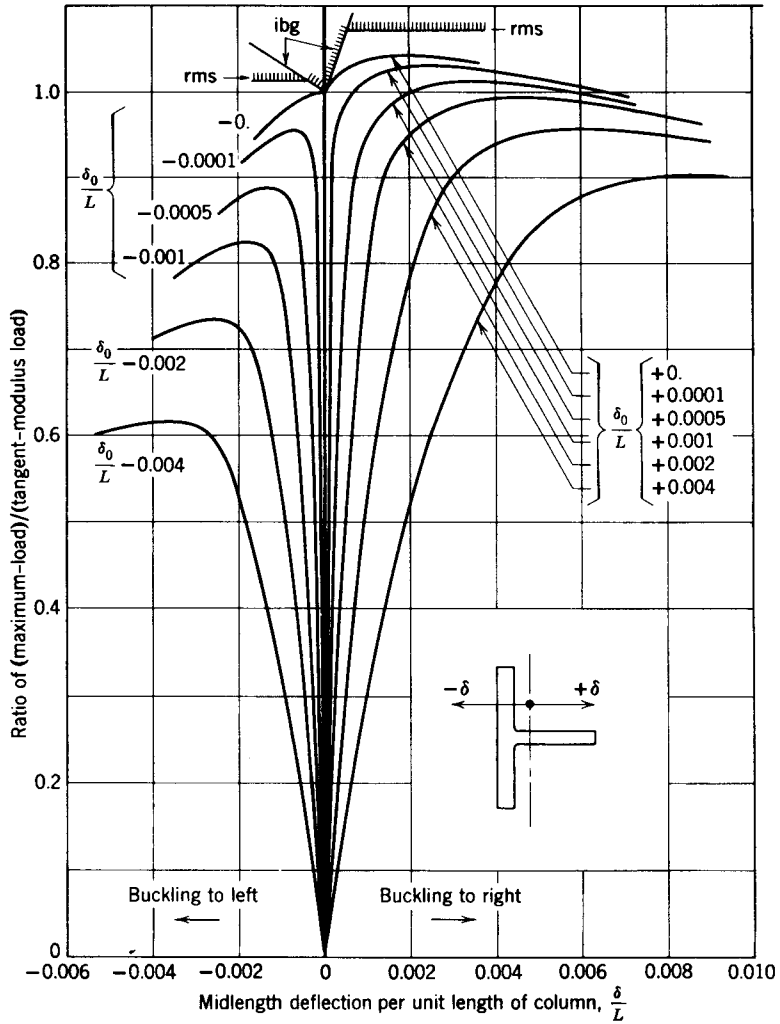

Fig. 3.30 Theoretical behavior of straight and initially curved T-section columns of aluminum alloy (Hariri, 1967).

Test data from Brungraber and Clark (1962) have been summarized by Sharp (1993) and are compared to straight-line approximations of predictions based on the tangent-modulus theory in Fig. 3.31 for columns with longitudinal welds and in Fig. 3.32 for columns with transverse welds. The measured values of the heat-affected areas were in the calculations for the data in these figures. In the absence of measured values the heat-affected zone may be assumed to be a width of 1 in. (25 mm) on either side of the center of a groove weld or the heel of a fillet weld. For columns with transverse welds that affect

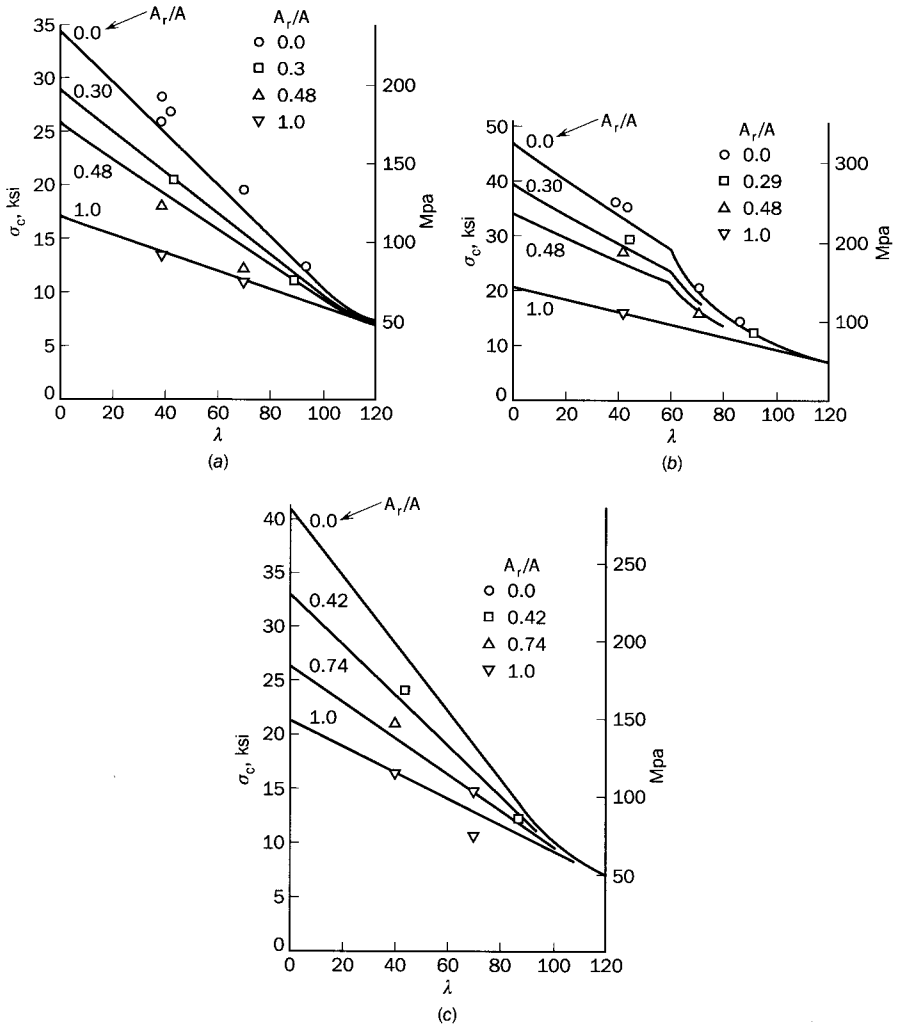

Fig. 3.31 Columns with longitudinal welds: (*a*) 5154-H32 rectangular sections; (*b*) 6061-T6 rectangular sections; (*c*) 5456-H321 rectangular sections (Sharp 1993).

the entire cross section, the strength reduction is dependent on the location of the welds and the amount of material of reduced strength (Lai and Nethercot, 1992, and Fig. 3.32). In general, heat-treatable alloys have a greater loss of strength due to welding than do non-heat-treatable alloys.

Design of Aluminum-Alloy Columns.

North American and Australian Design Practice (AA, 1994; SAA, 1979; CSA, 1980). The design formulas are based on the tangent-modulus formula, simplified to a straight line in the inelastic range which can be expressed as

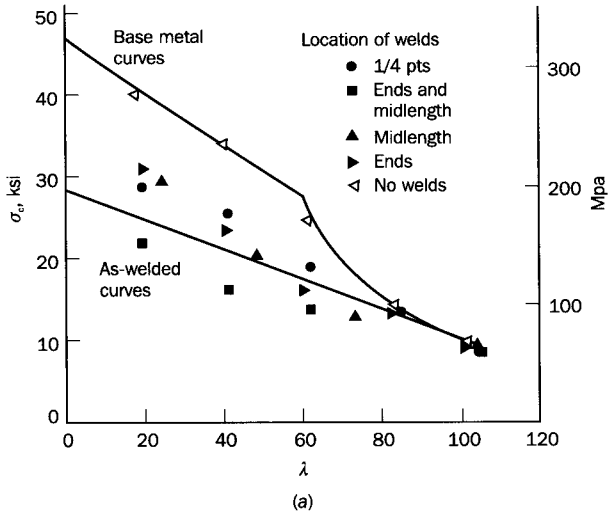

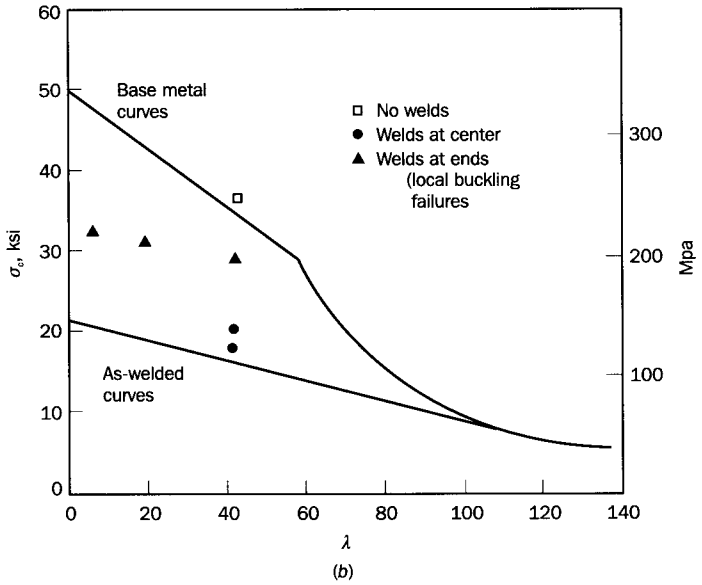

Fig. 3.32 Columns with transverse welds: (*a*) 6061-T6 rectangular sections [0.5 × 2.0 in. and 0.25 × 2.0 in. (12.7 × 50.8 mm and 6.3 × 50.8 mm]; (*b* 6061-T6 tubes 3 in. (76 mm) outside diameter, 0.25 in. (6.4 mm) wall (Sharp, 1993).

$$\frac{\sigma_c}{\sigma_y} = \alpha^2(1 - k\alpha\lambda) \qquad \text{for } \lambda < C \tag{3.21}$$

in which $\lambda = (KL/r)/\pi g$ and $g = (E/\sigma_y)^{1/2}$. For fully heated-treated alloys,

$$\alpha = (1 + 2/g)^{1/2} \tag{3.22a}$$
$$k = 0.31 \tag{3.22b}$$
$$C = 1.3/\alpha \tag{3.22c}$$

and for non-heat-treated alloys,

$$\alpha = (1 + 3/g)^{1/2} \tag{3.23a}$$
$$k = 0.38 \tag{3.23b}$$
$$C = 1.75/\alpha \tag{3.23c}$$

In no case can the stress exceed the yield strength. This classification is based on values of the ratios $\sigma_{0.2}/\sigma_{0.1}$ of 1.04 for fully heat-treated alloys and 1.06 for non-heat-treated alloys. For $\lambda > C$ the Euler formula is used.

Figures 3.33 and 3.34 compare the foregoing formulas with the results of tests on aluminum columns (Clark and Rolf, 1966). The test specimens were considered to have fixed ends (flat ends on rigid platens), and the deviations from straightness were less than $0.001L$. The effective-length factor K was assumed to be 0.5 in plotting the test results.

Allowable stresses for building design in the specifications are obtained by applying a constant factor of safety of 1.95 to the straight-line and Euler formulas. Thus the specifications do not directly consider the initial crookedness, which is specified by the Aluminum Association as $L/480$ for standard structural shapes but as $L/960$ for most other extruded shapes. Batterman and Johnston (1967) showed that a small initial crookedness can appreciably reduce the factor of safety, especially in the transition region between elastic and inelastic buckling. Figure 3.35 illustrates the results of calculations for columns of 6061-T6 alloy with $\delta_0 = 0.001L$. In a discussion of the specification, Hartmann and Clark (1963) noted that the effects of small amounts of initial crookedness or eccentricity may be offset by the use of conservative values of the equivalent-length factor as a basis for the specification formulas. To illustrate this, Batterman and Johnston (1967) considered the hypothetical case of a column with typical material properties and ends restrained such that throughout loading to maximum strength, the column segment between inflection points is always $0.9L$. For bending about the weak (y–y) axis and an initial crookedness of $0.001L$, the theoretical safety factor is plotted in Fig. 3.36 both for this case and for the case of pinned ends. Thus for a relatively slight amount of end restraint, the safety factor varies from values slightly above 2.2 in the short column range to a minimum of 1.97 at $L/r = 67$. It then increases to slightly above 2.2 at $L/r = 120$. The effect of the initial crookedness in reducing

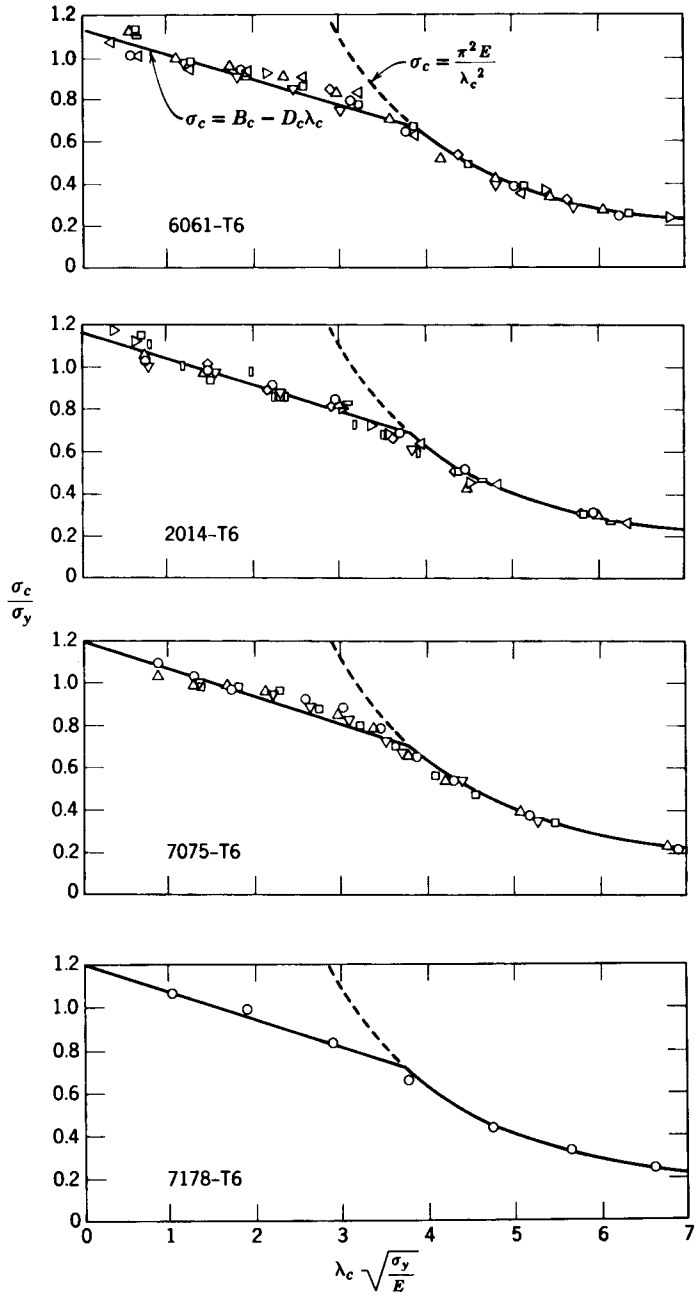

Fig. 3.33 Column strength of aluminum alloys (artificially aged) (Clark and Rolf, 1966).

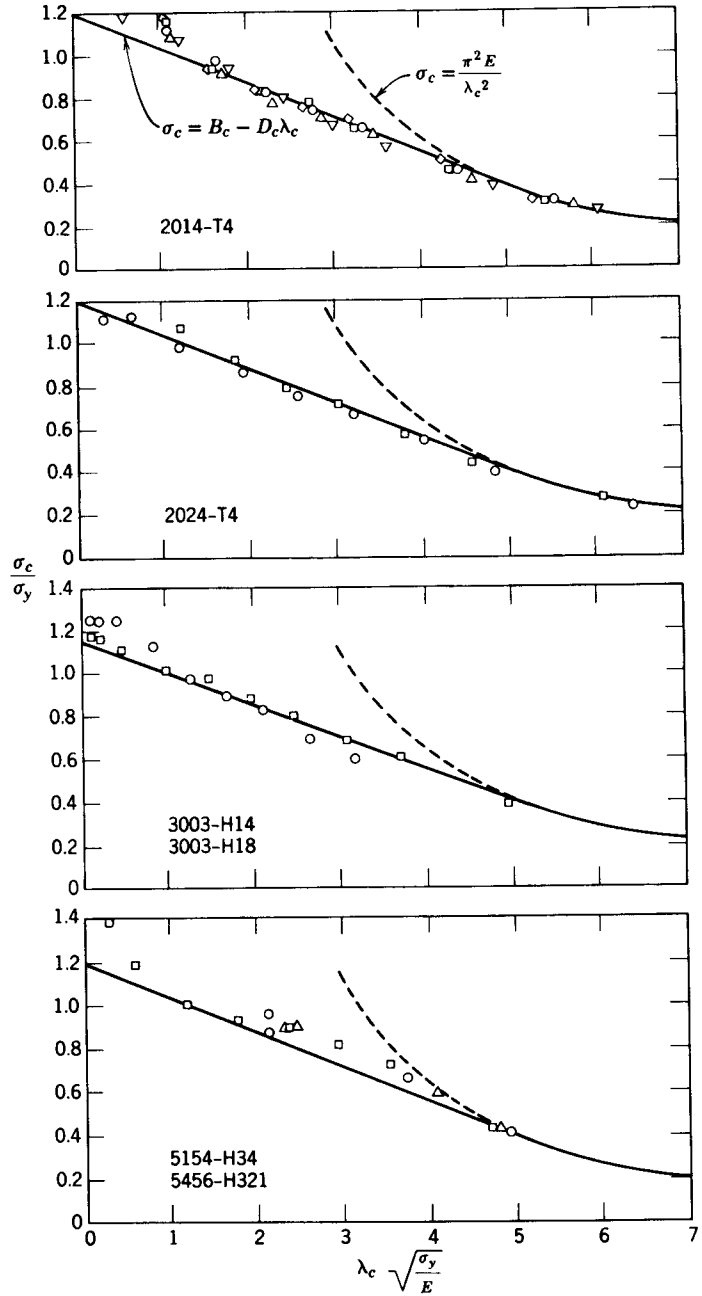

Fig. 3.34 Column strength of aluminum alloys (not artificially aged) (Clark and Rolf, 1966).

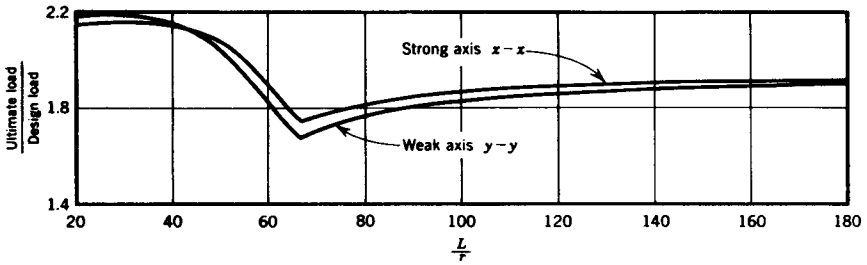

Fig. 3.35 Design load factor for wide-flange shapes of aluminum-alloy columns with $\delta_0 = 0.001L$ (Batterman and Johnston, 1967).

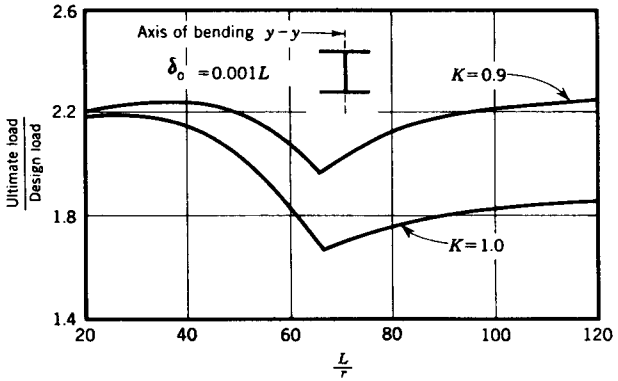

Fig. 3.36 Comparison of safety factors for columns with and without end restraint (Batterman and Johnston, 1967).

the safety factor from 1.95 to 1.67 is thus offset if the column is restrained at the ends such that an actual K value of 0.9 is produced. In the load and resistance factor design version of the Aluminum Association (AA, 1994) specification, a variable resistance factor is used to account for the effects of initial crookedness.

European Design Practice. An earlier British code (ISE, 1962) adopted the Perry–Robertson formula, which can be expressed as

$$\frac{\sigma_c}{\sigma_y} = \frac{1}{2\lambda^2}\{(1+\eta+\lambda^2) - [(1+\eta+\lambda^2)^2 - 4\lambda^2]^{1/2}\} \tag{3.24}$$

The factor η is based on test results (Baker and Roderick, 1948) and thus incorporates all sources of imperfection and nonlinearity present in the tests. Two values are used, $0.0015L/r$ for heat-treated and $0.003L/r$ for non-heat-treated alloys. In a later code (BSI, 1991) straight-line formulas of the type

used in North America were adopted. A recent British limit-states design specification, BS 8118 (SAA, 1991), provides curves relating the critical stress σ_{cr} to the slenderness ratio KL/r for three representative aluminum alloys for use by designers.

Research by Mazzolani and Frey (1980) and Bernard et al. (1973) provided the background information on imperfections, residual stresses, and the influence of welds, which lead to the preparation of the ECCS recommendations (ECCS, 1978a), which resulted eventually in the Eurocode rules. The Ramberg–Osgood formula was used to model the stress-strain relationship in the form

$$\epsilon = \frac{\sigma}{E} + 0.002\left(\frac{\sigma}{\sigma_{0.2}}\right)^n \tag{3.25}$$

Steinhardt's suggestion (1971) that n is equal to the value of the yield strength in kN/cm^2 gives close agreement with test results (n is a coefficient that reflects the shape of the stress-strain curve).

Three curves have been adopted, using values of n of 20, 15, and 10 to represent the various alloy types. Included in the computer evaluation were initial imperfections of both curvature and eccentricity, as well as unsymmetrical sections. The curves are shown in Fig. 3.37. The uppermost curve is for

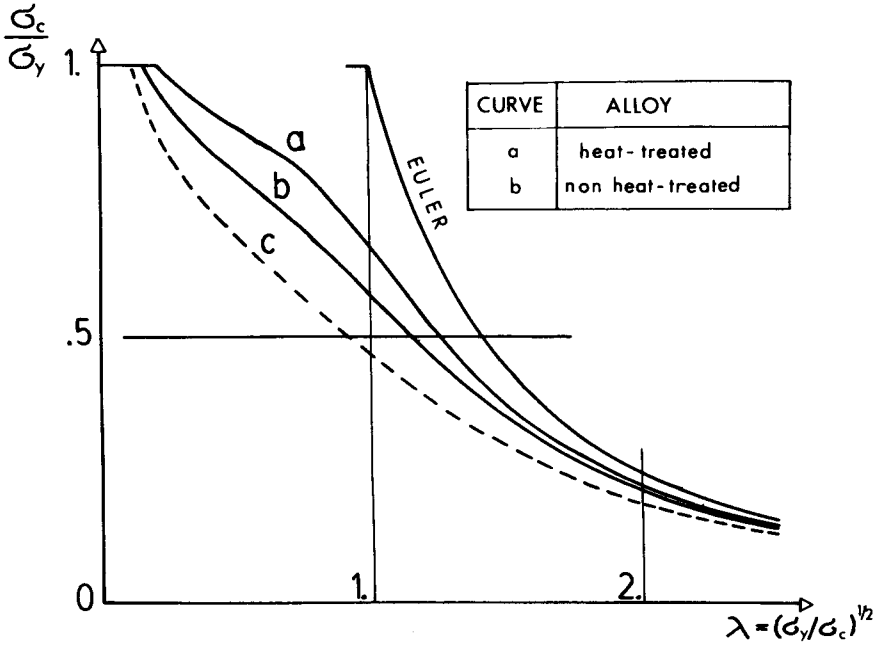

Fig. 3.37 Basic column-buckling curves (ECCS aluminum structures.)

heat-treated, symmetrical, open or solid sections, with the lowest curve for all hollow sections and all non-heat-treated sections other than symmetric open or solid sections. This lowest curve lies substantially below those in other standards, as it represents an extreme combination of adverse influences.

3.2.8 Stainless steel columns

Stainless steel has been used primarily in nonstructural applications, such as the roof sheeting of the chapel of the U.S. Air Force Academy in Colorado Springs, Colorado, and the covering used for the Gateway Arch in St. Louis, Missouri. Stainless steel has also been used in many cold-formed steel structures applications, and a design specification has been developed for such purposes (ASCE, 1991).

The past several years have seen increasing attention being paid to the potential use of stainless steel for structural purposes. Although the availability of plates and hot-rolled shape products is still limited, and current production is only by a few mills in Japan and South Africa, the need for high-corrosion resistance structural elements in many infrastructure applications indicate that use is likely to grow substantially. Although cost is a major issue—current structural stainless steel prices reflect an approximate ratio of 5:1 compared to carbon and other steels—it is readily conceivable that certain uses may justify the higher price.

Research and development work for stainless steel structural elements is limited at this time and has been conducted primarily at Rand Afrikaans University in Johannesburg, South Africa. The following descriptions therefore reflect a state-of-the-art assessment of materials and what is known about the performance of stainless steel columns.

Stainless Steel Materials. Stainless steel is the common name applied to a range of iron-based alloys whose prime corrosion-resisting element is chromium. The minimum chromium content is approximately 11% the maximum around 30%. Carbon content ranges from 0.02 to 0.12%, which is another reason stainless steel is significantly different from the usual structural steel, where carbon content typically lies around 0.15 to 0.25%. In addition, specific stainless steels utilize alloying elements such as manganese, nickel, and titanium. The stainless steels are typically characterized as either *austenitic* or *ferritic*, as defined by their metallurgical (crystalline) structure. The austenitic steels have high chromium and nickel contents; the ferritic steels contain medium to low contents of chromium (11 to 18%) and have no nickel.

A typical stress-strain curve for stainless steel is shown in Fig. 3.38. It is noted that there is no yield plateau; the curve reflects a steel that behaves in increasingly nonlinear fashion; and the overall ductility is generally very high (elongations at rupture are commonly 50% and more). Figure 3.38 does not reflect an additional important property of stainless steel: Unlike carbon steel, there are clear differences in the properties associated with longitudinal tension

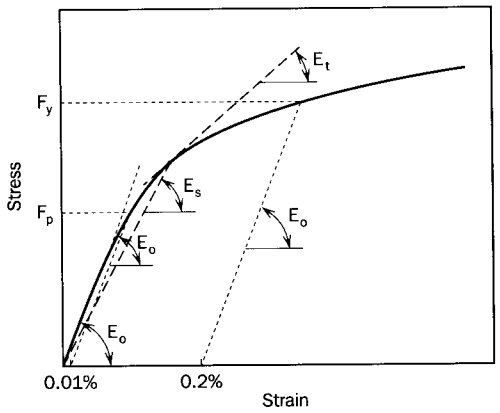

Fig. 3.38 Typical stress-strain behavior of stainless steel (van den Merwe and van der Berg, 1992).

and compression, as well as with transverse tension and compression. Nevertheless, the shape and characteristic properties of all stainless steels are as illustrated in the figure.

Representative values of yield and ultimate tensile (compressive) stresses and the modulus of elasticity are as follows (van den Berg and van der Merwe, 1992; Bredenkamp et al., 1994):

- *Yield stress in tension*: 40 to 55 ksi (275 to 380 MPa)
- *Yield stress in compression*: 45 to 65 ksi (310 to 450 MPa)
- *Initial modulus of elasticity*: 29,000 ksi (200 GPa)

Stainless steel type 3CR12 is currently being investigated for use in hot-rolled shapes (Bredenkamp et al., 1994).Its stress-strain characteristics are somewhat different from the usual austenitic and ferritic steels, as illustrated by Fig. 3.39. In particular, the linearly elastic range is large and there appears to be a clear yield plateau. The average yield and tensile strengths are 40 and 65 ksi (276 and 448 MPa), and the average E value is 30,000 ksi (207 GPa). The elongation at rupture is approximately 30%.

Residual Stresses. Data on residual stresses in hot-rolled and welded built-up stainless steel structural shapes are very limited at this time. Most of the work that has been done has focused on welded shapes (Bredenkamp et al., 1992; Bredenkamp and van den Berg, 1995); work on hot-rolled shapes is in progress (Bredenkamp et al., 1994). Figure 3.40 gives an example of the residual stress distribution in a welded wide-flange shape with 180 × 6 mm flanges ($7 \times \frac{1}{4}$ in.) and 90 × 4.5 mm web ($3\frac{1}{2} \times \frac{3}{16}$ in.), and Fig. 3.41 shows the

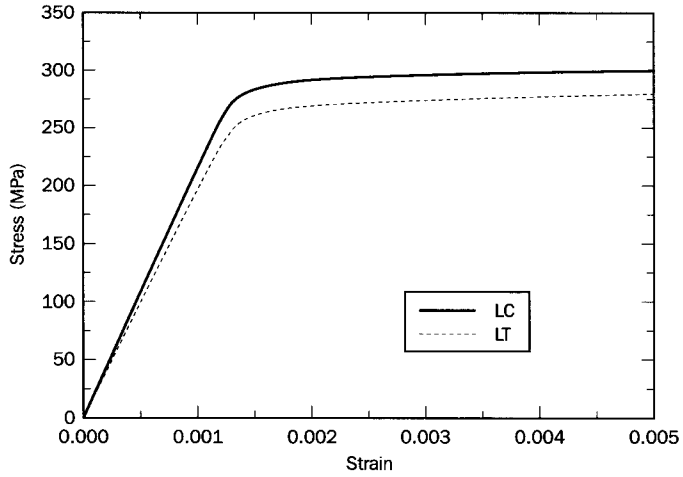

Fig. 3.39 Analytical stress-strain curves for type 3CR12 steel (Bredenkamp et al., 1994).

stub column curve for the same shape (Bredenkamp et al., 1992). The magnitudes of the residual stresses are comparable to similar-sized carbon steel welded shapes; however, the range of elastic response of the stub column is very limited.

Residual-stress distribution data for hot-rolled shapes are not available currently in the form used for the welded shape in Fig. 3.40. Theoretical data are available for one specially rolled shape (Bredenkamp et al., 1994); the cross section had 55 × 4.4 mm flanges ($2\frac{5}{32} \times \frac{5}{32}$ in.) and 89 × 3.6 mm net depth web ($3\frac{1}{2} \times \frac{9}{64}$ in.).

Column Strength. No initial out-of-straightness data are available currently (1997) for welded or hot-rolled shapes. It is therefore not possible to evaluate the maximum strength of stainless steel columns. On the other hand, experimental data are available (Bredenkamp et al., 1992, 1994; Bredenkamp and van den Berg, 1995); these have been compared with predictions using the SSRC curves, the Perry–Robertson curve, and a tangent-modulus solution. An example is given in Fig. 3.42, showing the column data for the hot-rolled shape in 3CR12 stainless steel.

It appears that the tangent-modulus–based solution gives the best prediction of strength, but the data on the testing procedure indicate that a uniform strain alignment was used for the specimen. This would reflect the response of a perfectly straight column, hence the good correlation with tangent-modulus theory. However, in the absence of additional data, the current recommendation for stainless steel columns is to use the tangent-modulus approach (van der Merwe and van den Berg, 1992; ASCE, 1991), as for cold-formed columns.

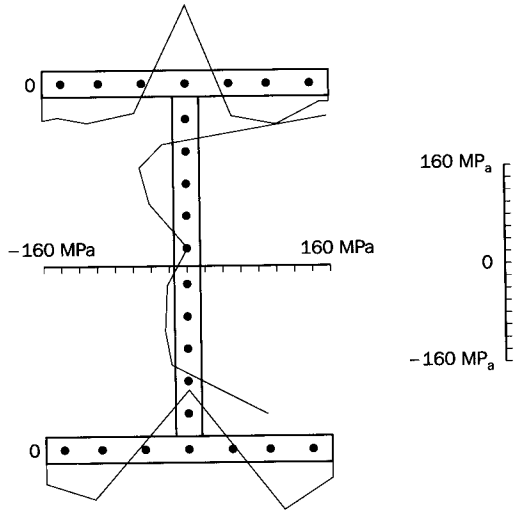

Fig. 3.40 Residual stress pattern for a welded stainless steel I-shape (Bredenkamp et al., 1992).

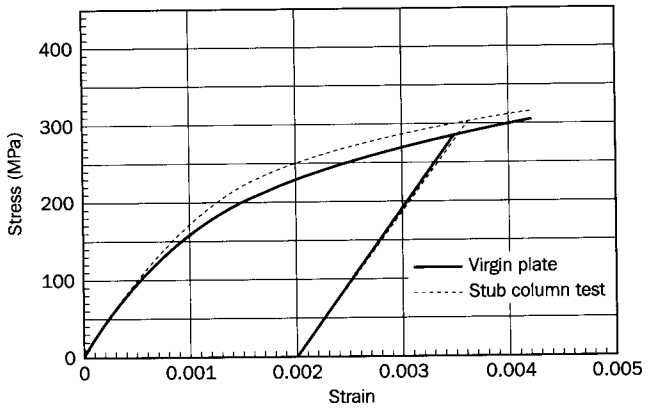

Fig. 3.41 Analytical stress-strain curves for a welded stainless steel I-shape (Bredenkamp et al., 1992).

3.2.9 Development of Column Strength Criteria

The following gives a description of data and computational techniques that are needed for the development of maximum-strength column curves and other results for pinned-end, centrally loaded columns. Further details can be found in the references of Batterman and Johnston (1967), Bjorhovde (1972, 1988, 1992), Chen and Atsuta (1976), Chen and Han (1985), Chernenko and Kennedy (1991), Kennedy and Gad Aly (1980), and Albert et al. (1995).

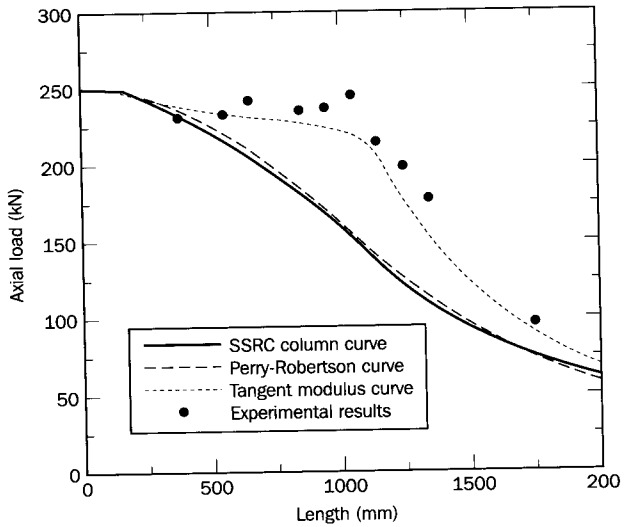

Fig. 3.42 Experimental and theoretical buckling loads for type 3CR12 stainless steel columns (Bredenkamp et al, 1994).

When detailed strength and performance data are not available for a specific column shape, it is possible for individual researchers or code-writing bodies to develop column curves of types that are similar to those that have been presented in this guide. The following gives a brief outline of the assumptions that should be used, the type of data that are required, and the computational technique that is suitable for these types of problems.

Data That Are Needed. The following data are needed for the computation of the maximum strength of columns:

1. Type of material and its material properties (i.e., yield stress, yield strain, modulus of elasticity).
2. Distribution of the residual stresses in the cross section, including variation through the thickness, if the shape is large or is tubular.
3. Variation of the yield stress throughout the cross section. This is in most cases needed only for welded built-up shapes and cold-formed shapes, where the yield stress at a weld or a cold-formed corner, for example, may differ significantly from the nominal properties.
4. In case the material is of a type or grade that exhibits nonlinear stress-strain characteristics (e.g., stainless steel), a complete, typical stress-strain curve is required.
5. Maximum value of the initial out-of-straightness.

Assumptions for the Analysis. The following assumptions are normally conservative in nature, with the result that computed column strengths are usually somewhat less than those obtained in actual tests:

1. Material is linearly elastic, perfectly plastic.
2. The initial and all subsequent deflection shapes of the column can be described by a half sine wave.
3. The residual stresses are constant in an element of the cross section along the full length of the column.
4. Sections that are originally plane remain so for the range of deflections that is suitable for column studies.
5. Yielded fibers in the cross section will unload elastically.
6. The yield stress may vary across the width and through the thickness of the component plates of the cross section but does not vary along the length of the column.
7. In line with assumption 2, only stresses and strains at midheight of the column are considered in the analysis.

It should be pointed out that if detailed yield-stress and other material data are not available for the elements in the cross section, the results of a stub column test can be used. If this is not available, tension test results for various parts of the shape can be used; the properties to utilize in the computations should then be based on a weighted average.

Computational Technique. Maximum column strength requires the solution of an inelastic, nonlinear problem. It is best achieved through an incremental, iterative computation algorithm. Internal force and moment equilibrium are established for every load and deflection level, requiring iteration over the cross section to determine when individual fibers yield, unload, or continue to load. The computations are carried to a level where the column cannot take any additional load when an additional amount of deflection is imposed; this constitutes the maximum strength level. It is recommended that the incrementation procedure be based on deflection increments rather than load, due to the convergence problems that may be encountered as the maximum load is approached when load increments are used. The procedure above leads to the development of the load-deflection curve for the columns with a given slenderness ratio or length. To obtain the complete column curve, it must be repeated for a range of lengths. As an illustration of the basic steps in the column strength computations, Fig. 3.43 gives a flowchart that indicates the necessary major parts of the solution.

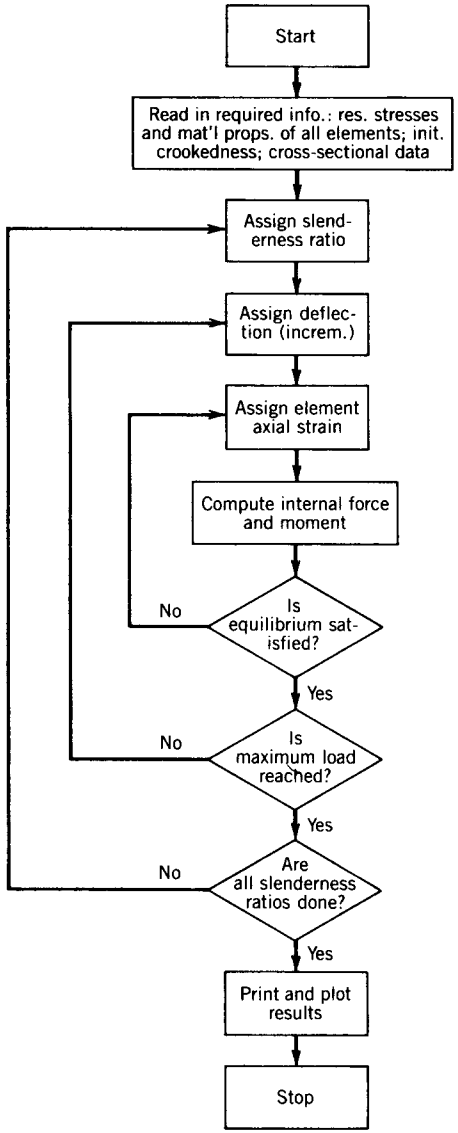

Fig. 3.43 Flowchart for maximum column strength computation.

3.3 TAPERED COLUMNS

3.3.1 Introduction

Tapered structural members are beams, columns, or beam-columns which have a continuously varying cross section along their longitudinal axes. Such structural components are used in many applications in practice, such as gable

frames, towers, and architecturally exposed steel columns in stores, halls, or airports. Because of the variation of the flexural, axial, and torsional stiffness in the member, the stability analysis is considerably more complicated than that of prismatic members. One of the earliest solutions to the problem of buckling of tapered columns is due to Timoshenko (1908). Since then a vast amount of research has been performed on the many aspects of tapered elements. In this section the stability of axially loaded tapered columns, acting either individually or as members in a rigid frame, is discussed.

Design engineers have ample information to determine the elastic critical load of tapered columns of perfect geometry. Considerably less is known about the effects of initial imperfections and residual stresses on buckling in the inelastic range. In design the maximum column capacity is usually obtained by first calculating the elastic critical load of the tapered column, next determining the length of a prismatic pinned-end Euler column which buckles under the same critical load, and finally, calculating the inelastic capacity by the applicable column strength equation with this effective length (AISC, 1993). Such a column equation includes the effects of both material and geometric nonlinearity. The pertinent geometric properties of the tapered column are taken at the least cross section of the tapered column. This approach is conservative since it assumes the same extent of yielding in all other cross sections, even though they are of larger area than the smallest reference section.

3.3.2 Elastic Critical Load of Tapered Columns

The elastic buckling of tapered columns can be determined by solving the differential equation of linear buckling, where the moment of inertia is an algebraic function of the longitudinal coordinate of the member. This analytically exact solution is possible only for special cases of the variation of the moment of inertia, and it involves considerable mathematical manipulation. Thus only the simpler problems are solved by this approach in textbooks such as those by Timoshenko and Gere (1961) or Bleich (1952). This mathematically exact method was also used by Gere and Carter (1962) and Ermopoulos (1986) to develop extensive charts and formulas for direct use by design engineers. Fogel and Ketter (1962) also developed extensive charts for the strength of tapered beam-columns, with the first yield as the limit state.

The other methods of solution for the elastic buckling load of tapered columns are the numerical and energy methods. The energy methods are presented in many textbooks, such as that by Timoshenko and Gere (1961), for example. The numerical methods are the *numerical integration method* (also known as the *method of successive approximations*, or *Newmark's method*) (Gere and Carter, 1962; Wang, 1967), the *finite difference method* (Girijavalabhan, 1969), and the *finite integral method* (Kitipornchai and Trahair, 1972). Modern methods of solution employ the *finite element method*, discretizing the member into many prismatic segments (Lee et al, 1972), or

using trapezoidal beam elements (Gallagher, 1975; Karabalis and Beskos, 1983; Chan, 1990; Bradford and Cuk, 1988).

There are many further references on the buckling of tapered columns, beams, and beam-columns. Many of these are summarized in the English edition of the Japanese *Handbook of Structural Stability* (CRCJ, 1971), which presents very extensive charts and tables for many different cross sections, boundary conditions, and taper configurations. Additional formulas and tables are given in *Formulas for Stress and Strain* (Roark and Young, 1975). The charts in Gere and Carter (1962) apply to eight types of cross section and to four kinds of boundary conditions. Ample data are thus available in the literature to the design engineer for the determination of the elastic critical load of individual tapered columns.

The elastic buckling of rigid frames containing tapered columns has also attracted considerable research attention, by Wang (1967), Lee at al. (1972), and others (see CRCJ, 1971). The work of Lee and his associates at the University of New York at Buffalo is considered in more detail in the next section.

The problem of the inelastic buckling of tapered columns has received relatively little attention, with one exception. Appl and Smith (1968) solved the case of tapered aluminum columns with a Ramberg–Osgood type of stress-strain curve by a power series solution of the differential equation of buckling. They also conducted tests on 44 specimens and found excellent correlation with the theoretical prediction. More research is needed on the inelastic buckling capacity of tapered steel columns.

3.3.3 Buckling of Web-Tapered I-Section Steel Columns

Following is a discussion of research conducted for about a decade starting at 1966 by Lee and his associates at the University of New York at Buffalo. This research was a continuation of earlier work at Columbia University under the direction of Butler (Butler and Anderson, 1963; Butler, 1966). Both of these projects were under the technical guidance of a joint committee of the Structural Stability Research Council (SSRC) and the Welding Research Council (WRC). The broad assignment of this research was to develop design criteria for rigid frames composed of web-tapered steel members. A more extensive discussion of the results of this work, including the stability of beams, beam-columns, columns, and frames, is presented in Chapter 9 of the fourth edition of this guide.

For the linearly tapered member, the depth at any distance z from the smaller end can be expressed as

$$d_z = d_0\left(1 + \frac{z}{l}\gamma\right) \tag{3.26}$$

where d_0 represents the smallest depth at $z = 0$, and γ represents the tapering ratio. For a prismatic member, $\gamma = 0$; for a member whose depth at the large end is three times that of its smaller end, $\gamma = 2$. This geometry is defined in Fig. 3.44*a* and the loading condition is illustrated in Fig. 3.44*b*.

Since it was found to be virtually impossible to nondimensionalize the many parameters in tapered sections, solutions were obtained for members possessing five smaller end cross-sectional dimensions, given in Fig. 3.45. These cover all the range of tapered members used in present-day practice. Other variables of the solutions were obtained for member length, moment ratios, taper ratios,

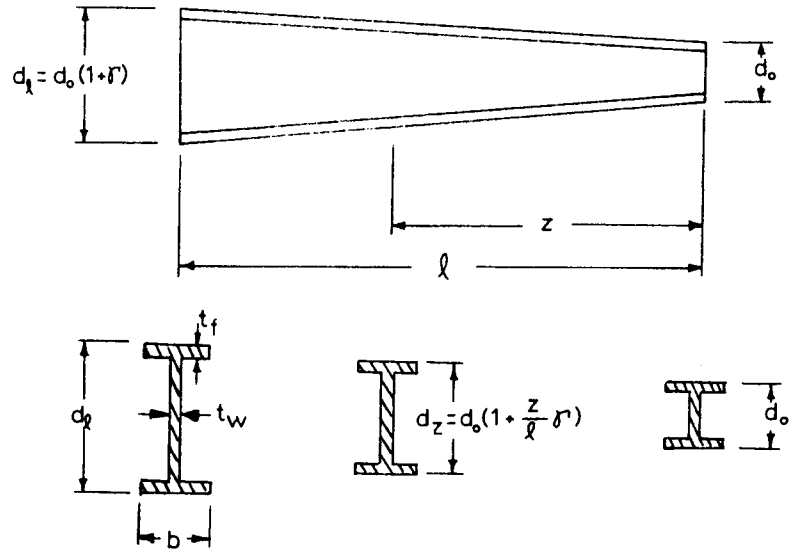

Fig. 3.44a (*a*) Geometry of linearly tapered I-beam (b, t_f, and t_w are all constant).

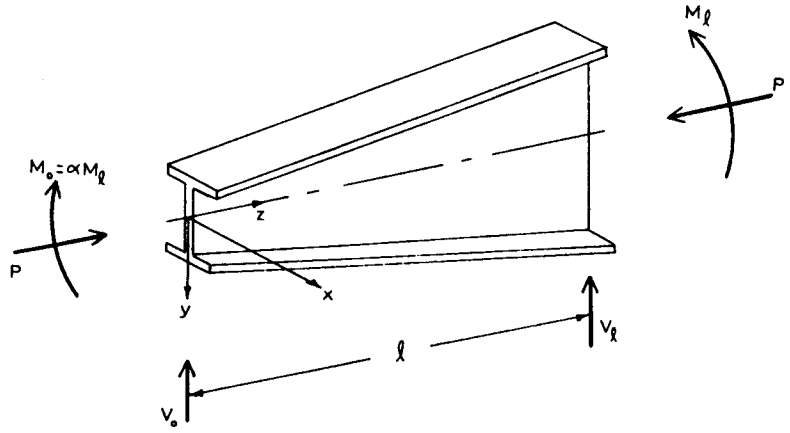

Fig. 3.44b (*b*) The presumed loading on a simply supported linearly tapered I-beam.

	I	II	III	IV	V
		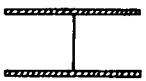		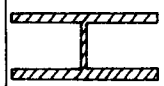	
d_o	6.00 in.	6.00 in.	6.00 in.	6.00 in.	12.00 in.
b	4.00	12.00	4.00	12.00	6.00
t_f	0.25	0.25	0.75	0.75	0.25
t_w	0.10	0.10	0.25	0.25	0.10

Fig. 3.45 Dimensions of the smaller end of linear tapered I-beam presumed.

eccentricities, axial loads, and end moments. These are described by Lee et al. (1972, 1981).

Several avenues of approach are available for the development of design approximations. First, using multivariable curve-fitting techniques, polynomial expressions containing all the variables could be developed. A second approach could start from the assumption that adequate solutions are now available for prismatic members. Then modifying factors could be developed and introduced into the prismatic formulas. The factors can be calculated from

$$\frac{\text{strength of tapered member}}{\text{strength of prismatic member of the smaller cross section}} = f(\gamma, d_0, b, t, w, l) \quad (3.27)$$

with the restriction that when $\gamma = 0$ (prismatic), $f = 1.0$.

Although both approaches require curve-fitting techniques, the second approach offers two appealing advantages to the designers. First, they will be using the same formulas (AISC, 1993) for prismatic members but with a factor. Second, the factor will give an intuitive feeling for the increase in strength over a prismatic section.

There are two modes of general failure to be considered in the design of axially loaded tapered members of doubly symmetrical cross section: (1) strong-axis buckling and (2) weak-axis buckling.

Considering elastic buckling, a function f (Eq. 3.27) is required, such that

$$P_{\text{taper}} = P_{\text{prismatic}} f(\gamma, d_0, b, t, w, l) \quad (3.28)$$

where

$$P_{\text{prismatic}} = \frac{\pi^2 E I_{x_0}}{l^2}$$

Since column-type buckling can occur about either the strong or weak axis of the cross section, the function f will be different for each case. Observing that the variation of the weak-axis radius of gyration along the length of a web-tapered member (flange width is constant) is small, no modification factor is necessary. Thus

$$(P_{ey})_\gamma = \frac{\pi^2 E I_{y_0}}{l^2} \qquad \text{(weak axis)} \quad (3.29)$$

If the member is braced against weak-axis buckling, then buckling will occur about the strong axis. For this case, let $f = 1/g^2$ so that

$$(P_{ex})_\gamma = \frac{\pi^2 E I_{x_0}}{(gl)^2} \quad (3.30)$$

Equation 3.30 implies that the buckling load for a tapered column of length l can be considered equivalent to that of a prismatic column having a cross section equal to that of the smaller end of the tapered column and a length equal to gl (Fig. 3.46). Note that for axially loaded tapered columns the critical stress will always occur at the smaller end and the stress will decrease toward the larger end.

Seeking a function of simple form with relatively small error and assuming a curve fitted to the data,

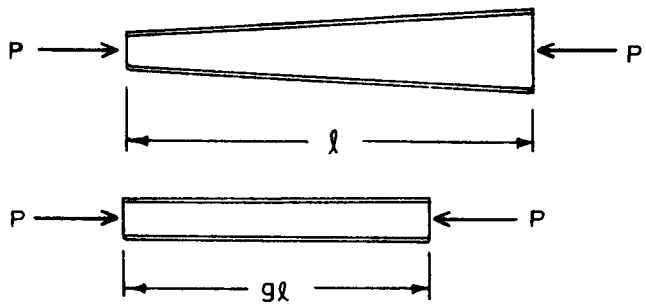

Fig. 3.46 Tapered column and prismatic column having the same smaller end cross section and the same critical load.

$$g = \sqrt{\frac{(\pi^2 EI_{x_0}/l^2)}{(P_{ex})_\gamma}}$$

where the sections indicated in Fig. 3.45 were used to establish the range of variation. After examining the resulting fitted functions, the following was chosen (see Lee et al., 1972):

$$g = 1.000 - 0.375\gamma + 0.080\gamma^2(1.000 - 0.0775\gamma) \tag{3.31}$$

In general, these elastic formulas are applicable for slenderness ratios greater than a certain limiting ratio. For members with lesser slenderness values, buckling will occur in the inelastic range and the formula will overpredict the critical load. Since there are available at this date no inelastic solutions, one possible procedure for solving problems in this range is to use the AISC column curve (Eq. 3.19) with an effective length gl.

If the column is restrained at either or both ends, the buckling load as developed above will be different. A restrained column of height l can be considered as a pin-ended column of length $K_\gamma l$, where K_γ is the effective length factor. In this consideration the function g has been absorbed into the effective length factor K_γ. Thus K_γ is interpreted as relating a restrained tapered column of height l to a pin-ended prismatic column of length $K_\gamma l$.

The effective length is determined by considering a rectangular rigid frame (Fig. 3.47) composed of prismatic beams and tapered columns. The top beam is

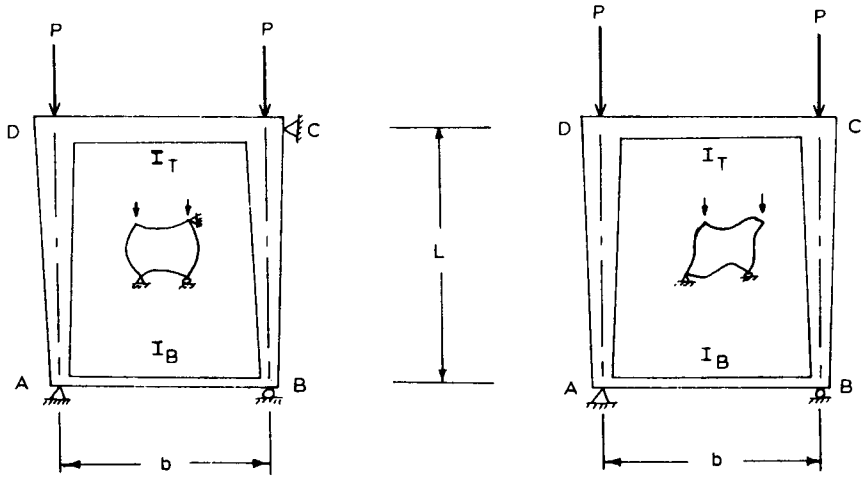

Fig. 3.47 Rectangular frame composed of linearly tapered I-shaped columns and prismatic I-beams used to determine the effective column length: (*a*) no sidesway; (*b*) with sidesway.

assumed to have a moment of inertia I_T; the bottom beam, I_B. The loads are assumed to act at the centroid of the columns. The frame has two support conditions in the plane of the frame: (*a*) supported at A, B, and C (sidesway prevented) and (*b*) supported at A and B (sidesway permitted). Finally, it is to be understood that only buckling in the plane of the frame is considered (i.e., strong-axis buckling of the tapered columns).

The effective length $K_\gamma l$ was calculated from

$$K_\gamma = \sqrt{\frac{\pi^2 EI_{x_0}}{P_{cr} l^2}} \tag{3.32}$$

where P_{cr} is the critical load acting on the frame in Fig. 3.47. Thus Eq. 3.30 can be written to include end restraints,

$$(P_{ex})_\gamma = \frac{\pi^2 EI_{x_0}}{(K_\gamma l)^2} \tag{3.33}$$

Curves relating end restraint to the effective length factor K_γ are given in Fig. 3.48 *a* and *b* for $\gamma = 3$. Additional charts of this kind are provided in the commentary to the AISC allowable stress design specification (AISC, 1989).

In many single-story rigid frames the girders are designed to be multisegment members, for reasons of economy. A typical frame is shown in Fig. 3.49. The design of such a frame requires additional information. First, to determine the end restraint at the top of the column, it is necessary to estimate the I/L value of the girder. Second, if the girder AB is to be checked, the effective-length factors in terms of the end-restraint parameters must also be provided. Design information for both of these has been developed by Lee et al. (1979). Their application in design may be found in the book by Lee et al. (1981).

3.4 BUILT-UP COLUMNS

3.4.1 Introduction

The effect of shear in built-up columns sets apart the design of these members from that of other columns. The importance of designing the elements connecting the main longitudinal components for shear was tragically demonstrated by the failure of the first Quebec Bridge during construction in 1907. Bridge-design practice in the United States today reflects the lessons learned from the extensive research that followed that failure. Wyly (1940) concluded that about three-fourths of the early failures of laced columns resulted from local rather than general column failure. Moreover, the critical load for a built-up column is less than that of a comparable solid column because the effect of shear on deflections is much greater for the former. Thus the shear in built-up

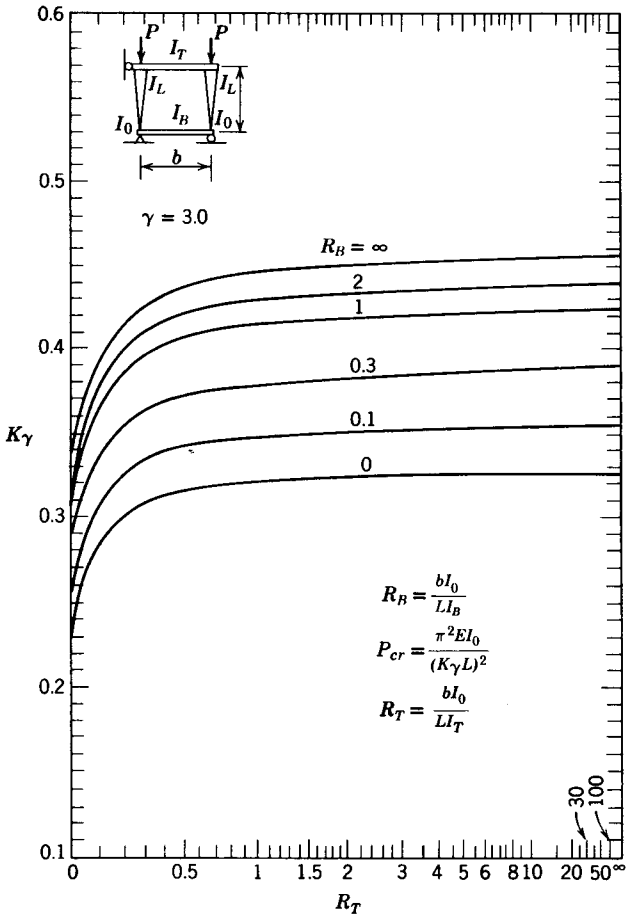

Fig. 3.48a (*a*) Effective-length factors for tapered columns: sidesway prevented ($\gamma = 3.0$).

columns needs to be evaluated to (1) determine the possible reduction in the buckling load, and (2) design the lacing bars, battens, and their connections.

Three common types of built-up columns are illustrated in Fig. 3.50. They are used when the loads to be carried are large, or when a "least weight' member or a member with about the same radius of gyration in orthogonal directions is desired. Laced or "latticed" columns (Fig. 3.50*a*) are frequently used in guyed antenna towers, in derrick booms, and in space exploration vehicles. In modern bridge construction, perforated cover-plated columns (Fig. 3.50*c*) are likely to be used rather than laced columns. Of the three, battened columns (Fig. 3.50*b*) are the least resistant to shear and may experience an appreciable reduction in axial strength. They are not generally used for

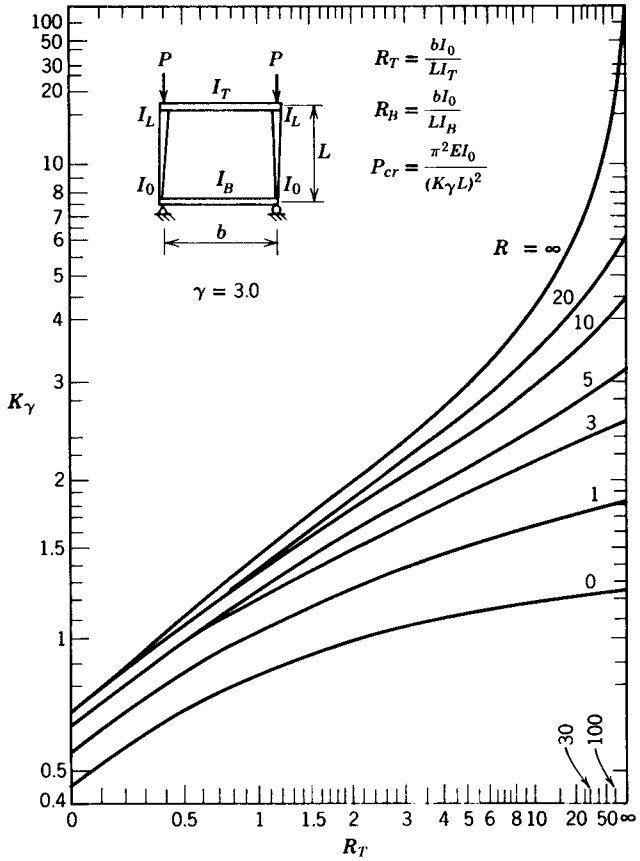

Fig. 3.48b (*b*) Effective-length factors for tapered columns: sidesway permitted ($\gamma = 3.0$).

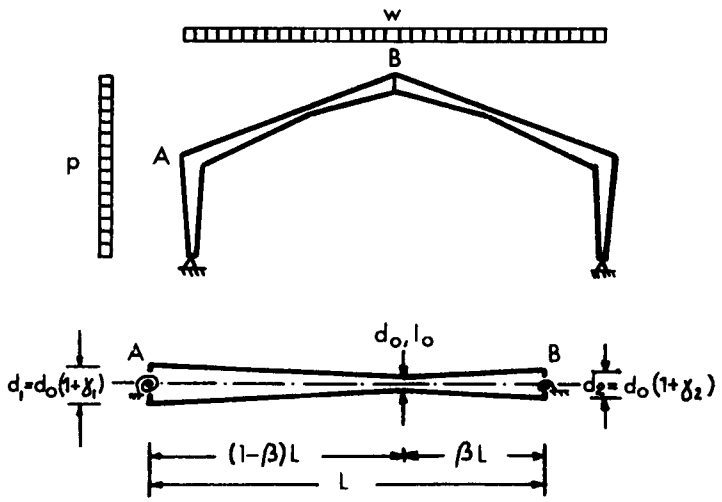

Fig. 3.49 Typical rigid frame with doubly tapered rafter.

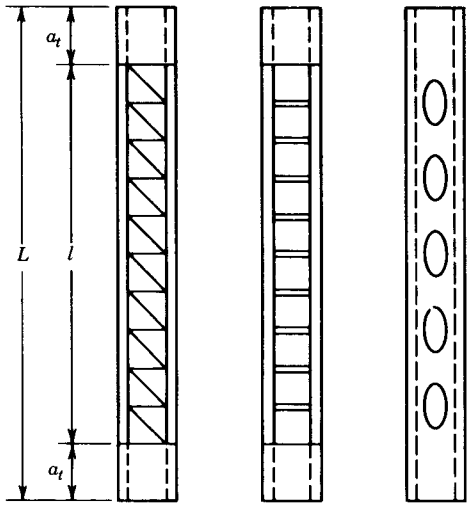

Fig. 3.50 Built-up columns.

either bridge or building construction in the United States. Box columns with perforated cover plates designed to specification rules require no special considerations for shear effects.

Engesser (1891) considered the effect of shear on the reduction of the Euler load of an axially loaded column. This has been reevaluated by Ziegler (1982). Bleich (1952) and Timoshenko and Gere (1961) discuss both aspects of the shear effects. Additional references are given in the third edition of this guide (Johnston, 1976).

The shear in a column may be caused by:

1. Lateral loads from wind, earthquake, gravity, or other causes
2. The slope of the column with respect to the line of thrust due both to unintentional initial curvature and the increased curvature during buckling
3. The end eccentricity of the load due to either end connections or fabrication imperfections

The shear due to lateral is combined with the estimated allowance for the shear caused by the other effects. The slope effect is most important for slender columns and the eccentricity effect for short columns. Worldwide, the design requirements for shear in built-up columns vary widely (Beedle 1991). The Eurocode 3 (ECS, 1993) recommends evaluating shear on the basis of the end slope due to a specified initial out-of-straightness, magnified by the effect of axial load and added to the transverse shear due to the applied loads.

The AASHTO and AREA bridge specifications provide an empirical formula for shear to be added to that due to the weight of the member or the external forces:

$$V = \frac{P}{100}\left[\frac{100}{(l/r)+10} + \frac{(l/r)F_y}{3{,}300{,}000}\right] \tag{3.34}$$

where

V = normal shearing force, lb (N)
P = allowable compressive axial load on members, lb (N)
l = length of member, in. (m)} radius of gyration of section about the axis perpendicular to plane of lacing or perforated plate, in. (m)
r = radius of gyration of section about the axis perpendicular to plane of lacing or perforated plate, in. (m)
F = specified minimum yield point of type of steel being used, psi (MPa)

When the yield strength is expressed in MPa, the coefficient 3300 becomes 22,750.

The AISC specification for buildings (1993a) calls for the calculation of an increased slenderness ratio for use in the column formula to account for the shear effect. The design formula is based on the research by Zandonini (1985) and Aslani and Goel (1991). In Canada, highway bridge specifications (CSA, 1980) require a shear force of 2.5% of the axial force to be added to that due to lateral loads.

3.4.2 Effect of Shear Distortion on Critical load

Shear distortion reduces the axial compressive capacity of built-up columns. The shear flexibility of battened or laced structural members can be characterized by the shear flexibility parameter, μ (Lin et al., 1970). The parameter μ takes account of the added distortion due to axial force or bending in the web elements. It is assumed that the end stay plates do not contribute to the shear flexibility. The effect of shear on the elastic critical load is depicted in Fig. 3.51 for three basic end conditions:

1. Both ends hinged (subscript h)
2. One end fixed, one hinged (subscript f, h)
3. Both ends fixed (subscript f)

One enters Fig. 3.51 with a chosen a_t/L and a calculated shear parameter value of μ. The load ratio P_{cr}/P_e can then be read for the appropriate end conditions, after which the equivalent-length factor may be calculated by the equation

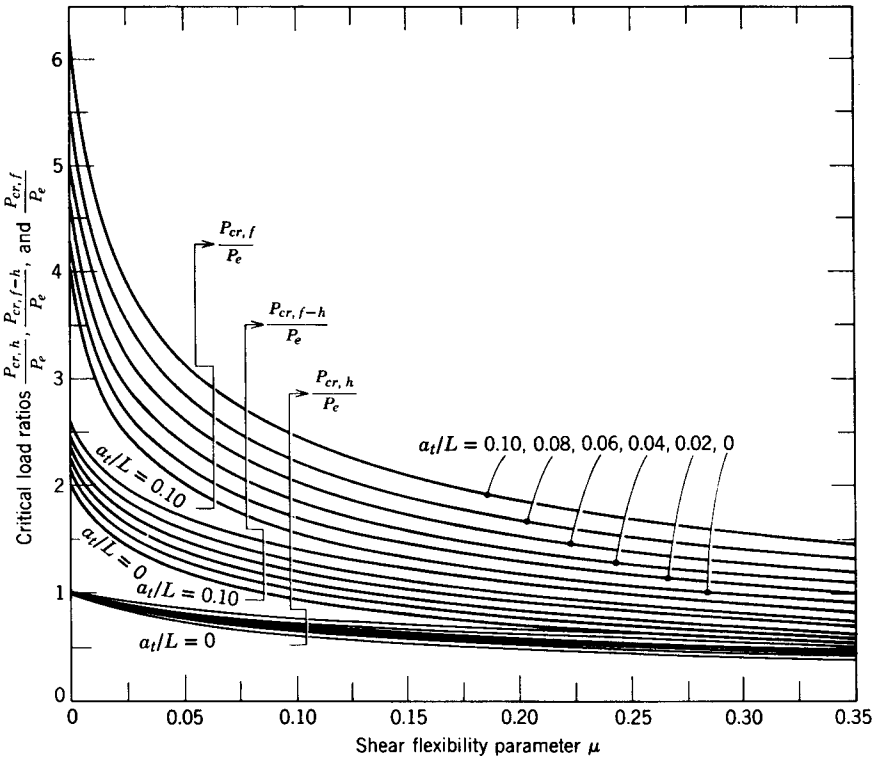

Fig. 3.51 Critical loads of columns with various end conditions, constant shear flexibility μ, and rigid stay plates.

$$K = \sqrt{\frac{P_e}{P_{cr}}} \tag{3.35}$$

In Eq. 3.35 and Fig. 3.51 P_{cr} is the elastic critical load of the given open-web or open-flange column, and $P_e = \pi^2 EI/L^2$, the Euler load for a solid-wall column with both ends hinged. Compressive resistance is then obtained for a given specification as a function of KL/r by formula or table.

3.4.3 Laced Columns

For a typical laced member (Fig. 3.50*a*), consisting of two main longitudinal elements, two planes of diagonal lacing and transverse struts, Lin et al. (1970) provide the following formula for the shear flexibility factor μ:

$$\mu = \frac{\xi_b}{1+\xi_a}\left(\frac{b}{l}\right)^2 \frac{A_c}{A_d}\left\{\frac{b}{\xi_a a}\left[1+\left(\frac{\xi_a a}{b}\right)^2\right]^{3/2} + \frac{b}{\xi_a a}\frac{A_d}{A_c}\right\} \tag{3.36}$$

The notation used in Eq. 3.36 is described by Figs. 3.50*a* and 3.52. The third edition of this guide (Johnston, 1976) provides an illustrative example of the application of Eq. 3.36 to a typical design.

In view of the usual small effect of shear in laced columns, Bleich (1952, p. 174) has suggested that a conservative estimate of the influence of 60° or 45° lacing, as generally specified in bridge-design practice, can be made by modifying the effective-length factor K (determined by end-restraint conditions) to a new factor K', as follows:

$$K' = \begin{cases} K\sqrt{1+\dfrac{300}{(KL/r)^2}} & \text{for } KL/r > 40 \\ 1.1K & \text{for } KL/r \le 40 \end{cases} \tag{3.37}$$

The change in K is significant only for small KL/r values, in which case there is little change in the compressive strength.

Bridge design practice in the United States (AASHTO, 1996; AREA, 1979) requires that the slenderness ratio of the portion of the flange between lacing bar connections have a slenderness ratio of no more than 40 or more than two-thirds that of the entire member. Canadian bridge specifications (CSA, 1980) change the foregoing limits to 60 and three-fourths, respectively.

The lacing bars and their connections must be designed to act either in tension or compression, and the rules for general column design apply to them as well. In exceptional cases, such as very large members, double diagonals can be designed as tension members and the truss system completed by compression struts. The importance of adequate and tight-lacing bar connections has been demonstrated by test (Hartmann et al., 1938).

Crane booms frequently consist of latticed columns. Vroonland (1971) analyzed nonuniform booms under combined lateral and axial loads and included the effects of deflections and intermediate lateral supports. Brolin et al. (1972) tested four booms, varying from 60 to 200 ft in length, to destruction. The

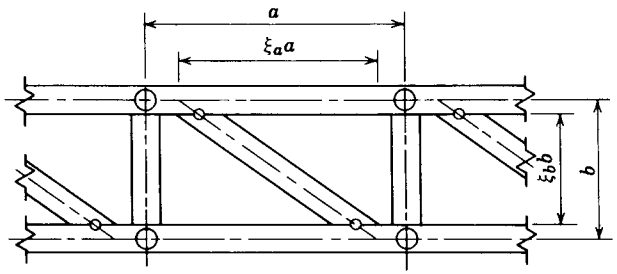

Fig. 3.52 Typical panel of a laced structural member. Circles indicate where hinges were assumed in the analysis.

failure loads were in good agreement with the analyses of Vroonland. Failures occurred when the compressive force in an individual chord member reached the failure load predicted for the unsupported length between brace points.

Interest in laced members has recently been renewed by the needs of the space industry for minimum weight members to carry very small loads. Figure 3.53 illustrates a member with three longitudinal tubular chords (longerons) with tension diagonals and transverse compression struts. The overall and chord slendernesses are about the same and are very large.

Miller and Hedgepeth (1979) studied the deleterious effects of initial out-of-straightness of the column as a whole combined with that of the chords between struts. They provide charts that predict the maximum buckling load as a fraction of the Euler bifurcation load of a perfectly straight member. For slenderness ratios of both the member and chord of about 279, the maximum load is less than 50% of the Euler load. Crawford and Benton (1980) studied similar members and got comparable results. These studies indicate that for latticed members with very large slenderness ratios the interaction of local and overall out-of-straightness is the dominating factor, not the effect of shears.

3.4.4 Battened Columns

Figure 3.54 shows the basic elements of a battened column consisting of two main longitudinal chords rigidly connected by battens in one, two, or more planes. The battens act as the web and transmit shear from one chord to the other by flexural action in combination with local bending of the chords.

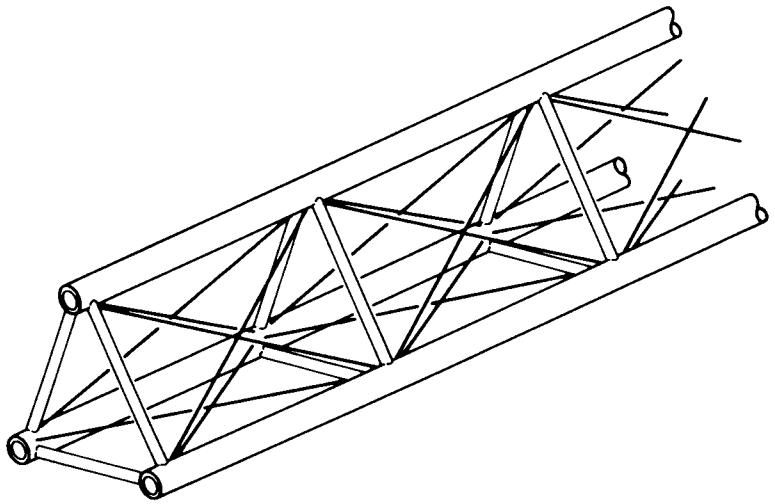

Fig. 3.53 Triangular latticed column.

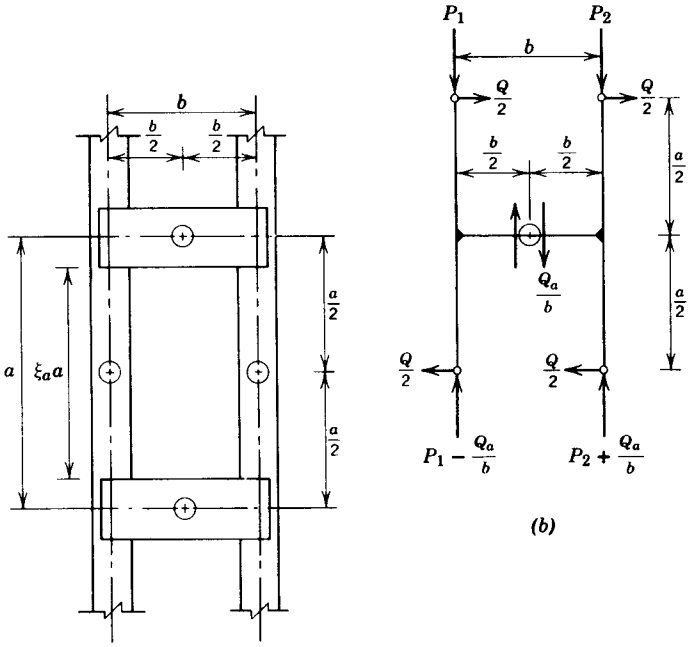

Fig. 3.54 Typical panel of battened structural member: (*a*) geometrical configuration; (*b*) force equilibrium. Circles indicate assumed points of inflection.

A battened column is more flexible in shear than either a laced column or even a column with perforated cover plates. It acts as a Vierendeel truss. The effect of shear distortions can be significant and should be considered in calculating the compressive strength of the column. Battened columns are generally not allowed in current U.S. design specifications but are in Canada. As well, battened columns are frequently used for antenna towers and on occasion for secondary members. The lower portion of columns in mill buildings that support crane runway girders may look like battened columns, but because the connections of the battens to the chords are not rigidly framed, they really are spaced columns, as discussed in Section 3.4.5.

The typical unit of a battened column has a length a center to center of battens and a width b between centroids of the chords. The properties of the battened column are characterized by the shear shape factors and moments of inertia of the battens and chords.

In developing the shear flexibility effect for the highly redundant battened member, Lin et al. (1970) assumed points of inflection for symmetric members at the midpoints of the battens and midway between the battens for the chords. The analysis is conservative because the overall continuity of the longitudinal members is neglected. The shear flexibility parameter is then given by

$$\mu = \left[\frac{1}{(l/r_c)^2} + \left(\frac{b}{2l}\right)^2\right]\left[\frac{A_c}{A_b}\left(\frac{ab}{6r_b^2} + 5.2\frac{a}{b}\eta_b\right) + 2.6\xi_a\eta_c + \frac{\xi_a^3}{12}\left(\frac{a}{r_c}\right)^2\right] \quad (3.38)$$

The nomenclature for Eq. 3.38 is shown in Fig. 3.54 and (additionally) as follows:

A_c, A_b = area of a single longitudinal and all batten elements within a length a respectively
r_c, r_b = radius of gyration of longitudinal and batten elements, respectively
η_c, η_b = shear shape factors for the longitudinal and batten elements, respectively, where the shear shape factor is the ratio of the total cross-sectional area to the shear area (Timoshenko and Gere, 1961)
l = length of column between end tie plates

Equation 3.38 accounts for the amplification of deflection in the column segments between battens. These may be neglected if the slenderness ratio of the chord segment between battens, $\xi_a a/r_c$, does not exceed $80\sqrt{f_a}$ where f_a is the average stress in ksi at the specified load level. This limit is considerably more stringent than the batten spacing requirements in some specifications. Because it is likely to be impractical to determine the partial rigidity of semirigid batten connections experimentally, it is recommended that whenever semirigid connections exist, the column be considered to be a spaced column.

Example 3.1: Battened Column As shown in the Fig. 3.55, batten flange stiffeners have been included to eliminate local web distortion and to ensure that

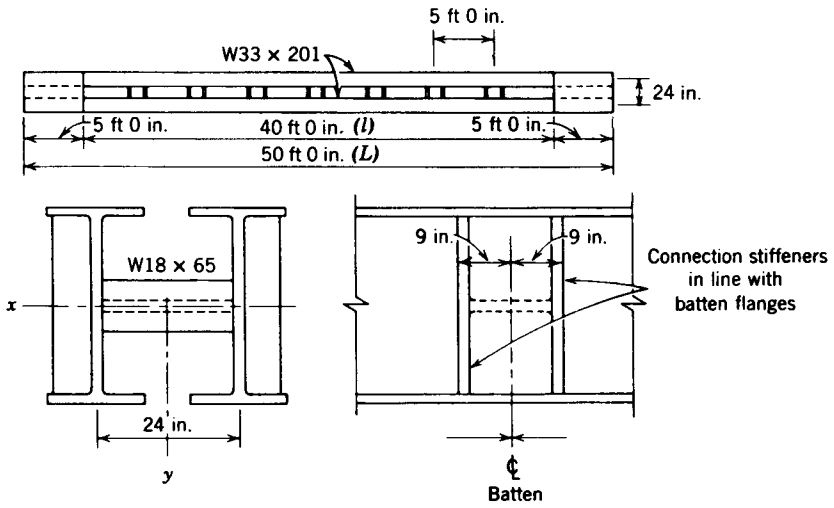

Fig. 3.55 Example details.

the battens are fully effective. If such stiffeners were not provided, the column could be treated as a spaced column. From the AISC manual,

W33 × 201 (longitudinal)
$A_c = 59.1\,\text{in}^2$
$r_c = r_y = 3.56\,\text{in.}$
$r_x = 14.0\,\text{in.}$
$I_y = 749\,\text{in}^4$
W18 × 65 (batten)
$A_b = 19.1\,\text{in}^2$
$r_b = r_x = 7.49\,\text{in.}$
$a = 60\,\text{in.}$
$b = 24\,\text{in.}$
$\xi_a = \dfrac{60 - 18}{60} = \dfrac{42}{60} = 0.70$
$l = 480\,\text{in.}$
$L = 600\,\text{in.}$
$\eta_c = 1.6$
$a/L = 0.10$
$\eta_b = 2.6$

For the combined cross section,

$$I_y = \frac{59.1 \times 24^2}{2} + 2 \times 749 = 18{,}519\,\text{in}^4$$

$$r = \sqrt{\frac{18{,}519}{2 \times 59.1}} = 12.5\,\text{in.} < r_x$$

Substituting Eq. 3.38 yields

$$\mu = \left[\frac{1}{(480/3.56^2} + \left(\frac{24}{2 \times 480}\right)^2\right] \times \left[\frac{59.1}{19.1}\left(\frac{60 \times 24}{6 \times 7.49^2} + 5.2 \times \frac{60}{24} \times 2.6\right) + 2.6 \times 0.7 \times 1.6 - \frac{0.70^3}{12}\left(\frac{60}{3.56}\right)^2\right]$$

$$= 0.088$$

The critical load ratio for three sets of end conditions is obtained from Fig. 3.51 and the effective-length factor is evaluated from Eq. 3.35. The results are given in Table 3.1. If no reduction were made, the value of KL/r for the hinged–hinged case would be $600/12.5 = 48$.

Bleich (1952) gives the following approximate formula for the effective length of a battened column with both ends hinged:

$$\frac{KL}{r} = \sqrt{\left(\frac{L}{r}\right)^2 + \frac{\pi^2}{12}\left(\frac{a}{r_c}\right)^2} \tag{3.39}$$

where L/r is the slenderness ratio of the column as a whole and a/r_c is the slenderness ratio of one chord center-to-center of battens. Bleich estimates that the buckling strength of a steel column having an L/r of 110 is reduced by about 10% when $a/r_c = 40$, and by greater amounts for larger values of a/r_c.

For example 3.1, $a/r_c = 60/3.56 = 16.9$ and Eq. 3.39 gives

$$\frac{KL}{r} = \sqrt{\left(\frac{600}{12.5}\right)^2 + \frac{\pi^2}{12}(16.9)^2} = 50.4$$

which is lower than the 53.8 determined by Eqs. 3.38 and 3.35.

The unconservative assumption has been made that the addition of two stay plates gives the end regions full rigidity with respect to shear. At the same time, the effective KL/r is slightly decreased because of the increase in bending resistance due to the stay plates in the end regions. The two effects are offsetting and may be neglected. The design of the chords and the batten plates and their connections should take account of the local bending resulting from specified shear forces.

The batten plates and their connections to the chords are designed for the combination of shear Qa/nb and moment at the connection of

$$M_b = \frac{Qa}{2n} \tag{3.40}$$

TABLE 3.1 Results for Example 3.1

End Conditions	P_{cr}/P_c (Fig. 3.51)	K	KL/r	$\phi_c F_{cr}$ (AISC) (ksi)	
				$F_y = 36$ ksi	$F_y = 50$ ksi
Hinged–hinged	0.80	1.12	53.8	26.3	34.4
Hinged–fixed	1.45	0.83	39.9	28.1	37.8
Fixed–fixed	2.52	0.63	30.3	29.2	39.9

where Q is the shear required by specification plus shear due to any transverse loading, a the distance center-to-center of battens, and n the number of parallel planes of battens.

The strength of the chords should be checked for the combination of axial load, based on the strength for zero length, and the bending moment:

$$M_c = \frac{Q\xi_a a}{4} \tag{3.41}$$

3.4.5 Stay Plates and Spaced Columns

End stay plates in battened columns may contribute significantly to the buckling strength. Their importance is revealed by the study of a spaced column, defined herein as the limiting case of a battened column in which the battens are attached to the longitudinal column elements by hinged connections. The battens then act simply as spacers, with no shear transmitted between the longitudinal elements. Without end stay plates, the buckling strength of such a spaced column is no greater than the sum of the critical loads of the individual longitudinal components of the built-up member. The strengthening effect of the end stay plates arises from two sources: (1) a shortening of the length within which the column components can bend about their own axes, and (2) the forcing of the longitudinal components to buckle in a modified second-mode shape and thus have an elastic-buckling coefficient that may approximate four times that of the first mode. The buckling load of a spaced column with end tie plates is a lower bound to the buckling load of the battened column (also with tie plates) but with low or uncertain moment resistance in the connections between battens and the longitudinal components. Such columns are sometimes used in mill building construction. In addition to their contribution to column strength, end tie plates perform their usual role of distributing the applied forces or moment to the component elements of either laced or battened columns. They also provide a means of transmitting load to another member or to a footing. With regard to the distance along the column between spacer elements, the same rule as for battens should provide a conservative basis for design.

Example 3.1 involved a battened column. If the stiffener plates to provide rigidity of the batten connections were omitted, the behavior would approach the conditions assumed for the spaced column because the attachment of the battens to the column webs would not transmit moment effectively.

Using the notation adopted for battened columns, the moment of inertia of the two longitudinals about the y–y axis would be, as in Example 3.1.

$$I = \frac{A_c b^2}{2} + 2I_c$$

where I_c is the moment of inertia of one of the individual longitudinal elements.

The ratio I/I_c in mill building columns is usually at least 40 and could be greater than 100. This ratio is used as a parameter for the determination of the buckling load of a spaced column with end tie plates.

Four modes of buckling for spaced columns without sidesway are treated in Johnston (1971), as illustrated in Fig. 3.56. Spaced columns with sideways permitted also are treated briefly.

For the hinged-end condition the spaced column with end stay plates buckles either in S-curvature (mode A) (Fig. 3.56*a*) or in mode B curvature (Fig. 3.56*b*), depending on the values of I/I_c and a_t/L. It will be noted that in S-curvature there is no differential change of length of the two longitudinal column components between the end tie plates; thus they buckle under identical loads $P/2$, and the critical load is independent of the ratio I/I_c. When the column buckles in mode B curvature (Fig. 3.56*b*), the component on the concave side (at the center) shortens more than on the convex; thus there arises overall moment resistance due to the difference in the direct component forces. This is added to the separate moments induced in the components as a result of their own curvature. The critical loads for S-curvature buckling could be less than those for mode B curvature when the ratio I/I_c is relatively small and a_t/L is large.

In practice, the base of a column will usually be fixed to a footing, and S-curvature buckling cannot take place. Buckling will be in mode C as illustrated in Fig. 3.56*c*, but as I/I_c gets large it will tend toward the shape with both ends fixed, as illustrated in Fig. 3.56*d*. In fixed-end buckling (Fig. 3.56*d*), as in mode A, the moment resistance is simply the sum of the moments in the component parts, with no contribution due to differential direct forces as in Fig. 3.56*b* or *c*.

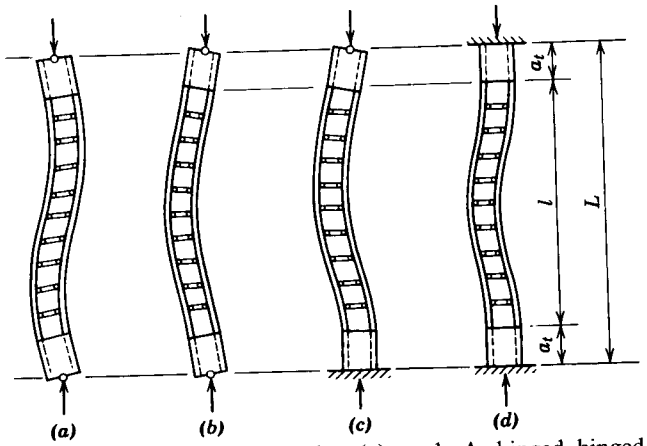

Fig. 3.56 Spaced column buckling modes: (*a*) mode A, hinged–hinged; (*b*) mode E, hinged–hinged; (*c*) mode C, hinged–fixed; (*d*) mode D, fixed–fixed.

The fixed-end case is the simplest to evaluate, since the critical load is simply twice the critical load of a longitudinal component, length l, with both ends fixed, that is, the Euler load with an equivalent length of $0.5l$ multiplied by 2.

Added moment resistance in a spaced column due to differential changes in component length occurs only when the end rotations are different in magnitude and/or sense, as in Fig. 3.56*b* and *c*. Within length l between the tie plates there is no shear transfer between longitudinals; hence the differential direct forces and the resisting moment that they contribute must remain constant within l.

Although Johnston (1971) gives critical load information for a variety of end conditions, including the four shown in Fig. 3.56, fixed-base and hinged-top case, Fig. 3.56*c* is possibly of greatest practical application. In terms of the overall length $L = l + 2a_t$ the equation for elastic critical load is written

$$P_{cr} = \frac{CEI_c}{L^2} \tag{3.42}$$

in which C is termed the elastic-buckling coefficient. For the determination of approximate critical loads in the inelastic range or for evaluation of compressive strengths by column-design formulas, it is convenient to determine the effective-length factor K, for use in the equation

$$P_{cr} = \frac{2\pi^2 EI_c}{(KL)^2} \tag{3.43}$$

where

$$K = \pi\sqrt{\frac{2}{C}} \tag{3.44}$$

Elastic-buckling coefficients C for the hinged–fixed case are plotted in Fig. 3.57, whose use will now be illustrated.

Example 3.2 Identical with Example 3.1 but omitting batten-flange stiffeners and considering the design as a spaced column,

$$\frac{a_t}{L} = \frac{5}{50} = 0.10 \qquad \frac{I}{I_c} = \frac{18{,}519}{749} = 24.7$$

From Fig. 3.57, $C = 100$. By Eq. 3.44,

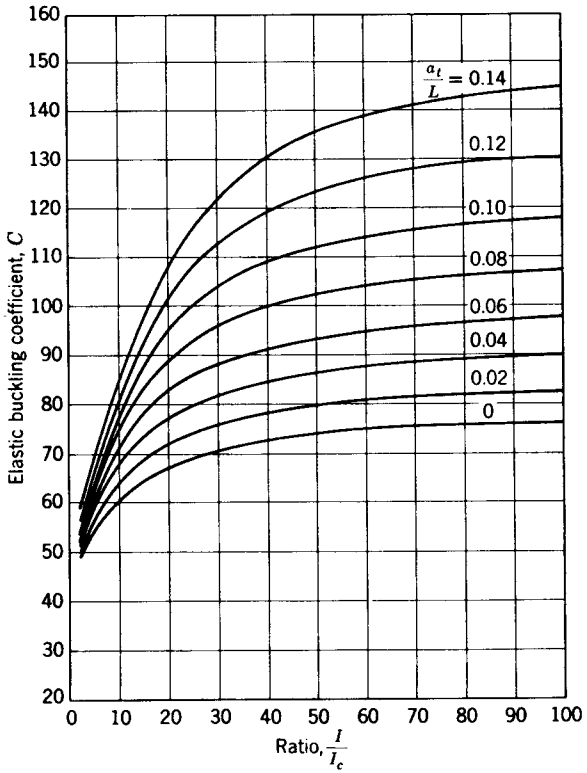

Fig. 3.57 Elastic buckling coefficients, one end hinged, one end fixed (mode C of Fig. 3.56).

$$K = \pi\sqrt{\frac{2}{100}} = 0.445$$

$$\frac{KL}{r_c} = \frac{0.445 \times 600}{3.56} = 75.0$$

(Note that K is now referenced to L/r_c, not L/r.) By AISC specification (1993, Tables 3-36 and 3-50):

	$\phi_c F_{cr}$ ksi	
F_y	Spaced Column	Battened (Example 3.1)
36	22.8	28.1
50	28.2	37.8

In a limited number of tests of spaced columns (Freeman, 1973) the maximum failure loads fell short of the predicted, due in part to open holes in the bolted specimens and to deformation of the end stay plates. Pending further tests, it is recommended that only half of the length of the end stay plates be considered effective and that 90% of the theoretical failure loads be used as a basis for design.

3.4.6 Columns with Perforated Plates

White and Thürlimann (1956) provide (in addition to the results of their own research) a digest of investigations at the National Bureau of Standards (Stang and Greenspan, 1948) and give recommendations for the design of columns with perforated cover plates. The following design suggestions for such columns are derived from the White–Thürlimann study and from AASHTO specifications (1996).

When perforated cover plates are used, the following provisions govern their design:

1. The ratio of length, in direction of stress, to width of perforation should not exceed 2.
2. The clear distance between perforations in the direction of stress should not be less than the distance between points of support [i.e., $(c - a) \geq d$ in Fig. 3.58*a*].
3. The clear distance between the end perforation and the end of the cover plate should not be less than 1.25 times the distance between points of support.
4. The point of support should be taken as the inner line of fasteners or fillet welds connecting the perforated plate to the flanges. For plates butt welded to the flange edge of rolled segments the point of support may be taken as the weld whenever the ratio of the outstanding flange width to flange thickness of the rolled segment is less than 7. Otherwise, the point of support should be taken as the root of the flange of the rolled segment.
5. The periphery of the perforation at all points should have a minimum radius of $1\frac{1}{2}$ in. (38 mm).
6. The transverse distance from the edge of a perforation to the nearest line of longitudinal fasteners, divided by the plate thickness, that is, the b/t ratio of the plate adjacent to a perforation (see Fig. 3.58), should conform to minimum specification requirements for plates in main compression members.

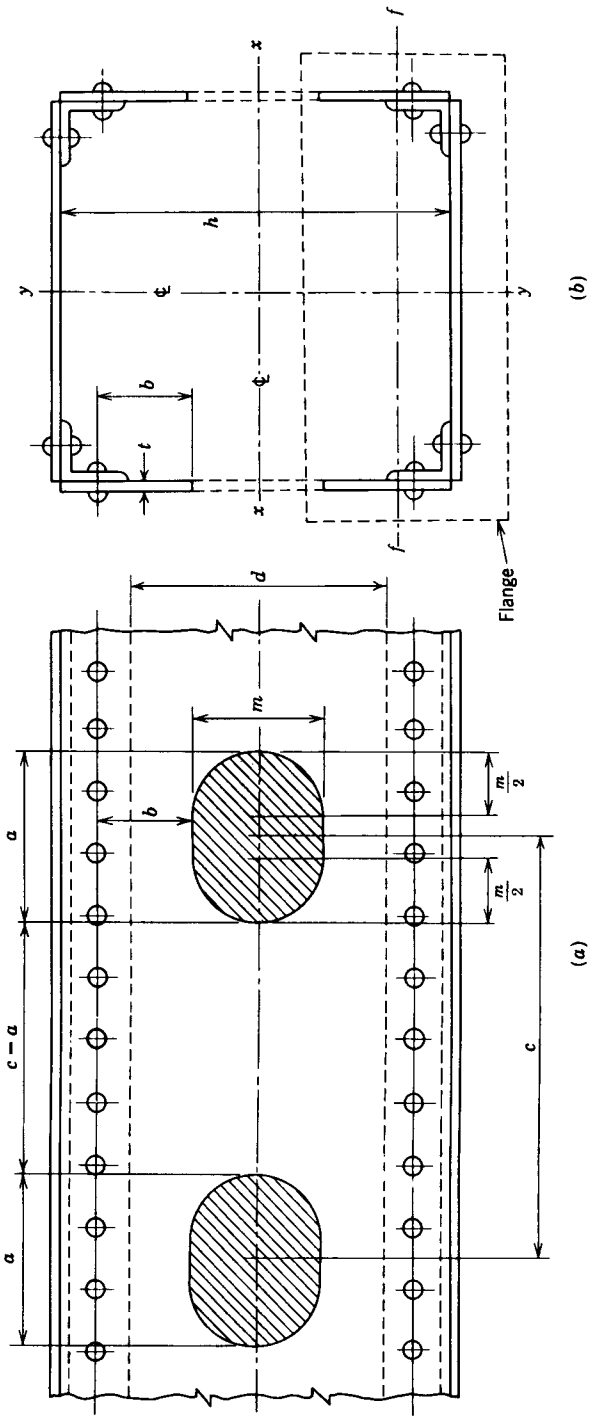

Fig. 3.58 Column with perforated web plates.

3.5 MILL BUILDING COLUMNS

3.5.1 Introduction

Mill buildings are industrial structures within which machinery or products are moved about by overhead traveling cranes. The cranes travel on runway girders that are supported by column brackets or by stepped columns.

Mill building columns are designed by a variety of semiempirical procedures which, on the basis of experience, have produced generally satisfactory results. The design procedure presented herein is based on a modification of AISC building specification procedures. It is assumed that the user of this chapter also has available the AISE Technical Report No. 13 (AISE, 1979), which classifies mill building structures, suggests design-load combinations, defines terms, and provides design information such as the equivalent length factors of stepped columns. Some common types of mill building columns are illustrated in Fig. 3.59. Figure 3.59*a* shows a column of uniform section for the entire length with the crane runway girders supported by column brackets. Figure 3.59*b* shows a stepped column, with the lower shaft a single heavy wide-flange section. The upper shaft, supporting the roof structure is a lighter wide-flange shape.

Figure 3.59*c* represents, in the lower shaft, either a battened column or a spaced column, as differentiated in Section 3.4. The battened column is one in which the two longitudinal column elements are connected by battens with moment-resisting end connections. These are to be spaced close enough and designed with sufficient strength and rigidity as to make the two longitudinals act very nearly as segments of a single section and thus achieve integral beam-column action. But in some mill building columns, the battens are little more than spacers, and the longitudinal elements are simply forced to deflect in the same curve. Their effective lengths as separate columns are, however, appreciably reduced by end tie plates (see Section 3.4).

Figure 3.59*d* shows a laced column, often used between two crane aisles. With adequate lacing bars the two lower shaft segments act substantially with integral action (see Section 3.4). Lacing is particularly appropriate when the longitudinal elements are spaced some distance apart, in which case eccentricity of load may be large. However, any of the types illustrated in Fig. 3.59 may be used for either interior or exterior columns.

The determination of internal moments, shears, and direct forces is a preliminary to the design of a stepped column. For manual analysis, Murray and Graham (1957) have developed a widely used method in which it is assumed, for crane loadings, that the column is hinged at the top, midway between points of attachment to the roof structure. The neglect of top rotational restraint increases the calculated moment at the footing, which is assumed fixed, and thus compensates roughly for sidesway that may take place at the top. Huang (1968a) has developed graphs that facilitate analysis by the Murray procedure. Alternatively, the complete bent may be analyzed by the slope-

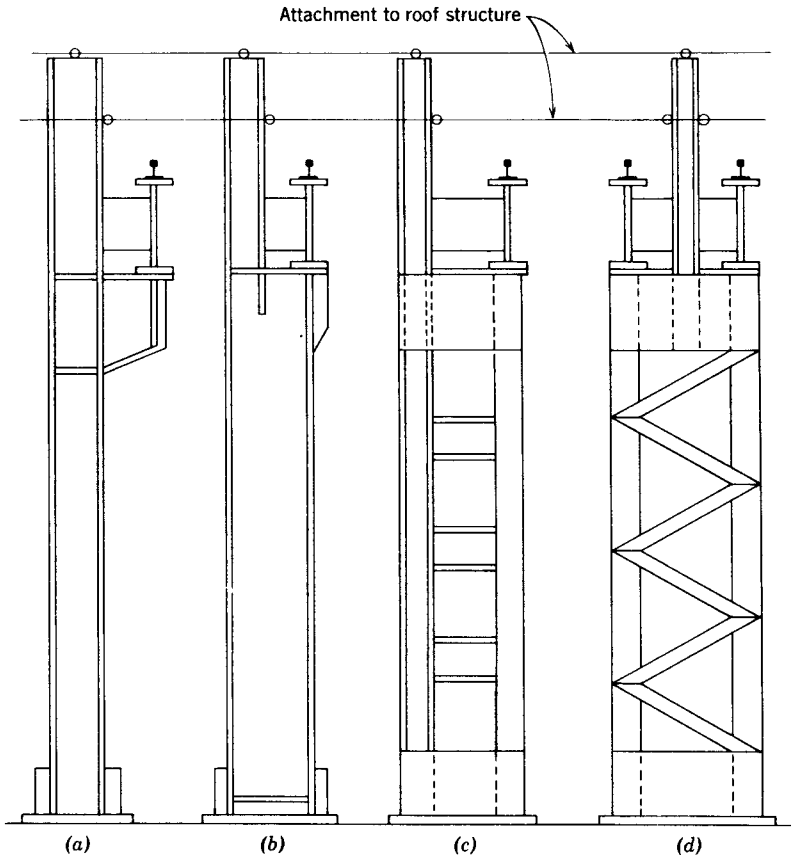

Fig. 3.59 Types of mill building columns.

deflection or moment-distribution procedures, for which coefficients for stepped members are given by Maugh (1963). A more complete analysis must take account of the fact that individual bents are not free to sway independently but are partially restrained by their neighbors through cross-bracing in the plane of the roof. Usually, for wind loads, the columns are either assumed rotationally fixed at the top or considered to be supported by two hinges as shown in Fig. 3.59, with the hinges assumed to have equal sideways displacements.

Given an analysis of bending moments resulting from a particular load condition, the design check may then be made by a modification of the AISC interaction formula for combined stress due to compression and biaxial bending. It is assumed herein that integral column action is achieved in the lower shaft by means of a continuous web plate or by properly designed battens or lacing. Stepped spaced columns, on the other hand, do not achieve

integral action, but nevertheless can provide an economical and satisfactory solution for mill building application, especially if adequate end stay plates are introduced to reduce the effective lengths of the components (see Section 3.4).

3.5.2 Effective Length of Stepped Columns

The effective length, or more properly the equivalent length, of a uniform or prismatic column having the same buckling characteristics as that of the stepped column is needed to determine the axial compressive resistance and the Euler buckling load for potential modes of failure by buckling or bending about the x–x axis (see Fig. 3.60). Tables to determine effective length factors are provided in the AISE guide (AISE, 1979) for a range of the three parameters defined in Fig. 3.60 for the cases when the column base is either fixed or hinged and the column top is hinged. The parameter a is the ratio of the length of the upper (reduced) segment to the total length. The parameter B is the ratio of the moment of inertia (about the centroidal x–x axes) of the combined (lower) column cross section to that of the upper section. The parameter P_1/P_2 is the ratio of the axial force acting in the upper segment (roof and upper wall loads) to that applied to the lower segment (crane girder reactions with an allowance for lower wall loads and the column weight). Other notation is given in Fig. 3.60 as well. The AISE tables give ranges for a from 0.10 to 0.50, for B from 1.0 to 100, and for P_1/P_2 from 0.0 to 0.25. Huang (1968b) provides values of the effective length factors in graphs over a somewhat different range of parameters for stepped columns with fixed bases and hinged tops and for values of P_1/P_2 up to 1.0 Further values tabulated for the effective-length factors for stepped columns are given in Timoshenko and Gere (1961), the English edition of the Japanese *Handbook of Structural Stability* (CRCJ, 1971) and in Roark and Young (1975), among many other sources.

3.5.3 Design Procedure for Stepped Columns

The interaction equations used for the design of stepped columns depend on the potential modes of failure and therefore on how the columns are braced. Stepped columns are usually laterally unsupported over the entire length from top to bottom for buckling or bending about the x–x axis. For buckling about the weak, y–y axis, lateral support is usually provided at the level of the crane runway girder seat, location B in Fig. 3.60. Therefore, the following potential failure modes exist:

1. Bending of the overall column in-plane about the x–x axis. It is for this case that the equivalent length for the stepped column is needed in order that the compressive resistance and the Euler buckling load may be determined.
2. Buckling about the y–y axis of the lower segment.

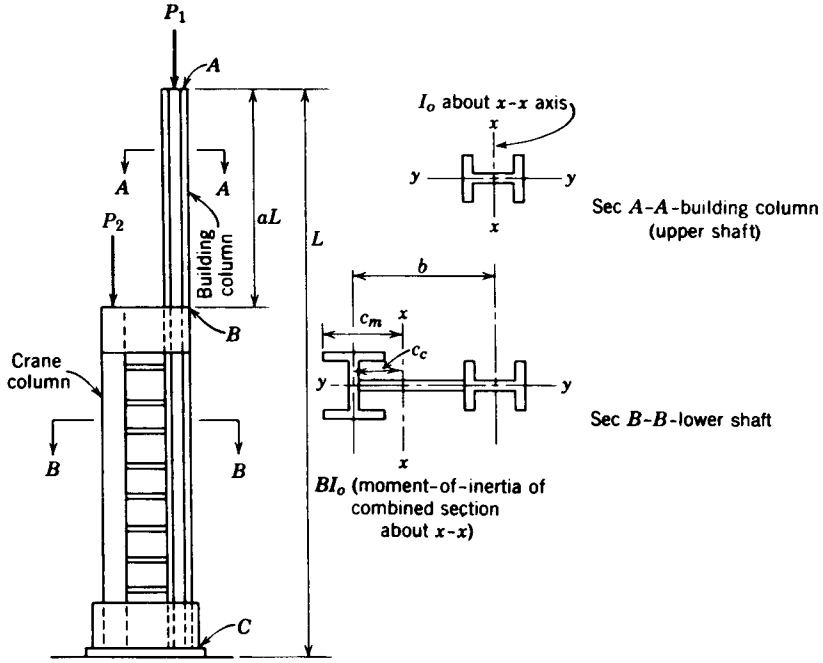

Fig. 3.60 Notation for stepped columns (AISE, 1979).

3. Yielding of the cross section of the lower segment.
4. Buckling about the y–y axis of the upper (reduced) segment of the column.
5. Yielding of the cross section of the upper segment.

The interaction equations for axial compression and biaxial bending are:

$$\frac{P_u}{\phi P_n}+\frac{8}{9}\left(\frac{M_{ux}}{\phi_b M_{nx}}+\frac{M_{uy}}{\phi_b M_{ny}}\right)\le 1.0 \qquad \text{for } P_u/\phi P_a \ge 0.2 \qquad (3.45a)$$

$$\frac{P_u}{2\phi P_n}+\left(\frac{M_{ux}}{\phi_b M_{nx}}+\frac{M_{uy}}{\phi_b M_{ny}}\right)\le 1.0 \qquad \text{for } P_u/\phi P_n \le 0.2 \qquad (3.45b)$$

where

$$B_{1x}=\frac{C_{mx}}{(1-P_u/P_{ex})}\ge 1.0 \qquad (3.45c)$$

and there is a parallel term for B_{1y} related to the y–y axis.

Values for the various terms are needed. It is conservatively assumed that the moments M_{uy} due to eccentric crane girder reactions are all taken by the lower segment and therefore the moments about the y–y axis in the upper segment are zero.

Following the AISC–LRFD procedures, failure modes 1, 2, and 3 are considered together as are modes 4 and 5. When using the AISC–LRFD equations for failure modes 1, 2, and 3 combined, the following values are suggested. The factored axial load, P_u, is $P_1 + P_2$, and M_{ux} and M_{uy} are the maximum modified factored moments within the length. Based on AISE (1979), C_{mx} is taken as 0.85 when all bents are under simultaneous wind load with sidesway. For crane load combinations, with only one bent under consideration, take C_{mx} equal to 0.95. Because it has been assumed that the lower segment takes all the moments about the y–y axis, $C_{my} = 0.6$ when the base is pinned and 0.4 when the base is fixed about the y–y axis. The compressive resistance is the least of ϕP_{nx} of the equivalent column and ϕP_{ny} of the bottom segment, taking, in this case, $K = 0.8$ if the base is considered to be fully fixed, and $K = 1.0$ if the base is considered to be pinned. The factored moment resistance $\phi_b M_{nx}$ is based on the possibility of lateral torsional buckling and $\phi_b M_{ny}$ is the full cross-sectional strength. This being the case, both factors B_{1x} and B_{1y} as given previously are limited to a value of 1.00 or greater. The value of P_{ex} is as determined for the equivalent column and P_{ey} is based on 0.8 of the lower segment for a fixed base and 1.0 of the lower segment if the base is hinged. When using the AISC–LRFD equations for failure modes 4 and 5 combined for the upper segment, the values suggested parallel those for the lower segment with the exceptions that there are moments only about the x–x axis and C_{mx} depends directly on the shape of the moment diagram.

The five failure modes could also be checked independently when the values for checking are as follows: For bending failure about the x–x axis, failure mode 1 (the predominant moments are about the x–x axis), the factored axial load is $P_1 + P_2$, and M_{ux} and M_{uy} are the maximum modified factored moments within the length. C_{mx} is taken as 0.85 when all bents are under simultaneous wind load with sidesway. For crane load combinations, with only one bent under consideration, take C_{mx} equal to 0.95. Because it has been assumed that the lower segment takes all the moments about the y–y axis, $C_{my} = 0.6$ when the base is pinned and 0.4 when the base is fixed about the y–y axis. The value of B_1 is not restricted. The compressive resistance is the least of ϕP_{nx} of the equivalent column and ϕP_{ny} of the bottom segment with $K = 0.8$ if the base is taken to be fully fixed, and with $K = 1.0$ if the base is taken as pinned. The factored moment resistances, $\phi_b M_{nx}$ and $\phi_b M_{ny}$, are the full cross-sectional strengths. The value of P_{ex} is as determined for the equivalent column and P_{ey} is based on 0.8 of the lower segment for a fixed base and 1.0 of the lower segment if the base is hinged.

The values for checking the last four potential failure modes, modes 2 to 5 independently, for y–y axis buckling and for cross-sectional strength are as follows: The factored force effects, P_u, M_{ux}, and M_{uy} are those for the appro-

priate segment. When checking for cross-sectional strength, the resistances ϕP_y, M_{ux} and M_{uy} are the full factored cross-sectional strengths for the appropriate segment. When checking for y–y axis buckling, ϕP_{ny} is based on y–y axis end conditions for the segment being considered. The effective length is the full length AB for the upper segment, and the length BC for the lower segment if full fixity does not exist, and 0.80 of the length BC if fully fixed at the base. In Eq. 3.45, M_{nx} is the appropriate lateral torsional buckling strength taking the shape of the moment diagram into account, and M_{ny} is the full cross-sectional strength. C_{mx} and C_{my} have minimum values of 1.0 because the variation of moment has been accounted for in finding the moment resistance. The value of P_{ex} is that determined for the equivalent column and P_{ey} is taken as that for the appropriate segment.

3.5.4 Design Trends and Research Needs

An LRFD approach to the design of crane columns has been presented, based on AISE modifications to the AISC–LRFD specifications, that is, applicable to members for which the two longitudinal components of the lower segment can be considered to act integrally. When both these components carry very large loads and are therefore heavy, it may be economical to design the lower segment as a spaced column. The use of adequate end tie plates in such a spaced column reduces the effective lengths and increases the buckling load of the components.

The design of a column with constant cross section subject to lateral loads and moments applied at a bracket, as shown in Fig. 3.59*a*, has been considered by Adams (1970). The upper and lower segments are treated as separate beam-columns.

In the example given here the lateral support provided by the girts attached to one flange of the column has not been considered. Horne and Ajmani (1971) and Albert et al. (1995) take this into account. Research is needed into the effect of the dynamic component of the crane loads on the behavior of mill building columns.

3.6 GUYED TOWERS

Guyed towers are used for communication structures, electrical transmission structures (ASCE 1972), and more recently, for compliant offshore platforms and wind energy conversion systems. They consist of a mast supported at one or more levels by guy cables that are anchored at the base. The masts are generally three-dimensional steel trusses of either triangular or square cross section, but occasionally, may be of circular cross section. The loading on a guyed tower may include:

1. Self-weight
2. Initial guy tensions (also called guy pretensions)
3. Wind, ice, and earthquake loads
4. Loads due to falling ice, sudden rupture of guy cables, conductors, ground wire, and so on
5. For communication towers, loads on antennas
6. For electrical transmission towers, loads on conductors and ground wire
7. For compliant offshore platforms, operational loads and wave loading
8. Transportation and erection loads

The annual failure rate of existing towers was estimated by Magued et al. (1989) to be 55/100,000. This is considered to be high when compared to other structures. Contrary to most other structures for which the dead load is the major load, wind loads and combined wind and ice loads are the major loads on towers (Wahba et al., 1993).

The complete design of a guyed tower includes consideration of vibration and fatigue phenomena in which ice-covered cables tend to vibrate with large amplitudes perpendicular to the direction of wind. Galloping generally results from some form of icing on the cables when there is sufficient energy to produce large oscillations and failure of the tower may result. Saxena et al. (1989) reported that there were many incidents where some form of ice storms accompanied with moderate wind speed led to the collapse of several transmission and communication towers. Considerable work has been done on the prediction of dynamic behavior and the effect of wind and ice loads on such towers (McCaffrey and Hartman, 1972; Novak et al., 1978; Nakamoto and Chiu, 1985; Saxena et al., 1989). Simplified methods for estimating the dynamic response using a series of static patch loads have been developed (Gerstoft and Davenport, 1986; Davenport and Sparling, 1992). McClure et al. (1993) identified sudden ice shedding and earthquakes as some of the other causes of concern for the safety of these towers.

The following deals only with buckling aspects of guyed tower design. Although instability may not be the failure mode of all guyed towers, the possibility of general instability of a guyed tower should be investigated by the designer (Hull, 1962; Goldberg and Gaunt, 1973; Williamson, 1973; Chajes and Chen, 1979; Chajes and Ling, 1981; Costello and Phillips, 1983).

Because the governing equilibrium equations are not linear homogeneous equations, instability is not a bifurcation problem but occurs as a large deformation for a small increase in applied load. The stability of a guyed tower is influenced principally by (1) the cross-sectional area of guy cables, (2) the second moment of area (moment of inertia) of the cross section of mast, and (3) the initial tension in the guy cables. For the case of buckling of a guyed tower, the axial stiffness of the guy cables is, perhaps, more important than the bending stiffness of the mast. The buckling load can be increased effectively by

increasing the cross-sectional area of guy cables up to the point where the mast would buckle in a number of half-waves equal to the number of guy levels. To increase the buckling load further, the second moment of area (i.e., the bending stiffness) of the mast must be increased. An increase in guy pretensions has both beneficial and detrimental effects on the stability of guyed towers. An increase in guy pretensions is beneficial as it results in reduced deflections of the mast. On the other hand, an increase in guy pretensions is detrimental as it increases the compressive force on the mast, thus reducing its resistance to buckling. Initially, the increase in guy pretensions results in an increase in buckling load, because of reduced tower deflections. However, after a certain stage, the increase in the buckling load produced by increasing guy pretensions will be more than offset by the decrease in the buckling load due to increasing compressive force on the mast.

The analysis of a guyed tower is complicated because of its geometrically nonlinear behavior even at low load levels. This nonlinearity is due to the increase in axial stiffness of guy cables with increasing tension and the decrease in the bending stiffness of the mast due to the increase in compressive forces. A guyed tower is usually analyzed by approximating it as an equivalent continuous beam-column on nonlinear elastic supports (Cohen and Perrin, 1957; Rowe, 1958; Dean 1961; Livesley and Poskitt, 1963; Goldberg and Meyers, 1965; Odley, 1966; Williamson and Margolin, 1966; Rosenthal and Skop, 1980; Ekhande and Madugula, 1988). Recently, Issa and Avent (1991) presented a method to obtain the forces in all individual members of the mast directly by the use of discrete field mechanics techniques. Sometimes the analytical model for the guyed tower analysis may be a finite element representation using beam-column elements for the mast and cable elements for the guys (IASS, 1981).

Two basic approaches are used for the second-order elastic analysis (geometric nonlinear analysis): the stability function approach and the geometric stiffness approach. This type of analysis includes both P–Δ (chord rotation) and P–δ (member curvature) effects, thus eliminating the need for moment amplification factors. The use of member effective-length factors (K-factors) is also not required when design is carried out in accordance with CAN/CSA-S16.1-94 (CSA, 1994). As all the force resultants acting on the ends of the members are established from the second-order analysis, the member design is based on its actual length. The member is designed assuming that $K = 1$. The tower legs can be designed as beam-columns in the usual manner.

3.7 RESEARCH NEEDS

It is generally accepted that the research of the last half-century has shown that the maximum-strength criterion is the soundest basis for the assessment of column strengths and therefore for the development of column curves. There is also a significant body of opinion that multiple column curves can better reflect the real strength of columns. Because of the reduced scatter when fewer shapes or types of cross sections are assigned to a particular curve, economy, in general, is achieved while maintaining or even increasing reliability.

However, much of the data that form the basis for current column curves were developed for manufacturing processes that may be outdated. Changes have taken place both in the chemistry of the steel and in the processes for producing shapes. With computer technology, manufacturers are now able to control both the chemistry and the rolling processes, to say nothing of the cooling processes, to closer tolerances than heretofore. No doubt the controls have reduced the variability in strengths and geometric properties that extend to out-of-straightnesses and even probably to residual stresses. The attendant question that needs to be addressed is the shift in the bias coefficient, if indeed such has taken place.

What is therefore required is that current statistical data be gathered on the variation of material properties (e.g., yield strengths, ultimate strengths, and moduli of elasticity), together with the variation of geometric properties. These then are combined statistically with current data on out-of-straightnesses and residual stress variations, both of which may also have changed due to advancements in the manufacturing process, all the while making full use of computer simulations (Kennedy and Chernenko, 1991). The result could well be a set of column curves, fully statistically based, that better predict the actual behavior, leading simultaneously to increased and enhanced understanding, economy, and safety.

On another front, computer analyses should be applied to members and frames so that essentially manual calculations based on simplified models, with restrictions on the members that can be considered, would no longer be necessary. For example, models could be developed to assess the strength of stepped crane columns of arbitrary shape under arbitrary loading without the need of design charts and their inherent design simplifications and even without the use of interaction equations. Advanced methods of analysis are bound to have even greater applications.

REFERENCES

AA (1994), *Specifications for Aluminum Structures*, Aluminum Association, Washington D.C.

AASHTO (1996), *Standard Specification for Highway Bridges*, 16th ed., American Association of State Highway and Transportation Officials, Washington, D.C.

Ackroyd, M. H. (1979), "Nonlinear Inelastic Stability of Flexibly Connected Plane Steel Frames," PhD. dissertation, University of Colorado, Boulder, Colo.

Ackroyd, M. H., and Bjorhovde, R. (1981), "Effect of Semi-rigid Connections on Steel Column Strength" (discussion), *J. Constn. Steel Res. (London)*, Vol. 1, No. 3, pp. 48–51.

Adams, P. F. (1970), "Segmental Design of Steel Beam-Columns," *Proc. Can. Struct. Eng. Conf.*, Toronto, Ontario, Canada.

AISC (1979), *Specification for the Design Fabrication and Erection of Structural Steel for Buildings*, American Institute of Steel Construction, Chicago.

AISC (1989), *Specification for Structural Steel Buildings: Allowable Stress Design and Pastic Design*, American Institute of Steel Construction, Chicago.

AISC (1993), *Load and Resistance Factor Design Specification for Structural Steel Buildings*, American Institute of Steel Construction, Chicago.

AISE (1979), "Guide for the Design and Construction of Mill Buildings," *AISE Tech. Rep. No. 13*, Association of Iron and Steel Engineers, Pittsburgh, Pa.

Albert, C., Srna, P., Kennedy, S. J., and Kennedy, D. J. L. (1995), "Inelastic Distortional Strength of Steel Beam-Columns," *Int. Conf. Struct. Stab. Design*, Oct. 30–Nov. 1, Australian Institute of Steel Construction, Sydney, Australia.

Alpsten, G. A. (1970), "Residual Stresses and Strength of Cold-Straightened Wide Flange Shapes," *Jernkontorets Ann.*, Vol. 154 (in Swedish).

Alpsten, G. A. (1972a), "Prediction of Thermal Residual Stresses in Hot Rolled Plates and Shapes," *9th Congr. IABSE, Final Rep.*, May, pp. 1–13.

Alpsten, G. A. (1972b), "Residual Stresses, Yield Stress and Column Strength of Hotrolled and Roller-Straightened Steel Shapes," *Colloq. Column Strength*, Paris.

Alpsten, G. A., and Tall, L. (1970) "Residual Stresses in Heavy Welded Shapes," *Weld. J.*, Vol. 49.

Appl. F. M., and Smith, J. O. (1968), "Buckling of Inelastic Tapered Pin-Ended Columns," *ASCE J. Eng. Mech. Div.*, Vol. 94, No. EM2, pp. 549–558.

AREA (1979), *Specification for Steel Railway Bridges*, AREA Manual for Railway Engineering, American Railway Engineering Association, Chicago, Chap. 15.

ASCE (1972), "Guide for the Design of Aluminum Transmission Towers," Task Committee on Lightweight Alloys of the Committee on Metals of the Structural Division, American Society of Civil Engineers, *Proc. ASCE.*, Vol. 98, No. ST12.

ASCE (1991), *Specification for the Design of Cold-Formed Stainless Steel Structural Members*, ANSI-ASCE Standard No. ASCE-8-90, American Society of Civil Engineers, New York.

Aslani, F. and Goel, S. C. (1991), "An Analytical Criterion for Buckling Strength of Built-up Compression Members," *AISC Eng. J.*, Vol. 28, No. 4, pp. 159–168.

Baker, J. F., and Roderick, J. W. (1948), "The Strength of Light Alloy Struts," *Res. Rep. No. 3*, Aluminum Development Association, London.

Barakat, M. A., and Chen, W. F. (1990), "Practical Analysis of Semi-rigid Frames," *AISC Eng. J.*, Vol. 27, No. 2, pp. 54–68.

Batteman, R. H., and Johnston, B. G. (1967), "Behavior and Maximum Strength of Metal Columns," *ASCE J. Struct. Div.*, Vol. 93, No. ST2, pp. 205–230.

Beedle, L. S. ed. (1991), *Stability of Metal Structures: A World View*, Structural Stability Research Council, Bethlehem, Pa.

Beedle, L. S., ed. (1993), *Semi-rigid Connections in Steel Frames*, Council on Tall Buildings and Urban Habitat, McGraw-Hill, New York.

Beedle, L. S., and Tall, L. (1960), "Basic Column Strength," *ASCE J. Struct. Div.*, Vol. 86, No. ST5, pp. 139–173.

Beer, H., and Schultz, G. (1970), "Theoretical Basis for the European Column Curves," *Constr. Met. No. 3*, p. 58.

Beer, G., and Tall, L. (1970), "The Strength of Heavy Welded Box Columns," *Fritz Eng. Lab. Rep. No. 337.27*, Lehigh University, Bethlehem, Pa., Dec.

Bernard, A., Frey, F., Janss, J., and Massonnet, C. (1973), "Research on the Buckling Behavior of Aluminum Columns," *IABSE Mem.*, Vol. 33-1, pp. 1–33 (in French).

Birkemoe, P. C. (1977a), "Column Behavior of Heat-Treated Cold-Formed Hollow Structural Shapes," *Stability of Structures Under Static and Dynamic Loads, Proc. 2nd Int. Colloq.*, Washington, D.C.

Birkemoe, P. C. (1977b), "Development of Column Curves for H.S.S.," *Int. Symp. Hollow Struct. Sec.* CIDECT, Toronto, Ontario, Canada.

Bjorhovde, R. (1972), "Deterministic and Probabilistic Approaches to the Strength of Steel Columns," Ph.D. dissertation, Lehigh University, Bethlehem, Pa., May.

Bjorhovde, R. (1977), "Strength and Behavior of Cold-Formed H.S.S. Columns," *Struct. Eng. Rep. No. 65*, University of Alberta, Edmonton, Alberta, Canada, Dec.

Bjorhovde, R. (1978), "The Safety of Steel Columns," *ASCE J. Struct. Div.*, Vol. 104, No. ST3, pp. 463–477.

Bjorhovde, R. (1980), "Research Needs in Stability of Metal Structures," *ASCE J. Struct. Div.*, Vol. 106, No. ST12, pp. 2425–2442.

Bjorhovde, R. (1981), "End Restraint and Column Stability" (discussion), *ASCE J. Struct. Div.*, Vol. 107, No. ST8, pp. 1696–1700.

Bjorhovde, R. (1984), "Effect of End Restraint on Column Strength: Practical Applications," *AISC Eng. J.*, Vol. 21, No. 1, pp. 1–13.

Bjorhovde, R. (1988), "Columns: From Theory to Practice," *AISC Eng. J.*, Vol. 25, No. 1, pp. 21-34.

Bjorhovde, R. (1991), "The Strength of Heavy Columns," *J. Constr. Steel Res.*, Vol. 19, No. 4, pp. 313–320.

Bjorhovde, R. (1992), "Compression Members," in *Constructional Steel Design: An International Guide* (ed. P. J. Dowling, J. E. Harding, and R. Bjorhovde), Elsevier Applied Science, London, Chap. 2.3.

Bjorhovde, R., and Birkemoe, P. O. (1979), "Limit States Design of H.S.S. Columns," *Can. J. Civ. Eng.*, Vol. 8, No. 2, pp. 276–291.

Bjorhovde, R., and Tall, L. (1971), "Maximum Column Strength and the Multiple Column Curve Concept," *Fritz Eng. Lab. Rep. No. 338.29*, Lehigh University, Bethlehem, Pa., Oct.

Bjorhovde, R., Brozzetti, J., Alpsten, G. A., and Tall, L. (1972), "Residual Stresses in Thick Welded Plates," *Weld J.*, Vol. 51, No. 8, pp. 392–405.

Bleich, F. (1952), *Buckling Strength of Metal Structures*, McGraw-Hill, New York.

Bradford, M. A. and Cuk, P. E. (1988), "Elastic Buckling of Tapered Monosymmetric I-Beams," *ASCE J. Struct. Eng.*, Vol. 114, No. 5, pp. 977–996.

Bredenkamp, P. J. and van den Berg, G. J. (1995), "The Strength of Stainless Steel Built-up I-Section Columns," *J. Constr. Steel Res.*, Vol. 34, No. 2–3, pp. 131–144.

Bredenkamp, P. J., van den Berg, G. J., and van der Merwe, P. (1992), "Residual Stresses and the Strength of Stainless Steel I-Section Columns," *Proc. SSRC 1992 Annu. Tech. Session*, Pittsburgh, Pa., Apr.

Bredenkamp, P. J., Human, J. J., and van den Berg, G. J. (1994), "The Strength of Hot-Rolled Stainless Steel Columns," *Proc. SSRC 1994 Annu. Tech. Session*, Apr., Milwaukee, Wis.

Brockenbrough, R. L. (1992), "Material Behavior," in *Constructional Steel Design: An International Guide* (ed. P. J. Dowling, J. E. Harding, and R. Bjorhovde), Elsevier Applied Science, London, Chaps. 1.1 and 1.2.

Brolin, C. A., Durscher, H. E., and Serentha, G. (1972), "Destructive Testing of Crane Booms," *SAE Trans.*, Vol. 81, Pap. 720784.

Brozzetti, J., Alpsten, G. A., and Tall, L. (1970a) "Residual Stresses in a Heavy Rolled Shape 14WF730," *Fritz Eng. Lab. Rep. No. 337.1*, Lehigh University, Bethlehem, Pa., Jan.

Brozzetti, J., Alpsten, G. A., and Tall, L. (1970b), "Welding Parameters, Thick Plates and Column Strength," *Fritz Eng. Lab. Rep. No. 337.21*, Lehigh University, Bethlehem, Pa., Feb.

Brungraber, R. J., and Clark, J. W. (1962), "Strength of Welded Aluminum Columns," *Trans. Am. Soc. Civ. Eng.*, Vol. 127, Part 11, pp. 202–226.

BSI (1991), *Structural Use of Aluminum*, BS 8181, British Standards Institution, London.

Butler, D. J. (1966), "Elastic Buckling Tests on Laterally and Torsionally Braced Tapered I-Beams," *Weld. J. Res. Suppl.*, Vol. 45, No. 1.

Butler, D. J., and Anderson, G. C. (1963), "The Elastic Buckling of Tapered Beam Columns," *Weld J. Res. Suppl.*, Vol. 42, No. 1.

Chajes, A. and Chen, W. S. (1979), "Stability of Guyed Towers," *ASCE J. Struct. Div.*, Vol. 105, No. ST1, pp. 163–174.

Chajes, A. and Ling, D. (1981), "Post-buckling Analysis of Guyed Towers," *ASCE, J. Struct. Eng.*, Vol. 107, No. 12, pp. 2313–2323.

Chan, S. L., (1990), "Buckling Analysis of Structures Composed of Tapered Members," *ASCE J. Struct. Eng.*, Vol. 116, No. 7, pp. 1893–1906.

Chapuis, J., and Galambos, T. V. (1982), "Restrained Crooked Aluminum Columns," *ASCE J. Struct. Div.*, Vol. 108, No. ST3, pp. 511–524.

Chen, W. F. (1980), "End Restraint and Column Stability," *ASCE J. Struct. Div.*, Vol. 105, No. ST11, pp. 2279–2295.

Chen, W. F., ed. (1987), "Joint Flexibility in Steel Frames," Special Issue, *J. Const. Steel Res.*, Vol. 8.

Chen, W. F., ed. (1988), *Steel Beam-to-Column Building Connections*, Elsevier Applied Science, London.

Chen, W. F., and Atsuta, T. (1976), *Theory of Beam-Columns*, Vol. 1, McGraw-Hill, New York.

Chen, W. F., and Han, D. C. (1985), *Tubular Members in Offshore Structures*, Pitman, London.

Chen, W. F., and Kishi, N. (1989), "Semi-rigid Steel Beam-to-Column Connections: Data Base and Modeling," *ASCE J. Struct. Eng.*, Vol. 115, No. 1, pp. 105–119.

Chen, W. F., and Lui, E. M. (1985), "Stability Design Criteria for Steel Members and Frames in the United States," *J. Constr. Steel Res.*, Vol. 5, No. 1, pp. 51–94.

Chen, W. F., and Lui, E. M. (1991), *Stability Design of Steel Frames*, CRC Press, Boca Raton, Fla.

Chen, W. F., and Sohal, I. S. (1995), *Plastic Design and Second-Order Analysis of Steel Frame*, Springer-Verlag, New York.

Chen. W. F., Goto, Y., and Liew, J. Y. R. (1966), *Stability Design of Semi-rigid Frames*, Wiley, New York.

Chernenko, D. E., and Kennedy, D. J. L. (1991), "An Analysis of the Performance of Welded Wide Flange Columns," *Can. J. Civil Eng.*, Vol. 18, pp. 537–555.

Clark, J. W., and Rolf, R. L. (1966), "Buckling of Aluminum Columns, Plates and Beams," *ASCE J. Struct. Div.*, Vol. 92, No. ST3, pp. 17–38.

Cohen, E., and Perrin, H. (1957), "Design of Multi-level Guyed Towers: Structural Analysis," *ASCE J. Struct. Div.*, Vol. 83, No. ST5, pp. 1356-1 to 1356-29.

Column Research Committee of Japan, ed. (1971), *Handbook of Structural Stability*, Engl. ed., Corona Publishing Company, Tokyo.

Costello, G. A., and Phillips, J. W. (1983), "Post-buckling Behavior of Guyed Towers," *ASCE J. Struct. Eng.*, Vol. 109, No. 6, pp. 1450–1459.

Crawford, R. F., and Benton, M. D. (1980), "Strength of Initially Wavy Lattice Columns," *AIAA J.*, Vol. 18, No. 5, p. 581.

CSA (1980), *Specification for Design of Highway Bridges*, CAN3-S6-M78, Canadian Standards Association, Rexdale, Ontario, Canada.

CSA (1994), *Limit States Design of Steel Structures*, CAN/CSA-S16.1-94, Canadian Standards Association, Rexdale Ontario, Canada.

Davenport, A. G., and Sparling, B. F. (1992), "Dynamic Gust Response Factors for Guyed Towers," *J. Wind Eng. Ind. Aerodyn*, Vol. 41–44, pp. 2237–2248.

Dean, D. L. (1961), "Static and Dynamic Analysis of Guy Cables," *ASCE J. Struct. Div.*, Vol. 87, No. ST1, pp. 1–21.

DeFalco, F., and Marino, F. J. (1966), "Column Stability in Type 2 Construction," *AISC Eng. J.*, Vol. 3, No. 2, pp. 67–71.

Disque, R. O. (1973), "Inelastic K-Factor in Column Design," *AISC Eng. J.*, Vol. 10, No. 2, pp. 33–35.

Disque, R. O. (1975), "Directional Moment Connections: A Proposed Design Method for Unbraced Steel Frames," *AISC Eng. J.*, Vol. 12, No. 1, pp. 14–18.

Duberg, J. E., and Wilder, T. W. (1950), "Column Behavior in the Plastic Strength Range," *J. Aeronaut. Sci.*, Vol. 17, No. 6, p. 323.

Dux, P. F., and Kitipornchai, S. (1981), "Inelastic Beam-Buckling Experiments," *Res. Rep. No. CE24*, Department of Civil Engineering, University of Queensland, St. Lucia, Australia.

ECCS (1978a), *European Recommendation for Aluminium Structures*, Committee T2, European Convention for Constructional Steelwork, Brussels, Belgium.

ECCS (1978b), *European Recommendations for Steel Structures*, European Convention for Constructional Steelwork, Brussels, Belgium.

ECS (1992), *Eurocode 3: Design of Steel Structures*, European Committee for Standardization, Brussels, Belgium.

Ekhande, S. G., and Madugula, M. K. S. (1988), "Geometric Nonlinear Analysis of Three-Dimensional Guyed Towers," *Comput. Struct.*, Vol. 29, No. 5, pp. 801–806.

Engesser, F. (1891), "Die Knickfestigkeit gerader Stabe," *Zentralbl. Bauverwaltung*, Vol. 11.

Ermopoulos, J. C. (1986), "Buckling of Tapered Bars Under Stepped Axial Loads," *ASCE J. Struct. Eng.*, Vol. 112, No. 6, pp. 1346–1354.

Essa, H. S., and Kennedy, D. L. J. (1993), "Distortional Buckling of Steel Beams," *Struct. Eng. Rep. No. 185*, Department of Civil Engineering, University of Alberta, Edmonton, Alberta, Canada.

Fogel, C. M., and Ketter, R. L. (1962), "Elastic Strength of Tapered Columns," *ASCE J. Struct. Div.*, Vol. 88, No. ST5, Proc. Pap. 3301, pp. 67–106.

Freeman, B. G. (1973), "Tie Plate Effects in Weakly Battened Columns," Ph.D. dissertation, Department of Civil Engineering, University of Arizona, Tucson, Ariz.

Frey, F. (1969), "Effect of the Cold-Bending of H-Shaped Rolled Steel Sections on Column Strength," *IABSE Mem.*, Vol. 291, pp. 101–124 (in French).

Frye, M. J., and Morris, G. A. (1975), "Analysis of Flexibly Connected Steel Frames," *Can. J. Civ. Eng.*, Vol. 2, No. 3, pp. 280–291.

Fukumoto, Y., Nethercot, D. A., and Galambos, T. V. (1983), "Experimental Data for the Buckling of Steel Structures–NDSS Stability of Metal Structures," *Proc. 3rd Int. Colloq. SSRC*, Toronto, Ontario, Canada, May, pp. 609–630.

Gallagher, R. H. (1975), *Finite Element Fundamentals*, Prentice Hall, Upper Saddle River, N.J.

Gere, J. M., and Carter, W. O. (1962), "Critical Buckling Loads for Tapered Columns," *ASCE J. Struct. Div.*, Vol. 88, No. ST1, Proc. Pap. 3045, pp. 1–11.

Gerstoft, P., and Davenport, A. G. (1986), "A Simplified Method for Dynamic Analysis of a Guyed Mast," *J. Wind Eng. Ind. Aerodyn.*, Vol. 23, pp. 487–499.

Girijavallabhan, C. V. (1969), "Buckling Loads of Nonuniform Columns," *ASCE J. Struct. Div.*, Vol. 95, No. ST11, pp. 2419–2431.

Goldberg, J. E. (1954), "Stiffness Charts for Gusseted Members Under Axial Load," *Trans. ASCE*, Vol. 119, p. 43.

Goldberg, J. E., and Gaunt, J. T. (1973), "Stability of Guyed Towers," *ASCE J. Struct. Div*, Vol. 99, No. ST4, pp. 741–756.

Goldberg, J. E. and Meyers, V. J. (1965), "A Study of Guyed Towers," *ASCE J. Struct. Div.*, Vol. 91, No. ST4, pp. 57–76.

Goto, Y., Suzuki, S. and Chen, W. F. (1993), "Stability Behavior of Semi-rigid Sway Frames," *Eng. Struct.*, Vol. 15, No. 3, pp. 209–219.

Hall, D. H. (1981), "Proposed Steel Column Design Criteria," *ASCE J. Struct. Div.*, Vol. 107, No. ST4, pp. 649–670.

Hariri, R. (1967), "Post-buckling Behavior of Tee-Shaped Aluminum Columns," Ph.D. dissertation University of Michigan, Ann Arbor, Mich., June.

Hartmann, E. C., and Clark, J. W. (1963), "The U.S. Code," *Proc. Symp. Alum. Struct. Eng.*, London, June 11–12, The Aluminum Federation.

Hartmann, E. C., Moore, R. L., and Holt, M. (1938), "Model Tests of Latticed Structural Frames," *Alcoa Res. Lab. Tech. Pap. No. 2.*

Hong, G. M. (1991), "Effects of Non-central Transverse Welds on Aluminum Columns," in *Aluminum Structures: Recent Research and Development*, Elsevier Applied Science, London.

Horne, M. R., and Ajmani, J. L. (1971), "Design of Columns Restrained by Side-Rails and the Post-buckling Behavior of Laterally Restrained Columns," *Struct. Eng.*, Vol. 49, No. 8.

Howard, J. E. (1908), "Some Results of the Tests of Steel Columns in Progress at the Watertown Arsenal," *Proc. A.S.T.M.*, Vol. 8, p. 336.

Huang, H. C. (1968a), "The Design of Mill Building Columns," *Iron Steel Eng.*, Vol. 45, No. 3, p. 97.

Huang, H. C. (1968b), "Determination of Slenderness Ratios for Design of Heavy Mill Building Stepped Columns," *Iron Steel Eng.*, Vol. 45, No. 11, p. 123.

Huber, A. W. (1956), "The Influence of Residual Stress on the Instability of Columns," Ph.D. dissertation, Lehigh University, Bethlehem, Pa., May.

Hull, F. H. (1962), "Stability Analysis of Multi-level Guyed Towers," *ASCE J. Struct. Div.*, Vol. 88, No. ST2, pp. 61–80.

IASS (1981), *Recommendations for Guyed Masts*, Working Group 4, International Association for Shell and Spatial Structures, Madrid, Spain, 106 pp.

ISE (1962), *Report on the Structural Use of Aluminum*, Institution of Structural Engineers, London.

Issa, R. R. A., and Avent, R. R. (1991), "Microcomputer Analysis of Guyed Towers as Lattices," *ASCE J. Struct. Div.*, Vol. 117, No. 4, pp. 1238–1256.

Jacquet, J. (1970), "Column Tests and Analysis of Their Results," *Constr. Met.*, No. 3, pp. 13–36.

Johnston, B. G. (1963), "Buckling Behavior Above the Tangent Modulus Load," *Trans. A.S.C.E.*, Vol. 128, Part 1, pp. 819-848.

Johnston, B. G. (1964), "Inelastic Buckling Gradient," *ASCE J. Eng. Mech. Div.*, Vol. 90, No. EM5, pp. 31–48.

Johnston, B. G. (1971), "Spaced Steel Columns," *ASCE J. Struct. Div.*, Vol. 97, No. ST5, p. 1465.

Johnston, B. G. ed. (1976), *Guide to Stability Design Criteria for Metal Structures*, 3rd ed., Wiley, New York.

Jones, S. W., Kirby, P. A., and Nethercot, D. A. (1980), "Effect of Semi-rigid Connections on Steel Column Strength," *J. Constr. Steel Res.*, Vol. 1, No. 1, pp. 35–46.

Jones, S. W., Kirby, P. A., and Nethercot, D. A. (1982), "Columns with Semi-rigid Joints," *ASCE J. Struct. Div.*, Vol. 108, No. ST2, pp. 361–372.

Karabalis, D. L. and Beskos, D. E. (1983), "Static, Dynamic and Stability Analysis of Structures Composed of Tapered Beams," *Comput. Struct.*, Vol. 16, No. 6, pp. 731–748.

Kato, B. (1977), "Column Curves for Cold-Formed and Welded Tubular Members," *2nd Int. Colloq. Stab. Steel Struct.*, Liege, Belgium, pp. 53–60.

Kennedy, D. J. L. and Gad Aly, M. (1980), "Limit States Design of Steel Structures Performance Factors," *Can. J. Civil Eng.*, Vol. 7, No. 1., pp. 45–77.

King, W. S., and Chen, W. F. (1993), "LRFD Analysis for Semi-rigid Frame Design," *AISC Eng. J.*, Vol. 30, No. 4, pp. 130–140.

King, W. S., and Chen, W. F. (1994), "Practical Second-Order Inelastic Analysis of Semi-rigid Frames," *ASCE J. Struct. Eng.*, Vol. 120, No. 7, pp. 2156–2175.

Kishi, N., and Chen, W. F. (1986), "Data Base of Steel Beam-to-Column Connections," *Struct. Eng. Rep. No. CE-STR-86-26*, School of Civil Engineering, Purdue University, West Lafayette, Ind., 2 vols.

Kishi, N., and Chen, W. F. (1990), "Moment-Rotation Relations of Semi-rigid Connections with Angles," *ASCE J. Struct. Eng.*, Vol. 116, No. 7, pp. 1813–1834.

Kishi, N., Chen, W. F., Goto, Y., and Matsuoka, K. G. (1993a), "Design Aid of Semi-rigid Connections for Frame Analysis," *AISC Eng. J.*, Vol. 30, No. 3, pp. 90–103.

Kishi, N., Goto, Y., Chen, W. F., and Matsuoka, K. (1993b), "Analysis Program for the Design of Flexibly Jointed Frames," *Comput. Struct.*, Vol. 49, No. 4, pp. 705–713.

Kishima, V., Alpsten, G. A., and Tall, L. (1969), "Residual Stresses in Welded Shapes of Flame-Cut Plates in ASTM A572(50) Steel," *Fritz Eng. Lab. Rep. No. 321.2*, Lehigh University, Bethlehem, Pa., June.

Kitipornchai, S., and Trahair, N. S. (1972), "Elastic Stability of Tapered I-Beams," *ASCE J. Struct. Div.*, Vol. 98, No. ST3, pp. 713–728.

Korol, R. M., Rutenberg, A. and Bagnariol, D. (1986), "On Primary and Secondary Stresses in Triangulated Trusses," *J. Constr. Steel Res.*, Vol. 6, pp. 123–142.

Lai, Y. F. W., and Nethercot, D. A. (1992), "Strength of Aluminium Members Containing Local Transverse Welds," *Eng. Struct.*, Vol. 14, No. 4, p. 241.

Lee, G. C., Morrell, M. L., and Ketter, R. L. (1972), "Design of Tapered Members," *Weld. Res. Counc. Bull. No. 173*, June.

Lee, G. C., Chen, Y. C., and Hsu, T. L. (1979), "Allowable Axial Stress of Restrained Multisegment Tapered Roof Girders," *Weld. Res. Counc. Bull. No. 248*, May.

Lee, G. C., Ketter, R. L., and Hsu, T. L. (1981), *The Design of Single Story Rigid Frames*, Metal Building Manufacturer's Association, Cleveland, Ohio.

Lin, F. J., Glauser, E. C., and Johnston, B. G. (1970), "Behavior of Laced and Battened Structural Members," *ASCE J. Struct. Div.*, Vol. 96, No. ST7, p. 1377.

Lindner, J., and Gietzelt, R. (1984), "Imperfectionsannahmen für Stützenschief-stellungen," *Stahlbau*, Vol. 53, No. 4, pp. 97–101.

Livesley, R. K., and Poskitt, T. J. (1963), "Structural Analysis of Guyed Masts," *Proc. Inst. of Civil Eng. (London)*, Vol. 24, pp. 373–386.

Loov, R. (1996), "A Simple Equation for Axially Loaded Steel Column Design Curves," *Can. J. Civil Eng.*, 23, pp.

Lui, E. M., and Chen, W. F. (1983a), "Strength of H-Columns with Small End-Restraints," *Struct. Eng.*, Vol. 61B, No. 1, Part B, pp. 17–26.

Lui, E. M., and Chen, W. F. (1983b), "End Restraint and Column Design Using LRFD," *Eng. J. Am. Ins. Steel Constr.*, Vol. 20, No. 1, pp. 29–39.

Lui, E. M., and Chen, W. F. (1984), "Simplified Approach to the Analysis and Design of Columns with Imperfections," *AISC Eng. J.*, Vol. 21, No. 2, pp. 99–117.

Lui, E. M., and Chen, W. F. (1988), "Behavior of Braced and Unbraced Semi-rigid Frames," *Solids Struct.*, Vol. 24, No. 9, pp. 893–913.

Madsen, I. (1941), "Report of Crane Girder Tests," *Iron Steel Eng.*, Vol. 18, No. 11, p. 47.

Magued, M. H., Bruneau, M., and Dryburgh, R. B. (1989), "Evolution of Design Standards and Recorded Failures of Guyed Towers in Canada," *Can. J. Civ. Eng.*, Vol. 16, No. 5, pp. 725–732.

Masur, E. F. (1954), "Lower and Upper Bounds to the Ultimate Loads of Buckled Trusses," *Q Appl. Math.*, Vol. 11, No. 4, p. 385.

Maugh, L. C. (1963), *Statically Indeterminate Structures*, 2nd ed., Wiley, New York.

Mazzolani, F. M. (1985), *Aluminium Alloy Structures*, Pitman, Marshfield, Mass.

Mazzolani, F. M., and Frey, F. (1977), "Buckling Behavior of Aluminium Alloy Extruded Members," *2nd Int. Colloq. Stabil. Steel Struct.*, Liege, Belgium, pp. 85–94.

Mazzolani, F. M., and Frey, F. (1980), "The Bases of the European Recommendations for the Design of Aluminum Alloy Structures," *Alluminio*, No. 2.

McCaffrey, R. J., and Hartman, A. J. (1972), "Dynamics of Guyed Towers," *ASCE J. Struct. Div.*, Vol. 98, No. ST6, pp. 1309–1323.

McFalls, R. K., and Tall, L. (1970), "A Study of Welded Columns Manufactured from Flame-Cut Plates," *AWS Weld. J.* Vol. 49, No. 4, pp. 141s–153s.

McClure, G., Guevara, E., and Lin, N. (1993), "Dynamic Analysis of Antenna-Supporting Towers," *Proc. Annu. Conf. Can. Soc. Civ. Eng.*, June 8–11, Fredericton, New Brunswick, Canada, pp. 335–344.

Michalos, J., and Louw, J. M. (1957), "Properties for Numerical Analysis of Gusseted Frameworks," *Proc. Am. Railw. Eng. Assoc.*, Vol. 58, p. 1.

Miller, R. K., and Hedgepeth, J. M. (1979), "The Buckling of Latticed Columns with Stochastic Imperfections," *Int. J. Solids Struct.*, Vol. 15, pp. 71–84.

Murray, J. J., and Graham, T. C. (1957), "The Design of Mill Buildings," *Iron Steel Eng.*, Vol. 34, No. 2, p. 159.

Nakamoto, R. T., and Chiu, A. N. L. (1985), "Investigation of Wind Effects on Guyed Towers," *ASCE J. Struct. Div.*, Vol. 111, No. 11, pp. 2320–2332.

Nethercot, D. A., and Chen, W. F. (1988), "Effects of Connections on Columns," *J. Constr. Steel Res.*, Vol. 10, pp. 201–239.

Novak, M., Davenport, A. G., and Tanaka, H. (1978), "Vibration of Towers Due to Galloping of Iced Cables," *ASCE J. Eng. Mech. Div.*, Vol. 104, No. EM2, pp. 457–473.

Odley, E. G. (1966), "Analysis of High Guyed Towers," *ASCE J. Struct. Div.*, Vol. 92, No. ST1, pp. 169–197.

Osgood, W. R. (1951), "The Effect of Residual Stress in Column Strength," *Proc. First U.S. Natl. Congn. Appl. Mech.*, June, p. 415.

Razzaq, Z., and Chang, J. G. (1981), "Partially Restrained Imperfect Columns," *Proc. Conf. Joints Struct. Steelwork*, Teesside, England. Apr., Pentech Press, Chichester, West Sussex, England.

Roark, R. J., and Young, W. C. (1975), *Formulas for Stress and Strain*, McGraw-Hill, New York.

Romstad, K. M., and Subramanian, C. V. (1970), "Analysis of Frames with Partial Connection Rigidity," *ASCE J. Struct. Div.*, Vol. 96, No. ST11, pp. 2283–2300.

Rondal, J., and Maquoi, R. (1979), "Single Equation for SSRC Column Strength Curves," *ASCE J. Struct. Div.*, Vol. 105, No. ST1, pp. 247–250.

Rosenthal, F., and Skop, R. A. (1980), "Guyed Towers Under Arbitrary Loads," *ASCE J. Struct. Div.*, Vol. 106, No. ST3, pp. 679–692.

Rotter, J. M. (1982), "Multiple Column Curves by Modifying Factors," *ASCE J. Struct. Div.*, Vol. 108, No. ST7, pp. 1665–1669.

Rowe, R. S. (1958), "Amplification of Stress and Displacement in Guyed Towers," *ASCE J. Struct. Div.*, Vol. 84, No. ST6, pp. 1821.1–1821.20.

SAA Australian Standard (1979), *Rules for the Use of Aluminium in Structures*, AS1664, Standards Association of Australia, North Sydney, New South Wales, Australia.

Salmon, E. H. (1921), *Columns*, Oxford Technical Publishers, London.

Saxena, R., Popplewell, N., Trainor, P. G. S., and Shah, A. H. (1989), "Vibration of Complex Guyed Towers," *Proc. ASME 12th Bienn. Conf. Mech. Vib. Noise*, Montreal, Quebec, Canada, Sept. 17–21, pp. 1–7.

Sfintesco, D. (1970), "Experimental Basis for the European Column Curves," *Constr. Met.*, No. 3, p. 5.

Sfintesco, D., ed. (1976), *ECCS Manual on the Stability of Steel Structures*, 2nd ed., European Convention for Constructional Steelwork, Brussels, Belgium.

Shanley, F. R. (1947), "Inelastic Column Theory," *J. Aeronaut. Sci.*, Vol. 14, No. 5, p. 261.

Sharp, M. L. (1993), *Behavior and Design of Aluminum Structures*, McGraw-Hill, New York.

Shen, Z.-Y., and Lu, L.-W. (1983), "Analysis of Initially Crooked, End Restrained Columns," *J. Constr. Steel Res.*, Vol. 3, No. 1, pp. 10–18.

Sherman, D. R. (1976), *Tentative Criteria for Structural Applications of Steel Tubes*, American Iron and Steel Institute, Washington, D.C.

Stang, A. H., and Greenspar, M. (1948), "Perforated Cover Plates for Steel Columns: Summary of Compression Properties," *U.S. Nat. Bur. Stand. J. Res.*, Vol. 40, No. 5 RP.

Steinhardt, G. (1971), "Aluminum in Engineered Construction," *Aluminum*, No. 47 (in German).

Sugimoto, H., and Chen, W. F. (1982), "Small End Restraint Effects in Strength of H-Columns," *ASCE J. Struct. Div.*, Vol. 108, No. ST3, pp. 661–681.

Tall, L. (1964), "Recent Developments in the Study of Column Behavior," *J. Inst. Eng. Aust.*, Vol. 38, No. 12.

Tall, L. (1966), "Welded Built-up Columns," *Fritz Eng. Lab. Rep. No. 249.29*, Lehigh University, Bethlehem, Pa., Apr.

Tide, R. H. R. (1985), "Reasonable Column Design Equations," *Proc. SSRC Annu. Tech. Session*, Cleveland, Ohio, Apr. 1S17.

Timoshenko, S. P. (1908), "Buckling of Bars of Variable Cross Section," *Bull. Polytech. Inst.*, Kiev, Ukraine.

Timoshenko, S. P., and Gere, J. M. (1961), *Theory of Elastic Stability*, 2nd ed., McGraw-Hill, New York.

Tomonaga, K. (1971), "Actually Measured Errors in Fabrication of Kasumigaseki Building," *Proc. 3rd Reg. Conf. Plan. Des. Tall Build.*, Tokyo, Sept.

Trahair, N. S. (1977), *The Behavior and Design of Steel Structures*, Chapman & Hall, London.

van den Berg, G. J., and van der Merwe, P. (1992), "Stainless Steel in Structural Applications," in *Constructional Steel Design: World Developments* (ed. P. J. Dowling, J. E. Harding, R. Bjorhovde, and E. Martinez-Romero), Elsevier Applied Science, London.

van der Merwe, P., and van den Berg, G. J. (1992), "Design Criteria for Stainless Steel Structural Members," *Proc. Conf. Appl. Stainless Steel '92*, Stockholm, Sweden, June.

Vinnakota, S. (1982), "Planar Strength of Restrained Beam-Columns," *ASCE J. Struct. Div.*, Vol. 108, No. ST11, pp. 2496–2516.

Vinnakota, S. (1983), "Planar Strength of Directionally and Rotationally Restrained Steel Columns," *Proc. 3rd Int. Colloq. Stab. Met. Struct.*, Toronto, May, pp. 315–325.

Vinnakota, S. (1984), "Closure," *ASCE J. Struct. Div.*, Vol. 110, No. ST2, pp. 43–435.

Vroonland, E. J. (1971), "Analysis of Pendant-Supported Latticed Crane Booms," *SAE Trans.*, Vol. 80, Pap. 710697.

Wahba, Y. M. F., Madugula, M. K. S., and Monforton, G. R. (1993), "Combined Wind and Ice Loading on Antenna Towers," *Can. J. Civ. Eng.*, Vol. 20, No. 6, pp. 1407–1056.

Wang, C.-K. (1967), "Stability of Rigid Frames with Non-uniform Members," *ASCE J. Struct. Div.*, Vol. 93, No. ST1, pp. 275–294.

White, M. W., and Thürlimann, B. (1956), "Study of Columns with Perforated Cover Plates," *AREA Bull. No. 531.*

Williamson, R. A. (1973), "Stability Study of Guyed Towers Under Ice Loads," *ASCE J. Struct. Div.*, Vol. 99, No. ST12, pp. 2391–2408.

Williamson, R. A., and Margolin, M. N. (1966), "Shear Effects in Design of Guyed Towers," *ASCE J. Struct. Div.*, Vol. 92, No. ST5, pp. 213–233.

Wyly, L. T. (1940), "Brief Review of Steel Column Tests," *J. West. Soc. Eng.*, Vol. 45, No. 3, p. 99.

Yang, H., Beedle, L. S., and Johnston, B. G. (1952), "Residual Stress and the Yield Strength of Steel Beams," *Weld. J., Res. Suppl.*, Vol. 31, pp. 224–225.

Yu, W. W. (1992), *Cold-Formed Steel Design*, 2nd ed., Wiley, New York.

Yura, J. A. (1971), "The Effective Length of Columns in Unbraced Frames," *AISC Eng. J.*, Vol. 8, No. 2, pp. 37–42.

Zandonini, R. (1985), "Stability of Compact Built-up Struts: Experimental Investigation and Numerical Simulation," *Costruzioni Metalliche*, No. 4.

Ziegler, H. (1982), "Arguments for and Against Engesser's Buckling Formulas," *Ing. Arch.*, Vol. 52, pp. 105–113.

CHAPTER FOUR

PLATES

4.1 INTRODUCTION

Figure 4.1 shows a number of cross-sectional shapes for metal compression or flexural members. Except for the hollow cylinder (Fig. 4.1*a*), all of the members are composed of connected elements which, for purposes of analysis and design, can be treated as flat plates. When a plate element is subjected to direct compression, bending, shear, or a combination of these stresses in its plane, theoretical critical loads may be evaluated indicating that the plate may buckle locally before the member as a whole becomes unstable or before the yield stress of the material is reached. Such behavior is characterized by distortion of the cross section of the member. The almost inevitable presence of initial out-of-planeness may result in a gradual growth of cross-sectional distortion with no sudden discontinuity in real behavior at the theoretical critical load.

The theoretical critical load for a plate is not necessarily a satisfactory basis for design, since the ultimate strength can be much greater than the critical buckling load. For example, a plate loaded in uniaxial compression, with both longitudinal edges supported, will undergo stress redistribution as well as develop transverse tensile membrane stresses after buckling that provide post-buckling support. Thus additional load may often be applied without structural damage. Initial imperfections in such a plate may cause bending to begin below the buckling load, yet unlike an initially imperfect column, the plate may sustain loads greater than the theoretical buckling load.

This chapter considers local buckling theory and postbuckling behavior for plates with or without stiffeners which are used in open sections made up of

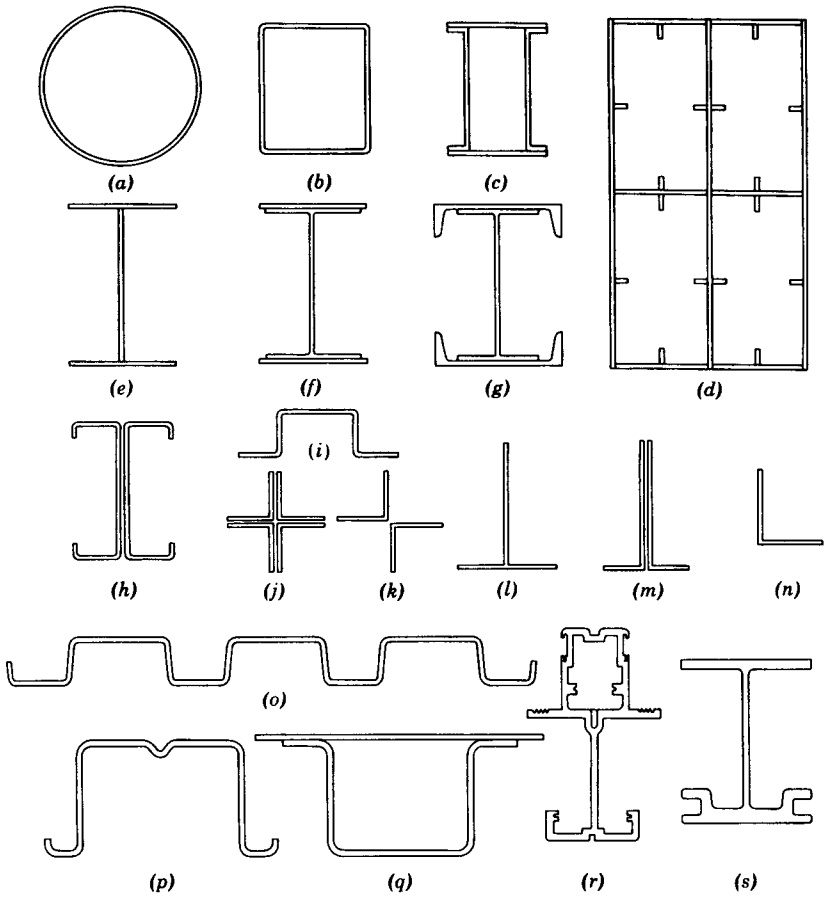

Fig. 4.1 Compression or flexural members.

plate elements and rectangular tubes. Interaction between plate elements in a section is discussed. Interaction between local plate buckling and overall member buckling is treated in Chapter 13. Buckling of hollow cylinders, with or without stiffeners, is treated in Chapter 14. Design applications of thin-walled metal construction are covered in Chapter 13, and plate buckling and post-buckling problems in relation to plate girder and box girder design are discussed in Chapters 6 and 7.

4.2 LOCAL BUCKLING AND POSTBUCKLING STRENGTH OF PLATES

An examination of the buckling behavior of a single plate supported along its edges is an essential preliminary step toward the understanding of local buckling behavior of plate assemblies. The buckling stresses are obtained from the

concept of bifurcation of an initially perfect structure. In practice, the response of the structure is continuous, due to the inevitable presence of initial imperfections. Thus the critical stress must be viewed as a useful index to the behavior, and plates can continue to carry additional loads well after initial buckling. Postbuckling resistance in plates is due to the redistribution of axial compressive stresses and, to a lesser extent, to the membrane tension and shear that accompany the out-of-plane bending of the plate in both the longitudinal and transverse directions. The longitudinal stresses tend to concentrate in the vicinity of the longitudinally supported edges, which are the stiffest parts of the buckled plate. As a result, yielding begins along these edges, which limits the load-carrying capacity.

4.2.1 Uniaxial Uniform Compression

Buckling Strength

Long Rectangular Plates. In 1891, Bryan (1891) presented the analysis of the elastic critical stress for a rectangular plate simply supported along all edges and subjected to a uniform longitudinal compressive stress. The elastic critical stress of a long plate segment is determined by the plate width-to-thickness ratio b/t, by the restraint conditions along the longitudinal boundaries, and by the elastic material properties. It is expressed as

$$\sigma_c = k\frac{\pi^2 E}{12(1-\nu^2)(b/t)^2} \tag{4.1}$$

in which k is a *buckling coefficient* determined by a theoretical critical-load analysis. It is a function of plate geometry and boundary conditions such as those shown in Fig. 4.2.

When the member cross section is composed of various connected elements (see Fig. 4.1) a lower bound of the critical stress can be determined by assuming, for each plate element, a simple support condition for each edge attached to another plate element or a free condition for any edge not so attached. The smallest value of the critical stress found for any of the elements is a lower bound of the critical stress for the cross section. This stress will be conservative because the element providing the lower bound will be restrained by the more stable adjoining plate elements if longitudinal edge joints provide effective continuity. More complete information on k-factors as influenced by the interaction between plate components can be found in a number of references (Bleich, 1952); (Stowell et al., 1952; Gerard and Becker, 1957/1958; Timoshenko and Gere, 1961).

Short Plates. When a plate element is relatively short in the direction of the compressive stress (i.e. $a/b \ll 1$), the critical stress may be conservatively estimated by assuming that a unit width of plate behaves like a column.

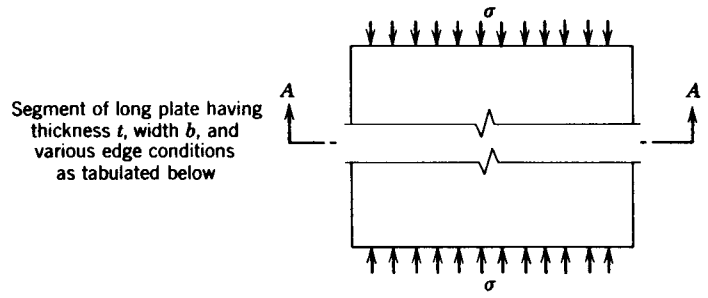

Case	Description of edge support	k
1	Both edges simply supported	4.00
2	One edge simply supported, the other fixed	5.42
3	Both edges fixed	6.97
4	One edge simply supported, the other free	0.425
5	One edge fixed, the other free	1.277

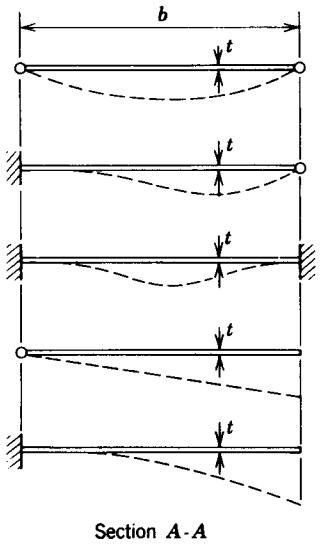

Fig. 4.2 Coefficients k for Eq. 4.1.

Inelastic buckling. Bleich (1952) generalized the expression for the critical stress of a flat plate under uniform compressive stress in either the elastic or inelastic range in the following manner:

$$\sigma_c = k\frac{\pi^2 E\sqrt{\eta}}{12(1-\nu^2)(b/t)^2} \tag{4.2}$$

in which $\eta = E_t/E$. This modification of Eq. 4.1 to adapt it to a stress higher than the proportional limit is a conservative approximation to the solution of a complex problem that involves a continuous updating of the constitutive relations depending on the axial stress carried (Stowell, 1948; Bijlaard, 1949, 1950).

Postbuckling Strength. Local buckling causes a loss of stiffness and a redistribution of stresses. Uniform edge compression in the longitudinal direction results in a nonuniform stress distribution after buckling (Fig. 4.3) and the buckled plate derives almost all of its stiffness from the longitudinal edge supports.

Elastic postbuckling stiffness is measured in terms of the apparent modulus of elasticity E^* (the ratio of the average stress carried by the plate to the average strain) (see Fig. 4.4). The values of E^* for long plates ($a \gg b$) for some typical longitudinal edge conditions are given by Allen and Bulson (1980). The values given below are sufficiently accurate up to twice the critical stress.

- *Simply supported longitudinal edges.* Sides straight but free to move laterally:

$$E^* = 0.5E \tag{4.3a}$$

Sides free to move:

$$E^* = 0.408E \tag{4.3b}$$

- *Clamped longitudinal edges.* Sides straight but free to move laterally:

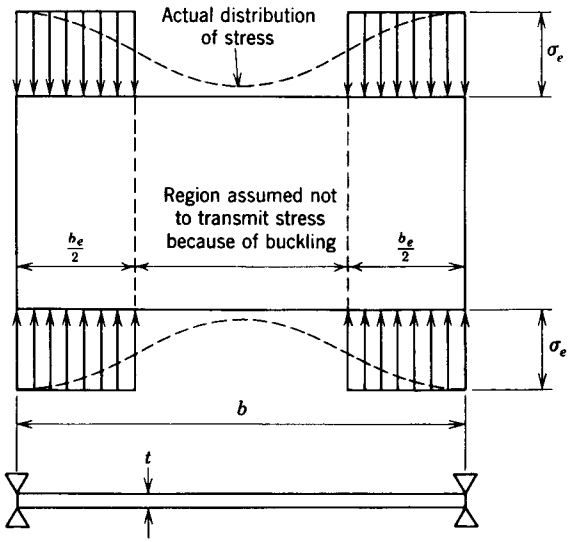

Fig. 4.3 Definition of effective width.

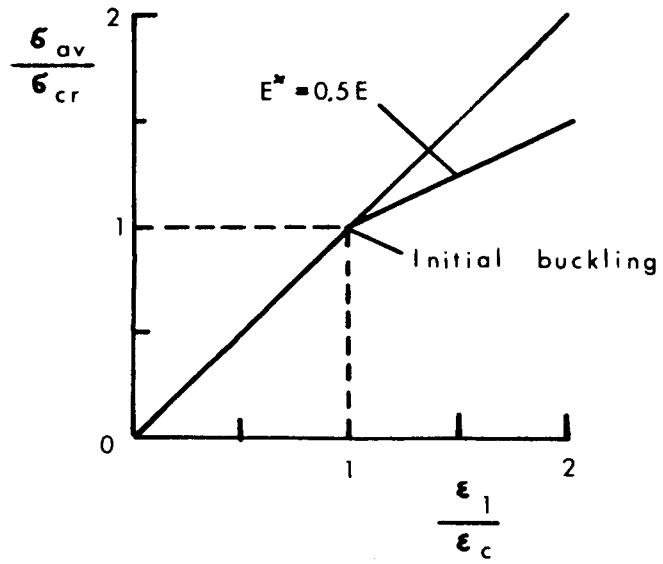

Fig. 4.4 Postbuckling stiffness of plates having simply supported edges (Allen and Bulson, 1980).

$$E^* = 0.497E \tag{4.3c}$$

- *One longitudinal edge simply supported, the other free*

$$E^* = 0.444E \tag{4.3d}$$

A very important semiempirical method of estimating the maximum strength of plates is by the use of the *effective width* concept. The fact that much of the load is carried by the region of the plate in the close vicinity of the edges suggests the simplifying assumption that the maximum edge stress acts uniformly over two "strips" of plate and the central region is unstressed (Fig. 4.3). Thus only a fraction of the width is considered effective in resisting applied compression. The concept of effective width is, however, not confined to calculation of postbuckling strength of uniformly compressed plates but has become the means of allowing for local buckling effects in columns, panels, or flexural members that have the dual function of supporting loads and acting as walls, partitions, bulkheads, floors, or roof decking. In a plate structure, use of the effective width leads to an effective cross section consisting of portions of members meeting along a junction. It is near these junctions that the plates will begin to yield preceding failure.

The effective-width concept has been used in design specifications for many years. Specifications of the AISI (1996), the Aluminum Association (1994), and

the AISC (1993) all permit the use of an effective width in the design of members having plate elements with b/t ratios greater than the limits for full effectiveness.

The effective-width concept seems to have had its origin in the design of ship plating (Murray, 1946). It had been found that longitudinal bending moments in ships caused greater deflections than those calculated using section properties based on the gross area of the longitudinal members. Deflections could be calculated more accurately by considering only a strip of plate over each stiffener having a width of 40 or 50 plate thicknesses as effective in acting with the stiffeners in resisting longitudinal bending.

The advent of all-metal aircraft construction provided another opportunity for the use of the effective-width concept , since it was advantageous to consider some of the metal skin adjacent to stiffeners as being part of the stiffener in calculating the strength of aircraft components. Cold-formed members used in steel buildings also provide useful applications of stiffened-sheet construction. A discussion of the effective-width concept as applied to cold-formed steel design has been prepared by Winter (1983).

Tests by Schuman and Back (1930) of plates supported in V-notches along their unloaded edges demonstrated that, for plates of the same thickness, increasing the plate width beyond a certain value did not increase the ultimate load that the plate could support. It was observed that wider plates acted as though narrow side portions or effective load-carrying areas took most of the load. Newell (1930) and others were prompted by these tests to develop expressions for the ultimate strength of such plates. The first to use the effective-width concept in handling this problem was von Kármán (1932). He derived an approximate formula for the effective width of simply supported plates, and in an appendix to his paper, Sechler and Donnell derived another formula based on slightly different assumptions. Subsequently, many other effective-width formulas have been derived, some empirical, based on approximate analyses, and some based on the large-deflection plate-bending theory, employing varying degrees of rigor.

For plates under uniform compression, stiffened along both edges parallel to the direction of the applied compression stress, von Kármán (1932) developed the following approximate formula for effective width, based on the assumption that two strips along the sides, each on the verge of buckling, carry the entire load:

$$b_e = \left[\frac{\pi}{\sqrt{3(1-\nu^2)}}\sqrt{\frac{E}{\sigma_e}}\right]t \tag{4.4}$$

Combining Eqs. 4.4 and 4.1, for $k = 4$ (simple edge supports), the formula suggested by Ramberg et al. (1939) is obtained (see Fig. 4.3 for notation):

$$\frac{b_e}{b} = \sqrt{\frac{\sigma_c}{\sigma_e}} \tag{4.5}$$

From Fig. 4.3, the average stress is

$$\sigma_{av} = \frac{b_e}{b}\sigma_e \tag{4.6}$$

Substituting Eq. 4.5 into Eq. 4.6 with the edge stress equal to the yield stress ($\sigma_e = \sigma_y$) gives us

$$\sigma_{av} = \sqrt{\sigma_c \sigma_y} \tag{4.7}$$

As a result of many tests and studies of postbuckling strength, Winter (1947) and Winter et al. (1950) suggested the formula for effective width that was adopted in the 1946 through 1962 editions of the AISI specifications for light-gage cold-formed steel:

$$\frac{b_e}{t} = 1.9\sqrt{\frac{E}{\sigma_e}}\left(1 - 0.475\sqrt{\frac{E}{\sigma_e}\frac{t}{b}}\right) \tag{4.8}$$

or, alternatively, in the form of Eq. 4.5,

$$\frac{b_e}{b} = \sqrt{\frac{\sigma_c}{\sigma_e}}\left(1 - 0.25\sqrt{\frac{\sigma_c}{\sigma_e}}\right) \tag{4.9}$$

Equations 4.8 and 4.9 are basically the same as Eqs. 4.4 and 4.5, respectively, but include a correction coefficient determined from tests and reflecting the total effect of various imperfections, including initial deviations from planeness. Equation 4.8 was found to be satisfactory also for austenitic stainless steel in the annealed and flattened condition (Johnson and Winter, 1966) and for quarter- and half-hard type 301 stainless steel (Wang, 1969; Wang et al., 1975).

Introducing the coefficient $B = b/t\sqrt{\sigma_e/E}$, Winter's formula, Eq. 4.8, can be written as

$$\frac{b_e}{b} = \frac{1.90}{B} - \frac{0.90}{B^2} \tag{4.10}$$

A formula proposed by Conley et al. (1963) is nearly the same as that proposed by Winter and can be expressed as

$$\frac{b_e}{b} = \frac{1.82}{B} - \frac{0.82}{B^2} \tag{4.11}$$

A useful form of Eq. 4.10 or 4.11 is obtained by introducing the material yield strength into the dimensionless parameter B. If $\bar{B}$ is defined as

$$\bar{B} = B\sqrt{\frac{\sigma_y}{\sigma_e}} = \frac{b}{t}\sqrt{\frac{\sigma_y}{E}} \tag{4.12}$$

and if σ_{av}/σ_e is substituted for b_e/b, and both sides of the equation are multiplied by σ_e/σ_y, Eq. 4.11 can be written

$$\frac{\sigma_{av}}{\sigma_y} = \frac{1.82}{\bar{B}}\sqrt{\frac{\sigma_e}{\sigma_y}} - \frac{0.82}{\bar{B}^2} \tag{4.13}$$

By introducing discrete values of $\bar{B}$ into Eq. 4.13, and relationships shown in Fig. 4.5 between σ_{av}/σ_y and σ_e/σ_y for B values greater than 1.0 were determined. It was assumed that there would be no loss of plate effectiveness for values of $\bar{B} \leqslant 1.0$ and thus the straight line from (0, 0) to (1.0, 1.0) was drawn for $\bar{B} = 1.0$. Lines of constant $\bar{B}$ when plotted fully are tangent to the $\bar{B} = 1.0$ line, and only their upper portions are shown. Thus for any given strength level

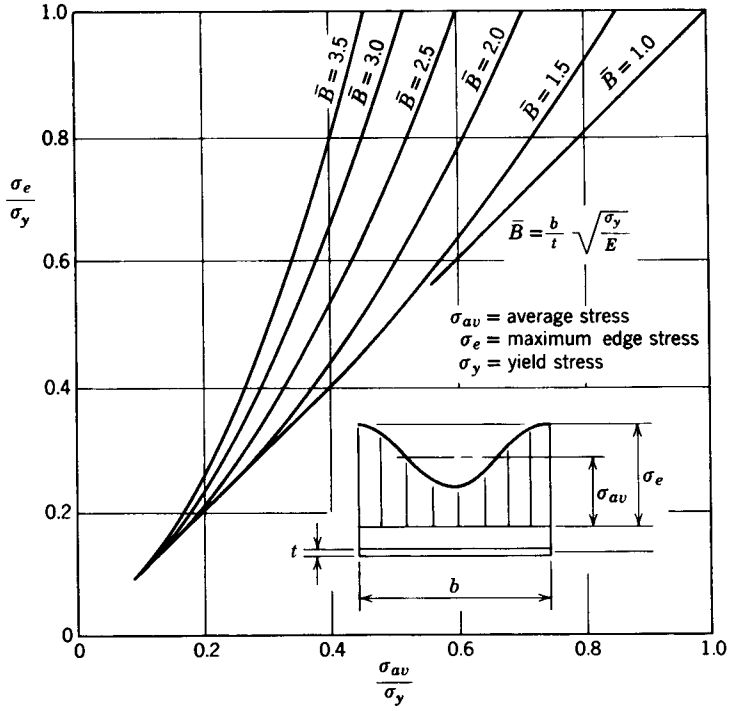

Fig. 4.5 Chart for determining σ_e/σ_y.

of plate steel, a relationship between average stress after buckling and the maximum or edge stress of the plate panel is established as a function of the actual b/t ratio. This relationship is valid for stiffened plates in which the ratio of stiffener cross-sectional area to plate-panel cross-sectional area is small. If the cross section of a structural member includes a buckled plate, the effective-width approach should be used in computing deflections, in determining the location of the neutral axis, or in ohter calculations where the effective moment of inertia or radius of gyration of the member is important.

In the 1968 and later editions of the AISI specification for cold-formed steel members (American Iron and Steel Institute 1996), the coefficients in Eqs. 4.8 and 4.9 were reduced slightly, giving the following expressions for effective width:

$$\frac{b_e}{t} = 1.9\sqrt{\frac{E}{\sigma_e}}\left(1.0 - 0.415\sqrt{\frac{E}{\sigma_e}\frac{t}{b}}\right) \tag{4.14a}$$

or

$$\frac{b_e}{b} = \sqrt{\frac{\sigma_c}{\sigma_e}}\left(1.0 - 0.22\sqrt{\frac{\sigma_c}{\sigma_e}}\right) \tag{4.14b}$$

The limiting value of b/t when all of the width is considered to be effective is obtained by setting b_e equal to b. The AISI value thus obtained from Eq. 4.14 is $(b/t)_{\text{lim}} = 221/\sqrt{\sigma}$. AISC values of effective width (1978) are slightly more liberal than those of AISI.

Considering that Eq. 4.14a is an appropriate formula for determining the effective design width of stiffened compression elements with a k value of 4.0, a generalized formula for different stiffened compression elements with various rotational edge restraints can be written as follows:

$$\frac{b_e}{t} = 0.95\sqrt{\frac{kE}{\sigma_e}}\left(1 - 0.209\sqrt{\frac{kE}{\sigma_e}\frac{t}{b}}\right) \tag{4.15}$$

Use of Eq. 4.14 or similar expressions involves the concept of effective section properties varying with the stress level. The significance of this is discussed in Chapter 13.

In the calculation of the ultimate compression load for plates supported along the two unloaded edges, σ_e is taken equal to the compressive yield stress for steel. For aluminum alloys and magnesium alloys, σ_e is taken as 0.7 times the yield strength, as determined by the offset method. However, if the buckling stress σ_c exceeds 0.7 times the yield strength, the load capacity as determined by inelastic plate-buckling analysis may be taken as $bt\sigma_c$ in which σ_c is determined by Eq. 4.2 and the effective width need not be calculated. The use

of the ultimate compressive buckling load in specifications for aluminum structures is discussed later in this section.

Equation 4.14b can be used to determine a nondimensional ultimate-strength curve for steel plates in the postbuckling range. The average stress on the plate at ultimate load, σ_{av}, is the ultimate load divided by the total area. From Eq. 4.14b,

$$\sigma_{av} = \frac{P_{ult}}{bt} = \sqrt{\sigma_c \sigma_y}\left(1.0 - 0.22\sqrt{\frac{\sigma_c}{\sigma_y}}\right) \tag{4.16}$$

In Fig. 4.6 the average stress at ultimate load, by Eq. 4.16, is compared with the uniform-edge compression stresses to cause buckling. A method for predicting the strength of simply supported plates, taking into account initial out-of-flatness, is given by Abdel Sayed (1969) and Dawson and Walker (1972). Out-of-flatness, residual stress, and strain hardening are considered by Dwight and Ratcliffe (1968).

For a plate supported along only one longitudinal edge, the effective width has been experimentally determined by Winter as

$$\frac{b_e}{b} = 1.19\sqrt{\frac{\sigma_c}{\sigma_e}}\left(1 - 0.30\sqrt{\frac{\sigma_c}{\sigma_e}}\right) \tag{4.17}$$

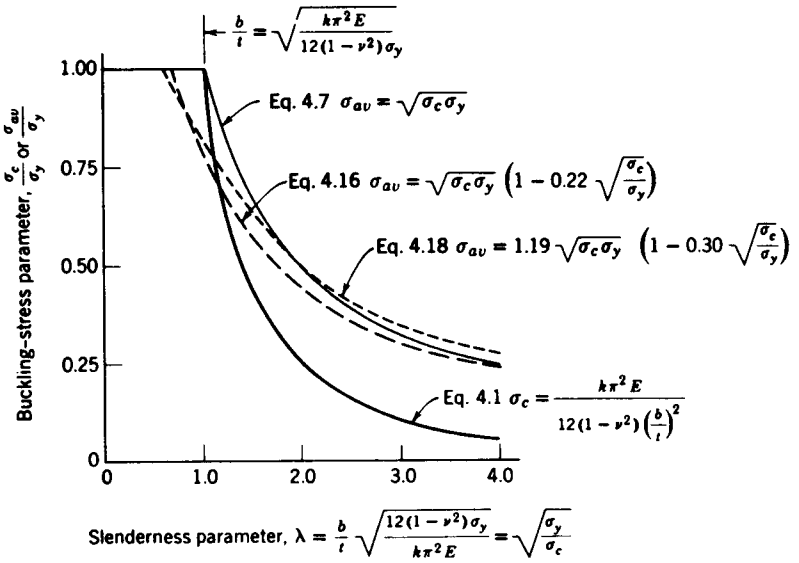

Fig. 4.6 Nondimensional buckling curves for plates under uniform edge compression (adapted from Brockenbrough and Johnston, 1974).

This equation has also been confirmed by an analysis carried out by Kalyanaraman (Kalyanaraman et al., 1977; Kalyanaraman and Pekoz, 1978). The average stress at ultimate load can then be expressed as

$$\sigma_{av} = 1.19\sqrt{\sigma_c \sigma_y}\left(1 - 0.30\sqrt{\frac{\sigma_c}{\sigma_y}}\right) \tag{4.18}$$

Equation 4.18 is also shown in Fig. 4.6. This curve actually falls above and to the right of Eq. 4.16, but it must be remembered that in the elastic range σ_c for a plate supported on both longitudinal edges is about eight times as large as that for the same plate supported along only one longitudinal edge.

After a statistical study of the available test data, Lind et al. (1976) suggest a compact expression for the effective width at ultimate load in the form

$$\frac{b_e}{t} = 1.64\sqrt{\frac{E}{\sigma_y}} \tag{4.19}$$

and this formula has been incorporated into the Canadian specifications (CSA, 1974). This can be compared to von Kármán's expression (Eq. 4.4) developed in 1932 with a coefficient of 1.9 instead of 1.64 if $\nu = 0.3$ is used. In subsequent work by Roorda and Venkataramaiah (1979), the available experimental data was reworked and it was concluded that a Winter-type effective-width equation was more appropriate. The current CSA specification (CAN3-S136-M84) uses Eq. 4.14a for calculation of effective width for stiffened compression elements with $k = 4.0$ and for unstiffened compression elements with $k = 0.5$. In the case of unstiffened compression elements, although less accurate than Eq. 4.17, the results are considered adequate for design. Kalyanaraman et al. (1977) found reasonable agreement with tests.

Jombock and Clark (1962) list 14 effective-width formulas, along with their sources, and discuss the assumptions on which they are based. Since the effective-width concept is also well developed in current specifications and commentaries, it is suggested that reference be made thereto for further information on this topic.

As an alternative to the effective-width concept for wide, thin plates, another approach is to use the average stress at failure and the actual (unreduced) plate width. This is the basis for allowable stresses on thin sections in the Aluminum Association specifications (AA, 1994). In applying these specifications the designer does not, in general, calculate an effective width but uses instead an allowable stress that has been derived by applying a factor of safety to the average stress at failure for plate elements. For plates that buckle in the inelastic stress range, the average stress at failure is considered to be the same as the local-buckling stress, since plates of these proportions have little post-buckling strength (Jombock and Clark, 1968). Inelastic local-buckling strength

for aluminum plates is represented in the specifications by the following straight-line approximation to Eq. 4.1 (Clark and Rolf, 1966):

$$\sigma_c = B_p - D_p k_1 \frac{b}{t} \tag{4.20}$$

where

$$B_p = \sigma_y \left[1 + \frac{(\sigma_y)^{1/3}}{k_2} \right]$$

$$D_p = \frac{(B_p)^{3/2}}{k_3 (E)^{1/2}}$$

$$k_1 = \sqrt{\frac{12(1-\nu^2)}{k}}$$

For aluminum alloys that are artificially aged (temper designations beginning with T5, T6, T7, T8, or T9), $k_2 = 11.4\,\text{ksi}^{1/3}$ ($78.6\,\text{MPa}^{1/3}$) and $k_3 = 10$. For other aluminum alloys (temper designations beginning with 0, H, T1, T2, T3, or T4), $k_2 = 7.6\,\text{ksi}^{1/3}$ ($52.4\,\text{MPa}^{1/3}$) and $k_3 = 10\sqrt{2/3}$.

Equation 4.20 has been shown to agree well with the results of tests on aluminum plate elements (Clark and Rolf, 1966; Jombock and Clark, 1968). For plates that buckle elastically, the average stress at failure is represented for purposes of the aluminum specification as

$$\sigma_{av} = \sqrt{\sigma_e \sigma_c} \tag{4.21}$$

Equation 4.21 corresponds to Eq. 4.7. Jombock and Clark (1968) demonstrated that the edge stress at failure σ_e for aluminum plates could be represented by a function of the intercept B_p in Eq. 4.20. This results in a simple relationship between the ultimate-strength curves corresponding to elastic and inelastic buckling. Generally, this edge stress at failure for aluminum alloys is about $0.7\sigma_y$.

The formulas used in the Aluminum Association specifications (AA, 1994) are illustrated in Fig. 4.7. Comparisons with test results were published by Jombock and Clark (1968). The use in these specifications of the average stress at failure for thin sections results in some simplification, since the designer does not have to calculate an effective width. However, it sacrifices some of the flexibility of the effective-wdith approach and does not give as accurate a picture of the true physical behavior. For example, the average stress-at-failure method does not treat the change in moment of inertia of a member when its compression elements are in the postbuckling range, and hence does not lend itself to calculation of deflections. Therefore, the Aluminum Association specifications include an effective-width formula to be used in calculating deflections in the postbuckling range.

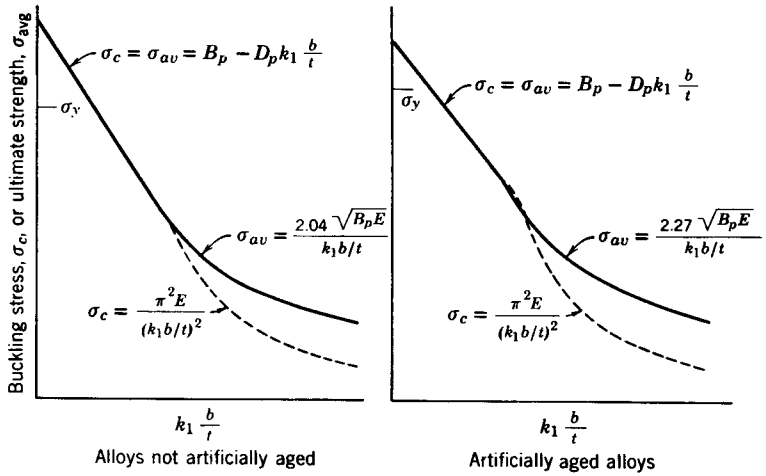

Fig. 4.7 Equations for buckling stress and ultimate strength of plates used in Aluminum Association specifications (AA, 1994).

Certain box-girder-bridge structural failures in the early 1970s have interjected a warning due to designers of plate structures that many aspects of plate behavior need further investigation. For example, the concepts of effective width and average stress at failure consider plate strains only up to the maximum plate capacity—that is, the ultimate load as characterized by reaching the yield stress at the edge. Research has shown that inelastic strains beyond the point may lead to a sudden and substantial reduction of the plate's load-carrying capacity (Dwight and Moxham, 1969; Dwight, 1971).

4.2.2 Compression and Bending

Buckling Strength. When compression plus bending loads are applied to a structural member, plate elements of the member can be subjected to in-plane stresses which vary along the loaded edges of the plate, from a maximum compressive stress, σ_1, to a minimum stress, σ_2, as shown in Fig. 4.8. For this situation, elastic critical plate stresses are dependent on the edge-support conditions and the ratio of bending stress to uniform compression stress. Values of k_c that can be substituted for k in Eq. 4.1 are tabulated in Fig. 4.8 for several cases. For intermediate stress ratios (σ_{cb}/σ_c), values of k_c can be estimated by linear interpolation. For plates with a free edge the k_c values vary slightly with Poisson's ratio. In the inelastic range, an estimate of the buckling stress can be obtained by using k_c for k in Eq. 4.2. Diagrams for buckling coefficients for rectangular plates under combined bending and

Loading	Ratio of Bending Stress to Uniform Compresion Stress σ_{cb}/σ_c	Minimum Buckling Coefficient, $*k_c$					
		Unloaded Edges Simply Supported	Unloaded Edges Fixed	Top Edge Free: Bottom Edge Simply Supported	Top Edge Free: Bottom Edge Fixed	Bottom Edge Free: Top Edge Simply Supported	Bottom Edge Free: Top Edge Fixed
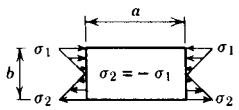 $\sigma_2 = -\sigma_1$	∞ (pure bending)	23.9	39.6	0.85	2.15		
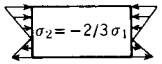 $\sigma_2 = -2/3\sigma_1$	5.00	15.7					
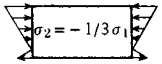 $\sigma_2 = -1/3\sigma_1$	2.00	11.0					
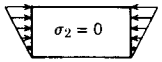 $\sigma_2 = 0$	1.00	7.8	13.6	0.57	1.61	1.70	5.93
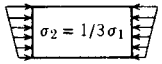 $\sigma_2 = 1/3\sigma_1$	0.50	5.8					
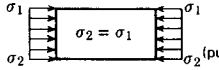 $\sigma_2 = \sigma_1$	0.0 (pure compression)	4.0	6.97	0.42	1.33	0.42	1.33

*Values given are based on plates having loaded edges simply supported and are conservative for plates having loaded edges fixed.

Fig. 4.8 Buckling coefficients for long flat plates under compression and bending (Brockenbrough and Johnston, 1974; Bijlaard, 1957).

compressive stresses in two perpendicular directions are given by Yoshizuka and Naruoka (1971).

Postbuckling Strength. Plate elements and channel sections subjected to prescribed loading and displacement eccentricity have been studied by Rhodes and Harvey (1971, 1976). These solutions are based on the assumption of a fixed buckling mode and are thus, in principle, restricted in their applicability to the immediate vicinity of bifurcation, but for the case of single plates have been shown to be in reasonable agreement with experimental results up to three times the critical load.

In the case of simply supported plates under eccentric loading P, the failure loads for plates with various loading eccentricities can be accurately predicted by a simple expression of the form (Rhodes and Harvey, 1977).

$$\bar{P}_{\text{ult}} = \frac{pb}{\pi^2 D} = \frac{\bar{\sigma}_y + 11.4}{b(e/b) + 0.85} \tag{4.22}$$

where $D = Et^3/12(1-\nu^2)$, $\bar{\sigma}_y = \sigma_y(b^2 t/\pi^2 D)$, and e is the distance from the point of load application to the remote edge of the plate.

A study has been carried out by Usami (1982) on elastic postbuckling of plates in compression and bending using compatibility equations and the energy method. Based on the numerical results, effective-width formulas in combined compression and bending have been derived. It is shown that Winter's formula (Eq. 4.14) forms a good lower bound. Based on Usami's results, the following empirical formula was proposed to predict the postbuckling strength, σ:

$$\frac{\sigma}{\sigma_e} = \sqrt{\frac{\sigma_c}{\sigma_e}}\left[(1 + 0.1\xi_0) - (0.22 + 0.05\xi_0)\sqrt{\frac{\sigma_c}{\sigma_e}}\right] \tag{4.23a}$$

in which $\xi_0 = 0$ for pure compression and 2.0 for pure bending, and ξ_0 can be calculated from

$$k = \begin{cases} \dfrac{8.4}{2.1 - \xi_0} & \text{for } 0 \leqslant \xi_0 \leqslant 1.0 \\ 10\xi_0^2 - 13.736\xi_0 + 11.372 & \text{for } 1.0 \leqslant \xi_0 \leqslant 2.0 \end{cases} \tag{4.23b}$$

for different geometric boundary conditions. This equation reduces to Winter's equation with $\xi_0 = 0$. If the plate yield stress σ_y is substituted for σ_e, σ becomes the ultimate stress of the plate.

Based on an experimental study, LaBoube and Yu (1982) have found that the postbuckling strength of beam web elements subjected to pure bending stress is a function of web slenderness ratio, the bending stress ratio of the web, the width-to-thickness ratio of the compression flange, and the yield point of the steel. The effective depth equations for beam webs have been developed through a statistical analysis to predict the ultimate bending capacity of cold-formed steel beams when used in conjunction with the assumed bending stress distribution.

The Aluminum Association specifications (AA, 1994) treat postbuckling strength of webs in bending by means of an average stress approach similar to that used for plates in compression. This approach is compared with test results by Jombock and Clark (1968).

4.2.3 Shear

Buckling Strength. When a plate is subjected to edge shear stresses as shown in Fig. 4.9, it is said to be in a state of *pure shear*. Tension and compression stresses exist in the plate, equal in magnitude to the shear stress and inclined at 45°. The destabilizing influence of compressive stresses is resisted

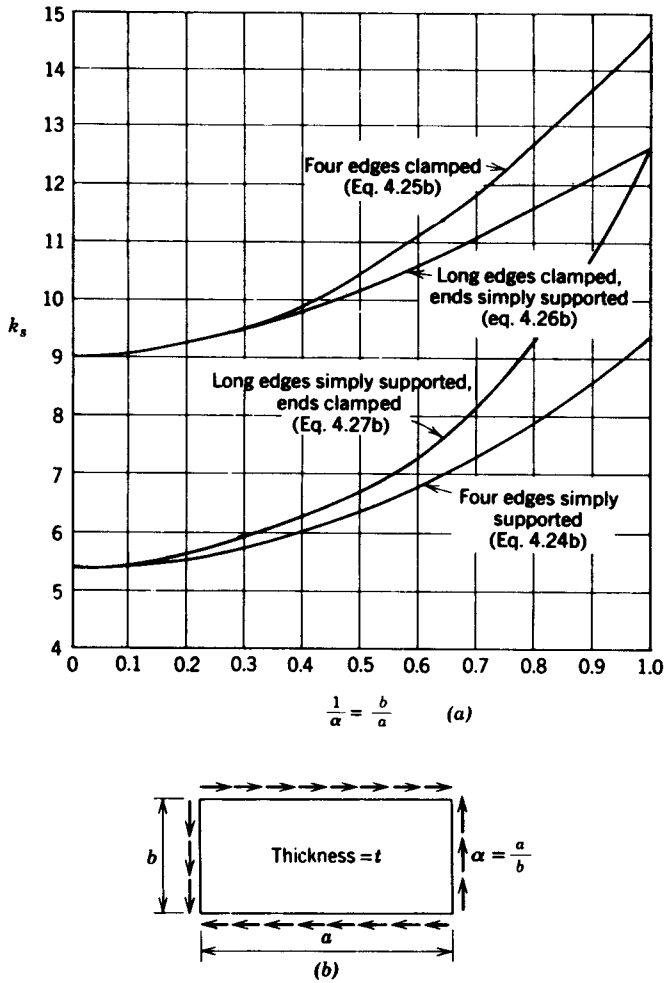

Fig. 4.9 Buckling coefficients for plates in pure shear. (Side b is the short side.)

by tensile stresses in the perpendicular direction. Unlike the case of edge compression, the buckling mode is composed of a combination of several waveforms and this is part of the difficulty in the buckling analysis for shear.

The critical shear stresses can be obtained by substituting τ_c and k_s for σ_c and k in Eq. 4.1, in which k_s is the buckling coefficient for shear buckling stress. Critical-stress coefficients k_s for plates subjected to pure shear have been evaluated for three conditions of edge support. In Fig. 4.9 these are plotted with the side b, as used in Eq. 4.1, always assumed to be shorter than side a. Thus α is always greater than 1 and by plotting k_s in terms of $1/\alpha$, the complete range of k_s can be shown and the magnitude of k_s remains manageable for small values

of α. However, for application to plate-girder design it is convenient to define b (or h in plate-girder applications) as the vertical dimension of the plate-girder web for a horizontal girder. Then α may be greater or less than unity and empirical formulas for k_s together with source data are as follows:

Plate Simply Supported on Four Edges. Solutions developed by Timoshenko (1910), Bergmann and Reissner (1932), and Seydel (1933) are approximated by Eqs. 4.24a and 4.24b, in which $\alpha = a/b$:

$$k_s = \begin{cases} 4.00 + \dfrac{5.34}{\alpha^2} & \text{for } \alpha \leqslant 1 \quad (4.24a) \\ 5.34 + \dfrac{4.00}{\alpha^2} & \text{for } \alpha \geqslant 1 \quad (4.24b) \end{cases}$$

Plate Clamped on Four Edges. In 1924, Southwell and Skan obtained $k_s = 8.98$ for the case of the infinitely long rectangular plate with clamped edges. For the finite-length rectangular plate with clamped edges, Moheit (1939) obtained

$$k_s = \begin{cases} 5.6 + \dfrac{8.98}{\alpha^2} & \text{for } \alpha \leqslant 1 \quad (4.25a) \\ 8.98 + \dfrac{5.6}{\alpha^2} & \text{for } \alpha \geqslant 1 \quad (4.25b) \end{cases}$$

Plate Clamped on Two Opposite Edges and Simply Supported on the Other Two Edges. A solution for this problem has been given by Iguchi (1938) for the general case, and by Leggett (1941) for the case of the square plate. Cook and Rockey (1963) later obtained solutions considering the antisymmetric buckling mode which was not considered by Iguchi. The expressions below were obtained by fitting a polynomial equation to the Cook and Rockey results as shown in Fig. 2.36 of the book by Bulson (1970). For long edges clamped,

$$k_s = \begin{cases} \dfrac{8.98}{\alpha^2} + 5.61 - 1.99\alpha & \text{for } \alpha \leqslant 1 \quad (4.26a) \\ 8.98 + \dfrac{5.61}{\alpha^2} - \dfrac{1.99}{\alpha^3} & \text{for } \alpha \geqslant 1 \quad (4.26b) \end{cases}$$

and for short edges clamped,

$$k_s = \begin{cases} \dfrac{5.34}{\alpha^2} + \dfrac{2.31}{\alpha} - 3.44 + 8.39\alpha & \text{for } \alpha \leqslant 1 \quad (4.27a) \\ 5.34 + \dfrac{2.31}{\alpha} - \dfrac{3.44}{\alpha^2} + \dfrac{8.39}{\alpha^3} & \text{for } \alpha \geqslant 1 \quad (4.27b) \end{cases}$$

Curves for $\alpha \geqslant 1$ are plotted in Fig. 4.9. If the predicted critical stress in shear is greater than the proportional limit of the material, the buckling will be inelastic.

Postbuckling Strength. The initial mode of buckling in pure shear, which takes the form of a half wave in the tension direction and at least one full wave in the compression direction (Fig. 4.10*a*), undergoes a change in the advanced postbuckling range, eventually taking the form of a family of diagonal folds (Fig. 4.10*b*). These folds carry significant tensile stresses developed in the postbuckling range and the displacement pattern is called a *tension field.*

The maximum shear load that can be applied before failure occurs due to a breakdown of the material in the tension field, and it is influenced by the rigidity of the edge members supporting the plate. This problem is dealt with in greater detail in Chapter 6. For a plate with infinitely stiff edge members, the maximum shear strength can be estimated by the formula (Allen and Bulson, 1980)

$$\bar{V}_u = \tau_c bt + \tfrac{1}{2}\sigma_{ty} bt \qquad (4.28)$$

where

$$\sigma_{ty} = \sqrt{\sigma_y^2 - 0.75\tau_c^2} - 1.5\tau_c \qquad \text{provided that } \tau_c \ll \sigma_y$$

Stein and Manue (1989) presented buckling and postbuckling results for plates loaded by in-plane shear. The buckling results had been plotted to show the effects of thickness on the stress coefficient for aluminum plates. Results were given for various length-to-width ratios. Postbuckling results for thin plates with transverse shearing flexibility were compared to results from classical theory. The plates were considered to be long with side edges simply supported, with various in-plane edge conditions and the plates were subjected to a constant shearing displacement along the side edges.

Elangovan and Prinsze (1992) carried out a numerical investigation, using a finite element buckling analysis to determine the critical shear stress of flat rectangular plates with two opposite edges free. Plate sizes and the boundary conditions at the two edges loaded in shear were the parameters considered in their study. Results showed a considerable difference in the buckling strength

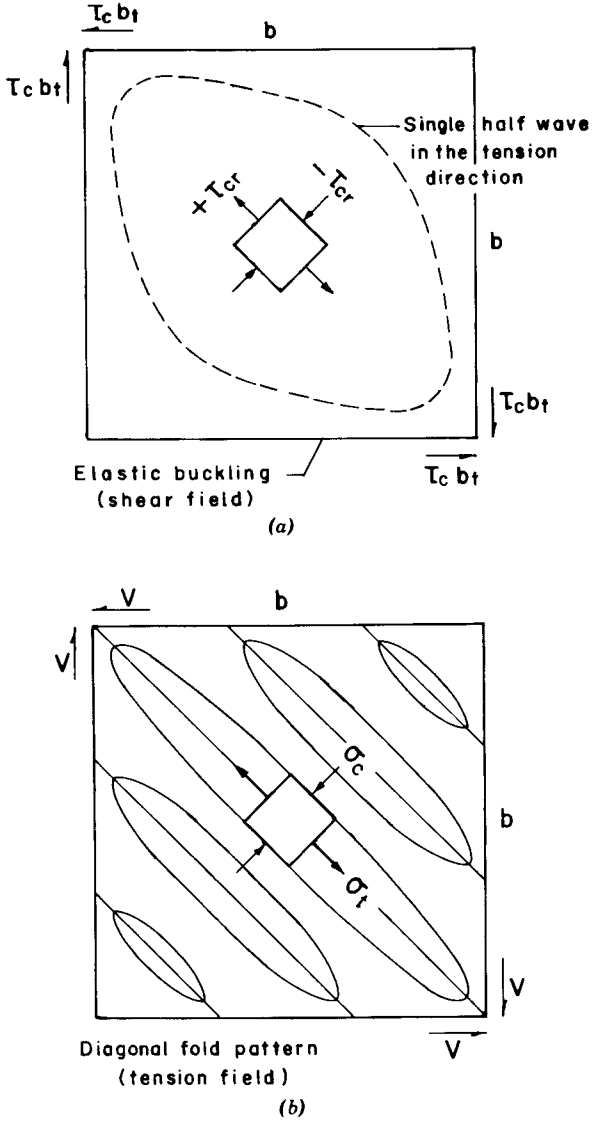

Fig. 4.10 Shear and tension fields (square plate).

of plates if the in-plane displacement normal to the loaded edges were restrained either at one or at both of those edges.

4.2.4 Combined Stresses

Shear Combined with Direct Stress. The case of shear combined with longitudinal compression, with all sides simply supported, was treated by

Iguchi (1938). His results are approximated by the following interaction equation, also shown graphically in Fig. 4.11:

$$\frac{\sigma_c}{\sigma_c^*} + \left(\frac{\tau_c}{\tau_c^*}\right)^2 = 1 \tag{4.29}$$

where σ_c^* and τ_c^* denote critical stress, respectively, under compression or shear alone.

Equation 4.29, shown in Fig. 4.11, is for ratios of a/b greater than unity. Batdorf and associates (Batdorf and Houbolt, 1946; Batdorf and Stein, 1947) have shown that when the loaded side b is more than twice as long as a, Eq. 4.29 becomes overly conservative. This situation is the exception in actual practice, and Eq. 4.29 may be accepted for engineering design purposes.

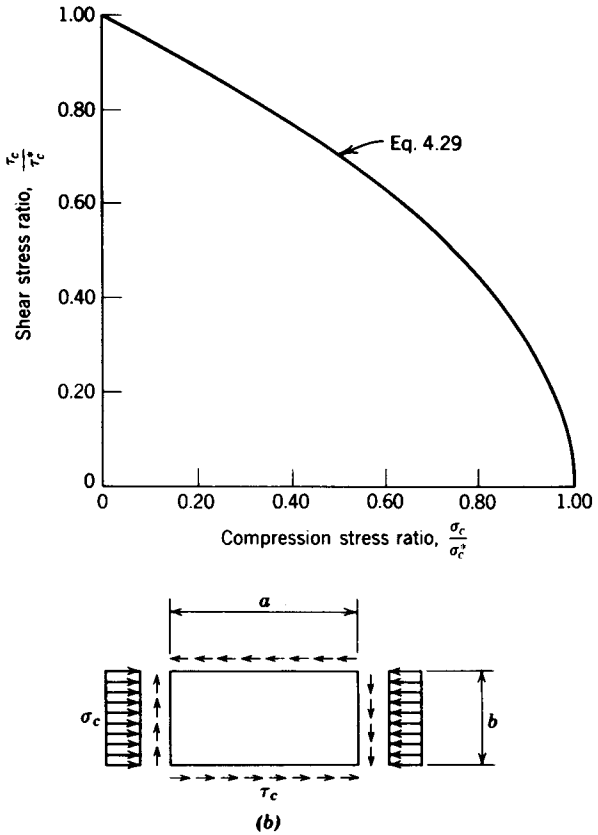

Fig. 4.11 Interaction curve for buckling of flat plates under shear and uniform compression.

The work of Stowell (1949) and Peters (1954) may be referred to with regard to buckling in the inelastic range under combined compressive and shear stress for loads applied in constant ratio. Peters found that a circular stress-ratio interaction formula as expressed by Eq. 4.30 was conservative and agreed better with test results than Eq. 4.29

$$\left(\frac{\sigma_c}{\sigma_c^*}\right)^2 + \left(\frac{\tau_c}{\tau_c^*}\right)^2 = 1 \tag{4.30}$$

Shear Combined with Bending. For a plate simply supported on four sides, under combined bending and pure shear, Timoshenko (1934) obtained a reduced k_c as a function of τ_c/τ_c^* for values of $\alpha = 0.5$, 0.8, and 1.0, where τ_c is the actual shearing stress and τ_c^* is the buckling stress for pure shear. This problem was also solved by Stein (1936) and Way (1936), whose results for four values of α are plotted in Fig. 4.12. Chwalla (1936a) suggested the following approximate interaction formula, which agrees well with the graphs of Fig. 4.12.

$$\left(\frac{\sigma_{cb}}{\sigma_{cb}^*}\right)^2 + \left(\frac{\tau_c}{\tau_c^*}\right)^2 = 1 \tag{4.31}$$

For a plate simply supported on four sides, under combined bending and direct stress at the ends (of dimension b), combined with shear, an approximate evaluation of the critical combined load is obtained by use of a three-part interaction formula, Eq. 4.32 (Gerard and Becker, 1957/1958).

$$\frac{\sigma_c}{\sigma_c^*} + \left(\frac{\sigma_{cb}}{\sigma_{cb}^*}\right)^2 + \left(\frac{\tau_c}{\tau_c^*}\right)^2 = 1 \tag{4.32}$$

The foregoing problem, with the further addition of vertical compressive force along the top and bottom edges of length a, has been treated by McKenzie (1964) with results given in the form of interaction graphs. The results are in good agreement with the special case of Eq. 4.32. Interaction equation 4.32, valid when a/b is greater than unity, is shown graphically in Fig. 4.13, as presented in Brockenbrough and Johnston (1974).

Information on the postbuckling strength of plate elements subjected to the combined action of shear and compression is limited. A semiempirical method for the determination of stress levels at which permanent buckles occur in a long plate with simply supported edges under the combined action of uniform axial compression and shear has been suggested by Zender and Hall (1960). Some additional information on postbuckling strength of plates subjected to the combined action of shear and bending can be found in Chapters 6 and 7.

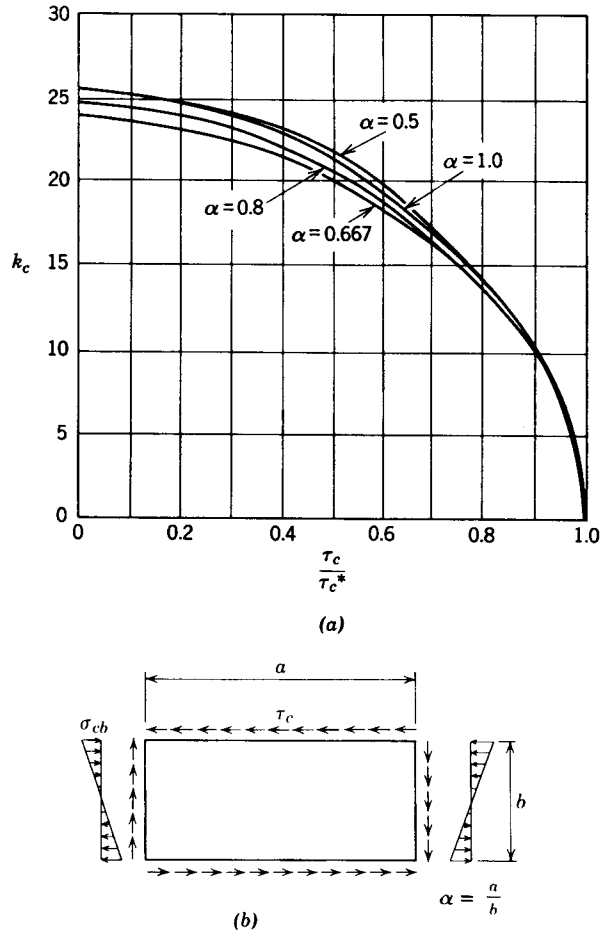

Fig. 4.12 Buckling coefficients for plates in combined bending and shear.

4.2.5 Effects of Perforation on Buckling Strength

Designers frequently find it necessary to introduce openings in the webs of girders and other large plate structures. The introduction of an opening changes the stress distribution within the member and will, in many instances, also change the mode of failure. Buckling is a key aspect in the behavior of thin perforated plates.

Plates in Compression. The problem of a square plate with a central hole having either simply supported or clamped-edge conditions has been studied by Levy et al. (1947), Kumai (1952), Schlack (1964), Kawai and Ohtsubo (1968), and Fujita et al. (1970).

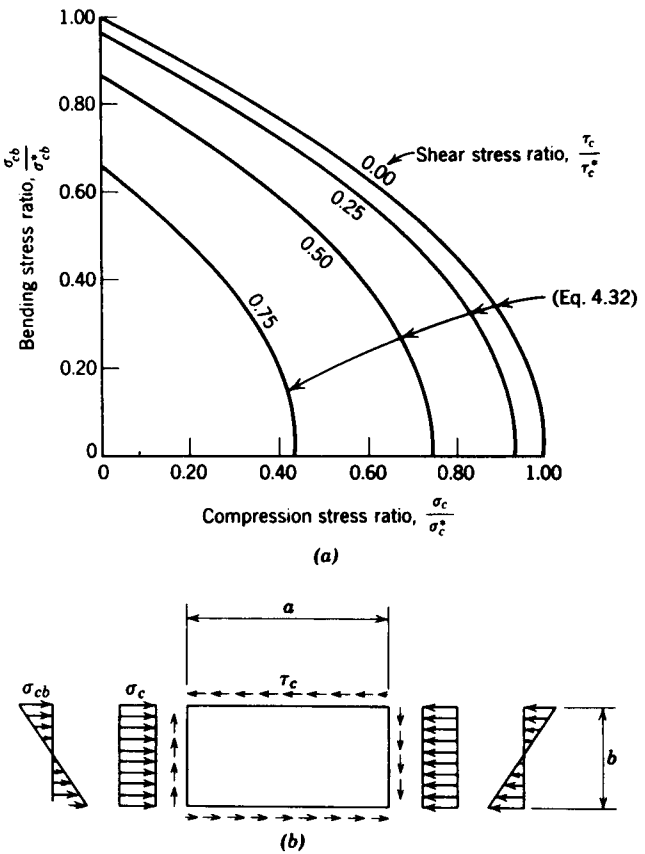

Fig. 4.13 Interaction curve for buckling of flat plates under shear, compression, and bending.

Figure 4.14 gives the ratios of the buckling coefficients of simply supported square plates with circular holes (k_{pc}/k) and square holes (k_{ps}/k) to the coefficient of unperforated plates. For a given size of perforation, the reduction in the critical load for a plate having a square hole is greater than that with a circular hole (Yang, 1969). It has been demonstrated that by suitably reinforcing the hole, it is possible to increase the critical stress beyond that of the unperforated plate (Levy et al., 1947). Clamped-edge conditions have been considered by Schlack (1964) and Kumai (1952).

The buckling behavior of perforated plate elements with only one longitudinal edge supported (compression flanges) perforated by circular holes has been investigated by Yu and Davis (1973). On the basis of limited experimental results, stress reduction factors have been recommended for the design of cold-formed steel members.

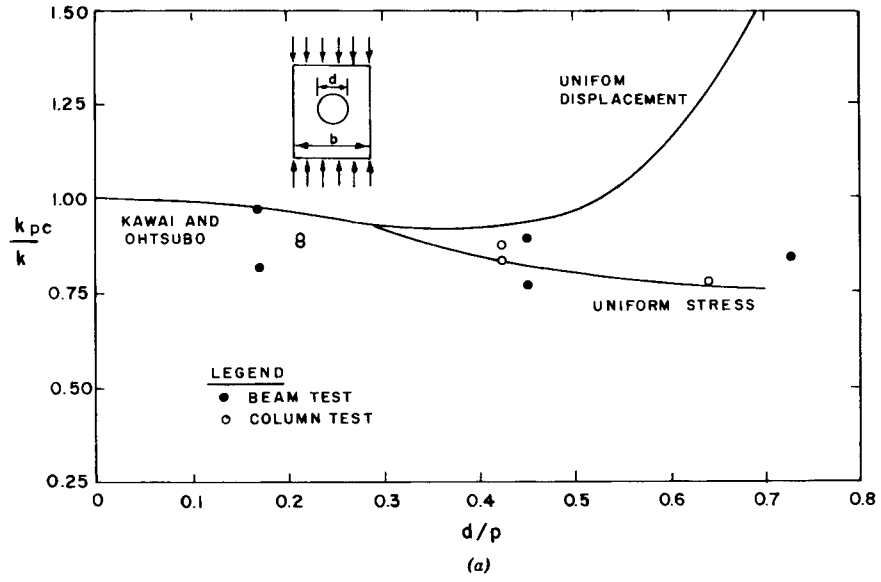

Fig. 4.14 Buckling of plates with holes: (*a*) effect of d/b ratio on buckling coefficient and comparison of test data with theoretical buckling coefficients; (*b*) effect of h_1/b ratio on buckling coefficient and comparison of test data with theoretical bucking coefficients (Yu and Davis, 1973).

Based on test data, a modified equation of effective width was presented by Yu and Davis (1973) to account for the postbuckling strength of compression flanges supported along two longitudinal edges. That equation is similar to the original effective-width equation, with some additional parameters to take into account the effects of perforation.

May and Ganaba (1988) used the finite element analysis to determine the elastic buckling loads for plates with and without openings. The formulation is based on Mindlin plate theory. The eight-node serendipity element was used to model the membrane behavior of the plate to determine the in-plane stress distribution throughout the plate due to the edge loading. The heterosis plate bending element was used in formulation of the governing equations of the stability problems. The elastic buckling loads for plates with and without openings and different edge loading conditions were determined. The openings considered were circular and square located at the center of the plate.

Nemeth and Michael (1990) presented an experimental study of the buckling and postbuckling behavior of square and rectangular compression-loaded aluminum plates with centrally located circular, square, and elliptical cutouts. The results indicated that the plates exhibit overall trends of increasing buckling strain and decreasing initial postbuckling stiffness with increasing cutout width. Results showed that the reduction in initial postbuckling stiffness due to a cutout generally decreases as the plate aspect ratio increases. Also, the square plates with elliptical cutouts having large cutout width/plate width ratio generally lose prebuckling and initial postbuckling stiffness as the cutout height increases.

Brown (1990) presented results for concentrated loading applied to perforated plates of different aspect ratios. Two different in-plane restraint conditions and four edge conditions had been analyzed. The results had been obtained by the application of conjugate load-displacement method of elastic stability analysis, and show how simple modifications to plate geometry, particularly with respect to perforation aspect ratio and support conditions, can effect major changes to the elastic critical load.

Square Plates in Shear. The buckling of a square plate with a central circular cutout has been examined by Rockey et al. (1969) using the finite element method. The relationship between the buckling stress of the plate and the relative size of the hole (d/b) was obtained for both simply supported and clamped-edge conditions. Rockey's work suggests a simple linear relationship between the critical stress and the d/b ratio in the form

$$\tau_{cp} = \tau_c\left(1 - \frac{d}{b}\right) \tag{4.33}$$

where τ_{cp} and τ_c are the critical stresses for the perforated plate and unperforated plate, respectively. The relationship holds good for both clamped and

simply supported end conditions (Fig. 4.15). The behavior of plates with cutouts reinforced by a ring formed by a pressing process was also studied by Rockey, both analytically and experimentally (Rockey, 1980). It was found that the buckling stress increases with t_r/t, the ratio of the depth of the lip to the plate thickness, and the larger the hole, the greater must be the t_r/t ratio to achieve a buckling strength equal to that of the unperforated plate. The magnitudes of the residual stresses formed in the lip and in the plate adjacent to the hole increase, however, with the depth of the lip and this tends to reduce both the buckling and ultimate strengths; and thus the ratio between the ultimate and the buckling loads is not significantly affected as t_r/t is increased beyond a certain value.

Shear buckling of square perforated plates was also investigated by Grosskurth et al. (1976) using the finite element approach. They considered the case of uniform shear deformation instead of uniform shear stress and obtained critical stresses that were in closer agreement with, although higher than, the experimental values.

Shear Webs with Multiple Holes. The problem of a long shear web with holes has received some attention in the literature. Based on the available data, Michael (1960) has suggested semiempirical expressions for the critical stress in terms of d/a and a/b (notation indicated in Fig. 4.16). These are

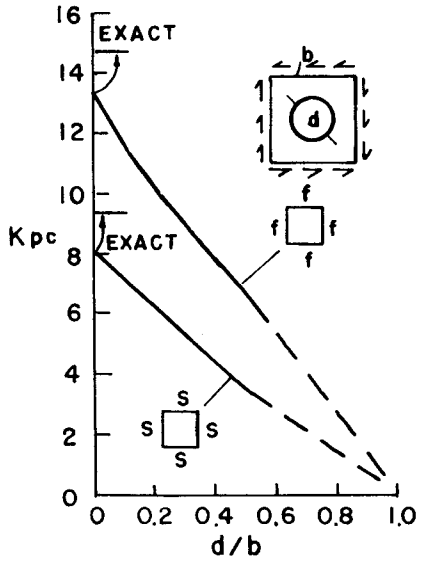

Fig. 4.15 Simply supported and clamped plates with hole under shear loading (Rockey et al., 1969).

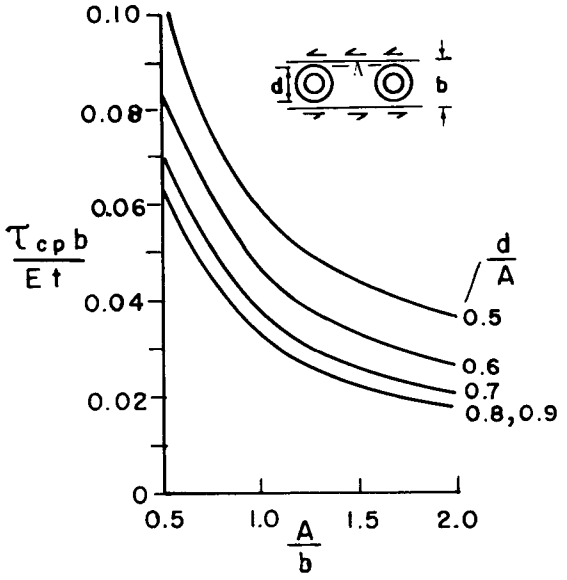

Fig. 4.16 Critical shear stress for webs with holes (Michael, 1960).

plotted graphically in Fig. 4.16 and are applicable for the web fixed along the top and bottom edges.

Webs with Holes Under Combined Loading. Redwood and Uenoya (1979) have investigated the problem of webs with holes subjected to combined bending and shear. Using the finite element approach for the solution of the plane stress problem and a Rayleigh–Ritz procedure for the buckling analysis, they studied the problem of shear webs with aspect ratios from 1.5 to 2.5 with circular or rectangular holes. They suggested an interaction formula for τ_c and σ_{cb} (critical values of the maximum shear and bending stresses, respectively) in the form

$$\left(\frac{\tau_c}{\tau_{cp}}\right)^2+\left(\frac{\sigma_{cb}}{\sigma_{cbp}}\right)^2=1.0 \tag{4.34}$$

in which τ_{cp} and σ_{cbp} are the pure shear and pure bending critical stresses of the plate with the hole. These, in turn, can be expressed in terms of the corresponding critical stresses of plates without holes (τ_c^*, σ_{cb}^*) and the relative sizes of the holes with respect to the plate dimensions. With the notation indicated in Fig. 4.17, the expressions for plates with rectangular holes take the form

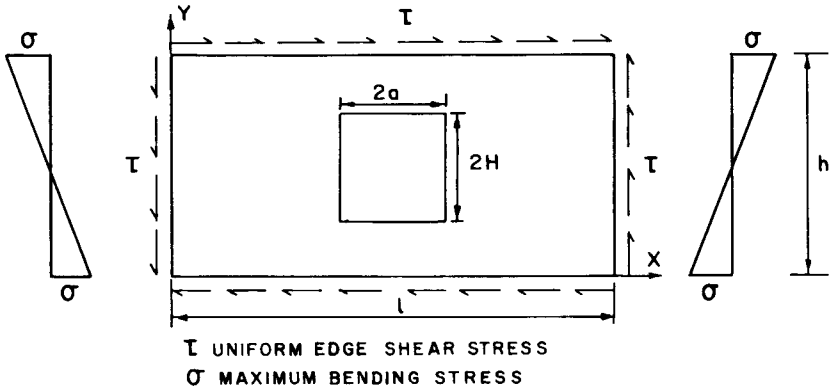

Fig. 4.17 Perforated rectangular plate under combined action of shear and bending.

$$\sigma_{cbp} = \left[1.02 - 0.04\left(\frac{a}{H}\right)\right]\sigma^*_{cb} \qquad \text{but} \leqslant \sigma^*_{cb} \qquad (4.35a)$$

$$\tau_{cp} = \left[1.24 - 1.16\left(\frac{2H}{h}\right) - 0.17\left(\frac{a}{H}\right)\right]\tau^*_c \qquad \text{but} \leqslant \tau^*_c \qquad (4.35b)$$

and for circular holes,

$$\sigma_{cbp} = \sigma^*_{cb} \qquad (4.36a)$$

$$\tau_{cp} = \left[1.15 - 1.05\left(\frac{2R}{h}\right)\right]\tau^*_c \qquad \text{but} \leqslant \tau^*_c \qquad (4.36b)$$

where R is the radius of the hole.

The values of σ^*_{cb} and τ^*_c can be obtained from a knowledge of the aspect ratio and boundary conditions of the plate. For example, for a simply supported plate with an aspect ratio of 2, these stresses are given with sufficient accuracy by the following expressions:

$$\sigma^*_{cb} = 23.90\sigma^*_c \qquad (4.37a)$$

$$\tau^*_c = 6.59\sigma^*_c \qquad (4.37b)$$

in which

$$\sigma^*_c = \frac{\pi^2 E}{12(1-\nu^2)}\left(\frac{t}{h}\right)^2$$

4.2.6 Inelastic Buckling Analysis of Plates

Lau and Hancock (1989) presented a method of inelastic buckling analysis of thin-walled structural members and plates. The method was based on the spline finite strip method of structural analysis. The analysis took into account

the nonlinear material stress-strain properties, strain hardening, and residual stresses. The plastic theories used in the study were the flow theory of plasticity and the deformation theory of plasticity. The method of inelastic buckling analysis was applied to a variety of instability problems, including plates, cold-formed columns, hot-rolled columns, and welded T-section beams.

Azhari and Bradford (1993) presented a complex eigenvalue finite strip method of analysis that includes inelasticity. The method can handle shear effects as well as the flow and deformation theories of plasticity. The method was used to study the initial local buckling of flat plates with and without residual stresses using both the flow and deformations theories. A method for estimating the rotation capacity of a plastic hinge before the onset of local buckling was also given.

4.2.7 Plastic Buckling of Plates

Inoue et al. (1993) studied an analytical evaluation of the effective plastic shear modulus of fully yielded steel plates at the instant of buckling. It was assumed that yielding of steel was to follow the Tresca yield criterion and that plastic deformation of a steel plate was to be caused by slips. The Tresca yield criterion provides lower bending stiffnesses than those obtained from the von Mises yield criterion, but it does not lower the plastic shear modulus of the material at any point on the yield plateau. They proposed a new theory that assumes a nonuniform distribution of slips depending on the orientation of an infinite number of possible slip planes at each point in the plate. The twisting of the plate is then accompanied by distortion of its sectional shape, and this mode of buckling is shown to provide a considerable reduction in the effective plastic shear modulus. Applying these sectional stiffnesses and solving differential equilibrium equations leads to a lower bifurcation strength, which provides much better correlations with experimental results than those of previous predictions.

4.2.8 Biaxially Compressed Plates

Pavlovic and Baker (1989) presented an exact solution for the stability of a rectangular plate under biaxial compression. The case when both longitudinal and transverse stresses were uniform was used as a starting point to investigate the much more complex problem of partial loading on two opposite edges. A parametric study was carried out covering different plate geometrics, load ratios, and varying edge lengths over which the applied load acted. The limiting cases of very long and very wide plates were considered in the study, as was the problem in which two opposite edges were subjected to concentrated forces.

Isami and Hidenori (1989) presented a new, unified approach to the ultimate strength of biaxially compressed rectangular plates in the elastoplastic range. For a given strain ratio in two directions compressed biaxially, the elastoplastic buckling strength is obtained from the elastoplastic material behavior and the

residual stresses in two directions. Then elastoplastic ultimate strength is predicted in terms of the imperfection sensitivity in the neighborhood of the particular point, where the elastoplastic postbuckling curve intersects the pathological failure mechanism curve. The ultimate strength was found to be in good agreement with previous numerical results.

Sivakumaran et al. (1992) studied the postbuckling behavior and the ultimate strength of simply supported, thin, rectangular, steel plates subjected to partial biaxial compressive loads. The analytical technique accounted for large deflections, elasto-perfectly plastic material behavior, residual stresses, and initial out-of-plane deflections. The method of analysis was based on the principle of minimum potential energy and the Rayleigh–Ritz solution procedure. The solution procedure had been applied in an incremental step-by-step manner. The influences of initial imperfections such as out-of-plane deflections and residual stresses and the plate width-to-thickness ratio on the behavior and the ultimate strength of such plates had been discussed, and the results of the parametric study were presented in graphical form and summarized by simple design curves.

4.3 INTERACTION BETWEEN PLATE ELEMENTS

In the preceding section, attention has been confined to the behavior of a single plate element supported along one or both of its longitudinal edges. The structural sections employed in practice (Fig. 4.1) are composed of plate elements arranged in a variety of configurations. It is clear that the behavior of an assembly of plates would be governed by an interaction between the plate components. In this section the mechanics of such an interaction and its implication in design are discussed briefly.

4.3.1 Buckling Modes of a Plate Assembly

Unlike a single plate element supported along the unloaded edges, a plate assembly can buckle in one of several possible modes. For the case of axial compression, the buckling mode can take one of the following forms:

- *Mode I.* This is the purely local buckling mode discussed earlier. The mode involves out-of-plane deformation of the component plates with the junctions remaining essentially straight, and it has a wavelength of the same order of magnitude as the widths of the plate elements.
- *Mode II.* The buckling process may involve in-plane bending of one or more of the constituent plates as well as out-of-plane bending of all the elements, as in a purely local mode. Such a buckling mode is referred to as a *stiffener buckling mode*, *local torsional mode*, or *orthotropic mode*, depending on the context. The associated wavelengths are considerably greater than those of mode I, but there is a half-wavelength at which the critical stress is a minimum.
- *Mode III.* The plate structure may buckle as a column in flexural or flexural-torsional mode with or without interaction of local buckling.

Attention in this chapter will be primarily on the mode I type of buckling. Column behavior (mode III) and interaction between local and overall modes of buckling are treated in Chapter 13 and elsewhere in this guide.

4.3.2 Buckling of a Plate Assembly

A prismatic plate structure is often viewed simply as consisting of *stiffened* and *unstiffened* plate elements. The former are plate elements supported on both of their longitudinal edges by virtue of their connection to adjacent elements, while the latter are those supported only along one of their longitudinal edges. Thus the critical local buckling stress of a plate assembly may be taken as the smallest of the critical stresses of the plate elements, each treated as simply supported along its junctions with other plates. However, such a calculation must be used with caution for the following reasons:

1. The results can be unduly conservative when the plate structure consists of elements with widely varying slendernesses. This is the result of neglecting the rotational restraints at the functions.
2. The results are inapplicable unless it is ensured that all the plate elements buckle locally (i.e., the junctions remain essentially straight). If, on the other hand, mode II or III type of buckling is critical, the result of such a simplified calculation would be on the unsafe side.

The intervention of stiffener buckling (mode II) is usually averted in practice by designing "out" the stiffener buckling mode by the provision of stiffeners (edge or intermediate) of adequate rigidity. This is appropriate because of the limited postbuckling resistance associated with the mode II type of buckling. A design approach for edge and intermediate stiffeners has been proposed by Desmond et al. (1981a and b).

Optimal design of the cross section would be one that made all the component plates equally stiff with due regard to their condition (i.e., whether they were stiffened or unstiffened. This would also ensure that all the elements participate equally in the local buckling process, thus making it realistic to use design concepts such as the effective width.

In plastic design of steel structures, it is necessary that the moment capacity of the member not be impaired by local buckling until the required rotation is achieved. This can be achieved by limiting the width-to-thickness ratios of elements that are vulnerable to local buckling in the inelastic range. Such limiting width-to-thickness ratios have been proposed for flanges of I-beams

by Lay (1965). Further studies of this topic can be found in the following references: Dawe and Kulak (1984, 1986), Kuhlmann (1989) and Kemp, (1996). Such provisions are also available in design specifications (American Institute of Steel Construction 1993).

Figure 4.18 gives the variations of the local buckling coefficients k_w for a wide-flange I-section, a box section and a Z- or channel section, respectively, with respect to the geometrical properties of the member. Each of these charts is divided into two portions by a dashed line running across it (Kroll et al., 1943). In each portion, buckling of one of the elements dominates over the other, but the propertions exactly on the dashed line represent the most structurally efficient configuration, in that there occurs a complete participation of all plates in the local-buckling process. Additional charts and related information may be found in the references such as the Japanese *Handbook of Structural Stability* (CRCJ, 1971).

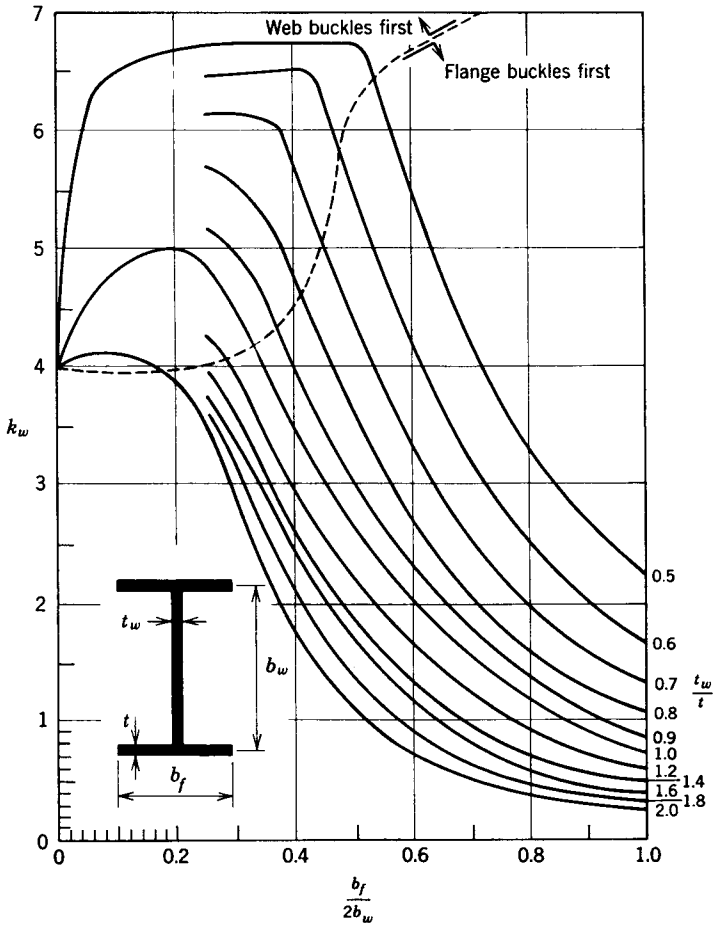

Fig. 4.18a Plate-buckling coefficient k_w for wide-flange columns (Kroll et al., 1943).

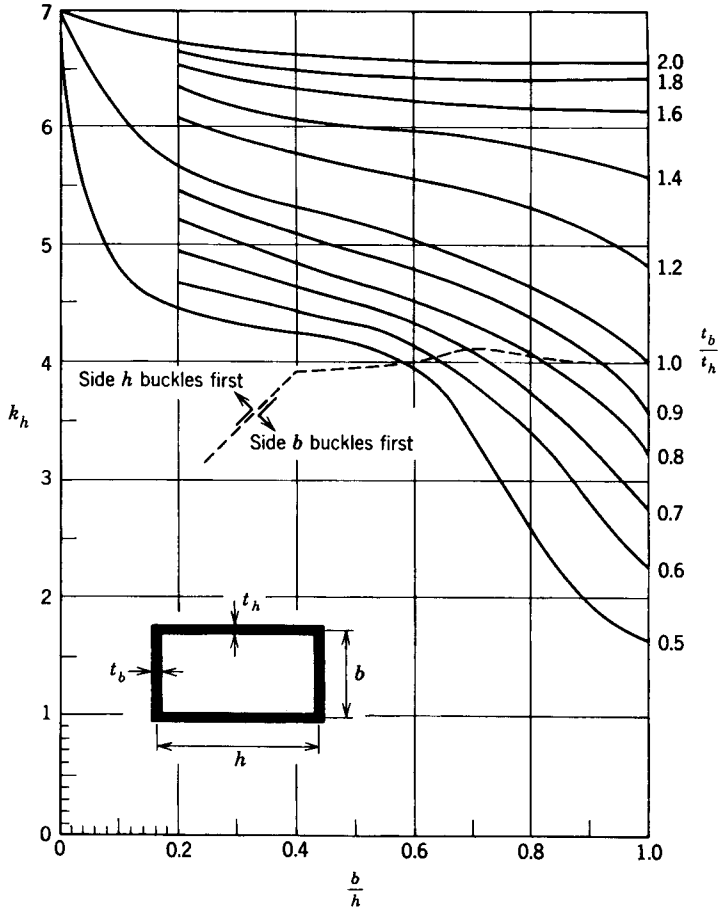

Fig. 4.18b Plate-buckling coefficient k_h for side h of rectangular box column (Kroll et al., 1943).

4.3.3 Postbuckling of a Plate Assembly

Interaction between the elements of a plate assembly is inescapable because of the equilibrium and compatibility conditions that must be satisfied at the junction. In the case of local buckling it is possible to simplify these conditions considerably, as has been shown by Benthem (1959). The smallness of the in-plane displacements in comparison to the out-of-plane displacements makes it possible to assume that normal displacements are zero for each plate element meeting at a corner. Also, because of the smallness of the bending rigidity in

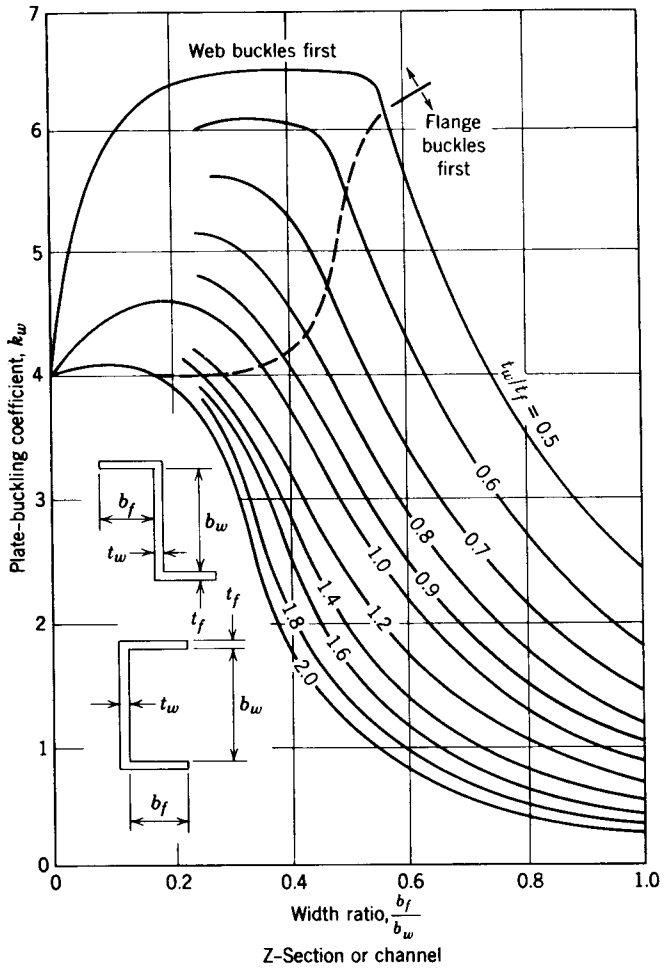

Fig. 4.18c Plate-buckling coefficient k_w for Z-sections and channels (Kroll et al., 1943).

comparison to the extensional rigidity, it is possible to assume that the in-plane membrane meets another plate element at an angle (Walker, 1964; Graves-Smith, 1968; Rhodes and Harvey, 1971; Tien and Wang, 1979).

In the postbuckling range in-plane displacements and membrane stresses dominate the behavior of the buckled plates. The interactions between plate elements along the junctions become very complex. The problem is compounded when interaction between overall and local buckling is considered. The problem has become a major subject for research during the past two decades.

The earlier references on interaction of local and overall buckling in the postbuckling range include those by Bijlaard and Fisher (1952), Cherry

(1960), Graves-Smith (1969), Klöppel et al. (1969), Sharp (1970), and Škaloud and Zornerova (1970). Research in this field has also been carried out by Rhodes and Harvey (1976), Graves-Smith and Sridharan (1978, 1980), Kalyanaraman (1978), Thomasson (1978), Little (1979), Rhodes and Loughlan (1980), Hancock (1980, 1981), Sridharan and Graves-Smith (1981), Fukumoto and Kubo (1982), and Sridharan (1982). Using the concept of effective width, the problem has been investigated by DeWolf et al. (1974), Wang and Pao, (1981), and Desmond et al. (1981a and b). The application aspect of this subject is discussed further for thin-walled members in Chapter 13.

4.4 LOCAL BUCKLING AND POSTBUCKLING STRENGTH OF STIFFENED PLATES

This section deals with the buckling and ultimate strength of stiffened flat plates under various combinations of loadings. The behavior of the stiffened plate as a unit is emphasized rather than the stability of its individual elements. However, in design, the structural properties of all of the components must be considered.

Stiffened plates can fail through instability in essentially two different ways. In one, overall buckling, the stiffeners buckle along with the plate, and in the other, local buckling, the stiffeners form nodal lines and the plate panels buckle between the stiffeners. In either case the stiffness of the combination may be such that initial buckling takes place at fairly low stress levels. Nevertheless, a significant amount of postbuckling strength may remain in the stiffened plate, provided that proper attention is given to the design and fabrication of the structural details. A great deal of information on this subject can be found in the *Handbook of Structural Stability* (CRCJ, 1971) and in a book by Troitsky (1976).

4.4.1 Uniaxial Compression

Buckling Strength. It is often economical to increase the compressive strength of a plate element by introducing longitudinal and/or transverse stiffeners (Fig. 4.19). In the following paragraphs methods are presented for determining the compressive strength of stiffened plate panels. The edges of the plate are assumed to be simply supported in all cases, and it is also assumed that individual elements of the panel and stiffeners are not subject to instability.

Longitudinal Stiffeners. Seide and Stein (1949), Bleich and Ramsey (1951), and Timoshenko and Gere (1961) have presented charts and tables for determining the critical stress of plates simply supported on all edges and having one, two, or three equally spaced longitudinal stiffeners parallel to the direction of the

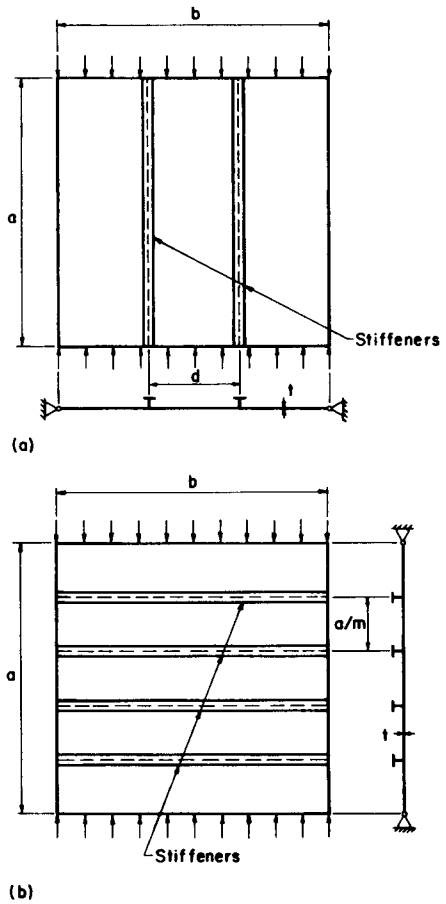

Fig. 4.19 Stiffened plate panels; (*a*) panel with longitudinal stiffeners; (*b*) panel with transverse stiffeners.

applied compressive load. The solutions of Seide and Stein are also useful for other numbers of equally spaced stiffeners. In all of these solutions the stiffeners are assumed to have zero torsional rigidity.

A conservative method of analysis proposed by Sharp (1966) divides the analysis of the stiffened plate into two parts: one applying to short panels in which the buckled configuration takes the form of a single half-wave in both the longitudinal and transverse directions and another applying to long panels in which several longitudinal waves may occur along with a single half-wave in the transverse direction. In very short panels, the stiffener and a width of plate equal to the stiffener spacing, d, are analyzed as a column of length, a, with a slenderness ratio

$$\left(\frac{L}{r}\right)_{eq} = \frac{a}{r_e} \tag{4.38}$$

where r_e is the radius of gyration of the section consisting of a stiffener plus a width of plate equal to d.

In long panels the critical stress is larger than that calculated by the use of Eq. 4.38. In this case an equivalent slenderness ratio is defined for use in column strength formulas,

$$\frac{L}{r_{eq}} = \sqrt{6(1-\nu^2)}\frac{b}{t}\sqrt{\frac{1+(A_s/bt)}{1+\sqrt{(EI_e/bD)+1}}} \tag{4.39}$$

where

$b = Nd$ = overall width of longitudinally stiffened panel
N = number of panels into which the longitudinal stiffeners divide the plate
I_e = moment of inertia of section consisting of the stiffener plus a width of plate equal to d
A_s = cross-sectional area of stiffener

$$D = \frac{Et^3}{12(1-\nu^2)}$$

The smaller of the values from Eqs. 4.38 and 4.39 is used in the analysis, and it is assumed that the plate is fully effective over the panel width d. For greater values of d, buckling of the stiffeners and of the plate between the stiffeners would need consideration.

A flat aluminum sheet with multiple longitudinal stiffeners, or a formed stiffened sheet, subjected to a uniform longitudinal compression (Sherbourne et al., 1971) will buckle into waves of length ψb, in which b is the plate width and $\psi = 1.8(I_x/t^3)^{1/4}$, where I_x is the moment of inertia in the strong direction and t is the plate thickness.

For a formed aluminum stiffened sheet this becomes $\psi = 1.8(\rho r_x/t)^{1/2}$, in which ρ is the ratio of the developed sheet width to the net width, and r_x is the radius of gyration in the strong direction.

If the spacing, a, of transverse supports is less than ψb, the elastic critical stress is given approximately by

$$\frac{\sigma_c = \pi^2 E[1+(a/\psi b)^4]}{(a/r_x)^2} \tag{4.40a}$$

If the spacing exceeds ψb, then

$$\frac{\sigma_c = 2\pi^2 E}{(\psi b/r_x)^2} \tag{4.40b}$$

The Canadian standard (CSA, 1983), using this method, reduces the design procedure to determining the equivalent slenderness ratios, which are, respectively, for the two cases,

$$\lambda = \frac{a/r_x}{[1 + (a/\psi b)^4]^{1/2}} \tag{4.41a}$$

$$= \frac{0.7\psi b}{r_x} \tag{4.41b}$$

Transverse Stiffeners. The required size of transverse stiffeners for plates loaded in uniaxial compression has been defined by Timoshenko and Gere (1961) for one, two, or three equally spaced stiffeners, and by Klitchieff (1949) for any number of stiffeners. The stiffeners as sized provide a nodal line for the buckled plate and thus prohibit overall buckling of the stiffened panel. The strength of the stiffened panel would be limited to the buckling strength of the plate between stiffeners. These authors also give formulas for calculating the buckling strength for smaller stiffeners. The required minimum value of γ given by Klitchieff is

$$\gamma = \frac{(4m^2 - 1)[(m^2 - 1)^2 - 2(m^2 + 1)\beta^2 + \beta^4]}{2m5m^2 + 1 - \beta^2\alpha^3} \tag{4.42}$$

where

$$\beta = \frac{\alpha^2}{m} \qquad \alpha = \frac{a}{b} \qquad \gamma = \frac{EI_s}{bD}$$

and m is the number of panels, $m - 1$ the number of stiffeners, and EI_s flexural rigidity of one transverse stiffener.

An approximate analysis that errs on the conservative side but gives estimates of the required stiffness of transverse stiffeners for plates, either with or without longitudinal stiffeners, may be developed from a consideration of the buckling of columns with elastic supports.

Timoshenko and Gere (1961) show that the required spring constant, K, of the elastic supports for a column, for the supports to behave as if absolutely rigid, is given by

$$K = \frac{mP}{Ca} \tag{4.43}$$

where

$$P = \frac{m^2\pi^2(EI)_c}{a^2}$$

and C is the constant depending on m, which decreases from 0.5 for $m = 2$ to 0.25 for infinitely large m, $(EI)_c$ the flexural stiffness of column, m the number of spans, and a the total length of column. In the case of a transversely stiffened plate (fig. 4.19*b*), a longitudinal strip is assumed to act as a column which is elastically restrained by the transverse stiffeners. Assuming also that the loading from the strip to the stiffener is proportional to the deflection of the stiffener, the spring constant for each column support can be estimated. For a deflection shape of a half sine wave the spring constant is

$$K = \frac{\pi^4(EI)_s}{b^4} \tag{4.44}$$

Equating Eqs. 4.43 and 4.44 and inserting the value given for P results in the following:

$$\frac{(EI)_s}{b(EI)_c} = \frac{m^3}{\pi^2 C(a/b)^3} \tag{4.45}$$

In the case of panels without longitudinal stiffeners $(EI)_c = D$ and the left side of Eq. 4.45 is γ.

Values of C are tabulated by Timoshenko and Gere (1961) for $m \leqslant 11$. As shown by Fig. 4.20, these values are given approximately by

$$C = 0.25 + \frac{2}{m^3} \tag{4.46}$$

In Table 4.1 values calculated using Eq. 4.45 are compared to corresponding values tabulated by Timoshenko and Gere (1961) for one, two, and three stiffeners and to those calculated by Eq. 4.41 for 10 stiffeners. Equation 4.45 is always conservative and is highly accurate for cases in which several stiffeners subdivide the panel.

Longitudinal and Transverse Stiffeners. For a combination of longitudinal and transverse stiffeners, Gerard and Becker (1957/1958) give figures showing the minimum value of γ as a function of α for various combinations of equally stiff longitudinal and transverse stiffeners. The same procedure used to establish Eq. 4.45 can also be applied to this case. The difference in the development is that the spring constant, K, of the support is dependent on the number of longitudinal stiffeners as illustrated below. The flexural stiffness $(EI)_c$ in these

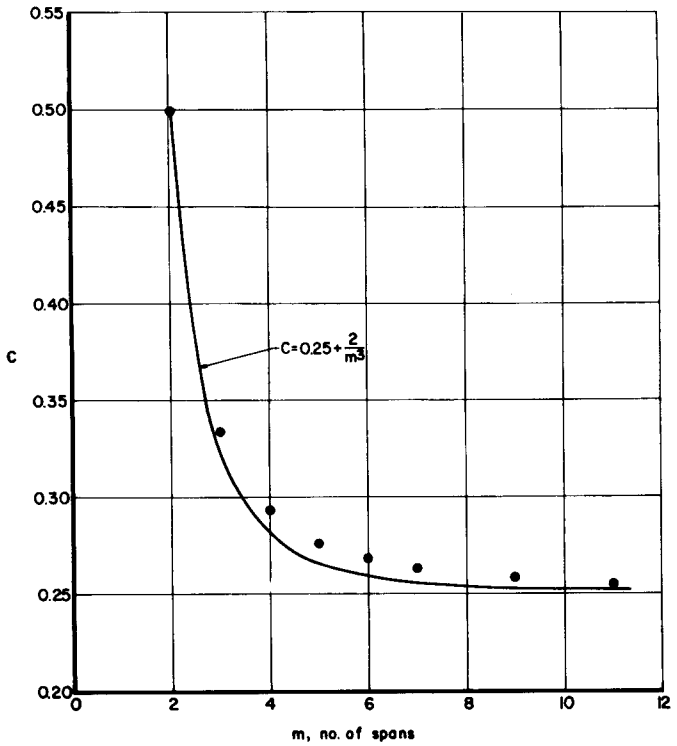

Fig. 4.20 Buckling of columns with elastic supports.

cases is equal to the average stiffness per unit width of the plate-longitudinal stiffener combination.

Number and Spacing of Longitudinal Stiffeners	Spring Constant, K	$\dfrac{(EI)_s}{b(EI)_c} = \gamma$
One centrally located	$\dfrac{48(EI)_s}{b^3}$	$\dfrac{0.206m^3}{C(a/b)^3}$
Two equally spaced	$\dfrac{162}{5}\dfrac{(EI)_s}{b^3}$	$\dfrac{0.152m^3}{C(a/b)^3}$
Four equally spaced	$\dfrac{18.6(EI)_s}{b^3}$	$\dfrac{0.133m^3}{C(a/b)^3}$
Infinite number equally spaced	$\dfrac{\pi^4(EI)_s}{b^3}$	$\dfrac{m^3}{\pi^2 C(a/b)^3} = \dfrac{0.1013m^3}{C(a/b)^3}$

The required size of transverse stiffeners in a panel also containing longitudinal stiffeners is thus approximately

TABLE 4.1 Limiting Values of γ for Transverse Stiffeners

	One Stiffener		Two Stiffeners		Three Stiffeners		Ten Stiffeners	
a/b Ratio	Timoshenko and Gere (1961)	Eq. 4.45	Timoshenko and Gere (1961)	Eq. 4.45	Timoshenko and Gere (1961)	Eq. 4.45	Eq. 4.42	Eq. 4.45
0.5	12.8	1.30	65.5	65.5	177.0	177.0	4170	4220
0.6	7.25	7.5	37.8	38.0	102.0	122.0	2420	2440
0.8	2.82	3.2	15.8	16.0	43.1	43.2	1020	1030
1.0	1.19	1.6	7.94	8.20	21.9	22.1	522	528
1.2	0.435	0.94	4.43	4.73	12.6	12.8	301	304
$\sqrt{2}$	0	0.57	2.53	2.90	7.44	7.85	185	187

$$\frac{(EI)_s}{b(EI)_c} = \frac{m^3}{\pi^2 C(a/b)^3}\left(1 + \frac{1}{N-1}\right) \tag{4.47}$$

This formula yields essentially the same values as does the formula presented for aluminum panels in the *Alcoa Structural Handbook* (Aluminum Company of America, 1960). With this size of transverse stiffener the strength of the panel is limited to the buckling strength of the longitudinally stiffened panel between transverse stiffeners.

Stiffener Type. The methods of analysis described above are directly applicable to open-section stiffeners having negligible torsional stiffness and are conservative when applied to stiffeners with appreciable torsional stiffness. The influence of torsional stiffness on overall panel buckling has been studied by Kusuda (1959) for the case of one longitudinal or one transverse stiffener. Stiffeners with large torsional rigidity also provide partial or complete fixity of the edges of subpanel plating, thereby increasing their critical stresses.

It has been shown by Lind (1973) and Fukumoto et al. (1977) that the stiffener type affects the buckling mode as well as the ultimate carrying capacity of the stiffened plate. It has also been shown by Tvergaard (1973), and Fok et al. (1977) that local imperfections of stiffeners influence significantly the overall buckling behavior of stiffened plate panels.

Postbuckling Strength. Buckling of a stiffened-plate panel may occur by primary instability with a half wavelength which is on the order of the panel length, or by local instability with a half-wavelength which is on the order of the width of plate elements of the plate and stiffeners. As plate panel length increases, the ultimate stress decreases, until at large slenderness ratio the panel fails in flexure as a long column. The ultimate strength in the long-column range can be predicted by the Euler column formula, where the radius of gyration is computed for the combined section of the stiffener and the effective width of the plating. At an intermediate slenderness ratio there is a transition in the mode of failure from the purely local mode to one dominated by overall panel failure. In the transition zone the panel fails through a combination of the primary buckling and flexural modes and may involve stiffener twisting.

It is well known that plates supported at their edges are often able to sustain compressive load far in excess of their buckling loads. The margin between the buckling load and the ultimate load in plates, known as the postbuckling strength, depends on whether the critical stress is reached below or above the proportional limit of the material. If the buckling stress is well below the proportional limit, the ultimate load may be many times greater than the buckling strength, depending on the aspect ratio, a/b, of the plate element. As the buckling stress approaches the yield strength of the material, the reserve strength in the postbuckling range approaches zero.

Initial buckling modes of stiffened flat panels vary with the slenderness ratio of the panel and with the type of construction: monolithic or built-up. In the following, as a basis for evaluating postbuckling strength, a brief discussion is given regarding predictions of initial buckling stresses and ultimate strength.

Local Instability Mode. The initial buckled form has one transverse sinusoidal half-wave, with perhaps a number of longitudinal half-waves. As the compressive load is increased, the central portion of the transverse half-wave becomes flattened, and, as shown in Fig. 4.21 the transverse deformation is no longer a simple sinusoidal curve. The well-known effective-width approach to the analysis of the postbuckling strength of a flat plate is based on the stress distribution associated with this buckled form, as discussed in detail in Section 4.2.

Another change of buckled form is possible when a rectangular flat plate, simply supported on all sides, is subjected to uniform edge compression and is free to expand laterally. A dynamic snap from one buckled form to another may occur by a sudden change of wavelength of buckles along the direction of compression. The behavior of the flat plate in this sense is analogous to the elastic postbuckling of a column supported laterally by a nonlinear elastic medium (Tsien, 1942; Stein, 1959; Koiter, 1963). A column supported laterally by a finite number of nonlinear elastic restraints buckles initially into m sinusoidal half-waves over its length; then subsequently the buckled form may become unstable, and the column may snap into n half-waves, with n being greater than m. The exact analysis of transition between the two modes of buckling is not known at present. Sherbourne et al. (1971) determined the terminal wavelength for flat plates at the ultimate capacity.

Failure Strength of Very Short Stiffened Panels. For a short stiffened plate with the slenderness ratio smaller than 20, Gerard and Becker (1957/1958) note that the failure stress is independent of the panel length. The average stress at failure in this slenderness range is known as the crippling, crushing, or local-failure stress, and will be represented by $\bar{\sigma}_f$. Gerard and Becker (1957/1958) present a method for determining the crippling stress of short longitudinally

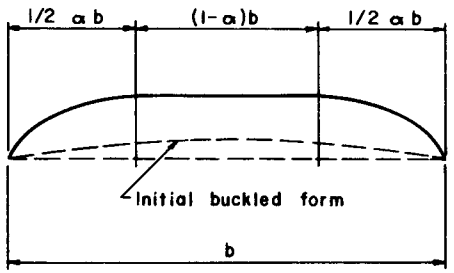

Fig. 4.21 Initial and final buckled shapes.

stiffened panels. However, for most cases, the yield stress of the material can be considered the failure stress for short stiffened panels.

Ultimate Strength of Intermediate and Long Stiffened Panels. Gerard and Becker (1957/1958) describe a method to predict the buckling failure of stiffened panels based on a curve analogous to the Johnson parabola shown in Fig. 4.22. At stresses lower than the local buckling stress σ_c and the proportional limit σ_{pl}, the Euler column equation is used. In the transition range between $L/r = 20$ and the long column, a parabola of the following form is used:

$$\bar{\sigma}_c = \bar{\sigma}_f \left[1 - \frac{\sigma_c}{\sigma_e}\left(1 - \frac{\sigma_c}{\bar{\sigma}_f}\right)\left(\frac{\sigma_{20}^{1/2} - \sigma_e^{1/2}}{\sigma_{20}^{1/2} - \sigma_c^{1/2}}\right)^2 \right] \tag{4.48}$$

where $\bar{\sigma}_c$ is the failure stress, $\sigma_e = \pi^2 E/(L/r)^2$ the Euler stress for the panel, $\bar{\sigma}_f$ the failure stress for a short stiffened panel, and σ_{20} the Euler stress evaluated at $L/r = 20$. Many direct-reading column charts have been prepared for panel ultimate strength. The type of plot is shown in Fig. 4.23. Gerard and Becker (1957/1958) have provided references and examples of this work.

In the determination of panel strength it is necessary to estimate the effective column length of the plate-stiffener combinations as well as the effective width of plating that acts in conjunction with the stiffener. When the critical stress for the individual panel of plating between stiffeners is greater than the critical stress for the stiffened panel, the plating may be assumed completely effective, and the effective column length of the panel is determined by the end conditions. When the critical stress for the individual plating panel is significantly less than that for the stiffened panel as a unit, the ultimate strength of the stiffened plate is considered to be the lesser of (1) the load that causes the stress at the juncture of plate and stiffener to reach the yield strength of the material, or (2) the column strength of the stiffener in conjunction with an effective width of plating that is less than the actual width of plating between stiffeners.

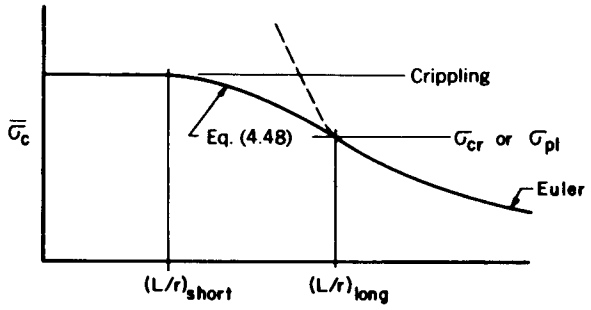

Fig. 4.22 Column curve for stiffened panels.

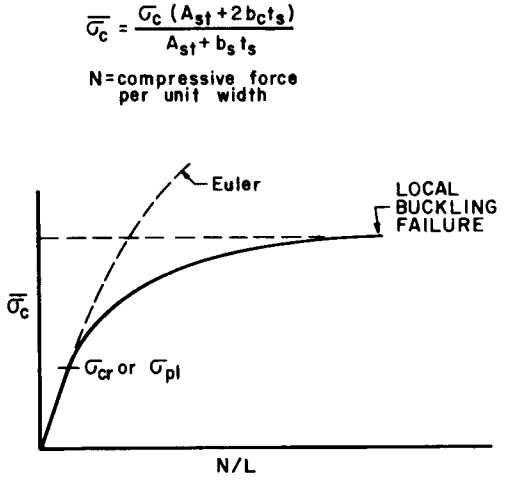

Fig. 4.23 Column chart by Gerard and Becker (1957/1958).

The application of the first criterion for ultimate strength assumes that the stiffener is stiff enough to allow the plate-edge stress to reach the yield stress before the stiffener buckles as a column and that the stress distribution across the buckled plate can be determined, while the second criterion assumes that the effective column length of the stiffener and the effective width of the associated plating can be properly determined and that residual stresses and distortions due to fabrication are properly accounted for with regard to column buckling. The effective-width concept is treated in Section 4.2.

To provide a better understanding of the behavior of stiffened plates, a theoretical study was carried out by Wittrick (1968). The collapse of box-girder bridges in the early 1970s precipitated a great interest in research on various aspects of box girders, especially the interactive buckling of an assembly of plates and the ultimate strength of a stiffened plate. The research efforts in many ways were centered around the Merrison Committee (1973). Murray (1975) reported on analysis and design procedure for the collapse load for the stiffened plates. Crisfield (1975) presented a finite element formulation for the large-deflection elastic–plastic full-range analysis of stiffened plating. A simple approach for the design of stiffened steel compression flanges was proposed by Dwight and Little (1976).

A theoretical and experimental study on the inelastic buckling strength of stiffened plates was reported by Fukumoto et al. (1977). Residual stresses were considered and the stiffened plates treated had relatively low width-to-thickness ratios and with relatively rigid stiffeners. It was found that partial yielding in the flat stiffeners considerably reduced the buckling strength of a stiffened plate. In the case of plates stiffened by T-type stiffeners, the strength reduction due to partial yielding in the stiffeners was much less pronounced. This is

probably due to the fact that the T-stiffeners were more rigid and less susceptible to initial imperfections than were the flat stiffeners. Murray (1973) has indicated that based on experimental results there is often little margin of strength above the load at which yielding first occurs in a stiffener. This phenomenon can lead to a triggering effect which results in a sudden failure of the stiffened plate. Such a viewpoint is also shared by Horne and Narayanan (1977).

Horne and Narayanan (1975, 1977) have proposed a design method for the prediction of collapse loads of stiffened plates subjected to axial compression. They have compared the results obtained from their method, methods proposed by other researchers, and experiments. The results are all close to the observed strength. Horne and Narayanan's method is based on the British Perry–Robertson column formula and consists of analyzing the stiffened plates as a series of isolated columns comprising a stiffener and the associated effective width of plating. The criterion for plate failure is the attainment of yielding stress at the plate stiffener boundary. The criterion for the stiffener-initiated failure is by yielding or by instability of the stiffener.

Little (1976) and Elsharkawi and Walker (1980) have studied the effects of continuity of longitudinal stiffeners on the failure mode and strength of stiffened plates consisting of several bays between cross frames. Little has indicated that there is a tendency for longitudinal continuity to be strengthened where failure occurs in the plate, and weakened where failure occurs in the stiffener. A simplified design method to account for the effects of continuity has been proposed by Elsharkawi and Walker (1980).

Desmond et al. (1981a,b) have presented an experimental study of edge-stiffened compression flanges and intermediately stiffened compression flanges. The compression elements are either adequately stiffened, partially stiffened, or unstiffened. A stiffener requirement that provides the minimum stiffener stiffness to support these compression flanges adequately is presented. The effective-width approach derived from the experiments appears to give satisfactory predictions for the ultimate strength of the members tested. Nguyen and Yu (1982) have reported a study on longitudinally reinforced cold-formed steel beam webs. Based on the experimental results, an effective-width procedure is proposed to predict the ultimate strength of such members subjected to bending. Additional information on this subject matter is presented in Chapters 6 and 7.

4.4.2 Compression and Shear

Buckling Strength

Initial Buckling. Analytical and experimental results on the buckling behavior of stiffened plates under combined compression and shear are relatively scarce. Recourse is therefore usually made to data for unstiffened plates supplemented with whatever data are available for the type of longitudinally stiffened construction considered to be most important in practice, that is, that shown in Fig. 4.24. The case of unstiffened rectangular plates under combined compressive and shear stresses has been presented in Section 4.2.4, which showed that a simple parabolic relationship of the form of Eq. 4.49 was satisfactory for engineering purposes for all ranges of elastic restraint from free rotation to complete fixity. The relationship takes the form

$$R_c + R_s^2 = 1 \tag{4.49}$$

where R_c is the ratio of compressive stress when buckling occurs in combined shear and direct stress to compressive stress when buckling occurs in pure compression and R_s is the ratio of shear stress when buckling occurs in combined shear and direct stress to shear stress when buckling occurs in pure shear.

Johnson (1957) treated the problem of long plates with one and two stiffeners acted on by axial compression and shearing stresses. The stiffeners were assumed to have bending stiffness only and the resulting interaction curves show discontinuities which reflect the mode into which the plate buckles. When the bending stiffness ratio of the stiffener to that of the plate (EI/bD) is low, the buckle goes through the stiffener. However, when the stiffness ratio is increased so that nodal lines occur along the stiffener lengths, buckling takes place without deflection along the stiffeners. In this case another interaction relation exists between compressive and shearing stresses. Another somewhat more limited study of the interaction relationship of infinitely wide stiffened plates under compression and shearing stresses was reported by Harris and Pifko (1969). In this study the finite-element method was used. The stiffeners were assumed to have both bending and torsional stiffness, and the grid refinement used was judged to be adequate to ensure accurate results. The results shown in Fig. 4.25 were compared to the parabolic expression (Eq. 4.49).

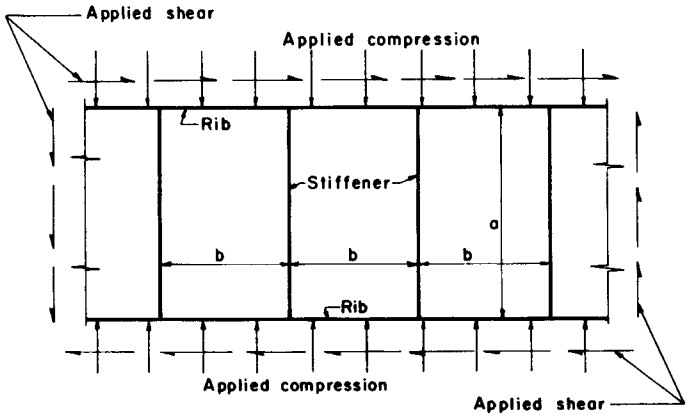

Fig. 4.24 Longitudinally stiffened plate under combined compression and shear stresses.

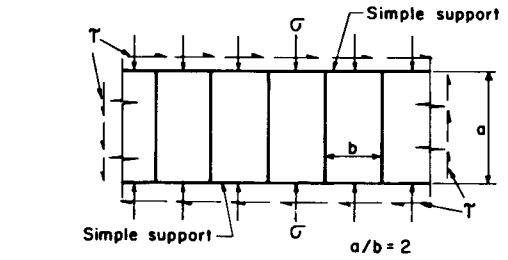

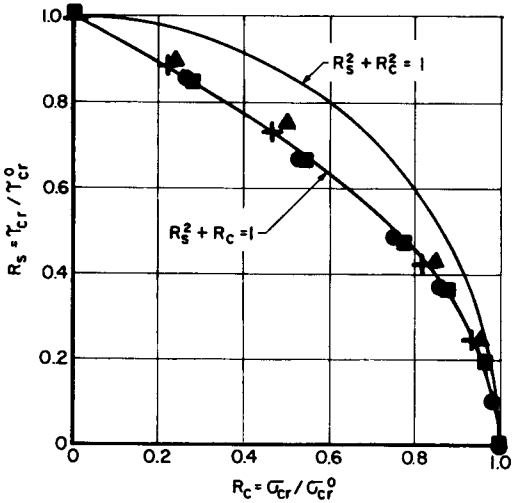

A/bt	EI/bD	CJ/bD	Symbol
0.4	100	0	●
0.4	100	1	+
0.4	100	10^6	▲
0.4	1000	0	■

Fig. 4.25 Analytical interaction relations for infinitely wide stiffened plate under combined compression and shearing stresses.

Except for the case of assumed large torsional stiffness ratio ($GJ/bD = 10^6$) the analytical points follow the parabolic relationship very well.

Buckling in the Inelastic Range. Analytic prediction of the interaction relationship for stiffened panels which buckle in the inelastic range under combined compression and shear are practically nonexistent in the literature. One such computation reported by Harris and Pifko (1969) was made for an integrally stiffened panel made of aluminum 2024-T351 and having the dimensions shown in Fig. 4.26. The predicted interaction curves are shown in this figure for both the elastic case, which agrees very well with the parabolic relationship

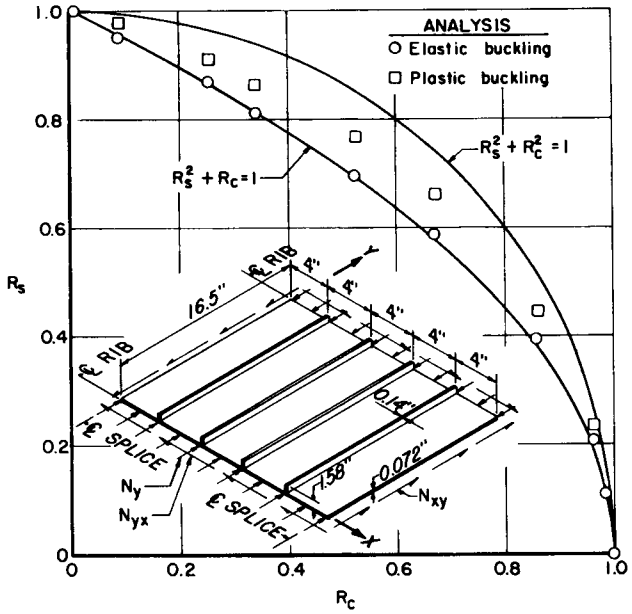

Fig. 4.26 Analytically predicted elastic and inelastic interaction curves for an integrally stiffened panel.

(Eq. 4.49), and the inelastic-buckling case. Because of the limited nature of the data, no general relationship for the inelastic-buckling case can be derived. However, it should be noted from Fig. 4.26 that the circular relationship lies above the analytical curve of the inelastic-buckling case.

Postbuckling Strength. Postbuckling behavior is complex, and exact treatment of the problem has not yet been achieved. Because of the importance of predicting the strength of stiffened panels loaded beyond initial buckling in the aircraft industry semiempirical methods have been in existence for many years. In the case of light stiffened plates under combined compression and shear, the structure will usually take a considerable load in excess of the initial buckling load of the plate. Chapter 6 covers the design aspects of using these postbuckling or tension-field theories; hence no discussion of these methods is made here.

4.5 BUCKLING OF ORTHOTROPIC PLATES

Problems related to rectangular plates with stiffeners parallel to one or both pairs of sides can be solved approximately by methods applicable to orthotro-

pic plate theory. An orthotropic plate is one whose material properties are orthogonally aniostropic; a uniformly stiffened plate is reduced to this case by effectively "smearing' the stiffness characteristics of its stiffeners over the domain of the plate. Clearly, the theory is best applicable when the spacing of the stiffeners is small.

The calculation of buckling strength of orthotropic plates is based on the solution of the following differential equation governing the small deflection $w(x, y)$ of the buckled plate:

$$D_1\frac{\partial^4 w}{\partial x^4}+2D_3\frac{\partial^4 w}{\partial x^2\partial y^2}+D_2\frac{\partial^4 w}{\partial y^4}+N_x\frac{\partial^2 w}{\partial x^2}+N_y\frac{\partial^2 w}{\partial y^2}+2N_{xy}\frac{\partial^2 w}{\partial x\partial y}=0 \qquad (4.50)$$

where

$$D_1=\frac{(EI)_x}{1-\nu_x\nu_y}$$

$$D_2=\frac{(EI)_y}{1-\nu_x\nu_y}$$

$$D_3=\tfrac{1}{2}(\nu_y D_1+\nu_x D_2)+2(GI)_{xy}$$

in which N_x, N_y, and N_{xy} are in-plane forces per unit width (Fig. 4.27), $(EI)_x$ and $(EI)_y$ are flexural stiffnesses, per unit width, of beam strips in the x and y directions, respectively; ν_x and ν_y are flexural Poisson ratios; and $2(GI)_{xy}$ is a measure of torsional stiffness.

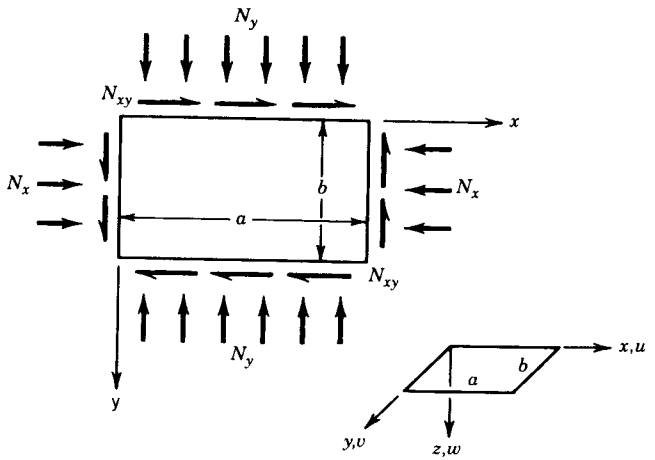

Fig. 4.27 Plate subjected to axial and shear stress.

Theoretical buckling data for several cases of rectangular plates with supported edges ($w=0$), under uniform in-plane loadings, N_x, N_y, and N_{xy}, applied singly or in certain combinations, are presented. The following are some of the additional notations that will be employed: a and b are the lengths of plate in x and y directions, respectively (see Fig. 4.27); m(integer) is the number of buckles or half-waves in the x-direction when the buckle pattern is sinusoidal in that direction; and n(integer) is the number of buckles or half-waves in the y-direction when the buckle pattern is sinusoidal in the y-direction.

Case I. Uniaxial Compression in x-Direction, Loaded Edges Simply Supported, Unloaded Edges Elastically Restrained Against Rotation. In this case, referring to Fig. 4.27, N_x is the only loading, the edges $x=0$, a are simply supported, and the edges $y=0$, b are each elastically restrained against rotation by a restraining medium whose stiffness (moment per unit length per radian of rotation) is K. The quantity Kb/D_2 to be denoted by ϵ, will be used as a dimensionless measure of this stiffness. An exact solution for this case leads to the following formula defining the value of N_x that can sustain a buckle pattern containing m sinusoidal half-waves in the x-direction:

$$\frac{N_x b^2}{\pi^2 D_3}=\left(\frac{b}{a/m}\right)^2\frac{D_1}{D_3}+2+f_1\left(\epsilon,\left(\frac{a/m}{b}\right)^2\frac{D_2}{D_3}\right) \qquad (4.51)$$

where f_1 is the function plotted in Fig. 4.28. If $(a/mb)^2(D_2/D_3)>0.4$, Eq. 4.51 can be very closely approximated by the formula

$$\frac{N_x b^2}{\pi^2 D_3}=\left(\frac{b}{a/m}\right)^2\frac{D_1}{D_3}+2+f_2(\epsilon)+\left(\frac{a/m}{b}\right)^2\frac{D_2}{D_3}f_3(\epsilon) \qquad (4.52)$$

where f_2 and f_3 are the functions plotted in Fig. 4.29. The buckling load is the smallest N_x obtained by substituting different integer values of m ($m=1,2,3,\ldots$) into Eq. 4.51 or, if it applies, Eq. 4.52. In performing this minimization, one should take into account the fact that for most practical restraining media the stiffness K is not fixed but is a function of the half-wavelength a/m of the edge rotation. K may also depend on the axial load in the restraining medium, therefore on N_x, necessitating a trial-and-error calculation to determine N_x for any selected m. Negative values of K are physically possible but are excluded from consideration in Figs. 4.28 and 4.29. Unequal restraints along the edges $y=0$ and b can be handled approximately by first assuming the $y=0$ constraint to be present at both edges, then the $y=b$ constraint, and averaging the two values of N_x thus obtained.

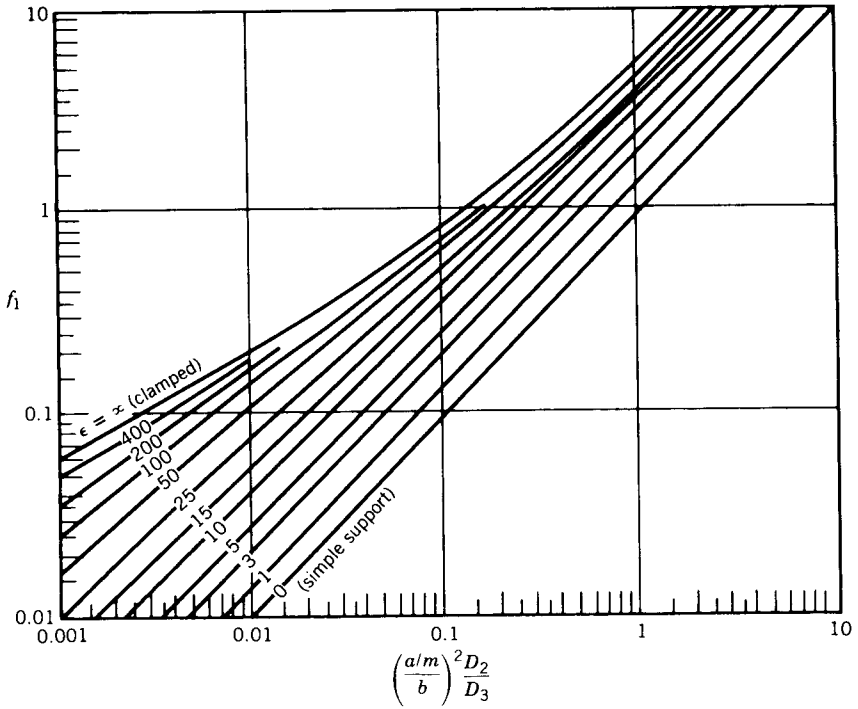

Fig. 4.28 Function f_1 in Eq. 4.51.

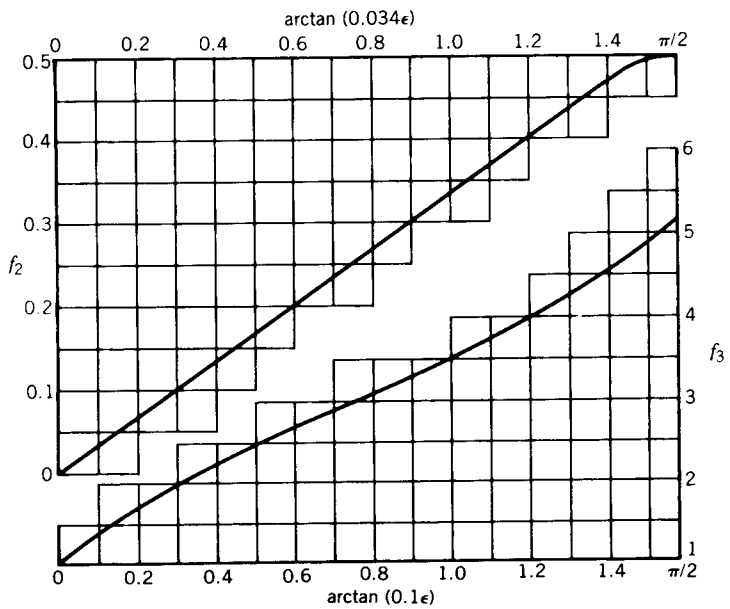

Fig. 4.29 Functions f_2 and f_3 in Eq. 4.52.

Case II. Biaxial Compression, All Edges Simply Supported. When all four edges are simply supported, combinations of N_x and N_y that can sustain a buckle pattern of m sinusoidal half-waves in the x-direction and n sinusoidal half-waves in the y-direction are defined exactly by the interaction equation

$$\frac{1}{n^2}\frac{N_x b^2}{\pi^2 D_3} + \frac{1}{m^2}\frac{N_y a^2}{\pi^2 D_3} = \left(\frac{b/n}{a/m}\right)^2 \frac{D_1}{D_3} + 2 + \left(\frac{a/m}{b/n}\right)^2 \frac{D_2}{D_3} \tag{4.53}$$

In using Eq. 4.53, one must substitute different combinations of m and n until that combination is found which minimizes N_x for a given N_y, N_y for a given N_x, or N_x and N_y simultaneously for a given ratio between them. It can be shown (Libove, 1983) that these minima will occur with at least one of the two integers equal to unity. Therefore, only the combinations $m = 1$; $n = 1, 2, 3, \ldots$ and $n = 1$; $m = 2, 3, \ldots$ need to be tried. The condition

$$\frac{N_y b^2}{\pi^2 D_2} < 1 \tag{4.54}$$

is sufficient to ensure that $n = 1$ will govern. In that case, with N_y regarded as given, Wittrick (1952) has shown that the N_x required for buckling is defined by

$$\frac{N_x b^2}{\pi^2 D_3} = 2 + (k-2)\left[\frac{D_1 D_2}{D_3^2}\left(1 - \frac{N_y b^2}{\pi^2 D_2}\right)\right]^{1/2} \tag{4.55}$$

where k is the function plotted as curve (a) in Fig. 4.30. The case of the infinitely long plate ($a/b = \infty$) is of interest as the limiting case of a very long plate. For that case it can be deduced from Eq. 4.53 that if $N_x b^2/\pi^2 D_3 \leqslant 2$, the longitudinal compression N_x is too small to sustain a multi-lobed buckle pattern, and the plate will buckle in a cylindrical mode (i.e., as a wide plate-column of length b) when $N_y b^2/\pi^2 D_2 = 1$. On the other hand, if $N_x b^2/\pi^2 D_3 > 2$, the buckle pattern will be sinusoidally lobed in the x-direction with a half-wave length-to-width ratio of

$$\frac{a/m}{b} = \left[\frac{D_2}{D_1}\left(1 - \frac{N_y b^2}{\pi^2 D_2}\right)\right]^{-1/4} \tag{4.56}$$

and the buckling will occur when N_x and N_y satisfy Eq. 4.55 with k set equal to 4. The interaction curve of Fig. 4.31 summarizes the results just given for the case $a/b = \infty$.

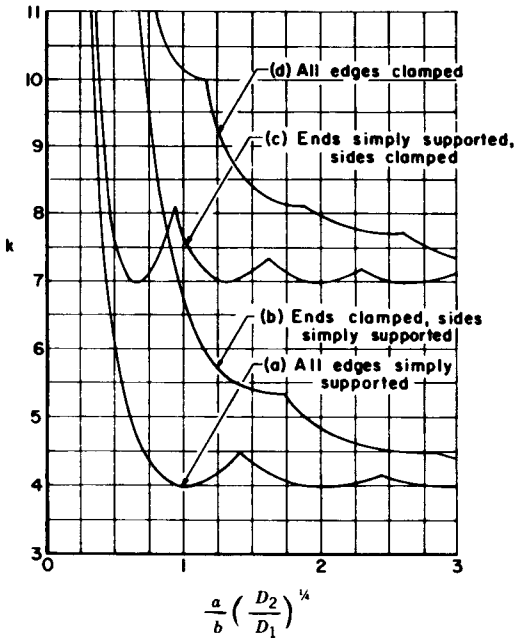

Fig. 4.30 Buckling coefficients for orthotropic plates.

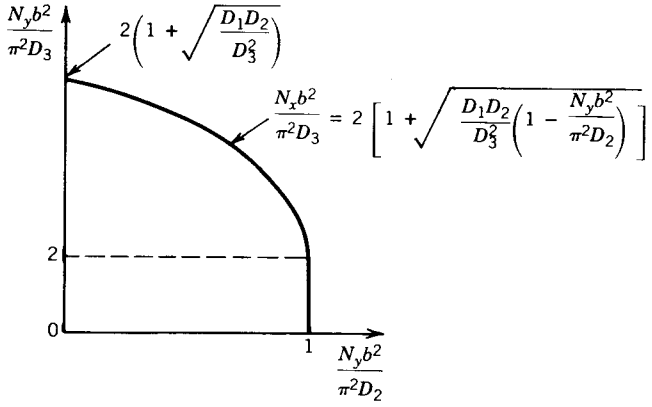

Fig. 4.31 Interaction curve for orthotropic plates.

Case III. Compression in x-Direction Applied to Clamped Edges, Limited Compression in y-Direction Applied to Simply Supported Edges. Referring to Fig. 4.27, and considering the case in which the edges $x = 0$, a are clamped, the edges $y = 0$, b are simply supported, N_{xy} is absent, and N_y satisfies the inequality (Eq. 4.54). Then, with N_y regarded as given, the value of N_x required to cause buckling is defined by Eq. 4.55 with k taken from curve (b) of Fig. 4.30 (Wittrick, 1952).

Case IV. Uniaxial Compression, Loaded Edges Simply Supported, Unloaded Edges Clamped. Here N_x is the only loading, the edges $x = 0$ and a are simply supported, and the other two edges are clamped. The exact solution for this case is contained in the subcase $\epsilon = \infty$ of case I. An approximate solution is given by Wittrick (1952) in the form

$$\frac{N_x b^2}{\pi^2 \sqrt{D_1 D_2}} = k - c\left(1 - \frac{D_3}{\sqrt{D_1 D_2}}\right) \tag{4.57}$$

where $c = 2.4$ and k is taken from curve (c) of Fig. 4.30. Equation 4.57 is virtually equivalent to Eq. 4.52 and must therefore be subject to the same restriction, [i.e., $(a/mb)^2(D_2/D_3) > 0.4$].

Case V. Uniaxial Compression, All Edges Clamped. Wittrick (1952) gives an approximate solution for this case in the form of Eq. 4.57 with $c = 2.46$ and k taken from curve (d) of Fig. 4.30.

Case VI. Shear, Various Boundary Conditions. Theoretical data for the shear flow N_{xy} required to cause buckling of rectangular orthotropic plates have been collected by Johns (1971). Three of his graphs are reproduced in Fig. 4.32. They apply, respectively, to the boundary conditions of (a) all edges simply supported; (b) edges $y = 0$ and $y = b$ simply supported, the other two edges clamped; and (c) all edges clamped. In Fig. 4.32, k_s stands for $N_{xy}b^2/\pi^2 D_1^{1/4} D_2^{3/4}$.

To make use of the buckling data presented above, one must of course, know the values of the elastic constants appearing in Eq. 4.50. These constants are best determined experimentally, by tests such as those described by Libove and Batdorf (1948) and Becker and Gerard (1963). If the plates are of a simple enough construction, the constants can also be evaluated theoretically. For example, for a sheet of thickness t and shear modulus G orthogonally stiffened by x-wise stiffeners of torsional stiffness C_1 spaced a distance b_1 apart, and y-wise stiffeners of torsional stiffness C_2 spaced a distance a_1 apart, $(EI)_x$ may be taken as the flexural stiffness of the composite beam consisting of one x-wise stiffener and its associated width b_1 of sheet, divided by b_1, while $(EI)_y$ is computed in an analogous manner using a y-wise stiffener and its associated width a_1 of sheet. For such plates, ν_x and ν_y may usually be taken as zero with little error, and then

$$D_3 = 2(GI)_{xy} = \frac{Gt^3}{6} + \frac{1}{2}\left(\frac{C_1}{b_1} + \frac{C_2}{a_1}\right) \tag{4.58}$$

(The factor $\frac{1}{2}$ in this formula is sometimes erroneously omitted.) Plates with integral wafflelike stiffening may also be modified as orthotropic plates,

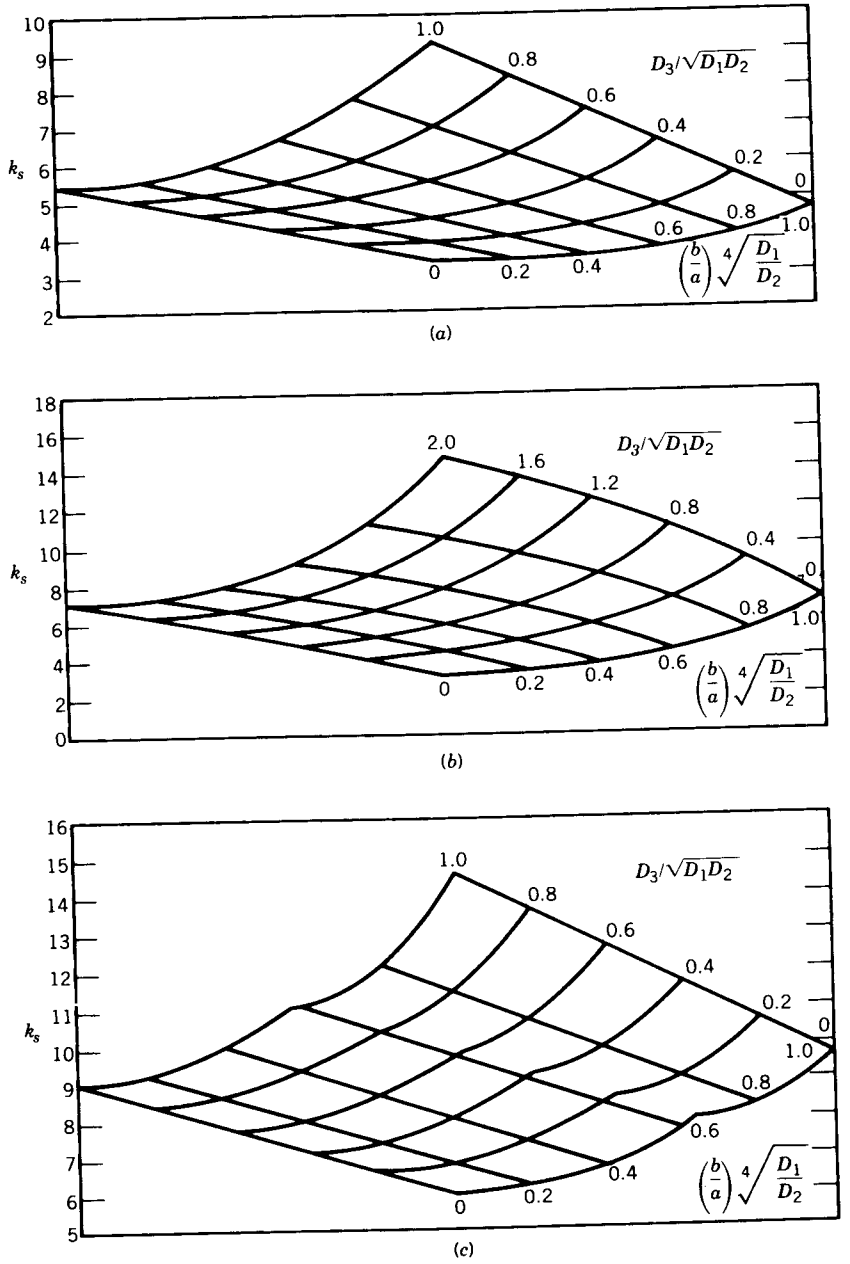

Fig. 4.32 Shear buckling coefficients for orthotropic plates. [Adapted from Johns (1971), printed with the permission of Her Majesty's Stationery Office.]

provided that the ribbings are so oriented as to create axes of elastic symmetry parallel to the plate edges; formulas for estimating the elastic constants of such plates are derived by Dow et al. (1954). Corrugated-core sandwich plates with the corrugations parallel to the x or y axis can similarly be treated as orthotropic plates, and formulas for their elastic constants are developed by Libove and Hubka (1951); however, for such sandwich plates, deflections due to transverse shear, neglected in the present discussion, may sometimes be important. It is common practice to treat a corrugated plate also as an orthotropic plate, and the appropriate elastic constants when the profile of the plate is sinusoidal are discussed by Lau (1981). However, there are indications (Perel and Libove, 1978) that modelling the corrugated plate as an orthotropic plate may lead to an underestimate of its shear buckling strength.

The orthotropic plate model has an additional shortcoming when applied to stiffened plates, namely its neglect of any coupling between in-plane forces and out-of-plane deflections. That is, underlying Eq. 4.50 is the tacit assumption that there exists a reference plane in which the forces N_x, N_y, and N_{xy} can be applied without producing any curvatures or twist. In the case of a sheet with identical stiffening on both sides, there does of course exist such a plane—it is the middle surface of the sheet. If the stiffening is one-sided, however, it is usually not possible to find a reference plane that will eliminate completely the coupling between in-plane forces and out-of-plane deflections. It has been shown (Whitney and Leissa, 1969; Jones, 1975) that such coupling, occurring in the context of composite laminated plates, can have a marked effect on the buckling loads. Therefore, it is very likely that in metal plates with one-sided stiffening it can also have a marked effect on the buckling loads. A thorough investigation of this effect, using an appropriately generalized orthotropic plate theory, would be a worthwhile subject for future research.

Finally, orthotropic plate theory is incapable of modeling local buckling, that is, buckling in which the buckle wavelengths are of the same order as the stiffener spacings or the widths of the plate elements of which the stiffeners are composed. Wittrick and Horsington (1984) have developed more refined approaches that can account for local buckling and modes of buckling in which local and overall deformations appear in conjunction. Their methods are applicable to plates with unidirectional stiffening possessing certain boundary conditions and subjected to combinations of shear and biaxial compression.

4.6 LATERALLY LOADED PLATES IN COMPRESSION

Plates with stiffeners in the direction of the axial load that are also subjected to a distributed lateral load are commonly encountered as the bottom plates in ships. A study based on a large-deflection postbuckling theory (Supple, 1980) shows that lateral pressure produces effects similar to initial geometric imper-

fections with a long buckling wavelength. It is shown that a sufficiently high pressure induces stable postbuckling in the long-wave mode.

The stiffened plating is supported on heavy transverse structural members which may be assumed to be rigid. The panels have width-to-length ratios of about 2.5 to 4.0, and there is essentially no interaction in the transverse direction and thus the panel undergoes cylindrical bending. It behaves as if it were a wide beam-column under axial and lateral loads. It is convenient to isolate one longitudinal stiffener together with a plate of the width equal to the spacing of the stiffeners, b, and to consider that all other stiffeners behave in a similar manner. Such a beam-column is shown in Fig. 4.33.

Ultimate-strength analysis, that is, the determination of the maximum values of the lateral and axial loads that can be sustained by the member, requires a consideration of:

1. The yield strength of plate and stiffener materials
2. Large-deflection theory
3. Partial plastification of the section
4. Postbuckling and post-ultimate-strength behavior of the plate

The complexity of the problem, in particular, consideration of items 2, 3, and 4 suggests that numerical methods be used. Some solutions have been obtained for standard wide-flange shapes by Ketter (1962), and Lu and Kamalvand (1968) in the form of interaction curves between the axial and lateral loads. Unfortunately, these results cannot be used for plating since items 1 and 4 were not considered. Another complication is that the wide-flange sections are doubly symmetrical, whereas the section shown in Fig. 4.33 is singly symmetrical with a very large top flange.

This means, for example, that although it was possible to nondimensionalize the results for wide-flange sections in terms of L/r and make them applicable

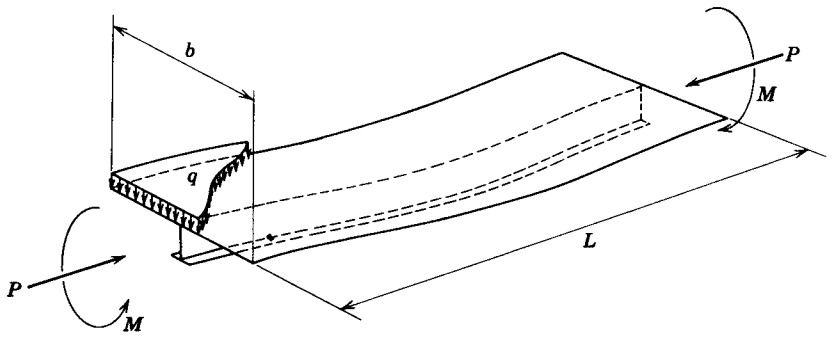

Fig. 4.33 Idealized beam-column.

with a very small error to any wide-flange section, the unsymmetrical section of the stiffened panel must be treated as a special case for every combination of relative proportions.

Nomographs for the ultimate strengths of stiffened plates with a yield point of 47 ksi and the ranges of geometrical and loading parameters commonly encountered in ship structures are given by Vojta and Ostapenko (1967).

REFERENCES

AA (1994), *Aluminum Design Manual*, Aluminum Association, Washington, D.C.

Abdel-Sayed, G. (1969), "Effective Width of Thin Plates in Compression," *ASCE J. Struct. Div.*, Vol. 95, No. ST10, pp. 2183–2204.

AISC (1993), *Load and Resistance Factor Design for Structural Steel Buildings*, American Institute of Steel Construction, Chicago.

AISI (1996), *Specification for the Design of Cold-Formed Steel Structural Members*, American Iron and Steel Institute, Washington, D.C.

Allen, H. G., and Bulson, P. S. (1980), *Background to Buckling*, McGraw-Hill, Maidenhead, Berkshire, England.

Aluminum Company of America (1960), *Alcoa Structural Handbook* (also *Handbook of Design Stresses for Aluminum*), Alcoa, Pittsburgh, Pa.

Azhari, M., and Bradford, M. A. (1993), "Inelastic Initial Load Buckling of Plates with and Without Residual Stresses," *J. Eng. Struct.*, Vol. 15, No. 1, 1993, pp. 31–39.

Batdorf, S. B., and Houbolt, J. C. (1946), "Critical Combinations of Shear and Transverse Direct Stress for an Infinitely Long Flat Plate with Edges Elastically Restrained Against Rotation," *NACA Rep. No. 847.*

Batforf, S. B., and Stein, M. (1947), "Critical Combinations of Shear and Direct Stress for Simply Supported Rectangular Flat Plates," *NACA Tech. Note No. 1223.*

Becker, H., and Gerard, G. (1963), "Measurement of Torsional Rigidity of Stiffened Plates," *NASA Tech. Note No. D-2007.*

Benthem, J. P. (1959), "The Reduction in Stiffness of Combinations of Rectangular Plates in Compression After Exceeding the Buckling Load," *NLL-TR S-539.*

Bergman, S., and Reissner, H. (1932), "Über die Knickung von rechteckigen Platten bei Schubbeanspruchung," *Z. Flugtech Motorluftschiffahrt*, Vol. 23, p. 6.

Bijlaard, P. P. (1949), "Theory and Tests on Plastic Stability of Plates and Shells," *J. Aeronaut. Sci.*, Vol. 16, pp. 529–541.

Bijlaard, P. P. (1950), "On the Plastic Buckling of Plates," *J. Aeronaut. Sci.*, Vol. 17, p. 493.

Bijlaard, P. P. (1957), "Buckling of Plates Under Nonhomogeneous Stress," *ASCE J. Eng. Mech. Div.*, Vol. 83, No. EM3, Proc. Paper 1293.

Bijlaard, P. P., and Fisher, G. P. (1952), "Column Strength of H Sections and Square Tubes, in Post Buckling Range of Component Plates," *NACA Tech. Note No. 2994.*

Bleich, F. (1952), *Buckling Strength of Metal Structures*, McGraw-Hill, New York.

Bleich, F., and Ramsey, L. B. (1951), *A Design Manual on the Buckling Strength of Metal Structures*, Society of Naval Architects, Washington, D.C.

Brockenbrough, R. L., and Johnston, B. G. (1974), *U.S. Steel Design Manual*, 2nd ed., U.S. Steel Corporation, Pittsburgh, Pa.

Brown, C. J. (1990), "Elastic Buckling of Perforated Plates Subjected to Concentrated Loads," *J. Comput. Struct.*, Vol. 36, No. 6, pp. 1103–1109.

Bryan, G. H. (1891), "On the Stability of a Plane Plate Under Thrusts in Its Own Plane, with Applications to the 'Buckling' of the Sides of a Ship," *Proc. London Math. Soc.*, Vol. 22.

Bulson, P. S. (1970), *Stability of Flat Plates*, American Elsevier, New York.

Cherry, S. (1960), "The Stability of Beams with Buckled Compression Flanges," *Struct. Eng.*, Vol. 38, No. 9.

Chwalla, E. (1936a), "Beitrag zur Stabilitätstheorie des Stegbleches vollwandiger Träger," *Stahlbau*, Vol. 9, p. 81.

Chwalla, E. (1936b), "Die Bemessung der waagerecht ausgesteiften Stegbleche vollwandiger Träger," *Prelim Publ. IABSE, 2nd Cong.*, Berlin-Munich, p. 957.

Clark, J. W., and Rolf, R. L. (1966), "Buckling of Aluminum Columns, Plates and Beams," *ASCE J. Struct. Div.*, Vol. 92, No. ST3, pp. 17–38.

Conley, W. F., Becker, L. A., and Allnutt, R. B. (1963), "Buckling and Ultimate Strength of Plating Loaded in Edge Compression: Progress Report 2. Unstiffened Panels," *David Taylor Model Basin Rep. No. 1682.*

Cook, I. T., and Rockey, K. C. (1963), "Shear Buckling of Rectangular Plates with Mixed Boundary Conditions," *Aeronaut. Q.*, Vol. 14.

CRCJ (Column Research Committee of Japan) (1971), *Handbook of Structural Stability*, Corona Publishing Co., Tokyo.

Crisfield, M. A. (1975), "Full Range Analysis of Steel Plates and Stiffened Plating Under Uniaxial Compression," *Proc. Inst. Civ. Eng.*, Part 2, pp. 1249–1255.

CSA (1974, 1984), *Cold Formed Steel Structural Members*, CSA Standard S136, Canadian Standards Association, Rexdale, Ontario, Canada.

CSA (1983), *Strength Design in Aluminum*, CAN3-S157-M83, Canadian Standards Association, Rexdale, Ontario, Canada.

Dawe, J. L., and Kulak, G. L. (1984), "Local Buckling of W-Shaped Columns and Beams," *ASCE J. Struct. Eng.*, Vol. 110, No. 6, pp. 1292–1304.

Dawe, J. L., and Kulak, G. L. (1986), "Local Buckling of Beam-Columns," *ASCE J. Struct. Eng.*, Vol. 112, No. 11, pp. 2447–2461.

Dawson, R. G., and Walker, A. C. (1972), "Post-buckling of Geometrically Imperfect Plates," *ASCE J. Struct. Div.*, Vol. 98, No. ST1, pp. 75–94.

Desmond, T. P., Peköz, T., and Winter, G. (1981a), "Edge Stiffeners for Thin-Walled Members," *ASCE J. Struct. Div.*, Vol. 107, No. ST2, Proc. Pap. 16056, pp. 329–354.

Desmond, T. P., Peköz, T., and Winter, G. (1981b), "Intermediate Stiffeners for Thin Walled Members," *ASCE J. Struct. Div.*, Vol. 107, No. ST4, Proc. Pap. 16194, pp. 627–648.

DeWolfe, J. T., Peköz, T., and Winter, G. (1974), "Local and Overall Buckling of Cold Formed Members," *ASCE J. Struct. Div.*, Vol. 100, No. ST10, pp. 2017–2306.

Dow, N. F., Libove, C., and Hubka, R. E. (1954), "Formulas for the Elastic Constants of Plates with Integral Waffle-like Stiffening," *NACA Rep. No. 1195.*

Dwight, J. B. (1971), "Collapse of Steel Compression Panels," *Proc. Conf. Dev. Bridge Des. Constr.*, Crosby Lockwood, London.

Dwight, J. B., and Little, G. H. (1976), "Stiffened Steel Compression Flanges, a Simpler Approach," *Struct. Eng.*, Vol. 54, No. 12, pp. 501–509.

Dwight, J. B., and Moxham, K. E. (1969), "Welded Steel Plates in Compression," *Struct. Eng.*, Vol. 47, No. 2.

Dwight, J. B., and Ratcliffe, A. T. (1968), "The Strength of Thin Plates in Compression," in *Thin-Walled Steel Structures* (ed. K. C. Rockey and H. V. Hill), Crosby Lockwood, London.

Elangovan, P. T., and Prinsze, M. (1992), "Critical Shear Stress of Flat Rectangular Plates with Free Edges," *J. Thin-Walled Struct.*, Vol. 13, No. 5, pp. 409–425.

Elsharkawi, K., and Walker, A. C. (1980), "Buckling of Multibay Stiffened Plate Panels," *ASCE J. Struct. Div.*, Vol. 106, No. ST8, pp. 1695–1716.

Fok, W. C., Walker, A. C., and Rhodes, J. (1977), "Buckling of Locally Imperfect Stiffeners in Plates," *ASCE J. Eng. Mech. Div.*, Vol. 103, No. EM5, pp. 895–911.

Fujita, Y., Yoshida, K., and Arai, H. (1970), "Instability of Plates with Holes," 3rd Rep., *J. Soc. Nav. Archit. Jpn.*, Vol. 127, pp. 161–169.

Fukumoto, Y., and Kubo, M. (1982), "Buckling in Steel U Shaped Beams," *ASCE J. Struc. Div.*, Vol. 108, No. ST5, pp. 1174–1190.

Fukomoto, Y., Usami, T., and Yamaguchi, K. (1977), "Inelastic Buckling Strength of Stiffened Plates in Compression," *IABSE Period.* 3/1977, *IABSE Proc.* p-8/77, pp. 1–15.

Gerard, G., and Becker, H. (1957/1958), "Handbook of Structural Stability," six parts, *NACA Tech. Notes Nos. 3781–3786.*

Graves-Smith, T. R. (1968), "The Postbuckled Behavior of Thin Walled Columns," *8th Cong. IABSE*, New York, pp. 311–320.

Graves-Smith, T. R. (1969), "The Ultimate Strength of Locally Buckled Columns of Arbitrary Length," in *Thin-Walled Steel Structures* (ed. K. C. Rockey and H. V. Hill), Crosby Lockwood, London.

Graves-Smith, T. R., and Sridharan, S. (1978), "A Finite Strip Method for the Buckling of Plate Structures Under Arbitrary Loading," *Int. J. Mech. Sci.*, Vol. 20, pp. 685–693.

Graves-Smith, T. R., and Sridharan, S. (1980), "The Local Collapse of Elastic Thin-Walled Columns," *J. Struct. Mech.*, Vol. 13, No. 4, pp. 471–489.

Grosskurth, J. F., White, R. N., and Gallagher, R. H. (1976), "Shear Buckling of Square Perforated Plates," *ASCE J. Eng. Mech. Div.*, Vol. 102, No. EM6, Proc. Pap. 12641, pp. 1025–1040.

Hancock, G. J. (1980), "Design Methods for Thin-Walled Box Columns," *Rep. No. 359*, University of Sydney, Sydney, Australia.

Hancock, G. J. (1981), "Interaction Buckling of I-Section Columns," *ASCE J. Struct. Div.*, Vol. 107, No. ST1, pp. 165–181.

Harris, H. G., and Pifko, A. B. (1969), "Elastic-Plastic Buckling of Stiffened Rectangular Plates," *Proc. Symp. Appl. Finite Elem. Methods Div. Eng.*, Vanderbilt University, Nashville, Tenn., Nov.

Horne, M. R., and Narayanan, R. (1975), "An Approximate Method for the Design of Stiffened Steel Compression Panels," *Proc. Inst. Civ. Eng.*, Part 2, Vol. 59, pp. 501–514.

Horne, M. R., and Narayanan, R. (1977), "Design of Axially Loaded Stiffened Plates," *ASCE J. Struct. Div.*, Vol. 103, No. ST11, pp. 2243–2257.

Iguchi, S. (1938), "Die Knickung der rechteckigen Platte durch Schubkräfte," *Ing. Arch.*, Vol. 9, p. 1.

Inoue, T., and Kato, B. (1993), "Analysis of Plastic Buckling of Steel Plates," *Int. J. Solids Struct.*, Vol. 30, No. 6, pp. 835–856.

Isami, T., and Hidenori, K. (1990), "New Strength Prediction Method for Biaxially Compressed Plates," *Proc. 39th Jpn. Nat. Congr. Appl. Mech. Theor. Appl. Mech.*, Vol. 39, University of Tokyo Press, Tokyo, pp. 109–118.

Johns, D. J. (1971), "Shear Buckling of Isotropic and Orthotropic Plates: A Review," *Tech. Rep. R&M No. 3677*, British Aeronautical Research Council, London.

Johnson, A. E., Jr. (1957), "Charts Relating the Compressive and Shear Buckling Stress of Longitudinally Supported Plates to the Effective Deflectional Stiffness," *NACA Tech. Note No. 4188.*

Johnson, A. L., and Winter, G. (1966), "Behavior of Stainless Steel Columns and Beams," *ASCE J. Struct. Div.*, Vol. 92, No. ST5, p. 97.

Jombock, J. R., and Clark, J. W. (1962), "Postbuckling Behavior of Flat Plates," *Trans. Am. Soc. Civ. Eng.*, Vol. 127, Part I, pp. 227–240.

Jombock, J. R., and Clark, J. W. (1968), "Bending Strength of Aluminum Formed Sheet Members," *ASCE J. Struct. Div.*, Vol. 94, No. ST2, pp. 511–528.

Jones, R. M. (1975), *Mechanics of Composite Materials*, Scripta, Silver Spring, Md., pp. 264–267.

Kalyanaraman, V., and Peköz, T. (1978), "Analytical Study of Unstiffened Elements," *ASCE J. Struct. Div.*, Vol. 104, No. ST9, pp. 1507–1524.

Kalyanaraman, V., Peköz, T., and Winter, G. (1977), "Unstiffened Compression Elements," *ASCE J. Struct. Div.*, Vol. 103, No. ST9, pp. 1833–1848.

Kawai, T., and Ohtsubo, H. (1968), "A Method of Solution for the Complicated Buckling Problems of Elastic Plates with Combined Use of Raleigh–Ritz Procedure in the Finite Element Method," *Proc. 2nd Air Force Conf. Matrix Methods Struct. Mech.*, Oct.

Kemp, A. R. (1996), "Inelastic Local and Lateral Buckling in Design Codes," *ASCE J. Struct. Eng.*, Vol. 122, No. 4, pp. 374–382.

Ketter, R. L. (1962), "Further Studies on the Strength of Beam-Columns," *Trans. ASCE*, Vol. 127, No. 2, p. 224.

Klitchieff, J. M. (1949), "On the Stability of Plates Reinforced by Ribs," *J. Appl. Mech.*, Vol. 16, No. 1.

Klöppel, K., Schmied, R., and Schubert, J. (1969), "Ultimate Strength of Thin Walled Box Shaped Columns Under Concentric and Eccentric Loads: Post Buckling Behavior of Plate Elements and Large Deformations Are Considered," *Stahlbau*, Vol. 38, pp. 9–19, 73–83.

Koiter, W. T. (1963), "Introduction to the Post-buckling Behavior of Flat Plates," *Int. Colloq. Comportement Posteritiques Plaques Utilisée Constr. Metall.*, Institute of Civil Engineering, Liege, Belgium.

Kroll, W. D., Fisher, G. P., and Heimerl, G. J. (1943), "Charts for the Calculation of the Critical Stress for Local Instability of Columns with I, Z, Channel and Rectangular Tube Sections," *NACA Wartime Rep. No. L-429.*

Kuhlmann, U. (1989), "Definition of Flange Slenderness Limits on the Basis of Rotation Capacity Values," *J. Constr. Steel Res.*, Vol. 14, No. 1, pp. 21–40.

Kumai, T. (1952), "Elastic Stability of a Square Plate with a Central Circular Hole Under Edge Thrust," *Rep. Inst. Appl. Mech. Kyusyn Univ.*, Vol. 1, No. 2, p. 1.

Kusuda, T. (1959), "Buckling of Stiffened Panels in Elastic and Strain-Hardening Range," *Rep. No. 39*, Transportation Technical Research Institute (Unyn-Gijutsu Kenkyrijo Mejiro, Toshima-Ku), Tokyo.

LaBoube, R. A., and Yu, W. W. (1982), "Bending Strength of Webs of Cold-Formed Steel Beams," *ASCE J. Struct. Div.*, Vol. 108, No. ST7, pp. 1589–1604.

Lau, J. H. (1981), "Stiffness of Corrugated Plate," *ASCE J. Eng. Mech. Div.*, Vol. 17, No. EM1, pp. 271–275.

Lau, S. C. W., and Hancock, G. J. (1989), "Inelastic Buckling Analysis of Beams, Columns and Plates Using the Spline Finite Strip Method," *J. Thin-Walled Struct.*, Vol. 7, No. 3–4, pp. 213–238.

Lay, M. G. (1965), "Flange Local Buckling in Wide-Flange Shapes," *ASCE J. Struct. Div.*, Vol. 91, No. ST6, pp. 49–66.

Legget, D. M. A. (1941), "The Buckling of a Square Panel in Shear When One Pair of Opposite Edges Is Clamped and the Other Pair Simply Supported," *Tech. Rep. R&M No. 1991*, British Aeronautical Research Council, London.

Levy, S., Wolley, R. M., and Knoll, W. D. (1947), "Instability of Simply Supported Square Plate with Reinforced Circular Hole in Edge Compression,' *J. Res. Natl. Bur. Stand.*, Vol. 39, pp. 571–577.

Libove, C. (1983), "Buckle Pattern of Biaxially Compressed Simply Supported Orthotropic Rectangular Plates," *J. Compos. Mater.*, Vol. 17, No. 1, pp. 45–48.

Libove, C., and Batdorf, S. B. (1948), "A General Small-Deflection Theory for Flat Sandwich Plates," *NACA Rep. No. 899.*

Libove, C., and Hubka, R. E. (1951), "Elastic Constants for Corrugated-Core Sandwich Plates," *NACA Tech. Note No. 2289.*

Lind, N. C. (1973), "Buckling of Longitudinally Stiffened Sheets," *ASCE J. Struct. Div.*, Vol. 99, No. ST7, pp. 1686–1691.

Lind, N. C., Ravindra, M. K., and Schorn, G. (1976), "Empirical Effective Width Formula," *ASCE J. Struct. Div.*, Vol. 102, No. ST9, pp. 1741–1957.

Little, G. H. (1976), "Stiffened Steel Compression Panels: Theoretical Failure Analysis," *Struct. Eng.*, Vol. 54, No. 12, pp. 489–500.

Little, G. H. (1979), "The Strength of Square Steel Box-Columns: Design Curves and Their Theoretical Basis," *Struct. Eng.*, Vol. 57.

Lu, L. W., and Kamalvand, H. (1968), "Ultimate Strength of Laterally Loaded Columns," *ASCE J. Struct. Div.*, Vol. 94, No. ST6, pp. 1505–1524.

May, I. M., and Ganaba, T. H. (1988), "Elastic Stability of Plates with and Without Openings," *J. Eng. Comput.*, Vol. 5, No. 1, pp. 50–52.

McKenzie, K. I. (1964), "The Buckling of Rectangular Plate Under Combined Biaxial Compression, Bending and Shear," *Aeronaut. Q.*, Vol. 15, No. 3, pp. 239–246.

Merrison Committee (1973), "Inquiry into the Basis of Design and Method of Erection of Steel Box Girder Bridges (Interior Design and Workmanship Rules)," Merrison Committee, London.

Michael, M. E. (1960), "Critical Shear Stress for Webs with Holes," *J. R. Aeronaut. Soc.*, Vol. 64, p. 268.

Moheit, W. (1939), "Schubbeulung rechteckiger Platten mit eingespannten Rändern," Thesis, Technische Hochschule Darmstadt, Leipzig, Germany.

Murray, J. M. (1946), "Pietzker's Effective Breadth of Flange Reexamined," *Engineering*, Vol. 161, p. 364.

Murray, N. W. (1973), "Buckling of Stiffened Panel Loaded Axially and in Bending," *Struct. Eng.*, Vol. 51, No. 8, pp. 285–301.

Murray, N. W. (1975), "Analysis and Design of Stiffened Plates for Collapse Load," *Struct. Eng.*, Vol. 53, No. 3, pp. 153–158.

Nemeth, J. and Michael, P. (1990), "Buckling and Postbuckling Behavior of Compression-Loaded Isotropic Plates with Cutouts," *Proc. 31st Struct. Dyn. Mater. Conf.*, April 2–4 Part 2, American Institute of Aeronautics and Astronautics, New York, pp. 862–876.

Newell, J. S. (1930), "The Strength of Aluminum Alloy Sheets," *Airway Age*, Vol. 11, p. 1420; Vol. 12, p. 1548.

Nguyen, R. P., and Yu, W. W. (1982), "Longitudinally Reinforced Cold-Formed Steel Beam Webs," *ASCE J. Struct. Div.*, Vol. 108, No. ST11, pp. 2423–2442.

Pavlovic, M. N., and Baker, G. (1989), "Effect of Non-uniform Stress Distribution on the Stability of Biaxially Compressed Plates," *Int. J. Struct. Mech. Mater. Sci.*, Vol. 28, No. 1–4, pp. 69–89.

Perel, D., and Libove, C. (1978), "Elastic Buckling of Infinitely Long Trapezoidally Corrugated Plates in Shear," *Trans. ASME J. Appl. Mech.*, Vol. 45, pp. 579–582.

Peters, R. W. (1954), "Buckling of Long Square Tubes in Combined Compression and Torsion and Comparison with Flat-Plate Buckling Theories," *NACA Tech. Note No. 3184.*

Ramberg, W., McPherson, A. E., and Levy, S. (1939), "Experiments on Study of Deformation and of Effective Width in Axially Loaded Sheet-Stringer Panels," *NACA Tech. Note No. 684.*

Redwood, R. G., and Uenoya, M. (1979), "Critical Loads for Webs with Holes," *ASCE J. Struct. Div.*, Vol. 105, No. ST10, pp. 2053–2068.

Rhodes, J., and Harvey, J. M. (1971), "Effects of Eccentricity of Load or Compression on the Buckling and Postbuckling Behavior of Flat Plates," *Int. J. Mech. Sci.*, Vol. 13, pp. 867–879.

Rhodes, J., and Harvey, J. M. (1976), "Plain Channel Section Struts in Compression and Bending Beyond the Local Buckling Load," *Int. J. Mech. Sci.*, Vol. 8, pp. 511–519.

Rhodes, J., and Harvey, J. M. (1977), "Examination of Plate Post Buckling Behavior," *ASCE J. Eng. Mech. Div.*, Vol. 103, No. EM3, pp. 461–480.

Rhodes, J., and Loughlan, J. (1980), "Simple Design Analysis of Lipped Simple Columns," *Proc. 5th Int. Spec. Conf. Cold-Formed Steel Struct.*, St. Louis, Mo.

Rockey, K. C. (1980), "The Buckling and Post-buckling Behavior of Shear Panels Which Have a Central Circular Cut Out," in *Thin Walled Structures* (ed. J. Rhodes and A. C. Walker), Granada, London.

Rockey, K. C., Anderson, R. G., and Cheung, Y. K. (1969), "The Behavior of Square Shear Webs Having a Circular Hole," in *Thin-Walled Steel Structures* (ed. K. C. Rockey and H. V. Hill), Crosby Lockwood, London.

Roorda, J., and Venkataramaiah, K. R. (1979), "Effective Width of Stiffened Cold-Formed Steel Plates," *Can J. Civ. Eng.*, Vol. 6, No. 3.

Schlack, A. L. (1964), "Elastic Stability of Pierced Square Plates," *Exp. Mech.*, p. 167.

Schuman, L., and Back, G. (1930), "Strength of Rectangular Flat Plates Under Edge Compression," *NACA Tech. Rep. No. 356.*

Seide, P., and Stein, M. (1949), "Compressive Buckling of Simply Supported Plates with Longitudinal Stiffeners," *NACA Tech. Note No. 1825.*

Seydel, E. (1933), "Über das Ausbeulen von rechteckigen isotropen oder orthogonala-nisotropen Platten bei Schubbeanspruchung," *Ing. Arch.*, Vol. 4, p. 169.

Sharp, M. L. (1966), "Longitudinal Stiffeners for Compression Members," *ASCE J. Struct. Div.*, Vol. 92, No. ST5, pp. 187–212.

Sharp, M. L. (1970), "Strength of Beams or Columns with Buckled Elements," *ASCE J. Struct. Div.*, Vol. 96, No. ST5, pp. 1011–1015.

Sherbourne, A. N., Marsh, C., and Lian, C. Y. (1971), "Stiffened Plates in Uniaxial Compression," *IABSE Publ.*, Vol. 31-I, Zurich, pp. 145–178.

Sivakumaran, K. S., Lu, S. (1992), "Collapse Behavior of Thin Rectangular Plates Subjected to Partial Biaxial Compression," *J. Thin-Walled Struct.* Vol. 14, No. 4, pp. 307–325.

Škaloud, M., and Zornerova, M. (1970), "Experimental Investigation into the Interaction of the Buckling of Compressed Thin-Walled Columns with the Buckling of Their Plate Elements," *Acta Tecnica CSAV No. 4.*

Southwell, R. V., and Skan, S. (1924), "On the Stability Under Shearing Force of a Flat Elastic Strip," *Proc. R. Soc.*, Vol. A105.

Sridharan, S. (1982), "A Semi-analytical Method for the Post-Local-Torsional Buckling Analysis of Prismatic Plate Structures," *Int. J. Numer. Methods Eng.*, Vol. 18, pp. 1685–1607.

Sridharan, S., and Graves-Smith, T. R. (1981), "Postbuckling Analysis with Finite Strips," *ASCE J. Eng. Mech. Div.*, Vol. 107, No, EM5, pp. 869-888.

Stein, O. (1936), "Stabilität ebener Rechteckbleche unter Biegung and Schub," *Bauingenieur*, Vol. 17, p. 308.

Stein, M. (1959), "The Phenomenon of Change in Buckle Pattern in Elastic Structures," *NACA Tech. Note No. R-39.*

Stein, M. (1989), "Effect of Transverse Shearing Flexibility on Postbuckling on Plates in Shear," *AIAA J.*, Vol. 27, No. 5, pp. 652–655.

Stowell, E. Z. (1948), "A Unified Theory of Plastic Buckling of Columns and Plates," *NACA Tech. Note No. 1556.*

Stowell, E. Z. (1949), "Plastic Buckling of a Long Flat Plate Under Combined Shear and Longitudinal Compression," *NACA Tech. Note No. 1990.*

Stowell, E. Z., Heimerl, G. J., Libove, C., and Lundquist, E. E. (1952), "Buckling Stresses for Flat Plates and Sections," *Trans. Am. Soc. Civ. Eng.*, Vol. 117, pp. 545–578.

Supple, W. J. (1980), "Buckling of Plates Under Axial Load and Lateral Pressures," in *Thin Walled Structures* (ed. J. Rhodes and A. C. Walker), Granada, London.

Thomasson, P.-O. (1978), "Thin-Walled C-Shaped Panels in Axial Compression," *Document D.I. 1978*, Swedish Council for Building Research, Stockholm.

Tien, Y. L., and Wang, S. T. (1979), "Local Buckling of Beams Under Stress Gradient," *ASCE J. Struct. Div.*, Vol. 105, No. ST8, pp. 1571–1588.

Timoshenko, S. (1910), "Einge Stabilitätsprobleme der Elastizitätstheorie," *Z. Math. Phys.*, Vol. 58, pp. 337.

Timoshenko, S. (1934), "Stability of the Webs of Plate Girders," *Engineering*, Vol. 138, p. 207.

Timoshenko, S. P., and Gere, J. M. (1961), *Theory of Elastic Stability*, 2nd ed., McGraw-Hill, New York.

Troitsky, D. S. C. (1976), *Stiffened Plates, Bending, Stability and Vibrations*, Elsevier, New York.

Tsien, H. S. (1942), "Buckling of a Column with Nonlinear Lateral Supports," *J. Aeronaut. Sci.*, Vol. 9, No. 4.

Tvergaard, V. (1973), "Imperfection-Sensitivity of a Wide Integrally Stiffened Panel Under Compression," *Int. J. Solids Struct.*, Vol. 9, pp. 177–192.

Usami, T. (1982), "Post Buckling of Plates in Compression and Bending," *ASCE J. Struct. Div.*, Vol. 108, No. ST3, pp. 591–609.

Usami, T., and Fukumoto, Y. (1982), "Local and Overall Buckling of Welded Box Columns," *ASCE J. Struct. Div.*, Vol. 108, No. ST3, pp. 525–542.

Vojta, J. F., and Ostapenko, A. (1967), "Ultimate Strength Design Curves for Longitudinally Stiffened Plate Panels with Large b/t," *Fritz Eng. Lab. Rep. No. 248.19*, Lehigh University, Bethlehem, Pa.

von Kármán, T., Sechler, E. E., and Donnell, L. H. (1932), "Strength of Thin Plates in Compression," *Trans. A.S.M.E.*, Vol. 54, No. APM-54-5, p. 53.

Walker, A. C. (1964), "Thin Walled Structural Forms Under Eccentric Compressive Load Actions," Doctoral thesis, University of Glasgow, Glasgow, Scotland.

Wang, S. T. (1969), "Cold-Rolled Austenitic Stainless Steel: Material Properties and Structural Performance," *Cornell Univ. Dept. Struct. Eng. Rep. No. 334.*

Wang, S. T., and Pao, H. Y. (1981), "Torsional-Flexural Buckling of Locally Buckled Columns," *Int. J. Comput. Struct.*, Vol. 11.

Wang, S. T., Errera, S. J., and Winter, G. (1975), "Behavior of Cold Rolled Stainless Steel Members," *ASCE J. Struct. Div.*, Vol. 101, No. ST11, pp. 2337–2357.

Wang, S. T., Yost, M. I., and Tien, Y. L. (1977), "Lateral Buckling of Locally Buckled Beams Using Finite Element Techniques," *Int. J. Comput. Struct.*, Vol. 7.

Way, S. (1936), "Stability of Rectangular Plates Under Shear and Bending Forces," *J. Appl. Mech. ASME.* Dec. Vol. 3, No. 4, pp. A131–A135.

Webb, S. E., and Dowling, P. J. (1980), "Large Deflection Elasto-plastic Behavior of Discretely Stiffened Plates," *Proc. Inst. Civ. Eng.*, Part 2, Vol. 69, pp. 375–401.

Whitney, J. M., and Leissa, A. W. (1969), "Analysis of Heterogeneous Anisotropic Plates," *Trans. ASME J. Appl. Mech.*, Vol. 36, pp. 261–266.

Winter, G. (1947), "Strength of Thin Steel Compression Flanges," *Trans. ASCE*, Vol. 112, p. 527.

Winter, G. (1983), "Commentary on the 1968 Edition of the Specification for the Design of Steel Structural Members," in *Cold-Formed Steel Design Manual*, American Iron and Steel Institute, Washington, D.C.

Winter, G., Lansing, W., and McCalley, R. B. (1950), "'Four Papers on the Performance of Thin Walled Steel Structures," *Eng. Exp. Strn. Rep. No. 33*, Cornell University, Ithaca, N.Y., pp. 27–32, 51–57.

Wittrick, W. H. (1952), "'Correlation Between Some Stability Problems for Orthotropic and Isotropic Plates Under Bi-axial and Uni-axial Direct Stress," *Aeronaut. Q.*, Vol. 4, pp. 83–99.

Wittrick, W. H. (1968), "A Unified Approach to the Initial Buckling of Stiffened Panels in Compression," *Aeronaut. Q.*, Vol. 19, p. 265.

Wittrick, W. H., and Horsington, R. W. (1984), "Buckling and Vibration of Composite Folded Plate Structures of Finite Length in Combined Shear and Compression," *Proc. R. Soc. London*, Vol. A392, pp. 107–144.

Yamaki, N. (1959/1960), "Postbuckling Behavior of Rectangular Plates with Small Initial Curvature Loaded in Edge Compression," *J. Appl. Mech. ASME*, Vol. 26, pp. 407–414; Vol. 27, pp. 335–342.

Yang, H. T. Y. (1969), "A Finite Element Formulation for Stability Analysis of Doubly Curved Thin Shell Structures," Doctoral thesis, Cornell University, Ithaca, N.Y.

Yoshizuka, J., and Naruoka, M. (1971), "Buckling Coefficient of Simply Supported Rectangular Plates Under Combined Bending and Compressive Stresses in Two Perpendicular Directions," *Stahlbau*, Vol. 40, p. 217.

Yu, W. W., and Davis, C. S. (1973), "Cold Formed Steel Members with Perforated Elements," *ASCE J. Struct. Div.*, Vol. 99, No. ST10, p. 2061.

Zender, W., and Hall, J. B., Jr. (1960), "Combinations of Shear Compressive Thermal and Compressive Load Stresses for the Onset of Permanent Buckles in Plates," *NASA Tech. Note No. D-384.*

CHAPTER FIVE

BEAMS

5.1 INTRODUCTION

Beams, girders, joists, and trusses subjected to flexure have much greater strength and stiffness in the plane in which the loads are applied (major principal axis) than in the plane of the minor principal axis. Unless these members are properly braced against lateral deflection and twisting, they are subject to failure by lateral–torsional buckling prior to the attainment of their full in-plane capacity. They are especially prone to this type of buckling during the construction phase, where braces are either absent or different in type from the permanent ones.

Lateral–torsional buckling is a limit state of structural usefulness where the deformation of a beam changes from predominantly in-plane deflection to a combination of lateral deflection and twisting while the load capacity remains first constant, before dropping off due to large deflections and yielding. Lateral–torsional buckling can be avoided by properly spaced and designed lateral bracing, or by using cross sections which are torsionally stiff, such as box-shaped sections or open-section beam groups connected intermittently by triangulated lacing or by diaphragms or by ensuring that the required design moment does not exceed the lateral–torsional buckling capacity.

The principal variable affecting lateral–torsional buckling strength is the distance between lateral braces. Other variables are: the type and position of the loads, the restraints at the ends and at intermediate locations, the type of cross sections, continuity at supports, the presence or absence of stiffening devices that restrain warping at critical locations (Ojalvo and Chambers,

1977), the material properties, the magnitude and distribution of the residual stresses, prestressing forces, initial imperfections of geometry and loading, discontinuities in the cross section (e.g., change of section, holes, and copes), cross-sectional distortion, and interaction between local and overall buckling.

The analytical aspects of determining the lateral–torsional buckling strength are quite complex, and closed-form solutions exist only for the most simple cases. However, research in this field has been conducted intensively since the mid-nineteenth century, and current research interest continues at a high level. The literature in the field is extensive. A review of the early work was given by Johnston (1976), while Lee (1960), Nethercot (1983), and Trahair and Bradford (1988), provide reviews of the modern development. The theory and the design applications are covered extensively in textbooks in various languages. Some of the English-language texts are those of Bleich (1952), Timoshenko and Gere (1961), Vlasov (1961), Chajes (1974), Brush and Almroth (1975), Heins (1975), Allen and Bulson (1980), Galambos (1968), and Trahair (1993).

Lateral-torsional buckling behavior is presented graphically in a plot relating strength (critical moment) and unbraced length. The solid curve in Fig. 5.1 illustrates schematically the variation of the critical load when a bifurcation-type instability occurs for a perfectly straight beam. The dashed curve represents the case when initial imperfections are present. There are three ranges of behavior: (1) elastic buckling, which governs for long beams (of importance during construction); (2) inelastic buckling, when instability occurs after some portions of the beam have yielded; and (3) plastic behavior, where the unbraced length is short enough so that buckling occurs after the plastic moment is reached. The last two ranges are of importance for the completed structure.

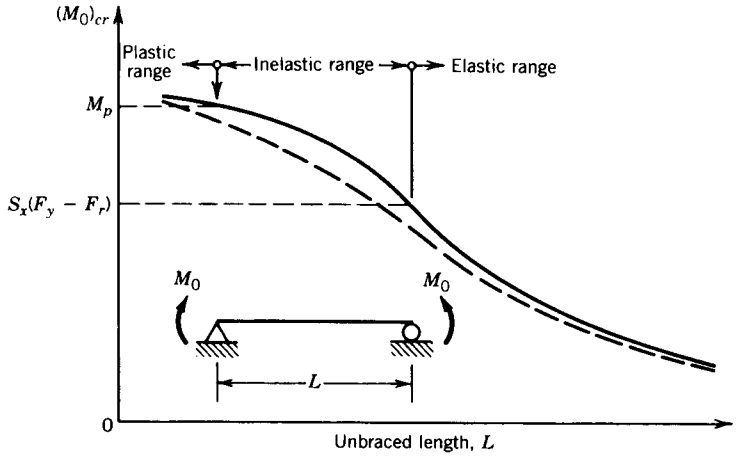

Fig. 5.1 Beam buckling curves.

5.2 ELASTIC LATERAL-TORSIONAL BUCKLING

5.2.1 Simply Supported Doubly Symmetric Beams of Constant Sections

Uniform Moment. This case is the simplest configuration, and buckling analysis leads to a closed-form solution (Timoshenko and Gere, 1961). The ends of the beam are prevented from lateral deflection ($u = 0$) and twisting ($\phi = 0$), but they are free to rotate laterally ($u'' = 0$) and the end cross section is free to warp ($\phi'' = 0$). The critical buckling moment is given by

$$M_{0cr} = \frac{\pi}{L}\sqrt{EI_yGJ}\sqrt{1 + W^2} \tag{5.1}$$

where

$$W = \frac{\pi}{L}\sqrt{\frac{EC_w}{GJ}} \tag{5.2}$$

L is the span length, E and G are the elastic and shear moduli, respectively, and I_y, J, and C_w are, respectively, the minor axis moment of inertia, the St.-Venant torsion constant, and the warping constant. The second square root in Eq. 5.1 represents the effect of warping torsional stiffness. The ratio $G/E = 0.385$ for steel and 0.376 for aluminum. The cross-sectional constants I_y, J, and C_w are listed in handbooks or they can be derived [see, e.g., Bleich (1952) or Galambos (1968)] for doubly symmetric open sections. For rectangular solid or boxed beams, W may be taken as zero.

Nonuniform Bending. If the end moments are unequal (Fig. 5.2), numerical or approximate solutions are required to obtain the buckling load. The most extensive early work for this case was performed by Massonnet (1947), Horne (1954), and Salvadori (1955, 1956), and their results have been verified many times by other researchers using various numerical techniques. Salvadori (1955) found that a simple modifier to Eq. 5.1 can account for the effect of moment gradient:

$$M_{cr} = C_bM_{0cr} \tag{5.3}$$

where M_{0cr} is obtained from Eq. 5.1 and C_b is the *equivalent uniform moment factor*. Various lower-bound formulas have been proposed for C_b, but the most commonly accepted are the following:

$$C_b = 1.75 + 1.05\kappa + 0.3\kappa^2 \leqslant 2.56 \tag{5.4a}$$

$$\frac{1}{C_b} = 0.6 - 0.4\kappa \tag{5.4b}$$

$$M_{cr} = C_bM_{0cr}$$

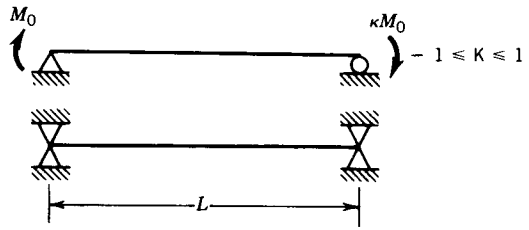

Fig. 5.2 Nonuniform moment.

The moment ratio κ (Fig. 5.2) is defined as positive when the end moments cause double curvature deflection. The value of C_b is mildly dependent on W [Eq. 5.2; also Nethercot (1983)], especially when κ approaches +1; however, either Eq. 5.4a or 5.4b is accurate enough for most purposes.

Equations 5.4a and 5.4b are applicable for use with linearly varying moment diagrams between brace points. Kirby and Nethercot (1979) presented an alternative equation for C_b which applies to any shape of the moment diagram curve between the brace points. Their equation is

$$C_b = \frac{12.5M_{\max}}{2.5M_{\max} + 3M_A + 4M_B + 3M_C} \tag{5.4c}$$

where $M_{\max}$ is the absolute value of the unbraced moment in the unbraced segment, and M_A, M_B, and M_C are the absolute value of the moments at the quarter point, center, and three-quarter point, respectively, in the unbraced segment.

When transverse loads are applied between the ends of the beam (Fig. 5.3), without intermediate lateral braces, it is important to consider the location of the applied load with respect to the midheight. The value of C_b may be computed from the following equation (Nethercot and Rockey, 1972; Nethercot, 1983):

$$C_b = AB^{2y/h} \tag{5.5}$$

where A and B are taken from Fig. 5.3, h is the beam depth, and y is the distance from the midheight to the point of load application. The distance y is negative for loading applied above midheight, and positive for loading applied below midheight. Comparison with accurate numerical solutions indicates that the critical buckling loads computed by Eq. 5.5 are within 5% of the true solution.

Loading	BMD	M	A	B
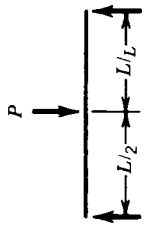	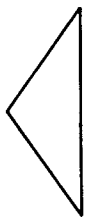	$\frac{PL}{4}$	1.35	$1 - 0.180W^2 + 0.649W$
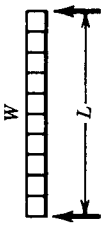	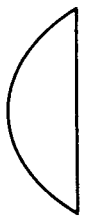	$\frac{wL^2}{8}$	1.12	$1 - 0.154W^2 + 0.535W$
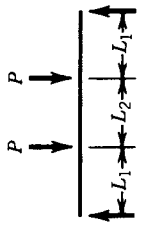		PL_1	$1 + \left(\frac{L_1}{2L_1 + L_2}\right)^2$	$1 - 0.465W^2 + 1.636W$

Fig. 5.3 Coefficients for transverse loads.

The effect of load location can be appreciated from the following example for a simply supported beam under uniform load, using a W24 × 55 steel beam of 576 in. (14.63 m) length:

$E = 29{,}000$ ksi (200,000) MPa $\quad G/E = 0.385$
$I_y = 29.1\,\text{in}^4\ (12.1 \times 10^6\,\text{mm}^4) \quad J = 1.18\,\text{in}^4\ (0.49 \times 10^6\,\text{mm}^4)$
$C_w = 3870\,\text{in}^6\ (1.015 \times 10^{12}\,\text{mm}^6)$
$W = 0.503 \quad M_{0cr} = 644$ in.-kips (731 kN-m)
$A = 1.13 \quad B = 1.230$ (Fig. 5.3)
$w_{cr} = 8M_{cr}/L^2$

- *Top flange loading*: $w_{cr} = 0.171$ kip/ft (2.50 kN/m), $\quad y = -h/2$
- *Midheight loading*: $w_{cr} = 0.211$ kip/ft (3.08 kN/m) $\quad y = 0$
- *Bottom flange loading*: $w_{cr} = 0.259$ kip/ft (3.78 kN/m) $\quad y = h/2$

The effects of load height and load condition can also be approximated by taking $B = 1.4$. This leads to the following expression:

$$C_b = \frac{12.5M_{\max}}{2.5M_{\max} + 3M_A + 4M_B + 3M_C}(1.4^{2y/h}) \tag{5.6}$$

5.2.2 End-Restrained Doubly Symmetric Beams of Constant Section

End restraint has a pronounced effect on the elastic lateral-torsional buckling strength of beams. Special cases of idealized end conditions are shown in Fig. 5.4. Nethercot and Rockey (1972) have presented the following method of solution for the two loading cases of Fig. 5.5.

$$M_{cr} = CM_{0cr} \tag{5.7}$$

where $C = A/B$ for top-flange loading, $C = A$ for loading through the midheight, and $C = AB$ for bottom-flange loading, and A and B are determined by the equations in Fig. 5.5.

In restraint condition II of Fig. 5.4 the end is free to rotate laterally but is prevented from warping. Such a condition can be effectively achieved by welding boxed stiffeners (*tube-type warp restraints*, Fig. 5.6; Ojalvo and Chambers, 1977) at or near the end support. Other warp-restraining stiffeners have been also recommended and their effectiveness has been analyzed (Vacharajittiphan and Trahair, 1974; Ojalvo and Chambers, 1977; Heins and Potocko, 1979; Szewczak et al., 1983; Lindner, 1995). The effect of end plates was studied by Lindner and Gietzelt (1983). The effect of warp prevention is illustrated

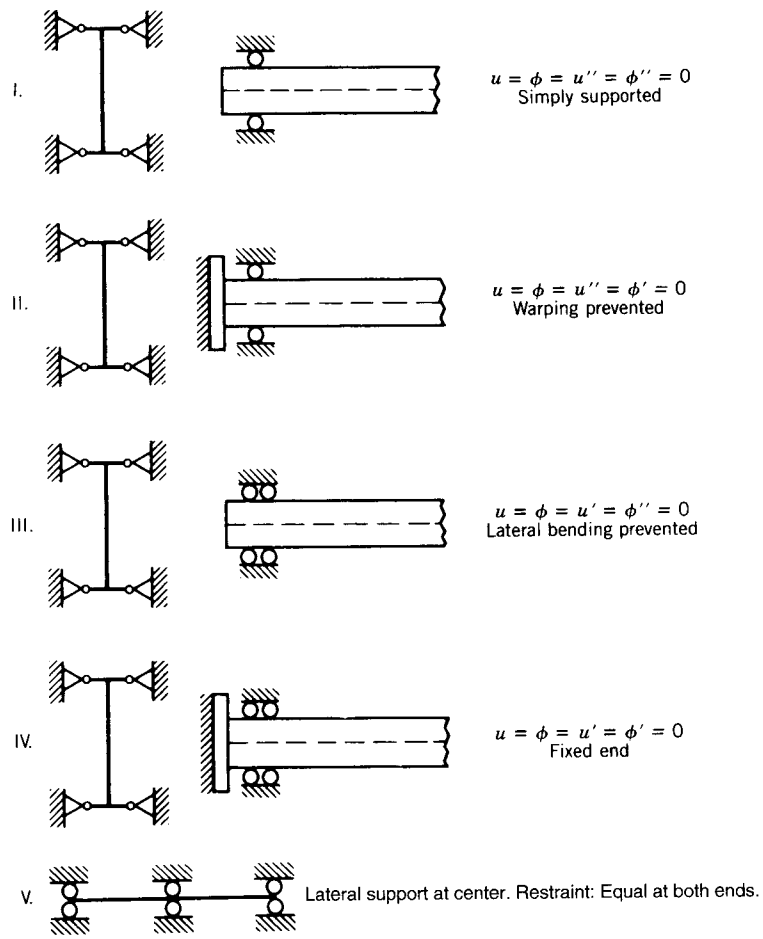

Fig. 5.4 Idealized end restraints.

Loading	Restraint	A	B
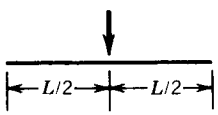	I	1.35	$1 - 0.180W^2 + 0.649W$
	II	$1.43 + 0.485W^2 + 0.463W$	$1 - 0.317W^2 + 0.619W$
	III	$2.0 - 0.074W^2 + 0.304W$	$1 - 0.207W^2 + 1.047W$
	IV	$1.916 - 0.424W^2 + 1.851W$	$1 - 0.466W^2 + 0.923W$
	V	$2.95 - 1.143W^2 + 4.070W$	1
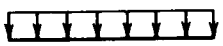	I	1.13	$1 - 0.154W^2 + 0.535W$
	II	$1.2 + 0.416W^2 + 0.402W$	$1 - 0.225W^2 + 0.571W$
	III	$1.9 - 0.120W^2 + 0.006W$	$1 - 0.100W^2 + 0.806W$
	IV	$1.643 - 0.405W^2 + 1.771W$	$1 - 0.339W^2 + 0.625W$
	V	$2.093 - 0.947W^2 + 3.117W$	$1.073 + 0.044W$

Fig. 5.5 Restraint categories.

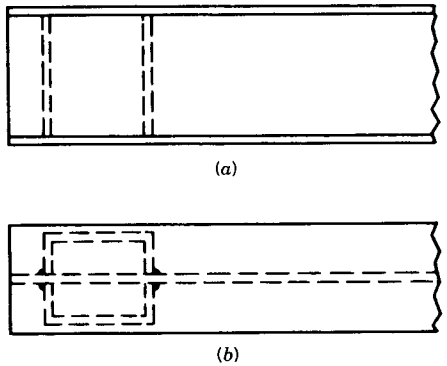

Fig. 5.6 Tube-type warp restraints.

for the W24 × 55 steel beam of ($W = 0.503$; $M_{0cr} = 644$ in.-kips; $A = 1.507$; $B = 1.230$) 576 in. length under uniformly distributed load:

Top-flange loading: $w_{cr} = 0.228$ kip/ft (3.33 kN/m)
Midheight loading: $w_{cr} = 0.281$ kip/ft (4.10 kN/m)
Bottom-flange loading: $w_{cr} = 0.346$ kip/ft (5.05 kN/m)

When the initial elastic buckling load for the case of warping prevented is compared to the case of free warping, as computed previously, it can be seen that the former has a 33% higher buckling load. For other lengths and other sections this ratio is different, of course, but the point is made that the buckling load can be increased substantially with a modest expenditure.

Bracing will contribute significantly to increasing the strength of the beam. In simply supported and continuous beams, lateral and torsional bracing is provided not only at the supports but also at intermediate points, and lateral buckling analysis is performed on each unbraced segment, using Eq. 5.3 along with the equivalent uniform moment factor C_b (Eqs. 5.4). The reader is referred to Chapter 12 for the requirements to design the bracing. The load corresponding to the smaller critical moment is then a conservative lower bound to the elastic buckling load because each unbraced segment is assumed to be laterally and torsionally simply supported. Accounting for the end restraint of the adjacent segments on the critical segment can substantially increase the buckling load (Nethercot, 1983). Considerable research was performed on analyzing the effects of continuity (Vacharajittiphan and Trahair, 1975; Nethercot, 1973a; Powell and Klingner, 1970; Trahair, 1969; Salvadori, 1955; Hartmann, 1967). Trahair (1977) and Trahair and Bradford (1988) have recommended the following simple and conservative method, which is based on the analogy that the buckling behavior of continuous beams is the same as the behavior of end-restrained columns. Thus the nomographs for nonsway

columns (Johnston, 1976) can be used to obtain the effective length of the beam segment. This method assumes that lateral restraint and warping restraint are identical, and that in-plane restraint is accounted for by the in-plane bending moment diagram (BMD). Following are the steps needed for the analysis:

1. Compute the in-plane BMD (Fig. 5.7*a*).
2. Determine C_b (Eq. 5.4) and M_{cr} (Eq. 5.3) for each unbraced segment in the beam, using the actual unbraced length as the effective length in Eq. 5.1, and identify the segment with the lowest critical load. The critical loads for buckling assuming simply supported ends for the weakest segment and the two adjacent segments are P_m, P_{rL}, and P_{rR}, respectively (Fig. 5.7*b*).
3. Compute the stiffness ratios for the three segments as follows: for the critical segment

$$\alpha_m = \frac{2EI_y}{L_{bcr}}$$

and for each adjacent segment

$$\alpha_r = n\frac{EI_y}{L_b}\left(1 - \frac{P_m}{P_r}\right)$$

where $n = 2$ if the far end of the adjacent segment is continuous, $n = 3$ if it is pinned, and $n = 4$ is it is fixed.

4. Determine the stiffness ratios $G = \alpha_m/\alpha_r$ and obtain the effective length factor K from the nonsway restrained column nomographs.

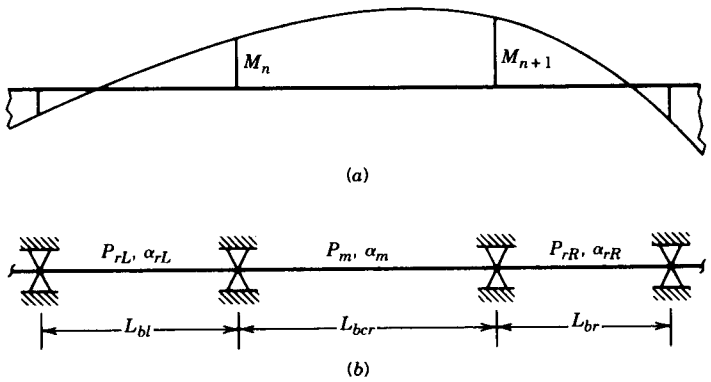

Fig. 5.7 Computation of the effect of end restraint: (*a*) in-plane BMD; (*b*) braced segments.

5. Compute the critical moment and the buckling load of the critical segment from the equation

$$M_{cr} = \frac{C_b\pi\sqrt{EI_yGJ}}{KL}\sqrt{1 + \frac{\pi^2 EC_w}{GJ(KL)^2}} \tag{5.8}$$

The method is illustrated by the example of Fig. 5.8. When the end restraint of the critical segment is accounted for, the buckling load is increased by 34%. When the lateral and the warping end restraints are unequal, the following general approximate method may be used:

$$M_{cr} = \frac{C_b\pi\sqrt{EI_yGJ}}{K_yL}\sqrt{1 + \frac{\pi^2 EC_w}{GJ(K_zL)^2}} \tag{5.9}$$

For example, for end condition II in Fig. 5.4, $K_y = 1.0$ ($u'' = 0$) and $K_z = 0.5$ ($\phi' = 0$). When one end is pinned and the other fixed, $K_z = 0.7$. More exact values of K_z and K_y for many end-restraint combinations are given by Vlasov (1961). Solutions obtained by numerical methods for special cases of end restraint are tabulated in many papers (e.g., Austin et al., 1957; Clark and Hill, 1960). Approximate solutions with coefficients are also given by Clark and Hill (1960).

5.2.3 Monosymmetric Beams

The methods and formulas in Section 5.2.2 apply to doubly symmetric beams of uniform section, for example, wide-flange shapes, solid rectangular bars, and rectangular tubes (for the latter sections, $C_w = 0$), and for channels where bending about the major axis is in the plane of the shear center (Fig. 5.9). For monosymmetric beams where bending is in the plane of symmetry (Fig. 5.10), the shear center S and the centroid C do not coincide, and the general formula for the critical moment is given by the following formula (Galambos, 1968):

$$M_{cr} = \frac{C_b\pi^2 EI_y\beta_x}{2(K_yL)^2}\left\{1 \pm \sqrt{1 + \frac{4}{\beta_x^2}\left[\frac{C_wK_y^2}{I_yK_z^2} + \frac{GJ(K_yL)^2}{\pi^2 EI_y}\right]}\right\} \tag{5.10}$$

The only term not defined previously is β_x, the coefficient of monosymmetry. The general expression for β_x is

$$\beta_x = \frac{1}{I_x}\int_A y(x^2 + y^2)dA - 2y_0 \tag{5.11}$$

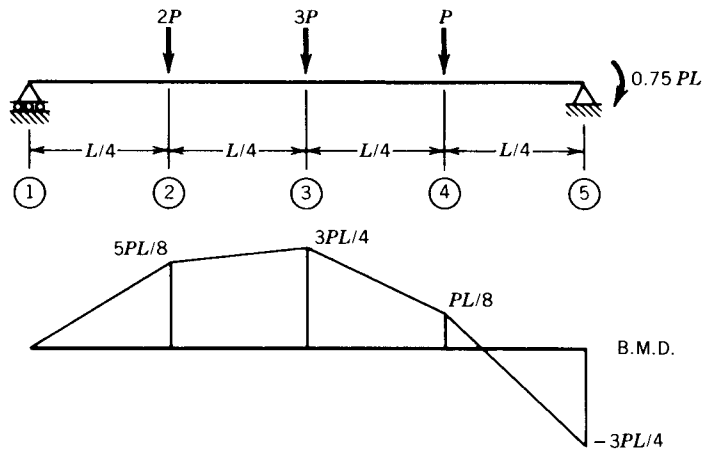

Segment	M_{max}	C_b (Eq. 5.4a)	M_{cr} (Eq. 5.3) [in.-kips (kN-m)]	P_{cr} [kips (kN)]
1-2	$0.625PL$	1.75	8411 (950)	22.43 (99.8)
2-3	$0.75PL$	1.083	5205 (588)	11.57 (51.5)
3-4	$0.75PL$	1.583	7608 (860)	16.91 (72.2)
4-5	$0.75PL$	1.933	9291 (1050)	20.65 (91.9)

$L = 600$ in. (15.24 m); W24 × 55; $I_y = 29.1$ in^4 (12.1×10^6 mm^4)
$J = 1.18$ in^4 (0.491×10^6 mm^4); $C_w = 3870$ in^6 (1.039×10^{12} mm^6). Critical segment: 2–3.

(*a*)

$$\alpha_{12} = \frac{3EI_y}{L/4}\left(1 - \frac{11.57}{22.43}\right) = 1.453\left(\frac{4EI_y}{L}\right)$$

$$\alpha_{23} = \frac{2EI_y}{L/4} = 2\left(\frac{4EI_y}{L}\right)$$

$$\alpha_{34} = \frac{2EI_y}{L/4}\left(1 - \frac{11.57}{16.91}\right) = 0.632\left(\frac{4EI_y}{L}\right)$$

$$G_2 = 2/1.453 = 1.4$$

$$G_3 = 2/0.632 = 3.2$$

From nonsway nomograph: $K = 0.85$.

$$M_{cr} = 6990 \text{ in.-kips } (790 \text{ kN-m})$$

$$P_{cr} = 15.53 \text{ kips } (69.1 \text{ kN})$$

(*b*)

Fig. 5.8 Example of end restraint.

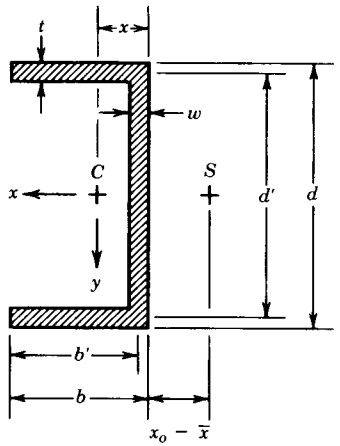

d' = shear center
C = centroid
S = shear center
$\bar{x}$ = ABS(x)
$d' = d - t$
$b' = b - w/2$

$$\alpha = \frac{1}{2 + d'w/(3b't)}$$

$$x_0 = -\bar{x} - b'\alpha$$

$$C_w = (d')^2(b')^3t\left[\frac{1 - 3\alpha}{6} + \frac{\alpha^2}{2}\left(1 + \frac{d'w}{6b't}\right)\right]$$

$$J = \tfrac{1}{3}(2b't^3 + d'w^3)$$

Fig. 5.9 Torsional properties for channels.

where I_x is the major-axis moment of inertia, y_0 is the shear center distance (Fig. 5.10), which is negative if the larger flange is in compression, x and y are centroidal coordinates, and integration is over the whole sectional area A. The value of $\beta_x = 0$ for doubly symmetric shapes, such as an I shape, and for a channel. The formula for β_x for a general I-shaped monosymmetric beam is given in Fig. 5.10. For a T-shaped beam (tee) or a double-angle beam, $C_w = 0$ and β_x is determined from the formula in Fig. 5.10, with either $b_2 = t_2 = w$ or $b_1 = t_1 = w$, depending on whether the flange or the stem is in compression.

For practical purposes β_x of the section shown in Fig. 5.10 can be approximated by (Kitipornchai and Trahair, 1980; for an exact expression, see Nethercot, 1983, p. 25)

$$\beta_x = 0.9d'\left(\frac{2I_{yc}}{I_y} - 1\right)\left[1 - \left(\frac{I_y}{I_x}\right)^2\right] \tag{5.12}$$

where d' is the distance between the centers of areas of the two flanges, I_{yc} the minor-axis moment of inertia of the compression flange, and I_y the minor-axis moment of inertia of the whole cross section. For a tee, $I_{yc} = I_y$ if the flange is in compression and $I_{yc} = 0$ if the stem is in compression. In cases when $K_y = K_z = K$, Eq. 5.10 can be written as (Trahair, 1977)

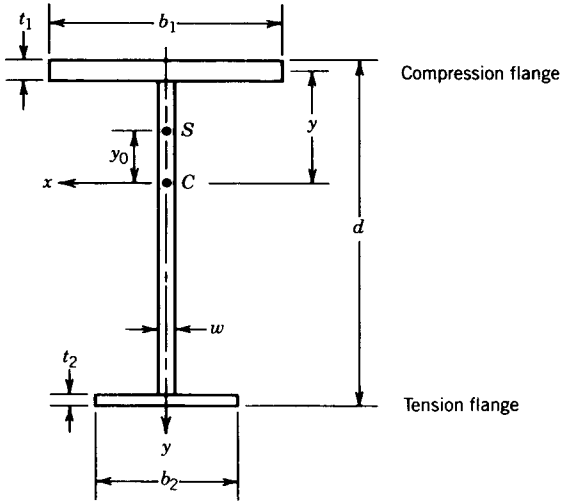

$$\alpha = \frac{1}{1 + (b_1/b_2)^3(t_1/t_2)}$$

$$d' = d - (t_1 + t_2)/2$$

$$C_w = (d')^2 b_1^3 t_1 \alpha / 12$$

$$\bar{y} = \text{ABS}(y)$$

$$y_0 = -\bar{y} - \alpha d'$$

$$\beta_x = \frac{1}{I_x}\left\{(d' - \bar{y})\left[\frac{b_2^3 t_2}{12} + b_2 t_2 (d' - \bar{y})^2 + \frac{w}{4}(d' - \bar{y})^3\right]\right.$$

$$\left. - \bar{y}\left(\frac{b_1^3 t_1}{12} + b_1 t_1 \bar{y}^2\right) - \frac{w\bar{y}^4}{4} - 2y_0\right.$$

$$J = \frac{1}{3}(b_1 t_1^3 + b_2 t_2^3 + d' w^3)$$

Fig. 5.10 Torsional properties for monosymmetric I-beams.

$$M_{cr} = \frac{\pi C_b}{KL}\left[\sqrt{EI_y GJ}(B_1 + \sqrt{1 + B_2 + B_1^2})\right] \tag{5.13}$$

where

$$B_1 = \frac{\pi \beta_x}{2(KL)}\sqrt{\frac{EI_y}{GJ}} \tag{5.14a}$$

$$B_2 = \frac{\pi^2 E C_w}{(KL)^2 GJ} \tag{5.14b}$$

for tee-shaped sections, $B_2 = 0$.

For sections with $0.1 \leqslant I_{yc}/I_y \leqslant 0.9$, the factor C_b is determined by the equation (Helwig and Yura, 1995)

$$C_b = \frac{12.5M_{\max}}{2.5M_{\max} + 3M_A + 4M_B + 3M_C}(1.4^{2y/h})R \tag{5.15}$$

where for beams under single curvature bending $R = 1$; for beams under reverse curvature between brace points

$$R = 0.5 + 2\left(\frac{I_{y\text{-top}}}{I_y}\right)^2 \tag{5.16}$$

$I_{y\text{-top}}$ is the moment of inertia of the top flange about the minor axis of the section. The following two conditions must be satisfied in case of reverse bending:

$$C_b M_{cr\text{-top}} \leqslant M_{\text{top}} \quad \text{and} \quad C_b M_{cr\text{-bottom}} \leqslant M_{\text{bottom}} \tag{5.17}$$

where $M_{cr\text{-top}}$ and $M_{cr\text{-bottom}}$ are the respective capacities calculated by treating the top flange as the compression flange and the bottom flange as the compression flange. M_{top} and M_{bottom} are the maximum moments from the applied loading causing compression in the top and bottom flanges, respectively. If there is more than one change of curvature between the brace points, intermediate bracing is recommended to avoid this condition. Sections outside the range $0.1 \leqslant I_{yc}/I_y \leqslant 0.9$ are approximately tee shapes for which C_b should not exceed the value of 100.

Charts, tables, and approximate formulas for a variety of end-restraint conditions and transverse loadings applied at, below, and above the shear center are presented by Clark and Hill (1960), Melcher (1994), and Anderson and Trahair (1972), and for tapered doubly symmetric and nonsymmetric beams by Kitipornchai and Trahair (1972, 1975a), Nethercot (1973b), Kitipornchai and Dux (1985), and Gupta et al. (1996).

5.2.4 Cantilever Beams

Solutions in the form of tables, charts, and approximate formulas for the lateral–torsional buckling load of cantilevers are available for a variety of loading conditions, including transverse loads applied at the level of either flange (Clark and Hill, 1960; Timoshenko and Gere, 1961; Massey and McGuire, 1971; Nethercot and Rockey, 1972; Nethercot, 1973c, 1983; Trahair, 1977; Trahair and Bradford, 1988). Despite the fact that the upper flange of the cantilever is in tension, it is the flange that deforms more in the buckled shape, and lateral stability is further reduced as the point of load

application is raised relative to the shear center. While in a careful analysis recourse can be had to the published solutions, some of which are cited above, Nethercot (1983) has shown that for most applications the simple effective-length method is satisfactory:

$$M_{cr} = \frac{\pi}{KL}\sqrt{EI_y GJ}\sqrt{1 + \frac{\pi^2 EC_w}{(KL)^2 GJ}} \tag{5.18}$$

where the effective-length factors for various restraint conditions at the tip and at the root of the cantilever are given in Fig. 5.11. Both end load and uniformly distributed load have been considered.

5.2.5 Summary of Elastic Lateral–Torsional Buckling

The preceding sections of this chapter have presented formulas for the solution of various cases of loading, beam geometry, and end restraint. These formulas are sufficient for developing design criteria in structural specifications and for solving most of the usual and unusual cases encountered in practice. Since most of the cases of lateral–torsional buckling are not amenable to closed-form solution, the original solutions are numerical, and many papers were cited to enable the user of this guide to obtain the answers, which were presented in the form of charts, tables, and special-purpose approximate expressions. Recourse can also be had to solutions that can be adapted to programmable calculators and microcomputers. These methods are based on various energy methods (e.g., Bleich, 1952; Salvadori, 1955; Timoshenko and Gere, 1961; Vlasov, 1961), finite difference methods (Galambos, 1968; Vinnakota, 1977b), finite integral methods (Brown and Trahair, 1968), and finite element methods (Barsoum and Gallagher, 1970; Powell and Klingner, 1970). As computers are increasingly becoming part of the structural engineer's workstation, these computerized numerical methods will be used more and more in lieu of the approximate equations. Thus it is vital that structural engineers possess a thorough understanding of the basic aspects of the theory of lateral–torsional buckling as it is explained in textbooks on stability theory.

The lateral stability of trusses was investigated by Horne (1960), and approximate solutions and a lower-bound design equation for light factory-made trusses (steel joists) are given by Hribar and Laughlin (1968) and Galambos (1970). Lateral buckling of the unsupported compression chord of trusses is discussed in Chapter 15.

The previous discussion in this chapter considered solutions for the elastic lateral–torsional buckling of ideally perfect beams under perfect in-plane loading, using linear buckling theory. This theory has been quite adequate for the development of design rules and it has been substantiated extensively by tests. However, there have also been a number of investigations which have considered the effects of initial geometric imperfections (Vinnakota, 1977a;

Restraint Conditions		Effective length	
At root	At tip	Top flange loading	All other cases
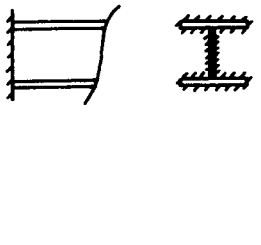	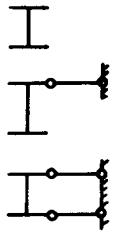	1.4 L	0.8 L
		1.4 L	0.7 L
		0.6 L	0.6 L
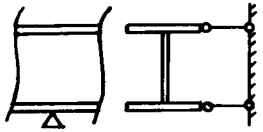	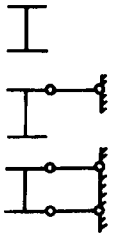	2.5 L	1.0 L
		2.5 L	0.9 L
		1.5 L	0.8 L
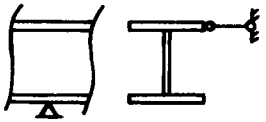	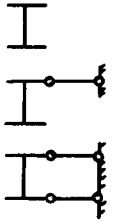	7.5 L	3.0 L
		7.5 L	2.7 L
		4.5 L	2.4 L

Fig. 5.11 Effective-length factors for cantilevers.

Nethercot, 1983), prebuckling curvature (Trahair and Woolcock, 1973), and postbuckling strength (Masur and Milbrandt, 1957; Woolcock and Trahair, 1974, 1976). A challenge to part of the theory of monosymmetric beams, called the *Wagner hypothesis*, has been presented by Ojalvo (1981). It should be noted that end connections such as partial end plates (Lindner, 1985) and coped ends (Yura and Cheng, 1985; Cheng et al., 1988; Cheng and Yura, 1988; Lindner, 1994) can influence the buckling load significantly.

The linear buckling theory assumes that the original shape of the cross section does not distort and that local buckling (Chapter 4) and lateral-tor-

sional buckling occur independently. If the plate elements of the cross section are relatively thin, as is the case of light-gage cold-formed beams (Chapter 13), there is a possibility of combined cross-sectional distortion and lateral-torsional and/or local buckling. This effect was investigated by Goldberg et al. (1964), Rajasekaran and Murray (1973), Plank and Wittrick (1974), Akay and Johnson (1977), and Hancock (1978). Lateral-torsional buckling of rolled or welded I-beams is not normally significantly affected by distortion (Hancock, 1978).

5.3 INELASTIC LATERAL–TORSIONAL BUCKLING

Buckling in the elastic range (Fig. 5.1) is important for relatively slender beams, and in practical terms this means that it is more useful when considering the strength of beams during the construction phase. However, an understanding of elastic buckling is also important for another reason: It serves as the model of the analysis of inelastic beams, which buckle laterally and torsionally after some portions of the beam have exceeded the yield strain. Most of the research on inelastic lateral-torsional buckling has used the tangent-modulus theory of inelastic buckling by investigating the stability of an equivalent elastic beam that has its stiffness properties (minor-axis bending stiffness, St.-Venant torsional stiffness, and warping torsional stiffness) reduced due to in-plane flexure prior to buckling. Since stability is checked for the stiffness just prior to buckling (tangent modulus), theoretically this analysis gives a lower bound to the buckling load. However, this is masked by the presence of unavoidable initial geometric imperfections, and for practical purposes tests have shown that the tangent-modulus approach is a satisfactory model. The pattern of yielding prior to buckling is affected by the magnitude and the distribution of residual stresses, and so in effect even a doubly symmetric beam will act as a monosymmetric beam in the inelastic range.

Because the extent of yielding varies from section to section in a beam under nonuniform flexure, the stiffness and monosymmetry parameters are not uniform along the length of the beam, and for continuous beams and frames, in-plane plastic force redistribution plays a significant role. By necessity, then, inelastic analysis is always performed by a numerical method.

Research on inelastic lateral–torsional buckling of beams has been performed vigorously since the 1940s, and research continues in the 1990s, especially on problems related to continuous systems. The first paper on the subject was authored by Neal (1950), and the residual stress effect was first considered by Galambos (1963). The combined effects of residual stresses and geometrical imperfections on inelastic lateral-torsional buckling of beams were considered by Lindner (1974), Vinnakota (1977a), and Celigoj (1979). A large number of analytical and experimental studies have been performed on the inelastic buckling of beams, and this is not the place to present a full discussion. Such a review has been given by Trahair (1977, 1983, 1993; Trahair and Bradford, 1988), who presents a detailed recapitulation of the theory, the assumptions, the methods of analysis, experimental verifications, and tabulated and graphical results. All tests reported in the literature have been analyzed statistically and reported by Fukumoto (Fukumoto and Kubo, 1977; Fukumoto et al., 1980; Fukumoto and Itoh, 1981).

Another aspect of the problem of lateral–torsional buckling of beams is the determination of the maximum permissible unbraced length so that the plastic moment can be attained and maintained for a sufficiently long rotation capacity so as to permit the development of a plastic mechanism (Lay and Galambos, 1965, 1967).

The research on inelastic lateral–torsional buckling is complex, involving extensive numerical calculations and carefully conducted expensive experiments. The significance of this work to the user of this guide lies in the fact that it provides the basis for the development of design rules.

5.4 BRACING REQUIREMENTS

It is evident that the single most important element in preventing the lateral–torsional buckling of beams is the spacing, stiffness, and strength of the bracing. For bracing to be fully effective, it must prevent both twisting and lateral deflection of the cross section of the beam.

The spacing of lateral bracing determines the buckling load (see the equations for the various conditions discussed above in this chapter). Lateral bracing usually exists in the final structure through the medium of the slab or the roof, which is supported directly on the beam, or through secondary members framing into the beam. In regions of negative moment where only the tension flange is braced, it is necessary to provide lateral bracing for the compression flange. Lateral bracing available to the final structure is generally more than adequate to prevent lateral and torsional displacement at the points of support. However, during construction the amount of bracing provided is usually very scant, and therefore it is necessary to determine its required minimum stiffness and strength. The subject of beam bracing is discussed further in Section 12.9.

5.5 DESIGN OF LATERALLY UNSUPPORTED BEAMS

Design against lateral–torsional buckling is an important aspect of the design process because of the sudden and possibly catastrophic nature of failure. This is especially so during construction, as pointed out before. Lateral–torsional buckling is a complex problem, depending on many parameters which are not well defined at the time of design. In detailed analysis, such as the investigation of failures, it is necessary to perform a careful computation involving all the parameters that can be estimated. In design calculations which are governed by structural codes (specifications), it is usually adequate to provide simple rules

based on conservative assumptions regarding the end restraints. Most design specifications assume simple end conditions ($u = u'' = \phi = \phi'' = 0$) of each braced segment, and a variable moment based on the moment diagram as determined by planar structural analysis. The critical elastic moment is thus determined by Eq. 5.3 with M_{0cr} computed by Eq. 5.1. Inelastic buckling is usually determined by specifying some type of empirical curve which gives essentially the elastic solution for long beams, and which terminates at $M_{cr} = M_p$, the plastic moment, for short beams.

Various approximations have been used in specifications to simplify the calculation of M_{0cr} (Eq. 5.1), and these have been described in numerous textbooks on structural steel design. Following is a discussion of the methods of treating lateral–torsional buckling in modern design specifications (Beedle, 1991).

The basis of these modern methods of design is the proper determination of the appropriate elastic critical load, based on the methods discussed earlier in this chapter for conservative end restraints. The resulting critical moment is M_E. The following empirical methods are used to determine the buckling load in the inelastic range:

1. It is assumed that beams and columns act similarly in the inelastic range, so the lateral–torsional buckling strength is determined by the appropriate column formula for an equivalent slenderness parameter

$$\lambda_{eq} = \sqrt{\frac{M_p}{M_E}} \tag{5.19}$$

For example, the multiple column curves (see Chapter 3) may be expressed as

$$\frac{F_{cr}}{F_y} = \frac{Y - \sqrt{Y^2 - 4\lambda^2}}{2\lambda^2} \leqslant 1.0 \tag{5.20}$$

where

$$Y = 1 + \alpha(\lambda - 0.15) + \lambda^2 \quad \text{and} \quad \lambda = \lambda_{eq} \tag{5.21}$$

and $\alpha = 0.103$, 0.293, and 0.662, respectively, for SSRC column categories 1, 2, and 3 (Chapter 3). Other column curve equations could be used, of course. Depending on whether or not the column curve includes initial imperfections, this also reflects on the beam-curve.

This approach is used in many of the lateral–torsional buckling specifications around the world including Eurocode 3.

2. The German specifications for stability use an empirical beam formula of the form

$$\frac{M_{cr}}{M_p} = \left(\frac{1}{1 + \lambda_{eq}^{2n}}\right)^{1/n} \tag{5.22}$$

where n is a coefficient that equals 2.5 to 1.5, depending on the criteria set by the various national code-writing bodies in western Europe (Beedle, 1991).

3. The AISC load and resistance factor design (LRFD) (AISC, 1993) specification uses a straight-line transition from the elastic buckling curve at $M_{cr} = M_r$, $L = L_r$ to $M_{cr} = M_p$, $L = L_p$, where

$$M_r = S_x(F_y - F_r) \tag{5.23}$$

(S_x is the elastic section modulus, F_y the yield stress, and F_r the compressive residual stress); L_r is determined from Eq. 5.1 for $M_{0cr} = M_r$, and $C_b = 1.0$; and

$$L_p = 1.762\sqrt{\frac{E}{F_y}}\, r_y \tag{5.24}$$

The lateral–torsional buckling strength is then determined for simply supported beams under uniform moment by the following formulas:

$$M_{cr} = \begin{cases} M_p & \text{for } L \leqslant L_p \quad (5.25a) \\ C_b\left[M_p - (M_p - M_r)\dfrac{L - L_p}{L_r - L_p}\right] \leqslant M_p & \text{for } L_p \leqslant L \leqslant L_r \quad (5.25b) \\ M_E & \text{for } L \geqslant L_r \quad (5.25c) \end{cases}$$

The application of the three methods is shown by the example given in Fig. 5.12, and the three approaches are compared to each other and to analytically obtained results (Kitipornchai and Trahair, 1975b; Vinnakota, 1977a) in Fig. 5.13. The information in Fig. 5.13 pertains to a W10 × 22 beam ($E = 29{,}000$ ksi; $G/E = 0.385$, $F_y = 43.5$ ksi, and $F_r = 12.6$ ksi). When the beam is subject to uniform moment, the ECCS and the LRFD method give essentially the same result; in nonuniform bending the ECCS approach is more conservative than the LRFD method. Of the three methods the LRFD approach is closest to the prediction of inelastic buckling analyses (Yura et al., 1978).

Further discussion of design methods and of other variations of the empirical approach are given by Nethercot and Trahair (1983) and Galambos (1983). The experimental statistical data for inelastic beam tests have been given by Fukumoto and co-workers (Fukumoto and Kubo, 1977; Fukumoto et al., 1980; Fukumoto and Itoh, 1981), who also examine the ECCS beam equation (Eq. 5.19) in the light of these tests. Galambos (1983) also uses the Fukumoto data to arrive at resistance factors for beam design according to the AISC–LRFD beam strength formulas (Eqs. 5.25).

Simply supported beam under uniform moment

W24 × 55; $L = 150$ in. (3.81 m); $C_b = 1.00$

$F_y = 36$ ksi (248 MPa); $F_r = 10$ ksi (69 MPa); $E = 29{,}000$ ksi (200,000 MPa)

$G/E = 0.385$

$I_y = 29.1$ in.^{4} (12.1×10^6 mm^4); $S_x = 114$ in^3 (1.87×10^6 mm^3); $Z_x = 134$ in^3 (2.19×10^6 mm^3)

$r_y = 1.34$ in. (34 mm); $J = 1.18$ in^4 (0.491×10^6 mm^4); $C_w = 3870$ in^6 (1.039×10^{12} mm^6)

$$M_{0cr} = M_E = \frac{\pi}{L}\sqrt{EI_yGJ}\sqrt{1 + \frac{\pi^2 ECw}{GJL^2}} = 4806 \text{ in.-kips (543 kN-m)}$$

$M_p = F_y Z_x = 4824$ in.-kips (545 kN-m); $\lambda = \sqrt{M_p/M_E} = 1.00$

(1) *Equivalent column method*

SSRC column curve no. 2: $\alpha = 0.293$

$Y = 1 + \alpha(\lambda - 0.15) + \lambda^2 = 2.253$

$$\frac{M_{cr}}{M_p} = \frac{Y - \sqrt{Y^2 - 4\lambda^2}}{2\lambda^2} = 0.609$$

$M_{cr} = 2938$ in.-kips (332 kN-m)

(2) *European beam formula*, $n = 2.5$

$$\frac{M_{cr}}{M_p} = \left(\frac{1}{1 + \lambda^{2n}}\right)^{1/n} = 0.756$$

$M_{cr} = 3656$ in.-kips (413 kN-m)

(3) *AISC LRFD method*

$M_r = S_x(F_y - F_r) = 2964$ in.-kips (335 kN-m)

$$M_r = \frac{\pi}{L_r}\sqrt{EI_yGJ}\sqrt{1 + \frac{\pi^2 EC_w}{GJL_r^2}}$$

Solve for $L_r = 198.1$ in. (5.03 m) > $L = 150$ in. (3.81 m)

$$L_p = \frac{300 r_y}{\sqrt{F_y}} = 67.0 \text{ in. (1.70 m)} < L = 150 \text{ in. (3.81 m)}$$

$M_{cr} = C_b[M_p - (M_p - M_r)(L - L_p)/(L_r - L_p)] \le M_p$

$M_{cr} = 3646$ in.-kips (412 kN-m)

Fig. 5.12 Example of design methods.

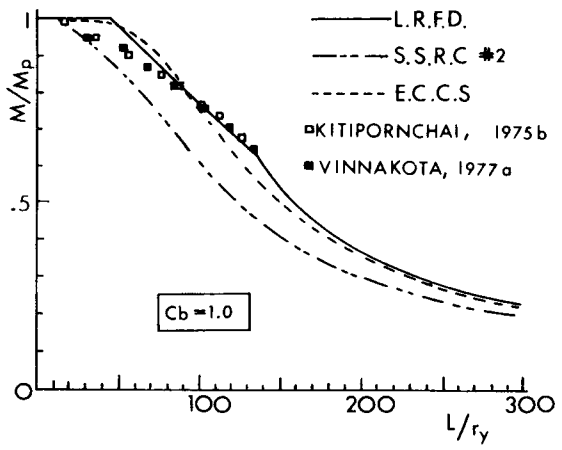

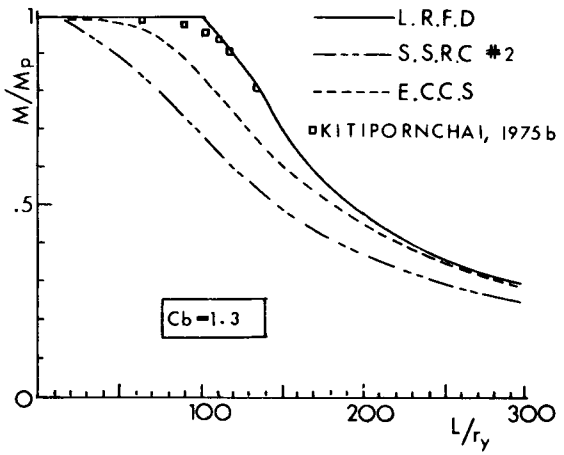

Fig. 5.13 Comparison of design methods and analytical solutions.

REFERENCES

AISC (1993), *Load and Resistance Factor Design for Structural Steel Buildings*, American Institute of Steel Construction, Chicago.

Akay, H. V., and Johnson, C. P. (1977), "Local and Lateral Buckling of Beams and Frames," *ASCE J. Struct. Div.*, Vol. 103, No. ST9, pp. 1821–1832.

Allen, H. G., and Bulson, P. S. (1980), *Background to Buckling*, McGraw-Hill, Maidenhead, Berkshire, England.

Anderson, J. M., and Trahair, N. S. (1972), "Stability of Monosymmetric Beams and Cantilevers" *ASCE J. Struct. Div.*, Vol. 98, No. ST1, pp. 269–286.

Austin, W. J., Yegian, S., and Tung, T. P. (1957), "Lateral Buckling of Elastically End-Restrained Beams," *Trans. ASCE*, Vol. 122, pp. 374–409.

Barsoum, R. S., and Gallagher, R. H. (1970), "Finite Element Analysis of Torsional and Flexural-Torsional Stability Problems," *Int. J. Numer. Methods Eng.*, Vol. 2, pp. 335–352.

Beedle, L. S., ed. (1991), *Stability of Metal Structures*: A World View, 2nd ed., Structural Stability Research Council, Bethlehem, Pa.

Bleich, F. (1952), *Buckling Strength of Metal Structures*, McGraw-Hill, New York.

Brown, P. T., and Trahair, N. S. (1968), "Finite Integral Solutions of Differential Equations," *Civ. Eng. Trans. Inst. Eng. Aust.*, Vol. CE10, No. 2.

Brush, D. O., and Almroth, B. O. (1975), *Buckling of Bars, Plates and Shells*, McGraw-Hill, New York.

Celigoj, C. (1979), "Influence of Initial Deformations on the Carrying-Capacity of Beams," *Stahlbau* Vol. 48, pp. 69–75, 117–121 (in German).

Chajes, A. (1974), *Principles of Structural Stability Theory*, Prentice Hall, Upper Saddle River, N.J.

Cheng, J. J., Yura, J. A., and Johnson, J. P. (1988), "Lateral Buckling of Steel Beams," *ASCE J. Struct. Eng.*, Vol. 114, No. ST1, pp. 1–15.

Cheng, F. F., and Yura, J. A., (1988), "Lateral Buckling Tests on Coped Steel Beams," *ASCE J. Struct. Eng.*, Vol. 114, No. ST1, pp. 16–30.

Clark, J. W., and Hill, H. N. (1960), "Lateral Buckling of Beams," *ASCE J. Struct. Div.*, Vol. 86, No. ST7, pp. 175–196.

Fukumoto, Y., and Itoh, Y. (1981), "Statistical Study of Experiments on Welded Beams," *ASCE J. Struct. Div.*, Vol. 107, No. ST1, pp. 89–104.

Fukumoto, Y., and Kubo, M. (1977), "An Experimental Review of Lateral Buckling of Beams and Girders," *Proc. Int. Colloq. Stab. Struct. Under Static Dyn. Loads*, Structural Stability Research Council, Bethlehem, Pa., Mar.

Fukumoto, Y., Itoh, Y., and Kubo, M. (1980), "Strength Variation of Laterally Unsupported Beams," *ASCE J. Struct. Div.*, Vol. 106, No. ST1, pp. 165–182.

Galambos, T. V. (1963), "Inelastic Lateral Buckling of Beams," *ASCE J. Struct. Div.*, Vol. 89, No. ST5, pp. 217–244.

Galambos, T. V. (1968), *Structural Members and Frames*, Prentice-Hall, Upper Saddle River, N. J.

Galambos, T. V. (1970), "Spacing of Bridging for Open-Web Steel Joists," *Tech. Dig. No. 2*, Steel Joist Institute, Myrtle Beach, S.C.

Galambos, T. V. (1983), "A World View of Beam Stability Research and Practice," *Proc. SSRC Annu. Meet.*, Toronto, May.

Galambos, T. V. (1989), "Impact of Code Differences on the Stability Design of Beams," *Proc. SSRC*, New York, Apr., pp. 57–71.

Goldberg, J. E., Bogdanoff, J. L., and Glantz, W. D. (1964), "Lateral and Torsional Buckling of Thin-Walled Beams," *Proc. IABSE*, Vol. 24, pp. 92–100.

Gupta, P., Wang, S. T., and Blandford, G. E. (1966), "Lateral–Torsional Buckling of Non-prismatic I-Beams," *ASCE J. Struct. Eng.*, Vol. 122, No. 7, pp. 748–755.

Hancock, G. J. (1978), "Local Distortional and Lateral Buckling of I-Beams," *ASCE J. Struct. Div.*, Vol. 104, No. ST11, pp. 1787–1800.

Hartmann, A. J. (1967), "Elastic Lateral Buckling of Continuous Beams," *ASCE J. Struct. Div.*, Vol. 93, No. ST4, pp. 11–28.

Heins, C. P. (1975), *Bending and Torsional Design in Structural Members*, Lexington Books, Lexington, Mass.

Heins, C. P., and Potocko, R. A. (1979), "Torsional Stiffening of I-Girder Webs," *ASCE J. Struct. Div.*, Vol. 105, No. ST8, pp. 1689–1700.

Helwig, T. A., and Yura, J. A. (1995), *Bracing for Stability*, Structural Stability Research Council, Bethlehem, Pa., and American Institute of Steel Construction, Chicago.

Horne, M. R. (1954), "The Flexural–Torsional Buckling of Members of Symmetric I-Sections Under Combined Thrust and Unequal Terminal Moments," *Q. J. Mech. Appl. Math.*, Vol. 7, Part 4.

Horne, M. R. (1960), "The Elastic Stability of Trusses," *Struct. Eng.*, Vol. 38.

Hribar, J. A., and Laughlin, W. P. (1968), "Lateral Stability of Welded Light Trusses," *ASCE J. Struct. Div.*, Vol. 94, No. ST3, pp. 809–832.

Johnston, B. G., ed. (1976), *Guide to Stability Design Criteria for Metal Structures*, Wiley, New York.

Kirby, P. A., and Nethercot, D. A. (1979), *Design for Structural Stability*, Wiley, New York.

Kitipornchai, S., and Dux, P. F. (1985), "Buckling and Bracing of Elastic Beams and Cantilevers," in *Handbook of Civil Engineering*, Technomic, Lancaster, Pa.

Kitipornchai, S., and Trahair, N. S. (1972), "Elastic Stability of Tapered I-Beams," *ASCE J. Struct. Div.*, Vol. 98, No. ST3, pp. 713–728.

Kitipornchai, S., and Trahair, N. S. (1975a), "Elastic Stability of Tapered Monosymmetric Beams," *ASCE J. Struct. Div.*, Vol. 101, No. ST8, pp. 1661–1678.

Kitipornchai, S., and Trahair, N. S. (1975b), "Inelastic Buckling of Simply Supported Steel I-Beams," *ASCE J. Struct. Div.*, Vol. 101, No. ST7, pp. 1333–1348.

Kitipornchai, S., and Trahair, N. S. (1980), "Buckling Properties of Monosymmetric I-Beams," *ASCE J. Struct. Div.*, Vol. 106, No. ST5, pp. 941–958.

Lay, M. G., and Galambos, T. V. (1965), "Inelastic Steel Beams Under Uniform Moment," *ASCE J. Struct. Div.*, Vol. 91, No. ST6, pp. 67–94.

Lay, M. G., and Galambos, T. V. (1967), "Inelastic Beams Under Moment Gradient," *ASCE J. Struct. Div.*, Vol. 93, No. ST1, pp. 381–400.

Lee, G. C. (1960), "A Survey of the Literature on the Lateral Instability of Beams," *Weld. Res. Counc. Bull. No. 63*, Aug.

Lindner, J. (1974), "Influence of Residual Stresses on the Load-Carrying Capacity of I-Beams," *Stahlbau*, Vol. 43, pp. 39–45, 86–91 (in German).

Lindner, J. (1985), "Influence of Parameters of Lateral Bracing on the Load-Carrying Capacity of Beams," *Proc. SSRC Annu. Tech. Session*, Cleveland, Ohio, Apr.

Lindner, J. (1994), "Influence of Construction Details on the Load-Carrying Capacity of Beams," *Proc. SSRC Annu. Tech. Session*, Bethlehem, Pa., June, pp. 65–77.

Lindner, J. (1995), "Influence of Constructional Detailing on the Lateral–Torsional Buckling Capacity of Beam-Columns," in *Structural Stability and Design*, A.A. Balkema, Rotterdam/Brookfield, pp. 61–66.

Lindner, J., and Gietzelt, R. (1983), "Influence of End Plates on the Ultimate Load of Laterally Unsupported Beams," in *Instability and Plastic Collapse of Steel Structures (M. R. Horne Conf.)*, Manchester, Granada, London, pp. 538–546.

Massey, C., and McGuire, P. J. (1971), "Lateral Stability of Nonuniform Cantilevers," *ASCE J. Eng. Mech. Div.*, Vol. 93, No. EM3, pp. 673–686.

Massonnet, C. (1947), "Buckling of Thin-Walled Bars with Open Cross Section," *Hommage Fac. Sci. Appl. Univ. Liege* (ed. G. Thone) (in French).

Masur, E. F., and Milbrandt, K. P. (1957), "Collapse Strength of Redundant Beams After Lateral Buckling," *J. Appl. Mech. ASME*, Vol. 24, No. 2.

Melcher, J. (1994), "Note on the Buckling of Beams with Monosymmetric Section Loaded Transversally to Its Plane of Symmetry," *Proc. SSRC Annu. Tech. Session*, Lehigh University, Bethlehem, Pa., pp. 61–75.

Neal, B. G. (1950), "The Lateral Instability of Yielded Mild Steel Beams of Rectangular Cross Section," *Philos. Trans. R. Soc. London*, Vol. A242.

Nethercot, D. A. (1973a), "Buckling of Laterally and Torsionally Restrained Beams," *ASCE J. Eng. Mech. Div.*, Vol. 99, No. EM4, pp. 773–792.

Nethercot, D. A. (1973b), "Lateral Buckling of Tapered I-Beams," *IABSE Publ.*, Vol. 33-II, pp. 173–192.

Nethercot, D. A. (1973c), "The Effective Lengths of Cantilevers as Governed by Lateral Buckling," *Struct. Eng.*, Vol. 51, No. 5.

Nethercot, D. A. (1983). "Elastic Lateral Buckling of Beams," in *Beams and Beam Columns: Stability in Strength* (ed. R. Narayanan), Applied Science Publishers, Barking, Essex, England.

Nethercot, D. A., and Rockey, K. C. (1972), "A Unified Approach to the Elastic Lateral Buckling of Beams," *AISC Eng. J.*, Vol. 9, No. 3, pp. 96–107.

Nethercot, D. A., and Trahair, N. S. (1983), "Design of Laterally Unsupported Beams," in *Beams and Beam-Columns: Stability and Strength* (ed. R. Narayanan), Applied Science Publishers, Barking, Essex, England.

Ojalvo, M. (1981), "Wagner Hypothesis in Beam and Column Theory," *ASCE J. Eng. Mech. Div.*, Vol. 107, No. EM4, pp. 649–658.

Ojalvo, M., and Chambers, R. S. (1977), "Effects of Warping Restraints on I-Beam Buckling," *ASCE J. Struct. Div.*, Vol. 103, No. ST12, pp. 2351–2360.

Plank, R. J., and Wittrick, W. H. (1974), "Buckling Under Combined Loading of Thin Flat-Walled Structures by a Complex Finite Strip Method," *Int. J. Numer. Methods Eng.*, Vol. 8, No. 2.

Powell, G., and Klingner, R. (1970), "Elastic Lateral Buckling of Steel Beams," *ASCE J. Struct. Div.*, Vol. 96, No. ST9, pp. 1919–1932.

Rajesekaran, S., and Murray, D. W. (1973), "Coupled Local Buckling in Wide-Flange Beam-Columns," *ASCE J. Struct. Div.*, Vol. 99, No. ST6, pp. 1003–1024.

Salvadori, M. G. (1955), "Lateral Buckling of I-Beams," *Trans. ASCE*, Vol. 120, p. 1165.

Salvadori, M. G. (1956), "Lateral Buckling of Eccentrically Loaded I-Columns," *Trans. ASCE*, Vol. 121, p. 1163.

Szewczak, R. M., Smith, E. A., and DeWolf, J. T. (1983), "Beams with Torsional Stiffeners," *ASCE J. Struct. Div.*, Vol. 109, No. ST7, pp. 1635–1647.

Timoshenko, S. P., and Gere, J. M. (1961), *Theory of Elastic Stability*, McGraw-Hill, New York.

Trahair, N. S. (1969), "Elastic Stability of Continuous Beams," *ASCE J. Struct. Div.*, Vol. 95, No. ST6, pp. 1295–1312.

Trahair, N. S. (1977), "Lateral Buckling of Beams and Beam-Columns," in *Theory of Beam-Columns*, Vol. 2, (ed. W. F. Chen and T. Atsuta), McGraw-Hill, New York, Chap. 3.

Trahair, N. S. (1983), "Inelastic Lateral Buckling of Beams," *Beams and Beam-Columns: Stability and Strength* (ed. R. Narayanan), Applied Science Publishers, Barking, Essex, England.

Trahair, N. S. (1993), *Flexural–Torsional Buckling of Structures*, CRC Press, Boca Raton, Fla.

Trahair, N. S., and Bradford, M. A. (1988), *The Behaviour and Design of Steel Structures*, 2nd edn. Chapman & Hall, London.

Trahair, N. S., and Woolcock, S. T. (1973), "Effect of Major Axis Curvature on I-Beam Stability," *ASCE J. Eng. Mech. Div.*, Vol. 99, No. EM1, pp. 85–98.

Vacharajittiphan, P., and Trahair, N. S. (1974), "Warping and Distortion of I-Section Joints," *ASCE J. Struct. Div.*, Vol. 100, No. ST3, pp. 547–564.

Vacharajittiphan, P., and Trahair, N. S. (1975), "Analysis of Lateral Buckling in Plane Frames," *ASCE J. Struct. Div.*, Vol. 101, No. ST7, pp. 1497–1516.

Vinnakota, S. (1977a), "Inelastic Stability of Laterally Unsupported Beams," *Comput. Struct.*, Vol. 7, No. 3.

Vinnakota, S. (1977b), "Finite Difference Methods for Plastic Beam-Columns," in *Theory of Beam-Columns*, Vol. 2 (ed. W. F. Chen and T. Atsuta), McGraw-Hill, New York, Chap. 10.

Vlasov, V. Z. (1961), *Thin-Walled Elastic Beams*, Israel Program for Scientific Translations, Jerusalem.

Woolcock, S. T., and Trahair, N. S. (1974), "Post-buckling of Determinate I-Beams," *ASCE J. Eng. Mech. Div.*, Vol. 100, No. EM2, pp. 151–172.

Woolcock, S. T., and Trahair, N. S. (1976), "Post Buckling of Redundant I-Beams," *ASCE J. Eng. Mech. Div.*, Vol. 102, No. EM2, pp. 293–312.

Yura, J. A., and Cheng, J. (1985), "Lateral and Local Instability of Coped Beams," *Proc. SSRC Annu. Tech. Session*, Cleveland, Ohio, Apr.

Yura, J. A., Galambos, T. V., and Ravindra, M. K. (1978), "The Bending Resistance of Steel Beams," *ASCE J. Struct. Div.*, Vol. 104, No. ST9, pp. 1355–1370.

CHAPTER SIX

PLATE GIRDERS

6.1 INTRODUCTION

This chapter deals with the buckling and strength of plate girders. Curved and box girders are not covered. Considerations of buckling involve not only lateral–torsional buckling and local buckling of the flange, as in the case of beams, but buckling of the web as well. The web is often reinforced with transverse stiffeners, and occasionally with longitudinal stiffeners, to increase its resistance to buckling, and design involves finding a combination of plate thickness and stiffener spacing that will be economical in material and fabrication.

The strength of a centrally loaded column is usually only slightly larger than the theoretical buckling load, but the strength of a stiffened plate can be much larger than its buckling load. Nevertheless, buckling was accepted as a basis for design of plate-girder webs almost exclusively until the early 1960s. This was due principally to the fact that formulas for predicting buckling are relatively simple and have been known for many years, while suitable analyses of postbuckling strength are relatively new. However, the postbuckling strength was acknowledged in most specifications by using smaller factors of safety for web buckling than for yielding or failure of other elements.

The source of the postbuckling strength of stiffened plate-girder webs in shear was explained by Wilson (1886). He had observed in his early experience (25 years before) that railroad plate-girder bridges with webs $\frac{3}{16}$ in. thick and stiffeners at intervals of 5 ft were "bearing up well under use." He discovered: "By means of a paper model with a very thin flexible web, that when stiffeners

were properly introduced the web no longer resisted by compression, but by tension, the stiffeners taking up the duty of compressive resistance, like the posts of a Pratt truss, and dividing the girder into panels equivalent to those of an open truss, the web in each panel acting as an inclined tie." Wilson says that using this theory he obtained "results that quite agreed with practical examples," but he does not explain his analysis.

Wagner (1931) developed a diagonal-tension theory of web shear. Wagner's work was extended by Kuhn (1956) for applications in aircraft design. Extensive studies, both analytical and experimental, were made in the late 1950s by Basler and Thürlimann on the postbuckling behavior of web panels in bending as well as in shear (Basler and Thürliman, 1960a,b, 1963; Basler et al., 1960; Yen and Basler, 1962; Basler, 1963a,b); Practical procedures were developed and have been adopted in many specifications. Widespread interest in the subject has resulted in a number of modifications to the Basler–Thürlimann approach to achieve better correlation between theory and tests.

Two approaches to the design of plate-girder webs are used: (1) design based on buckling as a limiting condition, with a relatively low factor of safety to allow for postbuckling strength, and (2) design based on yielding or ultimate strength as a limiting condition, with the same factor of safety as for yielding or ultimate strength of other structural members.

Steel plate shear walls have been used in North America and Japan. Steel savings as much as 50% have been achieved in structures employing a steel plate shear wall system rather than a moment-resisting frame. When the alternative is reinforced concrete walls, the steel system offers reduced foundation costs. This feature makes steel plate shear walls particularly adaptable for upgrading the lateral load resistance of an existing structure without overstressing its foundation.

In a steel plate shear wall, the building columns correspond to the flanges in a plate girder and the floor beams correspond to the girder vertical stiffeners. Therefore, the stiffness of the boundary members relative to the thickness of the plate is high and a complete tension field will be developed. It is important in design that the columns be strong enough such that they will not fail before the plate develops its full tension field.

Girders with corrugated webs have been used in buildings in Sweden and Germany and in bridges in France (Combault, 1988). A summary of the research and development in beams and girders with corrugated webs was reported by Elgaaly and Dagher (1990). The corrugations increase the out-of-plane stiffness of the web and eliminate the need to use vertical stiffeners. Girders with corrugated webs were tested to failure and analyzed under shear, Elgaaly et al. (1992, 1993) and Hamilton (1995b); the failure was due to buckling of the web. It was noted from the experimental and the analytical results that buckling of the web is local for coarse corrugations and global for dense corrugations. Simple buckling formulas to calculate the buckling load of the web were suggested, which are based on local buckling of the corrugation

subpanels as isotropic flat plates or global buckling of the entire web panel as an orthotropic plate.

6.2 WEB BUCKLING AS A BASIS FOR DESIGN

Where buckling is taken as the basis for design of plate-girder webs the maximum stress in the web, computed by conventional beam theory, should not exceed the buckling stress divided by a factor of safety. A number of formulas and extensive charts and tables have been developed for the buckling analysis of stiffened and unstiffened plates. Buckling of rectangular plate panels is discussed in Chapter 4.

The geometric parameters that determine buckling of plate-girder webs are the web thickness t, the web depth h between flanges, and the spacing a of transverse stiffeners. Four limiting values of web slenderness must be established:

1. A limiting value of h/t to control flexural buckling of a web with no longitudinal stiffener
2. A limiting value of h/t to control flexural buckling of a web with a longitudinal stiffener
3. A limiting value of h/t to control shear buckling of a web with no transverse stiffeners
4. A limiting value of a/t to control shear buckling of a web with transverse stiffeners

These limits are chosen to give a small factor of safety against buckling. It is usually assumed that the web panel is simply supported at the flanges and stiffeners. For example, if a factor of safety of 1.25 with respect to bend buckling of a web with no longitudinal stiffener is desired, the limiting value of h/t is found from Eq. 4.1 as

$$1.25f_b = \frac{23.9\pi^2 E}{12(1-\nu^2)(h/t)^2} \tag{6.1}$$

where f_b is the service-load bending stress and $k = 23.9$ is from Fig. 4.8. Equation 6.1 gives

$$\frac{h}{t} = \frac{23{,}000}{\sqrt{f_{b,\text{psi}}}} = 4.2\sqrt{\frac{E}{f_b}} \tag{6.2}$$

This is the limiting value of the allowable stress design method of the 1994 AASHTO specifications. The limit can also be expressed in terms of F_y, as in the 1994 AREA formula

$$\frac{h}{t} = \frac{32{,}500}{\sqrt{F_{y,\text{psi}}}} = 6.04\sqrt{\frac{E}{F_y}} \tag{6.3}$$

Equations 6.2 and 6.3 give almost the same results for a web whose bending stress f_b equals the allowable value $0.55F_y$. Limiting values of h/t for cases 2 and 3 can be derived similarly. However, the derivation of formulas for spacing of transverse stiffeners (case 4) is less simple because of the dependence of k_s on the aspect ratio $\alpha = a/h$ (Gaylord and Gaylord, 1972). AREA neglects this dependence and arrives at a simple formula of the same form as Eqs. 6.2 and 6.3.

$$\frac{a}{t} = \frac{10{,}500}{\sqrt{f_{v,\text{psi}}}} \tag{6.4a}$$

where f_v is the average calculated service-load shear stress in psi. AASHTO, by assuming that $k_s = 5(1 + 1/\alpha^2)$ for all values of α, limits the allowable shear stress from web buckling in a web panel to

$$f_v = \frac{7 \times 10^7(1 + 1/\alpha^2)}{(h/t)^2} \leqslant \frac{1}{3}F_y \tag{6.4b}$$

Equation 6.4b can be rewritten in the following form:

$$\frac{a}{t} = \frac{8370}{\sqrt{f_v - [8370/(h/t)]^2}} \tag{6.4c}$$

Equations 6.4b and 6.4c contain the term of web depth-to-thickness ratio, h/t, and these equations should therefore provide more accurate results than Eq. 6.4a.

The procedures given above for control of web slenderness are generally conservative and, in some cases, extravagant, because they neglect the post-buckling strength of the web.

6.3 SHEAR STRENGTH OF PLATE GIRDERS

In evaluating the behavior of a plate girder subjected to shear it is assumed that the web is plane and the material is elastic–plastic. Such a web buckles at a stress that can be predicted theoretically. The load at this stage corresponds to the beam-action strength of the girder. Subsequent to buckling the stress dis-

tribution in the web changes and considerable postbuckling strength may be realized because of the diagonal tension that develops. This is called the *tension-field action*. Even without transverse stiffeners a plate girder can develop a shear stress at the ultimate load which is several times the shear-buckling stress. Figure 6.1 shows the general distribution of the tension field that develops in a plate girder with transverse stiffeners. This stress distribution has been verified experimentally (Basler et al., 1960; Clark and Sharp, 1971; Steinhardt and Schröter, 1971).

The tension field in the girder with stiffeners is anchored by the flanges and stiffeners. The resulting lateral load on the flanges is illustrated in Fig. 6.2, and it is clear that this causes the flanges to bend inward. Therefore, the nature of the tension field is influenced by the bending stiffness of the flanges. For example, if the stiffness of the flanges is large relative to the web, the tension field may be uniform over the entire panel. With continued increase in load the tensile membrane stress combines with the shear-buckling stress to cause yielding of the web, and failure of the panel occurs upon formation of a mechanism involving a yielded zone in the web and plastic hinges in the flanges. Figure 6.3 shows three possible failure modes, involving (1) a beam mechanism in each flange, (2) a panel mechanism, and (3) a combined mechanism. The additional shear associated with the formation of a failure mechanism involving plastic hinges in the flanges is called the frame action (Cescotto et al., 1981).

Wagner (1931) used a complete, uniform tension field to determine the strength of a panel in pure shear. The flanges are assumed to be rigid and the web very thin. This model corresponds to that shown in Fig. 6.3*b* except that there are no plastic hinges, since the flanges are infinitely stiff. The Wagner analysis has been found to be quite satisfactory for aircraft structures.

Basler and Thürlimann (Basler, 1963) were the first to formulate a successful model for plate girders of the type used in civil engineering structures. They assume that the flanges are too flexible to support a lateral loading from the

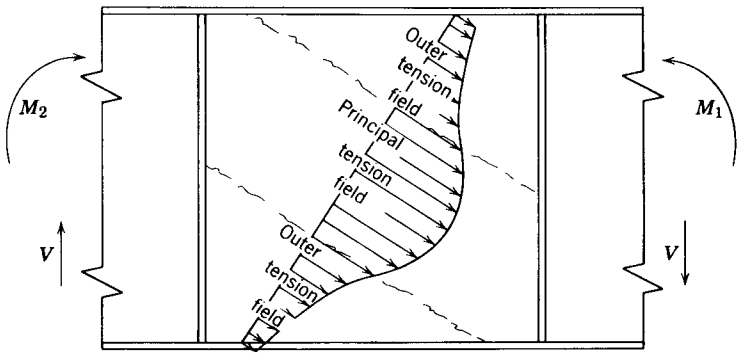

Fig. 6.1 Tension-field action.

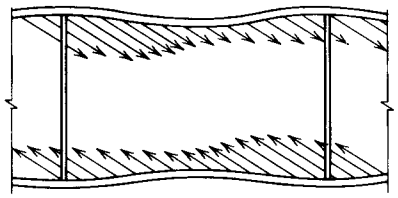

Fig. 6.2 Flange resistance.

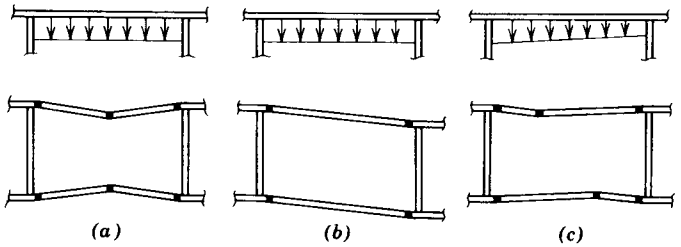

Fig. 6.3 Frame action.

tension field, so that the yield band shown in Table 6.1 determines the shear strength. The inclination and width of the yield band are defined by the angle θ, which is chosen so as to maximize the shear strength. The shear stress τ_u for the optimal value of θ was found to be*

$$\tau_u = \tau_{cr} + \tfrac{1}{2}\sigma_t \sin\theta_d \tag{6.5}$$

where τ_{cr} is the shear-buckling stress, σ_t the tension-field stress, and θ_d the angle of panel diagonal with flange. Combining the beam shear τ_{cr} and the postbuckling tension σ_t and substituting the results in the Mises yield condition gives

$$\sigma_t = -\tfrac{3}{2}\tau_{cr}\sin 2\theta + \sqrt{\sigma_{yw}^2 + (\tfrac{9}{4}\sin^2 2\theta - 3)\tau_{cr}^2} \tag{6.6}$$

The maximum value of τ_u is then found by substituting σ_t from Eq. 6.6 into Eq. 6.5.

To obtain a simpler solution Basler assumes that σ_t and τ_{cr} are additive, as they would be if σ_t acted at 45°, and uses the resulting combination of principal stresses in a linear approximation of the Mises yield condition. This gives

$$\sigma_t = \sigma_{yw}\left(1 - \frac{\tau_{cr}}{\tau_{yw}}\right) \tag{6.7}$$

*Basler gives the result in terms of the aspect ratio α instead of θ_d.

TABLE 6.1 Various Tension Field Theories for Plate Girders

Investigator	Mechanism	Web Buckling Edge Support	Unequal Flanges	Longitudinal Stiffener	Shear and Moment
Basler (1963-a)			Immaterial	Yes, Cooper (1965)	Yes
Takeuchi (1964)	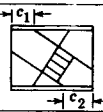		Yes	No	No
Fujii (1968, 1971)	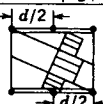		Yes	Yes	Yes
Komatsu (1971)	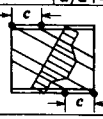		No	Yes, at mid-depth	No
Chem and Ostapenko (1969)			Yes	Yes	Yes
Porter et al. (1975)	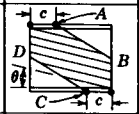		Yes	Yes	Yes
Hoglund (1971-a, b)	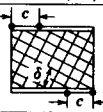		No	No	Yes
Herzog (1974-a, b)	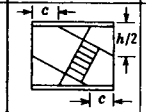	Web buckling component neglected	Yes, in evaluating c	Yes	Yes
Sharp and Clark (1971)			No	No	No
Steinhardt and Schroter (1971)			Yes	Yes	Yes

where σ_{yw} and τ_{yw} are the web yield stresses in tension and shear, respectively. Values of τ_u by this approximation are less than those by Eq. 6.6, but an investigation of girders with a wide range of proportions showed that the maximum difference was less than 10%. Substituting σ_t from Eq. 6.7 into Eq. 6.5 gives

$$\tau_u = \tau_{cr} + \tfrac{1}{2}\sigma_{yw}\left(1 - \frac{\tau_{cr}}{\tau_{yw}}\right)\sin\theta_d \tag{6.8}$$

Basler assumes that inelastic buckling will occur if τ_{cr} exceeds $0.8\tau_{yw}$ and takes the inelastic buckling stress τ_{cri} to be

$$\tau_{cri} = \sqrt{0.8\tau_{cr}\tau_{yw}} \quad 0.8\tau_{yw} \leqslant \tau_{cr} \leqslant 1.25\tau_{yw} \tag{6.9}$$

This value is to be substituted for τ_{cr} in Eq. 6.8.

It was shown first by Gaylord (1963) and later by Fujii (1968a) and Selberg (1973) that Basler's formula gives the shear strength for a complete tension field instead of the limited band of Table 6.1. The correct formula for the limited band is

$$\tau_u = \tau_{cr} + \sigma_{yw}\left(1 - \frac{\tau_{cr}}{\tau_{yw}}\right)\frac{\sin\theta}{2 + \cos\theta_d} \tag{6.10}$$

Therefore, Basler's formula overestimates the shear strength of a girder whose flanges are incapable of supporting lateral load from a tension field.

Many variations of the postbuckling tension field have been developed since the Basler–Thürlimann solution was published. The principal characteristics of most of these are shown in Table 6.1 and are discussed in the following paragraphs. The table shows the tension field, the positions of the plastic hinges if they are involved in the solution, the edge conditions assumed in computing the shear-buckling stress, and other features of the solutions. In all cases except the Fujii and Herzog models the shear-buckling strength is added to the vertical component of the tension field to give the contribution of the web to the shear strength of the girder panel.

Takeuchi (1964) appears to have been the first to make an allowance for the effect of flange stiffness of the yield zone in the web. He located the boundaries of the tension field at the distances c_1 and c_2 from diagonally opposite corners of the panel (Table 6.1). These distances were assumed proportional to the respective flange stiffnesses I_{f1} and I_{f2} and were chosen to maximize the shear strength. However, shear strengths determined in this way were not in good agreement with test results (Konishi et al., 1965). Lew and Toprac (1968) used this model in their investigation of hybrid plate girders and determined c_1 by a formula established to give agreement with available test results.

Fujii (1968a,b) assumes a tension field encompassing the whole panel, together with beam mechanisms in each flange with the interior hinge at midpanel (Table 6.1). The web compression in the direction perpendicular to the pincipal tension is assumed equal to the compression in that direction at the initiation of buckling. Tresca's yield condition is then used to determine the magnitude of the tension. If the flanges can resist the tributary web stress with the web in the yield condition, the web yields uniformly over the panel, but if they cannot, there is a central band of yielding with a smaller tension equal to that which the flange can support in the outer triangular portions. Inelastic shear buckling of the web is assumed to begin at $\tau_{cr} = 0.5\tau_{yw}$, and to vary parabolically from that point to τ_{yw} at $h/t = 0$. The theory was extended to include unsymmetrical girders (Fujii, 1971).

Komatsu (1971) gives formulas for four modes of failure. Failure in the first mode occurs in the manner shown in Table 6.1, where the inner band yields under the combined action of the buckling stress and the postbuckling tension field, while the smaller tension in the outer bands is the value that can be supported by the girder flange as a beam mechanism with the interior hinge at the distance c determined by an empirical formula based on tests. The inclination of the yield band is determined so as to maximize the shear, as in Basler's solution, but the optimum inclination must be determined by trial. In the second mode, which is a limiting case of the first mode, the interior hinge develops at midpanel, and the web yields uniformly throughout the panel. In the third mode of failure the flanges are assumed to remain elastic while allowing complete yielding of the web. An optimum value of the tension-field inclination must also be found by trial for this case. The fourth case is a limiting case in which a Wagner field develops along with a panel mechanism of the flanges.

Chern and Ostapenko (1969) proposed the tension field shown in Table 6.1, where the principal band is determined by yielding, taking into account the stress that exists at buckling. A panel mechanism is assumed to develop in the flanges. The resulting ultimate shear strength V_u is given as

$$V_u = \tau_{cr}A_w + \frac{1}{2}\sigma_t A_w[\sin 2\theta - (1-\rho)\alpha + (1-\rho)\alpha\cos 2\theta] + \frac{2}{a}(m_{pb} + m_{pt}) \tag{6.11}$$

where ρ is the ratio of outer-band tension to inner-band tension, m_{pb} and m_{pt} are the resisting moment of bottom and top flange, and α is the panel aspect ratio. Equation 6.6 is used to determine σ_t. In computing m_p the flange is assumed to act with an effective width of web b_e given by

$$b_e = 12.5t\left(0.8 - \frac{\tau_{cr}}{\tau_{yw}}\right) \quad \frac{\tau_{cr}}{\tau_y} \leqslant 0.8 \tag{6.12}$$

Two categories of shear buckling are used to determine τ_{cr} in Eq. 6.6 (1) elastic buckling, assuming the web panel fixed at the flanges and simply supported at the stiffeners, and (2) inelastic buckling if τ_{cr} for elastic buckling exceeds $0.5\tau_{yw}$. The authors differentiate V_u with respect to θ to develop a formula for the optimum value of θ, which must be solved by trial.

The tension field of Porter et al. (1975) shown in Table 6.1 consists of a single band and is a development of one suggested earlier by Rockey and Škaloud (1972) in which the tension band was taken in the direction of the panel diagonal. The tensile membrane stress together with the buckling stress causes yielding, and failure occurs when hinges form in the flanges to produce a combined mechanism that includes the yield zone $ABCD$. The vertical component of the tension field is added to the shear at buckling and combined with the frame action shear. The resulting ultimate shear strength is

$$V_u = \tau_{cr}A_w + \sigma_t A_w\left(\frac{2c}{h} + \cot\theta - \cot\theta_d\right)\sin^2\theta + \frac{4m_p}{c} \tag{6.13}$$

The coordinate c of the plastic hinge is

$$c = \frac{2}{\sin\theta}\sqrt{\frac{m_p}{\sigma_t t}} \quad 0 \leqslant c \leqslant a \tag{6.14}$$

where m_p is the plastic moment of resistance of the flange. The flange is assumed to act with an effective width of web b_e given by

$$b_e = 30t\left(1 - 2\frac{\tau_{cr}}{\tau_{yw}}\right) \quad \frac{\tau_{cr}}{\tau_{yw}} \leqslant 0.5 \tag{6.15}$$

Formulas to reduce m_p for the effect of the flange axial force are given. The authors suggest Eq. 6.6 for determining σ_t. The elastic shear-buckling stress is calculated with the four edges of the panel simply supported, but if this value exceeds $0.8\tau_{yw}$ inelastic buckling is assumed to occur, with τ_{cri} given by

$$\frac{\tau_{cri}}{\tau_{yw}} = 1 - 0.16\frac{\tau_{yw}}{\tau_{cr}} \tag{6.16}$$

The maximum value of V_u must be found by trial. However, for a given panel θ is the only independent variable in Eq. 6.13, and the maximum is not difficult to determine, particularly since the optimal value of θ usually lies between $\theta_d/2$ and 45° and τ_u is not sensitive to small changes from the optimum of θ. An assumption of $\theta = 0.667\theta_d$ will give either a very close approximation or an underestimation of the failure load.

If the flanges cannot develop moment, then $m_p = 0$ and Eq. 6.14 yields $c = 0$. Substituting this value in Eq. 6.13 and maximizing τ_u by differentiating with respect to θ the true Basler solution (Eq. 6.10) results. It is shown by

Porter et al. (1975) that Eq. 6.13 includes several other existing solutions as special cases. A procedure for evaluating the effect on V_u of the reduction in m_p due to flange axial forces is also given.

Höglund (1971a,b, 1973) has developed a theory for girders without intermediate transverse stiffeners which was later extended to girders with intermediate stiffeners. He used the system of bars shown in the figure in Table 6.1 as a model of the web. The compression bars in this system are perpendicular to the tension bars. When the angle δ between the tension bars and the flanges is decreased, the shear-buckling load for the system is increased. If the load is uniformly distributed, δ is varied along the girder because the shear varies. Calculated stresses in the bar system are in good agreement with stresses measured in test girders. The shear strength V_u is given by

$$V_u = V_w + \frac{4m_p}{c}\left(1 - \frac{M}{M_f}\right)^2 \quad M \leqslant M_f \tag{6.17}$$

where

V_w = shear strength of web (Table 6.2)
$c = a(0.25 + m_p/m_{pw})$
m_{pw} = plastic moment of web $(= \sigma_{yw} th^2/4)$
M = moment in panel
M_f = flange moment $= \sigma_{yf} A_f h$

TABLE 6.2 Values of V_w in Eq. 6.17[a]

$\sqrt{\tau_y/\tau_{cr}}$		
End Stiffeners Rigid[b]	End Stiffeners Nonrigid	V_w
Less than 0.8	Less than 0.8	$\tau_y ht$
0.8–2.75	0.8–1.25	$\tau_y ht \dfrac{1.8}{1+\sqrt{\tau_y/\tau_{cr}}}$
Over 2.75	—	$\tau_y ht \dfrac{1.32}{\sqrt{\tau_y/\tau_{cr}}}$
Over 2.75	Over 1.25	$\tau_y ht/\sqrt{\tau_y/\tau_{cr}}$

[a] τ_{cr} to be computed from Eq. 4.1 with k from Eqs. 4.24.
[b] See Eqs. 6.18 and Fig. 6.4.

The term involving M/M_f accounts for the reduction in the flange moment m_p and will depend on a mean value of M, but Höglund suggests that the largest value be used to simplify the problem.

It will be noted that V_w depends on the nature of the end stiffeners. End stiffeners can be considered rigid if Eqs. 6.18 are satisfied (see also Fig. 6.4).

$$\begin{aligned} e &\geqslant 0.18h \\ \frac{3000t}{\sqrt{\tau}} &\geqslant g > 0.18h \\ A_e &\geqslant 0.1ht \\ A_u &\geqslant \frac{V_u}{\sigma_y} - 12t^2 \\ A_{st} &\geqslant \frac{16m_p}{a\sigma_{y(st)}} \end{aligned} \tag{6.18}$$

In the second of these equations τ is in kilograms per square centimeter and t in centimeters. The term $3000t/\sqrt{\tau}$ is identical with the right side of Eq. 6.4a. A_{st} is the intermediate-stiffener area required to develop the tension field in the adjacent panel.

Herzog (1974a,b) takes the boundary of the tension field from midheight of the panel at the stiffeners to the plastic hinges in the flanges (Table 6.1). The distance c is based on an average, relative flange stiffness to allow for unequal flanges, and a chart, developed from a study of various test results, particularly those reported by Rockey and Škaloud (1968), is given to determine it. He gives three relatively simple formulas for the ultimate shear, one for each of three ranges of panel aspect ratio, together with a coefficient by which the results are to be multiplied to account for a longitudinal stiffener.

Clark and Sharp (1971) and Sharp and Clark (1971) proposed a tension field for thin-webbed aluminum girders which consists of a Basler field on which is superimposed a complete tension field inclined at 45° (Table 6.1). The flanges are assumed to be elastic beams continuous over the stiffeners and subjected to

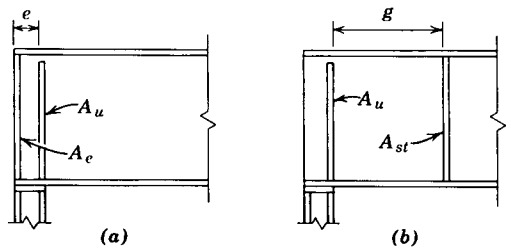

Fig. 6.4 End stiffeners.

a uniform load from the 45° field. The shear strength is the sum of the vertical components of the two tension fields and the shear at buckling. Basler's approximation of the von Mises yield condition is used to determine the combination of web stresses that cause yielding. In general, their procedure gives conservative results when compared with tests to ultimate load because it is based on general yielding of the web. However, it has been noted that aluminum girders generally do not develop plastic hinges in the flanges, and failure usually occurs by flange or stiffener buckling or, in riveted and bolted girders, by cracks developing at web holes because of the diagonal tension.

Steinhardt and Schröder (1971) have also suggested a tension field for aluminum girders (Table 6.1). The tension-field band is in the direction of the panel diagonal and its boundaries insersect the midpanel points of the flanges. The tension-field loading on the flange is assumed to vary sinusoidally with a maximum value at the stiffeners. Assuming flange bending to be elastic the corresponding tension-field distribution shown in the figure is derived. The resultant shear is found by adding the vertical component of the tension field to the shear at buckling. The theory was extended to girders of unsymmetrical sections.

Tables 6.3A and 6.3B give comparisons of predicted shear strengths according to Basler, Fujii, Ostapenko, Höglund, Rockey, and Komatsu with results of tests from a number of sources. In computing the values an axial-force reduction in the flange plastic moment is taken into account by Höglund and Rockey but not by Fujii, Ostapenko, and Komatsu. Furthermore, in the five cases in Table 6.3A when M/M_f exceeds unity Höglund has reduced his pure-shear values by Basler's shear-moment interaction formula. Two points should be kept in mind in evaluating the results in these tables: (1) definitions of ultimate strength differ among investigators, and (2) even girders that are identical in design and fabrication can differ considerably in ultimate strength. For example, the ultimate strengths of TG1 and TG1′ in Table 6.3B were 151 and 116.2 kN, respectively, yet these were tests on presumably identical halves of a single girder.

The results in Tables 6.3A and 6.3B are summarized in Table 6.4. Basler's formula gives the largest range of values; however, the others do not differ from Basler significantly. Chern and Ostapenko's formulas tend to overestimate shear strength more than the others; this is due in part to the neglect of shear-moment interaction. All but one of the first 10 girders in Table 6.3A were subjected to fairly large moment, and when they were compared by Chern and Ostapenko (1970b) with the Chern–Ostapenko shear-moment interaction formulas the following values of V_{ex}/V_u were obtained: 0.90, 0.92, 0.92, 0.97, 0.97, 0.95, 1.00, 0.96, and 0.91. The average of these 10 values is 0.95; the 10 values in Table 6.3A average 0.91.

Höglund's formulas give the most conservative results, particularly for slender webs (Table 6.3B). This conservatism is explained in part by the fact that he bases the axial-force reduction in flange plastic moment (Eq. 6.17) on the largest moment in the panel. Rockey uses an average flange stress in computing

TABLE 6.3A Shear Strength of Plate Girders

Source	Test Number	$\frac{a}{h}$	$\frac{h}{t}$	V_{ex}/V_u Basler[a]	Fujii[b]	Ostapenko[a]	Höglund[c]	$\frac{M}{M_f}$
Okumura et al.	G1	2.61	55	0.85	1.06	0.87	0.89	0.82
	G2	2.61	55	0.87	1.08	0.88	0.93	1.01
	G3	2.63	70	0.97	1.01	0.88	0.99	1.25
	G5	2.68	70	1.05	1.09	0.94	1.02	0.87
	G6	1.25	70	1.06	1.22	0.96	0.86	0.45
	G7	2.68	70	1.07	1.09	0.94	1.02	0.87
	G9	2.78	90	1.20	0.95	0.90	1.06	1.00
Nishino and Okumura	G1	2.67	60	1.04	0.94	0.98	1.03	0.97
	G2	2.67	60	0.98	1.11	0.93	0.98	1.25
	G3	2.67	77	1.00	0.98	0.86	0.96	1.09
Basler et al.	G6-T1	1.5	259	1.04	1.08	0.96	1.06	0.48
	G6-T2	0.75	259	0.95	0.97	0.94	1.06	0.62
	G6-T3	0.5	259	0.98	1.00	0.93	1.04	0.74
	G7-T1	1.0	255	0.98	1.05	0.96	1.12	0.59
	G7-T2	1.0	255	1.02	1.09	1.00	1.16	0.61
Cooper et al.	H1-T1	3.0	127	1.33	0.96	1.00	1.01	1.00
	H1-T2	1.5	127	1.08	0.92	0.97	1.06	0.60
Konishi et al.	B	1.0	267	0.81	1.02	0.79	1.18	0.53
Okumura and Nishino	G1-1	3.0	182	1.21	1.07	0.99	0.97	1.00
	G1-2	1.5	182	1.03	1.04	0.91	1.08	0.87
	G2-1	3.0	144	1.34	0.96	1.02	1.01	1.16
	G2-2	1.5	144	1.17	1.00	0.96	1.14	0.93
Mean value				1.05	1.03	0.94	1.03	
Standard deviation				0.14	0.07	0.05	0.08	

[a] From Chern and Ostapenko (1969).
[b] From Fujii (1971).
[c] From Höglund (1973).

this effect, and Basler found better correlation in predictions of shear-moment interaction when he used a reduced moment (Basler, 1963b).

Herzog presents in graphical form a comparison of shear strengths by his formulas with results of 96 tests by others, including all of those in Tables 6.3A and 6.3B. The mean value of the ratio V_{ex}/V_u is 1.036. However, the standard deviation is 0.16, and in one test (not in Tables 6.3) V_{ex}/V_u is 1.41, while Höglund's formula gives 1.04.

The simplest formulas are Basler's, Höglund's, and Herzog's, and of these Höglund's gives the most consistent results except for slender webs ($h/t > 300$). Fujii's formulas and Komatsu's also give good results, but they are more complicated. The formulas by Rockey, Evans, and Porter give good results but require the optimum inclination of the tension field to be determined by

TABLE 6.3B Shear Strength of Plate Girders

Source	Test Number	$\frac{a}{h}$	$\frac{h}{t}$	V_{ex}/V_u Rockey[a]	Höglund[b]	Komatsu[c]	$\frac{M}{M_f}$
Rockey and Škaloud	TG 14	1.0	316	1.02	1.29	—	0.70
	TG 15	1.0	316	1.00	1.29	—	0.53
	TG 16	1.0	316	1.07	1.11	—	0.38
	TG 17	1.0	316	0.99	1.12	—	0.34
	TG 18	1.0	316	0.92	1.15	—	0.33
	TG 19	1.0	316	0.92	1.16	—	0.32
Basler et al.	G6-T1	1.5	259	1.02	1.06	1.03	0.48
	G6-T2	0.75	259	1.14	1.06	0.97	0.62
	G6-T3	0.5	259	1.12	1.04	0.99	0.74
	G7-T1	1.0	255	1.08	1.12	0.96	0.59
	G7-T2	1.0	255	1.04	1.16	1.00	0.61
Škaloud	TG1[d]	1.0	400	—	1.27	1.10	0.65
	TG1′	1.0	400	—	0.97	0.84	0.50
	TG2	1.0	400	—	1.17	0.96	0.28
	TG2′	1.0	400	—	1.01	0.83	0.24
	TG3	1.0	400	—	1.13	1.00	0.20
	TG3′	1.0	400	—	1.12	1.00	0.20
	TG4	1.0	400	—	1.14	1.02	0.19
	TG4′	1.0	400	—	1.08	0.97	0.18
	TG5	1.0	400	—	1.11	0.99	0.15
	TG5′	1.0	400	—	1.08	0.96	0.14
Mean value				1.03	1.13	0.97	
Standard deviation				0.07	0.08	0.07	

[a]From Porter et al. (1975).
[b]From Höglund (1973).
[c]From Komatsu (1971).
[d]TG1, TG1′, and so on, are twin girders. End stiffeners nonrigid according to Höglund (Eqs. 6.18).

TABLE 6.4 Comparison of Test Results in Tables 6.3A and 6.3B

Investigator	Mean	Standard Deviation	Range of V_{ex}/V_u	Ratio Highest/Lowest
Basler	1.05	0.14	1.33–0.84	1.64
Fujii	1.03	0.07	1.22–0.92	1.33
Chern and Ostapenko	0.94	0.05	1.02–0.79	1.29
Höglund (Table 6.3A)	1.03	0.08	1.18–0.86	1.37
Höglund (Table 6.3B)	1.13	0.08	1.29–1.01	1.28
Rockey	1.03	0.07	1.14–0.92	1.24
Komatsu	0.97	0.07	1.10–0.83	1.32

trial. Chern and Ostapenko's formulas are complicated and also require a trial determination of the optimum inclination of the tension field.

Yonezawa et al. (1978) proposed an ultimate shear strength theory for plate girders with webs diagonally stiffened between vertical stiffeners. It is assumed that the ultimate shear strength consists of the sum of contributions from three sources: the beam shear force V_{cr} taken by the diagonally stiffened web, the shear force V_t taken by the tension field in the web, and the shear force V_s taken by the diagonal stiffener. Buckling coefficients, obtained from a finite difference solution of the differential equation for a buckled web with a diagonal stiffener under shear, are presented for the computation of the beam shear force. Coefficients for panels with both compression and tension type stiffeners with either fixed or pinned plate boundaries are given. Expressions for the tension field contribution are based on the work of Rockey et al. The shear force taken by the diagonal stiffener is determined by taking the vertical component of the force acting on the stiffener. Tests on two plate girders showed good agreement between theoretical and experimental ultimate loads. Studies on diagonally stiffened web were also performed at Liege (Jetteur, 1984).

In the case of tapered plate girders, the axial forces in the inclined flanges have vertical components. These components of force may either increase or decrease the shear force carried by the web depending on the direction of taper and on the direction of the applied shear. Shear buckling of simply supported plates of variable depth have been investigated by finite element analysis and charts for the buckling coefficient k have been prepared by Elgaaly (1973).

Two investigations have been reported on the ultimate shear strength of tapered web girders. Falby and Lee (1976) have proposed a method for estimating ultimate shear strength based on the Basler method. Their method is limited to small tapers and does not account for the effect on shear of the axial load in the inclined flange. Davies and Mandal (1979) extended Rockey's tension-field model to the case of tapered web girders. Their theory is not limited to small tapers and takes into account the influence of the axial force in the sloping flange. Good agreement is obtained between theoretical predictions and experimental collapse loads. The theory is applicable to loading conditions where the girder is loaded within the tip (the intersection point of the flanges). However, it appears that modifications must be made to the theory in order to deal with the more common loading case associated with continuous plate girders with tapered webs at the supports.

6.4 GIRDERS WITH NO INTERMEDIATE STIFFENERS

Plate girders with bearing stiffeners at the supports but with no intermediate stiffeners except for bearing stiffeners at heavy concentrated loads are of practical interest. The postbuckling strength of such girders can be significant. The

shear stress at ultimate load in three tests with web slendernesses h/t of 210, 210, and 300 (B1, K1, and B4 of Table 6.5) were 3.69, 4.00, and 4.68 times the theoretical shear-buckling stress assuming panel boundaries simply supported. Höglund's formula (Eq. 6.17), which was developed originally for such girders, is in good agreement with test results (Table 6.5).

The formulas by Ostapenko and Chern are in good agreement with tests on girders with panel aspect ratios of 5.5 if the tension-field contribution is assumed to be zero (Table 6.5); in other words, the ultimate shear is the sum of the critical shear, assuming the web fixed at the flanges, and the flange plastic-hinge contribution.

6.5 STEEL PLATE SHEAR WALLS

Although the postbuckling strength of steel plates under static loads has been investigated for over half a century, there are few if any, studies of the postbuckling behavior of thin steel plates under cyclic loading. Tests were conducted at the University of Alberta (Tromposch and Kulak, 1987), at the University of Maine (Elgaaly et al., 1991a and 1993a), and at the University of Wales in Cardiff (Roberts and Sabouri, 1991) to determine the hysteretic characteristics of thin steel plates under cyclic shear loading. All test results indicate that the behavior of thin steel plates which are adequately supported along their boundaries and are subjected to cyclic shear loading is stable in the

TABLE 6.5 Shear Strength of Girders with Long Panels

Source	Test No.	$\frac{a}{h}$	$\frac{h}{t}$	V_{ex}/V_{th} Höglund[a]	V_{ex}/V_{th} Chern and Ostapenko[b]
Carskaddan (1968)	C-AC2	5.5	143	0.99	1.02
	C-AC3	5.5	71	0.97	0.94
	C-AC4	5.5	102	1.04	1.02
	C-AC5	5.5	103	0.96	0.96
	C-AHI	5.5	69	1.03	1.00
Höglund (1971b)	B1[c]	[d]	210	1.14	—
	K1	[d]	210	0.94	—
	B4	[d]	300	1.05	—

[a] From Höglund (1973).
[b] From Chern and Ostapenko (1969).
[c] End stiffeners nonrigid according to Höglund (Eqs. 6.18).
[d] No intermediate transverse stiffeners.

postbuckling domain. Kulak (1985) modeled the thin steel plate by a series of inclined tension strips. The angle of inclination of these strips is a function of the panel width and height, plate thickness, cross-sectional area of the surrounding beams and columns, and the moment of inertia of the columns; and it can be determined using the principle of least work. The stress-strain relationship for the diagonal tension strips was assumed to be elastic–perfectly plastic. Test specimens were analyzed using this model; it was found that the model was able to predict only the initial behavior and the ultimate capacity to a reasonable degree of accuracy (Elgaaly et al., 1993b).

A complete diagonal tension field was assumed by Elgaaly et al. (1995a) and the web was replaced by tension strips in the diagonal direction, with an angle of inclination that varies between 40 and 45°. To obtain a good correlation between the analytical and experimental results, it was determined that a trilinear stress-strain relationship for the tension strips should be used (Fig. 6.5). Elgaaly et al. (1995a) noted from their test results that the strain distribution along the length of the equivalent tension strips is not uniform; higher strains were measured near the ends rather than near the center of the plate. This is due to the fact that the equivalent compression strips crossing the tension strips at the ends are shorter in length and will not buckle as early as the longer compression strips near the center of the plate. Hence, an analytical model was developed based on von Kármán's effective width concept (1932), and yielding was assumed to start at the ends of the tension strip and propagates toward its center.

The trilinear stress-strain (or load-elongation) curve derived by Elgaaly et al. (1995) is given by $\sigma_y 1 = (A + Bb_e/L)\sigma_y \leq \sigma_y$, where

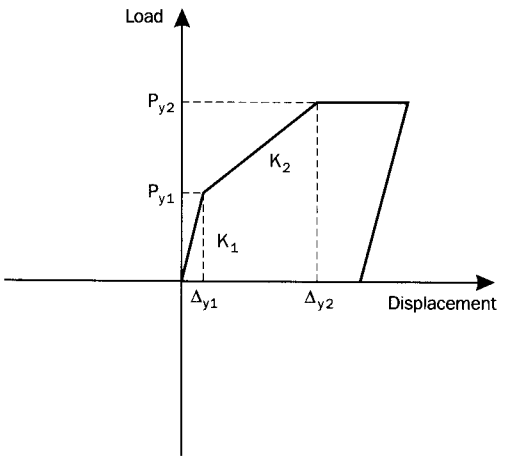

Fig. 6.5 Trilinear load (stress)–displacement (strain) curve.

$A = 1 - 1/\sqrt{3}$
$B = (2/3)^{0.5}$
$b_e = \left[\sqrt{k\pi^2 E/12(1-\nu^2)\tau_y}\right]t$
k = 14.58, shear buckling coefficient for a clamped square plate
t = thickness of the plate
τ_y = yield stress in shear ($= \sigma_y/\sqrt{3}$)
ν = Poisson's ratio
L = length of truss member
$E_2 = (\sigma_y - \sigma_{y1})E/[\sigma_y(2+\beta)/3 - \sigma_{y1}]$
σ_y = yield stress in tension
E = Young's modulus of elasticity
β = ratio of maximum strain to the strain at yield (5 to 15)

Elgaaly et al. (1995a) found that if the plate panel is bolted to the surrounding beams and columns, as is usually the case, the trilinear load-elongation (or stress-strain) relationship of the tension strip will be influenced by the behavior of the bolted connection. If the load that causes slippage of the bolted connection is less than the load that causes initiation of yielding at the ends of the tension member, the load that causes slippage will control. In other words, P_{y1} in Fig. 6.5 should be taken as the smaller value of

$$P'_{y1} = \sigma_{y1} \times \text{member cross-sectional area} \quad \text{and} \quad P''_{y1} = n(0.7fF_{ub}A_b)$$

where n is the number of bolts at one end of an equivalent strip, f the coefficient of friction, 0.33 to 0.5, F_{ub} the bolt ultimate strength in tension, and A_b the area of the bolt.

The ultimate load P_{y2} is controlled either by full yielding of the member as given before for the welded plate, tearing of the plate at the bolt holes, or shear failure of the bolts. The deflection Δ_{y2} shown in Fig. 6.5, includes the elongation of the strip, the slippage at the connection, and the bearing deformation of the plate and the bolts. The elongation of the strip due to elastic and plastic deformation can be approximated by $\sigma_y[(2+\beta)/3]L/E$. The slippage at the connection for a standard-size bolt hole can be taken as 0.125 in., and the bearing deformations can be taken as 0.2 to 0.3 times the bolt diameter (Kulak et al., 1987).

Furthermore, Elgaaly et al. (1995a) included a reduction in the stiffness of the strip in a bolted plate panel due to the eccentricity of the plate with respect to the webs of the surrounding beams and columns. The effects of residual stresses and local buckling of the compression flange of the surrounding beams and columns were also considered in the axial and moment stiffnesses and capacities of these members.

Comparisons between Elgaaly et al. (1991a, 1993a) experimental load-displacement envelopes and their analytical results using the stress-strain (or load-elongation) relationship, given above, for a welded and bolted specimens are given in Fig. 6.6. As can be noted, the agreement between the analytical and experimental results are very good.

6.6 BENDING STRENGTH OF PLATE GIRDERS

A plate girder subjected primarily to bending moment usually fails by lateral–torsional buckling, local buckling of the compression flange, or yielding of one or both flanges. Buckling of the compression flange into the web (vertical buckling) has been observed in many tests, and the following limiting value of the web slenderness h/t to preclude this mode of failure has been developed by Basler and Thürlimann (1963):

$$\frac{h}{t} \le \frac{0.68E}{\sqrt{\sigma_y(\sigma_y + \sigma_r)}}\sqrt{\frac{A_w}{A_f}} \tag{6.19}$$

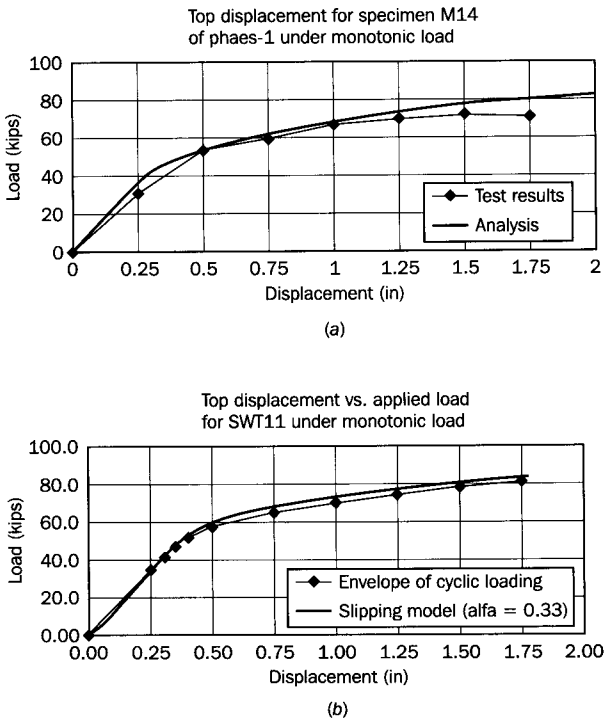

Fig. 6.6 Experimental and analytical load-displacement curves (a) Welded wall. (b) Bolted wall.

where A_w is the area of web, A_f the area of one flange, and σ_r the residual tension that must be overcome to achieve uniform yield in compression. In tests in which it has been observed, vertical buckling has occurred only after general yielding of the compression flange in the panel. Therefore, Eq. 6.19 may be too conservative, or even unnecessary, for girders of practical proportions. However, web slenderness must be limited to facilitate fabrication and to avoid fatigue cracking under repeated loads due to out-of-plane web flexing.

As in the case of shear, buckling of the web due to bending does not exhaust the panel capacity. However, the distribution of the bending stress changes in the postbuckling range and the web becomes less efficient. The solution to this problem by most investigators is based on the assumption that a portion of the web becomes ineffective. Basler and Thürlimann assume a linear distribution of stress on the effective cross section shown in Fig. 6.7, with the ultimate moment being reached when the extreme fiber compression reaches yield stress, or a critical stress if some form of buckling controls. The effective width b_e is assumed to be $30t$ for a web with $h/t = 360$. This is the limiting slenderness according to Eq. 6.19 with $A_w/A_f = 0.5$, $\sigma_y = 33$ ksi, and $\sigma_r = 16.5$ ksi. Bending strength is then assumed to increase linearly from the value for a girder whose web can reach yield stress in bending without buckling. This assumption gives

$$\frac{M_u}{M_y} = 1 - C\left[\frac{h}{t} - \left(\frac{h}{t}\right)_y\right] \tag{6.20}$$

where C is a constant and $(h/t)_y$ is the web slenderness that permits yielding in bending without buckling. In particular, the following formula was suggested:

$$\frac{M_u}{M_y} = 1 - 0.0005\frac{A_w}{A_f}\left(\frac{h}{t} - 5.7\sqrt{\frac{E}{\sigma_y}}\right) \tag{6.21}$$

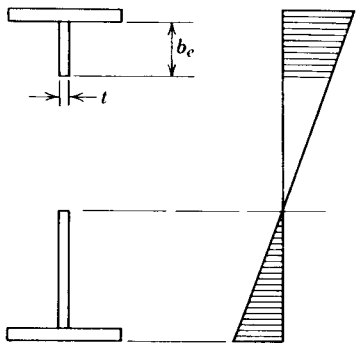

Fig. 6.7 Bending stresses.

The value of $(h/t)_y$ in this formula is somewhat larger than the theoretical value for hinge-edged panels and was chosen to give the limiting slenderness 170 which was prescribed at that time, for steel with $\sigma_y = 33$ ksi (228 MPa) by the AISC specification. Equation 6.21 has been found to be in good agreement with test results (Basler and Thürlimann, 1963; Maeda, 1971; Cooper, 1971) with girders with $h/t = 388$, 444, and 751.

Höglund (1973) assumes the effective width b_e in Fig. 6.7 to be $0.76t\sqrt{E/\sigma_{yf}}$ and considers an additional strip of web of $1.64t\sqrt{E/\sigma_{yf}}$, immediately above the neutral axis to be effective. The following formula for the effective section modulus was derived:

$$S_{\text{eff}} = S\left[1 - 0.15\frac{A_w}{A_f}\left(1 - 4.8\frac{t}{h}\sqrt{\frac{E}{\sigma_{yf}}}\right)\right] \qquad \frac{h}{t} \le 4.8\sqrt{\frac{E}{\sigma_{yf}}} \tag{6.22}$$

where S_{eff} is the effective section modulus and S is the section modulus of unreduced cross section. This equation was found to give a slightly larger reduction than Eq. 6.21, and was in good agreement with 11 tests ($0.96 < M_{\text{exp}}/M_{th} < 1.04$). For hybrid girders S_{eff} should be decreased by the amount ΔS given by

$$\Delta S = \frac{h^2 t}{12}\left(2 + \frac{\sigma_{yw}}{\sigma_{yf}}\right)\left(1 - \frac{\sigma_{yw}}{\sigma_{yf}}\right)^2 \qquad \frac{\sigma_{yw}}{\sigma_{yf}} \le 1 \tag{6.23}$$

Fujii's formulas (1968a, 1971) for the ultimate moment are more complicated and are restricted to laterally supported girders. They involve the parameter $(t/h)\sqrt{E/\sigma_{yf}}$ of the Höglund formula and the web bend-buckling stress. A multiplying coefficient for hybrid girders is given. A comparison of predicted values with results of tests on 10 nonhybrid girders gave $0.94 < M_{\text{exp}}/M_{th} < 1.11$.

Chern and Ostapenko (1970a) have developed formulas for hybrid girders with unequal flanges. The ultimate moment is the sum of the web-buckling moment based on an effective width similar to Basler's. The postbuckling moment is determined by yielding of the tension flange or by lateral or local buckling of the compression flange. A comparison of predicted values with results of tests gave $0.95 < M_{\text{exp}}/M_{th} < 1.15$ for 14 nonhybrid girders and $0.86 < M_{\text{exp}}/M_{th} < 1.13$ for 10 hybrid girders. In a later report (Ostapenko et al., 1971) the following modification of Basler's formula was proposed:

$$M_u = \frac{I}{y_c}\sigma_c\left\{1 - \frac{I_w}{I} + \frac{\sigma_{yw}}{\sigma_c}\left[\frac{I_w}{I} - 0.002\frac{y_c t}{A_c}\left(\frac{y_c}{t} - 2.85\sqrt{\frac{E}{\sigma_{yw}}}\right)\right]\right\} \tag{6.24}$$

where

I = moment of inertia of cross section
I_w = moment of inertia of web about centroidal axis of cross section
y_c = distance from neutral axis to compression edge of web
A_c = area of compression flange
σ_c = compression-flange buckling stress

$$\frac{y_c}{t} \geq 2.85\sqrt{\frac{E}{\sigma_{yw}}}$$
$$\sigma_{yf} \geq \sigma_{yw}$$

This equation has been found to give good correlation with test results. The ultimate moment in terms of the tension flange is

$$M_u = \frac{I\sigma_{yt}}{y_t}\left[1 - \frac{I_w}{I}\left(1 - \frac{\sigma_{yw}}{\sigma_{yt}}\right)\right] \tag{6.25}$$

where y_t is the distance from the neutral axis to the tension edge of the web.

Herzog (1973, 1974b) gives a formula for the general case of the unsymmetrical hybrid girder with one or more longitudinal stiffeners, which includes simple reduction coefficients for vertical, local, and lateral buckling of the compression flange. The ultimate moment is given by

$$M_u = \sigma_{yc}A_c\left(y_c + \frac{t_c}{2}\right) + \sigma_{yt}A_t\left(y_t + \frac{t_t}{2}\right) + \sigma_{ys}A_s y_s + \frac{\sigma_{yw}t_w}{6}[(1+\phi)y_c^2 + 2y_t^2] \tag{6.26}$$

where

$$\phi = \frac{\sigma_{ys}\sum A_s}{\sigma_{yw}A_w}$$

In Eq. 6.26, c, t, s, and w signify compression flange, tension flange, longitudinal stiffener, and web, respectively, and y and t are defined in Fig. 6.6. The distance y_c to the compression edge of the web is

$$y_c = \frac{2}{3+\phi}\left[h - 2\left(\frac{\sigma_{yc}A_c + \sigma_{ys}A_s - \sigma_{yt}A_t}{\sigma_{yw}t_w}\right)\right] \tag{6.27}$$

A comparison of predicted values by Eq. 6.26 with results of tests on 23 girders without longitudinal stiffeners gave $0.91 < M_{exp}/M_{th} < 1.19$, with a mean value 1.005 and standard deviation 0.095. Comparisons with tests on 26 longitudinally stiffened girders gave $0.90 < M_{exp}/M_{th} < 1.16$, with a mean value 1.036 and standard deviation 0.105.

6.7 COMBINED BENDING AND SHEAR

Assuming the shear in a girder to be carried only by the web, as in Basler's solution, shear is a maximum when the web is yielded uniformly, or, if shear buckling occurs at a smaller stress, when it has a fully developed tension field. These values are independent of the bending moment in the panel as long as the moment is less than $M_f = \sigma_{yf}A_f h$, which is the moment that can be carried by the flanges alone (AB in Fig. 6.8*a*). Any larger amount must be resisted in part by the web, which reduces the shear, until the shear capacity finally becomes zero for a panel in pure bending (BC in Fig. 6.8*a*). If the flange contribution to shear is taken into account, as in the more recent theories of shear strength, AB in Fig. 6.8*a* is not correct, because the flange axial force from the moment in the panel reduces the flange plastic moment m_p on which the flange contribution is based. This condition is represented by a line $A'B$, which can be defined, for example, by Höglund's formula (Eq. 6.17).

Basler's interaction diagram (1963b) is shown in Fig. 6.8*b*. The segment BC, for which a formula is given, corresponds to BC in Fig. 6.8*a* with $M_u = M_p$, but is assumed to be invalid for thin-webbed girders when M exceeds M_y. The

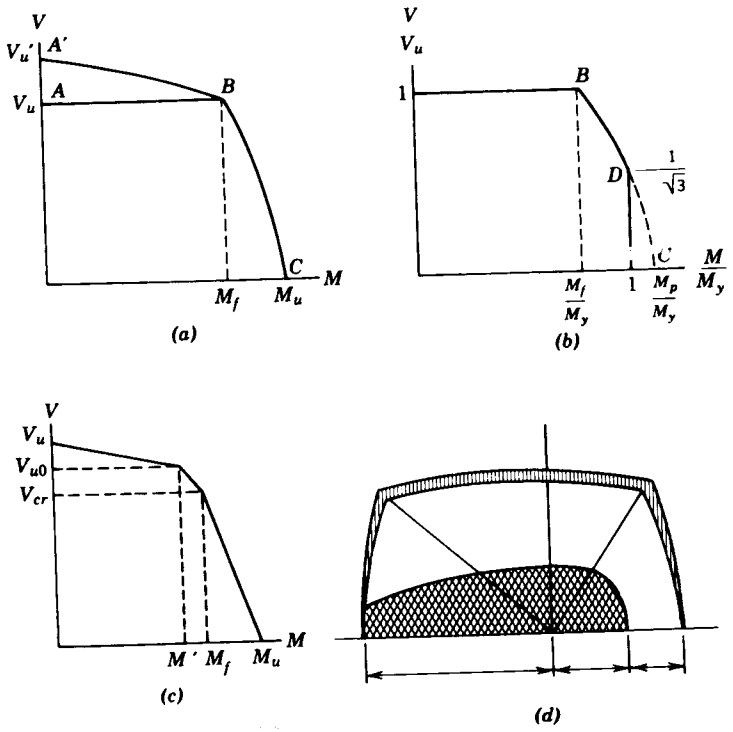

Fig. 6.8 Shear-moment interaction diagrams.

segment BC can be taken to be a straight line. Correlation with test results was good with M taken at $h/2$ from the high-moment end of the panel or at midpanel if $a < h$.

Herzog (1974a,b) assumes a trilinear diagram similar to Basler's. Fujii's interaction diagram is shown in Fig. 6.8*c*, where the additional point (M_f', V_{uo}) is for the case of a flange with no bending resistance (Fujii, 1971).

Chern and Ostapenko (1970b) assume the ultimate capacity will be dictated by failure of the web, instability of the compression flange, or yielding of the tension flange. The complete interaction behavior is represented schematically by the interaction curve of Fig. 6.8*d*. Curve Q_2–Q_1–Q_4 represents failure of the web, curve Q_2–Q_3 represents buckling of the compression flange, and curve Q_4–Q_5 represents yielding of the tension flange.

When web failure controls (region Q_2–Q_1–Q_4 of Fig. 6.8*d*) the total shear resistance V_{wc} is

$$V_{wc} = V_{crc} + V_{ec} + V_{fc} \tag{6.28}$$

in which V_{crc} is the beam-action shear, V_{ec} the tension-field shear, and V_{fc} the frame-action shear. The subscript c indicates that these shears are associated with combined stresses in the girder.

The beam-action shear is computed from

$$V_{crc} = A_w \tau_c \tag{6.29}$$

in which τ_c is obtained from the interaction equation

$$\left(\frac{\tau_c}{\tau_{cr}}\right)^2 + \frac{1+C}{2}\left(\frac{\sigma_{bc}}{\sigma_{cp}}\right) + \frac{1-C}{2}\left(\frac{\sigma_{bc}}{\sigma_{cp}}\right)^2 = 1 \tag{6.30}$$

in which C is the ratio of bending stresses in the tension and compression at the extreme fibers, σ_{bc} the maximum bending stress in the web, and σ_{cp} the critical buckling stress in the web under pure bending.

The tension-field shear V_{ec} in Eq. 6.28 is computed using the second term in Eq. 6.11 with $\rho = \frac{1}{2}$ and σ_t replaced by σ_{tc}. The tension-field stress σ_{tc} is found by using the combined stresses resulting from shear and bending in the yield criterion. As was done for the case of pure shear, an iteration procedure is used to find the maximum value of V_{wc}.

The frame-action shear is computed using the same frame mechanism as for the pure shear case (the third term in Eq. 6.11). The flange plastic moments in the combined shear and bending case, however, will be affected by the axial forces in the flanges. The resulting frame-action shear is

$$V_{fc} = \frac{1}{a}(m_{cl} + m_{cr} + m_{tl} + m_{tr}) \tag{6.31}$$

in which m_{cl} and m_{cr} are the plastic moments in the compression flange at the left and right sides of the panel, and m_{tl} and m_{tr} are the corresponding plastic moments in the tension flange. All of these moments are modified for the effect of axial force in the flange.

The other conditions for which failure occurs are depicted by curves Q_2–Q_3 and Q_4–Q_5 of Fig. 6.8*d*. Curve Q_2–Q_3 represents the case where buckling of the compression flange controls, in which case a completely developed tension field will not have formed. In the region represented by curve Q_4–Q_5, the tension flange starts yielding before the web plate reaches its ultimate shear strength. Yielding will penetrate into the cross section and the plastic strength of the girder panel will be the ultimate capacity.

The model postulated by Rockey et al. (Rockey, 1971a,b; Rockey and Škaloud, 1972; Rockey et al., 1973; Porter et al., 1975) for predicting the strength of girders without longitudinal stiffeners under bending and shear includes three additional factors not included in the pure bending and pure shear models. These factors are (1) the reduction in the shear buckling stress of the web due to the presence of bending stress, (2) the influence of the in-plane bending stress on the value of the diagonal tension-field stress at failure, and (3) the reduction of the magnitude of the plastic modulus of the flanges resulting from the axial compressive and tensile strength.

The buckling stress reduction is handled by using the interaction equation

$$\left(\frac{\sigma_{bc}}{\sigma_{cp}}\right)^2 + \left(\frac{\tau_c}{\tau_{cr}}\right)^2 = 1 \tag{6.32}$$

to determine the critical shear stress τ_c under combined bending and shear. Note that Eq. 6.32 is for the case of a symmetric cross section, which is a special case of Eq. 6.30 with $C = -1$.

After the panel has buckled the tension-field shear is computed by using a postbuckling shear force modified to include the effect of combined bending and shear. This involves modifying the tension field stress σ_1 to include both bending and shear stresses in the yield criterion and it also involves using an interaction equation to find the flange plastic moments m_f when axial stress resulting from bending acts in the flanges. The equations previously given for pure shear are then used with an iteration approach to determine the strength of the girder panel.

6.8 PLATE GIRDERS WITH LONGITUDINAL STIFFENERS

Longitudinal stiffeners (Fig. 6.9) can greatly increase the bending strength of plate girders. This additional strength can be attributed to control of the lateral deflection of the web which increases the flexural stress the web can carry and also improves the bending resistance of the flange due to greater web restraint.

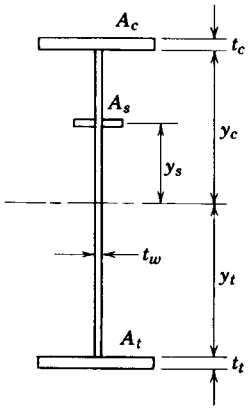

Fig. 6.9 Plate girders with longitudinal stiffeners.

Rockey and Leggett (1962) have determined that the optimum location for a longitudinal stiffener used to increase the flexural buckling resistance of a panel is 0.22 times the web depth from the compression flange if the web is assumed to be fixed at the flanges and simply supported at all four edges. Accordingly, 0.20 of the depth has been adopted nearly universally by design specifications as the accepted location for a longitudinal stiffener. Where a longitudinal stiffener at 0.20 of the web depth from the compression flange is provided, the value of k in the plate-buckling formula is increased from 23.9 to 129, which means that the elastic critical bending stress is more than five times as large as for a girder with no longitudinal stiffener. Since an unstiffened web of mild steel with a slenderness of about 170 develops yield-stress moment without buckling, a stiffened web can do the same with a slenderness $170\sqrt{123.9/23.9}$, or about 400. Tests show that an adequately proportioned longitudinal stiffener at $0.2h$ from the compression flange eliminates the bend-buckling loss in girders with web slendernesses as large as 450, so that the ultimate moment as determined by compression-flange buckling strength is attained (Cooper, 1967). Girders with larger slenderness are likely to require two or more longitudinal stiffeners to eliminate the web bend-buckling loss. Of course, the increase in bending strength of a longitudinally stiffened thin-web girder is usually small because the web contribution to bending strength is small. However, longitudinal stiffeners can be important in a girder subjected to repeated loads because they reduce or eliminate the transverse bending of the web, which increases resistance to fatigue cracking at the web-to-flange juncture and allows more slender webs to be used (Yen and Mueller, 1966).

The optimum location of a longitudinal stiffener that is used to increase resistance to shear buckling is at middepth. In this case the two subpanels buckle simultaneously and the increase in critical stress can be substantial. For example, $k = 9.34$ and 6.34 for a square panel and the corresponding subpanel, respectively, and the slenderness ratio h/t of the square panel is

twice that of the subpanel. Therefore, the elastic shear-buckling stress for the subpanel is 2.7 times as large as for the square panel. Of course, in a web with a longitudinal stiffener not at middepth the larger subpanel buckles first, and at a smaller critical stress than for the stiffener at middepth.

The postbuckling shear strength of longitudinally stiffened girders has been evaluated in two ways: Cooper (1967) assumes that each subpanel develops its own tension field after buckling, while Porter et al. (1975) assume that only one tension field is developed between the flanges and transverse stiffeners even if longitudinal stiffeners are used.

If each subpanel develops its own tension field as suggested by Cooper, the tension field shears for a girder stiffened as shown in Fig. 6.10, are

$$V_{p1} = \frac{\sigma_{t1} b_1 t}{2\sqrt{1+\alpha_1^2}} \qquad V_{p2} = \frac{\sigma_{t2} b_2 t}{2\sqrt{1+\alpha_2^2}} \tag{6.33}$$

in which b_1 and b_2 are the depths of the subpanels, σ_{t1} and σ_{t2} the diagonal tension stresses in the subpanels, and α_1 and α_2 the aspect ratios a/b_1 and a/b_2, respectively. Cooper goes on to develop the total shear strength after employing a modified form of the von Mises yield condition to evaluate the diagonal tension stresses. Chern and Ostapenko (1971) extended Cooper's model to include frame action of the flanges and of the longitudinal stiffener. The model used by Rockey et al. (1974) was suggested after it was observed from tests that an overall tension field develops in the web.

Figure 6.11 shows a test girder at failure. The inclined arrows painted on the web show the predicted angle of the tension field and are in good agreement with the axes of the buckles in both subpanels. The predicted positions of the flange plastic hinges, also painted on the girder, are in good agreement with the actual positions. The longitudinal stiffeners were at $h/4$ from the compression flange in the right-hand panel. Failure was in the right-hand panel, but it is

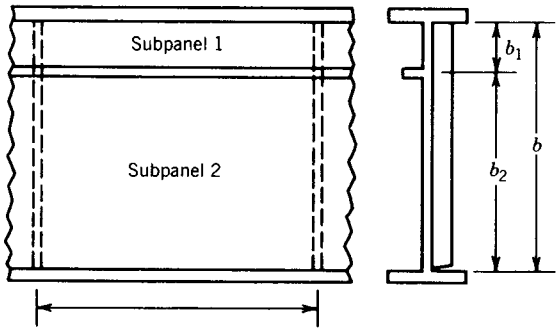

Fig. 6.10 Typical longitudinally stiffened panel.

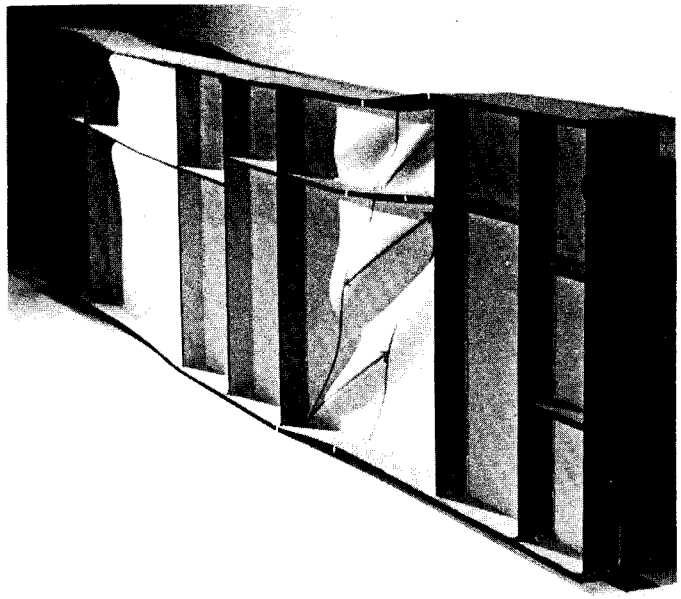

Fig. 6.11 Longitudinally stiffened girder at ultimate load in shear (Rockey et al., 1974).

clear that the other panel was not far behind. To obtain the tension-field shear resistance of a longitudinally stiffened girder the same approach is used for an unstiffened girder, but in computing the tension field stress associated with failure the critical beam-action shear corresponding to buckling of the largest subpanel is used in the yield criterion.

Where longitudinal stiffeners are used in the panel the shear strength under combined shear and bending is treated by Chern and Ostapenko and by Rockey et al. in much the same way as if the panel were under pure shear. However, modifications to the buckling stresses, tension-field stresses, and plastic moments in the flanges to account for the combined stress effects are included. As noted previously, Chern and Ostapenko include the contribution from the longitudinal stiffener in computing the frame-action strength and include the modification of the stiffener's plastic moment capacity to account for the combined stress effects in this case.

Interaction equations to compute the critical buckling stress for each subpanel are presented by Chern and Ostapenko. These equations are similar to Eq. 6.30. The subpanel tension-field stresses are then computed using the state of stress in each subpanel with the yield criterion. Finally, an iterative approach is used to find the shear strength.

Rockey et al. compute the buckling stress in the subpanels by an interaction approach applied to each subpanel stress condition as shown in Fig. 6.12. The

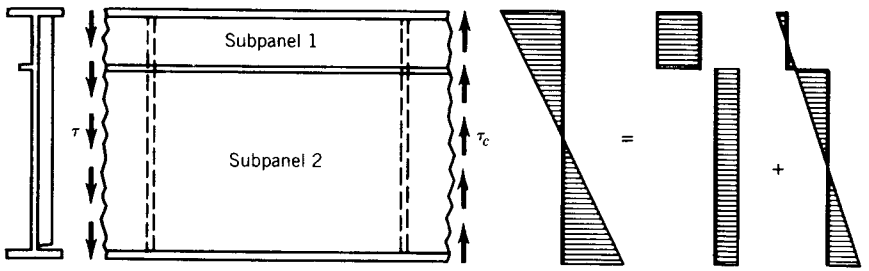

Fig. 6.12 Stress distribution in panels of plate girder under shear and bending.

state of stress in a subpanel is therefore a shear stress τ_c, a pure bending stress σ_{bc}, and an axial stress σ_{cc}. The buckling condition is

$$\frac{\sigma_{cc}}{\sigma_{crc}} + \left(\frac{\sigma_{bc}}{\sigma_{cp}}\right)^2 + \left(\frac{\tau_c}{\tau_{cr}}\right)^2 = 1 \tag{6.34}$$

The postbuckling strength of the panel is determined as if no longitudinal stiffeners were present.

Combined shear and bending of longitudinally stiffened girders with unequal flanges has been investigated by Chern and Ostapenko (1971). Their analysis for shear is based on their tension-field distribution for girders without longitudinal stiffeners with each subpanel treated independently as in Cooper's analysis, and taking into account the plastic moments of the flanges and stiffener and the axial-force reduction in flange plastic moment. The girder strength is determined by shear until the shear-strength curve intersects the curve for bending strength (Fig. 6.8*d*). The analysis involves some lengthy iterations so that it is not suitable for hand computation.

Of the three analyses discussed in this chapter Cooper's is the most conservative and the easiest to use. Rockey's method requires trial-and-error to determine the optimum inclination of the tension field and, for each trial, an iteration to determine the axial-force reduction in flange plastic moment. Finally, Chern and Ostapenko's solution involves so many iterative steps as to be manageable only by digital computer.

A large amount of experimental data is available from tests on transversely stiffened girders with and without longitudinal stiffeners. Many of these data can be found in the previously cited references.

The various theories for predicting the strength of plate girders in bending agree well with the experimental evidence. For example, Table 6.6 compares the theories of Cooper (1965) and Chern and Ostapenko (1970b) with experimental data for several girders with longitudinal stiffeners. As can be seen, there is a good correlation between theory and experimental results. For the nine bending test results compared with Cooper's theory, the average ratio of

TABLE 6.6 Bending Tests on Longitudinally Stiffened Girders[a]

Source of Data	Test Number	Aspect Ratio	Web Depth-to-Thickness Ratio	Experimental ÷ Theoretical	
				Cooper (1965)	Ostapenko and Chern (1970)
Massonnet (1962)	LB2	1.0	447	0.99	0.99
	LB3	1.0	447	1.00	1.00
	LB4	1.5	447	1.02	1.02
	LB5	0.75	447	1.02	1.02
	LB6	1.0	407	0.96	—
Dubas (1971)	D	0.6	299	1.00	—
	E	0.4	401	0.94	—
	3	0.6	300	1.02	—
	4	0.45	400	0.99	—

[a]All longitudinal stiffeners were located at one-fifth the web depth from the compression flange.

TABLE 6.7 Shear Test Results Compared with Cooper (1967) Theory

Test Number	Aspect Ratio	Web Depth-to-Thickness Ratio	Location of Longitudinal Stiffener from Compression Flange[a]	Experimental ÷ Theoretical Load
LS1-T2	1.0	256	0.33*b*	1.10
LS2-T1	1.0	275	0.33*b*	1.06
LS3-T1	1.5	276	0.33*b*	1.10
LS3-T2	1.5	276	0.33*b*	1.17
LS3-T3	0.75	276	0.33*b*	1.07
LS4-T1	1.0	260	0.2*b*	1.00
LS4-T2	1.0	260	0.5*b*	1.18

[a]*b* = web depth (Fig. 6.12).

test ultimate load to predicted ultimate load is 0.99. For four bending tests the Chern and Ostapenko ratio is 1.01.

Tables 6.7 through 6.9 give results of tests on longitudinally stiffened girders subjected to high shear. These results are compared with Cooper's theory (1967) in Table 6.7, Ostapenko and Chern's theory (1970) in Table 6.8, and the theory of Rockey et al. (1974) in Table 6.9. In Table 6.10 the aforementioned theories are compared for the series of tests reported by Cooper.

TABLE 6.8 Comparison of Ostapenko and Chern (1970) Theory with Various Test Results

Source of Data	Test Number	Aspect Ratio	Web Depth-to-Thickness Ratio	Location of Longitudinal Stiffener from Compression Flange[a]	Experimental ÷ Theoretical Load
Cooper (1967)	LS1-T2	1.0	256	0.33*b*	1.00
	LS2-T1	1.0	275	0.33*b*	0.94
	LS3-T1	1.5	276	0.33*b*	1.01
	LS3-T2	1.5	276	0.33*b*	1.00
	LS3-T3	0.75	276	0.33*b*	0.93
	LS4-T1	1.0	260	0.2*b*	1.08
Škaloud (1971)	UG5.1	1.77	400	0.26*b*	1.06
	UG5.2	1.15	400	0.26*b*	1.06
	UG5.3	1.46	400	0.26*b*	0.97
	UG5.4	1.77	264	0.26*b*	1.00
	UG5.5	0.83	264	0.26*b*	0.96
	UG5.6	1.77	264	0.26*b*	0.88
Porter et al. (1975)	F11-T1	1.39	365	0.2*b*	1.03
	F11-T2	1.20	365	0.2*b*	1.14
	F11-T3	1.00	365	0.2*b*	0.94

[a]*b* = web depth (Fig. 6.12).

As can be seen, Cooper's theory conservatively estimates the shear strength consistent with his assumptions. The Chern–Ostapenko and Rockey theories bracket the experimental data and are in good agreement with these tests. It is interesting to note that the average ratio of experimental to theoretical shears equals 1.0 for the Chern–Ostapenko theory based on the 15 tests reported. The standard deviation for these tests is 0.065. A similar comparison obtained using the theory of Rockey et al. gives an average of 1.0 with a standard deviation of 0.051 for 16 tests. More recent work on longitudinally stiffened plate girders design is reported by Maquoi et al. (1983). The buckling of the webs of longitudinally stiffened girders with unsymmetric flanges is treated by Frank and Helwig (1995).

6.9 END PANELS

The tension field in a plate-girder panel is resisted by the flanges and by the adjacent panels and transverse stiffeners. Since the panels adjacent to an interior panel are tension-field designed, they can be counted on to furnish the

TABLE 6.9 Comparison of Test Results with Theory of Rockey et al. (1974)

Girder Number	Aspect Ratio	Web Depth-to-Thickness Ratio	Location of Longitudinal Stiffener from Compression Flange[a]	Experimental ÷ Theoretical Load
SH1	1	387	0.50*b*	0.94
SH1	1	387	0.33*b*	0.99
SH2	1	387	0.20*b*	1.02
SH2	1	387	0.25*b*	1.02
SH2R	1	387	0.20*b*	0.93
SH2R	1	387	0.25*b*	0.93
SH4	1.33	400	0.25*b*	1.09
SH4	1.33	400	0.33*b*	1.07
SH5	1	370	0.25*b*	0.96
SH5	1	370	0.33*b*	0.98
SH7	1.67	295	0.33*b*	1.03
SH7	1.67	295	0.25*b*	1.03
SH8	1.67	295	0.50*b*	0.92
SH8	1.67	295	0.33*b*	1.05
SH9	1	375	0.50*b*	0.99
SH9	1	375	0.33*b*	1.04

[a] b = web depth (Fig. 6.12).

TABLE 6.10 Shear Strength of Longitudinally Stiffened Girders (Chern and Ostapenko, 1971; D'Apice et al., 1966)

Test Number (Cooper, 1967)	Aspect Ratio	Web Depth-to-Thickness Ratio	Location of Longitudinal Stiffener from Compression Flange[a]	Experimental ÷ Theoretical		
				Cooper (1967)	Rockey et al. (1974)	Ostapenko et al. (1971)
LS1-T2	1	256	0.33*b*	1.10	1.05	1.00
LS2-T1	1	275	0.33*b*	1.06	0.95	0.94
LS3-T1	1.5	276	0.33*b*	1.10	0.88	1.01
LS3-T2	1.5	276	0.33*b*	1.17	1.05	1.00
LS3-T3	0.75	276	0.33*b*	1.07	0.93	0.93
LS4-T1	1	260	0.20*b*	1.00	0.99	1.08
LS4-T2	1	260	0.50*b*	1.18	0.95	—

[a] b = web depth (Fig. 6.12).

necessary support. However, an end panel does not have such support and must be designed as a beam-shear panel unless the end stiffeners are designed to resist the bending effect of a tributary tension field. Basler (1963a) assumed that an end panel designed for beam shear can support a tension field in the adjacent interior panel, and this assumption has been generally accepted. This means that the end-panel stiffener spacing can be based on the shear-buckling stress as discussed by Škaloud (1962). If the end panel is designed for tension-field action an end post must be provided. A possible end post consists of the bearing stiffener and an end plate (Fig. 6.4*a*). According to Basler such an end post can be designed as a flexural member consisting of the stiffener and end plate and the portion of the web between, supported at the top and bottom flanges and subjected to the horizontal component of the tension field distributed uniformly over the depth. The required area A_e of the end plate, based on ultimate load considerations, is given by

$$A_e = \frac{(\tau - \tau_{cr})hA_w}{8e\sigma_y} \tag{6.35}$$

where e is the distance between bearing stiffener and end plate (Fig. 6.4). The bearing stiffener itself is designed to support the end reaction. According to tests reported by Schueller and Ostapenko (1970), web shear may control the design of the end post.

6.10 DESIGN OF STIFFENERS

6.10.1 Transverse Stiffeners

Transverse stiffeners must be stiff enough to preserve the straight boundaries that are assumed in computing shear buckling of plate-girder webs. Stein and Fralich (1950) developed a solution for this problem for an infinitely long web with simply supported edges and equally spaced stiffeners. Results were in fair agreement with tests on 20 specimens. Using their numerical data, Bleich developed a formula for the moment of inertia I of the stiffener which can be put in the following form:

$$I = 2.5ht^3\left(\frac{h}{a} - 0.7\frac{a}{h}\right) \qquad a \le h \tag{6.36}$$

The AASHTO formula for load-factor design is

$$I = Jat^3 \tag{6.37a}$$

in which

$$J = 2.5\left(\frac{h}{a}\right)^2 - 2 \leq 0.5 \tag{6.37b}$$

This is the same as Eq. 6.36 except that the coefficient of a/h in the second term in parentheses is 0.8 instead of 0.7.

In girders with longitudinal stiffeners the transverse stiffener must also support the longitudinal stiffener as it forces a horizontal node in the bend-buckling configuration of the web. According to an analysis by Cooper (1967), the required section modulus S_T of the transverse stiffener is given conservatively by $S_T = S_L h/a$, where S_L is the section modulus of the longitudinal stiffener. This requirement is reduced considerably in the AASHTO specification, where $S_T = S_L h/3a$.

Transverse stiffeners in girders that rely on a tension field must also be designed for their role in the development of the diagonal tension. In this situation they are compression members, and so must be checked for local buckling. Furthermore, they must have cross-sectional area adequate for the axial force F that develops. The value of F_s in Basler's solution is

$$F_s = \tfrac{1}{2}\sigma_t at(1 - \cos\theta_d) \tag{6.38a}$$

Substituting the value of σ_t from Eq. 6.7 gives

$$F_s = \tfrac{1}{2}\sigma_{yw} at\left(1 - \frac{\tau_{cr}}{\tau_{yw}}\right)(1 - \cos\theta_d) \tag{6.38b}$$

The AISC formula for the cross-sectional area A_s of stiffeners symmetrical about the plane of the web is derived from Eq. 6.38b by $A_s = F_s/\sigma_{ys}$. If stiffeners are one-sided A_s is multiplied by a factor to correct for eccentricity. The AASHTO formula, given here in the notation of this chapter, is a modification of Eq. 6.38b.

$$A_s = \left[0.15Bht(1 - C)\frac{V}{V_u} - 18t^2\right]\frac{\sigma_{yw}}{\sigma_{ys}} \tag{6.39}$$

In this formula C replaces τ_{cr}/τ_y in Eq. 6.38b, B is a factor to correct for one-sided stiffeners, and the term $18t^2$ is the area of a portion of the web assumed to act with the stiffener. The reduction in required area effected by V/V_u, where V is the design ultimate-load shear and V_u the shear strength of the panel, is also permitted by the AISC specification.

If longitudinally stiffened girders are assumed to develop independent tension fields in their subpanels, as Cooper assumes, then Eq. 6.39 can be used to determine transverse stiffener area if h is taken to be the depth of the deeper subpanel. (The stiffener area requirement by this equation will always be larger for the deeper subpanel.) On the other hand, if a panel of a longitudinally stiffened girder develops the same tension field as it would without the longitudinal stiffener, as Rockey's work appears to show, then transverse-stiffener area requirements are the same for both.

In addition to the effects of axial force from the tension field, British Standard BS 5400: Part 3 (BSI, 1982) accounts for the destabilizing forces arising from the action of stresses in the plane of the girder web on the initial displacements of the transverse stiffeners. This destabilizing effect is assessed by assuming that adjacent transverse stiffeners have initial displacements which alternate on each side of the girder web in a "sawtooth" progression. Horne (1980) has shown that the magnification of displacements, and the consequential bending stresses in the stiffeners, by the longitudinal and shear stress in the plate panels are equivalent to the effect produced by an imaginary axial force in the stiffeners. An approximate formula for a strut with an initial imperfection of length/750 is utilized for the design of the transverse stiffeners.

6.10.2 Longitudinal Stiffeners

A longitudinal stiffener must be stiff enough to maintain a node in a buckled web and must resist axial compression because of its location in the compression zone of the web. Therefore, both moment of inertia and cross-sectional area enter into a determination of its size. There have been a number of analytical investigations of this problem. Results are usually expressed in terms of three parameters: (1) $\gamma^* = EI/hD$, where I is the moment of inertia of the stiffener and $D = Et^3/12(1 - \nu^2)$ (2) $\delta = A_s/ht$, in which A_s is the area of the stiffener, and (3) the panel aspect ratio a/h. Empirical formulas involving these parameters for various positions of the stiffener have been developed from numerical data, and charts (Klöppel and Scheer, 1960) are available.

The AASHTO formula for moment of inertia of a longitudinal stiffener at $h/5$ from the compression flange is

$$I_s = ht^3(2.4\alpha^2 - 0.13)$$

It will be noted that this equation does not contain δ. However, it is in fairly good agreement with the values of γ^* by Dubas (1948) for $\delta = 0.10$ in the range $0.5 \leq \alpha \leq 1.6$, and since γ^* decreases with decrease in δ, it is a reasonable upper bound for girders of practical proportions. It is important to note that these values of γ^* are derived from linear-buckling analysis and give a stiffness that guarantees only the critical load.

In calculating γ^* a portion of the web should be considered as part of the cross section. Strain measurements reported by Massonnet (1962) showed a mean effective width of $20t$. Tests show that the theoretical values must be increased considerably to develop the ultimate strength. Massonnet found that they should be multiplied by a factor ranging from 3 for a longitudinal stiffener at middepth to 7 for one at $h/5$ from the compression flange. This conclusion has been verified by a number of other investigators (Rockey, 1971a,b; Dubas, 1971). Further extensions were proposed by Maquoi et al. (1983). It is

apparent, however, that there is a considerable range in the empirical multiplication factors. Difficulties may arise in practice in deciding on an appropriate factor to be used for a particular combination of applied stress and stiffener geometry.

An alternative approach to the design of a longitudinal web stiffener is to treat it as a column. This approach has been adopted in BS 5400: Part 3 (BSI, 1982). Axial loading of the strut includes the longitudinal stress due to girder bending moment plus an axial load equivalent to the destabilizing effect of shear stress and in-plane stress transverse to the stiffener. For the design of longitudinal stiffeners an effective width of web plate of $16t$ on each side of the stiffener is considered.

6.11 PANELS UNDER EDGE LOADING

Girders often support loads on the top flange which produce compression on the edge of the web. They may be distributed over large distances, in some cases the length of the girder, or over relatively small distances, in which case they can be taken as concentrated loads. Bearing stiffeners may be needed for concentrated loads, but in some cases the web can carry them unaided.

A number of studies of buckling of plate elements under edge loading have been made (Girkmann, 1936; Zetlin, 1955; Wilkesmann, 1960; Klöppel and Wagemann, 1964; Warkenthin, 1965; Kawana and Yamakoshi, 1965; Bossert and Ostapenko, 1967; Ostapenko et al., 1968; Rockey and Bagchi, 1970; Khan and Walker, 1972; Khan et al., 1977).

The ultimate strength of a web under edge loading may exceed the buckling load by a considerable margin, and several experimental investigations to determine ultimate strengths have been made. Bossert and Ostapenko (1967) and Ostapenko et al. (1968) used a finite difference analysis to determine the web-buckling stress for a panel subjected to bending and an edge load distributed uniformly over the panel. The web was assumed to be fixed at the flanges and simply supported at the stiffeners. Ten tests were made on three plate-girder specimens with aspect ratios varying from 0.8 to 1.6 and ratios of extreme-fiber bending stress to edge stress from 0 to 5. The resulting ultimate strengths are shown in Fig. 6.13. The horizontal line through the ordinate 3 gives a lower bound on the experimental strengths. The following formula for the allowable edge stress $\sigma_{e(\text{all})}$ gives a factor of safety of 2 on the lower-bound ultimate edge stress:

$$\sigma_{e(\text{all})} = \frac{1}{\sqrt{a/h}} \frac{24{,}000}{(h/t)^2} \frac{K}{\sqrt{F_y}} \tag{6.40}$$

where K is a coefficient given in Fig. 6.14.

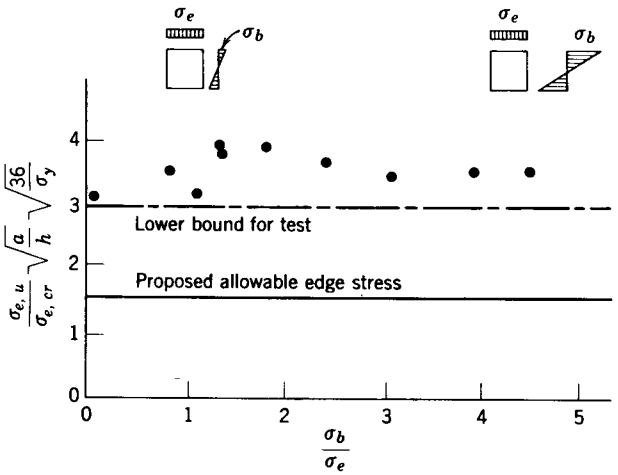

Fig. 6.13 Web plates under edge loading.

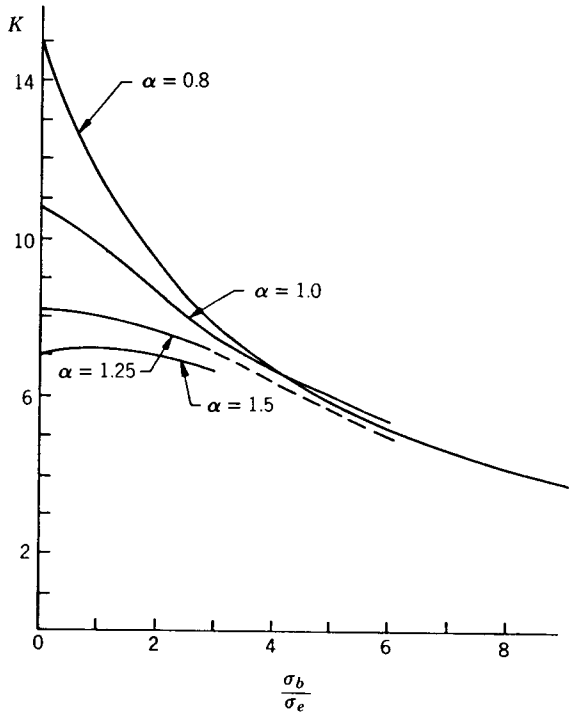

Fig. 6.14 Values of K in Eq. 6.40.

Rockey et al. (1972), Elgaaly and Rockey (1973), Elgaaly (1975, 1977), and Bagchi and Rockey (1975) used the finite element method to determine the buckling load of a plate simply supported on all four edges and subjected to a partial edge loading (patch loading). Results were also obtained for the cases of a panel with patch load and shear, and patch load and moment. Values of the coefficient k in the buckling formula (Eq. 4.1) were determined.

Results of patch-load tests on 20 trough-section beams of 15-ft span are reported by Elgaaly and Rockey (1973). The objective was to determine the interaction between edge loading and pure in-plane bending. The ratio c/a was 0.2 for all tests. It was found that the moment did not significantly reduce patch-loading strength until it exceeded 50% of the bending strength of the panel.

Elgaaly (1975) conducted tests on 18 trough-section beams of about 2 ft span, to determine the interaction between the ultimate strength under edge loading and shear. The ratio c/a was 0.2 for all tests and the panel slenderness ratio was 325 for 12 specimens and 200 for the remaining six. The results from the tests show that the presence of shear will reduce the ultimate load-carrying capacity of the web under edge loading, and an approximate relationship for this reduction was established. It was shown also that the postbuckling strength increases with the increase in the panel slenderness ratio. Furthermore, panels subjected to the combination of edge loading and shear exhibit a higher ultimate strength-to-buckling strength ratio than panels subjected to edge loading only.

The effect of flange thickness on web capacity under direct in-plane loading was also examined (Elgaaly, 1977) and results of patch-load tests on five welded girders are reported. The web dimensions were kept identical in all five girders (aspect ratio = 1 and slenderness ratio = 250). The c/a ratio was 0.2 for all tests. The results from these tests are given in Fig. 6.15.

A theoretical study (Roberts and Rockey, 1979) was carried out to determine the influence of a longitudinal stiffener on the ultimate capacity of a concentrated edge load. The study was restricted to the consideration of the buckling of a square plate panel reinforced by a single longitudinal stiffener at the one-fifth depth position. It was shown that the presence of the stiffener significantly increased the edge load. Values of buckling coefficients relating buckling resistance of the plate and the flexural rigidity of the longitudinal stiffener are provided.

The research described above is applicable to either flangeless panels or to beams with very thin flanges. However, in the case of plate girders and I-beams with reasonably thick flanges, it can be expected that the flanges will make a significant contribution to resisting local loading. On the basis of a preliminary series of tests Granholm (1960) and Bergfelt and Hövik (1968) concluded that web thickness was the most important parameter affecting the ultimate concentrated edge load, and proposed an empirical formula $P_u = 8.5t_w^2$ for mild steel (P_u is obtained in kN if t_w is given in millimeters). These tests had thin flanges and the failure mode was local yielding of the webs under the concentrated load. Further tests by Bergfelt (1976) on specimens with higher ratios of flange-to-web thickness showed that the failure load is also influenced by the bending stiffness of the flange and that failure involved a combination of yielding and buckling of the web. The ultimate load for the "weak" flange case where web yielding controls may be predicted by

$$P_u = 13\eta t_{fi} t_w \sigma_y \tag{6.41}$$

where t_{fi} is an equivalent flange thickness given by $t_{fi} = t_f(b/25t_f)^{1/4}$ to account for b/t values other than 25, and η is a parameter dependent on t_{fi}/t_w as follows:

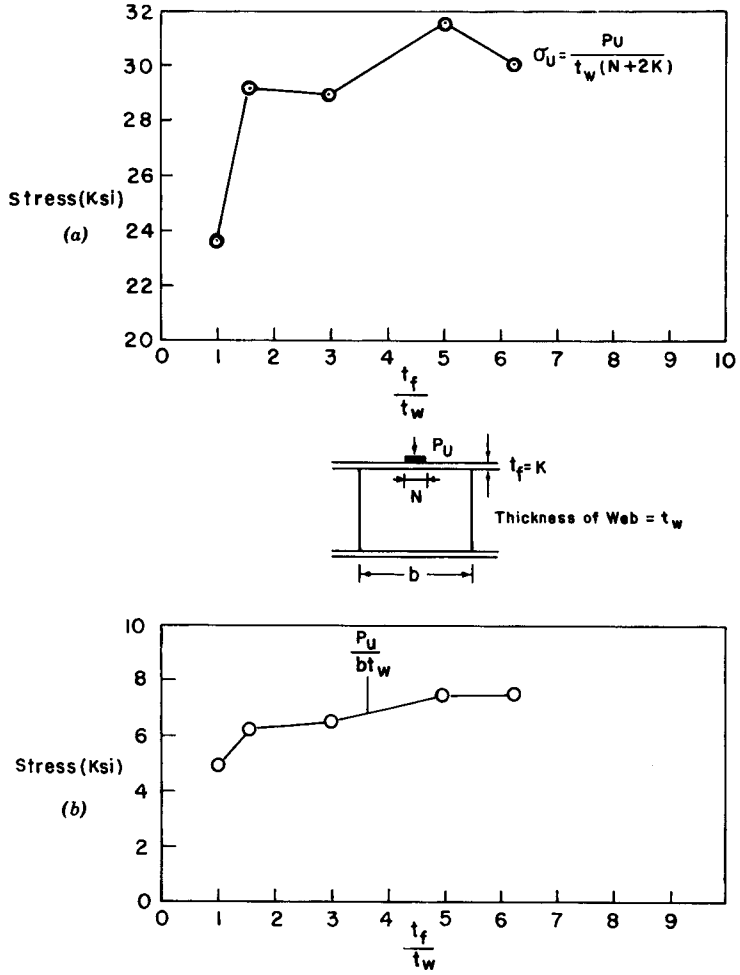

Fig. 6.15 Test results (Elgaaly, 1977).

t_{fi}/t_w	0.5	1.0	1.5	2.0
η	0.55	0.65	0.85	2.00

The theoretical basis for Eq. 6.41 is the treatment of the flange as a beam on an elastic foundation with plasticity accounted for by adjustments to the spring constants. Use of the η values, tabulated above, limits the ultimate load to a value associated with the start of rapidly increasing vertical deformation of the flange. For the "strong" flange case the following empirical formula shows good correlation with test results:

$$P_u = 0.6t_w^2(E\sigma_y)^{1/2}\left(1+\frac{0.4t_{fi}}{t_w}\right) \tag{6.42}$$

The ultimate concentrated load as given by Eqs. 6.41 and 6.42 is shown in Fig. 6.16. Where $t_{fi}/t_w = 2$ for mild steel both equations predict a failure load in close agreement with Granholm's original formula. Bergfelt's formulas are applicable when the load is concentrated as a sharp edge load. Where the load is distributed along a web length c the ultimate load given by Eqs. 6.41 and 6.42 should be multiplied by a factor $f(c)$ given by

$$f(c) = \frac{\gamma}{1-e^{-\gamma}\cos\gamma} \leq 1.3 \tag{6.43}$$

where $\gamma = c/2L$ and $L = 6.7t_f$.

The limitation of 1.3 on the factor $f(c)$ is imposed to reflect the observation that when the load is distributed along the web, buckling will occur before yielding and thus the distribution length has a small influence on the ultimate load. For combined bending moment and concentrated load it was observed

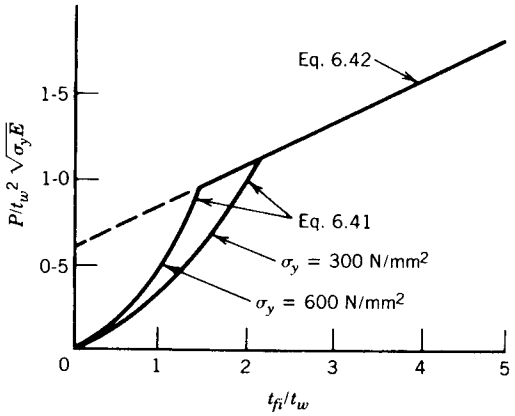

Fig. 6.16 Ultimate concentrated loads from Eqs. 6.41 and 6.42.

that a reasonable lower bound to test results is obtained when the value of P_u from Eqs. 6.41 and 6.42 is multiplied by the following correction factor proposed by Djubek and Škaloud (1976):

$$\left[1-\left(\frac{\sigma_b}{\sigma_y}\right)^2\right]^{1/2} \tag{6.44}$$

Roberts and Rockey (1979) developed a method based on the upper bound theorem of plastic collapse for predicting the ultimate value of a concentrated edge load. The assumed failure mechanism, involving plastic hinges in the flange and web, is shown in Fig. 6.17*a*. Equating external and internal work gives an expression from which the ultimate load P_u may be determined if the web hinge location α is known. The latter is chosen empirically to agree with test results. The solution presented by Roberts and Rockey (1979) contains an error in the expression which was pointed out and corrected by Chatterjee (1980). The mechanism solution overestimates the experimental collapse load when the loaded length c becomes too large. Consequently, upper limits are placed on c so that the correlation with test data is satisfactory. For stocky webs failure may be initiated by direct yielding of the web resulting in the vertical descent of the applied load and a failure mechanism of the type shown in Fig. 6.17*b*. For this type of failure the restrictions concerning the loaded length c do not apply. The actual value of the collapse load should be taken as the smaller of either the bending-type failure or the direct compression failure of the web. For the girders tested, rotation of the flange was prevented by the loading arrangement—the usual situation in most of the tests with concentrated loads. Hence the theoretical work in general is applicable to the case of flanges restrained against rotation. The mechanism solution was extended by Roberts and Chong (1981) to a loading condition in which the edge load is uniformly distributed between vertical stiffeners as indicated in Fig. 6.17*c*.

To account for the interaction between coexisting global bending and local bending stresses, a correction factor of the type given in Eq. 6.44 could be applied to the values of P_u predicted by the mechanism solution. The provisions for patch loading contained in BS 5400; Part 3 (BSI, 1982) are based on a modified version of the mechanism solution of Roberts and Rockey.

Herzog (1974b,c) analyzed the results of the 72 tests reported by Bergfelt and Hövik (1968), Bergfelt (1971), and Škaloud and Novak (1972) and developed the empirical formula

$$P = 100t^2\left[1.2+\frac{5I_f h}{AI_w t}\left(1+\frac{c}{h}\right)^2\left(0.85+0.01\frac{a}{h}\right)\right]\left[1-\left(\frac{\sigma_b}{\sigma_y}\right)^2\right]^{1/8} \tag{6.45}$$

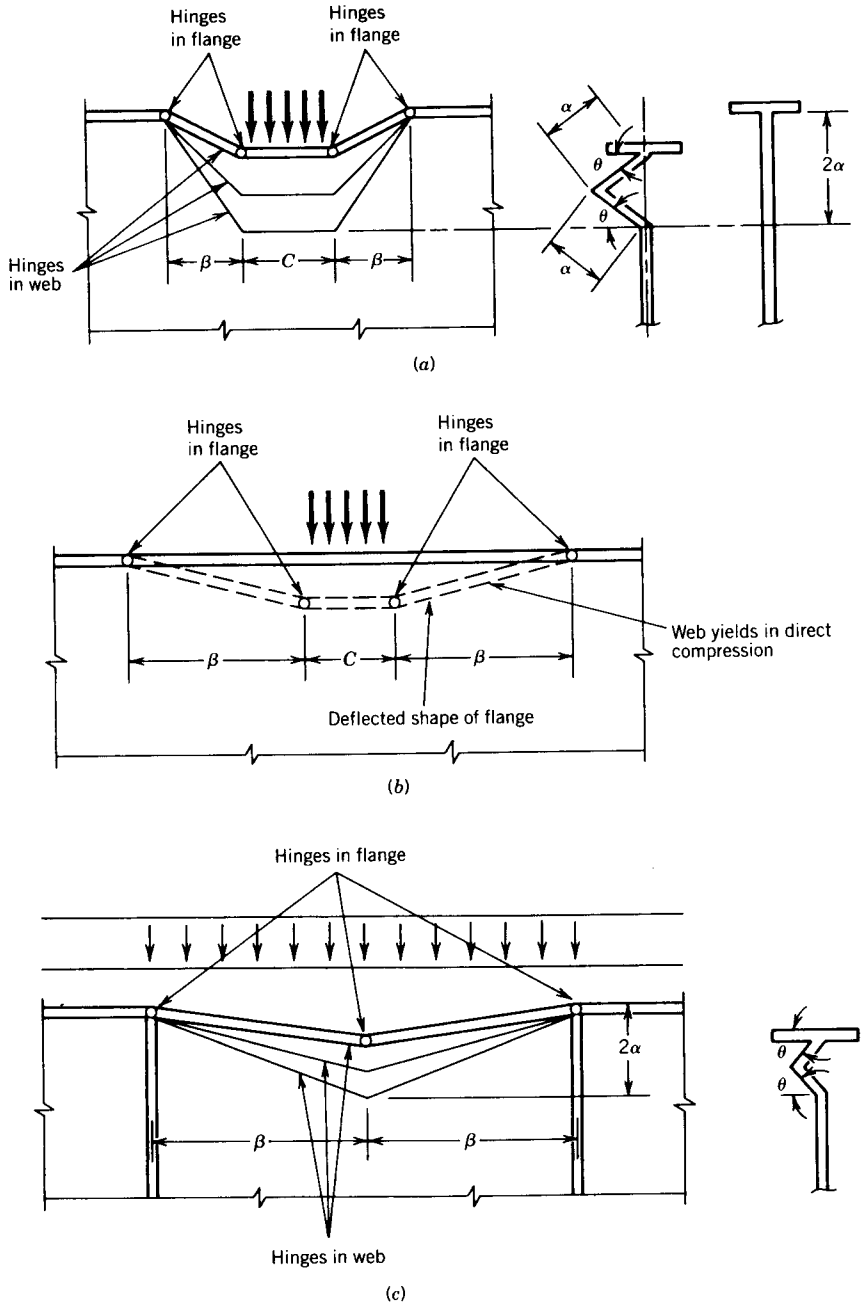

Fig. 6.17 Failure mechanism models.

The mean value of the ratios of test load to predicted load by this formula was 1.001 with a standard deviation of 0.141.

Recently, the effect of nearly concentrated edge loads on webs was investigated by Aribert et al. (1981) with emphasis on concentrated direct loads on the web of a wide-flange column resulting from the end moment of a connected beam. The studies on crippling of plate-girder webs, subjected to patch or distributed edge loading have been summarized by Elgaaly (1983), and design recommendations to prevent web crippling were suggested.

Further tests and finite element analyses were performed by Elgaaly et al. (1991b, 1992) to supplement the data available. Results of recent investigations in Europe and Japan (Shimizu et al., 1989a and b; Drdacky, 1991; Höglund 1991; Raoul et al., 1991; Spinassas et al., 1991) also add to the state of knowledge in this field. The formula to predict the ultimate capacity of webs when subjected to in-plane patch loading, developed by Roberts (1981), properly includes the effects of all the parameters that have influence on the capacity. This formula was adopted by AISC (1989, 1993) to determine the nominal strength of the web against crippling:

$$P_u = Kt_w^2\left[1 + 3\left(\frac{N}{d}\right)\left(\frac{t_w}{t_f}\right)^{1.5}\right]\left(\frac{F_{yw}t_f}{t_w}\right)^{0.5} \tag{6.46}$$

where

P_u = ultimate capacity
K = a constant
t_w = web thickness
N = width of patch
d = beam or web depth
t_f = loaded flange thickness
F_{yw} = yield stress of web material

The constant K was taken to be 135 for loads applied at a distance not less than $d/2$ from the end of the member, and 68 if the load is applied at a distance less than $d/2$ from the end. The choice of the distance $d/2$ appears to be arbitrary, and it creates a discontinuity. Furthermore, it was noted that for the case where the load is at a distance $0.5N$ from the end of the beam and N is less than d, the use of K equal to 68 is conservative. Some of this conservatism was eliminated in the latest edition of the AISC–LRFD specification (AISC, 1993), based on Elgaaly et al.'s (1991b) research results.

In case a longitudinal stiffener is provided to increase the capacity of the web under in-plane bending, the stiffener is usually placed at a distance equal to 0.2 to 0.25 times the web depth from the compression flange. The effect of the presence of such a stiffener on the behavior of the web under in-plane compressive edge loads was investigated at the University of Maine (Elgaaly

and Salkar, 1992) as well as at Shinshu University in Japan (Shimizu et al., 1991), Chalmers University in Sweden (Bergfelt, 1983), and the Building Research Institute of the Czech Technical University in Prague (Kutmanova et al., 1991). The conclusion that can be made, based on the aforementioned studies, is that the effect of such a stiffener on the ultimate capacity of the web, under in-plane compressive edge loading, is generally negligible. This is different from the conclusion reached by Rockey based on his theoretical studies on the effect of the longitudinal stiffener on the elastic web buckling under compressive edge loading, discussed earlier in this chapter.

Research work by Herzog, Skaloud, and Elgaaly reported by Elgaaly (1983) indicated that the following formula can be used to determine a reduction factor R which should be multiplied by the ultimate capacity of the web under edge loading to include the effect of the presence of global in-plane bending:

$$R = [1 - (f_b/F_y)^3]^{1/3}$$

where f_b is the actual global bending stress. Research work by Elgaaly (1975) indicated that the presence of global shear will reduce the ultimate capacity of the web under discrete edge compressive loads. This was based on the results from 18 tests conducted on slender webs ($d/t_w = 325$ and 200) with N/d equal to 0.2. General recommendations to estimate the reduction in the crippling strength due to the presence of global shear cannot be made due to the limited results that are available. More research work on the effect of the presence of global bending and/or shear on the ultimate capacity of the web under edge compressive loads is needed. The AISC specification does not address the effects of the presence of global bending and/or shear on the crippling load capacity of the web.

Eccentric Loads. Eccentricities with respect to the plane of the web are unavoidable in practice. Therefore, the strength of the web under eccentric loads needs to be examined. Research work was conducted at the University of Maine to study the effect of these possible eccentricities (Elgaaly and Nunan, 1989, Elgaaly et al. 1989, Elgaaly et al., 1991b 1992). The maximum eccentricity that was considered is equal to one-sixth times the width of the flange. The study includes both experimental and analytical work. From the test results it was found that there is no reduction in the ultimate capacity due to the eccentricity when the load was applied through a thick patch plate placed eccentrically with respect to the plane of the web; however, reductions occurred when the load was applied through a cylindrical roller; as shown in Fig. 6.18. To quantify the reduction in the strength due to the eccentricities, several rolled and built-up sections were tested, and finite element models for more beams were analyzed. As shown in Fig. 6.19, the reduction was found to be function of t_f/t_w and varies linearly with e/b_f, where e and b_f are the eccentricity and the flange width, respectively.

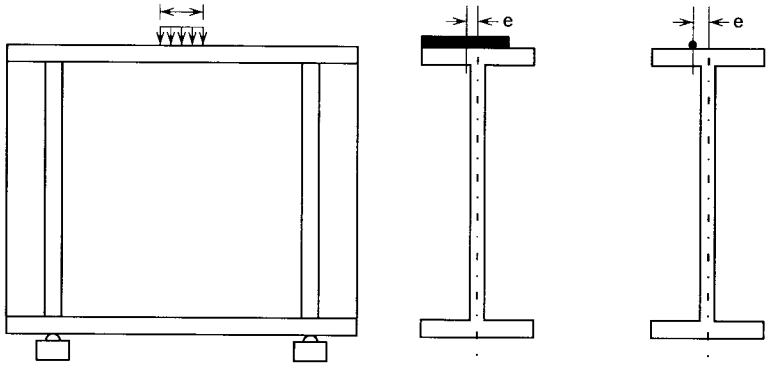

Fig. 6.18 Eccentric loads with respect to the plane of the web.

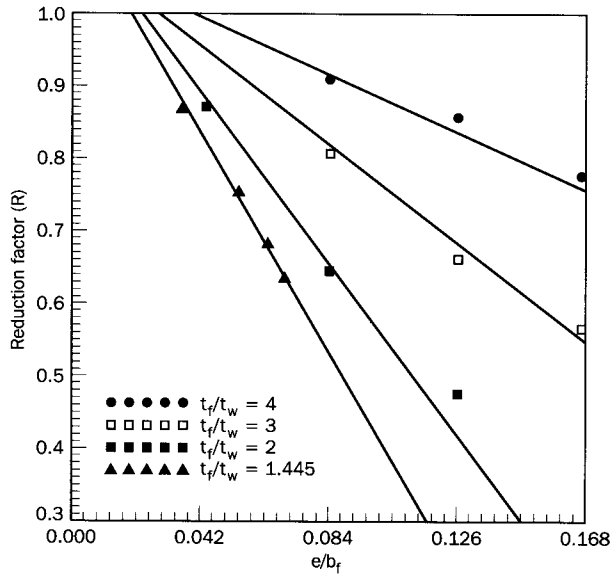

Fig. 6.19 Reduction in ultimate capacity due to load eccentricity.

A reduction factor R can be calculated using the formula

$$R = m\frac{e}{b_f} + c$$

where

$$R < 1.0$$

$$m = -0.45\left(\frac{t_f}{t_w}\right)^2 + 4.55\left(\frac{t_f}{t_w}\right) - 12.75$$

$$c = 1.15 - 0.025\left(\frac{t_f}{t_w}\right)$$

The straight-line equations for the reduction factor R are shown in Fig. 6.19 together with the test results. Since the reduction factor equation is empirical, it should be used only within the range of the test (experimental and analytical models) data: namely, f_f/t_w equal to 1 to 4 and e/b_f less than one-sixth.

Bearing Stiffeners. It appears that no research work was published on the behavior of stiffened webs under concentrated compressive loads. The AISC specification requires that stiffeners to prevent web crippling should be double-sided and extend at least one-half the web depth. According to the specification, stiffeners under concentrated compressive loads should be designed as axially loaded columns with an effective length equal to 0.75 of the web depth. Furthermore, the cross section of such a column should be taken as composed of the pair of stiffeners and a strip of the web having a width equal to 25 times the web thickness.

Tests and finite element analysis were conducted to study the behavior of the stiffened webs under concentrated edge loads (Elgaaly et al., 1992 and Elgaaly and Eash, 1993). The load was applied on the top flange using a roller, a patch plate, or a W-shape, as shown in Fig. 6.20. It was found that the behavior of the web and the failure loads were almost identical in the tests where the load was applied through a roller or the W-shape. In some tests the load was applied with a small eccentricity e_1 with respect to the vertical axis of the stiffener. In the case where the load was applied through a patch plate, the eccentricity had

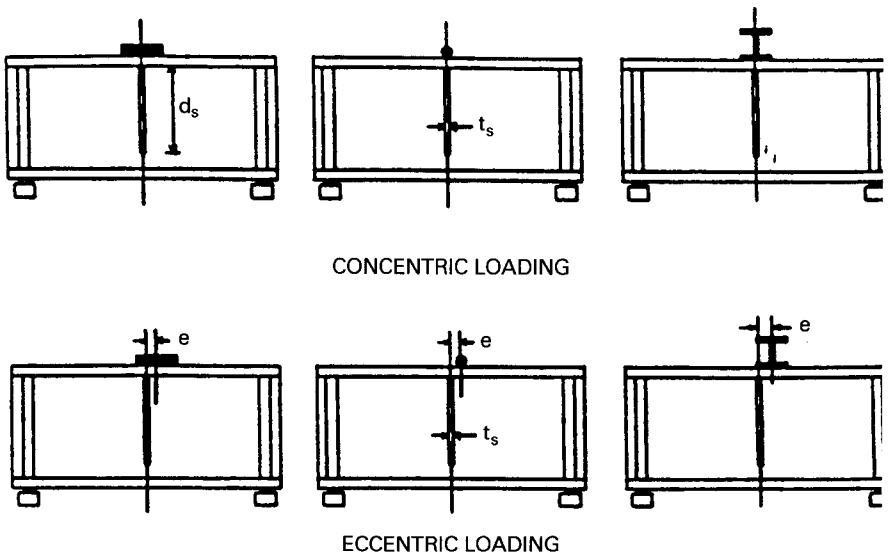

Fig. 6.20 Method of load application.

negligible effect on the results. The eccentricity, however, had an effect on the failure load and the web behavior when the load was applied through a roller.

In the case of deep stiffeners ($d_s/d > 0.75$), failure was due to the buckling of the stiffener (mostly global). It appears that the effective width of the web, which acts together with the stiffener, varies along the depth of the stiffener; and it is bigger near the load. The reduction in the failure load due to an eccentricity of 0.5 in. was found to be about 15%. In the case of the shallow stiffeners ($d_s/d < 0.5$), failure was due to local buckling of the stiffener, buckling of the web below the stiffener, or a combination thereof. The reduction in the failure load due to a 0.5 in. eccentricity was found to be about 6 to 14% for thin to thick stiffeners, respectively.

The requirements in the AISC specification regarding the design of end stiffeners, subjected to concentrated loads, are similar to the requirements for the design of an intermediate stiffener. The only difference is in the strip width of the web, which is to be considered effective with the stiffener. The width of this strip in the case of end stiffeners is only 12 times the web thickness, instead of 25 times the web thickness in the case of intermediate stiffeners.

A total of 31 tests were conducted to examine the behavior of the stiffened web over the support (Elgaaly et al., 1992 and Elgaaly and Eash, 1993). In few tests the support was eccentric with respect to the centerline of the stiffener. In Fig. 6.21, the failure loads are plotted vs. the depth of the stiffener relative to the beam depth d_s/d for stiffener thickness t_s equal to $\frac{3}{16}$, $\frac{1}{4}$, and $\frac{5}{16}$ in. As can be

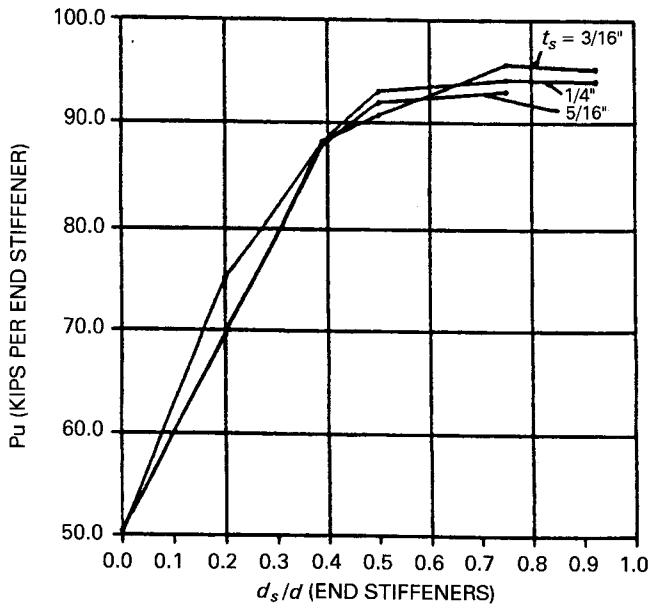

Fig. 6.21 Web with end stiffener ultimate capacity as a function of d_s/d and t_s.

noted from the figure, the ultimate capacity of the stiffened web reached a maximum value at a stiffener depth d_s equal to $0.75d$, and this maximum value was independent of the stiffener thickness. It has to be noted that the ultimate capacity correponds to the web panel shear capacity.

6.12 FATIGUE

Investigations have shown that the ultimate strength of thin-web plate girders under static load is not affected by initial out-of-flatness of the web (Shelestenko et al., 1970). On the other hand, fatigue cracks may develop at the web-to-flange juncture due to a lateral bending of the web under repeated loads (Maeda, 1971; Patterson et al., 1970). The magnitude of the initial deflection of the web and the extent to which the repeated stress exceeds the buckling stress appear to be the principal factors influencing the development of these tracks (Patterson et al., 1970; Parsanejad and Ostapenko, 1970). The factors are functions of the web slenderness and the panel aspect ratio.

According to the AASHTO specifications for load-factor design, webs without longitudinal stiffeners must have slenderness that satisfy the formula

$$\frac{h}{t} \leq \frac{36{,}500}{\sqrt{F_{y,\text{psi}}}} \tag{6.47}$$

If the girder has unequal flanges, h in this equation is replaced by $2y_0$, where y_0 is the portion of the web in compression. This limit may be somewhat conservative (Chern, and Ostapenko 1970a).

6.13 DESIGN PRINCIPLES AND PHILOSOPHIES

Despite the general recognition that the classical buckling theory is an inadequate guide to the prediction of the strength of plates panels in shear or compression, it must also be realized that comprehensive ultimate strength models are not yet fully developed. A situation exists, therefore, where some countries have opted to make use of ultimate strength theory when justified, while others prefer to rely in varying degrees on the use of the classical linear theory of plate buckling. Consequently, current design criteria for plate girders vary widely depending on the philosophy of design. It is interesting to compare the design provisions for plate girders adopted in various countries.

The current AISC specification and the allowable stress and load factor design methods of the AASHTO specification recognize the contribution of tension-field action. Design for shear is then based on simplified expressions of Basler's formulas. AASHTO allows the use of a single longitudinal stiffener located at one-fifth of the depth from the compression flange, its principal

function being the control of lateral web deflections. This reduction of out-of-plate deflections both improves the fatigue life of the web and permits the use of thinner web plates. The existing AASHTO provisions for transverse and longitudinal stiffeners prescribe minimum rigidities based on elastic buckling theory. These provisions are intended for moderate-span plate-girder bridges and are not adequate for long-span plate girders requiring very deep webs. For such cases, the problems requiring consideration include the design of deep webs with multiple longitudinal stiffeners, the development of new design methods for stiffener proportioning, the establishment of a procedure to account for axial load shedding from web to compression flange, and the development of a general ultimate strength method for transversely and longitudinally stiffened webs. Some of these problems have been investigated in a recent study carried out under the sponsorship of the Federal Highway Administration (FHWA, 1980).

In British Standard BS 5400: Part 3 (BSI, 1982) girders are classified into two categories: those without longitudinal web stiffeners and those with such stiffeners. For the former, experimental data were thought to be sufficiently complete to justify the use of tension-field theory and an adaptation of the Rockey model is used for the ultimate shear strength. For the latter, it was thought that ultimate strength criteria had not been sufficiently established for longitudinal web (or box girder flange) stiffeners to cope with the associated high shear deformations. Therefore, the design of webs in girders containing longitudinal stiffeners is based on web panel behavior which stops short of the tension-field mechanism. Individual plate panels are subject to checks for yielding and buckling. The buckling check uses coefficients based on a large-deflection, elastic-plastic numerical study of initially imperfect plates under various stress patterns. (Harding and Hobbs, 1979). Stiffener design is based on a strength criterion which attempts to assess the function of the stiffeners in controlling the stability of the plate panels.

6.14 GIRDERS WITH CORRUGATED WEBS

Elgaaly and Hamilton (1993) performed 42 tests on 21 beams. Four different corrugation configurations (Table 6.11) and two thicknesses were used. All of the beams failed due to buckling of the web. The test results are given in Tables 6.12 and 6.13, where τ_e is the experimental shear stress at failure. Failure in all the specimens except those made of dense corrugation was initiated by local buckling of one of the corrugation fields, which propagated to other fields. The failure was sudden and the load-carrying capacity drops at the failure load and the specimen exhibits some residual strength of about 75% of its ultimate capacity. In the case of dense corrugation the failure was due to global buckling of the panel as an orthotropic plate.

The ultimate shear stress τ_f from finite element analysis (Elgaaly et al., 1995b) and the test results τ_e are given in Tables 6.12 and 6.13; where τ_y is

TABLE 6.11 Corrugation Configurations for Test Specimens

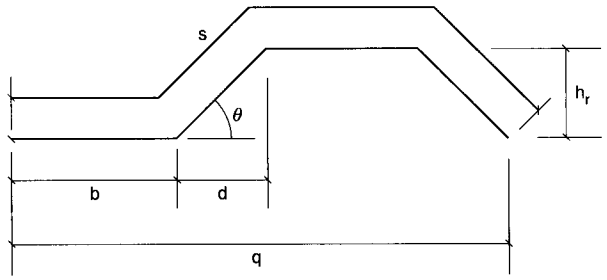

Panel Type	b [in. (mm)]	d [in. (mm)]	h_r [in. (mm)]	θ (deg)	s [in. (mm)]	q [in. (mm)]
UFS	0.78	0.47	0.56	50	3.0	2.5
	(19.8)	(11.9)	(14.2)		(76.2)	(63.5)
UF1X	1.50	1.00	1.00	45	5.83	5.0
	(38.1)	(25.4)	(25.4)		(148.1)	(127.0)
UFX-36	1.65	0.92	1.31	55	6.5	5.14
	(41.9)	(23.4)	(33.3)		(165.1)	(130.6)
UF2X	1.96	1.04	2.00	62.5	8.43	6.00
	(49.8)	(26.4)	(50.8)		(214.1)	(152.4)

the yield stress of the material. As can be noted from these tables; agreement between the analytical and experimental results is satisfactory. The average ratio between the analytical and experimental results is satisfactory. The average ratio between the analytical and the experimental results is 1.15. The primary reason that the analytical results are higher than the experimental results could be the presence of unavoidable out-of-plane initial imperfections in the test specimens.

In the local buckling mode, the corrugated web acts as a series of flat plate subpanels that mutually support each other along their vertical (longer) edges and are supported by the flanges at their horizontal (shorter) edges. These flat plate subpanels are subjected to shear; and the elastic buckling stress is given by

$$\tau_{cre} = k_s \frac{\pi^2 E}{12(1-\nu^2)(w/t)^2}$$

where

TABLE 6.12 Stresses Based on Local Buckling Versus Stresses From Finite Element Analysis[a]

Panel	τ_f (ksi)	τ_e (ksi)	τ_e/τ_f	τ_y (ksi)	τ_{ssf} (ksi)	τ_f/τ_{ssf}	τ_{fx} (ksi)	τ_f/τ_{fx}	τ_f/τ_a
V121216A	44.92	37.35	0.83	56.58	41.02	1.10	54.87[b]	0.82	0.94
V121216B	52.71	54.54	1.04	55.71	51.57[b]	1.03	65.29[b]	0.95[c]	0.99
V121221A	39.95	34.95	0.88	55.71	33.23	1.20	48.96[b]	0.82	0.97
V121221B	52.72	43.96	0.83	55.71	47.95[b]	1.10	61.00[b]	0.95[c]	1.02
V121232A	31.68	30.59	0.97	55.71	18.76	1.69	30.16	1.05	1.30
V121232B	43.97	37.32	0.85	53.69	27.84	1.58	43.85[b]	1.00	1.23
V121832A	24.11	25.63	1.06	58.89	18.76	1.29	30.16	0.80	0.99
V121832B	43.26	27.62	0.64	47.05	38.17[b]	1.13	48.40[b]	0.92[c]	1.02
V122421A	35.18	30.48	0.87	51.96	38.23	0.92	50.71[b]	0.69	0.79
V122421B	50.49	37.23	0.74	53.41	46.80[b]	1.08	59.53[b]	0.95[c]	1.01
V122432A	27.31	23.15	0.85	59.76	18.76	1.46	30.16	0.91	1.12
V122432B	33.01	29.96	0.91	53.12	27.66	1.19	43.47[b]	0.76	0.93
V181216B	40.12	48.61	1.21	51.78	36.98	1.09	50.06[b]	0.80	0.92
V181216C	55.46	49.91	0.90	56.82	51.07[b]	1.09	65.33[b]	0.98[c]	1.03
V181221A	34.79	32.18	0.93	48.39	30.65	1.14	44.01[b]	0.79	0.93
V181221B	47.57	40.74	0.86	50.74	44.09[b]	1.08	56.33[b]	0.94[c]	1.00
V181232A	23.57	27.42	1.16	46.19	15.98	1.48	25.92	0.91	1.13
V181232B	33.33	33.90	1.02	50.44	25.18	1.32	40.60[b]	0.82	1.01
V181816A	41.69	37.33	0.90	49.53	39.88[b]	1.05	51.00[b]	0.84[c]	0.93
V181816B	51.44	41.42	0.81	51.40	47.12[b]	1.09	60.26[b]	1.00[c]	1.04
V181821A	35.13	28.22	0.80	46.19	33.26	1.06	44.79[b]	0.78	0.90
V181821B	45.08	40.23	0.89	49.91	47.27[b]	1.07	54.01[b]	0.90[c]	0.98
V181832A	27.69	27.55	1.00	57.74	16.67	1.66	27.03	1.02	1.27
V181832B	31.68	33.30	1.05	48.57	25.18	1.26	39.84[b]	0.80	0.98
V241216A	40.83	28.32	0.69	49.53	39.73[b]	1.03	50.95[b]	0.82[c]	0.92
V241216B	49.36	40.30	0.82	49.23	49.11[b]	1.01	62.99[b]	1.00[c]	1.00
V241221A	36.09	30.16	0.84	51.05	30.41	1.19	45.15[b]	0.80	0.96
V241221B	46.69	39.57	0.85	53.48	45.08[b]	1.04	57.77[b]	0.87[c]	0.95
V241232A	26.87	26.41	0.98	56.38	17.19	1.56	28.05	0.96	1.19
V241232B	33.53	31.68	0.95	48.93	25.78	1.30	40.58[b]	0.83	1.01

[a] $\tau_a = 0.5(\tau_{ssf} + \tau_{fx})$, 1 ksi = 6.895 MPa.
[b] Inelastic buckling.
[c] τ_y controls.

k_s = buckling coefficient, which is a function of the panel aspect ratio (h/w) and the boundary support conditions
h = web depth
t = web thickness
w = flat plate subpanel width (the horizontal or the inclined, whichever is larger)

TABLE 6.13 Stresses Based on Global Buckling Using Orthotropic Plate Theory Versus Stresses from Finite Element Analysis[a]

Panel	τ_f (ksi)	τ_e (ksi)	τ_e/τ_f	τ_y (ksi)	τ_{cre} (ksi)	τ_{cri} (ksi)	τ_{cr} (ksi)	τ_f/τ_{cr}
V121809A	48.59	42.57	0.88	47.92	129.71	70.52	47.92	1.01
V121809C	54.72	41.50	0.76	56.00	122.76	74.16	56.00	0.98
V122409A	44.34	38.55	0.87	49.07	130.42	71.55	49.07	0.90
V122409C	56.87	41.51	0.73	51.96	125.69	72.28	51.96	1.10
V181209A	57.93	45.96	0.79	57.74	51.29	48.67	48.67	1.19
V181209C	56.78	46.20	0.81	49.58	53.58	46.10	46.10	1.23
V181809A	51.46	42.82	0.83	51.77	53.58	47.11	47.11	1.09
V181809C	45.87	39.57	0.86	46.79	54.12	45.01	45.01	1.02
V241209A	32.48	27.06	0.83	50.74	30.46	—	30.46	1.07
V241209C	32.28	29.72	0.89	51.96	30.74	—	30.74	1.08

[a] τ_{cr} = minimum (τ_y, τ_{cre}, τ_{cri}), 1 ksi = 6.895 MPa.

E = Young's modulus of elasticity
ν = Poisson's ratio

The buckling coefficient k_s is given by

$$k_s = \begin{cases} 5.34 + 2.31(w/h) - 3.44(w/h)^2 + 8.39(w/h)^3 & \text{for the longer edges simply supported and the shorter edges clamped} \\ 8.98 + 5.6(w/h)^2 & \text{in the case where all edges are clamped} \end{cases}$$

In case $\tau_{cre} > 0.8\tau_y$, inelastic buckling will occur and the inelastic buckling stress τ_{cri} can be calculated by $\tau_{cri} = (0.8\tau_{cre}\tau_y)^{0.5}$, where $\tau_{cri} \leq \tau_y$.

The local buckling stresses were calculated for the test specimens with the UF1X, UFX-36, and UF2X corrugation configurations, assuming two boundary conditions: simply supported along the longer edges and clamped along the shorter edges τ_{ssf}, and clamped along all four edges τ_{fx}. The calculated stresses are given in Table 6.12 and are compared with the corresponding stresses from the finite element analysis τ_f and the test results τ_e. An average local buckling stress $t_a = 0.5(\tau_{ssf} + \tau_{fx})$ was calculated for all the specimens and is included in the table. As can be noted, the average local buckling stresses τ_a agree reasonably well with the corresponding stresses from the finite element analysis τ_f; the average ratio τ_f/τ_a was calculated to be 1.015 for all the values given in Table 6.12.

When global buckling controls, the buckling stress can be calculated for the entire corrugated web panel, using orthotropic-plate buckling theory. The global elastic buckling stress τ_{cre} can be calculated from

$$\tau_{cre} = \frac{k_s[(D_x)^{0.25}(D_y)^{0.75}]}{th^2}$$

where

$D_x = (q/s)Et^3/12$
$D_y = EI_y/9$
$I_y = 2bt(h_r/2)^2 + [t(h_r)^3/6\sin\theta]$
k_s = buckling coefficient, equals 31.6 for simply supported boundaries and 59.2 for clamped boundaries
t = corrugated plate thickness

b, h_r, q, s, and θ are as shown in the figure given in Table 6.11.

In the aforementioned, when $\tau_{cre} > 0.8\tau_y$, inelastic buckling will occur and the inelastic buckling stress τ_{cri} can be calculated by $\tau_{cri} = (0.8\tau_{cre}\tau_y)^{0.5}$, where $\tau_{cri} \leq \tau_y$.

The global buckling stresses for the test specimens made of the UFS corrugation were calculated using the buckling formula for the orthotropic plate and a buckling coefficient k_s equal to 59. The results are given in Table 6.13 together with the experimental results and the results from the finite element analysis. The average value of the ratio between the finite element analysis results and those obtained from the orthotropic plate theory τ_f/τ_{cr} is 1.067.

Beams and girders with corrugated webs are economical to use and can improve the aesthetics of the structure. The beams manufactured and used in Germany for buildings have webs with a height-to-thickness ratio of 150 to 260. The corrugated webs of the two bridges built in France were 8 mm thick and the web height-to-thickness ratio was in the range 220 to 375. Such slender webs fail due to buckling, local and/or global.

For corrugated webs subjected to shear, the strength can be calculated, to a very good degree of accuracy, using the buckling stress formulas for flat isotropic or orthotropic plates. When the corrugation is coarse, the capacity of the panel will be controlled by local buckling of the flat segments of the corrugation, and as the corrugation becomes dense, global buckling of the whole panel as an orthotropic plate controls. For practical applications it is recommended that local and global buckling values be calculated and the smaller value controls.

6.15 RESEARCH NEEDS

1. *Combined shear, moment and axial force.* Plate girders in cable-stayed girder bridges, self-anchored suspension bridges, arches, and rigid frames are subjected to axial compression or tension in addition to shear and moment. Some of the analyses discussed in this chapter can be extended to cover this

situation, but there is little or no experimental research on the ultimate strength of plate-girder panels under combined shear, moment, and axial force. Consideration of multiple longitudinal stiffeners would be an important aspect of such research.

2. *Longitudinal stiffeners.* Design procedures for longitudinally stiffened girders should be studied with a view to simplifying the ultimate-strength analyses that show good correlation with test results. These investigations should cover multiple longitudinal stiffeners.

3. *Stiffeners.* Current methods for analysis and design of stiffeners are probably adequate, but further investigations would be worthwhile.

4. *Panels with variable depth.* More work is required to develop general design procedures for the ultimate strength of panels with variable depth.

5. *Webs with holes.* The buckling strength of a thin square plate with a central circular hole, clamped at its edges and subjected to pure shear, were determined analytically and experimentally by Grosskurth et al. (1976). Stability of webs containing circular or rectangular middepth holes was investigated by Redwood and Venoya (1979). The postbuckling strength of webs with holes needs to be investigated. Narayanan and Der-Avanessian (1985) cite seven references on this topic and refer to over 70 tests performed at the University of Cardiff.

6. *Fatigue.* Better knowledge of the fatigue behavior of slender web plates is needed to take full advantage of ultimate-strength design of plate-girder bridges and crane girders, particularly those with corrugated webs.

7. *Corrugated webs.* Vertically corrugated webs may be an economical alternative to thin webs. There is no theoretical or experimental information on the ultimate strength of such panels under patch loading.

8. *Composite girders.* The assumptions on which the analyses for shear and bending of plate-girder panels are based can be expected to apply to composite girders. The large stiffness and low tensile strength of a concrete slab, compared to a steel flange, may result in some differences in the panel behavior. Therefore, tests on thin-webbed composite girders are needed. Such tests have recently been conducted at the University of Texas at Austin by Frank.

REFERENCES

AISC (1989), *Specification for Structural Steel Buildings – Allowable Stress Design and Plastic Design*, American Institute of Steel Construction, Chicago II.

AISC (1993), *Load and Resistance Factor Design Specification for Structural Steel Buildings*, American Institute of Steel Construction, Chicago, II.

Aribert, J. M., Lachal, A., and Elnawawy, O. (1981). "Modelisation elasto-plastique de la résistance d'un profile en compression locale," *Constr. Met.*, No. 2.

Bagchi, D. K., and Rockey, K. C. (1975), "Postbuckling Behaviour of Web Plate Under Partial Edge Loading," *Proc. 3rd Int. Spec. Cold-Formed Steel Struct.*, University of Missouri–Rolla, Rolla, Mo., Nov. 24–25, Vol. 1, pp. 351–384.

Basler, K. (1963a), "Strength of Plate Girders in Shear," *Trans. ASCE*, Vol. 128, Part II, p. 683.

Basler, K. (1963b), "Strength of Plate Girders Under Combined Bending and Shear," *Trans. ASCE*, Vol. 128, Part II, p. 720.

Basler, K., and Thürlimann, B. (1960a), "Carrying Capacity of Plate Girders," *IABSE 6th Congr., Prelim, Publ.*, Vol. 16.

Basler, K., and Thürlimann, B. (1960b), "Buckling Tests on Plate Girders," *IABSE 6th Congr., Prelim. Publ.*, Vol. 17.

Basler, K., and Thürlimann, B. (1963), "Strength of Plate Girders in Bending," *Trans. ASCE*, Vol. 128, Part II, p. 655.

Basler, K., Yen, B. T., Mueller, J. A., and Thürlimann, B. (1960), "Web Buckling Tests on Welded Plate Girders," *Weld. Res. Counc. Bull. No. 64*, Sept.

Bergfelt, A. (1971), "Studies and Tests on Slender Plate Girders Without Stiffeners, *IABSE Colloq. Des. Plate Box Girders Ultimate Strength*, London.

Bergfelt, A. (1976), "The Behaviour and Design of Slender Webs Under Partial Edge Loading," *Int. Conf. Steel Plated Struct.*, Imperial College, London.

Bergfelt, A. (1983), "Girder Web Stiffening for Patch Loading," *Publ. S83:1*, Chalmers University of Technology, Goteborg, Sweden.

Bergfelt, A., and Hövik, J. (1968), "Thin-Walled Deep Plate Girders Under Static Load," *IABSE 8th Congr., Final Rep.*, New York, 1968.

Bossert, T. W., and Ostapenko, A. (1967), "Buckling and Ultimate Loads for Plate Girder Web Plates Under Edge Loading," *Fritz Eng. Lab. Rep. No. 319.1*, Lehigh University, Bethlehem, Pa., June.

BSI (1982), *Steel, Concrete and Composite Bridges*, British Standard BS 5400: Part 3, *Code of Practice for Design of Steel Bridges*, British Standards Institution, London.

Carskaddan, P. S. (1968), "Shear Buckling of Unstiffened Hybrid Beams," *ASCE J. Struct. Div.*, Vol. 94, No. ST8, pp. 1965–1992.

Cescotto, S., Maquoi, R., and Massonnet, C. (1981), "Sur Ordonnateur du comportement a la ruine des putres a âme pleine cisailles on flèches," *Constr. Met.*, No. 2, pp. 27–40.

Chatterjee, S. (1980), "Design of Webs and Stiffeners in Plate and Box Girders," *Int. Conf. Des. Steel Bridges*, Cardiff, Wales.

Chern, C., and Ostapenko, A. (1969), "Ultimate Strength of Plate Girder Under Shear," *Fritz Eng. Lab. Rep. No. 328.7*, Lehigh University, Bethlehem, Pa., Aug.

Chern, C., and Ostapenko, A. (1970a), "Bending Strength of Unsymmetrical Plate Girders," *Fritz Eng. Lab. Rep. No. 328.8*, Lehigh University, Bethlehem, Pa., Sept.

Chern, C., and Ostapenko, A. (1970b), "Unsymmetrical Plate Girders Under Shear and Moment," *Fritz Eng. Lab. Rep. No. 328.9*, Lehigh University, Bethlehem, Pa., Oct.

Chern, C., and Ostapenko, A. (1971), "Strength of Longitudinally Stiffened Plate Girders Under Combined Loads," *IABSE Colloq. Des. Plate Box Girders Ultimate Strength*, London.

Clark, J. W., and Sharp, M. L. (1971), "Limit Design of Aluminum Shear Web," *IABSE Colloq. Des. Plate Box Girders Ultimate Strength*, London.

Combault, J. (1988), "The Maupre Viaduct near Charolles, France," *Proc. AISC Eng. Conf.*, pp. 12.1–12.22.

Cooper, P. B. (1965), "Bending and Shear Strength of Longitudinally Stiffened Plate Girders," *Fritz Eng. Lab. Rep. No. 304.6*, Lehigh University, Bethlehem, Pa., Sept.

Cooper, P. B. (1967), "Strength of Longitudinally Stiffened Plate Girders," *ASCE J. Struct. Div.*, Vol. 93, No. ST2, pp. 419–452.

Cooper, P. B. (1971), "The Ultimate Bending Moment for Plate Girders," *IABSE Colloq. Des. Plate Box Girders Ultimate Strength*, London.

D'Apice, M. A., Fielding, D. J., and Cooper, P. B. (1966), "Static Tests on Longitudinally Stiffened Plate Girders," *Weld. Res. Counc. Bull. No. 117*, Oct.

Davis, G., and Mandal, S. N. (1979), "The Collapse Behaviour of Tapered Plate Girders Loaded Within the Tip," *Proc. Inst. Civ. Eng.*, Vol. 67, Part 2.

Djubek, J., and Škaloud, M. (1976), "Postbuckled Behaviour of Web Plates in the New Edition of Czechoslovak Design Specifications," *Int. Conf. Steel Plated Struct.*, Imperial College, London.

Drdacky, M. (1991), "Non-stiffened Steel Webs with Flanges Under Patch Loading," *Contact Loading and Local Effects in Thin-Walled Plated and Shell Structures: IUTAM 1990 Symposium in Prague*, Springer-Verlag, Berlin.

Dubas, C. (1948), "A Contribution to the Buckling of Stiffened Plates," *IABSE 3rd Congr., Prelim. Publ.*, Liege, Belgium.

Dubas, P. (1971), "Tests on Postcritical Behaviour of Stiffened Box Girders," *IABSE Colloq. Des. Plate Box Girders Ultimate Strength*, London.

ECCS (1976), "Conventional Design Rules Based on Linear Buckling Theory," *Proc. 2nd Int. Colloq. Stab., Introd. Rep.*, ECCS, Liege, Belgium.

Elgaaly, M. A. (1973), "Buckling of Tapered Plates Under Pure Shear," *Proc. Conf. Steel Struct.*, Timisaora, Romania, Oct.

Elgaaly, M. (1975), "Failure of Thin-Walled Members Under Patch Loading and Shear," *Proc. 3rd Int. Spec. Conf. Cold-Formed Steel Struct.*, University of Missouri–Rolla, Rolla, Mo., Nov. 24–25, Vol. 1, pp. 357–381.

Elgaaly, M. (1977), "Effect of Flange Thickness on Web Capacity Under Direct in-Plane Loading," *Proc. SSRC Annu. Tech. Session*, May.

Elgaaly, M. (1983), "Web Design Under Compressive Edge Loads," *AISC Eng. J.*, Vol. 20, No. 4, pp. 153–171.

Elgaaly, M., and Dagher, H. (1990), "Beams and Girders with Corrugated Webs," *Proc. SSRC Annu. Tech. Session*, Lehigh University, Bethlehem, Pa., pp. 37–53.

Elgaaly, M., and Eash, M. (1993) "Crippling of Beams over End Supports," a report submitted to the National Science Foundation.

Elgaaly, M., and Hamilton, R. (1993), "Behavior of Welded Girders with Corrugated Webs," a report submitted to the National Science Foundation, Civil Engineering Department, University of Maine, Orono, Maine.

Elgaaly, M., and Nunan, W. (1989), "Behavior of Rolled Section Web Under Eccentric Edge Compressive Loads," *ASCE J. Struct. Eng.*, Vol. 115, No. 7, pp. 1561–1578.

Elgaaly, M. A., and Rockey, K. C. (1973), "Ultimate Strength of Thin-Walled Members Under Patch Loading and Bending," *Proc. 2nd Spec. Conf. Cold-Formed Steel Struct.*, University of Missouri–Rolla, Rolla, Mo., Oct.

Elgaaly, M., and Salkar, R. (1991a), "Behavior of Webs Under Eccentric Compressive Edge Loads," *Contact Loading and Local Effects in Thin-Walled Plated and Shell Structures: IUTAM 1990 Symposium in Prague*, Springer-Verlag, Berlin.

Elgaaly, M., and Salkar, R. (1991b), "Web Crippling Under Edge Loading," *Proc. 1991 AISC Nat. Steel Constr. Conf.*

Elgaaly, M., and Salkar, R. (1992), "Web Behavior and Ultimate Capacity Under In-plane Compressive Loads" a report submitted to the National Science Foundation.

Elgaaly, M., Sturgis, J., and Nunan, W. (1989), "Stability of Plates Under Eccentric Edge Loads," *Proc. ASCE Struct. Congr.*

Elgaaly, M., Caccese, V., and Chen, R. (1991a), "Cyclic Behavior of Unstiffened Thin Steel Plate Shear Walls," a report submitted to the National Science Foundation, University of Maine, Orono, Maine.

Elgaaly, M., Salkar, R., and Du, C. (1991b), "Analytical Study of Web Crippling Under Edge Compressive Loads," *Proc. 5th Int. Conf. Comput. Exp. Meas.*, Montreal, Quebec, Canada, Elsevier, New York.

Elgaaly, M., Smith, D., and Hamilton, R. (1992), "Beams and Girders with Corrugated Webs," *Proc. 1992 NSF Struct. Geomech. Build. Syst. Grantees' Conf.*, San Juan, Puerto Rico, pp. 126–128.

Elgaaly, M., Caccese, V., and Martin, D. (1993a), "Experimental Investigation of the Behavior of Bolted Thin Steel Plate Shear Walls," a report submitted to the National Science Foundation, University of Maine, Orono, Maine.

Elgaaly, M., Caccese, V., and Du, C. (1993b), "Postbuckling Behavior of Steel Plate Shear Walls Under Cyclic Loads," *ASCE J. Struct. Eng.*, Vol. 119, No. ST2.

Elgaaly, M., Liu, Y., and Caccese, V. (1995a), "Thin Steel Plate Shear Walls, Research to Practice," *Proc. Conf. Research Transformed into Practice: Implementation of NSF Research*, ASCE Press, New York.

Elgaaly, M., Seshadri, A., and Hamilton, R. W., (1995b), "Beams with Corrugated Webs, Research to Practice," *Proc. Conf. Research Transformed into Practice Implementation of NSF Research*, ASCE Press, New York.

Falby, W. E., and Lee, G. C. (1976), "Tension-Field Design of Tapered Webs," *Am. Inst. Steel Constr.*, Vol. 13, No. 1., p. 11.

FHWA (1980), "Proposed Design Specifications for Steel Box Girder Bridges," *Rep. No. FHWA-TS-80-205*, U.S. Department of Transportation, Federal Highway Administration, Washington, D.C.

Frank, K. H., and Helwig, T. A. (1995), "Buckling of Webs in Unsymmetric Plate Girders," *AISC Eng. J.*, Vol. 32, No. 2, pp. 43–53.

Fujii, T. (1968a), "On an Improved Theory for Dr. Basler's Theory," *IABSE 8th Congr., Final Rep.*, New York.

Fujii, T. (1968b), "On Ultimate Strength of Plate Girders," *Jpn. Shipbuild. Mar. Eng.*, May.

Fujii, T. (1971), "A Comparison Between Theoretical Values and Experimental Results for the Ultimate Shear Strength of Plate Girders" *IABSE Colloq. Des. Plate Box Girders Ultimate Strength*, London.

Gaylord, E. H. (1963), "Discussion of K. Basler 'Strength of Plate Girders in Shear,'" *Trans. ASCE*, Vol. 128, Part II, p. 712.

Gaylord, E. H., and Gaylord, C. N. (1972), *Design of Steel Structures*, 2nd ed., McGraw-Hill, New York.

Girkmann, K. (1936), "Die Stabilität der Stegbleche vollwandiger Träger bei Berücksichtigung örtlicher Lastangriffe," *IABSE 3rd Congr., Final Rep.*, Berlin.

Granholm, C. A. (1960), "Tests on Girders with Thin Web Plates," *Rapp. 202*, Institutionen for Byggnadsteknik, Chalmers Tekniska Hogskola, Goteborg, Sweden (in Swedish).

Grosskurth, J. F., White, R. N., and Gallagher, R. H. (1976), "Shear Buckling of Square Perforated Plates," *ASCE J. Eng. Mech. Div.*, Vol. 102, No. EM6, pp. 1025–1040.

Harding, J. E., and Hobbs, R. E. (1979), "The Ultimate Behaviour of Box Girder Web Panels," *Struct. Eng.*, Vol. 57B, No. 9.

Herzog, M. (1973), "Die Traglast versteifter, dünnwändiger Blechträger unter reiner Biegung nach Versuchen," *Bauingenieur*, Sept.

Herzog, M. (1974a) "Die Traglast unversteifter und versteifter, dünnwändiger Blechträger unter reinem Schub und Schub mit Biegung nach Versuchen," *Bauingenieur*, Oct.

Herzog, M. (1974b), "Ultimate Strength of Plate Girders from Tests," *ASCE J. Struct. Div.*, Vol. 100, No. ST5, pp. 849–864.

Herzog, M. (1974c), "Die Krüppellast sehr dünner Vollwandträgerstege nach Versuchen," *Stahlbau*, Vol. 43, pp. 26–28.

Höglund, T. (1971a), "Behavior and Load-Carrying Capacity of Thin-Plate I Girders," *R. Inst. Technol. Bull.*, No. 93, Stockholm (in Swedish).

Höglund, T. (1971b), "Simply Supported Thin Plate I-Girders Without Web Stiffeners Subjected to Distributed Transverse Load," *IABSE Colloq. Des. Plate Box Girders Ultimate Strength*, London.

Höglund, T. (1973), "Design of Thin-Plate I Girders in Shear and Bending," *R. Inst. Technol. Bull. No. 94*, Stockholm.

Höglund, T. (1991), "Local Buckling of Steel Bridge Girder Webs During Launching," *Contact Loading and Local Effects in Thin-Walled Plated and Shell Structures: IUTAM 1990 Symposium in Prague*, Springer-Verlag, Berlin.

Horne, M. R. (1980), "Basic Concepts in the Design of Webs," *Int. Conf. Des. Steel Bridges*, Cardiff, Wales.

Jetteur, P. (1984), "Contribution a la solution de problème particuliers d'instabilité dans la grand poutres metallique," *Colloq. Publ. Fac. Sci. Appl. Liege No. 94.*

Kawana, K., and Yamakoshi, M. (1965), "On the Buckling of Simply Supported Rectangular Plates Under Uniform Compression and Bending," *J. Soc. Nav. Archit. West Jpn.*, Vol. 29, pp.

Khan, M. Z., and Walker, A. C. (1972), "Buckling of Plates Subjected to Localized Edge Loading," *Struct. Eng.*, Vol. 50, No. 6, pp. 225–232.

Khan, M. Z., Johns, K. C., and Hayman, B. (1977), "Buckling of Plates with Partially Loaded Edges," *ASCE J. Struct. Div.*, Vol. 103, No. ST3, pp. 547–558.

Klöppel, K., and Scheer, J. S. (1960), *Beulwerte ausgesteifter Rechteckplatten*, Wilhelm Ernst, Berlin.

Klöppel, K., Wagemann, C. H. (1964), "Beulen eines Bleches unter einseitiger Gleichstreckenlast," *Stahlbau*, Vol. 33, pp. 216–220.

Komatsu, S. (1971), "Ultimate Strength of Stiffened Plate Girders Subjected to Shear," *IABSE Colloq. Des. Plate Box Girders Ultimate Strength*, London.

Konishi, I., et al. (1965), "Theories and Experiments on the Load Carrying Capacity of Plate Girders," *Rep. Res. Comm. Bridges Steel Frames Weld. Kansai Dist. Jpn.*, July (in Japanese).

Kuhn, P. (1956), *Stresses in Aircraft and Shell Structures*, McGraw-Hill, New York.

Kulak, G. L. (1985), "Behavior of Steel Plate Shear Walls," *Proc. AISC Eng. Symp. Struct. Steel*, American Institute of Steel Construction, Chicago.

Kulak, G. L., Fisher, J. W., and Struik, J. H. A. (1987), *Guide to Design Criteria for Bolted and Riveted Joints*, Wiley, New York.

Kutmanova, I., Škaloud, M., Janus, K., and Lowitova, O. (1991), "Ultimate Load Behavior of Longitudinally Stiffened Steel Webs Subject to Partial Edge Loading," *Contact Loading and Local Effects in Thin-Walled Plated and Shell Structures: IUTAM 1990 Symposium in Prague*, Springer-Verlag, Berlin.

Lew, H. S., and Toprac, A. A. (1968), "Static Strength of Hybrid Plate Girders," *SFRL Tech. Rep.*, University of Texas, p. 550–11, Jan.

Maeda, Y. (1971), "Ultimate Static Strength and Fatigue Behavior of Longitudinally Stiffened Plate Girders in Bending," *IABSE Colloq. Des. Plate Box Girders Ultimate Strength*, London.

Maquoi, R., Jetteur, P., Massonnet, C., and Škaloud, M. (1983), "Calcule des âmes et semelles radier des ponts en acier," *Constr. Met.*, No. 4, pp. 15–28.

Massonnet, C. (1962), "Stability Considerations in the Design of Steel Plate Girders," *Trans. Am. Soc. Civ. Eng.*, Vol. 127, Part II, pp. 420–447.

Narayanan, R., Der-Avanessian, N. G.-V. (1985), "Design of Slender Webs Having Rectangular Holes," *ASCE J. Struct. Eng.*, Vol. III, No. 4, pp. 777–787.

Ostapenko, A., and Chern, C. (1970), "Strength of Longitudinally Stiffened Plate Girders," *Fritz Eng. Lab. Rep. No. 328.10*, Lehigh University, Bethlehem, Pa., Dec.

Ostapenko, A., Yen, B. T., and Beedle, L. S. (1968), "Research on Plate Girders at Lehigh University," *IABSE 8th Congr., Final Rep.*

Parsanejad, S., and Ostapenko, A. (1970), "On the Fatigue Strength of Unsymmetrical Steel Plate Girders," *Weld Res. Counc. Bull. No. 156*, Nov.

Patterson, P. J., Corrado, J. A., Huang, J. S., and Yen, B. T. (1970), "Fatigue and Static Tests of Two Welded Plate Girders," *Weld. Res. Counc. Bull. No. 155*, Oct.

Porter, D. M., Rockey, K. C., and Evans, H. R. (1975), "The Collapse Behavior of Plate Girders Loaded in Shear," *Struct. Eng.* Vol. 53, No. 8, pp. 313–325.

Raoul, J., Schaller, I., and Theillout, J. (1991), "Tests of Buckling of Panels Subjected to In-plane Patch Loading," *Contact Loading and Local Effects in Thin-Walled Plated and Shell Structures: IUTAM 1990 Symposium in Prague*, Springer-Verlag, Berlin.

Redwood, R. L., and Venoya, M. (1979), "Critical Loads for Webs with Holes," *ASCE J. Struct. Div.*, Vol. 105, No. ST10, pp. 2053–2068.

Roberts, T. M. (1981), "Slender Plate Girders Subjected to Edge Loading," *Proc. Inst. Civ. Eng.* Part 2, p. 71.

Roberts, T. M., and Chong, C. K. (1981), "Collapse of Plate Girders Under Edge Loading," *ASCE J. Struct. Div.*, Vol. 107, No. ST8, pp. 1503–1510.

Roberts, T. M., and Rockey, K. C. (1979), "A Mechanism Solution for Predicting the Collapse Loads of Slender Plate Girders When Subjected to In-plane Patch Loading," *Proc. Inst. Civ. Eng.*, Vol. 67, Part 2.

Roberts, T. M., and Sabouri, S. (1991), "Hysteretic Characteristics of Unstiffened Plate Shear Panels," *Thin-Walled Struct.*, Vol. 12.

Rockey, K. C. (1971a), "An Ultimate Load Method for the Design of Plate Girders," *IABSE Colloq. Des. Plate Box Girders Ultimate Strength*, London.

Rockey, K. C. (1971b), "An Ultimate Load Method of Design for Plate Girders," *Proc. Conf. Dev. Bridge Des. Constr.*, Crosby Lockwood, London.

Rockey, K. C., and Bagchi, D. K. (1970), "Buckling of Plate Girder Webs Under Partial Edge Loadings," *Int. J. Mech. Sci.*, Vol. 12.

Rockey, K. C., and Leggett, D. M. A. (1962), "The Buckling of a Plate Girder Web Under Pure Bending When Reinforced by a Single Longitudinal Stiffener," *Proc. Inst. Civ. Eng.*, Vol. 21.

Rockey, K. C., and Škaloud, M. (1968), "Influence of Flange Stiffness upon the Load Carrying Capacity of Webs in Shear," *IABSE 8th Congr., Final Rep.*, New York.

Rockey, K. C., and Škaloud, M. (1972), "The Ultimate Load Behavior of Plate Girders Loaded in Shear," *Struct. Eng.*, Vol. 50, No. 1.

Rockey, K. C., Elgaaly, M., and Bagchi, D. K. (1972), "Failure of Thin-Walled Members Under Patch Loading," *ASCE J. Struct. Div.*, Vol. 98, No. ST12, pp. 2739–2752.

Rockey, K. D., Evans, H. R., and Porter, D. M. (1973), "Ultimate Load Capacity of Stiffened Webs Subjected to Shear and Bending," *Proc. Conf. Steel Box Girders*, Institution of Civil Engineers, London.

Rockey, K. C., Evans, H. R., and Porter, D. M. (1974), "The Ultimate Strength Behavior of Longitudinally Stiffened Reinforced Plate Girders," *Symp. Nonlinear Tech. Behav. Struct. Anal.*, Transport and Road Research Laboratory, Crowthorne, Dec.

Schueller, W., and Ostapenko, A. (1970), "Tests on a Transversely Stiffened and on a Longitudinally Stiffened Unsymmetrical Plate Girder," *Weld Res. Counc. Bull. No. 156*, Nov.

Selberg, A. (1973), "On the Shear Capacity of Girder Webs," *Univ. Trondheim Rep.*

Sharp, M. L., and Clark, J. W. (1971), "Thin Aluminum Shear Webs," *ASCE J. Struct. Div.*, Vol. 97, ST4, pp. 1021–1038.

Shelestanko, L. P., Dushnitsky, V. M., and Borovikov, V. (1970), "Investigation of the Influence of Limited Web Deformation on the Ultimate Strength of Welded Plate Girders," *Res. Steel Compos. Superstruct. Bridges*, No. 76, Transport, Moscow (in Russian).

Shimizu, S., Yabana, H., and Yoshida, S. (1989a), "A Collapse Model for Patch Loaded Web Plates," *J. Constr. Steel Res.*, Vol. 13, pp. 61–73.

Shimizu, S., Horii, S., and Yoshida, S. (1989b), "The Collapse Mechanism of Patch Loaded Web Plates," *J. Constr. Steel Res.*, Vol. 14, pp. 321–337.

Shimizu, S., Horii, S., and Yoshida, S. (1991), "Behavior of Stiffened Web Plates Subjected to Patch Loads," *Contact Loading and Local Effects in Thin-Walled Plated and Shell Structures: IUTAM 1990 Symposium in Prague*, Springer-Verlag, Berlin.

Škaloud, M. (1962), "Design of Web Plates of Steel Girders with Regard to the Postbuckling Behavior (Analytical Solution), *Struct. Eng.*, Vol. 40, No. 12, p. 409.

Škaloud, M. (1971), "Ultimate Load and Failure Mechanism of Thin Webs in Shear," *IABSE Colloq Des. Plate Box Girders Ultimate Strength*, London.

Škaloud, M., and Novak, P. (1972), "Postbuckled Behavior and Incremental Collapse of Webs Subjected to Concentrated Load," *IABSE 9th Congr., Prelim, Publ.*, Amsterdam.

Spinassas, I., Raoul, J., and Virlogeux, M. (1991), "Parametric Study on Plate Girders Subjected to Patch Loading," *Contact Loading and Local Effects in Thin-Walled Plated and Shell Structures: IUTAM 1990 Symposium in Prague*, Springer-Verlag, Berlin.

Stein, M., and Fralich, R. W. (1950), "Critical Shear Stress of Infinitely Long Simply Supported Plate with Transverse Stiffeners," *J. Aeronaut. Sci.*, Vol. 17.

Steinhardt, O., and Schröter, W. (1971), "Postcritical Behavior of Aluminum Plate Girders with Transverse Stiffeners," *IABSE Colloq. Des. Plate Box Girders Ultimate Strength*, London.

Takeuchi, T. (1964), "Investigation of the Load Carrying Capacity of Plate Girders," M.S. thesis, University of Kyoto (in Japanese).

Tromposch, E. W., and Kulak, G. L. (1987), "Cyclic and Static Behavior of Thin Panel Steel Plate Shear Walls," *Struct. Eng. Rep. No. 145*, Department of Civil Engineering, University of Alberta, Edmonton, Alberta, Canada, Apr.

von Kármán, T., Sechler, E. F., and Donnell, L. H. (1932), "The Strength of Thin Plates in Compression," *Trans. ASME*, Vol. 54, No. 2.

Wagner, H. (1931), "Flat Sheet Metal Girder with Very Thin Metal Web," *NACA Tech. Memo. Nos. 604, 605, 606.*

Warkenthin, W. (1965), "Zur Beulsicherheit querbelasteter Stegblechfelder," *Stahlbau*, Vol. 34, p. 28.

Wilkesmann, F. W. (1960), "Stegblechbeulung bei Längsrandbelastung," *Stahlbau*, Vol. 29.

Wilson, J. M. (1886), "On Specifications for Strength of Iron Bridges," *Trans. ASCE*, Vol. 15, Part I, pp. 401–403, 489–490.

Yen, B. T., and Basler, K. (1962), "Static Carrying Capacity of Steel Plate Girders," *Highw. Res. Board Proc.*, Vol. 41.

Yen, B. T., and Mueller, J. A. (1966), "Fatigue Tests of Large-Size Welded Plate Girders," *Weld. Res. Counc. Bull. No. 118*, Nov.

Yonezawa, H., Miakami, I., Dogaki, M., and Uno, H. (1978), "Shear Strength of Plate Girders with Diagonally Stiffened Webs, *Trans. Jpn. Soc. Civ. Eng.*, Vol. 10.

Zetlin, L. (1955), "Elastic Stability of Plates Under Edge Loading," *Proc. ASCE*, Vol. 81.

CHAPTER SEVEN

BOX GIRDERS

7.1 INTRODUCTION

Box girders are used extensively for bridges (Fig. 7.1), heavy industrial buildings, offshore platforms, and other structures where large loads are frequently encountered. They are employed to best advantage when use is made of their considerable torsional stiffness. Although box girders may have a variety of cross-sectional shapes (Fig. 7.2) ranging from a deep narrow box to a wide shallow box (perhaps with many webs, some sloping) those occurring most frequently have flanges which are wider and more slender than in plate girder construction. The webs, on the other hand, may be of comparable slendernesses to those of plate girders. However, it is the extensive use of slender plate construction for flanges as well as webs which makes stability considerations so important in the case of box girders.

In this chapter aspects of the stability of box girders and their components, which are additional to those described in Chapter 6, are discussed. Most of these additional problems are a consequence of the use of wide flanges, that is, the influences of shear lag and lateral loading on the buckling of stiffened compression plates. Others relate to the need to provide diaphragms within a box, not only to retain the box shape but also to distribute forces to the support bearings. In the case of box girders, as opposed to plate girders, the bearings may not be positioned directly beneath and in line with the webs. Much of the information on web stability provided already in the context of plate girders is applicable to box girders, but there are important differences

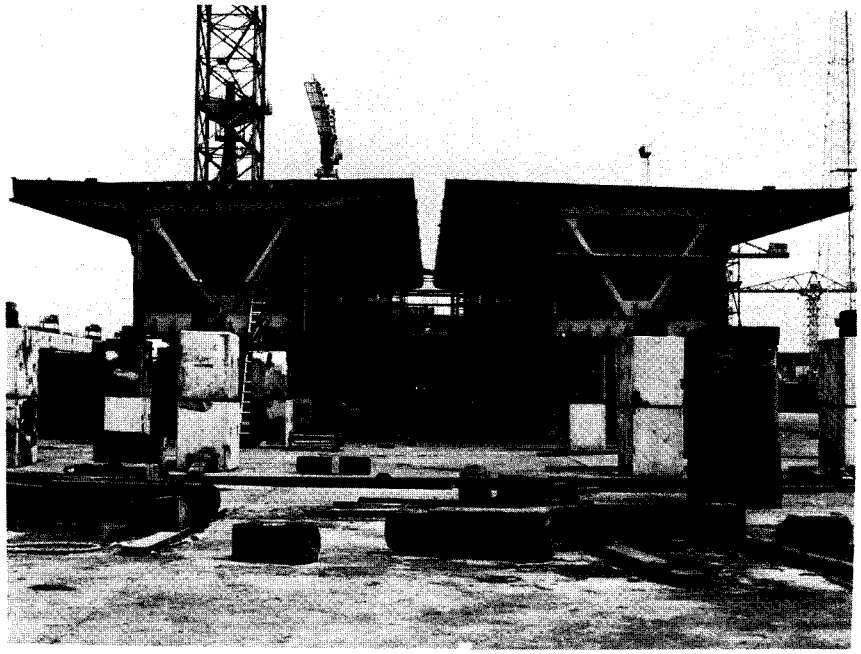

Fig. 7.1 Box girder bridges.

which are discussed. Some of the unresolved problems relating to box girders are also outlined.

7.2 BASES OF DESIGN

Up until the end of the 1960s the design of box girders was not codified in detail in any country. Although a wide variety of approaches was used for the design of box girder bridges, the basis generally adopted was to use a factor of safety on the buckling stress, more often than not the *critical elastic buckling stress*, of the component being designed. These factors of safety varied from country to country and were intended to cover not only the as-built condition but also conditions met during construction. In some cases they also reflected an appreciation of the postbuckling reserve of plates, with lower factors of safety being used than would be the case where no such reserve was anticipated.

Three major collapses that occurred during the erection of box girder bridges, at Milford Haven (1969), West Gate (1970), and Koblenz (1971) (Fig. 7.3), caused the entire basis of the design of box girders to be reviewed (ICE, 1973; "Inquiry," 1973) not only in Europe but also in the United States

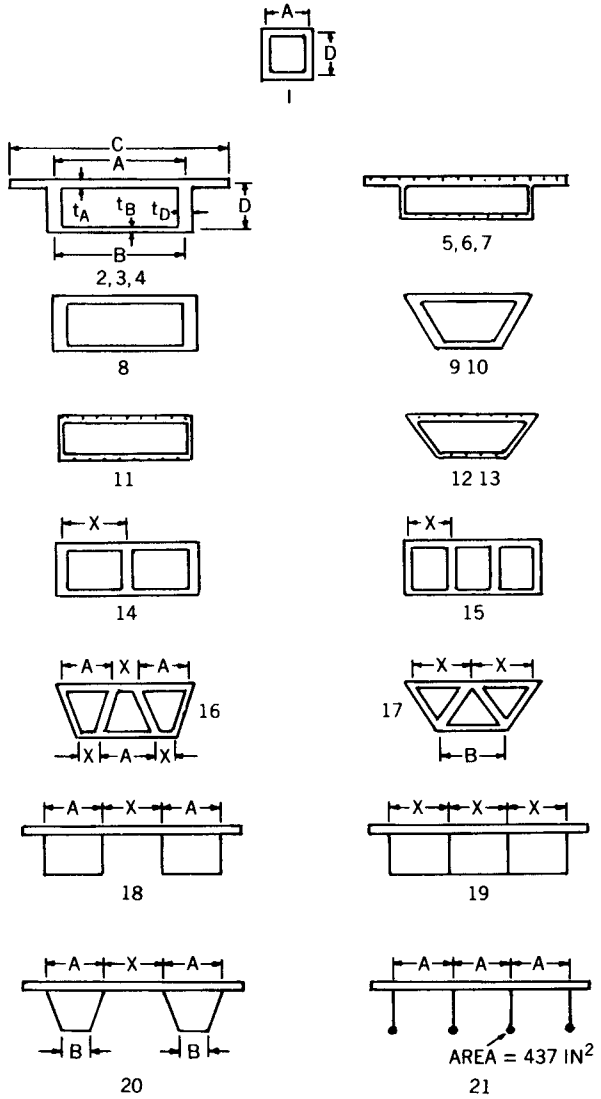

Fig. 7.2 Bridge cross sections.

and, since then, worldwide. The drafting of new rules in the wake of these tragedies coincided with the trend toward limit-state format codes involving a consideration of the ultimate limit state. Not surprisingly, therefore, emphasis was placed on the development of new design approaches based on the ultimate, or the *inelastic buckling strength*, of box girders and their components (Horne, 1977).

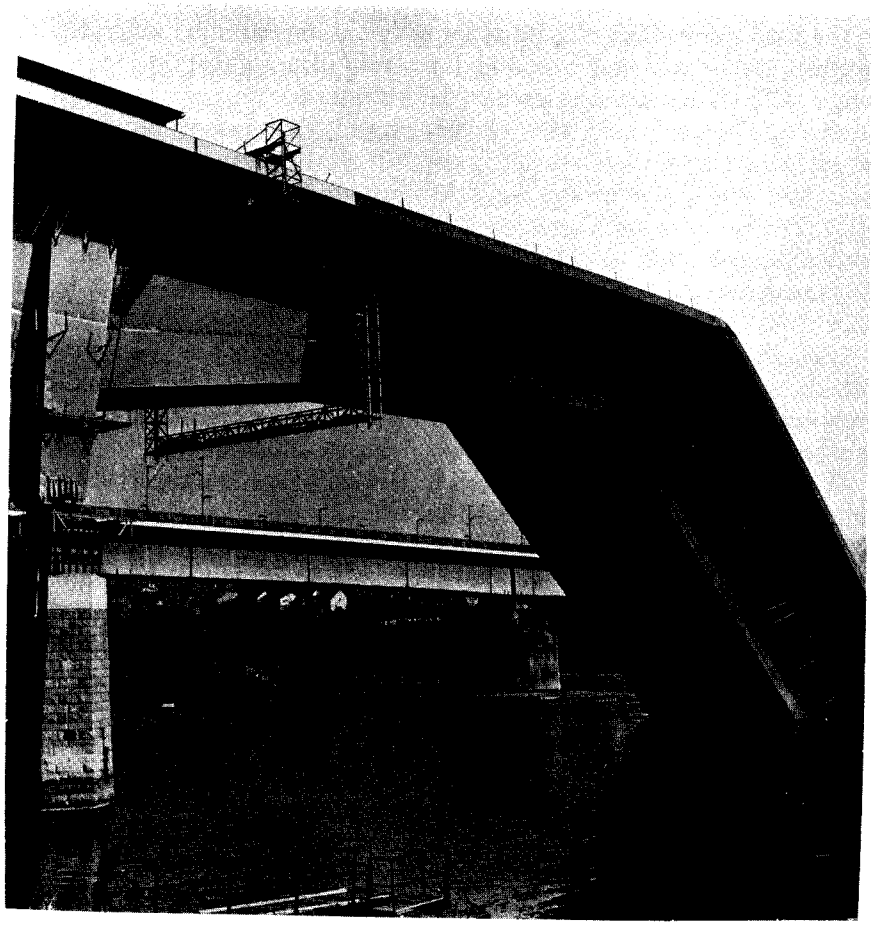

Fig. 7.3 Koblenz bridge collapse.

Influence of Initial Geometric Imperfections and Residual Stresses. Much attention was paid to the role of initial imperfections, both geometric and residual stresses, during the investigations of the strength of box girders and their components (Dowling et al., 1977b). Extensive measurements were made of residual stresses produced during box girder fabrication by using both destructive, but mainly nondestructive, methods. These were carried out in model boxes fabricated using techniques representative of full-scale techniques and also in actual box girder bridges under construction. Numerous surveys of the distribution of initial distortions in model and full-scale boxes were also made. Concurrent with these measurements fundamental studies on the prediction of residual stresses, and on their effects, together with the effects of geometric imperfections, were carried out in many places.

The weakening effect of both types of initial imperfection, separately and together, is now well understood and has been incorporated into the various design methods produced to predict the inelastic buckling strength of plated structures. The weakening effect of these imperfections is most pronounced in the range of intermediate slendernesses, that is, those slendernesses at which the critical buckling stress and the yield stress are roughly equal (Frieze et al., 1975). The knockdown in strength is most marked for plates of intermediate slenderness subjected to compressive stressing and is least pronounced for shear-loaded cases, being practically negligible for rectangular plates in pure shear.

Strength curves for plate panels used for design have normally been selected with allowances made for practical combinations of residual stresses and initial imperfections. Ultimate load design methods for stiffeners or stiffened plates also normally incorporate the effects of imperfections in their expressions. Typically, a level of compressive residual stress of the order of 10% of the yield stress, with an initial geometric imperfection which is related to fabrication tolerances, may be adopted by code drafters. In other cases a geometric imperfection is chosen which is considered on the basis of theoretical or experimental evidence to incorporate the combined weakening effect of residual stress and practical initial distortions. It has been shown that provided that the magnitude of the initial distortion chosen is big enough (and this is often of the same order as specified fabrication tolerances), the additional weakening effect of even the largest residual compressive stresses is small for practical plates.

The option of specifying levels of residual stresses to be calculated by designers and measured by fabricators is not a realistic one in terms of the economics of normal fabricated box girders and is avoided in specifications. As a result of the efforts made to reconsider the basis of design for box girders, new rules were produced in the United Kingdom, the United States, and Germany, among other countries. The first to be fully codified were the British rules; as of 1997 those of the United States were still in proposal form (Wolchuk and Mayrbourl, 1980). For this reason the basis of the design approach contained in BS 5400: Part 3, Design of Steel Bridges (BSI, 1983) is summarized here in more detail than is devoted to the other rules.

7.3 BUCKLING OF WIDE FLANGES

Box girder flanges are normally stiffened in both the longitudinal and transverse directions (Fig. 7.4). The unstiffened flanges of narrow box girders can be treated as plates, as described in Chapter 4, by using reduced effective widths to account for the effects of buckling. Possible modes of buckling occurring in an orthogonally stiffened plate are illustrated in Fig. 7.5. These include overall buckling of the stiffened flange, buckling of the longitudinally stiffened panels

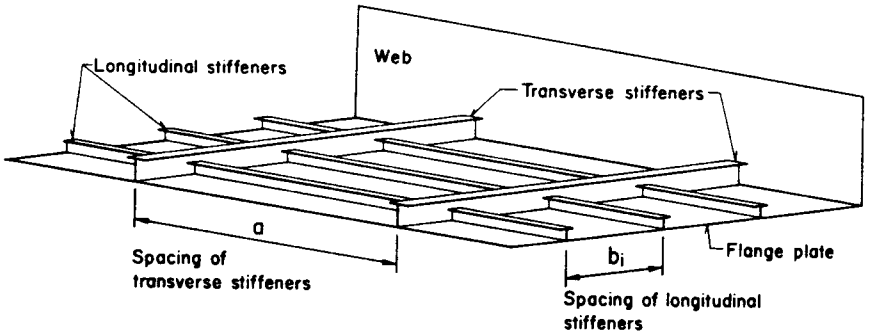

Fig. 7.4 Sample stiffened panel (compression flange).

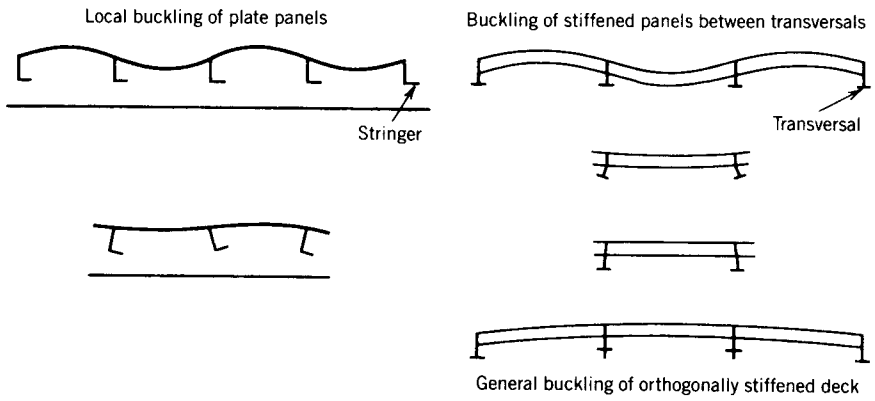

Fig. 7.5 Various forms of local buckling of stringers and transversals.

between transverse elements, various forms of local plate and stiffener buckling, and various combinations of these modes.

The linear elastic buckling of stiffened flanges with one or more stiffeners is covered in Chapter 4 and formed the basis of earlier design methods. Indeed, many codes still in use today are based on these methods together with the use of safety factors determined from test results. These are reviewed by Rockey and Evans (1980). In this chapter emphasis is placed on methods designed to predict the ultimate strength of such flanges, as these are being used to replace the elastic methods. It should be recognized, however, that even now the new rules for stiffened compression flanges are not based entirely on ultimate strength considerations, as pointed out by Dowling (Rockey and Evans, 1980).

In considering the inelastic buckling of wide stiffened flanges, three basic approaches can be adopted. In increasing order of complexity, the flanges can be treated as:

1. A series of disconnected struts
2. An orthotropic plate
3. A discretely stiffened plate

For most stiffened flanges the strut approach is sufficiently accurate and is suitable for design purposes. When the flange stiffening is lighter than normal, advantage can be taken of the postbuckling reserve of the stiffened plate and many methods have been produced based on this type of modeling, notably those of Massonnet and his co-workers (Maquoi and Massonnet, 1971; Jetteur, 1983). However, the flange geometry rarely justifies such an approach in practice, and the strut approach will, in any case, produce safe designs. The discretely stiffened plate approach is of interest mainly as an aid to understanding the flange behavior rather than as a design aid, although in the case of a flange stiffened by only one or two stiffeners, it can be used, in the absence of simpler approaches, to proportion compression flanges. Each of these methods is described in turn below.

7.3.1 The Strut Approach

The basis of this approach is to treat a plate stiffened by several equally spaced longitudinal stiffeners as a series of unconnected compression members or struts, each of which consists of a stiffener acting together with an associated width of plate that represents the plate between stiffeners (Fig. 7.6). Where transverse stiffeners are present, they are designed to be sufficiently stiff to ensure that they provide nodal lines acting as simple rotationally free supports to the ends of the longitudinal struts. Thus the equivalent buckling length of the longitudinal stiffeners is effectively the distance between transverse elements. Such an approach was suggested by Ostapenko and Vojta (1967) and Dowling and his co-workers, Moolani and Chaterjee (Dwight and Little, 1976); Dowling and Chatterjee, 1977; Dowling et al., 1977a; Chatterjee, 1978). Apart from the overall buckling of the longitudinal stiffeners between transverse

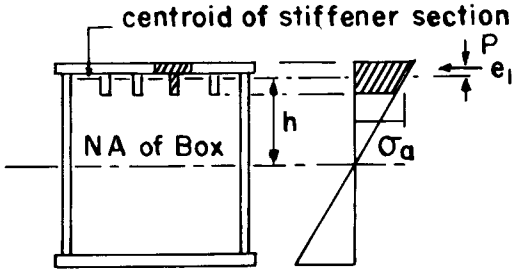

Fig. 7.6 Curvature of box girder.

stiffeners, allowance is made for reduction in effectiveness due to buckling of the plate between stiffeners.

Where the longitudinal stiffeners are open sections such as flat bars, tees, or angles, limitations are placed on their cross-sectional geometry to ensure that local buckling of the stiffeners does not precede the attainment of the ultimate strength of the flange. In the case of closed sections such as troughs or vees, used in orthotropic steel deck construction, the limitations on cross-sectional geometries are adjusted to allow for bending in the plane of the stiffener walls and to ensure that economical use of relatively thin walled sections is not precluded.

Limitations of stiffener cross sections are based on controlling the applied stresses under ultimate load to values that are fractions of the elastic critical buckling stresses. In BS 5400 the safety factor used is 2.25, which was derived as a suitable value for flat stiffeners but has been applied to all other types of stiffening. The limitations imposed in the proposed U.S. code (Wolchuk and Mayrbourl, 1980) are somewhat different and correspond to the requirement that the torsional buckling stress should be greater than the yield stress, with relaxations to allow for "thinning out" the stiffeners in low-stress zones. These two sets of criteria lead to the following restrictions:

Draft U.S. Rules

$$C_s \le \begin{cases} \dfrac{0.40}{\sqrt{F_y/E}} & \text{for } f_{\max} \ge 0.5F_y \quad (7.1) \\ \dfrac{0.65}{\sqrt{F_y/E}} & \text{for } f_{\max} \le 0.5F_y \quad (7.2) \end{cases}$$

where

$f_{\max}$ = maximum factored compression stress
C_2 = effective slenderness coefficient

$$= \frac{d}{1.5t_0} + \frac{w}{12t} \quad \text{for flats} \quad (7.3a)$$

$$= \frac{d}{1.35t_0 + 0.56r_y} + \frac{w}{12t} \quad \text{for tees or angles} \quad (7.3b)$$

For any outstanding part of a stiffener,

$$\frac{b'}{t'} \le \frac{0.48}{\sqrt{F_y/E}} \quad (7.4)$$

BS 5400. For flats,

$$\frac{h_s}{t_s}\sqrt{\frac{\sigma_{ys}}{355}} \leq 10 \tag{7.5}$$

or less than or equal to a higher value obtained from Fig. 7.7*a* when $b/t\sqrt{\sigma_y/355} \leq 30$. For angles;

$$\begin{aligned} b_s &\leq h_s \\ \frac{b_s}{t_s}\sqrt{\frac{\sigma_{ys}}{355}} &\leq 11 \\ \frac{h_s}{t_s}\sqrt{\frac{\sigma_{ys}}{355}} &\leq 7 \end{aligned} \tag{7.6}$$

or less than or equal to a higher value obtained from Fig. 7.7*b* when $(l_s/b_s)\sqrt{\sigma_{ys}/355} \leq 50$. In these formulas (see Fig. 7.8),

d, h_s = stiffener depth
b_s = width of angle

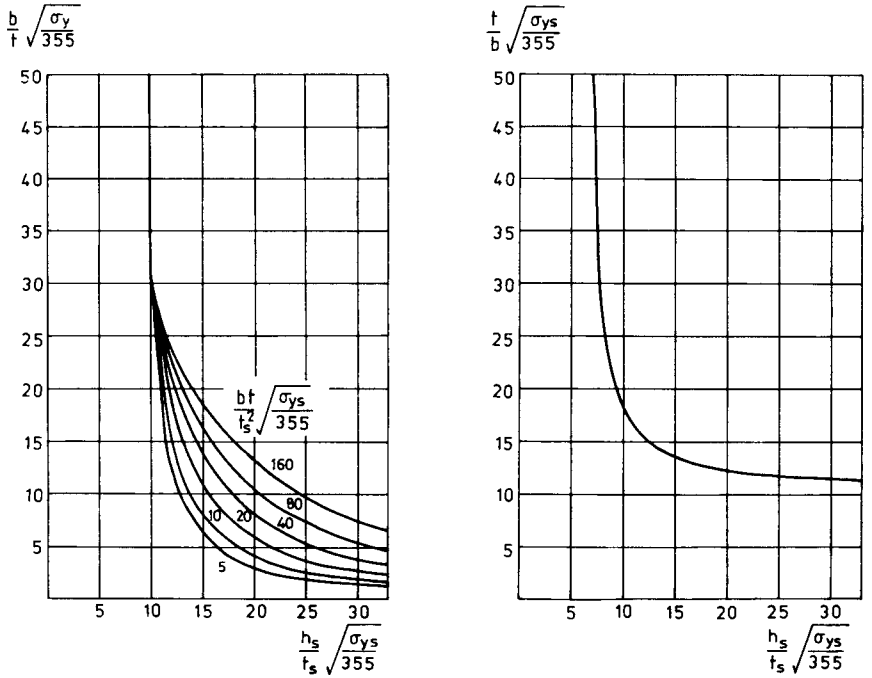

Fig 7.7 (*a*) Limiting slenderness for flat stiffeners; (*b*) limiting slenderness for angle stiffeners.

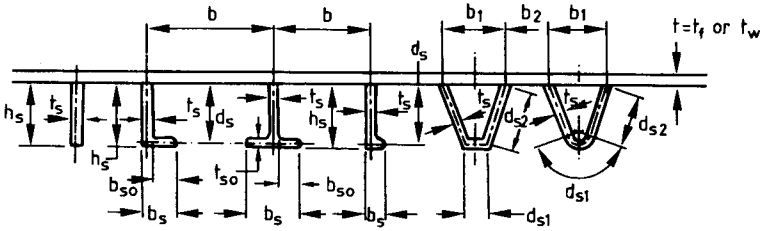

Fig. 7.8 Flange and web stiffeners.

t_0, t', t_s = stiffener thickness
t = plate thickness
w, b = spacing of stiffeners
l_s = span of stiffener between supporting members
r_y = radius of gyration of stiffener (without plate) about axis normal to plate
σ_{ys} = yield stress of stiffener, N/mm^2
σ_y = yield stress of plate, N/mm^2

Thus the design model relates to an orthogonally stiffened flange in which the controlling buckling mode envisaged is buckling of the longitudinally stiffened plate between transverse stiffeners, which may or may not be accompanied by local plate buckling between stiffeners. However, local buckling of the stiffener is suppressed, together with any participation of the transverse members in the overall buckled mode.

In accounting for the buckling of the repeating combined stiffener/plate "strut" allowance can be made for the effect of initial distortions and residual stresses caused by welding the stiffeners to the plate. The extensive amount of data now available on plate strength can be used to account for interstiffener plate buckling using either an effective width or effective stress approach. Normally, a simple effective width approach is used to account for both the reduced strength and stiffness of the compressed plate. Although there are approximations involved in selecting just one width to account for stiffness as well as strength, the gain in accuracy which could be obtained using a more complex approach is not considered to be sufficient for design.

The effective width used in BS 5400 is derived from the results of a parametric study and uses a strength-based effective width which accounts for practical levels of initial imperfections and compressive residual stresses. Figure 7.9 gives curves from BS 5400 which may be used to calculate the width of plate k_{cb} considered to act effectively with a stiffener. Knowing the cross-sectional properties of the strut, the calculation of the buckling strength of the strut can be obtained from a column buckling formula of the Perry–

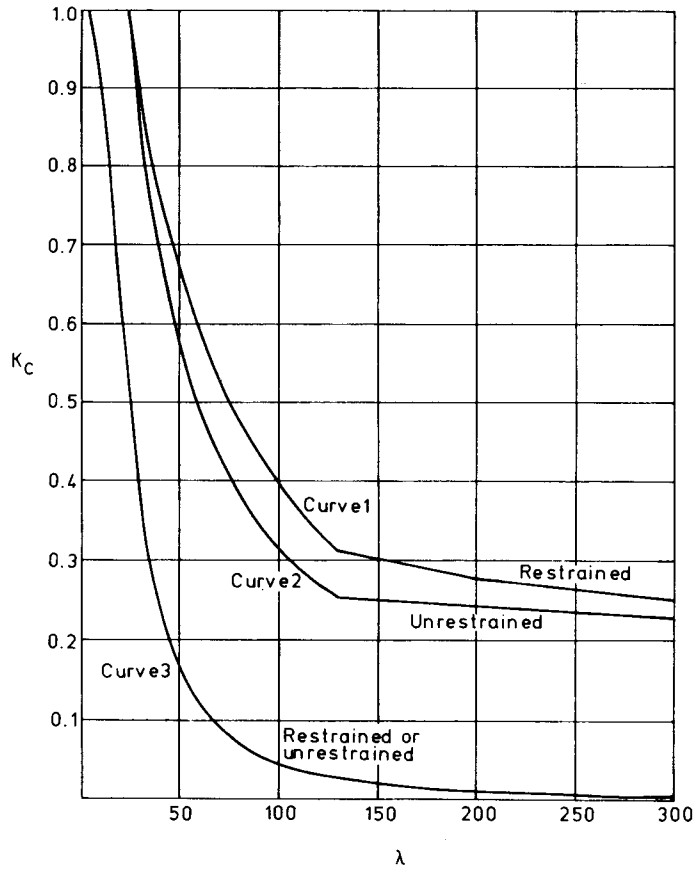

Note: The value of K_c to be used is the higher of the values obtained using either:

(a) curve 1 or 2 as relevant, with

$$\lambda = \frac{b}{t}\sqrt{\frac{\sigma_y}{355}} \quad \text{or}$$

(b) curve 3 with $\lambda = \frac{a}{t}\sqrt{\frac{\sigma_y}{355}}$

where

a is the panel dimension in the direction of stress considered
b is the panel dimension normal to the direction of stress.

Item (a) will always give the higher value for K_c where $a/b \geq 0.5$.

For $a/b < 0.5$, items (a) or (b) may give a higher value.

Fig. 7.9 Coefficient K_c for plate panels under direct compression.

Robertson type which relates to a pin-ended, initially crooked, axially loaded column,

$$\frac{\sigma_{su}}{\sigma_y} = \frac{1}{2}\left\{\left[1+(\eta+1)\frac{\sigma_E}{\sigma_y}\right] - \sqrt{\left[1+(\eta+1)\frac{\sigma_E}{\sigma_y}\right]^2 - \frac{4\sigma_E}{\sigma_y}}\right\} \tag{7.7}$$

where

σ_{su} = limiting applied axial stress on effective strut section
σ_E = Euler stress of effective strut
σ_y' = available yield stress of compressive extreme fiber = σ_{ys} when checking stiffener; = σ_{ye} i.e., an effective yield stress allowing for the presence of shear) when checking flange
η = $\Delta y/r_{se}^2$
Δ = maximum initial imperfection
y = distance from centroid to compressive extreme fiber
r_{se} = radius of gyration of effective section about axis parallel to plate

As the cross section is asymmetric, the possibility of failure in the two directions (one causing compressive failure of the plate, the other causing compressive yielding of the stiffener tip) must be checked. The magnitude of the initial crookedness in these two directions may well be different, although in BS 5400 the bow in the direction causing compression in the stiffener tip is taken to be as large as that in the opposite direction. This allows for the fact that compressive residual stresses caused by welding may be present at the stiffener tip, which are otherwise unaccounted for in the design procedure. The effect of end eccentricity of loading over the stiffener/plate strut is represented by a term in Δ given by $r_{se}^2/2y_{Bs}$. Here y_{Bs} is the distance from the centroid of the effective stiffener section to the neutral axis of the cross section of the complete beam.

The design of the stiffened flange is checked to ensure that

$$\frac{\sigma_a + 2.5\tau_1 k_{s1}}{k_{l1}\sigma_{ye}} \leq 1 \tag{7.8}$$

$$\frac{\sigma_a + 2.5\tau_1 k_{s2}}{k_{12}\sigma_{ye}} \leq 1 \tag{7.9}$$

using the curves plotted in Fig. 7.10. The first of these expressions checks for failure by yielding of the stiffener tip, and the second checks for buckling or yielding of the plate panel. If the longitudinal stress varies along the length of the stiffener, σ_a in the expressions above is taken at a point $0.4l$ from the end, where the stress is greater. In these formulas

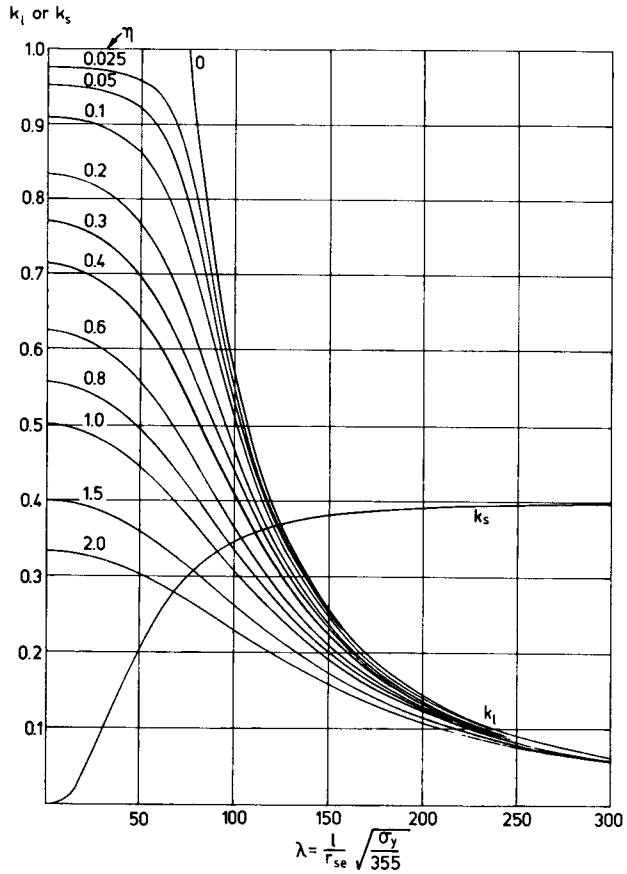

Fig. 7.10 Parameters for the design of longitudinal flange stiffeners.

σ_a = longitudinal stress at centroid of effective stiffener section
τ_1 = in-plane shear stress in flange plate due to torsion
σ_{ys} = yield stress of stiffener material
σ_{ye} = effective yield stress of flange plate material allowing for presence of shear
l = spacing of cross beams

A method proposed by Wolchuk and Mayrbourl (1980) in the proposed AASHTO code for box girders uses a format based on a German procedure (DAS, 1978) for calculating stiffened flange strength. Reproduced in Fig. 7.11, the method allows designers to check chosen sections rapidly and has the added advantage that it gives designers a good feel for the phenomenon controlling the strength (i.e., plate or stiffener buckling). The ultimate flange strength is computed as $P_u = F_u A_f$ or $F_u' A_f$, whichever is less, where

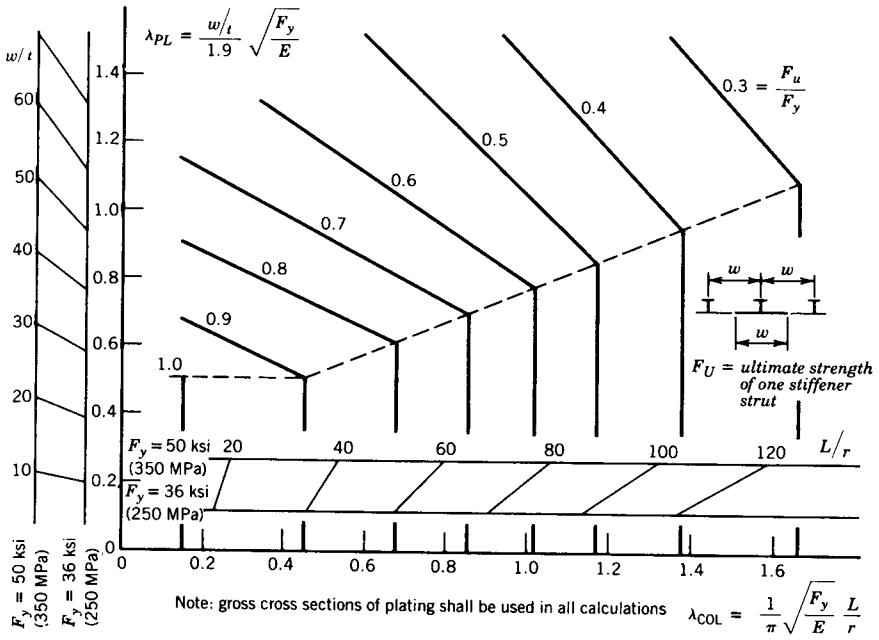

Fig. 7.11 Strength of stiffened flange in compression.

A_f = cross-sectional area of stiffened flange
F_u = ultimate strength of stiffener strut (stiffener with full width of associated plating)
F_u' = modified ultimate strength of stiffener strut under combined compression and shear
$= F_u$ for $f_v \le 0.175F_y$
$= 1.05F_u\sqrt{1 - 3f_v^2/F_y^2}$ for $f_v \ge 0.175F_y$
f_v = governing shear stress in flange

Design methods based primarily on the results of tests on stiffened panels have more recently been suggested by Japanese authors and were reviewed in the U.S.–Japan Seminar or Inelastic Instability of Steel Structures and Structural Elements held in Tokyo (Fujita and Galambos, 1981). One such proposed strength curve is given by

$$\frac{\sigma_u}{\sigma_y} = 1.24 - 0.54\bar{\lambda} \tag{7.10}$$

where

$$\bar{\lambda} = \frac{b}{t}\sqrt{\frac{\sigma_y}{E}\frac{12(1-\nu^2)}{\pi^2 k}} \tag{7.11}$$

and $k = 4n^2$ (n being the number of plate panels). It should be noted that this strength curve is chosen to agree with the *mean* of the test results obtained in Japan, as shown in Fig. 7.12.

In the case of stiffened flanges not subjected to normal loading, transverse stiffeners are designed to provide sufficient stiffness to ensure that they act as supports which are effectively rigid against movements normal to the plane of the flange plate but offer little resistance to rotation of the longitudinal stiffeners at their junctions. Thus they ensure that the effective buckling length of the latter does not exceed their span between adjacent transverse members. Where flanges form the deck of a box girder bridge which has to carry lateral loading the cross girders are primarily proportioned to resist the lateral loading and will normally have more than sufficient rigidity to constrain the stiffened panels in the manner envisaged.

The stiffness requirement for transverse members stipulated within BS 5400: Part 3 is based on limited experimental observations and provides a factor of safety of 3 against overall linear elastic buckling. The approximate expression produced for the minimum second moment of area required of a transverse stiffener and its effective width of attached flange is

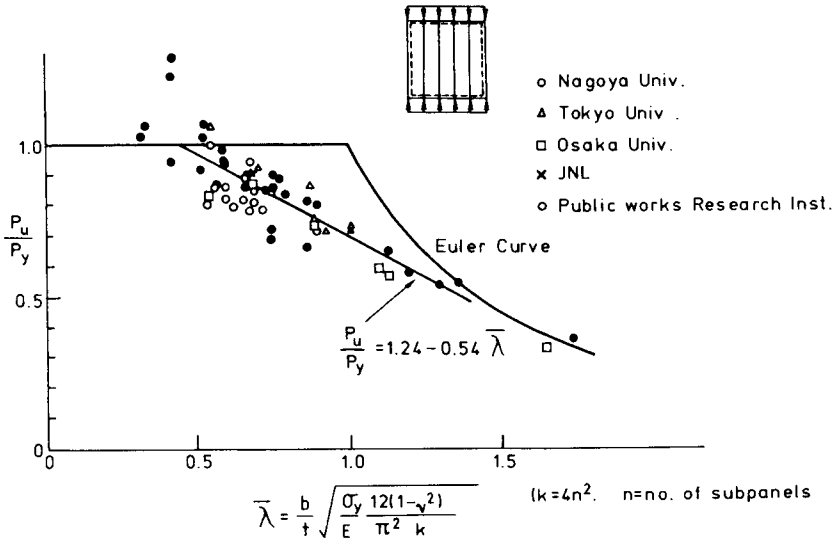

Fig. 7.12 Stiffened plate test results and proposed strength curve.

$$I_{be} = \frac{9\sigma_f^2 B^4 a A_f^2}{16KE^2 I_f} \tag{7.12}$$

where

σ_f = longitudinal compressive stress in flange
B = spacing of webs of main beam
a = cross-beam spacing
A_f = cross-sectional area per unit width of the flange
I_f = second moment of area per unit width of the flange
K = 24 for segments between *interior* webs of main beams and is determined from Fig. 7.13 in other cases

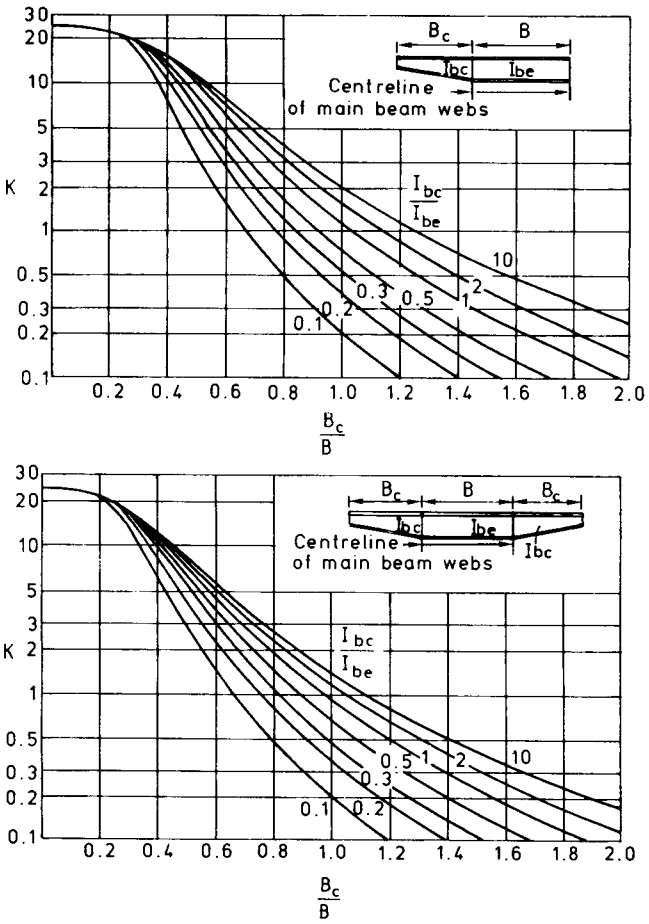

Fig. 7.13 Buckling coefficient K for transverse members.

In addition, the transverse member must be designed to carry any locally applied lateral loading as well as the normal component of in-plane loading in the flange caused by lack of alignment of the transverse members. Two simplified loading cases, selected to cover the latter effect, are stipulated as follows:

1. A uniformly distributed load per unit width of $\sigma_f A_f/200$
2. A concentrated load at a cantilever tip of $\sigma_f A_{sc}/160$, where A_{sc} is the cross-sectional area of the longitudinal stiffening member at the cantilever tip (σ_f and A_{sc} are in SI units)

In the proposed U.S. code the destabilizing effect of flange geometric imperfections is taken into account by assuming the transverse stiffeners or cross-frame members to be loaded by a uniformly distributed load of 1% of the average factored compressive force in the flange. The rigidity requirement is again covered by an expression for the minimum moment of inertia I_t derived from a linear elastic stability analysis of spring-supported compression bars, but substituting a factored applied axial stress f for the critical stress:

$$I_t = \frac{0.04b^3 A_f f}{Ea} \tag{7.13}$$

where

I_t = moment of inertia of transverse member including an effective width of flange plate
b = spacing between webs
A = cross-sectional area of compression flange
f = factored axial stress in compression flange
a = spacing of transverse members
E = Young's modulus

7.3.2 Orthotropic Plate Approach

Where there are several stiffeners (more than three) in a flange, advantage can be taken of the orthotropic plate idealization in which the actual discretely stiffened plate is replaced by an *ortho*gonally aniso*tropic* plate of constant thickness in which the stiffness of the stiffened plate is spread uniformly over its width. The potential advantage of this method is that the inherent plate action, ignored by the strut approach, can be mobilized. This, of course, has a particular advantage in the postbuckling range when transverse tensile membrane stresses in the plate restrain the rate of growth of out-of-plate deflections in the stiffeners. As the equations describing postbuckling behavior are nonlinear, the solutions generally involve an iterative procedure to produce the ultimate strength. The latter is assumed to be reached when a particular collapse criterion is satisfied. Collapse criteria suggested include the onset of yield at the flange/web junction, the mean stress along that edge reaching yield, yield at a stiffener tip at the center of the flange, or in-plane yield in the plate in the same region. These methods have been described in some detail by Maquoi and Massonnet (1971) and Jetteur (1983) and are reviewed in the book *Behaviour and Design of Steel Plated Structures*, issued by the ECCS (Dubas and Gehri, 1986). They suffer from the disadvantage that an iterative procedure is needed for their solution, although in some cases this has been greatly aided by the provision of design charts.

7.3.3 Discretely Stiffened Plate Approach

Analytical studies have been made of stiffened panels in which account has been taken of the discrete nature of the stiffening and which incorporate nonlinear geometrical and material effects. Both finite difference and finite element numerical formulations have been used for this purpose. The results, although giving insight into the interactive buckling of plate and stiffeners, have not been used to produce a general design method, although the analytical techniques can be used to analyze any particular design. Škaloud and Novotny (1965) gives the background for some available analyses.

Influence of Shear Lag oN Flange Buckling. Shear lag arises because the in-plane *shear* straining of a flange causes those parts most remote from a web to *lag* behind those in the vicinity of the web (Fig. 7.14). It is most marked in beams whose flanges are relatively wide compared to their length and therefore is of greater importance in box girder than in plate girder construction. It results in a nonuniform distribution of longitudinal stresses across the flange width, with bigger stresses occurring near flange/web junctions and smaller ones in the regions farthest removed from such junctions. The addition of stiffeners to a wide flange results in the nonuniformity becoming even more pronounced, even though the maximum stresses may be reduced. A systematic study of the factors influencing shear lag in box girder flanges has been reported by Moffatt and Dowling (1975, 1976) and forms the basis of the relevant rules in the proposed U.S. design specification (Fig. 7.15) and in the new British code. Similar studies have been reported by Abdel Sayed (1969) and others.

It is the nonuniform distribution of in-plane stresses in a box girder flange which is of interest from the point of view of structural stability. This form of distribution can increase or decrease the average stress, causing earlier buckling of the flange compared with the uniformly compressed case, depending on the degree of stiffening in the plate. On the other hand, it is clear that concentration of the applied stresses near the longitudinally compressed edges of the plate will encourage an earlier onset of yield at the edges than would uniform stressing across the flange width. The interaction of these two effects is complex

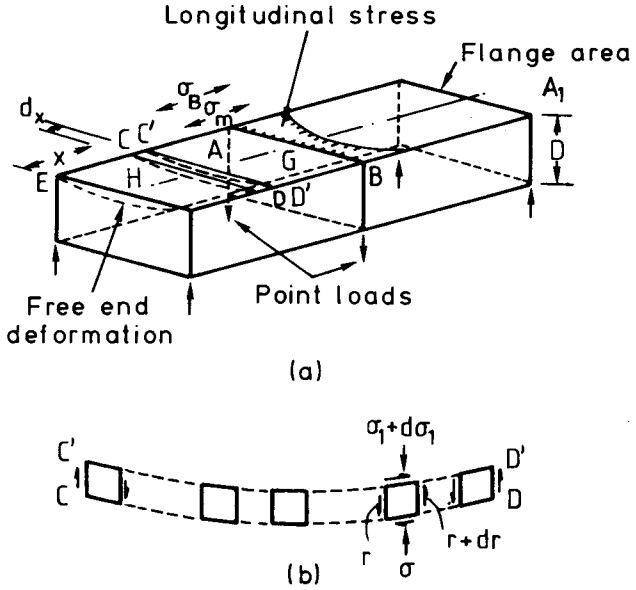

Fig. 7.14 Definition of shear lag.

and, indeed, is complicated further by the capacity of the stiffeners and plate panels to redistribute load. Tests (Dowling et al., 1977a; Frieze and Dowling, 1979) have shown, however, that for most practical cases shear lag can be ignored in calculating the ultimate compressive strength of stiffened or unstiffened flanges. This conclusion has been supported by the numerical studies of Lamas and Dowling (1980), Jetteur et al. (1984), and Burgan and Dowling (1985). Thus a flange may normally be considered to be loaded uniformly across its width. Only in the case of flanges with particularly large aspect ratios, or particularly slender edge panels or stiffeners, is it necessary to consider the flange stability in greater detail.

The limits given in BS 5400: Part 3 for neglecting shear lag in the calculation of the strength of unstiffened flanges is for flanges where the maximum longitudinal stress is more than 1.67 times the mean longitudinal stress. For cases in which this limit is exceeded the serviceability limit state has to be checked by including the effects of shear lag in the calculation of applied stresses.

Wolchuk, in the proposed U.S. code, suggests that shear lag may be ignored if the peak stress does not exceed the average stress by more than 20% and a uniform stress distribution is assumed for the calculation of the ultimate flange strength. Where these limits are exceeded it is suggested that the flange capacity at the web be increased to accommodate an additional force, computed as the load-factored stress is excess of 120% of the average stress multiplied by the flange area affected by the excess.

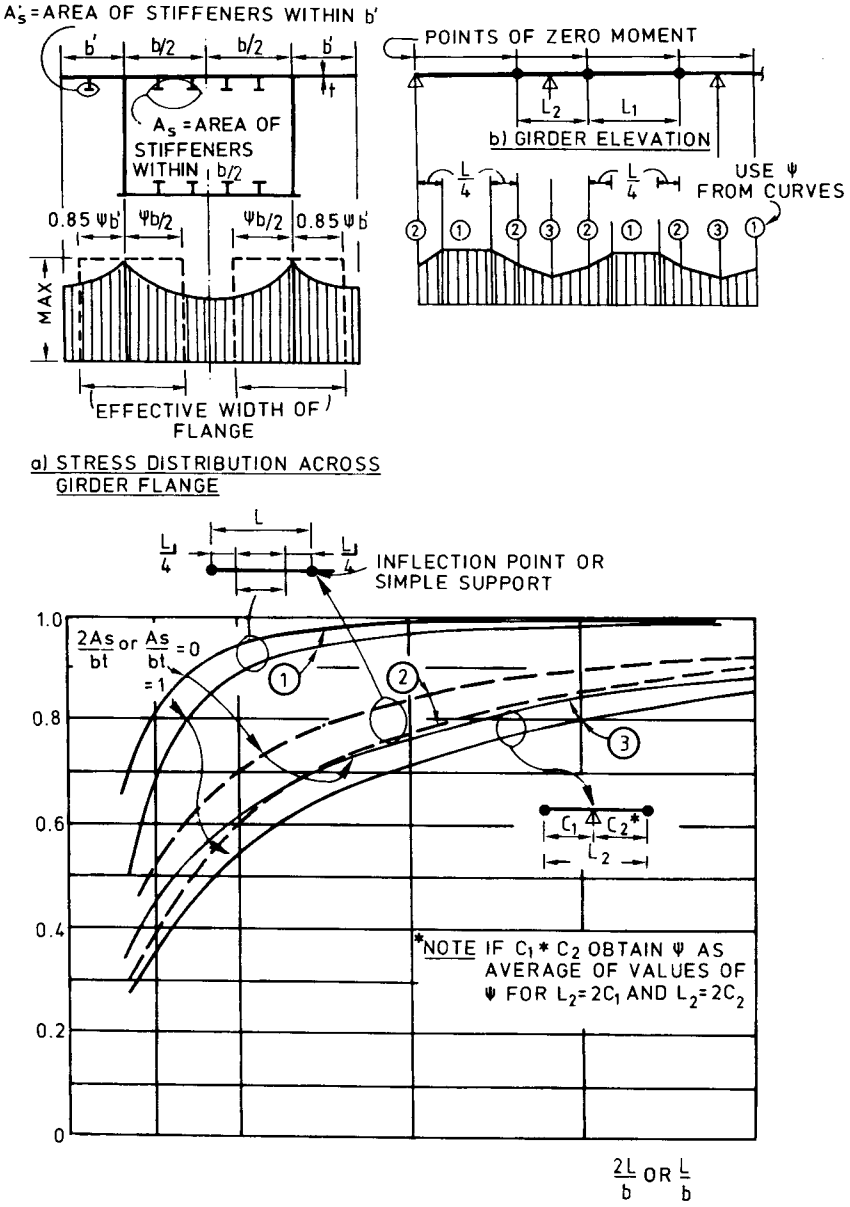

Fig. 7.15 Effective width of flange.

Influence of Lateral Loads. Lateral loads can be of interest in the context of bridges where the deck constitutes the top flange of the box girder. Where the box in question is a marine structure, such as a ship or an offshore platform, the lateral loading may be hydrostatic. In such cases the question arising is: What is the effect of the lateral loading on the stability of the stiffened plate acting as a compression flange to a box girder?

Plates such as those used in bridge decks to resist traffic loading are normally stocky and designed primarily to limit deflections under the lateral loading to very small acceptable values ($\ll t$). The presence of in-plane stresses due to participation of the plate as part of the box girder flange magnifies the deflections and bending stresses by a factor of approximately $1/(1-\sigma_a/\sigma_{cr})$. In the same way allowance can be made for the magnification of stresses in a compressed stiffened deck carrying lateral loading by also increasing the stresses due to the moments, when appropriate by this amplification factor.

In BS 5400: Part 3 stiffened compression flanges used to carry local wheel loading, such as steel bridge decks, may be designed for the ultimate limit scale ignoring the presence of the local loads. This is based on experimental evidence of a relatively limited nature. However, this is one of the few cases for which it is necessary to carry out a serviceability check using elastic analysis. This check is done to ensure that yielding under working load is prevented. The stresses in both the deck plate and the stiffeners are checked, including all elastic effects, such as shear lag, torsion, and in-plane stressing of the plate due to local bending of the stiffened plate under wheel loading. In calculating the stiffener stresses a distinction is made between the zones of hogging moment in the longitudinal stiffener over a transverse member and the sagging moment occurring between transverse members. Whereas in the latter case the full amplified stresses due to in-plane loading and local bending are combined, in the former only the in-plane stresses are amplified and added to the local bending stresses occurring at the longitudinal to transverse stiffener intersection.

The approximate expressions used to check the stiffener design are as follows: Over transverse members,

$$\frac{\sigma_a + 2.5\tau_1 k_{s1}}{k_{l1}\sigma_{ys}} + \frac{\sigma_{f0}}{\sigma_{ys}} \leq 1 \tag{7.14}$$

and between transverse members,

$$\frac{\sigma_a + 2.5\tau_1 k_{s2}}{k_{12}\sigma_{ye}} = \frac{\sigma_{fz}}{\sigma_{ye}} \leq 1 \tag{7.15}$$

where f_0 is the stress due to local bending at point on stiffener farthest from flange plate, σ_{fz} is the stress at midplane of flange plate due to local bending, and the other symbols are as defined earlier in this section.

The proposed U.S. code calls attention to the need to consider the effects of axial compression in the deck, combined with the effects of bending under lateral loading, when carrying out the design of orthotropic decks on the elastic basis but offers no guidance on how this may be done.

7.4 BENDING STRENGTH OF BOX GIRDERS

A box girder subjected primarily to bending moment will normally fail by buckling of the compression flange. Unlike plate girders, lateral torsional buckling rarely governs for practical box girders. Methods described in Section 7.3 can be used to calculate the compression flange strength.

In the simplest case the bending strength of box girders can be assumed to be contributed by the flanges alone and the moment of resistance can be calculated on the basis of the design force multiplied by the distance separating the flange centroids. Such an approach is allowed within BS 5400: Part 3 and greatly simplifies design.

To calculate the strength of the box girder, allowing for the contribution of the web, a linear distribution of stress over the depth of the cross section may be assumed. Effects of buckling in the web can be represented by using effective widths of web adjacent to the stiffeners as outlined in Chapter 4. The British Code BS 5400 also allows the use of the effective thickness approach for girders, which has the advantage that no recalculation of the position of the neutral axis is needed as is the case with the effective width approach. Cooper's expression for bending strength (1967) is used to give the effective thickness for unstiffened webs, and the full thickness is used for webs stiffened by effective longitudinal stiffeners. Failure is deemed to have occurred when the extreme fiber flange stress reaches the calculated ultimate stress of the compression flange σ_{lc}, or the yield stress of the tension flange σ_{yt}, whichever is the critical criterion. Thus in BS 5400

$$M_D = Z_{xc}\sigma_{lc} \quad \text{or} \quad Z_{xt}\sigma_{yt} \tag{7.16}$$

where Z_{xc} and Z_{xt} are the elastic moduli of the effective section for the extreme compression and tension fibers, respectively.

7.5 SHEAR STRENGTH OF BOX GIRDERS

The key difference between plate and box girders which may influnce the shear strength of the webs is the use of relatively thin flanges in box girders at the boundaries of the webs. Caution is needed in applying available tension field models, derived and verified in the context of plate girder webs, to the design of the webs of box girders. Of major concern is the relatively small amount of support against in-plane movement which may be afforded to the web by the

thin flange of a box girder, compared with the restraint offered by the thicker and narrower flange of a corresponding plate girder. In the latter case the out-of-plane bending rigidity and in-plane extensional rigidity of the flange to resist movement perpendicular to and parallel to the flange/web junction, respectively, is more effectively mobilized than in the case of thin flanged box girders.

7.5.1 Box Girders Without Longitudinal Stiffeners

In BS 5400: Part 3 (BSI, 1983) the tension-field model of Rockey and his co-workers (Porter et al., 1975) has been modified for application to both plate and box girders without longitudinal stiffeners (see Chapter 6). Thus for box girders with unstiffened flanges but with transverse stiffeners in the webs (or flanges)—a form of construction associated with relatively small boxes—advantage can be taken of postbuckling strength using a tension-field model. Limited use is made of the plastic frame mechanism action in the tension field to keep shear deformations within the limits for the whole girder. To do this the maximum possible shear capacity is limited to the shear yield capacity of the web alone. In the case of a box with thin unstiffened flanges, the width of flange taken as effective is $10t_f\sqrt{355/\sigma_{yf}}$ each side of the web, when the flange projects beyond the web. Where no such projection occurs the effect of frame action is neglected in the calculation of tension-field capacity (Harding and Dowling, 1981).

Wolchuk and Mayrbourl (1980) suggest, in applying the tension-field model to the transversely stiffened webs of box girders, the solution of Basler (1961), which is based on the assumption of negligible flange bending rigidity. This corresponds roughly to neglecting the frame action in the Rockey solution and reflects the caution needed for box girders, where the flanges are generally more slender than in plate girders. Thus the proposed U.S. code suggests that

$$V_u = V_B + V_T \tag{7.17}$$

with

$$V_B = Dt_w F_{vcr} \tag{7.18}$$

$$V_T = \frac{Dt_w F_T}{2(\sqrt{1+\alpha^2}+\alpha)} \tag{7.19}$$

where

D = depth of web between flanges, measured along web
d_0 = transverse stiffener separation
α = d_0/D
t_w = web thickness
F_{vcr} = critical buckling shear stress
F_T = tension-field stress

7.5.2 Box Girders with Longitudinal Stiffeners

In the case of box girders with longitudinal stiffeners very little experimental evidence is available to underpin the application of tension-field theories to web design. Code drafters are therefore doubly cautious on account of the unknown interaction between thin longitudinally stiffened webs and thin box girder flanges. Conservative approaches to design have been suggested which still take advantage of postbuckling reserve, albeit to a lesser extent than might be possible with a full plastic tension-field treatment.

In the British codified method (BSI, 1983) the stiffened web is checked on a panel-by-panel basis. The design procedure consists of calculating the longitudinal stresses using simple bending theory and gross areas. Shear forces are assumed to be distributed uniformly down a cross section. Each panel is then checked for yielding under combined compression, bending, and shear using the interaction formula

$$\left(\frac{\sigma_1 + 0.77\sigma_b}{\sigma_{yw}}\right)^2 + 3\left(\frac{\tau}{\sigma_{yw}}\right)^2 \le 1 \tag{7.20}$$

and for buckling using

$$\frac{\sigma_1}{\sigma_{yw}K_1} + \left(\frac{\sigma_b}{\sigma_{yw}K_b}\right)^2 + 3\left(\frac{\tau}{\sigma_{yw}K_q}\right)^2 \le 1 \tag{7.21}$$

where

σ_1 = mean longitudinal stress
σ_b = maximum longitudinal stress due to in-plane bending
τ = average shear stress
σ_{yw} = yield stress of web material
K_1, K_b, K_q = coefficients for ultimate plate strength

In checking yielding, any proportion of the longitudinal stresses σ_1 and σ_b, up to 60% maximum in a panel, can be shed to the flanges while maintaining overall equilibrium. In checking stability, up to 60% of these stresses can be shed from the restrained inner panels, but none can be shed from outer panels, which are considered to be unrestrained.

The proposed U.S. code uses the same approach as for webs stiffened transversely only, except that F_{vcr} is now calculated for each subpanel bounded by longitudinal and transverse stiffening and assumes the lowest value.

7.6 COMBINED BENDING AND SHEAR STRENGTH OF BOX GIRDERS

7.6.1 Box Girders Without Longitudinal Stiffeners

If the bending and shear strengths have been calculated without any contributions from the web and flanges, respectively, there is evidence to suggest that girders can safely resist these magnitudes of moment M_R and shear V_R acting simultaneously, so no interaction needs to be considered. For box girders with flanges and webs unstiffened longitudinally this approach provides a simple conservative estimate of combined bending and shear strength.

However, more often webs will have been considered to make some contribution to the bending strength M_D, and in the case where webs have been designed to take advantage of postbuckling strength, flanges may have been considered to contribute to the shear strength V_D through their framing action. BS 5400 proposes the use of an interactive diagram (Fig. 7.16) which can be used for box girders with no longitudinal stiffeners.

The proposed U.S. (Wolchak and Mayrbourl, 1980) specification for transversely stiffened web of box girders uses an interaction equation to calculate the critical buckling stress for combined shear, bending, and compression, in terms of ratios of the individual stress components to their critical buckling values when acting alone. Thus

$$\left(\frac{F_{vcr}}{F^0_{vcr}}\right)^2+\left(\frac{F_{bcr}}{F^0_{bcr}}\right)^2+\frac{F_{ccr}}{F^0_{ccr}}=1 \tag{7.22}$$

However, the stress components are interdependent and may be related as follows:

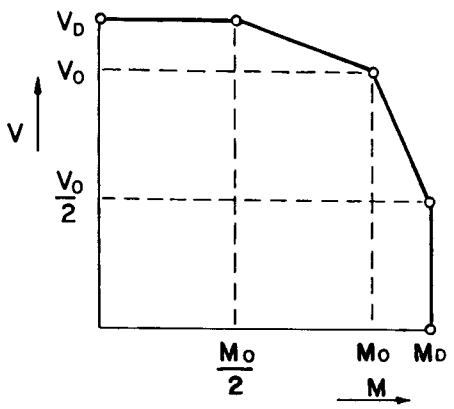

Fig. 7.16 Interaction between shear force and bending moment.

$$F_{bcr}=\frac{1-R}{2}\mu F_{vcr}$$
$$F_{ccr}=\frac{1+R}{2}\mu F_{vcr}$$

where

$$R=\frac{f_{2w}}{f_{1w}}$$
$$\mu=\frac{f_{1w}}{f_v}$$

f_{1w} = governing axial compressive stress at longitudinal edge of web panel
f_{2w} = axial stress at opposite edge of panel
f_v = governing shear stress = V/D_{tw}

These stresses are illustrated in Fig. 7.17. F°_{vcr}, F°_{bcr}, F°_{ccr} are the buckling stresses computed by assuming that only shear, bending, or compressive stresses, respectively, were present.

An additional flange force ΔF is added to the flange forces computed in accordance with elastic analysis. It includes that portion which must be transferred to the flanges from the webs after buckling, as well as a portion related to the use of tension-field action for the webs. These are for compression flanges:

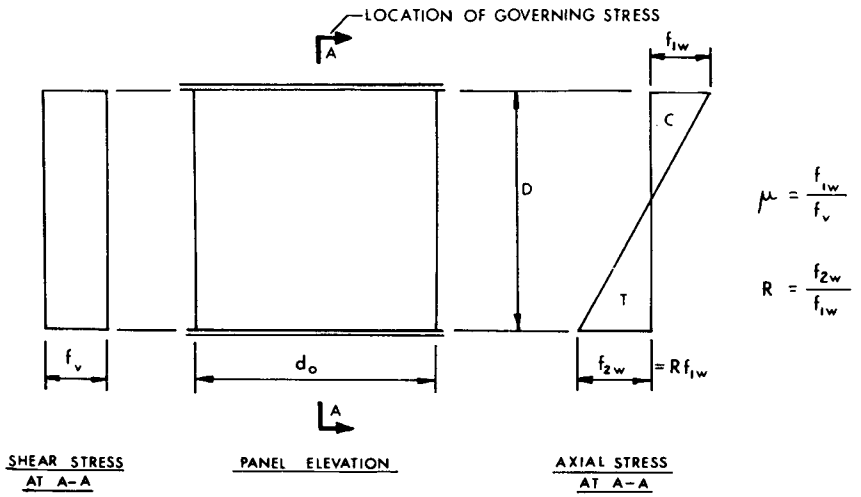

Fig. 7.17 Definition of μ and R for unstiffened and transversely stiffened webs.

$$\Delta F_1 = \left(1 - \frac{\sum V_B}{V_M}\right)\left[(f_{1R} - f_1)A_{fc} + \tfrac{1}{2} V_M \cot\left(\tfrac{1}{2}\theta_d\right)\right] \qquad (7.23)$$

and for tension flanges:

$$\Delta F_2 = \left(1 - \frac{\sum V_B}{V_M}\right)\left[(f_{2R} - f_2)A_{ft} - \tfrac{1}{2} V_M \cot\left(\tfrac{1}{2}\theta_d\right)\right] \qquad (7.24)$$

where

V_M = factored shear force acting coincident with maximum moment
ΣV_B = $\Sigma D t_w F_{vcr}$ = sum of buckling shear capacities of all webs at cross section considered
f_1, f_2 = stress in compression and tension flange, respectively, assuming fully participating webs
f_{1R}, f_{2R} = stresses assuming reduced moment of inertia of cross section
A_{fc}, A_{ft} = compression and tension flange area, respectively
θ_d = angle of inclination of web panel diagonal to the horizontal

7.6.2 Box Girders with Longitudinal Stiffeners

For box girders with longitudinally stiffened flanges and webs the situation is complicated by the scarcity of research information, in particular the lack of experimental data. Some redistribution of the longitudinal stress caused by bending or compression in a web is allowed within BS 5400: Part 3, as noted in Section 7.5 on the design of longitudinally stiffened webs for shear. The resultant stress distribution after such shedding must be such that the whole of the applied bending moment and axial force (if any) is transmitted and equilibrium is maintained. The percentage reduction in stress in the web panels participating in the shedding can vary from panel to panel but is assumed to be uniform within any one panel. No shedding is permitted from panels containing holes larger than a specified size. Similarly, stresses that cause yielding of the tension flange, but not buckling or yielding of the compression flange, may be redistributed within certain restrictions outlined in BS 5400: Part 3.

In summary, therefore, interaction between moment and shear in box girders with longitudinal stiffeners is dealt with by relieving the web of some of the longitudinally destabilizing compressive stresses caused by bending, and distributing the load to the compression flange while maintaining overall equilibrium of the cross section. In the proposed U.S. code combined bending and shear are treated in the same way for webs with and without longitudinal stiffeners. However, with longitudinal stiffening the formulas are applied to each subpanel in turn, rather than considering the overall web depth.

7.7 INFLUENCE OF TORSION ON STRENGTH OF BOX GIRDERS

The level of torsional stress induced in the webs and flanges of practical box girders does not of itself normally constitute an instability problem, athough tests on small thin-walled boxes subjected to torsion have shown that local instability of box corners can limit the strength in such cases. Allowance for the effects of the shears induced by torsion can be made in the design of the flanges by reducing the effective yield stress in the plate due to the presence of combined stresses, including torsional shear stresses, in the flange plate. In the design of the webs, additional shear stresses caused by torsion may be added to those associated with bending when calculating the total stresses applied to a web.

7.8 DIAPHRAGMS

Two types of diaphragms are encountered within box girders: intermediate diaphragms and load-bearing diaphragms. The former limit cross-sectional deformation, while the latter are provided at points of support to give load paths for vertical loads (web shears) and horizontal loads (flange shears) through to the support bearings, and to prevent buckling of the webs in the vicinity of these large concentrated loads. Intermediate diaphragms will not be covered here. Load-bearing diaphragms, on the other hand, need careful consideration in relation to buckling, just as support stiffeners do in the case of plate girders.

Most diaphragms are stiffened at the bearing locations with bearing stiffeners. These are often accompanied by short-length stub stiffeners immediately above the bearings, the role of which is to stiffen the diaphragm plate in the vicinity of the bearings so that localized redistribution of stress concentrations can occur through yielding of the plate. In longer diaphragms (Fig. 7.18), secondary stiffening can be provided to stabilize the diaphragm plate as an alternative to the use of very thick plate.

Transverse secondary stiffening may also be necessary to resist any transverse compression caused by the diaphragm's behavior as a deep beam, an action that is accentuated by the use of sloping webs. As the aim of any sensible design must be to eliminate the possibility of diaphragm buckling limiting the strength of the box girder it makes little sense to attempt to economize on diaphragm design and a conservative design approach is usually adopted.

Diaphragm design is treated in detail in BS 5400: Part 3. Only single-cell boxes, without steeply sloping webs and with diaphragms normal to the girder axis, are considered. Two approaches to design are contained within that specification, one for simple diaphragms and the other for diaphragms of more complicated geometries. In each case the design procedure involves three main features. These are:

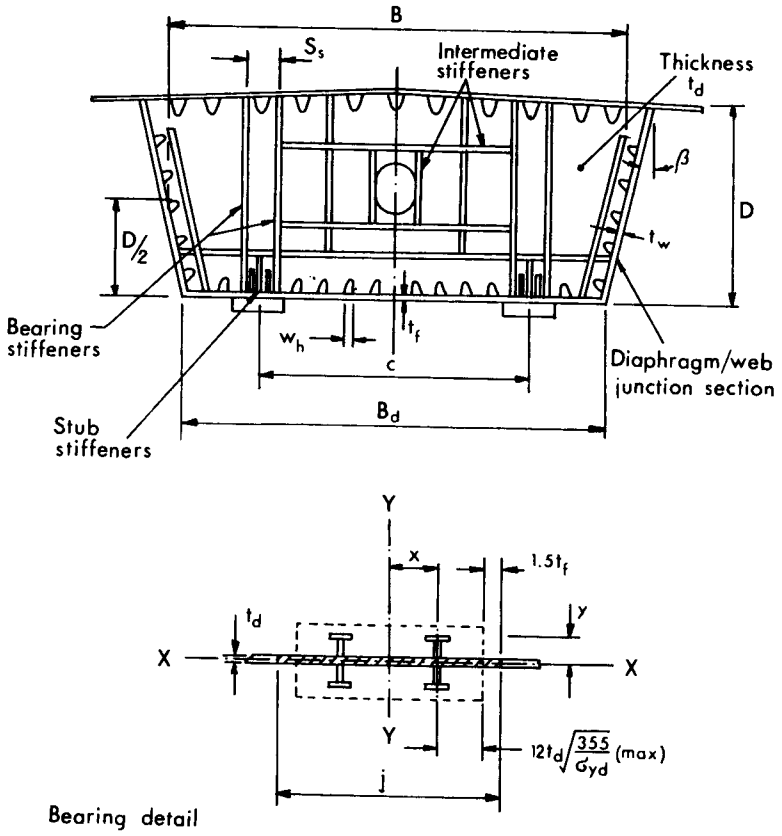

Fig. 7.18 Geometric notation for diaphragms.

1. Limitations of diaphragm geometry
2. Analysis of diaphragm stresses
3. Design checks on diaphragm yielding and buckling

The designer can choose to use diaphragms of simple layout, referred to as *unstiffened diaphragms*, even though they normally have full-height stiffeners at the bearing locations as well as a diaphragm plate (Fig. 7.19). The stiffeners, however, can be omitted in smaller boxes. For larger boxes the designer may opt for *stiffened diaphragms* with arrangements of bearing, stub, and secondary stiffening of the type referred to above.

The design method for the unstiffened diaphragms places greater restrictions on geometry and provides simple formulas for stress analysis, as well as simple yielding and buckling expressions for use in the design checks. Stiffened diaphragms, while still subject to limitations of geometry, albeit less restrictive

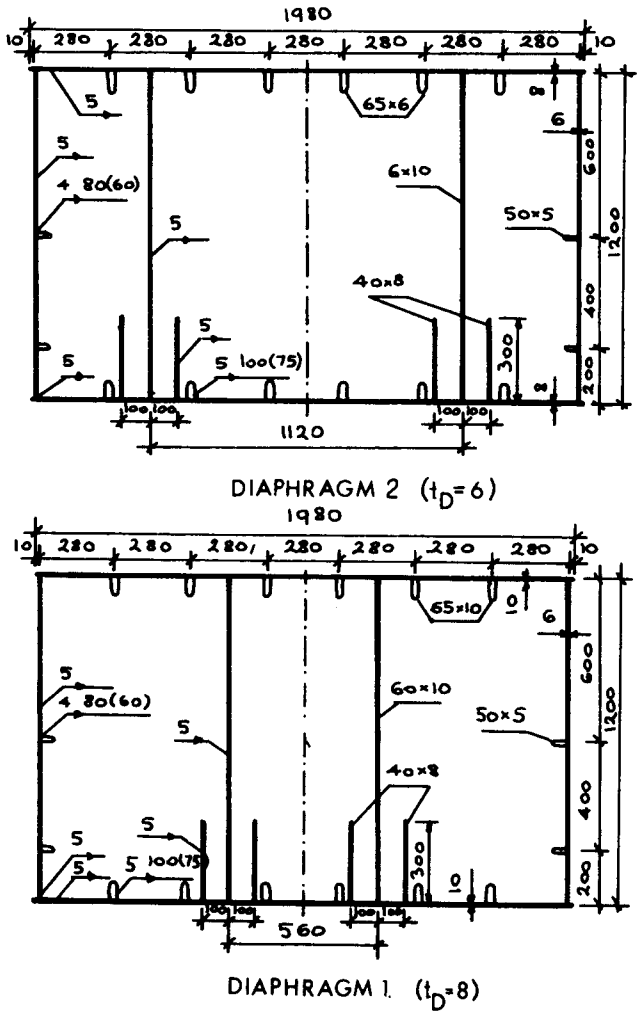

Fig. 7.19 Details of load-bearing diaphragms.

ones, normally require detailed computer analysis of stresses and detailed stiffener and plate panel failure checks.

7.9 UNSTIFFENED DIAPHRAGMS

Vertical stiffeners, which must be the full length of the diaphragm and positioned symmetrically on both sides of the diaphragm, are placed directly above bearings. These are provided solely to resist out-of-plane bending moments

caused by eccentricity of reactions with respect to the diaphragm midthickness. Such eccentricities may be due to fabrication tolerances or to longitudinal movements (temperature or otherwise) of the box girder. The stiffeners are loaded most heavily directly over the bearings with the loading tapering to zero at the intersection of the stiffener with the top flange, at which location they are normally attached to the flange stiffeners. The diaphragm plate resists all in-plane forces caused by bearing reactions, web and flange shear forces, and friction between diaphragm and bearings. The stiffeners are placed symmetrically to avoid addition to the stresses on the plate, which are calculated by ignoring the presence of the stiffeners.

7.9.1 Limitations on Diaphragm Geometry

To prevent torsional instability of the stiffeners, the limitations that relate to stiffeners in general are applied, examples of which are given in Section 7.3. To control the effects of openings, needed for access and services, limitations are placed on their positioning and sizing. To avoid complicated calculations, rules are given that allow holes of certain proportions to be used provided that they are sufficiently small not to affect plate stability. Holes are prohibited within the lower third of the diaphragm depth above bearings to allow some capacity for redistribution in a highly stressed area where the stresses may be further increased by the misalignment of bearings. Only one circular opening is allowed on each side of the vertical centerline of the diaphragm within the upper third of the depth, and its diameter is limited. Maximum sizes of cutouts for longitudinal stiffeners on the box walls are also given, and the stiffeners should be connected to the diaphragm plate.

7.9.2 Analysis of Diaphragm Stresses

A simplified model of the diaphragm interaction with other box girder components is used in the calculation of diaphragm stresses. Portions of flange are considered to act with the isolated diaphragm, which responds as a deep beam loaded by edge forces and supported by the bearings. The effective widths to be used in calculations are based on plane stress considerations (shear lag) alone and so may only be used when the transverse stiffness of the compression flange is not significantly reduced by transverse stresses, that is, provided that the calculated stresses do not exceed:

1. $\frac{1}{4}$ of flange longitudinal compressive strength
2. $\frac{1}{2}(t_f/b)^2E$, where t_f is the flange plate thickness and b is the spacing of longitudinal stiffeners

Otherwise, a reduced width of flange on either side must be used. It will be noted that no portion of the webs is included. This leads to a conservative

estimate of the stresses and greatly simplifies what is in reality a complicated problem due to the high level of both shear and bending stresses, which may coexist in the web at that location if the diaphragm is at an internal support.

For simple diaphragms the shear flows are simplified as shown in Fig. 7.20. Advantage has been taken of the ability of both plate panels and welds connecting the diaphragm and webs to redistribute shears applied in the nonuniform manner protected by elastic theory. This has enabled the shear flows to be taken as uniform. By also including the effects of inclined webs, the resulting reference stress is calculated using

$$\sigma_{R2} = \left[\left(\frac{K_d \sum R_v}{2} + \frac{T}{B}\right)x_R + Q_{fv}\frac{l_f}{2}\right]\frac{1}{Z_e} + \frac{\sum R_v \tan\beta}{2A_e} \tag{7.25}$$

where

K_d = 2 usually, and allows for boundary shears
B = average width of diaphragm
$\sum R_v$ = total vertical force transmitted to bearings
Q_{fv} = vertical force transmitted to diaphragm by a change of flange shape
l_f = horizontal distance from reference point to nearest edge of bottom flange
T = torque transmitted to diaphragm
Z_e, A_e = effective section modulus and area, respectively, of diaphragm and flanges at the vertical section through the reference point

Other symbols are shown in Fig. 7.21.

The vertical stress is calculated using

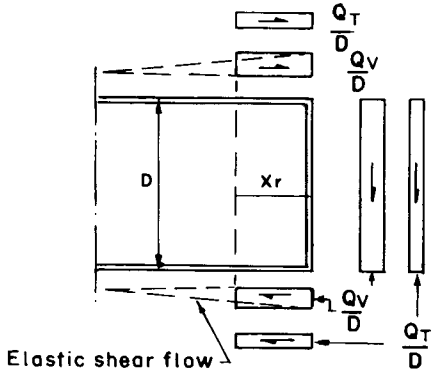

Fig. 7.20 Shear flows assumed to derive K_D.

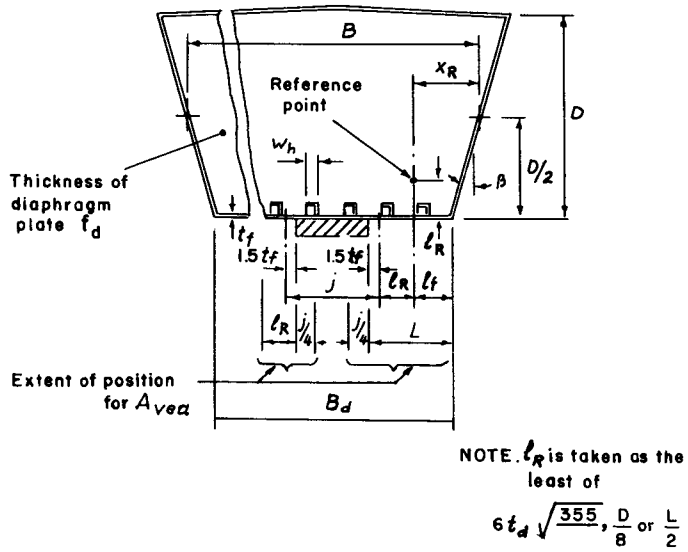

Fig. 7.21 Reference point and notation for unstiffened diaphragms.

$$\sigma_{R1} = \frac{R_v(1 + 4e/t_d)}{(j - \sum w_h)t_d} \tag{7.26}$$

for twin symmetrical bearings, where t_d is the diaphragm thickness and j is the effective width of contact of bearing pad allowing for load dispersion through flange (Fig. 7.21). With a single central bearing the vertical stress has an additional component, given by $0.77(T_b j/2I_{yd})$. Because maximum stressing in the vicinity of the bearings is very localized, a factor of 0.77 on yield is used here in the yield stress check to make some allowance for plastic redistribution. In these formulas

R_v = total vertical load transmitted to one bearing
T_b = torsional reaction at single central bearing
$\sum w_h$ = sum of widths of cutouts for stiffeners immediately above the flange and within width j
I_{yd} = second moment of area of width j of diaphragm plate, excluding cutouts
e = eccentricity of bearing reaction along span

The shear stress is given by

$$\tau_R = \left(\frac{\sum R_v}{2} + Q_{fv} + \frac{T}{2B}\right)\frac{1}{A_{vea}} + \frac{Q_h}{A_{he}} \tag{7.27}$$

where Q_h is the shear force due to transverse horizontal loads transmitted from top flange, A_{vea} the minimum net area of vertical cross section of diaphragm plating, and A_{he} the net area of horizontal cross section through reference point. Thus it is possible to calculate the combined stress at the reference point (Fig. 7.21).

7.9.3 Design Checks on Diaphragm Yielding and Buckling

The bearing stiffener is checked for yielding but not for buckling, as the plate itself is designed to take all in-plane forces from the webs and flanges. However, in the check for yielding the axial stresses above the bearings caused by the reactions at those locations are added to those caused by the out-of-plane moments. The effective area of contact of plate and stiffeners to be used in calculating these stresses is shown in Fig. 7.18.

The diaphragm plate is checked for both yielding and buckling. Use is made of approximate expressions for the elastic critical buckling of rectangular and trapezoidal plates loaded along their edges in checking the buckling strength of the diaphragm plate. Rotational restraint provided by flanges and webs to the diaphragm at their intersections is conservatively neglected. The empirical expressions allow for slope of webs, spacing and width of bearings, panel aspect ratio, and influence of top flange loading in coefficients K_1 to K_4.

The complete buckling check is

$$\sum R_v + \frac{T}{l_b} \le \frac{0.7KEt_d^3}{D} \tag{7.28}$$

where

$K = K_1K_2K_3K_4$
$K_1 = 3.4 + 2.2D/B_d$
$K_2 = 0.4 + j/2B_d$ for single central bearing
$= 0.4 + (c - j/3)/B_d$ for twin bearings
$K_3 = 1 - \beta/100$
$K_4 = 1 - \dfrac{fP_d}{\sum R_v + T/l_b}\left(\dfrac{2B}{B_d} - 1\right)$
c = distance between centers of bearings
$l_b = jK$ for single central bearings
$= c$ for twin bearings
$P_d = W_d \sum P/K_5$
W_d = uniformly distributed load applied to top of diaphragm
P = any local load applied to top of diaphragm
$K_5 = 0.4 + w/2B - B_d$
w = width of load P with allowance for dispersal through flange
$f = 0.55$ for $D/B \le 0.7$

$= 0.86$ for $D/B \geq 1.5$
with linear interpolation for intermediate values

Other symbols are dimensions defined in Figs. 7.18 and 7.20.

The reasoning behind the buckling check above is that the reactions applied to the diaphragm should not exceed 70% of the reactions causing critical buckling. This is based on the results of numerical parametric studies which suggest that provided the average stress above the bearing is contained, no further yielding due to buckling will occur in other parts until the diaphragm is loaded beyond 70% of the critical load. The stress in the vicinity of the bearings may attain average yield stress when the plate is loaded well below critical but is reduced as the stress approaches the cutoff level of 70% of critical load (see Fig. 7.22).

7.10 STIFFENED DIAPHRAGMS

The basis for the design of stiffened diaphragms differs from that of the "simple" unstiffened diaphragms in that the bearing stiffeners are designed not only to resist any out-of-plane moments but also to act as load-bearing stiffeners, in conjunction with narrow associated widths of diaphragm plate, to

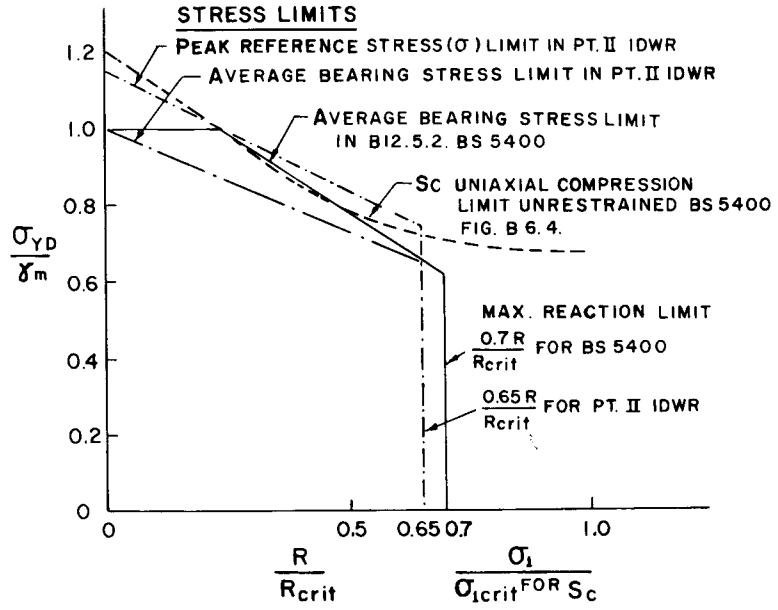

Fig. 7.22 Stress limits in simple plate diaphragms.

transmit vertical loads to the bearings. The plate panels are then designed for shear and transverse stress only. Secondary stiffeners are used to stabilize the plate by subdividing it into appropriately sized subpanels. Boundary stiffeners may also be provided at the web/diaphragm junctions to help resist tension field forces in the webs or to transmit reactions from cross girders or floor beams, with or without cantilevers, into the diaphragm.

7.10.1 Limitations on Diaphragm Geometry

The limitations on stiffeners to control stiffener buckling are the same as those for unstiffened diaphragms. Load-bearing stiffeners are not required to be symmetrical and can be welded to a single side, although they are still required to be full height. Unstiffened openings such as might be used in unstiffened diaphragms may be replaced by larger holes framed by stiffeners designed to resist destabilizing forces.

7.10.2 Analysis of Diaphragm Stresses

A rational analysis such as finite element analysis is often used to determine stresses in a stiffened diaphragm. Such an analysis would model the presence of stiffeners and openings with sufficient accuracy for design purposes. Alternatively, use can be made of the simplified analysis to determine the in-plane transverse stresses in the diaphragm plate. Secondary stiffeners are ignored in calculating diaphragm properties. Stresses must be calculated at the corners of each plate panel and any in-plane bending stresses due to Vierendeel action around large openings must be calculated separately and added to the other in-plane stresses. Load-bearing stiffeners, including a width of plating no more than 12 times the diaphragm thickness, are designed to carry linearly varying axial stresses compatible with the assumption of uniform shear flows and out-of-plane moments that decrease linearly with height.

7.10.3 Design Checks on Diaphragm Yielding and Buckling

Plate panels are checked for yield at all critical parts, ignoring vertical stresses. The panels are checked for buckling using ultimate strength interaction formulas originally devised for use in the design of longitudinally stiffened webs. Panels in the vicinity of the bearings are proportioned so that overall yield precedes buckling. Other panels are designed for buckling.

Load-bearing stiffeners are designed as struts, as in the case of longitudinally stiffened panels. A yield check is made for all sections, with some overstress, $1.33\sigma_{ys}$, permitted at the points of contact with bearings. Buckling checks are confined to the middle third of the height, where destabilizing effects are greatest in stiffeners of constant section. The destabilizing effects of transverse plate stresses are accounted for by means of an additional fictitious load in the stiffener. This load is taken as

$$P_{se} = \frac{\sigma_q l_s^2 t_d k_s}{a_{\max}} \tag{7.29}$$

where σ_q is the horizontal stress in the middle third of length l_s, l_s the length of stiffener between points of effective restraint, and $a_{\max}$ the spacing of vertical stiffeners; k_s is found from Fig. 7.9 using $l = l_s$.

Intermediate stiffeners are assumed to be free of axial stresses and applied moments and are proportioned to resist the destabilizing effect of transverse and shear stresses in the case of vertical stiffeners and shear stress alone in the case of horizontal stiffeners. A similar approach is used for stiffeners framing large holes, in which case the destabilizing terms are calculated assuming the hole to be absent.

7.11 RESEARCH NEEDS

Despite the enormous amount of research carried out on box girders in the 1970s there are still many aspects of the stability of box girders needing further attention, some of which are summarized below.

Flange Buckling

- Design rules are needed for flanges stiffened by one or two stiffeners. The strut approach may not be appropriate in such cases, as it neglects the transverse stiffness of the plate and is a poor model for a single stiffener.
- The limitations on cross-sectional shape to prevent local buckling of open and closed stiffeners need to be defined more accurately.
- There is a need for a simpler approach than those available for the buckling of lightly stiffened flanges which allows the postbuckling reserve of the stiffened flange to be taken into account.
- The limitations on redistribution of stresses caused by shear lag in the flange need to be defined more clearly for both simply and continuously supported box girders.
- A more rational ultimate load method for the design of laterally loaded flanges needs to be evolved.

Web Buckling

- Simple tension field design methods need to be developed for application to box girders which can include longitudinal stiffeners and the interaction among shear, bending, and axial stresses in the web.
- The application of corner stiffening to boxes as an aid to stabilizing the web and corner could be usefully investigated.

Diaphragms

- Simplification of the design approach to unstiffened diaphragms should be sought based on further research.
- Methods for the design of diaphragms should be produced to cover the cases of skew diaphrams and twin-walled diaphragms.
- The effects of interactions among diaphragm, flange, and web need more consideration

Behavior of Boxes

- The strength of longitudinally stiffened boxes under combined bending and shear needs closer attention in the future.
- The strength of stiffened boxes under combined bending, shear, and torsion also needs attention.

REFERENCES

Abdel-Sayed, G. (1969), "Effective Width of Steel Deck-Plate in Bridges," *ASCE J. Struct. Div.*, Vol. 95, p. 1459.

Basler, K. (1961), "Strength of Plate Girders in Shear," *ASCE J. Struct. Div.*, Vol. 87, p. 151.

BSI (1983), *Steel, Concrete and Composite Bridges*, British Standard BS 5400: Part 3, *Code of Practice for Design of Steel Bridges*, British Standards Institution, London.

Burgan, B. A., and Dowling, P. J. (1985), "The Collapse Behavior of Box Girder Compression Flanges—Numerical Modelling of Experimental Results," *CESLIC Rep. BG 83*, Imperial College, University of London.

Chatterjee, S. (1978), "Ultimate Load Analysis and Design of Stiffened Plates in Compression," Ph.D. thesis, Imperial College, University of London.

Cooper, P. B. (1967), "Strength of Longitudinally Stiffened Plate Girders," *ASCE J. Struct. Div.*, Vol. 93, p. 419.

DA Stahlbau (1978), "Beulsicherheitsnachweise für Platten," *DASt Richtlinie 12*, Deutscher Ausschuss für Stahlbau, Cologne, Germany.

Dowling, P. J., and Chatterjee, S. (1977), "Design of Box Girder Compression Flanges," *2nd Int. Colloq. Stabil.*, European Convention for Constructional Steelwork, Brussels, Belgium, p. 153.

Dowling, P. J., Harding, J. E., and Frieze, P. A., eds. (1977a) "Steel Plated Structures," *Proc. Intl. Conf. Imperial College*, 1976, Crosby Lockwood, London.

Dowling, P. J., Frieze, P. A., and Harding, J. E. (1977b), "Imperfection Sensitivity of Steel Plates Under Complex Edge Loading" *2nd Int. Colloq. Stabil., Steel Structures*, Liege, Belgium, p. 305.

Dubas, P., and Gehri, E., eds. (1986), *Behaviour and Design of Steel Plated Structures*, ECCS Technical Committee 8.3, Publ. No. 44, European Convention for Constructional Steelwork, Brussels, Belgium.

Dwight, J. B., and Little, G. H. (1976), "Stiffened Steel Compression Flanges: A Simpler Approach," *Struct. Eng.*, Vol. 54, p. 501.

Frieze, P. A., and Dowling, P. J. (1979), "Testing of a Wide Girder with Slender Compression Flange Stiffeners Under Pronounced Shear Lag Conditions," *CESLIC Rep. BG 49*, Imperial College, University of London.

Frieze, P. A., Dowling, P. J., and Hobbs, R. E. (1975), "Parametric Study of Plates in Compression," *CESLIC Rep. BG 39*, Imperial College, University of London.

Fujita, Y., and Galambos, T. V., eds. (1981), "Inelastic Instability of Steel Structures and Structural Elements," *U.S.–Jpn. Joint Sem.*, Tokyo.

Harding, J. E., and Dowling, P. J. (1981), "The Basis of the Proposed New Design Rules for the Strength of Web Plates and Other Panels Subject to Complex Edge Loading," in *Stability Problems in Engineering Structures and Components* (ed. T. H. Richards and P. Stanley), Applied Science Publishers, Barking, Essex, England, p. 355.

Horne, M. R. (1977), "Structural Action in Steel Box Girders," *CIRIA Guide 3*, Construction Industry Research and Information Association, London.

ICE (1973), "Steel Box Girder Bridges," *Proc. Int. Conf.*, Institute of Civil Engineers, London.

"Inquiry into the Basis of Design and Method of Erection of Steel Box Girder Bridges," (1973), *Report of the Committee and Appendices*, H.M. Stationery Office, London.

Jetteur, P. (1983), "A New Design Method for Stiffened Compression Flanges of Box Girders," in *Thin-Walled Structures* (ed. J. Rhodes and A. C. Walker), Granada, London, p. 189.

Jetteur, P., et al. (1984), "Interaction of Shear Lag with Plate Buckling in Longitudinally Stiffened Compression Flanges," *Acta Tech. CSAV*, No. 3, p. 376.

Lamas, A. R. G., and Dowling, P. J. (1980), "Effect of Shear Lag on the Inelastic Buckling Behaviour of Thin-Walled Structures," in *Thin-Walled Structures* (ed. J. Rhodes and A. C. Walker), Granada, London, p. 100.

Maquoi, R., and Massonnet, C. (1971), "Théorie non-lineaire de la resistance post-critique des grandes poutres en caisson raidies," *Mem. AIPC*, Vol. 31-II, p. 91.

Moffatt, K. R., and Dowling, P. J. (1975), "Shear Lag in Steel Box Girder Bridges," *Struct. Eng.*, Vol. 53, p. 439.

Moffatt, K. R., and Dowling, P. J. (1976), "Discussion," *Struct. Eng.*, Vol. 54, p. 285.

Ostapenko, A., and Vojta, J. F. (1967), "Ultimate Strength Design of Longitudinally Stiffened Plate Panels with Large b/t" *Fritz Eng. Lab. Rep. No. 248.18*, Lehigh University, Bethlehem, Pa., Aug.

Porter, D. M., Rockey, K. C., and Evans, H. R. (1975), "The Collapse Behaviour of Plate Girders in Shear," *Struct. Eng.*., Vol. 53, p. 313.

Rockey, K. C., and Evans, H. R., eds. (1980), "Design of Steel Bridges," *Proc. Int. Conf.*, University College, Cardiff, Granada, London.

Škaloud, M., and Novotny, R. (1965), "Uberkritisches Verhalten einer anfänglich gekrümmten gleichformig gedrückten, in der Mitte mit einer langsrippe versteiften Platte," *Acta Tech. CSAV*, p. 210.

Wolchuk, R., and Mayrbourl, R. M. (1980), "Proposed Design Specification for Steel Box Girder Bridges," *Rep. No. FHWA-TS 80-205*, U.S. Department of Transportation, Federal Highway Administration, Washington, D.C

CHAPTER EIGHT

BEAM-COLUMNS

8.1 INTRODUCTION

Beam-columns are defined as members subjected to a combination of axial force and bending moment. They therefore provide a link between the column under pure axial load discussed in Chapter 3 and the beam loaded only by moments, which was the subject of Chapter 5. Indeed, a case can be made for considering all members in frame structures as beam-columns, with columns and beams being the special cases that result when one load component becomes negligibly small. The bending moments in beam-columns may be generated as a result of transverse loading acting between the member's ends, from loading on adjacent members in rigidly framed structures or by the eccentricity of reactions and nominal axial forces in simply framed structures. When considering the behavior of beam-columns in rigidly framed structures it is normally necessary to consider also the influence of the surrounding members, which leads to the study of subassemblages and complete frames of Chapter 16. In the present chapter the subject is treated principally in terms of the response of an isolated member to a known system of end forces and moments.

Depending on the exact manner in which a beam-column is loaded and supported, its response may be categorized in a number of different ways. Perhaps the most fundamental feature is the presence (or absence) of a bracing system which is capable of preventing translation of one end relative to the other. Problems involving sway are more appropriately considered in the context of overall frame behavior. For nonsway beam-columns the three problem classes illustrated in Fig. 8.1 may be identified:

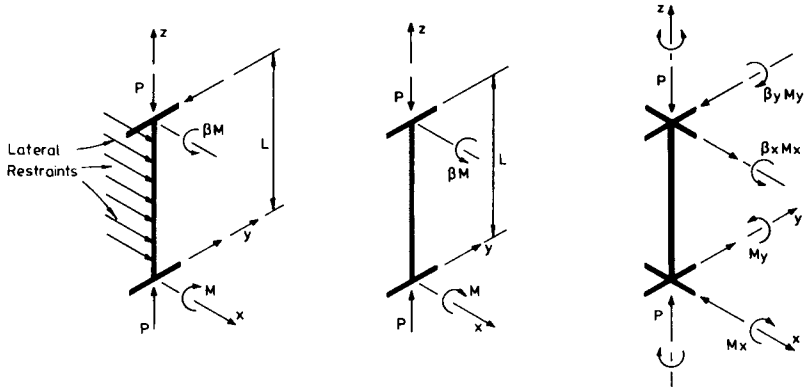

Fig. 8.1 Classes of beam-column behavior.

1. The thrust is applied with an eccentricity about the minor axis (or if the eccentricity is about the major axis, then the column is prevented from deflecting out of this plane by properly designed bracing), in which case the member will collapse by excessive deformation in this plane.
2. The thrust is applied with an eccentricity about the major axis, in which case the member will collapse by deflecting about the minor axis and twisting (i.e., similar to lateral–torsional beam buckling).
3. The thrust is applied with an eccentricity about both axes, in which case the member will collapse by combined bending and twisting.

Thus case 1 represents an interaction between column buckling and simple uniaxial beam bending, case 2 represents an interaction between column buckling and beam buckling, and case 3 represents the interaction of column buckling and biaxial bending. Clearly, case 3 is the most general case, with the others being more limited versions.

The analysis of various aspects of these problems has formed the subject of a very large number of research investigations. Initially these were confined to the elastic range, but the increasing availability of computers has meant that by including inelastic material behavior in conjunction with such features as residual stresses and initial deformations realistic maximum strength analyses may now be conducted. The development of the theory of beam-columns has been summarized by both Massonnet (1976) and Chen and Atsuta (1977). A more general review of the most significant developments prior to 1976 is available in the third edition of the guide (Johnston, 1976), while reviews devoted specifically to the biaxial problem have been provided by Chen and Santathadaporn (1968) and by Chen (1977a, 1981). In view of the availability of these comprehensive summaries of the general subject area of beam-columns, no general historical review will be presented herein. Rather, the chapter will concentrate

on an evaluation of the various design and analysis approaches that are available for each type of beam-column problem. In this way it is hoped that the material will be of direct use to designers needing to work beyond the limitations of codes of practice, to specification writing bodies engaged in the task of updating design codes, and to researchers concerned with advancing the understanding of particular aspects of the topic. Readers requiring a historical perspective on the subject are advised to consult the reviews referenced above, in which they will find more than 300 relevant papers listed.

8.2 STRENGTH OF BEAM-COLUMNS

The load-carrying capacity of a beam-column depends on several factors, which may conveniently be arranged under the three headings *load-related*, *member-related*, and *imperfection-related*. The first of these is readily appreciated if the strength of a beam-column subject to any combination of axial load P, major-axis moment M_x, and minor-axis moment M_y is displayed on a three-dimensional interaction diagram of the type shown as Fig. 8.2. Clearly, any point located on an axis will correspond to loading of one type only, while

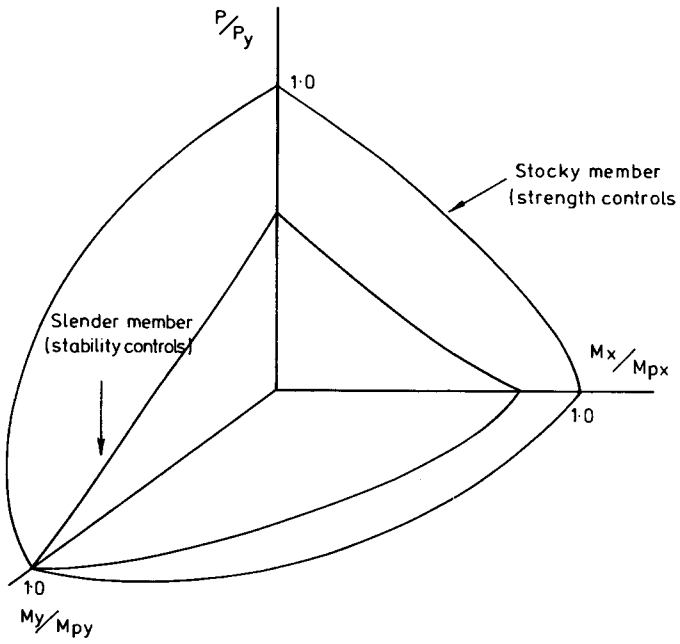

Fig. 8.2 Interaction surfaces for beam-columns.

the line or surface joining these endpoints will define strength under two or three load components, respectively.

In constructing diagrams of the form of Fig. 8.2, use is made of the member's strength as a column P_u and as a beam M_{ux} and M_{uy} in fixing the endpoints. Procedures for determining these quantities have previously been discussed in Chapters 3 (columns) and 5 (beams). These make use of several properties of the member (e.g., geometrical proportions, material strength, unbraced length, end support conditions, etc.). These same properties will also have some effect on the exact shape of the interaction curves or surfaces (i.e., their degree of concavity or convexity).

The various "imperfections" (e.g., lack of straightness in either plane, residual stresses, variation of material strength around the cross section, etc.) will also influence both the component strengths and the shapes of the interactions. The estimation of the strength of a beam-column therefore requires a knowledge of the form of Fig. 8.2 appropriate to the particular set of parameters present. Succeeding sections of this chapter will address this problem in terms of both the design-oriented procedures that have evolved to meet this need and the evidence, both theoretical and experimental, on which these have been based.

Traditionally, design methods for beam-columns fall into one of two categories: (1) those that use charts or tables to provide safe combinations of the applied load compontments, and (2) interaction formulas of the type

$$f\left(\frac{P}{P_u}, \frac{M_x}{M_{ux}}, \frac{M_y}{M_{uy}}\right) \leq 10 \tag{8.1}$$

which provide a smooth transition between end points corresponding to strength under only one form of loading. More recently, the availability of inexpensive microcomputers has meant that for special problems (e.g., beam-columns on unusual cross section for which the application of methods based on wide-flange shapes might be considered questionable), direct analysis is also a possibility.

Use of the interaction approach does, of course, imply that reliable estimates of the endpoints of the interaction, which depend on the strengths P_u, M_{ux}, and M_{uy} under only one component of the applied loading, are available. A word of caution is in order here, as changes in these endpoints (e.g., by the substitution of one column formula for another) can sometimes produce unexpectedly large changes in the predictions of an interaction equation. Although methods are available for obtaining accurate theoretical solutions to each of the problem types shown in Fig. 8.1, such methods always require the use of numerical procedures to follow the inelastic load-deflection behavior associated with the attainment of true maximum strength. They therefore cannot lead directly to design equations. Explicit forms of Eq. 8.1 for individual cases must therefore be developed either as modifications to formulas derived from

elastic analysis or on a wholly empirical basis. The suitability of such formulas then requires verification against available theoretical and experimental data.

8.3 UNIAXIAL BENDING: IN-PLANE STRENGTH

A convenient form of Eq. 8.1, which is used as the starting point for several design formulas, is

$$\frac{P}{P_u} + \frac{M}{M_u} \leq 1.0 \tag{8.2}$$

where P is the thrust at failure, P_u the ultimate load for the centrally loaded column for buckling in the plane of the applied moment, M the maximum bending moment at failure, and M_u the ultimate bending moment in the absence of axial load.

If the design basis is to be the attainment of first yield in an initially stress-free member, then P_u and M_u should be chosen accordingly (Johnston, 1976). For ultimate load design P_u and M_u should be taken as the column strength as discussed in Chapter 3 and the in-plane bending capacity (i.e., M_p, the fully plastic moment capacity).

While the correct value for P is the applied axial load, the determination of the appropriate value for M in any particular case is more difficult since it will be affected by the deformation of the member. This in turn will be a function principally of the form of the applied loading producing the moments, the level of thrust, and the member slenderness. Figure 8.3 illustrates the difference between a stocky column for which the maximum moment may sensibly be taken as the maximum primary moment (i.e., that calculated neglecting the

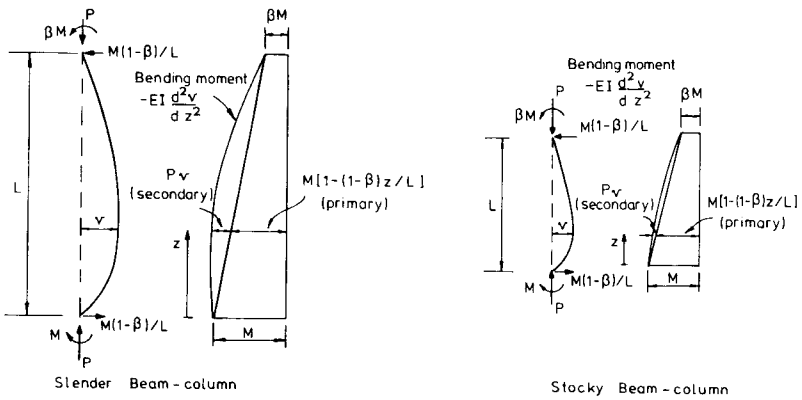

Fig. 8.3 Stocky and slender beam-columns.

effects of the axial load) and a slender column. For the latter the action of the thrust acting through the deflections produced by the primary moment leads to so-called secondary moments, the effect of which is to increase the moments as shown. The relative size of the primary and secondary moments will depend on the variables mentioned previously. In particular, for certain patterns of primary moment (e.g., double curvature bending produced by end moments M_1 and $-M_1$), the point of maximum moment may be located at the end(s) of the member even though its slenderness is large.

The maximum moment at midlength in a beam-column subjected to compression P and equal and opposite end moments M_0 is given approximately by (Johnston, 1976)

$$M_{\max} = M_0\left(\frac{1}{1 - P/P_e}\right) \tag{8.3}$$

in which P_e is the elastic critical load for buckling in the plane of the applied moments. The term in parentheses in Eq. 8.3 may be regarded as an amplification factor by which the first-order moment M_0 is multiplied to obtain the second-order moment $M_{\max}$. It causes $M_{\max}$ to increase nonlinearly as shown in Fig. 8.4.

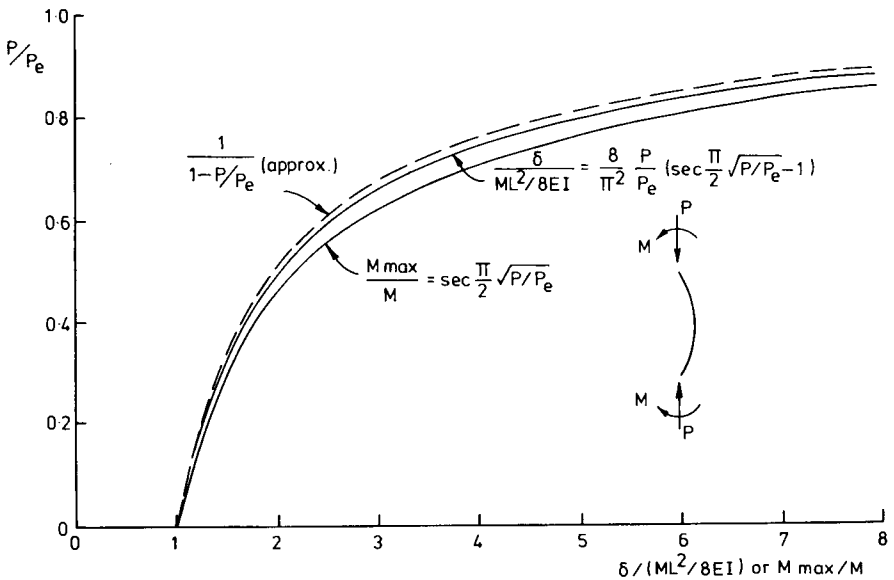

Fig. 8.4 Maximum deflection and moment in elastic beam-columns with equal end moments.

Although Eq. 8.3 is derived on the assumption of elastic behavior, its application in an ultimate load context is well established. Substituting it into Eq. 8.2 gives the design formula

$$\frac{P}{P_u} + \frac{M_0}{M_u(1 - P/P_e)} \leq 1.0 \tag{8.4}$$

which was first recommended by SSRC (Johnston, 1976) and which has been included in several national codes. A direct comparison between Eq. 8.4 and the early numerical solution of Galambos and Ketter (1961) for the case of a W8 × 31 section bent about its major axis is reproduced as Fig. 8.5 (Massonnet and Save, 1965). Additional solutions (see Table 8.1A) have shown that Eq. 8.4 provides an acceptable fit for all W shapes, including those fabricated by welding (Galambos, 1964). Equation 8.4 may also be used for W shapes bent about their minor axis, provided that P_u, M_u, and P_e are correctly specified, and Fig. 8.6 compares its predictions with numerical data (Lu et al., 1983). Test data for both cases as well as for other cross-sectional shapes are listed in Table 8.1B. Those listed for steel are, however, largely confined to rolled W-shapes; extensive test data on other manufactured shapes (e.g., tubes) or for any welded section appear to be lacking. For aluminum sections the coverage is wider, including several results for monosymmetric section (Klöppel and Barsch, 1973; Gilson and Cescotto, 1982). It is also noticeable that only a small proportion of the theoretical studies of Table 8.1A include an allowance for initial curvature and that existing data would appear to be confined to either W-shapes or to square and circular tubes.

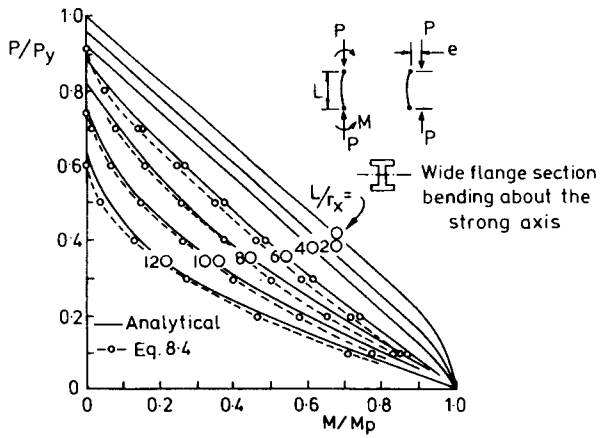

Fig. 8.5 Comparison of Eq. 8.4 with numerical results of Galambos and Ketter for major-axis bending of a W-section (after Massonnet and Save, 1965).

TABLE 8.1A Theoretical Solutions for the In-Plane Strength of Beam-Columns

Reference	Results for Direct Use	Initial Deflection	Cross Section	Residual Stress
Galambos and Ketter (1961)	Yes	No	W, x–x axis	Pattern a
Ketter (1962)	Yes	No	W, x–x axis	Pattern a
	Yes	No	W, x–x axis	Pattern a
Lu and Kamalvand (1968)	Yes	No	W, x–x axis	Pattern a
Chen (1971b)	Yes	No	W, x–x axis	None, pattern a
	Yes	No	W, y–y axis	None, pattern a
	Yes	No	Square tube	None
Chen (1971a)	Yes	No	W, x–x axis	None
	Yes	No	Rectangular tube	None
Chen (1970)	Yes	No	W, x–x axis	Pattern a
			Rectangular tube	None
Lu et al. (1983)	Yes	Height/1000	W, x–x axis	Pattern a
	Yes	Height/1000	W, y–y axis	Pattern a
Chen and Atsuta (1972b)	Yes	No	W, x–x axis	Pattern a
Cheong-Siat-Moy (1974a)	Yes	No	W, x–x axis	Pattern a
Cheong-Siat-Moy (1974b)	Yes	No	W, x–x axis	Pattern a
Ballio and Campanini (1981)	Yes	Height/1000	W, x–x axis	Pattern b
	Yes	Height/1000	W, y–y axis	Pattern b
	Yes	Height/1000	Square tube	Pattern b
	Yes	Height/1000	Circular tube	None
Ballio et al. (1973)	Yes	Height/1000	W, x–x axis	Pattern b
	Yes	Height/1000	W, y–y axis	Pattern b
	Yes	Height/1000	Square tube	Pattern a
	Yes	Height/1000	Square tube	Pattern b
Yu and Tall (1971)	Yes	No	W, x–x axis	Pattern a
			W, x–x axis	Pattern d
Young (1973)	Yes	Height/1000	W, x–x axis	Patterns b and c
			W, y–y axis	Patterns b and c
			Square tube	Pattern b

For beam-columns subjected to unequal end moments and/or transverse loading between points of support in the plane of bending, Eq. 8.4 may still be used provided that M_0 is replaced with an equivalent moment $M_{eq} = C_m M_0$, where C_m is a reduction factor and M_0 is taken as the maximum first-order moment. Since the C_m factor is also applicable to the other types of beam-column problems illustrated in Fig. 8.1, a full discussion of its basis will be delayed until Section 8.5. The more general form of the interaction equation is, therefore,

$$\frac{P}{P_u} + \frac{C_m M_0}{M_u(1 - P/P_e)} \leq 1.0 \tag{8.5}$$

Equation 8.5 refers to the conditions of failure resulting from instability due to excessive bending occurring within the member. However, when a beam-column is bent by moments producing plastic hinges at one or both ends, it is necessary to limit such terminal moments to within M_{pc}, the plastic-hinge moment modified to include the effect of axial compression. The determination of M_{pc}, by satisfying the requirements of equilibrium, is simple, if tedious, for

Load Cases	Comparison with Eq. 8.4
1 (β =1.0, 0)	Partial
1 (β = 1, 0.5, 0, −0.5, −1)	Partial
4	Partial
4, 2, 5, 6	Yes
4, 1 (β = 1)	No
4, 1 (β = 1)	No
4, 1 (β = 1)	No
4, 1 (β = 1)	No
4, 1 (β = 1)	No
3, 1 (β = 1), 2	No
3, 1 (β = 1), 2	No
1 (β = 1, 0.5, 0, −0.5, −1)	No
1 (β = 1, 0.5, 0, −0.5, −1)	No
1 (β = 1)	No
2, 4, 6	No
2, 7, 13	No
1 (β = 1, 0, −1)	Yes
9, 2, 4, 8	Yes
3, 10, 7	Yes
12, 11	Yes
1 (β = 1)	Yes
1 (β = 1)	Yes
1 (β = 1)	Yes
1 (β = 1)	Yes
1 (β = 1)	No
1 (β = 1)	No
1 (β = 1, 0, −1)	No
1 (β = 1, 0, −1)	No
1 (β = 1, 0, −1)	No

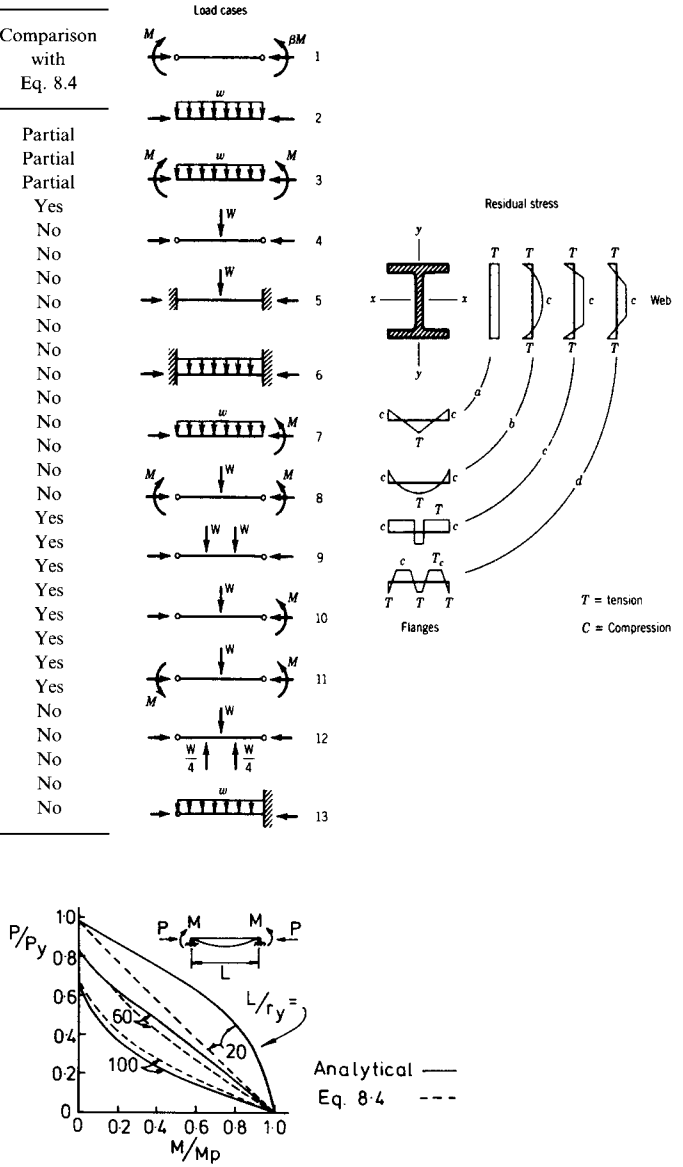

Fig. 8.6 Comparison of Eq. 8.4 with numerical results of Kanchanalai and Lu (1979) for minor-axis bending of a W-section.

rectilinear shapes. Expressions for M_{pc} for wide-flange shapes are available (ASCE, 1971a). These may be extended to other orthogonal shapes, in which case the superposition procedure developed by Chen and Atsuta for biaxially bent beam-columns can be applied (Chen and Atsuta, 1972a, 1974, 1977).

TABLE 8.1B Experimental Data on the In-Plane Strength of Beam-Columns

Reference	Number of Tests	L/r Range	Cross Section	Residual Stress	Load Cases	Comparison with Eq. 8.4	Comments
Johnston and Cheney (1942)	30	23–122	W, x–x axis	Pattern a	$1(\beta = 1)$	Galambos and Ketter (1961)	Major-axis failure
	30	26–126	W, y–y axis	Pattern a	$1(\beta = 1)$	No	
Galambos and Ketter (1961)	5	11–90	W, x–x axis	Pattern a	$1(\beta = 1)$	Yes	
Ketter et al. (1952, 1955)	14	28–120	W, x–x axis	Pattern a	$1(\beta = 1, 0)$	Yes	Some out-of-plane failures
Galambos and Ketter (1961)							
Yu and Tall (1971)	2	40	W, x–x axis	Patterns a and d	$1(\beta = 1)$	No	Braced about y–y axis
Mason et al. (1958)	24	36–117	Hat shape	Unknown pattern	$1(\beta = 1)$	Yes	
van Kuren and Galambos (1964)	36	22–116	W, x–x axis	Pattern a	$1(\beta = 1, 0.5, 0, -1)$	Yes	10 tests braced about y–y axis, several out-of-plane failures for the rest
van Kuren and Galambos (1964)	1	72	W, y–y axis	Pattern a	$1(\beta = 1)$	Yes	
Dwyer and Galambos (1965)	3	38–80	Square tube	Unknown pattern	$1(\beta = 1)$	Yes	
Bijlaard et al. (1955)	18	40–50	Square tube	Unknown pattern	$1(\beta = 1)$	No	Elastic end restraints
			W, x–x axis	Pattern a	$1(\beta = 1)$	No	
Lay and Galambos (1965)	7	30–60	W, x–x axis	Pattern a	$1(\beta = 1)$	No	End restraint from beams, braced about y–y axis
Gilson and Cescotto (1982)	18	35–68	T-shape	Aluminum	$1(\beta = 1)$	No	Comparisons with ECCS
Hill et al. (1956)	9		Circular tube	Aluminum	$1(\beta = 1)$	Mazzolani and Frey (1983)	
Clark (1955)	28		Square tube	Aluminum	$1(\beta = 1)$		
			Solid square				
Klöppel and Barsch (1973)	48	30–70	W, x–x axis	Aluminum	$1(\beta = 1)$	Mazzolani and Frey (1983)	
	48	30–82	Circular tube	Aluminum	$1(\beta = 1)$	Mazzolani and Frey (1983)	
	27	30–80	T shape	Aluminum	$1(\beta = 1)$	Mazzolani and Frey (1983)	

Expressions for M_{pc}, applicable for most wide-flange sections, are plotted non-dimensionally in Figs. 8.7 and 8.8. The accuracy of these curves has been verified by experiments. Simple approximate expressions to compute M_{pc} are also shown by dashed lines in Figs. 8.7 and 8.8. The limitation $M_0 \leq M_{pc}$ will lead to two additional interaction formulas as follows. For strong-axis bending,

$$\frac{P}{P_y} + 0.85\left(\frac{M_0}{M_p}\right) \leq 1.0 \quad M_0 \leq M_p \tag{8.6}$$

and for weak-axis bending,

$$\left(\frac{P}{P_y}\right)^2 + 0.84\left(\frac{M_0}{M_p}\right) \leq 1.0 \quad M_0 \leq M_p \tag{8.7}$$

An alternative to Eq. 8.7 suggested by Pillai (1974), which is easier to incorporate into the biaxial interaction formulas discussed in Section 8.6 due to its linear format, is compared with the "exact" results in Fig. 8.8.

$$\frac{P}{P_y} + 0.6\left(\frac{M_0}{M_p}\right) \leq 1.0 \quad M_0 \leq M_p \tag{8.8}$$

Several of the references listed in Tables 8.1A and 8.1B contain material that could be of direct use to the designer confronted with a problem outside the scope of standard design treatments. The most useful of these, together with other design-oriented references, are summarized from this point of view in Table 8.1C.

Although Eqs. 8.6 through 8.8 permit the in-plane strength of a beam-column containing a plastic hinge to be determined, for such members to function satisfactorily in plastically designed structures they must also possess sufficient ductility. Quantitative assessments of this are usually expressed in terms of rotation capacity R, the ratio of plastic rotation to the hypothetical rotation in an elastic member at the moment capacity given by Eqs. 8.6 through 8.8, as appropriate. For I-sections in major-axis bending, assuming a minimum acceptable value for $R = 3$, Kemp (1984) has proposed that slenderness be limited to

$$\frac{L}{r_x} \leq \sqrt{\frac{\pi^2 E}{\sigma_y}}(0.6 - 0.4\beta)\frac{1 - P/P_y}{1.5P/P_y} \tag{8.9}$$

This expression is a development of that suggested by Lay (1974), which is used in the Australian code (SAA 1990). A more general study of the interaction of axial force, end moment, slenderness, and rotation capacity is available

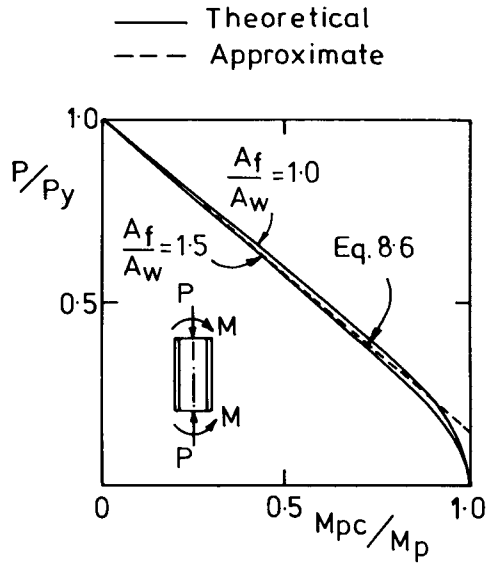

Fig. 8.7 Approximate interaction equation for a W-section (strong-axis bending, short column).

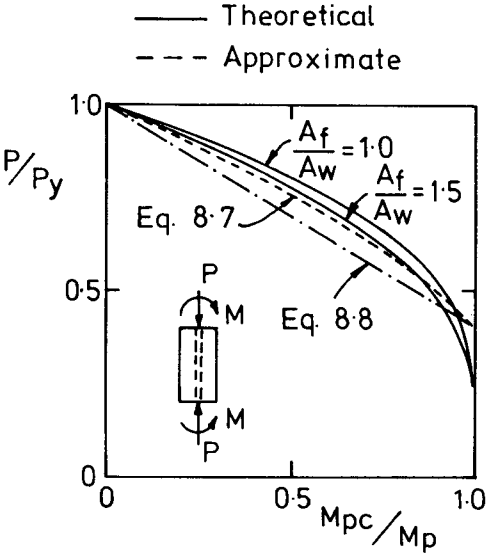

Fig. 8.8 Approximate interaction equation for a W-section (weak-axis bending, short column).

TABLE 8.1C Design-Oriented References on the In-Plane Strength of Beam-Columns

Reference	Direct Extension or Refinement of Eq. 8.4	Alternative to Eq. 8.4	Comments
Galambos and Ketter (1961)	Yes	—	Original basis for $\beta = 1, 0, -1$ cases
Ketter (1962)	Yes	—	Demonstrates dependence of C_m on axial load level
Lu and Kamalvand (1968)	Yes	—	Interaction curves and C_m values for lateral load cases
Chen and Atsuta (1977)	Yes	Yes	Numerous interaction curves, elastic C_m factors
Ballio and Campanini (1981)	Yes	—	C_m factors for a variety of cases, includes dependence of C_m on axial load level
Kanchananlai and Lu (1979)	Yes	Yes	Improvements for minor-axis bending of I-sections, extension to members in unbraced frames
Massonnet and Save (1965)	—	—	Verification of Eq. 8.4 against theory and tests
Galambos (1964)	Yes	—	General discussion of Eq. 8.4, including direct comparison with tests, simple presentation of numerical approaches suitable for direct programming
Young (1973)	—	Yes	Alternative presentation of results as basis for a different type of design approach
Galambos (1981)	Yes	Yes	Discussion of Eq. 8.4 against more recent alternatives
Adams (1970)	Yes	—	Direct extension of Eq. 8.4 to

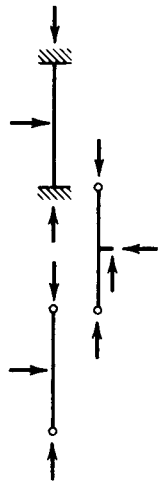

TABLE 8.1C *Continued*

Reference	Direct Extension or Refinement of Eq. 8.4	Alternative to Eq. 8.	Comments
McLellan and Adams (1970) Adams (1974)	Yes	—	General discussion of Eq. 8.4 and its application to members in frames
Mazzolani and Frey (1983)	Yes	Yes	Comparison with test data for aluminum beam-columns
Ojalvo and Fukumoto (1962)	—	Yes	Graphical presentation of theoretical results for $\beta = +1.0$, including full moment-rotation behavior
Galambos and Prasad (1962)	Yes	Yes	Tabular presentation of theoretical results for full range of P, β, L/r
Kemp (1984)	No	Yes	Considers beam-columns in plastically designed frames, provides limits on P, L/r, and β which will ensure satisfactory performance (rotation capacity)
Chen and Cheong-Siat-Moy (1980)	Yes	Yes	Covers application of interaction formula to members in unbraced frames
Cheong-Siat-Moy and Downs (1980)	Yes	Yes	Provides improved formulas for major and minor axis bending of members in unbraced frames
Djalaly (1975)	Yes	Yes	Suggests two modified amplification factors for major and minor axis bending of W sections, provides C factors for several cases
Roik and Wagenknecht (1976), Roik and Bergmann (1977)	—	Yes	Interaction curves for I ⊢ ◻ ◎ under various types of loading
Roik and Kindmann (1983)	—	Yes	Covers background to German beam-column interaction equations

in the work of van Manen (1982). The ductility of beam-columns is considered by Nakashima (1994) from the point of view of seismic behavior.

At this time (1997) it appears that the theory of the in-plane inelastic ultimate strength behavior of doubly and singly symmetric beam-columns bent in the plane of symmetry is well understood. Efficient numerical methods are available for the solution of beam-columns of any shape loaded by any kind of in-plane load (Chen and Atsuta, 1977, Vol. 1). Extensive comparisons have been made between the various interaction curves published in the literature and design interaction equations (Duan and Chen, 1989, 1990; Duan et al., 1989, Cai and Chen, 1991; Sohal and Syed, 1992). Equation 8.5, with some national variations, is still the basis of the design of beam-columns in most modern design specifications.

Following are in-plane interaction equations from several representative modern design specifications:

American Institute of Steel Construction (AISC, 1993)

$$\text{for } \frac{P_u}{\phi_c P_n} \leq 0.2: \qquad \frac{1}{2}\frac{P_u}{\phi_c P_n} + \frac{M_u}{\phi_b M_n} \leq 1.0 \tag{8.10a}$$

$$\text{for } \frac{P_u}{\phi_c P_n} \geq 0.2: \qquad \frac{P_u}{\phi_c P_n} + \frac{8}{9}\frac{M_u}{\phi_b M_n} \leq 1.0 \tag{8.10b}$$

Canadian Standards Association (CSA, 1994). For class 1 sections (suitable for plastic design)

$$\frac{P_u}{\phi P_n} + \frac{0.85 M_u}{\phi M_n} \leq 1.0 \tag{8.11}$$

For class 2 and 3 sections (not suitable for plastic design):

$$\frac{P_u}{\phi P_n} + \frac{M_u}{\phi M_n} \leq 1.0 \tag{8.12}$$

Australian Standard AS4100-90 (SAA, 1990). Same as Eq. 8.12.

Eurocode 3 (ECS, 1993). Same as Eq. 8.12, where

P_u = applied ultimate axial load on member
ϕ_c = 0.85 resistance factor for axial capacity of member
P_n = nominal axial capacity according to the respective specification
ϕ_b = 0.90 resistance factor for flexural capacity of member
M_n = nominal in-plane flexural capacity according to the respective specification

M_u = applied ultimate bending moment on member, amplified to account for second-order bending due to the product of the axial load and the deflection

ϕ = 0.90 = resistance factor

The nominal axial and flexural capacities, as well as the amplified applied bending moments, are different in each respective specification. Comparison can thus be made only for a specific member of a given size under a given set of loads. The curves in Fig. 8.9 compare the beam-column capacity of a W8 × 40 beam-column for the four current specifications listed above. Even though there are differences, the spread is reasonable. White and Clarke (1977) provided recently a very detailed comparison of the beam-column design philosophies, procedures and standards in The United States, Canada, Australia and Europe.

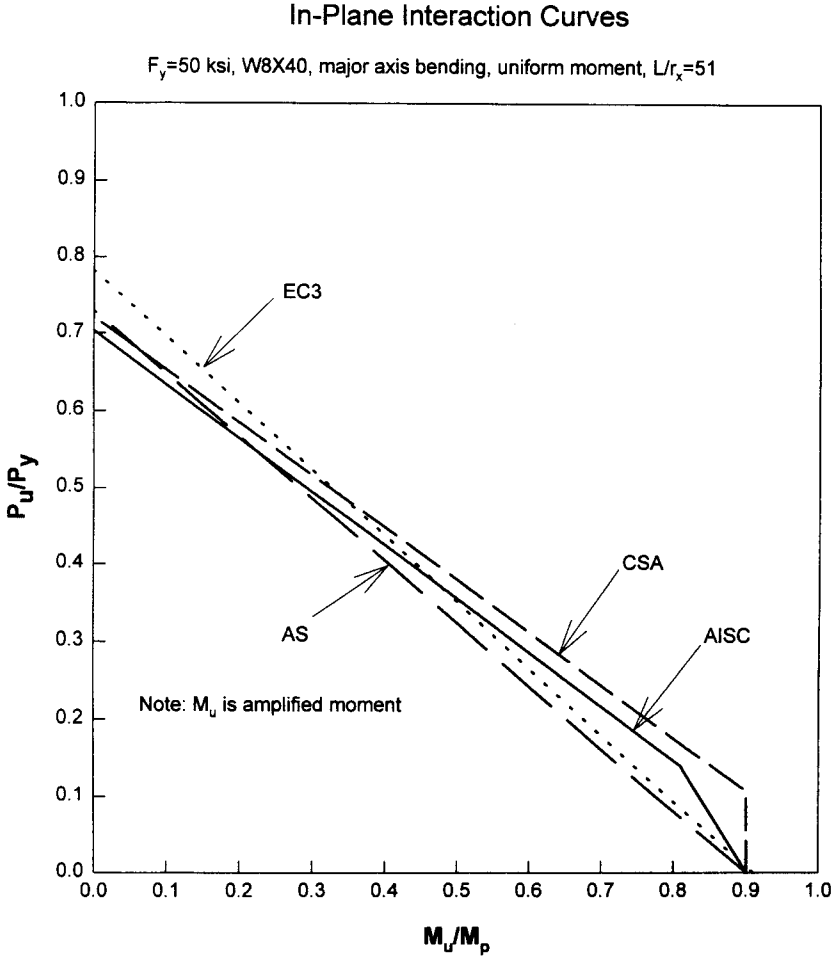

Fig. 8.9 In-plane interaction curves.

8.4 UNIAXIAL BENDING: LATERAL–TORSIONAL BUCKLING

When an I-section is bent about its major axis (i.e., in the plane of the web), there exists a tendency for it to fail by deflecting sideways and twisting, as explained in Chapter 5. The presence of an axial load when such a member is used as a beam-column will only serve to accentuate this tendency, since the preferred mode of failure under pure axial load would normally be by buckling about the minor axis. Beam-columns loaded in strong axis bending therefore exhibit an interaction between column buckling and beam buckling.

The elastic critical load for a member subject to compression P and equal and opposite end moments M_0 as shown in Fig. 8.1*b* is given by (Hill and Clark, 1951a,b; Horne, 1956; Salvadori, 1956; Campus and Massonnet, 1956; Chen and Atsuta, 1977);

$$\frac{M_0}{M_E} = \left[\left(1 - \frac{P}{P_{ey}}\right)\left(1 - \frac{P}{P_\phi}\right)\right]^{1/2} \tag{8.13}$$

where M_E is the elastic critical moment for lateral–torsional buckling as a beam (see Chapter 5).

P_{ey} = elastic critical load for minor-axis flexural buckling

P_ϕ = elastic critical load for pure torsional buckling (see Chapter 3).

Critical combinations of P and M_0 are shown plotted in Fig. 8.10.

If an approximate allowance is made for the effects of in-plane deflection (Chen and Atsuta, 1977), Eq. 8.13 becomes

$$\frac{M_0}{M_E} = \left[\left(1 - \frac{P}{P_{ex}}\right)\left(1 - \frac{P}{P_{ey}}\right)\left(1 - \frac{P}{P_\phi}\right)\right]^{1/2} \tag{8.14}$$

A linearized conservative alternative to Eq. 8.14 can be expressed as

$$\frac{P}{P_{ey}} + \frac{M_0}{M_E(1 - P/P_{ex})} \leq 1 \tag{8.15}$$

which is of the same form as Eq. 8.4 for in-plane failure except that the quantities appearing in the denominator P_{ey} and M_E now relate to out-of-plane failure.

By analogy with Eq. 8.5 the design version of Eq. 8.15 may be written as

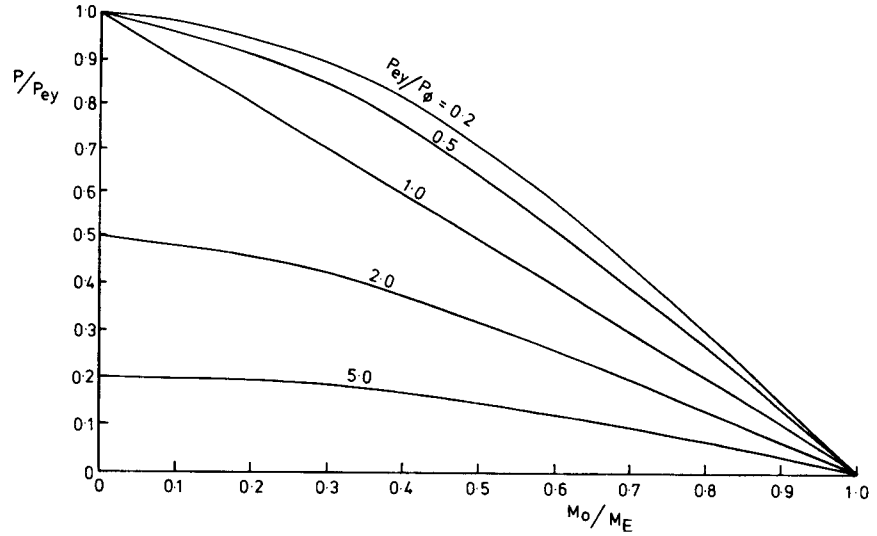

Fig. 8.10 Elastic critical-load combinations for beam-columns with equal end moments.

$$\frac{P}{P_{uy}} + \frac{C_m M_0}{M_u(1 - P/P_{ex})} \leq 1 \tag{8.16}$$

where

P = applied axial load
P_{uy} = axial load producing failure in the absence of bending moment, computed for weak-axis buckling
M_0 = maximum applied first-order moment
M_u = moment producing failure in the absence of axial load, allowing for lateral torsional buckling
C_m = reduction factor as discussed in Section 8.3

The problem of elastic and inelastic lateral–torsional buckling has received a great deal of attention from researchers. The references in Table 8.2A give a sampling of this work. This list is by no means complete, but it gives access to the formulas and charts necessary for most practically occurring situations. Furthermore, Trahair (1993) has summarized the research on the lateral–torsional buckling of beam-columns in his book *Flexural–Torsional Buckling of Structures*. It should be noted that most of the studies of biaxially loaded beam-columns discussed in Section 8.6 are capable of treating the laterally unbraced member subject to uniaxial bending as a special case.

TABLE 8.2A Theoretical Solutions for the Lateral–Torsional Buckling Strength of Wide-Flange Beam-Columns

Reference	Approach	Residual Stress	Load Cases	Comparison with Eq. 8.16	Comments	Results for Direct Use
Vinnakota (1977)	Maximum strength	Pattern a	1 ($\beta = 1$)	No		Yes
Fukumoto and Galambos (1966)	Tangent modulus	Pattern a	1 ($\beta = 1.0$)	No		Yes
Galambos et al. (1965)	Tangent modulus	Pattern a	1 ($\beta = 1.0$)	No		Yes
Miranda and Ojalvo (1965)	Tangent modulus	None	1 ($\beta = 1$)	No	Allows for prior in-plane deflection	Yes
Lim and Lu (1970)	Tangent modulus	None	1	No	Approx. extrapolation to maximum strength; includes minor-axis restraint, prior in-plane deflection, and continuous members	
Lindner and Wiechart (1978)	Maximum strength	Pattern b	1 ($\beta = 1, 0, -0.7$) 4, 2	No		Yes
Abdel-Sayed and Aglan (1973)	Tangent modulus	Pattern a	1 ($\beta = 1$)	No	Allows for prior in-plane deflection, sample results for aluminum section	
Bradford and Trahair (1985)	Maximum strength	Pattern b	Any in-plane loading	No	Finite element analysis (FEM)	Yes
Bradford and Trahair (1986)	Maximum strength	Measured in test	Continuous beam-column	No	FEM analysis of Cuk et al. (1986) tests	
Bradford et al. (1987)	Maximum strength	Patterns a and b	1,4	No	FEM analysis	Yes
Pi and Trahair (1992a,b)	Maximum strength	Any pattern	Any in-plane loading	No	Prebuckling deformations	Yes
Pi and Trahair (1994a,b)	Maximum strength	Any pattern	Any in-plane loading	No	All nonlinearity effects	Yes
Wang and Kitipornchai (1989)	Maximum strength	Any pattern	Any in-plane loading	No	Monosymmetric members	Yes
Kitiporchai and Wong (1988)	Elastic Buckling		In-plane loading	No	Elastic lateral–torsional buckling	Yes

TABLE 8.2A *Continued*

Reference	Approach	Residual Stress	Load Cases	Comparison with Eq. 8.16	Comments	Results for Direct Use
Jingping et al. (1988)	Maximum strength	Pattern a	2-4	No	Transversely loaded beam-columns	Yes
Trahair (1993)	Buckling and maximum strength	Any pattern	Any plane of loading	No	Summary of all available work on subject	Yes

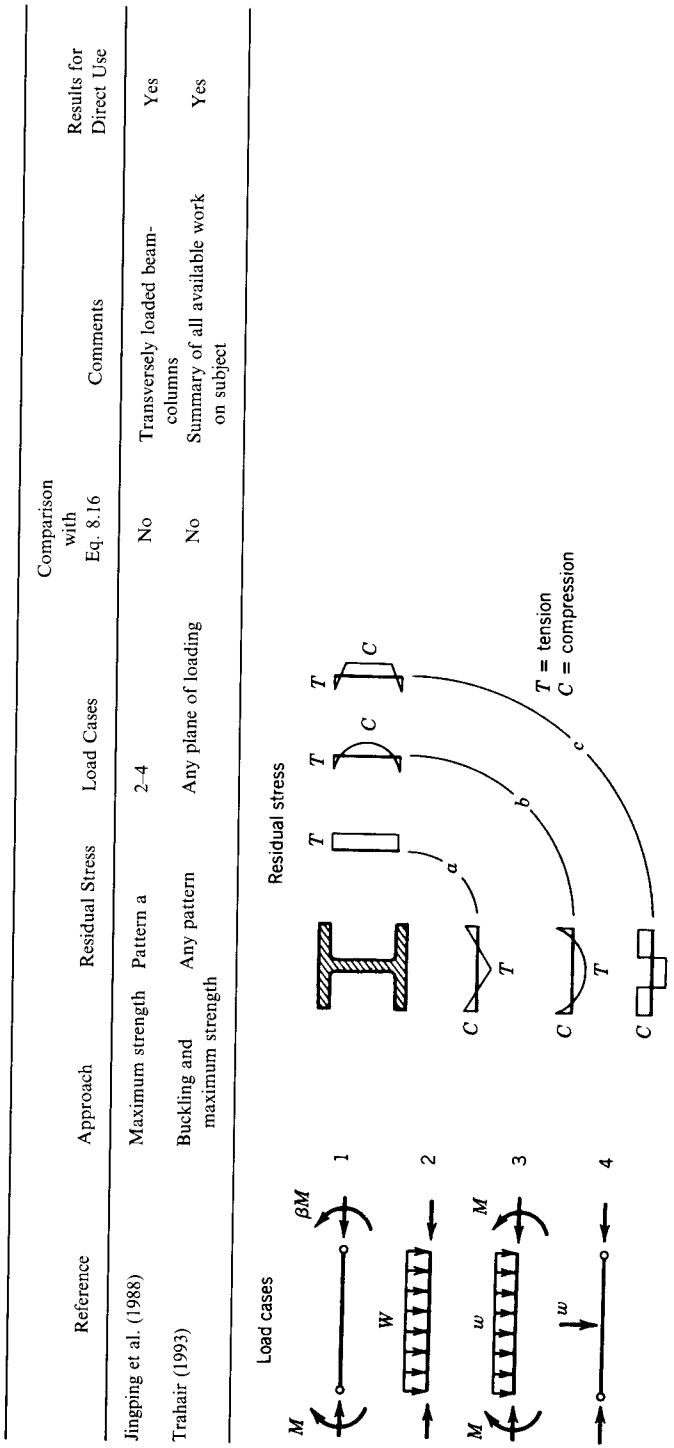

Several series of tests have been performed on laterally unbraced beam-columns, and these are reviewed in Table 8.2B. In addition to these investigations designed to study the problem, some of the test series reported in Table 8.1B contain instances of failure in a lateral–torsional mode, usually because inadequate bracing was provided.

When values of C_m of less than 1.0 are used in Eq. 8.16, it is, of course, also necessary to check cross-sectional strength using Eq. 8.6. References that expand on the use of Eq. 8.16 or present alternative design procedures are listed in Table 8.2C.

It should be remembered that lateral–torsional buckling is normally associated with torsionally weak sections bent in their stiffer principal plane. Therefore, certain classes of section (e.g., tubes) are not susceptible to this mode of failure. In such cases bending about both principal axes may be treated using the methods of Section 8.3.

Following are interaction equations for beam-columns failing by lateral–torsional buckling for several representative design specifications:

American Institute of Steel Construction (AISC, 1993)

$$\frac{1}{2}\frac{P_u}{\phi_c P_n}+\frac{M_u}{\phi_b M_n}\le 1.0 \qquad \text{for } \frac{P_u}{\phi_c P_n}\le 0.2 \tag{8.17a}$$

$$\frac{P_u}{\phi_c P_n}+\frac{8}{9}\frac{M_u}{\phi_b M_n}\le 1.0 \qquad \text{for } \frac{P_u}{\phi_c P_n}\ge 0.2 \tag{8.17b}$$

Canadian Standards Association (CSA, 1994). For class 1 sections (suitable for plastic design),

$$\frac{P_u}{\phi P_n}+\frac{0.85M_u}{\phi M_n}\le 1.0 \tag{8.18}$$

For class 2 and 3 sections (not suitable for plastic design),

$$\frac{P_u}{\phi P_n}+\frac{M_u}{\phi M_n}\le 1.0 \tag{8.19}$$

Australian Standard AS4100-90 (SAA, 1990)

$$\left(1-\frac{P_u}{\phi P_n}\right)\left(1-\frac{P_u}{\phi P_{oz}}\right)+\left(\frac{M_u}{\phi M_n}\right)^2\le 1.0 \tag{8.20}$$

Eurocode 3 (ECS, 1993)

TABLE 8.2B Experimental Data for the Lateral–Torsional Buckling Strength of Wide-Flange Beam Columns

Reference	Number of Tests	L/r Range	Load Cases	Comparison with Eq 8.16	Comments
Van Kuren and Galambos (1964)	26	22–116		Yes	Some in-plane failures
			$\beta = 1, 0.5, 0, -1$		
Lindner and Kurth (1982a)	70	58–169	$\beta = 1, 0.5, 0, -1$	No	High-strength steel
Campus and Massonnet (1956)	91	40–177	$\beta = 1, 0, -1$	Yes	See Nethercot (1983) for comparison
Djalaly (1971)	8	62–82	$\beta = 1, 0.5$	No	
Chagneau (1973)	8	60–80	$\beta = 1, 0.5$	No	
Hill (1951a,b)	59	28–183	$\beta = 1$	No	Aluminum
Gent and Sen (1977)	8	43–74	$\beta \approx 0.15$	No	Tests designed to investigate rotation capacity; some in-plane failures
Cuk et al. (1986)	14	$L/r_x = 98$	Framed member	No	Study effect of end restraint
Nakashima et al. (1990)	42	$L/r_y = 42$ to 91	Sway members	No	Study effect of lateral sway

TABLE 8.2C Design-Oriented References for the Lateral–Torsional Buckling Strength of Wide-Flange Beam-Columns

Reference	Direct Extension of Refinement of Eq. 8.16	Alternative to Eq. 8.16	Comments
Galambos (1981)	Yes	Yes	Discussion of Eq. 8.16 against more recent alternatives
Campus and Massonnet (1956)	Yes	—	Original basis for Eq. 8.16, derivation of comparison with test data
Mazzolani and Frey (1983)	Yes	Yes	Comparison with test data for aluminum beam-columns
Galambos et al. (1965)	—	Yes	Considers importance of in-plane deflections, alternative design approach
Djalaly (1973)	Yes	Yes	Eq. 8.16 and several alternatives compared with test data
Cuk and Trahair (1981)	Yes	—	Suggests that C_m depends on axial load level; basis is elastic critical loads
Bradford and Trahair (1985)	No	Yes	Formulas for Australian code (SAA, 1990)
Trahair and Bradford (1988)	No	Yes	General steel design text
Trahair (1993)	No	Yes	Summary of research on subject

$$\frac{P_u}{\phi P_n} + \frac{M_u}{\phi M_n} \leq 1.0 \tag{8.21}$$

Architectural Institute of Japan (AIJ, 1990)

$$\frac{P_u}{\phi P_n} + \frac{0.85 M_u}{\phi M_n} \leq 1.0 \tag{8.22}$$

The terms in these equations are defined as follows:

P_u = applied ultimate axial load on the beam-column
M_u = applied uniform ultimate moment on the member, obtained by either a second-order analysis or by approximate amplification factors multiplied to the first-order moments
ϕ_c = 0.85 = resistance factor for columns in AISC (1993)
ϕ_b = 0.9 = resistance factor for beams in AISC (1993)
ϕ = 0.9 = resistance factor
P_n = nominal axial capacity about minor axis of the wide-flange cross section according to the respective specification

M_n = nominal lateral–torsional bending capacity of the unbraced wide-flange shape in the absence of axial force according to the respective specification

The nominal axial and flexural capacities, as well as the amplified first-order applied moments, are determined differently in each respective design standard. Comparisons can thus be made only for a specific member under a specific loading condition. Such a comparison is shown in Fig. 8.11 for a W8 × 40 beam-column. At the left end of the interaction curves there is reasonable agreement of the axial capacity. However, on the right end, there is a considerable difference in the lateral–torsional flexural capacity between the different specifications. The interaction strength when both axial force and bending moment are present is thus somewhat divergent, especially when the axial force is low.

8.5 EQUIVALENT UNIFORM MOMENT FACTOR

When a beam-column is loaded by unequal end moments M_0 and βM_0, where $-1.0 \leq \beta \leq 1.0$, it is usually overconservative to use the value M_0 directly in the design formulas of Eq. 8.4 or 8.16. This is particularly true as β approaches -1.0 and the member tends to be bent in double curvature, since the design formulas are based on the case of uniform primary moment (i.e., $\beta = +1.0$). However, studies for both the in-plane case (Austin, 1961; Chen and Atsuta, 1977) and the lateral-torsional buckling problem (Horne 1956; Salvadori, 1956; Campus and Massonnet, 1956) have shown that a simple and reasonably accurate correction results if M_0 is replaced by a reduced value $C_m M_0$, where

$$C_m = 0.6 + 0.4\beta \geqslant 0.4 \tag{8.23}$$

Equation 8.23 is a simplified version of the several different formulas that have been proposed by various authors; for design purposes it is particularly convenient to use the same expression for both problem types as well as to ignore the relatively small effect on C_m of member slenderness.

For beam-columns subjected to other forms of loading (e.g., transverse loads between supports) extensive numerical results are available (Lu and Kamalvand, 1968; Chen and Atsuta, 1977; Ballio and Campanini, 1981) for the case where failure occurs by excessive bending. A simple approximation to these consists of replacing M_0 in Eq. 8.4 by the maximum value taken from a straight-line envelope of the actual (primary) moment diagram. More accurate values may, however, be obtained if the C_m factors given in Table 8.3 are used. Since these permit the use of moments below the maximum it becomes necessary to increase their values as the axial load decreases and the problem approaches a beam. Similar conclusions were reached by Djalaly (1975), who provides C_m factors for nine different load cases.

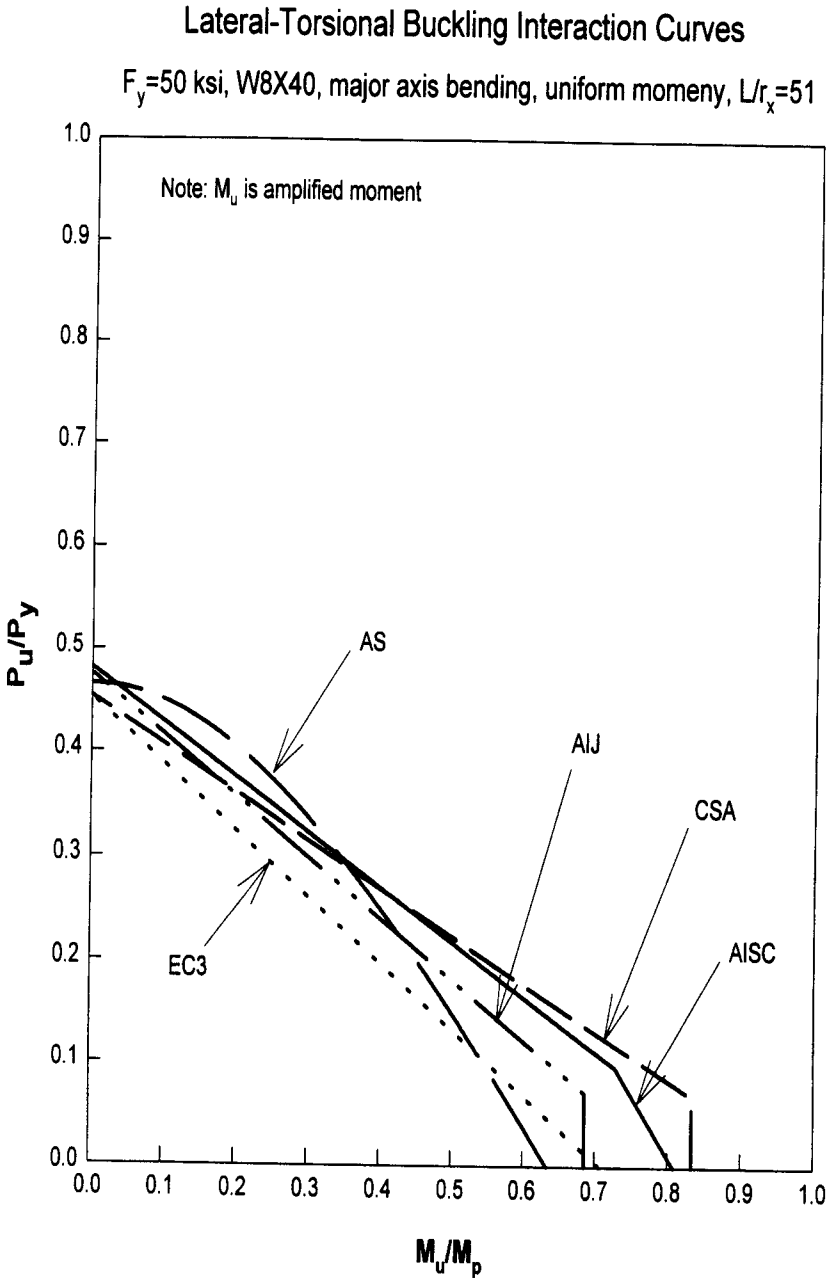

Fig. 8.11 Lateral–torsional buckling interaction curves.

TABLE 8.3 C_m Factors for Use with Eq. 8.5 for In-Plane Strength of Beam-Columns

Load Case	Formula for C_m	Limits
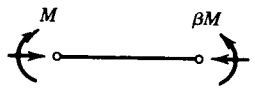	$0.6 - 0.4\beta$	$P/P_u \geq 0.4$
	$1 - \dfrac{1-(0.6-0.4\beta)}{0.4}\dfrac{P}{P_u}$	$P/P_u < 0.4$
	$0.5 + \dfrac{0.7M_m}{M_0}$	$P/P_e \geq 0.5$
	$1 - 2\left[1 - \left(0.5 + \dfrac{0.7M_m}{M_0}\right)\right]\dfrac{P}{P_e}$	$P/P_e < 0.5$
etc.	where M_0 = maximum moment in span, M_m = average moment	

Similar refinements to Eq. 8.23 for the laterally unbraced case have been suggested by Cuk and Trahair (1981) based on studies of elastic buckling. Extensive tabular and chart solutions have been obtained by many numerical studies, and these are summarized in Trahair's (1993) book and in the papers cited in Table 8.2A.

8.6 BIAXIAL BENDING

Both of the cases discussed in Sections 8.3 and 8.4 are special cases of the more general beam-column problem illustrated in Fig. 8.1*c*. Contributions in this area prior to 1975 are reviewed fully in the third edition of the guide, while more recent general reviews are available (Massonnet, 1976; Chen, 1977a, 1981; Chen and Atsuta, 1977). For design purposes it is convenient to separate consideration of the problem into two phases: (1) short columns, and (2) intermediate and slender columns, corresponding to the outer and inner failure surfaces of Fig. 8.2, respectively. Phase 1 will therefore concern itself with the strength of the cross section under combined axial load and major- and minor-axis moments. This is relevant for stocky columns, particularly those subjected to nonuniform moments, for which failure is likely to be governed by the local strength of the most heavily stressed cross section, assuming the individual component plates to be such that local buckling does not occur. More slender columns are likely to fail in an overall fashion, which in the present case will involve the interaction of column buckling and beam biaxial bending.

8.6.1 Strength of Short Columns

Provided that the cross section meets the requirements for compactness necessary to ensure against local buckling, its local strength will be governed by the

development of full plasticity. For the uniaxial case the location of the neutral axis may be determined from first principles (Chen and Atsuta, 1977); alternatively, Eqs. 8.6 and 8.7 for wide-flange sections or the formulas of Table 8.4 for other common shapes may be employed. No comparable simple expressions exist for the biaxial case. Moreover, determination of the location and angular disposition of the neutral axis, which satisfies the three conditions of equilibrium for applied load P and moments M_x and M_y, now involves so many possible cases as to be prohibitive for anything other than research purposes. Santathadaporn and Chen (1970) have derived interaction curves relating M_x to M_y for a series of values of P for wide-flange sections of varying width-to-depth ratio and varying flange thickness-to-depth ratio. For design purposes the average set of curves given in Fig. 8.12 will normally prove adequate. If a single design equation is required, this can be provided only

TABLE 8.4 Full Plastic Interaction for Uniaxial Bending

Cross Section	M_P	Interaction of P and M_0
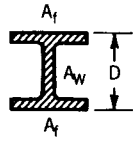	$\sigma_y A_f D\left(1 - \dfrac{A_w}{4A_f}\right)$	$\left(\dfrac{P}{P_y}\right)^{1.2} + \dfrac{M_0}{M_p} = 1$
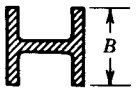	$\dfrac{\sigma_y A_f B}{2}$	$\left(\dfrac{P}{P_y}\right)^{2} + \left(\dfrac{M_0}{M_p}\right)^{1.2} = 1$
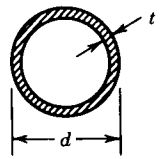	$\dfrac{1}{6}\sigma_y d^3\left[1 - \left(1 - \dfrac{2t}{d}\right)^3\right]$	$\left(\dfrac{P}{P_y}\right)^{1.7} + \dfrac{M_0}{M_p} = 1$
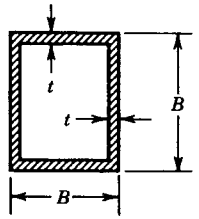	$\sigma_y t D^2\left(\dfrac{B}{D} + \dfrac{1}{2}\right)$	$\dfrac{D}{B} \geq 3 \quad \left(\dfrac{P}{P_y}\right)^{2} + \dfrac{M_0}{M_p} = 1$ $1 \leq \dfrac{D}{B} < 3 \quad \left(\dfrac{P}{P_y}\right)^{1.5} + \dfrac{M_0}{M_p} = 1$ $\dfrac{D}{B} < 1 \quad \left(\dfrac{P}{P_y}\right)^{1.2} + \dfrac{M_0}{M_p} = 1$

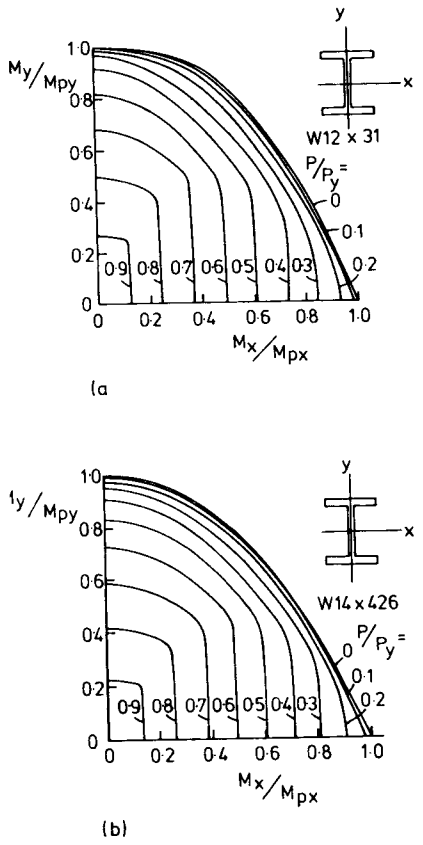

Fig. 8.12 Interaction curves for strength of short beam-columns under biaxial loading: (*a*) light W-section; (*b*) heavy W-section.

at the expense of accuracy, leading to significant underpredictions of the available strength in most cases. The most suitable linear expression is (Pillai, 1974)

$$\frac{P}{P_y} + 0.85\left(\frac{M_x}{M_{px}}\right) + 0.6\left(\frac{M_y}{M_{py}}\right) \leq 1 \tag{8.24}$$

in which the different coefficients for the two moment terms are a reflection of the different shapes of the uniaxial interactions as shown in Figs. 8.5 and 8.6. More accurate predictions may be obtained using (Chen and Atsuta, 1977; Tebedge and Chen, 1974)

$$\left(\frac{M_x}{M_{px}}\right)^{\alpha} + \left(\frac{M_y}{M_{py}}\right)^{\alpha} \leq 1 \tag{8.25}$$

in which M_{pcx} and M_{pcy} are the moment capacities about the respective axes, reduced for the presence of axial load; they may be obtained from Eqs. 8.6 and 8.7. The value of the exponent α is given by

$$\alpha = 1.6 - \frac{P/P_y}{2\ln(P/P_y)} \tag{8.26}$$

Figure 8.13, which compares Eqs. 8.24 and 8.25 with the average "exact" results of Santathadaporn and Chen (1970), shows how the interaction between the two moment terms becomes increasingly convex as the axial load increases. Equation 8.25 will therefore produce significant economies over Eq. 8.24 in situations where columns carrying very large axial loads must also withstand small moments.

Interaction curves for sections other than wide-flange shapes have been obtained by Chen and Atsuta (1974, 1977) using a superposition technique. Results for a number of different structural sections, including circular tubes and unsymmetrical shapes such as angles, are available in Chen and Atsuta (1974, 1977). These show that the degree of symmetry present in the interaction surface parallels the degree of symmetry of the section. Chen and Atsuta (1977) also contains a procedure (suitable for programming) for developing these

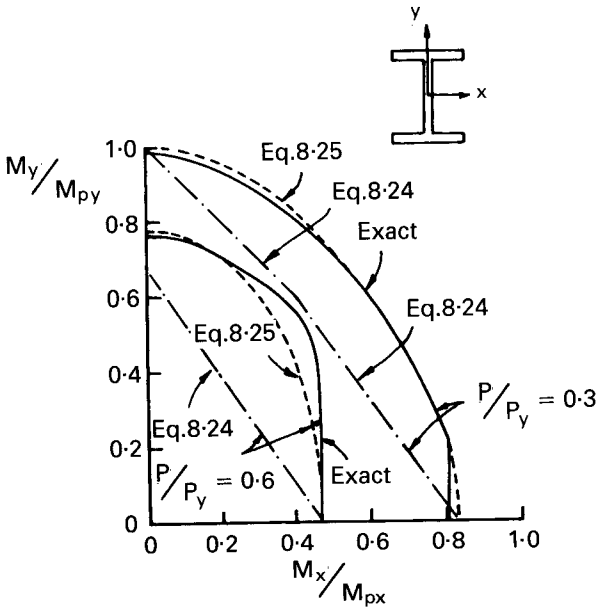

Fig. 8.13 Comparison of Eqs. 8.24 and 8.25 with numerical data of Chen and Atsuta for strength of biaxially loaded beam-columns.

surfaces. For standard angles a full set of interaction curves is available (Bez, 1983).

All of the foregoing discussion has assumed that yielding occurs only as a result of the direct stresses produced by compression and bending. However, the presence of any shear stresses due to St.-Venant torsion will have the effect of reducing cross-sectional capacity. This may be allowed for in a particularly simple manner (Morris and Fenves, 1969); Chen and Atsuta, 1972a, 1977); if the material is assumed to follow the von Mises yield criterion, all coordinates on the yield surface will be reduced by a factor

$$\sqrt{1-t^2} \tag{8.27}$$

in which $t = \tau/\tau_y$ the ratio of applied shear stress to the shear shield stress of the material.

8.6.2 Strength of Intermediate and Slender Columns

Slender columns in biaxial bending constitute the most formidable example of the beam-column problem. Over the years, successive investigations have produced increasingly refined analytical solutions, have conducted expensive and painstaking series of experiments, and have used this information as the basis for ever more reliable and accurate design procedures. Clearly, it is neither feasible nor appropriate to review all of these contributions; this is adequately covered by Chen and Santathadaporn (1968), Johnston (1976), Massonnet (1976), Chen and Atsuta (1977), and Chen 1977a, 1981). Rather, selected design approaches are presented and their relationship to the available theoretical and experimental data discussed. By means of Table 8.5 the reader is also guided to the sources of useful original data.

Since a design procedure for biaxial bending should reduce to that already recommended for uniaxial bending in the absence of one of the moment terms, a logical starting point is Eqs. 8.5 and 8.16. As shown in Figs. 8.5 and 8.10, these expressions provide good descriptions of the $P - M_x$ and $P - M_y$ interactions for wide-flange sections. The second edition of the Guide suggested an empirical combination of these two expressions to give

$$\frac{P}{P_u} + \frac{C_{mx}M_x}{M_{ux}(1 - P/P_{ex})} + \frac{C_{my}M_y}{M_{uy}(1 - P/P_{ey})} \leq 1 \tag{8.28}$$

An improvement for the particular case of hollow circular and square box sections suggested by Pillai (1970) is

$$\frac{P}{P_u} + C\left[\frac{C_{mx}M_x}{M_{ux}(1 - P/P_{ex})} + \frac{C_{my}M_y}{M_{uy}(1 - P/P_{ey})}\right] \leq 1 \tag{8.29}$$

in which

$$C = \frac{(e_x^2 + e_y^2)^{1/2}}{e_x + e_y}$$

For such sections both M_{ux} and M_{uy} may, of course, be taken as the full plastic moment capacities.

An alternative way of writing Eq. 8.28 is to use algebraic transposition (Chen, 1977b) to obtain

$$\frac{C_{mx}M_x}{M_{ucx}} + \frac{C_{my}M_y}{M_{ucy}} \leq 1 \tag{8.30}$$

in which M_{ucx} and M_{ucy} are the uniaxial moment capacities according to Eqs. 8.16 and 8.5, respectively (i.e., the value of M for a given P). This implies that the interaction between the moment terms is linear, whereas both test data and theoretical solutions for biaxially loaded columns indicate a convex interaction, as illustrated in Fig. 8.14.

As a development of their work on short columns. Tebedge and Chen (1974) proposed that a nonlinear expression similar to Eq. 8.25 also be used for slender columns. Thus Eq. 8.30 becomes

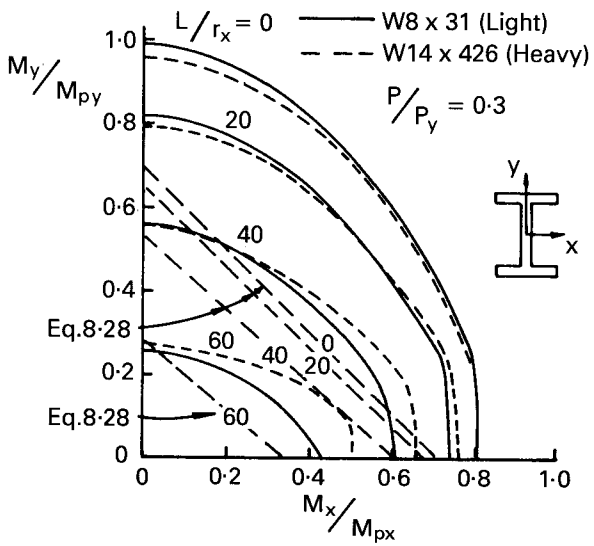

Fig. 8.14 Comparison of Eq. 8.28 with numerical data of Chen and Atsuta for stability of biaxially loaded beam-columns.

$$\left(\frac{C_{mx}M_x}{M_{ucx}}\right)^{\eta}+\left(\frac{C_{my}M_y}{M_{ucy}}\right)^{\eta}\leq 1.0 \tag{8.31}$$

Based largely on numerical studies covering I-sections with $B/D = 0.3$ (Ross and Chen, 1976) as well as H sections with $B/D = 1.0$ (Tebedge and Chen, 1974) Chen recommends that η be determined from

$$\eta = \begin{cases} 0.4+\dfrac{P}{P_y}+\dfrac{B}{D} & \text{for } B/D \geq 0.3 \\ 1.0 & \text{for } B/D < 0.3 \end{cases} \tag{8.32}$$

where B is the flange width and D is the section depth. For square box sections (Chen, 1977b) η should be taken as

$$\eta = 1.3+\frac{1000}{(L/r)^2}\frac{P}{P_u}\geq 1.4 \tag{8.33}$$

Use of Eq. 8.31 with η values greater than unity recognizes the convexity of the moment interaction as illustrated in Fig. 8.15.

A quantitative assessment of the accuracy of Eqs. 8.28 and 8.31, based on their ability to predict the strengths of the specimens in four series of tests (Chubkin, 1959; Klöppel and Winkelmann, 1962; Birnstiel, 1968; Anslijn, 1983) on biaxially loaded I-sections, has been made by Pillai (1980, 1981). In conducting this comparison, advantage was taken of the fact that the use of Eq. 8.31 is not tied to any particular method of determining M_{ucx} and M_{ucy}; the concept of combining uniaxial moment capacities can be used with any reasonable moment expression. For the 81 tests of Anslijn (1983) Pillai found that when used with column and beam buckling predictions from the then current AISC specification, Eq. 8.25 was an almost perfect predictor in terms of the mean value for P_{test}/P_{calc} of 1.050. However, with a standard deviation of 0.101, this meant that 31% of the test results were overpredicted. A more recent evaluation of the comparisons between the AISC design equations, numerical predictions, and test results is given by Duan and Chen (1989).

Theoretical procedures for assessing beam-column strength under biaxial loading are rather complex, so that even in the elastic range (Culver, 1966a,b) numerical solutions are required. Thus the results presented in any of the references listed in Table 8.5A will normally cover only a limited aspect of the problem. However, several series of large-scale tests have been conducted (see Table 8.5B), and these have proved invaluable in the evaluation of the various design approaches listed in Table 8.5C.

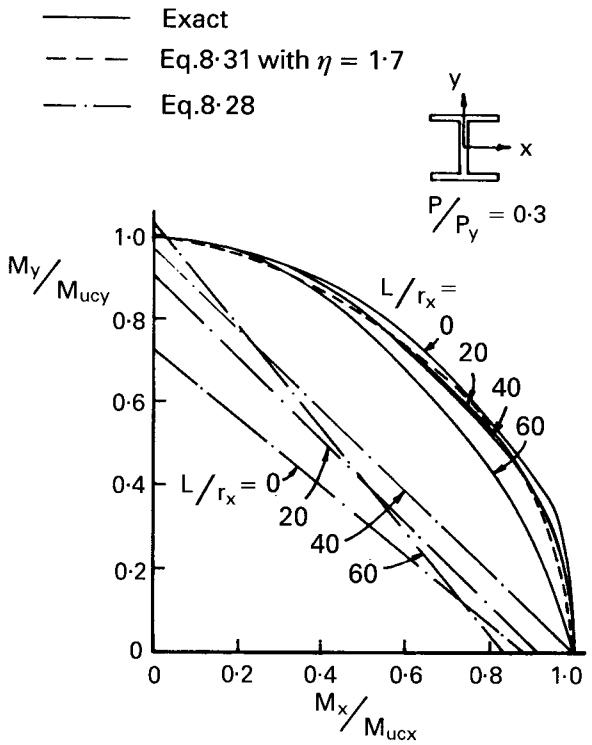

Fig. 8.15 Comparison of Eqs. 8.28 and 8.31 with numerical data of Chen and Atsuta for stability of biaxially loaded beam-columns.

8.7 DESIGN OF BEAM-COLUMNS

The behavior of metal beam-columns is quite complex. However, enough research has been performed on these members so that the elastic and plastic instability under static or dynamic loads is well understood. Analytical methods and tools are also available for the determination of the deformation and strength of beam-columns to any desired degree or accuracy and sophistication. These procedures still tend to be in the domain of research, and the structural designer is provided with empirical equations or charts that are based on research. Modern structural design specifications around the world have retained the generic form of the interaction formula of Eq. 8.1. For uniaxial flexure many of these design rules use the simple interaction form of Eq. 8.2. In every specification the moment M is always specified as the *second-order* (amplified) moment obtained either from a second-order structural analysis where equilibrium is formulated on the deformed configuration of the structure, or from an approximation using moments from a first-order

TABLE 8.5A Theoretical Solutions for the Biaxial Bending Strength of Beam-Columns[a]

Reference	Cross Section	Residual Stress	Slender Column	Load Cases	Results for Direct Use	Comments
Djalaly (1975)	W-shape	Pattern b	Yes		Yes	Tabulated results for one section
Virdi (1981)	Square and circular tubes	None	Yes	Any loading	No	Applicable to cases where torsional effects can be neglected
Lindner (1972), Lindner and Gietzelt (1982)	W-shape	Pattern b	Yes	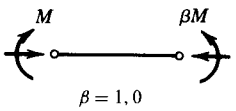	Yes	Tabulated results for one section: method explained in Lindner (1972): comparison with Eqs. 8.25, 8.28, 8.31
Hancock (1977)	W-shape	Pattern a	No		No	Cross section analysis only
Razzaq and McVinnie (1982)	Square tube	None	Yes	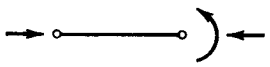	No	Column deflection curves
Vinnakota (1977)	W-shape	Pattern a	Yes	Any loading	Yes	Detailed study of initial deflections
Rajasekaran (1977)	W-shape	None	Yes	Any loading	No	General finite element approach
Opperman (1983)	T, L, I, C shapes	None	Yes	Any loading	No	General finite element approach
Ramm and Osterrieder (1983)	Any open section	None	Yes	Any loading	No	General finite element approach
Duan and Chen (1989)	W-shape	Pattern a	Yes	Any loading	Yes	Examine interaction equations and compare to test results

[a]This topic is discussed fully by Chen and Atsuta (1977); papers incorporated in the text have not been included in the list above.

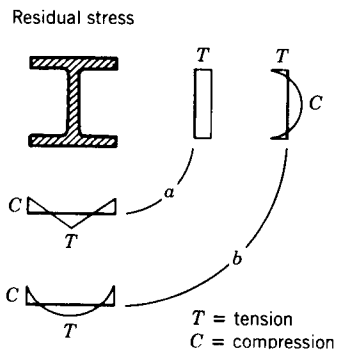

TABLE 8.5B Experimental Data for the Biaxial Strength of Beam-Columns

Reference	Number of Tests	Cross Section	L/r Range	Load Cases	Comments
Birnstiel (1968)	12	W-shapes	63–121	 $\beta_x = 1, \beta_y = 1$	Rolled, welded, and annealed sections
Chubkin (1959)	43	W-shapes	50–150	$\beta_x = 1, \beta_y = 1$	Residual stress data not available
Klöppel and Winkelmann (1962)	69	W-shapes	57–121	$\beta_x = 1, \beta_y = 1$	Variable residual stresses due to method of specimen manufacture
Anslijn (1983)	78	W-shapes	40–96	Various β_x, β_y	
Matthey (1982)	15	W-shapes		Various β_x, β_y	
Marshall and Ellis (1970)	29	Square tubes	27–135	Various β_x, β_y	Small-scale tests

TABLE 8.5C Design-Oriented References for the Biaxial Bending Strength of Beam-Columns

	Direct Extension or Refinement of Eqs.:				Alternative to Eqs.:				
Reference	8.24	8.25	8.28	8.31	8.24	8.25	8.28	8.31	Comments
Chen and Atsuta (1977)	Yes	Yes	Yes	Yes	—	—	—	—	Full discussion in Chapter 13, including review of all proposals up to 1976
Pillai (1980, 1981)	—	Yes	—	Yes	—	—	—	—	Assessment of Eqs. 8.25 and 8.31 against test data using various component data
Lindner and Gietzelt (1983)	—	Yes	Yes	Yes	Yes	Yes	Yes	Yes	Evaluation of various three-term formulas on basis of test data and theoretical results of Lindner and Gietzelt (1982b)
Nethercot (1983)	—	Yes	—	Yes	Yes	Yes	Yes	Yes	Review of available interaction formulas with comparisons
Djalaly (1975)	—	Yes	—	Yes	Yes	Yes	Yes	Yes	
Chen and Liu (1983)	—	Yes	Yes	Yes	—	—	—	—	Proposed unification of beam-column and column design; discussion of C_m factor
Chen (1981)	—	Yes	Yes	Yes	Yes	Yes	Yes	Yes	Inclusion of external pressure effects
Maquoi and Rondal (1982)	Yes	Yes	Yes	Yes	Yes	Yes	Yes	Yes	Design-oriented reorganization of ECCS interaction formulas
Chen (1982)	—	Yes	—	Yes	Yes	Yes	Yes	Yes	Covers box sections and fabricated tubes, limited verification of C_m factors
Duan and Chen (1989)	—	—	Yes	Yes	—	—	Yes	Yes	Verify AISC (1993) interaction equations

analysis which are multiplied by an *amplification factor*. Such factors are often of the type of Eq. 8.3. Depending on whether P_e, the elastic critical load, is evaluated for the member length or the story effective length, the amplification factor accounts empirically for the member or the frame instability. This versatility of the interaction equation approach makes it very useful in design. Further discussion of this topic is presented in Chapter 16, where frame stability will be treated in more detail.

A major international effort was undertaken by SSRC to collect the stability design rules from all regions of the world (Beedle, 1991). Most code-writing authorities have changed to the limit-states design format in the last two decades, using a set of load factors and resistance factors that are based on probabilistic principles. This new direction provided an opportunity to also revise the specific rules for the design of beam-columns. Even though the specification writers had access to the same basic research results, the detailed criteria for designing a beam and a column may look very different in different parts of the world, reflecting the preferences of the engineering culture for which the standards were promulgated. As can be seen from the comparisons presented in Figs. 8.9 and 8.11, the actual differences are not very large. The reasons for the differences are discussed by Beedle (1991). Further discussion of the evolution of the beam-column design criteria is found in Sputo (1993) and Kennedy et al. (1993). A worldwide specification has been proposed under the auspices of the International Standards Association (ISO, 1994).

8.8 SPECIAL TOPICS

The present chapter focused on beam-columns manufactured from hot-rolled steel wide-flange shapes. The behavior of beam-columns of cold-formed steel shapes is discussed in Chapter 14 of this guide. Many beam-columns are box-shaped. For these members it is often necessary to consider the interaction of local and overall buckling. The papers by Shen and Zhang (1991) and Sohal and Chen 1988 deal with this topic:

The design of beam-columns with tapered webs was the subject of an extensive set of research projects at the University of Buffalo in New York. This work was presented as Chapter 9 in the fourth edition of this guide. Further relevant references on the stability of tapered steel beam-columns are Butler and Anderson (1963), Culver and Preg (1968), Hsu and Lee (1981), and Bradford (1988). The postbuckling behavior of beam-columns was investigated by Kounadis and Ioannidis (1994).

Determination of the response of beam-columns to wave or earthquake motions is an important factor in assessing the strength of offshore structures. Therefore, considerable effort has recently been directed at developing certain of the techniques for assessing static strength listed in Table 8.1A into efficient methods for the cyclic inelastic analysis of steel tubular beam-columns (Chen, 1981; Han and Chen, 1983a,b). Computer programs based on these techniques have been verified against the results of large-scale tests and are now being used to generate data on cyclic response (Han and Chen, 1983a,b). For a full account of this topic, the reader is referred to the monograph by Chen and Han (1983).

REFERENCES

Abdel-Sayed, G., and Aglan, A. A. (1973), "Inelastic Lateral Torsional Buckling of Beam Columns," *Publ. IABSE*, No. 33–II, pp. 1–16.

Adams, P. F. (1970), "Segmental Design of Steel Beam-Columns," *Can. Struct. Eng. Conf.*

Adams, P. F. (1974), *The Design of Steel Beam-Columns*, Canadian Steel Industries Construction Council, Toronto, Ont. Canada.

AIJ (1990), *Standard for Limit State Design of Steel Structures*, Architectural Institute of Japan, Tokyo.

AISC (1993), *Load and Resistance Factor Design Specification for Structural Steel Buildings*, American Institute of Steel Construction, Chicago IL.

Anslijn, R. (1983), "Tests on Steel I Beam-Columns in Mild Steel Subjected to Thrust and Biaxial Bending," *CRIF Rep. MT 157*, Brussels, Belgium, Aug.

ASCE (1971a), "Plastic Design in Steel: A Guide and Commentary," *ASCE Manual of Engineering Practice*, No. 41, 2nd ed., American Society of Civil Engineers, New York.

Austin, W. F. (1961), "Strength and Design of Metal Beam-Columns," *ASCE J. Struct. Div.*, Vol. 87, No. ST4, pp. 1–34.

Ballio, G., and Campanini, C. (1981), "Equivalent Bending Moments for Beam-Columns," *J. Constr. Steel Res.*, Vol. 1, No. 3.

Ballio, G., Petrini, V., and Urbano, C. (1973), "The Effect of the Loading Process and Imperfections on the Load Bearing Capacity of Beam Columns," *Meccanica*, Vol. 8, No. 1.

Beedle, L. S., editor-in-chief (1991), *Stability of Metal Structures: A World View*, 2nd ed., Structural Stability Research Council, Bethlehem, Pa.

Bez, R. (1983), "Diagrams d'interaction de cornières metalliques," *Publ. ICOM 111*, Swiss Federal Institute of Technology, Lausanne, Switzerland, Mar.

Bijlaard, P. P., Fisher, G. P., and Winter, G. (1955), "Eccentrically Loaded, End-Restrained Columns," *Trans. Am. Soc. Civ. Eng.*, Vol. 120, p. 1070.

Birnstiel, C. (1968), "Experiments on H-Columns Under Biaxial Bending," *ASCE J. Struct. Div.*, Vol. 94, No. ST10, pp. 2429–2450.

Bradford, M. A. (1988), "Lateral Stability of Tapered Beam-Columns with Elastic Restraints," *Struct. Eng.*, Vol. 66, No. 22, pp. 376–384.

Bradford, M. A. and Trahair, N. S. (1985), "Inelastic Buckling of Beam-Columns with Unequal End-Moments," *J. Constr. Steel Res.*, Vol. 5, No. 3, pp. 195–212.

Bradford, M. A., and Trahair, N. S. (1986), "Inelastic Buckling Tests of Beam-Columns," *ASCE J. Struct. Eng.*, Vol. 112, No. 3, pp. 538–549.

Bradford, M. A., Cuk, P. E., Gizejowski, M. A., and Trahair, N. S. (1987), "Inelastic Lateral Buckling of Beam-Columns," *ASCE J. Struct. Eng.*, Vol. 113, No. 11, pp. 2259–2277.

Butler, D. J., and Anderson, G. C. (1963), "The Elastic Buckling of Tapered Beam-Columns," *Weld. J. Res. Suppl.*, Vol. 42, No. 1.

Cai, C. S., and Chen, W.-F. (1991), "Further Verification of Beam-Column Strength Equation," *ASCE J. Struct. Eng.*, Vol. 117, No. 2, pp. 501–513.

Campus, F., and Massonnet, C. (1956), "Recherches sur le flambement de colonnes en acier A37 a profil en double te sollicitées obliquement," *C. R. Rech. IRSIA*, Aprl.

Chan, S. L., Kitipornchai, S., and Al-Bermani, F. G. (1991), "Elasto-Plastic Analysis of Box-Beam-Columns Including Local Buckling Effects," *ASCE J. Struct. Eng.*, Vol. 117, No. 7, pp. 1946–1962.

Chen, W. F. (1970), "General Solution of Inelastic Beam-Column Problem," *ASCE J. Eng. Mech. Div.*, Vol. 96, No. EM4, pp. 421–442.

Chen, W. F. (1971a), "Approximate Solution of Beam Columns," *ASCE J. Struct. Div.*, Vol. 97, No. ST2, pp. 743–751.

Chen, W. F. (1971b), "Further Studies of an Inelastic Beam-Column Problem," *ASCE J. Struct. Div.*, Vol. 97, No. ST2, pp. 529–544.

Chen, W. F. (1977a), "Theory of Beam-Columns: The State-of-the-Art Review," *Proc. Int. Colloq. Stabil. Struct. Under Static Dyn. Loads*, SSRC/ASCE, Washington D.C., Mar.

Chen, W. F. (1977b), "Design of Box Columns Under Biaxial Bending," *2nd Int. Colloq. Stabil. Steel Struct.. Prelim. Rep.*, Liege, Belgium.

Chen, W. F. (1981), "Recent Advances in Analysis and Design of Steel Beam-Columns in U.S.A.," *Proc. U.S.–Jpn. Sem. Inelastic Instabil. Steel Struct. Elements*, Tokyo, May.

Chen, W. F. (1982), "Box and Cylindrical Columns Under Biaxial Bending," in *Axially Compressed Structures: Stability and Strength* (ed. R. Narayanan), Applied Science Publishers, Barking, Essex, England, Chap. 3.

Chen, W. F., and Atsuta, T. (1972a), "Interaction Equations for Biaxially Loaded Sections," *ASCE J. Struct. Div.*, Vol. 98, No. ST5, pp. 1035–1052.

Chen, W. F., and Atsuta, T. (1972b), "Column-Curvature Curve Method for Analysis of Beam-Columns," *Struct. Eng.*, Vol. 50, No. 6.

Chen, W. F., and Atsuta, T. (1974), "Interaction Curves for Steel Sections, Under Axial Load and Biaxial Bending," *EIC Eng. J.*, Vol. 17, No. A-3.

Chen, W. F., and Atsuta, T. (1977), *Theory of Beam-Columns*, Vols. 1 and 2, McGraw-Hill, New York.

Chen, W. F., and Cheong-Siat-Moy, F. (1980), *Limit States Design of Steel Beam-Columns*, Solid Mechanics Archives, Vol. 5, Noordhoff International Publishing, Leyden, The Netherlands.

Chen, W. F., and Han, D. J. (1983), *Tubular Members in Offshore Structures*, Pitman, London.

Chen, W. F., and Lui, E. M. (1983), "Design of Beam-Columns in North America," *Proc. 3rd Int. Colloq. Stab. Met. Struct.*, Toronto.

Chen, W. F., and Santathadaporn, S. (1968), "Review of Column Behaviour Under Biaxial Loading," *ASCE J. Struct. Div.*, Vol. 94, No. ST12, pp. 2999–3021.

Cheong-Siat-Moy, F. (1974a), "A Method of Analysis of Laterally Loaded Columns," *ASCE J. Struct. Div.*, Vol. 100, No. ST5, Proc. Pap. 10548, pp. 953–970.

Cheong-Siat-Moy, F. (1974b), "General Analysis of Laterally Loaded Beam-Columns," *ASCE J. Struct. Div.*, Vol. 100, No. ST6, Proc. Pap. 10625, pp. 1263–1278.

Cheong-Siat-Moy, F., and Downs, T. (1980), "New Interaction Equation for Steel Column Design," *ASCE J. Struct. Div.*, Vol. 106, No. ST5, pp. 1047–1062.

Chubkin, G. M. (1959), "Experimental Research on Stability of Thin Plate Steel Members with Biaxial Eccentricity," in *Analysis of Spatial Structures*, Vol. 5, Moscow, Paper 6.

Clark, J. W. (1955), "Eccentrically Loaded Aluminium Columns," *Trans. ASCE*, Vol. 120, p. 116.

CSA (1994), *Limit States Design of Steel Structures*, CAN/CSA-S16.1-94, Canadian Standards Association, Rexdale, Ontario, Canada.

Cuk, P., and Trahair, N. S. (1981), "Elastic Buckling of Beam-Columns with Unequal End Moments," *Civ. Eng. Trans. Inst. Eng. Aust.*, Vol. CE23, No. 2.

Cuk, P. E., Rogers, D. E., and Trahair, N. S. (1986), "Inelastic Buckling of Continuous Steel Beam-Columns," *J. Constr. Steel. Res.*, Vol. 6, No. 1, pp. 21–52.

Culver, C. G. (1966a), "Exact Solution of the Biaxial Bending Equations," *ASCE J. Struct. Div.*, Vol. 92, No. ST2, pp. 63–84.

Culver, C. G. (1966b), "Initial Imperfections in Biaxial Bending," *ASCE J. Struct. Div.*, Vol. 92, No. ST3, pp. 119–138.

Culver, G. C., and Preg, S. M., Jr. (1968), "Elastic Stability of Tapered Beam-Columns," *ASCE J. Struct. Div.*, Vol. 94, No. ST2, pp. 455–470.

Djalaly, H. (1971), "La Barre dans la Structure, *CTIOM Rep.*, Mar.

Djalaly, H. (1973), "Calcul de la résistance ultime des barres au flambement par flexion-torsion," *Constr. Met.*, No. 4.

Djalaly, H. (1975), "Calcul de la résistance ultime des beams comprîmées et flèchies," *Constr. Met.*, No. 4.

Duan, L., and Chen, W.-F. (1989), "Design Interaction Equation for Steel Beam-Columns," *ASCE J. Struct. Eng.*, Vol. 115, No. 5, pp. 1225–1243.

Duan, L., and Chen, W.-F. (1990), "Design Interaction Equation for Cylindrical Tubular Beam-Columns," *ASCE J. Struct. Eng.*, Vol. 116, No. 7, pp. 1794–1812.

Duan, L., Sohal, I., and Chen, W.-F. (1989), "On Beam-Column Moment Amplification Factor," *AISC Eng. J.*, Vol. 26, No. 4, pp. 130–135.

Dwyer, T. J., and Galambos, T. V. (1965), "Plastic Behaviour of Tubular Beam-Columns," *ASCE J. Struct. Div.*, Vol. 91, No. ST4, pp. 125–152.

ECS (1993), *Eurocode 3: Design of Steel Structures*, European Prestandard ENV 1993-1 -1, European Committee for Standardization, Brussels, Belgium.

Fukumoto, Y., and Galambos, T. V. (1966), "Inelastic Lateral-Torsional Buckling of Beam-Columns,' *ASCE J. Struct. Div.*, Vol. 92, No. ST2, pp. 41–62.

Galambos, T. V. (1964), "Combined Bending and Compression," in *Structural Steel Design*, (ed. L. Tall), Ronald Press, New York.

Galambos, T. V. (1981), "Beam-Columns," *ASCE Conv.*, New York, May.

Galambos, T. V., and Ketter, R. L. (1961), "Columns Under Combined Bending and Thrust," *Trans. ASCE*, Vol. 126, Part I, pp. 1–25.

Galambos, T. V., and Prasad, J. (1962), "Ultimate Strength Tables for Beam-Columns," *Weld. Res. Counc. Bull. No. 78*, June.

Galambos, T. V., Adams, P. F., and Fukumoto, Y. (1965), "Further Studies on the Lateral-Torsional Buckling of Steel Beam-Columns," *Fritz Eng. Lab. Rep. No. 205A.36*, Lehigh University, Bethlehem, Pa.

Gent, A. R., and Sen, T. K. (1977), "The Plastic Deformation Capacity of H-Columns at High Axial Loads," *Prelim. Rep. 2nd Int. Colloq. Stab. Steel Struct.*, Liege, Belgium.

Gilson, S., and Cescotto, S. (1982), "Experimental Research on the Buckling of Alu-alloy Columns with Unsymmetrical Cross-Section," Laboratorie de Mécanique des Materiaux et Théorie des Structures, Université de Liege, Liege, Belgium.

Han, D. J., and Chen, W. F. (1983a), "Behaviour of Portal and Strut Types of Beam-Columns," *Eng. Struct.*, Vol. 5, pp. 15–25.

Han, D. J., and W. F. (1983b), "Buckling and Cyclic Inelastic Analysis of Steel Tubular Beam-Columns," *Eng. Struct.*, Vol. 5, pp. 119–132.

Hancock, G. J. (1977), "Elastic-Plastic Analysis of Thin-Walled Cross-Sections," *6th Aust. Conf. Mech. Struct. Mater.*, Christchurch, New Zealand, Aug.

Hill, H. N., and Clark, J. W. (1951a), "Lateral Buckling of Eccentrically Loaded I- and H-Section Columns," *Proc. 1st Natl. Congr. Appl. Mech.*, ASME, New York.

Hill, H. N., and Clark, J. W. (1951b), "Lateral Buckling of Eccentrically Loaded I-Section Columns," *Trans. Am. Soc. Civ. Eng.*, Vol. 116, p. 1179.

Hill, H. N., Hartmann, E. C., and Clark, J. W. (1956), "Design of Aluminium Alloy Beam-Columns," *Trans. Am. Soc. Civ. Eng.*, Vol. 121.

Horne, M. R. (1956), "The Flexural-Torsional Buckling of Members of Symmetrical I-Section Under Combined Thrust and Unequal Terminal Moments," *Q. J. Mech. Appl. Math.*, No. 4.

Hsu, T. L., and Lee, G. C. (1981), "Design of Beam-Columns with Lateral–Torsional End-Restraints," *Weld. Res. Counc. Bull.*, No. 272, Nov.

ISO (1994), *Steel Structures: Materials and Design*, Draft ISO/TC 167/SC 1, International Organization for Standardization, Paris.

Jingping, L., Zaitian, G., and Shaofan, C. (1988), "Buckling of Transversely Loaded I-Beam-Columns," *ASCE J. Struct. Eng.* Vol. 114, No. 9, pp. 2109–2118.

Johnston, B. G. (1976), *Guide to Stability Design Criteria for Metal Structures*, 3rd ed., Wiley, New York.

Johnston, B. G., and Cheney, L. (1942), "Steel Columns of Rolled Wide Flange Sections," *Prog. Rep. No. 2*, American Institute of Steel Construction, Chicago, Nov.

Kanchanalai, T., and Lu, L. W. (1979), "Analysis and Design of Framed Columns Under Minor Axis Bending," *Eng. J. Am. Inst. Steel Constr.*, second quarter, pp. 29–41.

Kemp, A. R. (1984), "Slenderness Limits Normal to the Plane-of-Bending for Beam-Columns in Plastic Design," *J. Constr. Steel. Res.*, Vol. 4, pp. 135–150.

Kennedy, D. L. J., Picard, A., and Beaulieu, D. (1993), "Limit States Design of Beam-Columns: The Canadian Approach and Some Comparisons," *J. Constr. Steel Res.*, Vol. 25, No. 1–2, pp. 141–164.

Ketter, R. L. (1962), "Further Studies of the Strength of Beam-Columns," *Trans. Am. Soc. Civ. Eng.*, Vol. 127, Part II, pp. 224–466.

Ketter, R. L., Beedle, L. S., and Johnson, B. G. (1952), "Column Strength Under Combined Bending and Thrust," *Weld. J. Res. Suppl.*, Vol. 31, No. 12.

Ketter, R. L., Kaminsky, E. L., and Beedle, L. S. (1955), "Plastic Deformation of Wide-Flange Beam Columns," *Trans. Am. Soc. Civ. Eng.*, Vol. 120, p. 1028.

Kitipornchai, S., and Wang, C.-M. (1988), "Out-of-Plane Buckling Formulas for Beam-Columns/Tie Beams," *ASCE J. Struct. Eng.*, Vol. 114, No. 12, pp. 2773–2789.

Klöppel, K., and Barsch, W. (1973), "Versuche zum Kapitel Stabilitätsfälle der Neufassung von Din 4113," *Aluminium*, Vol. 10.

Klöppel, K., and Winkelmann, E. (1962), "Experimentale und theoretische Untersuchungen über die Traglast von zweiachsig assussermittig gedrückten Stahlstäben," *Stahlbau*, Vol. 31, p. 33.

Kounadis, A. N., and Ioannidis, G. I. (1994), "Lateral Post-buckling Analysis of Beam-Columns," *ASCE J. Eng. Mech.*, Vol. 120, No. 4, pp. 695–706.

Lay, M. G. (1974), *Source Book for the Australian Steel Structures Code AS1250*, Australian Institute of Steel Construction, Sydney, Australia.

Lay, M. G., and Galambos, T. V. (1965), "The Experimental Behaviour of Retrained Columns," *Weld. Res. Counc. Bull.*, No. 110, Nov.

Lim, L. C., and Lu, L. W. (1970), "The Strength and Behavior of Laterally Unsupported Columns," *Fritz Eng. Lab. Rep. No. 329.5*, Lehigh University, Bethlehem, Pa., June.

Lindner, J. (1972), "Theoretical Investigations of Columns Under Biaxial Loading," *Proc. Int. Colloq. Column Strength*, IABSE-CRC-ECCS, Paris.

Lindner, J., and Gietzelt, R. (1982), "Design of Biaxially Loaded Steel Beam-Columns," *Rep. 2061E*, Technical University of Berlin, Nov.

Lindner, J., and Gietzelt, R. (1983), "Discussion of Interaction Equations for Members in Compression and Bending," *Proc. 3rd Int. Colloq. Stab. Met. Struct.*, Paris, Nov.

Lindner, J., and Kurth, W. (1982), "Zum Biegedrillknicken Von Stützen aus, Ste 690," *Stahlbau*, Vol. 51.

Lindner, J. and Wiechart, G. (1978), "Zur Bemessung gegen Biegedrillknickung," *Beitrag Festschr. Otto Jungbluth*, 60 Jahre, Technische Hochschule, Darmstadt, Germany.

Lu, L. W., and Kamalvand, H. (1968), "Ultimate Strength of Laterally Loaded Columns," *ASCE J. Struct. Div.*, Vol. 94, No. ST6, pp. 1505–1524.

Lu, L. W., Shen, Z. Y., and Hu, X. R. (1983), *Inelastic Instability Research at Lehigh University: Instability and Plastic Collapse of Steel Structures* (ed. L. J. Morris), Granada, London.

Maquoi, R., and Rondal, J. (1982), "Sur la force portant des poutres colonnes," *Ann. Trav. Publics Belg.*, No. 5.

Marshall, P. J., and Ellis, J. S. (1970), "Ultimate Biaxial Capacity of Box Steel Columns," *ASCE J. Struct. Div.*, Vol. 96, No. ST9, pp. 1873–1888.

Mason, R. G., Fisher, G. P., and Winter, G. (1958), "Eccentrically Loaded, Hinged Steel Columns," *ASCE J. Eng. Mech. Div.*, Vol. 84, No. EM4, p. 1792.

Massonnet, C. (1976), "Forty Years of Research on Beam-Columns," *Solid Mech. Arch.*, Vol. 1, No. 2.

Massonnet, C., and Save, M. (1965), *Plastic Analysis and Design*, Vol. 1, *Beams and Frames*, Blaisdell, New York.

Matthey, P. A. (1982), "Flexion gauche non-symétrique de colonnes en double-te recherche expérimentale et simulation," *3rd Int. Colloq. Stab. Met. Struct. Prelim. Rep.*, Paris.

Mazzolani, F. M., and Frey, F. (1983), "ECCS Stability Code for Aluminium-Alloy Members: Present State and Work in Progress," *3rd Int. Colloq. Stab. Met. Struct., Prelim. Rep.*, Paris.

McLellan, E. R., and Adams, P. F. (1970), "Design of Steel Crane Columns or Columns Subjected to Lateral Loads," *EIC Trans.*, Vol. 70, No. A-6.

Miranda, C., and Ojalvo, M. (1965), "Inelastic Lateral–Torsional Buckling of Beam-Columns," *ASCE J. Eng. Mech. Div.*, Vol. 91, No. EM6, pp. 21–38.

Morris, G. A., and Fenves, S. J. (1969), "Approximate Yield Surface Equations," *ASCE J. Eng. Mech. Div.*, Vol. 95, No. EM4, pp. 937–954.

Nakashima, M. (1994), "Variation of Ductility Capacity of Steel Beam-Columns," *ASCE J. Struct. Eng.*, Vol. 120, No. 7, pp. 1941–1960.

Nakashima, M., Takanashi, K., and Kato, H. (1990), "Tests of Steel Beam-Columns Subject to Sidesway," *ASCE J. Struct. Eng.*, Vol. 116, No. 9, pp. 2516–2531.

Nethercot, D. A. (1983), "Evaluation of Interaction Equations for Use in Design Specifications in Western Europe," *Proc. 3rd Int. Colloq. Stab. Met. Struct.*, Toronto.

Ojalvo, M., and Fukumoto, Y. (1962), "Nomographs for the Solution of Beam-Column Problems," *Weld. Res. Counc. Bull.*, No. 78, June.

Opperman, H. P. (1983), "Refined Beam-Column Analysis," *Proc. 3rd Int. Colloq. Stab. Met. Struct.*, Paris.

Pi, Y. L., and Trahair, N. S. (1992a), "Prebuckling Deformations and Lateral Buckling: I. Theory," *ASCE J. Struct. Eng.*, Vol. 118, No. 11, pp. 2949–2966.

Pi, Y. L., and Trahair, N. S. (1992b), "Prebuckling Deformations and Lateral Buckling: II. Applications," *ASCE J. Struct. Eng.*, Vol. 118, No. 11, pp. 2967–2985.

Pi, Y. L., and Trahair, N. S. (1994a), "Non-linear Inelastic Analysis of Steel Beam-Columns: I. Theory," *ASCE J. Struct. Eng.*, Vol. 120, No. 7, pp. 2041–2061.

Pi, Y. L., and Trahair, N. S. (1994b), "Non-linear Inelastic Analysis of Steel Beam-Columns: II. Application," *ASCE J. Struct. Eng.*, Vol. 120, No. 7, pp. 2062–2085.

Pillai, U. S. (1970), "Review of Recent Research on the Behaviour of Beam-Columns under Biaxial Bending," *R. Mil. Coll. Can. Civ. Eng. Rep.*, Jan.

Pillai, U. S. (1974), "Beam Columns of Hollow Sections," *J. Can. Soc. Civ. Eng.*, Vol. 1.

Pillai, U. S. (1980), "Comparison of Test Results with Design Equations for Biaxially Loaded Steel Beam-Columns," *R. Mil. Coll. Can. Dep. Civ. Eng. Res. Rep.*, No. 80-2, Aug.

Pillai, U. S. (1981), "An Assessment of CSA Standard Equations for Beam-Column Design," *Can. J. Civ. Eng.*, Vol. 8.

Rajasekaren, S. (1977), "Finite Element Method for Plastic Beam-Columns," in *Theory of Beam-Columns* (ed. W. F. Chen and T. Atsuta), McGraw-Hill, New York, Chap. 12.

Ramm, E., and Osterrieder, P. (1983), "Ultimate Load Analysis of Three-Dimensional Beam Structures with Thin-Walled Cross Sections Using Finite Elements," *Proc. 3rd Int. Colloq. Stab. Met. Struct. Prelim. Rep.*, Paris.

Razzaq, Z., and McVinnie, W. W. (1982), "Rectangular Tubular Steel Columns Loaded Biaxially," *J. Struct. Mech.*, Vol. 10, No. 4.

Roik, K., and Bergmann, R. (1977), "Steel Column Design," *Prelim. Rep. 2nd Int. Colloq. Stab. Steel Struct.*, Liege, Belgium.

Roik, K., and Kindmann, R. (1983), "Design of Simply Supported Members by Means of European Buckling Curves for Uniaxial Bending with Compression," *Prelim. Rep. 3rd Int. Colloq. Stab. Met. Struct.*, Paris.

Roik, K., and Wagenknecht, R. (1976), "Traglastdiagramme zur Bemessung von Druckstaben mit doppellsymmetrischen Querschnitt aus Baustahl," *KIB/Berichte*, Vol. 27, Vulkan–Verlag, Essen, Germany.

Ross, D. A., and Chen, W. F. (1976), "Design Criteria for Steel I-Columns Under Axial Load and Biaxial Bending," *Can. J. Civ. Eng.*, Vol. 3, No. 2.

Salvadori, M. G. (1956), "Lateral Buckling of Eccentrically Loaded I-Columns," *ASCE Trans.*, Vol. 121, p. 1163.

Santathadaporn, S., and Chen, W. F. (1970), "Interaction Curves for Sections Under Combined Biaxial Bending and Axial Force," *Weld. Res. Counc. Bull.*, No. 148, Feb.

SAA (1990), *Australian Standard: Steel Structures*, AS 4100-1990, Standards Association of Australia, North Sydney, New South Wales, Australia.

Shen, Z., and Zhang, Q. (1991), "Interaction of Local and Overall Instability of Compressed Box-Columns," *ASCE J. Struct. Eng.*, Vol. 117, No. 11, pp. 3337–3355.

Sohal, I. S., and Chen, W.-F. (1988), "Local and Post-buckling Behavior of Tubular Beam-Columns," *ASCE J. Struct. Eng.*, Vol. 114, No. 5, pp. 1073–1090.

Sohal, I. S., and Syed, N. A. (1992), "Inelastic Amplification Factor for Design of Steel Beam-Columns," *ASCE J. Struct. Eng.*, Vol. 118, No. 7, pp. 1822–1839.

Sputo, T. (1993), "History of Steel Beam-Column Design," *ASCE J. Struct. Eng.*, Vol. 119, No. 2, pp. 547–557.

Tebedge, N., and Chen, W. F. (1974), "Design Criteria for Steel H-Columns Under Biaxial Loading," *ASCE J. Struct. Div.*, Vol. 100, No. ST3, pp. 579–598.

Trahair, N. S. (1993), *Flexural-Torsional Buckling of Structures*, E&FN Spon, London, Chap. 11.

Trahair, N. S., and Bradford, M. A. (1988), *The Behaviour and Design of Steel Structures*, 2nd ed., Chapman & Hall, London, Chap 7.

van Kuren, R. C., and Galambos, T. V. (1964), "Beam-Column Experiments," *ASCE J. Struct. Div.*, Vol. 90, No. ST2, pp. 223–256.

Van Manen, S. E. (1982), "Plastic Design of Braced Frames Allowing Plastic Hinges in the Columns," *Heron*, Vol. 27, No. 2.

Vinnakota, S. (1977), "Finite Difference Method for Plastic Beam-Columns," in *Theory of Beam-Columns*, (ed. W. F. Chen and T. Atsuta), McGraw-Hill, New York, Chap. 10.

Virdi, K. S. (1981), "Design of Circular and Rectangular Hollow Section Columns," *J. Constr. Steel. Res.*, Vol. 1, No. 4.

Wang, C.-M., and Kitipornchai, S. (1989), "New Set of Buckling Parameters for Monosymmetric Beam-Columns/Tie Beams," *ASCE J. Struct. Eng.*, Vol. 115, No. 6, pp. 1497–1513.

White, D. W. and Clarke, M. J. (1997), "Design of Beam-Columns in Steel Frames I: Philosophies and Procedures", *ASCE J. of Structural Engineering*, Vol. 123, No. 12, Dec., pp. 1556–1564.

White, D. W. and Clarke, M. J. (1997), "Design of Beam-Columns in Steel Frames I: Comparison of Standards", *ASCE J. of Structural Engineering*, Vol. 123, No. 12, Dec., pp. 1565–1574.

Young, B. W. (1973), "The In-Plane Failure of Steel Beam-Columns," *Struct. Eng.*, Vol. 51, No. 1.

Yu, C. K., and Tall, L. (1971), "A514 Steel Beam-Columns," *Publ. IABSE*, No. 31–II, pp. 185–213.

CHAPTER NINE

HORIZONTALLY CURVED STEEL I-GIRDERS

9.1 INTRODUCTION

During the past quarter century, there has been a notable increase in the number of horizontally curved steel bridges constructed throughout the world. This is due primarily to the ever-increasing emphasis on aesthetics coupled with land and or transportation alignment restrictions. Despite their extensive use, accurate prediction of the behavior of horizontally curved steel girders remains a task of formidable complexity. Research on the analysis and design of horizontally curved girders began with Saint Venant's (1843) memoir. Since then, thousands of pages of technical papers, reports, and books have been published in the literature concerning various applications in the fields of civil, mechanical, and aerospace engineering.

Despite the considerable progress begun almost a century and half ago, serious studies pertaining to the analysis and design of horizontally curved steel bridges began only a quarter of a century ago, when in 1969, the Federal Highway Administration formed the Consortium of University Research Teams (CURT). This team consisted of Carnegie-Mellon University, the University of Pennsylvania, the University of Rhode Island, and Syracuse University, whose research efforts, along with those at the University of Maryland, resulted in the initial development of working stress design criteria and tentative design specifications. The American Society of Civil Engineers and the American Association of State Highway and Transportation Officials (ASCE–AASHTO) Task Committee on Curved Girders (1977) compiled the results of most of the research efforts prior to

1976 and presented a single source set of recommendations pertaining to the design of curved I-girder bridges. The CURT research activity was followed shortly by the development of the load factor design criteria (Stegmann and Galambos, 1976; Galambos, 1978) adopted by AASHTO (1980), along with the working stress design criteria in the first guide specifications for horizontally curved highway bridges (AASHTO, 1987).

A survey of most published works pertaining to horizontally curved bridges was first presented by McManus et al. (1969), whose bibliography list contained 202 references, four of which dealt only with box girders. McManus's paper was discussed by other authors, who added additional references to the original list (Ketcheck, 1969; Tan et al., 1969; Pandit, 1970). Nine years later, the ASCE–AASHTO Task Committee on Curved Girders (1978a) presented a state-of-the-art report that provides 106 references dealing primarily with horizontally curved box girders. The committee also presented results of a survey pertaining to the geometry, design, detail, construction, and performance of box-girder bridges constructed in the United States, Canada, Europe, and Japan (ASCE–AASHTO Task Committee on Curved Girders, 1978b). The survey was an update of a more limited survey published by the AASHTO–ASCE Committee on Flexural Members (1973). Nakai and Yoo (1988) published a book that offers a comprehensive listing of numerous papers, with particular attention to the Japanese literature.

The current AASHTO guide specification for horizontally curved highway bridges (AASHTO, 1993) is based primarily on research work conducted prior to 1978. Since then, a significant amount of work has been conducted to enhance the specifications and to better understand the behavior of curved girders. A review of the literature was published by Zureick et al. (1993).

9.2 ANALYSIS METHODS

The analysis methods developed thus far for horizontally curved steel members can be classified into two major categories: approximate and refined methods. The approximate methods require minimal modeling effort on part of the designer and hence are adequate for preliminary analysis and design purposes. These include:

- The plane grid method
- The space frame method
- The V-load method

The refined methods, on the other hand, are somewhat more elaborate, computationally intensive, and time consuming in terms of modeling. Therefore, the methods that fall in this class should be used for the final or detailed analyses. Examples of such methods include:

- The finite element method
- The finite strip method
- The finite difference method
- Analytical solution to differential equations
- The slope deflection method

A brief description of each of these analytical methods is presented below; for further detail the reader is referred to Zureick et al. (1993).

9.2.1 Approximate Methods

Plane Grid Method. The structure of this method is modeled as an assemblage of two-dimensional grid members with one translational and two rotational degrees of freedom. This method does not account for nonuniform torsion (warping) and hence can be used only for initial member sizing.

Space Frame Method. This method was introduced in 1973 by Brennan and Mandel for the analysis of open and closed curved members. The curved members are idealized as three-dimensional straight members, while the diaphragms and lateral bracing are assumed as trusslike members that can carry only axial loads. The effects of warping is not usually included in this analysis, which makes this method practical for initial design purposes.

V-Load Method. This method uses equivalent straight girders with span lengths equal to the arc lengths instead of the individual curved girders by adding self-equilibrating vertical shear forces (acting on diaphragm locations) that take the curvature into account. These loads are dependent on the radius of curvature, bridge width, and diaphragm spacing (Poellot, 1987; Fiechtel et al., 1987).

9.2.2 Refined Methods

Finite Element Method. This approach discretizes the structure into small divisions (elements) where each element is defined by a specified number of nodes. The behavior of each element (and ultimately the structure) is assumed to be a function of its nodal quantities (displacements and/or stresses), which serve as the primary unknowns in this formulation. This is one of the most general and accurate methods to use since it does not put any limitation on the geometry, loads, or boundary conditions, and can be applied to open/closed girders and static and dynamic analysis. Additionally, the structure's response can always be improved by refining the mesh used and by increasing the number of nodes (or degrees of freedom) for each element. However, the rather involved modeling and analysis efforts required

by this method may in some cases make it impractical for preliminary analysis.

Finite Strip Method. In this numerical method, the curved bridge is divided into narrow strips in the circumferential direction which are supported in their radial direction. The analysis includes bending and membrane actions as well as warping and distortional effects (Hsu, 1989). Although this method provides some simplicity over the finite element method because of the smaller number of unknowns required, it does not offer the flexibility and versatility of the latter method.

Finite Difference Method. In this method, a grid is superimposed on the structure, and the governing differential equations are replaced by algebraic difference equations that are solved for each grid point.

Solution to the Governing Differential Equations (GDE). In this class an analytical solution to the GDE is obtained. The solution is usually a closed form or a convergent series solution, such as a Fourier series.

Slope Deflection Method. In this approach the partial differential equations are established in terms of slope-deflection equations and the solution is assumed to be a Fourier series. The analysis includes the effects of curvature, nonuniform torsion, and diaphragms. However, the solution is usually applicable to a certain number of spans and geometries.

9.2.3 Remarks on the Analytical Methods

From the published literature on the analysis methods for predicting the behavior of horizontally curved steel bridge girders (Zureick et al., 1993) it can be said that the plane grid and space frame methods treat curved members as straight members and hence are recommended to be used only for preliminary design purposes. The V-load method, which was applied to I-girders only, underestimates inner girder stresses and does not consider the bracing effect in the plane of the bottom flange. In addition, the reliability of these results is dependent on the selection of the transverse live-load distribution factors (Poellot, 1987). Thus the V-load method can only be recommended for preliminary analysis.

Among the refined methods, the finite element method is probably the most involved and time consuming. However, it is still the most general and comprehensive technique that has been applied to the static and dynamic elastic and inelastic analysis with different mechanical and thermal loading. Many general-purpose finite element-based software do incorporate a graphical interface to the existing computer codes, which expedite modeling and discretizing of the structure and allow the user to view results and modify the loading, boundary conditions, and/or configuration. The other refined methods are as good as the finite element method but are limited to certain configurations and boundary conditions, and they are generally more cumbersome to use.

9.3 STABILITY OF CURVED I-GIRDER BRIDGES

9.3.1 Flange-Slenderness Requirements

The combination of bending and warping in an I-shaped curved girder results in a nonuniform distribution of the stress across the compression flange width. Therefore, the outside part of the flange will buckle at a stress value different from that of the inside part. To study the buckling problem of a curved I-shape girder, Frampton (1968) and Culver and Frampton (1970) examined analytically the elastic buckling case, in which each half of the flange was treated separately as an isotropic sector plate free on one edge and rotationally restrained along the other edge by the web and the other half of the flange. The fundamental equation of buckling was then written in polar coordinates and solved numerically using the finite difference method. This investigation was later extended by Culver and Nasir (1969, 1971) to cover not only the elastic but also the inelastic flange local buckling behavior. In the inelastic range, the mathematical model was based on the assumption of orthotropic behavior. Their numerical results showed that the influence of curvature is very small for flange curvature ratios $1 \times 10^{-6} < b/R < 0.01$, where b is the half-width of the flange and R is the radius of the curved girder, and that as yielding spreads across the flange, both the buckling stress and the buckled wavelength decrease. The design recommendations resulting from this study suggested that the width-to-thickness ratio be limited to that set forth in the 1969 AISC Specification for straight rolled compact beams ($b/t \leq 1650/\sqrt{F_y}$, where F_y is in psi and b is the width of half of the flange). Culver (1971) presented a summary of his research related to proportioning the compression flange in a horizontally curved I-girder and pointed out that the total stress (warping plus bending) at the flange tip must be limited to $0.55F_y$ if the AASHTO b/t limit for straight girders is used for curved girders. In such a case, the factor of safety against local buckling for both straight and curved I-girders becomes essentially the same regardless of the ratio of bending to warping stress. This approach has been adopted in the AASHTO guide specification, where the flange local buckling criterion is based only on the b/t ratio. This approach was challenged recently by Kang and Yoo (1990), who used the finite element code MSC/NASTRAN to demonstrate that in a curved girder, local buckling of the flange is affected not only by the width-to-thickness ratio but also by the initial curvature and the warping normal stress. Komatsu and Kitada (1981) use an elastoplastic finite displacement analysis to study the ultimate strength of outstanding steel plates with initial imperfections. Results of this study were used to propose a slenderness ratio for a compact flange as follows (Nakai and Yoo, 1988; Kitada et al., 1986, 1993):

$$\lambda = \sqrt{\frac{F_y}{F_{cr}}} = \frac{b}{t}\sqrt{\frac{12(1-\nu^2)}{0.43\pi^2}\frac{F_y}{E}} \leq 0.5 \tag{9.1}$$

resulting in a limiting flange slenderness ratio:

$$\frac{b}{t} \leq 0.312\sqrt{\frac{E}{F_y}} \tag{9.2}$$

Again, it should be reminded that b is the width of half the flange, ν is Poisson's ratio, and E is the modulus of elasticity.

9.3.2 Web-Slenderness Requirements

The web-slenderness requirements for a curved I-girder differ from those of straight girders. These requirements are often based on the bending behavior, the shear behavior, a combination of the two, and the web out-of-lane deflections. Experimental data pertaining to the behavior of curved girders with unstiffened webs are limited to a depth-to-thickness ratio of 70. Therefore, designing curved unstiffened webs with a slenderness ratio substantially higher than 70 is undesirable. For stiffened webs, work has been conducted on curved I-girder with webs stiffened transversely, longitudinally, or both. These are addressed next.

Transversely Stiffened Web. Current AASHTO web-slenderness requirements for a curved I-girder are based on the analytical studies conducted by Culver et al. (1973a,b). In these studies the web panel was modeled as a series of isolated elastically supported cylindrical strips subjected to appropriate load distributions (Wachowiak, 1967). The stress state in each cylindrical strip was determined from the total potential energy of a nonlinear arch model using the Rayleigh–Ritz method. Numerical results were generated and a curve-fitting technique was used to develop the following web-slenderness requirement:

$$\frac{d}{t_w} \leq \frac{36,000}{\sqrt{F_y}}\left[1 - 8.6\left(\frac{a}{R}\right) + 34\left(\frac{a}{R}\right)^2\right] \tag{9.3}$$

where d and t_w are the depth and thickness of the web, respectively, and a is the distance between transverse stiffeners. An extension of this work was published a year later, when Culver et al. (1973) used a two-way shell model to check the accuracy of the isolated elastically supported cylindrical strips by treating the panel as a unit rather than as individual strips. The work also included the effects of longitudinal stiffeners.

During almost the same time, Abdel-Sayed (1973) studied analytically the prebuckling and elastic buckling behavior of curved webs, and proposed approximate conservative equations for the estimation of the critical load under pure normal stress, pure shear stress, and combined normal and shear stress. He used the linear theory of shells, neglected the effect of torsional rigidity of the flanges, and assumed the transverse stiffeners to be rigid in their directions (thus no strains could be developed along the edges of the panels) to obtain the governing differential equations that were solved using the Galerkin method.

In 1980, Daniels et al. summarized the Lehigh University five-year experimental research program on the fatigue behavior of horizontally curved bridges and concluded that the CURT slenderness limits were too severe. They developed an equation for load factor design in the form

$$\frac{d}{t_w} \leq \frac{36,500}{F_y}\left(1 - 4\frac{a}{R}\right) \leq 192 \tag{9.4}$$

which can also be written in the form

$$\frac{d}{t_w} \leq 6.7\sqrt{\frac{E}{F_y}}\left(1 - 4\frac{a}{R}\right) \leq 192 \tag{9.5}$$

and an equation for allowable stress design in the form

$$\frac{d}{t_w} \leq \frac{23,000}{\sqrt{f_b}}\left(1 - 4\frac{a}{R}\right) \leq 170 \tag{9.6}$$

or

$$\frac{d}{t_w} \leq 4.3\sqrt{\frac{E}{F_y}}\left(1 - 4\frac{a}{R}\right) \leq 170 \tag{9.7}$$

Equation 9.6 is now used in the 1993 AASHTO guide specifications for horizontally curved highway bridges.

In 1984, Mikami and Furunishi studied the nonlinear behavior of cylindrical web panels of horizontally curved plate girders subjected to pure bending and combined bending and shear. They used Washisu's nonlinear theory of shells to derive a set of differential equations that were solved by the finite difference method. Numerical values of the load, deflection, membrane stress, bending stress, and torsional stress were obtained for various values of the panel aspect ratio and the curvature. The work concluded that as the curvature increases, the membrane stress in the circumferential direction decreases. Furthermore, a curved panel under a combined bending and shear will experience higher bend-

ing stress and a lower level of circumfential membrane stress than those resulting from pure bending.

Transverse Stiffener Requirements. Culver et al. (1973) and Mariani et al. (1973) studied analytically curved web panels under pure shear using the Donnell shell equation and the Galerkin method. They concluded that the required stiffener rigidity for a curved web is less than that for a straight web if the panel aspect ratio a/d is less than 0.78. Here a is the distance between transverse stiffeners and d is the depth of the web. For $0.78 \leq a/d \leq 1$, the required stiffener rigidity increases with curvature in the amount $1 + (1/1775)[(a/d) - 0.78]Z^4$, where Z is a curvature parameter defined as $Z = (a^2/Rt)\sqrt{1-\nu^2}$, with $a/d \leq 1$. In these equations, R is the radius to the centerline of the web, t is the thickness of the web, and ν is Poisson's ratio. The study was limited to curved girders in which $0 \leq Z \leq 10$.

Nakai et al. (1984b, 1985b) presented analytically a beam-column model to estimate the strength of transverse stiffeners in curved girders. The analytical results were compared with experiments conducted by Nakai et al. (1984a), which led to a recommendation that the relative rigidity parameter β, defined as the ratio between required rigidity of a transverse stiffener in horizontally curved girders to that in straight girders (as specified in the Japanese specification), must be the following: For stiffeners attached to one side of the web plate,

$$\beta = \begin{cases} 1.0 + (\alpha - 0.69)Z[9.38\alpha - 7.67 - (1.49\alpha - 1.78)Z] & \text{for } 0.69 \leq \alpha \leq 1.0 \\ 1.0 & \text{for } \alpha < 0.69 \end{cases} \tag{9.8}$$

and for stiffeners attached to both sides of the web plate:

$$\beta = \begin{cases} 1.0 + (\alpha - 0.65)Z[12.67\alpha - 10.42 - (1.99\alpha - 2.49)Z] & \text{for } 0.65 \leq \alpha \leq 1.0 \\ 1.0 & \text{for } \alpha < 0.65 \end{cases} \tag{9.9}$$

where $\alpha = a/d$.

Longitudinally Stiffened Web. In a paper described earlier, Culver et al. (1973) generated numerical results from their analytical model and then used a curve-fitting approach to obtain the following slenderness requirement for a curved web stiffened with one longitudinal stiffener situated in the compressive stress region:

$$\frac{d}{t_w} \leq \frac{46{,}000}{f_b}\left(1 - 2.9\sqrt{\frac{a}{R}} + 2.2\frac{a}{R}\right) \tag{9.10}$$

where f_b is the computed flexural normal stress, in psi units.

9.3.3 Overall Buckling

A horizontally curved girder loaded normal to its plane of curvature will bend and twist simultaneously. Early works on the subject were developed by Vlasov (1961) and Dabrowski (1968), whose formulations were based on the undeformed structure. Culver and McManus (1971) and McManus (1972) presented a second-order analysis in which the equilibrium equations were formulated on the deformed structure. Results obtained in this study were compared to those of lateral buckling tests conducted by Mozer et al. (1971). The study recommended a set of formulas that were later adopted, and still are part of, the 1993 AASHTO guide specifications for horizontally curved bridges.

In 1978, Nishida et al. used the large deflection theory of curved members to derive the following approximate critical elastic moment for a curved beam subjected to two equal end moments:

$$M_{cr} \approx \sqrt{\left(1 - \frac{L^2}{\pi^2 R^2}\right)\frac{\pi^2 EI_y}{L^2}\left(GJ + \frac{\pi^2 EC_w}{L^2}\right)} \tag{9.11}$$

In Eq. 9.11, when R approaches infinity, M_{cr} approaches the elastic critical buckling moment for a straight girder. The symbols I_y, J, and I_w represent, respectively, the minor axis moment of inertia, the St.-Venant torsion constant, and the warping constant.

Yoo (1982) used the minimum potential energy principle to obtain solutions for the determination of the elastic flexural–torsional buckling loads for in-plane and out-of-plane buckling modes of thin-walled curved beams that do not undergo local buckling (Rajasekaran and Ramin, 1984). In 1983, Yoo and Pfeiffer investigated the elastic buckling of thin-walled curved members through a variational-based finite element formulation. Solutions to different cases pertaining to the stability of curved beams were obtained and compared against existing solutions obtained by Timoshenko and Gere (1961), Vlasov (1961), and Culver (1971). Numerical results obtained in this study were significantly different from those of Timoshenko, Vlasov, and Culver. The discrepancies were attributed to incorrect formulations in Timoshenko and Vlasov's cases, and to the fact that the governing differential equation was viewed as a deflection-amplification problem rather than a classical eigenvalue problem in Culver (1971). Later, Yoo and Pfeiffer (1984) presented a solution to the stability of curved beams with in-plane deformation and asserted their earlier conclusion related to the discrepancies with existing solutions including, this time, the work of Vacharajittiphahn and Trahair (1975), which are essentially based on Vlasov's formulation. In 1985, Yoo and Carbine carried out a series of laboratory tests on twelve W10 × 12

simply supported curved beam specimens subjected to concentrated loads. The length of each specimen was approximately 6.1 m (20 ft) with a subtended angle ranging from 0 to 30°. Specimens were loaded from the top flange in one case and from the bottom flange in another case. All specimens reached their ultimate loads, which were higher than the analytically predicted buckling load values from Yoo and Pfeiffer (1984). Bottom flange–loaded specimens had higher ultimate loads and showed lower cross-sectional deformations than those of top flange-loaded specimens. Papangelis and Trahair (1986, 1987) examined experimentally the work of Yoo and Yoo and Pfeiffer by conducting tests on circular aluminum arches. They concluded that the theoretical loads obtained from the work of Yoo differ substantially from various analytical and experimental results of various researchers (Stussi, 1943; Tokarz, 1968, 1971). The conflict among these curved beam theories was also discussed in a series of publications by Yang and Kuo (1986, 1987), who derived the nonlinear differential equations of equilibrium for horizontally curved I-beams by making use of the principle of virtual displacements to establish the equilibrium of a bar in its deformed or buckled configuration (see also Rajasekaran et al., 1988). Numerical results were obtained and compared with those resulting from Yoo's as well as Vlasov's theories. The authors attributed the discrepancy between their results and Yoo's to the fact that Yoo not only neglected both the radial stress effect and the contribution of shear stresses to the potential energy, but also substituted the curvature terms of the curved beam in the potential energy equation of a straight beam. In a recent paper published in 1991, Kuo and Yang further criticized the work of Vlasov and Yoo and supported their argument by solving numerically the buckling problem of a curved beam with solid cross section under uniform bending in one case and uniform compression in another case. Based on a finite element study, Kang and Yoo (1990) showed that initial curvature and warping do not affect lateral–torsional buckling strength of curved girders with a subtended angle between two adjacent cross bracings up to 0.1 rad, the maximum value allowed in the current ASSHTO guide specifications.

9.4 ULTIMATE STRENGTH AND DESIGN RECOMMENDATIONS

Culver and McManus (1971) studied analytically and experimentally the elastic and inelastic behavior of horizontally curved girders and made design recommendations that were essentially adopted in the AASHTO guide specifications. Fukomoto and Nishida (1981) tested six simply supported single curved I-beams under a concentrated load. Curvatures, including out-of straightness of these sections ($L/8R$), varied from 1/1379 to 1/97, with L and R being the curved arc length and the radius of the beam, respectively. Both numerical and experimental results of this investigation agreed quite well. For a curved I-girder under two equal end moments, it was shown that as the value

of the end moments increases, the horizontal displacement of the curved girder increases up to a value approximately equal to 0.8 of the flange width, then it reverses direction, while the vertical deflection as well as the angle of twist increases as the value of the end moment increases. It was also shown that early yielding due to residual stresses decreases the ultimate strength. The authors proposed an approximate ultimate strength formula that requires solution of the following quartic equation:

$$\lambda^4\delta^4 - \left\{\left[1 + \frac{P_E(d-t)}{2M_p}\frac{L^2}{2Rb_f}\right]\lambda^4 + 1\right\}\delta^2 - \frac{L^2}{2Rb_f}\delta + 1 = 0 \tag{9.12}$$

where

$$\lambda = \sqrt{\frac{M_p}{M_E}} \qquad \delta = \frac{M_u}{M_p} \qquad M_p \simeq F_y b_f t(d-t) \qquad P_E = \frac{\pi^2 E I_y}{L^2}$$

In 1983, Yoshida and Maegawa presented the finite displacement formulation of the transfer matrix to study the ultimate strength of horizontally curved I-beams. The analysis covers elastic and inelastic behavior, and the ensuing numerical results were in good agreement with the experiments conducted by Fukomoto and Nishida (1981).

Perhaps the simplest equation predicting the ultimate bending strength of a horizontally curved I-girder is that presented by Nakai et al. (1984c) and also by Kitada et al. (1993). The equation is of the form

$$M_u = \left(1.92 + 0.357\frac{L^2}{Rb_f}\right)M_a \tag{9.13}$$

where M_a is the allowable bending moment, as defined in the Japanese specifications for a straight I-girder subjected to bending and torsion. This equation is empirical and based on 19 tests in which the elements comprising the cross sections are classified as compact and the a/d ratio is less than 1. Furthermore, Eq. 9.13 was intended for curved girders with a curvature parameter $Z_o \approx a^2/8Rt_w \leq 1$.

In Japan, a set of design guidelines for horizontally curved bridges was compiled by the Hanshin Expressway Public Corporation (1988). These guidelines are based on the working stress design approach and recommend use of the following interaction equation when designing a horizontally curved steel girder:

$$\frac{f_b}{(F_{ba})_c} + \frac{f_w}{F_{bao}} \leq 1 \tag{9.14}$$

where f_b is the normal flexural stress, f_w the normal stress resulting from the nonuniform torsion due to curvature only, $(F_{ba})_c$ the allowable flexural compressive stress for a curved girder calculated as a reduction of the allowable stress of a straight I-girder according to the Japanese specification, and F_{bao} the yield stress of the steel.

To gain some insight into the performance of various ultimate strength equations presented thus far, an elementary parametric study was conducted with respect to one of the horizontally curved steel girder specimen tested by Nakai et al. (1984a). The specimen is labeled M2 whose cross-sectional dimensions, unbraced length (L), and the yield stress for both the flanges and the web are shown in Fig. 9.1. Results from the parametric study are plotted on a coordinate system in which the abscissa represents the unbraced length over the girder radius (L/R) and the ordinate represents the nondimensional ratio of the ultimate moment over the plastic moment, M_u/M_p. The ultimate moment M_u was calculated for specimen M2 using all four ultimate moment predictors as presented in (1) the AASHTO guide specifications for Horizontally Curved Highway Bridges (AASHTO, 1993), (2) the Hanshin Expressway Public Corporation (1988), (3) Fukumoto and Nishida's Eq. 13, and (4) Nakai et al.'s Eq. 14. It should be pointed out that the factors of safety were removed from all criteria so that a fair comparison could be made. Two cases for each predictor equation were considered. In the first case, M_u was calculated for a wide range of unbraced lengths while keeping the remaining geometrical and material properties of specimen M2 unchanged. In the second case, M_u was calculated for a wide range of radii while keeping the remaining geometrical and material data unchanged. The results plotted in Fig. 9.2 reveal that all predictors, except that of Nakai et al. (1984c), exhibit the same trend in the sense that as the L/r ratio increases, M_u decreases. Nakai et al.'s equation shows (1) an increase in M_u as L/R increases (when R was the variable), and (2) an initial increase in M_u as L/R increases (for low values of L/R with L being the variable), followed by a decrease in M_u as L/R increases. This anomalous behavior can be attributed to the fact that Nakai et al.'s equation is based on a curve-fitting approach valid for the limited data point used in the progression analysis. Further examination of Fig. 9.2 shows that the AASHTO approach is most conservative, followed by the Hanshin and Fukomoto criteria, respectively. In all cases the experimental test data were higher than the results from the predictors, perhaps due to the discrepancy of appropriately modeling the boundary conditions. Finally, all predictor equations resulted in two distinct ultimate moment values for a single L/R value, thus failing to predict a unique answer.

In addition to the bending strength, the ultimate strength of curved I-girders under shear and under combined shear and bending were addressed by Nakai et al. (1984a,b) and by Kitada et al., who concluded that Rockey and Škaloud's (1975) model for straight plate girders can be used to estimate the ultimate shear strength in curved girders as long as the curvature parameter $Z_o < 1$ (virtually all experiments conducted by the Japanese researchers had $a/d < 1$). Interaction curves related to the ultimate strength under combined

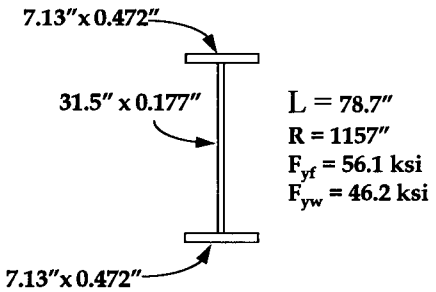

Fig. 9.1 Cross-sectional dimensions.

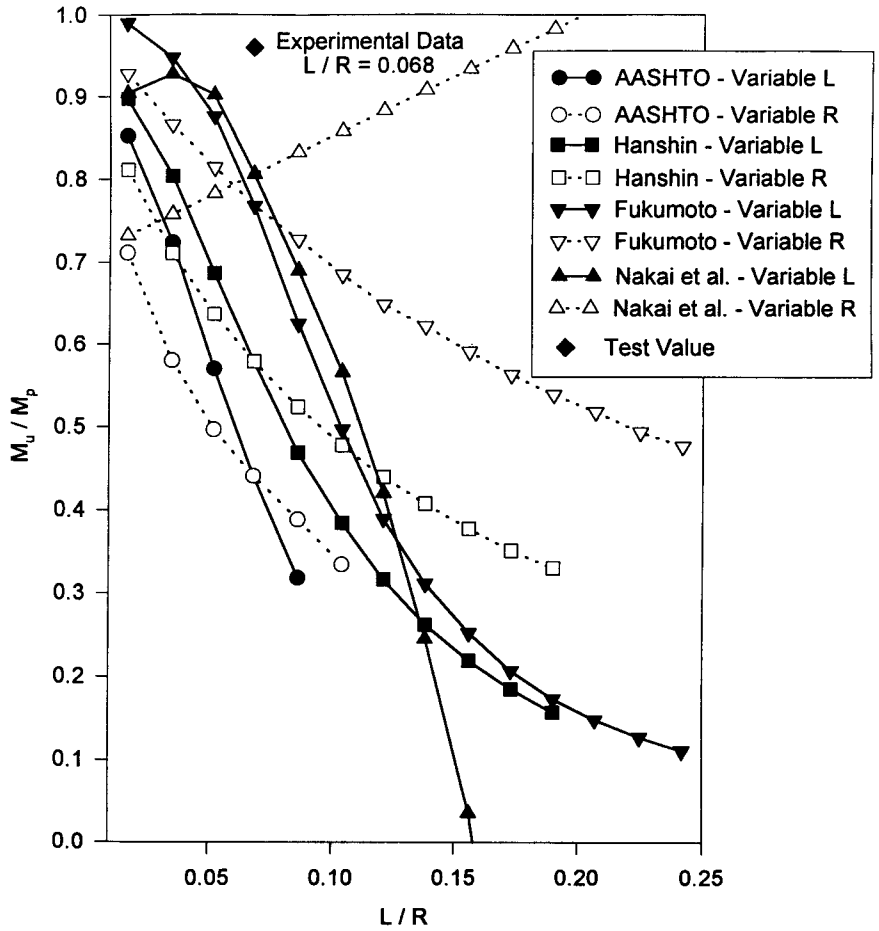

Fig. 9.2 Comparison of design theories with test result.

bending and shear were also provided. The Japanese technical papers by Mikami et al. (1980), Kuranishi and Hiwatashi (1981), and Nakai et al. (1984a, 1985a) form the basis for the ultimate strength studies discussed briefly earlier in this section.

9.5 DIAPHRAGMS, CROSS FRAMES, AND LATERAL BRACING

In 1986, Yoo and Littrell used the computer program SAP to study the effects of cross-bracing in curved bridges. A single-span curved bridge consisting of six 1.52-m (60-in.)-deep plate girders spaced 2.75 m (9 ft) apart was modeled using eight-noded brick elements and truss members. The bridge model was then analyzed under dead and live loads for different curvatures. The parametric study results were analyzed by linear and nonlinear regression and resulted in the development of the following design equation for the maximum bracing spacing:

$$S_{max} = L\left[-\ln\left(\frac{F_{ws}}{18.890}\frac{R}{L}\right)\right]^{-1.3364} \tag{9.15}$$

where F_{ws} is a factor for warping stress due to dead and live loads. It is usually selected arbitrarily but should be kept less than 0.5.

In 1989, Schelling et al. presented a study concerning the construction effects of bracing on curved I-girders. In this study the authors considered the response of single- and continuous-span, horizontally curved single- and multigirder bridges under the girder's self-weight and placement of the concrete deck. The effects of top and bottom lateral bracing systems during construction were also studied. The investigation resulted in a set of equations that define the dead-load distributions throughout the superstructure system analyzed by the two-dimensional grid method.

9.6 CONCLUDING REMARKS

It can be concluded from this chapter that the behavior of curved steel girders is one of the least understood structural forms and one of the few remaining unexplored frontiers of structural engineering research. Recognizing this fact, the Federal Highway Administration (FHWA), along with a number of state highway agencies in the United States, initiated studies with the primary objective of conducting fundamental analytical and experimental research examining the behavior of curved steel I-girders, addressing constructibility issues, and providing data for the eventual development of load and resistance factor design provisions for horizontally curved steel bridges. All these projects are currently ongoing.

9.7 REFERENCES

AASHTO (1980), *Guide Specifications for Horizontally Curved Highway Bridges*, American Association of State Highway Transportation Officials, Washington, D.C.

AASHTO (1987), *Guide Specifications for Horizontally Curved Highway Bridges, 1980*, as Revised by interim specifications for bridges, 1981, 1982, 1984, 1985, 1986, American Association of State Highway Transportation Officials, Washington, D.C.

AASHTO (1993), *Guide Specifications for Horizontally Curved Highway Bridges*, American Association of State Highway Transportation Officials, Washington, D.C.

AASHTO-ASCE Committee on Flexural Members (1973), "Survey of Curved Girder Bridges," *Civ. Eng.*, Vol. 43, No. 2, pp. 54–56.

Abdel-Sayed, G. (1973), "Curved Webs Under Combined Shear and Normal Stresses," *ASCE J. Struct. Div.*, Vol. 99, No. ST3, pp. 511–525.

ASCE–AASHTO Task Committee on Curved Girders (1977), "Curved I-Girder Bridge Design Recommendations," *ASCE J. Struct. Div.*, Vol. 103, No. ST5, pp. 1137–1167.

ASCE–AASHTO Task Committee on Curved Girders (1978a), "Curved Steel Box-Girder Bridges: A Survey," *ASCE J. Struct. Div.*, Vol. 104, No. ST11, p. 1697.

ASCE–AASHTO Task Committee on Curved Girders (1978b), "Curved Steel Box-Girder Bridges: State-of-the-Art," *ASCE J. Struct. Div.*, Vol. 104, No. ST11, pp. 1719–1739.

Brennan, P. J. and Mandel, J. A. (1973), "User's Manual: Program for Three-Dimensional Analaysis of Horizontally Curved bridges," *Syracuse Univ. Rep. Res. Proj. HPR-2(111)*, June.

Culver, C. G. (1971), "Flange Proportions for Curved Plate Girders," *J. Highw. Res. Board*, Vol. 354, pp. 61–66.

Culver, C. G., and Frampton, R. E. (1970), "Local Instability of Horizontally Curved Members," *ASCE J. Struct. Div.*, Vol. 96, No. ST2, pp. 245–265.

Culver, C. G., and McManus, P. (1971), *Instability of Horizontally Curved Members: Lateral Buckling of Curved Plate Girders*, Department of Civil Engineering, Carnegie-Mellon University, Pittsburgh, Pa., p. 203.

Culver, C. G., and Nasir, G. (1969), *Instability of Highway Curved Bridges: Flange Buckling Studies*, Carnegie-Mellon University, Pittsburgh, Pa., and Pennsylvania Department of Transportation, Bureau of Public Roads, Harrisburg, Pa.

Culver, C. G., and Nasir, G. (1971), "Inelastic Flange Buckling of Curved Plate Girders," *ASCE J. Struct. Div.*, Vol. 97, No. ST4, pp. 1239–1256.

Culver, C. G., Dym, C., and Brogan, D. (1972a), "Bending Behaviors of Cylindrical Web Panels," *ASCE J. Struct. Div.*, Vol. 98, No. ST10, pp. 2201–2308.

Culver, C. G., Dym, C., and Brogan, D. (1972b), *Instability of Horizontally Curved Members: Shear Buckling of Cylindrical Web Panels*, Carnegie-Mellon University, Pittsburgh, Pa.

Culver, C. G., Dym, C. L., and Uddin, T. (1973), "Web Slenderness Requirements for Curved Girders," *ASCE J. Struct. Div.*, Vol. 99, No. ST3, pp. 417–430.

Dabrowski, R. (1968), *Curved Thin-Walled Girders: Theory and Analysis (Gekrümmte dünnwandige Träger: Theorie und Berechnung)*, Springer Verlag, Berlin.

Daniels, J. H., Fisher, J. W., and Yen, B. T. (1980), "Fatigue of Curved Steel Bridge Elements: Design Recommendations for Fatigue of Curved Plate Girder and Box Girder Bridges," *Rep. No. FHWA-RD-79-138*, Federal Highway Administration, Washington, D.C., p. 60.

Fiechtl, A. L., Fenves, G. L., and Frank, K. H. (1987), "Approximate Analysis of Horizontally Curved Girder Bridges," *Final Rep. No. FHWA-TX-91-360-2F*, University of Texas at Austin, Center for Transportation Research, Austin, Texas, p. 96.

Frampton, R. (1968), "Local Instability of Horizontally Curved Members," Master's thesis, Carnegie-Mellon University, Pittsburgh, Pa.

Fukumoto, Y., and Nishida, S. (1981), "Ultimate Load Behavior of Curved I-Beams," *ASCE J. Eng. Mech. Div.*, Vol. 107, No. EM-2, pp. 367–385.

Galambos, T. V. (1978), "Tentative Load Factor Design Criteria for Curved Steel Bridges," *Res. Rep. No. 50*, School of Engineering and Applied Science, Civil Engineering Department, Washington University, St. Louis, Mo., May.

Hanshin Expressway Public Corporation (1988), "Guidelines for the Design of Horizontally Curved Girders," *draft report.*

Hsu, Y. T. (1989), "The Development and Behavior of Vlasov Elements for the Modeling of Horizontally Curved Composite Box Girder Bridge Superstructures," Ph.D. dissertation, University of Maryland, College Park, Md.

Kang, Y. J., and Yoo, C. H. (1990), "Flexural Stress of Curved Bridge Girders," *Proc. SSRC Annu. Tech. Session, Stability of Bridges*, St. Louis, Mo. Apr. 10–11: *Fritz Eng. Lab. Rep. No. 7*, Lehigh University, Bethlehem, Pa.

Ketchek, K. F. (1969), "Discussion of 'Horizontally Curved Girders: State of the Art' by McManus, P. F. et al.," *ASCE J. Struct. Div.*, Vol. 95, No. ST12, pp. 2999–3001.

Kitada, T., Ohminami, R., and Nakai, H. (1986), "Criteria for Designing Web and Flange Plates of Horizontally Curved Plate Girders," *Proc. SSRC Annu. Tech. Session, Stability of Plate Structures*, Washington, D.C. Apr. 15–16, pp. 119–130.

Kitada, T., Nakai, H., and Murayama, Y. (1993), "State-of-the-Art on Research, Design and Construction of Horizontally Curved Bridges in Japan," *Proc. SSRC Annu. Tech. Session*, Milwaukee, Wis.

Komatsu, S., and Kitada, T. (1981), "Ultimate Strength Characteristics of Outstanding Steel Plate with Initial Imperfection Under Compression," *Jpn. Soc. Civ. Eng.*, Vol. 314, pp. 15–27.

Kuo, S. R., and Yang, Y. B. (1991), "New Theory on Buckling of Curved Beams," *ASCE J. Eng. Mech. Div.*, Vol. 117, No. 8, pp. 1698–1717.

Kuranishi, S., and Hiwatashi, S. (1981), "Elastic Behavior of Web Plates of Curved Plate Girders in Bending," *Proc. Jpn. Soc. Civ. Eng.*, Vol. 315, pp. 1–11.

Mariani, N., Mozer, J. D., Dym, C. L., and Culver, C. G. (1973), "Transverse Stiffener Requirements for Curved Webs," *ASCE J. Struct. Div.*, Vol. 99, No. ST4, pp. 757–771.

McManus, P. F. (1972), "Lateral Buckling of Curved Plate Girders," Ph.D. dissertation, Carnegie-Mellon University, Pittsburgh, Pa.

McManus, P. F., Nasir, G. A., and Culver, C. G. (1969), "Horizontally Curved Girders: State of the Art," *ASCE J. Struct. Div.*, Vol. 95, No. ST5, pp. 853–870.

Mikami, I., and Furunishi, K. (1984), "Nonlinear Behavior of Cylindrical Web Panels," *ASCE J. Eng. Mech. Div.*, Vol. 110, No. EM2, pp. 230–251.

Mikami, I., Furunishi, K., and Yonezawa, H. (1980), "Nonlinear Behavior of Cylindrical Web Panels Under Bending," *Proc. Jpn. Soc. Civ. Eng.*, Vol. 288.

Mozer, J., Ohlson, R., and Culver, C. G. (1971), "Horizontally Curved Highway Bridges: Stability of Curved Plate Girders," *Rep. No. P2 res. Proj. HPR-2(111)*, Carnegie-Mellon University, Pittsburgh, Pa.

Nakai, H., and Yoo, C. H. (1988), *Analysis and Design of Curved Steel Bridges*, McGraw-Hill, New York, p. 768.

Nakai, H., Kitada, T., and Ohminami, R. (1984a), "Experimental Study on Ultimate Strength of Web Panels in Horizontally Curved Girder Bridges Subjected to Bending, Shear and Their Combinations," *Proc. SSRC Annu. Tech. Session, Stability Under Seismic Loading*, San Francisco, Apr. 10–11, pp. 91–102.

Nakai, H., Kitada, T., Ohminami, R., and Fukumoto, K. (1984b), "Experimental Study on Shear Strength of Horizontally Curved Plate Girders," *Jpn. Soc. Civ. Eng.*, Vol. 350, pp. 281–290.

Nakai, H., Kitada, T., Ohminami, R., and Fukumoto, K. (1984c), "A Proposition for Designing Transverse Stiffeners of Horizontally Curved Girders in Ultimate State," *Mem. Fac. Eng. Osaka City Univ.*, Vol. 25, pp. 111–131.

Nakai, H., Kitada, T., and Ohminami, R. (1985a), "Experimental Study on Bending Strength of Web Plates of Horizontally Curved Girder Bridges," *Jpn. Soc. Civ. Eng.*, Vol. 15, pp. 201–203.

Nakai, H., Kitada, T., Ohminami, R. (1985b), "Proposition for Designing Intermediate Transverse Stiffeners in Web Plate of Horizontally Curved Girders," *Jpn. Soc. Civ. Eng.*, Vol. 361/I-4, pp. 249–257.

Nishida, S., Yoshida, H., and Fukumoto, Y. (1978), "Large Deflection Analysis of Curved Members with Thin-Walled Open Cross-Section," *24th Symp. Struct. Eng.*, pp. 77–84.

Pandit, G. S., Ceradini, G., Grvarini, P., and Eremin, A. A. (1970), "Discussion of 'Horizontally Curved Girders: State of the Art' by McManus, P.F. et al.," *ASCE J. Struct. Div.*, Vol. 96, No. ST2, p. 433–436.

Papangelis, J. P., and Trahair, N. S. (1986), "Flexural-Torsional Buckling of Arches," *ASCE J. Struct. Div.*, Vol. 113, No. ST4, pp. 889–906.

Papangelis, J. P., and Trahair, N. S. (1987), "Flexural-Torsional Buckling Tests on Arches," *ASCE J. Struct. Div.*, Vol. 113, No. ST7, pp. 1433–1443.

Poellot, W. N. (1987), "Computer-Aided Design of Horizontally Curved Girders by the V-Load Method," *AISC Eng. J.*, Vol. 24, No. 1, pp. 42–50.

Rajasekaran, S., and Ramin, E. (1984), "Discussion of 'Flexural-Torsional Stability of Horizontally Curved Beams' by C. H. Yoo," *ASCE J. Eng. Mech. Div.* Vol. 110, No. EM1, pp. 144–148.

Rajasekaran, S., Sundaraajan, T., and Rao, K. S. (1988), "Discussion of 'Static Stability of Curved Thin-Walled Beams' by Yang, Y. B. and Kuo, S. R.," *ASCE J. Struct. Div.*, Vol. 114, No. ST5, pp. 915–918.

Rockey, K. C., and Škaloud, M. (1975), "The Ultimate Load Behavior of Plate Girder Loaded in Shear," *Struct. Eng.*, Vol. 53, No. 8, pp. 313–325.

Schelling, D., Namini, A. H., and Fu, C. C., (1989), "Construction Effects on Bracing on Curved I-Girders," *ASCE J. Struct. Div.*, Vol. 115, No. ST9, pp. 2145–2165.

Stegmann, T. H., and Galambos, T. V. (1976), "Load Factor Design Criteria for Curved Steel Girders of Open Section," *Res. Rep. 23*, Civil Engineering Department, Washington University, St. Louis, Mo., Apr.

Stussi, F. (1943), "Lateral Buckling and Vibration of Arches," *J. Int. Assoc. Bridge Struct. Eng.*, Vol. 7, pp. 327–343.

Tan, C. P., Shore, S., and Ketchek, K. (1969), "Discussion of 'Horizontally Curved Girders: State of the Art' by McManus, P. F. et al.," *ASCE J. Struct. Div.*, Vol. 95, No. ST12, pp. 2997–2999.

Timoshenko, S. P., and Gere, J. M. (1961), *Theory of Elastic Stability*, 2nd ed., McGraw-Hill, New York.

Tokarz, F. J. (1968), "Lateral Torsional Buckling of Arches," Ph.D. dissertation, Ohio State University, Columbus, Ohio.

Tokarz, F. J. (1971), "Experimental Study of Lateral Buckling of Arches," *ASCE J. Struct. Div.*, Vol. 97, No. ST2, pp. 545–559.

Vacharjittiphan, P., and Trahair, N. S. (1975), "Flexural–Torsional Buckling of Curved Members," *ASCE J. Struct. Div.*, Vol. 101, No. ST6, pp. 1223–1238.

Vlasov, V. Z. (1961), *Thin-Walled Elastic Beams*, National Science Foundation, Washington, D.C.

Wachowiak, J. (1967), "Die Berechung gekrümmter Stege von dünnwandigen Trägern auf Grund der Schalen Theorie," Ph.D. dissertation, Politechnika, Poland.

Yang, Y. B., and Kuo, S. R. (1986), "Static Stability of Curved Thin-Walled Beams," *ASCE J. Eng. Mech. Div.*, Vol. 112, No. ST8, pp. 821–841.

Yang, Y. B., and Kuo, S. R. (1987), "Effect of Curvature Stability of Curved Beams," *ASCE J. Struct. Div.*, Vol. 113, No. ST6, pp. 1185–1202.

Yang, Y. B., Kuo, S. R., and Yau, J. D. (1991), "Use of Straight-Beam Approach to Study Buckling of Curved Beams," *ASCE J. Struct. Div.*, Vol. 117, p. 1963.

Yoo, C. H. (1982), "Flexural–Torsional Stability of Curved Beams," *ASCE J. Eng. Mech. Div.*, Vol. 108, No. EM6, pp. 1351–1369.

Yoo, C. H., and Carbine, R. L. (1985), "Experimental Investigation of Horizontally Curved Steel Wide Flange Beams," *Proc. SSRC Ann. Tech. Session, Stability Aspects of Industrial Buildings*, Cleveland, Ohio, Apr. 16–17, pp. 183–191.

Yoo, C. H., and Littrell, P. C. (1986), "Cross-Bracing Effects in Curved Stringer Bridges," *ASCE J. Struct. Div.*, Vol. 112, No. ST9, pp. 2127–2140.

Yoo, C. H., and Pfeiffer, P. A. (1983), "Elastic Stability of Curved Members," *ASCE J. Struct. Div.*, Vol. 109, No. ST12, pp. 2922–2940.

Yoo, C. H., and Pfeiffer, P. A. (1984), "Buckling of Curved Beams with In-Plane Deformation," *ASCE J. Struct. Div.*, Vol. 110, No. ST2, pp. 291–300.

Yoshida, H., and Maegawa, K. (1983), "Ultimate Strength Analysis of Curved I-Beams," *ASCE J. Eng. Mech. Div.*, Vol. 109, No. 1, pp. 192–214.

Zureick, A., Naqib, R. and Yadlosky, J. M. (1993), "Curved Girder Bridge Research Project Intrim Report I: Synthesis" *Rep. No. FHWA-RD-93-129*.1

CHAPTER TEN

COMPOSITE COLUMNS AND STRUCTURAL SYSTEMS

10.1 INTRODUCTION

Composite structural members are members in which steel and concrete act together through mechanical interlock, friction, and adhesion. Composite members are designed to maximize the efficiency of the two materials by using, whenever possible, the concrete in compression and the steel in tension. In addition to exploiting the stress-strain characteristics of the two materials to increase the ultimate capacity of the member, composite systems attempt to gain additional benefits from the synergy of their interaction. For example, the concrete can be used to limit global and local buckling problems in the thinner steel elements, and the steel in tubular and round sections can be used to increase the confinement of the concrete and thus help to maintain its strength in the post-peak region.

Buildings are seldom constructed only of composite members. Most often, composite columns are used in the lateral load–resisting systems in combination with either other composite members to form composite systems, or with other types of structural elements to form hybrid systems (Goel and Yamanuchi, 1993; Yamanuchi et al., 1993; Deierlein, 1995; Deierlien and Leon, 1997). Composite members are very popular in floor systems where composite beams, stub girders, and composite joists and trusses are the most economical alternatives in mixed-use structures (Viest et al. 1996). The stability benefits derived from the presence of a floor slab for floor members are not addressed in this chapter. However, it should be noted that additional care needs to be taken in negative moment regions of composite flexural members to

ensure that the required rotational capacity is reached (Dekker et al. 1995). Thus, utilizing the beneficial aspects of composite action requires design checks that are different from those typical reinforced concrete or steel construction. Additional stability design provisions from composite beams with web openings and for composite joists and trusses are also available from an ASCE Task Group on Composite Design (ASCE 1994a; ASCE Task Committee, 1996).

In addition to floors systems, composite members are also being utilized as lateral load–resisting elements in braced and wall systems. In braced systems composite elements are desirable because they delay both global and local buckling, strengthening and stiffening the system significantly more than with conventional steel bracing (Liu and Goel, 1988). In wall systems composite members are being used to facilitate the connection between reinforced concrete walls and steel frames in hybrid systems, and to delay shear cracking and improve hysteretic performance in reinforced concrete systems (Harries et al., 1993; Shahrooz et al., 1993). Descriptions of composite and hybrid structural systems are given elsewhere (Griffis, 1986, 1992; NEHRP, 1994), and this chapter is concerned primarily with stability effects related to composite columns and their connections. Composite columns are formed either by encasing a steel shape in concrete (called *SRC construction*) or by filling a structural pipe or tube with concrete (*CFT construction*). There are many possible variations of composite columns (Figs. 10.1 and 10.2), but they are generally used in the following situations:

- As encased shapes in columns forming perimeter frames in high-rise structures. In this case prefabricated steel column "trees," consisting of one- or two-story columns and short beam stubs on either side, are often used as erection columns and later encased in concrete. In this case the encasement is used mainly to increase the stiffness of the columns and reduce the drift under wind or seismic loads. Examples of this type of application are the Gulf Tower and First City Tower in Houston (Griffis, 1992).
- As very large encased shapes or round concrete-filled sections acting as the corner columns for innovative structural systems in high-rise construction. In these systems the steel section is small and is used primarily for erection purposes in the case of encased shapes and for formwork in the case of concrete-filled tubes. Examples of this type of application are the Bank of China in Hong Kong, Two Union Square in Seattle, and the Norwest Center in Minneapolis (Griffis, 1992; Leon and Bawa, 1990).
- As encased shapes in special situations where the amount of steel required would exceed the maximum permitted by current codes in a concrete section.
- As transition columns between reinforced concrete and steel columns. This situation often arises in office buildings with a reinforced concrete parking garage occupying the first few floors and a lighter steel frame making up most of the upper stories.

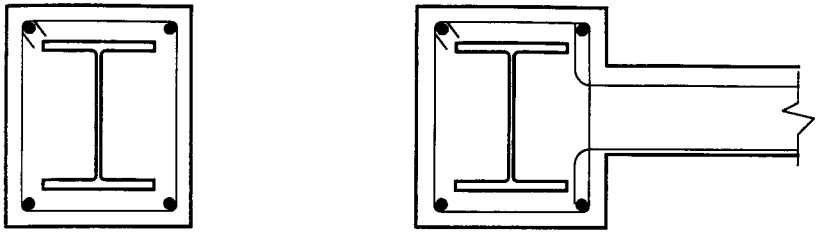

(a) Encased composite section as an isolated column or boundary element on a shear wall

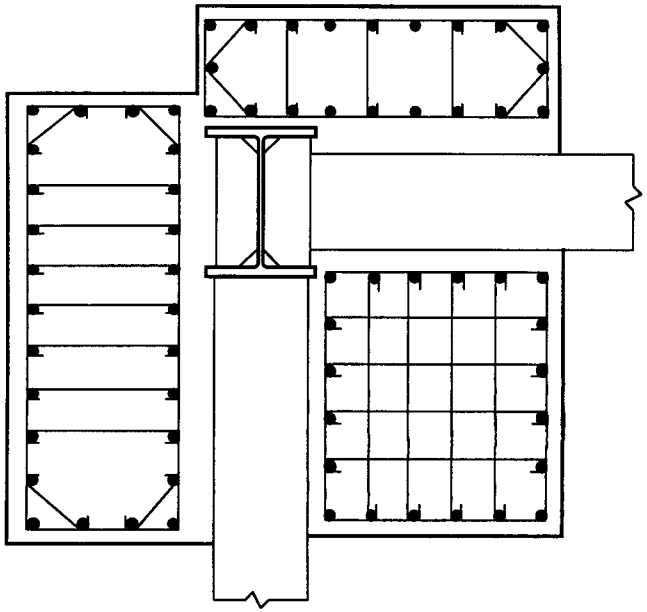

(b) Large encased composite section where steel column is used primarily as an erection column. Section shows full moment connection to two steel beams and three large reinforcing cages (not all details shown)

Fig. 10.1 Typical cross sections for encased composite columns.

- As concrete-filled tubes in structures with high story heights where the additional stiffness provided by the concrete reduces the slenderness ratio of the column.
- As columns in areas where impact and/or fire protection are crucial.
- As the main seismic load-resisting system. Extensive use is made of both encased shapes and concrete-filled sections in other countries, particularly Japan, for seismic design.

Until recently most applications of composite columns have been in high-rise structures. Applications of composite columns in low-rise structures in the

(a) Typical round and tubular composite sections

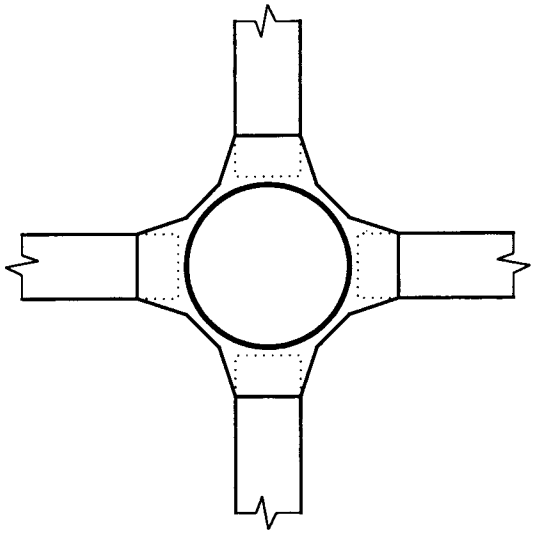

(b) Bidirectional moment connection to a concrete-filled tube utilizing flared stiffeners

Fig. 10.2 Typical cross sections for concrete-filled tubes.

United States is scant because of the perceived poor cost/benefit ratio. For SRC construction this is due to the need to have several construction trades on site and to the expense of forming reinforcing cages in situ. For CFT construction most problems arise from connections and fire protection. Many of these objections can be overcome with prefabrication and use of newer technologies (blind bolts for connections, for example). Moreover, as design provisions evolve and new design recommendations are adopted, it is likely that more extensive use of composite columns and other forms of composite construction will be made in the near future (see NEHRP 1994, chap. 7).

The advantages of composite construction were recognized early this century (Talbot and Lord, 1912), and most multistory buildings were built with composite columns for fire protection until lightweight, sprayed fireproofing became available. Recently, composite members and systems are becoming

popular again, primarily because of their stiffness characteristics (Griffis, 1992) and seismic resistance (Goel and Yamanuchi, 1993). Two excellent complementary references on composite construction for buildings have recently become available: one for fundamental mechanics issues (Oehlers and Bradford, 1995) and one for practical issues (Viest et al., 1996). The reader is referred to these for more detailed discussions of many of the issues addressed in this chapter. In addition, the proceedings of several recent international conferences provide an up-to-date overview of recent experimental research and analytical advances (Roeder, 1985a; Buckner and Viest 1988; Wakabayashi 1991; Easterling and Roddis, 1993; Javor, 1994; Buckner and Shahrooz, 1997). No attempt is made in this chapter to summarize this extensive literature. For older research, on which many of the current design provisions are based, the reader is referred to the third edition of this guide (Johnston, 1976). For a complete history of the development of composite construction, the reader is referred to Viest et al. (1996, Chap. 1).

10.2 CROSS-SECTIONAL STRENGTH OF COMPOSITE SECTIONS

Since real columns are seldom loaded in pure compression, it is useful to study composite column behavior from a beam-column standpoint. The flexural strength (M) at any given axial load (P) can be calculated by assuming a position of the neutral axis, drawing the stress distributions, and summing their moments about the plastic neutral axis. This locus of points is shown as solid lines in Fig. 10.3, which schematically illustrate the ultimate strength of SRCs and CFTs. The lines correspond to the "exact" solution when nonlinear constitutive models are used for both steel and concrete, and the effect of confinement is appropriately modeled. To compute the capacities, a process analogous to that for any reinforced concrete beam-column, in which the reinforcing bars are transformed into an equivalent thin steel section, can be used. This method is both tedious and computationally intensive, but computer programs based on subdividing the cross section into small elements (finite elements of fiber models) are available for both SRC and CFT sections (Mahin and Bertero, 1977; Gourley and Hajjar, 1994; El-Tawil et al., 1995; Gourley et al., 1995). Many commercial reinforced concrete computer design packages include some variation of the Mahin and Bertero (1977) approach as an option. In general, all these models assume strain continuity between the steel and concrete portions, an assumption that is not supported by much of the data from experimental programs where the interface behavior was monitored. This assumption, however, appears to have negligible influence on the ultimate strength and relatively small influence on the stiffness of the cross section and simplifies the problem considerably.

The parabolic shape of the interaction curves is similar for SRCs and CFTs (Fig. 10.3). For SRCs, the difference in flexural capacity between the balance point (point D) and the pure flexure case (point B) decreases as the amount of

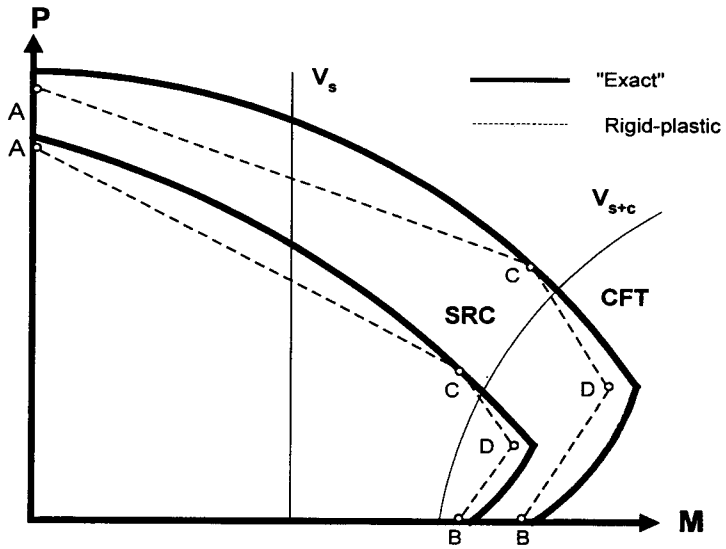

Fig. 10.3 Interaction curve for a composite section.

structural steel and longitudinal steel reinforcement increases. Increases in the yield strength of the structural steel, from, say, an A36 to an A572 material, significantly increase the capacity of the section at both points B and D. As one would expect, increases in concrete strength do not seem to have a major effect on the flexural strength at point B since steel yielding governs the strength, but they tend to increase the distance between points B and D in the interaction diagram. For most CFTs the shape in Fig. 10.3 is preserved since in the limit the CFT section can be modeled as a reinforced concrete section with distributed steel. For circular CFTs, however, the balance point tends to lie higher in the axial load axis than that of a comparable SRC or rectangular CFT section. In addition, for CFTs the difference in moment capacity between the balance and no axial load points tends to be higher as the concrete strength increases and/or the tube slenderness increases because the addition of axial load increases the contribution of the concrete compression block. These differences are illustrated, schematically, by the "exact" CFT and "exact" SRC curves in Fig. 10.3. It should also be noted that for CFTs the effect of the wall slenderness (D/t ratio) has a significant impact on the postpeak strength as the axial load level increases (Bridge and Webb, 1993). While the presence of the infill concrete tends to increase the resistance to local buckling by a factor of up to 1.5 above that of hollow sections (Matsui and Tsuda, 1987), failures controlled by concrete crushing tend to be very brittle since the beneficial effect of the confinement provided by the steel cannot be maintained. For square hollow sections, Bridge and O'Shea (1996a) found that the concrete infill provided

restraint to inward local buckling that enhanced the tube strength over that for a hollow bare steel tube, and that the enhancement could be taken into account using steel design specifications and codes that allowed for the increase in the elastic local buckling coefficient associated with the change in buckling mode. Contrary to some other research, O'Shea and Bridge (1996) found that the concrete infill did not enhance the axial strength of circular tubes as the buckling mode was predominantly outward.

Most analytical studies show that the differences between the results of this type of "exact" approach and those given by a simplified theory using rigid-plastic stress blocks such as those shown in Fig. 10.4, are small and insignificant for design (Roik and Bergman, 1992). This is shown schematically in

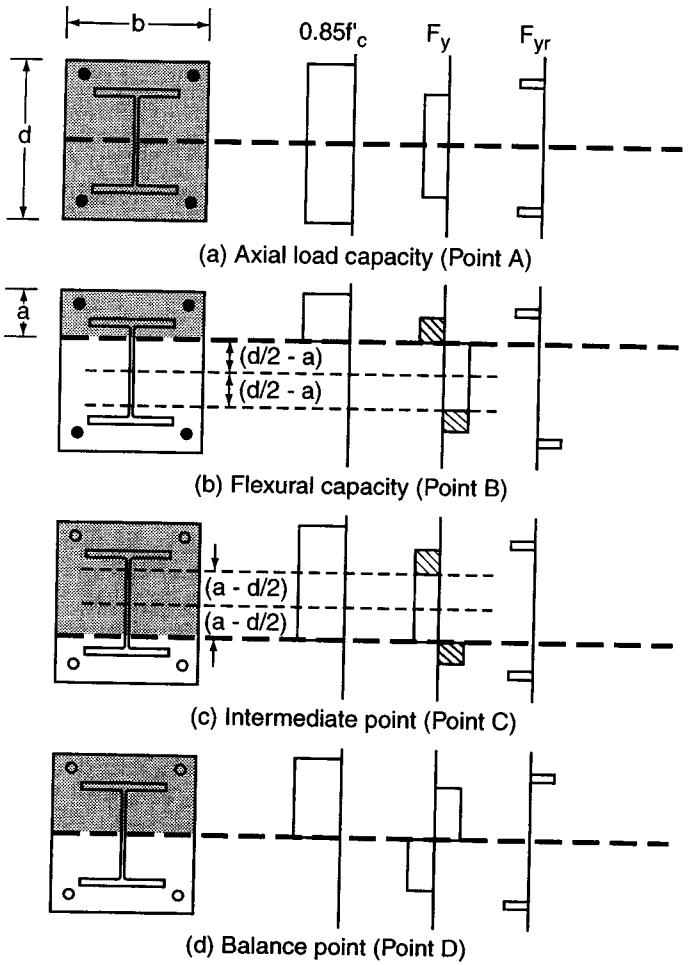

Fig. 10.4 Stress distributions for key points on the interaction diagram.

Fig. 10.3. The axial and flexural strengths are determined by assuming nominal yield strengths for the steel and 0.85 of the cylinder strength for the concrete. For encased shapes, Fig. 10.4 shows the plastic stress distribution for several of the points in the interaction surface shown in Fig. 10.3. The axial strength, P_u, is (Fig. 10.4a)

$$P_u = 0.85f_c'(db - A_s - A_r) + A_sF_y + A_rF_{yr} \tag{10.1}$$

where

f_c' = concrete cylinder strength
d = overall depth
b = width
F_y = Yield strength of steel shape
F_{yr} = yield strength of longitudinal reinforcement
A_s = area of the steel shape
A_r = area of longitudinal reinforcement

A simple and elegant solution for other important points in the interaction surface for the rigid plastic case can be found by following the procedure proposed by Roik and Bergmann (1989, 1992). Consider the typical case of an encased shape bent about its major axis and having only four bars as longitudinal reinforcement. If one assumes that the neutral axis lies in the web of the steel beam, the plastic stress distributions for points B through D in Fig. 10.3 correspond to the stress distributions in Fig. 10.4*b* through *d*. Points B and C correspond, respectively, to the case of no axial load and to an apparently arbitrary point in the interaction diagram above the balance point. In fact, points B and C correspond to the same moment because the stress blocks lying within the distance h_n in both Fig. 10.4*b* and *c* have their centroid at the plastic neutral axis and thus do not contribute to the plastic bending capacity of the section. In addition, it needs to be recognized from both Figs. 10.4*b* and *c* that the axial forces from the reinforcement and the shaded portions of the forces from the steel shape cancel out.

If one were to add the stress distributions in Figs. 104*b* and *c* and consider axial loads only, the total axial load (P_{conc}) would still be that at point C. From superimposing the stress blocks, this axial load will be that given by the concrete section alone under a uniform stress of $0.85f_c'$ since the contributions from the steel shape within the distance h_n also cancel out. Thus

$$P_{conc} = 0.85f_c'(bd - A_s - A_r) \tag{10.2}$$

The depth of the compression block, a, can then be calculated from Fig. 10.4*b* by assuming that the compressive force in the concrete is equal to the tensile force in the web of the steel shape within the distance $2h_n$. This leads to

$$a = \frac{t_w dF_y}{0.85f_c'b + 2t_wF_y} \tag{10.3}$$

A direct calculation for h_n, however, can be made by subtracting the stress distribution in Fig. 10.4*b* from that in Fig, 10.4*c*, and again considering only axial forces. In this case all stress blocks except those inside $2h_n$ disappear. Within this distance $2h_n$ the concrete will have a stress of $0.85f_c'$ while the steel will have a stress of $2F_y$. Since the total axial load is still P_{conc}, h_n is given by

$$h_n = \frac{P_{conc}}{2[0.85bf_c' + t_w(2F_y - 0.85f_c')]} \tag{10.4}$$

Knowing either h_n or a, the moment capacity of the section for both points B and C in Fig. 10.3 can easily be calculated.

The final point that needs to be defined is the balance point (point D). The maximum moment will be obtained when the neutral axis is at the centroid of the cross-section (Fig. 10.4*d*), since in this case all the forces are additive with respect to moment. From Fig. 10.4*d*, it is clear that all contributions to the axial load from the steel shape and reinforcement cancel out and that the axial load at this point thus corresponds to that of $0.85f_c'$ acting over half of the cross section, or $P_{CONC}/2$. The balance moment (M_{bal}) is given by

$$M_{bal} = Z_xF_y + 0.5bd^2f_c' + \sum_{i=1}^{n} A_{ri}d_{ri} \tag{10.5}$$

where Z_x is the plastic section modulus, A_{ri} the area of any rebar, and d_{ri} its distance to the plastic neutral axis.

Equations (10.1) through (10.5) permit a very quick and accurate calculation for the key points in the interaction curve. Although Fig. 10.4 and Eqs. (10.1) through (10.5) provide a solution for only the simplest case, the approach discussed above is general. It also applies for cases where the neutral axis is either in the flange of the steel shape or outside the steel shape, and for any number and bar-type distribution. Equations for bending about both axes and for concrete-filled shapes are given by Roik and Bergmann (1992) in a much more general format.

The use of simplified, ultimate strength approaches for calculating the ultimate strength of composite columns is not new. There is extensive analytical (Furlong, 1968; Knowles and Park, 1970; Chen and Chen, 1973; Virdi and Dowling, 1976; Duan and Chen, 1990; Gourley and Hajjar, 1994; Gourley et al., 1995) and experimental evidence for its use on both SRCs (Stevens, 1965; Furlong, 1967; Johnson and May, 1978; Ricles and Paboojian, 1994) and CFTs (Gardner and Jacobson, 1967 Knowles and Park, 1969; Neogi et al., 1969; Matsui and Tsuda, 1987; Cai, 1988; Shakir-Khalil and Zeghiche, 1989; Shakir-Khalil and Mouli, 1990; Ichinohe et al., 1991)

The two general approaches discussed above also apply for the case of biaxial bending. The exact approach only differs in that the assumed inclination of the neutral axis changes with respect to the principle axes of the cross section (El-Tawil et al., 1993). The validity of this approach has been verified experimentally (Morino et al., 1988, 1993) and analytically (Virdi and Dowling, 1973; Gourley and Hajjar, 1994). Although a rigid plastic approach is also possible in this case, it is not possible to derive simple, general equations for this case. A simplified approach utilizing the rigid plastic capacities computed for both principal axes has been proposed by Roik and Bergmann (1992) and adopted for the Eurocode (ECS 1994).

10.3 FORCE TRANSFER BETWEEN CONCRETE AND STEEL

Interaction between the steel and concrete portions of composite members results from a combination of chemical adhesion, friction, and mechanical interlock (mostly bearing). The most dependable composite action arises from the use of mechanical shear connectors (generally headed shear studs) that transfer the forces between the two materials by direct bearing and shear. From the strength standpoint, the studs need to be designed to transfer all the shear forces at the interface between the steel and concrete, consistent with the development of the plastic capacity of the cross section. This is labeled as full-strength shear connection. When fewer studs than these are provided, the system is said to be partial strength.

Although the concepts of full and partial strength are useful to describe the behavior of members such as composite beams where the two materials are in contact at a small and well-defined boundary, their application to composite columns is not straightforward. Studies have shown that the ultimate strength given by a rigid plastic approach is usually achieved by short composite columns under monotonic loading irrespective of whether or not mechanical force transfer is provided. Thus full strength is not as meaningful a design parameter in composite columns as it is in beams, except for the case where fatigue or seismic loadings govern the design. In such cases mechanical shear connectors should be provided since adhesion and friction are not reliable force transfer mechanisms under these types of loads.

Full and partial strength are different concepts from full and partial interaction. Full interaction implies continuity of strains and curvature across the steel concrete boundaries. Since most shear connectors provide a nonlinear shear strength versus slip behavior (i.e., some slip is needed before the resistance builds up) full interaction cannot be achieved in practice even at service load levels. In most practical cases the achievement of ultimate strength in composite systems requires substantial slip between the steel and concrete, resulting in severe discontinuities in the strain profile between the steel and concrete. Since most computer programs developed to calculate ultimate cross-sectional capacity rely on an assumption of strain compatibility between the

materials, one would expect that large discrepancies could occur between their predictions and available experimental results. However, this is not the case because at ultimate, while the strain discontinuities exist, their effect on the stresses is small since the materials are on fairly flat portions of their respective stress-strain curves. A powerful argument for proposing the use of rigid–plastic stress distributions for calculating composite member strength is that they circumvent the need to account for these discontinuities in interface strains. As long as the strains are larger than both the yield strain (F_y/E) for the steel and the strain consistent with the attainment of the maximum uniaxial strength (about 0.002 to 0.003) for the concrete, the stress distributions in Fig. 10.4 can be achieved. The use of rigid–plastic stress distributions also obviates the need to design for the perpendicular forces that develop at the interface if the steel and concrete are assumed to remain in contact. These forces are small except for areas adjacent to large concentrated loads (Robinson and Naraine, 1988), and can easily be handled by the horizontal projections (heads) of most mechanical connectors.

In both axially loaded specimens and flexural specimens, test results can be interpreted to imply that chemical adhesion provides a substantial contribution to the shear transfer in the service load range (Roeder, 1985b; Wium and Lebet, 1990a,b). Quantification of this effect is impossible given both the difficulties in measuring this property and the large scatter that can be expected from varying surface conditions, loading history, casting position, size effects, and concrete mix proportions, to name a few of the relevant variables.

At ultimate, and in the absence of mechanical shear connectors and adhesion, all the forces must be transferred by friction. The normal forces necessary for friction arise primarily from shear stresses and the differential expansion of the two materials under load. Shear stresses arise from moment gradients and the assumption of no vertical separation between the steel and concrete components (i.e., the assumption of equal curvatures in the steel and concrete portions). The differential expansion results from different values of Poisson's ratio (ν) and is dependent on the level of stress and the mix proportions. This effect is very different for SRCs and CFTs. At low levels of stress, the steel expands more than the concrete ($\nu \simeq 0.3$ for steel and $\nu \simeq 0.15$ to 0.20 for concrete in the elastic range). This does not result in any appreciable development of frictional forces unless all the load is introduced directly to the steel shape. As the concrete stresses increase over $0.5f_c'$, the dilatational behavior of the concrete begins to take over as microcracking progresses and the apparent ν of the concrete increases over that of the steel. In SRCs the confinement effect provided by ties is insignificant since the amounts of transverse reinforcement are volumetrically small and cross ties are typically not used. In CFTs, on the other hand, the expansion of the concrete is controlled by the steel section. For round tubes this results in large hoop stresses and the development of a very efficient confinement effect. This increases the nominal crushing strength of the concrete and helps maintain the strength in the post-peak regime of the stress-strain curve. The beneficial effects of the encasement

are present even in extreme cases where no shear connection is present and adhesion has been prevented with the use of lubricants (Orito et al., 1988). The hoop stresses, on the other hand, result in biaxial state of stress in the tube wall that can lead to early yielding or buckling. For rectangular and square CFTs the effect of confinement will be smaller because of the ineffectiveness of this type of cross section in developing hoop stresses. The amount of friction that can be developed depends primarily on the surface conditions, degree of compaction of the concrete, and any longitudinal out-of-straightness. While the experimental results for CFTs show this effect clearly (Virdi and Dowling, 1980), test results for SRCs are somewhat inconclusive in this area (Bryson and Mathey, 1973; Dobruszkes and Piraprez, 1981).

It should be clear from the discussion above that the force transfer between the steel and concrete portions of a composite member is a complex phenomenon. At this stage there are no mechanistic models that can address the numerous interactions described above adequately, nor are the experimental data needed to calibrate those models available. However, it is clear from the vast majority of the experimental results that a model that incorporates a sophisticated interface force transfer mechanism is not necessary to accurately predict the ultimate strength of a composite cross section. Rigid–plastic models such as the one described above or finite element and fiber model that assume no slip between the concrete and steel predict the ultimate strength equally well provided that the strains achieved in the model are large.

10.4 OTHER CONSIDERATIONS FOR CROSS-SECTIONAL STRENGTH

Designers should note that the latest information on high-strength concrete in compression indicates that the usual equivalent rectangular stress block, as shown in the stress distributions in Fig.10.4, may not be valid for high-strength concrete. The scant information on encased and concrete-filled composite columns with high-strength concrete (Prion and Boehme, 1989; Cederwall et al., 1990; Chen et al., 1992; Grauers, 1993) indicates that other types of stress distribution fit the results better as the concrete strength increases above 78 MPa (10 ksi). For SRCs this distribution tends to be triangular, just as it does for reinforced concrete sections (Collins et al., 1993), while for CFTs it is parabolic, reflecting the better postpeak confinement. The effect of transverse reinforcement on the concrete strength should generally be ignored when calculating ultimate strength, but designers should be conscious that transverse reinforcement will have a major effect on postpeak behavior. This if of particular importance under seismic loading, where strength and stiffness degradation will be influenced by the amount and distribution of transverse reinforcement. Designers should also understand that the confining effect decreases with increasing concrete strength since the amount of microcracking and resulting dilatatory behavior decreases with concrete strength. In addition, the effect of transverse steel is dependent on its spacing and presence of cross

ties for the case of encased sections and on the wall thickness for the case of concrete-filled tubes. O'Shea and Bridge (1996) have found that for the tube diameter-to-thickness ratios greater than 55 and concrete strengths in the range 110 to 120MPa, the steel tube provides virtually no confinement to the concrete when both the steel and concrete are loaded together. Confinement effects could be obtained only if the concrete was loaded and the steel was not bonded to the concrete. Unbonded tube construction has been considered by Orito et al. (1988).

The effect of shear on the ultimate axial and flexural strength depends primarily on the shear span (M/V) ration, the amount of axial load, and the detailing of the shear reinforcement. For a cross section with a large axial load and high shear span, it would appear that the shear resistance of the concrete and steel should be additive. Conversely, for a lightly loaded column with a low shear span, where a substantial portion of the concrete cross section may not be effective due to flexural or diagonal cracking, it would seem prudent to limit the shear strength to that of the steel section and the shear reinforcement. The differences in capacity computed from either set of assumptions are very large. This is illustrated schematically in Fig. 10.3, where the flexural capacity of any cross section can be limited by the capacity in shear given by either the steel alone (V_s) or the combined capacity (V_{s+c}). For this plot it was assumed that the column was in double curvature and that the ultimate moment capacity could be reached at either end ($V_s = 2M_{\text{ult}}/L = A_w F_{yw}$). For V_{s+c} note that the concrete capacity is dependent on the axial load, and thus the function is nonlinear.

The rigid–plastic stress distributions discussed in Section 10.2 are consistent with an assumption of uniform shear throughout the web. To calculate the ultimate strength properly, the web yield stress ($F_{y,\text{web}}$) should be reduced to

$$F_{y,\text{web}} = \sqrt{F_y - 2\tau_w^2} \tag{10.6}$$

$$\tau_w = \frac{V}{dt_w} \tag{10.7}$$

where V is the shear at the cross section d in the depth of the steel member and t_w is the thickness of the web of the steel section. Note that the shear will be the dominant failure mode in many columns used in seismic areas; for that design case, careful detailing for shear transfer is needed.

10.5 LENGTH EFFECTS

In principle, the design of a composite column for stability should be no different from that for a reinforced concrete or steel column. However, two

interrelated problems, one practical and one philosophical, arise when considering a composite section. The practical problem centers around how to compute an effective moment of inertia of the member for stability and drift calculations. This process is not straightforward because it is difficult to characterize the amount of cracking in the concrete. This cracking arises both from the type of loading and the long-term behavior of the concrete. Insofar as loading is concerned, the amount of cracking that can occur is a function of the level of axial load, how the loads are introduced into the column (i.e., connection details and sequence of construction), and the tensile capacity of the concrete. On the other hand, long-term effects such as creep and shrinkage are viscoelastic, time-dependent processes (Bradford and Gilbert, 1990; Oehlers and Bradford, 1995). Creep behavior is influenced primarily by the level of sustained axial load, the age at loading, and by material properties (type of cement, water/cement ratio, and aggregate characteristics). Shrinkage is influenced by both material properties and curing conditions (temperature, humidity). In general, these phenomena are important at the service level but do not play a major role at ultimate loading (Bridge, 1979, 1988; Nakai et al., 1991; Leon and Bawa, 1990). Creep and shrinkage can be important at both the member and system levels. An example of the latter are the forces that arise as the result of differential creep and shrinkage in high-rise structures that incorporate a perimeter frame and internal core walls. In practice, many of the problems associated with creep and shrinkage can be mitigated by proper material selection and careful construction sequences. At the design stage, however, many of these details are not known, and thus highly simplified and conservative approaches need to be taken. Most codes resort to assuming empirically that only a portion of the transformed area is effective when the ultimate strength is reached.

The philosophical problem is a much more serious one and arises from the very different approaches to stability calculations taken by the writers of codes for reinforced concrete and steel (Deierlein and Leon, 1996). The stability provisions for reinforced concrete structures (MacGregor, 1993), are based on calculating member forces using a second-order analysis where the beams and columns are assigned reduced stiffnesses to model the frame behavior as the applied load approaches the structural stability limit point. The resulting forces therefore account for inelastic second-order effects directly, and the calculated member forces are compared to the beam-column cross-section strengths. On the other hand, the steel design procedures (AISC, 1993; ASCE, 1997) use a second-order elastic analysis combined with an axial force–moment interaction equation to account for the inelastic amplification of forces. Included in this procedure is the need to determine the capacity of a column under pure axial loading taking into account the effective buckling length (KL) which is in turn a function of the sway stiffness of the frame. Thus the approaches differ in terms of (1) the assumptions used conducting the second-order analysis, and (2) the method of checking the member strength based on the cross-section capacity versus the member buckling capacity.

There are two additional complicating factors, at least in U.S. design practice, that arise from code differences. The first is that there is no set of consistent load factors for steel and concrete except in model codes for seismic design (NEHRP, 1994). The second is that there is no consistent methodology for handling the very common case of hybrid structural systems. Further research is needed to resolve these issues.

10.6 DESIGN APPROACHES

Over the years a large number of design approaches have been proposed for composite columns. Good summaries if these can be found in Furlong (1968, 1974, 1983, 1988), Basu and Sommerville (1969), Virdi and Dowling (1976), Roberts and Yam (1983), Roik and Bergmann (1985), Shakir-Khalil (1988), and Bradford (1995). There are numerous design codes that address the design of composite columns (AIJ, 1987; AISC, 1993; ECS, 1994; ACI, 1995). In the United States the design of composite columns by the AISC (1994) is based on the work of Furlong (1974) and the statistical studies of SSRC Task Group 20 (1979). The Eurocode 4 (ECS, 1994) procedure is based primarily on the work of Roik and Bergmann (1992), based on calibrations by Roik and Bergmann (1989) and Johnson (1997). The Japanese provisions (AIJ, 1987) are based on the work of Wakabayashi (1980).

10.6.1 AISC–LRFD Composite Column Design

For composite column design, the AISC–LRFD provisions currently use a method based on steel column design (AISC, 1993, Chap I). The idea behind this method is to turn the section properties of the composite column into equivalent steel ones. Three important variables need to be modified: the strength (F_{my}), the modulus of elasticity (E_m), and the radius of gyration (r_m). These modifications are as follows:

$$F_{ym} = F_y + c_1 F_{yr} \frac{A_r}{A_s} + c_2 f_c' \frac{A_c}{A_s} \tag{10.8}$$

$$E_m = E + c_3 E_c \frac{A_c}{A_s} \tag{10.9}$$

$$r_m = \max(r_{\text{steel}}, 0.3h_1) \tag{10.10}$$

where

A_c = area of concrete, in^2

A_r = area of longitudinal reinforcing bars, in^2
A_s = area of steel, in^2
E = modulus of elasticity of steel, ksi
E_c = modulus of elasticity of concrete = $w^{1.5}\sqrt{f_c}$, where w is the unit weight of concrete in lb/ft^3 and f_c' is in ksi
F_y = specified minimum yield stress of the steel shape, pipe, or tube, ksi
F_{yr} = specified minimum yield stress of the longitudinal reinforcing bars, ksi
f_c' = specified compressive strength of concrete, ksi
h_1 = overall thickness of entire composite cross section in the plane of buckling, in.

For concrete-filled tubing and pipe $c_1 = 1.0$, $c_2 = 0.85$, and $c_3 = 0.4$. For concrete-encased shapes $c_1 = 0.7$, $c_2 = 0.6$, and $c_3 = 0.2$ (SSRC, 1979). These modified properties are then used in the usual column and beam-column equations (AISC, 1993, Eqs. E-1 through E-4 and H-1-1). The AISC provisions are applicable to cross-sections with a reinforcement ratio (area of steel shape/area of concrete section) greater than 4%. For concrete-filled sections the minimum wall thickness is $b\sqrt{F_y/3E}$, where b is the width, for the rectangular section, and $D\sqrt{F_y/8E}$, where D is the diameter, for circular sections. These provisions are intended to ensure that the steel section yields before the concrete crushes or significant local buckling occurs.

The AISC states that the nominal beam-column flexural strength should be determined from the plastic stress distribution on the cross-section. The type of analysis is time consuming, and only recently have design aids become available for the case of encased sections (Griffis, 1993). The AISC specification, in its commentary, also gives an approximate formula for the flexural capacity at zero axial load (M_n) as

$$M_n = ZF_y + \frac{1}{3}(h_2 - 2C_r)A_rF_{yr} + \left(\frac{h_2}{2} - \frac{A_wF_y}{1.7f_c'h_1}\right)A_wF_y \tag{10.11}$$

where

A_w = web area of the encased steel shape ($A_w = 0$ for concrete-filled tubes)
Z = plastic section modulus of the steel section
c_r = average distance from face of the member to the longitudinal reinforcement
h_1 = width of the member perpendicular to the plane of bending
h_2 = width of the composite member parallel to the plane of bending

The AISC specifications also stipulate that if the axial load term in the interaction equations is below 0.3, the flexural strength should be determined by a straight-line transition between the M_n based on a plastic stress distribution at $P_u/\phi_cP_n = 0.3$ and the flexural strength at $P_u = 0$. If shear studs are required for the case of $P_u = 0$, shear studs are required up to $P_u/\phi_cP_n = 0.3$.

10.6.2 ACI Composite Column Design

ACI 318-95 addresses composite columns in Section 10.16 of ACI 318 (1995). In essence, ACI requires a sectional analysis similar to that for normal reinforced concrete columns in order to compute the cross-sectional strength. The length effects are treated the same as for a reinforced concrete column. The same limitations apply as the AISC–LRFD provisions for wall thicknesses, but the allowable reinforcement ratios are between 1 and 8%. As for reinforced concrete cross sections, the strength is limited to $0.8P_u$.

10.6.3 Eurocode 4 (ECS, 1994)

The design of composite columns by the Eurocode is a strength design method rather than the stress method currently used by AISC. Eurocode begins with a squash load calculated by combining the resistance of the steel, concrete, and reinforcement and then modifies that based on the slenderness of the column if necessary. The code also inserts partial safety factors during the course of the design calculations rather than using an overall ϕ factor as AISC does. The squash load, $N_{\text{pl,rd}}$ is calculated for encased shapes as

$$N_{\text{pl,rd}} = A_s\frac{F_y}{\gamma_s} + A_c\frac{0.85f_c'}{\gamma_c} + A_r\frac{F_{yr}}{\gamma_r} \tag{10.12}$$

for concrete-filled rectangular tubes as

$$N_{\text{pl,rd}} = A_s\frac{F_y}{\gamma_s} + A_c\frac{f_c'}{\gamma_c} + A_r\frac{F_{yr}}{\gamma_r} \tag{10.13}$$

and for concrete-filled circular tubes as

$$N_{\text{pl,rd}} = A_s\frac{F_y}{\gamma_s}\eta_2 + A_c\frac{f_c'}{\gamma_c}\left(1 + \eta_1\frac{tF_y}{df_c'}\right) + A_r\frac{F_{yr}}{\gamma_r} \tag{10.14}$$

where

A_c = area of concrete
A_r = area of longitudinal reinforcing bars
A_s = area of steel
F_y = specified minimum yield stress of the steel shape, pipe, or tube
F_{yr} = specified minimum yield stress of the longitudinal reinforcing bars
f_c' = specified compressive strength of concrete
γ_s = partial safety factor for the structural steel = 1.1
γ_c = partial safety factor for the concrete = 1.5
γ_r = partial safety factor for the reinforcing steel = 1.15

The benefit of good confinement conditions can only be taken into account in Eq. 10.14 if the column is short ($\lambda < 0.5$). The coefficients η_1 and η_2, which account for concrete confinement, are functions of the slenderness and the ratio of the eccentricity of the axial load to the tube diameter (e/d), which for axially loaded columns is zero, and are defined as

$$\eta_1 = \eta_{10}\left(1 - 10\frac{e}{d}\right) \geq 0.0$$

$$\eta_2 = \eta_{20} + (1 - \eta_{20})10\frac{e}{d} \leq 1.0$$

where

$$\eta_{10} = 4.9 - 18.5\lambda + 17\lambda^2 \geq 0.0$$

$$\eta_{20} = 0.25(3 + 2\lambda) \leq 1.0$$

Length effects are handled by the Eurocode with a different approach than in U.S. codes. In the AISC specification, length effects for composite columns are accounted for by finding a reduced interaction diagram just as for a steel column (Fig. 10.5*a*). The reduction is based primarily on the single column curve derived for steel sections. In the Eurocode, on the other hand, the slenderness parameter of the column is defined by

$$\lambda = \sqrt{\frac{A_s F_y + 0.85 A_c f_c' + A_r f_{yr}}{P_e}} \leq 2.0 \qquad (10.15)$$

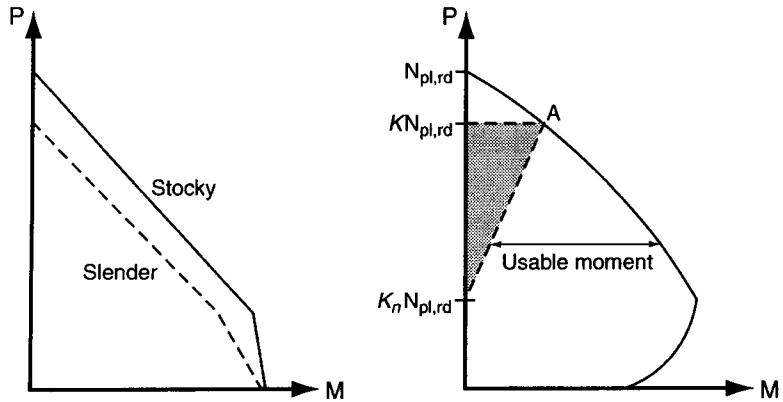

(a) AISC approach (b) Eurocode approach

Fig. 10.5 Comparison of AISC and Eurocode approaches to slenderness effects.

$$P_e = \frac{(EI)_e \pi^2}{(kl)^2} = N_{cr} \qquad (10.16)$$

where

kl = effective length of the column}
$(EI)_e$ = $E_s I_s + E_c I_c + E_r I_r$
E_s = modulus of elasticity of steel
E_c = modulus of elasticity of concrete ($E_c = 0.8E_{cm}/\gamma_c$, where E_{cm} is the secant modulus of concrete and γ_c is taken as 1.35)
E_r = modulus of elasticity of reinforcing steel
I_s = moment of inertia of steel
I_r = moment of inertia of reinforcing steel
I_c = moment of inertia of concrete (assumed to be uncracked)

Note that Eqs. 10.15 and 10.16 imply the use of the characteristic strengths and full-section properties, not some reduced values used for design (i.e., there are no c_1, c_2, and c_3 factors as in Eqs. 10.8 through 10.10 in AISC). In Eq. 10.12, the 0.85 can be neglected for concrete-filled tubes with $\lambda < 0.5$.

The Eurocode calculates a column's strength by reducing the squash load based on the slenderness of the column (Fig. 10.5*b*). Thus the design equation is

$$P_u \leq \kappa N_{\text{pl,rd}}$$

where P_u is the design axial load (kips) and κ is the reduction factor accounting for the column slenderness. The reduction factor κ is based on the European strut curves (Fig. 10.6) and is calculated by

$$\kappa = f_k - \sqrt{f_k^2 - \frac{1}{\lambda^2}} \leq 1.0 \qquad (10.17)$$

with

$$f_k = \frac{1 - \alpha(\lambda - 0.2) + \lambda^2}{2\lambda^2}$$

and $\alpha = 0.21$ for concrete-filled circular and rectangular hollow sections (curve a); $\alpha = 0.34$ for completely or partly concrete-encased I-sections with bending about the major axis of the profile (curve b); and $\alpha = 0.49$ for completely or partly concrete-encased I-section with bending about the minor axis of the profile (curve c). Thus the Eurocode uses multiple column curves derived for composite sections.

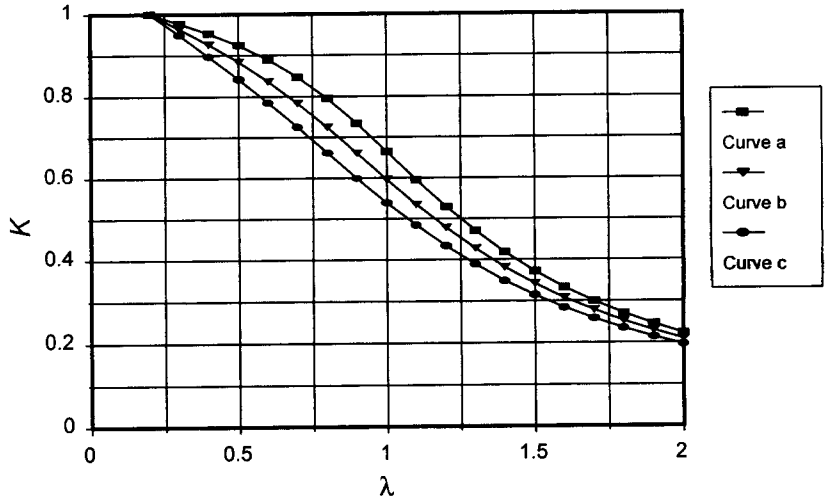

Fig. 10.6 European strut curves used in the Eurocodes.

The slenderness effects are then taken as the shaded region in Fig. 10.5*b*, leaving the usable flexural strength as the distance between the line joining K_n and point A in the failure envelope. Point k_n accounts for the effects of variable end moments and is given as

$$K_n = K\frac{1-r}{4} \qquad -1 < r < 1 \tag{10.18}$$

where r is the ratio of the end moments. For slender columns with small eccentricities the Eurocode also requires that the effect of creep be included in the calculations by modifying the modulus of elasticity of the concrete

Second-order analysis should be used if the second-order moments are a significant part of the system (>10%). The second-order moments can be obtained by multiplying the first-order moments by k, where k is defined as

$$k = \frac{\beta}{1-\dfrac{N}{N_{cr}}} \geq 1.0 \tag{10.19}$$

and

$$\beta = \begin{cases} 1.0 \text{ for bending moments from lateral loads in isolated (pinned) columns} \\ 0.66 + 0.44r \geq 0.44, \text{ where } r = \text{ratio of end moments } (M_{\min}/M_{\max}) \end{cases}$$

The Eurocode also has checks for local buckling of the steel in compression members. The limits for local buckling are based on a depth-to-thickness ratio of the section. For rectangular hollow steel sections with h being the greater overall dimension of the section,

$$\frac{h}{t} \leq 52\varepsilon$$

for circular hollow steel sections,

$$\frac{d}{t} \leq 90\varepsilon^2$$

and for partially encased I-sections

$$\frac{b}{t_f} \leq 44\varepsilon$$

where ε is based on the yield strength of the steel, and is defined as

$$\varepsilon = \frac{\sqrt{34.08}}{F_y}$$

with F_y in ksi. The 34.08 is the result of a conversion of units to ensure that ε is nondimensional. These calculations can be ignored for a section entirely encased in concrete, as the concrete will prevent the member from local buckling.

10.6.4 Comparison of Design Approaches

Figure 10.7 contrasts the results of the cross-sectional strength by an "exact" computer program, COSBIAN (Sanz-Picon, 1992; El-Tawil et al., 1993) and the AISC LRFD, ACI, and Eurocode methods. The figures show both the ultimate strength and design curves for each method. Two extreme cases of reinforcement ratios are shown. Column C-16.2 (fig. 10.7*a*) is a 26 in. × 26 in. column reinforced with an A36 W14 × 370 and 16 No. 6 bars (reinforcement ratio = 16.2%). Column C4.2 (Fig. 10.7*b*) is a 35 in. × 35 in. column reinforced with an A36 W14 × 176 and 15 No. 8 bars (reinforcement ratio = 4.2%). The concrete strength used is 3.5 ksi, the reinforcement yield strength was taken as 50 ksi, and the distance from the concrete surface to the centroid of the bars was 2 in.

For both cases the exact solutions from the program COSBIAN (Sanz-Picon, 1992), the ACI ultimate strength curve, and the simplified Eurocode curve are quite close. As one would expect, the AISC ultimate strength predictions are much better for the high reinforcement ratio and very conservative

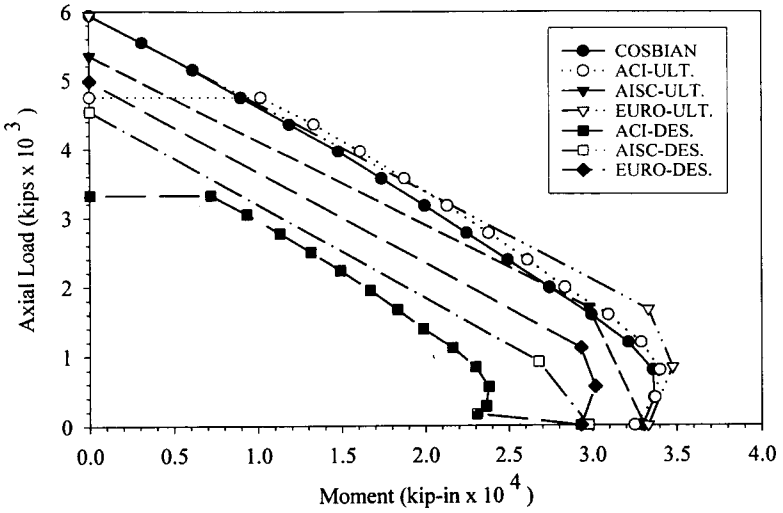

(a) C16-2 (high reinforcement ratio)

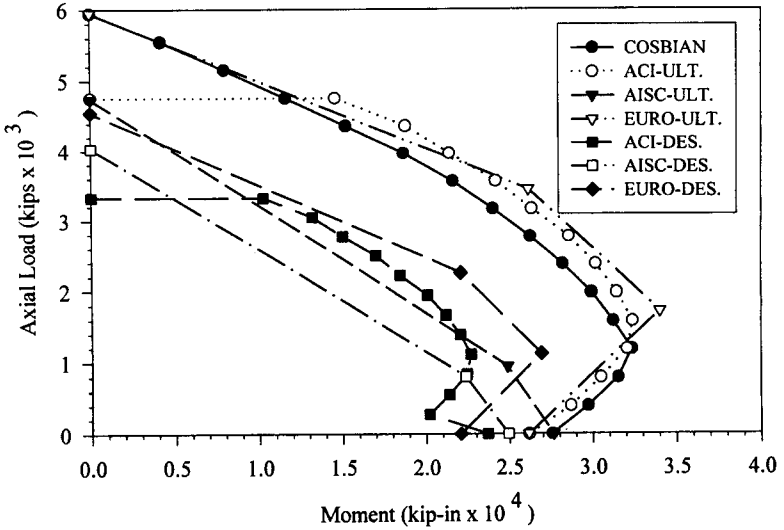

(b) C4-2 (low reinforcement ratio)

Fig. 10.7 Comparison of interaction diagrams (adapted from El-Tawil et al. 1993).

for the low reinforcement case. It should be noted that column C4-2 is just above the 4% limit imposed by AISC. For the design level the ACI method provides a more reasonable solution for the low reinforcement ratio, while the AISC method works best for the high reinforcement ratio. Both the AISC and ACI methods provide less capacity than the Eurocode approach.

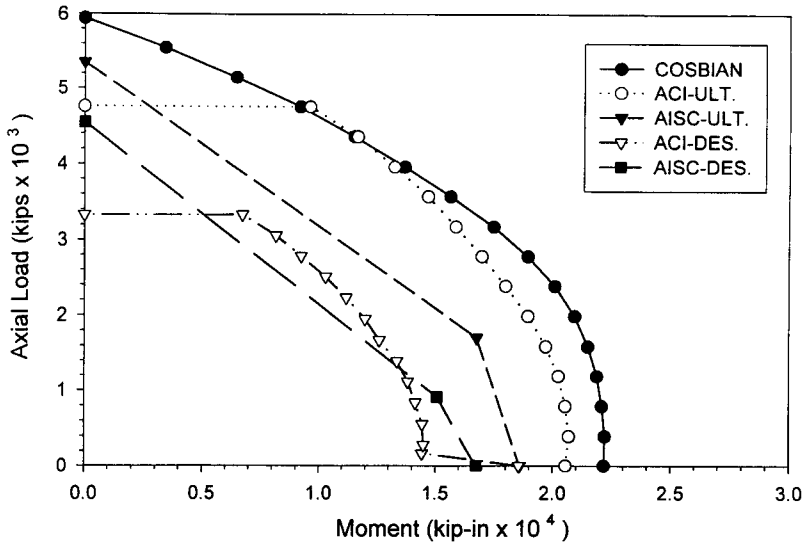

(a) C16-2 (high reinforcement ratio)

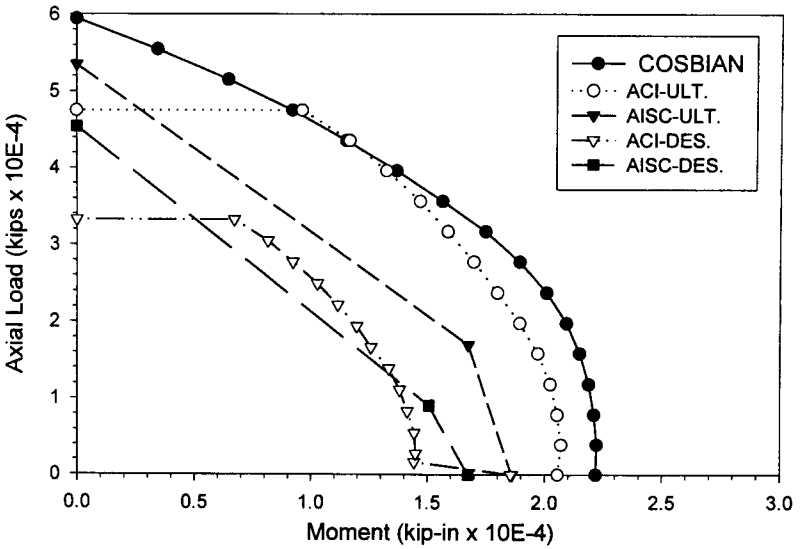

(b) - C4-2 (low reinforcement ratio)

Fig. 10.8 Biaxial interaction diagrams (El-Tawil et al., 1993).

Figure 10.8 shows the biaxial interaction diagram at 45° for the same columns as for the ACI and AISC methods. The biaxial curves show even larger differences for the AISC curves because of the simplified, bilinear relationship used by that specification. The AISC procedure will typically yield significantly lower ultimate moment values for the no-axial-load case, with the differences decreasing as the reinforcement ratio increases. The results look better for the ACI specification, but it should be noted that this comes at significant computational expense. Use of simplified relations for biaxial interaction in concrete (Bresler, 1960) will result in larger differences between the "exact' and the computed strength. These differences can be of the same magnitude as those for the AISC-LRFD specification.

Figure 10.9 shows a comparison of length effects for the same two columns. The calculations were run for L/r values of 0 and 40. Two load cases are shown: one for the case where the loads are applied simultaneously to the steel and concrete ($L/r = 0$, 40) and one for the case where a large axial load ($P = 1500$ kips) was applied to the steel column first ($L/r = 40$). The latter case is intended to simulate the loads on the steel section during the construction phase. The reductions resulting from the application of an axial load are small, generally below 6%. It is interesting to note that the Eurocode seems to give larger reductions in strength than either AISC or ACI.

10.7 DATABASES AND CALIBRATION

Several databases have been developed to test the accuracy of the AISC and the Eurocode design procedures (SSRC, 1979; Roik and Bergmann, 1989; Lundberg, 1993; Aho, 1996; Johnson, 1997). In addition, there are detailed studies dealing with the sensitivity and reliability of encased columns (Mirza and Skrabek, 1991, 1992). Figure 10.10 shows the results of comparing the AISC and Eurocode predictions to experimental results on selected encased sections taken from a database of over 1000 tests of composite columns (Aho, 1996). The mean for the AISC comparison, which included 139 tests, was 1.30 and the standard deviation was 0.27. The corresponding results for the Eurocode, which are based on 79 tests, are 1.11 and 0.20, respectively. For the same 79 tests the AISC procedure gave a mean of 1.22 and a standard deviation of 0.25. Form some 215 tests on axially and eccentrically loaded circular concrete-filled tubes, O'Shea and Bridge (1994) found that the ACI 318 design method gave a mean of 1.33 and a standard deviation of 0.28; the Eurocode method gave a better correlation, with corresponding values of 1.11 and 0.18. The large standard deviation obtained would seem to indicate that further refinement of the models used is needed. However, it should also be noted that these results are based on incomplete data for many tests, and that many of the tests present in the databases have not been corrected to account for unintended end restraint, second-order effects, or similar problems (Aho, 1996; Johnson, 1997).

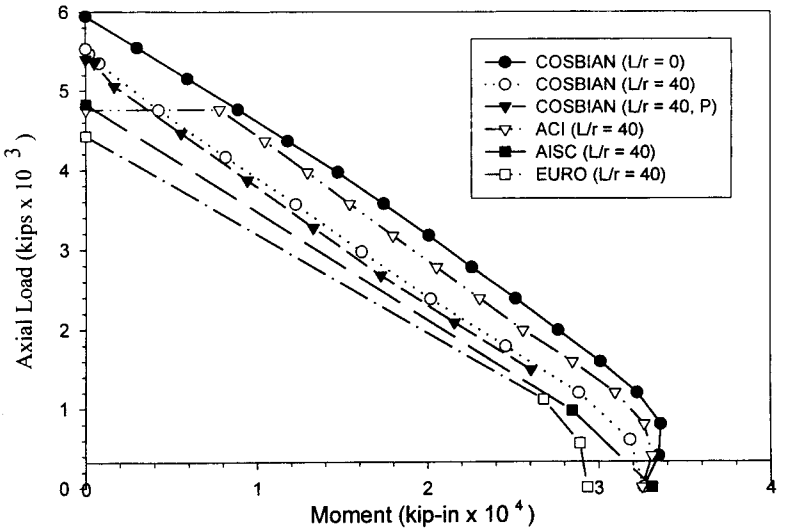

(a) - C16-2 (high reinforcement ratio)

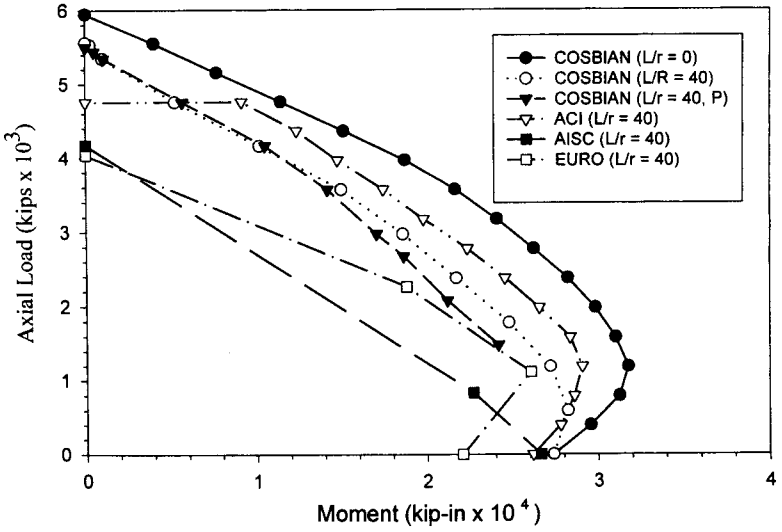

(b) - C2-6 (low reinforcement ratio)

Fig. 10.9 Slenderness effect (El-Tawil et al. 1993; Aho, 1996).

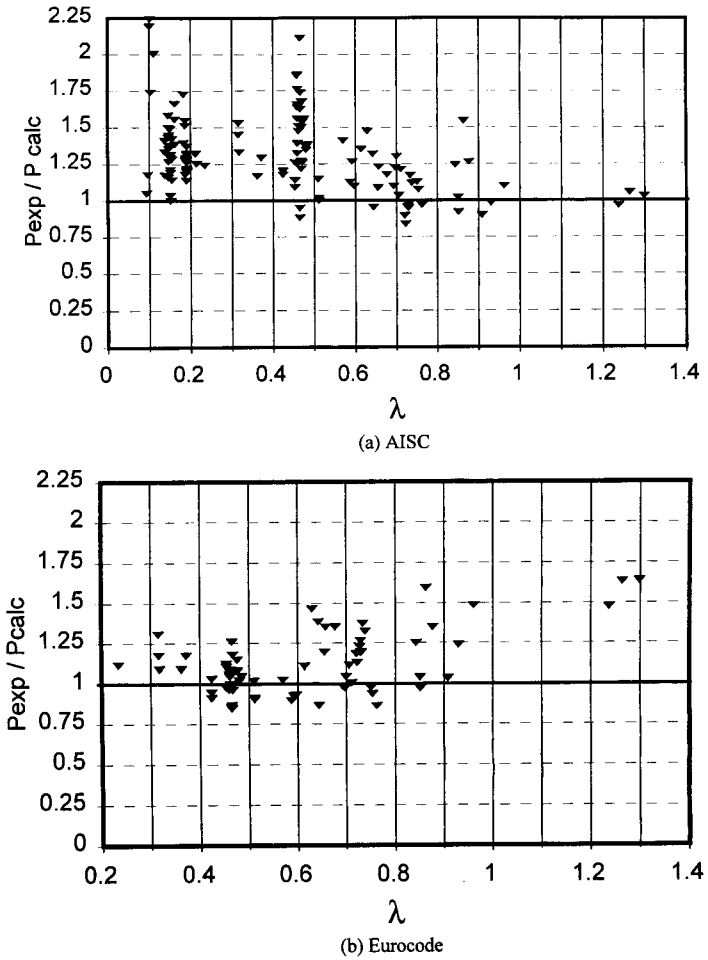

Fig. 10.10 Comparison of test results versus predictions for SRCs (Aho, 1996).

10.8 STRUCTURAL SYSTEMS AND CONNECTIONS FOR COMPOSITE AND HYBRID STRUCTURES

The new NEHRP provisions (NEHRP, 1994) recognize seven types of composite structural systems. Since many of them have a counterpart in steel and concrete, the prefix "C-" has been used to name the corresponding composite system:

Composite Partially Restrained Frames (C-PRF). C-PRFs consist of steel columns and composite beams joined by composite semirigid connections

(Leon, 1990, 1994 and Johnson and Hope-McGill, 1972, Kato and Tagami, 1985). In this case the connections utilize the slab and its reinforcement to provide negative moment capacity and stiffness to the system.

Composite Ordinary Moment Frames (C-OMF). C-OMFs include a variety of configurations where steel or composite beams are combined with steel, composite, or reinforced concrete columns (Deierlein et al., 1989; Sheik et al., 1989; ASCE Task Committee 1994). The team *ordinary* is used to indicate that little of the detailing required for critical structures is envisioned in this type of structure.

Composite Special Moment Frames (C-SMF). C-SMFs are similar to C-OMFs except that much more stringent detailing is required to provide behavior similar to that of a steel SMF (Minami, 1985). In this case the columns, if composite, are required to both meet all AISC requirements for b/t and h/t ratios and to have all the transverse reinforcement required for columns by Chapter 26 of ACI. As in most ductile frames, the columns and joints are required to develop the full strength of the beams so that a stable strong column–weak mechanism develops.

Composite Concentrically Braced Frames (C-CBF). C-CBFs are similar to their steel counterparts except that some of the members (beams, columns, and braces) are composite. There is considerable debate on the applicability of braced frames in areas of high seismicity because the tendency of the braces to buckle results in poor energy-dissipation characteristics if the structure goes inelastic. To alleviate the buckling problem several researchers have proposed to utilize composite braces (either encased shapes or concrete-filled tubes) where the stiffening effect of the concrete prevents local buckling (Liu and Goel, 1988).

Composite Eccentrically Braced Frames (C-EBF). As the name implies, C-EBFs are analogous to the usual eccentrically braced frame except that some of the members are composite. When the EBF concept was originally developed there was some concern as to whether the floor beams, which are in effect composite beams, could accommodate the large rotational ductilities demanded by the system without causing local failures. Extensive research has been carried out in this area, indicating that the floor elements are capable of withstanding the very large shear deformations required by short links (Ricles and Popov, 1989).

RC Walls Composite with Steel Elements. At least three possible variations of this system exist, and they correspond to cases of hybrid structures. The first utilizes concrete panels as infills in steel or composite frames. The second is where large steel sections are used as boundary elements in concrete shear walls. The third one is where steel or encased composite beams are used to tie two reinforced concrete shear walls (Sharooz et al., 1993; Harries et al., 1993).

Steel Plate-Reinforced Shear Walls. Since the early 1980s the concept of utilizing steel plate shear walls has been popular (Thorburn et al., 1983). The

concept is very similar to the use of plate girders in bridges, except that the main element is vertical rather than horizontal. These systems have been used successfully as retrofits in critical steel structures (hospitals), where access to the structure was severely limited by the need to keep it operating during the retrofit. The system basically behaves as a CBF with the tension field action taking the lateral loads. Composite steel shear walls, in which the steel plate is covered with concrete and composite action activated by mechanical connectors, have been postulated as a system with better energy dissipation capacity. Another variation could be a sandwich configuration where the space between two thin steel plates containing studs is filled with concrete. In this case the steel plates act as the formwork and could be welded directly to an existing steel frame. Great care is needed in connecting the plates to the boundary elements since the shear wall is such an efficient structural element that it can easily overstress the adjacent columns and beams.

The structural systems discussed above give a flavor of the many variations that can be developed by combining composite elements. The stability design of many of these systems has not been investigated extensively and thus the suggested design procedures are conservative (NEHRP, 1994). The design of connections in composite construction has recently been reviewed by Leon and Zandonini (1992).

10.9 SUMMARY

The discussion presented in this chapter indicates that although design provisions are available for composite columns, there are still significant gaps in our fundamental understanding of their behavior. While composite columns do not differ significantly in their stability behavior from steel or concrete members, the characterization of their cross-sectional strength and stiffness along the length of a given column is not simple. This is reflected in the relative poor correlation between test results and code predictions. There is clearly a need for more careful experimental work in long slender columns, particularly with respect to high-performance materials (HSC, HSS), scale effects, and biaxial bending. Work on short composite columns, where the behavior is influenced primarily by shear, is under way as part of the U.S.–Japan Program on Hybrid and Composite Structures (Yamanuchi et al., 1993), and design recommendations will hopefully be developed as part of that effort. Another fundamental issue, the degree of restraint provided by the hybrid and composite connections, has not been studied adequately and both analytical and experimental work is needed in this area. Finally, there is a need to better coordinate the various design approaches proposed by different organizations. The design of composite columns should result in a seamless integration between reinforced concrete and steel design, as recommended for concrete-encased columns by Muñoz and Hsu (1997).

REFERENCES

ACI (1995), *Building Code Requirements for Reinforced Concrete and Commentary*, ACI 318-95, American Concrete Institute, Detroit, Mich.

Aho, M. F. (1996), "A Database for Encased and Concrete-Filled Columns," M.S. thesis, School of Civil and Environmental Engineering, Georgia Institute of Technology, Atlanta, GA.

AIJ (1987), *Structural Calculations of Steel Reinforced Concrete Structures*, Architectural Institute of Japan, Tokyo.

AISC (1993), *Load and Resistance Factor Design Specification for Structural Steel Buildings*, American Institute of Steel Construction, Chicago.

ASCE Task Committee on Design Criteria for Composite Structures in Steel and Concrete (1994a), "Proposed Specification for Structural Steel Beams with Web Openings," *ASCE J. Struct. Eng.*, Vol. 118, No. 12, pp. 3315–3324.

ASCE Task Committee on Design Criteria for Composite Structures in Steel and Concrete (1994b), "Guidelines for Design of Joints Between Steel Beams and Reinforced Concrete Columns," *ASCE J. Struct. Eng.*, Vol. 120, No. ST8, pp. 2330–2357.

ASCE Task Committee on Design Criteria for Composite Structures in Steel and Concrete (1996), "Proposed Specification and Commentary for Composite Joists and Trusses," *ASCE J. Struct. Div.*, Vol. 122, No. ST4, pp. 350–358.

ASCE Task Group on Effective Length (1997), *Effective Length and Notional Load Approaches for Assessing Frame Stability: Implications for American Steel Design*, Committee on Load and Resistance Factor Design, American Society of Civil Engineers, New York.

Basu, A. K., and Sommerville, W. (1969), "Derivation of Formulae for the Design of Rectangular Composite Columns," *Proc. Inst. Civ. Eng.*, Suppl. Vol., pp. 233–280.

Bradford, M. A. (1995), "Design Strength of Slender Concrete-Filled Rectangular Steel Tubes," *ACI Struct. J.*, Vol. 93, No. 2, pp. 229–235.

Bradford, M. A., and Gilbert, R. I. (1990), "Time-Dependent Analysis and Design of Composite Columns," *ASCE J. Struct. Eng.*, Vol. 116, No. ST2, pp. 3338–3357.

Bresler, B. (1960), "Design Criteria for R. C. Columns Under Axial Load and Biaxial Bending," *ACI J.*, Vol. 57, No. 5, pp. 481–490.

Bridge, R. Q. (1979), "Composite Columns Under Sustained Loads," *ASCE J. Struct. Eng.*, Vol. 105, No. ST3, pp. 563–576.

Bridge, R. Q. (1988), "The Long-Term Behavior of Composite Columns," in *Composite Construction in Steel and Concrete*, (ed. D. Buckner and I. M. Viest), American Society of Civil Engineers, New York, pp. 460–471.

Bridge, R. Q., and O'Shea, M. D. (1996a), "Local Buckling of Square Thin-Walled Steel Tubes Filled with Concrete," *Proc. 5th Int. Colloq.*, Structural Stability Research Council, Chicago, pp. 63–72.

Bridge, R. Q., and Webb, J. (1993), "Thin Walled Circular Concrete Filled Steel Tubular Columns," in *Composite Construction in Steel and Concrete II*, ed. W. S. Easterling and W. M. K. Roddis, American Society of Civil Engineers, New York, pp. 634–649.

Bryson, J. O., and Mathey, R. G. (1973), "Surface Condition Effect on Bond Strength of Steel Beams Embedded in Concrete," *ACI J.*, Vol. 59, No. 3, pp. 39–46.

Buckner, C. D., and Shahrooz, B. eds. (1997), *Composite Construction in Steel and Concrete III*, American Society of Civil Engineers, New York.

Buckner, C. D., and Viest, I. M., eds. (1988), *Composite Construction in Steel and Concrete*, American Society of Civil Engineers, New York, 815 pp.

Cai, S.-H. (1988), "Ultimate Strength of Concrete-Filled Tube Columns," in *Composite Construction in Steel and Concrete* (ed. D. Buckner and I. M. Viest), American Society of Civil Engineers, New York, p. 702–727.

Cederwall, K., Engstrom, B., and Grauers, M. (1990), "High-Strength Concrete Used in Composite Columns," *Proc. 2nd Int. Symp. Utiliz. High-Strength Concrete* (ed. W. T. Hester), Berkeley, Calif, pp. 195–214.

Chen, W. F., and Chen, C. H. (1973), "Analysis of Concrete-Filled Steel Tubular Beam-Columns," *IABSE Publ. 33(II)*, pp. 37–52.

Chen, C., Astaneh-Asl., A., and Moehle, J. P. (1992), "Behavior and Design of High Strength Composite Columns," *Proc. Struct. Congr. X* (ed. J. Morgan), American Society of Civil Engineers, New York, pp. 820–823.

Collins, M. P., Mitchell, D., and MacGregor, J. G. (1993), "Structural Design Considerations for High-Strength Concrete," *Concrete Int.*, Vol. 15, No. 5, pp. 27–34.

Deierlein, G. G. (1995), "An Overview of the 1994 NEHRP Recommended Provisions for the Seismic Design of Composite Structures," *Proc. Struct. Congr. XIII* (ed. M. Sanayaei), Vol. 2, pp. 1305–1308.

Deierlein, G. G., and Leon, R. T. (1996), "Design Criteria for Composite Steel–Concrete Structures: Current Status and Future Needs," in ACI SP: *Hybrid and Composite Structures* (ed. B. Sharooz and G. Sabnis), American Concrete Institute Mich.

Deierlein, G. G., Sheikh, T. M., Yura, J. A., and Jirsa, J. O. (1989), "Beam-Column Moment Connections for Composite Frames, Part 2," *ASCE J. Struct. Eng.*, Vol. 115, No. ST11, pp. 2877–2896.

Dekker, N. W., Kemp, A. R., and Trinchero, P. (1995), "Factors Influencing the Strength of Continuous Composite Beams in Negative Bending," *J. Constr. Steel Res.*, Vol. 34, No. 2–3, pp. 161–186.

Dobruszkes, A., and Piraprez, E. (1981), "Détermination de l'adhérence naturelle acier-béton dans le cas de poutres mixtes composées d'un profilé métallique enrobe de béton," *Rep. MT 241*, CRST, Brussels, Belgium.

Duan, L., and Chen, W.-F. (1990), "Design Interaction Equations for Cylindrical Tubular Beam-Columns," *ASCE J. Struc. Eng.*, Vol. 116, No. ST7, pp. 1794–1812.

Easterling, W. S., and Roddis, W. M. K., eds (1993), *Composite Construction in Steel and Concrete II*, American Society of Civil Engineers, New York, 944 pp.

ECS (1994), *Eurocode 4: Design of Composite Steel and Concrete Structures*, European Committee for Standardization, Brussels, Belgium.

El-Tawil, S., Sanz-Picon, C. F., and Deierlein, G. G. (1993), "Evaluation of ACI 318 and AISC (LRFD) Strength Provisions for Composite Beam-Columns," *J. Constr. Steel Res.*, Vol. 34, No. 1, pp. 103–123.

El-Tawil, S., Sanz-Picon, C. F., and Deierlein, G. G. (1995), "Evaluation of ACI 318 and AISC (LRFD) Strength Provisions for Composite Columns," *J. Constr. Steel Res.*, Vol. 34, pp. 103–123.

Furlong, R. W. (1967), "Strength of Steel Encased Concrete Beam Columns," *ASCE J. Struct. Div.*, Vol. 93, No. ST5, pp. 113–124.

Furlong, R. W. (1968), "Design of Steel Encased Concrete Beam Columns," *ASCE J. Struct. Div.*, Vol. 94, No. ST1, pp. 267–281.

Furlong, R. W. (1974), "Concrete Encased Steel Beam Columns: Design Tables," ASCE J. Struct. Div., Vol. 100, No. ST9, pp. 1865–1883.

Furlong, R. W. (1983), "Column Rules of ACI, SSLC, and LRFD Compared," *ASCE J. Struct. Eng.*, Vol. 109, No. ST8, pp. 2375–2386.

Furlong, R. W. (1988), "Steel–Concrete Composite Columns: II," in *Steel–Concrete Composite Structures*, (ed. R. Narayanan), Elsevier Applied Sciences, New York, pp. 195–220.

Gardner, N. J., and Jacobson, E. R. (1967), "Structural Behavior of Concrete Filled Steel Tubes," *ACI J.*, Vol. 64, No. 11, pp. 404–413.

Goel, S. C., and Yamanuchi, H. (eds.) (1993), "Proceedings of the 1992 U.S.–Japan Workshop on Composite and Hybrid Structures," *Res. Rep. UMCEE 92-29*, Department of Civil and Environmental Engineering, University of Michigan, Ann Arbor, Mich.

Gourley, B. C. and Hajjar, J. F. (1994), "Cyclic Non-linear Analysis of Concrete-Filled Beam Columns and Composite Frames," *Rep. No. ST-94-3*, Department of Civil Engineering, University of Minnesota, Minneapolis, Minn.

Gourley, B. C., Hajjar, J. F., and Schiller, P. H. (1995), "A Synopsis of Studies of the Monotonic and Cyclic Behavior of Concrete-Filled Steel Tube Beam-Columns," *Rep. No. ST-93-5*, Department of Civil and Mineral Engineering, University of Minnesota, Minneapolis, Minn.

Grauers, M. (1993), "Composite Columns of Hollow Steel Sections Filled with High Strength Concrete," *Publ. 93:2*, Division of Concrete Structures, Chalmers University of Technology, Goteborg, Sweden.

Griffis, L. G. (1986), "Some Design Considerations for Composite-Frame Structures," *AISC Eng. J.*, Vol. 23, No. 2, pp. 59–64.

Griffis, L. G. (1992), "Composite Frame Construction." in *Constructional Steel Design*, (ed. P. J. Dowling et al.), Elsevier Applied Science, London, pp. 523–553.

Griffis, L. G. (1993), "Load and Resistance Factor Design of W-Shapes Encased in Concrete," *AISC Des. Guide 6 (D806)*, American Institute of Steel Construction, Chicago, 212 pp.

Harries, K., Mitchell, D., Cook, W. D., and Redwood, R. G., (1993), "Seismic Response of Steel Beams Coupling Concrete Walls," *ASCE J. Struct. Eng.*, Vol. 119, No. 12, pp. 3611–3629.

Ichinhoe, Y., Matsutani, T., Nakajima, M., Ueda, H., and Takada, K. (1991), "Elasto-plastic Behavior of Concrete Filled Steel Circular Columns," *Proc. 3rd Int. Conf.*

Steel-Concrete Compos. Struct., (ed. M. Wakabayashi), Fukuoka, Japan, pp. 131–136.

Javor, T., ed. (1994), *Steel-Concrete Composite Structures, Proc. 3, EXPERT-CENTRUM*, Bratislava, Slovakia, 623 pp.

Johnson, B. G., ed. (1976), *Guide to Stability Design for Metal Structures*, J. Wiley, New York.

Johnson, R. P. (1997), "Statistical Calibration of Safety Factors for Encased Concrete Columns," in *Composite Construction in Steel and Concrete III*, (ed. D. Buckner and B. Shahrooz), American Society of Civil Engineers, New York.

Johnson, R. P., and Hope-McGill, M. (1972), "Semi-rigid Joints in Composite Frames," *Prelim. Rep., 9th Congr. IABSE*, pp. 133–144.

Johnson, R. P., and May, I. M. (1978), "Tests on Restrained Composite Columns," *Struct. Eng.*, Vol. 56B, No. 2, pp. 21–27.

Kato, B., and Tagami, J. (1985), "Beam-to-Column Connection of a Composite Structure," in *Composite and Mixed Construction* (ed. C. Roeder), American Society of Civil Engineers, New York, pp. 205–214.

Knowles, R. B., and Park, R. (1969), "Strength of Concrete Filled Steel Tubular Columns," *ASCE J. Struct. Eng.*, Vol. 95, No. ST2, p. 2565–2587.

Knowles, R. B., and Park, R. (1970), "Axial Load Design for Concrete Filled Steel Tubes," *ASCE J. Struct. Eng.*, Vol. 96, No. ST10, pp. 2125–2153.

Leon, R. T. (1990), "Semirigid Composite Construction," *J. Constr. Steel Res.*, Vol. 15, No. 2, pp. 99–120.

Leon, R. T. (1994), "Composite Semi-rigid Construction," *AISC Eng. J.*, Vol. 31, 2nd quarter, pp. 57–67.

Leon, R. T., and Bawa, S. (1990), "Performance of Large Composite Columns," in *Mixed Structures, Proc IABSE Symp.*, Brussels, Vol. 50, IABSE, Zurich, pp. 179–184.

Leon, R. T., and Zandonini, R. (1992), "Composite Connections," in Constructional Steel Design, (ed. P. Dowling et al.), Elsevier Science Publishers, New York, pp. 501–520.

Liu, Z., and Goel, S. C. (1988), "Cyclic Load Behavior of Concrete-Filled Tubular Braces," *ASCE J. Struct. Eng.*, Vol. 114, No. 7, pp. 1488–1506.

Lundberg, J. E. (1993), "The Reliability of Composite Columns and Beam-Columns," *Struct. Eng. Rep. 93–2*, Department of Civil and Mineral Engineering, University of Minnesota, Minneapolis, Minn.

MacGregor, J. G. (1993), "Design of Slender Concrete Columns—Revisited," *ACI Struct. J.*, Vol. 90, No. 3, pp. 302–309.

Mahin, S., and Bertero, V. (1977), *RCCOLA: A Computer Program for R. C. Column Analysis: Users' Manual and Documentation*, Department of Civil Engineering, University of California, Berkeley, Calif.

Matsui, C., and Tsuda, K. (1987), "Strength and Behavior of Concrete-Filled Steel Square Tubular Columns with Large Width-Thickness Ratios," *Proc. Pac. Conf. Earthquake Eng.*, Vol. 2, Waimkei, New Zealand, pp. 1–9.

Minami, K. (1985), "Beam to Column Stress Transfer in Composite Structures," in *Composite and Mixed Construction* (ed. C. Roeder), pp. 215–226.

Mirza, S. A., and Skrabek, B. W. (1991), "Reliability of Short Composite Beam-Column Strength Interaction," *ASCE J. Struct. Div.*, Vol. 117, No. ST8, pp. 2320–2339.

Mirza, S. A., and Skrabek, B. W. (1992), "Statistical Analysis of Slender Composite Column Strength," *ASCE J. Struct. Div.*, Vol. 118, No. ST5, pp. 1312–1332.

Morino, S., Uchida, Y., and Ozaki, M. (1988), "Experimental Study of the Behavior of SRC Beam-Columns Subjected to Biaxial Bending," in *Composite Construction in Steel and Concrete* (ed. D. Buckner and I. M. Viest), American Society of Civil Engineers, New York, pp. 753–777.

Morino, S., Kawaguchi, J., Yazuzaki, C., and Kanazawa, S. (1993), "Behavior of Concrete-Filled Steel Tubular Three-Dimensional Subassemblages," in *Composite Construction in Steel and Concrete II*, (ed. W. S. Easterling and W. M. K. Roddis), American Society of Civil Engineers, New York, pp. 726–741.

Munoz, P. R. and Hse, C.-T. T. (1997), "Biaxially Loaded Concrete-Encased Composite Columns: Design Equation", *ASCE J. of Structural Eng.*, Vol. 123, No. 12, Dec. pp 1576–1585.

Nakai, H., Kurita, A., and Ichinose, L. H. (1991), "An Experimental Study on Creep of Concrete Filled Steel Pipes," *Proc. 3rd Int. Conf. Steel–Concrete Compos. Struct*, (ed. M. Wakabayashi), Fukuoka, Japan, pp. 55–60.

NEHRP (1994), "Composite Steel and Concrete Structure Design Requirements," in *NEHRP Recommended Provisions for Seismic Regulations for New Buildings*, FEMA 222/223, Federal Engineering Management Agency, Washington, DC, Chap. 7.

Neogi, P. K., Sen, H. K. and Chapman, J. C. (1969), "Concrete-Filled Tubular Steel Columns Under Eccentric Loading," *Struct. Eng.* Vol. 47, No. 5, pp. 187–195.

Oehlers, D. J., and Bradford, M. A. (1995), *Composite Steel and Concrete Structural Members: Fundamental Behavior*, Pergamon Press, Elmsford, N. Y.

Orito, Y., Sato, T., Tanaka, N., and Watanabe, Y. (1988), "Study of Unbonded Steel Tube Concrete Structure," in Composite Construction in Steel and Concrete (ed. D. Buckner and I. M. Viest), American Society of Civil Engineers, New York, pp. 786–804.

O'Shea, M. D., and Bridge, R. Q. (1994), "The Design of Circular Concrete Filled Steel Tubes," *Proc. Aust. Struct. Eng. Conf.*, Institution of Engineers Australia, Sydney, Australia, Vol. 2, pp. 607–612.

O'Shea, M. D., and Bridge, R. Q. (1996), "Circular Thin-Walled Tubes with High Strength Concrete Infill," in *Composite Construction in Steel and Concrete III*, (ed. D. Buckner and B. Shahrooz), American Society of Civil Engineers, New York.

Prion, H. G. L., and Boeheme, J. (1989), "Beam-Column Behavior of Steel Tubes Filled with High Strength Concrete," *Proc. 4th Int. Colloq. SSRC*, New York, pp. 439–450.

Ricles, J. M., and Paboojian, S. H. (1994), "Structural Performance of Steel Encased Composite Columns," *ASCE J. Struct. Div.*, Vol. 120, No. ST8, pp. 2474–2494.

Ricles, J. M., and Popov, E. P. (1989), "Composite Action in Eccentrically Braced Frames," *ASCE J. Struct. Eng.*, Vol. 115, No. 8, pp. 2046–2066.

Roberts, E. H. and Yam, L. C. P. (1983), "Some Recent Methods for the Design of Steel, Reinforced Concrete and Composite Steel–Concrete Columns in the UK," *ACI J.*, Vol. 80, No. 2, pp. 139–149.

Robinson, H., and Naraine, K. S. (1988), "Slip and Uplift Effects in Composite Beams," in *Composite Construction in Steel and Concrete* (ed. D. Buckner and I. M. Viest), American Society of Civil Engineers, New York, pp. 487–497.

Roeder, C. W., ed. (1985a), *Composite and Mixed Construction*, American Society of Civil Engineers, New York, 339 pp.

Roeder, C. W. (1985b), "Bond Stress of Embedded Steel Shapes in Concrete," in *Composite and Mixed Construction* (ed. C. Roeder), pp. 227–240.

Roik, K., and Bergmann, R. (1985), "Composite Columns: Design and Examples for Construction," in *Composite and Mixed Construction* (ed. C. Roeder), pp. 267–278.

Roik, K., and Bergmann, R. (1989), "Report on Eurocode 4: Clause 4.8 and 4.9—Composite Columns," *EC4/6/89*, Miniter für Raumordnung, Bauwesen, und Stadtgebau der Bundesrepublik Deutschland, RSII 1-6741028630, Bonn, Germany.

Roik, K., and Bergmann, R. (1992), "Composite Columns," in *Constructional Steel Design* (ed. P. Dowling et al.) Elsevier Science Publishers, New York, pp. 443–470.

Sanz-Picon, C. F. (1992), "Behavior of Composite Column Cross-Sections Under Biaxial Bending," M.Sc. thesis, Cornell University, Ithaca, N.Y.

Shahrooz, B. M., Remmetter, M. E., and Qin, F. (1993), "Seismic Design and Performance of Composite Shear Walls," *ASCE J. Struct. Eng.*, Vol. 119, No. ST11, pp. 3291–3309.

Shakir-Khalil, H. (1988), "Steel-Concrete Composite Columns: I," in *Steel–Concrete Composite Structures* (ed. R. Narayanan), Elsevier Applied Sciences, New York, pp. 163–194.

Shakir-Khalil, H., and Mouli, M. (1990), "Further Tests on Concrete-Filled Rectangular Hollow-Section Columns," *Struct. Eng.*, Vol. 68, pp. 405–413.

Shakir-Khalil, R., and Zeghiche, Z. (1989), "Experimental Behavior of Concrete-Filled Rolled Rectangular Hollow Section Columns," *Struct. Eng.*, Vol. 67, pp. 345–353.

Sheikh, T. M., Deierlein, G. G., Yura, J. A., and Jirsa, J. O. (1989), "'Beam-Column Moment Connections for Composite Frames, Part 1," *ASCE J. Struct. Div.*, Vol. 115, No. ST11, pp. 2858–2876.

SSRC Task Group 20 (1979), "A Specification for the Design of Steel–Concrete Composite Columns," *AISC Eng. J.*, Vol. 16, No. 4, pp. 101–115.

Stevens, R. F. (1965), "Encased Stanchions," *Struct. Eng.*, Vol. 42, No. 2, pp. 59–66.

Talbot, A. N., and Lord, A. R. (1912), "Tests of Columns: An Investigation of the Value of Concrete as Reinforcement for Structural Steel Columns," *Bull. 56*, University of Illinois Engineering Experiment Station, Champaign-Urbana, Ill.

Thornburn, L. J., Kulak, G. L., and Montgomery, C. J. (1983), "Analysis of Steel Plate Shear Walls," *Struct. Eng. Rep. No. 107*, University of Alberta, Edmonton, Alberta, Canada.

Viest, I. M. Colaco, J. P., Furlong, R. W., Griffis, L. G., Leon, R. T., and Wyllie, L. A. (1996), *Composite Construction: Design for Buildings*, ASCE-McGraw Hill, New York.

Virdi, K. S., and Dowling, P. J. (1973), "The Ultimate Strength of Composite Columns in Biaxial Bending," *Proc. Inst. Civ. Eng.*, Part 2, Vol. 55, pp. 251–272.

Virdi, K. S., and Dowling, P. J. (1976), "A Unified Design Method for Composite Columns," *IABSE Pub. 36*, pp. 165–1843.

Virdi, K. S., and Dowling, P. J. (1980), "Bond Strength in Concrete-Filled Steel Tubes," *IABSE Per. 3/1980.*

Wakabayashi, M. (1980), "Standards for the Design of Concrete Encased-Steel and Concrete-Filled Tubular Structures in Japan," *Proc. U.S.–Japan Sem. Compos, Struct. Mixed Struct. Sys.*, Gihodo Shuppan, Tokyo, pp. 69–84.

Wakabayashi, M., ed. (1991), *Steel–Concrete Composite Structures*, AICRSCCS, Fukuoka, Japan, 2 vols.

Wium, J. A., and Lebet, J. P. (1990a), "Pushout Tests on Embedded Steel Plates," *Publ. ICOM 240*, Ecole Polytechnique Fédérale de Lausanne, Lausanne, Switzerland.

Wium, J. A., and Leblet, J. P. (1990b), "Test for the Application of Forces on Short Composite Columns," *Publ. ICOM 241*, Ecole Polytechnique Fédérale de Lausanne, Lausanne, Switzerland.

Yamanuchi, H., Mahin, S. A., Goel, S. C., and Nishiyama, I. (1993), "U.S.–Japan Cooperative Earthquake Research Program on Composite and Hybrid Structures," *Proc. 1992 U.S.–Japan Workshop Compos. Hybrid Struct.*, U.S.–Japan Cooperative Research Program.

CHAPTER ELEVEN

STABILITY OF ANGLE MEMBERS

11.1 INTRODUCTION

Single angles in compression are used in many applications, such as web members in steel joists and trusses, members of latticed transmission towers or communication structures, elements of built-up columns, and bracing members. Bolted or welded members made of single angles are common in industrial plants to support pipes, cable trays, and heating, ventilating, and air-conditioning systems.

Single angles are popular because they can easily be connected to other structural members. They are almost always connected eccentrically at their ends. In most practical applications, angles are loaded through one leg only, thus introducing eccentricity with respect to the centroid of the cross section. At the same time, restraining moments at the ends of the member are also present due to the flexural rigidity of the connected elements. In a rational design philosophy, therefore, the detrimental effect of the end eccentricity and the advantageous effect of the end restraint on the compression capacity of the angle member should be addressed. Furthermore, due to the asymmetry of the angle cross section, the determination of the compression capacity under eccentric loading along with end restraints is complex. The end eccentricities cause biaxial flexural deformation of the strut at any given load; thus the problem is that of load-deformation response. Double angles are also frequently used as members in trusses and as bracing members. The ease with which connections can be made contribute to the popularity of their use. Angles are often used as beams in walkways, racks, equipment support frames,

pipe support systems plus other lightly loaded framing. Angles used in joists and trusses are often subjected to flexure from transverse loading.

In this chapter, single- and multiple-angle members subjected to compression and/or flexure are addressed. Experimental and analytical research and standard industry practice in the United States and abroad are also discussed.

11.2 REVIEW OF EXPERIMENTAL AND ANALYTICAL RESEARCH

The earliest tests on angles in compression in North America were performed by the National Bureau of Standards (1924). After a gap of 24 years, Foehl (1948) reported tests on seven single-angle steel columns. One leg at the end of each of these columns was welded to the stem of structural tee section, thus simulating the arrangement in the web of a long-span joist. The main objectives of these tests were to determine the effective slenderness ratios of these columns and to ascertain which leg of an unequal-leg angle should be placed perpendicular to the plane of the truss. It was concluded that the long leg should be placed in this position. At Washington University theoretical and experimental investigations were carried out on single-angle columns under biaxially eccentric loading (Trahair, 1969; Usami, 1970; Usami and Galambos, 1971; Leigh and Galambos, 1972). The test specimens were representative of the web members used in standard long span steel joists, with their ends welded to structural T-sections to simulate the chords of such joists. An analytical investigation was carried out by assuming that the column is made of an elastic–perfectly plastic material, and representing the out-of-plane end restraint by an elastic–plastic rotational spring and the in-plane end restraint by an elastic rotational spring; good correlation between the theoretical and experimental results was obtained. Usami and Fukumoto (1972) studied the behavior of angle members; it was found that the effect of residual stresses was not significant, a conclusion which agrees with the earlier finding of Ishida (1968). It was recommended that the maximum load of an eccentrically loaded angle bracing member can be taken as 58% of the maximum load of a corresponding concentrically loaded member.

The influence of end connections on the load-carrying capacity of web angle members was experimentally studied by Lorin and Cuille (1977). They found that increasing the yield strength of the gusset plate did not increase the load-carrying capacity of the member; however, doubling the thickness of the gusset plate from 0.4 in. to 0.8 in. increased the buckling load by approximately 40%.

El-Tayem and Goel (1986) reported on tests performed on cross-bracing systems made of single-angle members. Only one-half of the compression diagonal buckled about the weak principal axis. A theoretical model, including the end-restraint effect of the gusset connection and the restraint effect of the tension diagonal, was also presented to depict the results of the tests. The test results on the capacity of the compression diagonal was compared with the AISC specification (1989) compression capacity using the weak principal

axis slenderness ratio and one-half the length of the compression diagonal. The results indicate that the use of an effective-length factor K equal to 0.85 is acceptable without including the effect of the end eccentricity in the computation of the allowable loads.

Works by Culver (1966) and Dabrowski (1961) can be used to predict the elastic capacity of eccentrically connected single-angle struts. The effect of symmetrical end restraint (i.e., the same end restraint at both ends of the strut) was investigated by Trahair (1969) for the elastic case. Both equal and unequal leg angles were included in the study. The applicable equilibrium equations were solved using the finite integral method. The end condition considered is shown in Fig. 11.1. Line AB in this figure represents a knife-edge support; load P is assumed to be applied anywhere along line AB. The results of the analysis were compared with tests by Foehl (1948), and good agreement was found between the analysis and test results. It has to be noted that this investigation did not include the effects of initial deformations on the load-carrying capacity of the angle struts.

The results of tests conducted by Elgaaly et al. (1991, 1992) indicated that the design specifications for single angle members (AISC, 1989) can be conservative, while the ASCE (1988) design recommendations for transmission towers can be unconservative. Based on available test results, Adluri and Madugula (1992) reached the same conclusions with respect to the requirements of the AISC specifications. Finite element analysis provides a general

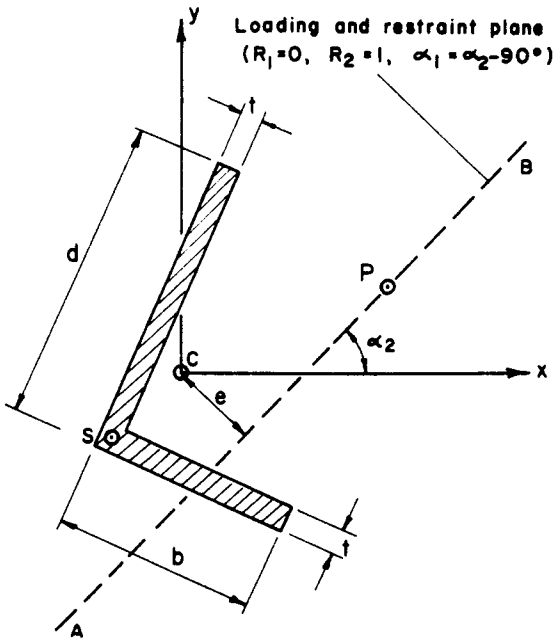

Fig. 11.1 Eccentrically loaded single-angle strut (Trahair, 1969).

tool for the determination of the load-carrying capacity of eccentrically connected angle struts. Two basic alternatives are available. The strut and its connections can be modeled using plate elements. This type of modeling has the advantage of including local plate buckling and cross-sectional distortion effects. However, the modeling and computational efforts involved in such an analysis can be justified only for isolated strut problems. The second approach relies on the beam-column theory of the open cross section. In this method beam elements are used, which makes it possible to model relatively large frame assemblies with minimum modeling and computation effort. Chunmei (1984) studied the inelastic buckling of single-angle struts using large deformation plate element analysis. The analysis results were in good agreement with test results.

A general finite beam element solution developed at Lehigh University (Hu et al., 1982; Lu et al., 1983) was used to predict the strength of unequal-leg angle struts loaded through gusset plates in the center of the outstanding leg. Figures 11.2 and 11.3 show the results from analysis of a $3 \times 2 \times \frac{1}{4}$ in. angle for two cases; with the long leg outstanding and with the short leg outstanding. A comparison of the results indicated that the long-leg-outstanding arrangement is not always the more favorable arrangement. In fact, higher ultimate capacity may be obtained with the short leg outstanding arrangement for relatively short

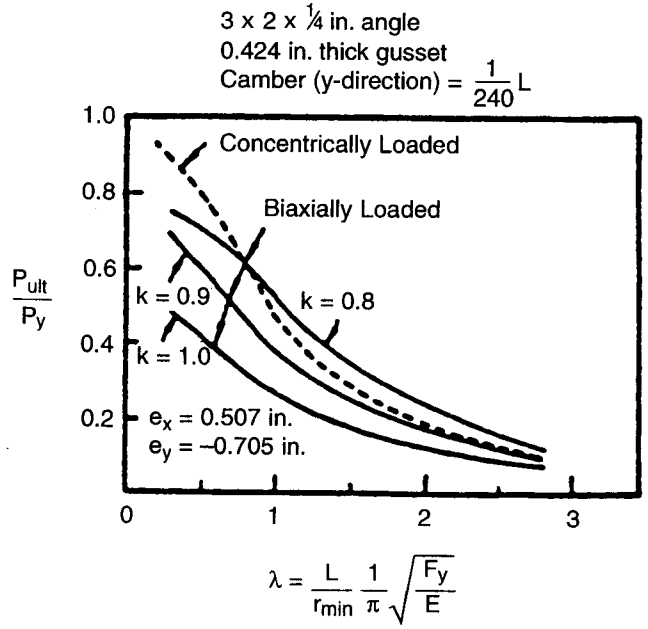

Fig. 11.2 Ultimate strength of single-angle columns loaded through gusset plates, short leg outstanding (Lu et al., 1983).

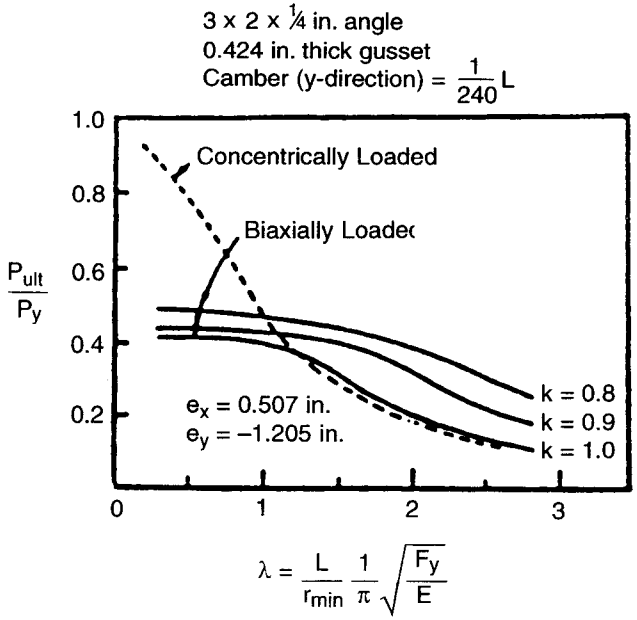

Fig. 11.3 Ultimate strength of single-angle columns loaded through gusset plates, long leg outstanding (Lu et al., 1983).

members. The results also indicated that end restraint can significantly increase the strength of an eccentrically loaded single-angle strut. Kitipornchai and Chan (1987) presented a finite beam element analysis for single-angle cross sections in the elastic range. End eccentricities and end restraints were included in the analysis. The formulation used the conventional beam stiffness matrix along with a geometry matrix specifically derived for the angle cross section. The equilibrium equations were solved in load steps accounting for the P–Δ effect, the results thus obtained were compared with the results of Trahair (1969), which did not include the P–Δ effect. Figure 11.4 shows that the P–Δ effect can have a significant influence on the load-carrying capacity of the eccentrically connected single-angle struts.

11.3 SINGLE-ANGLE COMPRESSION MEMBERS

11.3.1 Elastic Behavior

The elastic behavior is a special case of the stability of thin-walled members (Bleich 1952, Chap. 3; Vlasov, 1961, Chap. 6; Timoshenko and Gere, 1961, Chap. 5). Since the shear center is located at the intersection of the two angle legs, there is practically no warping rigidity and the warping constant C_w can

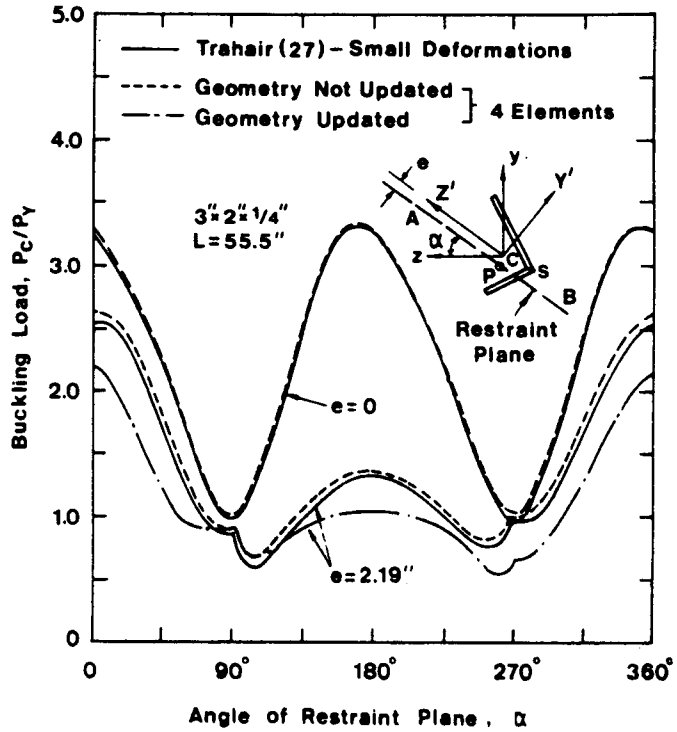

Fig. 11.4 Buckling of eccentrically loaded and restrained angle beam-columns (Kitipornchai and Chen, 1987).

be assumed to be zero. Angle members loaded through the centroid by a compressive axial force will buckle in flexural buckling about the minor principal axis of the cross section or in a torsional–flexural mode. The critical load P (Galambos, 1968) is the lowest root of the equation

$$(P_u - P)(P_z - P)(P_t - P) - P^2\left[(P_u - P)z_o^2 + (P_u - P)u_o^2\right]\frac{1}{r_o^2} = 0 \qquad (11.1)$$

where

$$P_u = \frac{\pi^2 EI_u}{L^2} \qquad (11.2)$$

$$P_z = \frac{\pi^2 EI_z}{L^2} \qquad (11.3)$$

$$P_t = \frac{GJ}{r_o^2} \qquad (11.4)$$

The terms in these equations are defined in Fig. 11.5, and L is the length of the column. For equal-leg angles $z_o = 0$ and Eq. 11.1 can be reduced to

$$P = \min(P_z, P_o) \tag{11.5}$$

where

$$P_o = \frac{(P_t + P_u) \pm \left[(P_t + P_u)^2 - 4P_uP_t\left(1 - u_o^2/r_o^2\right)\right]^{1/2}}{2\left(1 - u_o^2/r_o^2\right)} \tag{11.6}$$

11.3.2 End Restraint

Equations 11.2 and 11.3 apply only for pin-ended columns. Inevitably, some end restraint is introduced by the method of attachment of the angle to other members of the structure. Because this attachment is often to one leg only, the modeling of the end-restraint effect becomes complicated. Only a few solutions are available (Trahair, 1969; Kitipornchai and Lee, 1986). An acceptable design office solution is the use of effective-length factors so that Eqs. 11.2 and 11.3 are

$$P_u = \frac{\pi^2 EI_u}{(K_uL)^2} \tag{11.7}$$

$$P_z = \frac{\pi^2 EI_z}{(K_zL)^2} \tag{11.8}$$

where K_uL and K_zL are the effective length in the u and z directions, respectively.

11.3.3 Inelastic Behavior

Equations 11.2 and 11.3 (or Eqs. 11.7 and 11.8) are valid only in the elastic range. Inelastic behavior of angle columns has been investigated by Kitipornchai and Lee (1986) using the finite element method. A somewhat less elaborate solution is to replace the elastic modulus E in Eqs. 11.2 and 11.3 (or Eqs. 11.7 and 11.8) by the tangent modulus E_t. The shear modulus G in Eq. 11.4 remains unchanged. Approximate tangent-modulus representations for steel and aluminum are given in Chapter 3 of this guide. Use of the tangent modulus is complicated by the need for iteration. A simpler approximation is recommended in Appendix E3 of the AISC–LRFD specifications (AISC, 1993) and is described as follows:

1. Determine the elastic critical load P by Eq. 11.1 or 11.6, as appropriate.

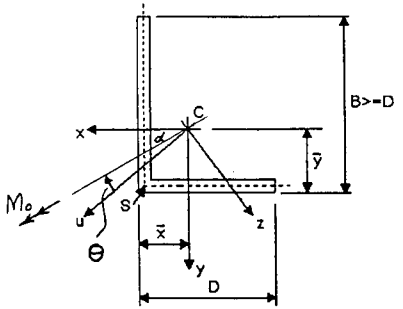

from the Handbook: $\alpha, \bar{x}, \bar{y}, I_x, I_y, r_z, A$

C: centroid (0,0)

S: shear center (u_o, z_o)

x,y: non-principal axes

u,z: principal axes

t: thickness of the angle

$x_o = \bar{x} - \frac{t}{2}$

$y_o = \bar{y} - \frac{t}{2}$

$I_z = A \cdot r_z^2$

$u_o = y_o \cdot \sin(\alpha) + x_o \cdot \cos(\alpha)$

$I_u = I_x + I_y - I_z$

$z_o = y_o \cdot \cos(\alpha) - x_o \cdot \sin(\alpha)$

$J = \frac{2 \cdot A \cdot t^2}{3}$

$d = D - \frac{t}{2}$

$r_o^2 = u_o^2 + z_o^2 + \frac{I_u + I_z}{A}$

$b = B - \frac{t}{2}$

$$C_1 = \frac{x_o^2}{2}\cdot\left[y_o^2 - (y_o - b)^2\right] + \frac{y_o^4 - (y_o - b)^4}{4} + \frac{y_o}{3}\cdot\left[x_o^3 - (x_o - d)^3\right] - y_o^3 \cdot d$$

$$C_2 = \frac{x_o}{3}\cdot\left[y_o^3 - (y_o - b)^3\right] - x_o^3 \cdot b + \frac{x_o^4 - (x_o - d)^4}{4} + \frac{y_o^2}{2}\cdot\left[x_o^2 - (x_o - d)^2\right]$$

$$\beta_z = \frac{t \cdot \left(C_1 \cdot \sin(\alpha) + C_2 \cdot \cos(\alpha)\right)}{I_z} - 2 \cdot u_o$$

$$\beta_u = \frac{t \cdot \left(C_1 \cdot \cos(\alpha) - C_2 \cdot \sin(\alpha)\right)}{I_u} - 2 \cdot z_o$$

Fig. 11.5 Definition of cross-sectional properties.

2. Compute an equivalent slenderness parameter:

$$\lambda_{eq} = \frac{1}{\pi}\left(\frac{L}{r}\right)_{eq}\sqrt{\frac{F_y}{E}} = \sqrt{\frac{AF_y}{P}} \tag{11.9}$$

3. Determine the buckling load using the formula in Section E2 of the AISC–LRFD specification.

Kitipornchai (1983) suggested the following approximations for the equivalent slenderness ratio from curve-fitting solutions to Equations 11.1 or 11.6: For equal-leg angles;

$$\left(\frac{L}{r}\right)_{eq} = 0.05\left(\frac{L}{r_z}\right) + 0.48\alpha_2 \leq \frac{L}{r_z} \tag{11.10}$$

and for unequal-leg angles;

$$\left(\frac{L}{r_z}\right)_{eq} = \left[\left(\frac{L}{r_z}\right)^3 - 8(\alpha_1 - 0.5)\alpha_2^2\frac{L}{r} + 0.76\alpha_2^3\right]^{1/3} \tag{11.11}$$

where $\alpha_1 = D/B$ and $\alpha_2 = B/t$.

Tests performed by Kennedy and Murty (1972) on hot-rolled angles showed that this method provided a satisfactory prediction of the strength. Similar confirmation has been provided by Marsh (1969), who found that his tests on slender equal-leg aluminum angles with single- and double-bolt connections were adequately predicted by

$$P_{cr} = \frac{0.9\pi^2 E}{(L/r)_{eq}^2} \tag{11.12}$$

where

$$\left(\frac{L}{r}\right)_{eq} = \sqrt{\left(\frac{5b}{t}\right)^2 + \left(\frac{KL}{r_y}\right)^2} \tag{11.13}$$

Upper limits of $0.50P_y$ (single bolts) and $0.67P_y$ (double bolts) were placed on P_{cr} ($P_y = AF_y$).

11.3.4 Eccentric Loading

The exact elastic solution of an angle with restrained ends and eccentric compressive load is complicated, and numerical methods must be employed (Trahair, 1969; Kitipornchai and Chan, 1987). Exact solutions for biaxially loaded columns with equal end eccentricities can be obtained by the method given by Culver (1966). If such columns have pinned ends, a simpler solution can be obtained by assuming the deflected shape to be a half sine wave (Dabrowski, 1961). This method is illustrated in Figs. 11.6 and 11.7, and the computations will result in midheight deformations, from which deflection limits can be checked.

When the axial compressive load is applied with eccentricities e_u and e_z (Fig. 11.6), the problem is no longer a bifurcation problem because deformation will occur with any axial load. It then becomes necessary to determine the resulting stresses, which may become amplified; or perhaps even reduced, as was found for single-angle beams by Thomas et al. (1973) due to the deflection and twist of the section. The problem of eccentrically loaded and end-restrained single-

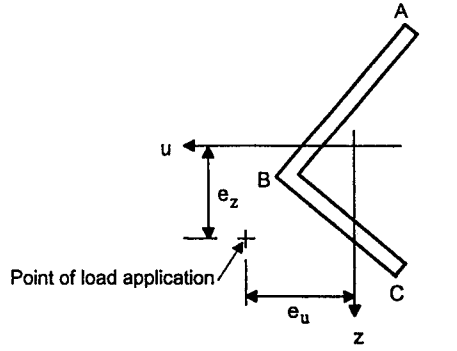

POINT	x	y
A	$\bar{x}$	$\bar{y}$-B
B	$\bar{x}$	$\bar{y}$
C	$\bar{x}$-D	$\bar{y}$

$$u = y * \sin(\alpha) + x * \cos(\alpha)$$

$$z = y * \cos(\alpha) - x * \sin(\alpha)$$

Fig. 11.6 Coordinates of the cross section in biaxial loading.

Given: L,P,e_u,e_z,cross-sectional dimensions

Step 1: Solve for A_o,B_o,C_o from the following three simultaneous equations

$$\begin{bmatrix} (P_z - P) & 0 & [-P\cdot(e_z - z_o)] \\ 0 & (P_u - P) & [P\cdot(e_u - u_o)] \\ [-P\cdot(e_z - z_o)] & [-P\cdot(e_u - u_o)] & [(P_t - P)\cdot r_o^2 - P\cdot(\beta_u\cdot e_z + \beta_z\cdot e_u)] \end{bmatrix} \cdot \begin{pmatrix} A_o \\ B_o \\ C_o \end{pmatrix} = \begin{bmatrix} \frac{-4\cdot P\cdot e_u}{\pi} \\ \frac{4\cdot P\cdot e_z}{\pi} \\ 0 \end{bmatrix}$$

A_o,B_o,C_o are deflections in the u and z directions and the angle of twist,respectively,at the column center.

$$P_z = \frac{\pi^2\cdot E\cdot I_z}{L^2} \qquad P_u = \frac{\pi^2\cdot E\cdot I_u}{L^2} \qquad P_z = \frac{G\cdot J}{r_o^2}$$

Step 2: compute the stresses at the extreme fibers (@ points A,B,C in Fig.11.6)

$$\sigma = -\frac{P}{A} + \frac{P\cdot u}{I_z}\cdot[-e_u + (e_x - z_o)\cdot C_o + A_o] - \frac{P\cdot z}{I_u}\cdot[e_z + (e_u - u_o)\cdot C_o + B_o]$$

Fig. 11.7 Method of determining the stresses at any point in the section.

angle struts for the special case of end restraint provided by tee stubs, which approximate the double-angle chord of a truss, was examined for the elastic case by Trahair (1969) for the limit state $\sigma_{max} = \sigma_y$ and for the inelastic case by Usami and Galambos (1971). Trahair compared his results with tests performed by Foehl (1948), and Usami and Galambos (1971) reported comparisons with a series of tests performed by them and with Foehl's tests. In both cases, good correlation was achieved between test and prediction. In a series of unpublished papers by Usami (1970), and Leigh and Galambos (1972), tests on the strength of single-angle eccentric webs in trusses were reported, and the results from the interaction equation,

$$\frac{P}{P_u} + \frac{Pe_u}{M_{uY}(1 - P/P_u)} + \frac{Pe_z}{M_{zY}(1 - P/P_u)} = 1 \tag{11.14}$$

were compared to test results and theoretical predictions. It was found that Eq. 11.14 gave a satisfactory if somewhat conservative prediction of the actual capacity, provided that the end eccentricities were reduced to account for end restraint from the other web members entering the panel point. P_u and P_z in Eq. 11.14 are defined by Eqs. 11.2 and 11.3, e_u and e_z are the eccentricities shown in Fig. 11.6, and M_{uY} and M_{zY} are the moments required to produce compressive yield in the extreme fiber when $P = 0$. Equation 11.14 has also been recommended for the design of single-angle web members of trusses whose ends are connected to the chords by welding or by using multiple bolted connections (Woolcock and Kitipornchai, 1980, 1986). Care is needed in deciding on appropriate end moment values if these are to reflect the effects of the load eccentricity accurately. A modification of Eq. 11.14 containing an additional torsional term has been suggested by Marsh (1972), who found that it gave good predictions of his tests on equal-leg angles under biaxially eccentric loading. While further clarification of the application of Eq. 11.14 would be useful, the evidence available suggests that it constitutes a reasonable basis for the design of angles required to function as beam-columns.

The other alternative is quite different, and its origin is with the designers of transmission towers. This alternative is applied to single-angle struts connected at their ends on one leg by bolts or by welding. The axial load is thus applied eccentrically, and the ends are restrained. For the design solution the slenderness ratio is modified for use in an appropriate column formula so as to account empirically for both the end eccentricity and the end restraints. Examples of this approach are given by both the ASCE (1988, 1992) ECCS (1976) recommendations. These methods have been reviewed by Kennedy and Madugula (1982). Support for the possible extension of this approach to a wider range of structures has been provided by Haaijer et al. (1981) on the basis of detailed finite element calculation for angles loaded (and restrained) through one leg.

In summary, present information on eccentrically loaded single-angle struts applicable for design office use indicates the utilization of the interaction equation (modified by the Q-factor reduction scheme of the AISC specification for local buckling, where applicable) in general, and the use of an empirical effective-length factor in particular for triangulated towers are appropriate. Theory, which has been validated by tests, is available to be used for the development of more accurate design criteria.

11.4 CURRENT INDUSTRY PRACTICE FOR HOT-ROLLED SINGLE-ANGLE MEMBERS IN THE UNITED STATES

11.4.1 ASCE Manual 10-90: Design of Latticed Steel Transmission Structures

For single-angle members used in transmission towers, the ASCE (1988, 1992) recognizes the importance of the eccentricity of load and the rotational restraints at the connections on the axial load-carrying capacity. An effective length factor K is included to accommodate the various end conditions of a single-angle member. Based on a review of many years of tower industry experience and the results of laboratory and full-scale tower tests, the ASCE design standard provides the following recommendations regarding effects of end eccentricity and rotational restraint on angle capacity:

A. For members with slenderness ratios less than 120, the end eccentricity plays the most predominant role. Conversely, compressive capacity of single-angle members with slenderness ratios greater than 120 is influenced primarily by the end rotational restraint. For members partially restrained against rotation at only one end,

$$\frac{Kl}{r} = 28.6 + 0.762\left(\frac{l}{r}\right);\ 120 < \frac{l}{r} < 225 \tag{11.15}$$

For members partially restrained against rotation at both ends,

$$\frac{Kl}{r} = 46.2 + 0.615\left(\frac{l}{r}\right);\ 120 < \frac{l}{r} < 250 \tag{11.16}$$

The same provisions are recommended for single-angle redundant members except that higher slenderness ratio limits are permitted. For a member to qualify for the use of the effective slenderness ratio above, the ASCE standard states that (1) the restrained member must be connected to the restraining member with at least two bolts and (2) the restraining member must have a stiffness factor (I/L) in the stress plane that equals or exceeds those of the restrained member. In other words, a single-bolt connection at either end of the single-angle member or at a point of intermediate support will not be considered as furnishing rotational restraint. Only a multiple-bolt connection detailed

to minimize eccentricity can be considered to offer partial rotational restraint if the restraining members are capable of resisting the rotation of the joint. Even with partial restraint, its impact on the allowable load is very significant. By using the provision above, a reduction of effective length up to 20% (i.e., $K = 0.8$) is permitted for members with qualified partial restraint at both ends.

B. For single-angle members that are connected by only one leg and have a slenderness ratio of less than 120, the ASCE design standard recommends that the effective slenderness ratio be taken as follows:

$$\frac{Kl}{r} = 30 + 0.75\left(\frac{l}{r}\right) \tag{11.17}$$

for members with a concentric load at one end and normal framing eccentricity at the other end, and

$$\frac{Kl}{r} = 60 + 0.5\left(\frac{l}{r}\right) \tag{11.18}$$

for members with normal framing eccentricities at both ends. Normal framing eccentricity at load transfer points implies that the centroid of the bolt pattern, except for some of the smaller angle sizes, is located between the heel of the angle and the centerline of the connected leg. These two design criteria imply that the normal end eccentricity may cause a reduction of axial load capacity by up to 20% for stocky single-angle struts. An even larger reduction of load-carrying capacity is possible when joint eccentricities exceed the normal framing eccentricity. In such a case, due consideration should be given to the additional bending stresses introduced in the member.

C. To guard against local buckling, the ratio of the flat width to thickness of the angle legs is limited to $80/\sqrt{F_y}$. Where this limit is exceeded, the effect of reduced local-buckling strength on the flexural buckling strength must be considered.

In some truss-type frames, single-angle bracing members are used as cross braces and connected by a single bolt at the crossover point of the two members. Tests have shown that if the tension member of the cross-bracing has at least 80% of the load of the compression member, the tension member provides partial support for the outstanding leg of the compression member. Under this condition, the controlling radius of gyration of equal-leg angles will be r_z. For unequal leg angles, with the long leg connected, the controlling radius of gyration may be r_z or r_y. If the load in the tension member is less than 80% of the load in the compression member, partial support for the outstanding leg at the centerline connection point is questionable.

11.4.2 Steel Joist Institute (1994): Standard Specifications for Steel Joists and Joist Girders

The SJI standard specification on web design requires that the slenderness ratio be limited to 200. For joist girders and K-series open-web steel joists, the effective-length factor is taken as 1.0 and no rotational restraint effects are considered. However, for long-span or deep long-span steel joists, the effective-length factor for compression web member is taken as 1.0 for buckling out-of-plane and 0.75 for in-plane buckling where moment-resistant weld groups are used at the ends of a crimped-end compression web member. Otherwise, the K-factor should be taken as 1.2 for in-plane buckling. An effective length less than the distance between intersection points could be justified because of the out-of-plane restraining influence of adjacent web members as the web member buckles. However, because web members are not always rigidly connected to each other at the joints, it is prudent not to count on out-of-plane end restraint in determining the effective length.

11.4.3 AISC Manual of Steel Construction, 9th Edition (ASD)

In 1989, a new AISC–ASD specification was issued to provide design guidance for allowable stress design of single-angle members AISC (1989a). The document was directed particularly to the design of hot-rolled, single-angle members with equal and unequal legs in tension, shear, compression, flexure, and for combined stresses. For axially loaded single-angle members allowable stresses were developed based on both flexural buckling and flexural–torsional buckling. For short, thin, or unequal leg angles, flexural–torsional buckling usually governs the compression strength. The allowable stress is determined using the regular column allowable formula with an equivalent slenderness ratio,

$$\left(\frac{Kl}{r}\right)_{\text{equiv}} = \pi\sqrt{\frac{E}{F_e}} \tag{11.19}$$

where F_e is the elastic buckling strength for the flexural–torsional mode. The angle end-restraint conditions should be considered in the determination of the member effective length. However, no guidelines were given as to how to account for the angle end restraint. Also not addressed by the AISC specification is the treatment of end eccentricity on the axial compression capacity of single angles.

However, the AISC steel construction manual (AISC 1989b) is more explicit in the treatment of eccentrically loaded single-angle struts. It recommends that bending about both principal axes caused by end eccentricity should be combined with the axial load effects using the AISC biaxial bending interaction formula. In the AISC steel construction manual biaxial example problem, the

maximum bending compressive stresses from each principal axis was combined in the interaction formula regardless of whether or not the maximum stresses occur at the same location. As a result, the design approach suggested by the AISC steel construction manual is rather conservative compared to the ASCE 10-90 design standards and the Steel Joist Institute standard.

In 1993, a new AISC–LRFD specification was issued for single angles AISC (1993b). Using the LRFD procedure for axially loaded angle members, it is required to examine only flexural buckling. While the specification recommends the use of the AISC–LRFD interaction formula, it indicates that the terms should reflect the stresses at a particular location on the cross section.

11.5 CURRENT INDUSTRY PRACTICE OUTSIDE THE UNITED STATES FOR THE DESIGN OF HOT-ROLLED ANGLES

Included in this section is a brief summary of industry practice of designing eccentrically loaded single-angle members in the ECCS recommendations (European Convention for Construction Steel Work), the BS 5950 (British Standard), the Australian practice, and the design standard for steel structures of the Architectural Institute of Japan.

11.5.1 ECCS Recommendations

The European practice for designing single-angle compression members can be found in the introductory report of ECCS (1976; often referred to as the "Stability Manual"), ECCS recommendations for steel construction (1978), and ECCS recommendations for angles in lattice transmission towers (1985). In all three ECCS references, the buckling strength for eccentrically loaded single-angle members are derived from the basic column compression strength curve by modifying the actual slenderness ratio according to the type of eccentricity and end restraint. For members with a nondimensional slenderness ratio λ, that is, defined as $(KL/r)\pi\sqrt{E/F_y}$ less than $\sqrt{2}$, the actual slenderness ratios are increased to account for the negative effect of end eccentricity. The effective nondimensional slenderness ratio is expressed both for buckling about the minor principal axis and for buckling about the two geometric axes.

At higher slenderness ratios, $\sqrt{2} < \lambda < 3$, the beneficial effect of the end restraint on buckling strength becomes more important than the negative effect of end eccentricity. Thus the actual slenderness ratios are decreased to account for this effect of end restraint.

The specific rules for determining the effective nondimensional slenderness ratios from the three ECCS references are summarized in Table 11.1 for members with $\lambda \leq \sqrt{2}$ and in Table 11.2 for members with $\lambda > \sqrt{2}$. Also listed in these two tables are the simplified rules from ECCS on the design of angle members in lattice transmission towers which are to be used in the initial design when end eccentricity, end restraints, and member continuity cannot be defined

TABLE 11.1 European Practice for Designing Single-Angle Compression Members[a]

References	Eccentricity at One End Only		Eccentricity at Both Ends	
	Buckling About Minimum Axis	Buckling About Geometric Axis	Buckling About Minimum Axis	Buckling About Geometric Axis
ECCS "Stability Manual" (1976)	$0.25 + 0.8232\lambda$	$0.35 + 0.7525\lambda$	$0.35 + 0.7525\lambda$	$0.50 + 0.6464\lambda$
ECCS "Recommendations for Steel Construction" (1978)	$0.60 + 0.57\lambda$	$0.60 + 0.57\lambda$	$0.60 + 0.57\lambda$	$0.60 + 0.57\lambda$
ECCS "Recommendations for Lattice Transmission Towers" (1985)	$0.25 + 0.8232\lambda$	$0.50 + 0.6464\lambda$	$0.50 + 0.6464\lambda$	$0.707 + 0.6464\lambda$
ECCS "Recommendations for Lattice Transmission Tower: Simplified Curve"	$0.50 + 0.6464\lambda$	$0.707 + 0.6464\lambda$	$0.50 + 0.6464\lambda$	$0.707 + 0.6464\lambda$

[a]Nondimensional effective slenderness ratio $\lambda_{\text{eff}} \leq \sqrt{2}$.

TABLE 11.2 European Practice for Designing Single-Angle Compression Members with End Restraints[a]

References	Restraint at One End Only		Restraint at Both Ends	
	Buckling About Minimum Axis	Buckling About Geometric Axis	Buckling About Minimum Axis	Buckling About Geometric Axis
ECCS "Stability Manual" (1976)	$0.35 + 0.7525\lambda$	$0.35 + 0.7575\lambda$	$0.50 + 0.6464\lambda$	$0.50 + 0.6464\lambda$
ECCS "Recommendations for Steel Construction' (1978)	$0.35 + 0.75\lambda$	$0.35 + 0.75\lambda$	$0.35 + 0.75\lambda$	$0.35 + 0.75\lambda$
ECCS "Recommendations for Lattice Transmission Towers" (1985)	$0.50 + 0.646\lambda$	$0.50 + 0.6464\lambda$	$0.50 + 0.6464\lambda$	λ
	Member continuous at one end and one end connected with multiple bolts		Member continous at both ends	
			$0.50 + 0.6464\lambda$	$0.707 + 0.6464\lambda$
			Member discontinuous at both ends but with multiple bolts at each end	
ECCS "Recommendations for Lattice Transmission Tower: Simplified Curve"			$0.50 + 0.6464\lambda$	$0.707 + 0.6464\lambda$

[a]Nondimensional effective slenderness ratio $\lambda_{\text{eff}} > \sqrt{2}$.
End restraint is assumed if the end connections have two or more connectors and the leg member (i.e., the supporting member) is stiffer than the connected (web) member.

clearly. Note that the basic approach of ECCS is very similar to those followed in the ASCE 10-90 standards and in Eurocode 3 (ECS, 1992).

11.5.2 BS 5950: Part I, 1985

For single-angle struts connected to a gusset or directly to another member at each end by two or more fasteners in line along the angle, or by an equivalent welded connection, the slenderness ratio, l/r, should be taken as not less than

$$\frac{0.85L}{r_z} \quad \text{or} \quad \frac{0.7L}{r_a} + 30 \tag{11.20}$$

where r_z is the radius of gyration about the minor principal axis and r_a is the radius of gyration about the axis parallel to the plane of the gusset or the supporting member. Consideration of the rotational restraint permits the use of an effective length factor of 0.85 while the end eccentricity effect is taken into account in the out-of-plane buckling.

If a single fastener end connection is used at each end of the single-angle strut, L/r should be taken as not less than

$$\frac{L}{r_z} \quad \text{or} \quad 0.7\frac{L}{r_a} + 30 \tag{11.21}$$

In other words, the rotational restraint effect is ignored in this case. In addition, it requires that the compression resistance be taken as not greater than 80% of the compression resistance of a corresponding concentrically loaded strut.

11.5.3 Australian Practice

A design approach was proposed by Woolcock and Kitipornchai (1986) to design single-angle web members. Basically, they recommended the combined stress interaction equation to be used for buckling and bending in the plane perpendicular to the truss. The out-of-plane bending moment at the end of each strut is calculated considering the eccentricity of the connection and the influence of adjacent web members. The current steel standard AS 4100-1990 also follows this approach.

11.5.4 Japanese Practice

The Design Standard for Steel Structures of the Architectural Institute of Japan recommends that single-angle web compression members of a truss be designed as pin-ended centrally compressed members, subjected to buckling about the minor principal axis. Where the end connection of web members is accomplished by a single fastener, the allowable compressive stress in these

members shall be reduced by half to account for the effect of end eccentricity and loss of end restraint.

11.6 DESIGN OF AXIALLY LOADED COLD-FORMED SINGLE ANGLES

The provisions of the ANSI–ASCE Standard 10-90 (*Design of Latticed Steel Transmission Structures*) (ASCE, 1992), the Canadian CSA-S136-M89 (*Cold-Formed Steel Structural Members*) (CSA, 1989), and the ECCS recommendations are summarized in this section.

11.6.1 ASCE Standard 10-90 (1992)

Historically, most transmission structures have been fabricated from hot-rolled steel angles. The availability of thinner hot-rolled sections is limited. Cold-formed angles are more readily available in thinner and smaller sections. They provide a feasible alternative for more economical structures. An excellent summary on the design of cold-formed angles for transmission towers is given by Gaylord and Wilhoite (1985).

Unlike hot-rolled sections, cold-formed angles are available in more varieties of shapes. Three of the more commonly used configurations are 90° angle, 60° angle, and lipped angle. The recommended design criteria for compression members using cold-formed angles are covered by the updated version of ASCE Manual 52, identified as ANSI–ASCE 19-90.

Design of cold-formed plain angles is identical to that of hot-rolled angles, except that the flat width should be taken as the leg width minus the thickness minus a maximum inside bend radius of two times the angle thickness. The ASCE standard (ASCE 10-90) requires the member to be checked for flexural and local buckling. The validity of these design criteria have been verified experimentally for cold-formed angles concentrically or eccentrically loaded (Gaylord and Wilhoite, 1985).

For symmetrical lipped angles, the member must be checked for flexural and torsional flexural buckling. This is because the local buckling strength of the lipped-angle leg is not equivalent to torsional buckling. The torsional-flexural buckling strength can be determined by the AISI specification for the design of cold-formed steel structural members, or using an equivalent radius of gyration, r_{tf}:

$$\frac{2}{r_{tf}^2} = \frac{1}{r_t^2} + \frac{1}{r_u^2} + \sqrt{\left(\frac{1}{r_t^2} - \frac{1}{r_u^2}\right)^2 4\left(\frac{U_o}{r_t r_u r_{ps}}\right)^2} \qquad (11.22)$$

where

r_t = equivalent radius of gyration for torsional buckling

$r_t = \sqrt{C_w + 0.4\mathrm{J}(KL)^2/I_{ps}}$
C_w = warping constant
J = St.-Venant torsional constant
KL = effective length
I_{ps} = polar moment of inertia of cross section about shear center
r_u = radius of gyration of cross section about U-axis
U_o = distance between centroid and shear center
$r_{ps} = \sqrt{I_{ps}/A}$ = polar radius of gyration about shear center

In addition, the edge stiffener should consist of a single lip bent at right angles to the stiffened element and meet a minimum lip depth requirement. Evaluation of torsional–flexural buckling requires determination of certain geometrical properties which are not encountered in flexural buckling. Procedures for computing the torsional constant, the warping constant, the location of the shear center, polar moment of inertia about the shear center, and other properties of cold-formed sections are given in the AISI *Cold-Formed Steel Design Manual* (AISI 1996) and in Madugula and Ray (1984a).

11.6.2 Canadian Standard CSA-S136-M89 (1994)

Cold-formed angles are designed as axially loaded columns. The design of concentrically loaded cold-formed members is discussed further in Chapter 13.

11.6.3 AISI Specification for the Design of Cold-Formed Steel Structural Members (AISI 1996)

In this specification cold-formed angles are to be designed for both axial load and flexure (see Chapter 13 for details of this procedure). The Australian cold-formed steel standard is similar to the AISI method.

11.6.4 European Practice

The axial strength of cold-formed angles is determined in the same way as for hot-rolled angles according to EECS recommendation (1978) except that the modulus of elasticity of cold-formed steel is taken as 210 GPa. Based on the work of Madugula et al. (1983) and Madugula and Ray (1984b), the computed failure loads using ECCS recommendations are either less than or very close to the experimental failure loads for eccentrically loaded cold-formed angles for all slenderness ratios. They are generally more conservative than those given in ASCE 10-90 (1992). Further, the ECCS recommendation gives essentially the same results as the ASCE 10-90 for the concentrically loaded cold-formed angles.

11.7 CONCLUDING REMARKS ON THE COMPRESSIVE STRENGTH OF ECCENTRICALLY LOADED SINGLE-ANGLE MEMBERS

The compressive strength of eccentrically loaded single-angle members has been studied over the years both analytically and experimentally. Where end restraints and eccentricities are clearly defined, the strength of the column can be predicted with good accuracy using either classical stability analysis or the finite element method. The latter method has yielded very good results in both the elastic and inelastic nonlinear range.

Both the experimental and analytical studies show that the compressive strength of single-angle members is weakened by end eccentricity in the lower slenderness ratio range. It has also been concluded that the end restraint can significantly increase the ultimate strength of single-angle members of higher slenderness ratios. One of the most difficult tasks for designers is to judge or to determine the end restraint and eccentricity condition for their specific application. Failure to consider the restraint effect could lead to an uneconomical design. On the other hand, ignoring the end eccentricity may sometimes result in an unsafe design. To ensure a safe and economical design of a structure made of single-angle members, designers must pay attention to minimizing framing eccentricity in detailing angle connections, while the beneficial effects of rotational restraints, where applicable, should not be ignored.

The empirical approach to include the effects of end restraints and joint eccentricities by modifying the member's effective slenderness ratio such as adopted by ASCE Standards 10-90, ECCS recommendations, and BS 5950 are very convenient to use. However, application of these design criteria to structures with uncertain end restraints or more excessive eccentricities should be exercised with great care. Where end restraint is poor and joint eccentricities are large, eccentricities must be taken into consideration by considering biaxial bending. For those cases the interaction equation in the AISC specification is recommended.

It appears that more research is needed to develop a general method for quantifying the effects of end eccentricity and end restraints on the member strength. Results would be useful to help designers to evaluate single-angle members with excessive eccentricities or with end restraints that are not covered by the various design specifications.

11.8 MULTIPLE ANGLES IN COMPRESSION

11.8.1 Introduction

Several different configurations of double angles are possible. The first, now used most frequently, is with the angles arranged in back-to-back configuration, basically forming a tee section, Fig. 11.8*a*. A second configuration, now used less frequently, is with the edges of the angles connected to form a boxed

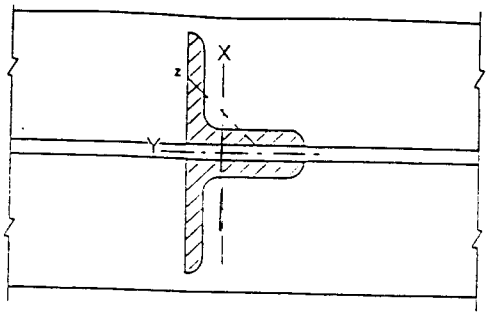

Back-to-back Angles

(*a*)

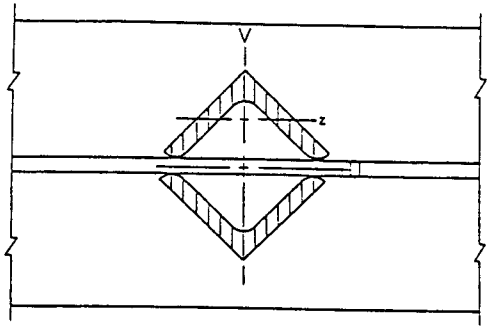

Boxed Angles

(*b*)

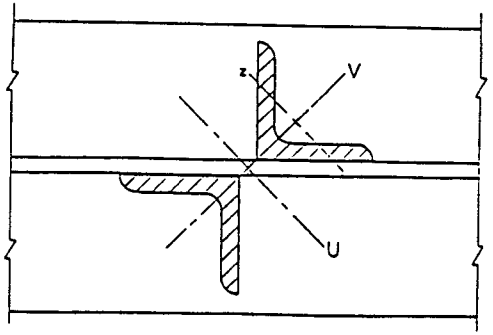

Starred Angles

(*c*)

Fig. 11.8 Double-angle configurations.

section, Fig. 11.8*b*. The third configuration, which seems to be gaining in popularity, is the starred angle compression member, Fig. 11.8*c*. The advantages and disadvantages of each configuration should be considered before a designer selects the appropriate double-angle configuration.

1. The back-to-back and boxed double angles have surfaces that are virtually inaccessible. This may be undesirable when maintenance is required, such as in the chemical industry, where a corrosive atmosphere exists, or where building hygiene is important, such as in the food or pharmaceutical industries. In starred angles all the surfaces are accessible for maintenance.
2. In back-to-back angles, bolts in connections can be used in double shear. In starred angles, bolts can be used only in single shear. Boxed angle connections have to be welded.
3. Boxed and starred angles tend to make more effective use of equal-leg angles than does the back-to-back configuration. The minimum moment of inertia of a boxed or starred angle made from equal-leg angles is about 60% greater than for the same angles in the back-to-back configuration.
4. Boxed angles seem to be preferred by some engineers and architects for aesthetic reasons; from a distance a boxed section has the appearance of a structural tube.
5. Starred angles are used as vertical web members in primary trusses which support secondary trusses in large industrial buildings. The nature of the cross section and the ease with which the connection can be made make these members desirable for this application. Such a connection at the exterior of a building is shown in Fig. 11.9*a*, and the cross section of the starred angle at the connection is shown in Fig. 11.9*b*.

11.8.2 Interconnection

Interconnectors. In some double-angle web members no interconnectors are used, except, of course, for the connection of the angles to the chords of the truss. The load-carrying capacity of such double angles is calculated as twice that of a single angle using the radius of gyration about the minor principal axis, the z-axis. This seems to be very conservative for slender back-to-back angles (Temple and Tan, 1988). It was found that the average failure load was as high as 2.2 times the load calculated according to the North American standards and specifications for a slender member and about 1.3 times the load calculated for angles of intermediate length. Since the double-angle web member is attached to the chord of the truss by one leg, the individual angle does not buckle about the z-axis, but at failure load the displacement in the y-direction at midheight (see Fig. 11.8*a*) was about five times that in the x-direction.

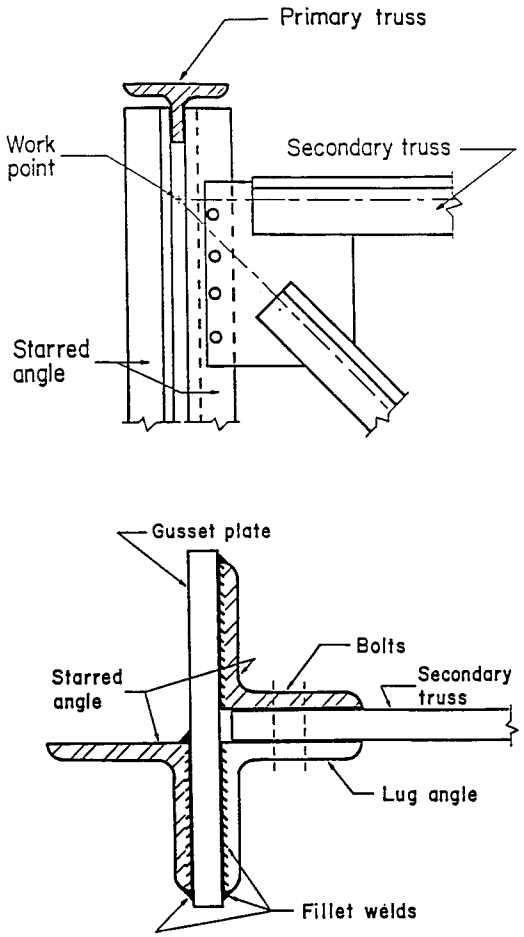

Fig. 11.9 End connections of starred-angle columns.

In most cases double angles are designed to act as an integral unit. Thus interconnectors, which normally consist of small bars but could be short lengths of angles, tubes, and so on, are used to connect the angles intermittently along the length of the member. Figure 11.10 illustrates various methods of connecting double angles. It seems that fabricators prefer small pieces of plates to other connectors, such as short lengths of angles, simply from the point of view of economy. Bolted connectors are seldom used except for bracing members.

Tests on starred angles (Temple et al., 1986) demonstrated that the type of connector did not affect the load-carrying capacity as long as the angles were firmly connected at the points of interconnection. It seems that fabricators will

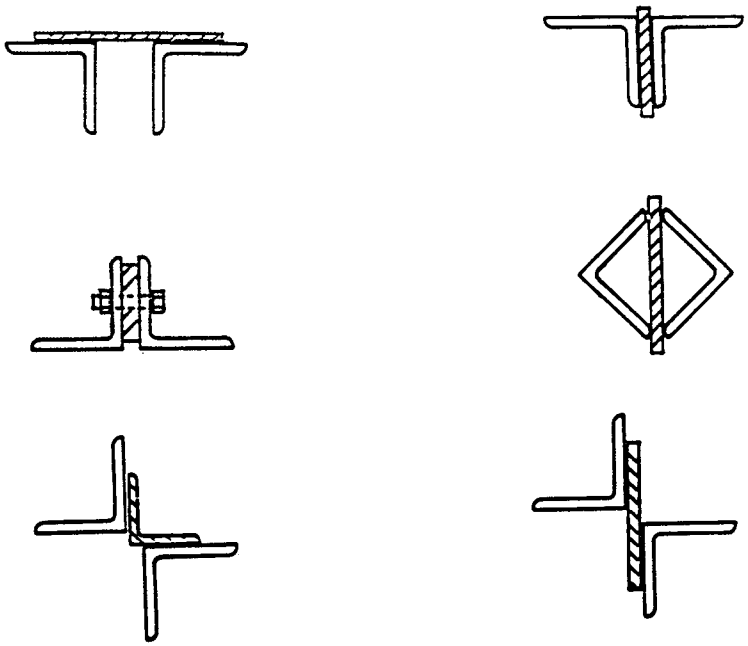

Fig. 11.10 Intermediate connectors between double-angles.

use a connector that is similar in thickness to the angles being connected and of dimensions that are of "manageable proportions." The connectors are then welded to the legs of the angles with the minimum-size weld specified by the applicable standard or specification for the thickness of material being used.

Interconnector Versus Batten. It has been proposed by Temple (1990) that when buckling of back-to-back angles occurs by flexural buckling about the x-axis (Fig. 11.8*a*) that the connector be termed an *interconnector*. The function of an interconnector is to make the two angles act together, that is, to deflect about the same amount in the y-direction, to maintain the back-to-back separation between angles from changing and to help restrain any rotation of the individual angles that might occur if no connectors were present. Tests have shown (Temple and Tan, 1988) that the forces and moments in the interconnectors are very small.

When torsional–flexural buckling of the back-to-back angles occur about the y-axis the connector behaves like a batten and hence should be designed for the appropriate moments and shears shown in Fig. 11.11 (Temple, 1990). It is realized that these forces are developed for flexural buckling only and not for torsional–flexural buckling. It seems that the shear force, expressed as a percentage of the compressive resistance, normally used in such calculations

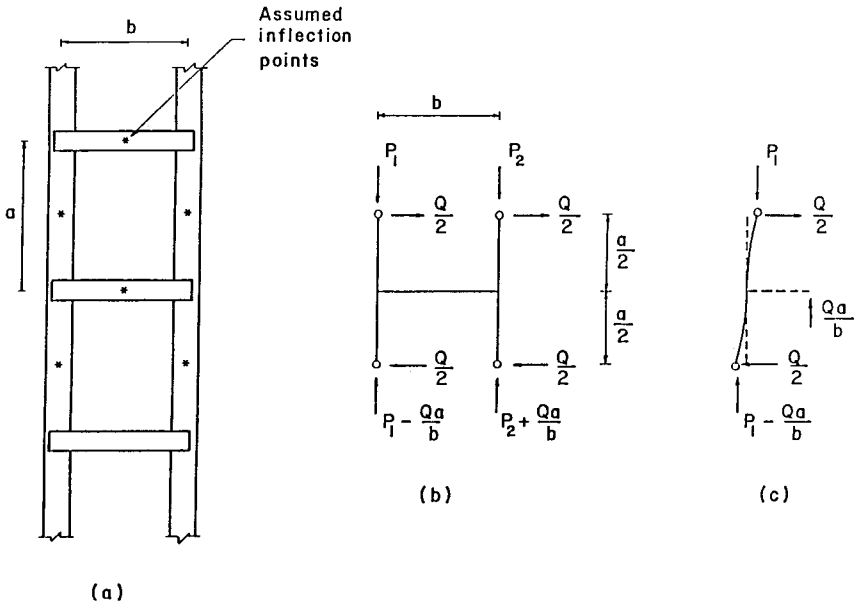

Fig. 11.11 Calculation of forces in intermediate connectors between double angles.

would be sufficient to handle the shear and moments developed in the connector from the flexural as well as torsional effects. The Canadian standard, CAN-S16.94 (CSA, 1994), has specified a shear force of 2.5% of the axial compressive force in the member under factored loads. The AISC's *Load and Resistance Factor Design Specification for Structural Steel Buildings* (AISC, 1993a) does not specify any requirements for battens. During a research project to determine the interconnection requirements of starred angles, Temple et al. (1986) determined the force that must be resisted by the connectors in such double angles. It was concluded that the force carried by such connectors was not great. Thus it is recommended that these connectors can be treated as interconnectors. As part of a research project on the interconnection of boxed angle compression members (Temple et al., 1987), connectors at the third points were strain gaged. It was determined that the connectors were under small compressive forces and could once again be treated as interconnectors.

Effect of Weld Pattern. In most cases connectors are welded to the legs of back-to-back angles as shown in Fig. 11.12*a*. In some cases, however, it is not convenient during fabrication to apply this "normal" weld pattern (Temple and Tan, 1988). In that case the welds are placed between the angles only as shown in Fig. 11.12*b*, referred to as a "special" weld pattern. Tests indi-

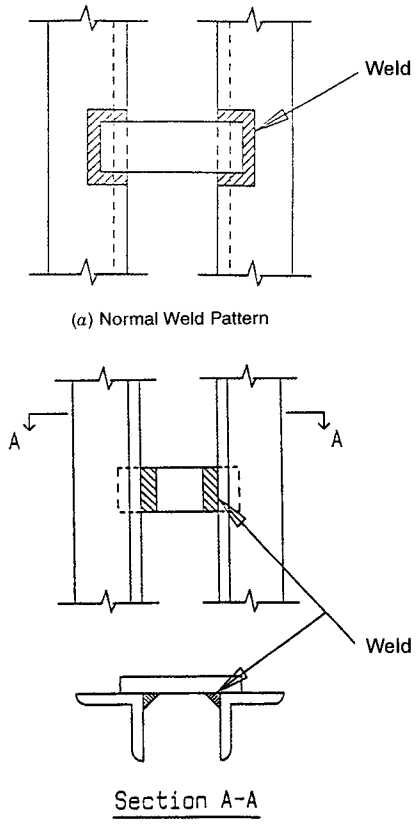

(*a*) Normal Weld Pattern

(*b*) Special Weld Pattern

Fig. 11.12 Welding of intermediate connectors between double angles.

cate that the load-carrying capacity is not affected significantly by the weld pattern. It would seem to be conservative to avoid, if possible, the special weld pattern, as it does not provide as much rotational restraint to the individual angles as does the normal weld pattern.

11.8.3 Interconnection Requirements in the North American Standards

The Canadian standard, S16.1 (CSA, 1994) and the American specification (AISC, 1993) have similar requirements for the connection of double-angle compression members. They require that the slenderness ratio of the individual angle between points of connection cannot exceed all of (CSA) or three-fourths of (AISC) the slenderness ratio of the built-up member. The AISC specification

provides an equation for an increased equivalent slenderness ratio to account for shear effect in separated members (AISC 1993a).

11.8.4 Connection Test Results

Test results for starred and boxed angle compression members, Temple et al. (1986) and Temple et al. (1987), indicate that the current Canadian requirements for the interconnection of these members are not adequate. For slender starred angles ($L/r = 122$) with zero interconnectors, which means that the angles were connected at the ends only, and with one interconnector at midheight, the failure loads were less than those specified by the applicable standards. The failure mode for these specimens consisted of buckling about the u-axis (Fig. 11.8*c*) but obviously not as an integral unit. With two or more interconnectors there was an abrupt change in the magnitude of the failure loads and in the failure mode. The failure loads were greater than those specified and the failure mode is one of the flexural buckling about the v-axis, the minor principal axis of the composite cross section. The number of interconnectors in these tests was varied from zero to five, but the use of more than two connectors did not significantly affect the failure loads.

In these tests the type of connector was varied and it was noted that the type of interconnector did not significantly affect the load-carrying capacity or failure mode as long as the angles were firmly attached at the point of connection. For starred angles of intermediate length ($L/r = 80$ or 40) there was not much difference in the load-carrying capacity as the number of connectors was changed from zero to one or two. There was, however, a difference in the failure mode, and this makes the use of two connectors desirable. These intermediate-length starred angles with two connectors buckled about the minor principal axis of the cross section, the v-axis, whereas with zero and one connector the starred angles failed by buckling about the u-axis.

The research project on the interconnector of starred angle compression members made from equal-leg angles concluded that two interconnectors, one at each of the third points, should be used. The research project on the connection requirements of boxed angles (Temple et al., 1987) concluded with results which are very similar to those in the starred angle research project. This is not surprising since rotating the individual angles by 180° results in the starred angle configuration. Again it was concluded that two interconnectors, one at each of the third points, should be used. In a research project on back-to-back angles, Temple and Tan (1988) demonstrated that for angles that buckle about the x-axis, one interconnector at midlength was sufficient to give back-to-back angles made from equal-leg angles a load-carrying capacity equal to or greater than that specified by the CSA standard (1994). It should be pointed out, however, that in these tests when one interconnector was used the

slenderness ratio of the individual angles between points of connection was only 78% of that for the double-angle member.

11.8.5 Load-Carrying Capacity

For singly symmetric sections such as back-to-back angles (Fig. 9*a*), instability can occur due to flexural buckling about the x-axis or to torsional-flexural buckling. If the section is doubly symmetric, as with starred and boxed angles (Fig 11.9*b* and *c*), buckling involves flexure about the x- or y-axis, or torsion about the shear center, which coincides with the centroid of the composite cross section. For the doubly symmetric sections the three failure modes are independent and the minimum load determines the load-carrying capacity. Tests conducted by Kennedy and Murty (1972) on double-angle struts with hinged- and fixed-end conditions under concentric loading confirmed the theoretical solutions commonly used to calculate flexural and flexural–torsional buckling loads of these specimens. Temple and Tan (1988) demonstrated that the load-carrying capacity of back-to-back angles buckling about the x-axis can be preferred by the then current North American standards and specifications. The torsional–flexural buckling load can be predicted by the procedure recommended in the AISC–LRFD specification (AISC 1993a). This procedure is demonstrated for back-to-back angles in a paper by Brandt (1988). He demonstrates that a simple comparison of the slenderness ratios about x and y for double angles can result in incorrect conclusions. Libove (1985) has studied sparsely connected built-up columns where the two identical elements are slightly separated and connected at a few points along their length. This includes back-to-back angles where buckling occurs at right angles to the axis of symmetry. He shows that satisfying the common rule that the slenderness ratio between points of connection should not exceed the slenderness ratio of the built-up member may result in a load-carrying capacity considerably less than the buckling load predicted using the composite cross section. Libove also cautions that the postbuckling behavior is unstable; that is, the load required to maintain a buckling configuration is less than that required to initiate it. New design provisions in the AISC specifications (AISC 1993a) were introduced to counteract this unconservatism.

Lorin and Cuille (1977) demonstrated that the substitution of a double angle for a larger angle, at relatively the same cost, makes for an improvement in the load-carrying capacity of 30 to 70%, the higher values obtained when the thickness of the gusset plates was doubled. Astaneh and Goel (1984) studied double-angle bracing members subjected to in-plane buckling due to severe cyclic load reversals. Eight full-size test specimens made of back-to-back double-angle sections were tested under constant-amplitude cyclic loading. Some specimens that were designed by code procedures failed during early cycles of loading. New design procedures were proposed, and these were adopted in the AISC specification (AISC 1993a).

11.9 ANGLES IN FLEXURE

Angles are sometimes used as purely flexure members or as struts subjected to transverse loading. Angles are often employed as beams in walkways, racks, equipment support frames, pipe support systems, plus other lightly loading framing. Pipe support systems composed of angles are used extensively in the nuclear power industry. The angles used are also often subjected to flexure from transverse loading. Support frames are often composed of members that become struts with small transverse load or beams with small axial load when subjected to seismic or wind loads.

11.9.1 Limit States

The ultimate strength of angle flexure members are determined by one of the following limit states: (1) yielding of the section, (2) local buckling of an angle leg, and (3) lateral torsional buckling. Deflection of angle flexural members represents a serviceability limit state that may govern over the strength limit state.

11.9.2 Yielding of the Section

Multiple angles in back-to-back, cruciform (or starred) configurations will yield at the tip of one of the angle legs, as will the single angle, provided that one of the other limit states does not control the strength of the section. Each of these shapes has a shape factor of at least 1.5. This means that the section has the potential of achieving an ultimate or plastic moment at least 50% more than the moment at first yield. It should be noted that in the composite sections it will be extremely difficult to achieve the full plastic moment unless substantial interconnection of components is employed. For the boxed composite section (composed of two equal-leg angles) first yield may occur along two faces simultaneously, in which case the shape factor is approximately 1.15. However, if loaded on a diagonal such that the neutral axis is along the other diagonal, the shape factor is 1.5. The plastic moment is about the same for both orientations, but the elastic section modulus is lower in the diagonally loaded orientation.

Based on the post yield behavior noted above, for single angles the use of $1.25F_yS$ has been deemed to be an acceptable nominal moment strength, according to the AISC–LRFD specification (AISC 1993b), provided that local or lateral–torsional buckling does not affect the behavior of the cross section. The AISC–ASD specification (1989) uses an allowable stress limit of $0.66F_y$ to reflect the benefit of the shape factor.

11.9.3 Local Buckling

When one of the legs of a single- or multiple-angle section has its tip at the maximum compression stress, local buckling of that leg may limit the section flexural capacity. The critical b/t ratio will depend on the variation of compressive stress along the leg. A uniform compression on a long plate element with one long edge free and the other hinged has a plate buckling coefficient of 0.43, as noted in Table 11.3. As the compression stress condition across the element becomes less severe, the buckling coefficient increases significantly. Rotational restraint at the supported edge will increase the buckling stress for each case. Each case in Table 11.3 can be obtained for angles in flexure as noted. For angle legs, the AISC–LRFD specification (AISC 1993b) sets the critical elastic stress at $0.534E/(b/t)^2$. This limit is used for axial load and for flexural loading when the tip of the angle has the maximum stress. This appears to be unconservative for axial load compared to the $0.39E$ value from Table 11.3. However, the use of overall leg length for b and the additional torsional stiffness due to the inside radius of hot-rolled angles increase the actual capacity above the theoretical. In addition, for unequal-leg angles the shorter leg

TABLE 11.3 Plate Buckling Coefficients for Equal-Leg Angles

Case	Stress Variation	K Coefficient	Steel $f_{cr}(b/t)^2$	Angle Orientation
1	$f_2 = f_1$	0.43	11,270	
2	$f_2 = 0$	0.57	14,940	
3	$f_2 = -f_1$	0.85	22,280	
4	$f_1 = 0$	1.70	44,560	

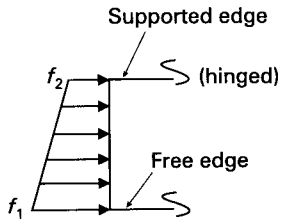

$$f_{cr} = \frac{K\pi^2 E}{12(1-\mu^2)(b/t)^2}$$

provides restraint to the critical longer leg, whereas the theoretical values consider a hinge at the supported edge.

11.9.4 Excessive Deflection

As with all structural members in flexure, deflection may be a controlling design condition for a member. The deflection-limiting L/b ratio varies significantly with orientation of the bending axis and with end-restraint conditions. For simply supported spans with $L/175$ deflection limit and major axis bending of an equal-leg angle, L/b can reach a value of about 50 before deflection controls over stress for A36 steel. If a total deflection of $L/360$ is used for an equal-leg angle bent about its minor axis, deflection will control when L/b exceeds about 12.

Often, angles are loaded parallel to one of their legs. If such an angle is laterally unbraced, it will deflect not only in the direction of the load but also perpendicular to that direction. The total deflection will be larger than that for a laterally braced angle. For an equal-leg angle that is laterally unbraced, the deflection in the loaded direction is 1.56 times that of the same angle when it is braced. In addition, the unbraced equal-leg angle will deflect perpendicular to the loaded direction 60% of the loaded direction amount. The resultant represents an 82% larger deflection than the laterally braced angle.

Twisting of angles can also be of concern. The shear center is at the intersection of the angle legs. Obviously, increasing load eccentricity and using thin angle legs will increase angle rotation. Angle rotation, in turn, can increase the normal stress as demonstrated by Leigh and Lay (1969) for angles bent about an axis parallel to a leg. However, for angles bent about a geometric axis, if L/t is kept below 800 for A36 steel, no increase in stress from twist will occur.

11.9.5 Lateral–Torsional Buckling

The general case is that of an unequal-leg angle that can be bent about any axis. This is illustrated in Fig. 11.5 with moment applied at angle θ from the u-axis. For the case of uniform bending moment M_0, and ignoring the warping stiffness such that the warping constant C_w is zero, the general equation for lateral–torsional buckling becomes

$$\phi''(GJ + \beta_u M_0 \cos\theta - \beta_z M_0 \sin\theta) + \phi\frac{M_0^2}{E}\left(\frac{\cos^2\theta}{I_z} + \frac{\sin^2\theta}{I_u}\right) + \frac{M_0^2 \sin\theta\cos\theta}{E}\left(\frac{1}{I_u} - \frac{1}{I_z}\right) = 0 \quad (11.23)$$

For the case of equal-leg angles the value of β_u becomes zero. Typically I_z, I_u, and J are expressed in terms of b and t (see Fig. 11.5 for definitions). $I_u = tb^3/3$, $I_z = tb^3/12$, $J = 2bt^3/3$, and $\beta_z = \sqrt{2}b$, by approximating the sec-

tion as two rectangular areas of length b and width t. In this case, the solution of Eq. 11.23 can be expressed in the following form:

$$M_0 = \frac{\sqrt{2}\pi^2 Eb^4 t}{6(1+3\cos^2\theta)L^2}\left[\sqrt{\sin^2\theta + \frac{4G(1+3\cos^2\theta)L^2t^2}{\pi^2 Eb^4}} - \sin\theta\right] \tag{11.24}$$

If M_0 is applied about the u, or major principal, axis ($\theta = 0$), this expression simplifies to

$$M_0 = \sqrt{\frac{2\pi}{6}}\sqrt{GE}\,\frac{b^2t^2}{L} \tag{11.25}$$

In terms of critical maximum bending stress F_{ob} for equal-leg angles, using I_u given above and $b/\sqrt{2}$ as the distance from the neutral axis,

$$F_{ob} = \frac{\pi\sqrt{GE}}{2(L/t)} \tag{11.26}$$

In the case of unequal-leg angles bent about the principal u-axis ($\theta = 0$), using the critical moment from Eq. 11.24 the critical moment M_0 becomes

$$M_0 = \frac{\pi^2 EI_z}{2L^2}\left[\sqrt{\beta_u^2 + \frac{4G}{3\pi^2 E}\left(\frac{Lt}{r_z}\right)^2} + \beta_u\right] \tag{11.27}$$

where β_u is the section property defined in Fig. 11.5. Its value should be taken as positive when the shorter angle leg (length D) is in compression and negative when the longer angle leg (length B) is in compression. Equations 11.26 and 11.27 both reflect the combined effects of lateral and torsional flexibility of the angle.

Often, angles are bent about one of the geometric axes (x or y). If this bending produces compression at the tip of the angle leg, lateral–torsional instability remains a potential problem. In Fig. 11.5 this situation occurs when $\theta = \alpha$ or $\alpha + 90°$ (i.e., when M_0 is applied about the x- or y- axis to produce compression at the top of the angle shown.

The critical moment for equal-leg angles can readily be evaluated using Eq. 11.24 by setting $\theta = 45°$, and can be expressed as

$$M_{0x} = \frac{\pi^2 Eb^4 t}{15L^2}\left(\sqrt{1 + \frac{20GL^2t^2}{\pi^2 Eb^4}} - 1\right) \tag{11.28}$$

The critical lateral–torsional moment can also be evaluated from Eq. 11.24 for an equal-leg angle bent about its z-axis. If $\theta = 90°$, the tips of the legs will be in compression, leading to

$$M_{0z} = \frac{\sqrt{2}\pi^2 Eb^4 t}{6L^2}\left(\sqrt{1 + \frac{16GL^2t^2}{\pi^2 Eb^4}} - 1\right) \tag{11.29}$$

The equations and procedures above are the bases for the criteria of both the allowable stress design and the load and resistance factor design criteria of the AISC specifications for single-angle members (AISC 1989a, 1993b). In the inelastic range of buckling a transition relationship is used: When $M_0 \le M_y$,

$$M_n = \left(0.92 - 0.17\frac{M_0}{M_y}\right)M_0 \tag{11.30}$$

and when $M_0 > M_y$,

$$M_n = \left(1.58 - 0.83\sqrt{\frac{M_y}{M_0}}\right)M_y \le 1.25M_y \tag{11.31}$$

where M_n is the nominal moment capacity, M_y the yield moment, and M_0 the elastic lateral–torsional buckling moment determined from the equations above. For allowable stress design the transition equations are scaled down and transformed into stress equations.

REFERENCES

Adluri, S. M. R., and Madugula, M. K. S. (1992), "Eccentrically Loaded Steel Angle Struts," *AISC Eng. J.*, Vol. 29, No. 2, pp. 59–66.

AISC (1989a), *Specification for Allowable Stress Design of Single-Angle Members* American Institute of Steel Construction, Chicago.

AISC (1989b), *Specification for Structural Steel Buildings, Allowable Stress Design and Plastic Design*, American Institute of Steel Construction, Chicago.

AISC (1993a), *Load and Resistance Factor Design Specification for Structural Steel Buildings*, American Institute of Steel Construction, Chicago.

AISC (1993b), *Specification for Load and Resistance Factor Design of Single-Angle Members*, American Institute of Steel Construction, Chicago.

AISI (1966a), *Cold-Formed Steel Design Manual*, American Iron and Steel Institute, Washington, DC

AISI (1966b), *Specification for the Design of Cold-Formed Steel Structures*, American Iron and Steel Institute, Washington, DC

ASCE (1988), *Guide for Design of Steel Transmission Towers*, ASCE Manual Eng. Pract. No. 52, American Society of Civil Engineers, New York.

ASCE (1992), *Design of Latticed Steel Transmission Structures*, ASCE Standard 10-90, American Society of Civil Engineers, New York.

Astaneh, A., and Goel, S. C. (1984), "Cyclic In-plane Buckling of Double Angle Bracing," *ASCE J. Struct. Div.*, Vol. 110, No. ST9, pp. 2036–2055.

Bleich, F. (1952), *Buckling Strength of Metal Structures*, McGraw-Hill, New York.

Brandt, G. D. (1988), "Flexural–Torsional Buckling for Pairs of Angles Used As Columns," *AISC Eng. J.*, first quarter.

BSI (1985), *Structural Use of Steelwork on Building*, BS5950, Part 1, British Standards Institute, London.

Chunmei, G. (1984), "Elastoplastic Buckling of Single Angle Columns," *ASCE J. Struct. Eng.*, Vol. 110, No. 6, pp. 1391–1395.

CSA Canadian Standards Association (1989), *Cold-Formed Steel Structural Members*, Toronto, Ontario, Canada.

CSA Canadian Standards Association (1994), *Limit States Design of Steel Structures*, S16.1, Toronto, Ontario, Canada.

Culver, C. G. (1966), "Exact Solution of the Biaxial Bending Equations," *ASCE J. Struct. Eng.*, Vol. 92, No. ST2, pp. 63–83.

Dabrowski, R. (1961), "Thin-Walled Members Under Biaxial Eccentric Compression," *Stahlbau*, Vol. 30, Dec., pp. 360–365.

ECS (1992), *Design of Steel Structures*, European Committee on Standardization, Brussels, Belgium.

ECCS (1976), "Manual of the Stability of Steel Structures," *2nd Colloq. Stab. Steel Struct.*, European Convention for Constructional Steelwork, Liege, Belgium.

ECCS (1978), *European Recommendations for Steel Construction*, European Convention for Constructional Steelwork, Brussels, Belgium.

ECCS (1985), *Recommendations for Angles in Lattice Transmission Towers*, European Convention for Construction Steelwork, Brussels, Belgium.

Elgaaly, M., Dagher, H., and Davids, W., (1991), "Behavior of Single Angle Compression Members," *ASCE J. Struct. Eng.*, Dec.

Elgaaly, M., Davids, W., and Dagher, H., (1992), "Nonslender Single Angle Struts," *AISC Eng. J.* first quarter.

El-Tayem, A., and Goel, S. C. (1986), "Effective Length Factor for the Design of X-Bracing Systems," *AISC Eng. J.*, first quarter.

Foehl, F. P. (1948), "Direct Method of Designing Single Angle Struts in Welded Trusses," in *Design Book of Welding*, Lincoln Electric Co., Cleveland, OH.

Galambos, T. V. (1968), *Structural Members and Frames*, Prentice Hall, Upper Saddle River, N.J.

Gaylord, E. H., and Wilhoite, G. M. (1985), "Transmission Towers: Design of Cold-Formed Angles," *ASCE J. Struct. Eng.*, Vol. 11, No. 8.

Haaijer, G., Carskaddan, P. S., and Grubb, M. A. (1981), "Eccentric Load Test of Angle Column Simulated with MSC/Nastran Finite Element Program," *Proc. SSRC Annu. Tech. Session*, Chicago.

Hu, X. R., Shen, Z. Y., and Lu, L. W. (1982), "Inelastic Stability Analysis of Biaxially Loaded Beam Columns by the Finite Elements Methods," *Proc. Int. Conf. Finite Element Methods*, Shanghai, China, Vol. 2, pp. 52–7.

Ishida, A. (1968), "Experimental Study on Column Carrying Capacity of SHY Steel Angles," *Yawata Tech. Rep. No. 265*, Dec. pp. 8584–8582, 8761–8763, Yawata Iron & Steel Co., Tokyo.

Kennedy, J. B., and Madugula, M. K. S. (1982), "Buckling of Single and Compound Angles," in *Axially Compressed Structures: Stability and Strength*, (ed. R. Narayanan), Applied Science Publishers, Barking, Essex, England, Chap. 6.

Kennedy, J. B., and Murty, M. K. S. (1972), "Buckling of Steel Angle and Tee Struts," *ASCE J. Struct. Div.*, Vol. 98, No. ST11, pp. 2507–2522.

Kitipornchai, S. (1983), "Torsional–Flexural Buckling of Angles: A Parametric Study," *J. Constr. Steel Res.*, Vol. 3, No. 3.

Kitipornchai, S., and Chan, S. L. (1987), "Nonlinear Finite Element Analysis of Angle and Tee Beam-Columns," *ASCE J. Struct. Eng.*, Vol. 113, No. 4, pp. 721–739.

Kitipornchai, S., and Lee, H. W. (1986), "Inelastic Buckling of Single Angle Tee and Double Angle Struts," *J. Constr. Steel Res.*, Vol. 6, No. 1, pp. 3–20.

Leigh, J. M., and Galambos, T. V. (1972), "The Design of Compression Webs for Longspan Steel Joists," *Res. Rep. No. 21*, Department of Civil Engineering, Washington University, St. Louis, Mo.

Leigh, J. M., and Lay, M. G., (1969), "The Design of Laterally Unsupported Angles," *BHP Tech. Bull.* (Melbourne, No. 3, Vol. 13, Australia), Nov.

Libove, C. (1985), "Sparsely Connected Built-Up Columns," *ASCE J. Struct. Div.*, Vol. 111, No. ST3, pp. 609–627.

Lorin, M., and Cuille, J. P. (1977), "An Experimental Study of the Influence of the Connections of the Transmission Tower Web Members on Their Buckling Resistance," *Proc. 2nd Int. Colloq. Stab. Prelim. Rep.*, Liege, Belgium, pp. 447–456.

Lu, L. W., Shen, Z. Y., and Hu, X. R. (1983), "Inelastic Instability Research at Lehigh University," *Michael R Horne Int. Conf. Instab. Plastic Collapse Steel Struct.*, University of Manchester, England.

Madugula, M. K. S., and Ray, S. K. (1984a) "Cross-Sectional Properties of Cold-Formed Angles," *Can. J. Civ. Eng.*, Vol. 11, No. 3.

Madugula, M. K. S., and Ray, S. K. (1984b) "Ultimate Strength of Eccentrically Loaded Cold-Formed Angles," *Can. J. Civ. Eng.*, Vol. 11, No. 2.

Madugula, M. K. S., Prabhu, T. S., and Temple, M. C. (1983), "Ultimate Strength of Concentrically Loaded Cold-Formed Angles," *Can. J. Civ. Eng.*, Vol. 10, No. 1.

Marsh, C. (1969), "Single Angle Members in Tension and Compression," *ASCE J. Struct. Div.*, Vol. 95, No. ST5, p. 1043.

Marsh, C. (1972), "Lateral Stability of Single Angle Beam-Columns," *CSSIC Proj. 712*, Sir George Williams University, Montreal, QE, Canada, Mar.

National Bureau of Standards (1924), "Results of Some Compression Tests of Structural Steel Angles," *Tech. Pap. No. 281*, U.S. Government Printing Office, Washington, D.C.

SAA (1990), *Steel Structures*, AS 4100, Standards Association of Australia, North Sydney, New South Wales, Australia.

SJI (1994), *Standard Specifications, Load Tables and Weight Tables for Steel Joists and Joist Girders*, 40th ed., Steel Joist Institute, Myrtle Beach, S.C.

Temple, M. C. (1990), "Connectors for Double Angles: Interconnectors or Battens," *Can. J. Civ. Eng.*, Vol. 17, No. 1, pp. 8–11.

Temple, M. C., and Tan, J. C. (1988), "Interconnection of Widely Spaced Angles," *Can. J. Civ. Eng.*, Vol. 15, No. 4, pp. 732–741.

Temple, M. C., Schepers, J. A., and Kennedy, D. J. L. (1986), "Interconnection of Starred Angle Compression Members," *Can. J. Civ. Eng.*, Vol. 13, No. 6, pp. 606–619.

Temple, M. C., McCloskey, D. C., and Calabresse, J. M. (1987), "The Interconnection of Boxed Angle Compression Members," *Can. J. Civ. Eng.*, Vol. 14, No. 4, pp. 534–541.

Thomas, B. F., Leigh, J. M., and Lay, M. G. (1973), "'The Behavior of Laterally Unsupported Angles," *Civ. Eng. Trans. Inst. Eng. Australia.*

Timoshenko, S. P., and Gere, J. M. (1961), *Theory of Elastic Stability*, Engineering Societies Monograph, McGraw-Hill, New York.

Trahair, N. S. (1969), "Restrained Elastic Beam-Columns," *ASCE J. Struct. Div.*, Vol. 95, No. ST12, pp. 2641–2664.

Usami, T. (1970), "Restrained Single-Angle Columns Under Biaxial Bending," *Res. Rep. No. 14*, Civil Engineering Department, Washington University, St. Louis, Mo., June.

Usami, T., and Fukumoto, Y. (1972), "Compressive Strength and Design of Bracing Members with Angle or Tee Sections," *Proc. Jpn. Soc. Civ. Eng.*, Vol. 201, May, pp. 31–50 (in Japanese).

Usami, T., and Galambos, T. V. (1971), "Eccentrically Loaded Single Angle Columns," *IABSE Publ. 31-/ii*, pp. 153–174.

Vlasov, V. Z. (1961), *Thin-Walled Elastic Beams*, Israel Program for Scientific Translation for NSF, Jerusalem (original Russian edition, 1959).

Woolcock, S. T., and Kitipornchai, S. (1980), "The Design of Single Angle Struts," *Steel Constr.*, Vol. 14, No. 4, p. 2.

Woolcock, S. T., and Kitipornchai, S. (1986), "Design of Single Angle Web Struts in Trusses," *ASCE J. Struct. Eng.*, Vol. 112, No. 6, pp. 1327–1345.

CHAPTER TWELVE

BRACING

12.1 INTRODUCTION

A general design guide for stability bracing of columns, beams, and frames is presented. The focus is on simplicity, not exact formulations. The design recommendations cover four general types of bracing systems: relative, discrete, continuous, and lean-on, as illustrated in Fig. 12.1. A relative brace controls the relative movement of adjacent stories or of adjacent points along the length of the column or beam. If a cut everywhere along the braced member passes through the brace itself, the brace system is relative, as illustrated by diagonal bracings, shear walls, or truss bracing. A discrete brace controls the movement only at that particular brace point. For example, in Fig. 12.1*b* the column is braced at points 1 by cross beams. A cut at the column midheight does not pass through any brace, so the brace system is not relative, but is discrete. Two adjacent beams with diaphragms or cross frames are discretely braced at the cross-frame locations. Continuous bracing is self-evident; there is no unbraced length. The special cases of diaphragm-braced columns and beams are discussed in Chapter 13. A beam or column that relies on adjacent structural members for support is braced in a lean-on system. Structural members that are tied or linked together such that buckling of the member would require adjacent members to buckle with the same lateral displacement characterize lean-on systems, as shown in Fig. 12.1*d*. In the sway mode, member A leans on member B.

An adequate brace system requires both strength and stiffness (Winter, 1960). A simple brace design formulation, such as designing the brace for

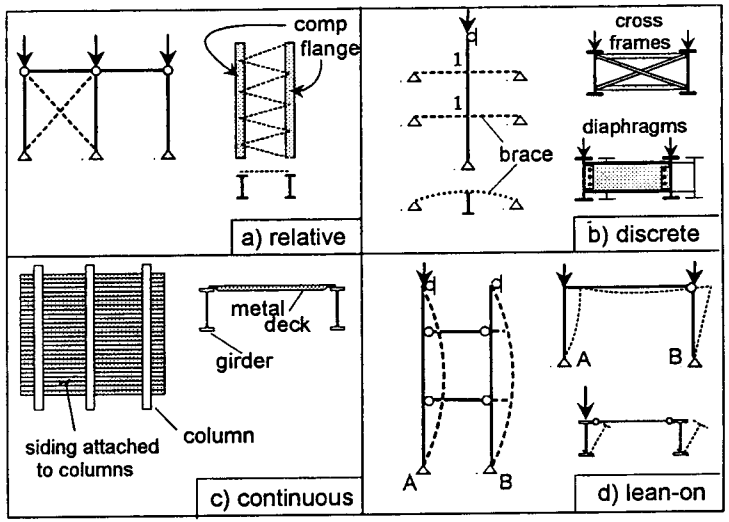

Fig. 12.1 Types of bracing systems.

2% of the member compressive force, addresses only the strength criterion. The magnitude of the initial out-of-straightness of the members to be braced has a direct effect on the bracing force. The brace stiffness also affects the brace force. Many published solutions provide stiffness recommendations only for perfectly straight structural systems. Such recommendations should not be used directly in design because very large brace forces may result, as will be shown subsequently.

12.2 BACKGROUND

A general discussion of stability bracing for beams, columns, and frames has been provided by Trahair and Nethercot (1984), Chen and Tong (1994), and Yura (1995). Before presenting the various bracing recommendations, some background material on the importance of initial out-of-straightness, connection stiffness, and member inelasticity on bracing effects is discussed along with the limitations of the design criteria.

12.2.1 Member Out-of-Straightness

Winter (1960) developed the concept of dual criteria for bracing design, strength, and stiffness, and he derived the interrelationship between them using simple models. He showed that the brace force is a function of the initial column out-of-straightness, Δ_0, and the brace stiffness, β. The concept is illustrated for the relative brace system shown in Fig. 12.2, where the brace, represented by the spring at the top of the column, controls the movement at the column top, Δ, relative to the column base. Summation of moments about point A gives $P\Delta_T = \beta L(\Delta_T - \Delta_0)$ where $\Delta_T = \Delta + \Delta_0$. If $\Delta_0 = 0$ (an initially perfectly plumb member), then $P_{cr} = \beta L$ which indicates that the load increases as the brace stiffness. The brace stiffness required in the sway mode to reach the load corresponding to Euler buckling between brace points, P_0, is called the *ideal stiffness*, β_i, where $\beta_i = P_0/L$ in this case.

For the out-of-plumb column, the relationship between P, β, and Δ_T is plotted in Fig. 12.3*a*. If $\beta = \beta_i$, P_0 can be reached only if the sway deflection gets very large. Unfortunately, such large displacements produce large brace forces, F_{br}, since $F_{br} = \beta\Delta$. For practical design, Δ must be kept small at the maximum factored load level. This can be accomplished by specifying $\beta > \beta_i$. For example, if $\beta = 2\beta_i$, then $\Delta = \Delta_0$ at P_0, as shown in Fig. 12.3*b*. The larger the brace stiffness, the smaller the brace force. For very stiff brace systems the brace force approaches $F_{br} = P_0\Delta_0/L$. The brace force is a linear function of the initial out-of-plumbness. The recommendations given later will assume a particular out-of-straightness and a brace stiffness at least twice the ideal stiffness.

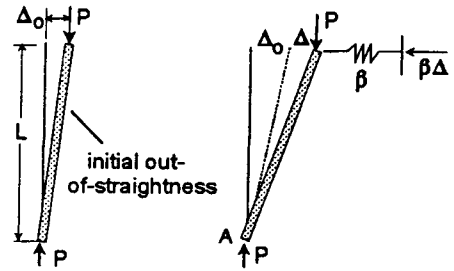

Fig. 12.2 Relative brace.

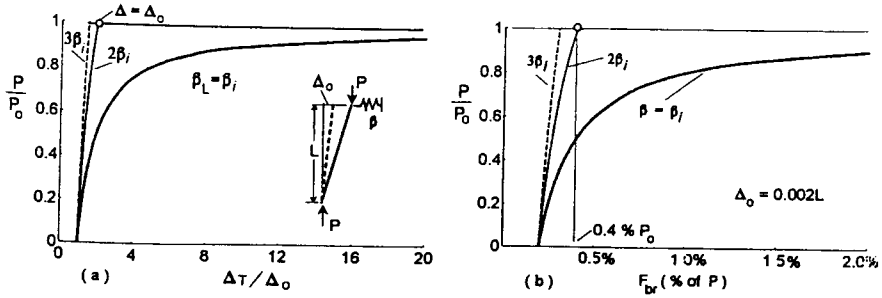

Fig. 12.3 Effect of initial out-of-plumbness.

12.2.2 Member Inelasticity

Most research on bracing requirements for structures are based on elastic concepts (Trahair and Nethercot, 1984). However, the design requirements for relative braces are merely a function of the load on the member and the distance between braces as illustrated above, not column elasticity or inelasticity. For discrete bracing systems Pincus (1964) used a simple theoretical model to demonstrate that the bracing stiffness requirements for inelastic columns are greater than those for elastic columns. However, experiments by Gil (1996) on inelastic columns with a midspan discrete brace showed no effect of column inelasticity on the bracing requirements. Also, Ales and Yura (1993) cast doubt on the Pincus solution, and their experiments on discrete bracing of inelastic beams verified Winter's approach. Nakamura (1988) presents a few beam experiments which also appear to follow the trends suggested by Winter's approach. Wang and Nethercot (1989) conducted a theoretical study of brace stiffness and strength requirements for beams with a concentrated load at midspan. Their study verified the Winter approach, especially on the need to use at least twice the ideal full bracing stiffness to reduce the brace forces. The brace forces were less than 1% of the flange force when the recommended stiffness was provided. The results appear to verify Winter's approach for use with inelastic beams, but the loading condition considered involved only a small amount of inelasticity near midspan.

For beams in the inelastic range, most research has been concerned with the spacing of the braces, not the properties of the braces. The Commentary on Plastic Design in Steel (ASCE, 1971) gives requirements for bracing at plastic-hinge locations. In the ASCE recommendations the lateral brace must have axial strength, axial stiffness, and flexural stiffness. Experiments on simply supported beams do not verify the need for flexural stiffness in the lateral braces. A design example illustrating both Winter's approach and the ASCE approach (neglecting the flexural stiffness requirement) is given in Salmon and Johnson (1996). Both approaches give the same-size brace in the example.

The few documented studies on discrete bracing requirements for inelastic beams and columns cited above indicate that inelasticity in the main members does not affect the bracing requirements. Undocumented bracing failures of test setups in experiments when instability occurs in the inelastic range, has contributed to the notion that inelastic structures require larger braces than elastic structures. However, when a lateral bracing failure occurs in a load test into the inelastic range, it usually happens *after* a local flange or web buckle occurs, which causes the W-shape beam to become unsymmetric. The loss of symmetry of the section causes shifts and inclinations of the principal bending axes which can cause very substantial lateral and torsional forces, much like those in channel sections not loaded through the shear center. Lateral bracing forces caused after local buckling occurs are very substantial but are beyond the scope of this presentation. However, since most local buckling occurs in the plastic range, bracing failures are often associated with inelasticity rather than local buckling.

In continuous and lean-on brace systems, the brace requirements are based on the elastic and/or inelastic stiffness of the members to be braced as will be given later. In these stability problems the effect of member inelasticity on the buckling solution can be reasonably approximated by using the tangent modulus stiffness E_T instead of the elastic modulus, E. The inelastic stiffness $E_T = \tau E$, where τ is the inelastic stiffness reduction factor. The elastic range is defined by the axial stress in the member, not the slenderness ratio. A member with low slenderness ratio (L/r) will respond elastically if the axial stress is low. In the AISC–LRFD specification an axial stress less $0.33F_y$ places the column in the elastic range. The AISC–LRFD manual (AISC, 1993) tabulates the stiffness reduction factor for various P/A stress levels. In LRFD, $\tau = -7.38(P/P_y)\log(1.176P/P_y)$, where P is the factored column load and P_y is the yield load, F_yA. The potential axial buckling capacity of a column is $\tau(0.877)\pi^2EI/(KL)^2$ for $P/P_y \geq \frac{1}{3}$. For $P/P_y < \frac{1}{3}$, $\tau = 1.0$. This τ factor will be used in some of the example problems.

12.2.3 Limitations

The brace requirements presented will enable a member to reach the Euler buckling load between the brace points (i.e., use $K = 1.0$). This is not the same as the no-sway buckling load as illustrated in Fig. 12.4 for the braced cantilever. The ideal brace stiffness is $1.0P_e/L$, corresponding to $K = 1.0$. A brace five times this stiffness is necessary to reach 95% of the $K = 0.7$ limit. Theoretically, an infinitely stiff brace is required to reach the no-sway limit. In addition, bracing required to reach specified rotation capacity or ductility limits is beyond the scope of this chapter.

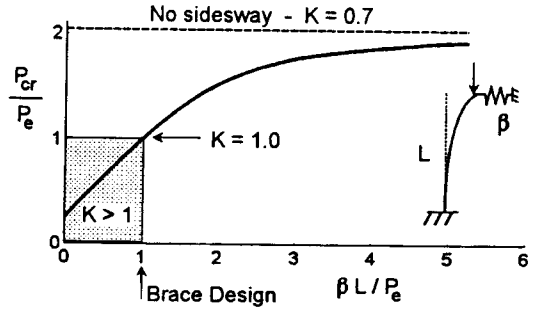

Fig. 12.4 Braced cantilever.

12.2.4 Brace System Stiffness

If they are flexible, brace connections should be considered in the evaluation of the bracing stiffness as follows:

$$\frac{1}{\beta_{sys}} = \frac{1}{\beta_{conn}} + \frac{1}{\beta_{brace}} \tag{12.1}$$

The brace system stiffness, β_{sys}, is less than the smaller of the connection stiffness, β_{conn}, or the stiffness of the brace, β_{brace}. When evaluating the bracing of rows of columns or beams, consideration must be given to the accumulation of the brace forces along the length of the brace, which results in a different displacement at each beam or column location. Medland and Segedin (1979) and Tong and Chen (1989) have studied interbraced structures. The solutions are fairly complex for design. In general, bracing forces can be minimized by increasing the number of braced bays and using stiff braces. Chen and Tong (1994) recommend bracing at least every eight bays.

12.3 SAFETY FACTORS, ϕ FACTORS, AND DEFINITIONS

The recommendations presented are based on ultimate strength. Column and beam loads are assumed to be factored loads. For brace stiffness formulations, a value of $\phi = 0.75$ is recommended in LRFD. If the load calculations are based on service loads as in ASD, a factor of safety of 2.0 can be applied to the factored load stiffness requirements. The strength requirements use the built-in safety factors or ϕ factors within each design specification. In LRFD, the design brace force will be based on factored loads and compared to the design strength of the brace and its connections. In ASD the brace force will be a function of the applied service loads, and this force will be compared to the allowable brace loads and connection capacity.

The displacement Δ_0 for relative and discrete braces is defined with respect to the distance between adjacent braces as shown in Fig. 12.5. In frames P is the sum of the column loads in a story to be stabilized by the brace. In the case of a discrete brace for a member, P would be the average load in the compression member above and below the brace point. The initial displacement Δ_0 is a small displacement from the straight position at the brace points caused by sources other than the gravity loads or compressive forces. For example, Δ_0 would be a displacement caused by wind or other lateral forces, erection tolerance (initial out-of-plumb), and so on. In all cases, the brace force recommendations are based on an assumed $\Delta_0 = 0.002L$. For other Δ_0 values use direct proportion. For torsional bracing of columns or beams, an initial twist β_0 of 1° is used. For cases where n columns, each with a random Δ_0, are to be stabilized by a brace system, Chen and Tong (1994) recommend an average

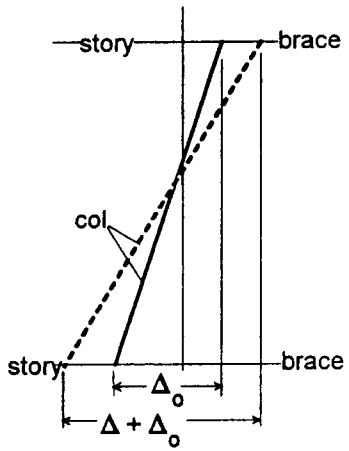

Fig. 12.5 Definitions.

$\Delta_0 = 0.002L/\sqrt{n}$ value, to account for the variation in initial out-of-straightness.

12.4 RELATIVE BRACES FOR COLUMNS OR FRAMES

Design recommendation:

$$\text{LRFD}, \phi = 0.75 \qquad \beta_{req'd} = \frac{2\Sigma P}{\phi L} \qquad F_{br} = 0.004\,\Sigma P$$

The design recommendation is based on an initial out-of-plumbness $\Delta_0 = 0.002L$ and a brace stiffness twice the ideal value shown in Fig. 12.4. Example 12.1 illustrates the bracing design. Each brace must stabilize 1500 kips. The floor is assumed to act as a rigid diaphragm and all Δ_0 are equal. The cos functions are necessary to convert the diagonal brace to an equivalent brace perpendicular to the column(s). Stiffness controls the design in this case. If Δ_0 is different from $0.002L$, change F_{br} in direct proportion to the actual Δ_0. If the brace stiffness provided, β_{act}, is different from $\beta_{req'd}$, F_{br} can be modified as follows:

$$F_{br} = 0.004\Sigma P \frac{1}{2 - \beta_{req'd}/\beta_{act}} \tag{12.2}$$

Example 12.1: Relative Brace–Tension System A typical brace must stabilize three bents. The factored load for each bent is

$$150 + 250 + 100 = 500 \text{ kips}$$

Design recommendations assume that F_{br} and Δ are perpendicular to the column.

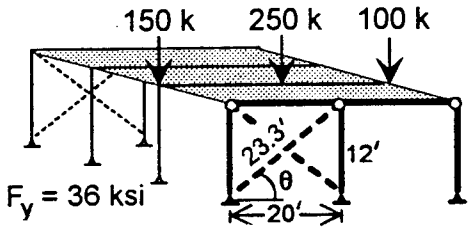

- Brace force

$$\frac{0.004(3 \times 500)}{\cos\theta} = 6.99 \text{ kips}$$

$\frac{5}{8}$-in. threaded rod OK

- Brace stiffness

$$\frac{A_b E}{L_b}\cos^2\theta = \frac{2(3 \times 500 \text{ kips})}{0.75(12)} \qquad A_{b_{\text{gross}}} = 0.364 \text{ in}^2$$

use $\frac{3}{4}\phi$, $A_g = 0.44 \text{ in}^2$.

12.5 DISCRETE BRACING SYSTEMS FOR COLUMNS

Design recommendation:

$$\text{LRFD}, \phi = 0.75 \qquad \beta_{\text{req'd}} = N_i \frac{2P}{\phi L} \qquad F_{br} = 0.01P$$

P = factored load, L = required brace spacing, n = number of braces, $N_i \approx 4 - (2/n)$

Discrete bracing systems can be represented by the model shown in fig. 12.6 for three intermediate braces. The exact solution taken from Timoshenko and Gere (1961) shows the relationship between P_{cr} and the brace stiffness, β. With no bracing $P_{cr} = \pi^2 EI/(4L)^2$. At low brace stiffness the buckling load increases substantially with the buckled shape a single (first-mode) wave. As the brace stiffness is increased, the buckled shape changes and additional brace stiffness becomes less effective. Full bracing occurs at $\beta_i L/P_e = 3.41 = N_i$. This ideal nondimensionalized stiffness factor N_i varies for equally spaced braces between 2.0 for one brace to 4.0 for a large number of braces. Thus 4.0 can be used conservatively for all cases. The design recommendation is based on full bracing assuming the load is at P_e.

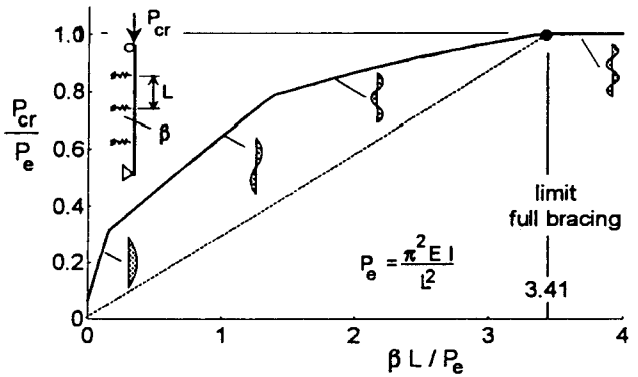

Fig. 12.6 Three discrete braces.

The discrete brace force requirement (Yura, 1993) was developed initially from Winter's rigid member model assuming zero moment at the node points which gives $F_{br} = 0.8\%P$ from solutions similar to those shown in Fig. 12.3. Tong and Chen (1987) and Plaut (1993) showed that Winter's model was unconservative for the case of a single brace at midspan so $F_{br} = 1\%P$ is recommended. This force assumes that a brace stiffness twice the ideal value is used. For other brace stiffnesses, the adjustment factor given in Eq. 12.2 can be used.

Typically, P may be less than P_e, so it is conservative to use the actual column load P to derive the design stiffness represented by the dashed line in Fig. 12.6. Note that the required brace stiffness is inversely proportional to the brace spacing L. In many applications there are more potential brace points than necessary to support the member forces required. Closer-spaced braces require more stiffness because the derivations *assume* that the unbraced length provided is just sufficient to support the column load. For example, say that three girts are available to provide weak-axis bracing to the columns. Say that the column load is such that only a single full brace at midspan would suffice. Then the required stiffness of the three-brace arrangement could be conservatively estimated by using the permissible unbraced length in the brace stiffness equation rather than the actual unbraced length. The continuous bracing formula given in the next section more accurately represents the true response of Fig. 12.6 for less than full bracing.

The design recommendation is based on twice the ideal stiffness to account for initial out-of-straightness. Example 12.2 illustrates the design procedure for a single discrete brace at the column midheight. The value of N_i is based on equal brace spacing and is unconservative for unequal spacing. For unequal spacing, N_i can be derived simply by using a rigid bar model between braces (Yura, 1994). For a single discrete brace at any location along the column length, with the longest segment defined as L and the shorter segment as aL, N_i can be determined as follows:

$$N_i = 1 + \frac{1}{a} \tag{12.3}$$

Example 12.2: Discrete Brace at Midheight A cross member braces the weak axis of W16 × 26 at midheight. Factored loads are shown.

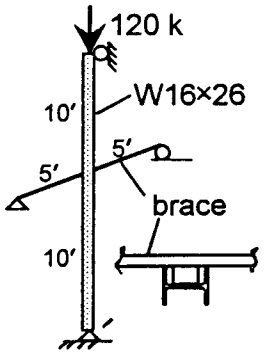

$$n = 1 \quad N_i = 2 \quad \beta_{\text{req'd}} = 2\left[\frac{2(120)}{0.75(120)}\right] = 5.33 \text{ kips/in.}$$

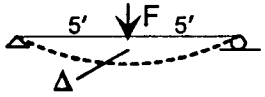

$$\beta = \frac{F}{\Delta} = \frac{48EI}{(10 \times 12)^3}$$

$$I_{\text{req'd}} = \frac{5.33(120)^3}{48(29{,}000)} = 6.4 \text{ in}^4$$

Try a C5 × 6.7:

$I_x = 7.5 \text{ in}^4$ $S_x = 3.5 \text{ in}^3$ $F_{br} = 0.01(120) = 1.2$ kips

$F_y = 36$ ksi $f_b = \dfrac{1.2(120)}{4(3.5)} = 10.3$ ksi OK

12.6 CONTINUOUS COLUMN BRACING

For a column braced continuously, Timoshenko and Gere (1961) give

$$P_{cr} = P_e\left(n^2 + \frac{\bar{\beta}L^2}{n^2\pi^2 P_e}\right) \tag{12.4}$$

where n is the number of half sine waves in the buckled shape as shown by the solid line in Fig. 12.7. As the brace stiffness per unit length $\bar{\beta}$ increases, the buckling load and n also increase. The switch in buckling modes for each n occurs when $\bar{\beta}L^2/\pi^2 P_e = n^2(n+1)^2$. Substituting this expression for n into Eq. (12.1) gives

$$P_{cr} = P_e + \frac{2L}{\pi}\sqrt{\bar{\beta}P_e} \tag{12.5}$$

Equation 12.5 is an approximate solution, shown dashed in Fig. 12.7, which gives the critical load for any value of $\bar{\beta}$ without the need to determine n. In the inelastic range use τP_e for P_e in Eq. 12.5.

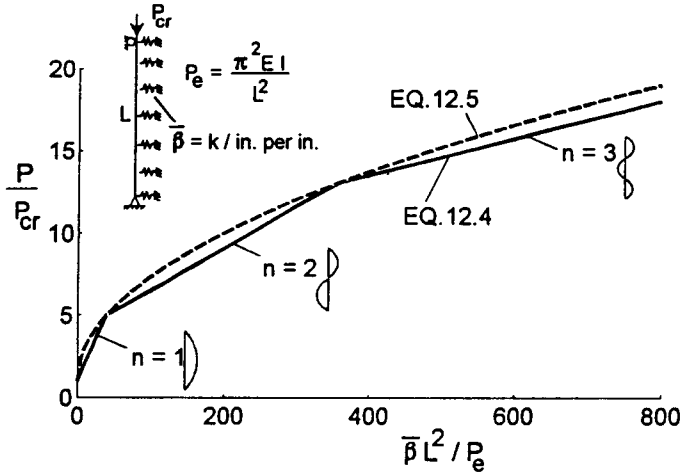

Fig. 12.7 Continuous bracing.

Equation 12.5 can also be used for discrete braces by defining $\bar{\beta} \equiv \beta\times$ number of braces/L and by limiting $P_{cr} \le \pi^2 EI/l^2$, where l is the distance between braces. This approach is accurate for two or more braces. For example, if there are two discrete braces, the ideal discrete brace stiffness is $\beta = 3P_e/l$, where $l = L/3$ and $P_{cr} = \pi^2 EI/l^2$. Using Eq.12.5 with $\bar{\beta} = 2(3P_e/l)/L$ gives $P_{cr} = 1.01(\pi^2 EI/l^2)$.

The bracing design recommendation given below is based on Eq. 12.5 with $\bar{\beta}$ adjusted by a factor of 2 to limit the brace forces, adding a ϕ_{br} value of 0.75 and using $P_0 = 0.85(0.877)\tau P_e$, which is the AISC–LRFD column design strength. The brace strength requirement $\bar{F}_{br} = \pi^2 P\Delta_T/L_0^2$, where L_0 is the maximum theoretical unbraced length that can support the column load, was developed by Zuk (1956). Taking $\Delta_T = 2\Delta_0$ and $\Delta_0 = 0.002L_0$ gives $\bar{F}_{br} = 0.04P/L_0$.

Design recommendation:

$$\text{LRFD, } \phi_c P_{cr} = P_0 + (L/\pi)\sqrt{2\phi_{br}\bar{\beta}P_0};\ F_{br} = 0.04P/L_0$$

where $P_0 = \phi_c(0.877)\tau P_e$, $\phi_c = 0.85$, $\phi_{br} = 0.75$

12.7 LEAN-ON SYSTEMS

When some members lean on adjacent members for stability support (bracing), the ΣP concept (Yura, 1971) can be used to design the members. The approach will be explained using the problem shown in Fig. 12.8, in which column A has

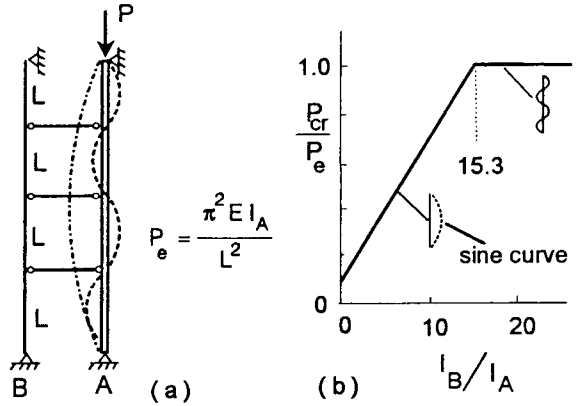

Fig. 12.8 Lean-on bracing.

a load P with three connecting beams attached between columns A and B. There are two principal buckling modes for this structure, the no-sway and the sway modes. If column B is sufficiently slender, the system will buckle in the sway mode, shown by the dot-dash line in Fig. 12.8*a*. In the sway mode the buckling strength involves the sum (ΣP_{cr}) of the buckling capacity of each column that sways because each column has the same deformation pattern. The system is stable in the sway mode if the sum of the applied loads (ΣP) is less than the ΣP_{cr}. This assumes that all the columns have the same height. If column B is sufficiently stiff, the buckling capacity may be controlled by the no-sway mode, shown dashed. Both modes must be checked.

An exact elastic solution, developed with the ANSYS computer program, shows that as I_B increases, P_{cr} increases linearly in the sway mode. At $I_B/I_A \geq 15.3$, column A buckles in the no-sway mode. The I_b value required to develop full bracing can be approximated using the ΣP concept. In the sway mode, the elastic capacities of columns A and B are $\pi^2 EI_A/(4L)^2$ and $\pi^2 EI_B/(4L)^2$, respectively. The desired P_{cr} corresponding to the no-sway mode is $\pi^2 EI_A/L^2$. Equating the sum of the sway capacities to the P_{cr} in the no-sway mode,

$$\frac{\pi^2 E(I_A + I_B)}{(4L)^2} = \pi^2 EI_A/L^2 \tag{12.6}$$

gives $I_B = 15I_A$, which is close to the exact solution of $I_B = 15.3I_A$. In the inelastic range, τ_i is used where τ_i is based on the axial load in each column, P_i. There can be axial load on all the columns.

Example 12.3, which is similar to a problem solved by Lutz and Fisher (1985), shows a W12 × 40 with its weak axis in plane supported by an adjacent

column W12 × 26 with the strong axis in-plane. The tie beams have shear-only end connections, so it is assumed that the tie beams do not contribute to the sway stiffness of the system. Sway is prevented at the top of the columns. The W12 × 40 has been sized based on buckling between the supports, $L = 8$ ft. The calculations show that the elastic W12 × 26 adjacent column can brace the weak-axis column, which is in the inelastic range. A W12 × 19 section would also be satisfactory.

Example 12.3: Lean-On System

AISC–LRFD specification, $F_y = 36$ ksi, factored loads. Is the W12 × 26 capable of bracing W12 × 40?

From the AISC manual, $\phi P_n = 317$ kips for $L = 8$ ft.

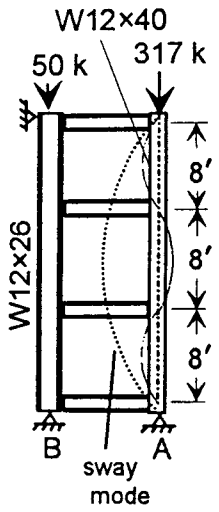

ΣP concept : W12 × 40, $A = 11.6$ in^2, $I_y = 44.1$ in^4

W12 × 26, $A = 7.65$ in^2, $I_x = 204$ in^4

Column A : $\dfrac{P_A}{F_y A} = 317/(36 \times 11.8)$

$= 0.746 > \frac{1}{3}$ $\quad \therefore$ inelastic

$\tau = -7.38(0.746) \log(1.176 \times 0.746) = 0.313$

$$\phi P_A = \frac{0.85(0.313)(0.877)\pi^2(29{,}000)(44.1)}{(288)^2}$$

$= 35.5$ kips

Column B : $\dfrac{P_B}{F_y A} = \dfrac{50}{36 \times 7.65} = 0.181 < \frac{1}{3}$ $\quad \therefore \tau = 1.0$

$$\phi P_B = \frac{0.85(0.877)\pi^2(29{,}000)(204)}{(288)^2} = 524 \text{ kips}$$

$\Sigma P = 35 + 524 = 559 > \Sigma P = 317 + 50$

$= 367$ kips OK

12.8 COLUMNS BRACED ON ONE FLANGE

Doubly symmetric columns will buckle in a flexural mode between brace points if the braces prevent both twist and displacement. If the brace detail does not prevent twist, such as rod bracing framing into the center of the web, the column can buckle in a torsional mode. Another common bracing detail that can result in twist of the section is shown in Fig. 12.9. Girts frame into the column flange which restrain weak-axis lateral displacement near the flange. If

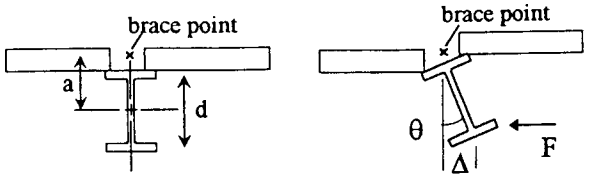

A) Lateral brace at flange B) Buckled shape

Fig. 12.9 Buckling about a restrained axis.

the girts are discontinuous, they will not provide any torsional restraint and the column may buckle by twisting about the lateral brace point as shown in Fig. 12.9*b*. The torsional buckling load, P_T, for a column with a lateral restraint (Timoshenko and Gere, 1961) is

$$P_T = \frac{\tau P_{ey}[(d^2/4) + a^2] + GJ}{a^2 + r_x^2 + r_y^2} \tag{12.7}$$

where a is the distance between the restrained axis and the centroid, d is the depth of the cross section, and P_{ey} is the Euler load based on the column length between points with zero twist. Other terms are as defined in Chapter 5. An infinitely stiff lateral brace at the brace point (zero displacement) was assumed in the derivation of Eq. 12.7. To compensate for finite stiffness, the maximum factored column load should not exceed 90% of P_T. Horne and Ajmani (1971, 1972) studied the more complex problem of beam-columns braced on one flange.

When the applied factored load is greater than P_T, torsional bracing must be provided. Two typical bracing schemes are shown in Fig. 12.10. When a moment connection is used, a partial-depth web stiffener is recommended to prevent web distortion. The design requirements for the torsional braces follow directly from the discrete column approach given in Section 12.5. A lateral brace force F is applied to the unrestrained flange in Fig. 12.9*b* resulting in a torsional moment $M_T = Fd$. Each flange is assumed to be supporting half the total column load. The angle of twist $\theta = \Delta/d$. Therefore, the torsional brace stiffness, $\beta_T = M_T/\theta = Fd^2/\Delta = \beta d^2$, where β is the discrete brace stiffness requirement from Section 12.5, with P equal to one-half the column load. The torsional brace moment for an assumed initial twist $\theta_0 = 1°$ is $0.0175\beta_T$.

12.9 BEAM BUCKLING AND BRACING

Before presenting the beam bracing recommendations, the suitability of assuming the inflection point as a brace point in restrained beams to define L_b will be

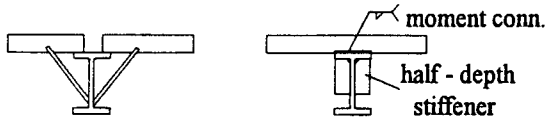

A) Struts B) Moment conn. w/ stiffener

Fig. 12.10 Typical torsional brace details.

discussed. In many cases where this issue is raised the top flange is laterally braced by the slab or joists all along the span, while the bottom flange is unbraced. An inflection point *cannot* be considered a brace point, as illustrated by the example shown in Fig. 12.11. One beam has a moment at one end ($C_b = 1.67$) with $L_b = L$, and the other beam has an inflection point at midspan ($C_b = 2.3$) with $L_b = 2L$. The $2L$ span with the inflection point will buckle at a load that is 68% of the beam with span L. If the inflection point is a brace point, the critical moment of both beams would be the same. The buckled shape of the $2L$ beam shows that the top flange and bottom flange move laterally in opposite directions at midspan. Even an actual brace on one flange at the inflection point does not provide effective bracing at midspan (Yura, 1993).

Some common cases of beams with top flange lateral bracing but neglecting torsional restraint were solved using a finite element computer program and approximate C_b formulas developed as given in Fig. 12.12. These C_b values can be used in design with L_b = span length if twist is positively controlled only at the supports. Two general cases are derived, top flange laterally braced with top flange gravity loading and top flange braced with uplift loading. Essa and

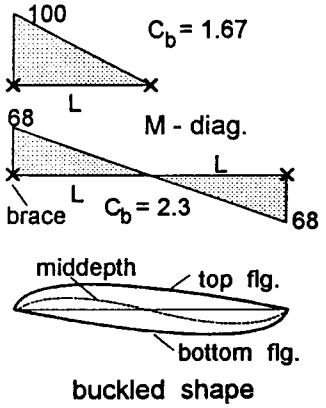

Fig. 12.11 Beam with inflection point.

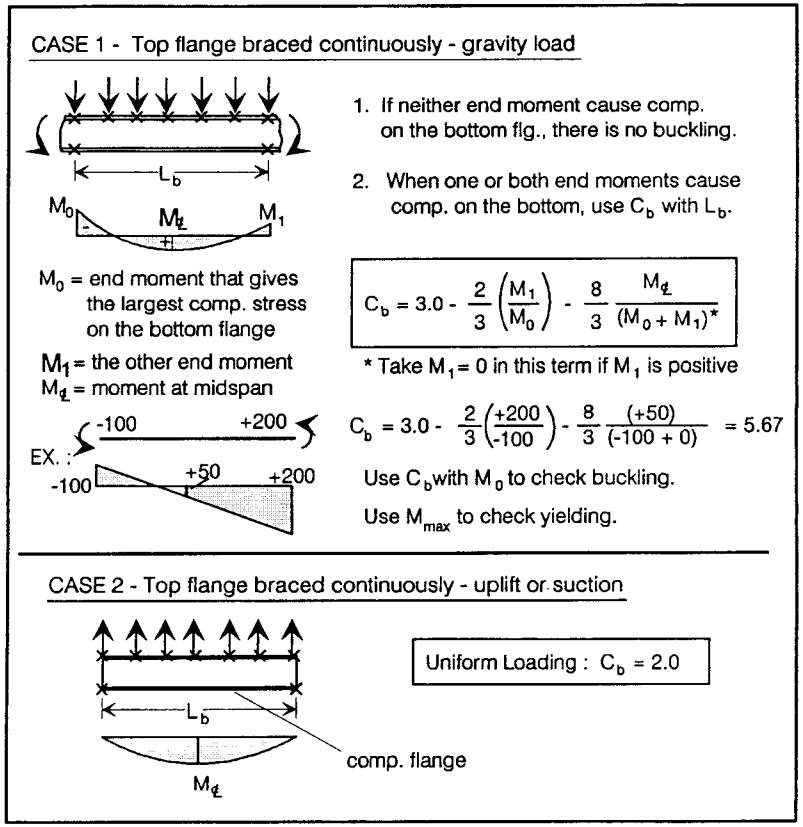

Fig. 12.12 C_b for braced beams.

Kennedy (1995) have presented design charts for suspended construction which also considers the torsional restraint provided by joists attached to the top flange.

12.10 BEAM BRACING

There are two general types of beam bracing, lateral and torsional. Bracing systems for beams must prevent the *relative* displacement of the top and bottom flanges (i.e. twist of the section). Lateral bracing (joists attached to the compression flange of a simply supported beam) and torsional bracing (cross frame or diaphragm between adjacent girders) can effectively control twist. Some bracing systems restrain lateral movement and twist simultaneously (slab attached to the top flange with shear studs). Mutton and Trahair (1973) and Tong and Chen (1988) have shown that combined lateral and torsional bracing is more effective than either lateral or torsional bracing acting alone for beams under uniform moment.

A general discussion of beam bracing and the development of the design recommendations herein are presented elsewhere (Yura, 1993). The provisions are limited to doubly and singly symmetric members loaded in the plane of the web. Lateral bracing can be relative, discrete, continuous, or lean-on; torsional bracing can be either relative or discrete. Only relative and discrete lateral bracing requirements are presented here. Continuous bracing is addressed by Trahair and Nethercot (1984) and Yura and Phillips (1992). Beams that are linked together lean on each other and the lateral buckling cannot occur at the links unless all the members buckle. In this case the beams in the structural system canot buckle until the sum of the maximum moment in each beam exceeds the sum of the individual buckling capacities of each beam (Yura et al., 1992). Buckling of an individual beam can occur only between the cross members in a lean-on system. No additional bracing requirements are necessary in lean-on systems.

If two adjacent beams are interconnected by a properly designed cross frame or diaphragm at midspan, that point can be considered a brace point when evaluating the beam buckling strength. Since the beams can move laterally at midspan, the effectiveness of such a bracing system is sometimes questioned. As long as the two flanges move laterally the same amount, there will be no twist. If *twist* is prevented, the beam can be treated as braced. Tests and theory confirm this approach (Flint, 1951; Yura et al., 1992).

12.10.1 Lateral Bracing

The effectiveness and size of a lateral brace depends on its location on the cross section, the moment diagram, the number of discrete braces in the span, and the location of the load on the cross section (Yura, 1993). These factors have been included in the recommendations. Lateral bracing is most effective when it is attached to the compression flange. The exception to this is for cantilevers, where top (tension) flange bracing is effective. Lateral bracing near the centroid of the cross section is ineffective.

The relative and discrete brace design provisions presented, which are based on Winter's approach, are applicable only for bracing attached near the top flange. The provisions also assume top flange loading, which is a worse case and can be used for any number of discrete braces. The compressive force is conservatively approximated as M_f/h. When the beam has an inflection point, lateral bracing must be attached to both flanges and the stiffness requirements are greater as given by the C_d factor in the brace requirements. For example, for a beam in reverse curvature as shown in Fig. 12.11, a brace on both the top and bottom flange at mid-span will require twice as much stiffness for each brace as a similar length beam with compression on only one flange. The brace force provisions are similar to those for columns (Section 12.4 and 12.5). A brace stiffness of twice the ideal value has been used in the development.

Lateral brace design recommendations: LRFD, $\phi = 0.75$

	Relative	*Discrete*
Stiffness:	$\beta_L = \dfrac{2.5M_f C_d}{\phi L_b h}$	$\beta_L = \dfrac{10M_f C_d}{\phi L_b h}$
Strength:	$F_{br} = \dfrac{0.004M_f C_d}{h}$	$F_{br} = \dfrac{0.01M_f C_d}{h}$

where M_f is the maximum moment; h is beam depth; L_b the unbraced length; and $C_d = 1.0$, single curvature; 2.0, reverse curvature.

The lateral bracing provisions are illustrated in Example 12.4, where a top flange relative brace truss system is used to stabilize the compression flange during construction of the composite plate girders. Each truss system is designed to stabilize two and one-half girders. The diagonal braces are assumed to support tension only.

Example 12.4: Relative Lateral Brace System

Design the diagonals of the top flange horizontal truss to stabilize the five 80-ft girders with the factored moments shown. $F_y = 36$ ksi.

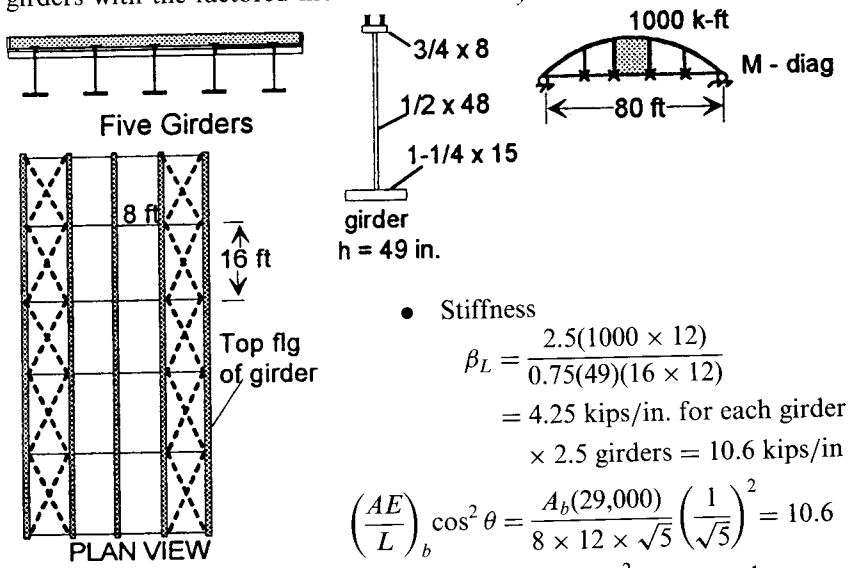

- Stiffness

$$\beta_L = \frac{2.5(1000 \times 12)}{0.75(49)(16 \times 12)}$$

$$= 4.25 \text{ kips/in. for each girder}$$

$$\times 2.5 \text{ girders} = 10.6 \text{ kips/in}$$

$$\left(\frac{AE}{L}\right)_b \cos^2\theta = \frac{A_b(29{,}000)}{8 \times 12 \times \sqrt{5}}\left(\frac{1}{\sqrt{5}}\right)^2 = 10.6$$

$$A_b = 0.393 \text{ in}^2 \leftarrow \text{controls}$$

- Strength

$$F_{br} = \frac{0.004(2.5)(1000 \times 12)}{49} = 2.45 \text{ kips}$$

$$A_b = \frac{2.45\sqrt{5}}{0.9 \times 36} = 0.17 \text{ in}^2$$

Use L2 × 2 × $\frac{1}{8}$; $A = 0.484$ in^2.

12.10.2 Torsional Bracing

Cross frames or diaphragms at discrete locations or continuous bracing provided by the floor system in through girders or pony trusses, or by metal decks and slabs, represent torsional bracing systems. In the development of the design recommendations (Yura, 1993), which are based on the work of Taylor and Ojalvo (1966), it was determined that factors that had a significant effect on lateral bracing had a substantially reduced effect on torsional bracing. The effects of the number of braces, top flange loading, and brace location on the cross section are relatively unimportant when sizing a torsional brace. A torsional brace is equally effective if it is attached to the tension flange or the compression flange. A moment diagram with compression in both flanges (reverse curvature) does not alter the torsional brace requirements.

On the other hand, the effectiveness of a torsional brace is greatly affected by cross-section distortion at the brace point, as illustrated in Fig. 12.13. The top flange is prevented from twisting by the torsional brace, but the web distortion permits a relative displacement between the two flanges. A stiffener at the brace location can be used to prevent the distortion. The design method considers web distortion and any stiffeners required.

Discrete braces and continuous bracing use the same basic design formula. The continuous bracing stiffness $\bar{\beta}_T = \beta_T n/L$, where β_T = discrete brace stiffness, n = number of braces, and L = span length. β_T and $\bar{\beta}_T$ defined as the torsional stiffnesses of the discrete and continuous bracing systems, respectively. The system stiffness β_T is related primarily to the stiffness of the brace, β_b, and the stiffness of the web plus any stiffeners, β_{sec}, by

$$\frac{1}{\beta_T} = \frac{1}{\beta_{sec}} + \frac{1}{\beta_b} \tag{12.8}$$

The β_b value for diaphragm systems is given in Fig. 12.14. The discrete web-stiffener detail can vary over the web as shown in Fig. 12.15. The stiffness of each portion of the web is given by

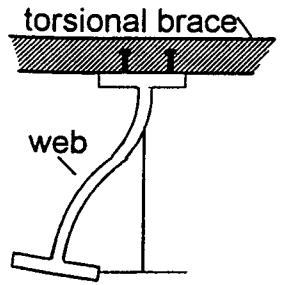

Fig. 12.13 Web distortion.

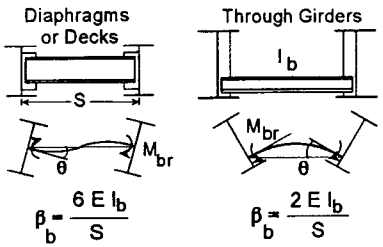

Fig. 12.14 Diaphragm β_b.

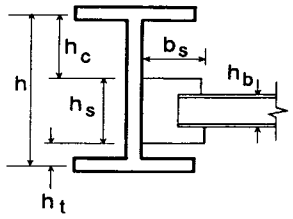

Fig. 12.15 Partially stiffened webs.

$$\beta_c, \beta_s, \beta_t = \frac{3.3E}{h_i}\left(\frac{h}{h_i}\right)^2\left[\frac{(1.5h_i)t_w^3}{12} + \frac{T_s b_s^3}{12}\right] \tag{12.9}$$

where $1/\beta_{\text{sec}} = \Sigma(1/\beta_i)$ and t_s is the thickness of the stiffener. For continuous bracing, replace $1.5h$ with 1 in. and neglect the t_s term if there is no stiffener. The portion of the web within h_b can be considered infinitely stiff. Equations 12.8 and 12.9 were developed from Milner and Rao (1978) and a finite element buckling program that considers cross-sectional distortion (Akay et al., 1977). For rolled sections ($h/t_w < 60$) cross-sectional distortion will not be significant if the diaphragm connection extends at least one-half the web depth.

Torsional brace design recommendations: LRFD, $\phi = 0.75$

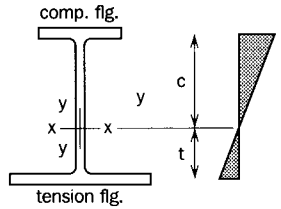

Stiffness: $\beta_T = \frac{\bar{\beta}_T L}{n} = \frac{2.4LM_f^2}{\phi n E I_{\text{eff}} C_{bb}^2}$

Strength: $M_{br} = F_{br} h_b = \frac{0.04LM_f^2}{nEI_{\text{eff}} C_{bb}^2}$

where M_f is the maximum moment, $I_{\text{eff}} = I_{yc} + (t/c)\, I_{yt}$, L is the length, n the number of span braces, and C_{bb} the moment modification factor for the full bracing condition.

For a singly symmetric section I_{yc} and I_{yt} are the out-of-plane moments of inertia of the compression and tension flanges, respectively. If the cross section is doubly symmetric, I_{eff} becomes I_y. The 2.4 factor in the stiffness requirement

comes from using twice the ideal stiffness and an additional 20% increase to account for top flange loading. The brace strength provision, M_{br}, assumes an initial twist of 1° (0.0175 rad) and is consistent with finite element studies (Helwig et al., 1993).

In Example 12.5 a diaphragm torsional bracing system is used for the problem given in Example 12.4. The C9 × 13.4 diaphragm will not brace the girders if a stiffener is not used. Even a much larger diaphragm cannot work without web stiffeners because of the web distortion. Similar example problems using cross frames are given elsewhere (Yura, 1993).

Example 12.5: Torsional Beam Bracing

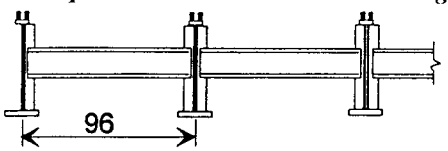

Same as Example 12.4 but use the diaphragm system shown. $M_{\max} = 1000$ kip-ft, $C_b = 1.0$; four braces, $F_y = 36$ ksi, $L = 80$ ft. The girder properties are as follows:

$h = 49.0 \quad c = 30.85 \quad t = 18.15$ in.

$I_x = 17{,}500 \quad I_{yc} = 32.0 \quad I_{yt} = 352 \text{ in}^4 \quad I_{\text{eff}} = 32 + \frac{18.15}{30.85}352 = 239 \text{ in}^4$

The strength is given by

$$M_{br} = \frac{0.04(80 \times 12)(1000 \times 12)^2}{4(29{,}000)239(1.0)^2} = 199 \text{ in-kips}$$

$$S_{x\ \text{req'd}} = \frac{199}{(0.9) \times (36)} = 6.16 \text{ in}^3$$

The stiffness of the diaphragms on the exterior girders is $6EI_{br}/S$. Since there are diaphragms on both sides of each interior girder, the stiffness is $2 \times 6EI_{br}/S$. The average stiffness available to each girder is $(2 \times 6 + 3 \times 12)/5 = 9.6EI_{br}/S$.

$$\beta_{T\ \text{req'd}} = \frac{2.4(80 \times 12)(1000 \times 12)^2}{(0.75)4(29{,}000)239(1.0)^2} = 15{,}960 \text{ in-kips/rad}$$

$$I_{br_{\min}} = \frac{15{,}960(96)}{(9.6)29{,}000} = 5.50 \text{ in}^4$$

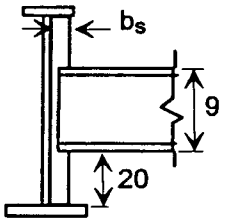

Try C9 × 13.4: $S_x = 12.5 \text{ in}^3 > 6.16$, $I_x = 47.9 \text{ in}^4$.

$$\beta_b = \frac{9.6(29{,}000)47.9}{96} = 138{,}900 \text{ in-kips/rad}$$

$$\frac{1}{15{,}960} = \frac{1}{138{,}900} + \frac{1}{\beta_{\text{sec}}} \qquad \beta_{\text{sec}} = 17{,}900 \text{ in-kips/rad}$$

$$\frac{1}{17{,}900} = \frac{2}{\beta_c} \qquad \beta_c = 2(179{,}000) = \frac{3.3(29{,}000)}{20}\left(\frac{49}{20}\right)^2\left[\frac{1.5(20)(0.5)^3}{12} + \frac{0.375b_s^3}{12}\right]$$

$$b_s = 3.10$$

Use a $\frac{3}{8} \times 3\frac{1}{2}$ in. stiffener.

12.11 FAULTY DETAILS

Numerous structural failures have occurred because of the structural arrangement shown in Fig. 12.16. The beam (or truss) is continuous over the top of the column. The critical components are: column in compression, compression in the bottom flange of the beam or chord of the truss, and no bottom flange

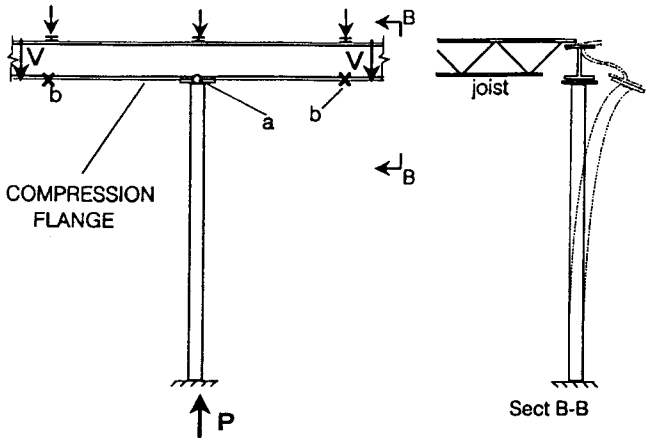

Fig. 12.16 Structural detail with probable instability.

bracing at point *a* and possibly points *b*. The sway at the top of the column shown in section B–B can result in a *k*-factor much greater than 2.0. The bottom flange of the beam can possibly provide bracing to the top of the column if there are braces at points *b* and consideration is given to the compression in the flange when evaluating its stiffness. In general, a brace, such as a bottom chord extension from the joist, should be used at point *a*. Beam web stiffeners at the column location will also be effective unless bottom flange lateral buckling is critical.

REFERENCES

AISC (1993), *Manual of Steel Construction: Load and Resistance Factor Design*, Vol. 1, 2nd ed., American Institute of Steel Construction, Chicago.

Akay, H. U., Johnson, C. P., and Will, K. M. (1977), "Lateral and Local Buckling of Beams and Frames," *ASCE J. Struct. Div.*, Vol. 103, No. ST9, pp. 1821–1832.

Ales, J. M., and Yura, J. A. (1993), "Bracing Design for Inelastic Structures," *Proc. SSRC Conf. "Is Your Structure Suitably Braced?"* Milwaukee, Wis., Apr., pp. 29–37.

ASCE (1971), *Commentary on Plastic Design in Steel*, ASCE Manual No. 41, 2nd ed., American Society of Civil Engineers, New York.

Chen, S., and Tong, G. (1994), "Design for Stability: Correct Use of Braces," *Steel Struct., J. Singapore Struct. Steel Soc.*, Vol. 5, No. 1, pp. 15–23.

Essa, H. S. and Kennedy, D. J. L. (1995), "Design of Steel Beams in Cantilever-Suspended-Span Construction," *ASCE J. Struct. Div.*, Vol. 121, No. 11, pp. 1667–1673.

Flint, A. R. (1951), "The Stability of Beams Loaded Through Secondary Members," *Civ. Eng. Public Works Rev.*, Vol. 46, No. 537-8, pp. 175–177, 259–260.

Gil, H. (1996), "Bracing Requirements for Inelastic Steel Members," Ph.D. dissertation, University of Texas at Austin, Austin, Texas, May, 156 pp.

Helwig, T. A., Yura, J. A., and Frank, K. H. (1993), "Bracing Forces in Diaphragms and Cross Frames," *Proc. SSRC Conf. "Is Your Structure Suitably Braced?"* Milwaukee, Wis., Apr., pp. 129–140.

Horne, M. R., and Ajmani, J. L. (1971), "Design of Columns Restrained by Side Rails," *Struct. Eng.*, Vol. 49, No. 8, pp. 329–345.

Horne, M. R., and Ajmani, J. L. (1972), "Failure of Columns Laterally Supported on One Flange," *Struct. Eng.*, Vol. 50, No. 9, pp. 355–366.

Lutz, A. L., and Fisher, J. (1985), "A Unified Approach for Stability Bracing Requirements," *AISC Eng. J.*, Vol. 22, No. 4, pp. 163–167.

Medland, I. C., and Segedin, C. M. (1979), "Brace Forces in Interbraced Column Structures," *ASCE J. Struct. Div.*, Vol. 105, No. ST7, pp. 1543–1556.

Milner, H. R., and Rao, S. N. (1978), "Strength and Stiffness of Moment Resisting Beam–Purlin Connections," *Civil Eng. Trans. Inst. Eng. Aust.*, Vol. CE 20, No. 1, pp. 37–42.

Mutton, B. R., and Trahair, N. S. (1973), "Stiffness Requirements for Lateral Bracing," *ASCE J. Struct. Div.*, Vol. 99, No. ST10, pp. 2167–2182.

Nakamura, T. (1988), "Strength and Deformability of H-Shaped Steel Beams and Lateral Bracing Requirements," *J. Constr. Steel Res.*, Vol 9, pp. 217–228.

Pincus, G. (1964), "On the Lateral Support of Inelastic Columns," *AISC Eng. J.*, Vol. 1, No. 4, pp. 113–115.

Plaut, R. H. (1993), "Requirements for Lateral Bracing of Columns with Two Spans," *ASCE J. Struct. Div.*, Vol. 119, No. 10, pp. 2913–2931.

Salmon, C. S., and Johnson, J. E. (1996), *Steel Structures: Design and Behavior*, 4th ed., Harper & Row, New York.

Taylor, A. C., and Ojalvo, M. (1966), "Torsional Restraint of Lateral Buckling," *ASCE J. Struct. Div.*, Vol. 92, No. ST2, pp. 115–129.

Timoshenko, S., and Gere, J. (1961), *Theory of Elastic Stability*, McGraw-Hill, New York.

Tong, G., and Chen, S. (1987), "Design Forces of Horizontal Inter-column Braces," *J. Constr. Steel Res.*, Vol. 7, pp. 363–370.

Tong, G., and Chen, S. (1988), "Buckling of Laterally and Torsionally Braced Beams," *J. Constr. Steel Res.*, Vol. 11, pp. 41–55.

Tong, G., and Chen, S. (1989), "The Elastic Buckling of Interbraced Girders," *J. Constr. Steel Res.*, Vol. 14, pp. 87–105.

Trahair, N. S., and Nethercot, D. A. (1984), "Bracing Requirements in Thin-Walled Structures," in *Developments in Thin-Walled Structures*, Vol. 2 (ed. J. R. Rhodes and A. C. Walker), Elsevier, New York, pp. 93–130.

Wang, Y. C., and Nethercot, D. A. (1989), "Ultimate Strength Analysis of Three-Dimensional Braced I-Beams," *Proc. Inst. Civ. Eng.*, Part 2, Vol. 87, Mar., pp. 87–112.

Winter, G. (1960), "Lateral Bracing of Columns and Beams," *Trans. ASCE*, Vol. 125, Part 1, pp. 809–825.

Yura, J. A. (1971), "The Effective Length of Columns in Unbraced Frames," *AISC Eng. J.*, Vol. 8, No. 2, pp. 37–42.

Yura, J. A. (1993), "Fundamentals of Beam Bracing," *Proc. SSRC Conf. "Is Your Structure Suitably Braced?"* Milwaukee, Wis., Apr., 20 pp.

Yura, J. A. (1994), "Winters Bracing Model Revisited," *50th Anniv. Proc. SSRC*, pp. 375–382.

Yura, J. A. (1995), "Bracing for Stability-State-of-the-Art," *Proc. Struct. Congr. XIII*, ASCE, Boston, Apr., pp. 88–103.

Yura, J. A., and Phillips, B. A. (1992), "Bracing Requirements for Elastic Steel Beams," *Res. Rep. 1239-1*, Center for Transportation Research, University of Texas at Austin, May, 73 pp.

Yura, J. A., Phillips, B., Raju, S., and Webb, S. (1992), "Bracing of Steel Beams in Bridges," *Res. Rep. 1239-4F*, Center for Transportation Research, University of Texas at Austin, October, 80 pp.

Zuk, W. (1956), "Lateral Bracing Forces on Beams and Columns," *ASCE J. Eng. Mech. Div.*, Vol. 82, No. EM3, pp. 1032.1–1032.11.

CHAPTER THIRTEEN

THIN-WALLED METAL CONSTRUCTION

13.1 INTRODUCTION

Thin-walled metal members are used as framing for light construction and as secondary members in heavy construction. Thin-walled metal panels and decks are widely used as floors, roofs, and walls. The increased use of cold-formed steel members is reflected in the existence of design specifications in Australia, China, East Europe, Japan, North America, and West Europe (Beedle, 1991).

New developments in research, design, and construction are presented in the proceedings of international specialty conferences, which meet periodically to discuss advances in all aspects of cold-formed steel structural systems (Rhodes and Walker, 1979; Yu and LaBoube, 1992).

Thin-walled steel members are usually cold-formed to shape from hot or cold-rolled sheet, strip, or plate. Aluminum sections are generally extruded or cold-formed. Cold-forming to shape may increase the yield and ultimate strength of the member because of strain hardening and strain aging (Karren and Winter, 1967; Uribe and Winter, 1970). This results in a higher yield strength for the material in the more severely cold-worked zones, such as corners, and in gradual yielding behavior of a cross section under load, even though the virgin material may exhibit sharp yielding characteristics. The strengthening effect of cold forming can be determined by test for any member, and specifications contain provisions for analytically determining the strength increase due to cold forming of cold-formed carbon and low-alloy steel members. Whether testing or analysis is used, the design approach is to modify

ordinary procedures to permit utilization of this increase in strength, recognizing the end service intended.

This chapter covers the behavior of flexural and compression members that is unique to thin-walled construction. Because of the thinness of the member elements, local buckling is an important consideration, and emphasis is given to aspects of buckling that affect member behavior.

13.2 FLEXURAL MEMBERS

13.2.1 Introduction

Thin-walled sections such as tubular members (Fig. 4.1*b*), I-sections (Fig. 4.1*h*), channels, Z-sections, hat sections (Fig. 4.1*i*), T-sections (Fig. 4.1*m*), and panels (Fig. 4.1*o*, *p*, *q*) are often used as flexural members in thin-walled construction. The depth of such members generally ranges from 1 to 12 in., and the thickness of material ranges from about 0.012 to about 0.5 in. or thicker.

In the design of thin-walled flexural members, consideration should be given to the following (Yu, 1991):

- Moment-resisting capacity and stiffness of the member
- Web design
- Bracing requirements

13.2.2 Moment Capacity

In thin-walled metal construction, the moment-resisting capacity of a flexural member is governed by one or a combination of the following factors:

- Yielding of material
- Local buckling of compression flange or web
- Lateral buckling

When the section geometry and loading result in bending in the plane of loading, and when local buckling or lateral buckling does not occur, flexural yielding is the limiting factor and traditional design concepts apply. However, the width-to-thickness ratios are frequently great enough to result in local buckling before the ultimate load is reached, and attention must be given to a cross section in which the normal stress distribution in a plane perpendicular to the longitudinal axis of the member varies because of local buckling. One may either consider the actual stress distribution and resort to the fundamental integrals governing flexural behavior, or replace the actual distribution with an assumed distribution, which will give the same results.

Where local buckling of individual compression elements is experienced, two different approaches have been used to facilitate design—one based on effective width, the other based on average or reduced stress—as described in Chapter 4. For each approach, the degree of edge restraint influences the behavior, and therefore the calculation procedure. Calculation procedures are generally based on either unstiffened or edge-stiffened compression elements. An unstiffened compression element is one that is stiffened at only one edge parallel to the direction of applied stress. A stiffened compression element is stiffened at both edges parallel to the direction of applied stress and is free at the other edge. Many of the design specifications are based on the effective-width approach (Beedle, 1991).

Equation 4.15 is used as the basis for determining the effective width of locally buckled elements. This equation is expressed by the following nondimensional form:

$$b_e = \frac{b(1 - 0.22/\lambda)}{\lambda} \tag{13.1}$$

where

b_e = effective width
b = flat width of plate
$\lambda = (\sigma_e/\sigma_{cr})^{1/2}$
σ_e = for ultimate-strength calculations, the maximum stress on the plate element computed for the moment causing first yield in the effective cross section; for deflection calculations, the maximum stress due to service loads.
σ_{cr} = plate buckling stress defined by Eq. 4.1, i.e.,

$$\sigma_{cr} = \frac{\pi^2 Ek}{12(1 - \nu^2)}\left(\frac{t}{b}\right)^2 \tag{13.2}$$

where E is the modulus of elasticity ($E = 29{,}500$ ksi for cold-formed steel), ν the Poisson's ratio ($\nu = 0.3$), t the plate thickness, and k the plate-buckling coefficient ($k = 4$ for stiffened elements; $k = 0.43$ for unstiffened elements, for partially stiffened elements an intermediate value for k is calculated).

When $b = b_e$, $\lambda = 0.673$, which is the limiting slenderness parameter below which the effective width is equal to the actual flat width. The effective-width criteria in the 1986 AISI specification are thus expressed by the following equations:

$$b = \begin{cases} b & \text{for } \lambda \le 0.673 \quad (13.3a) \\ \rho b & \text{for } \lambda > 0.673 \quad (13.3b) \end{cases}$$

where

$$\rho = \frac{1 - 0.22/\lambda}{\lambda} \tag{13.4}$$

and

$$\lambda = \frac{1.052}{\sqrt{k}} \frac{b}{t} \sqrt{\frac{\sigma_e}{E}} \tag{13.5}$$

This equation derives from Eqs. 13.1 and 13.2 with $\nu = 0.3$. Equation 13.6 is identical to the following formula in the 1980 AISI specification:

$$\frac{b_e}{t} = \frac{253}{\sqrt{\sigma}} \left(1 - \frac{55.3}{b\sqrt{\sigma}/t}\right) \tag{13.6}$$

where σ is the stress due to service loads, and $E = 29{,}500$ ksi, $\nu = 0.3$, $k = 4$, and the factor of safety is $\frac{5}{3}$. Equation 13.6 is the effective-width formula for a stiffened element, and is the same in both the 1980 and the 1986 versions of the AISI specifications. An average reduced allowable stress is used for unstiffened elements in the 1980 and earlier rules, while an effective-width criterion (with $k = 0.43$) is used in the 1986 edition.

The extension of the effective-width approach is based on research by DeWolf et al. (1974), Kalyanaraman et al. (1977), Kalyanaraman and Peköz (1978), Peköz et al. (1981a,b), Mulligan and Peköz (1983), and Loh (1985). A compilation of this research is presented by Peköz (1987). Yu (1991) also presents background discussion regarding the development of effective-width equations.

Research has been conducted on the inelastic reserve strength of cold-formed steel beams whose compression flanges are stiffened along both longitudinal edges. Results indicate that this inelastic reserve strength due to partial plastification of the cross section can be significant for many practical shapes (Reck et al., 1975). Design provisions in the AISI specification permit use of this reserve in design. Additional inelastic reserve capacity due to the redistribution of moments in statically indeterminate beams and profiled decks was studied by Unger (1973, Yener and Peköz (1980), Yu (1981), and Bryan and Leach (1984). The post-local-buckling behavior of continuous beams is discussed by Wang and Yeh (1974). Sloping edge stiffeners of beams have been studied by Peköz and He (1981), LaBoube (1983), and Cohen and Peköz (1987) and are the subject of current further research.

13.2.3 Lateral Buckling

In addition to yielding and local buckling, as discussed previously, the moment-resisting capacity of a thin-walled flexural member may be limited by lateral buckling of the beam between lateral supports. Theoretical and experimental treatments for lateral buckling of hot-rolled shapes and built-up members were discussed in Chapter 5. For thin-walled metal construction, the critical stress for lateral buckling of an I-beam having unequal flanges can be determined by the following formula (Winter, 1943, 1970):

$$\sigma_c = \frac{\pi^2 Ed}{2S_{xc}L^2} \left(I_{yc} - I_{yi} + I_y \sqrt{1 + \frac{4GJL^2}{\pi^2 EI_y d^2}} \right) \tag{13.7}$$

where

S_{sc} = compressive section modulus of the entire section about the major axis
I_{yc}, I_{yt} = moments of inertia of the compression and tension portion, respectively, of a section about its centroidal axis parallel to the web
E = modulus of elasticity
G = shear modulus
J = torsional constant of the section
d = depth of the section
L = unbraced length

For thin-walled steel sections, the first term under the radical in Eq. 13.7 usually exceeds the second term by a considerable margin (Winter, 1947). If the second term is omitted and considering that $I_y = I_{yc} + I_{yt}$, the following equation (Eq. 13.8) can be obtained for determination of critical stress for lateral buckling in the elastic range:

$$\sigma_c = \pi^2 EC_b \left(\frac{dI_{yc}}{L^2 S_{sc}} \right) \tag{13.8}$$

where C_b is a bending coefficient that can conservatively be taken as unity or calculated from $C_b = 1.75 + 1.05(M_1/M_2) + 0.3(M_1/M_2)^2$ but not more than 23. Here $M_1 < M_2$ and the ratio of M_1/M_2 is positive when M_1 and M_2 have the same sign (reverse curvature bending) and negative when they are of opposite signs (single curvature bending).

In the AISI specification the lateral buckling strength for I-section beams in the elastic range is based on Eq. 13.8. For Z-section beams, Eq. 13.8 is divided by 2. To account for local buckling on the overall lateral stability of a beam, the following is suggested (Peköz, 1987; AISI, 1989, 1991):

$$M_u = M_{cr} \frac{S_c}{S_f} \tag{13.9}$$

where M_u is the ultimate lateral–torsional buckling moment, S_f the elastic section modulus of the full reduced section for the extreme compression fiber, and S_c the elastic section modulus of the effective section calculated at

a stress M_{cr}/S_f in the extreme compression fiber. The critical moment is determined as follows:

$$M_{cr} = \begin{cases} M_y & \text{for } M_e \geq 2.78M_y \quad (13.10) \\ \left(\frac{10}{9}\right)\left(1 - \frac{10M_y}{36M_e}\right)M_y & \text{for } 2.78M_y > M_e > 0.56M_y \quad (13.11) \\ M_e & \text{for } M \leq 0.56M_y \quad (13.12) \end{cases}$$

where M_y is the moment causing yielding at the extreme compression fiber at the full section and M_e the elastic critical moment (Eq. 13.8 times S_f).

The solid curve in Fig. 13.1 shows the variation of the critical moment M with the unbraced length. The curve consists of three regions: yielding (Eq. 13.11), inelastic buckling (Eq. 13.12), and elastic buckling (Eq. 13.13). CSA (1989) uses a similar approach to lateral buckling except that the second term under the radical in Eq. 13.7 is retained. Previous study has indicated that equations developed for I-beams can also be used for channels with reasonable accuracy (Hill, 1954). For channels and other singly symmetric shapes, the 1986 AISI specification has deleted the yield plateau.

For a given $L/\sqrt{dI_{yc}}$ ratio, a Z-section will buckle laterally at a lower stress than will an I-beam or a channel section. A conservative design approach has been used in the AISI specification (1986), in which the critical moments for Z-sections in the elastic range are one-half of those permitted for I-beams or

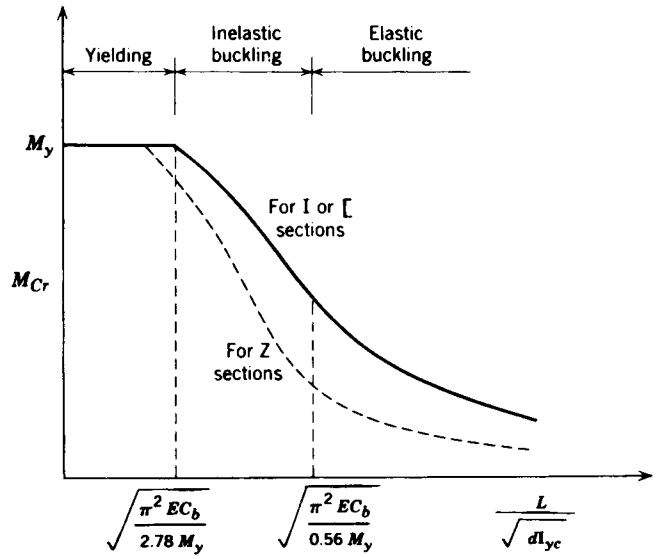

Fig. 13.1 Allowable compressive stress for lateral buckling of beams (Winter, 1970).

channels with the same $L/\sqrt{dI_{yc}}$ ratio. The lateral buckling curve for Z-shaped beams is shown as the dashed line in Fig. 13.1.

Based on studies of the torsional–flexural buckling of cold-formed steel sections under eccentric load (Peköz and Winter, 1969), the critical elastic buckling strength for both singly and doubly symmetric sections bending about the symmetry axis perpendicular to the web is given by

$$M_{cre} = C_b r_0 A \sqrt{\sigma_{ey}\sigma_t} \quad (13.13)$$

where $r_0 = \sqrt{r_x^2 + r_y^2 + x_0^2}$. r_x and r_y are radii of gyration of the cross section about the centroidal principal axis; x_0 is the distance from the shear center to the centroid along the principal x-axis, taken as negative; A is the full cross-sectional area. σ_{ey} and σ_t are defined below:

$$\sigma_{ey} = \frac{\pi^2 E}{(K_y L_y/r_y)^2}$$

$$\sigma_t = \frac{GJ + \pi^2 EC_w/(K_t L_t)^2}{Ar_0^2}$$

K_y, K_t = effective length factors for bending about the y-axis and for twisting
L_y, L_t = unbraced length for bending about the y-axis and for twisting

To account for inelastic behavior of such sections, the critical buckling moment is computed by the following equation when $M_{cre} > 0.5M_y$:

$$M_{cri} = M_y\left(1 - \frac{M_y}{4M_{cre}}\right) \quad (13.14)$$

Laterally unbraced steel box sections with length-to-width ratios up to $2500/\sigma_y$ and with web plates no less than $h/6$ apart can be used as beams without any stress reduction for lateral buckling because the St. Venant torsional stiffness of box sections is high, and the I_y/I_x ratio is higher than for I-sections (Winter, 1970).

For laterally unbraced hat sections bent about the x-axis, no stress reduction is necessary if $I_y > I_x$, because there is no tendency to buckle. When $I_y < I_x$ a conservative estimate of the critical elastic stress may be determined by regarding the compression portion of the section as an independent strut, which gives

$$\sigma_e = \frac{\pi^2 E}{(L/r_y)^2} \quad (13.15)$$

where r_y is the radius of gyration about the vertical axis of that portion of the hat section which is in compression. A more accurate analysis for such hat-shaped sections and for any other singly symmetric section is to use the equa-

tions given in Chapter 5. This is the approach required in the 1986 AISI specification for the design of singly symmetric section.

Recently completed work by Serrette and Peköz (1992) presents a solution to the problem of the unbraced compression flange by using the concepts of distortional buckling of the cross section.

13.2.4 Distortional Buckling

A mode of failure of thin-walled sections in compression and bending in which change of shape of the cross section and lateral and/or torsional movements occur simultaneously may occur especially in sections composed of high-strength steel. This mode of failure is called *distortional buckling*. The distortional mode of buckling occurs at longer half-wavelengths than local buckling and involves membrane displacements of the edge or intermediate stiffeners forming the section or of complete flanges. The distortional buckling modes, along with the local and the flexural–torsional modes, are shown for a rack section in compression and a channel section in bending in Figs. 13.2 and 13.3, respectively.

For the rack section shown in Fig. 13.2, a single distortional mode occurs at an intermediate half-wavelength. However, for the channel section shown in Fig. 13.3, two different types of distortional modes occur. The first occurs at shorter half-wavelengths and involves rotation of the flange about the flange–web junction. This mode is sometimes given the name *stiffener buckling*. The second occurs at longer half-wavelengths and involves distortion of the web

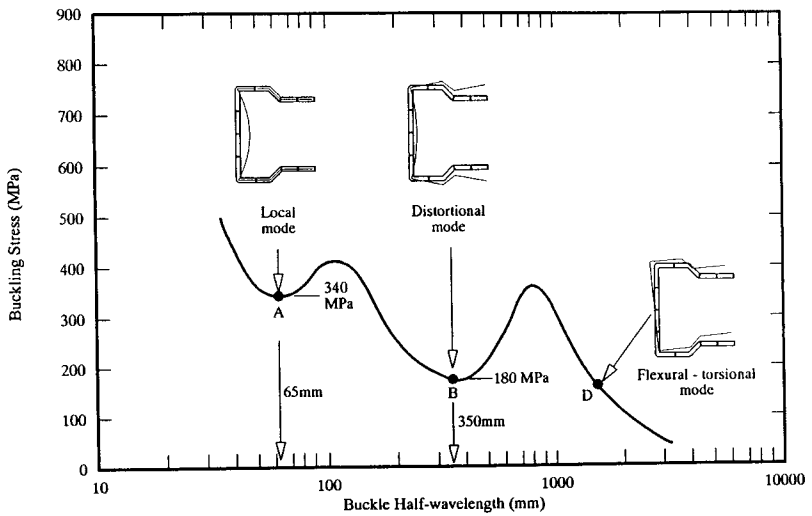

Fig. 13.2 Rack section column: buckling stress versus half-wavelength.

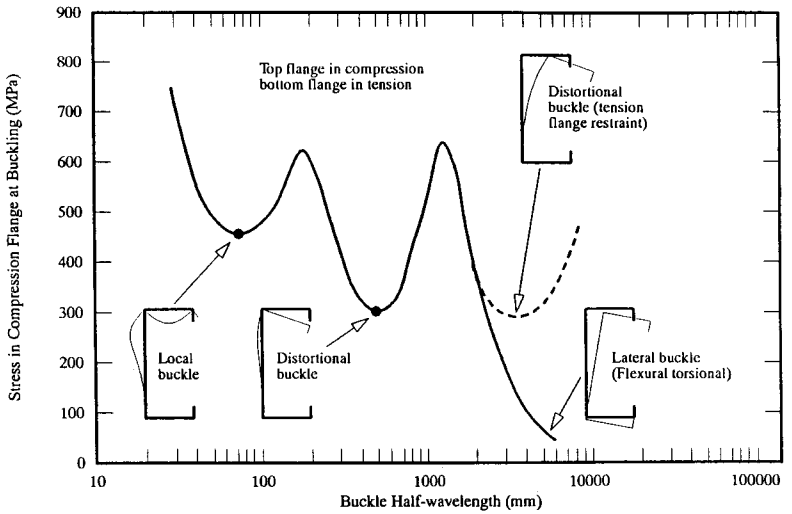

Fig. 13.3 Channel section: buckling stress versus half-wavelength for major-axis bending.

and transverse bending of the flange. It is closer in form to flexural–torsional buckling and a method for its analysis when applied to purlins restrained by sheeting has been provided by Peköz and Soroushian (1982). The distortional mode discussed in detail in this section is the type occurring at shorter half-wavelengths.

Research into the distortional mode of buckling has attracted considerable attention in recent years. Distortional buckling in steel storage rack sections was first discussed by Hancock (1985), where simple design charts for computing the buckling stress were presented. Further research including testing by Lau and Hancock (1988, 1990) resulted in a preliminary set of design curves based on the Johnson parabola (1976) for distortional buckling. These design charts and curves have recently been incorporated in the Australian steel storage rack standard (SAA, 1993). Simplified formulas for computing the elastic distortional buckling stress of sections with edge-stiffened elements were also provided by Lau and Hancock (1987). Charnvarnichbonkarn and Polyzois (1992) have modified the formulae for elastic buckling to predict the distortional buckling stress of Z-section columns. They have used the same design curves as proposed by Lau and Hancock (1988). Their method accurately predicted the distortional buckling strength of Z-section columns in compression. In neither the method of Lau and Hancock nor that of Charnvarnichbonkarn and Polyzois is allowance made for the postbuckling reserve of strength in the distortional model.

Early work on the distortional buckling mode in edge-stiffened elements and intermediate stiffened elements was performed by Desmond et al. (1981a,b). In

these two papers, the buckling mode was given the name *stiffener buckling mode* in cases where the stiffener was not adequate to prevent its deformation in a plane normal to the element that it supported. This is the same mode of buckling as that referred to as distortional buckling in this section. The design methods proposed for edge and intermediately stiffened elements by Desmond et al. have been incorporated in the AISI specification (1986). They account for the inability of the stiffener to prevent distortional buckling by reducing the local buckling coefficient for the plate element supported by the stiffener below 4.0 and then including this reduced buckling coefficient in the Winter effective-width formula used to compute the strength of the plate element. The design methods do not account for the restraint to distortional buckling provided by the web of the section. The use of the Winter effective-width formula allows for postbuckling in the distortional mode. However, as discussed in Kwon and Hancock (1992a), the design method in the AISI specification is unconservative for distortional buckling of channel sections in compression composed of high-strength steel of yield stress 550 MPa, so alternative design methods are necessary to design against distortional buckling in this case. Further, as discussed in Bernard et al. (1993b), the design method in the AISI specification (1986) may be unconservative for distortional buckling of decking panels with intermediate stiffeners composed of high-strength steel of yield stress of at least 550 MPa, so alternative design methods are necessary to design against distortional buckling in this case.

An alternative approach has been to account for the distortional mode of buckling of edge and intermediate stiffeners as a compressed strut on an elastic foundation where the elastic foundation is represented by a spring that depends upon the bending stiffness of adjacent parts of plane elements and on the boundary conditions of the element. This procedure has been adopted in Eurocode 3, Part 1.3 (ECS, 1992). The design strength of the stiffener is based on the conventional compression member design curve in the Eurocode with $\alpha = 0.13$. The method accounts for the elastic restraint of all elements in the section, including the web by incorporation of their flexibility in the elastic spring restraint. However, the method does not allow for any post-buckling reserve in the distortional buckling mode. A detailed discussion of this method applied to channel sections is given in Buhagiar et al. (1992).

Recent tests by Thoon et al. (1993) and Seah et al. (1993) have provided further data on distortional buckling of intermediately stiffened plate elements and lip-stiffened elements. In these papers the distortional buckling mode has been called stiffener buckling. The results of Thoon et al. are for steel with yield stress 181.5 to 343 MPa, and those of Seah et al. are for steel of yield stress ranging from 226.8 to 337.6 MPa.

A related problem is that of the buckling of the unsupported compression flanges of panel beams (decks with vertical upstands used to provide interlocking between adjacent panels). The distortional buckling mode involves rotation of the web–flange element about the axis of the web and tension flange. The mode is closer in form to that occurring at longer half-wavelengths in Fig. 13.3.

A design procedure for this type of distortional buckling has been provided by Serrette and Peköz (1992).

A detailed test program on a range of thin-walled cold-formed steel sections has been performed at the University of Sydney to determine the strength of sections failing in the pure distortional buckling mode, or the distortional buckling mode interacting with local buckling (mixed mode). The results of the tests are described for hat, channel and storage rack sections with yield stress in the range 200 MPa to 480 MPa in Lau and Hancock (1988, 1990), for channel sections with and without intermediate web stiffeners with yield stress in the range 585 MPa to 640 MPa by Kwon and Hancock (1992a, 1992b), and for trapezoidal decking sections with intermediate stiffeners and yield stress 650 MPa by Bernard et al. (1992a, 1993a).

Based on the University of Sydney tests, two different design curves have been proposed. The first uses a modification of the effective-width formula (13.1),

$$b_e = \frac{b(1 - 0.25/\lambda_d)}{\lambda_d} \tag{13.16a}$$

where

$$\lambda_d = \left(\frac{F_y}{\sigma_{crd}}\right)^{0.6} \tag{13.16b}$$

σ_{crd} is the buckling stress for elastic distortional buckling.
For sections in compression, b_e is applied to all elements, including lips. For sections in bending, an effective section modulus Z_e is computed to give the ultimate moment capacity M_u:

$$M_u = F_y Z_e \tag{13.17}$$

The effective section modulus is not based on the effective width of the individual elements but is given by

$$Z_e = \frac{Z(1 - 0.25/\lambda_d)}{\lambda_d} \tag{13.18}$$

where Z is the gross section modulus and λ_d is as defined in Eq. (13.16b). Comparison of Eq. (13.16) with the compression test results of Lau and Hancock (1988, 1990) and Kwon and Hancock (1992b) is given in Kwon and Hancock (1992b). Comparison of Eq. 13.17 with the flexural test results of Bernard et al. (1992a, 1993a) is given in Bernard (1993b).

The second design curve proposed uses a maximum stress (σ_{max}) given by

$$\sigma_{\max} = \begin{cases} F_y\left(1 - \dfrac{F_y}{4\sigma_{crd}}\right) & \sigma_{crd} \geq \dfrac{F_y}{2} \qquad (13.19a) \\ F_y\left[0.055\left(\dfrac{F_y}{\sigma_{crd}} - 3.6\right)^2 + 0.237\right] & \dfrac{F_y}{13} \leq \sigma_{crd} \leq \dfrac{F_y}{2} \qquad (13.19b) \end{cases}$$

Comparison of Eq. 13.18 with the compression test results of channel sections is given in Kwon and Hancock (1992b).

Local buckling can occur simultaneously with distortional buckling, or at a higher or lower load. The tests by Kwon and Hancock (1992a,b) were designed to determine whether adverse interaction occurred if local and distortional buckling were simultaneous or nearly simultaneous. No adverse interaction was found between local and distortional buckling for the channel sections tested so that the distortional buckling strength can be assessed independently of whether local buckling is occurring simultaneously.

The tests of trapezoidal decks by Bernard et al. (1992a,b, 1993a,b) included sections that underwent local buckling before and after distortional buckling. For sections with V-stiffeners, distortional buckling occurring before or in the approximate vicinity of local buckling could be predicted using the design formula proposed for distortional buckling alone. However, sections that underwent local buckling well before distortional buckling needed to be designed using conventional methods to account for local buckling as reported in Bernard et al. (1992a, 1993a,b). For the sections with flat hat stiffeners when distortional buckling occurred first, the design method (Eq. 13.17) adequately predicts the strength of the setions. However, sections that underwent local buckling before distortional buckling could not be predicted conservatively by Eq. 13.18, and a modified effective section method has been proposed by Bernard et al. (1992b).

13.2.5 Design of Webs

The design of webs of thin-walled beams is somewhat different than for hot-rolled members, because the width-to-thickness ratio of webs of thin-walled members is usually large and the use of bearing stiffeners is in most cases impractical. Nevertheless, design provision for webs with transverse stiffeners are included in the AISI specification (AISI, 1986; Nguyen and Yu, 1978).

In the design of webs, consideration should be given to (1) shear strength, (2) local buckling due to bending stress in the web, (3) effect of combined bending and shear, (4) web crippling, and (5) combined bending and web crippling. For webs having small width-to-thickness ratios, the shear strength of the web will be governed by the yield stress in shear determined by the Hencky–von Mises yield criterion; that is,

$$\tau_y = \frac{\sigma_y}{\sqrt{3}} \qquad (13.20)$$

As discussed in Chapter 4, for webs having relatively large width-to-thickness ratios, the strength of the web may be governed by shear buckling. The theoretical critical shear-buckling force in the elastic range can be determined using the values of k_s given in Eqs. 4.24a and 4.24b. For carbon steel ($E = 29{,}500$ ksi and $\nu = 0.3$),

$$V_{cr} = \frac{\pi^2 E k_s t^3}{12(1-\nu^2)h} = \frac{0.904 k_s E t^3}{h} \qquad (13.21)$$

where h is the flat width of the web and t is the web thickness.

For inelastic shear buckling, Basler (1961) presented the following equation:

$$\tau_{cri} = \sqrt{\tau_{pr}\tau_{cre}}$$

where τ_{pr}, the shear proportional limit, $= 0.8\tau_{r_y}$. By substituting the values from Eqs. 13.20 and 13.21 for τ_y and τ_{cre}, the following equation can be derived for inelastic shear buckling:

$$\tau_{cri} = \frac{0.64\sqrt{k_s E F_y}}{h/t} \qquad (13.22)$$

Design specifications (AISI, 1989, 1991; CSA, 1989) apply appropriate factors of safety or ϕ factors to Eqs. 13.20, 13.21, and 13.22 to arrive at minimum design strengths.

Webs of beams can buckle not only in shear but also because of the compressive stress caused by bending. For beams with the neutral axis at middepth, the web-buckling stress can be determined by Eq. 4.1 with $k = 23.9$. For $E = 29{,}500$,

$$\sigma_{cb}^* = \frac{640{,}000}{(h/t)^2} \qquad (13.23)$$

Although a web plate may buckle at a stress intensity given by Eq. 13.23, the load-carrying capacity of the plate may not be exhausted. LaBoube and Yu (1982) experimentally studied the behavior of web elements subjected to pure bending and determined that considerable postbuckling strength of the web is available and is a function of four key parameters: (1) web slenderness, h/t; (2) ratio of maximum compressive bending stress to maximum tensile bending stress in the web, f_c/f_t; (3) flange stiffness as defined by the flange slenderness ratio, w/t; and (4) the yield stress of the steel sheet, F_y. Subsequent research by Cohen and Peköz (1987) defined an appropriate effective width approach,

using Eq. 13.1, which is being utilized by design specifications in North America.

When high bending stresses and high shear stresses act simultaneously, as in cantilever beams and at supports of continuous beams, the webs of beams will buckle at a lower stress than if only one stress were present. For a combination of bending and shear, Eq. 4.30 can be used to predict buckling.

$$\left(\frac{\sigma_{cb}}{\sigma^*_{cb}}\right)^2+\left(\frac{\tau_c}{\tau^*_c}\right)^2 \le 1 \tag{13.24}$$

where σ_{cb} is the actual compressive stress at the junction of flange and web, τ_c is the actual average shear stress, and σ^*_{cb} and τ^*_c are the critical stresses for bending and shear, respectively, as determined above. Equation 13.24 has been adapted for design by replacing the critical stresses for bending and shear with permissible design strength values. The equation has also been presented in a load format by replacing the shear stress with shear force and bending stress with bending moment:

$$\left(\frac{M}{M_n}\right)^2+\left(\frac{V}{V_n}\right)^2 \le 1 \tag{13.25}$$

where M and V are the applied moments and shears, and M_n and V_n are the nominal strengths.

Webs with transverse stiffeners also are treated in the AISI specification. The economy of the thin flat webs is reduced by the fabrication costs associated with attaching stiffeners necessary to prevent premature local buckling. The use of "self-stiffened" corrugated webs could reduce fabrication costs and provide increased material efficiency. Design guidelines for both local and overall shear buckling are given by Shanley (1968) and Mertz and Matthiesen (1970). A study of the optimum attachment for a corrugated web to the beam flange was conducted by Sherman and Fisher (1971) and Hlavacek (1972). Corrugated webs are discussed further in Chapter 6.

The use of web stiffeners is frequently impractical in cold-formed steel construction, and without such stiffeners thin webs of beams may cripple due to the high local stresses caused by concentrated loads or reactions. Figure 13.4 shows the types of deformation that occur due to crippling of unrestrained single webs and restrained double webs. Theoretical analysis of web crippling is rather complicated (Bakker et al., 1990). Experimental investigations (Winter and Pian, 1946; Rockey et al., 1972; Hetrakul and Yu, 1978) have indicated that the web crippling strength of thin-walled beams depends on N/t, h/t, R/t, and σ_y, where t is the web thickness, N the bearing length, h the flat width of the web, σ_y the yield stress of the steel, and R the inside bend radius. The web crippling strength of multiweb deck sections was initially investigated by Yu (1980) and extended by Wing (1981) to include the effect of varying web slope

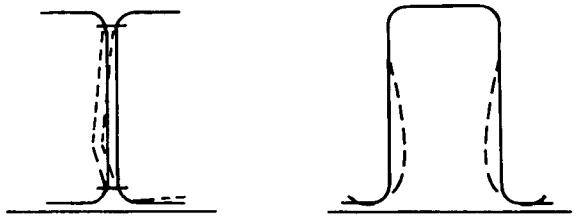

Fig. 13.4 Web crippling of beams.

and also the influence of large bend radius-to-thickness ratios. More recent work by Santaputra et al. (1989) addressed the web crippling behavior of high-strength (i.e., σ_y ranging from 30 to 165 ksi) cold-formed steel beams and decks.

13.3 COMPRESSION MEMBERS

13.3.1 Introduction

Thin-walled open sections are susceptible to flexural–torsional buckling and, in some unusual cases, torsional instability, whereas this mode of behavior is rather exceptional in hot-rolled steel construction. Due to the thinness of the component plate elements, the effect of local buckling may be of critical importance. Another problem peculiar to thin-walled construction is the sensitivity to imperfections in both the member and the connections. Imperfections in connections may lead to local crippling and hence reduce the overall load-carrying capacity. Fortunately, as discussed in Chapter 4, such members may have considerable post-local-buckling strength. With regard to overall flexural buckling, the behavior of cold-formed carbon and low-alloy steel members is similar to that of hot-rolled sections. This behavior, which is caused by the presence of residual cooling stresses in hot-rolled sections, is brought about by the effects of cold forming, which results in increased yield strength at affected zones such as corners. This results in an apparent gradual yielding behavior, as discussed in Section 13.1. However, a complication less easily dealt with may be the presence of through-the-wall residual stresses around the periphery of the section (McDermott, 1981).

13.3.2 Flexural Buckling

Slender compression members that are not susceptible to torsional, or flexural–torsional buckling will lose their stability by flexural buckling. Doubly symmetric sections and closed sections, axially loaded, do not have any tendency to twist if they are of dimensions commonly used in structures. Open sections may

buckle flexurally if their dimensions are as discussed in Section 13.3.5 of if they are restrained against twist.

Flexural buckling of a straight member occurs at an average stress of

$$\sigma_c = \frac{\pi^2 E_t}{(KL/r)^2} \tag{13.26}$$

The tangent modulus, E_t, is the slope of the stress-strain diagram at the buckling stress, σ_c. The exact shape of the stress-strain diagram—hence the variation of the tangent modulus with the stress level—depends on the process of forming the section as well as the properties of the virgin material. Thus it is impossible to predict the details of the shape of the stress-strain diagram for cold-formed members. For columns of small or moderate slenderness ratios (i.e., when the buckling stress is at a level where the stress-strain relationship is nonlinear) a simple but sufficiently accurate approach has been followed, similar to the CRC basic column curve treatment of the influence of residual cooling stresses in hot-rolled column behavior. Early tests (Karren and Winter, 1967) have shown that for the range of slenderness ratios in question, the flexural buckling stress for carbon and low-alloy steel members can be approximated by

$$\sigma_c = \sigma_y - \frac{\sigma_y^2}{4\pi^2 E}\left(\frac{KL}{r}\right)^2 \tag{13.27}$$

If the column is slender enough to buckle at a stress level where the stress-strain relation is linear, the buckling stress can be obtained from

$$\sigma_c = \frac{\pi^2 E}{(KL/r)^2} \tag{13.28}$$

The limiting value of the slenderness ratio $(KL/r)_{\text{lim}}$, determining which type of behavior is to be expected can be found by equating the buckling stresses according to Eqs. 13.27 and 13.28. Thus

$$\left(\frac{KL}{r}\right)_{\text{lim}} = \pi\sqrt{\frac{2E}{\sigma_y}} \tag{13.29}$$

Because cold-formed thin-walled columns are sensitive to imperfections and end eccentricities resulting from connection details, design specifications generally require a larger margin of safety for design, (i.e., a larger factor of safety or smaller ϕ factor). The 1996 version of the AISI specification recognized the imperfection sensitivity explicitly and adopted the new column equations (Eq. 3.19) which include an initial imperfection of height/1500 in their development and which are also in the AISC LRFD Specification (AISC, 1993).

Studies (Peköz, 1980; Dat and Peköz, 1980; Weng and Peköz, 1988) have shown that for certain sections Eq. 13.27 may overestimate the strength. It was found that even though the cold-forming increases the yield stress, the proportional limit is lowered and hence the buckling load is lowered. Dat and Peköz (1980) give column curves based on analytical and experimental studies involving cold-formed steel columns. Weng and Peköz (1987) present a design procedure that recognizes the reduced stiffness of cold-formed steel columns, which results from the forming process. Based on the work of Dat and Peköz (1980), the RMI specification (1979) requires greater design factors of safety. Guiaux (1974) and Ingvarsson (1975, 1977) present the results of research on cold-formed tubular sections. Recent studies of cylindrical tubular sections is summarized by Yu (1991) and in Chapter 14.

13.3.3 Effect of Local Buckling on Column Strength

Results of early studies on interaction between local and overall buckling were presented by Bijlaard and Fisher (1952a,b). More recently, this problem has received a significant amount of attention. Graves-Smith (1969) treats the post-local-buckling behavior within the scope of the large deflection plate theory and accounts for the inelasticity effects both locally and overall. The overall buckling load is computed using the tangent modulus approach based on the stiffnesses of the locally buckled plate elements. Although the method is basically general the author treats only the case of a square tubular column. Hancock (1981) and Sridharan and Benito (1984) have investigated the interaction problem using the finite strip method. Thomasson (1978) and Konig and Thomasson (1980) treat the post-local-buckling behavior with an effective-width approach and the column strength is determined on the basis of an initial column imperfection. The ultimate load is defined as either the load that causes yielding or the maximum load that can be sustained. Mulligan and Peköz (1983) studied singly symmetric columns.

The foregoing approaches necessitate computer calculations. A computationally simpler approach is presented by DeWolf et al. (1974, 1976) and Kalyanaraman et al. (1977). In these studies an effective-width approach is used to find stiffnesses that depend on the value of the axial load. The stiffnesses thus obtained are used with a modified tangent modulus approach to obtain the overall buckling load. A more recent experimental study is presented by Braham et al. (1980).

A simple but conservative treatment is provided by the use of a form factor as recommended by the AISI specifications (1980). Sections consisting of stiffened elements, sections consisting of unstiffened elements, and combinations of these two types of sections exhibit different types of behavior. This method is described in detail in the third edition of this guide. The AISI (1980) form factor method has the advantage of simplicity and appears to have performed

well historically. Recent tests have indicated, however, that its performance in predicting maximum strength is uneven, ranging from the excessively conservative to the unconservative.

The singly symmetric column which is not fully effective is a unique and difficult problem. Not only are the effective section properties reduced by local buckling, but the effective centroid shifts along the axis of symmetry. Thus an initially concentrically loaded column becomes a beam column. Testing such a column which is truly concentrically loaded throughout its loading history appears difficult if not impossible. Furthermore, the centrally loaded singly symmetric column appears to exist in practice only if it is fully effective and is loaded at its ends uniformly around the periphery. In practice, it may be difficult to be assured that such conditions will exist. Consequently, many columns that have no obvious moment applied to their ends may be, in actual fact, beam columns.

Springfield and Trestain developed a design method for the CSA Standard CAN3-S136-M84, which differed radically from the essentially similar methods of the 1974 CSA and 1980 AISI. Those methods tended to overpredict stiffened column strength for slender columns in which local buckling supposedly was not a factor but clearly was having an effect. For design office use, the iterative approach utilizing effective section properties was unsuitable. The key features of the new method were the use of gross section properties to determine slenderness and buckling stress, and the determination of effective area at this buckling stress rather than at F_y as used previously. The method predicted the DeWolf et al. (1974) test results with remarkable accuracy. The column curve developed by Lind for the 1974 CSA standard was retained. This is geometrically similar to the AISC column curve, in which a Johnson parabola extends from F_y, tangential to an Euler curve lowered to 0.833 (equivalent to 1.6/1.92) of the standard value. This reflects the unlikely event of real columns ever reaching the Euler load of a perfect column. Other important aspects were the adoption of the effective-width approach for all sections, stiffened and unstiffened, and, based on Trestain's (1982) evaluation of available test data, the use of a lower resistance factor for single symmetrical sections ($\phi = 0.75$ versus 0.90). In recognition of the dramatic reduction in stiffness of unstiffened channels as the effective flange width is reduced, the effective stress is limited to the unstiffened flange local buckling stress.

The 1984 CSA method was incorporated into the unified approach proposed by Peköz (1986) for the 1986 AISI specification. Further evaluation by Peköz using more recent test data has led to further refinement: in particular, the use of the effective centroid rather than the gross centroid as the origin for determination of eccentricity of load.

The 1986 AISI specification uses an effective cross-sectional area, as follows:

$$P_u = A_e F_u \tag{13.30}$$

where A_e is the effective area at stress F_u and F_u is the ultimate stress determined by the following equations:

$$F_u = \begin{cases} F_y\left(1 - \dfrac{F_y}{4\sigma_e}\right) & \text{for } F_u > \dfrac{F_y}{2} \quad (13.31) \\ \sigma_e & \text{for } F_u \le \dfrac{F_y}{2} \quad (13.32) \end{cases}$$

where σ_e is the elastic flexural buckling stress (Eq. 13.26) or the elastic flexural-torsional buckling stress. Equation 13.31 is identical to Eq. 13.27 for the case of flexural buckling. The form factor approach is used in the RMI specification (1979) for design of columns with perforations. The form factor Q is determined by stub column tests.

13.3.4 Wall Studs

Thin-walled sections are frequently used as wall studs. Wall studs may carry either axial force, bending moment, or both axial and bending forces. For such members, the buckling strength in the plane parallel to the sheathing may be increased greatly by the bracing effect of the sheathing. This is quite beneficial, since, in general, this direction is the weaker direction of the wall stud. Simaan and Peköz (1976) indicated that the bracing effect of sheathing may be utilized if the following criteria are satisfied:

1. The strength and rigidity of the wall material is adequate to prevent excessive deflection or buckling of the wall studs.
2. The spacing between fasteners joining each stud to the sheathing should be such that the stud will not buckle between the attachments.
3. The fasteners are capable of developing the required forces.

A further description of bracing requirements is given in Section 13.5.

Recent work by Miller and Peköz (1990) investigated the behavior of all stud assemblies having discrete braces, in addition to the wall sheathing, as well as the influence of eccentric loads and the presence of web perforations in the stud. They concluded that the Simaan model has limitations that merit further review.

13.3.5 Flexural–Torsional Buckling

Concentrically loaded columns can buckle by (1) flexure about one of the principal axes, (2) twisting about the shear center (torsional buckling), or (3) a combination of both flexure and twisting, called flexural–torsional buckling. Torsional buckling is a possible failure mode for point symmetric sections. Flexural–torsional buckling must be checked for open sections that are singly

symmetric and for sections that have no symmetry. Open sections that are doubly symmetric or point symmetric are not subject to flexural–torsional buckling because their shear center and centroid coincide. Closed sections also are immune to flexural-torsional buckling.

One can explain the nature of flexural–torsional buckling with the aid of Fig. 13.5. At buckling, the axial load can be visualized to have a lateral component (qdz) as a consequence of the column deflection. The torsional moment of this lateral component about the shear center of the open section shown in the figure causes twisting of the column. The degree of interaction between the torsional and flexural deformations determines the amount of reduction of the buckling load in comparison to the flexural buckling load. Therefore, as the distance between the shear center and the point of application of the axial load increases, the twisting tendency increases and therefore the flexural–torsional buckling load decreases. Flexural–torsional buckling can be a critical mode of failure for thin-walled open sections because of their low torsional rigidity. The theory of elastic flexural–torsional instability is well developed (Goodier, 1942; Vlasov, 1959; Timoshenko and Gere, 1961; Galambos, 1968). Flexural–torsional buckling of singly symmetric thin-walled open sections under concentric and eccentric loading also has been studied in detail, and design aids have been

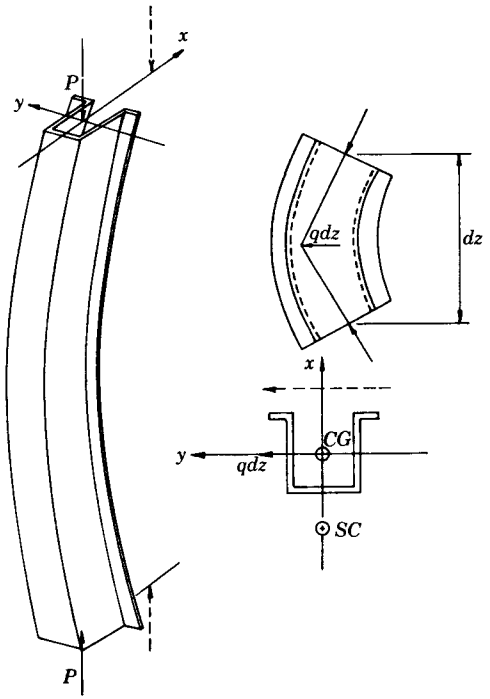

Fig. 13.5 Forces causing flexural–torsional buckling.

devised (Klöppel and Schardt, 1958; Pfluger, 1961; Chajes and Winter, 1965; Chilver, 1967; Peköz, 1969; Peköz and Winter, 1969). For the inelastic domain, approximate approaches have been developed and adequately substantiated by tests (Chajes et al., 1966). The AISI specification (1980, 1986) for carbon steel contains flexural–torsional buckling provisions based on the work of Chajes and Winter (1965), Peköz (1969), and Peköz and Winter (1969).

Equations for Elastic Flexural–Torsional Buckling. Differential equations of equilibrium for the general case of biaxial eccentricities have been solved by Thürlimann (1953), Vlasov (1959), Dabrowski (1961), Prawel and Lee (1964), Culver (1966), and Peköz and Winter (1969) using different procedures of solution. If the section is singly symmetric, such as the sections shown in Fig. 13.6, and is acted on by an axial load not in the plane of symmetry; or if the section is not symmetric, the solution of the differential equations indicates that as the axial load increases the member continuously twists and deflects biaxially. The principal axes, twist angle ϕ and deflections u and v are shown in Fig. 13.7. Analogous to small deflection flexural beam-column theory, infinite deflections and rotation are predicted for a certain value of the axial load.

However, if the section is singly symmetric and the axial load is applied through the centroid, the behavior of the member is described by three homogeneous differential equations, two of which are coupled. If the member is assumed to be hinged at both ends, namely, $u'' = v'' = \phi'' = 0$, the solution of the one uncoupled equation gives the critical load for buckling in the direction of the symmetry axis (taken here as the x-axis):

$$P_{ye} = K_{11} E I_y \frac{\pi^2}{L^2} \tag{13.33}$$

where I_y is the moment of inertia about the y-axis and L is the length of the column. K_{11} and other K values determined by the Galerkin method for various boundary conditions are given by Peköz (1969). The discussion here will be limited to hinged ends.

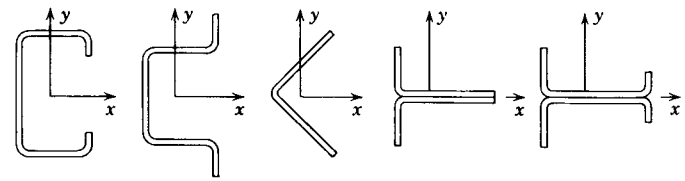

Fig. 13.6 Some singly symmetric sections and coordinate axis orientation.

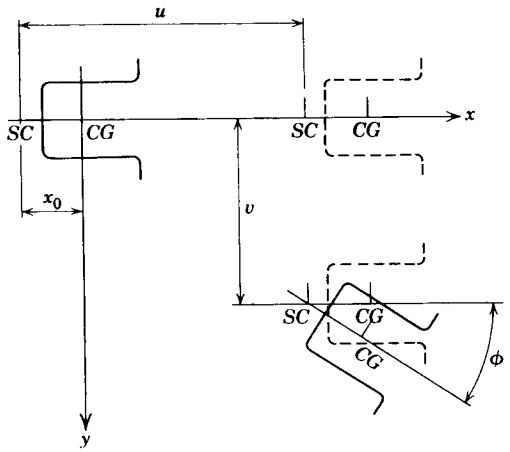

Fig. 13.7 Principal axes and deflection components.

The two coupled equations describing deformations v and ϕ result in a single buckling load P_{TF} for the flexural–torsional mode. The same buckling mode also occurs in the more general case of the load acting eccentrically in the plane of symmetry. Then the member continuously deflects as a beam-column in the plane of symmetry (x-direction), but is subject to flexural–torsional buckling out of this plane under load P_{TF} given in this case by Eq. 13.34. (The solution for a concentric load is obtained by setting $e_s = 0$ in this equation.)

$$P_{TF} = \frac{(P'_{\phi e} + \alpha P_{xe}) \pm \sqrt{(P'_{\phi e} + \alpha P_{xe})^2 - 4\gamma P_{xe} P'_{\phi e}}}{2\gamma} \tag{13.34}$$

where

$$\alpha = 1 + e_x \beta_2 \frac{A}{I_0} \tag{13.35}$$

$$\gamma = \frac{A}{I_0}(x_0 - e_x)^2 + e_x \beta_2 \frac{A}{I_0} + 1 \tag{13.36}$$

$$P'_{\phi e} = P_{\phi e} \alpha \tag{13.37}$$

$$P_{\phi e} = \frac{A}{I_0}\left(E C_w \frac{\pi^2}{L^2} + GJ\right) \tag{13.38}$$

$$P_{xe} = E I_x \frac{\pi^2}{L^2} \tag{13.39}$$

$$\beta_2 = \frac{1}{I_y}\left(\int_A x^3 dA + \int_A x y^2 dA\right) - 2x_0 \tag{13.40}$$

and where

e_x = eccentricity with respect to the center of gravity
x_0 = x-coordinate of the shear center
I_x = moment of inertia about the x-axis
I_0 = polar moment of inertia about the shear center
A = area of the cross section
C_w, J = warping and St.-Venant torsional constants for the cross section, respectively.

The parameter $P_{\phi e}$ has the physical meaning that it is the concentric torsional buckling load if the displacements u and v are prevented, $P'_{\phi e}$ is the corresponding value for eccentric loading, and P_{xe} designates the load for buckling in the direction of the y-axis if displacements ϕ and u are prevented.

For discussion purposes infinite elasticity is assumed in this section. With this assumption P_{ye} is the limiting eccentric axial force for member capacity in the plane of symmetry, and the following types of behavior can be defined depending on relative magnitudes of P_{ye} and P_{TF}. If P_{ye} is less than P_{TF}, the member will behave purely as a flexural beam-column without twisting, and deflection in the plane of symmetry will increase gradually. At an axial load equal to P_{ye}, infinite deflection without twisting is indicated by the solution.For concentric loading, if P_{ye} is less than P_{TF} the member will buckle flexurally about the y-axis. On the other hand, for concentric loading or eccentric axial loading in the plane of symmetry, if P_{ye} is greater than P_{TF}, buckling will occur by the lateral deflection (v) and twisting (ϕ) at an axial load equal to P_{TF}, the flexural–torsional buckling load.

When there is no axial load, the Galerkin method solution (Peköz, 1969) of the general differential equations of equilibrium gives the following expression for the critical moments, M_{CR}:

$$M_{CR} = -\frac{P_{xe}\beta_2}{2}\left(1 \pm \sqrt{1 + \frac{4I_0 R}{\beta_2^2 A}}\right) \tag{13.41}$$

where $R = P_{\phi e}/P_{xe}$. This equation yields one positive and one negative value of M_{CR}, which will be denoted M_{CR+} and M_{CR-}, respectively.

Design Simplifications. The preceding section has been restricted to the classic flexural–torsional stability of single symmetric thin-walled sections. In this section the general behavior of such sections is discussed on the basis of an assumed elastic–plastic stress-strain diagram.

In the precritical stages, the member does not twist; therefore, the maximum fiber stresses at subcritical loads can be found simply from the secant formula or any other appropriate beam-column formula. It is assumed that for the thin-walled sections in question, the attainment of the yield stresses represents the

limit of load-carrying capacity; that is, the plastic reserve capacity, if any, is negligible. This point has been verified experimentally (Peköz 1969; Peköz and Winter, 1969). Therefore, elastic flexural torsional buckling is a possible mode of failure only if the axial load P_{yd} that causes incipient yielding (e.g., as predicted by the secant formula) is larger than P_{TF}.

Extensive numerical studies were carried out on a variety of singly symmetric open sections and are reported by Peköz (1969). Figure 13.8 is a typical sample of the plots given in that reference that illustrates the complex behavior of such compression members.

For positive eccentricities, numerical studies indicate that both yielding and instability need to be considered. The following expression is shown in the reference to give very satisfactory results:

$$\frac{1}{P_{TFO}} + \frac{e_x}{M_{CR+}} = \frac{1}{P_{TF}} \tag{13.42}$$

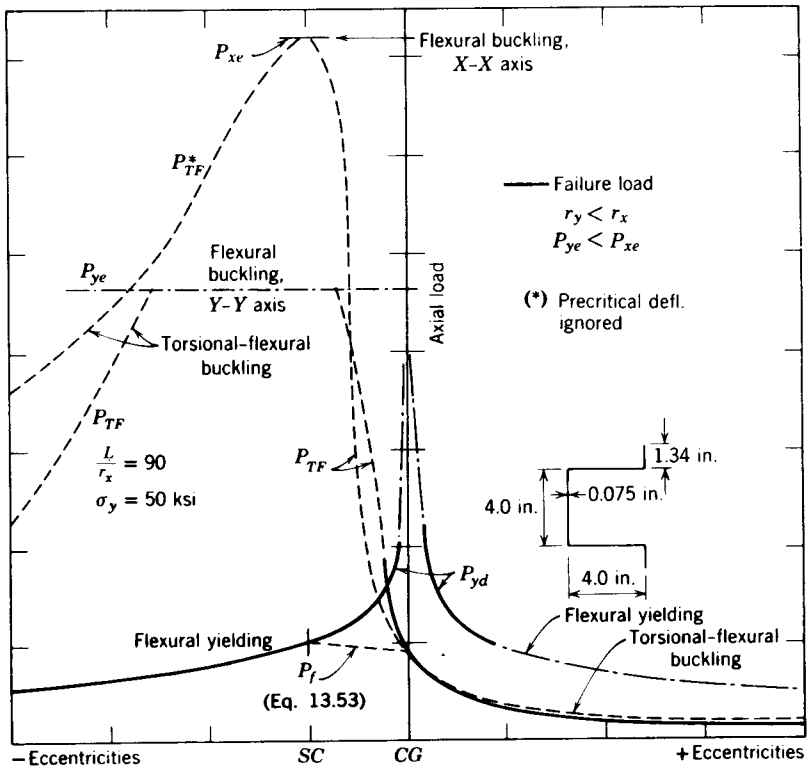

Fig. 13.8 Failure modes and loads (Peköz, 1969).

in which P_{TF} is the flexural–torsional buckling load for an eccentricity e_x; P_{TFO} the flexural–torsional buckling load for concentric loading, regardless of whether it is the governing mode; and M_{CR+} the positive critical moment when there is no axial load, regardless of whether it is the governing mode (see Eq. 13.41). With the aid of charts given by Peköz (1969) for computing P_{TFO} and M_{CR+}, this equation is much more convenient to use than Eq. 13.34.

For negative eccentricities greater than x_0—that is, if the point of application of the axial load is on the side of the shear center opposite from the center of gravity—numerical studies on hat, channel, lipped channel, angle, and lipped angle sections of typical dimensions and yield stresses below 50 ksi (345 MPa) indicate that flexural–torsional buckling is not a governing mode of failure. For such eccentricities, these members fail by yielding after deflecting in the direction of the symmetry axis as a beam-column. However, for singly symmetric I-sections both yielding and flexural–torsional buckling need to be investigated. For these sections, the following interaction equation may be used:

$$\frac{1}{P_{xe}} + \frac{e_x - x_0}{M_{CR-}} = \frac{1}{P_{TF}} \tag{13.43}$$

in which M_{CR-} is the negative critical moment when there is no axial load, regardless of whether it is the governing mode (see Eq. 13.41).

If a section when concentrically loaded can fail in flexural–torsional buckling, then flexural–torsional buckling is also a possible mode of failure for some range of eccentricities between the centroid and the shear center. It is seen from Fig. 13.8 that in this region, between shear center and centroid, the two branches of the failure curve (yielding on the left and flexural–torsional buckling on the right) show a definite and sharp peak. This means that small changes or inaccuracies in eccentricity can produce large reductions in load capacities. For this reason it seems reasonable and conservative—in design—to disregard the uncertain high carrying capacity in the region of the peak, and to base design values on the dashed straight cutoff shown in Fig. 13.8. In this range of eccentricities, the following linear interpolation formula between the axial load, P_3, applied at the shear center, which causes yielding or buckling and the concentric flexural–torsional buckling load, P_{TFO}, gives a realistic and conservative flexural–torsional buckling load, P_F.

$$P_F = P_{TFO} + \frac{e_x}{x_0}(P_S - P_{TFO}) \tag{13.44}$$

For singly symmetric I-sections, P_s is the smaller of the yield load P_{yd} or the buckling load P_{xe}, whereas for the other open sections, only yielding need be considered, as explained previously.

Additional Design Considerations. In addition to the points discussed in the preceding section, the following need to be considered in the design of thin-walled members to resist flexural–torsional buckling.

First is the inelastic stability behavior for members of relatively low slenderness ratios. Chajes et al. (1966) studied this problem and reported that an expression similar to the CRC column curve is satisfactory for concentric flexural–torsional buckling. The AISI specifications reflect this approach for both concentric and eccentric loading.

Second is the frequent case of unequal eccentricities at opposite ends of the member. Peköz (1969) presents the results of an extensive study of this subject and makes the conclusion that application of a modification factor, C_{TF}, to the second term of Eq. 13.42 is quite accurate. The value C_{TF} is the same as C_m discussed in Chapter 8, except that it does not have 0.4 as its lower limit.

Third, the influence of precritical beam-column deflections on the flexural–torsional buckling load is an important consideration. Again, on the basis of an analytical and experimental treatment of the subject, Peköz (1969) recommends the use of an amplification factor $1/(1 - P/P_{ye})$ for the moments.

Fourth, is the wandering centroid problem where centrally loaded, singly symmetric columns become beam-columns upon local buckling and the shifting of the neutral axis. In an extensive statistical study, Peköz (1986) established good correlation with test results if a concentrically loaded column is defined as a member loaded through its effective centroid. The effective centroid is calculated at the reduced column stress F_u from Eq. 13.31 or 13.32. This approach is used in the North American design specifications.

Fifth, is the behavior of biaxially loaded beam-columns. The 1980 AISI specification did not permit the calculation of singly symmetric beam-columns bending about the symmetry axis. The designer had to resort to tests. Based primarily on the work of Loh (1985), Mulligan and Peköz (1983), and Peköz (1986), the 1986 AISI specification determines the capacity of biaxially loaded open sections using an interaction equation with eccentricities measured from the effective centroid. The method is similar to procedures adopted previously by the RMI (1969) standard and followed in the CSA (1989) standard. Lipped channel sections used in the endwalls of metal buildings and the columns in industrial storage racks are a few examples of members subjected to such loads.

13.4 DIAPHRAGM ACTION OF THIN-WALLED PANELS

Thin-walled metal panels are often used as wall cladding, roof decking, and floor decking, where their primary structural function is to carry loads acting normal to their surface. Properly designed and interconnected metal roof, wall, and floor systems are also capable of resisting shear forces in their own planes, referred to as diaphragm action. Considerable progress has been made in predicting the shear strength and stiffness of a diaphragm composed of such panels. Publications by ECCS (1977), Easley (1977), Ha et al. (1979), Atrek and Nilson (1980), Bryan and Davies (1981) and SDI (1988) are among the contributions to the literature on the subject. The strength and stiffness of a diaphragm also can be determined from the load-deflection relationship obtained from a shear diaphragm test as described by ASTM E455. Procedures have been established for making use of this shear resistance in designing buildings to resist forces caused by wind, seismic action, and other lateral loads (Bryan and Davies, 1981, SDI, 1988; AISI, 1989). The shear strength and rigidity of thin-walled panels can be utilized in folded plate structures (Nilson, 1960), hyperbolic paraboloids (Gergely et al., 1971), and other shell roof structures (Bresler et al., 1968). Procedures have been developed that recognize the ability of diaphragms assembled from such panels to transfer load from a heavily loaded frame to less heavily loaded adjacent frames in a single-story structure, thus reducing the required maximum frame size (Luttrell, 1967; Bryan and Davies, 1981). Research has also assessed the influence of thin-walled metal cladding on the behavior of multistory buildings (Miller, 1972; El-Dakhakhni and Daniels, 1973). In addition, theory and test results both have shown that the shear strength and rigidity of properly connected diaphragms can be very effective as bracing for individual beams and columns.

13.5 BRACING REQUIREMENTS

13.5.1 Types of Bracing

Structural bracing may be divided into two general types, according to its function: (1) bracing provided to resist secondary loads on structures, such as wind bracing, and (2) bracing provided to increase the strength of individual structural members by preventing them from deforming in their weakest direction (Winter, 1958). In the latter instance, there are again two different cases: (1) bracing applied to prevent buckling and thereby increase the unstable strength of the member, and (2) bracing applied to counteract stable but detrimental types of deformation. As examples of the latter, channel- and Z-shaped beams loaded in the plane of the web twist or deflect laterally, with consequent loss of strength unless they are properly braced (Murray and Elhouar, 1985).

For bracing against buckling to be effective in an actual situation, it must possess not only the requisite strength but also a definite minimum rigidity. However, the required strength cannot be computed uniquely, except on the basis of assumed imperfections of shape and/or loading of the member to be braced (Winter, 1958). Bracing may be *continuous*, such as that provided by wall panels, roof decking, or floor systems, or it may be noncontinuous or *discrete*, such as cross-bracing. For discrete bracing the spacing of the braced points also is important. Finally, bracing may also be distinguished according to its behavior: (1) that which provides restraint through resistance to axial

deformation, as does cross-bracing, and (2) that which provides restraint through resistance to shear deformation, as do diaphragms (Fig. 13.9).

13.5.2 Diaphragm-Braced Columns

In the elastic range the predicted weak-axis buckling load of an ideal axially loaded I-section column or wall stud with directly attached symmetrical diaphragm bracing (Larson, 1960; Pincus and Fisher, 1966) is determined as

$$P = P_{yy} + Q \tag{13.45}$$

where P_{yy} is the weak-axis buckling load of the unbraced column and Q is the shear rigidity of the diaphragm contributing to the support of the column. The shear rigidity can be expressed as

$$Q = A_d G_{\text{eff}} \tag{13.46}$$

where A_d is the cross-sectional area of the diaphragm normal to the column axis and contributing to the support of the member and G_{eff} is the effective shear modulus of the diaphragm. The theory can be extended into the inelastic range using the tangent-modulus expression for the weak-axis buckling load (Errera et al., 1967). Thus

$$P = \frac{\pi^2 E_t^* I_y}{L^2} + Q \tag{13.47}$$

in which E_t^* is the tangent modulus associated with the increased buckling load, P. It is emphasized that Eqs. 13.45 and 13.47 predict the increased weak-axis buckling loads of ideal members; only the stiffness of the bracing is considered.

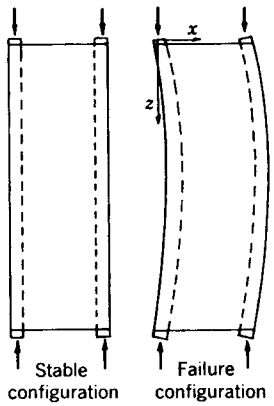

Fig. 13.9 Members with diaphragm bracing.

For real members, initial imperfections and the strength of the bracing must also be taken into consideration.

The theory and experimental verification have been extended to the case of diaphragm bracing connected to girts, which, in turn, are connected to columns (Apparao et al., 1969; Massicotte et al., 1985), and to diaphragm-braced columns of singly-symmetric and point-symmetric sections, such as channels and zees used as wall studs (Simaan, 1973).

Errera and Apparao (1976b) have presented a procedure for the design of I-shaped columns with diaphragm bracing provided by cold-formed steel panels. The procedure covers axially loaded I-section columns with shear diaphragms on both flanges or on one flange only. It also covers the case of axially loaded I-section columns braced by girts, which in turn are braced by diaphragms, as usually encountered in most metal building construction.

The AISI specification bases the bracing requirements for load bearing wall studs on the diaphragm behavior of the sheathing. Closed-form expressions are given if identical sheathing is attached to both flanges of the stud. For other cases, reference is made to the theoretical investigations of these types of stability problems as documented by Simaan and Peköz (1976). A study by Zhang and Peköz (1982) explored the case of wall studs subjected to axial and lateral loads.

13.5.3 Diaphragm-Braced Beams

The same type of diaphragm action is useful also in counteracting lateral-torsional buckling of beams. For ideal I-section beams braced directly by diaphragms on the compression flange, the critical lateral-buckling moment can be estimated as (Errera et al., 1967)

$$M_{cr} = M_0 + 2Qe \tag{13.48}$$

where M_0 is the lateral-buckling moment of the unbraced beam, e the distance between the center of gravity of the beam cross section and the plane of the diaphragm, and Q the shear rigidity of the diaphragm contributing to the support of the member, as defined previously. Again, it is emphasized that Eq. 13.48 predicts the buckling load of an ideal member. For real members the initial imperfections and the strength of the bracing must be taken into consideration. Design procedures for real beams with diaphragm bracing have been presented by Nethercot and Trahair (1975) and Errera and Apparao (1976a).

Because of their asymmetry channels and Z-sections used as beams and loaded in the plane of the web will continuously twist or deflect laterally with consequent loss of strength unless they are properly braced. When both flanges of such beams are connected to deck or sheathing material in such a manner as to restrain lateral deflection effectively, no further bracing is required. For other cases the AISI specification defines the maximum spacing

and the required strength of extensional braces to prevent such deformations. This has been the subject of a recently completed study by Ellifritt et al. (1992). The spacing is such that rotation between bracing points will be small enough to be unobjectionable, and the additional stresses associated with the rotation will not reduce the carrying capacity of the member. The required strength of the bracing is based on statics, using an approximate method of analysis which was checked against test results (Winter et al., 1949; Zetlin and Winter, 1955). Here again, more recent research (Celebi et al., 1971) has led to procedures for analyzing the strength and deflections of diaphragm-braced channels and Z-sections, and current efforts are aimed at developing suitable design procedures for both gravity and uplift loading (Peköz and Soroushian, 1982; Brooks and Murray, 1990).

13.6 STAINLESS STEEL STRUCTURAL MEMBERS

Cold-formed stainless steel sections have been widely used architecturally in buildings because of their superior corrosion resistance, ease of maintenance, and pleasing appearance. Typical applications include column covers, curtain-wall panels, mullions, door and window framing, roofing and siding, stairs, elevators and escalators, flagpoles, signs, and many others. Since 1968, their use for structural load-carrying purposes has been increased due to the availability of the AISI and ASCE design specifications (AISI, 1974; ASCE, 1990).

The first edition of the *Specification for the Design of Cold-Formed Stainless Steel Structural Members* was issued by American Iron and Steel Institute in 1968 on the basis of the research conducted by Johnson and Winter (1966) at Cornell University. This specification was revised in 1974 to reflect the results of additional research (Wang and Errera, 1971) and the improved knowledge of material properties and structural applications. This 1974 edition of the AISI specification contained design information on annealed and cold-rolled grades of sheet and strip stainless steels, types 201, 202, 301, 304, and 316.

Since 1984, additional studies on stainless steel members and connections have been conducted in the United States (van der Merwe, 1987; Lin, 1989), South Africa (van den Berg, 1988; van den Berg and van der Merwe, 1992; van der Merwe and van den Berg, 1992), Australia (Rasmussen and Hancock, 1993a,b), United Kingdom (Dier, 1992), and Japan. In 1990, a new ASCE standard, *Specification for the Design of Cold-Formed Stainless Steel Structural Members* (ASCE, 1990; Lin et al., 1992; Yu and Lin, 1992), was published by the American Society of Civil Engineers to supersede the AISI specification. This new ASCE specification is based on both limit-states design and allowable stress design and is applicable to the use of four types of austenitic stainless steels (types 201, 301, 304, and 316) and three types of ferritic stainless steels (annealed types 409, 430, and 439). In the United Kingdom, the *Concise Guide to the Structural Design of Stainless Steel* was published by the Steel Construction Institute (Burgan, 1992).

The main reason for having a different specification for stainless steel structural members is because stainless steel has the following differing characteristics compared with carbon steel:

1. Anisotropy
2. Nonlinear stress-strain relationship
3. Low proportional limit
4. Pronounced response to cold work

Figure 13.10 shows the stress-strain curves of annealed, half-hard, and full-hard stainless steels. Because of the differences in mechanical properties and structural uses between stainless steel and carbon steel, the ASCE specification for stainless steel design contains modified design provisions for (1) local buckling of flat elements, (2) w/t limitations, (3) deflection calculations, (4) service stress limitations, (5) lateral buckling of beams, (6) column buckling, and (7) connections. In general, the factors of safety used for the allowable stress design of stainless steels are somewhat larger than those used for carbon

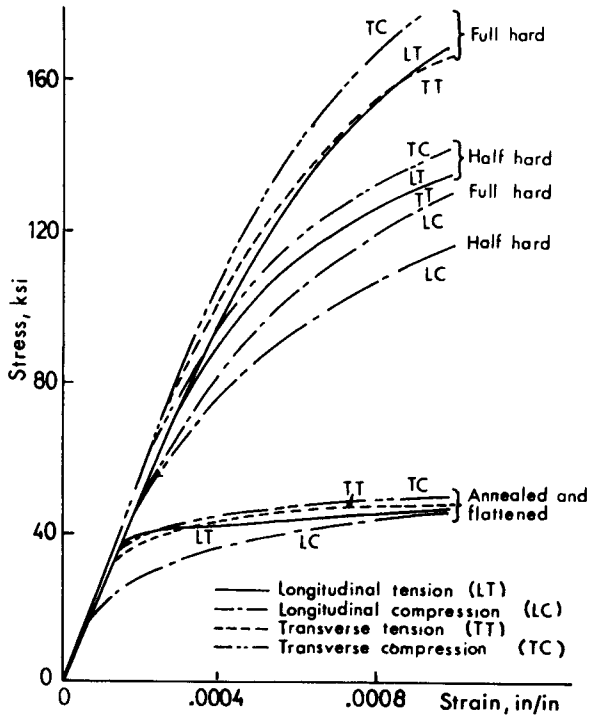

Fig. 13.10 Stress-strain curves of annealed half-hard, and full-hard stainless steels (Wang, 1969; Johnson and Kelsen, 1969).

steel. Due consideration has been given to the development of the load and resistance factor design criteria.

13.7 ALUMINUM MEMBERS

13.7.1 Effective Widths

Postbuckling strengths of thin aluminum plate elements are generally based on the von Kármán concept that the width, b_e, for which the elastic buckling stress (Eq. 4.1)

$$\sigma_{cr} = \frac{\pi^2 Ek}{12(1-\nu^2)(b/t)^2} = \frac{\pi^2 E}{(mb/t)^2} \tag{13.49}$$

is equal to the yield stress gives a limiting capacity which remains constant for all other widths. Thus, from Eq. 13.49,

$$b_e = \frac{\pi t}{m}\sqrt{\frac{E}{\sigma_y}} \tag{13.50}$$

For a simply supported plate the buckling coefficient $k = 4$, so $m = 1.63$ and $b_e = 1.93t\sqrt{E/\sigma_y}$.

This is not entirely consistent with the treatment for buckling of thin walls, which for the elastic-plastic range uses the equivalent slenderness ratio, mb/t, in an expression of the type

$$\sigma_c = \left(B_p - \frac{D_p mb}{t}\right) \tag{13.51}$$

This expression represents the true limiting stress (Jombock and Clark, 1968), and the maximum load carried by a plate element in the elastic-plastic range is

$$P = \sigma_c bt = \left(B_p - \frac{D_p mb}{t}\right)bt \tag{13.52}$$

The effective width, defined as that width which when multiplied by the yield stress and the thickness, gives the failing load for the element, then becomes

$$b_e = \frac{b}{\sigma_y}\left(B_P - \frac{D_P mb}{t}\right) \tag{13.53}$$

As b increases the highest load that can be carried occurs when

$$\frac{b}{t} = \frac{B_p}{2D_p m} \tag{13.54}$$

giving

$$P = \frac{B_p^2 t^2}{4D_p m} \tag{13.55}$$

This load capacity remains reasonably constant for all higher values of b/t. Jombock and Clark (1968) provide values for B_p and D_p which can be represented as

$$B_p = \sigma_y \alpha^2 \tag{13.56}$$

$$D_p = \frac{\sigma_y k\alpha}{g} \tag{13.57}$$

where

$g = (E/\sigma_y)^{1/2}$
$\alpha = (1 + 2/g^{2/3})^{1/2}$ for fully heat-treated alloy
$\alpha = (1 + 3/g^{2/3})^{1/2}$ for other alloys
$k = 0.1$ for fully heat-treated alloys
$k = 0.12$ for other alloys

The effective width is then

$$b_e = b\alpha(\alpha - kmb/t) \tag{13.58}$$

with a maximum value of

$$b_e = \alpha^3 gt/4mk \tag{13.59}$$

Jombock and Clark (1968), on the basis of limiting strain, provided a theoretical foundation for the model above, which has been adopted in North American codes (AA, 1994; CSA, 1984). This model gives a continuous transition from compact to thin-walled elements without discontinuities or changes in the form of the design expression.

Postbuckling behavior of elements supported on the long, unloaded edges, to which the model above applies, differs from that of outstanding, flange-type elements, in that, for the latter, initial elastic buckling precipitates the collapse of single unsymmetrical elements, while there may be some reserve capacity in symmetrical sections which can be represented by the treatment for edge-supported elements using an appropriate value of the coefficient m, usually 5.

The limiting stress on unstiffened elements of an unsymmetrical section such as a channel or Z, is obtained using the expression

$$\frac{mb}{t} < C \qquad \sigma = B - D\left(\frac{mb}{t}\right) \tag{13.60}$$

$$\frac{mb}{t} < C \qquad \sigma = \pi^2 E \Big/ \left(\frac{mb}{t}\right)^2 \tag{13.61}$$

where the value of m lies between 3 and 5, depending on the degree of edge restraint, and C is the slenderness parameter separating elastic and inelastic buckling.

In symmetrical sections, such as I- and double-channel shapes the effective width will be given by Eqs. 13.58 and 13.59 using $m = 5$, unless local buckling can precipitate overall flexural or lateral-torsional buckling, which will occur when the critical stresses for the different buckling modes are close in value.

13.7.2 Effective Section at Service Loads

A margin of over 1.5 between service loads and the ultimate load is usual; thus the extent of any local buckling in service will be small and confined to zones of maximum moment. For this reason, the influence of local buckling on deflections under service loads has been neglected in some codes. If a calculation is to be made, the difficulty of computing deflections with a varying and initially unknown effective moment of inertia is usually resolved by assuming that the effective section at the point of highest moment applies throughout. The effective width b_e of the elements comprising the effective section are obtained using the actual width b and the ratio of the critical stress σ_c to the applied stress σ computed on the basis of a fully effective section, thus:

$$b_e = b\left(\frac{\sigma_c}{\sigma}\right)^{1/2} \tag{13.62}$$

13.7.3 Torsional Buckling

Angles. A single angle may fail by flexure or torsional buckling; only by a special proportion of heavy root bulbs and very thin legs can local buckling be made to occur. To optimize shapes, bulbs and root fillets are added to increase the torsional rigidity such that the equivalent slenderness ratio for torsional buckling is around 60. Because of the interaction of torsion with flexure about the stronger axis, is it not effective to design sections of equal inertia about the two principal axes, and the optimum is an equal-leg right-angle section for both plain and bulb shapes. This is also true of double angles, designed to balance torsional and flexural buckling, in which case equal-leg angles are again very close to the optimum.

Eccentrically Loaded Columns. Unsymmetrical open sections loaded axially fail in combined torsion and flexure. Should they be loaded through the shear center, the modes are uncoupled and torsional buckling can be eliminated. Use has been made of this in T-sections for diagonals which, when bolted through the flanges, are loaded through the shear center. This allows much thinner sections to be used with a considerable increase in efficiency despite the moment due to the eccentricity. The optimum form is a lipped shape to control local buckling of the flanges.

Single angles loaded through one leg fail by lateral-torsional buckling in the manner of a beam-column (Marsh, 1969) and the design procedure adopted by CSA (1983) and ASCE (1972) treat this interaction by using an effective slenderness ratio:

$$\left(\frac{KL}{r}\right)_{\text{eff}} = \left[\left(\frac{5b}{t}\right)^2 + \left(\frac{KL}{r_v}\right)^2\right]^{1/2} \tag{13.63}$$

where $5b/t$ is the slenderness ratio for torsional buckling of angles and KL/r_v is the slenderness ratio for flexural buckling.

Postbuckling Strength. In general, the critical stress for a column failing by torsional buckling represents the maximum capacity of the member. This is always true of pin-ended unsymmetrical sections, as the application of the load through the centroid requires a uniform stress in the section for equilibrium. Should the column be loaded by fixed platens, the axis of load application can shift as the member twists, causing an increase in stress toward the shear center (Smith, 1955). Symmetrical sections, such as a cruciform, even when pin-ended, can accept a higher stress at the center as the member twists, giving a higher critical load than that obtained for a uniform stress.

REFERENCES

AA (1994), *Specifications for Aluminum Structures*, Aluminum Association, Washington, D.C.

AISC (1989), *Specification for the Design, Fabrication and Erection of Structural Steel for Buildings*, American Institute of Steel Construction, Chicago.

AISC (1993), *Load and Resistance Factor Design Specification for Structural Steel Buildings*, American Institute of Steel Construction, Chicago, IL.

AISI (1967), *Design of Light Gage Steel Diaphragms*, American Iron and Steel Institute, Washington, D.C.

AISI (1974), *Stainless Steel Cold-Formed Structural Design Manual*, American Iron and Steel Institute, Washington, D.C.

AISI (1980, 1986, 1989, 1996), *Specification for the Design of Cold-Formed Steel Structural Members*, American Iron and Steel Institute, Washington, D.C.

AISI (1986, 1996), *Cold-Formed Steel Design Manual*, American Iron and Steel Institute, Washington, D.C.

AISI (1991), *Load and Resistance Factor Design Specification for the Design of Cold-Formed Steel Structural Members*, American Iron and Steel Institute, Washington, D.C.

Apparao, T. V. S. R., Errera, S. J., and Fisher, G. P. (1969), "Columns Braced by Girts and a Diaphragm," *Proc. ASCE*, Vol. 95, No. ST5, pp. 965–990.

ASCE (1990), *Specification for the Design of Cold-Formed Stainless Steel Structural Members*, ANSI/ASCE 8-90, American Society of Civil Engineers, New York.

ASCE, Task Committee on Light-Weight Alloys (1972), "Guide for the Design of Aluminum Transmission Towers," *ASCE J. Struct. Div.*, Vol. 98, No. ST12, pp. 2785–2804.

ASTM (1996), *Standard Method for Static Load Testing of Framed Floor, Roof and Wall Diaphragm Construction for Buildings*, ASTM E455, American Society for Testing and Materials, Philadelphia, Pa.

Atrek, E., and Nilson, A. H. (1980), "Non-linear Analysis of Cold-Formed Steel Shear Diaphragms," *ASCE J. Struct. Div.*, Vol. 106, No. ST3, pp. 693–710.

Bakker, M., Peköz, T., and Stark, J. (1990), "A Model for the Behavior of Thin-Walled Flexural Members under Concentrated Loads," *Proc. 10th Int. Spec. Conf. Cold-Formed Steel Struct.*, University of Missouri–Rolla, Rolla, Mo.

Basler, K. (1961), "Strength of Plate Girders in Shear," *ASCE J. Struct. Div.*, Vol. 87, pp. 151–180.

Beelde, L. S., ed. (1991), *Stability of Metal Structures: A World View*, 2nd ed., Structural Stability Research Council, Bethelem, Pa.

Bernard, E. S., Bridge, R. Q., and Hancock, G. J. (1992a), "Tests of Profiled Steel Decks with V-Stiffeners," *11th Int. Spec. Conf. Cold-Formed Steel Struct.*, St. Louis, Mo.

Bernard, E. S., Bridge, R. Q., and Hancock, G. J. (1992b), "Intermediate Stiffeners in Cold Formed Profiled Steel Decks: Part I. 'Flat Hat' Shaped Stiffeners," *Res. Rep. No. R658*, School of Civil and Mining Engineering, University of Sydney, Sydney, Australia.

Bernard, E. S., Bridge, R. Q., and Hancock, G. J. (1993a), "Intermediate Stiffeners in Cold Formed Profiled Steel Decks: Part I. 'V' Shaped Stiffeners," *ASCE, J. Struct. Eng.*, Vol. 119, No. 8, pp. 2277–2293.

Bernard, E. S., Bridge, R. Q., and Hancock, G. J. (1993b), "Design of Decking Panels with Intermediate Stiffeners," *Res. Rep. No. R676*, School of Civil and Mining Engineering, University of Sydney, Sydney, Australia, Apr.

Bijlaard, P. P., and Fisher, G. P. (1952a), "Interaction of Column and Local Buckling in Compression Members," *NACA Tech. Note No. 2640*, Mar.

Bijlaard, P. P., and Fisher, G. P. (1952b), "Column Strength of H-Sections and Square Tubes in Post-buckling Range of Component Plates," *NACA Tech. Note No. 2994*, Aug.

Braham, M., Rondal, J., and Massonnet, C. E. (1980), "Large Size Buckling Tests on Steel Columns with Thin-Walled Rectangular Hollow Sections," in *Thin-Walled Structures* (ed. J. R. Rhodes and A. C. Walker), Granada, London.

Bresler, B., Lin, T. Y., and Scalzi, J. B. (1968), *Design of Steel Structures*, Wiley, New York.

Brooks, S. D., and Murray, T. M. (1990), "A Method for Determining the Strength of Z- and C-Purlin Supported Standing Seam Roof Systems," *Proc. Spec. Conf. Cold-Formed Steel Struct.*, University of Missouri–Rolla, Rolla, Mo.

Bryan, E. R., and Davies, J. M. (1981), *Steel Diaphragm Roof Decks*, Wiley, New York.

Bryan, E. R., and Leach, P. (1984), "Design of Profiled Sheathing as Permanent Formwork," *Tech. Note No. 116*, Construction Industry Research and Information Association, London.

Buhagiar, D., Chapman, I. C. and Dowling, P. I. (1992), "Design of C-Sections against Deformational Lip Buckling," *Proc. 11th Int. Spec. Conf. Cold-Formed Steel Struct.*, St. Louis, Mo., pp. 75–94.

Burgan, B. A. (1992), *Concise Guide to the Structural Design of Stainless Steel*, Steel Construction Institute, Berkshire, England.

Celebi, N., Peköz, T., and Winter, G. (1971), "Behavior of Channel and Z-Section Beams Braced by Diaphragms," *Proc. First Spec. Conf. Cold-Formed Steel Struct.*, University of Missouri–Rolla, Rolla, Mo., Aug.

Chajes, A., and Winter, G. (1965), "Torsional-Flexural Buckling of Thin-Walled Members," *ASCE J. Struct. Div.*, Vol. 91, No. ST4, pp. 103–124.

Chajes, A., Fang, P. J., and Winter, G. (1966), "Torsional–Flexural Buckling, Elastic and Inelastic, of Cold Formed Thin-Walled Columns," *Cornell Eng. Res. Bull.*, No. 66-1.

Charnvarnichbonkarn, P., and Polyzois, D. (1992), "Distortional Buckling of Cold-formed Steel Z-Section Columns," *Proc. 11th Int. Spec. Conf. Cold-Formed Steel Struct.*, St. Louis, Mo., pp. 353–378.

Chilver, A. H. (1967), *Thin-Walled Structures*, Wiley, New York.

Cohen, J. M., and Peköz, T. B. (1987), "Local Buckling Behavior of Plate Elements," *Res. Rep.*, Department of Structural Engineering, Cornell University, Ithaca, N.Y.

CSA (1983), *Strength Design in Aluminum*, CAN3-S157-M83, Canadian Standards Association, Rexdale, Ontario, Canada.

CSA (1989), *Cold-Formed Steel Structural Members*, CAN3S136-M84, Canadian Standards Association, Rexdale, Ontario, Canada.

Culver, C. G. (1966), "Exact Solution of the Biaxial Bending Equations," *ASCE J. Struct. Div.*, Vol. 92, No. ST2, pp. 63–84.

Dabrowski, R. (1961), "Dünnwandige Stabe unter zweiachsig aussermittigem Druck," *Stahlbau*, Vol. 30, p. 360.

Dat, D. T., and Peköz, T. (1980), "Strength of Cold-Formed Steel Columns," *Report No. 80-4*, Department of Structural Engineering, Cornell University, Ithaca, N.Y., Feb.

Desmond, T. P., Peköz, T. and Winter, G. (1981a), "Edge Stiffeners for Thin-Walled Members," *ASCE J. Struct. Eng.*, Vol. 107, No. 2, pp. 329–353.

Desmond, T. P., Peköz, T., and Winter, G. (1982b), "Intermediate Stiffeners for Thin-Walled Members," *ASCE J. Struct. Eng.*, Vol. 107, No. 4, pp. 627–648.

DeWolf, J., Peköz, T., and Winter, G. (1974), "Local and Overall Buckling of Cold Formed Steel Members," *ASCE J. Struct. Div.*, Vol. 100, No. ST10, pp. 2017–2036.

DeWolf, J., Peköz, T., and Winter, G. (1976), "Closure to 'Local and Overall Buckling of Cold-Formed Steel Members," *ASCE J. Struct. Div.*, Vol. 102, No. ST2, pp. 451–454.

Dier, A. F. (1992), "Structural Stainless Steel: Behavior and Design Code Development," in *Applications of Stainless Steel '92*, Vol. 1, Stockholm, Sweden, pp. 245–259.

Easley, J. T. (1977), "Strength and Stiffness of Corrugated Metal Shear Diaphragms," *ASCE J. Struct. Div.*, Vol. 103, No. ST1, pp. 169–180.

ECCS (1977), "European Recommendations for the Stressed Skin Design of Steel Structures," *ECCS-XVII-77-1 E*, European Convention for Constructional Steelwork, Brussels, Belgium, Mar. (English version published by Constrado, Croydon, England.)

ECS (1992), "Cold Formed Thin Gauge Members and Sheeting," *Eurocode, CEN/TC250/SC3-PT IA, 3(1.3)*, European Committee for Standardization, Brussels, Belgium.

El-Dakhakhni, W. M., and Daniels, J. H. (1973), "Frame–Floor–Wall System Interaction in Buildings," *Fritz Eng. Lab., Rep. No. 376.2*, Lehigh University, Bethlehem, Pa.

Ellifritt, D., Sputo, T., and Haynes, J. (1992), "Flexural Capacity of Discretely Braced C's and Z's," *Proc. 11th Int. Spec. Conf. Cold-Formed Steel Struct.*, University of Missouri–Rolla, Rolla, Mo.

Errera, S. J., and Apparao, T. V. S. R. (1976a), "Design of I-Shaped Beams with Diaphragm Bracing," *ASCE J. Struct. Div.*, Vol. 102, No. ST4, pp. 769–783.

Errera, S. J., and Apparao, T. V. S. R. (1976b), "Design of I-Shaped Columns with Diaphragm Bracing," *ASCE J. Struct. Div.*, Vol. 102, No. ST9, pp. 1685–1702.

Errera, S. J., Pincus, G., and Fisher, G. P. (1967), "Columns and Beams Braced by Diaphragms," *ASCE J. Struct. Div.*, Vol. 93, No. ST1, pp. 295–318.

Galambos, T. V. (1968), *Structural Members and Frames*, Prentice Hall, Upper Saddle River, N.J.

Gergely, P., Banavalkar, P. V., and Parker, J. E. (1971), "The Analysis and Behavior of Thin-Steel Hyperbolic Paraboloid Shells," *Cornell Univ. Dept. Struct. Eng. Rep. No. 338*, Sept.

Goddier, J. N. (1942), "Flexural-Torsional Buckling of Bars of Open Section," *Cornell Univ. Eng. Exp. Sta. Bull. No. 28*, Jan.

Graves-Smith, T. R. (1969), "The Ultimate Strength of Locally Buckled Columns of Arbitrary Length," in *Thin Wall Steel Structures* (ed. K. C. Rockey and H. V. Hill), Crosby Lockwood, London, pp. 35–60.

Guiaux, P. (1974), "Buckling Test on Cold Formed Hollow Sections, Square and Circular," *Rep. No. 741181E(2C)*, Structural Test Laboratories of the Civil Engineering Faculty of the University of Liege, Belgium.

Ha, K. H., El-Hakim, N., and Fazio, P. P. (1979), "Simplified Design of Corrugated Shear Diaphragms," *ASCE J. Struct. J. Div.*, Vol. 105, No. ST7, pp. 1365–1378.

Hancock, G. J. (1981), "Nonlinear Analysis of Thin Sections in Compression," *ASCE J. Struct. Div.*, Vol. 107, No. ST3, pp. 455–472.

Hancock, G. J. (1985), "Distortional Buckling of Steel Storage Rack Columns," *ASCE J. Struct. Eng.*, Vol. 111, No. 12, pp. 2770–2783.

Hetrakul, N., and Yu, W. W. (1978), "Structural Behavior of Beam Webs Subjected to Web Crippling and a Combination of Web Crippling and Bending," *Rep. No. 78-4*, University of Missouri–Rolla, Rolla, Mo., June.

Hill, H. N. (1954), "Lateral Buckling of Channels and Z-Beams," *Trans. ASCE*, Vol. 119, p. 829.

Hlavacek, V. (1972), "The Effect of Support Conditions on the Stiffness of Corrugated Sheets Subjected to Shear," *Acta Tech. CSAV, Prague*, Nov. 2.

Ingvarsson, L. (1975), "Cold-Forming Residual Stress, Effect on Buckling," *Proc. 3rd Int. Spec. Conf. Cold-Formed Steel Struct.*, Vol. I, Department of Civil Engineering, University of Missouri–Rolla, Rolla, Mo., Nov. 1, pp. 85–120.

Ingvarsson, L. (1977), "Cold-Forming Residual Stresses and Box Columns Built Up by Two Cold-Formed Channels Sections Welded Together," *Bull. No. 121*, Department of Statics and Structural Engineering, Royal Institute of Technology, Stockholm.

Johnson, A. L., and Kelsen, G. A. (1969), "Stainless Steel in Structural Applications," *Stainless Steel for Architecture*, ASTM STP, American Society for Testing and Materials, Philadelphia, p. 454.

Johnson, A. L., and Winter, G. (1966), "Behavior of Stainless Steel Columns and Beams," *ASCE J. Struct. Div.*, Vol. 92, No. ST5, pp. 97–118.

Johnston, B. G. (1976), *Guide to Stability Design Criteria for Metal Structures*, 3rd ed., Wiley, New York.

Jombock, J. R., and Clark, J. W. (1968), "Bending Strength of Aluminum Formed Sheet Members," *ASCE J. Struct. Div.*, Vol. 94, No. ST2, pp. 511–528.

Kalyanaraman, V., and Pekoz, T. (1978), "Analytical Study of Unstiffened Elements," *ASCE J. Struct. Div.*, Vol. 104, No. ST9, pp. 1507–1524.

Kalyanaraman, V., Pekoz, T., and Winter, G. (1977), "Unstiffened Compression Elements," *ASCE J. Struct. Div.*, Vol. 105, No. ST9, Proc. Pap. 13197, pp. 1833–1848.

Karren, K. W., and Winter, G. (1967), "Effects of Cold-Forming on Light Gage Steel Members," *ASCE J. Struct. Div.*, Vol. 93, No. ST2, pp. 433–470.

Klöppel, K., and Schardt, R. (1958), "Beitrag zur praktischen Ermittlung der Vergleichsschlankheit von mittig gedrückten Stäben mit einfachsymmetrischem offenem dünnwandigem Querschnitt," *Stahlbau*, Vol. 27, p. 35.

Konig, J., and Thomasson, P. O. (1980), "Thin-Walled C-Shaped Panels in Axial Compression or in Pure Bending," in *Thin-Walled Structures* (ed. J. R. Rhodes and A. C. Walker), Granada, London.

Kwon, Y. B., and Hancock, G. J. (1992a), "Design of Channels Against Distortional Buckling," *Proc. 11th Int. Spec. Conf. Cold-Formed Steel Struct.*, St. Louis, Mo., pp. 323–352.

Kwon, Y. B., and Hancock, G. J. (1992b), "Strength Tests of Cold-formed Channel Sections Undergoing Local and Distortional Buckling," *ASCE, J. Struct. Eng.*, Vol. 117, No. 2, pp. 1786–1803.

LaBoube, R. A. (1983), "Z-Purlin Edge Stiffeners," *Res. Rep., Butler Manufacturing Company*, Kansas City, Mo., Mar.

LaBoube, R. A., and Yu, W. W. (1982), "Bending Strength of Webs and Cold-Formed Steel Beams," *ASCE J. Struct. Div.*, Vol. 108, No. ST7, pp. 1589–1604.

Larson, M. A. (1960), "Discussion of 'Lateral Bracing of Columns and Beams' by George Winter," *Trans. ASCE*, Vol. 125, pp. 830–838.

Lau, S. C. W., and Hancock, G. J. (1987), "Distortional Buckling Formulas for Channel Columns," *ASCE J. Struct. Eng.*, Vol. 113, No. 5, pp. 1063–1078.

Lau, S. C. W., and Hancock, G. J. (1988), "Distortional Buckling Tests of Cold-Formed Channel Sections," *Proc. 9th Int. Spec. Conf. Cold-Formed Steel Struct.*, St Louis, Mo., pp. 45–73.

Lau, S. C. W., and Hancock, G. J. (1990), "Inelastic Buckling of Channel Columns in the Distortional Mode," *Thin-Walled Struct.*, Vol. 10, pp. 59–84.

Lin, S. H. (1989), "Load and Resistance Factor Design of Cold-Formed Stainless Steel Structural Members," Ph.D. Thesis, University of Missouri–Rolla, Rolla, Mo.

Lin, S. H., Yu, W. W., and Galambos, T. V. (1992), "ASCE LRFD Method for Stainless Steel Structures," *ASCE J. Struct. Div.*, Vol. 118, No. ST4, pp. 1056–1070.

Loh, T. S. (1985), "Combined Axial Load and Bending in Cold-Formed Steel Members," *Cornell Univ. Dept. Struct. Eng. Rep. No. 85-3*, Feb.

Luttrell, L. C. (1967), "Strength and Behavior of Light Gage Steel Shear Diaphragm," *Cornell Univ. Eng. Res. Bull. No. 67-1.*

Marsh, C. (1969), "Single Angles in Tension and Compression," *ASCE J. Struct. Div. Tech. Note*, Vol. 95, No. ST5, pp. 1043–1049.

Massicotte, B., Beaulieu, D., and Picard, A. (1985), "Bracing of Columns by Girt Diaphragm Systems in Light Industrial Buildings," *Proc. SSRC Annu. Tech. Session.*

McDermott, R. J. (1981), "Column Strength of Cold Formed Tubular Sections," M.S. thesis, Lehigh Unviersity, Bethlehem, Pa.

Mertz, K. L., and Mathiesen, R. B. (1970), "Design of Corrugated Shear-Transmitting Members," *AISI Proj. 149*, School of Engineering and Applied Science, University of California, Los Angeles, Dec.

Miller, C. J. (1972), "Analysis of Multistory Frames with Light Gage Steel Panel Infills," Dissertation (also *CU Rep. No. 349*), Cornell University, Ithaca, N.Y., Aug.

Miller, T. H., and Peköz, T. (1990), "Studies of the Behavior of Cold-Formed Steel Wall Stud Assemblies," *Proc. 10th Int. Spec. Conf. Cold-Formed Steel Struct.*, University of Missouri–Rolla, Rolla, Mo.

Mulligan, G. P., and Peköz, T. (1983), "Influence of Local Buckling on the Behavior of Singly Symmetric Cold-Formed Steel Columns," *Cornell Univ. Dep. Struct. Eng. Rep. No. 83-2*, Mar.

Murray, T. M., and Elhouar, S. (1985), "Stability Requirements of Z-Purlin Supported Conventional Metal Building Roof Systems," *Proc. Annu. SSRC Tech. Session*, Structural Stability Research Council, Bethlehem, Pa.

Nethercot, D. A., and Trahair, N. S. (1975), "Design of Diaphragm-Braced I-Beams," *ASCE J. Struct. Div.*, Vol. 101, No. ST10, pp. 2045–2062.

Nguyen, R. P., and Yu, W. W. (1978), "Webs for Cold-Formed Steel Flexural Members: Structural Behavior of Transversely Reinforced Beam-Webs," *Final Rep.*, University of Missouri–Rolla, Rolla, Mo., July.

Nilson, A. H. (1960), "Shear Diaphragms of Light Gage Steel," *ASCE J. Struct. Div.*, Vol. 86, No. ST11, pp. 111–140.

Peköz, T. B. (1969) (with a contribution by N. Celebi), "Torsional–Flexural Buckling of Thin-Walled Sections Uner Eccentric Load," *Cornell Eng. Res. Bull. No. 69.1*, Sept.

Peköz, T. (1980), "Design of Cold-Formed Steel Storage Racks," in *Thin-Walled Structures* (ed. J. R. Rhodes and A. C. Walker), Granada, London.

Peköz, T. (1986), "Development of a Unified Approach to the Design of Cold-Formed Steel Members," *Res. Rep.*, Committee of Sheet Steel Producers, American Iron and Steel Institute, Washington, D.C., May.

Peköz, T. B. (1987), "Development of a Unified Approach to the Design of Cold-Formed Steel Members," *Rep. CF 87-1*, American Iron and Steel Institute, Washington, D.C.

Peköz, T., and He, B. K. (1981), "Experiments on Z-Purlins to Explore Effectiveness of Sloping Edge Stiffeners," *Proc. Rep.*, Department of Structural Engineering, Cornell University, Ithaca, N.Y., Jan.

Peköz, T., and Soroushian, P. (1982), "Behavior of C- and Z-Purlins Under Wind Uplift," *Proc. 6th Int. Conf. Cold-Formed Steel Struct.*, St. Louis, Mo., Nov.

Peköz, T. B., and Winter, G. (1969), "Torsional–Flexural Buckling of Thin-Walled Sections Under Eccentric Load," *ASCE J. Struct. Div.*, Vol. 95, No. ST5, pp. 941–964.

Peköz, T., Desmond, T. P., and Winter, G. (1981a), "Intermediate Stiffeners for Thin-Walled Members," *ASCE J. Struct. Div.*, Vol. 107, No. ST4, pp. 627–648.

Peköz, T., Desmond, T. P., and Winter, G. (1981b), "Edge Stiffeners for Thin-Walled Members," *ASCE J. Struct. Div.*, Vol. 107, No. ST2, pp. 329–353.

Pfluger, A. (1961), "Thin-Walled Compression Members," *Mitt. Inst. Statik Tech. Hochsch. Hannover*, Part 1 (1959); Part 2 (1959); Part 3 (1961).

Pincus, G., and Fisher, G. P. (1966), "Behavior of Diaphragm-Braced Columns and Beams," ASCE J. Struct. Div., Vol. 92, No. ST2, pp. 323–350.

Prawel, S. P., Jr., and Lee, G. C. (1964), "Biaxial Flexure of Columns by Analog Computers, *ASCE J. Eng. Mech. Div.*, Vol. 90, No. EM1, Proc. Pap. 3805, pp. 83–112.

Rasmussen, K. J. R., and Hancock, G. J. (1993a), "Design of Cold-Formed Stainless Steel Tubular Members: I. Columns," *ASCE J. Sruct. Eng.*, Vol. 119, No. ST8, pp. 2349–2367.

Rasmussen, K. J. R., and Hancock, G. J. (1993b), "Design of Cold-Formed Stainless Steel Tubular Members: II. Beams," *ASCE J. Struct. Eng.*, Vol. 119, No. ST8, pp. 2368–2386.

Reck, H., Pekoz, T., and Winter, G. (1975), "Inelastic Strength of Cold-Formed Steel Beams," *ASCE J. Struct. Div.*, Vol. 101, No. ST11, pp. 2193–2204.

Rhodes, J., and Walker, A. C., eds. (1979), "Thin-Walled Structures," *Proc. Int. Conf.*, University of Strathclyde, Glasgow, Granada, London.

RMI (1979), *Specification for the Design, Testing and Utilization of Industrial Steel Storage Racks*, Rack Manufacturers Institute.

Rockey, K. C., Elgaaly, M. A., and Bagchi, D. K. (1972), "Failure of Thin-Walled Members Under Patch Loading," *ASCE J. Struct. Div.*, Vol. 98, No. ST12, pp. 2739–2752.

SAA (1993), *Steel Storage Racking*, AS4084. Standards Association of Australia, North Sydney, New South Wales, Australia.

Santaputra, C., Parks, M. B., and Yu, W. W. (1989), "Web Crippling Strength of Cold-Formed Steel Beams," *ASCE J. Struct. Eng.*, Vol. 115, No. ST10, pp. 2511–2527.

SDI (1988), *Diaphragm Design Manual*, Steel Deck Institute, St. Louis, Mo.

Seah, L. K., Rhodes, J. and Lim, B. S. (1993), "Influence of Lips on Thin-Walled Structures," *Thin-Walled Struct.*, Vol. 16, pp. 145–147.

Serrette, R., and Peköz, T. (1992), "Local and Distorsional Buckling of Thin-Walled Beams," *Proc. 11th Int. Spec. Conf. Cold-formed Steel Struct.*, St. Louis, Mo., pp. 63–74.

Shanley, F. R. (1968), "Investigation of Shear-Transmitting Members: Design of a Test Beam," *Rep. No. 68-20*, Department of Civil Engineering, University of California, Los Angeles, Apr.

Sherman, D. R., and Fisher, J. M. (1971), "Beam with Corrugated Webs," *Proc. First Int. Spec. Conf. Cold-Formed Steel Struct.*, University of Missouri–Rolla, Rolla, Mo., Aug.

Simaan, A. (1973), "Buckling of Diaphragm-Braced Columns of Unsymmetrical Sections and Application to Wall Studs Design," Dissertation, Cornell University, Ithaca, N.Y.

Simaan, A., and Peköz, T. (1976), "Diaphragm-Braced Members and Design of Wall Studs," *ASCE J. Struct. Div.*, Vol. 102, No. ST1, pp. 77–92.

Smith, R. E. (1955), "Column Tests on Some Proposed Aluminium Standard Structural Sections," *Rep. No. 25*, Aluminum Development Association, London.

Sridharan, S., and Benito, R. (1984), "Columns: Static and Dynamic Interactive Buckling," *ASCE J. Eng. Mech. Div.*, Vol. 110, No. EM1, pp. 49–65.

Thomasson, P. O. (1978), "Thin-Walled C-Shaped Panels in Axial Compression," *Res. Doc. DI:1978*, Swedish Council for Building, Stockholm, Sweden.

Thoon, K. H., Rhodes, J., and Seah, L. K. (1993), "Tests on Intermediately Stiffened Plate Elements and Beam Compression Elements," *Thin-Walled Struct.*, Vol. 16, pp. 111–143.

Thürlimann, B. (1953), "Deformation of and Stresses in Initially Twisted and Eccentrically Loaded Columns of Thin-Walled Open Cross-Section," *Rep. No. E696-3*, Brown University, Providence, R.I., June.

Timoshenko, S. P., and Gere, J. M. (1961), *Theory of Elastic Stability*, 2nd ed., McGraw-Hill, New York.

Trestain, T. W. J. (1982), "A Review of Cold Formed Steel Column Design," *Rep. No. 81109-1, CSCC Proj. DSS 817*, Canadian Sheet Steel Building Institute, Toronto, Ontario, Canada, Dec.

Unger, von B. (1973), "Ein Beitrag zur Ermittlung der Traglast von querbelasterten Durchlaufträgern mit dünnwandigem Querschnitt, insbesondere von durchlaufenden Trapezblechen für Dach und Geschossdecken," *Stahlbau*, Vol. 42.

Uribe, J., and Winter, G. (1970), "Cold-Forming Effects in Thin-Walled Steel Members," *Cornell Eng. Res. Bull. No. 70-1.*

Van den Berg, G. J. (1988), "The Torsional-Flexural Buckling Strength of Cold-Formed Stainless Steel Columns," D. Eng. thesis, Rand Afrikaans University, Johannesburg, South Africa.

Van den Berg, G. J., and van der Merwe, P., eds. (1992), *Collective Papers of the Chromium Steels Research Group*, Vol. 1, Rand Afrikaans University, Johannesburg, South Africa.

Van der Merwe, P. (1987), "Development of Design Criteria for Ferritic Stainless Steel Cold-Formed Structural Members and Connections," Ph.D. thesis, University of Missouri–Rolla, Rolla, Mo.

Van der Merwe, P., and van den Berg., G. J. (1992), "Criteria for Design of Stainless Steel Structures," in *Applications of Stainless Steel '92*, Vol. 1, Stockholm, Sweden, pp. 565–575.

Vlasov, V. Z. (1959), *Thin-Walled Elastic Beams*, 2nd ed. (translation from Russian; available from the Office of Technical Services, U.S. Department of Commerce, Washington, D.C.).

Wang, S. T. (1969), "Cold-Rolled Austenitic Stainless Steel: Material Properties and Structural Performance," *Cornell Univ. Dept. Struct. Eng. Rep. No. 334*, July.

Wang, S. T., and Errera, S. J. (1971), "Behavior of Cold Rolled Stainless Steel Members," *Proc. First Spec. Conf. Cold-Formed Steel Struct.*, University of Missouri–Rolla, Rolla, Mo.

Wang, S. T., and Yeh, S. S. (1974), "Post-Local-Buckling Behavior of Continuous Beams," *ASCE J. Struct. Div.*, Vol. 100, No. ST6, pp. 1169–1188.

Weng, C. C., and Peköz, T. (1987), "Flexural Buckling of Cold-Formed Steel Columns," *Res. Rep.*, Department of Structural Engineering, Cornell University, Ithaca, N.Y.

Weng, C. C., and Peköz, T. (1988), "Compression Tests of Cold Formed Steel Columns," *Proc. 9th Int. Spec. Conf. Cold-Formed Steel Struct.*, University of Missouri–Rolla, Rolla, Mo.

Wing. B. A. (1981), "Web Crippling and the Interaction of Bending and Web Crippling of Unreinforced Multi-web Cold Formed Steel Sections," Master's thesis, University of Waterloo, Waterloo, Ontario, Canada.

Winter, G. (1943), "Lateral Stability of Unsymmetrical I-Beams and Trusses in Bending," *Trans. ASCE*, Vol. 108, pp. 247–260.

Winter, G. (1947), "Discussion of 'Strength of Beams as Determined by Lateral Buckling," by Karl deVries," *Trans. ASCE*, Vol. 112, pp. 1212–1276.

Winter, G. (1958), "Lateral Bracing of Columns and Beams," *ASCE J. Struct. Div.*, Vol. 84, No. ST2, p. 1561.

Winter, G. (1970), *Commentary on the 1968 Edition of Light Gage Cold-Formed Steel Design Manual*, American Iron and Steel Institute, Washington, D.C.

Winter, G., and Pian, R. H. J. (1946), "Crushing Strength of Thin Steel Webs," *Cornell Univ. Eng. Exp. Sta. Bull. No. 35*, Part 1.

Winter, G., Lansing, W., and McCalley, R. B., Jr. (1949), "Performance of Laterally Loaded Channel Beams," *Colston Pap.*, Vol. II (reprinted in "Four Papers on the Performance of Thin Walled Steel Structures," *Cornell Univ. Eng. Exp. Sta. Rep. No. 33*).

Yener, M., and Peköz, T. (1980), "Inelastic Load Carrying Capacity of Cold-Formed Steel Beams," *Proc. 5th Int. Conf. Cold-Formed Steel Struct.*, St. Louis, Mo., Nov.

Yu, W. W. (1980), "Web Crippling and Combined Web Crippling and Bending of Steel Decks," *1st Prog. Rep.* (May 1980); *2nd Prog. Rep.* (Aug. 1980), University of Missouri–Rolla, Rolla, Mo.

Yu, W. W. (1981), "Web Crippling and Combined Web Crippling and Bending of Steel Decks," *Civ. Eng. Study 81-2*, University of Missouri–Rolla, Rolla, Mo.

Yu, W. W. (1991), *Cold-Formed Steel Design*, 2nd ed. Wiley-Interscience, New York.

Yu, W. W., and LaBoube, R. A. (1992), "Recent Research and Developments in Cold-Formed Steel," *Proc. 11th Int. Spec. Conf. Cold-Formed Steel Struct.*, University of Missouri–Rolla, Rolla, Mo.

Yu, W. W., and Lin, S. H. (1992), "Development of Design Standards for Stainless Steel Structures," in *Applications of Stainless Steel '92*, Vol. 1, Stockholm, Sweden, pp. 555–564.

Zetlin, L., and Winter, G. (1955), "Unsymmetrical Bending of Beams With and Without Lateral Bracing," *Proc. ASCE*, Vol. 81, pp. 774.1–774.20.

Zhang, Y., and Peköz, T. (1982), "An Exploratory Study on the Behavior of Cold-Formed Steel Wall Studs," *Cornell Univ. Dept. Struct. Eng. Rep. No. 82-14*, Sept.

CHAPTER FOURTEEN

CIRCULAR TUBES AND SHELLS

14.1 INTRODUCTION

A variety of structures consist of or include thin-walled cylinders that are subject to buckling. The round cylinder provides the most efficient shape available for centrally loaded columns with no lateral support between ends. Such columns are used in three-dimensional loading applications such as transmission towers, reticulated shells, and offshore platforms. Stiffened and unstiffened cylindrical shells (cylinders with large diameter-to-thickness ratios) are used as grain storage bins, liquid storage tanks, pressure vessels, and caissons for underwear construction.

Tubes and shells may be subject to axial compression, bending, twisting, or external or internal pressure, any one of which can cause failure. Depending of the dimensions of the cylinder, either local or overall buckling failures can occur. If the diameter of the cylinder is relatively large, longitudinal and/or ring stiffeners are often used to provide additional strength. Notation for the geometric parameters defining both an unstiffened and stiffened cylinder is given in Fig. 14.1.

Cylinders with relatively small diameter-to-thickness (D/t) ratios are usually referred to as tubes or pipes, and cylinders with large (D/t) ratios most often are called shells. Typically, shells are stiffened. When a single descriptive term is required, *cylinder* or *tubular member* is used.

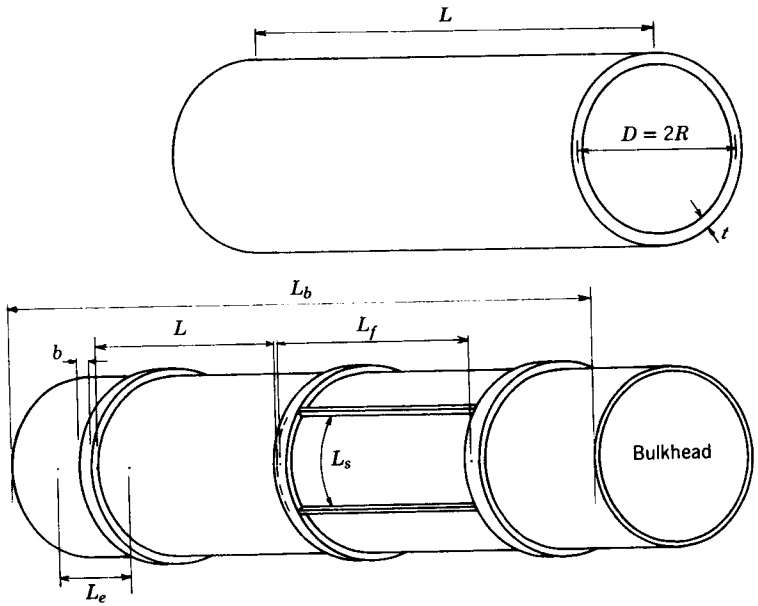

Fig. 14.1 Dimensional notation.

14.1.1 Production Practice

The behavior of a tubular member is influenced to some extent by whether it is manufactured in a pipe or tubing mill or fabricated from plate. The distinction is important primarily because of the differences in geometric imperfections and residual stress levels that result from the two production methods (Schilling, 1965). In general, fabricated cylinders may be expected to have considerably larger magnitudes of imperfections (in diameter, ovality, and lack of straightness) than the mill products.

Manufactured cylinders are made as seamless pipe, or with continuous seam welds of various types or in the case of nonferrous metals, by extrusion. Each of these methods includes a hot- or cold-formed finishing treatment to obtain the proper size and circular shape (Graham, 1965; U.S. Steel, 1964; Sherman, 1992).

Fabricated tubes and shells are produced by welding or mechanically joining plates of cold- or hot-formed materials such as carbon steel, high-strength low-alloy steel, constructional alloy steel, or structural aluminum alloys. Fabricated structural members are frequently made by butt welding a series of short cans with the longitudinal welds on adjacent cans separated by rotating the cans.

14.1.2 Stress-Strain Curves and Residual Stresses

The basic stress-strain curve of a tubular section can be either (1) linear up to a yield-point stress with subsequent plastic straining at essentially constant

stress, or (2) linear up to a proportional limit, less than yield strength, with subsequent gradual nonlinear transition to a yielding plateau or nonlinear softening prior to failure (Schilling, 1965). These two general categories of stress-strain behavior are illustrated by the solid curves in Fig. 14.2. The presence of residual stresses will change the effective stress-strain relationships to the dashed curves in Fig. 14.2. Generally, hot-finished cylinders will have sharp-yielding stress-strain curves, whereas cold-finished cylinders exhibit gradual-yielding behavior. Cold work in any cold-finished operation causes a change in stress-strain behavior from the basic material properties. Cylinders made of materials such as certain stainless steels and aluminum alloys will also have gradual-yielding stress-strain curves regardless of the production practice employed.

Residual stresses most commonly arise from the cooling effects after hot finishing, from the welding practices employed, or by the prevention of spring-back introduced during forming operations. Longitudinal residual stresses in

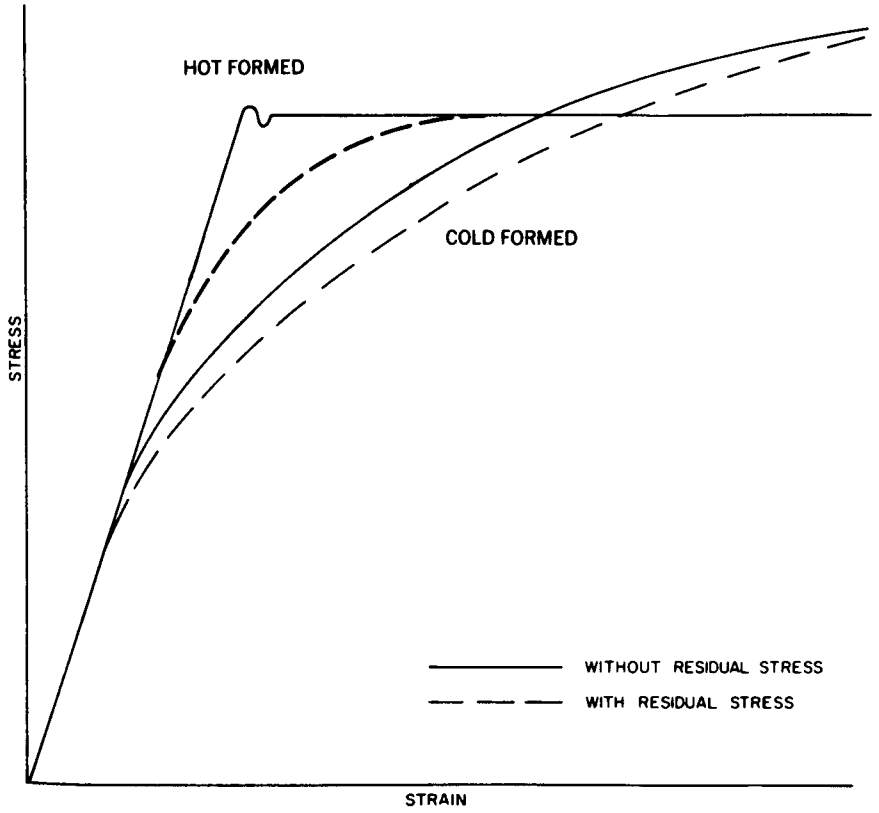

Fig. 14.2 Two geneal types of stress-strain curves.

manufactured cylinders may result from nonuniform plastic flow through the thickness of the cylinder wall. Because of the foregoing, the exact shape of the stress-strain curve, the proportional limit, and the yield strength of a tubular member are rather unpredictable.

Residual stresses can be measured (Denton and Alexander, 1963a,b; Sherman, 1969) and in certain cases, the effects of cold work can be determined (Kuper and Macadam, 1969). Measurements on members fabricated for a column testing (Chen and Ross, 1978) program gave the longitudinal and through-thickness circumferential residual stress patterns shown in Fig. 14.3. The pattern and general magnitude have been confirmed (Prion and Birkemoe, 1988). Manufactured cold-formed pipes have similar patterns unless the finishing operation has a stress-relieving effect. Hot-formed and hot-finished cylinders generally have very low residual stresses.

14.2 DESCRIPTION OF BUCKLING BEHAVIOR

14.2.1 Factors Affecting Buckling

Buckling load predictions for cylindrical members are more complicated than for wide-flange sections due to the larger number of variables. The variety of geometric proportions is quite large since the cylindrical shape is used as a structural member with large length-to-diameter (L/D) and small D/t ratios or as a shell structure where L/D is frequently less than 1 and D/t may be 100 times larger than for some unstiffened members. In many applications, circumferential and/or longitudinal stiffeners are used to increase the buckling strength. Their size, spacing, and position on the inside or outside of the cylinder will affect the performance of the cylinder.

Cylinders are made by several different procedures, which result in different magnitudes and patterns of both longitudinal and circumferential residual stresses. As in any structural element, the residual stresses can play an important role in determining the buckling strength. The method of producing the cylinder and the acceptable tolerances also influence the degree of initial imperfection that is present. Tests and theory have shown that the elastic local buckling strength of thin-walled cylinders is very sensitive to geometric imperfections and in some cases, to the boundary conditions. Tests of thin cylinders under axial loading resulted in failures at buckling strengths considerably less than the theoretical elastic capacity. These discrepancies have generally been attributed to specimen imperfections and poorly modeled boundary conditions; however, in many cases the observed buckling capacities cannot be totally correlated with measured imperfection levels.

Quantitative predictions of buckling strengths must include all the loadings associated with metal members: axial compression, flexural bending and shear, and torsion. In addition, the enclosed nature of the cylinder causes pressure to be an important type of loading. Only axial loadings cause an overall general

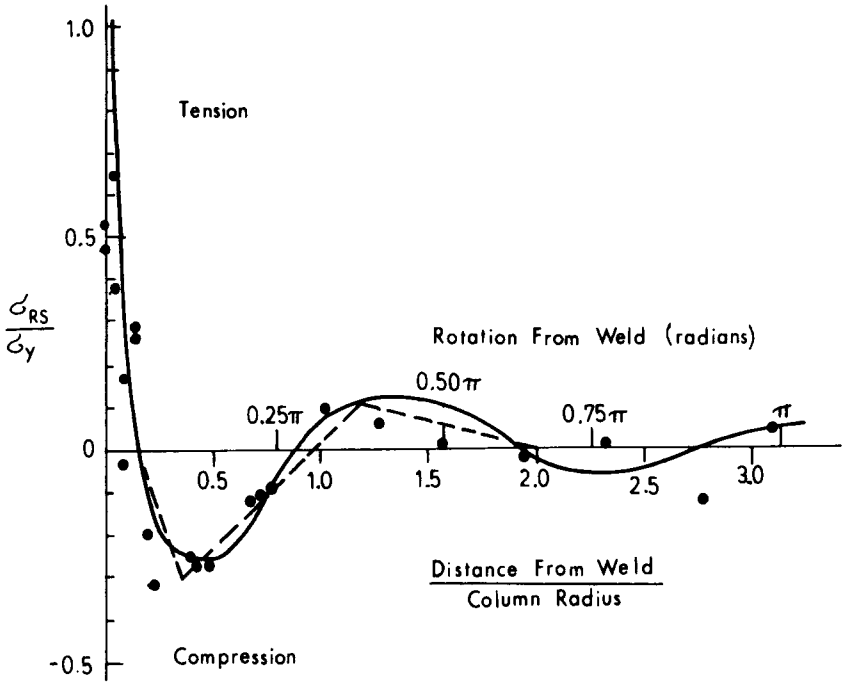

Fig. 14.3 Measured residual stresses in fabricated pipe: (*a* longitudinal residual stress distribution obtained from method of sectioning; (b) average circumferential residual stress pattern (Chen and Ross, 1978)

buckling of a cylindrical member since circular beams are not subject to lateral-torsional buckling. Tubular columns and beam-columns are included in Chapters 3 and 8. This chapter therefore concerns only the local buckling modes, except as they may interact with general buckling. The local buckling mode is a type of shell buckling in unstiffened cylinders. For cylinders stiffened with circumferential and/or longitudinal stiffeners, the local buckling mode

may be shell or panel buckling between heavy stiffeners or may include buckling of light stiffeners in a wave configuration.

14.2.2 Buckling Equations

The stability of cylinders has been studied analytically and experimentally for a number of years. As a result of these studies and the wide variation in types of cylinders, a large number of empirical and semiempirical expressions have been proposed for predicting the buckling strength. Many of these were presented in the third edition of the guide as part of a historical description of progress. This edition presents only those that are best supported by recent research. These equations represent the classical approach to the stability of cylinders.

Miller (Miller, 1983; Miller et al., 1983) has proposed the use of a unified equation format. In this format, the linear elastic bifurcation buckling stress is reduced by a series of "knockdown" (reduction) factors to obtain a realistic critical stress:

$$F_i = \eta K_i \alpha_{ij} \sigma_{iej} \tag{14.1}$$

In this equation, σ_{iej} is the theoretical elastic buckling stress for a particular loading, i, with j being either x or c representing axial and circumferential stresses, respectively. The terms η, K, and a are the three "knockdown" factors that are used.

1. η is a *plasticity factor* that reflects the residual stress levels and shape of the stress-strain curve. This factor is unity if buckling is purely elastic.
2. K is a *slenderness factor* that accounts for the length and theoretical boundary conditions.
3. α is a *capacity reduction factor* used to adjust for deviations between theory and tests. It accounts for the effects of imperfections in the boundary conditions and shell dimensions.

The knockdown factors are derived empirically and are normally a lower bound to test data. This approach requires an extensive database to account for all the parameters that exist in cylinders. However, the effects of various parameters are included in specific terms. In addition to clarifying the influence of the parameters, this approach also facilitates modifications as additional research becomes available. Miller (1984) presents a large number of design equations for the factors applicable to various loading conditions in unsiffened and stiffened cylinders. Sections 14.3 through 14.7 represent the classical approach.

14.3 UNSTIFFENED OR HEAVY-RING-STIFFENED CYLINDERS

14.3.1 Axial Compression

The instability modes for an axially compressed cylinder are overall column buckling and local wall buckling, either of which can be elastic or inelastic. The type of buckling to which a particular cylinder is susceptible is dependent both on the ratio of length to radius of gyration, L/r, and the ratio of cylinder diameter to wall thickness, D/t. Generally, column buckling is controlled by the L/r ratio, while shell buckling is dependent on the D/t ratio. For example, a cylinder with a large L/r and sufficiently small D/t will buckle as an elastic column, whereas a cylinder with a moderate to large D/t can buckle in either an inelastic or an elastic shell buckling mode. In many cases it is difficult to predict which of the four types of buckling a particular cylinder will exhibit.

Cylinders with heavy ring stiffeners that do not distort with the local buckle exhibit behavior between the rings which is similar to that of unstiffened cylinders. Closely spaced rings can enhance the local buckling strength. They will influence column buckling only in slenderness ranges where an interaction between column and local buckling exists. The general elastic stability theory for cylinders includes the spectrum from pure column to pure local buckling. The specific topic of realistic column buckling that reflects the stress-strain characteristics, residual stresses, and out-of-straightness of cylindrical columns is covered in Chapter 3. Therefore, this section is devoted to the discussion of local buckling of unstiffened cylinders and of cylindrical shells between theoretically rigid ring stiffeners. Guidelines for sizing fully effective ring stiffeners are provided in Section 14.4, and Section 14.7 contains a discussion of the interaction between column and local buckling.

Elastic Shell Buckling. The buckling of axially compressed cylindrical members was first approximately analyzed by Lorenz in 1908, and then in succeeding years more accurately by Timoshenko (1910), Southwell (1914), and Flügge (1932). Test results indicated, however, that actual cylinders buckled at loads well below those predicted by these early theoretical solutions. All of these solutions were based on small-deformation theory. In 1934, Donnell realized that a linear analysis was inadequate and suggested the need for a method of analysis that would account for large deformations. The first correct large-deflection solution was obtained by von Kármán and Tsien in 1941. Since then, numerous large-deflection investigations of axially compressed cylinders have been carried out. Of paramount importance among these was the analysis of Donnell and Wan (1950), who showed that initial imperfections are responsible for much of the discrepancy between linear theory and experimental results. The entire development of the theory of axially compressed cylindrical members is reviewed by Hoff (1966), who has himself made several important contributions to the subject. A comprehensive study of all aspects of the buckling of cylindrical shells has been pre-

pared by Gerard and Becker (1957). It includes theories, test results, and design recommendations.

The surface of a short cylinder buckles like an infinitely wide plate. The critical stress depends on L/D, D/t, and on the boundary conditions of the edges. As L/D decreases, the critical stress approaches that for a plate strip of unit width discussed in Chapter 4. Longer cylinders buckle into a series of diamond shaped bulges and the critical stress depends only on D/t. Still longer cylinders buckle as Euler columns where L/r is the parameter.

The theoretical elastic buckling stresses are summarized below with

$$Z = 2\left(\frac{L}{D}\right)^2\left(\frac{D}{t}\right)\sqrt{1-\nu^2} \tag{14.2}$$

used as a parameter to delineate the regions of behavior. For platelike buckling,

$$Z < 2.85 \qquad \sigma_{xc} = k_c \frac{\pi^2 E}{12(1-\nu^2)(L/t)^2} \tag{14.3a}$$

$$k_c = \begin{cases} \dfrac{12Z^2}{\pi^4} & \text{for simply supported edges} \quad (14.3b) \\ 4 + \dfrac{3Z^2}{\pi^4} & \text{for fully clamped edges} \quad (14.3c) \end{cases}$$

For diamond-shaped bulges,

$$2.85 \le Z < \frac{1.2(D/t)^2}{C} \qquad \sigma_{xc} = \frac{2CE}{D/t} \tag{14.4a}$$

where

$$C = \frac{1}{\sqrt{3(1-\nu^2)}} \tag{14.4b}$$

For the column buckling,

$$Z \ge \frac{1.2(D/t)^2}{C} \qquad \sigma_{xc} = \frac{\pi^2 E}{(L/r)^2} \tag{14.5}$$

Boundary conditions at the ends have little influence on Eq. 14.4 except when the edges are simply supported but can move freely in the tangential direction (Batdorf et al., 1947a; Almroth, 1966), in which case the buckling stress is half as large as the classical one.

Imperfections. The classical buckling stress given by Eq. 14.4 is a theoretical value assuming a geometrically perfect cylinder. The results of numerous compression tests (Lundquist, 1933; Donnell, 1956; Stein, 1968) show that actual cylinders may buckle elastically and fail at stresses as low as 30% of the critical stress given by Eq. 14.4. This discrepancy is due to the unstable postbuckling strength of such shells, which makes them extremely sensitive to small initial imperfections (such as deviations from the perfect geometrical shape) or due to residual stresses. The load that an axially loaded shell can support drops sharply subsequent to the onset of buckling, and the maximum load attained by the imperfect specimen is significantly below the critical load given by classical theory. Consequently, different values of C are recommended for applications where the normal degree of imperfections differ.

For manufactured or fabricated structural members, the value of C in Eq. 14.4a should be 0.165. This is approximately one-fourth of the theoretical value of Eq. 14.4b and was recommended by Plantema in 1946. Plantema's value was based on tests of manufactured members and recent tests of fabricated members with D/t in the range of 350 to 450 (Stephens et al., 1982, 1983) correlate with this value. The test members that form the basis for the recommended values had an out-of-roundness limit of 1%, $(D_{\max} - D_{\min})/D_{\text{nominal}}$. Usually, structural members do not have proportions for which the critical local buckling stress would be increased by boundary conditions as in Eq. 14.3.

Considerable research has been conducted to determine realistic values of C to be used in place of Eq. 14.4b for cylinders with large D/t ratios and aerospace-quality tolerances. Donnell and Wan (1950) developed theoretical curves for imperfect cylinders that are shown in Fig. 14.4. The parameter U in their curves is a measure of the initial imperfection of the cylinder.

An empirical curve (also in Fig. 14.4) developed by Batdorf et al. (1947a) for cylinders with D/t greater than 1000 merges with the Donnell-Wan curve for $U = 0.00025$. The NASA publication (Weingarten et al., 1968) suggests that

$$C = 0.6[1.0 - 0.9(1.0 - e^{-\theta})] \tag{14.6a}$$

where

$$\theta = 0.0442\sqrt{\frac{D}{t}} \tag{14.6b}$$

for D/t less than 3000. This relation is also plotted in Fig. 14.4 and is somewhat more conservative than the empirical curve by Batdorf and associates. Figure 14.4 also shows that the value of 0.165 recommended for C in structural members is conservative for D/t values less than 1000.

The NASA publication (Weingarten et al., 1965) also suggests that the effect of typical imperfections in short cylinders can be included by using $1.67CZ$ in

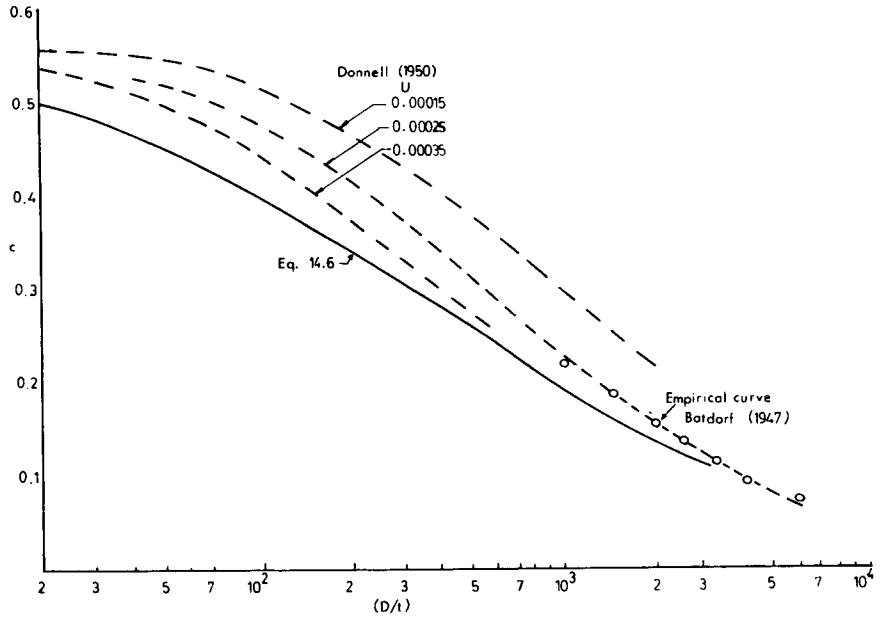

Fig. 14.4 Elastic buckling coefficient, C, for axially compressed cylinders.

place of Z in the K coefficients of Eqs. 14.3b and 14.3c. An earlier NACA guide (Gerard, 1957) presented different expressions for the short cylinder coefficients, but these differ by only a few percent from the values obtained using the modified Z.

A design procedure is proposed by Clark and Rolf (1964) for aluminum tubes. Based on the empirical relation,

$$C = \frac{1}{\sqrt{3(1-\nu^2)}(1+0.02\sqrt{D/t})^2} \tag{14.7a}$$

and when $\nu = 0.33$ for aluminum

$$C = \frac{0.612}{(1+0.02\sqrt{D/t})^2} \tag{14.7b}$$

They suggest the following formula for moderately long cylinders:

$$\sigma_{xc} = \frac{\pi^2 E}{8(D/t)(1+0.02\sqrt{D/t})^2} \tag{14.8}$$

For a cylinder whose length is less than its mean radius, they suggest using either Eq. 14.8 or the buckling equation for a flat-plate column, whichever gives the higher stress. Equation 14.8 is used in the Aluminum Association specification (AA, 1994).

Equation 14.8 can be presented in terms of an "equivalent slenderness ratio," which is substituted into the Euler column formula to obtain Eq. 14.9. This equivalent slenderness ratio is

$$(kL/r)_{\text{equiv}} = 2.829\sqrt{\frac{D}{t}}\left(1+0.02\sqrt{\frac{D}{t}}\right) \tag{14.9}$$

By substituting this value in the column formula (Eq. 14.5), the ultimate buckling strength can be determined for alloys for which ready-to-use formulas are not available.

Inelastic Shell Buckling. The inelastic buckling stress of cylindrical shells and tubes is usually obtained in one of two ways. Either the elastic formula is used with an effective modulus in place of the elastic modulus, or empirical relations are developed for specific classes of materials. The former approach is applicable only when the material stress-strain curve varies smoothly. This method has a long history of use and discussion (Gerard, 1956; Harris et al., 1957; Clark and Rolf, 1964; Weingarten et al., 1968). When the cylinder geometry and material properties are such that the computed buckling stress is in the plastic range, it is suggested that E in the elastic buckling equations be replaced by an effective modulus

$$E_{\text{eff}} = \sqrt{E_s E_t} \tag{14.10}$$

where E_s and E_t are the secant and tangent moduli, respectively.

As is usually the case when the effective modulus approach is used, a direct solution for the critical stress is not possible, and a graphical or spreadsheet trial-and-error approach is helpful.

The effective-modulus approach is applicable to homogeneous materials such as aluminum alloys and stainless steels, while the inelastic buckling of cylinders made from structural steels is more conveniently handled with an empirical formula. Even for aluminum alloys, however, Clark and Rolf (1964) point out that a shortcoming of the effective-modulus approach is that each different alloy requires its own design curve. They therefore propose that the following single equation can be used for all aluminum alloys:

$$\sigma_{xc} = B_t - D_t\sqrt{\frac{D}{2t}} \tag{14.11a}$$

where

$$B_t = \sigma_2\left[1 + 4.6\left(\frac{1000\sigma_2}{E}\right)^{0.2}\left(\frac{\sigma_2}{\sigma_1} - 1\right)\right] \tag{14.11b}$$

$$D_t = \frac{B_t}{0.9}\left(\frac{B_t}{E}\right)^{1/3}\sqrt{\frac{\sigma_2}{\sigma_1}} - 1 \tag{14.11c}$$

The quantities σ_1 and σ_2 are the values of the compressive yield strength at 0.1 and 0.2% offset (kips per square inch), respectively. To avoid curves that do not intersect the elastic curve, the ratio of σ_2/σ_1 is taken to be 1.06 in Eqs. 14.11b and 14.11c for those cases where the actual ratio exceeds this value. Equation 14.11 is applicable to any material whose stress-strain curve can be represented by the Ramberg–Osgood–Hill three-parameter relation

$$\varepsilon = \frac{\sigma}{E} + 0.002\left(\frac{\sigma}{\sigma_2}\right)^n \tag{14.14a}$$

where

$$n = \frac{0.301}{\log_{10}(\sigma_2/\sigma_1)} \tag{4.12b}$$

Equation 14.11a is shown by Clark and Rolf (1964) to agree well with both test results and the inelastic design criteria developed by Gerard (1956).

When dealing with cylinders made from carbon or low-alloy steel, the empirical approach is used exclusively. Several major experimental programs have been conducted since 1933. Figure 14.5 shows the experimental test data from Wilson and Newmark (1933), Wilson (1937), Plantema (1946), Ostapenko and Guzelman (1976, 1978), Ostapenko and Grimm (1980), Marzullo and Ostapenko (1978), Birkemoe et al. (1983), Prion and Birkemoe (1988) for thin-wall cylinders. All data from Wilson (1937) and Wilson and Newmark (1933) are shown for cylinders having thicknesses greater than or equal to $\frac{1}{4}$ in. while only the data for thicknesses less than $\frac{1}{4}$ in. that failed at a stress below the proportional limit are shown.

The considerable scatter in the data is probably due to differences in methods of making the cylinder that result in variation in imperfections, residual stresses, and material characteristics. There may also have been differences in test methods, data interpretation, and particularly in how the yield strength was determined.

As a result of the scatter in the test data, a number of different equations applicable to intermediate-length cylinders have been proposed for predicting the critical stress as a function of the wall slenderness. The equations vary in complexity and values of the critical stress depending on the philosophy of the proposer and the database used. The slenderness parameters are usually either D/t or a nondimensional local-buckling parameter, α, which for a circular cylinder can be expressed as

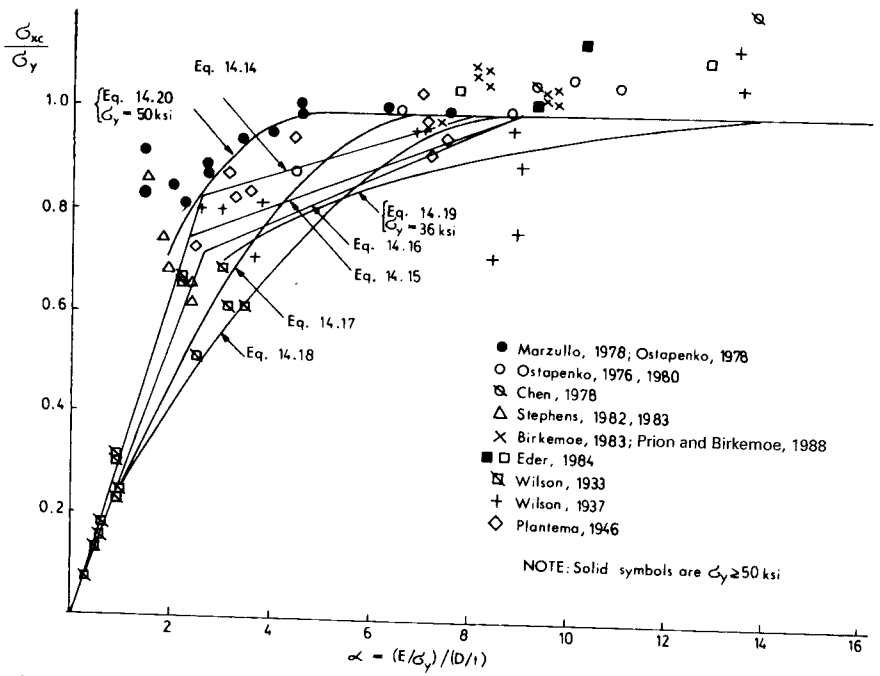

Fig. 14.5 Inelastic buckling equations and data for axially loaded cylinders.

$$\alpha = \frac{E/\sigma_y}{D/t} \tag{14.13}$$

Table 14.1 contains a listing of the various proposed equations. They are compared to one another and to the test data in Fig. 14.5. These equations have been converted from the original sources to express the ultimate strength in terms of α as required.

Equations 14.14 through 14.16 have a similar form with a linear dependence of α. Plantema proposed Eq. 14.14 in 1946 based on tests of manufactured tubes, and the AISI adopted the more conservative Eq. 14.15 after considering a larger database that included manufactured cylinders. Equation 14.16 is an even more conservative relation fitted to the pre-1976 data. The American Water Works Association adopted Eq. 14.17 with a safety factor of 2 on the basis of the fabricated cylinder tests conducted in the 1930s. Equation 14.18 also uses the quadratic form but is closer to a lower bound on the test data. The API equation (14.19) and the most recent equation (14.20), which was derived as a best fit to a series of tests on fabricated cylinders with several strength levels, contain the yield strength as part of the slenderness parameter in addition to α.

TABLE 14.1 Various Equations Proposed for the Critical Stress in Axially Loaded Steel Cylinders

Reference	Equation for σ_{xc}/σ_y	Limits	Equation Number
Plantema (1946)	1.0	$\alpha \geq 8$	14.14a
	$0.75 + 0.031\alpha$	$2.5 \leq \alpha < 8$	14.14b
	0.33α	$\alpha < 2.5$	14.14c
AISI specification (1996)	1.0	$\alpha \geq 9.1$	14.15a
	$0.665 + 0.0368\alpha$	$2.27 \leq \alpha \leq 9.1$	14.15b
SSRC Guide, 3rd ed. (1976)	1.0	$\alpha \geq 9.1$	14.16a
	$0.61 + 0.043\alpha$	$2.57 \leq \alpha < 9.1$	14.16b
	0.28α	$\alpha < 2.57$	14.16c
AWWA (1967)		$\sigma_y = 30$ ksi, $t \geq \frac{1}{4}$ in.	
Timoshenko (1910)	1.0	$\alpha \geq 7.25$	14.17a
Tokugawa (1929)	$0.27\alpha - 0.019\alpha^2$	$\alpha > 7.25$	14.17b
Marshall (1971)	1.0	$\alpha \geq 9.1$	14.18a
	$0.22\alpha - 0.0121\alpha^2$	$\alpha < 9.1$	14.18b
API (1989)	1.0	$\alpha \geq \frac{E/\sigma_y}{60}$	14.19a
	$1.64 - 0.23/(\sigma_y\alpha/E)^{0.25}$ not to exceed 0.3α	$\alpha > \frac{E/\sigma_y}{60}$	14.19b
Ostapenko and Grimm (1980)	1.0	$\alpha \geq 0.07/\gamma$	14.20a
	$38(\gamma\alpha) - 400(\gamma\alpha)^2 + 2020(\gamma\alpha)^3$ where $\gamma = (\sigma_y/E)^{2/3}$	$\alpha < 0.07/\gamma$	14.20b

The tests on fabricated cylinders conducted since 1976 fall considerably higher in Fig. 14.5 than the 1930s tests. This may reflect improved fabricating technology and indicates that lower-bound equations for the total data base may be overly conservative. At the same time, the scatter in the data probably does not warrant a complex best-fit expression for predicting the strength. Therefore, Eq. 14.15 is recommended as a reasonable estimation of a lower bound for the inelastic axial buckling stress of currently produced fabricated or manufactured steel tubes and pipe.

14.3.2 Cylindrical Shells Subjected to Bending

The buckling behavior of cylinders in bending differs from that of axially compressed cylinders in that bent cylinders have a stress gradient which is

not present in axially compressed cylinders and the cross section tends to ovalize (Brazier, 1927; Ades, 1957; Gellin, 1980). Donnell (1934) found that the elastic buckling stress in bending is somewhat higher than the critical stress for axial compression. Flügge (1932) and Timoshenko and Gere (1961) reached the same conclusion. Other investigators (Wilson and Olson, 1941; Weingarten and Seide, 1961; Yao, 1962) have indicated that there is not much difference between the critical stress in bending and in axial compression. Until this disagreement is resolved, it is recommended that Eq. 14.4 with $C = 0.165$ as in axial compression be used for determining the critical bending stress of cylinders that buckle elastically.

Inelastic buckling in flexure includes not only the nonlinear behavior below the material yield stress as in axial compression, but also the region between the yield moment and where the maximum stress is at yield while the strain level increases. This is a significant region because of the relatively high shape factors in cylinders, that is,

$$\frac{Z}{S} = \frac{4}{\pi}\left(1 + \frac{t}{D}\right) \tag{14.21}$$

where Z is the plastic-section modulus and S is the elastic-section modulus. Typical values for tubes listed in the AISC manual range from 1.30 upward. About 96% of the plastic moment can be developed at only twice the yield strain.

Data for the inelastic flexural capacity of steel tubes with a uniform bending moment are plotted in Fig. 14.6. Since local buckling after the yield moment has been reached is a function of strain rather than stress, the plot is in terms of normalized moment capacity rather than critical stress. The earliest tests on hot-formed pipe reported by Schilling (1965) indicated that the plastic moment could be achieved for $\alpha > 8.33$, which is approximately the same limit as that used in Eq. 14.14 for achieving the full yield strength of axially loaded cylinders. Although this was used to define a plastic moment for a number of years, the length that was machined to obtain the reduced thickness was too short to allow free ovalization and, as shown by Sherman in tests for moment capacity at fixed ends (Sherman, 1986), this resulted in high moment capacities. Later tests that also included cold-formed (Jirsa et al., 1972; 1972; Sherman, 1976; Korol, 1978) and fabricated pipe (Sherman, 1992) did not always reach the plastic moment when α exceeded 8.33. This is logical because the inelastic strain required for a plastic moment is much greater than that required for the yield capacity under axial load. In addition, pipes ovalize somewhat in bending, thereby producing additional geometric imperfection and biaxial stress conditions.

The moment capacities in Fig. 14.6 can be reasonably represented by a "best-fit" linear expression in terms of α similar to the form of Eq. 14.15 for critical axial stresses.

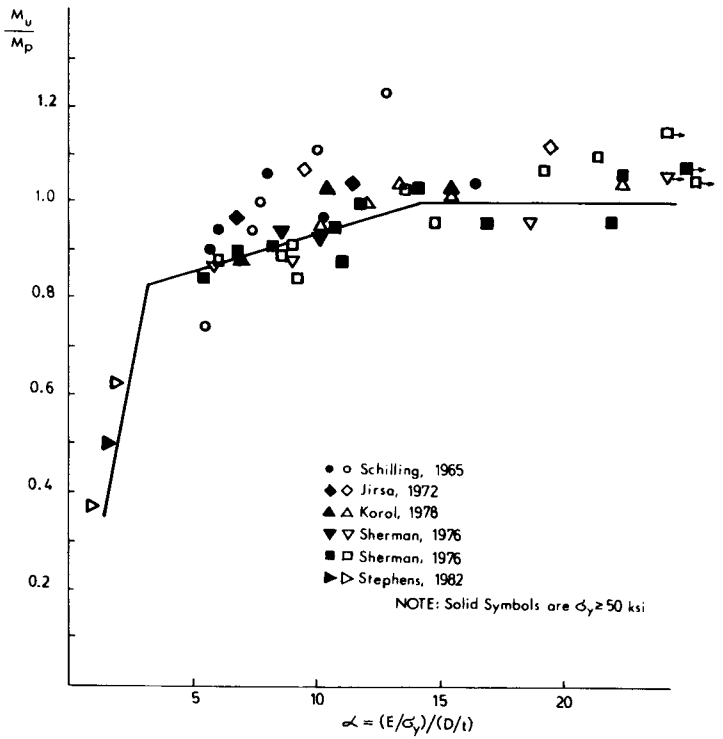

Fig. 14.6 Moment-capacity data.

$$M_u/M_p = \begin{cases} 1.0 & \text{for } \alpha \geq 14 \quad (14.22a) \\ 0.775 + 0.016\alpha & \text{for } \alpha < 14 \quad (14.22b) \end{cases}$$

Equation 14.22b is valid until the moment capacity is determined by elastic buckling,

$$M_u = \sigma_{xc} S \tag{14.22c}$$

where σ_{xc} is from Eq. 14.4. A lower bound to the data is obtained if the values in Eqs. 14.22a and 14.22b are multiplied by 0.9. Another equation that results in a continuous curve using the slenderness parameter $(E/F_y)^{0.5}(t/R)^{1.5}$ has been proposed by Kulak (1994).

Clark and Rolf (1964) developed the following criterion for aluminum and materials with a similar stress-strain curve.

$$\sigma_{tb} = B_{tb} - 0.707 D_{tb}\sqrt{\frac{D}{t}} \tag{14.23}$$

where σ_{tb} is the bending stress in the tube (maximum value of bending moment divided by section modulus) and B_{tb} and D_{tb} are coefficients given by

$$B_{tb} = 1.5\left[1 + 4.6\left(\frac{1000\sigma_y}{E}\right)^{0.2}\left(\frac{\sigma_2}{\sigma_1} - 1\right)\right]\sigma_y \tag{14.24a}$$

$$D_{tb} = \frac{B_{tb}}{2.7}\left(\frac{B_{tb}}{E}\right)^{1/3} \tag{14.24b}$$

In the formulas above, σ_y (kips per square inch) is either the tensile or compressive yield strength in the axial direction, whichever is lower, and σ_1 and σ_2 (kips per square inch) are the values of the compressive yield strength at 0.1 and 0.2% offset, respectively. The ratio σ_2/σ_1 should be taken to be 1.06 for those cases where the actual ratio exceeds this value. When $(D/2t) > (B_{tb} - B_t)^2/(D_{tb} - D_t)^2$, the formulas for axial compression should be used instead of Eq. 14.23. The coefficients B_t and D_t are defined in Eqs. 14.11b and 14.11c.

14.3.3 Cylindrical Shells Subjected to Torsion

The elastic shear buckling stress, τ_c, due to torsion in cylinders of any length can be expressed as (Batdorf et al., 1947b)

$$\tau_c = K_s \frac{\pi^2 E}{12(1-\mu^2)(L/t)^2} \tag{14.25a}$$

As in the case of axial loading, the value of K_s depends on the cylinder proportions and, for short cylinders, on the boundary conditions. The value of K_s can be expressed in terms of the parameter Z defined in Eq. 14.2.

For short cylinders ($Z < 50$), end conditions are of major importance. For a simply supported short cylinder,

$$K_s = 5.35 + 0.213Z \tag{14.25b}$$

and for a short tube having full end fixity,

$$K_s = 8.98 + 0.10Z \tag{14.25c}$$

where Z is defined by Eq. 14.2. With intermediate-length cylinders, for $100 \leq Z \leq 19.2(1-\mu^2)(D/t)^2$,

$$K_s = 0.85Z^{0.75} \tag{14.25d}$$

for all end conditions. For very long cylinders, as recommended by Timoshenko and Gere (1961),

$$K_s = \frac{0.406Z}{(1-\mu^2)^{0.25}(D/t)^{0.5}} \tag{14.25e}$$

Schilling (1965) presents test data for some alloy steels whose stress-strain curve approaches that of a sharp-yielding material. From these data he concludes that the critical shear stress for these steels can be approximated by the shear yield strength τ_y when the parameter $(\tau_y/E)(D/t)^{1.25}(L/D)^{0.5}$ is less than 1.076 and by the elastic shear buckling stress when the same parameter exceeds 1.076.

Studies of postbuckling behavior of intermediate-length cylinders loaded in torsion (Nash, 1957) show that the maximum load that an initially imperfect cylinder can resist is less than the classical shear buckling load. However, the drop in load subsequent to buckling is very small compared to that which takes place with axial compression. Hence the failure stress of an actual imperfect cylinder is only slightly lower than the critical stress predicted by linear theory. Schilling (1965) recommends that the theoretically obtained torsional buckling stress of intermediate-length cylinders loaded in torsion be reduced by 15% to account for initial imperfections.

For materials such as aluminum alloys and stainless steels, which have gradually yielding stress-strain curves, the buckling stress in the inelastic range can be obtained by replacing E, in the elastic formulas, by E_s, the secant modulus at $\sigma = 2\tau_c$ (Gerard, 1957).

In the Aluminum Association specification (AA, 1994), an equivalent slenderness ratio is used to obtain the shear buckling stress for tubes subjected to torsion. In the elastic range the buckling stress is given by

$$\tau_c = \frac{\pi^2 E}{\lambda^2} \tag{14.26a}$$

in which λ, the equivalent slenderness ratio, is approximated by

$$\lambda = 3.73\left(\frac{D}{t}\right)^{0.75} W^{0.5} \tag{14.26b}$$

The coefficient W is equal to unity for long, unstiffened tubes, and

$$W = 0.561\frac{\sqrt{L/D}}{(D/t)^{0.25}} \tag{14.26c}$$

for tubes where the clear length L between circumferential stiffeners is such that the value of W from Eq. 14.26c is less than unity.

For the inelastic buckling of aluminum tubes, Clark and Rolf (1964) propose the following relation:

$$\tau_c = B_s - D_s\lambda \tag{14.27a}$$

in which λ is given by Eq. 14.26b, and B_s and D_s are coefficients defined as follows:

$$B_s = \tau_2\left[1 + 5.8\left(\frac{1000\tau_2}{E}\right)^{1/3}\left(\frac{\tau_2}{\tau_1} - 1\right)\right] \tag{14.27b}$$

$$D_s = \frac{B_s}{2}\sqrt{\frac{B_s}{E}\left(\frac{\tau_2}{\tau_1} - 1\right)} \tag{14.27c}$$

in which τ_1 and τ_2 are the shear yield strengths at 0.1 and 0.2% offsets, respectively, expressed in kips per square inch. To avoid inelastic buckling curves that do not intersect the elastic curve, the ratio τ_2/τ_1 is taken to be 1.06 for those cases where the actual ratio exceeds this value. It is permissible to substitute σ_2/σ_1 for τ_2/τ_1 where σ_1 and σ_2 are determined from the compressive stress-strain curve. Good agreement is shown to exist between test results for five different aluminum alloys and Eq. 14.27.

14.3.4 Cylindrical Shells Subjected to Transverse Shear

Little information is available on the subject of local instability of shells or tubes subjected to transverse shear. It seems logical, however, that because of the presence of a stress gradient, tubes loaded in transverse shear will buckle at a higher stress than similar tubes loaded in torsion. Schilling (1965) suggests that for manufactured tubes the critical shear stress in transverse shear be taken as 1.25 times the critical stress in torsion when buckling is elastic. In the inelastic range, he advises using the same critical stress for transverse shear as is used for torsion.

14.3.5 Cylindrical Shells Subjected to Uniform External Pressure

The strength of a shell under external pressure depends on its L/D and D/t ratios and upon the physical properties of the material. It also depends on the amount of deviation of the shell from a true circular form. Failure of a shell can occur by yielding or by buckling at stresses which may be considerably below the yield point. The effective length of the shell can be reduced by the addition of circumferential stiffeners.

A thinness factor has been presented (Windenburg and Trilling, 1934) that is indicative of the mode of failure to be expected.

$$K = \left(\frac{D}{t}\right)^{0.75}\sqrt{\left(\frac{L}{D}\right)\left(\frac{\sigma_y}{E}\right)} \tag{14.28}$$

where L is the unsupported length of shell between stiffeners or between the ends of the cylinder (Fig. 14.1) and D is the diameter to midthickness ratio of the cylindrical shell. For approximation purposes, elastic instability is likely to occur in the range $K > 1.2$, plastic-shell instability in the range 0.8 to 1.2, and shell yielding if $K < 0.8$.

If the shell stiffeners are placed a large enough distance apart, the shell region between stiffeners will behave under pressure as though no stiffeners were present. The shortest length of cylinder for which the strengthening effect of the stiffeners can be ignored is defined as the *critical length.*

A distinction can also be made in regard to the support conditions at the ends of the cylinder. If the pressure produces longitudinal stresses in addition to circumferential stresses, the cylinder is hydrostatically loaded. However, if end conditions do not produce longitudinal pressure stresses, the cylinder is defined as being loaded by lateral pressure only.

Elastic Buckling. Solutions for the critical elastic pressure of cylinders with finite length were first developed in the early 1900s (Southwell, 1915; von Mises, 1931, 1933). In the intervening years, modifications have been made to account for realistic boundary conditions (Von Sanden, 1949) and to provide simpler equations that closely approximate the exact solution in certain ranges of cylinder proportions. The most exact theory is that of Reynolds (1962), which includes the influence of elastic stiffening rings at the boundaries on both the prebuckling and buckling deformations. This theory agrees well with the test results presented by Hom and Couch (1961) and by Reynolds (1962) and should be used for comparison of theory and experiment. However, the simpler but more conservative equations of von Mises are recommended for general use.

The von Mises equation for lateral pressure (Windenburg and Trilling, 1934, Eq. 2) is given by

$$p_c = 2E\frac{t}{D}\left\{\frac{(t/D)^2}{3(1-\nu^2)}\left[n^2 - 1 + \frac{\lambda^2(2n^2-1-\mu)}{n^2+\lambda^2}\right] + \frac{\lambda^4}{(n^2-1)(n^2+\lambda^2)^2}\right\} \tag{14.29a}$$

where n is the number of circumferential lobes formed at collapse and

$$\lambda = \frac{\pi D}{2L} \tag{14.29b}$$

The von Mises equation for the more common hydrostatic pressure case can be approximated by

$$p_c = \frac{2E(t/D)}{n^2 + (\lambda^2/2) - 1}\left\{\frac{(t/D)^2}{3(1-\nu^2)}[(n^2+\lambda^2)^2 - 2n^2 + 1] + \frac{\lambda^4}{(n^2+\lambda^2)^2}\right\} \tag{14.30}$$

Equation 14.30 is a simplified version of Eq. 6 of the Windenburg and Trilling (1934) paper and agrees with it closely for all shell geometries. The correct value of n in Eq. 14.29 or 14.30 is that which makes p_c a minimum.

In certain ranges of L/D, the number of lobes in the buckling mode may be known or one of the terms in the expression for critical pressure becomes negligible. This leads to reasonable simplifications of the more complex equations so that iterative solutions for n can be avoided. Table 14.2 contains a summary of these equations when Poisson's ratio is equal to 0.3. Simplified equations are provided only for the case of hydrostatic external pressure. The range of validity for each of the equations is defined in terms of L/D, or more conveniently by a parameter.

$$\theta = [12(1-\nu^2)]^{0.25}\frac{L}{D}\sqrt{\frac{D}{t}} \tag{14.37a}$$

or

$$\theta = 1.818\frac{L}{D}\sqrt{\frac{D}{t}} \qquad \text{for } \nu = 0.3 \tag{14.37b}$$

In a few cases, the equations are still relatively complex, but approximate values of the critical pressure can be obtained by using a simpler expression from an adjacent range, as is evident in Fig. 14.7.

Figure 14.7 is a plot of the buckling pressure coefficient γ as determined from Eqs. 14.30 through 14.36 for values of the shell geometry parameter θ where

$$\gamma = \frac{p_{\phi c}}{p^*} \tag{14.38a}$$

and

$$p^* = \frac{8E(t/D)^2}{3(1-\nu^2)} \tag{14.38b}$$

The value p^* is the theoretical critical end pressure for a cylinder compressed only at its ends (see Eq. 14.4). The buckling coefficient γ is single valued for all values of θ, except when approaching D/t values where $n = 2$. Test results fromWindenburg and Trilling (1934), Hom and Couch (1961), and Reynolds (1962) are also shown in Fig. 14.7.

TABLE 14.2 Summary of Equations for the Elastic Buckling of a Perfect Cylinder with Poisson's Ratio (ν) = 0.3[a]

Pressure	Reference	Critical Pressure, p_c	
Lateral External	Windenburg and Trilling (1934)	$\frac{2E}{D/t}\left\{\frac{0.366}{(D/t}\left[n^2-1+\frac{\lambda^2(2n^2-1.3)}{n^2+\lambda^2}\right]+\frac{\lambda^4}{(n^2-1)(n^2+\lambda^2)^2}\right\}$	Eq. 14.29a

Hydrostatic External							
θ		L/D					
From	To	From	To			Equation	Number
0	0.8	0	$\frac{0.44}{\sqrt{D/t}}$		Very short	$\frac{3.615E}{(D/t)^3(L/D)^2}$	14.31
0.8	1.4	$\frac{0.44}{\sqrt{D/t}}$	$\frac{0.77}{\sqrt{D/t}}$	SSRC Guide 3rd ed. (1976)		$\frac{3.615E}{(D/t)^2}\left[0.448(L/D)^2(D/t)+\frac{1}{(L/D)^2(D/t)}\right]$	14.32
1.4	2.0	$\frac{0.77}{\sqrt{D/t}}$	$\frac{1.1}{\sqrt{D/t}}$	Windenburg and Trilling (1934)	Short	$\frac{2.0E}{(D/t)(n^2+0.5\lambda^2-1)}\left\{\frac{0.367}{(D/t)^2}[(n^2+\lambda^2)^2-2n+1]+\frac{\lambda^4}{(n^2+\lambda^2)^2}\right\}$	14.30
2.0	10.0	$\frac{1.1}{\sqrt{D/t}}$	$\frac{5.5}{\sqrt{D/t}}$	Windenburg and Trilling (1934)		$\frac{2.6E}{(D/t)^{2.5}[(L/D)-0.45(t/D)^{0.5}]}$	14.33
10	D/t	$\frac{5.5}{\sqrt{D/t}}$	$0.55\sqrt{D/t}$		Intermediate	$\frac{2.6E}{(L/D)(D/t)^{2.5}}$	14.34
D/t	$4D/t$	$0.55\sqrt{D/t}$	$2.1\sqrt{D/t}$	SSRC Guide 3rd ed. (1976)		$\frac{2.0E}{(D/t)(3+0.5\lambda^2)}\left\{\frac{0.367}{(D/t^2}[(4+\lambda^2)^2-7]+\frac{\lambda^4}{(4+\lambda^2)^2}\right\}$	14.35
$4D/t$	–	$2.1\sqrt{D/t}$	–	Bryant (1954)	Long	$\frac{2.2E}{(D/t)^3}$	14.36

[a] L is the distance between a major bulkhead and a ring stiffener or successive ring stiffeners, n is the integer at which p_c is a minimum, $\lambda = 0.5\pi/(L/D), \theta = 1.818(L/D)(\sqrt{D/t})$.

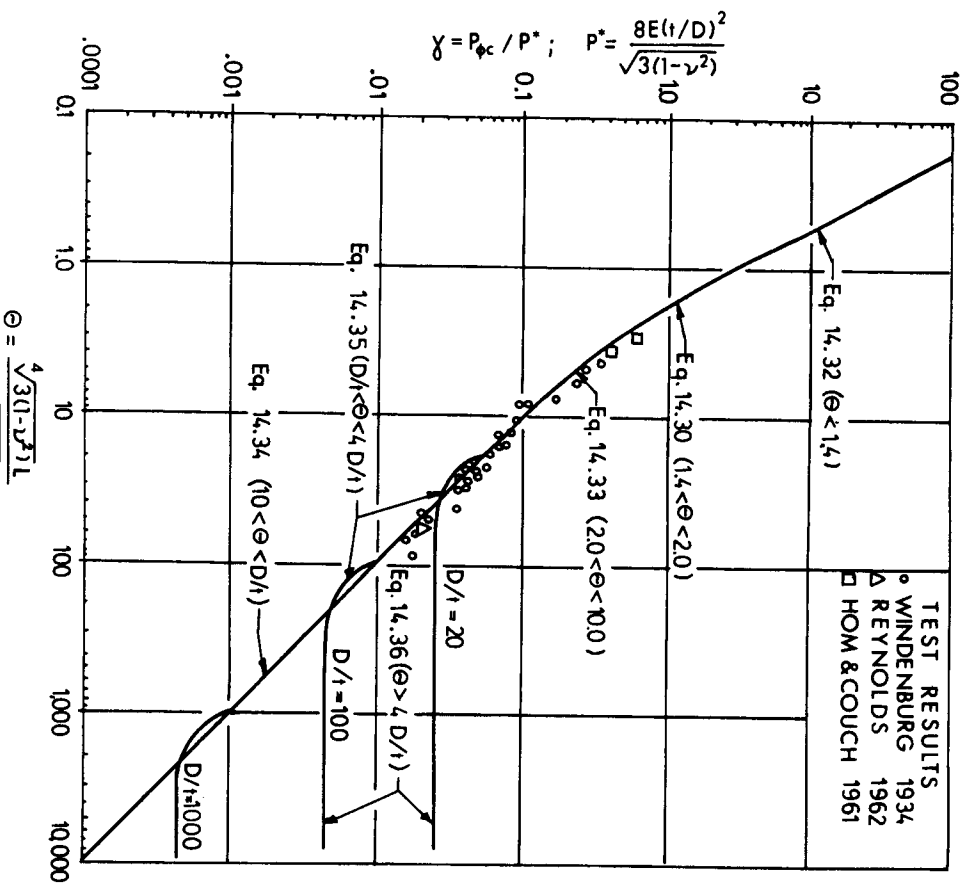

Fig. 14.7 Elastic buckling coefficients for circular cylinders under hydrostatic pressure ($\nu = 0.3$).

A hemispherical head, rather than a flat plate, is often used to close the ends of a cylinder. If the heads remains stable while the cylindrical section buckles, Harari and Baron (1970, 1971) have shown that the cylinder can be treated as a longer cylinder with a length of $D/2n$ added for each head, where n is the buckling mode of the equivalent cylinder.

Inelastic Buckling. During the 1960s a number of studies were conducted (Holmquist and Nadai, 1939; Gerard and Becker, 1957; DeHeart and Basdekas, 1960; Heise and Esztergar, 1970), particularly at the David Taylor

Model Basin (Reynolds, 1960; Hom and Couch, 1961; Lunchick, 1961a,b, 1963; Krenzke and Kiernan, 1963; Pulos, 1963; Boichot and Reynolds, 1964) on the inelastic collapse of cylinders under external pressure.These have included theoretical and experimental studies to develop predictive equations or semigraphical procedures. However, the most general approach consistent with plastic buckling theory is to substitute a reduced modulus, $\sqrt{E_s E_s}$, or a tangent modulus, E_s, for E in the elastic equations of Table 14.2. Determination of the tangent or secant moduli is complicated by the biaxial stress condition that exists under hydrostatic pressure. One approach is to assume that the distortion energy criterion applies to the plastic range, so that the stress intensity σ_i, can be defined as

$$\sigma_i = (\sigma_\phi^2 + \sigma_x^2 - \sigma_\phi \sigma_x)^{0.5} \tag{14.39a}$$

where

$$\sigma_\phi = -\frac{pD}{2t} \quad \text{and} \quad \sigma_s = -\frac{pD}{4t} \tag{14.39b}$$

From a representative stress-strain curve of the material used in the cylinder, the values of the desired moduli that correspond to σ_i are determined.

As in the case of columns, the use of the tangent modulus provides the lower limit load when it is used in the elastic buckling expression (Heise and Esztergar, 1970). Another limit is the plastic collapse pressure when the circumferential stress is at yield:

$$p_p = \frac{2\sigma_y}{D/t} \tag{14.40}$$

One practical way of determining the critical pressure is to use the charts in the ASME code (1980). The charts include elastic buckling, elastic-plastic buckling, and plastic collapse for several different materials. They have been developed from the theoretical elastic equations, with the tangent modulus for the particular material and a uniform factor of safety of 3. Figure 14.8*a* is a chart that includes the length and D/t terms in the critical stress equations. Knowing L/D and D/t for the cylinder, the factor A is determined, and this corresponds to σ_y/E. The material curve in fig. 14.8*b* is for carbon steel or low-alloy steels with yield strength greater than 30 ksi. Entering the chart with factor A, factor B is determined. In the ASME code, the allowable pressure is computed from B. However, multiplying by 3 to remove the factor of safety, the critical pressure is

$$p_c = \frac{4B}{D/t} \tag{14.41}$$

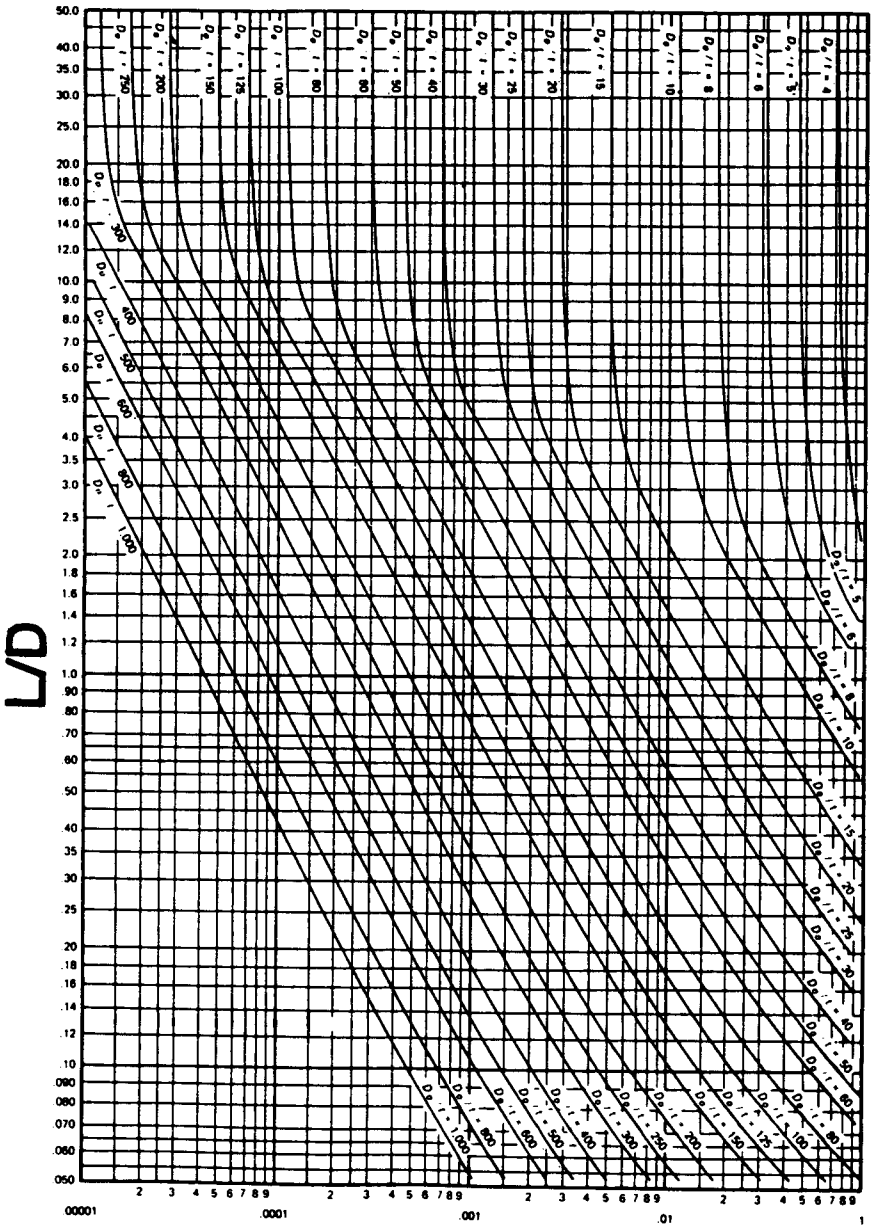

(a)

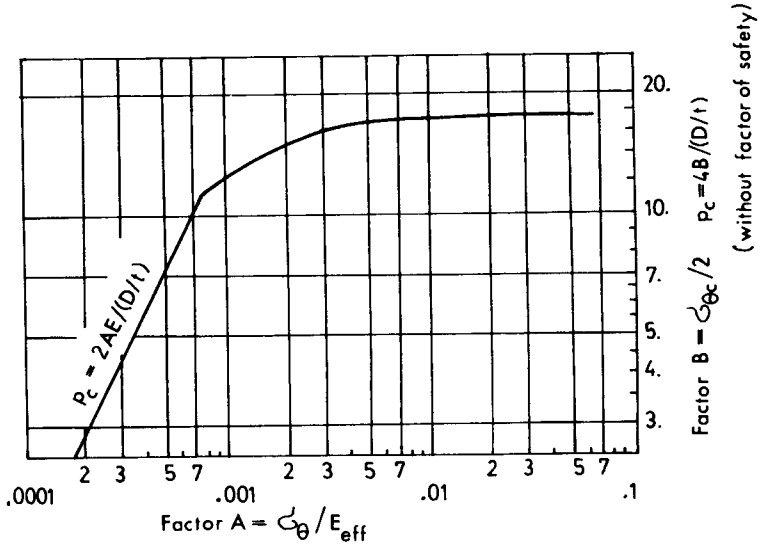

(b)

Fig. 14.8 ASME charts for buckling under hydrostatic pressure: (*a*) geometry terms from elastic equations: (*b*) material curve for carbon and low-alloy steels with $\sigma_y \geq 30$ ksi.

or the critical circumferential stress is

$$\sigma_{\phi c} = 2B \tag{14.42}$$

The reduced modulus is given by $E_R = 2B/A$.

The horizontal portion of the material line in Fig. 14.8*b* represents the plastic collapse at a circumferential yield stress of 35 ksi. The other extreme of elastic buckling of long cylinders is also represented. The vertical portions of the D/t lines in Fig. 14.8*a* correspond to long cylinders, and the value of A for this case is given by

$$A = \frac{1.1}{(D/t)^2} \tag{14.43}$$

If this is substituted in the equation for the elastic portion of the material line in fig. 14.8*b*, Eq. 14.36 in Table 14.2 is obtained.

The difficulty with the ASME charts is that a class of materials is included in one chart regardless of the yield strength. For example, Fig. 14.8*b* is for carbon and low-alloy steels with specified yield strengths of 30 ksi and over. To obtain a better estimate for the inelastic buckling pressure of cylinders with a different yield strength, new curves would have to be estimated between the elastic limit and yield.

Effects of Imperfections. The effect of initial imperfections has been studied by several investigators. Most analyses of the effects of initial imperfections are based on the assumption that the initial out-of-roundness is similar in form to one of the assumed buckling modes and the critical pressure is assumed to be the pressure at which the extreme fibers of the shell begin to yield.

Timoshenko and Gere (1961, Eq. e, p. 296) have developed a formula for determining the elastic critical pressure for cylinders of infinite length having a definable eccentricity. The hydrostatic pressure p_y at which yielding begins can be determined from the following equation:

$$p_y^2 - \left[\frac{2\sigma_y t}{D} + \left(1 + \frac{1.5De_0}{t}\right)p_c\right]p_y + \frac{2\sigma_y t}{D}p_c = 0 \tag{14.44}$$

where e_0 is the out-of-roundness $= (D_{\max} - D_{\min})/D = 4e/D$ (see Fig. 14.2), where e is the radial eccentricity and p_c is the critical pressure determined by Eqs. 14.30 through 14.36 (with E or E_t as appropriate). This equation is applicable only when the buckling mode is such that $n = 2$. For situations where the critical n is greater than 2, Kendrick's (1953b) equations should be used in place of Eq. 14.44.

The use of the equations with out-of-roundness produces more conservative approximations of test data than the theoretical elastic or inelastic equations. However, they do not eliminate the scatter, as would be the case if imperfections were its only source (Heise and Esztergar, 1970). It has been shown (Heise and Esztergar, 1970) that imperfections have less influence on cylinders with low D/t that buckle inelastically than on those that buckle elastically.

A value of $e_0 = 0.01$ has been adopted for fabricated tubes by the American Petroleum Institute (API, 1977) and the ASME (1980). This value of e_0 does not appear explicitly in the design equations but it has been considered in establishing the uniform factor of safety in both specifications.

Expressions and procedures for considering the out-of-roundness effect in shells with finite length have been developed by several investigators (Sturm, 1941; Holt, 1952; Bodner and Berks, 1952; Donnell, 1956; Galletly and Bart, 1957). The problem of an initial deflection of the shell in the longitudinal direction (out-of-straightness) has also been analyzed (Wu et al., 1953; Lunchick and Short, 1957).

An important aspect is the method of determining or defining the initial imperfection. Several methods have been proposed (Galletly and Bart, 1957), but the most satisfactory from a theoretical point of view is to use the maximum radial deviation from a perfect circle, e, measured over an arc length, A, corresponding to one-half lobe length.

$$A = \frac{\pi D}{2n} \tag{14.45}$$

where n is the lobar number in Eq. 14.30. Based on this imperfection measurement, the corrective method of Galletly and Bart (1957) is the most effective, although it does not account for all test data scatter (Heise and Esztergar, 1970).

For design purposes, imperfections are usually considered by specifying permissible out-of-roundness. An empirical expression (Windenburg, 1960) for the maximum e/t value so that the collapse pressure will not be less than 80% of that corresponding to a perfect shell is

$$\frac{e}{t} = \frac{0.018}{n}\frac{D}{t} + 0.015n \tag{14.46}$$

This procedure has been incorporated into the ASME code (1980), where the maximum permissible deviation and the length over which it is to be measured are presented in graphical form.

14.4 GENERAL INSTABILITY OF RING-STIFFENED CYLINDERS

Under static conditions, a ring-stiffened shell may fail in one or more of the three possible instability modes shown in Fig. 14.9. These are:

1. Axisymmetric collapse of the shell between adjacent ring stiffeners. This mode is a combination of yielding and axisymmetric buckling and is characterized by accordion-shaped pleats around the circumference of the shell.
2. Asymmetric or lobar buckling of the shell between adjacent ring stiffeners. This mode is characterized by the forming of two or more dimples of lobes around the circumference.
3. General instability or overall collapse of the entire shell and stiffeners (not column buckling). This mode is characterized by large dished-in portions of the stiffened shell, wherein the shell and stiffeners deflect together. The occurrence of this mode is strongly influenced by the shape, moment of inertia, and circularity of the stiffening rings and the ratio of the overall length to the radius of the cylinder.

The first two instability modes were the topic of the preceding section of this chapter and the third is the topic of this section.

Ring stiffeners have little influence on column buckling strengths of cylinders and the column curves for fabricated cylinders in Chapter 3 are applicable. Therefore, the purpose of ring stiffeners is primarily to enhance the local buckling strength of a cylinder. To accomplish this, their spacing L must be

(a)

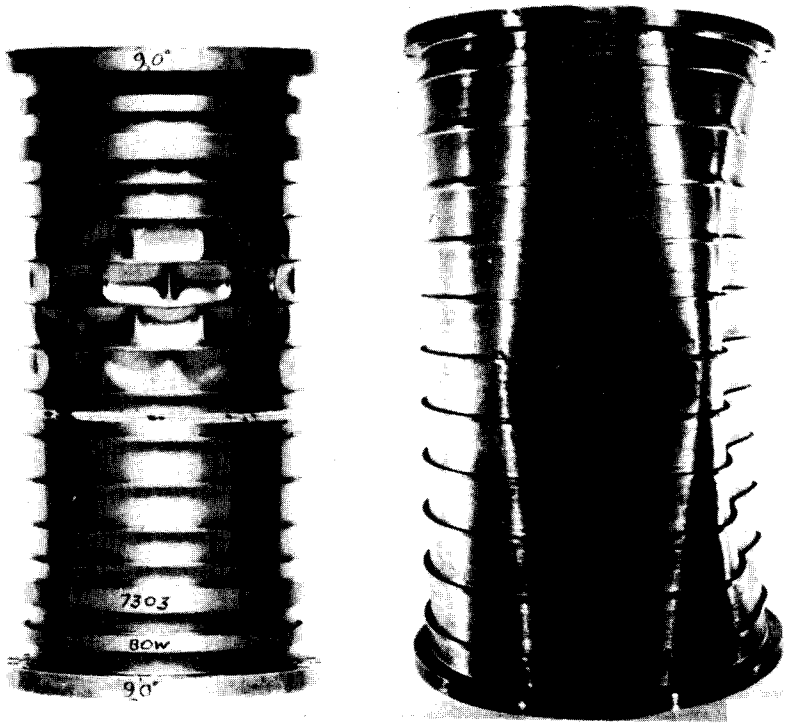

(b) (c)

Fig. 14.9 Buckling modes for ring-stiffened cylinders: (*a*) local buckling (axisymmetric); (*b*) local buckling (asymmetric); (*c*) general instability (overall collapse).

small enough to influence the strength predictions in the equations of Section 14.3 (i.e., L must be a term in the equation).

If the stiffeners have sufficient stiffness and strength, the failure will be in one of the first two instability modes and the collapse load a function of L. Lighter stiffeners, on the other hand, will lead to the third instability mode and its collapse load will be between that of an unstiffened long cylinder and one whose stiffeners are spaced L.

14.4.1 Nonpressure Loadings

Very little information is available on the general instability of ring-stiffened cylinders under nonpressure loads. This is probably due to the infrequent occurrence of conditions that would produce this mode. Under axial load, the critical length implied by the limit for Eq. 14.3 is $L/D < 1.22/\sqrt{D/t}$. This is an extremely small spacing relative to the critical length for pressure loading and would seldom be encountered in practice. Ring stiffeners are a very inefficient method of reinforcing a cylinder for axial loads. Ring stiffeners can be more effective in flexure because they reduce ovalization prior to local buckling. However, the spacing would have to be very small, as in the case of axial load, and would be considered only for regions of steep moment gradients. In the event that closely spaced ring stiffeners are present, their stiffness should be considered as uniformly distributed and the general buckling strength under axial load or flexure estimated using orthotropic shell theory.

The maximum (critical) spacing beyond which properly sized rings are no longer effective indicated in Eq. 14.25 for torsional loading is $L/D = 3.03\sqrt{D/t}$, which is considerably greater than that for the axial load requirements of Eq. 14.5. Therefore, it would appear that stiffeners could be effective in increasing the local buckling strength of torsion and similarly cylinders subject to transverse shear. However, little published information is readily available to determine the minimum size for a stiffener to be fully effective or to determine the general buckling strength if lighter stiffeners are used for either case. As a practical matter, it would seem that ring stiffeners are seldom used, or needed, to increase the buckling capacity of cylinders in torsion or shear.

14.4.2 Uniform External Pressure

Ring stiffeners are most frequently used to increase the local buckling strength of cylinders subject to external pressure. According to Table 14.2, the critical spacing is $L/D = 2.1\sqrt{D/t}$ for the hydrostatic loading case. A review of the state of the art in the design of ring-stiffened cylindrical shells under hydrostatic pressure was presented by Pulos in 1963. This report includes those formulations that have found extensive use. A later survey was made by Basdekas (1966) of the analytical and empirical procedures for the determination of dynamic as well as static strengths of cylindrical, spherical, and spheroidal shells. Meck (1965) also presents, in a concise form, the elastic and inelastic solutions for shell buckling and general instability.

Elastic General Instability. The elastic instability of ring-stiffened cylinders has been considered in the orthotropic shell theory (Bodner, 1957; Becker, 1958; Timoshenko and Gere, 1961, p. 499; Ball, 1962) and by a *split-rigidity method* (Tokugawa, 1929; Bryant, 1954) in which the formula for critical pressure consists of a shell term and a stiffener term. The most acceptable solution is that of Kendrick (1953a), whose theoretical predictions have been confirmed experimentally (Reynolds, 1957). However, these equations cannot be readily solved without the aid of a computer or graphical procedures (Reynolds, 1957; Reynolds and Blumenberg, 1959; Ball, 1962).

Although somewhat less exact than Kendrick's solution, the most widely used design equation is that of Bryant (1954) modified for the position of the stiffener on the inside or outside of the shell (Krenzke and Kiernan, 1963).

$$p_c = \frac{2E}{D/t}\frac{\lambda^4}{(n^2 + (\lambda^2/2) - 1)(n^2 + \lambda^2)^2} + \frac{EI_e(n^2 - 1)}{L_f R_0 R_c^2} \tag{14.47}$$

where

$\lambda = \pi D/2L_b$
R_0 = outside radius of shell
R_c = radius to centroidal axis of the combined stiffeners and shell of effective width L_e (see Fig. 14.1)
n = number of circumferential lobes existing at collapse
L_f = center-to-center spacing of stiffening rings
L_b = length of shell between bulkheads (or stiffening elements with sufficient stiffness to act as bulkheads) (see Fig. 14.1)
I_e = effective moment of inertia about the centroid of a section comprising one stiffener plus an effective width of shell, L_e

The effective width of a shell acting as part of the stiffener may be determined by

$$L_e = F_1 L + b \tag{14.48a}$$

where L is the unsupported length of the shell between stiffeners and

$$F_1 = \frac{2\cosh\theta - \cos\theta}{\theta \sinh\theta - \sin\theta} \tag{14.48b}$$

where $\theta = 1.818L/D\sqrt{D/t}$ when $\mu = 0.3$ (Eq. 14.37) and $b =$ contact width between stiffener and shell. The value L_e can be approximated by $1.1\sqrt{Dt} + b$ when $\theta > 2$, and $L + b$ when $\theta < 2$.

The first term in Eq. 14.47 is the shell term and is identical to the last term of Eq. 14.30. It is important only for shells with large D/t and low L/D ratios. The second term of Eq. 14.47 is the Levy formula for determining the critical uniform radial load on a circular ring [see discussion of Timoshenko and Gere (1961, pp. 287–392)] and in many cases is sufficiently accurate for design purposes.

The correct value of n is that which gives a minimum value of p in Eq. 14.47. The number of waves in a buckle pattern is determined by the restraint of adjoining stiffeners, heads, or diaphragms and the distance between them (spacing). When there are no effective restraints, $n = 2$. However, where heads, diaphragms, and/or large stiffeners are used to restrain the ends or are spaced along the length of the cylinder between which intermediate smaller rings are attached, n becomes greater but will be less than 10 for most shells of interest. The ASME code (1980) does not recognize the restraint at the ends of a vessel and assumes that $n = 2$. Use of this approximation in design can lead to very conservative ring sizes.

Except for large value of θ where n equals 2 and the second term of Eq. 14.47 is dominant, the desired stiffener size for a particular pressure must be determined by trial procedures. However, the largest effective stiffener size achieved is when the critical general buckling pressure of Eq. 14.47 is equal to that from the appropriate equation in Table 14.2 for buckling of the shell between stiffeners.

The formula for general instability developed by Bryant (1954) is dependent on the distance between large rings (any diaphragm or bulk-head is equivalent to a large ring in preventing buckling). In practice, many designs involve small, uniform rings evenly spaced, and at greater intervals of spacing there may be incorporated intermediate heavy rings, again of uniform but different cross section. Although theoretical solutions for the critical pressure with this stiffening arrangement have been formulated (Kendrick, 1953a,b; Reynolds, 1957), an empirical equation (Blumenberg, 1965) that agrees quite well with test results is recommended:

$$p_c = \frac{(I_E - I_c)(p_F - p_B)}{I_{FE} - I_e} + p_B \tag{14.49}$$

where

$$I_{FE} = \frac{p_F L_f R_0 R_d^2}{E(n^2 - 1)}$$

and n is the number of buckling lobes as determined by using p_B.

I_E = moment of inertia of large stiffener plus effective width of shell L_E
I_{FE} = value of I_E that makes the large stiffener fully effective, that is, equivalent to a bulkhead
L_e = L_e of Eq. 14.48
$L_E = F_1 L(A_s/A_S) + b$
L_f = center-to-center spacing of large stiffeners
P_F = critical pressure determined by Eq. 14.47, where $L_b = L_f$
p_B = critical pressure determined by Eq. 14.47 assuming the large stiffeners are the same size as the small stiffeners
R_d = radius to centroidal axis of the large stiffener plus effective width of shell L
A_s = area of small stiffener plus total area of shell between small stiffeners
A_S = area of large stiffener plus total area of shell between small stiffeners
$R_0 = b$, and I_c as in Eq. 14.47 and F_1 from Eq. 14.48b

Inelastic General Instability. Reynolds (1971) states that all the inelastic results can be summed up by one simple formula that came from the work of Bijlaard (1949). If the elastic buckling pressure of a structure can be expressed in the form

$$p_c = E(C_a + C_b) \tag{14.50}$$

in which C_a is a term that represents the membrane stiffness and C_b the bending stiffness of a stiffened cylinder, the inelastic buckling pressure can be written as

$$p_c = \sqrt{E_s E_t} C_a + E_t C_b \tag{14.51}$$

where E_s and E_t are the secant and tangent moduli, respectively, in the inelastic region. Therefore, $\sqrt{E_s E_t}$ would be used in place of E in the first term of Eq. 14.47, whereas E_t would replace E in the second term of Eq. 14.47.

Determination of the moduli to be used in Eq. 14.51 requires a knowledge of the stress field at the stiffener and in the shell midway between stiffeners. Since first yielding at the stiffeners is localized, it does not appreciably alter the elastic distribution of stresses between the stiffener region and the shell between stiffeners (Lunchick, 1959). Therefore, using $\nu = 0.3$ and assuming that the stiffener width is negligible compared to the spacing between stiffeners, the circumferential stresses are given by (Pulos and Salerno, 1961).

$$\sigma_\phi = \begin{cases} -\dfrac{0.85pR_0L_e}{A_f + L_e t} & \text{at the stiffener} \quad (14.52a) \\ -\dfrac{pD}{2t}\left[1 - \dfrac{0.85A_f}{A_f + L_e t}F(\theta)\right] & \text{in the shell} \quad (14.52b) \end{cases}$$

where

$$F(\theta) = \begin{cases} 1 & \text{for } \theta \leq 1 \\ 1.33 - 0.33\theta & \text{for } 1 < \theta < 4 \\ 0 & \text{for } \theta \leq 4 \end{cases}$$

and θ is defined in Eq. 14.37.

The longitudinal stresses at both locations are given by

$$\sigma_x = -\frac{pD}{4t} \tag{14.52c}$$

As in the case of inelastic buckling of unstiffened cylinders, the stress intensity of Eq. 14.39 based on the distortion energy yield criterion is calculated at the two locations and the moduli are determined from a representative stress-strain curve of the material. The ASME charts similar to Fig. 14.8*b* may also be used to determine a reduced modulus $E_r = 2B/A$.

More precise equations and charts for determining the circumferential stress when the stiffener width is not negligible are available from Krenzke and Short (1959) and Pulos and Salerno (1961) to be used in place of Eqs. 14.52a and 14.52b. Also, a more exact formulation of a collapse pressure based on a three-hinge mechanism of failure of the shell between stiffeners is presented by Lunchick (1959).

Effect of Imperfection. In addition to the effects of shell imperfections discussed under unstiffened cylinders, the initial out-of-roundness of the stiffener rings is equally important in determining the redution in the general instability strength of a stiffened shell under external pressure. Analytical studies of the effects of stiffener out-of-roundness were first considered by Kendrick (1953a,b). Hom (1962), assuming a more realistic out-of-roundness function, developed a method for determining the maximum bending stress introduced in the stiffener flange by stiffener eccentricity. Hom also developed an approximate formula for this bending stress.

$$\sigma_b = \pm\frac{16}{\pi}\left[\frac{Ee_f e}{D^2}(n^2 - 1)\frac{p}{p_c - p}\right] \tag{14.53}$$

where

n = number of circumferential buckling lobes (corresponding to n from Eqs. 14.47 and 14.49
e_f = distance from midthickness of the shell to the extreme fiber of stiffener, positive for internal stiffener and negative for external stiffener
p = applied pressure
p_c = critical pressure for perfect ring-stiffened cylinder (Eq. 14.47 or 14.49)
e = radial eccentricity from a true circle

Equation 14.53 is applicable only in the elastic range.

Another type of stress is introduced if the stiffener is initially tilted or twisted. In this case the radial forces do not pass through the centroid of the cross section of the stiffener, and a twisting moment results. When the radial stress in the web and the circumferential stress in the flange become excessive, yielding can result and cause crippling of the stiffeners, thereby precipitating collapse in the general instability mode. For outside stiffeners these radial forces induce a twist that tends to reduce the initial tilt, whereas for internal stiffeners this radial force tends to increase the tilt.

The total stress in the flange is the sum of the hoop stress σ_ϕ, the bending stress σ_b in the plane of the ring, and any tilt-induced stress. A method for calculating the latter stress is given by Wenk and Kennard (1956).

Torsional buckling of the stiffeners has also been considered by Farmer (1966) and Wah (1967). They make the overly conservative assumptions that the shell offers no resistance to twisting and that the torsional failure of the stiffener is independent of the in-plane stiffener buckling mode. A comparison of their predicted buckling pressures with test results (Blumenberg, 1965) indicates that their formula is ultraconservative. Experience indicates that if the stiffeners are symmetrical sections and are proportioned to satisfy the compact section requirements of the AISC specification, torsional buckling will not occur.

Inelastic Action. Because of the complexity of the effects that inelastic action has on the correct prediction of critical buckling pressures of imperfect cylinders, no definitive guidance is available to offer the designer at this time.

14.5 STRINGER- OR RING-AND-STRINGER-STIFFENED CYLINDER

Stringer (longitudinal) stiffeners are primarily used to increase the axial or bending load capacities of cylinders. They can be used either alone or in combination with ring stiffeners. Due to the greater number of parameters involved and the multiple potential mechanisms of failure, it is virtually impossible to achieve a universal set of design formulas substantiated by tests. Therefore, this section of the chapter is limited to a general discussion of the methods that can be used to evaluate the critical axis stress and critical pressure.

14.5.1 Nonpressure Loadings

Stiffeners may be placed on the outside of the shell (positive eccentricity), on the inside of the shell (negative eccentricity), or a combination of both may be employed, such as stringers on the outside and rings on the inside. However, Hutchinson and Amazigo (1967) point out that based on large-deflection

theory, shells with external stiffening are more sensitive to imperfections. Quite to the contrary, Singer (1967) claims that stiffened shells are relatively insensitive to imperfections. The conflicting results are typical and illustrate why only a general discussion of the action of stiffened cylinders axial loading is included.

To check the design of a stiffened cylindrical shell subjected to axial compression, the following forms of failure should be considered:

1. Overall column buckling or yielding
2. Local buckling encompassing several stiffeners
3. Local buckling between stiffeners (panel buckling)
4. Buckling of individual stiffeners
5. Local yielding of the shell or the stiffeners

The possibility of overall column buckling can be studied by including the stringers in the calculation of the radius of gyration of the column cross section. Circumferential stiffeners have no direct effect on the overall column-buckling mode.

In many cases, close stringer spacing allows their being treated as if they were uniformly distributed on the shell's circumference. Under this assumption, the stiffened shell can be modeled as an equivalent orthotropic shell. This approach is often used to investigate the possiblity of local buckling encompassing several stiffeners. If closely spaced, ring stiffeners can similarly be considered as being uniformly distributed along the axial direction; however, their spacing is normally such that they should be considered discretely spaced.

Spacing of longitudinal stiffeners (stringers) must be close enough to prevent panel buckling between the stiffeners. If both the stringers and the rings are sufficiently rigid, the cylinder can be treated as a series of curved panels each of which is supported along four edges. The buckling behavior of these curved panels is very similar to that of an entire cylinder. If the panel is short and its curvature is small, the panel buckles essentially as if it were a flat plate (as treated in Chapter 4) and the critical stress is given by Eq. 14.54.

$$\sigma_{sc} = \frac{k\pi^2 E}{12(1-\nu^2)(L_s/t)^2} \tag{14.54a}$$

where

$$K = \begin{cases} \left(\dfrac{L_s}{L} + \dfrac{L}{L_s}\right)^2 & \text{for } L/L_s < 1 \quad (14.54b) \\ 4.0 & \text{for } L/L_s \geq 1 \quad (14.54c) \end{cases}$$

In the above, L is the axial distance between circumferential stiffeners and L_s is the circumferential distance between longitudinal stringers (Fig. 14.1).

Long panels of sufficient curvature behave in the same manner as do moderately long cylinders. To obtain a rough estimate of the elastic buckling strength of moderately curved panels, Timoshenko and Gere (1961) suggest that Eq. 14.4 be used. When the axial and circumferential dimensions of the panel are about equal and the central angle subtended by the panel is less than $\frac{1}{2}$ rad, C may be taken equal to 0.6.

Buckling of individual stiffeners can be investigated by treating the stiffener and an effective width of the shell as a column. For example, the critical load of a typical stringer and the effective shell skin is obtained by assuming the stringer to behave like a column on an elastic foundation. The circumferential rings act as the foundation, and depending on their spacing and area, the foundation is considered to be continous or made up of elastic or rigid point supports.

Local yielding of the shell or stiffeners is perhaps more of a stress-analysis problem than a stability problem, but it must be given consideration. The designer must keep one point in mind when adding stiffeners to overcome a shell-stability problem. It is possible that the added stiffener is so rigid compared to the shell (that it is supposed to reinforce) that the stiffener becomes the main load-carrying component of the assemblage. For a further discussion of stiffened-plate behavior, refer to Chapter 4.

14.5.2 Uniform External Pressure

Stringer stiffeners are not generally used to increase the critical external pressure of a cylinder. Ring stiffeners are preferred for pressure loading, but in cases when the cylinder must withstand several loading conditions, stringer stiffeners may also be present. If stringers are spaced more closely than the buckling wave length of the shell, they will increase the critical pressure. Test programs are currently under way to study the influence of size and spacing of stringer stiffeners on the critical pressure, but little definitive information is presently available.

14.6 EFFECTS ON COLUMN BUCKLING

The basic column curves for tubular members subjected to axial compression are discussed in Chapter 3. The designer should, however, be aware of situations when these require some modification or interpretation to ensure that the proper critical axial stress is predicted.

14.6.1 Interaction Between Column and Local Buckling

For many practical applications, when the D/t ratio of a member is such that local buckling is probable, the KL/r ratio of the member may be such that column buckling is also an important consideration. One way to establish the allowable load for such a member is to use an allowable load based on the smaller of the loads derived from local buckling and overall column behavior.

A different and recommended approach (Marshall, 1971) is also used when designing light-gage cold-formed steel structural members for determining allowable loads for sections whose geometry and material properties are such that both local buckling and column buckling are important considerations. This approach is best explained with an example. Referring to Fig. 14.10, assume that a column is to be designed according to curve A; however, assume that theoretically, local-buckling limits the useful column loading to 30 ksi. In this approach, the local-buckling strength is substituted for σ_y in the appropriate column formula to yield the curve C. A similar approach is taken by AISC in appendix C of its specification. For a more complete discussion of both possible methods of analysis, refer to Chapter 4 for a simple treatment with respect to flat plates.

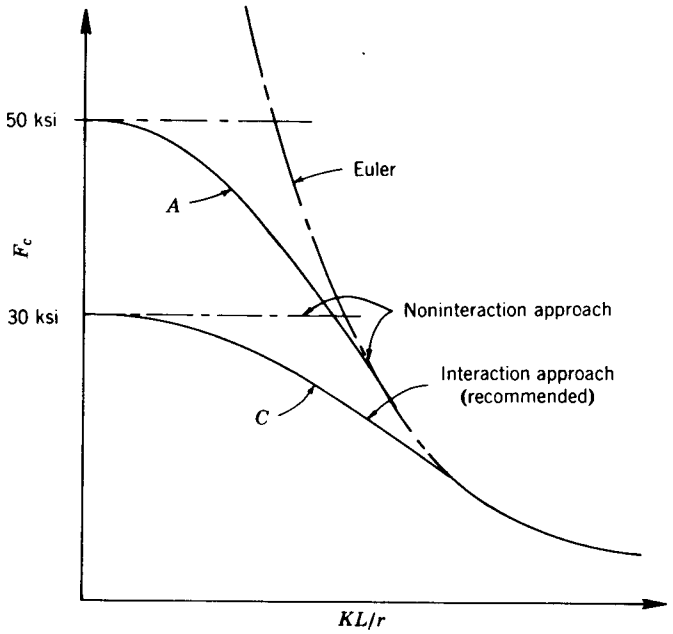

Fig. 14.10 Interaction of local buckling and column buckling.

14.6.2 Effect of Fluid Pressure on Overall Column Buckling

The influence of pressure on the overall stability of tubular members is normally not a structural consideration; however, in the oil industry, tubular members transmitting fluids from deep oil and gas wells have experienced failures of this type (Lubinski, 1951; Lubinski et al., 1962). In this type of problem, the cylinder is not closed ended and the pressure does not create longitudinal stresses.

The fact that pressures can influence column stability was recognized by Prescott (1946) and was discussed more recently in publications with theoretical derivations (Seide, 1960, Flügge, 1973) and has been experimently confirmed (Palmer and Baldry, 1974).

A free-body diagram of an element of an open-ended cylindrical member subjected to internal pressure is shown in Fig. 14.11. It can be seen that an effective axial compressive force on the element results from the internal pressure. This force can influence the stability of the column by adding to or subtracting from any preexisting axial force.

Figure 14.12 shows an example where internal pressurization alone can cause a cylindrical tube to buckle. In this illustration, two frictionless pistons at the tube ends contain the fluid within the tube. The pressure force on the pistons is restrained by the cable connecting the two pistons. With no external pressure or applied load, the effective buckling force is $p_1 A_1$. In this illustration the end conditions are essentially pinned and the elastic buckling pressure will be given by the corresponding Euler formula:

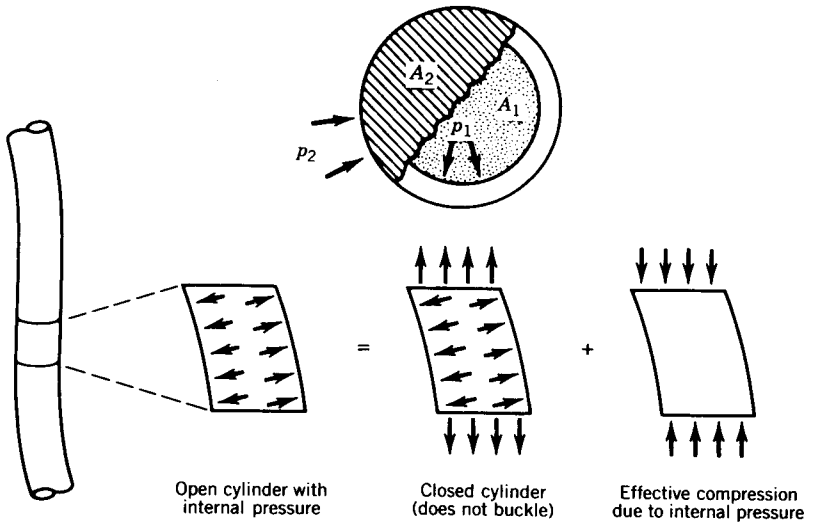

Fig. 14.11 Equilibrium of column subjected to internal pressure.

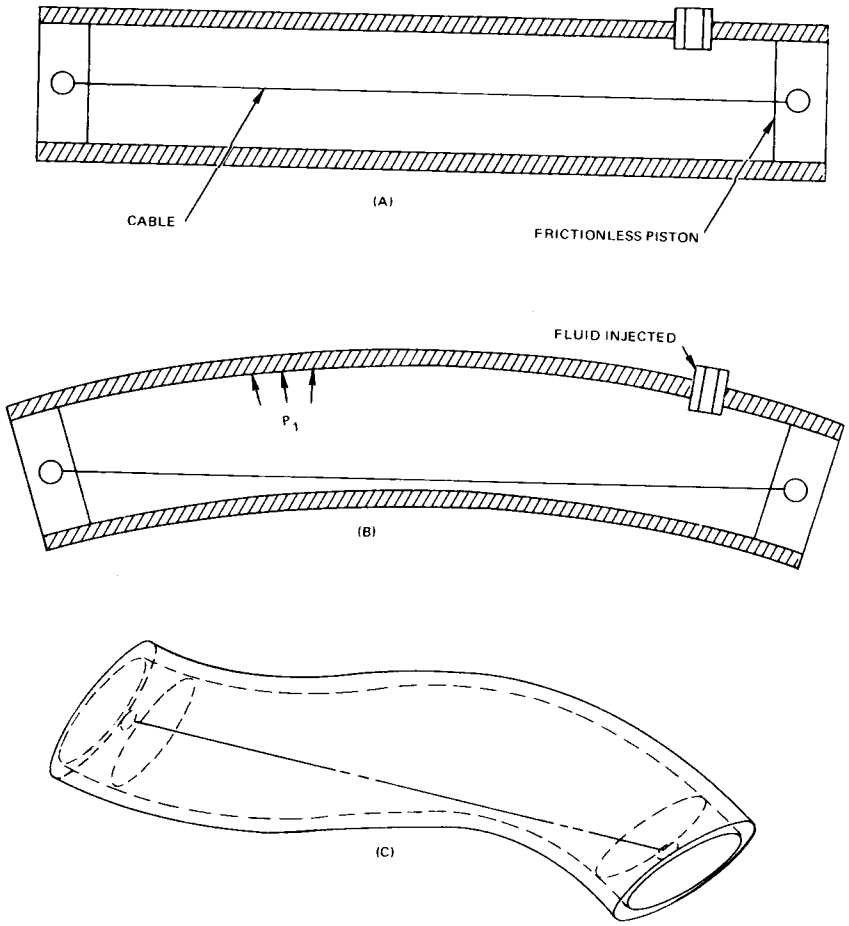

Fig. 14.12 Buckling under internal pressure.

$$p_1 = \frac{\pi^2 EI}{A_1 L^2} \tag{14.55}$$

The buckled shape will be sinusoidal until, with continued fluid injection, the inner wall contacts the cable. At that point the buckling will stop in the plane shown and additional pressurization will cause a deformation out of plane that leads to a helical shape for the buckled tube.

In contrast, a close-ended cylinder subjected to internal pressure will not suffer general instability as the compressive force will be balanced by the tensile force from the end closures. The resulting effective force is zero.

In a membrane shell where the walls of the shell are incapable of maintaining compression, internal pressurization will allow the pressurized membrane to support a column load by virtue of a prestressing effect in the membrane. A good example is a cylindrical rubber balloon, which has column strength only if inflated.

The axial tension force $p_2 A_2$ and other effects resulting from external pressure acting alone can be deducted from the free-body diagram of Fig. 14.11. Hence in the presence of external and internal pressures, the overall stability of the column will depend on an effective compressive force given by

$$P_e = P + p_1 A_1 - p_2 A_2 \tag{14.56}$$

where

P_e = effective-buckling force
P = any preexisting axial compression in the column
p_1 = internal pressure
p_2 = external pressure
A_1 = internal area of the cylinder
A_2 = external area of the cylinder

14.7 CYLINDERS SUBJECTED TO COMBINED LOADINGS

14.7.1 Combined Nonpressure Loadings

Gerard and Becker (1957) present intraction formulas together with experimental verification for several conditions of combined nonpressure loadings. Included among these are: (1) axial compression and bending; (2) axial compression and torsion; (3) axial compression, bending, and torsion; and (4) bending and torsion. Although a slightly different interaction equation is proposed for each case, Schilling (1965) suggests that a single formula can be conservatively applied to all these combinations. He proposes the relation

$$\frac{\sigma}{\sigma_{xc}} + \left(\frac{\tau}{\tau_c}\right)^2 = 1 \tag{14.57}$$

in which σ and τ are the normal and shear stress, respectively, that must be applied simultaneously to cause failure; σ_{xc} is the critical stress for axial compression; and τ_c is the critical stress for torsion or transverse shear applied alone. If both axial compression and bending are present, it is conservative to consider σ as the sum of the two normal stresses. Schilling implies that this procedure is sufficiently accurate for use in both the elastic and inelastic stress ranges.

14.7.2 Axial Stress in Combination with Internal or External Pressure

Since radial stresses may be neglected in structural cylinders of usual proportions (D/t exceeding about 12), this topic is concerned with the interaction of hoop stresses caused by pressure and axial stresses resulting from a combination of axial load, bending, and hydrostatic pressure. In the general case, shear stresses may also be present. The overall problem is illustrated in Fig. 14.13, where the general yield failure of thick-walled cylinders based on the maximum strain energy theory is shown. Ellipses have been plotted for Poisson's ratio of 0.3 and 0.5.

The applicability of this criterion to the general yielding situation has been demonstrated analytically and experimentally (Holmquist and Nadai, 1939) and has been further validated by some 200 tests with oil well casings having yield strengths from 30 to 80 ksi (Edwards and Miller, 1939). It was found that Poisson's ratio varied between 0.3 and 0.5 during inelastic action and an average value of 0.4 was recommended. However, a somewhat simpler method of evaluating yield is to determine a stress intensity

$$\sigma_i = (\sigma_\phi^2 + \sigma_x^2 - \sigma_\phi \sigma_x + 3\tau^2)^{0.5} \tag{14.58}$$

where σ_ϕ is the circumferential stress, σ_x is the total axial stress resulting from any combination of load, bending, and hdyrostatic pressure, and τ is the shear stress at the same location as the maximum σ_x. The yield criterion obtained by equating σ_i to the uniaxial yield stress is the Hencky–von Mises distortion energy criterion that corresponds to the ellipse in Fig. 14.13 for Poisson's ratio equal to 0.5.

The four quadrants of Fig. 14.13 represent the types of interaction between axial stress and pressure. In addition to general yielding, instability interactions must also be considered. An overview of the general problem is obtained by recognizing that the positive intercepts of the ellipse in Fig. 14.13 are not subject to reductions due to instability (pure tension for the abscissa intercept and pure internal pressure for the ordinate). The negative intercepts, however, will not be achieved in thin cylinders due to buckling under axial compression or external pressure. The instability interaction in the four regions is discussed in the following.

Tension in Combination with Internal Pressure. Since there is no instability mode in this region, only the yield criterion need be considered. The general criterion of Eq. 14.58 may be used, or it would be reasonable and only slightly conservative to neglect the interaction and consider the effects separately.

Tension in Combination with External Pressure. This combination of loading can lead to a phenomenon referred to as a propagating buckle. An

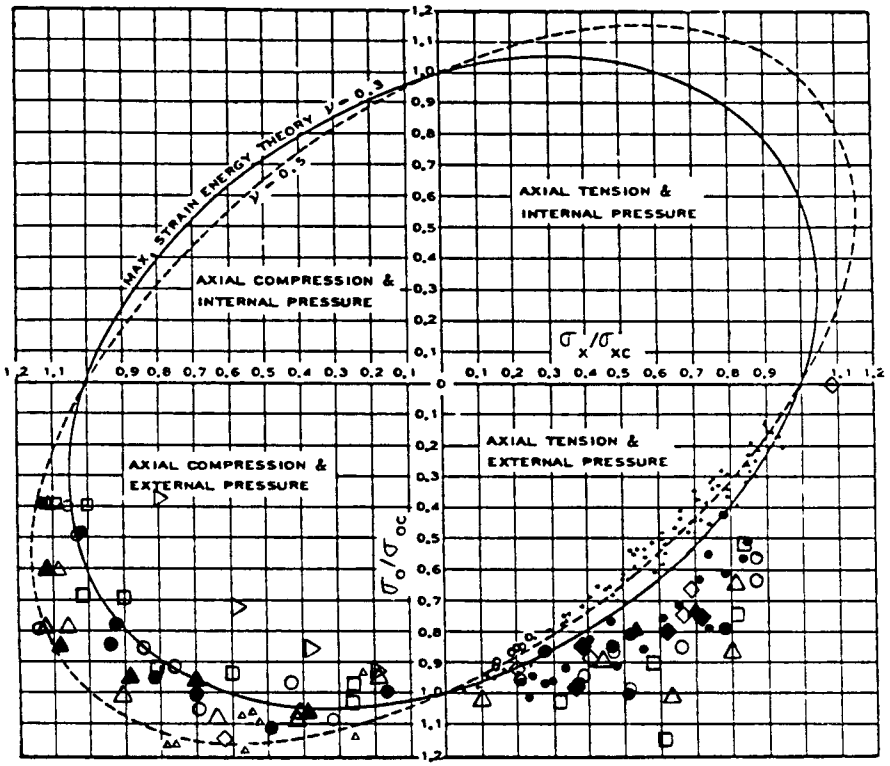

Fig. 14.13 Normalized ellipse of biaxial yield stresses and data for combined pressure and axial load.

indentation develops at a point around the circumference and spreads along the length of the cylinder.

Since the tension component does not lead directly to a stability failure, the results of the interaction are usually expressed in terms of a reduced critical external pressure stress, $\sigma'_{\phi c}$. Two approaches are used to obtain $\sigma'_{\phi c}$, one being a standard interaction equation and the other a reduced yield strength in the critical pressure (or stress) equations.

The interaction approach assumes an elliptic relation similar to the form for general yielding. However, the normalization of the hoop stress is based on the critical stress for pressure only rather than on yield. This results in

$$\left(\frac{\sigma_x}{\sigma_y}\right)^2 + \left(\frac{\sigma'_{\phi c}}{\sigma_{\phi c}}\right)^2 + \frac{\sigma_x}{\sigma_y}\frac{\sigma'_{\phi c}}{\sigma_{\phi c}} = 1 \tag{14.59}$$

where σ_x is the imposed axial stress, $\sigma_{\phi c}$ the reduced critical hoop stress $= p'_c/D2t$, σ_y the yield stress, and $\sigma_{\phi c}$ the critical hoop stress when no axial loading is imposed. This normalization has been used to plot the data in Fig. 14.13, where it can be observed that it is conservative for the collapse failures.

The API (1989) procedure uses an effective loop yield stress σ_{yr}, obtained by solving

$$\left(\frac{\sigma_{yr}}{\sigma_y}\right)^2 + \frac{\sigma_{yr}}{\sigma_y}\frac{\sigma_x}{\sigma_y} + \left(\frac{\sigma_x}{\sigma_y}\right)^2 = 1 \tag{14.60}$$

The critical pressure can be obtained as the value of p_y in Eq. 14.44 using σ_{yr} or in place of σ_y. It is also possible to use in empirical design curves that include inelastic and out-of-roundness effects in place of Eq. 14.44.

A variation on the reduced-yield approach is to base the inelastic properties on the stress intensity:

$$\sigma_i = [(\sigma'_{\phi c})^2 + \sigma_x^2 - \sigma_x \sigma'_{\phi c}]^{0.5} \tag{14.61}$$

Again the collapse pressure is based on Eq. 14.44 and the p_c term is based on the equations of Table 14.2 using a reduced modulus of elasticity

The approaches used with Eqs. 14.60 and 14.61 are not as conservative as the interaction equation (E1. 14.59). It is also important to note that all of the methods just discussed are for ultimate conditions. Actual design is more complicated in that different factors of safety are desirable for tension yielding and pressure collapse. Iterative solutions are required to obtain optimal designs from given tension and hydrostatic design loads.

Compression in Combination with External Pressure. For very stocky cylinders for which failure occurs by general yielding, Fig. 14.13 indicates that it would be conservative and reasonable to ignore the interaction between axial compression and external pressure. However, for cylinders the larger D/t ratios, for which both external pressure and axial loading may result in a collapse failure mode, the two stresses acting on a preexisting imperfection often have an additive effect. The construction shown in Fig. 14.14 has been suggested (Johns et al., 1975, 1976). This construction is conservative when compared to available bending and collapse test data (Johns et al., 1975, 1976) and with axial compression and external pressure tests (Miller and Vojta, 1984).

Compression in Combination with Internal Pressure. The exact design of cylinders subjected to a combination of axial compression and internal pressure is a very complicated procedure. The following offers an approximate procedure that should be sufficiently accurate for most design purposes.

Many tests have been conducted (Lo et al., 1951; Fung and Sechler, 1957; Gerard, 1957; Seide, 1960; Baker et al., 1968; Mungan, 1974) which show that internal pressure increases the axial-buckling stress as long as the failure stress remains elastic. A graphical method has been developed by Baker for determining this increase. The following equation (from Baker, 1951), when used in conjunction with Fig. 14.15 can be used for cylinders when the effective stress σ_i (from Eq. 14.61) is less than the proportional limit.

$$\sigma_x < \sigma_{xc} + 2\overline{\Delta C}\frac{Et}{D} \tag{14.62}$$

with σ_{xc} determined from Section 14.3.1 and $\overline{\Delta C}$ from Fig. 14.15. When σ_i is greater than the proportional limit, the second term is no longer valid and therefore

$$\sigma_x \leq \sigma_{xc} \tag{14.63}$$

with σ_x determined from Section 14.3.1.

14.8 STRENGTH AND BEHAVIOR OF DAMAGED AND REPAIRED TUBULAR COLUMNS

There are presently (1997) over 3500 major offshore fixed platforms devoted to the mining of crude oil in U.S. waters alone (Ricles et al., 1995). These structures are constructed from steel tubular members and they exist in a hazardous environment, being constantly in danger of collision with marine vessels and dropped objects, which can cause damage consisting of *dent damage* and *out-of-straightness*. Some of these dents may be quite large, resulting in significant changes of the original cross section. The marine environment also exposes the

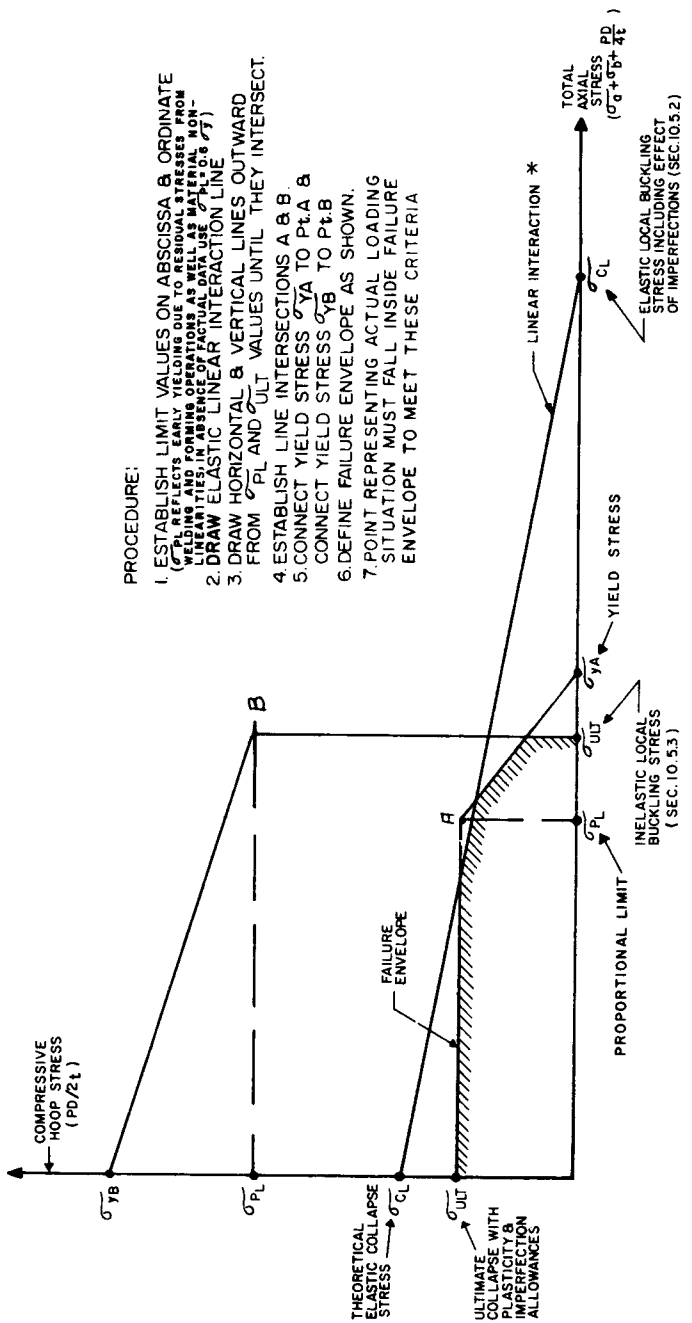

* ALTERNATIVELY THE PARABOLIC RELATIONSHIP GIVEN BY $\left[\frac{\sigma_x}{\sigma_{xc}}\right]+\left[\frac{\sigma_\phi}{\sigma_{\phi c}}\right]^2 \leq 1$

Fig. 14.14 Construction of composite failure envelope for interaction of combined compressive loadings.

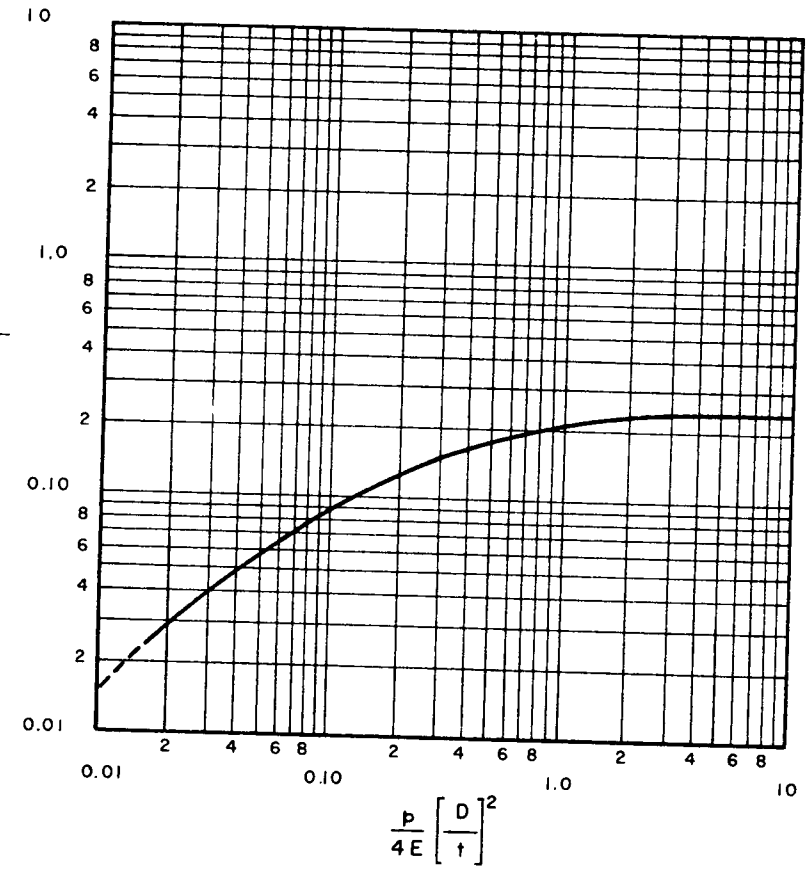

Fig. 14.15 Increase in axial compressive elastic buckling stress due to internal pressure (Baker et al., 1968).

tubes to corrosion, requiring the use of counteractive corrosion measures, such as cathodic protection systems or protective coatings. Despite these precautions there are numerous cases reported of platform members that have sufferend corrosion damage.

Because it is essential that the structural integrity of the platforms be maintained during their intended lifetime, it is necessary to be able to assess the remaining strength of a damaged tubular member and to provide a satisfactory repair procedure if that strength is inadequate. The strength of members with dents, both with and without out-of-straightness, has been a subject of extensive research since the late 1970s (Smith et al., 1981; Padula and Ostapenko, 1989; MacIntyre, 1991; Landet and Lotsburg, 1992; Duan et al., 1993; Salman, 1994). A tabular historic description and evaluation of this research has been prepared by Salman (1994). The strength of severely corroded tubular columns

was extensively studied by Padula and Ostapenko (1989), Ostapenko et al. (1993) and Hebor and Ricles (1994). The significant corrosion damage occurs in patches anywhere on the surface of the tube. Damaged tubes are strengthened when necessary by internal or external grouting and around the damaged portions of the member. Research on such tubes is reported in Parsanejad (1987), Parsanejad and Gusheh (1992), Ricles et al. (1994, 1995) and Ricles (1995). Computer methods for the analysis of the strength of internally grout repaired damaged members are available in Ricles (1995), and formulas for ultimate strength have been developed by Parsanejad (1987), Parsanejad and Gusheh (1992), and Ricles et al. (1994) for damaged and repaired tubular steel members.

REFERENCES

AA (1994), "Specifications for Aluminum Structures," Aluminum Association, Washington, D.C., Apr.

Ades, C. F. (1957), "Bending Strength of Tubing in Plastic Range," *J. Aeronaut. Sci.*, Vol. 24, pp. 605–610.

AISC (1993), *Load and Resistance Factor Design Specification for Structural Steel Buildings*, American Institute of Steel Construction, Chicago, IL.

AISI (1991), *Load and Resistance Factor Design Specification for Cold-Formed Structural Steel Members*, American Iron and Steel Institute, Washington, D.C.

Almroth, B. O. (1966), "Influence of Edge Conditions on the Stability of Axially Compressed Cylindrical Shells," *AIAA J.*, Vol. 4, No. 1, pp. 134–140.

API (1977), *API Specification for Fabricated Structural Steel Pipe*, API Spec. 2B, 3rd., American Petroleum Institute, Division of Production, Washington, D.C., Nov.

API (1989), *API Recommended Practice for the Planning, Design, and Construction of Fixed Offshore Platforms*, RP2A, 18th ed., American Petroleum Institute, Division of Production, Washington, D.C., September.

ASME (1980), *Boiler and Pressure Vessel Code*, Section VIII, *Pressure Vessels*, Div. 1, American Society of Mechanical Engineers, Washington, D.C., New York.

AWWA (1967), *AWWA Standard for Steel Tanks—Standpipes, Reservoirs, and Elevated Tanks—for Water Storage, AWWA D100-67*. American Water Works Association, Denver, Colo.

Baker, E. H., et al. (1968), *Shell Analysis Manual*, NASA CR-912, Apr.

Ball, W. E. (1962), "Formulas and Curves for Determining the Elastic General-Instability Pressures of Ring-Stiffened Cylinders," *David Taylor Model Basin Rep. No. 1570*, Jan.

Basdekas, N. L. (1966), "A Survey of Analytical Techniques for Determining the Static and Dynamic Strength of Pressure-Hull Shell Structure," *David Taylor Model Basin Rep. No. 2208*, Sept.

Batdorf, S. B. (1947), "A Simplified Method of Elastic Stability Analysis for Thin Cylindrical Shells," *NACA Rep. No. 874.*

Batdorf, S. B., Schildcrout, M., and Stein, M. (1947a), "Critical Stress of Thin-Walled Cylinders in Axial Compression," *NACA Tech. Note No. 1343.*

Batdorf, S. B., Schildcrout, M., and Stein, M. (1947b), "Critical Stress of Thin-Walled Cylinders in Torsion," *NACA Tech. Note No. 1344*, July.

Becker, H. (1958), "General Instability of Stiffened Cylinders," *NACA Tech. Note No. 4327*, July.

Bijlaard, P. P. !949), "Theory and Tests on the Plastic Stability of Plates and Shells," *J. Aeronaut. Sci.*, Vol. 16, No. 9.

Birkemoe, P. C., Prion, H. G. L., and Sato, J. A. (1983), "Compression Behavior of Unstiffened Fabricated Steel Tubes," *ASCE Annu. Conv. Struct. Cong.*, Oct.

Blumenberg, W. F. (1965), "The Effect of Intermediate Heavy Frames on the Elastic General-Instability Strength of Ring-Stiffened Cylinders Under External Hydrostatic Pressure," *David Taylor Model Basin Rep. No. 1844*, Feb.

Bodner, S. R.(1957), "General Instability and Ring-Stiffened Circular Cylindrical Shell Under Hydrostatic Pressure," *J. Appl. Mech.*, Vol. 24, No. 2, pp. 269–277.

Bodner, S. R., and Berks, W. (1952), "The Effect of Imperfections on the Stresses in a Circular Cylindrical Shell Under Hydrostatic Pressure," *PIRAL Rep. No. 210*, Polytechnic Institute of Brooklyn, New York, Dec.

Boichot, L., and Reynolds, T. E. (1964), "Inelastic Buckling Tests of Ring-Stiffened Cylinders Under Hydrostatic Pressure," *David Taylor Model Basin Rep. No. 1992*, May.

Brazier, L. G. (1927), "On the Flexure of Thin Cylindrical Shells and Other Thin Sections," *Proc. R. Soc. London*, Vol. A116, pp. 104–114.

Bryant, A. R. (1954), "Hydrostatic Pressure Buckling of a Ring-Stiffened Tube," *Rep. No. R-306*, Naval Construction Research Establishment, Washington, D.C.

Chen, W. F., and Ross, D. A. (1978), "Tests of Fabricated Tubular Columns," Fritz Eng. Lab., *Rep. No 393.8*, Lehigh University, Bethlehem, Pa., Sept.

Clark, J. W., and Rolf, R. L. (1964), "Design of Aluminum Tubular Members," *ASCE J. Struct. Div.*, Vol. 90, No. ST6, p. 259.

DeHeart, R. C., and Basdekas, N. L. (1960), "Yield Collapse of Stiffened Circular Cylindrical Shells," *Report under NOMR Contract NR 2650(00), Proj. NR 064-435*, Southwest Reseach Institute, San Antonio, Tx, Sept.

Denton, A. A., and Alexander, J. M. (1963a), "On the Determination of Residual Stresses in Tubes," *J. Mech. Eng. Sci.*, Vol. 5, No. 1, pp. 75–88.

Denton, A. A., and Alexander, J .M. (1963b), "New Method for Measurement of Local Residual Stresses in Tubes," *J. Mech. Eng. Sci.*, Vol. 5, No. 1, pp. 89–90.

Donnell, L. H. (1934), "A New Theory for the Buckling of Thin Cylinders Under Axial Compression and Bending," *Trans. ASME*, Vol. 56.

Donnell, L. H. (1956), "Effect of Imperfections on Buckling of Thin Cylinders Under External Pressure," *J. Appl. Mech.*, Vol. 23, No. 4, p. 569.

Donnell, L. H., and Wan, C. C. (1950), "Effect of Imperfections on Buckling of Thin Cylinders and Columns Under Axial Compression," *J. Appl. Mech.*, Vol. 17, No. 1.

Duan, L., Chen, W. F., and Loh, J. T. (1993), "Moment-Curvature Relationships for Dented Tubular Sections," *ASCE J. Struct. Eng.*, Vol. 119, No. ST3, pp. 809–831.

Eder, M. F., Grove, R. B., Peters, S. W., and Miller, C. D. (1984), "Collapse Tests of Fabricated Cylinders Under Combined Axial Compression and External Pressure," *Final Rep., American Petroleum Institute Proj. 83-46*, CBI Industries, Inc., Research Laboratory, Plainfield, Ill., Feb.

Edwards, S. H., and Miller, C. P. (1939), "Discussion on the Effect of Combined Longitudinal Loading and External Pressure on the Strength of Oil-Well Casing," *Drilling and Production Practice*, American Petroleum Institute, Washington, D.C., pp. 483–502.

Farmer, L. E. (1966), "Method for Determining Buckling Loads of Circular Stiffening Rings Including Consideration of Torsional Displacement," *AEDC-TR-66-188*, Engineering Support Facility, Washington, D.C., Sept.

Flügge, W. (1932), "Die Stabilität der Kreiszylinderschale," *Ing. Arch.*, Vol. 3.

Flügge, W. (1973), *Stresses in Shells*, 2nd ed., Springer-Verlag, New York, pp. 459–463.

Fung, Y. C., and Sechler, E. E. (1957), "Buckling of Thin Walled Circular Cylinders Under Axial Compression and Internal Pressure," *J. Aeronaut. Sci.*, Vol. 24, pp. 351–356.

Galletly, G. D., and Bart, R. (1957), "Effect of Boundary Conditions and Initial Out-of-Roundness on the Strength of Thin-Walled Cylinders Subjected to External Hydrostatic Pressure," *David Taylor Model Basin Rep. No. 1066*, Nov.

Gellin, S. (1980), "The Plastic Buckling of Long Cylindrical Shells Under Pure Bending," *Int. J. Solids Struct.*, Vol. 16, pp. 397–407.

Gerard, G. (1956), "Compressive and Torsional Buckling of Thin-Walled Cylinders in Yield Region," *NACA Tech. Note No. 3726.*

Gerard, G. (1957), "Plastic Stability Theory of Thin Shells," *J. Aeronaut. Sc.*, Vol. 24, No. 4, p. 269.

Gerard, G., and Becker, H. (1957), "Handbook of Structural Stability: Part 3. Buckling of Curved Plates and Shells," *NACA Tech. Note No. 3783*, Aug.

Graham, R. R. (1965), "Manufacture and Use of Structural Tubing," *J. Met.*, Vol. 17.

Harari, A., and Baron, M. L. (1970, 1971), "Buckling of Vessels Composed of Combinations of Cylindrical and Spherical Shells," *J. Appl. Mech.*, July 1970, pp. 393–398; July 1971, pp. 571–572.

Harris, L. A., et al. (1957), "The Stability of Thin-Walled Unstiffened Circular Cylinders Under Axial Compression Including the Effects of Internal Pressure," *J. Aeronaut. Sci.*, Vol. 24, No. 8, pp. 587–596.

Hebor, M., and Ricles, J. M. (1994), "Residual Strength and Repair of Corroded Marine Steel Tubulars," *ATLSS Rep. No. 94-10*, Lehigh University, Bethlehem, Pa.

Heise, O., and Esztergar, E. P. (1970), "Elastoplastic Collapse of Tubes Under External Pressure," *J. Eng. Ind.*, Vol. 92, pp. 735–742.

Hoff, N. J. (1966), "The Perplexing Behavior of Thin Cylindrical Shells in Axial Compression," *Isr. J. Technol.*, Vol. 4, No. 1.

Holmquist, J. L., and Nadai, A. (1939), "A Theoretical and Experimental Approach to the Problem of Collapse of Deep-Well Casing," in *Drilling and Production Practice*, American Petroleum Institute, Washington, D.C., pp. 392–420.

Holt, M. (1952), "A Procedure for Determining the Allowable Out-of-Roundness for Vessels Under External Pressure," *ASME Trans.*, Vol. 74, p. 1225.

Hom, K. (1962), "Elastic Stress in Ring-Frames of Imperfectly Circular Cylindrical Shells Under External Pressure Loading," *David Taylor Model Basin Rep. No. 1505*, May.

Hom, K., and Couch, W. P. (1961), "Hydrostatic Tests of Inelastic and Elastic Stability of Ring-Stiffened Cylindrical Shells Machined from Strain-Hardening Material," *David Taylor Model Basin Rep. No. 1501*, Dec.

Hutchinson, J. W., and Amazigo, J. C. (1967), "Imperfection-Sensitivity of Eccentrically Stiffened Cylindrical Shells," *AIAA J.*, Vol. 5, No. 3, pp. 392–401.

Jirsa, J. O., et al. (1972), "Ovaling of Pipelines Under Pure Bending," Pap. 1569, *4th Annu. Offshore Technol. Conf.*, Houston, Texas, May.

Johns, T. G., Mesloh, R. E., Winegardner, R., and Sorenson, J. E. (1975), "Inelastic Buckling of Cylinders Under Combined Loads," Pap. 2209, *7th Annu. Offshore Technol. Conf.*, Houston, Texas, May.

Johns, T. G., Sorenson, J. E., Mesloh, R. E., and Attenbury, T. J. (1976), "Buckling Strength of Offshore Platforms Program: Phase I," Battelle Institute, Columbus, Ohio.

Johnston, B. G.(1976), *Guide to Stability Design Criteria for Metal Structures*, Structural Stability Research Council, Wiley, New York, NY.

Kendrick, S. (1953a), "The Deformation Under External Pressure of Circular Cylindrical Shells with Evenly Spaced Equal Strength Nearly Circular Ring Frames," *Rep. No. R-259*, Naval Construction Research Establishment, Washington, D.C., Oct.

Kendrick, S. (1953b), "The Buckling Under External Pressure of Circular Cylindrical Shells with Evenly Spaced Equal Strength Circular Ring Frames: Part III," *Rep. No. R-259*, Naval Construction Research Establishment, Washington, D.C., Oct.

Kiziltug, A. Y., Grove, R. B., Peters, S. W., and Miller, C. D. (1985), "Collapse Tests of Short Tubular Columns Subjected to Combined Loads," *Final Rep. Contract No. UI-851604*, CBI Industries, Chicago, IL, Dec.

Korol, R. M. (1978), "Inelastic Buckling of Circular Tubes in Bending," *ASCE J. Eng. Mech. Div.*, Vol. 104, No. EM4, Pap. 13944, pp. 939–952.

Krenzke, M. A., and Kiernan, T. J. (1963), "Structural Development of a Titanium Oceanographic Vehicle for Operating Depths of 15,000 to 20,000 feet," *David Taylor Model Basin Rep. No. 1677*, Sept.

Krenzke, M. A., and Short, R. D. (1959), "Graphical Method for Determining Maximum Stresses in Ring-Stiffened Cylinder Under External Hydrostatic Pressure," *David Taylor Model Basin Rep. No. 1348*, Oct.

Kulak, G. L. (1994), "Tubular Members: Large and Small," *Proc. 50th Anniv. Conf.*, Structural Stability Research Council, Bethlehem, Pa.

Kuper, E. J., and Macadam, J. N. (1969), "Quantitative Effects of Strain Hardening on the Mechanical Properties of Cold-Formed Electric Welded Steel Tubing," *Proc. 10th Mech. Working Steel Process. Conf.*, American Institute of Mining, Metallurgical, and Petroleum Engineers, New York.

Landet, E., and Lotsburg, I. (1992), "Laboratory Testing of Ultimate Capacity of Dented Tubular Members," *ASCE J. Struct. Eng.*, Vol. 118, No. 4, pp. 1071–1089.

Lo, H., Crate, H., and Schwartz, E. B. (1951), "Buckling of Thin Walled Cylinders Under Axial Compression and Internal Pressure," *NASA Rep. No. 1027* (formerly 2021).

Lorenz, R. (1908), "Achsensymmetrische Verzerrungen im dünnwandigen Hohlzylinder," *Z. Ver. Dtsch. Ing.*, Vol. 52, No. 43.

Lubinski, A. (1951), "Buckling of Rotary Drilling Strings: Part III," *World Oil*, May, pp. 122–132.

Lubinski, A., Althouse, W. S., and Logan, J. L. (1952), "Helical Buckling of Tubing Sealed in Packers," *J. Petrol. Technol.*, June, pp. 655–670.

Lunchick, M. E. (1959), "Yield Failure of Stiffened Cylinders Under Hydrostatic Pressure," *David Taylor Model Basin Rep. No. 1291*, Jan.

Lunchick, M. E. (1961a), "Plastic Axisymmetric Buckling of Ring-Stiffened Cylindrical Shells Fabricated from Strain-Hardening Materials and Subjected to External Hydrostatic Pressure," *David Taylor Model Basin Rep. No. 1392*, Jan.

Lunchick, M. E. (1961b), "Graphical Methods for Determining the Plastic Shell-Buckling Pressures of Ring-Stiffened Cylinders Subjected to External Hydrostatic Pressure," *David Taylor Model Basin Rep. No. 1437*, Mar.

Lunchick, M. E. (1963), "Plastic General-Instability Pressure of Ring-Stiffened Cylindrical Shells," *David Taylor Model Basin Rep. No. 1587*, Sept.

Lunchick, M. E., and Short, R. D. (1957), "Behavior of Cylinders with Initial Shell Deflection," *David Taylor Model Basin Rep. No. 1130*, July.

Lundquist, E. E. (1933), "Strength Tests of Thin-Walled Duraluminum Cylinders in Compression," *NACA Rep. No. 473.*

MacIntyre, J. (1991), "An Analytical Study of Damaged Tubular Member Behavior," Ph.D. thesis, University of Toronto, Toronto, Ontario, Canada.

Marshall, P. W. (1971), "Design Criteria for Structural Steel Pipe," *Column Res. Conc. Proc.*

Marzullo, M. A., and Ostapenko, A. (1978), "Tests on Two High-Strength Steel Large-Diameter Tubular Columns," Pap. 3086, *Proc. 10th Offshore Technol. Conf.*, Houston, Texas, May.

Meck, H. R. (1965), "A Survey of Methods of Stability Analysis of Ring-Stiffened Cylinders Under Hydrostatic Pressure," *J. Eng. Ind.*, Aug., p. 385.

Miller, C. D. (1982), "Summary of Buckling Tests on Fabricated Steel Cylindrical Shells in USA," in *Buckling of Shells in Offshore Structures* (ed. Harding, J. E., Dowling, P. J. and Angelidis, C. M.), Granada, London, pp. 429–472.

Miller, C. D. (1983), "Research Related to Bucling of Nuclear Containment," *7th Int. Conf. Struct. Mech. Reactor Technol.*, Chicago, Aug.

Miller, C. D. (1984), "API Bulletin on Stability Design of Shells" (draft), *Am. Petrol. Inst. Bull.*, Vol. 2u, Sept.

Miller, C. D., and Vojta, J. F. (1984), "Strength of Stiffened Cylinders Subjected to Combinations of Axial Compression and External Pressure," *Proc. SSRC Annu. Tech. Session.*

Miller, C. D., Kinra, R. K., and Marlow, R. S. (1982), "Tension and Collapse Tests of Fabricated Steel Cylinders," Pap. 4218, *Proc. 14th Offshore Technol. Conf.*, Houston, Texas, May.

Miller, C. D., Grove, R. B., and Vojta, J. F. (1983), "Design of Stiffened Cylinders for Offshore Structures," *AWS Weld. Offshore Struct. Conf.*, New Orleans, La., Dec.

Mungan, I. (1974), "Buckling Stress States of Cylindrical Shells," *ASCE Struct. Div.*, Vol. 100, No. ST11, pp. 2289–2306.

Nash, W. A. (1957), "Buckling of Initially Imperfect Shells Subject to Torsion," *J. Appl. Mech.*, Vol. 24, No. 1.

Ostapenko, A., and Grimm, D. F. (1980), "Local Buckling of Cylindrical Tubular Columns Made of A-36 Steel," *Fritz Eng. Lab. Rep. No. 450-7*, Lehigh University, Bethelem, Pas., Feb.

Ostapenko, A., and Gunzelman, S. X. (1976), "Local Buckling of Tubular Steel Columns," *Proc. Methods Struct. Analysis*," Vol. 2, American Society of Civil Engineers, New York, p. 549.

Ostapenko, A., and Gunzelman, S. X. (1978), "Local Buckling Tests on Three Steel Large-Diameter Tubular Columns," *Proc. 4th Int. Conf. Cold-Formed Steel Struct.*, St. Louis, Mo., June, p. 409.

Ostapenko, A., Wood, B., Chowdhury, A., and Hebor, M. (1993), "Residual Strength of Damaged and Deteriorated Tubular Members in Offshore Structures," *ATLSS Rep. No. 93-03*, Lehigh University, Bethlehem, Pa.

Padula, J. A., and Ostapenko, A. (1989), "Axial Behavior of Damaged Tubular Columns," *Fritz Eng. Lab. Rep. No. 408.11*, Lehigh University, Bethlehem, Pa.

Palmer, A. C., and Baldry, J. A. S. (1974), "Lateral Buckling of Axially Constrained Pipelines," *J. Petrol. Technol.*, Nov., pp. 1283–1284.

Parsanejad, S. (1987), "Strength of Grout-Filled Damaged Tubular Members," *ASCE J. Struct. Eng.*, Vol. 113, No. 3, pp. 590–603.

Parsanejad, S., and Gusheh, P. (1992), "Behavior of Partially Grout-Filled Damaged Tubular Members," *ASCE J. Struct. Eng.*, Vol. 118, No. 11, pp. 3055–3066.

Plantema, F. J. (1946), "Collapsing Stress of Circular Cylinders and Round Tubes," *Rep. No. S.280*, National Luchtfaart Laboratorium, Amsterdam.

Prescott, J. (1946), *Applied Elasticity*, 1st American ed., Dover, New York, pp. 552–554.

Prion, H. G. L., and Birkemoe, P. C. (1988), "Experimental Behaviour of Unstiffened Fabricated Tubular Steel Beam-Columns," *Publ. No. 88-3*, Department of Civil Engineering, University of Toronto, Toronto, Ontario, Canada.

Pulos, J. G. (1963), "Structural Analysis and Design Considerations for Cylindrical Pressure Hulls," *David Taylor Model Basin Report No. 1639*, Apr.

Pulos, J. G., and Salerno, V. L. (1961), "Axisymmetric Elstic Deformations and Stresses in a Ring-Stiffened, Perfectly Circular Cylindrical Shell Under External Hydrostatic Pressure," Structural Mechanics Laboratory, *David Taylor Model Basin Rep. No. 1497*, Sept.

Reynolds, T. E. (1957), "A Graphical Method for Determining the General Instability Strength of Stiffened Cylindrical Shells," *David Taylor Model Basin Rep. No. 1106*, Sept.

Reynolds, T. E. (1960), "Inelastic Local Buckling of Cylindrical Shells Under External Hydrostatic Pressure," *David Taylor Model Basin Rep. No. 1392*, Aug.

Reynolds, T. E. (1962), "Elastic Local Buckling of Ring-Supported Cylindrical Shells Under Hydrostatic Pressure," *David Taylor Model Basin Rep. No. 1614*, Sept.

Reynolds, T. E. (1971), "Stability of Cylindrical Shells," *Graduate Course on Analysis and Design of Cylindrical Shells Under Pressure*, Catholic University of America, Washington, D.C., June.

Reynolds, T. E., and Blumenberg, W. F. (1959), "General Instability of Ring-Stiffened Cylindrical Shells Subjected to External Hydrostatic Pressure," *David Taylor Model Basin Rep. No. 1324*, June.

Ricles, J. M. (1995), "Analysis of Internally Grout Repaired Damaged Members," in *Analysis and Software of Cylindrical Members*, (ed. W. F. Chen and S. Toma), CRC Press, Boca Raton, Fla., Chap. 7.

Ricles, J. M., Gillum, T., and Lamport, W. (1994), "Grout Repair of Dented Offshore Tubular Bracing: Experimental Behavior," *ASCE J. Struct. Eng.*, Vol. 120, No. 7, pp. 2086–2107.

Ricles, J. M., Bruin, W. M., Sooi, T. K., Hebor, M. F., and Schönwetter, P. C. (1995), "Residual Strength Assessment and Repair of Damaged Offshore Tubulars," *Proc. 27th Offshore Technol. Conf.*, OTC Pap. 7807, May 1–4, Houston, Texas, pp. 41–59.

Salman, W. A. (1994), "Damage Assessment of Tubular Members in Offshore Structures," Ph.D. thesis, University of Toronto, Toronto, Ontario, Canada.

Schilling, C. G. (1965), "Buckling Strength of Circular Tubes," *ASCE J. Struct. Div.*, Vol. 91, No. ST5, p. 325.

Seide, P. (1960), "The Effect of Pressure on the Bending Characteristics of an Actuator System," *J. Appl. Mech.*, Sept., p. 429.

Sherman, D. R. (1969), "Residual Stress Measurement in Tubular Members," *ASCE J. Struct. Div.*, Vol. 95, No. ST4, Pap. 6502, pp. 635–637.

Sherman, D. R. (1976), "Tests of Circular Steel Tubes in Bending," *ASCE J. Struct. Div.*, Vol. 102, No. ST11, Pap. 12568.

Sherman, D. R. (1986), "Inelastic Flexural Buckling of Cylinders," *Steel Structures: Recent Research Advances and Their Application to Design* (ed. M. N. Pavlovic), Elsevier Applied Science, New York, Sept.

Sherman, D. R. (1992), "Tubular Members," in *Constructional Steel Design: An International Guide*, Elsevier Applied Science, New York, Dec.

Singer, J. (1967), "The Influence of Stiffener Geometry and Spacing on the Buckling of Axially Compressed Cylindrical and Conical Shells," *Prelim.Prepr. Pap., 2nd IUTAM Symp. Theory Thin Shells*, Copenhagen, Sept.

Smith, C. S., Somerville, J. W., and Swan, J. W. (1981), "Residual Strength and Stiffness of Damaged Steel Bracing Members," *Proc. 13th Offshore Technol. Conf.*, OTC Paper 3981, Houston, Texas.

Southwell, R. V. (1914), "On the General Theory of Elastic Stability," *Philos. Trans. R. Soc. London*, Ser. A, No. 213.

Southwell, R. V. (1915), "On the Collapse of Tubes by External Pressure," *Philos. Mag.*, Part 1, Vol. 25, May 1913, pp. 687–698; Part 2, Vol. 26, Sept. 1913, pp. 502–511; Part 3, Vol. 29, Jan. 1915, pp. 66–67.

Stein, M. (1968), "Some Recent Advances in the Investigation of Shell Buckling," *AIAA J.*, Vol. 6, No. 12.

Stephens, M. J., Kulak, G., and Montgomery, C. J. (1982), "Local Buckling of Thin-Walled Tubular Steel Members," *Struct. Eng. Dept. Rep. No. 103*, University of Alberta, Edmonton, Alberta, Canada, Feb.

Stephens, M. J., Kulak, G., and Montgomery, C. J. (1983), "Local Buckling of Thin-Walled Tubular Steel Members," *Proc. 3rd Int. Colloq. Stab. Met. Struct.* (George Mem. Session), Toronto, Ontario, Canada, May.

Sturm, R. G. (1941), "A Study of the Collapsing Pressure of Thin-Walled Cylinders," *Univ. Ill. Eng. Exp. Sta. Bull.*, No. 329.

Timoshenko, S. (1910), "Einige Stabilitäts-Probleme der Elastizitäts-Theorie," *Z. Math. Phys.*, Vol. 58, No. 4.

Timoshenko, S., and Gere, J. M. (1961), *Theory of Elastic Stability*, McGraw-Hill, New York.

Tokugawa, T. (1929), "Model Experiments on the Elastic Stability of Closed and Cross-Stiffened Circular Cylinders Under Uniform External Pressure," *Proc. World Eng. Congr.*, Tokyo, Vol. 29, pp. 249–279.

U.S. Steel (1964), *The Manufacture of Steel Tubular Products*, U.S. Steel Corporation, Pittsburgh, Pa.

Vojta, J. F., and Miller, C. D. (1983), "Buckling Tests on Ring and Stringer Stiffened Cylindrical Models Subject to Combined Loads," *Final Rep., Contract No. 11896*, Vol. 1, Main Report, 3 Volume Appendix, CBI Industries, Inc., Chicago, IL, Apr.

Von Kármán, T., and Tsien, H. S. (1941), "The Buckling of Thin Cylindrical Shells Under Axial Compression," *J. Aeronaut. Sci.*, Vol. 8, No. 8.

Von Mises, R. (1931), "The Critical External Pressure of Cylindrical Tubes" (Der kritische Aussendruck zylindrischer Röhre), *VDI-Z.*, Vol. 58, No. 19, 914, pp. 750–755; *David Taylor Model Basin Transl. 5*, Aug. 1931.

Von Mises, R. (1933), "The Critical External Pressure of Cylindrical Tubes Under Uniform Radial and Axial Load" (Der kritische Aussendruck für allseits belastete zylindrische Röhre), Stodolas Festschrift, Zurich, 1929, pp. 418–430; *David Taylor Basin Transl. 5*, Aug. 1933.

Von Sanden, K., and Tolke, F. (1949), "On Stability Problems in Thin Cylindrical Shells" (Über Stabilitätsprobleme dünner, kreiszylindrischer Schalen), *Ing. Arch.*, Vol. 3, 1932, pp. 24–66; *David Taylor Model Basin Transl. 33*, Dec. 1949.

Wah, T. (1967), "Buckling of Thin Circular Rings Under Uniform Pressure," *Int. J. Solids Struct.*, Vol. 3, pp. 967–974.

Weingarten, V. I., and Seide, P. (1961), "On the Buckling of Circular Cylindrical Shells Under Pure Bending," *Trans. ASME, J. Appl. Mech.*, Vol. 28, No. 1.

Weingarten, V. I., et al. (1965), "Elastic Stability of Thin-Walled Cylindrical and Conical Shells Under Combined Internal Pressure and Axial Compression," *AIAA J.*, Vol. 3, No. 6, pp. 118–125.

Weingarten, V. I., et al. (1968), "Buckling of Thin-Walled Circular Cylinders," *NASA SP-8007*, Aug.

Wenk, E., and Kennard, E. H. (1956), "The Weakening Effect of Initial Tilt and Lateral Buckling of Ring Stiffeners on Cylindrical Pressure Vessles," *David Taylor Model Basin Rep. No. 1073*, Dec.

Wilson, W. M. (1937), "Tests of Steel Columns," *Univ. Ill. Eng. Exp. Sta. Bull. No. 292.*

Wilson, W. M., and Newmark, N. M. (1933), "The Strength of Thin Cylindrical Shells as Columns," *Univ. Ill. Eng. Exp. Sta. Bull. No. 255.*

Wilson, W. M., and Olson, F. D.(1941), "Tests on Cylindrical Shells," *Univ. Ill. Eng. Exp. Sta. Bull. No. 331*, Sept.

Windenburg, D. F. (1960), "Vessels Under External Pressure," in *Pressure Vessel and Piping Design*, American Society of Mechanical Engineers, New York, pp. 625–632.

Windenburg, D. F., and Trilling, C. (1934), "Collapse by Instability of Thin Cylindrical Shells Under External Pressure," *Trans. ASME*, Vol. 56, No. 11, p. 819.

Wu, T. S., Goodman, L. E., and Newmark, N. M. (1953), "Effect of Small Initial Irregularities on the Stresses in Cylindrical Shells," *Univ. Ill. Struct. Res. Ser.*, No. 50, April.

Yao, J. C. (1962), "Large Deflection Analysis of Buckling of a Cylinder Under Bending," *Trans. ASME J. Appl. Mech.*, Vol. 29, No. 4.

CHAPTER FIFTEEN

MEMBERS WITH ELASTIC LATERAL RESTRAINTS

15.1 INTRODUCTION

Compression members are sometimes restrained laterally between their ends by intermittent elastic lateral supports. Typical examples include (1) the unbraced compression flange of a girder whose tension flange is laterally restrained by a bridge–floor or building–roof system; and (2) the top chord of a pony truss, for which vertical clearance requirements prohibit direct lateral bracing. The methods of design presented in this chapter can also be used for guyed towers.

In the case of the girder, the web prevents the top flange from buckling in the vertical plane, and intermittent elastic lateral restraints may be provided in the plane normal to the web by means of vertical stiffeners in combination with the contiguous framing elements in the floor or roof system adjacent to the tension flange. In a truss supporting a floor or roof system in the plane of the tension chord members, the panel points provide vertical support and elastic restraint for the compression chords as a whole.

Although not as widely used as in the past, the pony truss has served as the prototype through the years for the development of theory and design procedures that currently may find applications in other similar situations. The behavior during buckling of a member with intermittent elastic lateral supports lies between two limiting extremes. If the elastic restraints are very stiff, nodal points can be induced at each restraint location; the the restraints are very flexible, buckling can be in the shape of a single half-wave over the full member length as long as the ends of the member are laterally restrained. The actual

buckled shape consists of a number of half-waves not greater than the total number of spaces between supports.

The design of a compression member with intermittent elastic lateral supports may be based on the computed critical load; or because of initial crookedness and because of moments introduced by bending of the floor beams, it could be based on combined-stress calculations that include the effect of deflection. The latter approach is a rational one but has not as yet been simplified sufficiently to make it a practical design procedure. On the other hand the critical-load analysis gives only an upper bound to the actual strength of the member unless initial out-of-straightness is considered. Current design procedures require evaluation of the stiffness supplied by the compression chord lateral support system. This stiffness forms the basis for evaluating the integrity of the compression chord. The critical load of the chord with elastic lateral supports at the panel points is then determined, and the design load is found by dividing this critical load by a suitable factor of safety.

Using the pony truss as the prototype, a procedure of analysis is developed to determine the critical load of a member with discrete elastic lateral restraints. To a lesser extent the combined-stress procedure is reviewed in this chapter. The design of pony truss transverse frames (floor beams, truss verticals, and connecting knee braces) has a direct bearing on both procedures. Proper design of transverse frames is essential to the safety of the pony-truss bridge. Toward the end of the nineteenth century the failure of several pony-truss bridges focused attention on the top-chord buckling problem. Engesser (1885, 1893), was the first to present a simple, rational, and approximate formula for the required stiffness, C_{req}, of elastic supports equally spaced between the ends of a hinge-ended column of constant section. An equivalent uniform elastic support was assumed in the Engesser analysis.

Early developments are reviewed by Bleich (1952); Hu (1952), using the energy method, has studied the problem of elastically supported chords. He considered nonuniform axial forces, variable chord cross sections, and spring stiffness for both simple and continuous pony-truss bridges. Holt (1951, 1952, 1956, 1957), in work sponsored by the Column Research Council, presented a method of analysis for determining the critical load of a pony-truss top chord which is essnetialy "exact" in that it includes most of the secondary effects that influence the behavior of the pony truss. In a similar manner, Lee and Clough (1958) and Elgaaly and Khalifa (1970) studied the stability of pony-truss bridges.

The effect of the floor-system deflections on the top-chord stresses was studied in another CRC-sponsored project by Barnoff and Mooney (1957). Tests on models of pony-truss bridges have been conducted by Holt (1957). Oliveto (1980) described a computer program and considered both elastic and inelastic buckling of colunns partially restrained at intervals. Medland and Segedin (1979) evaluated brace forces for an initially crooked member.

15.2 BUCKLING OF THE COMPRESSION CHORD

The buckling problem of the compression chord of a pony truss can be reduced to that of a column braced at intervals by elastic springs whose spring constants corresponded to the stiffness of the truss transverse frames. The top-chord axial compression and the top-chord stiffness will vary from panel to panel, and the stiffness of the transverse frames may also vary from panel point to panel point, thus complicating the theoretical problem. In addition, there are secondary factors such as the following:

1. The stiffening effect of the truss diagnonals
2. The torsional stiffness of the chord and web members
3. The initial crookedness of the chord and the eccentricity of the axial load
4. For non-parallel-chord trusses, the effect of chord curvature.

Engesser's solution (1885, 1893), is based on the following simplifying assumptions:

1. The top chord, including the end posts, is straight and of uniform cross section.
2. Its ends are taken as pin-connected and rigidly supported.
3. The equally spaced elastic supports have the same stiffness and can be replaced by a continuous elastic medium.
4. The axial compressive force is constant through the chord length.

Engesser's analysis can be applied with reasonable accuracy to the case where the lateral support is supplied by equally spaced springs provided that the half-wavelength of the buckled shape of the continuously supported member is at least 1.8 times the spring spacing; this will be true if the bar is stable as a two-hinged column carrying the same axial load and having a length no less than 1.3 times the spring spacing.

Engesser's solution for the required stiffness of a pony-truss tranverse frame is

$$C_{req} = \frac{P_c^2 l}{4EI} \tag{15.1}$$

where C_{req} is the elastic transverse frame stiffness at a panel point that is required to ensure that the overall chord having panel lengths l and flexural rigidity EI will attain buckling load P_C. If the proportional limit of the column material is exceeded, E should be replaced by the tangent modulus E_t.

The Euler equation for critical stress with E_t replacing E can be written as follows for a column of length l:

$$E_t I = \frac{P_c (Kl)^2}{\pi^2} \tag{15.2}$$

Taking l in this equation as the panel length of the pony-truss compression chord, we can substitute Eq. 15.2 into El. 15.1, obtaining the required spring constant as

$$C_{\text{req}} = \frac{\pi^2 P_c}{4K^2 l} \tag{15.3}$$

This equation has been shown [see Hu (1952, p. 275)] to be adequate when the half-wavelength of the buckled chord is no less than $1.8l$; and this limiting value corresponds to a K factor of 1.3. It is not applicable to short bridges with a small number of panels:

The load P_C can be considered as both of the following:

1. The buckling load of the entire compression chord laterally supported by the transverse frames and pinned at the ends.
2. The buckling load of the portion of the compression chord *between* the transverse frames with end restraints producing effective length factor K.

According to Engesser's formulation, the maximum compression-chord buckling load and the corresponding required spring constant of each support can be determined as follows for a member of a given cross-sectional area A:

1. Determine the critical load P for the member between spring supports using the expression

$$P_c = A\sigma_c \tag{15.4}$$

   Obtain σ_C from an appropriate column-strength curve, taking the equivalent column slenderness ratio as Kl/r, with $K = 1.3$ and r estimated on the basis of probable shape and size of member.
2. Determine the spring constant C_{req} such that the buckling load of the chord member as a whole is equal to P_C:

$$C_{\text{req}} = 1.46\frac{P_c}{l} \tag{15.5}$$

It may be noted that Eq. 15.5 follows from Eq. 15.3, taking

$$\frac{\pi^2}{4K^2} = \frac{\pi^2}{4(1.3)^2} = 1.46$$

The Engesser simplifying assumption of taking the chord ends as pin-connected may result in significantly unsafe errors in C_{req}, particularly in the case of short pony-trusses. Holt (1952, 1956) provides an alternative design procedure that does not require this simplifying assumption. Holt's solution for the buckling load of the compression chord of a pony truss is based on the following assumptions (see Fig. 15.1):

1. The transverse frames at all panel points have identical stiffness.
2. The radii of gyration of all top-chord members and end posts are identical.
3. The top-chord members are all designed for the same allowable unit stress; hence their areas and (from step 2) their moments of inertia are proportional to the compression forces.
4. The connections between the top chord and the end posts are assumed pinned.
5. The end posts act as cantilever springs supporting the ends of the top chords.
6. The bridge carries a uniformly distributed load.

The results of Holt's studies are presented in Table 15.1, which gives the reciprocal of the effective-length factor K as a function of n (the numbers of panels) and Cl/P_c (where C is the furnished stiffness at the top of the least-stiff transverse frame). Where applicable, Table 15.1 provides a rapid design aid in checking the stability of a pony-truss compression chord. The procedure is as follows:

1. Design the floor beams and web members for their specified loads.
2. Calculate the spring constant C furnished at the upper end of the cross frame having the least transverse stiffness.
3. Calculate the value of parameter Cl/P_c, where P_c is the maximum design chord stress mutiplied by the desired factor of safety.
4. Enter the table with n and Cl/P_c and find the corresponding value of $1/K$ for a compression-chord panel, interpolating as necessary.

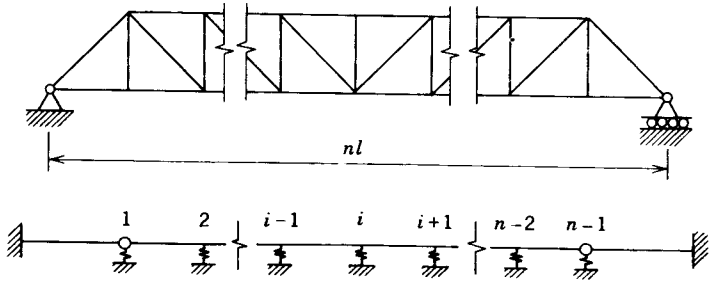

Fig. 15.1 Pony truss and analogous top chord.

TABLE 15.1 $1/K$ for Various Values of Cl/P_c and n

	n							
$1/K$	4	6	8	10	12	14	16	Lutz-Fisher (1985, Eq. 15-8)
1.000	3.686	3.616	3.660	3.714	3.754	3.785	3.809	4.000
0.980		3.284	2.944	2.806	2.787	2.771	2.774	3.730
0.960		3.000	2.665	2.542	2.456	2.454	2.479	3.478
0.950			2.595					
0.940		2.754		2.303	2.252	2.254	2.282	3.244
0.920		2.643		2.146	2.094	2.101	2.121	3.026
0.900	3.352	2.593	2.263	2.045	1.951	1.968	1.981	2.822
0.850		2.460	2.013	1.794	1.709	1.681	1.694	2.372
0.800	2.961	2.313	1.889	1.629	1.480	1.456	1.465	1.993
0.750		2.147	1.750	1.501	1.344	1.273	1.262	1.673
0.700	2.448	1.955	1.595	1.359	1.200	1.111	1.088	1.401
0.650		1.739	1.442	1.236	1.087	0.988	0.940	1.169
0.600	2.035	1.639	1.338	1.133	0.985	0.878	0.808	0.970
0.550		1.517	1.211	1.007	0.860	0.768	0.708	0.798
0.500	1.750	1.362	1.047	0.847	0.750	0.668	0.600	0.648
0.450		1.158	0.829	0.714	0.624	0.537	0.500	0.519
0.400	1.232	0.886	0.627	0.555	0.454	0.428	0.383	0.406
0.350		0.530	0.434	0.352	0.323	0.292	0.280	0.309
0.300	0.121	0.187	0.249	0.170	0.203	0.183	0.187	0.226
0.293	0							
0.259		0						
0.250			0.135	0.107	0.103	0.121	0.112	0.157
0.200			0.045	0.068	0.055	0.053	0.070	0.100
0.180			0					
0.150				0.017	0.031	0.029	0.025	0.056
0.139				0				
0.114					0			
0.100						0.003	0.010	0.025
0.097						0		
0.085							0	
0								0

5. Determine the value of Kl/r for the compression-chord panel (note that this value of Kl/r is to be applied to all panels).
6. Determine the allowable top-chord compressive unit stress corresponding to this value of Kl/r, using the appropriate column curve or table.

Value of $1/K$ of les than 0.5(i.e., $K > 2$) are only of academic interest, since the usual bridge proportions and transverse-frame stiffnesses lead to values of $1/K$ greater than 0.5.

Hu (1952) developed the curves shown in Fig. 15.2. These curves give the stiffness of the compression-chord transverse supports that is required to make each panel of the chord buckle as one half-wave. Hu's results for a chord of constant section $[(EI)_{end}/(EI)_{middle} = 1.0$ in Fig. 15.2] can be compared with Holt's work for $1/K = 1$ (first line of Table 15.1) for the cases $n = 4.6$, and 8, which were considered by both investigators. Hu's results give stiffness requirements approximately 7% less than those of Holt for $n = 4$, and 5% greater for $n = 6$ or 8. Thus the results are in reasonable agreement, even though the procedures are somewhat different. Hu (1952) also studied the effects caused by parabolic variation of the length of the pony-truss verticals and the effect of parabolic variation of C. In both cases the value of C_{req} will be less than that for the case where C has the same value at each transverse frame.

Because of the uncertainties involved in the analysis of pony-truss top chords, it is reasonable to require a factor of safety for overall top-chord buckling somewhat greater than that used for designing hinged-end columns. The transverse-frame spring constant C that is actually furnished can be determined for the frame loaded as shown in Fig. 15.3 by means of the following equation:

$$C = \frac{E}{h^2[(h/3I_C) + (b/2I_B)]} \tag{15.6a}$$

The first term within the denominator brackets represents the contribution of the truss vertical, and the second term represents the contribution of the floor

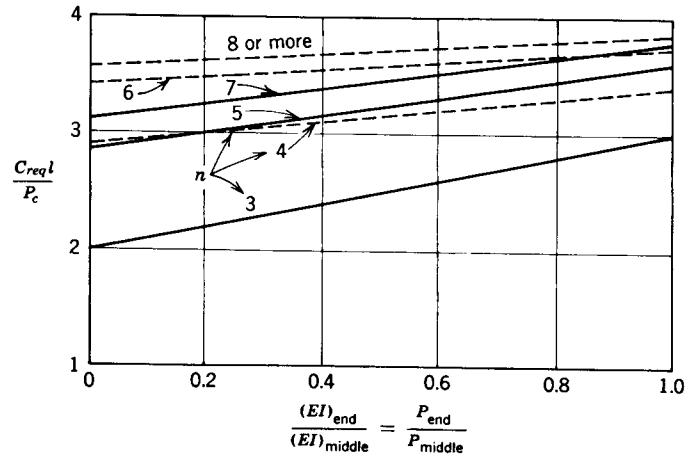

Fig. 15.2 Effect of variation in compression chord on transverse stiffness requirements.

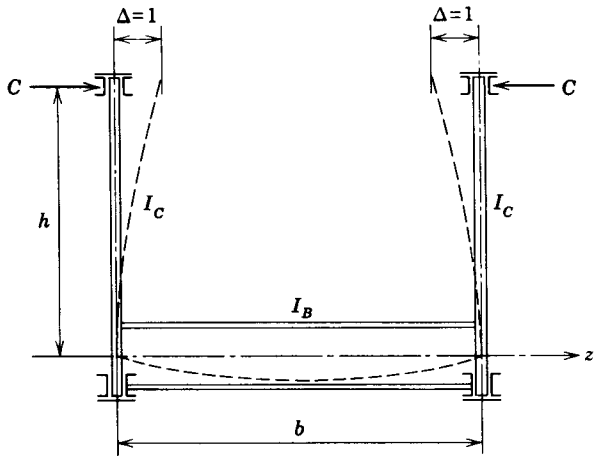

Fig. 15.3

beam. Thus the contributions of the top-chord torsional strength and the web-diagonal bending strength to the frame stiffness are neglected in this equation. It is evident that if the floor beam is very stiff in comparison with the truss vertical, the frame stiffness is approximately

$$C = \frac{3EI_C}{h^3} \tag{15.6b}$$

When the two chords tend to move in the same direction, the stiffness C will be greater than that given by eq. 15.6a; therefore, C as found from Eq. 15.6a is always the lower bound.

If the diagonals of the truss system are effectively fixed at their base, their contribution to C in Eq. 15.6a may be included by introducing the additional term $L_d^3/3I_d$ into the denominator. The values L_d and I_d represent the length and moment of inertia, respectively, of the diagonal members. In this case C becomes

$$C = \frac{E}{h^2\{h/[(3I_C + 3I_d(h/L_d)^3] + (b/2I_B)\}} \tag{15.6c}$$

15.3 EFFECT OF SECONDARY FACTORS ON BUCKLING LOAD

The consideration of secondary factors involves procedures that require a large amount of computation. Most of these procedures use the usual methods of indeterminate structural analysis to set up a system of simultaneous, linear,

homogeneous equations. The stability criterion is that the determinant of the coefficients of this system of equations must vanish.

Holt (1952) considered the following secondary factors:

1. Torsional stiffness of the chord and the web members
2. Lateral support given to the chord by the diagonals
3. Effect of web-member axial stresses on the restraint provided by them
4. Effect of non-parallel-chord trusses
5. Error introduced by considering the chord and end posts to be a single straight member

Holt's analysis show that the error in the critical load introduced by neglecting all of these factors is quite small and that satisfactory results in calculating the compression-chord buckling load can be obtained by assuming that the chord is a straight elasticity braced column whose length is the total length of the chord and end posts. These conclusions are in agreement with those reached by Schibler (1946), who finds that the torsional stiffness of the top chord and the support furnished by the web diagonals increase the chord buckling strength only slightly.

15.4 TOP-CHORD STRESSES DUE TO BENDING OF FLOOR BEAMS AND TO INITIAL CHORD ECCENTRICITIES

The compression chord of a pony truss is displaced laterally at some panel points as a result of live load on the bridge and because of initial crookedness and unintentional eccentricities of the chord. Such lateral deflections will, of course, reduce the maximum load capacity of the chord (and of the bridge). just as end eccentricity and initial curvature will reduce the compression strength of any column).

Lutz and Fisher (1985) did consider initial out-of-straightness for elasticially restrained members in the same manner as Winter (1960) did for fully braced members, namely by requiring the actual stiffness supplied to be twice the ideal required stiffness. They followed the simplifying assumptions made by Engesser discussed earlier and rewrote Eq. 15.3 in the form

$$C_{\text{req}} = 2.5\frac{P_c l}{L_e^2} \tag{15.7}$$

where $L_e = Kl$ and $\pi^2/4 \simeq 2.5$. They then extended the applicability to K-factors of less than 1.3 and as low as 1.0. Their empirical required stiffness expression is

$$C_i = \left[2.5 + 1.5\left(\frac{l}{L_e}\right)^4\right]\frac{P_c l}{L_e^2} \tag{15.8}$$

At $K = 1$ each spring would provide full bracing to the compression chord, which requires a stiffness of $4P_c/l$. They proposed that due to initial out-of straightness, the actual stiffness should be twice the required stiffness given above [see Winter (1960) and accompanying discussion by Green].

Design procedures that take account theoretically of such imperfections are not presently available. It is difficult to take them into account, because of both the complexity of the necessary calculations and the lack of knowledge with regard to probable initial imperfections. The calculations involve the top-chord stiffness in both bending and torsion.

Holt (1957) has developed an empirical procedure for estimating bending moments in the top chord and end posts that is in agreement with his test results. He recommends that the end post be designed as a simple cantilever beam to carry the axial load combined with a transverse load of 0.5% of the axial load, applied at the upper end. Tentatively, a value of 1% should probably be used.

15.5 DESIGN PROCEDURES

In the design of half-through (pony) truss spans, AASHTO specifications (1994) require that "the top chord shall be considered as a column with elastic lateral supports at the panel points. The critical buckling force of the column, so determined, shall exceed the maximum force from dead load, live load and impact in any panel of the top chord by not less than 50 percent." Thus a load factor of 1.5 is considered adequate, and this is less than that required by the same specification in the determination of allowable compressive stresses in hinged-end columns. This is presumably justified on the basis that all pony-truss top-chord compression members cannot be stressed simultaneously up to the same proportion of the critical buckling load. However, it seems evident that in cases where maximum compressive stress may occur simultaneously in the entire length of the compression chord, the safety factor should be higher than that used for general column design, rather than lower.

German buckling specifications base the design of pony-truss compression chords on the Engesser solution for the buckling load, with the recommendation that K be kept the same for all panels and between limits of 1.2 and 3.0. The formula for required transverse-frame stiffness is given as

$$C_{\text{req}} = \frac{2.50}{K_m^2}\frac{P_c}{l} \tag{15.9}$$

For $K_m = 1.3$, Eq. 15.9 gives very nearly the same result as Eq. 15.5, which is to be expected since both equations are based on Engesser's solution.

For design of the web verticals, the AASHTO specification (1994) reads: "The vertical truss members and the floorbeams and their connections in half-through truss spans shall be proportioned to resist a lateral froce of not less

than 300 pounds per linear foot (4350 N/m) applied at the top-chord panel points of each truss." The problem of the lateral stability of a pony-truss compression chord will now be illustrated by means of a design example, using, in part, AASHTO specifications (1994).

Example 15.1 Consider a pony truss that has 12 panels of 13 ft 4 in. for a span of 160 ft. (see Fig. 15.4). The transverse frame is shown in the sketched cross section. The W27 × 84 floor beams are required by bridge deck loads. The top chord is a 10 in. by 10 in. box section, with wall thickness to be determined by design requirements for a maximum compressive force of 360 kips (dead load, live load, and impact). The verticals are W10 rolled sections.

According to AASHTO requirements, the lateral force to be resisted at the upper panel points is

$$0.3\text{kip/ft} \times 13.33\text{ ft} = 4\text{ kips}$$

The maximum moment in the transverse frame will be at the joint of the web vertical and the floor beam and is

$$M = 4\text{ kips} \times 120\text{ in.} = 480\text{ kip-in.}$$

Using this moment and assuming that the maximum tension in the web vertical due to the bridge load is 24 kips in the region where the compression chord is most highly stressed, a W10 × 33 vertical with $I = 170\text{ in}^4$ is selected.

The I of the floor beam is 2850 in.^{4}, and from Eq. 15.6a the transverse-frame spring constant is

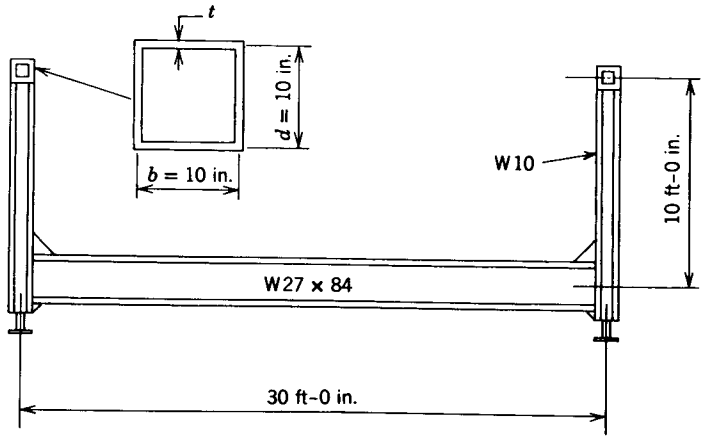

Fig. 15.4

$$C = \frac{29{,}000}{120^2[120/(3 \times 170) + 360/(2 \times 2850)]} = 6.75 \text{ kips/in.}$$

Assuming that the factor of safety against buckling to be 2.12 (only 1.50 is required by AASHTO), the compression chord must be designed for a buckling strength of $P = 2.12 \times 360$ kips. AASHTO uses a factor of safety of 2.12 for the allowable stress design of concentrically loaded columns. If a square built-up tubular section is considered for the compression chord, its properties can be approximate as:

- *Area*: $A = 4td$
- *Moment of inertia*: $I = \dfrac{Ad^2}{6}$
- *Radius of gyration*: $r = \dfrac{d}{\sqrt{6}}$

If d, the distance between wall centerlines, is taken as 10 in., $r = 10/\sqrt{6} = 4.08$ in.

Using Holt's procedure, Kl/r is determined from Table 15.1. Using the actual supplied C and $P_c = 763$ kips, we obtain

$$\frac{Cl}{P_c} = \frac{6.75(160)}{763} = 1.415$$

Entering Table 15.1 in the column for $n = 12$ panels and $Cl/P_c = 1.415$, $1/K$ falls between 0.750 and 0.800. Interpolation reveals $1/K = 0.776$ or $K = 1.288$. Considering the built-up 10-in. tube, yields

$$\frac{Kl}{r} = \frac{1.288(160)}{4.08} = 50.5$$

$$F_a = 16.930 - 0.53(50.5)^2 = 15.580 \text{ psi}$$

The required $A = 360/15.58 = 23.1$ in^2 and $t = 0.577$ in. with $d = 10$ in. Had the number of panels been 8 instead of 12, the thickness t required would have increased to 0.603 in. using Holt's procedure.

Using the Lutz–Fisher's expression gives

$$C_{\text{req}} = 2C_i = \frac{[5 + 3(l/L_e)^4]P_c l}{L_e^2}$$

or since $l/L_e = 1/K$,

$$\frac{C_i l}{P_c} = \left[2.5 + 1.5\left(\frac{1}{K}\right)^4\right]\left(\frac{1}{K}\right)^2$$

which is included as the last column in Table 15.1. With $C_{\text{req}} = 6.75$,

$$\frac{C_i l}{P_c} = \frac{(6.75/2)(160)}{763} = 0.708$$

From Table 15.1, $1/K = 0.52$ or $K = 1.923$. Thus $Kl/r = 1.923(160)/4.08 = 75.4$ for the 10-in. tube, and $F_a = 16{,}930 - 0.53(75.4)^2 = 13{,}916$ psi.

Required $A = 360/13.92 = 25.86$ in^2 and $t = 25.86/(4 \times 10) = 0.646$ in. Using the Holt procedure one could end up with a design with $d = 9.5$ in. using a $\frac{5}{8}$-in. plate. With the Lutz–Fisher procedure, which considers out-of-straightness, one would need a $\frac{5}{8}$-in. plate with $d = 10.25$ in.

15.6 PLATE GIRDER WITH ELASTICALLY BRACED COMPRESSION FLANGE

Although most of the research and references presented herein concern the pony-truss bridge, the design recommendations that have been given are also applicable to the design of plate girders with elastically braced compression flanges. Such girders will customarily have full-depth vertical stiffeners serving the dual function of web stiffener and top-flange transverse support. The lack of girder diagonal members is of no concern since Eq. 15.6a does not include the contribution of truss diagonals. In applying the design procedure to girders, one-third of the compression area of the web should be added to the area of the compression flange and introduced as the equivalent area of the top chord in the formulas as developed for the pony truss. This compression area should be reduced by multiplying by the plate girder bending strength reduction factor (if less than 1) for slender webs. The same section may be used in calculating I_C. If girders are used in an arrangement differing from the section shown in Fig. 15.3 an independent calculation of C must be made appropriate to the framing arrangement that is used.

15.7 GUYED TOWERS

In determining the effective-length factor K for use in the design of a guyed tower, Springfield* has used Table 15.1 together with an adaptation of the pony-truss analysis. He reports on the appliction to a "mast" with guys at nine levels, as follows:

*June 9, 1971, letter to the editor, from J. Springfield, of C.D. Carruthers & Wallace Consultants Ltd., Toronto, Canada.

Stiffnesses (of restraints) are not constants, but vary according to the magnitude of lateral displacement. The procedure we have adopted is as follows:

1. Compute the spring constants C at each guy level. This is done by dividing the horizontal guy reaction by the displacement under maximum wind load. The average spring stiffness is chosen rather than the instantaneous stiffness because the buckling mode could reduce the displacements at guy points, thus reducing the spring stiffness.
2. Calculate the parameter Cl/P_c for each column segment between guys. The smaller value of C is chosen from the top or bottom of the segment. l is the length of the column segment and P_c is the maximum column segment design load multiplied by the appropriate factor-of-safety.
3. The value of K for each segment is determined in turn from Table 15.1 (a total of nine K values). In its application, we have asumed a continuous compression strut with nine spans. Each span has identical spring supports of magnitude equal to the C value for the column segment being considered. The spacing of these supports is uniform, this distance being the length of column segment under consideration.

Holt assumes that the strut is fixed at each end and pinned at the first interior supports. Our approximation would be fairly good for the interior spans, but could be in error for the discontinuous ends, especially at the top end, where both joint displacement and rotation are possible.

The range of Cl/P_c for our mast is 1.3 to 2.3 and the corresponding range of K is 1.7 to 1.1. We have also applied Engesser's analysis for comparison, which shows the close agreement of C required for K values between 1.7 and 1.3. For K values smaller than 1.3, a rapid divergence appears as expected.

It is, of course, recognized that the complete design of guyed towers is a very complex problem, involving effects that may include preloading of guys, vertical movement of gusts, vortex shedding, and other vibration dynamic problems. The foregoing is only a brief summary of the column-buckling aspects of the design problem as approached in an approximate and simplified manner.

REFERENCES

AASHTO (1994), *AASHTO LRFD Bridge Design Specifications*, American Association of State Highway and Transportation Officials, Washington, D.C.

Barnoff, R. M., and Mooney, W. G.(1957), "The Effect of Floor System Participation on Top Chord Stresses in Single Span Pony Truss Bridges," in *Stability of Bridge Chords Without Lateral Bracing," Column Res. Counc. Rep. No. 5.*

Bleich, F. (1952), *Buckling Strength of Metal Structures*, McGraw-Hill, New York.

Elgaaly, M. A., and Khalifa, M. E., Jr. (1970), *Stability of Pony-Truss Bridges*, on file, Institution of Structural Engineers, London, June.

Engesser, F. (1885), "Die Sicherung offener Brücken gegen Ausknicken," *Centralbl. Bauverwaltung*, 1884, p. 415; 1885, p. 93.

Engesser, F. (1892), *Die Zusatzkräfte und Nebenspannungen eiserner Fachwerkbrücken*, Vol. II, Berlin.

Holt, E. C. (1951), "Buckling of a Continuous Beam-Column on Elastic Supports," Stability of Bridge Chords without Lateral Bracing, *Column Res. Counc. Rep. No. 1.*

Holt, E. C. (1952), "Buckling of a Pony Truss Bridge," Stability of Bridge Chords without Lateral Bracing, *Column Res. Counc. Rep. No. 2.*

Holt, E. C. (1956), "The Analysis and Design of Single Span Pony Truss Bridges," in *Stability of Bridge Chords Without Lateral Bracing, Column Res. Counc. Rep. No. 3.*

Holt, E. C. (1957), "Tests on Pony Truss Models and Recommendations for Design," in *Stability of Bridge Chords Without Lateral Bracing, Column Res. Conc. Rep. No. 4.*

Hu, L. S. (1952), "The Instability of Top Chords of Pony Trusses," Dissertation, University of Michigan, Ann Arbor, Mich., 1952.

Lee, S. L., and Clough, R. W. (1958), "Stability of Pony Truss Bridges," *Publ. Int. Assoc. Bridge Struct. Eng.*, Vol. 18, p. 91.

Lutz, L., and Fisher, J. (1985), "A Unified Approach for Stability Bracing Requirements," *AISC Eng. J.*, Vol. 22, No. 4, p. 163.

Medland, I. C., and Segedin, C. M. (1979), "Brace Forces in Interbraced Column Structures," *ASCE J. Struct. Div.*, Vol. 105, No. ST7, pp. 1543–1556.

Oliveto, G. (1980), "Inelastic Buckling of Columns Partially Restrained Against Sway and Rotation," *Eng. Struct.*, Vol. 2, pp. 97–102.

Schibler, W. (1946), "Das Tragvermögen der Druckgurte offener Fachwerkbrücken mit parallelen Gurten," *Inst. Baustatik E.T.H. Zurich Mitt.*, No. 19.

Winter, G. (1960), "Lateral Bracing of Columns and Beams" with discussions, *Trans. ASCE*, Vol. 125, pp. 807–845.

CHAPTER SIXTEEN

FRAME STABILITY

16.1 INTRODUCTION

Simply stated, frame stability requires that all structural members and connections of the frame have adequate strength to resist the applied loads where *static* equilibrium is satisfied on the deformed geometry of the structure.* In practice, this rather straightforward requirement presents complications for the design engineer, due largely to the limitations of conventional analysis methods to accurately calculate the inelastic deformations and internal forces as structures approach their strength (stability) limit state. Moreover, even where the best of analysis models are available, the designer still must account for uncertainties introduced by variability in the magnitude and distribution of loads and in the strength and stiffness of members, connections, foundations, and so on.

Contemporary design standards for steel structures generally treat frame stability through strength and stability criteria for beam-columns. Design provisions usually include a combination of (1) second-order moment amplification factors applied to the required member strengths, (2) one or more column curves to calculate the nominal strengths of members in "pure" axial compression, (3) nominal strength equations for members under major- or minor-axis bending actions, and (4) moment-axial force strength interaction equations. A complicating factor in beam-column design is the indeterminate nature of the

*This chapter is limited to consideration of stability under static loads. Dynamic stabilty is covered in Chapter 20.

internal member forces and of the restraints and destabilizing effects between individual members and the frames of which they are a part. Devices such as effective-length (K) factors and notional loads have been used for approximating these member–frame interactions. However, such methods usually introduce simplifying behavioral assumptions, such as artificial distinctions between braced and unbraced frames, the likelihood of all columns in a story failing simultaneously, the combination of in-plane and out-of-plane member stability effects, and so on.

In 1981, SSRC published Technical Memorandum No. 5, which while recognizing the interdependence of member and system stability, recommended that "in design practice, the two aspects of stability of individual members and elements of the structure and stability of the structure as a whole, be considered independently." Motivated in part by several landmark papers of the 1970s outlining the use of second-order (P–Δ) analysis for evaluating frame stability (e.g., Wood et al., 1976a,b; LeMessurier, 1976, 1977; MacGregor and Hage, 1977), the intent of this recommendation was to reduce reliance on effective-length methods as the primary basis for dealing with frame stability. Today (1998), all major design specifications include the use of second-order analysis, although a common and unified approach to frame stability design has yet to emerge.

Some design specifications, such as the Canadian standard for steel structures, CAN3-S16.1 (CSA, 1994), have eliminated use of the effective-length concept (i.e., K-factors) (Kennedy et al., 1990). Checks for in-plane and out-of-plane stability of beam-columns are based on the actual member lengths, and frame stability is checked solely through second-order analysis procedures. Where second-order analysis is used, CAN-16 requires the application of fictitious or "notational" lateral forces with factored gravity load combinations to account for inelastic effects and geometrical frame imperfections. The Australian standard follows a similar approach. In addition, CAN-S16.1 limits the use of elastic analysis to cases where the ratio of second-order effects to first-order effects is less than 1.4.

Alternatively, the AISC–LRFD specification (AISC, 1993) continues to use column effective-length factors in combination with second-order analysis to account for frame stability effects in beam-column member design. This is done in recognition of the limitations of elastic analysis to model the stability of frames with large axial column forces where the inelastic reduction of stiffness is significant. By maintaining effective-length checks, the AISC–LRFD approach avoids the imposition of any limits on the use of elastic second-order analysis (Yura, 1995). Eurocode 3 (ECS, 1993) requires application of notional horizontal loads with all load combinations, including lateral load combinations. White and Clarke (1997) show that this approach also properly accounts for the limitations of elastic analysis to model the stability of frames.

The intent of this chapter is to address frame stability in the context of computer analysis methods, which can model real behavior more accurately

and thereby reduce reliance on semiempirical methods to deal with the interaction of member and system stability effects. For in-plane behavior of rigidly connected frames, the theory and formulations for conducting accurate second-order inelastic analyses are fairly well established. Thus, for planar frames with members fully supported out-of-plane, it is feasible to model inelastic member and frame stability directly in a single analysis. In fact, the Australian AS4100 standard (SAA, 1990) explicitly permits the checking of in-plane member and frame stability solely on the basis of what it terms an *advanced analysis*, an accurate nonlinear analysis that accounts for inelastic spread-of-plasticity and initial imperfection effects. However, further work remains before the same can be said of modeling the more complex aspects of three-dimensional member of behavior that involves inelastic torsional-flexural effects. Therefore, most practical approaches for stability design still require the separation of in-plane frame and member behavior from out-of-plane member stability checks.

Overview of Chapter. The chapter begins in Section 16.2 with a review of the various types of elastic and inelastic second-order analyses and behavioral assumptions implied in these methods. Most of this discussion assumes access to modern frame analysis software. Next, in Section 16.3 basic aspects of frame behavior are reviewed by means of an example, followed by discussion of specific behavioral effects and modeling issues related to frame stability. In Section 16.4, the appliction and limitations of various types of elastic and inelastic analysis methods for evaluating frame and member stability are discussed. This is followed in Section 16.5 by a brief summary and comparison of frame and beam-column design provisions from four steel design standards. The chapter concludes with brief comments on the current status and future developments in frame stability.

16.2 METHODS OF ANALYSIS

An overview of analysis methods to calculate frame response is shown by the schematic load-deflection curves in Fig. 16.1. These plots relate the magnitude of applied gravity and lateral loads to the drift of the frame. The basic distinctions between the methods of analysis represented by each curve are (1) whether equilibrium is satisfied on the undeformed or deformed geometry of the structure, and (2) whether member plastification is considered. Following are brief descriptions of analysis types represented in the figure.

1. *First-order elastic analysis.* This is the most basic method of analysis, in which the material is modeled as linear-elastic and equilibrium is expressed on the undeformed configuration of the structure. Although currently the most

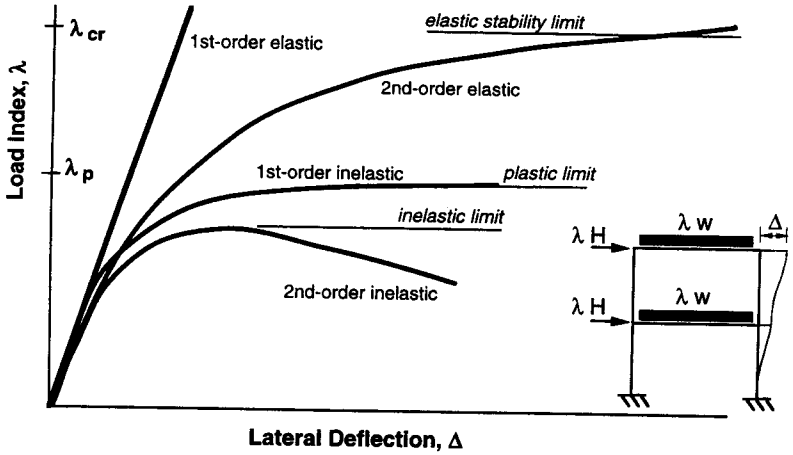

Fig. 16.1 Schematic comparison of load-deflection behavior.

prevalent method used in routine design, first-order elastic analysis provides no direct measure of frame stability.

2. *Second-order elastic analysis.* Here the material is still linear-elastic, but equilibrium is calculated on the deformed geometry of the structure. For most frames the load-deflection curve obtained from a rigorous second-order elastic analysis asymptotically approaches the load level referred to as the *elastic stability limit* of the structure. The *elastic stability limit* calcualted by a second-order incremental analysis is similar but distinct from the *elastic critical load* (λ_{cr}) calculated by a classical stability (or eigenvalue) analysis. Differences in the two limits arise because the elastic stability load corresponds to equilibrium in the deformed configuration, whereas the elastic critical load is calculated as a bifurcation from equilibrium from the undeformed geometry. Additionally, elastic loads are usually calculated for idealized conditions that may not represent the actual loading.

3. *First-order inelastic analysis.* This models the effects of member plastification under incremental loading, but since it is limited to first-order response, equilibrium is satisfied only for the undeformed geometry of the structure. The inelastic effects may be handled by techniques ranging from simple elastic–perfectly plastic hinge models to more detailed models that include spread of plasticity or distributed plasticity effects. Where the material representation is elastic–perfectly plastic (i.e., where strain hardening is neglected), the load-response curve from a first-order inelastic analysis asymptotically approaches the *plastic limit load*, which is identical to the load, λ_p, calculated by a plastic mechanism analysis.

4. *Second-order inelastic analysis.* This models the decrease in stiffness due to both member plastification and large deflections. Subject to the limitations

of behavioral effects considered in the analysis and accurate modeling of inelastic force redistributions, the *inelastic stability limit load* obtained by a second-order inelastic analysis is the most accurate representation to the true strength of the frame.

In the following sections, the two-fundamental aspects of nonlinear analysis and second-order and inelastic behavior are described. Also included is a review of computer-based critical load (eigenvalue) methods.

16.2.1 Second-Order Analysis

Referring to the simple frames shown in Fig. 16.2, the basic issue in second-order analysis is to calculate internal force equilibrium in the deformed condition. For the frame in Fig. 16.2*a*, a first-order analysis under gravity loads will yield bending moments in the beam equal to those for a simple span condition with zero moments in the column. Equilibrium of the deflected shape requires larger moments in the beam and nonzero moments in the

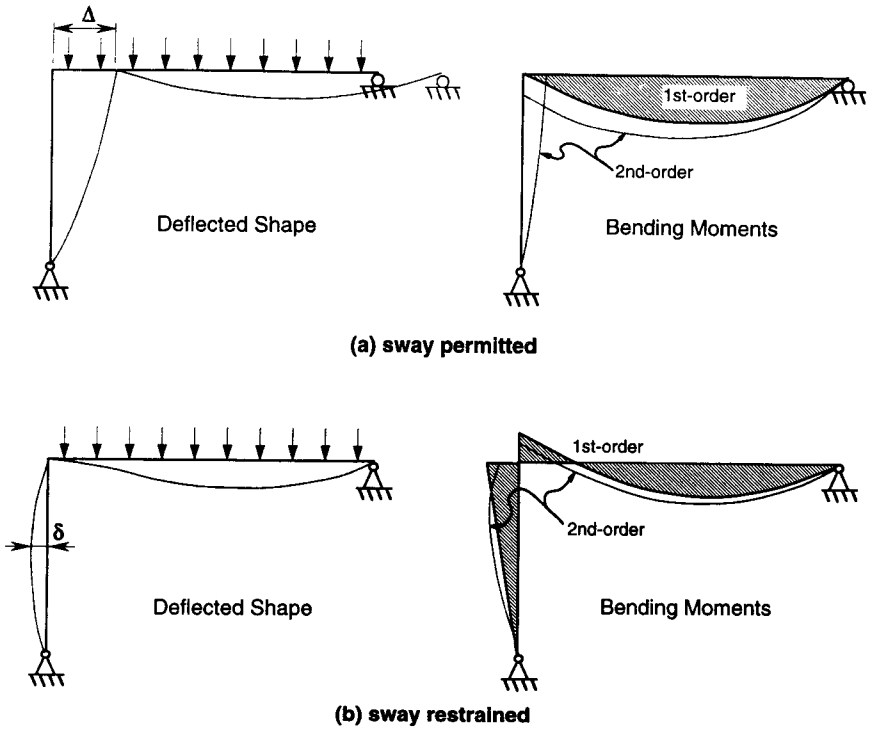

Fig. 16.2 Second-order P–Δ and P–δ moments.

column. These additional moments are due primarily to the P–Δ *effect*, where Δ is the lateral drift of the frame and P is the total vertical load that translates through Δ. LeMessurier (1977) has presented a similar example to this that demonstrates the extent of these second-order effects in a frame of realistic proportions.

For the frame in Fig. 16.2*b*, where sidesway is prevented, second-order moments are created in the beam and column arising from the lateral deflection (δ) along the column. The additional moment in the column is equal to the column load P times the deflection δ, hence the name P–δ *effect*. There is a reduction in the negative moment at the end of the beam due to the loss in rotational restraint of the column caused by the P–δ effect. This in turn increases the maximum positive moment within the beam span and may shift the location of maximum moment in the column. Further aspects of the second-order effects in a frame similar to this are discussed by Kanchanalai and Lu (1979).

Some points worth noting about these two examples, and about the calculation of frame second-order forces in general, are:

1. Second-order behavior affects moments in the beams and connections as well as in the columns. Moreover, the axial forces and shears of all members change due to second-order effects. However, in sway frames the changes in axial forces and shears are usually of lesser consequence than the amplification of moments.

2. The second-order moments do not necessarily have the same distribution as the first-order moments, and hence the total moments are not simply an amplification of the first-order moments. As described in the literature (LeMessurier, 1977; Kanchanalai and Lu, 1979), and as incorporated in many design specifications, there are many practical cases where second-order moments may be calculated by amplifying the first-order moments. However, the accurate calculation of the second-order forces using these methods may become fairly involved, generally requiring decomposition of the first-order moments into sidesway and nonsidesway moments, calculation of separate amplification factors for sidesway and nonsidesway, and combination of all the calculated terms (e.g., see the commentary to AISC–LRFD, 1993). Furthermore, these methods are ineffective and cumbersome for calculating the maximum second-order moments in beams with distributed gravity loads. Fortunately, with modern analysis programs, it is relatively easy to conduct direct second-order analyses with little computational expense, thereby avoiding the need for approximate procedures.

3. All structures, whether braced or unbraced, will experience both P–Δ and P–δ effects. While the examples in Fig. 16.2 are extreme cases dominated by one of the effects, both P–Δ and P–δ are present in each frame. In the frame of Fig. 16.2*a*, second-order P–Δ effects cause flexure of the left column, which in turn generates P–δ moments. In Fig. 16.2*b* there will be a slight joint transla-

tion due to axial shortening of the beam that will cause small P–Δ effects. In many practical cases one or the other of these effects might safely be ignored, but it is important to keep in mind that in most building frames the distinction between sway and nonsway moments is not as well defined as in these examples.

4. Linear superposition of effects does not hold for second-order analysis. Considering the frame in Fig. 16.2*a*, the deflections and internal forces from an analysis under lateral loads that caused a lateral deflection Δ, cannot be linearly combined with gravity effects. Rather, the two loads (gravity plus lateral) must be applied simultaneously in a single analysis. Moreover, since second-order effects are generally nonlinear (i.e., second-order internal forces and deflections under factored loads do not scale linearly from a second-order analysis under service loads), all second-order analyses should be made under factored loads.

Theoretical Stiffness Formulation. Various strategies to model geometric nonlinear effects can be developed based on conventional first- or second-order direct stiffness formulations and the use of incremental or incremental/iterative solution procedures. Formulations for second-order analysis can generally be expressed in the following form:

$$\{dF\} - \{dR\} = [K]\{d\Delta\} \tag{16.1}$$

where $\{dF\}$ is a vector of incremental applied nodal forces; $\{dR\}$ a vector of unbalanced nodal forces, calculated as the difference between the resultant of the current internal member forces and the applied loads; $[K]$ the stiffness matrix, which expresses an approximate linearized relationship between the nodal forces and the nodal displacements; and $\{d\Delta\}$ a vector of incremental nodel displacements and rotations. The features that distinguish the second-order analysis based on Eq. 16.1 from a first-order analysis are that the matrix equations are formulated in terms of incremental forces and displacements, and the unbalanced forces are calculated on the deformed geometry at the end of the linear loading step or iteration. As shown in Fig. 16.3, Eq. 16.1, which is generally nonlinear in the displacements through the term $\{dR\}$, can be solved in a piecewise linear fashion by applying successive increments of applied loads $\{dF_i\}$. For any force increment $\{dF_i\}$, a displacement increment $\{d\Delta_i^1\}$ can be computed based on the linear stiffness relationships, and then the actual internal nodal forces and the corresponding force imbalance $\{dR_i^1\}$ can be calculated. If the imbalance $\{dR_i^1\}$ is significant, Eq. 16.1 can be solved iteratively for successive values $\{dR_i^j\}$ and $\{d\Delta_i^j\}$, $j = 2, 3, 4, \ldots$, until the equilibrium error represented by the unbalanced force vector is negligible. If the force increments $\{dF_i\}$ are small enough, iterations will not be necessary to obtain an accurate solution and the nonlinear solution becomes a pure or "simple" incremental method.

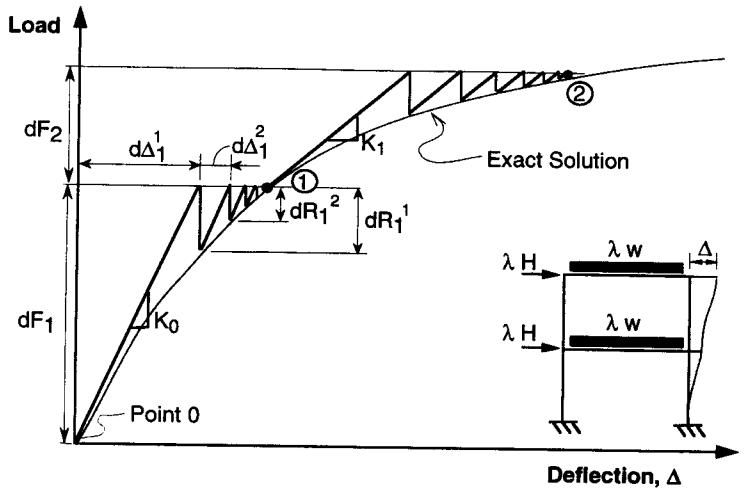

Fig. 16.3 Schematic representation of incremental–iterative solution procedure.

Figure 16.3 illustrates iteration at constant levels of load where a specified $\{dF_i\}$ is applied to the structure and iterations are conducted at a constant load until convergence is achieved. This type of procedure is commonly referred to as a Newton–Raphson incremental–iterative solution. Conventional Newton–Raphson procedures are not sufficient for continuing the solution through a stability limit load and into a postcollapse portion of the structural response. Therefore, alternative solution schemes such as arc-length or displacement control methods can be useful to the engineer in certain situations. Chen and Lui (1991) and Clarke (1994) provide useful overviews of several common solution approaches, and further details on solution methods are provided in the texts by Crisfield (1991), Yang and Quo (1994), and Bathe (1996).

Various formulations and their resulting stiffness matrices $[K]$ can be employed for the second-order solution represented by Eq. 16.1. The simplest of all approaches is to use the ordinary first-order elastic stiffness $[K_e]$ and to obtain the geometric nonlinear solution in a purely incremental–iterative fashion by updating the geometry after every step of the analysis. By this approach, the incremental internal member forces at the end of every solution step are calculated by substituting the member incremental displacements back into the linear elastic element stiffness equations associated with the deformed geometry of the structure. However, this approach in general will require a large number of small increments $\{dF_i\}$, as well as discretization of all the members with significant axial force into several elements. Furthermore, when formulated in this way, the global equations would not be able to detect bifurcation

points due to geometric instabilities. Therefore, this approach of using only the first-order elastic stiffness $\{K_e\}$ in Eq. 16.1 is not practical and is not recommended.

Two methods often employed to capture second-order behavior in the element stiffness relationships are referred to as the stability function and geometric approaches. The *stability function approach* is developed directly from the differential equations for flexure, where the equilibrium equations are formulated on the deformed member, assuming small deformations. The reader is referred to Chen and Lui (1991) and White and Hajjar (1991) for details of the derivation and application of the stability function approach. The *geometric stiffness approach* is derived from basic principles of virtual work, assuming interpolation or shape functions for the member's displacements. The virtual work derivation for second-order behavior differs from a conventional first-order derivation through consideration of higher-order terms in equations relating strains to member displacements. This approach is more extendible to a wide range of problems, including formulations for three-dimensional and inelastic analyses. When simplified into final matrix form, stiffness relationships obtained from either method are usually of comparable accuracy for assessing second-order effects in practical frames.

Popular virtual work (or energy) formulations for second-order frame analysis are based on updating the structural geometry at the end of each linearized solution step. In a formal nonlinear mechanics context, such methods are referred to as an updated Lagrangian procedure (e.g., Crisfield, 1991; Yang and Quo, 1994; Bathe, 1996). Based on this approach, the structure stiffness matrix of Eq. 16.1 takes on the following form:

$$[K] = [K_e] + [K_g] \tag{16.2}$$

where $[K_e]$ is the standard linear elastic stiffness matrix and $[K_g]$ is referred to as the geometric stiffness matrix. The net effect of updating the geometry and including the geometric stiffness terms is a change in the incremental (or tangent) stiffness associated with the internal member forces in the deformed equilibrium state. In Fig. 16.3 this changes the stiffness from K_0 to K_1 after the first load increment. In addition to improving the accuracy and efficiency of the solution, the geometric stiffness terms $[K_g]$ enable calculation of buckling loads, and for dynamic analyses they reflect the change in the natural period of vibration due to second-order effects.

The basic geometric stiffness for a two-dimensional prismatic beam-column member, based on cubic Hermitian interpolation of the transverse displacements and linear interpolation of the axial displacements is shown in Fig. 16.4*a*. A subset of the geometric stiffness terms corresponding to rigid-body rotation, sometimes called the *external geometric stiffness*, is shown in Fig. 16.4*b*. The terms in Fig. 16.4*b* account for the change in direction of the axial and shear forces in the member associated with rotation of the member chord which at the member level can be thought of as the P–Δ effect.

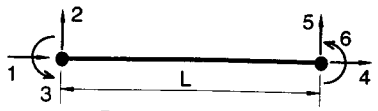

$P = +F_4$

$V = +F_2 = (M_3 + M_6)/L$

degrees of freedom and sign convention

0	V/L	0	0	-V/L	0
V/L	6P/5L	P/10	-V/L	-6P/5L	P/10
0	P/10	2PL/15	0	-P/10	-PL/30
0	-V/L	0	0	V/L	0
-V/L	-6P/5L	-P/10	V/L	6P/5L	-P/10
0	P/10	-PL/30	0	-P/10	2PL/15

(a) full matrix for two-dimensional beam-column

	V/L			-V/L	
V/L	P/L		-V/L	-P/L	
	-V/L			V/L	
-V/L	-P/L		V/L	P/L	

(b) external matrix for two-dimensional beam-column

Fig. 16.4 Geometric stiffness matrices.

Comparing the two matrices, the additional terms in Fig. 16.4*a* reflect the change in flexural stiffness of the member due to the presence of axial load, independent of sidesway displacements (i.e., the reduction in stiffness due to the P–δ effects along the member). Note that by omitting the terms involving shear (V) from the external geometric stiffness matrix (Fig. 16.4*b*), the geometric stiffness matrix for a pin-ended strut is obtained. The strut element matrix is often used in analysis programs to model interstory P–Δ effects.

The geometric stiffness shown in Fig. 16.4*a* represents the P–Δ effects exactly, but in general, it only approximates the P–δ effects. This can be deduced by considering that the assumed element shape functions represent rigid-body rotation of the member exactly but only approximate the actual transverse displacements (δ) of a member subjected to significant axial force. Although the representation of P–δ effects is not exact, the geometric stiffness matrix in Fig. 16.4*a* is sufficient to capture the geometric nonlinear behavior accurately in most frames where P–Δ effects dominate the behavior. For example, White and Hajjar (1991) have shown that the maximum error in the geometric stiffness terms is less than 1% for cases where the axial member force is less than 40% of the Euler buckling load ($P_e = \pi^2 EI/L^2$) of the member. This is a limit that is satisfied in most practical situations. Otherwise, second-order stiffness terms within 1% of the exact solution can be obtained by discretizing members into two or three elements (Allen and Bulson, 1980; White and Hajjar, 1991). Three elements are needed for the most severe cases of members whose ends are restrained against sidesway where the δ displacements dominate the geometric nonlinear response. Otherwise, for most sway frames, discretization of members into one or two elements will usually suffice for accurately modeling the elastic stiffness.

While member end forces calculated using the geometric stiffness terms of Fig. 16.4 will reflect P–Δ effects and the influence of P–δ on the member stiffnesses, calculation of second-order moments along the member length due to P–δ requires either a specialized member force calculation technique or discretization of the member into several elements. For example, as described by White and Hajjar (1991) and Liew (1992), exact analytical equations for the maximum moment within the span are reasonably simple and can be implemented as part of a computerized procedure without great difficulty. Alternatively, for members not subjected to transverse loads, the additional moments induced by P–δ effects can be calculated approximately using the standard amplification equation,

$$M^* = \frac{C_m}{1 - P/P_e} \qquad M_2 > M_1 \tag{16.3a}$$

$$C_m = 0.6 - \frac{0.4M_1}{M_2} \tag{16.3b}$$

$$P_e = \frac{\pi^2 EI}{L^2} \tag{16.3c}$$

where M^* is the maximum second-order moment, including both P–Δ and P–δ effects; M_1 and M_2 are the smaller and larger member end moments, respectively, including P–Δ effects, with M_1/M_2 positive for reversed-curvature bending; P is the axial compression in the member; and EI and L are member properties related to the axis of bending.

These equations are essentially the same as the "no-translation" (B1) force amplificaion factor in the AISC–LRFD specification (AISC, 1993), except that P_e in Eq. 16.3c is based on the actual member length. The general accuracy of these equations for any M_1/M_2 is shown in Fig. C–C1.2 of the AISC–LRFD specification commentary (AISC, 1993).

Approximate Second-Order Methods. With the capablities of current computer hardware and software, there is little reason not to do a rigorous second-order analysis of the type outlined above. For most practical cases, accurate second-order design forces can be obtained by applying the loads in one or two increments, and only a few iterations are required to converge to an accurate solution. However, for elastic analysis of building frames where deformations are usually not very large, it is often acceptable to utilize simplified methods to account for second-order effects. For example, Wilson and Habibullah (1987) present an approximate but computationally efficient method for modeling second-order effects in frames subjected to lateral loads. Their method uses fictitious lateral forces to capture interstory P–Δ effects that dominate the second-order sidesway response of most building frames. For three-dimensional structures with rigid floor diaphragms constraints, these forces include second-order torques applied about the vertical axis to account for P–Δ effects induced by relative floor rotations. Assuming that gravity loads are constant during the analysis and that lateral frame displacements are not too large, Wilson and Habibullah show that the P–Δ analysis under lateral loads is practically linear. This permits application of their method with only minor changes to standard linear analysis routines. A related method to this is the *negative brace method*, in which fictitious braces with negative stiffness coefficients inserted between floors to approximate P–Δ effects (Rutenberg, 1981, 1982). The brace stiffnesses are calculated using the gravity load, which is assumed constant during the analysis. An advantage of the negative brace technique is that it can be used with software that does not have built-in features for second-order analysis. It is important to note that simplified P–Δ procedures such as these do not include P–δ effects and, given the assumption of small deflections, they are limited in their ability to model very slender structures that respond nonlinearly to second-order effects.

Most design specifications provide factors to obtain approximate values of second-order moments by amplification of first-order moments. For example, Chapter C of the AISC–LRFD specification (1993) includes separate amplification factors (B1 and B2) to account for P–δ and P–Δ effects. The application and development of these factors are discussed at length in the commentary to the specification and will not be repeated here. It is important to recognize that these factors are approximate, and that in many situations they may not capture the full extent of second-order effects. For example, since the factors are developed for two-dimensional subassemblies with idealized boundary and loading conditions, they are clumsy to apply in frames that have interdepen-

dent P–δ and P–Δ effects and for irregular and three-dimensional structures. Moreover, they do not account directly for amplification of girder moments and/or axial forces in braces and columns.

16.2.2 Inelastic Analysis

For the present discussion, inelastic behavior will be limited to consideration of rigidly connected steel frame structures where the primary effect is yielding of members due to combined axial load and bending moments. Using an incremental stiffness analysis, such as described above for second-order analysis (Eq. 16.1), inelastic effects may be included by modifying the incremental stiffness matrix [K] to account for member plastification. Inelastic models are usually implemented in the same manner, whether the analysis is first- or second-order; however, combined inelastic and second-order effects near the strength limit state generally require more robust solution methods. In addition, since inelastic behavior is load path dependent, this necessitates an incremental solution procedure to trace the applied load history.

Types of inelastic beam-column models can be broadly classified, depending on the degree to which they model the progression of yielding in the members due to the combined effects of axial load, moments, and residual stresses. Basic methods that do not model any spread of plasticity in the member are often termed *plastic hinge* or *concentrated plasticity models*, and those that do model gradual yielding through member cross sections and along their length are termed *spread-of-plasticity*, *distributed plasticity*, or *plastic zone models*. For evaluating frame stability, an important distinction between concentrated and distributed plasticity methods is that the latter capture reductions in member stiffness prior to full plastification, which significantly affects second-order deformations and forces.

Basic aspects of inelastic behavior are illustrated by the frame in Fig. 16.5, which is subjected to proportional vertical and lateral loads. In this example second-order effects are not considered. Response curves, shown solid in Fig. 16.5*c* and *d*, correspond to an elastic–perfectly plastic hinge analysis, while the dashed lines correspond to a distributed plasticity analysis. Assuming that the columns plastify before the beam, the first hinge will form at the top of the right-hand column due to combined moment and axial compression. Upon further loading, the plastic limit load is reached with the formation of a second hinge in the left column that creates a sidesway mechanism. Referring to Fig. 16.5*d*, the first hinge is detected when the combination of axial load and moment at the top of the right column (pt. 1) reaches the full plastification yield criterion of the cross section. The internal bending moment diagram at this stage is shown by the solid line in Fig. 16.5*b*. As shown in Fig. 16.5*c*, the structure continues to carry additional load until a second hinge forms at the top of the left column, indicated as pt. 2 in the figure. Referring to Fig. 16.5*b* and *d*, during loading from point 1 to 2, the right column sheds some of its moment so that it can support additional axial

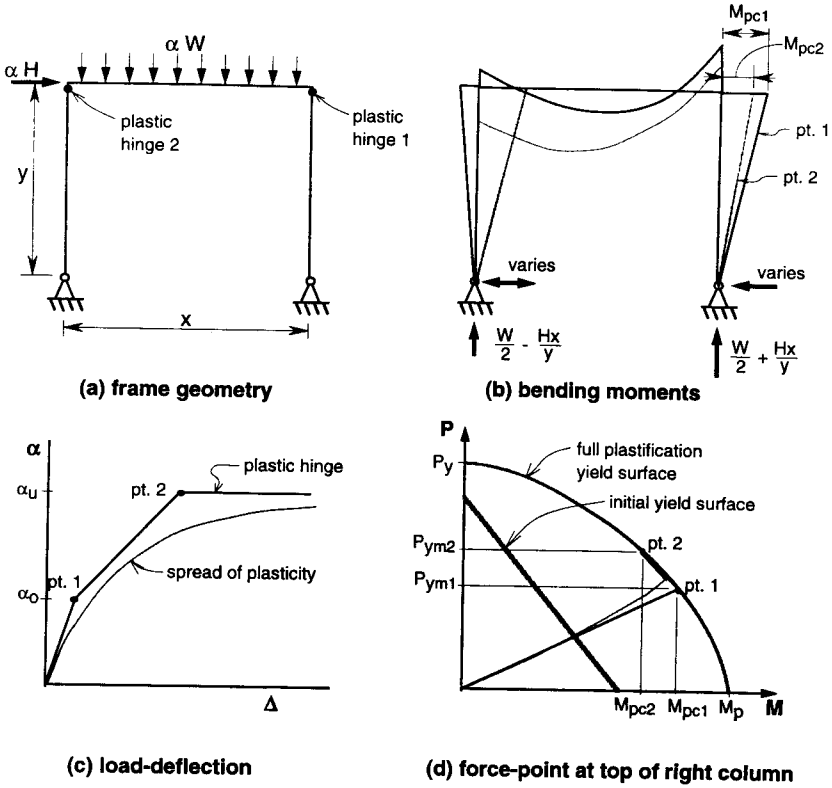

Fig. 16.5 Example of elastic–plastic force redistribution.

load. The increased axial load is directly proportional to the vertical column base reactions, which, as shown in Fig. 16.5*b* are statically determinate. By the time the second hinge forms in the left column the axial load resisted by the right column increases from P_1 to P_2, and in adherence with the yield criteria the moment decreases from M_1 to M_2.

In accordance with the upper-bound plasticity theorem, the limit load obtained using first-order analysis, whether an elastic–perfectly plastic hinge or a distributed plasticity analysis, will be equal to that obtained by a plastic mechanism analysis. This is assuming that the analyses are all made using the same full-plastification criterion and that strain hardening is neglected. On the other hand, limit loads based on different types of second-order inelastic analyses are, in general, not equal to each other because of the interaction of spread-of-plasticity and second-order effects. In some frames this interaction can lead to large differences in second-order inelastic limit points obtained from plastic hinge versus distributed plasticity analyses.

Plastic-Hinge Methods. For framed structures, plastic-hinge analyses are usually based on a yield criterion that considers longitudinal normal stresses due to axial loads and moments, often neglecting shear stresses due to shear forces and torsion. Although in theory it is possible to develop exact expressions for member-cross-section yield criteria (see, e.g., Chen and Atsuta, 1976), most plastic-hinge methods rely on simplified force interaction expressions to approximate the yield surface. For two-dimensional analyses either piecewise linear or continuous functions are commonly used, whereas for three-dimensional analyses, continuous functions are usually preferred over multifaceted surfaces. The following is an example of a yield surface similar to one originally developed by Orbison et al. (1982) for three-dimensional analyses:

$$1.15p^2 - 0.15p^6 + m_z^2 + m_y^4 + 3.67p^2m_z^2 + 3.0p^6m_y^2 + 4.65m_z^4m_y^2 = 1.0 \quad (16.4)$$

where $p = P/P_y$, $m_z = M_z/M_{zp}$ (strong-axis bending), and $m_y = M_y/M_{yp}$ (weak-axis bending). As described by Orbison et al., features of this yield surface equation that make it amenable to computer-based inelastic analyses are that it is a smooth, continuous, and convex function. This yield surface was obtained through calibration to model accurately the biaxial bending of light- to medium-weight H-shaped sections. Other examples of the development of yield surface functions include Attalla et al. (1994) and Duan and Chen (1990).

The stiffness equation for a plasic-hinge analysis has the same form as Eq. 16.1 but where the stiffness matrix $[K]$ is updated during the analysis to reflect formation of plastic hinges in the structure, and the unbalanced force vector $\{dR\}$ corrects for instances where the calculated element forces from the previous analysis increment violate the member yield criterion. An example of a rudimentary analysis procedure that models plastic hinges by inserting the equivalent of "real" hinges into the structure is described by Chen and Sohal (1995). Alternative formulations utilize plasticity theory to develop element tangent stiffness matrices that more rigorously account for the interaction of axial forces and bending moments in determining the direction of plastic deformations (e.g., Orbison et al., 1982; Porter and Powell, 1971).

Distributed Plasticity Models. At the member cross section, spread of plasticity can be idealized as a nonlinear moment-curvature response. Shown in Fig. 16.6*a* are two force interaction surfaces, the inner of which signifies the initiation of yielding calculated as a function of the cross-section area (A), elastic section moduli (S_y and S_z), residual stresses (F_{rc}), and the material yield strength (F_y). The outer or full-plastification surface follows the same yield surface criteria as described previously for elastic–plastic hinge analyses. Considering a member under constant axial force and increasing moment (Fig. 16.6*b*), the resulting moment-curvature behavior is shown in Fig. 16.6*c*, where ϕ_e and ϕ_p refer to the elastic and plastic curvatures, and

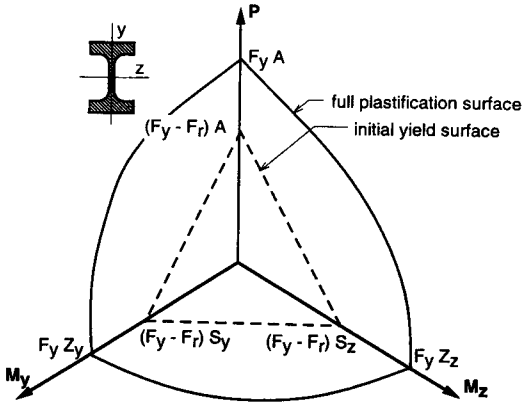

(a) initial and full plastification yield surfaces

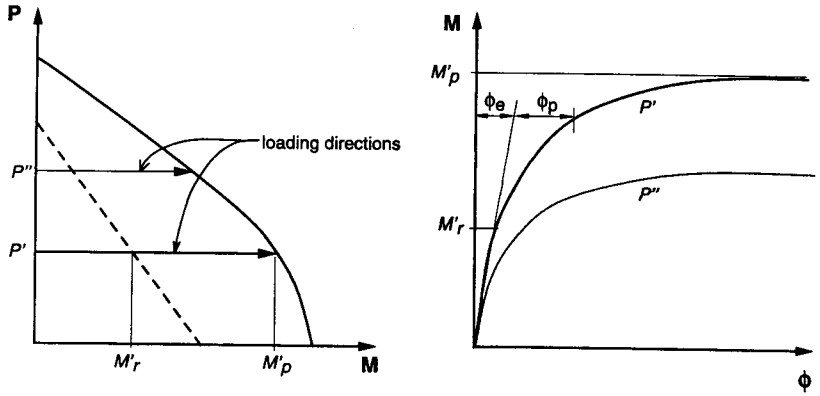

(b) member loading direction **(c) moment-curvature response**

Fig. 16.6 Inelastic cross-section behavior.

M_{rc} and M_{pc} refer to the initial and full plastification moments in the presence of an axial force P. The nonlinear response shown in Fig. 16.6*c* reflects spread of plasticity through the member cross section for bending about one axis under two levels of axial loads. Note that the departure from linearity begins sooner and is more significant for members with larger axial load. In general, the behavior shown in Fig. 16.6*b* and *c* can be extended to include nonlinear moment-curvature response about both bending axes under any arbitrary sequence of loading.

In addition to yielding through the cross section, spread of plasticity involves a progression of yielding along the length of the member. The length of the plastified regions are based on the initiation of yielding as calculated

using an initial yield surface such as shown in Fig. 16.6*a*. Using force-deformation response from the cross sections such as shown in Fig. 16.6*c*, the stiffness of the member can be calculated by numerically integrating the inelastic cross-section properties along the length of the member. Many methods have been proposed for implementing spread-of-plasticity effects in frame analysis software, ranging from detailed fiber-type models to more computationally efficient ones based on variants of the plastic-hinge concept (i.e., by using stress-resultant or force-deformation models).

Fiber-type models involve discretization of the member cross sections into small areas that are considered as longitudinal fibers of the member. By applying the assumption that plane sections originally normal to the reference axis of the member remain plane and normal (with the exception of warping deformations due to nonuniform torsion), the strains in the longitudinal fibers can be calculated from the axial strain and curvatures of the section. Then, by relating the strains to stresses using an appropriate constitutive law and considering the residual stresses, the cross-section forces can be obtained by numerically integrating the stresses over the cross section (i.e., a simple numerical integration rule would be $P = \Sigma\sigma_i A_i$, $M_y = \Sigma\sigma_i A_i z_i$, and so on, where A_i is the area of fiber i, σ_i is the stress in each fiber, and z_i is the distance from the fiber to the centroidal bending axis). At any level of loading, inelastic cross-section stiffness can also be calculated by integration. For example, the tangent flexural stiffness can be calculated simply as $\Sigma E_i A_i z_i^2$, where E_i is determined from the stress-strain constitutive law for the material. Neglecting strain hardening and considering elastic–perfectly plastic material behavior, E_i for any fiber will either be equal to the elastic modulus or zero. Axial and flexural stiffness of the cross section obtained in this way are then integrated along the length of the member to develop element tangent stiffness matrices. Examples of fiber element implementations include Alvarez and Birnstiel (1967), El-Zanaty et al. (1980), and Clarke (1994). While the basic formulations for fiber element methods are fairly straightforward, their direct implementation can require excessive computational requirements. In seeking an intermediate solution that has the computational efficiency of elastic–perfectly plastic hinge methods and the accuracy of spread-of-plasticity fiber methods, several researchers have recently proposed what can be called *quasi-hinge* or *stress-resultant constitutive models* (e.g., Liew et al., 1993; Attalla et al., 1994; El-Tawil and Deierlein, 1996). Although subject to some limitations of required calibration, such methods have been shown to make spread-of-plasticity analyses practical for large (realistic) building frames.

16.2.3 Critical Load Analysis

Given that for most buildings the elastic critical loads are considerably higher than the inelastic limit point, critical load analyses in themselves are often of limited practical value for frame design. They have proved useful in determining amplification factors to approximate second-order effects; however, with modern second-order analysis software, such methods are of less importance. As described below, while methods have been proposed to improve critical load analyses to reflect inelastic behavior, most of these still only provide an estimate of the upper-bound stability limit of a frame under a given loading. Methods of critical load analysis are reviewed here briefly given their traditional role in stability analysis and because they are still useful as screening tools for stability limits.

Using a stiffness matrix formulation, critical loads of frames and other structures may be calculated by the following eigenvalue problem:

$$[K + \mu_i K_g]\{\Delta_i\} = \{0\} \tag{16.5}$$

where $[K]$ is the structural stiffness matrix, $[K_g]$ the geometric stiffness matrix, μ_i the eigenvalue (critical load index), and $\{\Delta_i\}$ the eigenvector (buckled mode shape). $[K_g]$ is typically of the same form as the geometric stiffness matrix described previously for a second-order analysis; however, in this case the member forces that comprise the geometric stiffnesses are calcualted by a first-order analysis under a prescribed external load distribution $\{F\}$. Thus the resulting critical load is unique for the given loading condition, and the distribution of internal forces, upon which the critical load is based, are calculated for the undeformed geometry of the structure. Note that in most cases, the loading applied for critical load analysis is an idealized representation of the gravity loads that may not necessarily reflect the internal force distribution at the true limit point of the structure.

The critical load calculated by Eq. 16.5 is equal to the following:

$$\{F_{cr,i}\} = \mu_i\{F\} \tag{16.6}$$

where $\{F_{cr,i}\}$ is proportional to the prescribed load vector $\{F\}$. The subscript i in Eqs. 16.5 and 16.6 refers to the fact that there are as many buckling loads (eigensolutions) to the problem as there are number of degrees of freedom in Eq. 16.5. While the lower critical value is usually the one of interest, there may be instances where higher buckling modes provide useful information.

In addition to the rigorous solutions follownig the eigenvalue equations presented above, many simplified methods of determining critical loads of frames have been proposed (e.g., Stevens, 1967; Horne, 1975; Nair, 1987; ASCE, 1997). Most of these are based on story-by-story checks with other simplifying behavioral assumptions.

Tangent-Modulus Adjustment. In most applications, the structural stiffness used in Eq. 16.5 is the elastic stiffness, and the resulting critical load $\{F_{cr,i}\}$ corresponds to elastic buckling. However, by modifying $[K]$ using a

tangent-modulus adjustment one can obtain critical loads that more closely represent the actual limit state of the structure under pure axial loading. As described by Ziemian (1991), Eq. 16.5 can be adjusted to approximate the reduction in column stiffness due to axial compression and residual stresses in a similar manner to the method for adjusting effective column buckling lengths that was originally suggested by Yura (1971) and is included in the AISC–LRFD manual (AISC, 1993). In this approach, the $[K]$ matrix in Eq. 16.5 is based on member stiffnesses that are calculated using a tangent modulus for each member (E_t) that is consistent with the axial force in that member at the critical load $\{F_{cr}\}$. Values of E_t can be calculated using either tangent-modulus formulas derived from the assumed residual stresses in the member, or semiempirical formulas derived from inelastic column curves. The column stiffness reduction factors given in Part 3 of the AISC–LRFD manual (AISC, 1993) are one example of the latter type of adjustment. Since the terms in the stiffness matrix $[K]$ are now dependent on the magnitude of the applied load vector $\{F_{cr}\}$, the tangent-modulus adjustment necessitates an iterative solution procedure to solve Eq. 16.5. It is important to recognize that while this adjustment will result in critical loads closer to the inelastic limit point, the adjustment still does not take into account the loss in stiffness due to plastification of members under combined axial load and bending and the formation of plastic hinges.

16.3 FRAME BEHAVIOR

Technical Memorandum No. 5 of the SSRC, which outlines general principles for stability design of metal structures, states that

> the procedure for the establishment of the load carrying capacity of frames, members, or elements on the basis of maximum strength should be based on a mathematical model which incorporates:
> 1. Experimentally determined physical characteristics, such as residual stresses, material nonlinearities, . . . rationalized as may be appropriate.
> 2. A statistically appropriate combination of acceptance characteristics that are specified in supply, fabrication, and erection standards, such as out-of-straightness . . . material properties, and erection tolerances.
> 3. Effect of boundary conditions, such as restraint applied to the end of members.

These fundamental guidelines form the starting point for assessing the most important attributes of frame behavior pertaining to stability design, and for evaluating how different methods of analysis and associated design procedures

account for this behavior. In the following sections, considerations for analyzing frame behavior are described through a simple example, followed by a more comprehensive summary of behavioral effects and modeling issues that may affect the evaluation of frame and member stability.

16.3.1 Planar Frame Example

Frame behaivor and methods of stability analyses are reviewed by considering the frame shown in Fig. 16.7, which is based on studies by Iffland and Birnstiel (1982) and Ziemian et al. (1992a). The frame geometry and loading are representative of low-rise industrial structures, where stability effects are accentuated by a high ratio of gravity to lateral load. Member sizes shown in Fig. 16.7 represent a least-weight design based on second-order inelastic analyses to satisfy minimum strength and service-load criteria. Note that the leftmost W8 column of the frame is intentionally made smaller than the other columns and is stabilized by leaning on the stronger W14 columns.

The frame members are proportioned according to the following design criteria:

1. *Serviceability.* The roof and interstory drift indices under service wind loads are limited to 1/400 and 1/250, respectively, and the beam deflection index under service live load is limited to 1/360. In addition, plastic hinges are not permitted to form under service loads.
2. *Strength.* A second-order inelastic analysis is used to check that the frame can safely resist the factored load. In this check the following ASIC–LRFD (1993) criteria are applied: Load combinations of gravity

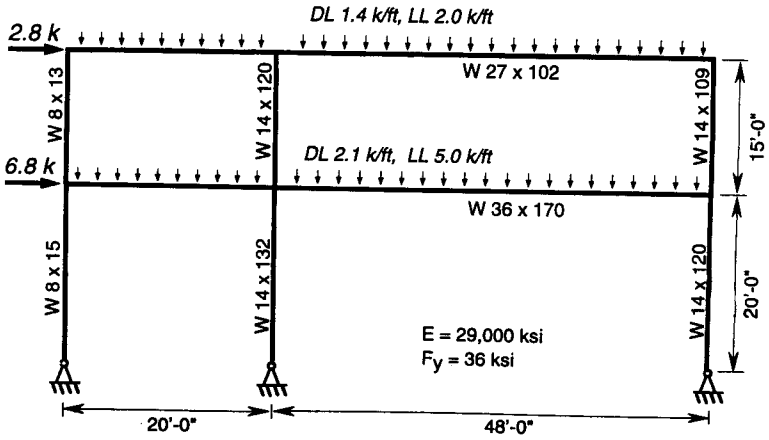

Fig. 16.7 Example frame: geometry and loading.

and wind loads include $1.2D + 1.6L$ and $1.2D + 0.5L + 1.3W$; the full plastification strengths of member cross sections are reduced by resistance factors ($\phi = 0.9$ for axial tension and plastic moments, $\phi = 0.85$ for axial compression); all members meet section slenderness and material criteria for compact plastically designed structures.

Implied by these criteria is the assumption that second-order inelastic analysis alone suffices for checking strength and stability of the frame and its members. Thus, subject to the assumptions that all members are rigidly connected and fully braced out-of-plane, the nonlinear analysis eliminates the need to check member strengths by beam-column force interaction equations, such as in Chapter H of the AISC–LRFD specification (1993).

Response of the frame under gravity load ($1.2D + 1.6L$) is summarized in the plot of the applied load ratio versus displacement and the plastic-hinging sequence shown in Fig. 16.8*a*. Because of its nonsymmetric geometry, the frame begins to sway to the left until the first hinge forms at an applied load of 74% of the full factored load. Upon further loading, more hinges form and the frame stiffness changes dramatically, such that it begins to deflect to the right. Finally, with formation of the sixth hinge at a load ratio of 1.0 (100% of the factored load), the frame reaches its inelastic stability limit and fails by swaying back to the left. Results of this plastic-hinge analysis are compared to those of a spread-of-plasticity (plastic zone) analysis in Fig. 16.8*b*. Also shown in Fig. 16.8*b* is a diagram indicating the percentage of cross-section yielding calculated at the inelastic limit point from the spread-of-plasticity analysis. Although the spread-of-plasticity solution indicates a less abrupt load-deformation response, both analyses give essentially the same stability limit strength. This is despite the fact that there is significant spread of plasticity in several columns and beams (Fig. 16.8*b*) that is not accounted for in the hinge analysis (Fig. 16.8*a*).

The following observations are made from these analyses:

- At the inelastic limit point, a classical *plastic mechanism* has not yet formed. Rather, the instability is a function of the combined destabilizing effects of member plastification and geometric nonlinear behavior.
- The distribution of internal moments at the limit point is quite different from the first-order distribution. As described by Ziemian et al. (1992a), plastic hinge formations cause unloading of moments and/or axial forces in some members under increasing external load.
- Stability at the limit point is based solely on satisfying the equilibrium on the deformed geometry with maximum internal forces limited to the fully plastified strength of the member cross sections. As noted above, the nominal yield strengths are reduced to design strengths by application of the AISC–LRFD resistance factors to account for statistical variations in cross section strengths.

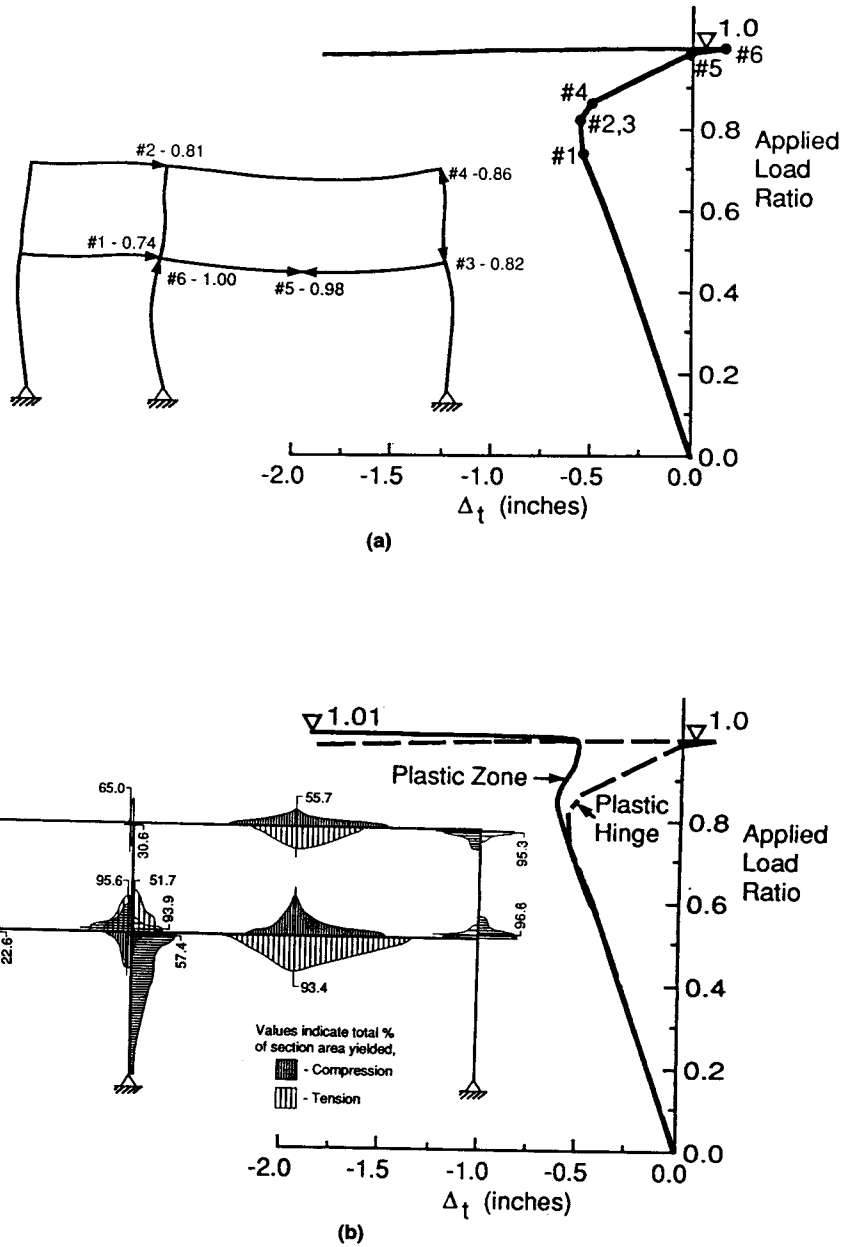

Fig. 16.8 Example frame: (*a*) second-order elastic–plastic hinge analysis under factored gravity loads; (*b*) comparison of spread-of-plasticity (plastic zone) and plastic hinge results (Ziemian, 1991).

Response curves for the frame under the factored gravity and wind loads using the four methods of analysis described previously are shown in Fig. 16.9. Under gravity loading (Fig. 16.9*a*), there is only slight (1%) difference in the limit point obtained using a first- versus second-order inelastic analysis. This is due to the fact that the net lateral displacement and resulting P–Δ effects are small at the limit load. There are significant inelastic P–δ effects in the light bottom-story column on the left-hand side, but these are not large enough to

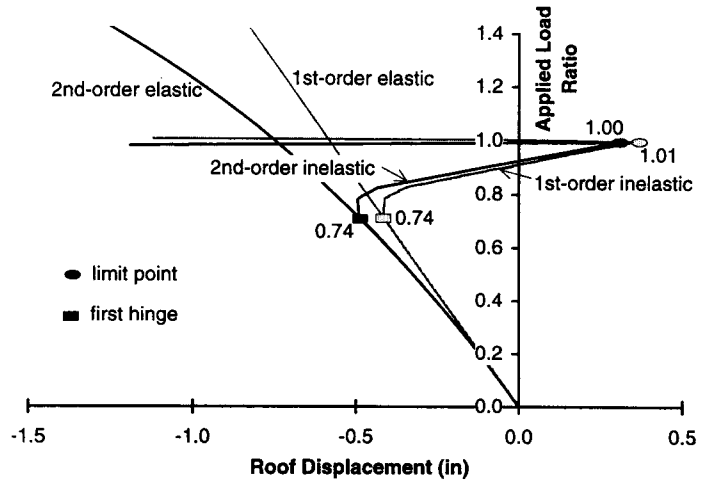

(*a*)

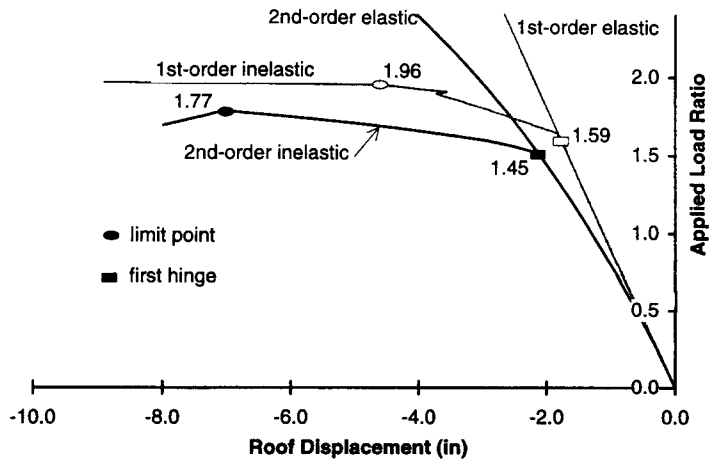

(*b*)

Fig. 16.9 Comparison of analysis results for two-story frame: (*a*) gravity loading; (*b*) gravity plus wind loading.

precipitate a "braced buckling" failure of that member prior to sway failure of the frame. As a result, lateral sway of the frame does not have a significant effect until the point when the abrupt sidesway collapse occurs. On the other hand, under combined gravity and lateral loading (Fig. 16.9*b*), the second-order behavior reduces the inelastic limit strength by approximately 10%. These observations depend on the specific characteristics of this frame, and relative differences between first- and second-order response should not be generalized to other cases.

The analyses above do not include the effects of geometric imperfections. Based on maximum fabrication and erection tolerances, the geometric imperfection effects can be checked by imposing a uniform out-of-plumbness of $H/500$ on both stories of the building. To check for the significance of these imperfections, second-order plastic-hinge analyses were rerun for cases where the initial geometry was modified to include an $H/500$ story imperfection. For the governing gravity load case the sidesway imperfections do change the initial elastic sway of the frame, but cause essentially no change in the inelastic strength limit for either the gravity or gravity plus wind load combinations.

Assuming that the second-order inelastic analyses provide an accurate representation of the stability limit strength of the frame, it is instructive to contrast these results with those from second-order elastic analyses. The second-order elastic response curves are superimposed on the inelastic curves in Fig. 16.9, although for presentation they have been truncated well below the elastic stability limit point. Had the full curves been plotted, they would asymptotically approach the elastic *stability limit loads* at an applied load ratio of 3.4 times the factored gravity loads (Fig. 16.9*a*) and at 6.6 times the factored gravity plus wind loads (Fig. 16.9*b*). Note that these limits, which are calculated on the deformed geometry, are close but not exactly equal to the *elastic critical load* ratios of 3.2 and 6.3 calculated by elastic eigenvalue analyses. The elastic limit load ratios of 3.4 and 6.6 are roughly three and one-half times larger that the corresponding second-order inelastic limit load ratios of 1.00 and 1.77. Differences between the elastic and inelastic limit points are considered to be one measure of the significance of geometric imperfection and spread-of-plasticity effects on frame behavior.

While elastic stability limits are often cited as a measure of frame stability, for most practical frames the internal force distribution and deformations at the elastic stability limit can be very different from those at the inelastic limit. Consider, for example, the two bending moment diagrams from the second-order elastic analysis of the frame under gravity loads shown in Fig. 16.10*a* and *b*. The moment distribution in Fig. 16.10*a* is at an applied load ratio of 1.0 (i.e., a load equal to the factored design load of $1.2D + 1.6L$) and in Fig. 16.10*b* is for a load ratio of 3.2 close to the elastic limit load. Comparing the two diagrams in Fig. 16.10, it is apparent that for some members the second-order behavior increases the first-order moments, whereas in other members the first- and second-order effects counteract one another. These counteracting effects are one reason why the frame was not sensitive to out-of-plumb imper-

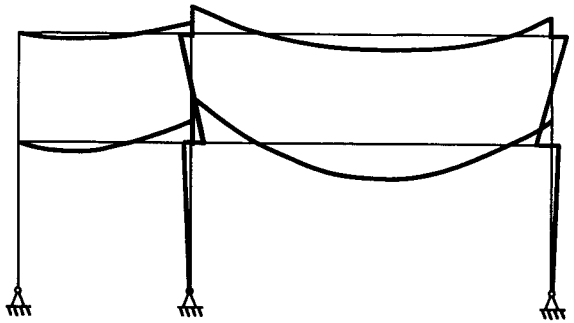

(a) factored design loads, applied load ratio = 1.0

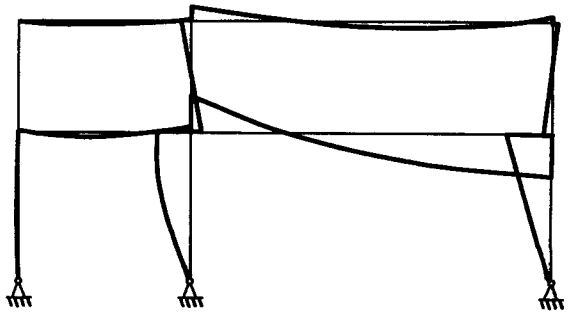

(b) near elastic limit load, applied load ratio = 3.2

Fig. 16.10 Bending moments from second-order elastic analysis under gravity loads.

fections. Finally, the highly nonlinear nature of the response near the stability limit load is why limits are often imposed on the use of approximate methods to calculate second-order forces by amplifying results from first-order analyses. For example, Eurocode 3 (ECS, 1993) limits the use of simplified second-order amplification factors to cases where the ratio of the critical load of the frame to the factored design load, F_{cr}/F_u, is less than 4. This translates to a limit on the second-order amplification factor of $AF < 1.33$, assuming that $\Delta F = 1/(1 - F_u/F_{cr})$.

The significance of second-order effects on the frame can be evaluated considering the data for the first-story drift and column moments calculated by first- and second-order elastic analyses summarized in Table 16.1. Under gravity load the second-order story drift amplification is 44%, while the second-order column moments vary from +4 to −11% compared to the first-order values. Under gravity plus wind, the deflections increase +17%, while the change in moments range between +8 and −93%. This is an example in which distributed gravity loads, differences in the relative column stiffnesses,

TABLE 16.1 Comparison of Elastic First- and Second-Order Analysis Results at Factored Design Loads for Bottom Story

Loading	Story Drift (in.)			Column Moments (kip-in.)								
				Left Column			Center Column			Right Column		
	First-Order	Second-Order	Percent Change	First-Order	Second-Order	Percent Change	First-Order	Second-Order	Percent Change	First-Order	Second-Order	Percent Change
$1.2D + 1.6L$	0.36	0.52	44	28	29	3	3540	3690	4	3570	3180	−11
$1.2D + 0.5L + 1.3W$	0.93	1.09	17	70	72	3	3190	3450	8	330	22	−93

and gravity-induced sidesway make it cumbersome to calculate second-order forces accurately using approximate member-based amplification factors. Instead, it is cleearly preferable to calculate these effects using a rigorous second-order computer analysis.

A final point regarding these analysis results is that a large amplification of deflections and moments due to elastic second-order effects does not necessarily result in a large change in the inelastic limit strength of the frame. This is an important point since most member-based design checks require an increase in member capacity to resist second-order moments that are often calculated in proportion to the drift amplification. Such procedures would be inconsistent for the previous frame, where despite rather large changes in the calculated first- and second-order *elastic* deflections and moments, the difference between the first- and second-order *inelastic* limit loads was much less. Referring back to Fig. 16.9, the second-order effects decrease the inelastic limit point by only 1% for the gravity load case and 10% for the gravity plus wind load case.

This example highlights some fundamental, yet sometimes subtle aspects of behavior that can affect the stability design of a relatively simple frame. The example is also intended to draw attention to aspects of behavior of indeterminate frames that are not necessarily captured in single-bay (often, single-story) frames that are the focus of much of the literature on frame stability. As this example shows, there are important aspects of behavior of practical frame systems that are not captured in simpler, less redundant structures. Finally, the example demonstrates some of the inherent limitations of applying elastic stability theory to structures where the strength limit state is reached at inelastic limit loads that are much lower than elastic limit loads.

16.3.2 Factors Influencing Frame Stability

Summarized in Tables 16.2A and 16.2B are various factors whose effect on frame stability should be considered in design. The tables are adapted from similar summaries previously compiled by Birnstiel and Iffland (1980), McGuire (1992), and White and Chen (1993), and they follow the principles of Technical Memorandum No. 5. As indicated, the factors are distinguished between those related to the physical attributes of the structure and loading (Table 16.2A) and how the response phenomena are modeled in analysis and design (Table 16.2B). The categorization of the factors is imperfect since many of the effects are interrelated, but the listing is intended to provide some guidance on behavioral effects that may influence behavior on typical building frames. The tables are by no means a comprehensive list of all possible effects that may arise in practice, and the degree to which various factors are significant for a given structure will vary from case to case. Whereas some factors are considered routinely in analysis, others are included in design implicitly through specification provisions and established practice.

TABLE 16.2A Factors Affecting Steel Frame Stability: Physical Attributes of Structure and Loading

Frame geometry and configuration
Centerline framing dimensions
Member geometry and material
Connection details
Foundation and support conditions
Shear connections to slab
Infill walls or secondary structural elements
Finite member and joint size effects
Out-of-plane bracing elements
Material properties
Elastic moduli
Expected versus nominal strengths
Ductility and fracture toughness
Geometric imperfections
Erection out-of-plumbness
Member out-of-straightness
Incidental connection or loading eccentricities
Internal residual stresses
From manufacturing/fabrication processes
From erection fit-up
From construction sequencing
From incidental thermal loadings or support settlement
Loading
Magnitude and distribution
Loading rate and duration

Following is a summary of how the varius factors from Tables 16.2A and 16.2B are addressed in the second-order elastic–plastic hinge analysis for the frame example presented in Section 16.3.1.

1. *Physical attributes and basic modeling.* The structure is modeled as a rigidly jointed planar frame using centerline dimensions of the ideal geometry. It is assumed that (1) the beam-column connections are fully restrained moment connections (2) the frame geometry and member proportions are such that the finite joint size and panel zone deformations are not significant, (3) column foundations provide negligible rotational restraint and that any minor settlements will not affect frame behavior significantly and (4) member properties are based on the bare steel members, assuming that they are designed neglecting composite action with the slab. Obviously, each of these assumptions is a simplification of the actual behavior and could be reconsidered in a more refined analysis. Residual stresses are not considered in the

TABLE 16.2B Factors Affecting Steel Frame Stability: Modeling Parameters and Behavioral Assumptions

Linear elastic response
Flexural, axial, and shear deformations of members
Deformations of connections and beam-column panel zones
Uniform torsion and/or nonuniform warping torsion deformations in members
Foundation and support movement
Dynamic and inertial effects
Geometric nonlinear response
P–δ effects: Influence of axial force on stiffness and internal moments of beam-columns
P–Δ: effects: influence of relative joint displacements on forces and displacements
Local buckling and cross-section distortion
Finite-rotation effects (three-dimensional structures)
Material nonlinear response
Member plastification under the action of axial force and biaxial bending (spread of plasticity versus plastic hinge idealizations)
Member plastification due to shear forces, uniform torsion, and nonuniform warping torsion (bi-moments)
Yielding in connection components and joint panels
Fracture of members and connections
Strain-hardening behavior
Cyclic plasticity effects
Load path effects, shakedown, and incremental collapse

plastic-hinge analysis, an assumption that is justified by the close agreement with the more refined spread-of-plasticity analysis, which did include residual stresses in the members (Fig. 16.8*b*). Erection out-of-plumb was also shown to have a negligible effect on the inelastic limit point, and other geometric imperfections are assumed to be insignificant.

2. *Response phenomena.* The basic analysis model includes axial and flexural deformations in the members. Members are compact, and thus local buckling can be neglected. All members are assumed to be braced out-of-plane, and thus torsional-flexural effects are not considered. Although this assumption is generally true for the beams, it is usually not true for columns and additional checks on the out-of-plane stability of the columns should be made. Loads are assumed to be static and are applied proportionally. The geometric nonlinear response, modeled through an updated Lagrangian approach, includes both the P–Δ and P–δ effects. In this case, each column was discretized into two elements to capture the P–δ amplification of moments with reasonable accuracy. Material nonlinear effects are included through an elastic–perfectly plastic hinge model that is based on the full plastification cross-section strength of members considering the interaction of axial force and bending moments.

Nominal yield strengths are used in the yield surface equations; strain hardening is neglected, and steel ductility and toughness are assumed sufficient to avoid fracture under the required inelastic deformation demands. Note that while in this case, the accuracy of the plastic-hinge analysis is verified by comparison to more detailed spread-of-plasticity analyses, it is not anticipated that such detailed verification would necessarily be applied in practice. Further discussion and guidance on gaging the significance of spread of plasticity is included in Sections 16.4 and 16.5.

3. *Uncertainties.* Variability in the loads and member strengths is considered by incorporating the AISC–LRFD load and resistance factors in the analysis. Resistance factors are included by reducing the yield surface criteria in the plastic-hinge model. The potential for incremental collapse under repeated loading is assumed small, although this has not been verified. Some discussion of repeated load effects is given in Section 16.4.2.

Since it is impractical and often unnecessary to include all behavioral effects in the analysis, the engineer must judge the degree to which the analysis accurately models the important stability effects to ensure a safe design. The remainder of this chapter includes further disucssion of a few of the more important factors.

16.3.3 Modeling of Initial Geometric Imperfections

Geometric imperfections are often idealized as the combination of member out-of-straightness and frame out-of-plumbness. However, the true imperfections in actual structures are less straightforward, being complicated by (1) actual column piece lengths and splice locations, (2) beam length and connection fit-up tolerances, (3) finite member size effects, (4) unavoidable eccentricities at connections and foundtions, (5) three-dimensional geometry, (6) imperfect load placement, and so on. Therefore, frame imperfections cannot be idealized with the same precision that is done, for example, in modeling out-of-straightness in axially loaded columns. Fortunately, for most frames the applied lateral loads and resulting member forces are large enough that initial geometric imperfections are not critical. Nevertheless, the engineer should consider the types and magnitude of imperfections that may occur and ecide whether they are significant to stability of the structure.

Fabrication and Erection Tolerances. In the absence of more accurate information, evaluation of imperfection effects should be based on the permissible fabrication and erection tolerances specified in the appropriate building code. In U.S. practice, for example, limits of member out-of-straightness and frame out-of-plumbness are prescribed in the *Code of Standard Practice for Steel Buildings and Bridges* (AISC, 1992). The basic limits specified by AISC that should be fairly representative of good practice elsewhere are as follows:

- *Member out-of-straightness*: $\delta_0 < L/1000$, where L is the distance between brace points.
- *Interstory out-of-plumbness*: $\Delta < h/500$, where h is the story height.
- *Maximum lack of verticality*: $\Delta_{0,max} < 25$ mm below the 20th floor, $\Delta_{0,max} < 50$ mm above the 20th floor.

Given that variations in beam lengths will tend to be random and are smaller than the maximum out-of-plumbness, all columns in a given story will tend to lean in the same direction.Moreover, to control the total lack of verticality, it is likely that the interstory out-of-plumbness will alternate directions up the height of the building. In general, one could expect the actual imperfections to be less than the maximum permissible values given above. Note, for example, that the maximum member out-of-straightness of $L/1000$ is 50% larger than the out-of-straightness of $L/1500$ assumed in the development of SSRC-column curve 2P, which is the basis of the column curve in the AISC–LRFD specification (AISC, 1993). However, given the absence of a reliable database of measured frame imperfections, it is suggested that where initial imperfection effects are found to be important, the *maximum erection tolerances* be used as the basis of frame stability checkes in design. In particular, checks for individual story instabilities should be checked using the maximum out-of-plumb tolerance.

Modeling of Imperfections with Notional Loads. The most direct method of modeling geometric imperfections is by incorporating the imperfections into the geometrical description of the analytical model. Alternatively, the internal forces caused by initial imperfections can be calculated by applying equivalent lateral forces, or what are sometimes called *notional loads*,* to the frame. Consider, for example, the bar–spring structure shown in Fig. 16.11*a* which includes an initial out-of-plumbness Δ_0. In Fig. 16.11*b* the initial imperfection is represented by the notional load of $P\Delta_0/h$ which produces internal first-order sway forces that are statically equivalent to those induced by vertical load P in Fig. 16.11*a*. By solving equilibrium on the deformed geometry for both cases, it can be shown that the resulting total second-order forces are equal, although the final deformed geometries differ by Δ_0. The resulting moment in the rotational spring is $M_s = 0.5P\Delta_0/(1–0.5Ph/k)$ where the denominator term represents the second-order amplifiction of the first-order spring moment, $M_{s1} = 0.5P\Delta_0$. These observations for this simple bar–spring structure generally hold true for elastic second-order moments

*The term *notional load* applies to any type of artificial load that is used to account indirectly for behavior effects not otherwise considered in the analysis. As described in Section 16.4.1, aside from their use to model initial geometric imperfections, notional loads are sometimes used to model spread-of-plasticity behavior, including the combined effects of residual stresses and initial geometric imperfections. The present discussion is limited to the use of notional loads for modeling initial geometric imperfections.

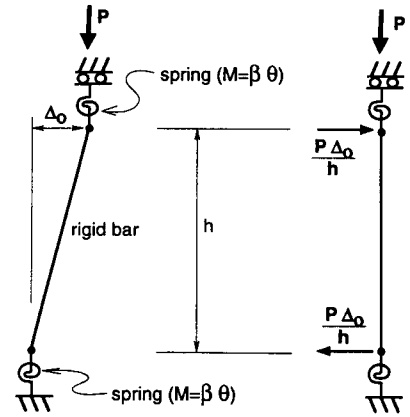

(a) imperfect geometry **(b) equivalent notional loads**

Fig. 16.11 Modeling of out-of-plumb imperfections with notional loads.

created by initial out-of-plumbness in frames (ASCE, 1997). Moreover, verification studies using spread-of-plasticity analyses have shown that notional loads can accurately represent initial out-of-plumbness effects for inelastic second-order analysis (Clarke and Bridge, 1992, 1996).

Notional loads can be used to model story out-of-plumbness, as shown in Fig. 16.12*a*, where the story notional load F_{n1} is equal to

$$F_{n1} = \frac{\Delta_0}{h}\Sigma P_u \tag{16.7}$$

and where ΣP_u is equal to the summation of factored gravity loads carried by the columns of the story in question, including all "gravity" or "leaning" columns that may not be part of the lateral load resisting frame. As shown in Fig. 16.12*b*, where a uniform out-of-plumbness is assumed over the building height, the net notional loads are equivalent to applying forces based on the load at each floor that accumulate over the height of the frame.

In concept, member out-of-straightness can also be modeled by notional loads by applying either point or distributed loads along the member such that the first-order moments induced by the notional loads are equivalent to those induced by the member axial load P_u acting through the initial imperfection δ_0. For example, a transverse point load of $4P_u\delta_0/l$ applied at midheight of a pin-ended column would be equivalent to the maximum moment caused by the out-of-straightness imperfection.

When to Include Story Out-of-Plumbness in Analysis. As noted in the two-story frame example of Section 16.3.1, in many cases the effects of initial imperfections are insignificant. Factors contributing to this behavior in the

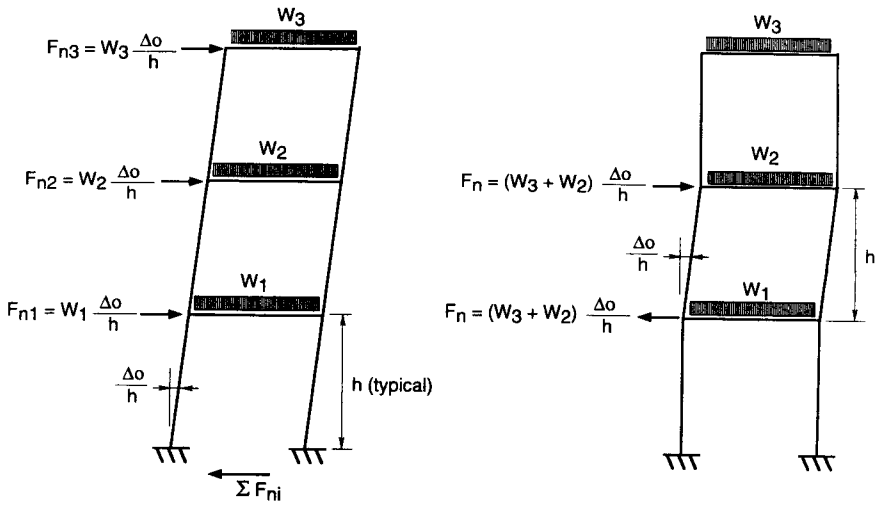

(a) uniform frame out-of-plumb **(b) isolated story out-of-plumb**

Fig. 16.12 Notional loads to simulate out-of-plumb imperfections.

two-story frame are that (1) the unsymmetric geometry caused a significant first-order sway of $\Delta = h/670$ under gravity loads, (2) significant moments and shears are present in the columns due to gravity loads, and (3) the ratio of applied column axial loads to nominal compressive strengths were relatively small. However, as described in Section 16.4.1, the effects of initial imperfections can be quite significant where these conditions are not present, (i.e., where column axial forces are large but the sidesway moments and deflections are small).

Regardless of whether a structure is sensitive to initial imperfections, for symmetric structures under gravity loads it is useful to include some initial imperfections to perturb the analysis, if it is desired to assess the strength directly from the analysis independent of the specification interaction equation checks. However, within the context of the AISC–LRFD and other design approaches based on the calculation of column-buckling loads, the effect of geometric imperfections are included implicitly in the calculation of the column axial capacities. Therefore, one does not need to include geometric imperfections within a second-order analysis to determine forces for design by these approaches. This can be particularly important for second-order analyses in order to detect possible sway instabilities and avoid bifurcationlike behavior. For this reason, and because of the potentially serious consequences of overlooking large forces induced by imperfections in frames governed by gravity loads, it is recommended to consider out-of-plumbness imperfections in the analysis of all frames under gravity loads. The imperfections could be included

either by modifying the assumed frame geometry or by applying equivalent notional loads in combination with the factored gravity loads. The justification for this is that it is relatively easy to do and avoids uncertainties about when initial imperfections may or may not be important. For analyses under combined lateral loads and gravity loads, the significance of imperfections can be gaged by considering the relative magnitude of the factored lateral loads to the equivalent notional loads of $0.002\Sigma P_u$ for an $h/500$ imperfection. Where the factored lateral loads are significantly larger than the equivalent notional load and/or where the frame has considerable overstrength, due to minimum stiffness requirements for serviceability conditions, it may be justified to neglect the initial out-of-plumbness when calculating the required member design forces.

Clarke and Bridge (ASCE, 1997) note that the stability of multistory frames is often governed by a critical story, implying that the pattern of imperfections shown in Fig. 16.12*a* would be an appropriate one to use. They also note, however, that it is generally conservative to specify a uniform out-of-plumbness equal to the maximum interstory values over the entire height of the building (e.g., Fig. 16.12*b*). For buildings up to three stories tall, applying a uniform out-of-plumbness would be consistent with the maximum lack-of-verticality limit, and for the sake of simplicitly, this approach could be followed in taller structures. Studies by Clarke and Bridge indicate that in multistory frames that are not extremely slender, it is reasonable and not overtly conservative to assume a uniform out-of-plumbness of $h/500$ over the entire height of the structure. In slender frames a more accurate strategy is warranted since a uniform out-of-plumbness applied up the entire building may generate unrealistically large overturning effects near the base of the frame.

When to Include Member Out-of-Straightness. The question of when to include member out-of-straightness in analysis is related to two considerations: (1) whether or not separate beam-column stability checks are included in the design method, and (2) whether the out-of-straightness has a significant effect on behavior. As described in Section 16.5, in the absence of analysis programs to handle torsional-flexural member response, all current design specifications require separate member stability checks which include allowances for member imperfections. In such cases, member out-of-straightness need not be considered in analysis. However, when separate member stability checks are not made, member out-of-straightness should be included in the analysis when it may have a significant effect on the behavior.

The significance of member out-of-straightness is related to the following: (1) the relative magnitude of applied axial force to primary bending moments in the member, (2) whether the primary bending moments cause single or reverse curvature bending, and (3) the slenderness of the member. These factors can be evaluated by considering the relative magnitudes of second-order moments induced by the applied factored loading M_u to the second-order moment induced by the imperfection, which is approximately equal to $M^* = \delta_0 P_u/(1 - P_u/P_{cr})$, where $P_{cr} = \pi^2 EI/L^2$. Where this ratio of M^*/M_u

is small (say less than 5%), the imperfection effects can probably be neglected. In addition to the simple ratio of moment magnitudes (M^*/M_u), the importance of imperfections will depend on whether the two moments are coincident along the member. Assuming that the maximum imperfection is at midlength of the member, the imperfections will probably have minimal impact where the maximum applied moments are at the member ends. Liew (1992) has proposed using the ratio of P_u/P_{cr} as an alternative measure of the effect of member imperfections. Liew's study, which is based on consideration of column strength relations from various specifications and standards and distributed plasticity studies of isolated beam-columns and frames, suggests that out-of-straightness effects are small (on the order of 5%) where $P_u/P_{cr} \leq 0.2$.

16.3.4 Joint and Connection Effects

Referring to Fig. 16.13, the three basic aspects of beam-column joints that affect frame behavior are (1) the finite size of the joint, (2) shearing deformations of the joint panel, and (3) rotational deformations at the beam-to-joint connections. Since the stiffening effect of the finite joint size offsets the flexibility of the joint panel and connection deformations, common practice often ignores all of these effects and instead, models frames using centerline dimensions and rigid joints. Alternatively, for frames with fully welded or bolted moment connections, where the relative rotation between the beams and columns is negligible, the combined effects of finite joint size and panel of deformations may be approximated by modeling some fraction of the finite joint as rigid, using member end offsets (e.g., a common value is to assume an effective rigid joint size of one-half the true size of the joint). However, to evaluate frame stability accurately, joints and connections should be modeled directly in the analysis, where their effects may be significant. Fortunately, with modern computer software this is feasible to do through combinations of rigid end links (member end offsets) and internal spring elements.

Joint panel flexibility is most significant under lateral loads and other situations where unbalanced beam and column forces result in shearing distortion as shown in Fig. 16.13*b*. As described by Krawinkler (1978), behavior of the joint panel can be expressed in terms of the shear distortion and the net shear force in the joint. The joint shear is a function of the moments and shears in the beams and columns. Sometimes joint shear is expressed in terms of a joint moment so that the joint panel zone flexibility can be modeled using a rotational spring connecting the beams to the column. For further information on equations to calcualte the joint stiffness, the reader is referred to Krawinkler (1978) and Krawinkler et al. (1995). As shown in Fig. 16.12*b*, connection deformation is more localized and is caused by moment transferred between the beam to panel zone region of the column. For information on calculating the stiffness of connections, the reader is referred to Chapter 3 of this guide.

As shown schematically in Fig. 16.14, force-deformation relationships for both joint panels (M_j versus γ_j) and connections (M_c versus θ_c) are generally

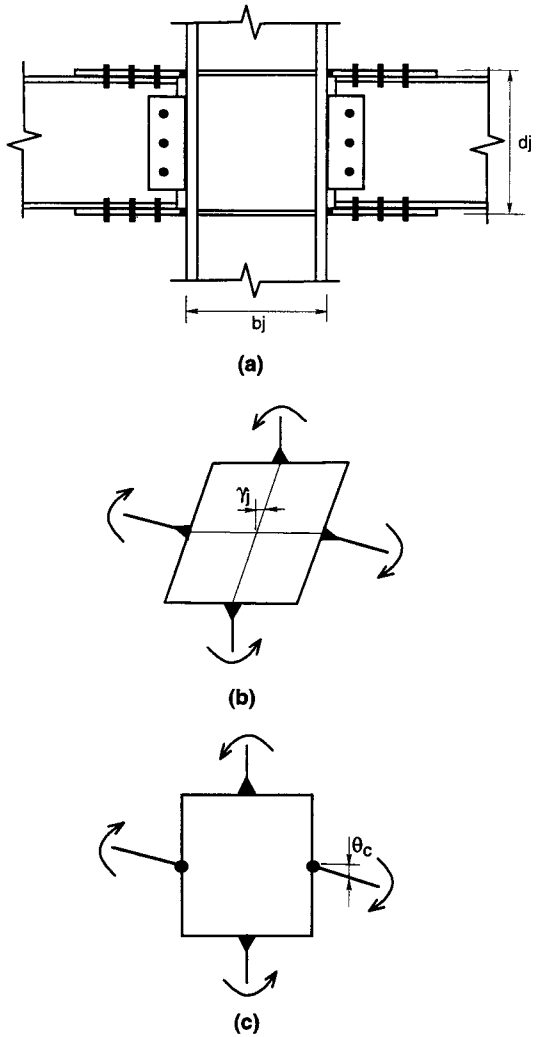

Fig. 16.13 Schematic representation of (*a*) beam-to-column connection, (*b*) joint panel behavior, and (*c*) beam connection behavior.

nonlinear. However, for design using analyses that are nominally elastic it is reasonable to approximate the connection and joint response through linear secant-stiffness relationships that represent the behavior for the limit state under consideration. For example, in analyses to evaluate serviceability conditions, the secant stiffness should be based on the maximum forces and deformations that would occur under service loads. On the other hand, for evaluating frame stability, the stiffnesses should be representative of maximum limiting conditions under the full factored loads. Obviously, the selection of

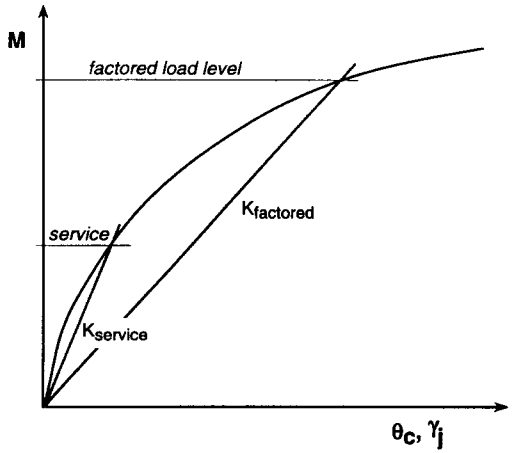

Fig. 16.14 Idealized force-deformation response of connections and joint panels.

appropriate stiffnesses should be done with care and may require several iterations to be sure that the calculated response (joint/connection forces and deformations) correspond with values originally assumed. By modeling these effects in second-order analyses, the deformations and forces associated with the joint and connection flexibility will be accounted for in design.

16.3.5 Three-Dimensional Frame Stability Behavior and Analysis

While discussion up to this point has dealt with two-dimensional frames, the influence of second-order effects induced by global torsion of the structure must be considered. Torsional stability may be particularly critical in mid- to high-rise buildings, where the lateral force-resisting system may be concentrated around the service core near the center of the building and where there are a large number of gravity or leaning columns. To consider this behavior, assume that as shown in Fig. 16.15*a*, the lateral response of a building with rigid floors is characterized by two translational and one rotational degrees of freedom (U_y, U_x, and θ_z) located at the center of stiffness of the framing system. In terms of second-order response, the translation P–Δ effects of individual columns (u_x and u_y) will create a torque whose magnitude is a function of the distance between the column and the center of stiffness. Nair (1975) has investigated this behavior for the idealized structural configurations shown in Fig. 16.15*b*, whose lateral systems have varying ratios of lateral to torsional stiffness. His study shows that in structures such as configuration I, a global torsional instability would be the critical mode of failure. Such instabilities are not captured by two-dimensional analyses or stability design methods that consider only behavior of the frame in two orthogonal directions. To

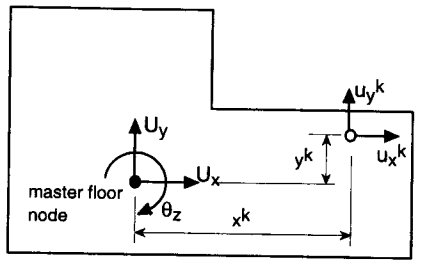

(a) floor displacement vectors and displacement vectors of element k

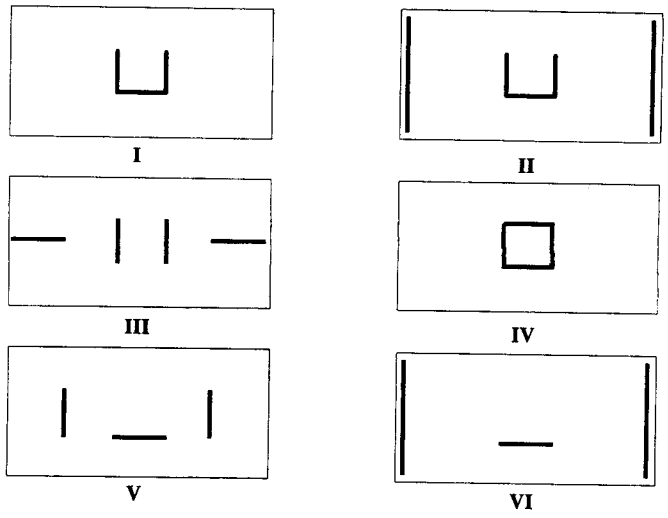

(b) alternate floor plan locations of lateral load frames

Fig. 16.15 Three-dimensional second-order effects in buildings (adapted from Nair, 1975).

investigate this mode of response accurately requires three-dimensional second-order analysis, including consideration of building out-of-plumbness and/or eccentricities of the lateral loading that will accentuate torsional response.

In general, the basic concepts of geometric nonlinear analysis described in Section 16.2.2 for two-dimensional structures can be extended into three dimensions. However, the rigorous development of appropriate geometric stiffness terms and transformation equations requires consideration of some subtle but significant theoretical issues associated with the kinematics of finite three-dimensional rotations. Specifically, these relate to the fact that finite rotations about more than one axis are noncommutative and do not follow conventional vector transformation equations. In building frames special treatment of finite

rotations can often be ignored since the only large second-order rotations are about a single axis, the vertical building axis, and out-of-plane failure is not considered within the analysis. The method of modeling story P–Δ effects proposed by Wilson and Habibullah (1987) makes use of this assumption. However, where three-dimensional rotations about more than one axis are possible, such as the case where torsional–flexural member behavior is considered (Section 16.3.6) finite-rotation effects should be considered. For further information on this subject, the reader is referred to Argyris (1982), Yang and McGuire (1986a,b), Chen (1994), Yang and Quo (1994), and Nukala (1997).

16.3.6 Torsional-Flexural Member Response

As discussed previously, standard frame analysis software is incapable of modeling out-of-plane memer instabilities (e.g., lateral beam buckling, lateral–torsional column buckling, etc.), and it is primarily for this reason that SSRC Technical Memorandum No. 5 recommends that separate checks be made for frame and member instabilities. However, progress is being made in research to develop frame analysis methods that include torsional–flexural member response and would thereby enable a single analysis that would capture both frame and member instabilities in a single analysis. In addition to basic attributes of an accurate second-order analysis, behavioral features that must be modeled to check accurately for member instabilities include (1) accurate representation of torsional member behavior, including the effects of warping and warping restraint; (2) member plastification under the combined effects of axial load, biaxial bending, and bi-moments generated by warping restraint; and (3) second-order finite rotation effects. A key aspect of analytical formulations to capture torsional–flexural member response are beam-column element stiffness with extra degrees of freedom related to warping and bi-moment effects. For further information on developments related to this topic, the reader is referred to Yang and McGuire (1986a,b), Yang and Quo (1994), Pi and Trahair (1994), Attala (1995), Attalla et al. (1996), and Nukala (1997).

16.4 FRAME STABILITY DESIGN USING SECOND-ORDER ANALYSIS

Considering the format of the AISC–LRFD specification (AISC, 1993) as an example,* strength and stability checks for design can be considered in terms of the following equation:

$$\Sigma\gamma_i Q_i < \phi R_n \tag{16.8}$$

*The LRFD format is used for discussion purposes because due to the nonlinear nature of stability effects, stability analyses should be made using factored loads (i.e., design loads that include a safety allowance for overloading).

where the left-hand side consists of the effects of factored loads on a structural member or connection and the right-hand side represents the design resistance or design strength of that element. In Eq. 16.8, Q_i refers to the internal forces created by an applied load (e.g., dead load, live load, wind, etc.), R_n is the nominal member or connection strength, and γ_i and ϕ are factors to account for the variability in the loads and resistance. Where stability effects are not involved, load effects calculated by analysis and represented on the left side of Eq. 16.8 are clearly separated by the design resistance on the right side. However, the design check for frame stability is complicated by splitting what is in essence an analysis problem between the two sides of Eq. 16.8. For example, in the AISC–LRFD specification, the member forces calculated on the basis of an elastic analysis using factored loads (left-hand side of Eq. 16.8) are compared to member strengths (on the right-hand side) that are based on inelastic behavior. Therefore, the inelastic deflections implicit in the determination of the design resistance's are not compatible with the elastic deflections calculated in the structural analysis. Where inelastic stability effects are significant, this issue is generally addressed either through calibration of the strength formulas of the design standard (as is the case in the AISC–LRFD specification) or by considering the effects of the inelasticity on the design behavior directly within the analysis. The latter approach, which is the goal behind more sophisticated second-order inelastic frame analysis methods, permits more direct checks for frame stability by accounting for the inelastic amplification of internal forces explicitly in the analysis (i.e., in the factored load terms on the left side of Eq. 16.8) as well as the member cross-section strengths associated with this inelastic behavior (i.e., the strength terms on the right side of Eq. 16.8).

In this section, guidance for using different types of second-order elastic and inelastic analyses for frame stability checks is described. The basic requirement for second-order analyses are that equilibrium under the factored loads should be solved for on the deformed configuration of the structure. The degree to which inelastic deformations influence the response at factored design loads is a central consideration, especially because most commercial programs prevalent in design practice consider only second-order *elastic* analysis. As described below, while second-order elastic analysis methods with simple member design checks are sufficient for the design of many regular building structures, there are instances when inelastic effects can be significant. Current design specifications deal with the limitations of elastic analysis through calibration of beam-column interaction equations that involve semiempirical techniques such as effective buckling length factors, application of notional loads, adjustments to member stiffnesses, and finally, limitations on the applicability of elastic analysis.

In the following sections, three specific approaches to the direct assessment of frame stability are considered. Each requires as a basis a rigorous second-order analysis which includes geometric nonlinear effects arising from both interstory drifts (P–Δ) and member curvature (P–δ). Where significant, initial

frame out-of-plumbness is included. With the primary intent to explore fundamental issues in behavior and design, the discussion is presented in a generic manner that is not linked to any specific design specification. The following three basic categories of elastic and inelastic analyses are studied:

1. *Elastic analysis with a first-hinge limit point.* Members and connections are modeled as normally elastic. Residual stresses and gradual plastification effects are not modeled, although approximate procedures for accounting for their effects are suggested. This method is closest to procedures for elastic analysis in existing design specifications.
2. *Elastic–perfectly plastic hinge analyses.* Members are modeled assuming elastic properties up to the point that they reach a fully plastic condition under combined axial loads and bending moments. Fully yielded sections are modeled using plastic hinges that enforce a yield surface criterion and allow for elastic unloading. This is essentially an extension of procedures used in the elastic first-hinge limit-point approach.
3. *Inelastic distributed plasticity analyses.* Gradual yielding of members prior to full plastification is modeled through either an explicit fiber element analysis or a refined plastic-hinge model. This approach comes closest to modeling the true limit-state behavior of the structure.

The following discussion of these approaches to analysis and design is limited to basic cases of rigidly connected planar frames under monotonic loading. It is assumed that (1) the member cross sections are sufficiently compact that local buckling does not significantly influence member inelastic deformability and/or strength, and (2) out-of-plane member failures are prevented. Therefore, cross-section plastic strengths are the sole limit on forces that can be developed in the members. As described in Section 16.5, these restrictions are relaxed to a certain extent in contemporary design standards, which implement these methods of analysis by use of member strength design equations that in some cases limit the forces to values less than the cross-section plastic strength. However, the essential qualities of the three analysis methods can be understood more clearly by adopting these restrictions.

16.4.1 Design Based on Elastic Analysis with a First-Hinge Check

Where a structure behaves elastically up to the formation of the first plastic hinge, stability effects can be accounted for up to this point using a rigorous second-order elastic analysis, including consideration of geometric imperfections. Thus one approach to design using elastic analysis is to define the strength limit state as when either (1) the fully plastic yield condition is reached in one or more members of the structure, or (2) the nominal strength of a connection, foundation, or other structural element is reached. Such an approach is referred to herein as a *first-hinge limit-state design*. In the context

of an LRFD approach, this method implies that the left-hand side of design Eq. 16.8 is equal to the induced member forces (axial load and bending) calculated by a second-order elastic analysis under the factored loads, and the right side is equal to the nominal full plastification strength of the member reduced by an appropriate strength reduction or ϕ factor. This approach will include both frame and in-plane member stability checks, provided that initial geometric imperfections are taken into account and inelastic effects (prior to the formation of the first plastic hinge) are not significant.

Referring back to the load-deformation response of the two-story frame shown in Fig. 16.9*a*, the first-hinge limit-state design would imply the frame strength under gravity load to be equal to 0.74 times the factored combination $1.2D + 1.6L$. Considering that the frame continues to carry load until reaching a factored gravity load ratio of 1.0, one obvious disadvantage of the first-hinge limit-point criterion is that the excess capacity afforded by inelastic force redistribution is neglected. However, it is important to recognize that the conservatism implied by this approach is inherent in all design specifications that are based on elastic analysis. The conservatism is offset by the simplicity of the method.

As evidenced by the agreement between plastic hinge analysis and the distributed plasticity analysis in Fig. 16.8*b*, the assumption of predominantly elastic response prior to formation of the first hinge is valid for this frame. The fact that spread-of-plasticity effects and initial imperfections were not significant in the frame are dependent in part on the fact that the column members are subject to strong-axis bending and the frame is nonsymmetrical. In a follow-up study, Ziemian and Miller (1997) investigated similar frames but with columns subjected to minor-axis bending and found similar results suggesting that elastic second-order analysis with a first-hinge limit criterion would also be a sufficient check for in-plane stability of those frames.

Contrary to the good correlation reported above between elastic–plastic hinge and spread-of-plasticity analyses, there are cases where the simple second-order elastic analysis approach would be unconservative, due to significant plastification prior to the formation of the first hinge. An example where such behavior is evident is shown in Fig. 16.16 for two portal frames that are similar to ones studied previously by El-Zanaty et al. (1980) and Attalla et al. (1994). The response curves shown in Fig. 16.16*b* and *c* contrast solutions obtained using plastic hinge versus distributed plasticity analyses for cases where the members are loaded in major- or minor-axis bending, respectively. These analyses were performed using elastic–plastic and quasi-plastic hinge software developed by Attala et al. (1994). As indicated in Fig. 16.16*a*, the applied loading consists of proportionally applied vertical loads (P) and a horizontal load of αP, where values of $\alpha = 0.0001, 0.01, 0.05$, and 0.15 were investigated. The case with $\alpha = 0.0001$ represents essentially pure gravity load where the small lateral load is applied to perturb the behavior of the perfectly symmetrical frame. Given the low degree of redundancy and the symmetry in these frames, the formation of the first plastic hinge essentially coincides with the inelastic limit

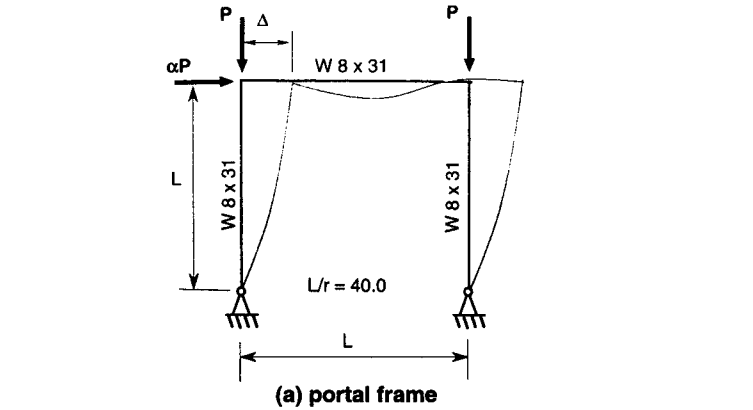

(a) portal frame

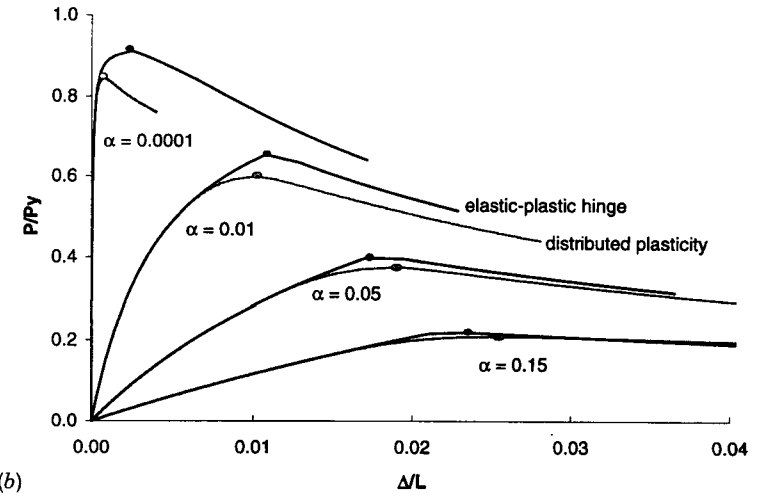

(*b*)

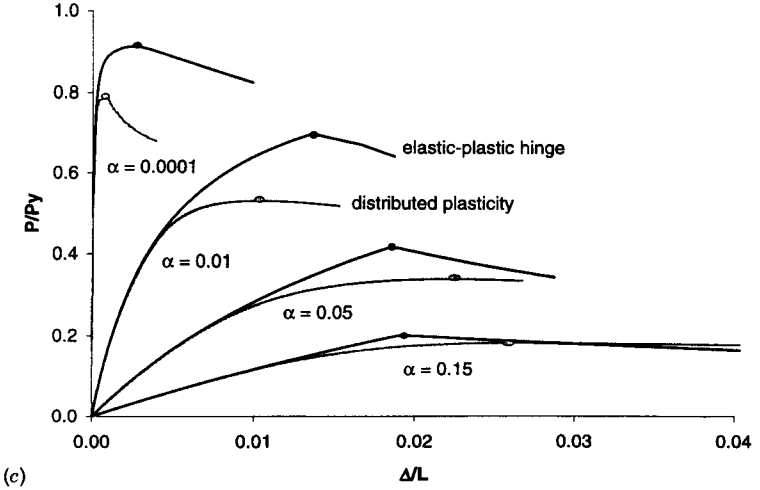

(*c*)

Fig. 16.16 Load-deformation response from plastic hinge and distributed plasticity analyses: (*a*) portal frame; (*b*) strong-axis bending; (*c*) weak-axis bending.

point for the elastic–perfectly plastic hinge analyses. Of concern in Fig. 16.16*b* and *c* are the large differences between the maximum lateral loads calculated by the elastic–perfectly plastic analyses compared to those of the distributed plasticity analyses. As shown in the figures, the differences are largest for members subjected to minor-axis bending with higher column loads. In the most extreme cases (minor-axis bending with $\alpha = 0.0001$ and 0.01), the limit load is reached well before the columns reach their fully plastic condition. This is evident from the fact that the descending branches of the load-deformation response curves do not coverage beyond the limit point.

The limit point of the curves in Figs. 16.16*b* and *c* are plotted in Figs. 16.17*a* and *b* in terms of normalized values of the average axial column force and maximum first-order moments in the columns (i.e., P/P_y and $\alpha PL/2M_p$, respectively). Results from similar analyses that included an initial out-of-plumb of $\Delta = h/500$ are also plotted in Fig. 16.17. Data from the distributed plasticity analyses with initial imperfections can be considered as representative of the true nominal in-plane strength of the frames. Thus comparisons with these data provide a measure of the errors introduced by neglecting spread-of-plasticity effects and/or initial imperfections. For example, comparing results for analyses with and without imperfections, the data show that imperfections alone are significant only for cases with small lateral loads (e.g., where $\alpha = 0.0001$). On the other hand spread-of-plasticity effects combined with initial imperfections play a more significant role. Tabulated values of the errors for the two sets of plastic-hinge analyses (with and without imperfections) are summarized in Table 16.3. As indicated in this table, where both initial imperfections and spread-of-plasticity effects are neglected (error index 1), differences from the exact solution vary from 7 to 34% for members under strong-axis bending and 12 to 51% for members under weak-axis bending. Referring to error index 2, inclusion of initial imperfections reduces the errors significantly for the cases with low lateral load, but even with this adjustment errors are still unacceptably large for most cases.

Differences of the type shown for the portal frame are important because they indicate the need for limitations on the application of second-order elastic analysis as the sole means of evaluating stability effects in design. Keep in mind, however, that the portal frame example represents an extreme case that was devised to investigate the limitations of elastic and elastic–perfectly plastic hinge analyses. As listed in Table 16.3, behavioral indices that might be used to gage the sensitivity of a frame stability to inelastic effects and initial imperfections include axial force levels in the columns (P/P_y), the ratio of elastic second- to first-order deflections ($\Delta_{2nd}/\Delta_{1st}$), and the ratio of the elastic critical load to the applied gravity load (P_{cr}/P). The data show that in the most sensitive cases with $\alpha = 0.0001$, the gravity-induced axial column forces are simultaneously approaching both the squash load and elastic critical load of the columns, and in the absence of significant lateral loads, the $\Delta_{2nd}/\Delta_{1st}$ ratios are extremely high for these cases. On the other hand, for cases with high lateral loads ($\alpha = 0.15$), all three indices are in a more reasonable range

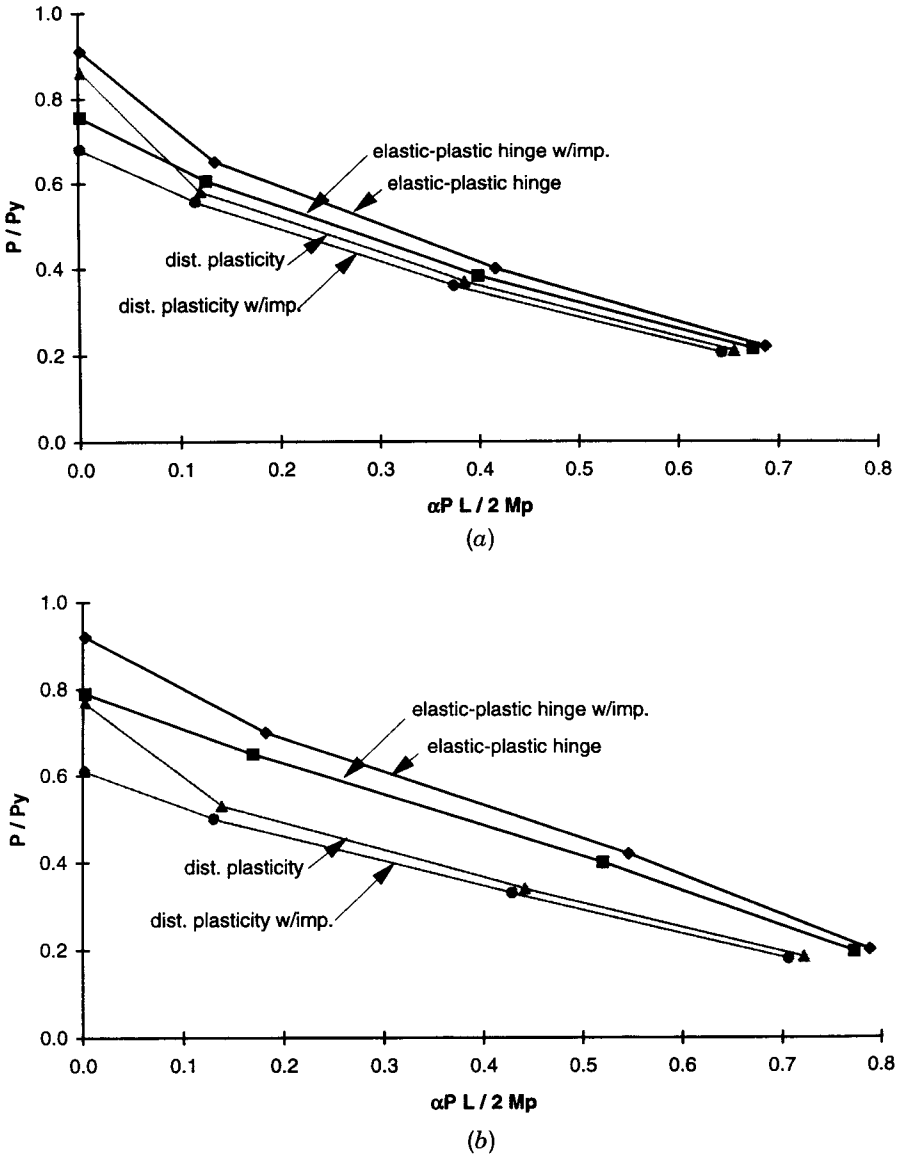

Fig. 16.17 Comparison of maximum strengths for portal frame: (*a*) strong-axis bending; (*b*) weak-axis bending.

where second-order effects are significant but not excessive. However, note that none of the three indices reflect the difference in errors associated with strong-axis versus weak-axis bending conditions. Moreover, even for this simple frame, there is no clear relationship between the behavioral indices and the errors introduced by spread-of-plasticity and initial imperfections.

TABLE 16.3 Portal Frame Example: Error and Behavioral Indices[a]

	Strong-Axis Bending				Weak-Axis Bending			
	0.0001*P*	0.01P	0.05*P*	0.15*P*	0.0001*P*	0.01*P*	0.05*P*	0.15*P*
% Error index 1	34	17	11	7	51	40	27	12
% Error index 2	11	9	6	5	30	30	21	9
Behavior index: P_u/P_y	0.91	0.65	0.40	0.22	0.92	0.70	0.42	0.20
Behavior index: $\Delta_{2nd}/\Delta_{1st}$	60	3.3	1.7	1.4	64	3.9	1.8	1.3
Behavior index: P_{cr}/P_u	1.0	1.4	2.3	4.2	1.0	1.3	2.2	4.6

[a]Error index 1 is the percentage difference between the plastic-hinge analysis with ideal geometry compared to the distributed plasticity analysis with out-of-plumb imperfections. Error index 2 is the percentage difference between the plastic-hinge analysis compared to the distributed plasticity analysis where both include out-of-plumb imperfections. Behavior indices are all based on loads and deformations calculated by the elastic–plastic hinge analyses.

In considering what should be the limits on second-order elastic analysis, it is instructive to compare features of the two-story-frame example where second-order elastic analysis is reasonably accurate (Figs. 16.7 to 16.9) to the portal frames (Figs. 16.16 and 16.17) where it is not:

1. *Ratio of elastic critical load to applied loads.* For the two-story frame, the elastic critical load is equal to 4.7 times the factored gravity load at the first-hinge limit point, whereas for the portal frames (Table 16.3) the same ratios range from 4.6 down to 1.0.

2. *Ratio of second-order to first-order elastic response.* As reported in Table 16.1, for the gravity load case of the two story frame, the difference between second- and first-order drift is 44% and the difference in moments is less than 11%. Recall that in the two story frame, the gravity loads contributed a lot to the first-order moments and drifts due to the non symmetrical geometry and the large gravity-induced moments in the beams. The second-order deflection increase of 44% in the two story frame is close to the ratio of $\Delta_{2nd}/\Delta_{1st} = 1.4$ reported in Table 16.3 for the portal frames with $\alpha = 0.15$. The ratios of $\Delta_{2nd}/\Delta_{1st}$ are much higher for the portal frames with lower lateral loads since the vertical loads do not cause significant first-order moments in this frame.

3. *Ratio of applied column load to squash load.* For the two-story frame, the maximum column loads at the first-hinge limit are approximately $P/P_y = 0.2$ to 0.4, compared to the ratios of 0.2 to 0.9 in the portal frames.

4. *Shape factor and inelastic bending stiffness of members.* Larger inelastic stiffness reductions occur in wide-flange columns subjected to minor- versus major-axis bending due to yielding at the flange tips due to the applied plus residual stresses. This is apparent in the portal frame example, where errors are much larger for the weak-axis bending cases, even though the other behavioral indices (P_u/P_y, $\Delta_{2nd}/\Delta_{1st}$, and P_{cr}/P_u) are roughly equal for the two column orientations.

5. *Redundancy.* Due to redundancy in the two-story frame, there is still considerable elastic restraint after the first plastic hinge forms, and as a result up to 40% more gravity load can be carried before reaching the inelastic limit load. On the other hand, in the portal frame examples the inelastic limit strength of the frames essentially coincides with the formation of the first hinge. Thus the portal frame results essentially reflect the behavior of individual beam-columns, as opposed to that of an indeterminate frame system with inelastic redistribution.

6. *Type of loading applied to the members.* In multistory frames, columns are often subjected to reverse-curvature bending, where yielding under combined bending and axial loads will tend to concentrate at the member ends. This is especially true for frames where sidesway instability governs. Thus the spread of yielding along members in many frames would be less severe than in the pinned-base portal frame, where the columns are in single curvature.

Given that many building frames will more closely resemble the two-story example than the simple portal frames, system stability checks based on second-order elastic analysis alone can often provide a reliable approach in engineering practice. However, there are limits on the accuracy of second-order elastic analysis, specifically in cases where inelastic effects become dominant in frames with (1) low redundancy, (2) large ratios of second- to first-order effects, (3) columns with large axial compressive loads, and (4) columns subjected to minor axis bending. White and Hajjar (1997) show further that large leaning column loads are another factor that can amplify inelastic effects. While some precise quantitative limits on the applicability of second-order elastic analysis have been proposed, none of these address all the factors noted above. For example, the Canadian standard (CSA, 1994) limits the use of second-order elastic analysis to cases where the elastic amplification of drifts and/or moments is less than 1.4. Similarly, Horne (1975) and several European standards (Anderson, 1993) limit use of elastic analysis based on the ratio of the elastic critical load to the plastic collapse load of the structure (λ_{cr}/λ_p). Horne (1975) suggests that when $\lambda_{cr}/\lambda_p > 10$, there is no interaction between elastic and inelastic second-order effects and for $4 < \lambda_{cr}/\lambda_p < 10$ the interaction is probably minimal. Springfield (1987) shows that by conservatively substituting the strength limit state for the plastic collapse load, the lower limit of $\lambda_{cr}/\lambda_p = 4$ corresponds to a second-order amplification factor of 1.38, which is close to the value of 1.4 in the Canadian standard. Springfield also notes that while the limit of 1.4 is reasonable for structures subjected to significant lateral load, this limit can be overly restrictive for structures dominated by gravity load effects where the first-order sway moments or drifts are negligible. This circumstance is recognized in the second-order analysis provisions in ACI-318 (95) (ACI, 1995) for slender reinforced concrete columns, which with certain restrictions permits amplification ratios up to 2.5 (as opposed to 1.4) for cases dominated by gravity loads.

While second-order amplification terms are useful guides for the safe limits of elastic analysis to evaluate frame stability, other parameters, such as those mentioned above, should be considered. A summary of these factors is presented in Table 16.4. So, for example, in redundant structures with lightly loaded columns subjected primarily to major-axis bending, it is likely that a second-order elastic analysis is sufficient to capture in-plane frame and member stability effects even for cases with second-order amplification higher than 1.4. However, when a combination of the parameters from Table 16.4 suggests that the stability of the structure is susceptible to spread-of-plasticity effects, it is necessary to account for these effects directly within the frame analysis and/or through calibrated design procedures.

As described below, alternatives to a rigorous distributed plasticity analysis to account for spread-of-plasticity effects using elastic analysis are (1) the modified stiffness approach, and (2) the notional load approach. Both methods are intended only to adjust for modest inelastic effects representative of the condition of frames under factored loads, and they are not meant to model inelastic force redistribution associated with hinging of the members. Neither of these approaches intended to be applied to check forces or deformations under service loads.

Modified Stiffness Approach. One approach to approximate modest spread-of-plasticity effects in an "elastic" second-order analysis is to reduce the stiffness of members in which gradual plastification could be significant. This would apply primarily to column members subjected to significant axial compression, but gradual plastification effects could also be significant in other highly stressed members with uniformly distributed (single curvature) moments. As described by MacGregor (1993), such an approach has been adopted in the ACI-381 code (1995) provisions for slender columns. Similar ideas were previously proposed for steel structures by Cheong-Siat-Moy (1978).

In considering a modified stiffness approach for steel structures, it is instructive to review the ACI-318 (1995) provisions for frames with slender reinforced concrete columns which use essentially a first-hinge limit-point approach. In ACI-318, required member strengths under factored loads (P_u and M_u) are determined by a second-order elastic analysis and checked against the design strength of the member cross section. The design strength is essentially the axial force–moment interaction surface reduced by appropriate resistance for axial

TABLE 16.4 Suggested Guides to the Limits of Second-Order Elastic Analysis to Evaluate Frame Stability

- *Ratio of elastic first-order to second-order effects.* Where the loading and/or structural configuration are such that first-order sidesway effects (moments, drifts, etc.) are significant, the ratio of second-order to first-order effects is one legitimate measure of the accuracy of elastic analysis to model stability limit states. Subject to adjustment by the other parameters noted below, maximum ratios of second- to first-order effects between 1.2 and 1.4 appear to be reasonably conservative limits of when distributed plasticity effects become significant. Limits such as these may not be appropriate for structures dominated by gravity loads, where first-order sidesway effects are small and economical column designs may require consideration of distributed plasticity effects.
- *Structural redundancy.* Highly redundant structures will, in general, have a larger margin between the onset of plastification and the inelastic limit than nonredundant structures or redundant structures where the stability is limited by a failure within a localized region of the structure. In many cases the onset of inelasticity in a few members will have a small influence on the overall response of the frame, and the overall frame behavior will remain predominantly elastic until larger load levels are reached.
- *Load magnitudes and moments in columns.* If $P/P_y \leq 0.2$, the existence of substantial distributed plasticity along the length of the column is not possible unless the column is loaded under large single-curvature bending. Moreover, in the absence of large moments, residual stress effects in combination with axial compression will not have a significant effect on column stiffness for $P/P_y \leq 0.6$.
- *Leaning columns.* If a large percentage of the gravity load is supported by leaning columns, reductions in the lateral stiffness of the structure due to distributed yielding are amplified. In the absence of extensive data on this, it is reasonable to assume that if loads supported by leaning columns are less than about twice the vertical loads supported by the lateral-load resisting columns, the amplification of distributed plasticity effects by the leaning columns should be negligible.
- *Strong-axis versus weak-axis bending.* For H-shaped sections subjected to weak-axis bending, the cross-section flexural rigidity decreases dramatically as yielding progresses inward from the flange tips. Furthermore, the general extent of the full-plastification surface is greater relative to the initial yield surface for weak-axis bending of these shapes, as reflected by the shape factor for the case of bending alone. Due to this fact, the distribution of plasticity along the member length when the full-plastification strength is reached is generally greater for weak-axis bending.

load and bending. A key aspect of the second-order analysis is that the flexural stiffnesses of beams and columns are chosen to give calculated deflections that are close to those at the strength limit of the structure under factored loads. This implies that member stiffnesses are chosen to include the effects of concrete cracking and creep as affected by the distribution and duration of axial forces and moments.

In lieu of more precise calculations, ACI-318 specifies values of stiffnesses for various types of members to use in the second-order analysis. For the overall frame analysis to calculate P–Δ effects, flexural stiffnesses of $0.35E_cI_g$ for beams and $0.7E_cI_g$ for columns are recommended, where E_c is the short-term elastic modulus of concrete and I_g is the gross moment of inertia. These values are intended to represent average properties throughout the structure. For calculating moments along the length of individual columns due to P–δ effects, a lower value of $0.4E_cI_g$ is suggested for the local moment amplification term. This is in recognition of the probabilistic nature of these estimated values, and the lower-bound values should be used for checks of individual members, whereas for overall system behavior values closer to the means can be used. The stiffness values as given above are for use in checking stability under combined gravity plus lateral loads. When checking stability under dead loads or other sustained loads, the stiffness values are reduced further to account for long-term creep effects by the factor $1/(1 + \beta d)$, where βd is the ratio of sustained to total factored load. Beyond calculating second-order effects in this manner, ACI-318 includes provisions that specify (1) minimum beam-column design moments, (2) threshold slenderness criteria below which stability effects do not need to be considered, (3) rules for distinguishing between sway and nonsway frames, and (4) a limit on the maximum permissible ratio of second- to first-order effects (e.g., $\Delta_{2nd}/\Delta_{1st} < 2.5$). The second-order limit of 2.5 is intended as a check for sidesway stability of frames dominated by gravity load effects.

One method to approximate stiffness reductions in steel members with high axial load is through a tangent modulus derived from column curve formulas (Orbison et al., 1982; Ziemian et al., 1992a; White and Chen, 1993). For example, the inelastic stiffness reduction implied by the AISC–LRFD column curve is shown in Fig. 16.18*a*. Since the tangent-modulus adjustment of Fig. 16.18*a* does not affect members with $P/P_y < 0.5$, this adjustment alone would not reduce the errors shown in Figs. 16.16 and 16.17 significantly except for the cases with little bending. This is beause the differences in these columns are due to the plastification under the combined action of axial compression and bending. For example, as shown in Fig. 16.18*b* for a column with $P/P_y = 0.5$, the flexural stiffness in minor-axis bending drops off rapidly under the action of axial load and moment. Thus for second-order analysis the modified—or reduced—stiffness must consider the combined effects of axial load, bending moments, residual stresses, and the member shape factor.

To investigate the feasibility of a modified stiffness approach, the portal frame examples from above (Fig. 16.16) were reanalyzed with a second-order plastic-hinge analysis using reduced column stiffnesses of $0.8EI$ for strong-axis bending and $0.6EI$ for weak-axis bending. These values were chosen to be in line with data such as shown in Fig. 16.19 and because they give good results in the portal frame example. First-hinge limit points from these analyses are shown in Fig. 16.19 which are analogous to the data shown in Fig. 16.17. Included are data from the following analyses:

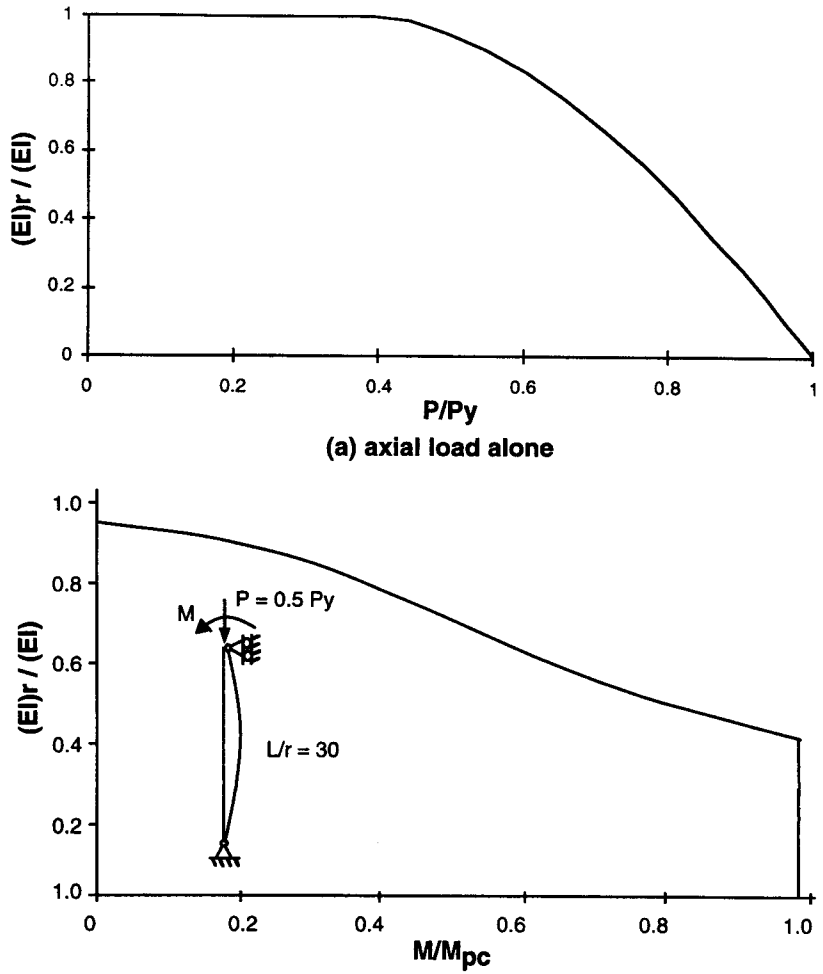

Fig. 16.18 Effect of axial load and bending on flexural stiffness of beam-columns.

- *DP*: distributed plasticity analysis
- *Elastic*: plastic-hinge analysis with elastic properties
- *M-elastic*: plastic-hinge analysis with modified column stiffness

All analyses are second-order and include an initial frame out-of-plumb of $h/500$. Also plotted are results from an alternative notional load procedure (NL-elastic) taht will be discussed below. As shown in the figures, for both strong- and weak-axis bending the modified stiffness approach (M-elastic) results in nearly perfect agreement with the more accurate distributed plasticity (DP) solutions.

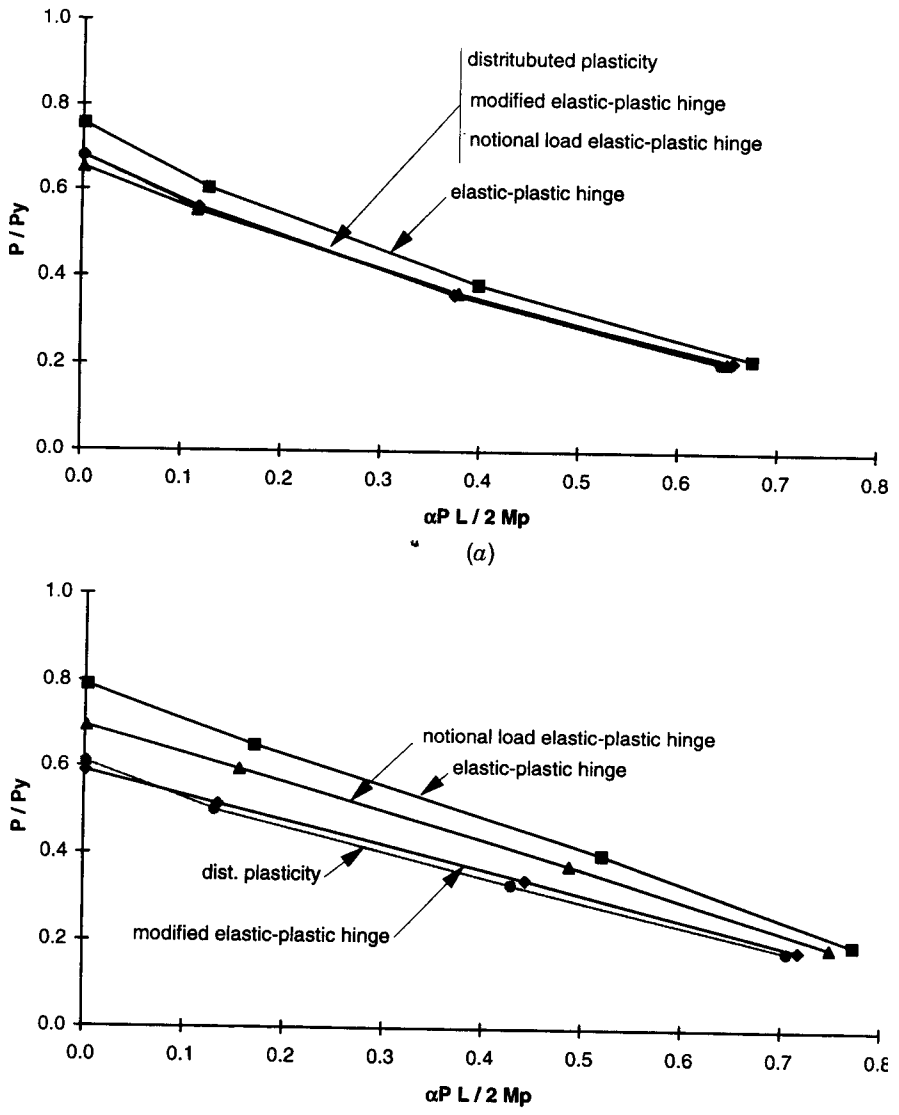

Fig. 16.19 Comparison of strengths for portal frame with modified stiffness and notional load approaches: (*a*) strong-axis bending; (*b*) weak-axis bending.

Although stiffness reduction ratios are input as constants that do not vary with axial load, as shown in Fig. 16.19, the results are fairly accurate for axial loads ranging from about $P/P_y = 0.2$ to 0.6. The reason for this is that as shown in Fig. 16.18*a*, the drop in stiffness due to axial load alone is small up to about $P/P_y = 0.5$ or so. Presumably, the effective stiffness should be

reduced further for cases with $P/P_y > 0.6$, perhaps by using a tangent-modulus adjustment (Fig. 16.18*a*) in combination with the 0.6 and 0.8 factors noted above.

As noted above, the portal frame examples are devised to accentuate a worst-case test for the limits of elastic analysis. Thus the stiffness reductions used above are probably more severe than would be appropriate for more redundant frames. However, one virtue of the modified stiffness method is that conservative errors due to underestimating the stiffness tend to be self-limiting in structures that are insensitive to stability effects. For this reason the relative change in second-order response due to a modest change in stiffness can be used as an indicator of a potential stability problem. Consider the data in Table 16.5, where amplification factors ($\Delta_{2nd}/\Delta_{1st}$) are summarized for analyses of the portal frame using the full and modified stiffnesses (rows A and B). Row C lists ratios reflecting the increase in the second-order amplification factor due to the decrease in stiffness. Considering, for example, the strong-axis bending case with $\alpha = 0.15$, the fact that the second-order effects do not increase due to the stiffness reduction of −20% (i.e., the change ratio in row C = 1.0) indicate that the frame is not sensitive to stability effects. On the other hand, for frames with $\alpha = 0.0001$, the change in the ratios for second-order effects (row C = 1.4 and 2.3) are in excess of the percentage reduction in stiffness (1/0.8 = 1.25 and 1/0.6 = 1.67), indicating that these structures are very sensitive to stability and spread-of-plasticity effects.

Notional Load Approach. Another approach that has been proposed for approximating inelastic effects in second-order elastic analyses is through the application of notional loads. The basic concept is similar to that described in Section 16.3.3 for modeling imperfections, except that for modeling spread-of-plasticity effects there is no theoretical basis to calculate appropriate values of the notional loads. Rather, the notional loads must be determined empirically through calibration to data from distributed plasticity analyses and/or tests. Notional load methods have, in fact, been implemented in several standards, including AS 4100-1990, CSA-S16.1-M94, and

TABLE 16.5 Comparison of $\Delta_{2nd}/\Delta_{1st}$ Index for Elastic and Reduced Stiffness Analyses

	Strong-Axis Bending ($\beta = 0.8$)				Weak-Axis Bending ($\beta = 0.6$)			
	0.0001*P*	0.01P	0.05*P*	0.15*P*	0.0001*P*	0.01*P*	0.05*P*	0.15*P*
(A) Full elastic (EI)	5.3	2.8	1.7	1.4	6.3	3.3	1.7	1.3
(B) Modified (β EI)	7.4	3.4	1.8	1.4	14.6	5.2	2.1	1.4
(C) Change ratio = *A*/*B*	1.4	1.2	1.1	1.0	2.3	1.6	1.2	1.1

Eurocode 3. In such cases the notional loads specified are calibrated to include both imperfections and inelastic effects (residual stresses and spread of plasticity). Further information on these code provisions is given in Section 16.5.

In one study of notional loads, Liew et al. (1994) proposed values equal to 0.5% of the gravity load ($0.005\Sigma P$) to account for the combined effects of initial out-of-plumbness imperfections and inelastic effects. The value of 0.5% is two and one-half times the value of 0.2% that would be appropriate for modeling imperfections alone. Coincidentally, the value of 0.5% is the same as that used in CSA-S16.1 (see Section 16.5) and it has been justified by a number of other case studies (e.g., Springfield, 1991; Clarke and Bridge, 1992, 1996; ASCE, 1997).

An example of results from the calibration studies using a portal frame by Liew et al. is shown in Fig. 16.20. The portal frame in this example was taken from earlier studies by Kanchanalai (1977) that were used in the development of the beam-column interaction equations in AISC–LRFD, but otherwise the plots in Fig. 16.20 are similar in nature to those shown in Figs. 16.17 and 16.19. Curves shown in Fig. 16.20 are from the following types of second-order analyses: (1) distributed plasticity solutions as developed by Kanchanalai, (2) elastic–plastic hinge analyses without notional loads, and (3) elastic–plastic

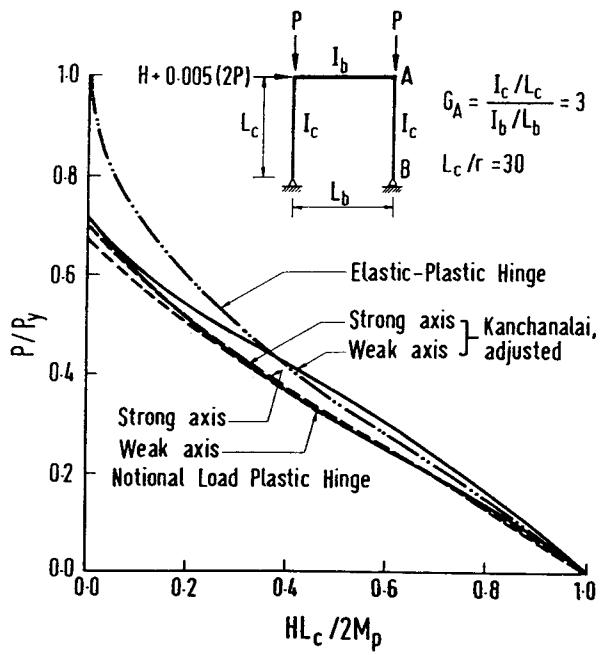

Fig. 16.20 Evaluation of strengths from notional load approach (Liew et al., 1994).

hinge analyses with notional loads equal to 0.5% of the vertical load. Note that while the notional load is applied in addition to the lateral load H, it is not included in the normalized first-order moment plotted on the horizontal axis. The elastic–plastic hinge analyses conducted by Liew et al. are essentially the same as those described for the previous examples, except that in this case the cross-section yield surface is based on the bilinear interaction formulas of the AISC–LRFD specification. As shown in Fig. 16.20, for low values of axial load (e.g., $P/P_y < 0.3$) with second-order amplification values less than about 1.4, the elastic–plastic hinge analysis without notional loads gives fairly accurate results. For larger axial loads where the elastic–plastic analysis is unconservative, the notional load compensates for inelastic and out-of-plumbness effects so as to produce an accurate solution.

It is interesting to compare Liew et al.'s results in Fig. 16.20 to similar analyses made for the portal frame example discussed previously. Referring back to Fig. 16.19, elastic–plastic hinge analysis results using 0.5% notional loads (NL-elastic) are plotted along with data from the distributed plasticity and modified stiffness analyses. In this case the notional load analyses are fairly accurate for strong-axis bending, although for weak-axis bending, the notional load results are up to about 20% unconservative compared to the distributed plasticity analyses. The primary reason that these results differ from those of Liew et al. is that in these analyses the hinge criterion is based on a more accurate yield surface (Eq. 16.3) rather than the AISC–LRFD interaction equations which are known to give conservative values of the weak-axis bending strength. Thus these examples demonstrate that calibrations of notional loads (and any other empirical procedures) must consider the specific yield criterion that is used. For example, notional load values calibrated for one set of interaction equations in a given specification will not necessarily be correct for another set of interaction equations. Obviously, an alternative way of calibrating the notional loads would be to use a higher notional load for weak-axis bending in a similar manner to the way that different stiffness reductions were used for major- and minor-axis bending in the modified stiffness approach.

The results in Figs. 16.19 and 16.20 are for frames in which second-order moments are largest at the ends of the columns. For cases where beam-columns may fail in a braced-buckling mode by P–δ effects, notional loads can be applied along the length of the member. For example, Liew et al. (1994) propose using a notional load of 1% of the axial member force applied at midspan of the column.

16.4.2 Design with Elastic–Perfectly Plastic Hinge Analysis

As demonstrated by the two-story-frame example (Fig. 16.8), for indeterminate structures the first-hinge limit criterion is a conservative estimate of the true inelastic limit strength of the frame. Often, the strength increase due to inelastic force redistribution beyond formation of the first hinge is on the order of 10 to

30%. Therefore, second-order elastic–plastic hinge analyses can enable the design of lighter and perhaps more cost-effective structures. More important, however, inelastic analyses provide insight on failure modes that ultimately control the strength limit-state behavior and thus improve the accuracy and rerliability of the strength evaluation. When utilizing inelastic force redistribution beyond the first hinge, there are certain behavioral considerations that must be addressed in design. Beyond those described for the elastic first-hinge approach in Section 16.4.1 (i.e., spread of plasticity and residual stress effects, initial imperfections, out-of-plane member failures), these additional considerations include (1) evaluating hinge rotation demands and capacities, (2) considering the increased potential for incremental collapse, and (3) proper modeling of strain hardening or softening.

Hinge Rotation Demands and Capacities. Where inelastic force redistribution is relied upon, a check should be made to verify that the inelastic rotation demands can be accommodated by the members and connections. In rigidly jointed steel frames, the basic modes of failure that will limit member deformation capacities include local flange or web buckling, lateral–torsional member buckling, and fracture of the member or its connections. While each of these modes of failure is treated independently in design standards, the modes of failure are often quite interrelated. For example, as described by Kemp (1986), the rotation capacity of steel H-shaped members is highly dependent on the interactive effects of local flange and web buckling and lateral buckling. Thus, while codes often prescribe independent slenderness limits for flange compactness, web compactness, and lateral bracing, in actuality the underlying behavior is highly coupled.

For the design of ordinary proportioned frames under gravity and wind loads, available evidence suggests that member compactness requirements such as those contained in the plastic design provisions of the AISC–LRFD specification (1993) provide adequate deformation capacity required for the structure to reach the inelastic limit point (Ziemian et al., 1992a,b). Such provisions usually address section compactness criteria (b/t and d/t), lateral bracing criteria (L/r), and specified material requirements. In a study that included both low-rise planar structures and a midrise three-dimensional structure. Ziemian et al. report that the maximum required plastic-hinge rotations under gravity and wind loads were less than 0.01 rad, which were on the order of half of the inelastic deformation capacity implied in the AISC–LRFD provisions for plastic design. This study did not address the potential for fractures at beam-column connections, which as experiences from the Northridge earthquake have shown, should not be discounted. However, there are several reasons why fracture is less likely under gravity and wind loading compared to cases where seismic design governs. First, the maximum plastic rotation demands of 0.01 rad calculated by Ziemian et al. are considerably less than values of 0.02 to 0.04 rad that are considered as representative of the maximum hinge rotation demands for seismically designed frames. Moreover, for gravity

and wind load design, repeated inelastic cyclic loading of the members and connections is not anticipated. Finally, the probable overstrength in the structure due to yield stresses that exceed the nominal values, strain hardening, composite beam action, and secondary structural elements will usually reduce plastic-hinge rotation demands under the factored design loads compared to those predicted by an elastic–perfectly plastic analysis of the bare frame.

Consideration of Incremental Collapse. Under repeated loading at levels that cause significant yielding, there is the potential for frames to fail due to incremental accumulation of lateral deflections at loads less than the inelastic monotonic limit load. This has implications for design by plastic-hinge analysis, where the factored load combinations including live, wind, or other variable loads can approach the inelastic limit strength of the frame. Checks for incremental collapse are related to shakedown analysis, the *shakedown load* being a value below which the structure will converge to a stable elastic state under repeated loading. Thus, for a given loading condition, the shakedown load lies between the load at which the first hinge forms and the inelastic limit point.

Previous studies dating back to research on plastic design in the 1950s and 1960s (Popov and McCarthy, 1960; WRC/ASCE, 1961; Neil, 1977; Horne, 1979) indicate that incremental collapse is probably not of concern for plastically designed building frames under variable gravity and wind loads. Since then, not much has been published related to the likelihood of incremental collapse. However, in considering the application of modern computer-based second-order plastic-hinge analysis to evaluate the inelastic limit strength of frames, the potential for incremental collapse should not be discounted. Shakedown limit or incremental collapse analyses should be considered where there is the likelihood of repeated load excursions beyond the yield point (e.g., cases where the ratio of live to dead load is large and/or where the design strength is governed by lateral loads).

Classical methods for evaluating shakedown (e.g., Neil, 1977; Horne, 1979; Konig, 1987) are generally impractical for evaluating frames of realistic proportions and loading conditions, especially when second-order effects are significant. Recently, Guralnick et al. (1984, 1986, 1991) have proposed an energy-based approach to evaluate incremental collapse that is more amenable to modern computer techniques than classical shakedown methods and can include second-order effects directly. The basic premise of this method is to evaluate shakedown through a convergence study of inelastic energy dissipation in a structure under repeated loading. A condition of shakedown is reached when there is a stabilization of the accumulation of plastic energy under repeated cycles of loading. While the method requires somewhat sophisticated computer analysis programs (e.g., plastic hinge analyses with features for cyclic loading), it does provide a systematic means for evaluating whether incremental collapse will occur under the applied loads.

Strain Hardening. The question of whether to include strain hardening in an inelastic analysis is one that depends both on the basic design philosophy and circumstances specific to the structure being analyzed. For example, the AISC–LRFD specification and most other steel design standards do not explicitly allow any increase in member strengths associated with strain hardening (i.e., member strengths are limited to their plastic strength calculated with the minimum specified material yield strength). Accordingly, for designs that meet the intent of these specifications, hinges should be modeled as elastic–perfectly plastic, thereby limiting the member resistances to the plastic yield strength of the cross section. This means that where numerical solution requirements necessitate that some small residual stiffness be included at the plastic hinges, such values should be kept to a minimum. For example, Eurocode 3 suggests keeping strain-hardening values on the order of 0.01% of the elastic stiffness. Neglecting beneficial effects of strain hardening tends to offset the destabilizing influence of local buckling and other effects that are not modeled in plastic hinge analyses.

16.4.3 Design with Spread-of-Plasticity Analysis

Any analysis model that accurately represents the effects of distributed plasticity due to combined axial force, bending, and residual stresses is termed a *spread-of-plasticity* analysis method. The intent for applying spread-of-plasticity analysis methods in design is that the nominal residual stress effects and initial geometric imperfections should be modeled explicitly whenever they are important. This avoids the introduction of ad hoc modifications of the sort that might be used with elastic–plastic hinge methods, thereby relieving the engineer of the need to make assumptions that create uncertainty in the analysis. Of course, where it can be shown that one or both effects have a negligible influence on behavior, then as with elastic analysis they need not be included in the analysis. The Australian steel design specification, AS4100 (SAA, 1900), has in fact codified provisions that permit the engineer to use what is termed an "advanced" spread-of-plasticity analysis as the sole basis for evaluating the in-plane stability of members and frames (i.e., in such cases member interaction equations for evaluating in-plane stability are not required).

Initial imperfections should as a minimum include frame out-of-plumbness, and when separate member stability checks are not used, member out-of-straightness should also be included in the analysis. As described in Chapter 3 on columns, residual stresses in members can vary significantly depending on the member sizes and details of the particular manufacturing process. In the absence of more specific information, the residual stresses shown in Fig. 16.21 are considered as representative of typical wide-flange shapes. This pattern also has a precedent for use in design since it formed the basis of parametric studies used in the calibration and development of the AISC–LRFD beam-column interaction equations (Kanchanalai, 1977).

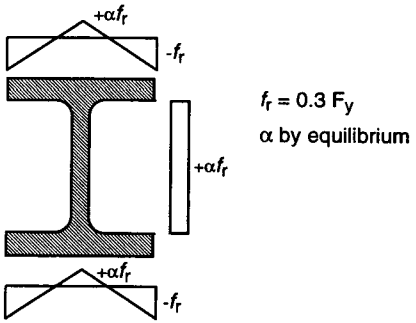

Fig. 16.21 Idealized residual stresses for H-shaped members.

With spread-of-plasticity methods it is important to check the inelastic deformation demands in plastified regions of the frame and to limit strain hardening to values that will not overestimate the nominal member strengths. Depending on the specific formulation employed in spread-of-plasticity analysis, the treatment of strain hardening and inelastic deformation demands will differ from those described above for plastic hinge methods. For example, in spread-of-plasticity methods that utilize a detailed fiber element approach, strain hardening is generally specified in terms of an assumed uniaxial stress versus strain relationship. On the other hand, in quasi-hinge methods, strain hardening may be included indirectly in force versus generalized strain relations of the cross sections, or in terms of some residual member stiffness. Whatever the method for specifying a "hardening" parameter, a check should be made at the end of the analysis to see that the member forces do not significantly exceed the full cross-section plastification criteria.

16.5 OVERVIEW OF CURRENT CODE PROVISIONS

In this section, modern frame stability design provisions from several major design standards and specifications are reviewed. This overview is not intended to provide an in-depth explanation of the provisions. Rather, the goal is to further describe and contrast various methodologies for evaluating frame stability and to consider the interdependence between design provisions and methods of analysis. The discussion is limited to static elastic analysis and limit-states design assessment of sway or nonsway frames, composed of members of bisymmetrical cross section, loaded by in-plane forces only. It is assumed that the beam-columns are braced out-of-plane at their ends but otherwise can fail either in an out-of-plane mode. The examples presented in this section are based on more detailed comparisons of beam-column and frame stability design provisions by White and Clarke (1997).

The specifications/standards considered are AISC–LRFD (AISC, 1993), CAN/CSA-S16.1-M94 (CSA, 1994), Eurocode 3 (ECS, 1993), and AS4100-1990 (SAA, 1990). There are subtle and major differences in the approaches to frame stability assessment in each of these documents pertaining to (1) the adopted load and resistance factors (i.e., partial safety factors for actions and resistances; (2) the nominal loads or actions selected for design within the jurisdiction of each of these standards; (3) column strength formulas, including the number of column curves provided; (4) beam strength formulas; (5) the number, format, and "shape" of interaction curves considered for calculating interaction effects between bending and axial compression; (6) use or non-use of effective-length (i.e., K factors; and (7) modification of moments to account for geometric imperfection and/or distributed plasticity effects through application of notional loads. However, all of these documents are the same in that they require the calculation of second-order elastic forces, either through direct analysis or through approximate amplification of the first-order elastic forces. Thus they are comparable to the first-hinge limit-state design approach described in Section 16.4.1. Table 16.6 compares and contrasts a few of the aspects of these different approaches related to beam-column and frame stability design checks. As can be seen in Table 16.6, the largest differences in the design approaches are between the AISC–LRFD specification and the other three standards.

16.5.1 Basic Approach of AISC–LRFD Specification

A key difference between AISC–LRFD and the other design standards is that AISC–LRFD uses only one interaction equation to assess both in-plane and out-of-plane member behavior. The AISC–LRFD beam-column interaction equation implicitly accounts for geometric imperfections and residual stress effects by using a column strength curve that is based on effective lengths for member/frame stability assessment. The considerations of strength and stability are treated together in the single LRFD interaction equation. The basic concept behind this approach is illustrated in Fig. 16.22, where it is shown that the AISC–LRFD beam-column interaction curve is fit between two "anchor points" representing the nominal strength under pure compression ($P_{n,KL}$) and bending (M_n). These points are determined as follows:

1. *Nominal compression strength,* $P_{n,KL}$: This represents the nominal axial strength of the column as limited by the effects of lateral buckling either in or out of the plane of the frame. By the most rigorous definition, the nominal axial strength is determined considering the limit of stability of the framing system, or of a local subassembly within the framing system, where all the columns are concentrically loaded such that the distribution of column forces is comparable to that which would occur under the factored design load. The nominal resistance is calculated using a single column curve that is a function

TABLE 16.6 Comparison of Design Checks for Beam-Column and Frame Stability

	AISC–LRFD	CAN/CSA-S16.1	Eurocode 3	AS4100
Number of column curves	1	2	4	5
Resistance factors	0.85 axial, 0.9 bending	0.9	1/1.1 = 0.91	0.9
Basic method of analysis	Second-order elastic	Second-order elastic	First- or second-order elastic	Second-order elastic
Force interaction checks for member stability and strength	Single interaction equation, the terms of which account for the mode of failure; no distinction between strength and stability checks	Three separate interaction equations for in-plane and out-of-plane stability and cross-section strength	Three separate interaction equations for in-plane and out-of-plane stability and cross-section strength	Three separate interaction equations for in-plane and out-of-plane stability and cross-section strength
Consideration of section compactness (class 1 = plastic design, class 2 = compact)	No distinction between class 1 and 2 sections	All interaction curve strengths are increased for class 1 sections	No change in strengths for class 1 versus 2 sections	In-plane and out-of-plane stability limits are increased for class 1 sections
Limitations on analysis methods and interaction equations	No limits	P–Δ amplitude < 1.4; otherwise, a second-order distributed plasticity analysis is required	Use of simplified second-order factors limited to cases where P–Δ amplitude < 1.33	Use of simplified second-order factors limited to cases where P–Δ amplitude < 1.4
Effective buckling lengths for sway frames	$K \geq 1$, determining using effective-length nomographs or other rational analysis	$K = 1$	$K \geq 1$ when first-order analysis is used; $K = 1$ when second-order analysis is used	$K = 1$
Notional loads	Not recognized	Notional loads used to calculate minimum gravity moments; $F_n = 0.005\Sigma W$	Notional loads applied simultaneously with all loads; $F_n \leq 0.005\Sigma W$	Notional loads applied simultaneously with gravity loads; $F_n = 0.002\Sigma W$

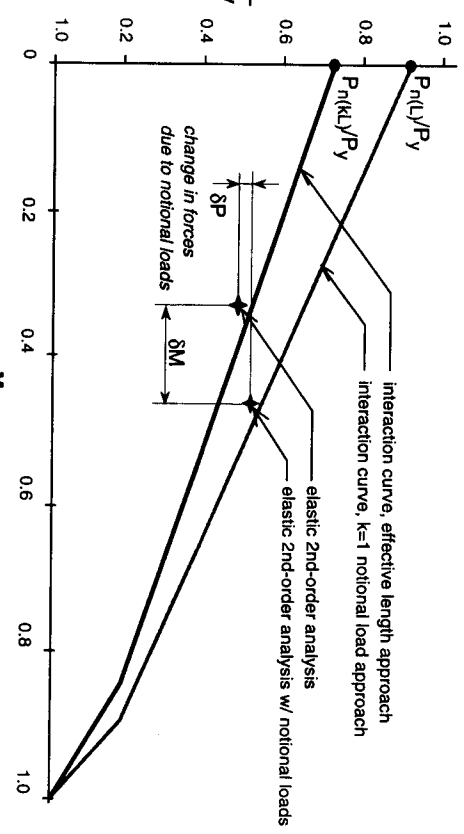

Fig. 16.22 Distinction between effective length and notional load approaches (adapted from White and Clarke, submitted).

of in-plane and out-of-plane effective buckling lengths.* The effective lengths are usually calculated by simplified alignment charts that may be adjusted to reflect the effective inelastic stiffness of columns at the strength limit state. There are many complicating aspects to proper calculation of effective lengths and their use in the AISC–LRFD design provisions, which are not addressed here. The reader is referred to a recent ASCE Steel–LRFD committee report (ASCE, 1997) for a thorough assessment of the state of the art with regard to these topics.

2. *Nominal bending, strength, M_n:* The nominal moment strength is determined for bending in the plane of the frame considering the potential for inelastic lateral buckling out of plane. The nominal strength equation for calculating lateral buckling is based on the distribution of bending moments in the member based on second-order elastic analysis and assuming that the ends of the member are fully restrained against translation and torsional rotation but free to warp and to rotate in or out of plane. Thus the beneficial effects of continuity with other framing members are neglected.

For cases governed by in-plane stability, the AISC–LRFD beam-column design equations are calibrated to results from distributed plasticity analyses of

*For the examples presented in this section, the out-of-plane buckling lengths are taken as the actual length of the member.

small nonredundant frames, including geometric imperfections and residual stresses (Yura, 1988; Yura et al., 1996; ASCE, 1997). Calculated strengths for cases involving both in- and out-of-plane failures are also verified against test data (Kanchanalai, 1977; Yura et al., 1996). The calibration is based on the presumption that member forces are calculated by second-order *elastic* analysis without any requirements to model inelastic effects or initial frame out-of-plumbness. Referring to Fig. 16.22, inelastic and out-of-plumbness effects are largely taken into account by reliance on effective buckling lengths for calculating $P_{n,KL}$, thereby reducing the nominal member resistance to account for frame stability effects.

16.5.2 Basic Approach of Other Design Standards and Contrasting of Methods

Frame and beam-column stability checks in the Canadian, Eurocode, and Australian standards use the actual member length, or in some cases, an effective length less than the actual member length for calculation of the column strength term in the design interaction equations. This nominal compression strength, denoted by $P_{n,L}$ in Fig. 16.22, is generally based on multiple column curves. The nominal moment strength, M_n, is generally calculated in the same way as by the AISC–LRFD specification. Contrary to AISC–LRFD, the frame stability assessment is based entirely on the calculation of member forces using second-order elastic analysis, where notional loads are required to account for frame-out-of-plumbness and inelastic effects. Thus the interaction equations with $K = 1$ or $K < 1$ are only intended to check member stability. As shown in the figure, the difference between the nominal strength curve based on $P_{n,L}$ and $P_{n,KL}$ reflects the increase in second-order elastic moments associated with the notional loads, which can be thought of as the increase in moments associated with inelastic deformations and column out-of-plumbness.

Member forces from second-order elastic analyses under the factored loads in combination with the notional loads are used in conjunction with all member strength interaction equations, which for the Canadian and Australian standards consist of separate interaction equations to check (1) cross-section strength, (2) in-plane member strength, and (3) out-of-plane strength. Major differences between the Canadian, European, and Australian standards are the magnitude of the notional loads, whether or not notional loads should be applied in conjunction with other lateral loads, and the use of effective lengths of less than 1 in assessing the member stability. Eurocode 3 and CSA-S16.1 use maximum values of notional loads equal to $0.005\Sigma P$ that are intended to account for both inelastic and out-of-plumbness effects, whereas AS4100 specifies a lower value of $0.002\Sigma P$, which reflects only the out-of-plumbness. Eurocode 3 is the only specification which requires that the notional loads be applied in combination with all loads, whereas CSA-S16.1 and AS4100 only require that notional loads be used in the factored gravity load check. Eurocode 3 is also the only one that allows the use of K factors of less than 1 in

the member stability checks for a sway frame. Beyond these conceptual differences, there are many additional differences in the provision formats and "shapes" of the interaction curves of the three standards. For example, CSA-S16.1 and AS4100 provide "enhanced" strength interaction formulas for members that have class 1 (i.e., plastic design type) cross sections, whereas the American and European documents do not distinguish between the design strengths for class 1 and class 2 type sections.

16.5.3 Examples of Strength Interaction Curves

A simple example comparing results obtained using the design specifications is presented to provide some appreciation for the issues involved in accurate stability assessment. The example consists of a single column which, as shown in Fig. 16.23, has end rotational restraints representative of conditions in a sway frame. The column is oriented with its web in the plane of the frame but is laterally unbraced about both axes. The W200 × 46 (W8 × 31) column is typical of a light- to medium-weight wide-flange column section that satisfies the compactness and/or class 1 provisions of all the specifications and standards. Design strengths calculated according to the four standards are shown in the interaction plots of Fig. 16.24*a* through *d*. In general, the specification calculations were based on a rigorous interpretation of the relevant provisions, and the values shown in Figs. 16.24 are the *design strengths* that include the appropriate resistance or partial safety factors. Second-order elastic analyses for specification checks were made using procedures developed by LeMessurier (1977), which include both P–Δ and P–δ effects. Results from exact spread-of-plasticity analyses are also shown in Figs. 16.24. One set of results are for two-dimensional analyses that modeled only the in-plane behavior, and the second set is from three-dimensional analyses, which considered both in-plane and out-of-plane effects, including torsional–flexural response. The distributed plasticity analyses included both initial imperfections (out-of-plumbness

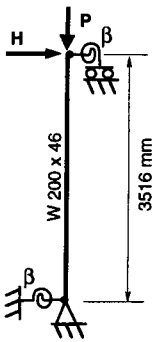

Material	E = 200,000 MPa Fy = 250 MPa
Slenderness	In-plane L/r = 40 Out-of-plane L/r = 69
Imperfections	Plumbness Δo/500 Straightness δo/1000
End Restraint	β = 22,700 kN-m

Fig. 16.23 Beam-column design example.

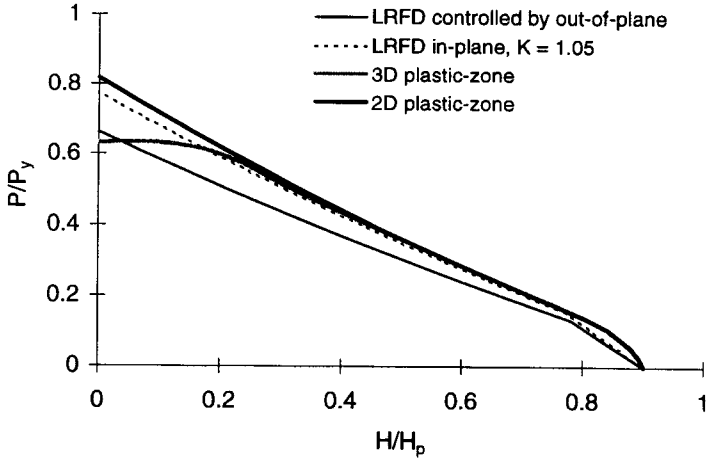

(*a*)

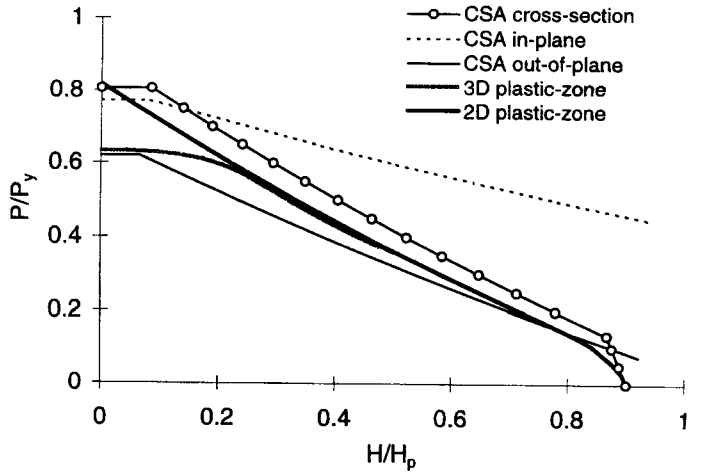

(*b*)

Fig. 16.24 Design strengths for nonredundant sway column: (*a*) AISC–LRFD; (*b*) CSA-S16.1; (*c*) Eurocode 3; (*d*) AS4100.

$\Delta_0 = L/500$ in the plane of the frame, and member out-of-straightness $\delta_0 = L/1000$ in both directions) and residual stresses ($f_{r,\max} = 0.3F_y$).

In-Plane Versus Out-of-Plane Effects. Comparing results for the two- and three-dimensional plastic zone analyses, the behavior is governed by in-plane effects for cases where the axial load $P/P_y < 0.5$, whereas for higher axial loads the strength is limited by out-of-plane instability. This situation is common in many designs of planar frames with H-shape members subjected

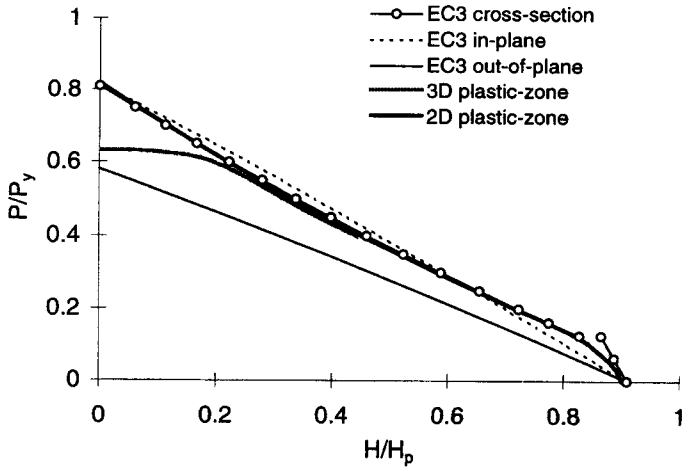

(*c*)

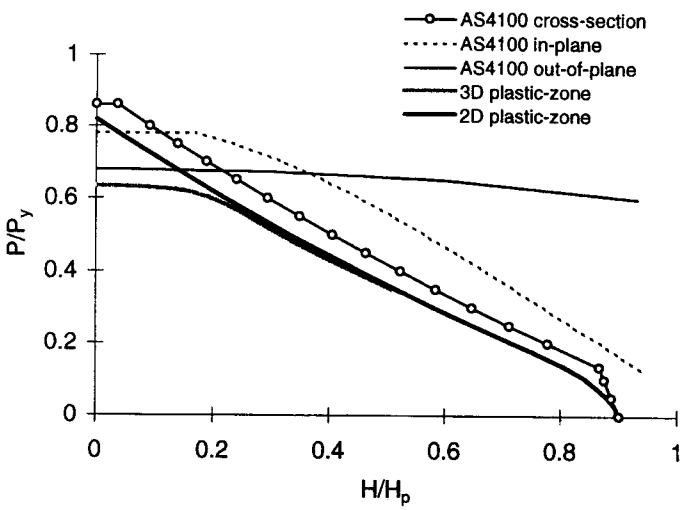

(*d*)

Fig. 16.24 continued (*c*) Eurocode 3; (*d*) AS4100.

to strong-axis bending but unbraced out-of-plane over the story height. All of the strength interaction plots, with the exception of the one from AS4100, are controlled by the out-of-plane strength check, although none of these distinguish the transition from in-plane to out-of-plane behavior. The AS4100 provisions (Fig. 16.24*d*) are perhaps the most representative of the actual strength since they suggest a transition in failure modes at about $P/P_y = 0.68$. However, the AS4100 results consistently overestimate the true

strength, whereas the other three standards provide conservative answers over nearly the entire range of values. Given that the out-of-plane slenderness of the column ($L_{cy}/r_y = 68.9$) satisfies the plastic design (class 1) requirements of all the specifications, it is somewhat contradictory that the AISC–LRFD, CSA-S16.1, and Eurocode 3 equations indicate that the members are governed by their out-of-plane strength for all values of axial load. Thus this example highlights the potential conservatism in out-of-plane strength checks, even for frames composed of fairly stocky members with small ratios of r_x/r_y subjected to nearly full reversed-curvature bending.

In-Plane Behavior. Comparisons of two-dimensional plastic zone solutions with in-plane and cross-section strength checks provide an indication of how well the code provisions capture the in-plane behavior. In particular, cross-section checks combined with elastic second-order analysis essentially follow the concepts of the first-hinge design approach described in Section 16.4.1. Overall, the AISC–LRFD and Eurocode 3 provisions provide the best agreement with the spread-of-plasticity analysis for in-plane behavior, although the two codes take different approaches (i.e., AISC–LRFD uses an effective-length factor and Eurocode 3 uses the notional load method). The CSA–S16.1 and AS4100 standard lead to significantly different results which are related to the following points:

1. In concept, the cross-section strength checks of Eurocode 3, CSA-S16.1, and AS4100 are essentially based on a first-hinge limit-state approach using forces from a second-order analysis with notional loads. In other words, the strength check for this case is based on the strength of a member with $P_n = P_y$ and $M_n = M_p$. The difference in accuracy between the Eurocode 3 and the other standards is due primarily to the fact that the Eurocode 3 requires the notional load to be applied in combination with other design lateral loads, whereas CSA-S16.1 and AS4100 only include the notional load in the gravity load check (i.e., where $H = 0$). Thus the calculated moments are larger and the strength interaction curve is lower than the other two over the entire range of P/P_y values. This is also the reason for the "cap" at the top of the interaction curves for the CSA-S16.1 and AS4100 cross-section checks in Fig. 16.24*b* and *d*. In a sense, the notional load applied only to the gravity check is essentially the same as capping the axial strength to account for some minimum eccentricity.

2. The peak axial strength values from the cross-section check per Eurocode 3 and CSA-S16.1 match the distributed plasticity and AISC–LRFD values very well, indicating that the assumed notional loads of $0.005P$ are appropriate for this case. On the other hand, the value of $0.002P$ used in AS4100 (see Fig. 16.24*d*), which represents only the out-of-plumbness effect, overestimates the strength since it does not take account of inelastic stiffness reduction.

3. The in-plane member strength checks of Eurocode 3, CSA-S16.1, and AS4100 are designed to detect cases where the maximum moment due to the combined effects of axial load, applied moments, and member out-of-straightness occurs along the length of the member. This may occur, for example, with relatively slender members or where moments cause single curvature. This is not the case in this example, where the maximum moments occur at the member end. The CSA-S16.1 and AS4100 provisions for in-plane member strength use a moment-modification term that reflects the fact that under reverse curvature, the critical moment away from the member ends can be less than the maximum moments at the ends. Therefore, for this example the CSA-S16.1 and AS4100 in-plane member curves lie above the in-plane cross-section strength curves. On the other hand, the Eurocode 3 provisions take a more conservative approach that utilizes the maximum end moments with the resulting in-plane member and cross-section curves being very similar.

Qualification of Results. It is important to note that because the column stiffness and rotational restraints in this example were chosen to be representative of typical buildings, system stability has a much smaller effect than it did in the portal frame examples discussed in Section 16.4. Consider, for example, that the effective inelastic in-plane buckling length factor $K = 1.05$ calculated per AISC–LRFD is very close to the actual member length used in the other standards. Additionally, the ratio of the applied load to the critical buckling load is relatively large. For example, for the limiting case where $P = 0.8P_y$, the ratio of $P_{cr}/P_y = 4.3$. Assuming that the elastic second-order amplification factor is approximately equal to $1/(1 - P/P_{cr})$, the limiting value of P_y/P_{cr} implies an upper bound of elastic second-order magnification of about 1.3, which is below the limit imposed on the use of elastic analysis in CSA-S16.1. Therefore, the comparisons shown in Fig. 16.24 are not necessarily indicative of the accuracy of the specification provisions for more slender systems.

16.5.4 Summary

All four of the specifications described above share the common requirement for determining member forces using second-order elastic analysis. Most also permit the use of amplification factors to approximate second-order effects using first-order elastic analyses, although for the reasons noted earlier in this chapter, with the availability of modern computers and software it is preferable to perform explicit second-order analyses. Of the four specifications, only AISC–LRFD continues to require use of the effective-length concept for calculating the nominal axial strength of the column to assess in-plane frame stability. This requirement is intended as a means to overcome the limitations

of elastic analysis to capture inelastic effects associated with residual stresses and spread of plasticity. The others (Eurocode 3, CSA-S16.1, and AS4100) rely solely on second-order elastic analyses coupled with the application of notional loads as the primary method for checking frame stability. In recognition that commonly available frame analysis programs do not model torsional–flexural member instabilities, all of the specifications maintain reliance on beam-column interaction equations for out-of-plane member instabilities.

16.6 CONCLUDING REMARKS

Although second-order analysis methods now prevalent in design practice go a long way toward addressing the problem of frame stability, they are still limited in their ability to model inelastic instability of frame and member behavior. This is particularly true for out-of-plane member response involving torsional–flexural behavior. Therefore, in the near term, design practice will continue to rely on methods that combine second-order elastic analysis with semiempirical member design equations and procedures to design for frame and member stability. As described in this chapter, current design standards include a number of useful approaches, although none of these provide a fully satisfactory solution to address the range of conditions encountered in design practice.

A key question in dealing with frame stability is the interplay between member and frame instability and whether they can be addressed together or separately. In this regard it is important to distinguish between cases governed by in-plane versus out-of-plane stability effects. Cases that can be dealt with considering only in-plane behavior are planar frames whose members are either (1) fully braced in the out-of-plane direction, or (2) oriented with their weak axes in the plane of bending such that out-of-plane failure is unlikely. In all other cases, out-of-plane or combined in- and out-of-plane behavior must be considered.

In-plane behavior. Available second-order analysis methods are capable of modeling in-plane member and frame instabilities in a single analysis. In particular, spread-of-plasticity analyses that include rigorous second-order routines to pick up both P–Δ and P–δ effects can be used as the sole basis for calculating strength and stability limit states of the frame and its members. Such analyses must, of course, include the effects of initial geometric imperfections, joints and connections, and so on, where they are significant. Short of performing detailed spread-of-plasticity analyses and, subject to certain limitations, elastic analyses can be used to calculate the first-hinge limit state for in-plane behavior. Similarly, elastic–plastic analyses can be used to calculate the inelastic limit state, including the beneficial effects of force distribution beyond formation of the first hinge. The major limitation or qualification for such analyses is that they can be applied only where either elastic inelastic second-order deformations are small or where such deformations are accounted for by using semiempirical procedures such as the modified stiffness or notional load procedures described in Section 16.4. As with spread-of-plasticity analyses, any methods that do not include separate member checks must take rigorous account of both P–Δ and P–δ effects, considering any significant initial geometric imperfections. In the absence of definitive guidelines to quantify the limitations and adjustments to elastic analyses, most current design standards require that member force interaction equations for in-plane behavior be used in conjunction with second-order elastic analysis methods.

Out-of-plane Behavior. A majority of frames encountered in design practice are ones in which members can fail in an out-of-plane torsional–flexural mode probably under combined axial load and major axis bending. Torsional–flexural behavior also arises in space frames where members are subjected to biaxial bending. At the present time, practical analysis techniques to account for this mode of behavior, which involves modeling of nonuniform (or warping) torsion, are not generally available. It is largely for this reason that current design standards require separate member-based strength and stability checks. However, especially in the cae of planar frames, out-of-plane member behavior and design equations to check for this have much less interaction with overall frame behavior than do in-plane member checks. For example, considering the AISC–LRFD equations, in the out-of-plane direction the effective column length is usually equal to the actual column length. Similarly, notional story loads used in other standards only apply for in-plane behavior and do not affect the out-of-plane checks. Therefore, for out-of-plane behavior there is more justification in separately treating member and frame stability checks.

Final Remarks on Frame Stability. With modern computer-based methods, there are few reasons not to conduct rigorous elastic second-order analyses that include as a minimum story P–Δ effects, and preferably, member P–δ effects. Such analyses should be three-dimensional, taking into account the following factors to the extent that they are significant: (1) gravity loads carried by both the lateral resisting systems and "gravity" or "leaning" columns, (2) connection and joint flexibility and finite sizes, (3) initial geometric imperfections—both in elevation and plan, and (4) other modeling considerations. Without a clear consensus on the limits of elastic analysis to model inelastic stability effects, current codes and standards feature a variety of methods, many of which have vestiges of earlier times when system second-order analyses were not as practical as they are today. It has been the intent of this chapter (particularly Section 16.4) to clarify the major issues and set a direction for the development of more consistent and rational approaches for frame stability that are more straightforward and take better advantage of existing and emerging analysis and limit-states design methods.

REFERENCES

ACI (1995), *Building Code Requirements for Structural Concrete and Commentary*, ACI 318-95, American Concrete Institute, Farmington Hills, Mich.

AISC (1992), *Code of Standard Practice for Steel Buildings and Bridges*, American Institute of Steel Construction, Chicago.

AISC (1993), *Load and Resistance Factor Specification for Structural Steel Buildings*, American Institute of Steel Construction, Chicago.

Allen, H. G., and Bulson, P. S. (1980), *Background to Buckling*, McGraw-Hill, New York, 582 pp.

Alvarez, R. J., and Birnstiel, C. (1969), "Inelastic Analysis of Multistory Multibay Frames," *ASCE J. Struct. Div.*, Vol. 95, No. ST11, pp. 2477–2503.

Anderson, D. (1993), "Plastic Hinge Based Methods for Advanced Analysis and Design of Steel Frames: European Standards and Guides," in *Plastic Hinge Based Methods for Advanced Analysis and Design of Steel Frames*, Structural Stability Research Council, Lehigh University, Bethlehem, Pa., pp. 25–40.

Argyris, J. H. (1982), "An Excursion into Large Rotations," *Comput. Methods Appl. Mech. Eng.*, Vol. 32, pp. 82–155.

ASCE Technical Committee on LRFD (1997), *Effective Length and Notional Load Approaches for Assessing Frame Stability: Implications for American Steel Design*, American Society of Civil Engineers, New York.

Attalla, M. R. (1995), "Inelastic Torsional–Flexural Behavior and the Three-Dimensional Analysis of Steel Frames," Ph.D. thesis, CEE, Cornell University, Ithaca, N.Y.

Attalla, M. R., Deierlein, G. G., and McGuire, W. (1994), "Spread of Plasticity: A Quasi-plastic Hinge Approach," *ASCE J. Struct. Eng.*, Vol. 120, No. 8, pp. 2451–2473.

Attalla, M. R., Deierlein, G. G., and McGuire, W. (1996), "Inelastic Torsional–Flexural Effects in Steel Structures: Theory and Applications," *Proc. 5th Int. Colloq. Stabil. Met. Struct.*, Structural Stability Research Council, Lehigh University, Bethlehem, Pa., pp. 11–20.

Bathe, K. (1996), *Finite Element Procedures*, Prentice-Hall, Upper Saddle River, N.J.

Birnstiel, C., and Iffland, J. S. B. (1980), "Factors Influencing Frame Stability," *ASCE J. Struct. Div.*, Vol. 106, No. ST2, pp. 491–504.

Chen, C. S. (1994), "Geometric Nonlinear Analysis of Three-Dimensional Structures," M.S. thesis, CEE, Cornell University, Ithaca, N.Y., pp. 197.

Chen, W. F., and Atsuta, T. (1976), *Theory of Beam-Columns: In-Plane Behavior and Design*, Vol. 1, McGraw-Hill, New York.

Chen, W. F., and Lui, E. (1991), *Stability Design of Steel Frames*, CRC Press, Boca Raton, Fla.

Chen, W. F., and Sohal, I. (1995), *Plastic Design and Second-Order Analysis of Steel Frames*, Springer-Verlag, New York.

Cheong-Siat-Moy, F. (1978), "Frame Design Without Using Effective Column Length," *ASCE J. Struct. Div.*, Vol. 104, ST1, pp. 23–33.

Clarke, M. (1994), "Plastic-Zone Analysis of Frames," in *Advanced Analysis of Steel Frames* (ed. W. F. Chen and S. Toma), CRC Press, Boca Raton, Fla.

Clarke, M., and Bridge, R. (1992), "The Inclusion of Imperfections in the Design of Beam-Columns," *Proc. 1992 Annu. Tech. Session*, Structural Stability Research Council, Lehigh University, Bethelem, Pa., pp. 327–346.

Clarke, M., and Bridge, R. (1996), "The Design of Steel Frames Using the Notional Load Approach," *Proc. 5th Colloq. Stabil. Met. Struct.*, Structural Stability Research Council, Lehigh University, Bethlehem, Pa., pp. 33–42.

Crisfield, M. A. (1991), *Nonlinear Finite Element Analysis of Solids and Structures*, Wiley, New York.

CSA (1994), *Limit States Design of Steel Structures*, CAN/CSA-S16.1-M94, Canadian Standards Association, Rexdale, Ontario, Canada.

Duan, L., and Chen, W. F. (1990), "A Yield Surface Equation for Doubly Symmetrical Sections," *Eng. Struct.*, Vol. 12, No. 2, pp. 114–119.

ECS (1993), *Eurocode 3: Design of Steel Structures*, ENV 1993-1-1:1992E, European Committee for Standardization, Brussels, Belgium.

El-Tawil, S., and Deierlein, G. G. (1996), "Inelastic Analysis of Mixed Steel–Concrete Systems," *Proc. 5th Int. Colloq. Stab. Met. Struct.*, Structural Stability Research Council, Lehigh University, Bethelem, Pa., pp. 53–62.

El-Zanaty, M. H., Murray, D. W., and Bjorhovde, R. (1980), "Inelastic Behavior of Multistory Steel Frames," *Struct. Eng. Rep. No. 83*, University of Alberta, Edmonton, Alberta, Canada.

Guralnick, S. A., Singh, S., and Erber, T. (1984), "Plastic Collapse, Shakedown and Hysteresis," *ASCE J. Struct. Eng.*, Vol. 110, No. 9.

Guralnick, S. A., Erber, T., Stefanis, J., and Soudan, O. (1986), "Plastic Collapse, Shakedown, and Hysteresis of Multistory Steel Structures," *ASCE J. Struct. Eng.*, Vol. 112, No. 12.

Guralnick, S. A., Erber, T., Soudan, O., and Jixing He (1991), "Incremental Collapse of Framed Structures Subjected to Constant Plus Cyclically Varying Loads," *ASCE J. Struct. Eng.*, Vol. 117, No. 6.

Horne, M. R. (1975), "An Approximate Method for Calculating the Elastic Critical Loads of Multi-story Plane Frames," *Struct. Eng.*, Vol. 15, No. 6, pp. 242–248.

Horne, M. R. (1979), *Plastic Theory of Structures*, 2nd ed., Pergamon Press, Elmsford, N.Y.

Horne, M. R., and Merchant, W. (1965), *The Stability of Frames*, Pergamon Press, Elmsford, N.Y.

Iffland, J. S. B., and Birnstiel, C. (1982), "Stability Design Procedures for Building Frameworks," *AISC Proj. No. 21.62*, American Institute of Steel Construction, Chicago.

Kanchanalai, T. (1977), "The Design and Behavior of Beam-Columns in Unbraced Steel Frames," *AISI Proj. No. 189, Rep. No. 2*, Civil Engineering/Structures Research Laboratories, University of Texas, Austin, Texas, 300 pp.

Kanchanalai, T., and Lu, L.-W. (1979), "Analysis and Design of Framed Columns Under Minor Axis Bending," *AISC Eng. J.*, second quarter, pp. 29–41.

Kemp, A. (1986), "Factors Affecting the Rotational Capacity of Plastically Designed Members," *Struct. Eng.*, Vol. 64B, No. 2, pp. 28–35.

Kennedy, D. J. L., Picard, A., and Beaulieu, D. (1990), "New Canadian Provisions for the Design of Steel Beam-Columns," *Can. J. Civ. Eng.*, Vol. 17, pp. 873–893.

Konig, J. A. (1987), *Shakedown of Elastic–Plastic Structures*, Elsevier, New York.

Krawinkler, H. (1978), "Shear in Beam-Column Joints in Seismic Design of Steel Frames," *AISC Eng. J.*, Vol. 15, No. 3, pp. 82–91.

Krawinkler, H., Alali, A., Thiel, C. C., and Dunlea, J. M. (1995), "Analysis of a Damaged Four-Story Building and an Undamaged Two-Story Building," in *SAC Rep. 95-04, Technical Report: Analytical and Field Investigations of Buildings Affected by the Northridge Earthquake*, SAC Joint Venture, Sacramento, Calif., Chap. 3.

LeMessurier, W. J. (1976), "A Practical Method of Second-Order Analysis: Part 1. Pin Jointed Systems," *AISC Eng. J.*, Vol. 13, No. 4, pp. 89–96.

LeMessurier, W. J. (1977), "A Practical Method of Second-Order Analysis: Part 2. Rigid Frames," *AISC Eng. J.*, Vol. 14, No. 2, pp. 49–67.

Liew, J. Y. R. (1992), "Advanced Analysis for Frame Design," Ph.D. dissertation, School of Civil Engineering, Purdue University, West Lafayette, Ind.

Liew, J. Y. R., White, D. W., and Chen, W. F. (1993), "Second-Order Refined Plastic Hinge Analysis for Frame Design, Parts 1 and 2," *ASCE J. Struct. Eng.*, Vol. 119, No. 11, pp. 3196–3237.

Liew, J. Y. R., White, D. W., and Chen, W. F. (1994), "Notional-Load Plastic-Hinge Method for Frame Design," *ASCE J. Struct. Eng.*, Vol. 120, No. 5, pp. 1434–1454.

MacGregor, J. (1993), "Design of Slender Concrete Columns, Revisited," *ACI Struct. J.*, Vol. 90, No. 3, pp. 302–309.

MacGregor, J., and Hage, S. E. (1977), "Stability Analysis and Design of Concrete Frames," *ASCE J. Struct. Div.*, Vol. 103, No. ST10, pp. 1953–1970.

McGuire, W. (1992), "Computer-Aided Analysis," in *Constructional Steel Design: An International Guide* (ed. P. J. Dowling, J. E. Harding, and R. Bjorhovde), Elsevier Applied Science, New York, pp. 915–932.

Nair, R. S. (1975), "Overall Elastic Stability of Multistory Buildings," *ASCE J. Struct. Div.*, Vol. 10, No. ST12, pp. 2487–2503.

Nair, R. S. (1987), "Tall Building Stability: Practical Considerations," *Proc. Struct. Congr. ASCE*, pp. 582–594.

Neil, B. G. (1977), *The Plastic Methods of Structural Analysis*, 3rd ed., Chapman & Hall, London.

Nukala, P. K. V. V. (1997), "Three-Dimensional Inelastic Analysis of Steel Frames," Ph.D. thesis, School of Civil Engineering, Purdue University, West Lafayette, Ind.

Orbison, J. G., McGuire, W., and Abel, J. F. (1982), "Yield Surface Applications in Nonlinear Steel Frame Analysis," in *Computer Methods in Applied Mechanics and Engineering*, Vol. 33, North-Holland, Amsterdam, pp. 557–573.

Pi, Y.-L., and Trahair, N. (1994), "Nonlinear Inelastic Analysis of Steel Beam-Columns: Theory and Applications," *ASCE J. Struct. Eng.*, Vol. 120, No. 7, pp. 2041–2085.

Popov, E. P., and McCarthy, R. E. (1960), 'Deflection Stability of Frames Under Repeated Loads," *ASCE J. Eng. Mech. Div.*, Vol. 86, No. EM1, pp. 61–78.

Porter, F. L., and Powell, G. H. (1971), "Static and Dynamic Analysis of Inelastic Frame Structures," *EERC Rep. No. 71-3*, University of California, Berkeley, Calif.

Rutenberg, A. (1981), "A Direct P–Delta Analysis Using Standard Plane Frame Computer Programs," *Comput. Struct.*, Vol. 12, No. 1–2, pp. 97–102.

Rutenberg, A. (1982), "Simplified P–Delta Analysis for Asymmetric Structures," *ASCE J. Struct. Div.*, Vol. 108, No. ST9, pp. 1995–2013.

SAA (1990), *Steel Structures*, AS4100 Standards Association of Australia, Australian Institute of Steel Construction, Sydney, Australia.

Springfield, J. (1987), "Frame Stability: A Canadian Designer's Approach," *Proc. Struct. Congr. ASCE*, pp. 595–610.

Springfield, J. (1991), "Limits on Second-Order Elastic Analysis," *Proc. SSRC Annu. Tech. Session*, Structural Stability Research Council, Lehigh University, Bethelem, Pa., pp. 89–99.

Stevens, L. K. (1967), "Elastic Stability of Practical Multi-story Frames," *Proc. Inst. Civ. Eng.*, Vol. 36, pp. 99–117.

White, D. W., and Chen, W.F., ed. (1993), *Plastic Hinge Based Methods for Advanced Analysis and Design of Steel Frames*, Structural Stability Research Council, Lehigh University, Bethlehem, Pa.

White, D. W., and Clarke, M. (1997), "Design of Beam-Columns in Steel Frames: I. A Study of Philosophies and Procedures," *ASCE J. Struct. Eng.*, Vol. 123, No. 12, Dec. pp. 1556–1564.

White, D. W., and Hajjar, J. (1991), "Application of Second-Order Elastic Analysis to LRFD: Research to Practice," *AISC Eng. J.*, Vol. 28, No. 4, pp. 133–148.

White, D. W., and Hajjar, J. (1997), "Design of Frames Without Consideration of Effective Length," *Eng. Struct.*, Vol. 19, No. 10, pp. 787–810.

Wilson, E. L., and Habibullah, A. (1987), "Static and Dynamic Analysis of Multi-story Buildings Including *P*–Delta Effects," *Earthquake Spectra*, Vol. 3, No. 2, pp. 289–298.

Wood, B. R., Beaulieu, D., and Adams, P. F. (1976a), "Column Design by *P*–Delta Method," *ASCE J. Struct. Div.*, Vol. 102, No. ST2, pp. 411–527.

Wood, B. R., Beaulieu, D., and Adams, P. F. (1976b), "Further Aspects of Design by *P*–Delta Method," *ASCE J. Struct. Div.*, Vol. 102, ST3, pp. 487–500.

WRC/ASCE (1961), *Commentary on Plastic Design in Steel*, a joint committee report, American Society of Civil Engineers, New York.

Yang, Y. B., and McGuire, W. (1986a), "Stiffness Matrix for Geometric Nonlinear Analyais," *ASCE J. Struct. Eng.*, Vol. 112, No. 4, pp. 853–877.

Yang, Y. B., and McGuire, W. (1986b), "Joint Rotation and Geometric Nonlinear Analysis," *ASCE J. Struct. Eng.*, Vol. 112, No. 4, pp. 853–877.

Yang, Y. B., and Quo, S. R. (1994), *Theory and Analysis of Nonlinear Framed Structures*, Prentice Hall, Upper Saddle River, N.J.

Yura, J. A. (1971–1972), "The Effective Length of Column in Unbraced Frames, *AISC Eng. J.*, Apr. 1971, pp. 37–42; "Closure to Discussion by Peter Adams," Jan. 1972, pp. 40–46.

Yura, J. A. (1988), *Elements for Teaching Load and Resistance Factor Design, Combined Bending and Axial Load*, American Institute of Steel Construction, Chicago.

Yura, J. A. (1995), "A Critique of Stability Effects in Steel Frames," *Restructuring: America and Beyond, Proc. Struct. Congr. XIII, ASCE*, pp. 1793–1796.

Yura, J. A., Kanchanalai, T., and Chotichanathawenwong, S. (1996), "Verification of Steel Beam-Column Design Based on the AISC–LRFD Method," *Proc. 5th Int. Colloq. Stab. Met. Struct.*, Structural Stability Research Council, Lehigh University, Bethelem, Pa., pp. 21–30.

Ziemian, R. D. (1991), "Advanced Methods of Inelastic Analysis in the Limit States Design of Steel Structures," Ph.D. thesis, CEE, Cornell University, Ithaca, N.Y.

Ziemian, R. D., and Miller, A. R. (1997), "Inelastic Analysis and Design: Frames With Members in Minor-Axis Bending," *ASCE J. Struct. Eng.*, Vol. 123, No. 2, pp. 151–157.

Ziemian, R. D., McGuire, W., and Deierlein, G. G. (1992a), "Limit States Steel Design with Second-Order Inelastic Analysis: Planar Frame Studies," *ASCE J. Struct. Eng.*, Vol. 118, No. 9, pp. 2532–2549.

Ziemian, R. D., McGuire, W., and Deierlein, G. G. (1992b), "Limit States Steel Design with Second-Order Inelastic Analysis: 3DH High-Rise Frame Study," *ASCE J. Struct. Eng.*, Vol. 118, No. 9, pp. 2550–2567.

CHAPTER SEVENTEEN

ARCHES

17.1 IN-PLANE STABILITY OF ARCHES

The analysis and design of arches may be broadly classified according to their response to load and their in-plane mode of failure. These characteristics depend on the type of arch, such as:

- Slender arches, generally of solid-web rolled or built-up sections, subject primarily to axial force in the arch rib (analogous to axially loaded columns)
- Slender arches subject to significant bending and deformation, due primarily to asymmetric loading (analogous to beam-columns)
- Stocky arches, frequently of truss form, used because of high bending loads, in which failure will be due primarily to chord or flange failure arising from axial load and excessive bending (similar to any truss subject to axial load and moment)
- Arches composed of arch ribs and deck stiffening girders

These categories are treated separately in this chapter. Finally, attention is given to out-of-plane buckling.

When the loads acting on an arch are increased proportionally, it loses its stability as a certain critical value of the load is attained. In the case of elastic structures under conservative loads the critical load always corresponds to either a birfurcation point or a stability limit point. Various possible load-

deformation plots for arches, called *equilibrium paths*, are shown in Fig. 17.1. Each point on a path represents an equilibrium configuration of the structure.

Figure 17.1*a* shows an equilibrium path for an unsymmetric problem in which the arch boundary conditions and/or the manner of loading may be unsymmetrical. The point on the equilibrium path at which the load is a relative maximum is called a limit point.

Figure 17.1*b* illustrates possible load-deformation relationships for a symmetrical and symmetrically loaded arch. Here the primary or fundamental equilibrium path is intersected by a secondary path. The primary branch represents a symmetric deflected mode and the secondary branch an antisymmetric mode. Points at which equilibrium paths intersect one another are called bifurcation points. If an antisymmetrical mode does not first become dominant, the arch eventually will become unstable when the load-deflection curve reaches a limit point. Then the arch buckles in a symmetrical mode. However, Fig. 17.1*b* shows the antisymmetrical mode dominating. Note that the load drops beyond the bifurcation point. This is the usual behavior when the arch buckles by sidesway, but it is possible for the load to increase slightly after bifurcation in which case the maximum load is attained at a limit point after large movements in the plane of the arch (Fig. 17.1*c*). In case of an unstable, rapidly

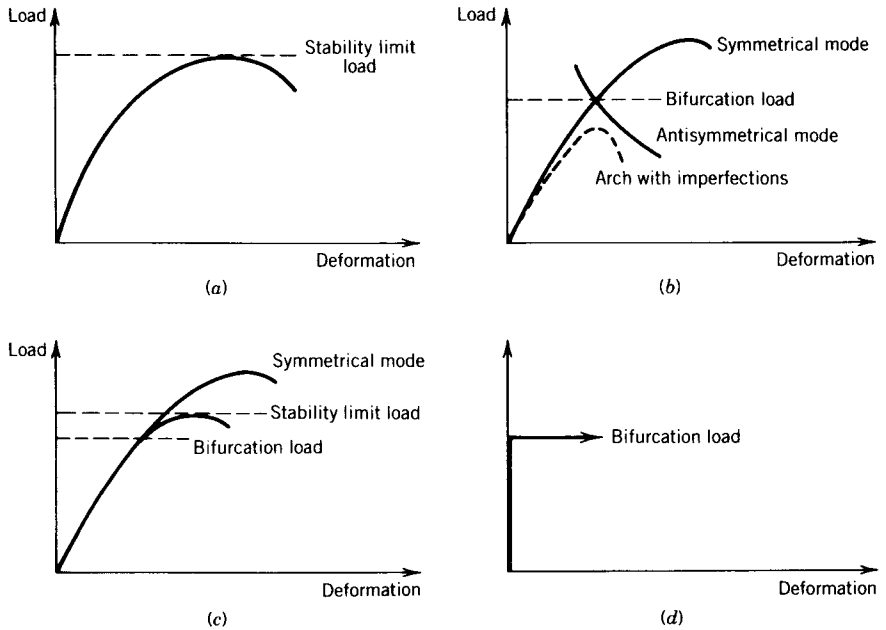

Fig. 17.1 Some possible load-deformation paths for arches. (*a*) Nonlinear stability: Unsymmetrical or unsymmetrically loaded arch. (*b*) Nonlinear stability: symmetrical and symmetrically loaded arch. (*c*) Nonlinear stability: symmetrical and symmetrically loaded arch. (*d*) Linear stability: negligible prebuckling deformation.

descending postbuckling path the arch is sensitive to geometric imperfections or load eccentricity. The associated drop in critical load is shown in Fig. 17.1*b* (dashed curve), and the buckling load at the bifurcation point is replaced by the snap load at the limit point on the dashed curve. The degeneration of a bifurcation point into a limit point due to the presence of imperfections suggests that bifurcation is an exception rather than the rule.

Arch structures are most efficient if they carry their load in such a way that the funicular curve coincides with the centroidal axis of the rib, so that there will be axial compression but no bending of the arch rib. Such a rib experiences only very small displacements before buckling. Circular arches subjected to uniform normal pressure, commonly called hydrostatic loading, parabolic arches subjected to uniform load on a horizontal projection and catenary arches with load uniformly distributed along the arch axis are some examples of arches under pure axial compression. In the ideal situation such structures undergo birfurcation buckling. These bifurcation problems are far more amenable to analysis because they permit a linearization of the equilibrium equations for the prebuckling, or fundamental state. The linearization is based on the assumption of very small displacements and the equilibrium path is horizontal (Fig. 17.1*d*), as in small-deflection column theory. For practical design loadings, however, the funicular curves normally do not coincide with the centroidal axis and in such cases the arch experiences substantial bending moments and displacements before buckling. Studies that take into account these prebuckling deformations are nonlinear stability problems, as illustrated by Fig. 17.1*a–c*.

17.2 IN-PLANE LINEAR STABILITY

Early papers on arch stability were devoted to linear stability problems. This work by Gaber, Stüssi, Kollbrunner, Hilman, Dischinger, and Dinnik is summarized by Austin (1971) and Timoshenko and Gere (1961). Consider the buckling of arches of constant cross section (herein termed uniform arches) in which the arch is the funicular curve for the loading. The critical values of distributed load and horizontal reaction of fixed two-hinged and three-hinged symmetric arches are summarized in Table 17.1 for the following cases: (1) parabolic arches subjected to vertical load uniformly distributed on a horizontal projection, (2) catenary arches under uniform vertical load along the arch axis, and (3) circular arches subjected to uniform normal pressure, commonly called hydrostatic loading. In each of these cases, for geometrically perfect arches, the loading causes pure axial compression (no bending) at every cross section of the arch. The arches are free to buckle in their plane without restraint. Axial compressive strain has been neglected in the analyses reported since it has a very small effect for slender arches. Buckling is a bifurcation phenomenon from an undeflected position, as shown in Fig. 17.1*d*. The critical

TABLE 17.1 Critical Load Parameter and Critical Horizontal Reaction Parameter for Uniform Elastic Arches in Pure Compression[a]

$\frac{h}{L}$	Three-Hinged Arch		Two-Hinged Arch		Fixed Arch	
	qL^3/EI	HL^2/EI	qL^3/EI	HL^2/EI	qL^3/EI	HL^2/EI
Parabolic arches subjected to vertical load uniformly distributed on a horizontal projection						
0.10	22.5	28.1	29.1	36.3	60.9	76.2
0.15			39.5	32.9	85.1	70.9
0.20	39.6	24.8	46.1	28.8	103.1	64.5
0.25			49.2	24.6	114.6	57.3
0.30	49.5	20.6	49.5	20.6	120.1	50.0
0.35			47.8	17.1	120.6	43.1
0.40	45.0	14.1	45.0	14.1	117.5	36.7
0.50	38.2	9.6	38.2	9.6	105.3	26.3
Catenary arches subjected to vertical load uniformly distributed along the arch axis						
0.10			28.7	36.3	60.1	76.2
0.15			38.3	32.8	82.7	70.9
0.20			43.5	28.5	98.0	64.3
0.25			44.8	24.1	105.9	56.9
0.30			43.2	19.8	107.4	49.4
0.35			39.7	16.1	104.0	42.1
0.40			35.3	12.9	97.2	35.4
0.50			26.5	8.2	79.3	24.5
Circular arches subjected to normal load uniformly distributed along the arch axis						
0.10	22.2	26.7	28.4	34.1	58.9	70.7
0.20	33.5	17.6	39.3	20.6	90.4	47.5
0.30	34.9	9.3	40.9	10.9	93.4	24.9
0.40	30.2	3.4	32.8	3.7	80.7	9.1
0.50	24.0	0	24.0	0	64.0	0

[a] h, rise; L, span; q, critical intensity of distributed load; H, critical horizontal reaction at supports; E, Young's modulus of elasticity; I, moment of inertia of the cross section.

values in Table 17.1 are given for a range of rise-to-span ratios from 0.10 to 0.50.

In Table 17.1 the critical values for two-hinged and fixed parabolic and catenary arches were taken from Austin and Ross (1976). The remaining values were taken from Timoshenko and Gere (1961). Kollbrunner (1936, 1942) showed that the elastic critical values obtained experimentally are in close agreement with the theoretical values reported in Table 17.1.

The fundamental modes that correspond to the critical values given in Table 17.1 are shown in Fig. 17.2. The fixed and two-hinged arches always buckle into

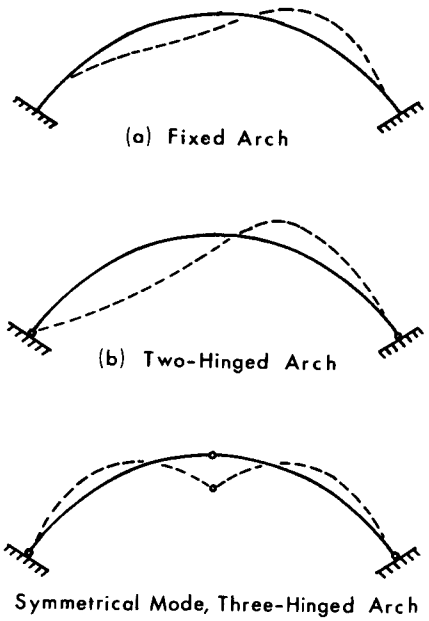

Fig. 17.2 Fundamental buckling-mode shapes.

an antisymmetrical mode in which the arch sways sideways, with the crown moving horizontally and becoming a point of contraflexure (Fig. 17.2*a* and *b*). In the case of a three-hinged arch, for low rise-to-span ratios the buckling is symmetric, as shown in Fig. 17.2*c*; the crown moves downard. For high rise-to-span ratios the three-hinged arch buckles in an antisymmetrical mode like that of the two-hinged arch and at the same critical load.

In the buckling behavior of uniform arches of low and moderate span-to-depth ratios under pure axial compression which buckle by sidesway there is a similarity with the buckling behavior of straight columns. For example, a fixed arch that buckles into two waves with a point of contraflexure at the crown (Fig. 17.2*a*) has a mode shape from support to crown similar to that of a fixed-hinged column, and the critical axial thrust at the quarter-point of the arch agrees fairly well with the critical compressive force in the end-loaded, fixed-hinged column whose length is equal to the arc length of the arch from support to crown. This interpretation is developed fairly extensively in the third edition of the guide but is not repeated here because it is not useful, except as a very broad concept, for elastic buckling of slender arches under more general loadings which do not produce pure axial compressive force in the arches. It is used, however, in ultimate strength studies and as a design tool, as will be described.

The elastic buckling of nonuniform parabolic arches subjected to vertical loading distributed uniformly on a horizontal projection has been studied for moment-of-inertia variations, $I = I_c \sec\phi$ and $I = I_c \sec^3\phi$ in which $I_c =$

moment of inertia at crown and ϕ = angle between the tangent to the arch axis and the horizontal. These studies are reported in the third edition of the guide. However, it is apparent that it is not feasible to give tables for all possible practical flexural stiffness distributions even if such values were available. Therefore, a simple approximate procedure for extrapolating uniform arch-buckling information to nonuniform arches for antisymmetrical buckling is useful. In this procedure the critical load on a nonuniform arch is considered to be equal to that for a similar uniform arch with an "equivalent" moment of inertia computed in the following manner. Imagine that one-half of the nonuniform arch (from support to crown) is straightened out to form a simply supported beam and loaded with a concentrated load at midspan. Compute the deflection at midspan. The equivalent uniform moment of inertia of this nonuniform arch then is equal to the moment of inertia of a simply supported prismatic beam of the same span and loading that deflects at the center the same amount. The same equivalent value of moment of inertia is recommended for fixed two- and three-hinged arches. The result of such a computation is discussed in the third edition of the guide. Similar procedures developed by Aas-Jakobsen are described by Forrester in a discussion of Austin's paper (1971).

Stiffened arches are deck structures that consist of an arch connected to an overhead horizontal girder by closely spaced columns. As discussed in the third edition of this guide, for two- and three-hinged, low-rise parabolic arches subjected to uniform load on a horizontal projection the critical load and critical horizontal reaction can be closely approximated by the use of the values in Table 17.1, using for the moment of inertia, I, an equivalent I equal to the sum of the arch and girder moments of inertia. This simple concept recognizes that the arch and girder buckle together.

17.3 IN-PLANE NONLINEAR ELASTIC STABILITY

Section 17.2 has treated arches subjected to special loadings that produced only axial compression. Since the arches were considered to be inextensible, there were no prebuckling deflections for these cases. However, actual design loadings on arches usually produce both axial compression and bending moment on a general cross section of the arch rib. These internal forces cause a change in shape of the arch before buckling occurs. This makes the problem nonlinear even though the material is deforming elastically.

17.3.1 Symmetrical Loadings on Symmetrical Arches

The general deformational behavior of symmetrical arches symmetrically loaded is shown in Fig. 17.1*b* and has been described above. Buckling data are given in Table 17.2 for two-hinged and fixed parabolic and circular arches subjected to uniform vertical load uniformally distributed along the arch axis.

TABLE 17.2 Elastic Buckling Coefficients for Uniform Arches with Vertical Load Uniformly Distributed Along Arch Axis[a]

		Two-Hinged Arch			Fixed Arch		
θ (deg)	h_i/L	qL^3/EI	HL^2/EI	h_c/h_i	qL^3/EI	HL^2/EI	h_c/h_t
		Parabolic arches–antisymmetrical modes					
	0.10	28.6	36.3	1.002	60.4	76.1	1.003
	0.15	38.2	32.9	1.004	83.4	70.8	1.006
	0.20	43.4	28.8	1.006	99.3	64.3	1.010
	0.25	44.9	24.5	1.008	107.7	57.0	1.013
	0.30	43.5	20.5	1.009	109.6	49.5	1.015
	0.35	40.4	16.96	1.009	106.4	42.5	1.017
	0.40	36.5	13.98	1.009	100.0	36.2	1.017
	0.50	28.5	9.51	1.008	83.0	25.9	1.017
		Circular arches—antisymmetrical modes					
50	0.1109	31.2	35.6	0.994	64.8	75.2	0.992
70	0.1577	39.5	32.0	0.989	83.4	70.0	0.983
90	0.2071	44.0	27.4	0.981	95.5	63.3	0.969
106.26	0.2500	44.5	23.2	0.974	99.9	57.0	0.966
120	0.2887	42.8	19.34	0.968	99.8	51.2	0.938
140	0.3501	37.1	13.75	0.959	93.8	42.1	0.910
160	0.4196	28.9	8.72	0.953	81.9	32.6	0.880
180	0.5000	20.0	4.78	0.950	66.0	23.4	0.854
		Circular arches—symmetrical modes					
50	0.1109	63.0	74.6	0.88	90.9	110.6	0.94
70	0.1577	77.6	66.8	0.81	110.0	98.5	0.91
90	0.2071	85.6	57.9	0.75	119.4	85.7	0.88
106.26	0.2500	87.7	50.5	0.69	120.3	75.2	0.85
120	0.2887	86.7	44.3	0.64	117.2	66.7	0.82
140	0.3501	81.7	35.1	0.57	107.5	54.2	0.78
160	0.4196	73.8	27.1	0.45	93.5	43.1	0.73
180	0.5000	64.4	19.07	0.34	77.2	32.5	0.67

[a] h_i, initial rise of arch; h_c, height of arch at crown at instant of buckling; θ, angle of opening of the circular arch.

These data are from Austin and Ross (1976). Similar data are available in this paper also for a single concentrated load at midspan. In these studies axial strains have been neglected since their influence is very small for slender arches.

The antisymmetrical buckling critical loads for circular arches are shown to be less than the symmetrical buckling critical loads in Table 17.2. The same is true for parabolic arches, although the symmetrical buckling critical loads are not available. Antisymmetrical buckling usually governs but not always. Fixed

circular arches with a single concentrated load at the crown buckle symmetrically. This is also true for fixed parabolic arches with concentrated load at the crown, except for deep arches with a rise-to-span ratio greater than about 0.40. Note in Table 17.2 that the ratio h_c/h_i is close to unity for the arches that buckle by sidesway, which indicates that the profile at the instant of buckling was nearly the same as the unloaded profile for these cases.

The critical conditions for antisymmetrical buckling often are expressed in terms of horizontal reactions; this is especially meaningful for flatter arches. In Fig. 17.3 graphs are shown of the critical horizontal reaction coefficient versus the rise-to-span ratio for the antisymmetrical buckling solutions given in Tables 17.1 and 17.2. Note in Fig. 17.3 that the critical horizontal reactions are quite insensitive to the arch shape and to a lesser extent to the loading; they vary primarily with the rise-to-span ratio. This is particularly true for the fixed

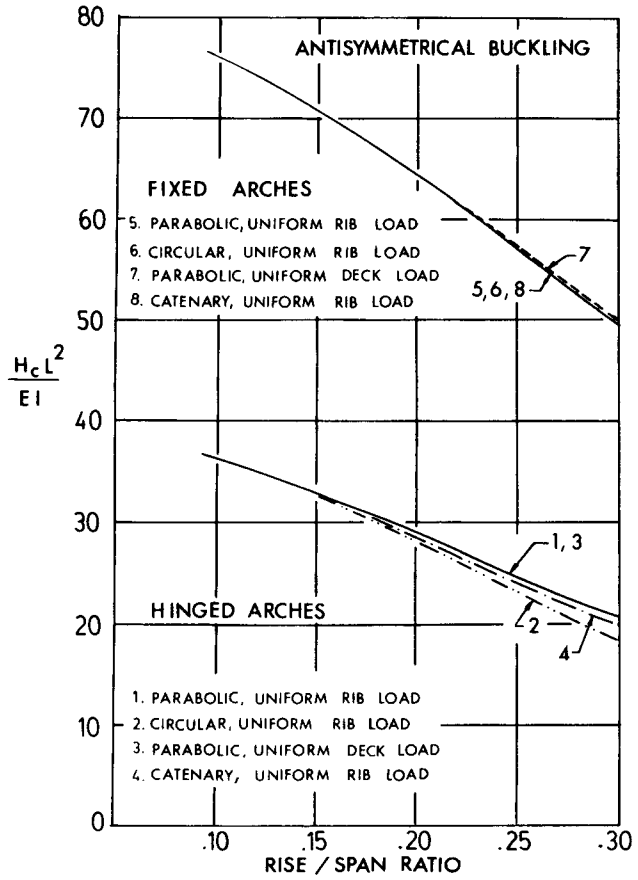

Fig. 17.3 Variation of critical horizontall reaction with rise-to-span ratio.

arches; the curves for three different shapes all with uniform rib loading lie on a single line and the parabolic arch with uniform deck loading case is very close. The rise-to-span ratios vary from 0.10 to 0.30, which includes the most practical range for bridges. The curves separate more for larger rise-to-span ratios. These results suggest that the curves of Fig. 17.3 can be used to make close estimates of the critical horizontal reaction for other symmetrical loadings. Note that the horizontal reaction in Fig. 17.3 is the exact value obtained by nonlinear analysis for some of the cases. However, the horizontal reactions given by a first-order solution for the same load agree closely with these values.

17.3.2 Unsymmetrical Loading

The general deformational behavior of unsymmetrically loaded arches is shown in Fig. 17.1*a* and has been described above. Several studies have been made of the most important practical loading, which comprise a uniformly distributed dead load (on a horizontal projection), q, plus a uniformly distributed live load, p, extending a variable distance from one abutment, as shown in Fig. 17.4. These studies were for parabolic arches.

The first studies by Deutsch (1940), Harries (1970) and Kuranishi and Lu (1972), used half-span live load. Kuranishi and Lu noted that for elastic buckling the total dead plus live load intensity, $w = p + q$, at buckling seemed roughly equal to the buckling value for uniform load over the entire span. Recently, studies have been made by Chang (1973) and Harrison (1982) in which the length of the live load s was varied. The results by Chang are given in Tables 17.3 and 17.4. Parabolic hinged and fixed arches are considered with span-to-depth ratios of 0.15 and 0.25 and live load-to-dead load ratios of ∞, 0.50, 0.15, and 0, covering the range of practical values. Note that the live load-to-dead load ratio = 0 corresponds to uniform symmetrical load, the arch buckling is by bifurcation, and the values are the same as reported in Table 17.1.

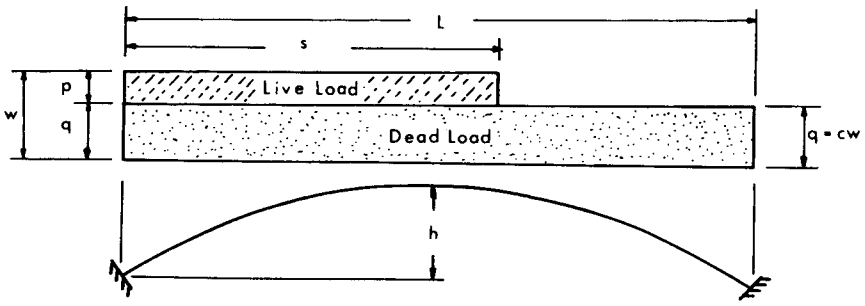

Fig. 17.4 Unsymmetrical loading.

TABLE 17.3 Minimum Elastic Buckling Coefficients for Uniform Hinged- and Fixed-Ended Parabolic Arches Under Distributed Dead and Live Loads

$\frac{h}{L}$	$\frac{p}{q}$	Hinged-Ends			Fixed Ends		
		s/L	wL^3/EI	HL^2/EI	s/L	wL^3/EI	HL^2/EI
0.15	∞	0.72	34.0	26.6	0.72	71.7	58.1
	0.50	0.67	35.5	29.4	0.66	75.9	62.2
	0.15	0.63	36.8	30.8	0.63	78.4	66.1
	0	—	39.5	32.9	—	85.1	70.9
0.25	∞	0.77	44.7	22.5	0.73	99.3	49.5
	0.50	0.68	46.0	23.3	0.66	104.0	51.9
	0.15	0.64	47.0	23.9	0.64	107.5	54.4
	0	—	49.2	24.6	—	114.6	57.3

TABLE 17.4 Elastic Buckling Coefficients for Uniform Hinged- and Fixed-Ended Parabolic Arches Under Distributed Dead and Half-Span Live Load ($s=0.50L$)

$\frac{h}{L}$	$\frac{p}{q}$	Hinged Ends		Fixed Ends	
		wL^3/EI	HL^2/EI	wL^3/EI	HL^2/EI
0.15	∞	42.4	22.4	96.2	46.7
	0.50	37.1	28.4	80.2	60.4
	0.15	37.3	30.6	80.0	65.2
	0	39.5	32.9	85.1	70.9
0.25	∞	56.4	19.3	131.4	41.0
	0.50	48.3	22.8	109.8	50.4
	0.15	47.7	23.8	109.1	53.7
	0	49.2	24.6	114.6	57.3

In Table 17.3 the minimum total load intensity, w is tabulated along with the corresponding horizontal reaction, H, and length of live load, s. These results were obtained with a numerical solution using 24 equal divisions in the arch rib, with the load length being incremented one panel at a time. The values of w and H were found accurately, but the loaded length, s, is only approximate. Table 17.4 gives the corresponding values for half-span live loading ($s = 0.50$). The following conclusions can be drawn for pratical ranges. The minimum total buckling load is obtained when the live load acts over from 63 to 68% of the span. The buckling value of the total load s is minimized for high live-to-dead load ratios but does not drop below about 89% of the full-span buckling value for the practical range. This is remarkably constant. Half-span loading is a good approximation for the partial loading case, as the corresponding elastic buckling load is not greater than about 6% more than the absolute minimum, in the practical range.

It should be noted that high live loads acting over partial spans produce very large moments and deformations. The elastic limit load is reached only after very large displacements which completely distort the arch, as discussed by Harrison (1982) and by Yabuki and Vinnakota (1984). When inelastic behavior is considered the limit loads for these cases are very much less than the elastic buckling values reported above, as discussed in the next section.

17.4 IN-PLANE ULTIMATE LOAD

17.4.1 Limit Analysis of Stocky Arches

The limit analysis of arches was presented by Onat and Prager in 1953 and by Galli and Franciosi in 1955. Following their investigations several researchers reported on the collapse load of arches (Stevens 1957; Coronforth and Childs, 1967). However, in these studies the collapse loads were obtained by the upper and lower bound methods assuming rigid–plastic behavior. These methods, based on the localized plastic-hinge concept, cannot consider the longitudinal spread of yielding zones nor the effect of deflections on moments. Hence the studies are valid only for structures with very stocky cross sections subjected to predominant flexural moments. In 1957, Stevens experimentally checked the validity of this approach on models of circular, elliptic, and parabolic arches with two-hinged and fixed support conditions. He found that a reasonably accurate estimate of the collapse load can be obtained by limit analysis for arches under a concentrated load. However, the experimental collapse load for an arch under half-span loading is considerably less than the calculated value.

17.4.2 Slender Arches in Pure Compression

Slender two-hinged and fixed arches with loadings that produce pure axial compression buckle by sidesway with a node at the crown (Fig. 17.2*a* and *b*). The behavior is very much like that of a column and it is common to express the buckling strength of such arches in terms of the axial thrust at the quarter point of the arch, P, as described earlier. The elastic critical value can be expressed as

$$P_c = \pi^2 EI(kS)^2 \tag{17.1}$$

where S is the length of curved centroidal axis of arch rib from support to crown, E the Young's modulus, and I the moment of inertia of the arch rib. The effective-length factor k depends on the support fixity condition, the rise-to-span ratio, and the shape of the arch profile. The values of k for arches are

tabulated in the third edition of this guide and have values close to the well-known corresponding values for a column with a hinge at one end (crown) and a fixity condition at the other end which corresponds to the arch support condition.

Komatsu and Shinke (1977) have made inelastic ultimate strength studies for a two-hinged parabolic arch subjected to uniform load. Residual stress and initial crookedness were considered, and rise-to-span ratios = 0.10, 0.15, and 0.20 were used with a wide range of other parameters. It was found that the ultimate value of the thrust at the quarter point of the arch was accurately predicted with the usual column curves adjusting for yield points, effective lengths, and so on. Thus one could use for arches the standard relationships employed to relate the inelastic ultimate strength of columns to the elastic critical values.

17.4.3 Slender Arches Under Symmetrical Load

In this case the loading produces on a general cross section combined axial compressive force and bending moment. Then the arch acts much like a beam-column. It has been shown by Shinke et al. (1975) that the most demanding practical loading for low bridge arches of uniform cross section is the unsymmetrical loading discussed in the preceding section and shown in Fig. 17.4 with $s = 0.50$. The general deformational behavior is shown in Fig. 17.1*a*, in which the buckling failure is a limit-point phenomenon. Arches of practical proportions develop extensive inelastic action before failure. However, the limit load is reached before the displacements become so large that consideration of nonlinear geometry is necessary. To accurately predict the load-carrying capacity of steel arch structures it is necessary to consider the effects of the spread of yielding zones in the cross section and along the longitudinal axial direction of the rib, the effects of initial residual stresses, and, of course, the amplification of the moments caused by the displacements. The following studies considered uniform arches subjected to uniform dead load over the entire span and half-span live load (as in Fig. 17.4, except as noted).

In 1970 Harries reported some analytical results on the ultimate strength of two-hinged parabolic steel arches in which the effects of prebuckling deformations and the spread of yielding zones were considered. Elastic–plastic deformations were calculated. Harries considered rectangular sections and circular tubes.

Kuranishi and Lu in 1972 reported extensive parametric studies on the load-carrying capacity of two-hinged parabolic steel arches having either rectangular or idealized sandwich cross sections (approximating a wide-flange or box cross section). Residual stresses and strain hardening were taken into account. They found, as did Harries, that when the effect of yielding is considered, the strength of an arch can be drastically reduced under unsymmetrical loads. The buckling load is less when the live load acts over only one-half the span instead

of over the entire span, and the larger the live load-to-dead load ratio the smaller the buckling load becomes.

In a restudy of the ultimate solutions of the previous paper, Kuranishi (1973) examined the ratio of the ultimate load to the elastic limit load found by a second-order analysis for the sandwich cross section which approximates I and box cross sections. He shows that the inelastic ultimate load lies between the load at initial yielding and about 93% of this value for a practical range of live load-to-dead load ratios. He concludes that one could design efficiently by using second-order elastic analyses and keeping the maximum stress below 90% of the yield stress. The same could not be said for a solid rectangular section where the ultimate load always exceeded the load at first yielding.

Shinke et al. (1975) studied analytically the behavior of two-hinged and fixed parabolic arches of solid rectangular, pipe, and box cross sections. In this first study residual stresses and strain hardening were not considered. They compare the ultimate strength of several cases of uniform live load symmetrically distributed about the centerline with arches having an unsymmetrically distributed load in the pattern of Fig. 17.4, and find that for the same dead- and live-load intensities unsymmetrically distributed load always governs. They also investigated the effect of length of live load, s, and found that the buckling load is least when the length of live load, s, is roughly equal to one-half the span. With this loading, then, a parametric study was made of the ultimate strength of a box section. In a second study the same authors (Shinke et al., 1977) consider the effect of residual stresses and initial crookedness of the arch rib. Residual stresses are shown to be important, while initial crookedness is not important for unsymmetrical loading. An extensive series of experiments on two-hinged and fixed parabolic arches of solid rectangular cross section are also reported. The analytical results and experiments agree well.

More recently, Kuranishi and Yabuki (1979) and Yabuki (1981) have published numerical studies on the load-carrying capaicty of two-hinged parabolic steel arches with thin-walled box cross sections. These works have been summarized by Yabuki and Vinnakota (1984).

The strength of arches with stiffening girders has been studied by Shinke et al. (1980), Kuranishi et al. (1980), and Yabuki (1981). Both propose formulas to estimate the ultimate load.

Studies of the effects of the unsymmetrical distributed load of Fig. 17.4 supplemented by a single concentrated load at the quarter point of the span as per Japanese highway specifications have been made by Yabuki and are summarized by Yabuki and Vinnakota (1984).

The limit load depends on the following factors: rise-to-span ratio, live load-to-dead load ratio, slenderness ratio, yield stress, type of cross section (box section, wide-flange, rectangle, etc.), and residual stress magnitudes and patterns. There are many variables, so that it does not seem possible to present a comprehensive and definite coverage in the space available. Therefore, only a

brief review of the major points will be given. This has been extracted from the paper by Yabuki and Vinnakota (1984).

The effects of some of these parameters on the ultimate load-carrying capacity of two-hinged, parabolic, uniform arches subject to uniform dead load plus half-space live load are shown in Figs. 17.5 through 17.7. In these figures the ultimate or maximum load is expressed in terms of the ordinate $w_{\max}/w_y$, in which w_y is the magnitude of a uniformly distributed load ($p = 0$) that would cause the arch to yield at the springings under the direct axial thrust produced. Hence

$$w_y = \frac{2A\sigma_y}{L\sqrt{\frac{1}{16}(L/h)^2 + 1}} \tag{17.2}$$

where σ_y is the yield stress level of the material. In these diagrams $c = q/w$ (see Fig. 17.4 and $\lambda = L_s/r =$ slenderness ratio, in which L_s is the curved length of the arch axis).

Figure 17.5 shows the variation of maximum strength of steel arch ribs as a function of slenderness ratio for different load artios, c. The load-carrying capacity decreases with the slenderness ratio, which is one of the important parameters in predicting the load-carrying capacity of arches. The load-carrying capacity also decreases markedly as c decreases (i.e., as the live-load component increases) because the live load causes large bending moments and large displacements.

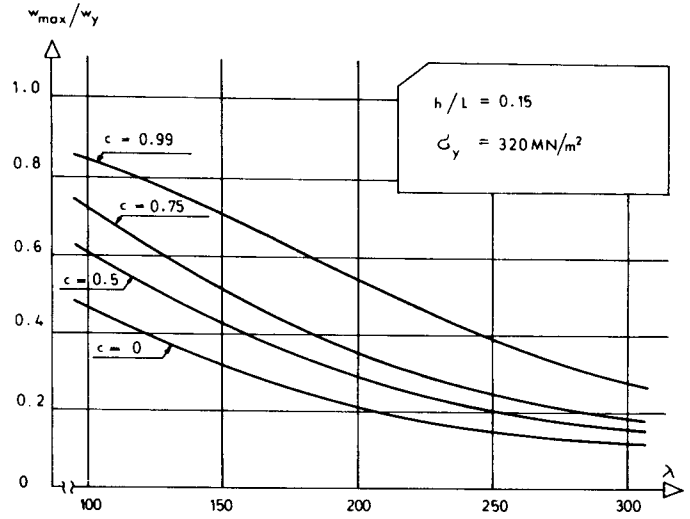

Fig. 17.5 Variation of load-carrying capacity as a function of slenderness ratio.

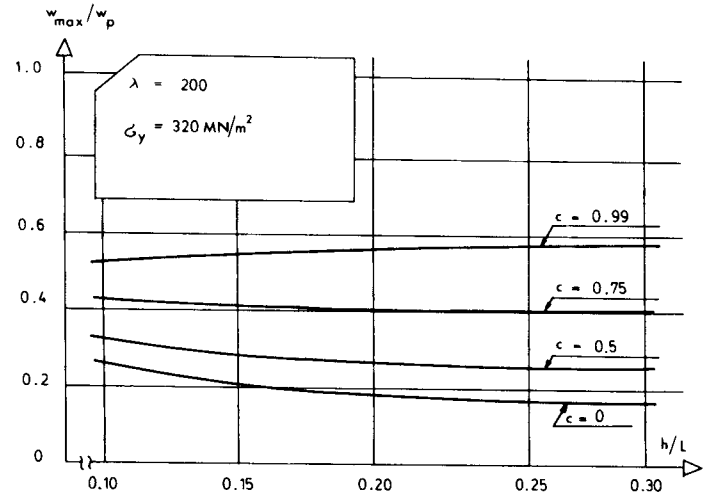

Fig. 17.6 Variation of load-carrying capacity as a function of rise-to-span ratio.

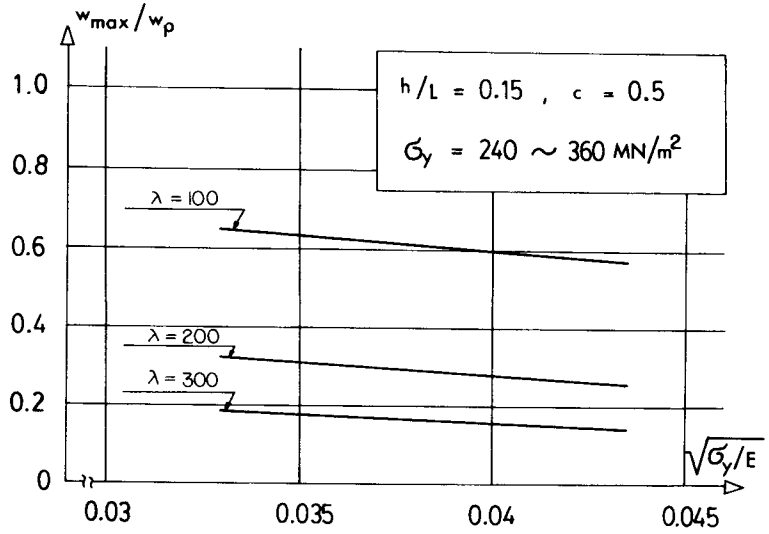

Fig. 17.7 Influence of yield-stress level of material on the load-carrying capacity of arches.

The influence of rise-to-span ratio on the load-carrying capacity of arch ribs with a slenderness ratio of 200 is shown in Fig. 17.6. I can be considered that the ultimate load, expressed in the nondimensional form with w_y given by Eq. 17.2, is not significantly affected by the rise-to-span ratio of the arch rib, especially for high values of c.

The reduction in ultimate strength of arch ribs due to the effect of residual stresses can be as much as 20%. The reduction becomes especially noticeable

when the arch is subjected to uniformly distributed load covering the entire span. The maximum variation of the ultimate strength using various distribution patterns for the residual stresses is within 10%. The reduction in ultimate strength becomes more significant as the level of compressive residual stress increases, and especially so when the compressive residual stress is greater than $0.4\sigma_y$.

The initial deformations of arch ribs result in a reduction of their ultimate strength. This reduction is important when the arch rib is subjected to uniformly distributed load covering the entire span. However, in the case of unsymmetrical load, which is the critical loading condition for arch rib structures, the deformations due to the loading become large so that the effects of the initial deformations are not significant. The nondimensional ultimate load intensity, $w_{\max}/w_y$, decreases in proportion to the square root of the yield stress level of the material as shown in Fig. 17.7.

The maximum compressive strains occurring in the flange plates of box sections of arch ribs under the ultimate load were examined. Based on these computed strains, the following remarks are made. The maximum strain occurring at a cross section of the arch subjected to unsymmetrical load is higher than its value when the arch rib is subjected to uniformly distributed load covering the entire span. The difference between the two becomes significant when the slenderness ratio becomes large. If the arch rib has to keep its load-carrying capacity up to the ultimate state without premature local buckling of the flange plates, they are required to endure strains four times as large as the yield strain ε_y. However, the flange plates of practical thin-walled box ribs might buckle by strains under $4\varepsilon_y$. Assuming that the critical strain of the cross section is $2\varepsilon_y$, tentatively, the ultimate strength reduction due to this limitation on critical strain becomes large as the loading pattern becomes unsymmetrical and the slenderness ratio becomes small.

The ultimate strength of stiffened two-hinged arch structures is analogous to that of two-hinged arches, if the arch and the stiffening girder behave as an entirely integrated structure. Let λ_T be the slenderness ratio of the stiffened arch structure defined by

$$\lambda_T = \frac{L_s}{\sqrt{(I + I_g)/A}} \tag{17.3}$$

where I_g is the moment of inertia of stiffening girder. The ultimate strength of a stiffened arch structure with a slenderness ratio $\lambda = \lambda_T$ is always somewhat greater than that of a two-hinged arch whose slenderness ratio $\lambda = \lambda_T$. However, judging from the analytical results the two may be considered to be equal to each other for all practical purposes. It is generally not required that attention be given to the *local failure* of arch rib members (buckling between the columns connecting the arch and the stiffening girder) for the unsymmetrical loading case, if a check is made for their strength for constant

uniformly distributed load. The *local failure strength* of arch rib members can be determined by the basic column strength curve, when they have straight members between columns. However, for curved members, it is advisable to reduce this strength by 15%. Pi and Trahair (1996) studied the inelastic in-plane strength of steel arches using a finite element program that takes into account the effects of arch curvature, large deformations, material inelasticity, initial crookedness and residual stresses.

17.5 DESIGN OF ARCHES FOR IN-PLANE STABILITY

Arches of considerable span are normally not of uniform cross section but are composed of segments with different cross-sectional properties. Each of the segments must be designed for the loads which produce the maximum stresses in that segment. Many arch structures are complex structural systems such as deck bridge arches in which the arch rib is connected to the roadway girder by columns rigidly attached. Studies of the behavior of uniform free standing arches may be of limited usefulness in these cases. A general approach is to factor the loads, use a second-order elastic analysis for the entire system and keep the maximum combined stresses for each segment below some reference stress. Kuranishi (1973) recommends this procedure with the maximum stress less than 90% of the yield stress, as stated previously.

Design procedures for arches based on the ultimate inelastic strength studies reviewed in Section 17.4 have been proposed by Kuranishi (1973), Komatsu and Shinke (1977), and Kuranishi and Yabuki (1984b). Kuranishi proposed an interaction-type formula similar to beam-column formulas for two-hinged parabolic arches under unsymmetrical loading. Komatsu and Shinke presented practical formulas for the planar ultimate load intensity of two-hinged and fixed parabolic steel arches as a function of the normal thrust calculated at a quarter point of the arch rib by first-order elastic analysis. They also recommended that the ultimate load capacity of arch ribs with varying and/or hybrid cross-section can be evaluated accurately by using mean values of the cross-sectional area and/or yield stress level of the material, calculated by averaging along the entire axial length of the rib. Kuranishi and Yabuki also presented accurate practical formulas for the in-plane ultimate strength of parabolic two-hinged steel arch ribs and steel arch bridge structures with a stiffening girder. These formulas are expressed in terms of bending moment and axial thrust (or stresses provided by these cross-sectional forces) at a quarter point of the rib, which are all calculated by the first-order elastic analysis. More recently, Sakimoto and Watanabe (1995) proposed a computer-aided design procedure that can determine the proportions of each member automatically so as to meet the ultimate strength requirement as a total structural system. The procedure is based on the tangent-modulus method and eigenvalue analysis.

17.6 OUT-OF-PLANE STABILITY OF ARCHES

When applied forces acting in the plane of a curved member reach a certain critical level, a combination of twisting and lateral bending causes the member to deform out of its original plane. The critical load is influenced by the nature and distribution of the loads, the shape of the axis of the member, the variation of the flexural and torsional stiffness of the cross sections along the axis of the member, and restraint available at the supports and elsewhere. For a steel arch, residual stresses resulting from uneven cooling after rolling and yielding of the material are also important factors. The multiplicity of parameters defeats attempts at formulating simply and widely applicable rules for the determination of buckling loads.

Subjects of research have progressed with time from elastic linear buckling of a single arch to ultimate strength of total systems—that is, from simple and idealized theoretical models to more practical models to be encountered in actual structures. Some of the available solutions that may be useful as a guide to the design of practical structures are presented in formulas and tables. Results from elastic linear buckling theory are shown in Sections 17.7 and 17.9, and in Sections 17.10 and 17.11 more recent results from ultimate strength analyses are presented.

Figure 17.8 shows notations and a coordinate system used for the descriptions in the following sections. Unless stated otherwise, the results presented apply to symmetric arches of constant cross section with doubly symmetric axes. The effect of warping torsional restraint was not included in the results presented except in Fig. 17.9. Warping torsional resistance is a negligible factor for closed-profile cross sections, while it is of importance for open profile cross sections. Results obtained by ignoring warping torsional restraint are conservative for open profile sections.

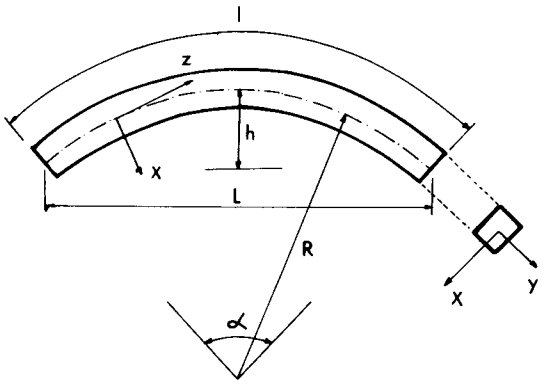

Fig. 17.8 Notation and coordinate system.

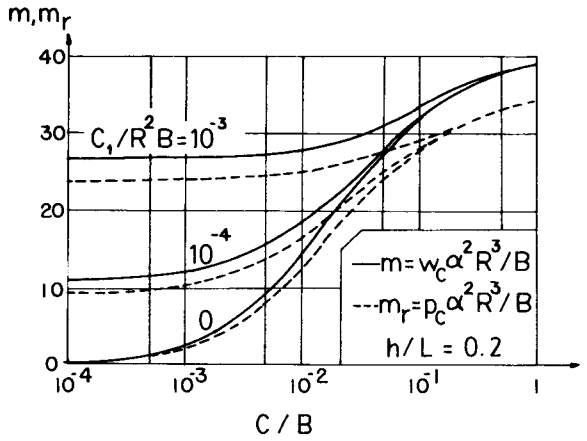

Fig. 17.9 Effects of the warping rigidity C_1.

Isolated arches supported so that their ends are free to rotate about the x-axis have very little lateral stability and should be avoided. Although results for this end condition were not given here in most cases, the practical significance of this fact should be emphasized, since in actual arches, completely rigid supports are difficult, if not impossible, to realize.

17.7 OUT-OF-PLANE BUCKLING OF CIRCULAR ARCHES

17.7.1 Uniform Moment

Equal couples, M, applied about the y-axis at the ends can cause buckling out of the x–z plane if the flexural stiffness about the y-axis is large in comparison to both the flexural stiffness about the x-axis, B, and the St.-Venant torsional rigidity of the cross section about the z-axis, C. If the ends are fixed against translation in the y direction but are free to rotate about the x and y axes the critical moment, M_c, is (Timoshenko and Gere, 1961)

$$M_c = \frac{B+C}{2R} \pm \sqrt{\left(\frac{B-V}{2R}\right)^2 + \frac{BC}{R^2}\frac{\pi^2}{\alpha^2}} \tag{17.4}$$

In this equation the plus (minus) sign corresponds to the lowest buckling moment which compresses the fibers on the concave (convex) side of the bar. The effects of warping torsional restraint and other boundary conditions are investigated by Kollár and Iványi (1966). Finite element analysis results for the inelastic buckling and ultimate strength of steel wide-flange arches were also presented by Pi and Trahair (1997).

17.7.2 End Forces Directed along the Chord

Two collinear forces applied to the ends of circular members can cause lateral buckling (Klöppel and Protte, 1961; Ojalvo et al., 1969). Forces directed away from each other (pull loads) will generally cause antisymmetric buckling about the center of the member, whereas forces directed toward each other (push loads) cause a symmetric buckling. The buckling load for ends hinged about the x-axis may be expressed in the form (Klöppel and Protte, 1961)

$$F_c = m\frac{B}{(R\alpha/2)^2} \tag{17.5}$$

When the central angle α is less than π and the warping torsional stiffness is negligible, the value m (minus sign for pull loads) was given by the following approximate equations: For pull loads;

$$m = a_0 + \frac{a_1}{\alpha} + \frac{a_2}{\alpha^2} \tag{17.6a}$$

and for thrust loads;

$$m = 2.47 + a_3\alpha + a_4\alpha^2 \tag{17.6b}$$

Some of the coefficients a_0 through a_4 are given in Table 17.5. The effect of the warping torsional stiffness was also studied by Klöppel and Protte (1961).

17.7.3 Uniformly Distributed Radial Forces

If the radial forces, p, are directed inward along the centroidal axis and the ends of the bar are free to rotate with respect to their principal axes x and y but unable to rotate with respect to the axis z, the buckling load p_c is (Timoshenko and Gere, 1961)

$$p_c = \frac{B}{R^3}\frac{(\pi^2-\alpha^2)^2}{\alpha^2[\pi^2+\alpha^2(B/C)]} \tag{17.7}$$

TABLE 17.5 Coefficients for Use in Eq. 17.6

C/B	a_0	a_1	a_2	a_3	a_4
0.01	0.052	−0.217	−0.36	−0.24	0.09
0.5	0.815	−6.313	−7.411	−0.034	0.069

An approximate equation for the case of built-in ends can be obtained by replacing the terms π^2 with $4\pi^2$ in Eq. 17.7, but this would not be accurate unless α is smaller than $\pi/2$ and C/B is greater than or equal to 0.5.

More comprehensive studies, including the effect of warping torsional restraint, are reported by Fukasawa (1983) and Kollár and Iványi (1966). Some of the theoretical results from Fukasawa (1983) are discussed in the next section.

17.7.4 Uniformly Distributed Vertical Forces

When the arch is fixed against rotation about the x-axis at its ends, the uniform load w_c at buckling may be expressed in the form (Demuts, 1969)

$$w_c = m\frac{B}{L^3} \tag{17.8}$$

Values of m are shown in Table 17.6.

The usual closed-profile cross section used in arches has a C/B ratio in the range 0.5 to 1.5 and for the open-profile cross section C/B is in the range 0.01 to 0.001. If the arch cross section has a thin-walled open profile, the warping torsional rigidity, C_1, also has a primary effect on the buckling loads, as shown in Fig. 17.9 (Fukasawa, 1963; Namita, 1968). In this figure the buckling coefficient $m = w_c\alpha^2R^3/B$ for uniform vertical loads, w, is shown by solid lines and the buckling coefficient $m_r = p_c\alpha^2R^3/B$ for uniform radial loads, p, is shown by broken lines. It is also found that the values m and m_r are related to each other by an approximate relation $m_r \simeq m[2(\sin\alpha/2)/\alpha]$ when the height span ratio, h/L, is not large (for $h/L \leqslant 0.2$).

TABLE 17.6 Approximate Values of m for use in Eq. 17.8

	Circular Arch				Parabolic Arch			
	Vertical Loads		Vertical Loads		Hanger Loads (Symmetric)		Column Loads (Antisymmetric)	
H/L \ C/B	0.01	0.5	0.01	0.5	0.01	0.5	0.01	0.5
0.1	18	28	16	28	39	70	12	18
0.2	17	39	15	39	35	110	12	29
0.3	13	38	13	37	28	116	10	32
0.4	9	30	11	30	24	104	8	31
0.5	5	20	9	24	20	87	6	28

17.8 OUT-OF-PLANE BUCKLING OF PARABOLIC ARCHES

17.8.1 Uniformly Distributed Vertical Loads

The uniformly distributed buckling load, w_c, again may be expressed in the form of Eq. 17.8. Representative values of m are given in Table 17.6 (Tokarz and Sandhu, 1972). The ratio $C/B = 0.01$ is typical of thin-walled open-profile cross sections for which warping torsional restraint is of importance. The effect of the warping torsional rigidity may be similar to what can be observed in a circular arch (see Fig. 17.9). Additional information is available in the papers by Stüssi (1943), Tokarz (1971), Kee (1961) and Papangelis and Trahair (1987a,b).

17.8.2 Parabolic Arches with Tilting Loads

It has been recognized by Stüssi (1943) and others that the buckling load of an arch is increased if the loads are applied to the arch by a system of vertical hangers connected to a laterally stiff roadway at the elevation of the chord as in the case of the through-type arch bridges. If the loads are applied by means of columns connected to a laterally stiff roadway above, the lateral deformations of the buckled arch will be antisymmetric about the crown when the arch is connected to the roadway at this point or if the columns are very short near the crown. Both hanger- and column-loaded parabolic arches were studied theoretically by Östlund (1954), Godden (1954), and Shukla and Ojalvo (1971). The buckling load w_c may be expressed by Eq. 17.8 using appropriate values of m from Table 17.6. It is assumed there that the ends of the arch are fixed against rotation about the x-axis. Östlund (1954) and Almeida (1970) reported that certain braced arches subjected to hanger loads are also controlled by antisymmetric buckling.

17.9 BRACED ARCHES AND REQUIREMENTS FOR BRACING SYSTEMS

Most arches used in practice are braced against lateral movement either continuously or at regularly spaced intervals. An arch rib connected continuously to a curved roof is an example of continuous bracing. Unless such arch ribs are unusually deep, lateral buckling will not be a problem. Twin arch ribs with a lateral bracing system often occur in arch bridges.

The elastic lateral buckling of twin arch ribs braced with transverse bars normal to the plane of the ribs has been studied by several investigators (Östlund, 1954; Kuranishi, 1961a; Almeida, 1970; Tokarz, 1971; Sakimoto and Namita, 1971). The following properties of the bracing system are important in the suppression of lateral buckling: (1) the location and spacing of the transverse bars; (2) the distance between the arch ribs, b; (3) the flexural stiffness of the bars, D_x, about the x-axis; and (4) the flexural stiffness of the bars, D_z, about the z-axis.

It was found that increasing the flexural stiffness D_x was a more effective way of suppressing lateral buckling than increasing the flexural stiffness D_z. The flexural stiffness D_z is less important except when the arch ribs have an open-profile cross section and the stiffness D_x or D_z is increased independently, the buckling load of twin arches increases and tends to attain an asymptotic value. While the magnitude of the asymptotic value depends on the properties of the bracing system listed above, the asymptotic value of the buckling load for a closely braced arch system can be obtained when $D_x \geq 10b(B/R)$ or $D_z \geq b(B/R)$, respectively (Östlund, 1954; Sakimoto and Namita, 1971).

When pairs of arch ribs are braced closely with such stiff transverse bars, the critical load per one arch rib of a set of braced arches can be increased up to 250% or more of that for the identical isolated single arch so far as elastic buckling is concerned. For actual bridge arches, however, this increase of the buckling strength will be limited by yielding of the material (see Fig. 17.13).

Wästlund (1960) and others have suggested a simple approximate method for the determination of the lateral buckling load of braced arches by utilizing a planar system which is obtained by straightening out the arch in a horizontal plane. The compressive force required to buckle the longitudinal ribs of the assumed planar system would be computed as for a column with batten lacing, and these compressive forces would be the approximations to the rib forces required to buckle the actual arch structure. The approximate method can be accurate for the arches of a torsionally stiff (closed) cross section, but it is unconservative for the arches of an open-profile cross section (Östlund, 1954).

The strength of braced arches in the plane of bracing is similar to the buckling strength of columns with lacing bars and battens, which is given by Timoshenko and Gere (1961) as

$$\frac{1}{P_{cr}} = \frac{1}{P_E} + \frac{1}{S} \tag{17.9}$$

where P_{cr} is the critical load of the column, P_E the critical load of the column with stiff lacing, and S the shear stiffness provided by the bracing bars or battens. While increasing the shear stiffness of the arch in the lateral plane increases the critical load, the increase is limited by the flexural buckling strength in the vertical plane. Therefore, there is a critical value for the shear stiffness, above which the buckling capacity is determined by the flexural strength. Based on extensive parametric studies based on a finite element program, Kuranishi (1993) presented the following relationship for the critical value of the shear stiffness:

$$\mu_{Scr} = \frac{\pi^2}{48} \frac{1}{(K_i\rho_i/K_o\rho_o)^2 - 1} \tag{17.10}$$

where

μ_S = ratio of the shear rigidity of the rib and bracing system in the plane containing the two ribs, to the flexural rigidity of the two arch ribs
μ_{Scr} = critical value of μ_S
ρ_o = out-of-plane slenderness ratio of the rib
K_o = out-of-plane effective length factor
ρ_i = in-plane slenderness ratio of an arch rib
K_i = in-plane effective length factor

Although twin arches braced with transverse bars might be a favorable structure from an aesthetic point of view, transverse bars cannot be a more effective bracing system than a bracing system of diagonal members for suppressing lateral buckling (Sakimoto, 1979; Sakimoto and Komatosu, 1982). If the lateral bracing consists of either diagonals, diagonals in combination with transverse bars, or a K system, out-of-plane buckling of the arch tends not to be a problem except for through-type arch bridges, which cannot have lateral bracing over the entire arch length. Through-type steel arches with double diagonal bracing system are discussed in the following section.

The stiffness of diagonal bracing members required for the necessary lateral stability of an arch system was studied by Sakimoto and Komatsu (1977a,b) and Kuranishi and Yabuki (1981) in relation to the ultimate strength of braced steel arches subjected to the combination of vertical and horizontal uniform loads.

17.10 ULTIMATE STRENGTH OF STEEL ARCHES SUBJECTED TO UNIFORMLY DISTRIBUTED VERTICAL LOADS

Since the arch is basically a compressive member, residual stresses resulting from welding and initial out-of-plane deflections have a significant influence on the strength of steel arches limited by lateral instability. The computer results obtained for typical theoretical models of square box cross sections show that (1) the residual stress may cause a reduction of strength of at most 20% for mild-steel arches and 10% for high-strength-steel arches, and (2) the initial out-of-plane deflections may reduce, at maximum, 15% of the strength of a perfectly plane arch (Sakimoto and Komatsu, 1977b; Komatsu and Sakimoto, 1977).

Some of the results are shown in Figs. 17.10 and 17.11. In these figures the vertical axis represents the ultimate unit strength, σ_u, divided by the yield stress, σ_y, and the horizontal axis shows the slenderness ratio, $\lambda = l_s/r_x$, in which l_s is the total curved length of the arch rib and r_x is the radius of gyration of the rib section about the x-axis. The term σ_{rc} denotes the maximum compressive residual stress assumed in trapezoidal distribution pattern and $\bar{v}_0$ denotes the amplitude of initial out-of-plane deflections assumed in the shape of a half-sine

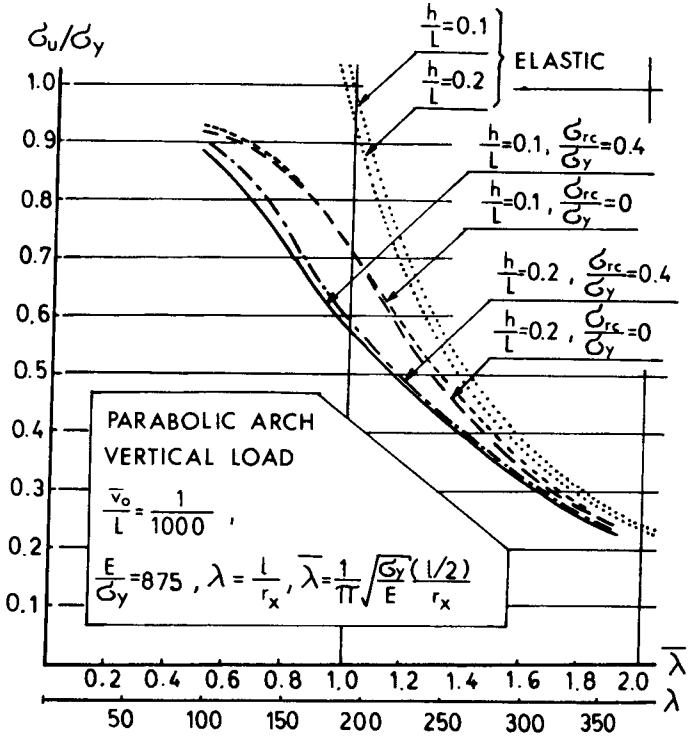

Fig. 17.10 Effects of residual stresses.

wave. Figure 17.12 shows that the effect of load directions is also very significant for steel arch bridges. In these figures elastic buckling curves of the identical arches (Shukla and Ojalvo, 1971; Tokarz and Sandhu, 1972) are also shown and noted as *elastic* for reference.

Extensive parametric studies (Sakimoto, 1979; Sakimoto and Komatsu, 1982) resulted in a simple approximate method for determining the strength of braced or unbraced steel arches which fail by lateral instability. Using an analogy between an arch and a column an equivalent slenderness function λ_a for the determination of the ultimate strength of through-type steel arches of box cross sections is defined as follows (Sakimoto and Komatsu, 1983a):

$$\lambda_a = \frac{1}{\pi}\sqrt{\frac{\sigma_y}{E}}\frac{l}{r_x}K_e K_l K_\beta \tag{17.11}$$

where σ_y is the lowest yield stress among those of different steel grades used in the arch rib and K_e, K_l, and K_β are effective-length factors.

The coefficient K_e relates to the rotational fixity of an arch rib at its ends with respect to the centroidal x-axis. For the clamped condition K_e is 0.5 and

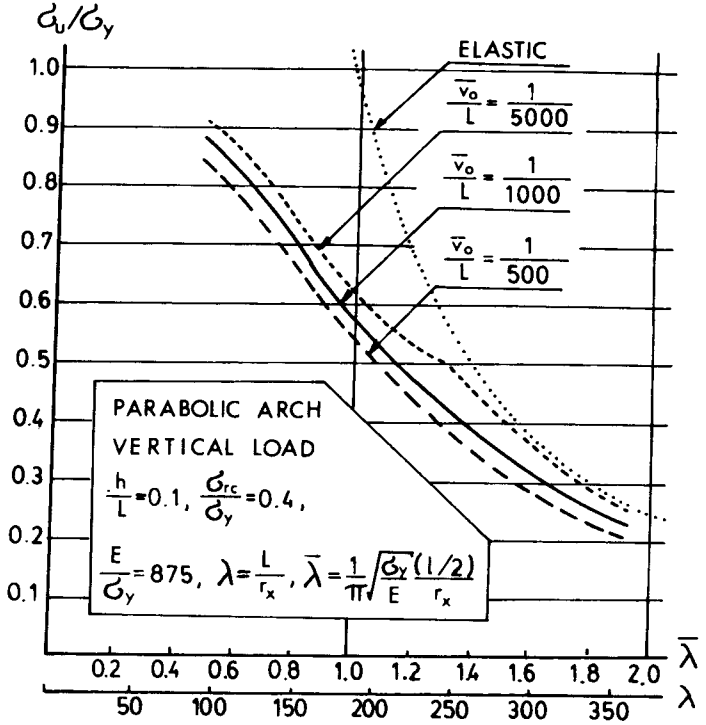

Fig. 17.11 Effects of initial lateral deflections.

for the hinged condition it is 1.0. The coefficient K_l relates to the direction of the loads and it is 0.65 for the tilting hanger case and 1.0 for nontilting hangers (i.e., for vertical loads). The coefficient K_β is related to the lateral restraint supplied by the bracing system and given by $K_\beta = 1 - \beta + (2r_x\beta/K_e b)$. The term β denotes a ratio of the length of braced portion to the total length of the arch rib. Since β is equal to zero for arches without bracing, K_β equals 1.0 for an isolated single arch.

The ultimate unit strength, σ_u, is computed for the column with the equivalent slenderness function, and this ultimate unit strength would be the approximation to the ultimate stress required to buckle the actual arch structure. The ultimate unit strength, σ_u, for arches is defined as the tangential thrust at the support, N_u, divided by the area A; that is, $N_u = A \cdot \sigma_u$. The thrust N_u is determined from a linear theory for the loaded arch. For a parabolic arch, for example, the uniformly distributed load per unit length of the arch span at the ultimate state, w_u, can be computed by a linear theory as follows:

$$w_u = \frac{2A\sigma_u}{L\sqrt{\frac{1}{16}(L/h)^2 + 1}} \tag{17.12}$$

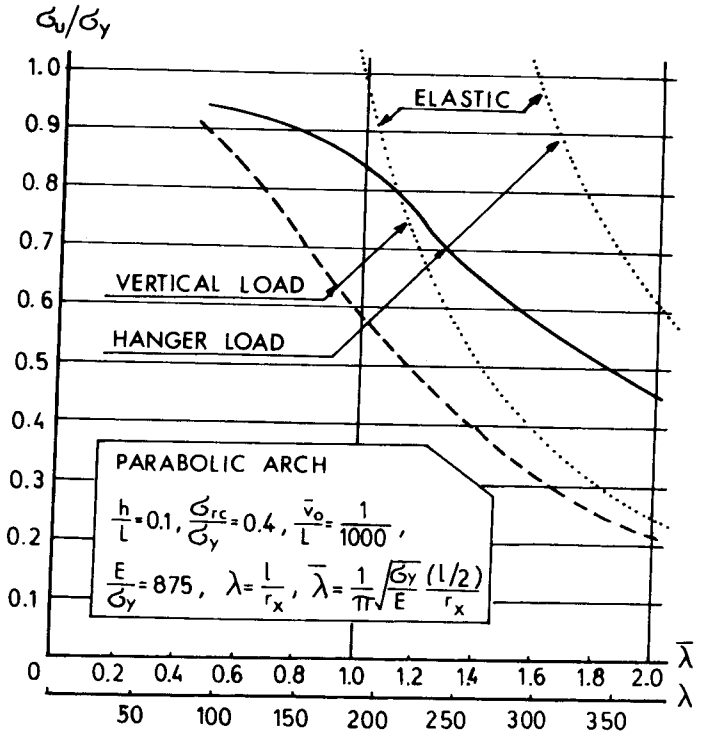

Fig. 17.12 Effects of load directions.

in which A is the cross-sectional area of an individual arch rib. Where the rib cross section varies, A and r_x are weighted average values for the entire curved length l.

Curve 2 of the SSRC multiple column curves or curve C of the ECCS multiple column curves or similar column curves are suggested as counterparts to the Japanese column curve which was used in this investigation (Sakimoto and Komatsu, 1983a). Applicably of the approximation method has been examined with computer simulations for a parabolic or a circular steel arch composed of box section arch members with the ratio of $h/L = 0.1$ and 0.2. One of the results is shown in Fig. 17.13, where curve 2 of SSRC multiple column formulas is used in the approximation method. Practical applications for actual steel bridges are presented in Sakimoto and Komatsu (1983b), Sakimoto and Yamao (1983), Sakimoto et al. (1989), and Sakimoto and Sakata (1990).

When overall lateral buckling is suppressed, only the buckling of the portions of the ribs between points of bracing need be considered. The slenderness limit for which the local instability of the arch segment may occur prior to overall lateral instability can be determined approximately from Eq. 17.11 as follows (Sakimoto and Komatsu, 1983a):

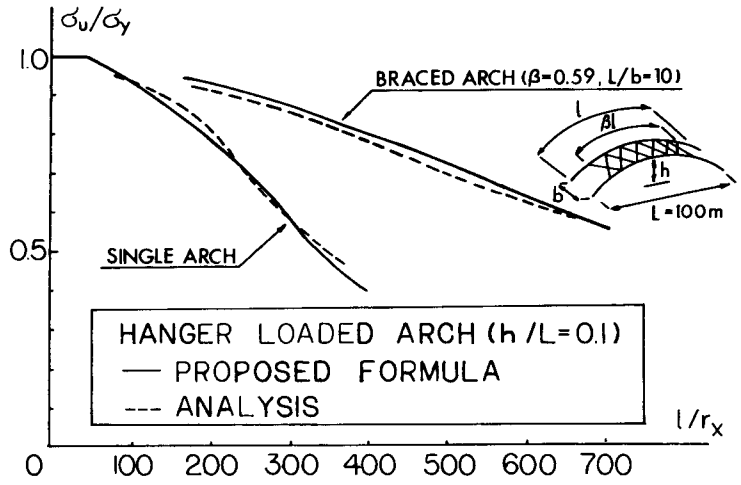

Fig. 17.13 Accuracy of the approximation method.

$$\frac{\sqrt{\sigma_y}}{E}\left(\frac{l_p}{r_x}\right)_{\max} \geq \frac{\sqrt{\sigma_y}}{E}\frac{l}{r_x}K_e K_l K_\beta \tag{17.13}$$

Here $(l_p/r_x)_{\max}$ denotes the slenderness ratio for the most slender of the arch segment having an unbraced length, l_p, between points of bracing, and the term σ_y in the left side of Eq. 17.13 is the yield stress of the arch segment where $(l_p/r_x)_{\max}$ occurs.

17.11 ULTIMATE STRENGTH OF STEEL ARCH BRIDGES SUBJECTED TO UNIFORM VERTICAL LOADS

In Section 17.10 the slenderness parameter is given in explicit form by Eq. 17.11 with effective-length coefficients. If a computer program is available to obtain spatial (three-dimensional) eigenvalues, the following procedure to determine the effective length is suggested by Sakimoto et al. (1992). Assuming linearity of the prebuckling state, the critical axial force of a member, N_{cr}, can be expressed as

$$N_{cr} = \alpha N_o = \frac{\pi^2 EI}{L_e^2} \tag{17.14}$$

where α is the smallest eigenvalue, N_o the reference axial force of the member for the reference vertical load P_o, and L_e the effective length. The slenderness parameter is defined as

$$\lambda_a = \frac{1}{\pi}\sqrt{\frac{\sigma_y}{E}}\frac{L_e}{r_x} = \sqrt{\frac{A\sigma_y}{\alpha N_o}} = \sqrt{\frac{1}{\alpha}} \tag{17.15}$$

if the reference load is taken as the squash load of the arch rib, $N_o = A\sigma_y$, where A is the cross-sectional area. By substituting this slenderness parameter into a column strength formula, as discussed in Section 17.10, the ultimate strength of the arch bridge can be obtained.

To verify the validity of this procedure, the ultimate strengths of the arch bridge models shown in Fig. 17.14, with properties described in Table 17.7, were computed by an elastoplastic finite displacement analysis. The ultimate normal stress σ_{n_u} can be given as $\sigma_{N_u} = N_u/A$, where N_u is the axial force at the springing calculated by linear theory for the ultimate load P_u.

In Fig. 17.15, σ_{N_u} values obtained are plotted as a function of the slenderness parameter λ_a given by Eq. 17.15 for each numerical model. The closeness between the calculated values and the column strength curves demonstrates the validity of this procedure.

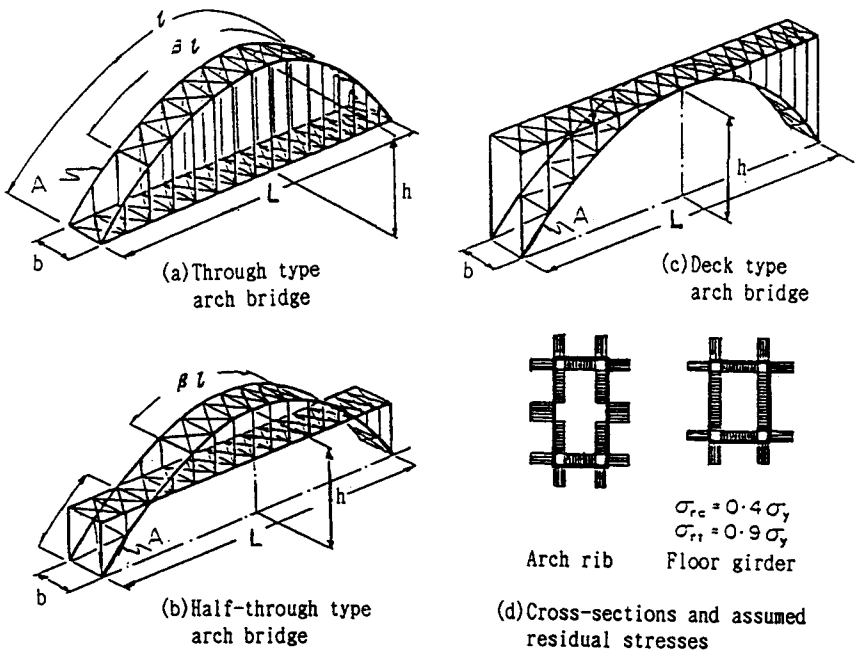

Fig. 17.14 Numerical models of arch bridges.

TABLE 17.7 Structural Properties of the Numerical Models

	Through-Type Arch Bridge	Half-through-Type Arch Bridge	Deck-Type Arch Bridge
Span length, L (m)	150	150	100, 200, 300
Rise, h (m)	22.5	22.5	20, 40, 60
Rise-to-span ratio, h/l	0.15	0.25	0.20
Arch rib distance, a (m)	20, 10, 5	20, 10, 5	5.2
Bending stiffness ratio, $\bar{I}$	0.1–3.0	0.1–3.0	0.1–1.0
Bracing ratio, β	0.48–0.86	0.64–0.88	1.0
Cross-sectional area, A (cm^2)	448	448	298.8–903.1

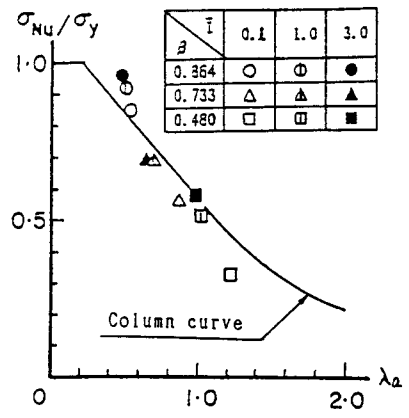

(a) Through type arch bridge

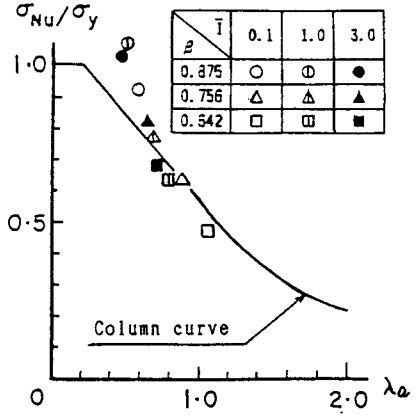

(b) Half-through type arch bridge

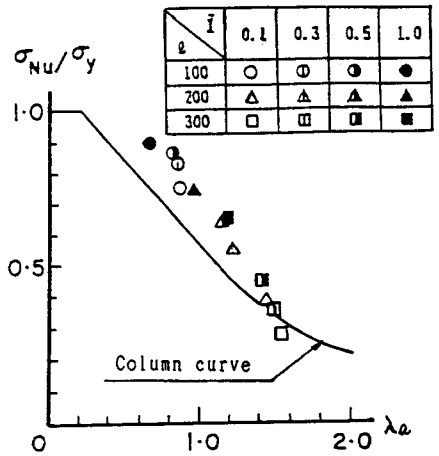

$\bar{I}$ = the ratio of the lateral flexura stiffness of the floor system to that of the twin arch ribs as a whole

(c) Deck type arch bridge

Fig. 17.15 Validity of the slenderness procedure using the eigenvalue.

17.12 ULTIMATE STRENGTH OF STEEL ARCH BRIDGES SUBJECTED TO VERTICAL AND LATERAL UNIFORM LOADS

The spatial elastic–plastic behavior and the ultimate load capacity of the through-type braced arch bridges of box cross sections was studied for a combination of the vertical and horizontal uniform loads by Sakimoto (Sakimoto and Komatsu, 1977a, 1979; Sakimoto et al., 1979). Computer analyses for various theoretical models resulted in a simple approximation method for the determination of the ultimate lateral strength of bridge arches braced partly over the central portion. By utilizing an analogy between a laterally loaded arch and a beam-column an interaction formula is proposed as follows:

$$\frac{N}{N_u}+\frac{M}{M_y[1-(N/N_e)]}\le 1.0 \tag{17.16}$$

Although this formula has a form similar to the interaction formula for a beam column, the meanings of the quantities should be understood according to the following definitions:

N = tangential end thrust computed by a linear theory for uniformly distributed design loads

N_u = tangential end thrust at inelastic lateral buckling of the arch under uniformly distributed vertical loads, which is determined by $N_u = A\sigma_u$ from the result of the former section

M = lateral end moment of the individual arch rib subjected to uniformly distributed horizontal loads, not including contribution of axial load interacting with deflections; this can be approximated by the value computed for the planar system which is obtained by straightening out the arch in a horizontal plane; a simple approximation formula for the determination of this moment is also given by Sakimoto and Komatsu (1979)

M_y = yield moment of the arch rib at the ends with respect to the x-axis

N_e = Euler buckling load computed for a hinged column of which the length and the cross section are identical to those of the arch rib at its unbraced end part.

The validity of the interaction formula has been verified by extensive computer simulations for various braced bridge arches of practical proportions. If the twin ribs are braced closely over the entire length of the arch, the second term of the left side of Eq. 17.16 becomes negligibly small. This means such a braced arch tends not to be a problem against usual lateral loads.

Deflections and stresses due to forces normal to the plane of the arch are increased by a contribution of axial load interacting with lateral deflections. Stüssi (1943) and others (Östlund, 1954; Wästlund, 1960) suggest that increased deflections and stresses may be estimated by multiplying the deflections and

stresses due to transverse force acting alone by the amplification factor $1/(1 - w/w_c)$, in which w is the intensity of the uniform load in the plane of the arch and w_c is the intensity of the in-plane load that would cause lateral buckling. While this amplification factor is at best only roughly approximate (Layrangues, 1959; Donald and Godden, 1961a,b), it may be convenient for use in a preliminary design.

The effect of lateral horizontal force on the in-plane strength of arch bridges was studied by Kuranishi and Yabuki (Kuranishi, 1961b; Yabuki and Kuranishi, 1973; Kuranishi and Yabuki, 1977). It was found that the in-plane strength of arch bridges braced closely over the entire length of the arch is not significantly affected by the lateral loads usually encountered in actual structures. Therefore, through-type steel arch bridges can be designed with a lateral bracing system (between arch ribs) of sufficient out-of-plane stiffness that the arch rib design will be determined primarily by the in-plane loads. For such a case lateral loads can be taken into account for practical purposes as a set of additional in-plane vertical loads. Thus the arch rib design can be made on the basis of a quasi-planar model subjected to the principal vertical loads with a small modification of these loads resulting from wind loads. The lateral bracing stiffness required to ensure that two-hinged arch bridges act basically as in-plane structures has been defined by Kuranishi, Yabuki, and Vinnakota (Kuranishi and Yabuki, 1981, 1984b; Yabuki et al., 1983).

REFERENCES

Almeida, P. N. (1970), "Lateral Buckling of Twin Arch Ribs with Transverse Bars," Dissertation, Ohio State University, Columbus, Ohio.

Austin, W. J. (1971), "In-Plane Bending and Buckling of Arches," *ASCE J. Struct. Div.*, Vol. 97, No. ST5, pp. 1575–1592.

Austin, W. J., and Ross, T. J. (1976), "Elastic Buckling of Arches Under Symmetrical Loading," *ASCE J. Struct. Div.*, Vol. 102, No. ST5, pp. 1085–1095.

Chang, C. K. (1973), "Effect of Loaded Length on the Buckling Strength of Slender Arches," Thesis, Rice University, Houston, Texas.

Coronforth, R. C., and Childs, S. B. (1967), "Computer Analysis of Two Hinged Circular Arches," *ASCE J. Struct. Div.*, Vol. 93, No. ST2, pp. 319–338.

Demuts, E. (1969), "Lateral Buckling of Circular Arches Subjected to Uniform Gravity Type Loading," Dissertation, Ohio State University, Columbus, Ohio.

Deutsch, E. (1940), "Das Knicken von Bogenträgern bei unsymmetrischer Belastung," *Bauingenieur*, Dec., pp. 353–360.

Donald, P. T. A., and Godden, W. G. (1961a), "A Numerical Solution to the Curved Beam Problem," *Struct. Eng.*, Vol. 41, pp. 179–186.

Donald, P. T. A., and Godden, W. G. (1961b), "The Transverse Behavior of Laterally Unsupported Parabolic Arches," *Struct. Eng.*, Vol. 41, pp. 187–191.

Fukasawa, Y. (1963), "Buckling of Circular Arches by Lateral Flexure and Torsion Under Axial Thrust," *Trans. Jpn. Soc. Civ. Eng.*, No. 96, pp. 29–47 (in Japanese).

Galli, A., and Franciosi, G. (1955), "Limit Analysis of Thin Arch Bridges with Stiffening Girders," *G. Genio Civ.*, Vol. 93, No. 11.

Godden, W. G. (1954), "The Lateral Buckling of Tied Arches," *Proc. Inst. Civ. Eng.*, Vol. 3, Part III, pp. 496–514.

Harries, H. (1970), "Traglast stahlerner Zweigelenkbogen mit ausgebreiteten Fliesszonen," *Stahlbau*, Vol. 6, pp. 170–177; Vol. 8, pp. 248–257.

Harrison, H. B. (1982), "In-Plane Stability of Parabolic Arches," *ASCE J. Struct. Div.*, Vol. 108, No. ST1, pp. 195–205.

Kee, C. F. (1961), "Lateral Inelastic Buckling of Tied Arches," *ASCE J. Struct. Div.*, Vol. 87, No. ST1, pp. 23–39.

Klöppel, K., and Protte, W. (1961), "A Contribution to the Buckling Problem of Circular Curved Bars," *Stahlbau*, No. 30, pp. 1–15 (in German).

Kollár, L. U., and Iványi, G. (1966), "Buckling of Shell Arches by the Energy Method," *Bautech. arch.*, pp. 1–23 (in German).

Kollbrunner, C. F. (1936), "Versuche über die Knicksicherheit und die Grundschwingungzahl vollwandiger Bogen," *Bautechnik*, Mar., pp. 186–188.

Kollbrunner, C. F. (1942), "Versuche über die Knicksicherheit und die Grundschwingungzahl vollwandiger Dreigelenkbogen, *Schweiz. Bauzg.*, Vol. 120, No. 10, pp. 113–115.

Komatsu, S., and Sakimoto, T. (1977), "Ultimate Load Carrying Capacity of Steel Arches," *ASCE J. Struct. Div.*, Vol. 103, No. ST12, pp. 2323–2336.

Komatsu, S., and Shinke, T. (1977), "Practical Formulas for In-Plane Load Carrying Capacity of Arches," *Proc. Jpn. Soc. Civ. Eng.*, No. 267, pp. 39–51 (in Japanese).

Kuranishi, S. (1961a), "The Torsional Buckling Strength of Solid Rib Arch Bridge," *Trans. Jpn. Soc. Civ. Eng.*, No. 75, pp. 59–67 (in Japanese).

Kuranishi, S. (1961b), "Analysis of Arch Bridge Under Certain Lateral Forces," *Trans. Jpn. Soc. Civ. Eng.*, No. 75, pp. 1–6 (in Japanese).

Kuranishi, S. (1973), "Allowable Stress for Two-Hinged Steel Arch," *Proc. Jpn. Soc. Civ. Eng.*, No. 213, pp. 71–75.

Kuranishi, S. (1993), "Stiffening Effect of Lateral Bracing of Steel Arch Bridges on Their In-Plane Strength," *Proc. SSRC Ann. Techn. Session*, Milwaukee, Wis.

Kuranishi, S., and Lu, L. W. (1972), "Load Carrying Capacity of Two-Hinged Steel Arches," *Proc. Jpn. Soc. Civ. Eng.*, No. 204, pp. 129–140 (in English).

Kuranishi, S., and Yabuki, T. (1977), "In-Plane Strength of Arch Bridges Subjected to Vertical and Lateral Loads," *2nd Int. Colloq. Stabl. Steel Struct., Prelim. Rep.*, Liege, Belgium, Apr., pp. 551–556.

Kuranishi, S., and Yabuki, T. (1979), "Some Numerical Estimations of Ultimate In-Plane Strength of Two-Hinged Steel Arches," *Proc. Jpn. Soc. Civ. Eng.*, No. 287, pp. 155–158.

Kuranishi, S., and Yabuki, T. (1981), "Required Out-of-Plane Rigidities of Steel Arch Bridges with Two Main Ribs Subjected to Vertical and Lateral Loads," *Techn. Rep. Tohoku Univ.*, Sendai, Japan, Vo. 46, No. 1.

Kuranishi, S., and Yabuki, T. (1984b), "Lateral Load Effect on Arch Bridge Design," *ASCE J. Struct. Eng.*, Vol. 110, No. 9, pp. 2263–2274.

Kuranishi, S., Sato, T., and Otsuki, M. (1980), "Load Carrying Capacity of Two-Hinged Steel Arch Bridges with Stiffening Deck," *Proc. Jpn. Soc. Civ. Eng.*, No. 300, pp. 121–130.

Layrangues, P. (1959), "Elastic Deformations and Forces in a Fixed End Symmetrical Circular Arch Subjected to a Constant Normal Force and a Uniformly Distributed Lateral Force," *Ann. Ponts Chaussees*, Vol. 129, pp. 323–343 (in French).

Namita, Y. (1968), "Second Order Theory of Curved Bars and Its Use in the Buckling Problem of Arches," *Trans. Jpn. Soc. Civ. Eng.*, No. 155, pp. 32–41 (in German).

Ojalvo, M., Demuts, E., and Tokarz, F. J. (1969), "Out-of-Plane buckling of Curved Members," *ASCE J. Struct. Div.*, Vol. 95, No. ST10, pp. 2305–2316.

Onat, E. T., and Prager, W. (1953), "Limit Analysis of Arches," *J. Mech. Phys. Solids*, Vol. 1, pp. 71–89.

Östlund, L. (1954), "Lateral Stability of Bridge Arches Braced with Transverse Bars," *Trans. R. Inst. Technol.*, Stockholm, No. 84.

Papangelis, J. P., and Trahair, N. S. (1987a), "Flexural–Torsional Buckling Tests on Arches," *ASCE J. Struct. Eng.*, Vol. 113, No. ST4, pp. 889–906.

Papangelis, J. P., and Trahair, N. S. (1987b), "Flexural–Torsional Buckling of Arches," *ASCE J. Struct. Eng.*, Vol. 113, No. ST7, pp. 1433–1443.

Pi, Y.-L., and Trahair, N. S. (1996), "In-Plane Inelastic Buckling Strengths of Steel Arches," *ASCE J. Struct. Eng.*, Vol. 122, No. ST7, pp. 734–747.

Pi, Y.-L., and Trahair, N. S. (1997), "Out-of-plane Inelastic Buckling and Ultimate Strength of Steel Arches," *Res. Rep. No. R737*, Department of Civil Engineering, University of Sydney, Australia.

Sakimoto, T. (1979), "Elasto-Plastic Finite Displacement Analysis of Three Dimensional Structures and Its Application to Design of Steel Arch Bridges," Dissertation, Osaka University, Osaka, Japan.

Sakimoto, T., and Komatsu, S. (1977a), "A Possibility of Total Breakdown of Bridge Arches Due to Buckling of Lateral Bracings," *2nd Int. Colloq. Stab. Steel Struct., Final Rep.*, Liege, Belgium, Apr., pp. 299–301.

Sakimoto, T., and Komatsu, S. (1977b), "Ultimate Load Carrying Capacity of Steel Arches with Initial Imperfections," *2nd Int. Colloq. Stabil. Steel Struct., Prelim. Rep.*, Liege, Belgium, Apr., pp. 545–550.

Sakimoto, T., and Komatsu, S. (1979), "Ultimate Strength of Steel Arches Under Lateral Loads," *Proc. Jpn. Soc. Civ. Eng.*, No. 292, pp. 83–94.

Sakimoto, T., and Komatsu, S. (1982), "Ultimate Strength of Arches with Bracing Systems," *ASCE J. Struct. Div.*, Vol. 108, No. ST5, pp. 1064–1076.

Sakimoto, T., and Komatsu, S. (1983a), "Ultimate Strength Formula for Steel Arches," *ASCE J. Struct. Div.*, Vol. 109, No. 3, pp. 613–627.

Sakimoto, T., and Komatsu, S. (1983b), "Ultimate Strength Formula for Central-Arch-Girder Bridges," *Proc. Jpn. Soc. Civ. Eng.*, No. 33, pp. 183–186.

Sakimoto, T., and Namita, Y. (1971), "Out-of-Plane Buckling of Solid Rib Arches Braced with Transverse Bars," *Proc. Jpn. Soc. Civ. Eng.*, No. 191, pp. 109–116.

Sakimoto, T., and Watanabe, H. (1995), "A New procedure for Frame Design", Proc. SSRC Annual Tech. Session, Pittsburgh, Pa. pp 23–31.

Sakimoto, T., and Yamao, T. (1983), "Ultimate Strength of Deck-Type Steel Arch Bridges," *3rd Int. Colloq. Stab. Met. Struct., Prelim. Rep.*, Paris, Nov.

Sakimoto, T., Yamao, T., and Komatsu, S. (1979), "Experimental Study on the Ultimate Strength of Steel Arches," *Proc. Jpn. Soc. Civ. Eng.*, No. 286, pp. 139–149.

Sakimoto, T., and Sakata, T. (1990), "The Out-of-Plane Buckling Strength of Through-Type Arch Bridges," *J. Constr. Steel Res.*, Vol. 16, pp. 307–318.

Sakimoto, T., Sakata, T., and Tsuruta, E. (1989), "Elasto-plastic Out-of-Plane Buckling Strength of Through Type and Half-Through Type Arch Bridges," *Struct. Eng./Earthquake Eng.*, Vol. 6, No. 2, pp. 307s–318s (*Proc. Jpn. Soc. Civ. Eng. No. 410/I-12*).

Sakimoto, T., Sakata, T., and Kobori, T. (1992), "An Effective Length Procedure for Out-of-Plane Buckling Strength Estimation of Steel Arch Bridges," *Proc. 3rd Pac. Struct. Steel Conf.*, Tokyo, pp. 251–258.

Shinke, T., Zui, H., and Namita, Y. (1975), "Analysis of In-Plane Elasto-plastic Buckling and Load Carrying Capacity of Arches," *Proc. Jpn. Soc. Civ. Eng.*, No. 244, pp. 57–69 (in Japanese).

Shinke, T., Zui, H., and Namita, Y. (1977), "Analysis of Experiment on In-Plane Load Carrying Capacity of Arches," *Proc. Jpn. Soc. Civ. Eng.*, No. 244, pp. 11–23 (in Japanese).

Shinke, T., Zui, H., and Nakagawa, T. (1980), "In-Plane Load Carrying Capacity of Two-Hinged Arches with Stiffening Girder," *Trans. Jpn. Soc. Civ. Eng.*, No. 301, pp. 47–59.

Shukla, S. N., and Ojalvo, M. (1971), "Lateral Buckling of Parabolic Arches with Tilting Loads," *ASCE J. Struct. Div.*, Vol. 97, No. ST6, pp. 1763–1733.

Stevens, L. K. (1957), "Carrying Capacity of Mild Steel Arches," *Proc. Inst. Civ. Eng.*, Vol. 6, pp. 493–514.

Stüssi, F. (1943), "Lateral-Buckling and Vibration of Arches," *Proc. Int. Assoc. Bridge Struct. Eng. Publ.*, Vol. 7, pp. 327–343 (in German).

Timoshenko, S. P., and Gere, J. M. (1961), *Theory of Elastic Stability*, 2nd ed., McGraw-Hill, New York.

Tokarz, F. J. (1971), "Experimental Study of Lateral Buckling of Arches," *ASCE J. Struct. Div.*, Vol. 97, No. ST2, pp. 545–559.

Tokarz, F. J., and Sandhu, R. S. (1972), "Lateral–Tosional Buckling of Parabolic Arches," *ASCE J. Struct. Div.*, Vol. 98, No. ST5, pp. 1161–1179.

Wästlund, G. (1960), "Stability Problems of Compressed Steel Members and Arch Bridges," *ASCE J. Struct. Div.*, Vol. 86, No. ST6, pp. 47–71.

Yabuki, T. (1981), "Study on Ultimate Strength Design of Steel Arch Bridge Structures," Dissertation, Tokoku University, Sendai, Japan (in Japanese).

Yabuki, T., and Kuranishi, S. (1973), "Out-of-Plane Behavior of Circular Arches Under Side Loadings," *Proc. Jpn. Soc. Civ. Eng.*, No. 214, pp. 71–82.

Yabuki, T., and Vinnakota, S. (1984), "Stability of Steel Arch-Bridges, A State-of-the-Art Report," *Solid Mech. Arch.*, Vol. 9, Issue 2, Noordhoff International Publishers, Leyden, The Netherlands.

Yabuki, T., Vinnakota, S., and Kuranishi, S. (1983), "Lateral Load Effect on Load Carrying Capacity of Steel Arch Bridge Structures," *ASCE J. Struct. Div.*, Vol. 109, No. 10, pp. 2434–2449.

CHAPTER EIGHTEEN

DOUBLY CURVED SHELLS AND SHELL-LIKE STRUCTURES

18.1 INTRODUCTION

A *shell-like metal structure* is one that resists loads in a manner similar to that of a thin shell. That is, a major mode of its resistance is by membrane actions by which forces are carried from point to point by biaxial tension or compression and by shear in the plane of the shell. In addition to the membrane resistance, the shell-like structure has bending resistance to help resist loads. Shell-like structures can be divided into two classes, although the distinction between them is often not obvious, continuous, and discrete. Continuous shell structures are basically curved plates, which may be stiffened in orthogonal or skew directions. Discrete shells are reticulated structures that are curved in space. Continuous shell structures are considered first.

A typical stiffened shell is shown in Fig. 18.1. Stiffening elements in the meridional direction are called *stringers*. They are usually small and spaced close together. Stiffening elements in the circumferential direction are called *ring stiffeners*. They are often large rings space fairly far apart. There are four modes in which buckling can occur for this structure. First, there is *local buckling*; the plate spanning between the stringers and stiffeners can buckle. Second, the shell plate and stringer combination spanning between the stiffeners can buckle; this is called *bay instability*. In the third form of instability, *general instability*, a large portion of the plate, stringers, and stiffeners buckles. In addition, the stringers or stiffeners may undergo *torsional buckling* as curved

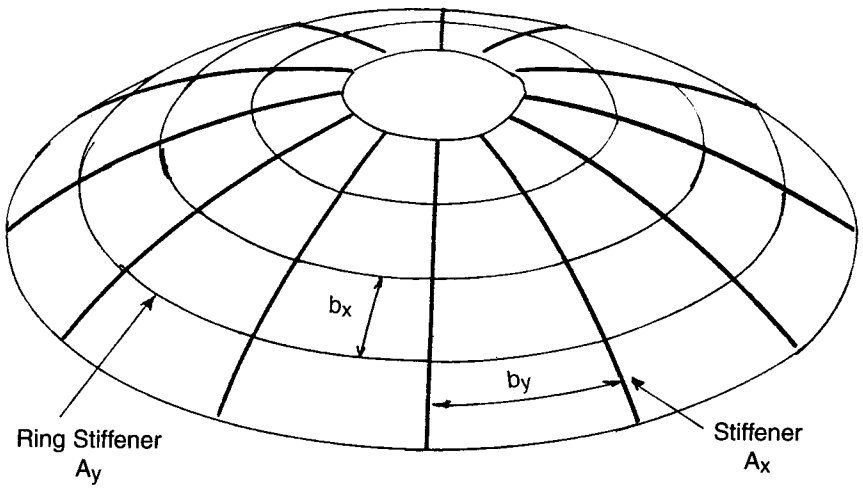

(*a*)

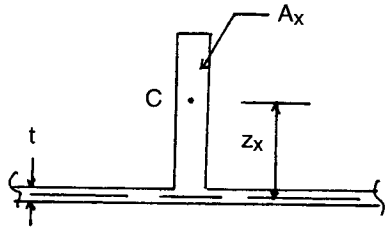

(*b*)

Fig. 18.1 (*a*) Geometry of a typical stiffened shell; (*b*) Geometry of stiffener.

columns. This form of instability is not unique to shell structures and is considered in other chapters of the guide.

Shell design codes usually address the first three buckling cases. There are two ways in which stiffened shells can be described. The first approach is to "smear" stiffeners and stringers across the shell plate and analyze the system as a continuous orthotopic plate. The second approach is to use the split rigidity concept. This approach is described here in conjunction with discrete shell structures.

The representation of shell stiffeners as orthotopic plates is presented in Flugge's text (1962), among others. The constitutive equations for the equivalent orthotopic shell, modified slightly, are as follows:

$$N_x = A_{11}\epsilon_x + A_{12}\epsilon_y - B_{11}\kappa_x \tag{18.1a}$$

$$N_y = A_{12}\epsilon_x + A_{22}\epsilon_y - B_{22}\kappa_y \tag{18.1b}$$

$$N_{xy} = A_{66}\epsilon_{xy} \tag{18.1c}$$

$$M_x = B_{11}\epsilon_x - D_{11}\kappa_x - D_{12}\kappa_y \tag{18.2a}$$

$$M_y = B_{22}\epsilon_y - D_{12}\kappa_x - D_{22}\kappa_y \tag{18.2b}$$

$$M_{xy} = D_{66}\kappa_{xy} \tag{18.2c}$$

where ϵ_x denotes the middle surface strain in the x-direction and κ_x denotes the middle surface curvature. The other ϵ and κ values are defined similarly.

The constants appearing in Eqs. (18.1) and (18.2) are as follows:

$$A_{11} = \frac{E_s t}{1-\mu^2}\frac{\bar{b}_y}{b_y} + E_x A_x \tag{18.3a}$$

$$A_{22} = \frac{E_s t}{1-\mu^2}\frac{\bar{b}_x}{b_x} + E_y A_y \tag{18.3b}$$

$$A_{12} = \frac{\mu E_s t}{q-\mu^2} \tag{18.3c}$$

$$A_{66} = \frac{G_s t}{2}\left(\frac{\bar{b}}{b_x} + \frac{\bar{b}_y}{b_y}\right) \tag{18.3d}$$

$$B_{11} = \frac{E_x A_x z_x}{b_y} \tag{18.3e}$$

$$B_{22} = \frac{E_y A_y z_y}{b_x} \tag{18.3f}$$

$$D_{11} = \frac{E_s t^3}{12(1-\mu^2)}\frac{\bar{b}_y}{b_y} + \frac{E_x I_x}{b_y} \tag{18.3g}$$

$$D_{22} = \frac{E_s t^3}{12(1-\mu)^2}\frac{\bar{b}_x}{b_x} + \frac{E_y I_y}{b_x} \tag{18.3h}$$

$$D_{12} = \frac{\mu E_s t^3}{12(1-\mu)^2} \tag{18.3i}$$

$$D_{66} = \frac{G_s t^3}{6}\left(\frac{\bar{b}_x}{b_x} + \frac{\bar{b}_y}{b_y}\right) + \frac{G_x J_x}{b_y} + \frac{G_y J_y}{b_x} \tag{18.3j}$$

where

t = shell thickness
E_s = modulus of elasticity of the shell plate
E_x = modulus of elasticity of the x stiffener
G_s = shear modulus of elasticity of the shell plate
G_x = shear modulus of elasticity of the x stiffener
μ = Poisson's ratio
$\bar{b}_i$ = effective length in the i-direction
z_i = distance from centroid of stiffening element to the center of the plate, outward positive

The effective lengths, $\bar{b}_i$, are introduced into these equations by some codes to take into account the fact that not all of the shell can be effective in interacting with stiffeners or stringers if these elements are spaced far apart (ASME, n.d.). Since stringers are usually smaller members placed close together, representing them by an orthotopic shell is accurate. However, this is not true for large stiffeners placed far apart. In this case, the stiffeners are separate units and, ideally, should be considered as such. Nonetheless, if one is attempting to solve the shell buckling problem with a closed-form solution, such as would appear in a design code, there is no alternative to the use of the smeared stiffness approach for all shell properties.

18.2 THE BASIC PROBLEM

The basic problem of shell stability can be seen from an investigation of the buckling of a spherical shell under external pressure. This problem will be sketched in some detail using a simplified analysis since many shell codes use equations similar to those to be discussed.

A doubly curved shallow shell segment is shown in Fig. 18.2. An attempt will be made to compute the bifurcation load for this segment under constant membrane stress resultants. The membrane forces, $\bar{N}_x$ and $\bar{N}_y$, are found by a linear elastic analysis of the shell. The membrane shear stress resultants are neglected; their inclusion complicates the mathematics but not the basic theory (Anderson and Bennet, 1981). The bifurcation equations describing buckling of the shell are three simultaneous equations for the buckled displacements, $u(x, y)$, $v(x, y)$, and $w(x, y)$:

$$\begin{aligned}\sum F_x = {} & \left(A_{11} - \frac{B_{11}}{R_x} - \frac{C_{11}}{R_x^2} + \frac{D_{11}}{R_x^2}\right)\frac{\partial^2 u}{\partial x^2} + \left(A_{66} + \frac{D_{66}}{R_x^2}\right)\frac{\partial^2 u}{\partial y^2} \\ & + \left(A_{12} + A_{66} + \frac{D_{12}}{R_x R_y} + \frac{D_{66}}{R_x R_y}\right)\frac{\partial^2 v}{\partial x\,\partial y} + \left(\frac{D_{11}}{R_x} - B_{11}\right)\frac{\partial^3 w}{\partial x^3} \\ & + \left(\frac{D_{12}}{R_x} + 2\frac{D_{66}}{R_x}\right)\frac{\partial^3 w}{\partial x\,\partial y^2} + \left(\frac{C_{11}}{R_x^2} - \frac{A_{11}}{R_x} - \frac{A_{12}}{R_y}\right)\frac{\partial w}{\partial x} = 0\end{aligned} \tag{18.4}$$

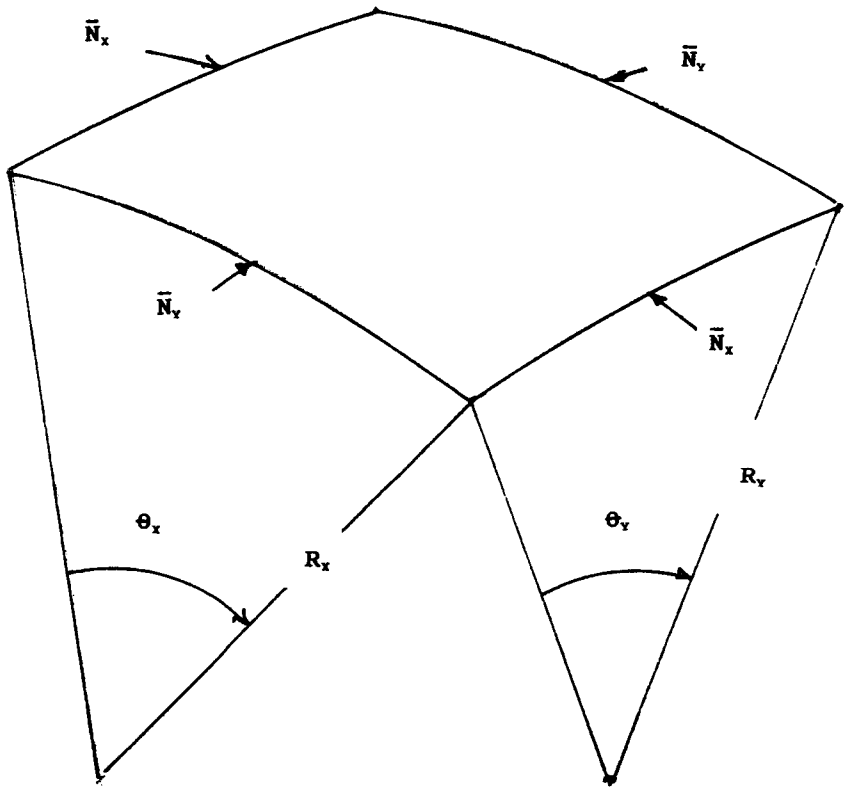

Fig. 18.2 Shallow shell segment.

$$\sum F_y = \left(A_{22} - \frac{B_{22}}{R_y} - \frac{C_{22}}{R_y} + \frac{D_{22}}{R_y^2}\right)\frac{\partial^2 v}{\partial y^2} + \left(A_{66} + \frac{D_{66}}{R_y^2}\right)\frac{\partial^2 v}{\partial x^2}$$
$$+ \left(A_{12} + A_{66} + \frac{D_{12}}{R_x R_y} + \frac{D_{66}}{R_x R_y}\right)\frac{\partial^2 u}{\partial x\,\partial y} + \left(\frac{D_{22}}{R_y} - B_{22}\right)\frac{\partial^3 w}{\partial y^3}$$
$$+ \left(\frac{D_{12}}{R_y} + 2\,\frac{D_{66}}{R_y}\right)\frac{\partial^3 w}{\partial x^2\,\partial y} + \left(\frac{C_{22}}{R_y^2} - \frac{A_{12}}{R_x} - \frac{A_{22}}{R_y}\right)\frac{\partial w}{\partial y} = 0 \qquad (18.5)$$

$$\sum F_z = -D_{11}\frac{\partial^4 w}{\partial x^4} - (4D_{66} + 2D_{12})\frac{\partial^4 w}{\partial x^2\,\partial y^2} - D_{22}\frac{\partial^4 w}{\partial y^4}$$
$$- \left(\frac{C_{11}}{R_x} + \frac{B_{11}}{R_x} - \bar{N}_x\right)\frac{\partial^2 w}{\partial x^2} - \left(\frac{C_{22}}{R_y} + \frac{B_{22}}{R_y} - \bar{N}_y\right)\frac{\partial^2 w}{\partial y^2}$$
$$- \left(\frac{A_{11}}{R_x^2} + 2\,\frac{A_{12}}{R_x R_y} + \frac{A_{22}}{R_y^2}\right)w$$
$$+ \left(C_{11} - \frac{D_{11}}{R_x}\right)\frac{\partial^3 u}{\partial x^3} - \left(2\,\frac{D_{66}}{R_x} + \frac{D_{12}}{R_x}\right)\frac{\partial^3 u}{\partial x\,\partial y^2}$$
$$+ \left(C_{22} - \frac{D_{11}}{R_x}\right)\frac{\partial^3 v}{\partial x^3} - \left(2\,\frac{D_{66}}{R_y} + \frac{D_{12}}{R_y}\right)\frac{\partial^3 v}{\partial x^2\,\partial y}$$
$$+ \left(\frac{A_{12}}{R_x} + \frac{A_{22}}{R_y} - \frac{B_{22}}{R_y^2} + \frac{\bar{N}_y}{R_y}\right)\frac{\partial v}{\partial y}$$
$$+ \left(\frac{A_{11}}{R_x} + \frac{A_{12}}{R_y} - \frac{B_{11}}{R_x^2} + \frac{\bar{N}_x}{R_x}\right)\frac{\partial u}{\partial x} = 0 \qquad (18.6)$$

These equations can be solved by Galerkin's method. The shell segment is assumed to be simply supported on all sides. u, v, and w can then be approximated by a double Fourier series:

$$u = \sum_{m=M_L}^{M_u}\sum_{n=N_L}^{N_u} \bar{B}_{mn}\cos\frac{m\pi x}{\theta_x R_x}\sin\frac{n\pi y}{\theta_y R_y} \qquad (18.7a)$$

$$v = \sum_{m=M_L}^{M_u}\sum_{n=N_L}^{N_u} \bar{C}_{mn}\sin\frac{m\pi x}{\theta_x R_x}\cos\frac{n\pi y}{\theta_y R_y} \qquad (18.7b)$$

$$w = \sum_{m=M_L}^{M_u}\sum_{n=N_L}^{N_u} \bar{A}_{mn}\sin\frac{m\pi x}{\theta_x R_x}\sin\frac{n\pi y}{\theta_y R_y} \qquad (18.7c)$$

where $\bar{A}_{mn}$, $\bar{B}_{mn}$, and $\bar{C}_{mn}$ are unknown amplitudes; and m and n are the meridional and circumferential half-wave numbers. M_u is the largest meridional half wave number and M_L is the smallest; N_u and N_L have similar definitions.

Substitution of Eqs. (18.7) into Eqs. (18.4) and (18.5) permits us to solve for $\bar{B}_{mn}$ and $\bar{C}_{mn}$ in terms of $\bar{A}_{mn}$. This requires the solution of two simultaneous algebraic equations for each choice of m and n. The results can be expressed as follows:

$$\bar{B}_{mn} = k_1\bar{A}_{mn} \qquad (18.8a)$$

$$\bar{C}_{mn} = k_2\bar{A}_{mn} \qquad (18.8b)$$

where k_1 and k_2 vary with the values of m and n as well as the physical constants describing the orthotropic shell.

The use of Eqs. (18.8) in Eq. (18.6), along with the requirement of nonvanishing $\bar{A}_{mn}$, results in an equation for the critical values of the stress resultants $\bar{N}_x$ and $\bar{N}_y$:

$$
\begin{aligned}
&-D_{11}\lambda_1^4-(4D_{66}+2D_{12})\lambda_1^2\lambda_2^2-D_{22}\lambda_2^4+\frac{2B_{11}}{R_x}\lambda_1^2+\frac{2B_{22}}{R_y}\lambda_2^2\\
&+\left(B_{11}-\frac{D_{11}}{R_x}\right)k_1\lambda_1^3+\left(B_{22}-\frac{D_{22}}{R_y}\right)k_2\lambda_2^3-\left(\frac{A_{11}}{R_x^2}+2\,\frac{A_{12}}{R_xR_y}+\frac{A_{22}}{R_y^2}\right)\\
&-(2D_{66}+D_{12})\left(\frac{k_1\lambda_1\lambda_2^2}{R_x}+\frac{k_2\lambda_1^2\lambda_2}{R_y}\right)-\left(\frac{A_{11}}{R_x}+\frac{A_{12}}{R_y}-\frac{B_{11}}{R_x^2}\right)k_1\lambda_1\\
&-\left(\frac{A_{12}}{R_x}+\frac{A_{22}}{R_y}-\frac{B_{22}}{R_y^2}\right)k_2\lambda_2-\left[\bar{N}_x\left(\lambda_1^2+\frac{k_1\lambda_1}{R_x}\right)+\bar{N}_y\left(\lambda_2^2+\frac{k_2\lambda_2}{R_y}\right)\right]=0
\end{aligned}
\tag{18.9}
$$

where

$$
\lambda_1=\frac{m\pi}{\theta_x R_x}\quad\text{and}\quad\lambda_2=\frac{n\pi}{\theta_y R_y}
\tag{18.10}
$$

Since the ratio of of $\bar{N}_x$ to $\bar{N}_y$ is known, Eq. (18.9) can be used to solve for the critical stress resultant, $\bar{N}_{cr}$. Note, however, that $\bar{N}_{cr}$ depends on the choice of m and n; every choice gives a different buckling load. The critical buckling stress resultant corresponds to the choice of m and n that minimizes N_{cr}. Unfortunately, this computation requires a great deal of trial and error; a computer must be used to complete the analysis.

It might be mentioned that with minor modifications, the same equations can be applied to cylindrical shells. Equations similar to Eq. (18.9) applied to cylinders are employed in Code Case N284 (ASME, n.d.) and the Eurocode (ECCS, 1988). For the case of a spherical shell under uniform pressure, $R_x = R_y = R$ and $\bar{N}_x = \bar{N}_y = pR/2$. The critical pressure found by using Eq. (18.9) corresponds closely to the classical buckling pressure for a complete sphere:

$$
p_{cr}=\frac{E}{\sqrt{3(1-\mu^2)}}\left(\frac{t}{R}\right)^2
\tag{18.11}
$$

At first glance, this result is surprising. It is due, however, to the fact that spherical shells buckle into a large number of waves in both directions. The value of n (or m) given by Timoshenko and Gere (1961) is

$$
n=3.46\sqrt{\frac{R}{t}}
\tag{18.12}
$$

Therefore, if the spherical segment is chosen long enough to develop the waves corresponding to Eq. (18.12), the buckling pressure will be the same as that for the complete sphere. The corresponding segment length must be greater than $1.82\sqrt{Rt}$. If the length of the spherical shell segment is less than $1.82\sqrt{Rt}$, the support conditions will affect the buckling pressure. Although Eq. (18.9) can still describe simply supported segments, it can no longer be applied independently of the boundary conditions.

Equation (18.9) is based on the assumptions of constant stress resultants, as well as simple support on all four sides of the shell segment. Very few loadings produce a constant membrane state over a significant portion of a shell. However, Eq. (18.9) can be used if the membrane state can be taken as constant over the buckling wave defined by Eq. (18.12). In addition, the assumption of simple support will be satisfactory for the buckling load if the shell segment is long enough for the buckling wave to develop.

The comparison of theory with experiment for clamped spherical shells under uniform pressure is very disappointing. Figure 18.3 shows the comparison. One might expect that the testing of any finite shell will differ somewhat from the results for a complete sphere, but the experiments show such scatter and low buckling pressures that the entire theory is suspect. Early researchers attributed the poor comparison between theory and experiment to the neglect of nonlinear terms in the shell equations (Kaplan, 1974). The results found by Budiansky (1959) and Huang (1964) when including these nonlinear terms are shown in Fig. 18.3. Although these analytical results are more accurate than the linear bifurcation theory and agree with the experiments of Krenzke and Kiernan (1963), they do not account for the large difference between theory and experiment.

The first satisfactory analysis of the problem, at least in a qualitative sense, was provided by Koiter (1970), who showed that the buckling load for spherical shells under uniform pressure is sensitive to small imperfections in the geometry of the shell. Koiter developed a perturbation analysis that helps the analyst to determine whether or not a structure is imperfection-sensitive. If a shell is imperfection-sensitive, its buckling load varies significantly with small imperfections. Koiter's theory has been developed extensively, and some form of it is necessary for any application of shell stability (Hutchinson and Budiansky, 1970; Fitch and Budiansky, 1970). It should be noted, however, that imperfection sensitivity depends on the shell geometry, the geometry of the imperfections, and the type of loading. For example, a spherical shell is imperfection-sensitive under uniform pressure, but it is not as imperfection-sensitive to a concentrated load at the apex (Kaplan, 1974).

Figure 18.3 has significance for the designer. Can the shell he or she is to design have less imperfection than the shells tested in various research labora-

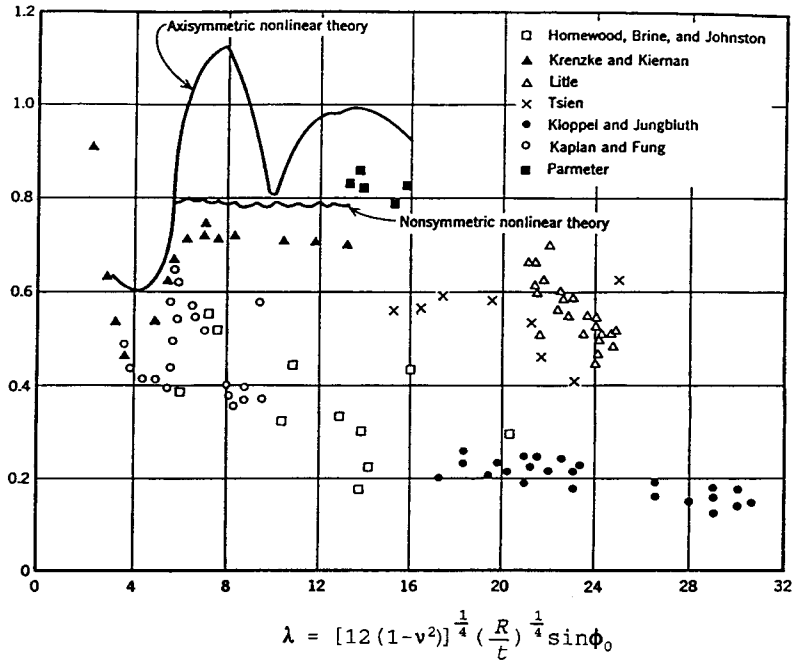

Fig. 18.3 Results of experiments of spherical shells.

tories? If the answer is no, what value should be chosen for the buckling pressure? Even if the shell can be fabricated with a great deal of precision, how close can the actual buckling pressure be to the theoretical value? This is the basic problem of shell stability. As can be seen, the application of shell stability is very much a semiempirical science.

18.3 FINITE ELEMENT METHOD

One of the problems that has plagued the analytical investigation of shell structures is the description of boundary conditions. Shell equations are so complex that some form of Fourier series or other polynomial series must be employed in their solution. When this is done, all boundary conditions on the shell are determined by the assumed series. Usually, one or two of the conditions may not be physically possible on a constructed shell. It is hoped, however, that their effect will be small. Unfortunately, the fact that all actual boundary conditions cannot be satisfied mathematically makes it impossible to verify the critical loads by comparison with experiments. For those cases where the boundary conditions will influence the shell buckling values, this makes it impossible to correlate analytical and experimental values. The finite element method allows one to avoid this problem because boundary conditions can be described correctly. (This is also a great advantage of the finite element method over traditional finite difference analyses.)

It should be noted that a linear bifurcation analysis for the buckling load usually requires two separate analyses. A stress analysis must be made to determine the membrane state due to the applied load. This state must then be input into the bifurcation program.

Two distinct forms of finite element analysis can be applied to shell structures. If the shell is a shell of revolution, special shell-of-revolution programs can be applied to both its stress analysis and eigenvalue computation. These programs have the defect that the stringers in the meridional direction must be modeled using the orthotropic shell properties described earlier. Stiffeners in the circumferential direction can be modeled directly in these program and need not be described by orthotropic shell properties. But if the shell is stiffened by large stiffeners spaced far apart in both directions, the shell-of-revolution computer codes must be employed with some care since the smearing of the stringers is not valid (Bushnell, 1977).

While stress analysis is relatively straightforward once one is familiar with the shell-of-revolution code being used, a problem does arise in the eigenvalue computation. One must choose the value of the circumferential wave number N corresponding to the buckling mode. Trial and error might be used where a first trial run is made with large jumps in the N values used but where N is allowed to vary over a large range. After the range of N values where buckling can occur is decided upon, a more refined analysis can be carried out with N values in that range. Investigators often use a small analytical program based on the analyses described in the preceding section to estimate the circumferential wave number prior to running the finite element code.

General-purpose computer codes can, of course, be applied to shell structures. They have the obvious advantage that both stiffeners and stringers can be modeled as discrete elements if so desired (Seide et al., 1979). A general-purpose finite element code would appear to be easier to use, in that the same model can be applied to both the stress and eigenvalue analyses. This advantage is more apparent than real, however. The node spacing in the circumferential direction must be fine enough to model the wave in that direction. This requires some estimate of N prior to setting up the finite element mesh. Of course, the mesh must also be fine in the meridional direction to describe the rapid change in stress resultants. However, this is also a problem when using shell-of-revolution programs.

A complete discussion of computer analyses of shell structures written for practising engineers is provided in the text by Bushnell (1985). A snapshot of the current state of the art of nonlinear shell analysis is provided in the collection of articles edited by Kratzig and Onate (1990). An extensive bibliography is given by Noor (1989).

18.4 DESIGN CODES

Existing design codes explicitly aid the designer of doubly curved shells in very few cases (Beedle, 1991). Most codes give design equations for spherical shells under internal pressure. A representative code is ASME Code Case N284. it will be discussed in some detail herein. The code case defines the local buckling stress as

$$\sigma_{xe} = \eta \alpha_x \sigma_{cr} = \eta \alpha_x C_x \frac{Et}{R} \tag{18.13}$$

where

$$Cx = \begin{cases} \dfrac{0.904}{M_x^2} + 0.1013 M_x^2 & \text{for } 1.5 M_x < 1.73 \\ 0.605 & \text{for } M_x \geq 1.73 \end{cases}$$

$$\alpha_x = \begin{cases} 0.837 - 0.014 M_x & \text{for } 1.5 < M_x < 1.73 \\ \dfrac{0.826}{M_x^{0.46}} & \text{for } 1.73 < M_x < 23 \\ 0.124 & \text{for } M_x > 23.6 \end{cases}$$

$$M_x = \frac{L_y}{\sqrt{RT}}$$

L_y = arc length of support in the circumferential direction

σ_{cr} is the linear elastic buckling stress; α_x is the capacity reduction factor, which takes into account the effect of initial imperfections; and C_x is a coefficient describing the linear elastic buckling load. As can be seen, when $M_x > 1.73$, the value of σ_{cr} is the same as that found for the complete sphere, Eq. (18.11).

η is the plasticity reduction factor. It is given by the equations:

$$\eta = \begin{cases} 1 & \text{for } \Delta \leq 0.55 \\ \dfrac{0.45}{\Delta} + 0.18 & \text{for } 0.55 < \Delta < 6.25 \\ \dfrac{1}{\Delta} & \text{for } \Delta \geq 6.25 \end{cases}$$

where

$$\Delta = \frac{\alpha_x \sigma_{cr}}{F_y} \qquad F_y = \text{yield stress}$$

ASME Code Case N284 also gives σ_{cr} values for the case where stiffeners are used. This defines a general shell instability. The relevant equation is

$$\sigma_{Ge} = \frac{1.944 E t_1^{0.25}}{R t_2^{0.75}} \left(\frac{I_1 E}{\bar{b}_2}\right)^{1/3} \left(\frac{I_2 E}{\bar{b}_1}\right)^{1/3} \tag{18.14}$$

where $t_1 > t_2$ and $I_{1E} > I_{2E}$. t_1 and t_2 are equivalent orthotropic thicknesses and I_{iE} are the equivalent moments of inertia of the orthotropic shell. If stiffeners act in only one direction, I_{2E} is taken as $\bar{b}_1(t^3/12)$.

Capacity reduction factors for general instability and stiffener instability are assumed to be the same as the values for the local buckling stress. This does not seem to be reasonable. It is doubtful whether stiffened shells buckling in either stiffener or general modes are as imperfection-sensitive as unstiffened shells. The choice of the capacity reduction factor is a serious problem because Eq. (18.13) is an ultimate strength formula. The buckling stress found from it must be reduced by an appropriate factor of safety. Hence application of the capacity reduction factors for unstiffened shells to stiffened shells can greatly reduce the design capacity of the stiffened shell.

Other double curved shells such as toroidal or elliptical shells may be analyzed in the code case as equivalent spherical shells using the meridional radius as the sphere radius. The ECCS Eurocode does consider torispherical end closures subject to uniform pressure. Conical shells are designed using the buckling equations for an equivalent cylindrical shell (Weingarten et al., 1960). There does not appear to be any code that discusses stability problems of hyperbolic shells.

Even though the ASME code case does not give much explicit help to the designer, as might be desired, it does spell out a rational design procedure that we can apply for any shell. Although it is basically an elastic procedure, it can be modified slightly to cast it into a limit-state design form. The steps recommended are as follows:

1. Carry out stress analyses of the shell for all those factored load combinations deemed important. Only the membrane stress resultants are used in linear stability analyses. Complete collections of membrane solutions for common shell forms under various loadings are given in Pfluger (1961) and Baker et al. (1972). If a computer analysis is used at this stage, one must be aware of discontinuity stresses near abrupt changes of cross section or fixed supports. One need only use membrane stress resultant values at a distance greater than $0.50\sqrt{RT}$ from the point of discontinuity.
2. Compute the capacity reduction factors and plasticity factors for the stress states computed in step 1. Note that the plasticity reduction factor depends on the membrane stress resultants causing buckling.

3. Carry out a linear bifurcation analysis for the membrane states found by dividing the membrane stress resultants computed in step 1 by the factors computed in step 2. The bifurcation analysis can be done by formula, where appropriate, using equations similar to Eq. (18.9) or full-fledged finite element analyses. If an analysis using equations similar to Eq. (18.9) is employed, several different states found from a single load combination may have to be evaluated since it is not obvious at which position on the shell the critical stress combination will occur, particularly if the shell thickness varies or the shell is made of several different shell types.

Use of a shell-of-revolution program for the linear bifurcation analysis may restrict the membrane states under investigation to axisymmetrical states. On the other hand, many important loads, both static and dynamic, yield asymmetric stress states. It has been found that it is conservative to use the largest asymmetric membrane stress resultants as axisymmetric stress states in the buckling equations (Klöppel and Roos, 1956). Note, however, that it is not a simple task to choose which asymmetric stress state is critical, so several may have to be checked. As noted in step 3, if the shell thickness varies or the shell is made of a combination of shapes, a large number of asymmetric stress states may have to be checked. A discussion of practical problems in applying the foregoing procedure is presented in Harstead et al. (1983).

While the foregoing procedure provides a reasonable design methodology, it suffers from an important defect, the lack of data concerning capacity reduction factors to be applied to the membrane stress states for various shell configurations or loading conditions. As stated earlier, one would expect that stiffened spherical shells would be less imperfection-sensitive than unstiffened shells. Therefore, their capacity reduction factor should be larger. Since no codes give these factors, their choice is up to the designer. Of course, one can be conservative and use factors based on the sphere under external pressure, but these values will lead to extremely conservative design.

18.5 DESIGN AIDS

The missing information in design codes must be supplemented by the literature available on shell stability. Although the amount of printed material on this topic is very large, very little of it is of immediate use to the designer. Three texts on the buckling of shells written with the designer in mind are Buchert (1985), Kollar and Dulacska (1985), and Samuelson and Eggwertz (1992). All present results of use to designers. The buckling of spheres and cylinders is covered in detail in all three texts as well as the problem of construction tolerances for these shells. In addition to these texts, the complete study of

spherical domes provided by Yamada (1983) should be mentioned. Formulas for stiffened domes under external pressure are presented and compared to an extensive series of texts. A review of torispherical shells is presented in Galletly (1985). An interesting aspect of the design of these shells is that the use of linear analysis procedures results in very conservative designs.

The major shell type where very little design information exists is shells of revolution with different radii of curvature in each direction, ellipsoids, and hyperboloids. Simple buckling values can be computed using Eq. (18.9), but this assumes that the shell is similar to spherical shells in that buckling occurs in waves of small wavelength. It appears, however, from Kollar and Dulacska (1984) and Buchert (1985) that behavior is similar to spherical shells, at least if the principal radii are similar. Buchert recommends the same capacity reduction factor as that for a sphere under external pressure.

Another practical design problem for metal shells is buckling due to temperature. While computation of the buckling stress can be carried out easily using either Eq. (18.9) or finite element codes, the choice of capacity reduction factor is very important. Use of the spherical shell values may be too conservative in many problems. Intuitively, since buckling is not due to gravity load but to restraint of deformation, one would expect that spherical shells would not be imperfection-sensitive under thermal buckling. Some discussion of this problem is presented in Samuelson and Eggwertz (1992) and in Bushnell (1985). Both references agree that the capacity reduction factors need not be chosen as conservatively as for spherical shells under external pressure. Explicit values are not given, however.

It would be ideal if data existed on initial imperfections so that existing computer codes could be used to compute capacity reduction fctors (Arbocz, 1990). This does not seem to be possible either now or in the foreseeable future. Therefore, the best that one can do is estimate imperfection sensitivity. Koiter's method has been incorporated in some computer codes (Riks et al., 1990). This might be of some help, but whether the Koiter approach can be used for quantitative analysis is an open question (Seide, 1974). An approach to imperfection sensitivity that may achieve quantitative results is that of Batista and Goncalves (1994). They assume that the actual shell instability is due to the loss of membrane stiffness in any classical buckling mode. Therefore, one can obtain a lower bound to the actual buckling load by taking the ratio of reduced potential energy in any mode to the total potential energy in the mode. This reduced potential energy depends on the shell geometry and loading and is achieved by neglecting those stabilizing terms in the total potential energy that are severely undermined by the combined effects of initial imperfections and nonlinear mode coupling developed during the buckling process. The classical buckling load multiplied by this ratio is the lower bound to the failure load. Results using this approach are very promising. Unfortunately, no commercial codes implement the procedure, but it could easily be employed in a postprocessor.

18.6 RETICULATED SHELLS

Reticulated shells are space trusses or frames that are curved in space to behave as shell structures. Obviously, the first step in designing these structures is the design of individual members and joints. The stress resultants in these members are usually found from a linear frame analysis, although one could also use a shell analogy (Benjamin, 1963) if the number of elements and joints is extremely large. One can expect, however, that these structures might have to be considered as shells. Therefore, the problem of overall instability must be looked at.

A good review of the current state of the art in reticulated shell analysis is presented in Gioncu (1992). It is possible to carry out complete nonlinear analyses for reticulated shells, but the designer is still faced with the problem encountered earlier, the relationship between the theoretical buckling loads found by analysis, linear or nonlinear, and the actual buckling loads one would find by actually testing the structure.

Buchert has addressed this problem with aid of the split rigidity concept (1973, 1985). It is also described in Galambos (1988). The shell properties are averaged in such a way that the moments of inertia of the discrete members in each direction are described by a bending thickness, t_B, while the discrete areas are described by a membrane thickness, t_M. Note that in general there will be different thicknesses in each direction. A typical formula obtained from assumptions of this type is the following, valid when the same properties exist in both orthogonal directions:

$$p_{cr} = 2.67\eta E\left(\frac{t_M}{R}\right)^2 \left\{ \left[0.210\left(\frac{\delta}{t_M}\right)^2 + 0.0715\left(\frac{t_B}{t_m}\right)^3 \right]^{1/2} - 0.459\,\frac{\delta}{t_M} \right\} \tag{18.15}$$

where δ is the combination of the imperfection in the dome segment and the deflection due to the applied loads. To compute the latter, one must be able to solve the shell equations for shells with the different bending and membrane thicknesses. Some solutions are provided in Buchert's text along with equations describing more complicated buckling cases (1985).

It should be noted that the split rigidity method may be used instead of the orthotropic shell approach to describe stiffened shells as well as lattice domes. The latter approach seems, however, to be more amenable to computer work, while the use of split rigidities is more useful for hand computations. The split rigidity concept has been criticized because some ingenuity is required to estimate the effective thicknesses when the stiffening elements are not orthogonally positioned. This is true, but, of course, a similar problem arises in replacing stiffener properties by orthotropic shell properties whenever the stiffeners are positioned arbitrarily. Another discrete approach to the reticulated shell problem is presented in Wright (1965). Yamada (1983) also provides equations for buckling of reticulated spherical shells using orthotropic shell properties.

A split rigidity or orthotropic shell approach is useful if one is assured that the reticulated shell is imperfection-sensitive. There are few published experimental data on this problem, and the few computer studies that address the imperfection-sensitivity problem are inconclusive (Battista et al., 1991; Morris, 1992; Batista and Alves, 1993; Kashani and Croll, 1994). It appears that some reticulated shells are imperfection-sensitive, while others are not. Buchert gives the following criterion: a reticulated shell is imperfection-sensitive when the critical buckling wavelength includes two or more members in every direction.

18.7 DESIGN TRENDS AND RESEARCH NEEDS

Although design codes and commercially available computer codes are available to aid one in the design of shell-like structures, the designs actually arrived at might be either too conservative or not conservative enough. Use of the capacity reduction factors for spherical shells under external pressure for other load conditions or shell geometries seems to be very conservative. On the other hand, design of reticulated shells without considering the problem of geometric imperfections errs in the other direction. Most of the research work done on buckling of shell structures has been carried out in the aerospace industry. Shell structures in this field are very thin and made of high-strength alloys. Civil engineering shells are thicker and made of steel. Little work has been carried out on shells of this type. The effect of geometric imperfections may not be as great, but the effect of inelastic behavior and residual stresses will become more pronounced. There currently exist very good computer codes for the analysis of shell structures, but for them to be useful, they must be used in conjunction with experimental data. At present, such data do not exist.

REFERENCES

Anderson, C. A., and Bennet, J. G. (1981), "Containment Buckling Program," submitted to 9th Water Reactor Safety Research Information Meeting, Washington, D.C., Oct., Los Alamos Scientific Laboratory, Los Alamos, N. Mex.

Arbocz, J. (1990), "About the State of the Art of Shell Design," *Int. Colloq. Stabil. Steel Struct., Budapest, Hungary*, Final Rep., pp. 213–226.

ASME (n.d.), *ASME Boiler and Pressure Vessel Code*, ANSI/ASME BVP-III-1-NE, Section III, Code Case N-284, American Society of Mechanical Engineers, New York.

Baker, E. H., Kovalevsky, L., and Rish, F. L. (1972), *Structural Analysis of Shells*, McGraw-Hill, New York.

Batista, R. C., and Alves, R. V. (1993), "Asymptotic Modal Analysis of Lattice Domes," *Proc. SSRC Ann. Techn. Session*, pp. 211–221.

Batista, R. C., and Goncalves, P. B. (1994), "Nonlinear Lower Bounds for Shell Buckling Design," *J. Construct. Steel Res.*, No. 28, pp. 101–120.

Batista, R. C., Antonini, R. C., and Alves, R. V. (1991), "An Asymptotic Modal Approach to Nonlinear Elastic Stability," *J. Comput. Struct.*, Vol. 38, No. 4, pp. 475–484.

Beedle, L. (editor-in-chief) (1991), *Stability of Metal Structures: A World View*, 2nd ed., Structural Stability Research Council, Lehigh University, Bethlehem, Pa.

Benjamin, B. S. (1963), *The Analysis of Braced Domes*, Asia Publishing House, New York.

Buchert, K. P. (1973), *Buckling of Shell and Shell-like Structures*, K. P. Buchert and Associates, Columbia, MO.

Buchert, K. P. (1985), *Split Rigidity Theory of Plates, Shells, and Stability*, 2nd ed., K. P. Buchert and Associates, Columbia, MO.

Budiansky, B. (1959), "Buckling of Clamped Spherical Shells," *Proc. Symp. Theory Thin Elastic Shells*, Delft, The Netherlands, pp. 64–94.

Bushnell, D. (1977), "BSOR4: Program for Stress, Buckling and Vibration of Complex Shells of Revolution," in *Structural Mechanics Software Series*, Vol. 1 (ed. N. Perrone and W. Pilkey) University of Virginia Press, Charlottesville, Va.

Bushnell, D. (1985), *Computerized Buckling Analysis of Shells*, Martinus Nijhoff, Dordrecht, The Netherlands.

ECCS (1988), *European Recommendations for Steel Construction: Buckling of Shells*, 3rd ed., Technical Committee 8, Structural Stability, European Convention for Constructional Steelwork, Brussels, Belgium.

Fitch, J. R., and Budiansky, B. B. (1970), "Buckling and Postbuckling Behavior of Spherical Caps Under Axisymmetric Load," *J. Am. Inst. Aeronaut. Astronaut.*, Vol. 8, pp. 686–693.

Flugge, W. (1962), *Stresses in Shells*, Springer-Verlag, Berlin.

Galambos, T. V., ed. (1988), *Guide to Stability Design Criteria for Metal Structures*, 4th ed., Wiley, New York, Chap. 18.

Galletly, G. D. (1985), "Torispherical Shells," in *Shell Structures: Stability and Strength* (ed. R. Narayan), Elsevier, New York.

Gioncu, V. ed. (1992), *Stability of Space Structures*, special issue, *Int. J. Space Struct.*, Vol. 7, No. 4.

Harstead, G. A., Morris, N. F., and Unsal, A. I. (1983), "Containment Vessel Stability Analysis," *Nucl. Eng. Des.*, May, pp. 303–318.

Huang, N. C. (1964), "Unsymmetrical Buckling of Thin Shallow Spherical Shells," *ASME J. Appl. Mech.*, Vol. 31, pp. 447–457.

Hutchinson, J. W., and Budiansky, B. (1970), "Postbuckling Theory," Appl. Mech. Rev., Vol. 23, pp. 1353–1366.

Kaplan, A. (1974), "Buckling of Spherical Shells," in *Thin Shell Structures: Theory, Experiment, and Design* (ed. Y. C. Fung and E. E. Sechler), Prentice Hall, Upper Saddle River, N.J., pp. 247–288.

Kashani, M., and Croll, J. G. A. (1994), "Lower Bounds for Overall Buckling of Spherical Space Domes," *ASCE J. Eng. Mech.*, Vol. 120, No. 5, pp. 949–970.

Klöppel, K., and Roos, E. (1956), "Contribution to the Buckling Problem of Thin-Walled Stiffened and Unstiffened Spherical Shells Under Full and Half-Sided Loading," *Stahlbau*, Vol. 25, Mar., pp. 49–60 (in German).

Koiter, W. T. (1977), "The Stability of Elastic Equilibrium," *Techn. Rep. No. AFFDL TR-70-25*, Air Force Flight Dynamics Laboratory, Wright Patterson AFB, Ohio (translation of 1946 thesis).

Kollar, L., and Dulacksa, E. (1984), *Buckling of Shells for Engineers*, Wiley, London.

Kratzig, W. B., and Onate, E., eds. (1990), *Computational Mechanics of Nonlinear Response of Shells*, Springer-Verlag, New York.

Krenzke, M. A., and Kiernan, T. J. (1963), "Elastic Stability of Near-Perfect Shallow Spherical Shells," *J. Am. Inst. Aeronaut. Astronaut.*, Vol. 1, pp. 2855–2857.

Litle, W. A. (1964), *Reliability of Shell Buckling Predictions*, Res. Monogr. No. 25, MIT Press, Cambridge, Mass.

Morris, N. F. (1992), "Application of a Koiter-Type Theory to Buckling of Lattice Domes," *Int. J. Space Struct.*, Vol. 7, No. 4, pp. 335–343.

Noor, A. K. (1989), "List of Books, Monographs, Conference Proceedings and Survey Papers on Shells," in *Analytical and Computational Models of Shells* (ed. A. K. Noor et al.), American Society of Mechanical Engineers, New York, pp. vii–xxxviii.

Pfluger, A. (1961), *Elementary Statics of Shells*, 2nd ed., F. W. Dodge Corporation, New York.

Riks, E., Brogan, F. A., and Rankin, C. C. (1990), "Numerical Aspects of Shell Stability Analysis," in *Computational Mechanics of Nonlinear Response of Shells* (ed. W. B. Kratzig and E. Onate), Springer-Verlag, New York, pp. 125–151.

Samuelson, L. A., and Eggwertz, S. (1992), *Shell Stability Handbook*, Elsevier, New York.

Seide, P. (1974), "A Reexamination of Koiter's Theory of Initial Postbuckling Behavior and Imperfection Sensitivity of Structures," in *Thin Shell Structures: Theory, Experiment, and Design* (ed. Y. C. Fung and E. E. Sechler), Prentice Hall, Upper Saddle River, N.J., pp. 247–288.

Seide, P., Weingarten, V., and Masri, S. (1979), "Buckling Criterion and Application of Criteria to Design of Steel Containment Shell," *NUREG/CR-0793*, May.

Timoshenko, S., and Gere, J. (1961), *Theory of Elastic Stability*, McGraw-Hill, New York.

Weingarten, V., Morgan, E., and Seide, P. (1960), "Final Report on Development of Design Criteria for Elastic Stability of Thin Metal Shells," *STL/TR-60–0000-19425*, Space Technology Laboratories, Inc.

Wright, D. T. (1965), "Membrane Forces and Buckling in Reticulated Shells," *ASCE J. Struct. Div.*, Vol. 91, pp. 173–202.

Yamada, M. (1983), "An Approximation on the Buckling Analysis of Orthogonally Stiffened Framed Spherical Shells Under External Pressure," in *Shell and Spatial Structures Engineering: Proc. Int. Symp. Shell Spat. Struct. COPPE, Federal University of Rio de Janeiro, Brazil, Sept.*, (ed. F. L. L. B. Carneiro et al.), Pentech Press, Plymouth, Devonshire, England, pp. 177–193.

CHAPTER NINETEEN

SELECTED TOPICS IN DYNAMIC STABILITY

19.1 INTRODUCTION

The stability of structures subjected to dynamic loads encompasses a wide and diverse class of problems. In general, a system can be defined as stable with respect to a particular perturbation if a small change in that perturbation results in an arbitrarily small change of a particular aspect of structural response during a desired period of time. In other words, a structural system may be:

- Stable with respect to one system of parameters and unstable with respect to the other
- Stable for a given time period and unstable thereafter

For example, a column subjected to an axial compression in excess of the statical Euler force may not buckle if the duration of the force application is sufficiently short. Conversely, a periodic axial force having a magnitude being only a fraction of the Euler force may cause unstable lateral motion for a certain range of frequencies.

It is always difficult to summarize a discipline that is not only diverse but which is still growing at an increasing rate. In the absence of similar texts it was decided to cover five distinctly different topics in hope to clarify at least some of the aspects of greatest practical interest, as follows:

1. Parametric resonance
2. Stability of impulsively loaded columns
3. Dynamic snap-through of shallow structures
4. Flow-induced instability
5. Suddenly loaded structures

19.2 PARAMETRIC RESONANCE

The phenomenon known as *parametric excitation* can be illustrated with an example of a simply supported column subjected to an harmonic axial force $P(t)$ (Fig. 19.1). Ordinarily, for a load intensity small in comparison with Euler's static buckling force, the expected response would consist of axial vibrations. However, for certain frequencies of the axial force $P(t)$, large and potentially dangerous transverse vibrations can occur. The occurrence of such a response characterized by motion that is typically orthogonal to the direction in which the external force is applied is referred to as parametric excitation. The exponential increase in the amplitude of these transverse vibrations is labeled as parametric resonance. For a comprehensive study of the phenomenon, see Mettler (1962), Bolotin (1964, 1968), Nemat-Nasser (1972), Schmidt (1975), and Ibrahim et al. (1978).

19.2.1 Formulation of the Problem

Neglecting the axial component of the motion, the equation of the small, elastic transverse vibrations of a column subjected to a time-dependent axial force $P(t)$ is

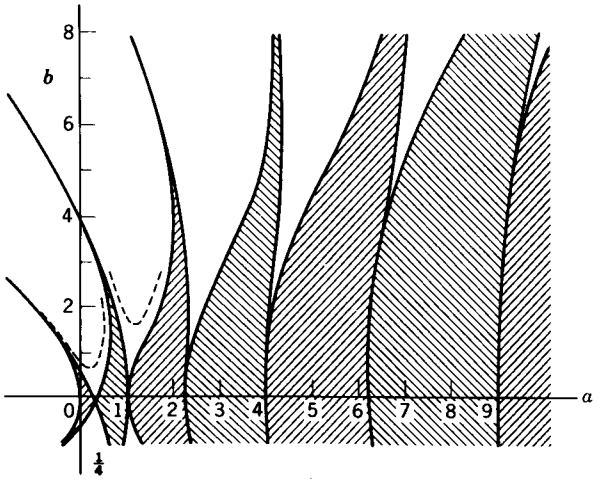

Fig. 19.1 Strutt's diagram.

$$EI\frac{\partial^4 w}{\partial x^4} + P(t)\frac{\partial^2 w}{\partial x^2} + m\frac{\partial^2 w}{\partial t^2} = 0 \tag{19.1}$$

where E, I, m, and $w(x, t)$ are the elastic modulus, moment of inertia, mass per unit length, and the transverse displacement correspondingly. Seeking the solution in the form of standing waves (i.e., in separable form) gives us

$$w(x, t) = X(x)f(t) \tag{19.2}$$

Equation 19.1 implies that

$$\ddot{f} + \omega^2\left[1 - \frac{P(t)}{P_e}\right]f = 0 \tag{19.3}$$

where P_e is the static buckling force and ω the free vibration frequency. It is recognized that the standing-wave solution is, strictly speaking, possible only if $X(x)$ is simultaneously the static buckling mode and the free vibration mode. This occurs only in case of the simply supported column and uniform radial loading of a circular ring. In all other cases the solution (Eq. 19.2) is approximate (in the sense of the Ritz or the Galerkin method).

The stability of the motion, as measured by the magnitude of the transverse displacement $w(x, t)$ in Eq. 19.2, depends on $f(t)$, which is the solution of the ordinary differential equation with periodic coefficients (Eq. 19.3). In case of deterministic loading, this governing equation is a Mathieu equation if

$$P(t) = P_0 + P_t \cos\theta t \tag{19.4}$$

and is a Hill equation if

$$P(t) = P_0 + \sum_k P_{tk} \cos k\theta t \tag{19.5}$$

Both Mathieu and Hill equations were investigated thoroughly in the past (McLachlan, 1947; Bolotin, 1964; Schmidt, 1975). In addition, Eq. 19.3 admits a closed-form solution for the case of the periodic impact loading (Krajcinovic and Herrmann, 1968; Hsu, 1972).

19.2.2 Regions of Instability

The qualitative study of the small parametric vibrations of an elastic structure reduces to the determination of the combinations of the load intensity (P_0, P_t) and the load frequency (defined by θ), for which the response amplitude starts to grow exponentially.

For arbitrary boundary conditions the partial differential equation (Eq. 19.1) admits a solution in terms of a sum of standing waves:

$$w(x, t) = \sum_{k=1}^{\infty} f_k(t)X_k(x) \tag{19.6}$$

where $X_k(x)$ satisfies boundary conditions at $x = 0$ and L. If X_k is chosen to represent the free vibration modes, Eq. 19.3 can be rewritten as (see Bolotin, 1964)

$$\ddot{f}_i = \omega_i^2\left[f_i - P(t)\sum_k a_{ik}f_k\right] = 0 \tag{19.7}$$

where

$$a_{ik} = -\frac{1}{m\omega_i^2}\int_0^L X_k X_i'' \, dx \qquad \int_0^L X_i X_k \, dx = \begin{cases} 1 & \text{if } i = k \\ 0 & \text{if } i \not\geq k \end{cases} \tag{19.8}$$

with L being the column length. If the loading function is given by Eq. 19.4, then Eq. 19.7 can be recast into

$$\ddot{f}_i = \omega_i^2\left[f_i - (P_0 + P_t\cos\theta t)\sum_k a_{ik}f_k\right] = 0 \tag{19.9}$$

The system of Eq. 19.9 of an infinite number of ordinary differential equations with periodic coefficients is coupled through the last term in the brackets. The solution of the system is greatly facilitated if the diagonal terms are much larger than the off-diagonal terms.

In the case of a simply supported beam or a circular ring, $a_{ik} = 0$ if $i \neq k$. Then with

$$a_{ii} = \frac{1}{P_i} \tag{19.10}$$

it is possible to write, instead of Eq. 19.9,

$$\ddot{f}_i + \Omega_i^2(1 - \mu_i\cos\theta t)f_i = 0 \tag{19.11}$$

where

$$\Omega_i = \omega_i\sqrt{1 - \frac{P_0}{P_i}} \qquad \mu_i = \frac{P_t}{2(P_0 - P_i)} \tag{19.12}$$

Introducing the simple transformation

$$2z = \theta t \quad a = \left(\frac{2\Omega}{\theta}\right)^2 \quad q = \mu\left(\frac{2\Omega}{\theta}\right)^2 \tag{19.13}$$

Eq. 19.11 can be rewritten in a typical form of a Mathieu equation,

$$\frac{d^2f}{dz^2} + (1 - 2q\cos 2z)f = 0 \tag{19.14}$$

The solutions of Eq. 19.14 are either

- *Stable*: decreasing in time $f(t+T) < f(t)$, or
- *Unstable*: increasing in time $f(t+T) > f(t)$

The regions of stable and unstable solutions in the (a, q) plane are separated by the loci of points representing harmonic solutions of (Eq. 19.14) $f(t+T) = f(t)$. These harmonic solutions are known as Mathieu functions $se_n(z)$ and $ce_n(z)$ of the integer order n. The graphical depiction of the stable and unstable regions (shaded in Fig. 19.1) is known as the *Strutt diagram*. The Mathieu functions defining the first two instability regions are listed in Table 19.1.

The analysis is much more complicated for columns other than those simply supported. The boundaries of the principal instability region can be computed approximately using the information in Table 19.2, where k is the elastic foundation modulus,

$$C_1 = 2\omega_1\left(\frac{mL^4}{EI}\right)^{1/2} \tag{19.15}$$

and

$$\left(\frac{\theta_*}{2\omega_1}\right)^2 = 1 - \frac{L^2}{EIC_2}(P_0 \pm \tfrac{1}{2}P_t) \tag{19.16}$$

TABLE 19.1 Boundaries of First Two Instability Regions (Bolotin, 1968)

Region	Function	Relation Between Ω_i and μ_i
1	$se_1(z)$	$(\theta_*/2\Omega)^2 = 1 + \mu + \frac{1}{8}\mu^2 + O(\mu^3)$
	$ce_2(z)$	$= 1 - \mu + \frac{1}{8}\mu^2 + O(\mu^3)$
2	$se_2(z)$	$= 1 + \frac{1}{3}\mu^2 + O(\mu^4)$
	$ce_2(z)$	$= 1 - \frac{5}{3}\mu^2 +)(\mu^4)$

TABLE 19.2 Boundary of the Principal Instability Region

Column	C_1	C_2	$P_c l^2/EI$
	7.04	2.66	2.47
	19.74	9.87	9.87
	30.84	21.3	20.2
	44.7	40.7	39.48
k	$19.74\sqrt{1+\beta}$	$9.87\sqrt{1+\beta}$	$9.87(n^2 + \beta/n^2)$, $\beta = \frac{kl^4}{\pi^4 EI}$ $n = 1, 0 \le \beta \le 4$ $n = 2, 4 \le \beta \le 36$ $n = 3, 36 \le \beta \le 144$

A closed-form solution of the problem was derived only in two cases:

1. For the step load the harmonic solutions (separating the stable from unstable regions) are obtained as the roots of the transcendental equation (Bolotin, 1968)

$$\left|\cos\frac{\pi p_1}{\theta}\cos\frac{\pi p_2}{\theta}-\frac{p_1^2+p_2^2}{2P_1P_2}\sin\frac{\pi p_1}{\theta}\sin\frac{\pi p_2}{\theta}\right|=0 \tag{19.17}$$

where

$$p_{1,2}=\Omega\sqrt{1\pm\frac{P_t}{P_0-P_{cr}}}$$

with Ω is defined by Eq. 19.12a, while π/θ is the duration of each step.

2. For the loading consisting of impulses repeating after a period T,

$$P(t)=P_0+P_t\sum_k\delta(\theta t-k\theta T)$$

where δ is the Dirac delta functional, the harmonic solutions are roots of the transcendental equation (see Krajcinovic and Herrmann, 1968)

$$\left|\frac{P_t}{2(P_{cr}-P_0)}\frac{\Omega_k T}{2\pi}\sin\Omega_k T+\cos\Omega_k T\right|=1 \tag{19.18}$$

where Ω_k is again defined by Eq. 19.12a.

It is important to notice that depending on the loading frequency, in all of these cases:

- The instability may occur when the combined load magnitude P_0+P_t does not exceed the static buckling force P_e.
- The column can remain stable even though P_0+P_t may exceed P_e.

19.2.3 Summary of Results for Linear Systems

Most of the research conducted in the past focused on the practically most important case of a harmonic load given by Eq. 19.4. The derived results can be summarized for the designer in the following way. The loading frequencies leading to an unstable response are located in regions defined by boundaries $ce_n(z)$ and $se_n(z)$ arranged in Table 19.1. For a properly designed structure

loaded dynamically ($P_t > P_0$, $P_e > P_0$) $|\mu| < 1$ from Eq. 19.12. Hence the first (principal) instability region is bounded by

$$1-\mu<\left(\frac{\theta_{cr}}{2\Omega}\right)<1+\mu \tag{19.19}$$

The higher critical loading frequencies are located within very narrow bands surrounding lines

$$\theta_{cr}=\frac{2\Omega_i}{n}\qquad n=3,4,5,\ldots \tag{19.20}$$

where Ω_i are frequencies of the natural vibrations of the structure subjected to a statical axial force P_0 (Eq. 19.12).

Linear or Viscous Damping. In case of viscous damping the governing equation (Eq. 19.11) must be amended by a term $2\eta f$, where 2η is the damping coefficient. The viscous damping has the effect of shrinking the instability regions without eliminating them. The critical loading frequencies belonging to the primary instability region satisfy the inequalities

$$1-\sqrt{\mu^2-4\eta^2}<\frac{\theta_{cr}}{2\Omega}<1+\sqrt{\mu^2-4\eta^2}$$

Combination Resonance. Investigation of multiple-degree-of-freedom systems (Cesari, 1973) revealed the existence of additional regions of unbounded response. The parametric combination resonance of order n occurs if

$$\theta_{cr}=\frac{1}{n}|\Omega_i\pm\Omega_j|\qquad i\not\gtrless j;\ n=1,2,\ldots$$

where Ω_i is the natural frequency of the ith mode (in the presence of the static force P_0).

Simultaneous Parametric and Forced Excitation. If an elastic column is subjected to a harmonic axial load of frequency θ and a harmonic transverse load of frequency θ_f, the instability will occur (Yamamoto and Saito, 1970) when

$$\Omega=\theta\pm\theta_f$$

Influence of Axial Motion. The governing equation (Eq. 19.1) was derived neglecting the displacements along the axis of the column (i.e., propagation

of compressive and tensile waves). The system of equations governing the coupled axial and transverse (parametric) elastic vibrations were derived by Bolotin (1964). A solution of this problem reveals fairly significant modification of the instability region provided that the natural frequency of axial vibrations is close to the frequency 2Ω (given by Eq. (19.12). This is a natural consequence of the fact that near resonance the dynamic axial force in the column becomes very large.

19.2.4 Summary

Trying to summarize almost a century of intensive work, single out the most salient features of a complex phenomenon, and highlight the points of paramount practical importance is in many ways an impossible task. It is quite possible that the equations in Table 19.1 contain all that a designer should know in the beginning phase of a design. If the structure is designed such that the (a, Z) point is well within the stable region of the Strutt diagram, and if the frequency of the axial force is not close to the frequency of axial vibrations, the chances are that no problems will occur. Yet a complex and significant structure may warrant a much more comprehensive study, including a variety of nonlinear effects.

19.3 STABILITY OF IMPULSIVELY LOADED COLUMNS

An impulsively loaded column is defined to be a structural member subjected to a compressive stress that depends significantly on inertia properties and on time. The term *impulse* is used here to encompass all of the various loading conditions that can create time dependent excitation such as impact, which specifically refers to collisions between two bodies where the mass effect of both bodies is considered (Goldsmith, 1960), boundary velocity, such as that produced in a constant-speed testing machine (Hoff, 1951), and force pulse, such as that caused by overpressure distribution from air-blast conditions (Kornhauser, 1964).

The duration of the excitation is probably the most important consideration in the study of the stability of impulsively loaded columns. It determines whether or not the effects of wave propagation must be considered to describe the response accurately. This in turn influences the numerical approach required for the solution. If the duration is sufficiently long, the axial force can be considered constant along the length, being a function of time only. (This is equivalent to the assumption of an infinite axial wave speed.) If the duration is sufficiently short, the longitudinal wave must be considered in the formulation. If, in addition to the duration being short, the strain rate is sufficiently high, elastic-plastic wave propagation may be present, and the consideration of material strain rate sensitivity may be required.

19.3.1 Classification

Theoretical and experimental studies concerned with the stability of a single member subjected to impulsive loading are classified in Table 19.3 according to the following characteristics: mathematical model, material, imperfections, loading, and solution technique.

19.3.2 Low-Velocity Excitation

The distinction between the buckling characteristics of the lower- and higher-speed excitation is significant. The lower-speed (strain rates on the order 10^{-1} to $10^{2}\,s^{-1}$), longer-duration forcing function produces buckling forms that involve the entire column length. The usual assumption made—that the axial wave traverses the column length a sufficient number of times so that the axial force is not a function of position along the length but is a function of time only—has been generally confirmed in several studies (Davidson, 1953; Sevin, 1960; Lindberg, 1965; Abrahamson and Goodier, 1966). Justification has also been established for neglecting the axial inertia effects under the restrictive conditions of elastic material property and sufficiently long load duration (Sevin, 1960; Hayashi and Sano, 1972a). This conclusion was also reached for the restriction of a sufficiently large material dissipation (McIvor and Bernard, 1973). In addition, the axial-flexural coupling effect (Davidson, 1953; Huffington, 1963) and the rotary inertia and shear deformation effects (Housner and Tsu, 1962; Huffington, 1963; Hayashi and Sano, 1972a,b) were found to be insignficant under these restrictions.

The classical conclusion of impulsive stability, discovered in the earliest work (Koning and Taub, 1934; Taub, 1934) and substantiated by many later analyses, is that the impulsive axial force can significantly exceed the static buckling load of the column without excessive lateral displacements due to the delaying effect of the column's inertia. The larger axial force overloads are associated with shorter duration, smaller initial imperfections, and larger slenderness values. However, the dynamic buckling load is never less than the static buckling load (Ari-Gur et al., 1980). Material damping can enhance the axial overload capacity (Suzuki, 1969).

The dynamic buckling mode shape, which grows with time for the axial overload condition, is strongly dependent on the magnitude of the axial force (Housner and Tsu, 1962; Lindberg, 1965) and the stress-strain function (Lee, 1978). For relatively slow loading rates and long durations, the fundamental mode, similar to the static configuration, dominates the shape, which is strongly influenced by the initial imperfections (Lee, 1981). For higher loading rates and shorter durations, the higher modes are excited (Housner and Tsu, 1962; Lindberg, 1965; Abrahamson and Goodier, 1966; McIvor and Bernard, 1973; Lee 1981) and the dominant shape falls between the highest and lowest modes associated with a critical load smaller than the applied axial load

TABLE 19.3 Summary of Studies

Reference	Model						Material			Imperfections					Loading				Solution					Comments
	BE	LI	AI	RI	SD	CS	LE	IE	VE	HS	GD	GV	RD	MI	BV	FP	IP	CF	AS	FE	FD	WP	ES	
Meier (1945)	×	×					×			×							×	×						Solution of equations of motion based on half-sine-wave shape
Hoff (1951)	×	×				×	×			×					×			×	×					Buckling of a column due to loading by a constant-speed testing machine
Chawla (1951)	×	×				×	×	×		×					×						×			Numerical solution to Hoff's problem (1951) extended to inelastic material
Hoff et al. (1951)	×	×				×	×			×					×			×	×		×			Extension of Hoff's problem (1951) to include a wider range of parameters
Gerard and Becker (1952)	×		×				×								×			×				×	×	Buckling of a column confined to a fraction of total length due to stress wave
Davidson (1953)	×	×				×	×			×				×					×				×	Study of mass impact through a spring connection to column
Schmitt (1956)	×	×					×			×					×				×			×		Numerical method based on wave travel used to solve equations of motion
Erickson et al. (1956)																							×	Experimental study used to verify Hoff's results (1951)
Hartz and Clough (1957)	×	×						×			×					×			×				×	Numerical study of columns loaded beyond the linear material range
Sevin (1960)	×	×	×			×	×			×					×						×			Numerical solution to coupled equations of motion to study the axial inertia effects
Hausner and Tsu (1962)	×	×		×	×		×				×					×	×	×						Detailed development of live column models
Huffington (1963)		×	×	×	×	×	×			×	×					×	×				×	×		Useful comparison of linear and nonlinear models
McIvor (1964)	×	×	×			×	×					×						×						Instability study of a column undergoing axial vibrations
Lindberg (1965)	×	×					×				×		×				×	×				×	×	Study of the effects of imperfections expressed in a random form
Abrahamson and Goodier (1966)	×	×						×			×	×					×	×				×	×	Linear strain hardening material used to study plastic buckling phenomenon
Malyshev (1966)	×	×					×										×	×				×	×	Study of the stability of an infinitely long column with step load (in Russian)
Kornev (1968)	×	×					×				×						×	×						Russian publication
Holzer and Eubanks (1969)	×	×					×				×	×				×			×					Displacement bounds are determined

TABLE 19.3 *Continued*

Suzuki (1969)	×	×				×			×	×					×				×					Solution of Hoff's problem (1951) with damping and different loading velocities
Holzer (1970)	×	×					×				×	×				×								Displacement bounds are determined
Holzer (1971)	×	×					×				×					×								Displacement bounds are determined
Plaut (1971)	×	×					×				×					×								Displacement bounds are determined
Malyi and Efimov (1972)		×		×	×		×				×				×			×				×		Exact solution to semi-infinite bar subjected to longitudinal impact (in Russian)
Hayashi and Sano (1972a)	×	×	×			×	×			×				×					×		×		×	Study of column buckling due to mass impact at low velocity—first report
Hayashi and Sano (1972b)	×	×	×	×	×	×	×			×				×							×		×	Study of column buckling due to mass impact at high velocity—second report
Malyi (1972)	×	×					×								×			×				×		Simplified solution to Malyi–Efimov problem (in Russian)
McIvor and Bernard (1973)	×	×	×			×			×		×					×			×					Axial-lateral motion coupling with material dissipation
Malyi (1973)	×	×					×				×				×			×				×		Russian publication
Kornev (1974)	×	×					×										×	×						Russian publication
Kiryukhin and Malyhi (1974)	×	×	×				×				×				×			×						Russian publication
Grybos (1975)		×	×	×	×	×	×							×				×	×					Defines parameters associated with critical velocity and impacting mass
Lee (1978)	×	×	×			×		×							×				×			×		Nonlinear axial strain and Ramberg–Osgood type of material function
Elishakoff (1978a)	×	×					×			×			×				×	×						Random imperfections as the amplitude of half sine wave
Elishakoff (1978b)	×	×					×						×				×		×					More general random imperfections than Elishakoff (1978a) utilizing Monte Carlo method
Amiro (1979)	×	×					×				×	×					×	×						Russian publication
Ari-Gur et al. (1980)	×	×	×			×	×				×			×							×		×	Study of column buckling due to mass impact with several different materials
Lee (1981)	×	×						×			×				×				×					Study of inelastic column buckling as an initial value-eigenvalue problem

Notes to Table 19.3

1. Model properties: equations of motion:
   BE = Bernoulli-Euler assumptions for bending
   LI = lateral inertia included
   AI = axial inertia included
   RI = rotary inertia included
   SD = shear deformation included
   CS = coupled strain-displacement relations
2. Material properties:
   LE = linear-elastic
   IE = inelastic
   VE = viscoelastic
3. Initial imperfections for flexural response:
   HS = half-sine-wave displacement function
   GD = general displacement function
   GV = general velocity function
   RD = random displacement variable
4. External loading condition:
   MI = mass impact, mass of impacting body considered
   BV = boundary velocity
   FP = finite pulse, finite duration
   IP = infinite pulse, including step load
5. Solution procedure:
   CF = closed-form solution to differential equations
   AS = approximate solution to differential equations
   FE = finite-element discretization
   FD = finite-difference discretization
   WP = wave propagation considered
   ES = experimental studies

Notes:
1. The order of papers in the classification is chronological
2. Boundary conditions arre not considered as a model property in the classification because they are frequently selected on the basis of convenience for a solution studied rather than a meaningful part of the model. For example, semi-infinite bars are frequently used in wave propagation studies to avoid the complexity of wave reflection and material unloading. End conditions are considered by Koning and Taub (1934).
3. All models considered have prismatic section properties: area and moment of inertia.

(Housner and Tsu, 1962). These modes are less influenced by imperfections (Lindberg, 1965; Hayashi and Sano, 1972a,b).

The inelastic impulsive buckling phenomenon is more complex because it includes the nonlinear material property and the possibility of energy dissipation due to unloading. Some numerical studies of these effects have been made (Chawla, 1951; Hartz and Clough, 1957; Abrahamson and Goodier, 1966; Lee 1981). It has been found that inelastic buckling is more abrupt than elastic buckling (Chawla, 1951).

19.3.3 High-Velocity Excitation

High-velocity excitation (strain rate on the order of 10^2 to $10^6\ s^{-1}$) is typically associated with impact, and its response is usually described by the propagation of stress waves. The axial stress function cannot be considered constant along the length since it is determined by the movement of the stress wave (i.e., the segment covered by the wave is fully stressed while the portion of the length head of the wave remains unstressed). The entire column length is no longer a parameter of stability since the propagating wave may cause buckling in a shorter segment of the member (Gerard and Becker, 1952). The higher the strain rate, the closer the buckled segment is to the end where impact occurs and the shorter the buckled segment (Hayashi and Sano, 1972b). The higher buckling modes that are excited under these conditions influence the buckled shape and the initial imperfections are not a factor (Lindberg, 1965; Hayashi and Sano, 1972a,b). Slender columns are more susceptible to high-velocity buckling (Abrahamson and Goodier, 1966).

Axial wave propagation caused by sufficiently high strain rates may involve both elastic and plastic wavefronts. Von Kármán and Duwez (1950) developed a solution to this problem for a uniaxial tensile wave, and although they did not address the stability problem, Lee (1978) used their solution procedure to study the stability of a column with an axial plastic compressive wave. Very few stability studies have been made for these conditions (Abrahamson and Goodier, 1966; Hayashi and Sano, 1972b; Lee, 1978). Some experimental testing has produced inelastically buckled shapes due to impact (Abrahamson and Goodier, 1966; Hayashi and Sano, 1972a,b). Under these severe conditions, material properties may be affected. Indication of strain rate sensitivity has been noted (von Kármán and Duwez, 1950), while other studies have indicated that the effect is negligible (Lee, 1978).

19.3.4 Numerical Solutions

The numerical solutions to the differential equations of motion have been based on various approximating procedures (see Table 19.3, "Solution"). The low-velocity solution is relatively uncomplicated, but the high-velocity solution is more difficult, particularly for the elastic–plastic wave problem with special consideration required for solution discontinuities. Hyperbolic systems that model wave propagation effects must account for the discontinuities that may exist at the characteristic lines (Belytschko, 1976a). In either category, the solution must be developed in a detailed evolutionary manner that is classified as a nonlinear transient analysis problem. Recent surveys are available that discuss the computer methods for the numerical solution to this class of problems (Belytschko, 1976b; Hughes, 1980). Finite difference and finite element discretization schemes are most commonly used (Belytschko, 1976a).

19.4 DYNAMIC SNAP-THROUGH OF SHALLOW STRUCTURES

Shallow structures or structural elements, such as arches or domes with low height-to-span ratios, can also be subjected to dynamic loads (e.g., from winds or earthquakes). Under extreme loading conditions, part or all of the structure may invert (snap-through). This part of the chapter considers the dynamic snap-through of shallow structures.

Critical values of the loads are usually defined by the Budiansky–Roth criterion (Holzer, 1976, 1979). First, a measure of the response is chosen, such as the area or volume displaced by the structure from its initial configuration, or the displacement of the crown. The maximum value of this response measure is then computed for increasing levels of load. If, at some load level, a small increase in load is accompanied by a large increase in the maximum response, this load is termed the critical load.

19.4.1 Types of Loads

Spatial Distribution. In most studies the load is assumed to be distributed uniformly over the structure. If the structure is symmetric, such as an arch symmetric about its center or a spherical cap symmetric about the vertical axis through its crown, it may have a particularly large resistance to snap-through under symmetric loads. The addition of small asymmetric components to the uniform load may cause a sharp drop in critical load (Gregory and Plaut, 1982). Therefore, results for a symmetric problem may be quite misleading if applied to an actual structure, which will not be perfectly symmetric in geometry, boundary conditions, and loading.

The effect of changes in the load distribution can be investigated by considering two or more independent loads. If two independent loads are applied in varying ratios, the critical load combinations can be plotted as interaction curves, and the effects of changes in the distribution of the combined loads can be studied. Such interaction curves have been determined for a shallow arch (Gregory and Plaut, 1982) and a lattice dome.

In general, as far as snap-through is concerned, the worst spatial distribution is probably a localized one, applied somewhere on one side of the structure. A snow load on one sector of a spherical roof, for example, may be much more dangerous than a fairly uniform load with the same pressure.

Temporal Variation. For blast loads, the duration is often assumed to be so short that the load is modeled as an impulse, which acts at an instant of time. An initial velocity is imparted to the structure, and the ensuing response is computed. Another common type of load is a step load with infinite duration. The load is applied at a certain time and then maintains the same magnitude during the motion. The determination of the structural response under these two types of loads is particularly simple, because the loads do not change with time after the instant of application (i.e., they are zero in the first case, and constant in the second).

Pulse loads, which act on the structure over some finite time interval, are considered in some investigations. They may be shaped like a half-sine wave, an N, or a triangle, for example. Right triangular pulses with varying time lengths of decay are treated by Kao and Perrone (1978). The critical value of the initial load magnitude decreases as the time length of the pulse increases, with the step load of infinite duration providing a lower bound on these critical values.

A few authors consider snap-through of shallow structures subjected to stochastic loads (Ariaratnam and Sankar, 1968; Pi et al., 1971). The probability distribution for the time of snap-through is determined. Another type of load which has been analyzed is a pulsating load (Huang, 1972; Huang and Plaut, 1981). The critical value becomes lower when the forcing frequency is near a resonance condition, as one would expect.

19.4.2 Types of Structures

Shallow arches under dynamic loads have been studied extensively. This is partly due to the simplicity of the mathematical formulation. Usually, the ends are assumed to be simply supported or clamped, and the initial shape to be circular or sinusoidal. Spherical caps have also received much attention. In most cases the edge is taken to be clamped.

The dynamic response of shallow space trusses (lattice domes) also has been investigated. The bars remain straight, so that the configuration can be defined by the locations of the joints. Snap-through can be local, with inversion of one portion of the structure, or global, with complete inversion. Finally, dynamic snap-through of shallow space frames, in which the joints are rigid, has been considered in one study (Belytschko et al., 1977). The analysis is much more complicated than that for trusses, since bending and torsion are involved as well as axial forces in the members.

In almost all of the investigations, the structures are assumed to be made of homogeneous, isotropic, linearly elastic material. An orthotropic spherical cap is considered in one paper (Alwar and Reddy, 1979). Another paper treats a spherical cap having elastic–plastic material behavior (Kao, 1980), while viscoelastic behavior is assumed in a couple of studies of dynamic snap-through of an arch (Johnson, 1980; Huang and Nachbar, 1968). Plasticity reduces the critical load significantly, while the presence of internal damping (viscoelasticity), and also of external damping (Mescall and Tsui, 1971), tends to raise the critical load.

The effect of structural imperfections is examined in several papers (Huang and Nachbar, 1968; Belytschko et al., 1977; Kao and Perrone, 1978; Kao, 1980). The imperfection usually is chosen as an initial displacement of the structure, such as a dimple in the spherical cap. Such imperfections generally

tend to decrease the critical load. The size of the decrease may be significant, even if the imperfection is small.

19.4.3 Numerical Techniques

There are two aspects to the numerical solution of a typical structural dynamics problem: spatial discretization and time integration (Ball, 1975). For a space truss, there are a finite number of degrees of freedom (the coordinates of the joints), so spatial discretization is not needed. For the other types of structures, various techniques are utilized, such as Galerkin's method, the finite difference method, and the finite element method.

After spatial discretization, the resulting equations of motion are usually integrated numerically over time to determine the structural response. The most popular methods are Newmark's beta method, Houbolt's technique, and the Runge–Kutta method. A Hamming predictor–corrector method and the finite difference method are also used sometimes.

19.4.4 Comparison with Critical Static Loads

For step loads with infinite duration, the critical values for dynamic snap-through are often compared to the critical values of the static problem. For a clamped spherical cap with a uniform load and no damping, the critical step load is usually about one-half of the critical static load. For an undamped shallow arch (Gregory and Plaut, 1982) and for a lattice dome, the decrease is often around 25%. However, the percentage difference depends on many factors, including the type of structure, its shallowness, the spatial distribution of the load, and the amount of damping.

19.5 FLOW-INDUCED INSTABILITY

Flow-induced vibrations have been known to man since ancient times. But systematic studies of the flow effect on circular cylinders were not made until about a century ago when Strouhal established the vortex shedding frequency for a single circular cylinder across a flow (Goldstein, 1965). Since the collapse of the Tacoma Narrows Bridge in 1940, flow-induced instability has attracted much attention. Recently, due to the use of high-strength materials and the development of advanced structural analysis techniques, structures have become progressively lighter and more flexible and consequently more prone to vibration and instability. Significant progress has been made in understanding the complex interaction phenomena of flow and cylinder motion. The increasing study is evidenced by many conferences (Naudascher, 1972; IAEA, 1977; Chen and Bernstein, 1979; Naudascher and Rockwell, 1980) directed to this subject and numerous publications, including reviews and books (Junger and Feit, 1972; Scanlan and Wardlaw, 1973; Mulcahy and Chen, 1974; Shin and Wambsganss, 1975; Mulcahy and Wambsganss, 1976; Chenoweth and Kistler, 1976; Chen, 1977a,b; King, 1977; Blevins, 1977; Scanlan and Simiu, 1978).

19.5.1 Instability Mechanisms

The dynamics of circular cylinders subject to flow is described by the following equation of motion (Chen, 1977b):

$$[M]\{\ddot{q}\} + [C]\{\dot{q}\} + [K]\{q\} = \{Q\} \tag{19.21}$$

where

$[M] = [M_s] + [M_f]$
$[M_s]$ = structural mass
$[M_f]$ = added mass of fluid
$[C] = [C_s] + [C_f] + [C_v]$
$[C_s]$ = viscous damping of structures
$[C_f]$ = viscous damping of fluid
$[C_v]$ = velocity-dependent damping of fluid
$[K] = [K_s] + [K_f]$
$[K_s]$ = structural stiffness
$[K_f]$ = fluid elastic stiffness
$[Q]$ = excitation forces

Instability of the system can be studied by setting $\{Q\}$ equal to zero. It is obvious that the fluid elastic stiffness (K_f) and flow velocity-dependent damping (C_v) are the important parameters in a stability analysis. In general, C and K are not symmetric; therefore, the system may be subjected to different types of instability.

Divergence (Buckling). Divergence of circular cylinders is caused by fluid elastic force, such as steady drag or lift force for flow across circular cylinders, and fluid centrifugal force for pipes conveying fluid. Divergence is a static phenomenon; it is associated with the characteristics of the matrix K only. Buckling of a pipe conveying steady flow is a typical example of divergence.

Fluid-Damping-Controlled Instability. Fluid-damping-controlled instability is the instability caused by fluid damping force. when the flow velocity is increased, the modal damping of a mode becomes zero and the system loses stability. The instability of the system is attributed to the matrix C_v. Galloping of transmission lines is a typical example of instability controlled by fluid damping.

Fluid Elastic-Stiffness-Controlled Instability. When the matrix K is not symmetric, the system may become dynamically unstable. This type of in-

stability is defined as fluid elastic-stiffness-controlled instability. Flutter of cantilevered pipes conveying fluid and whirling of tube arrays subject to cross flow are of flutter type instability. The instability is attributed to fluid elastic force.

Parametric Instability. When the matrices M, C, or K are periodic functions of time, parametric resonance and/or combination resonance may occur. This type of instability has been observed in pipes conveying pulsating flow and two-phase flow.

19.5.2 Coupling Effect of Fluid

When circular cylinders vibrate in a fluid, the motion of a cylinder will affect other cylinders because of fluid coupling; therefore, all cylinders will respond as a group rather than as an individual structural element. This type of motion is called coupled vibration. Significant progress has been made in the characterization of fluid coupling and coupled modes; those include two cylinders, tube rows, and tube arrays (Chen, 1975; Chen and Chung, 1976; Lubin et al., 1977; Chen and Jendrzejczyk, 1978).

For a structural system oscillating in a still fluid, the fluid coupling effect may be taken into account using the added mass matrix $[M_f]$ and viscous damping matrix $[C_f]$. The added mass, in general, can be calculated by the potential flow theory. A summary of potential flow results, including formulas, graphs, and a computer program, is available (Chen and Chung, 1976). For small oscillations, viscous damping can be calculated based on the linearized viscous flow theory. some of the data available are summarized in a recent review (Chen, 1981b).

19.5.3 Parallel-Flow-Induced Instability

Parallel flow may be either internal or external (Benjamin, 1961; Paidoussis, 1970, 1975; Paidoussis and Deksnis, 1970; Chen, 1971; Holmes, 1978). In some cases, both internal and external flows may exist at the same time. A review of this problem, including a list of over 100 references, was published by Chen in 1974).

In parallel flow, M_f, C_v, and K_f are important in determining the critical flow velocity. C_v and K_f are in general not symmetric; therefore, the system may be subjected to divergence and dynamic instability. Many intriguing phenomena of parallel flow-induced instability have been investigated in detail:

1. Destabilizing effect of velocity-dependent forces is an interesting phenomenon. The critical flow velocity at which large cylinder oscillations occur obtained from the equation of motion in the absence of a velocity-dependent force is higher than the critical flow velocity obtained by including the velocity-dependent force and letting it approach zero (Chen, 1971). Experimental verification of the analytical result is difficult because any practical system possesses velocity-dependent force.
2. Divergence is possible for a cantilevered, articulated pipe conveying fluid (Benjamin, 1961), but it is not possible for a cantilevered continuous pipe (Paidoussis, 1970; Paidoussis and Deksnis, 1970). This implies that a discrete model may not always be used as a model for a continuous system.
3. The system may be destabilized by increasing structural stiffness. For example, a cantilevered pipe may become unstable by divergence by placing an additional constraint at the free end; it is stable without the additional restraint (Chen, 1971).
4. A small change in system parameters may result in significant effects on system characteristics: for example, the sharp change in the critical flow velocity with mass ratio.
5. The linear theory predicts that dynamic instability is possible for a pipe supported at both ends (Paidoussis, 1975), while nonlinear theory shows that such a system can become unstable by divergence only (Holmes, 1978).

The general dynamic characteristics of cylinders subject to parallel flow are generally understood. Recent studies have been directed toward periodic flows, two-phase flow, and curved pipes.

19.5.4 Cross-Flow-Induced Instability

When a cylinder array in a cross flow oscillates, the flow field is disturbed. In return, cylinder motion may be enhanced and becomes unstable. Extensive studies have been published to establish the stability limit (Connors, 1970; Blevins, 1974; Chen 1977a, 1980, 1981a,b). A brief review of this subject area is available (Chen, 1980).

Various forms of instability are possible, depending on whether C_v or K_f is dominant. When C_v is dominant, the instability of a cylinder is attributed to the fluid force associated with its own motion. In this case, the system possesses a classical mode. On the other hand, when K_f is dominant, the instability is attributed to the fluid elastic coupling among different cylinders. The instability mode is not a classical normal mode. In general, C_v is dominant for a heavy fluid while K_f is dominant for a light fluid (Chen, 1981a).

The threshold flow velocity is generally determined by the equation

$$\frac{V}{fD} = k\left(\frac{2\pi\zeta M}{\rho D}\right)^{\alpha} \tag{19.22}$$

where

M = cylinder mass
ρ = fluid density
f = cylinder natural frequency
D = cylinder diameter
ζ = modal damping ratio
V = flow velocity
α, k = constants

The constant α is found to be 0.5 in most cases; however, recent test results show that it varies from about 0.03 to 1.0. The constant k depends on tube arrangements and has been determined by many investigators; it varies from 1 to 10.

The mathematical model for a single tube in a tube row was developed initially by Connors (1970). Fluid elastic coupling of adjacent tubes for tube arrays was included later to improve the model (Blevins, 1974); critical flow velocity can be calculated if the instability mode is known. Further development of the model to include inertia, damping, and fluid elastic couplings has been proposed (Chen, 1981a). Based on the full coupled equation, instability modes as well as critical flow velocities can be calculated.

19.5.5 Design Guides for Stability of Cylinder Arrays in Fluid

Some of the general design guidelines that can be applied in design of system components consisting of a group of circular cylinders are discussed in this section.

Still Fluid. The effect of still fluid is to contribute to fluid added mass and fluid damping. A design guide for calculating the added mass of circular cylindrical structures is available (Chen and Chung, 1976). For a group of n cylinders, each cylinder can move in two directions, the order of added mass matrix is $2n$. Once the added mass is known, it can be incorporated in the equation of motion for calculating the natural frequencies and mode shapes of coupled cylinder/fluid vibration.

It has been shown that $[M_f]$ is a symmetric matrix (Chen, 1975); therefore, there are $2n$ eigenvalues. Let the eigenvalues be designated γ_i, $i = 1$ to $2n$. γ_i plays an important role for coupled vibration of cylinder arrays. For example, let the natural frequency of a group of identical cylinders in vacuum be f_v, and mass per unit length m. The natural frequencies for a single cylinder and multiple cylinders are as follows: For a single cylinder in infinite fluid

$$f_s = \frac{f_v}{(1 + m_d/m)^{1/2}} \qquad m_d = \text{displaced mass of fluid}$$

For the coupled vibration of multiple cylinders

$$f_c = \frac{f_v}{(1 + \gamma_i/m)^{1/2}} \qquad \gamma_i = \text{eigenvalue of the added mass matrix } M_f$$

For a group of n cylinders, there are $2n$ natural frequencies in a frequency band corresponding to a single natural frequency of a single cylinder; the mode shapes are the same as the eigenvectors of the added mass matrix.

Parallel Flow. Any type of instability in a structural system is considered to be unacceptable, as it may lead to catastrophic failure. Fortunately, the critical flow velocity is usually very high and is unlikely to occur in practical system components. In general, it is of no concern except when the cylinders are extremely flexible.

Analysis of the critical flow velocity can be made using Eq. 19.21. The system may lose stability by divergence (static instability) or dynamic instability. The calculation procedure is straightforward if the matrices in Eq. 19.21 are known. The exact critical flow velocity is more of academic interest. An estimate of the critical flow velocity can be made rather easily. Let the critical load of the corresponding single cylinder subjected to a compressive force be P_{cr}. The critical flow velocity for cylinder arrays subjected to parallel flow is given approximately by

$$V = \left(\frac{P_{cr} - pA}{\gamma_i}\right)^{1/2} \tag{19.23}$$

where γ_i is the eigenvalue of the added mass matrix, A the cylinder cross section, and p the fluid pressure. If the critical flow velocity calculated by this method is much higher than the required flow velocity, no further analysis is needed.

Cross Flow. Based on the available data, the lowest critical flow velocity is determined from the equation

$$\frac{U}{fD} = k\left(\frac{2\pi\zeta M}{\rho D^2}\right)^{\alpha} \tag{19.24}$$

The values of k and α depend on the tube arrangement; available experimental data are summarized in a recent report (Chen, 1981b).

19.6 SUDDENLY LOADED STRUCTURES

As already seen, the term *dynamic stability* encompasses many classes of problems and it has been used, by the various investigators, in connection with a particular study. Therefore, it is not surprising that there are various interpre-

tations of the meaning of the term. The class of problems falling in the category of parametric excitation are the best defined, conceived, and understood problems of dynamic stability.

Moreover, many authors refer to problems of the *follower force* type as problems of dynamic stability (Bolotin, 1963; Herrmann, 1967). The primary reason for this is that critical conditions can be obtained (in many cases) only through the use of the kinetic or dynamic approach to static stability problems (flutter instead of divergence type of instability). In addition, problems of aeroelastic instability and flow-induced instability also fall under the general heading of dynamic stability.

A large class of structural problems that has received attention recently and does qualify as a category of dynamic stability is that of impulsively loaded configurations and configurations which are suddenly loaded with loads of constant magnitude and infinite duration. These configurations under static loading are subject to either limit-point instability or bifurcation instability with unstable postbuckling branch (violent buckling). The two types of loads may be thought of as mathematical idealizations of blast loads of (1) large decay rates and small decay times, and (2) small decay rates and large decay times, respectively. For these loads, the concept of dynamic instability is related with the observation that for sufficiently small values of the loading the system simply oscillates about the near-static equilibrium point and the corresponding amplitudes of oscillation are sufficiently small. If the loading is increased, some systems will experience large-amplitude oscillations or, in general, divergent type of motion. For this phenomenon to happen the configuration must possess two or more static equilibrium positions and "tunneling through" (Hsu, 1966) occurs by having trajectories that can pass through an unstable static equilibrium point. Consequently, the methodologies developed by the various investigators are for structural configurations that exhibit snap-through buckling when loaded quasistatically.

Solutions to such problems started appearing in the open literature in the early 1950s. Hoff and Bruce (1954) considered the dynamic instability of a pinned half-sine arch under a half-sine distributed load. In studying the axisymmetric behavior of a shallow spherical cap under suddenly applied loads, Budiansky and Roth (1962) defined the load to be critical, when the transient response increases suddenly with very little increase in the magnitude of the load. This concept was adopted by numerous investigators (Simitses, 1974) in the subsequent years because it is tractable to computer solutions. Conceptually, one of the best efforts in the area of dynamic buckling, under impulsive and suddenly applied loads, is the work of Hsu and his collaborators (1966, 1967). In his studies, he defined sufficiency conditions for stability and sufficiency conditions for instability, thus finding upper and lower bounds for the critical impulse or critical sudden load. Independently, Simitses (1965) in dealing with the dynamic buckling of shallow arches and spherical caps termed the lower bound as a minimum possible critical load (MPCL) and the upper bound as a minimum guaranteed critical load (MGCL). Finally, there exist a few reported investigations for the case of suddenly loaded systems with constant loads and finite duration (Zimcik and Tennyson, 1979; Simitses, 1980, 1982). Note that this entire class of problems falls in the category of dynamic analysis of conservative systems.

The concepts and methodologies used in estimating critical conditions are as follows:

1. *Equations-of-motion approach* (Budiansky and Roth, 1962). The equations of motion are (numerically) solved for various values of the load parameter (ideal impulse or sudden load), thus obtaining the system response. The load parameter, at which there exists a large (finite) change in the response, is called critical.

2. *Total energy–phase plane approach* [Hoff–Hsu (Hoff and Bruce, 1954; Hsu, 1966, 1967; Hsu et al., 1968)]. Critical conditions are related to characteristics of the system phase plane, and the emphasis is on establishing sufficient conditions for stability (lower bounds) and sufficient conditions for instability (upper bounds).

3. *Total potential energy approach* [Hoff–Simitses (Hoff and Bruce, 1954; Simitses, 1974, 1980, 1982)]. Critical conditions are related to characteristics of the system total potential. Through this approach, also, lower and upper bounds of critical conditions are established. This last approach is applicable to conservative systems only. The concepts and procedure related to the last approach are next explained, with some detail.

19.6.1 Concepts and General Procedure

The concept of dynamic stability is best explained through a single-degree-of-freedom system. First the case of ideal impulse is treated and then the case of constant load of infinite duration.

Ideal Impulse. Consider a single-degree-of-freedom system for which the total potential (under zero load) curve is plotted versus the generalized coordinate (independent variable) θ (see Fig. 19.2). Clearly, points A, B, C denote static equilibrium points and point B denotes the initial position ($\theta = 0$) of the system.

Since the system is conservative, the sum of the total potential, $\bar{U}_T^0$ (under zero load) and the kinetic energy, T^0 is the constant C, or

$$\bar{U}_T^0 + T^0 = C \tag{19.25}$$

Moreover (see Fig. 19.2), since $\bar{U}_T^0$ is zero at the initial position ($\theta = 0$), the constant C, can be related to some initial kinetic energy, T_i^0. Then

$$\bar{U}_T^0 + T^0 = T_i^0 \tag{19.26}$$

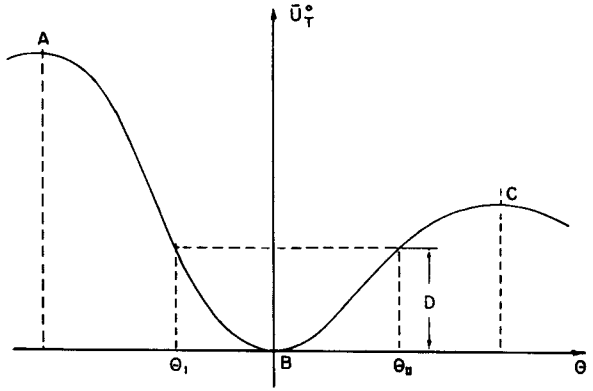

Fig. 19.2 Zero-load total potential curve.

Next, consider an ideal impulse applied to the system. Through the impulse-momentum theorem, the impulse is related to the initial kinetic energy T_i^0. Clearly, if T_i^0 is equal to D (see Fig. 19.2), or $\bar{U}_T^0(\Theta_{II})$, the system will simply oscillate between Θ_I and Θ_{II}. On the other hand, if the initial kinetic energy, T_i^0, is equal to the value of the total potential at the unstable static equilibrium point C, $U_T^0(C)$, then the system can reach point C with zero velocity ($T^0 = 0$), and there exists a possibility of motion escaping (passing position C) or becoming unbounded. Such a motion is termed *buckled motion* by Simitses (1965). In the case for which motion is bounded and the path may include the initial point (B), the motion is termed *unbuckled motion*. Through this, both a concept of dynamic stability is presented, and the necessary steps for estimating critical impulses are suggested. Note that once the unstable static equilibrium positions (points A and C) are established, the critical initial kinetic energy is estimated by

$$T_{i_{cr}}^0 = \bar{U}_T^0(C) \tag{19.27}$$

Moreover, since T_i^0 is related to the ideal impulse, the critical impulse is estimated through Eq. 19.27. Observe that an instability of this type can occur only when the system under zero load possesses unstable static equilibrium points. Furthermore, if position C corresponds to a very large and thus unacceptable position θ (from physical considerations), one may still use this concept and estimate a maximum allowable (and therefore critical) ideal impulse. For example, if one restricts motion to the region between Θ_I and Θ_{II}, the maximum allowable ideal impulse is obtained from Eq. 19.27 but with D or $\bar{U}_T^0(\Theta_{II})$ replacing $\bar{U}_T^0(C)$. Because of this, a critical or an allowable ideal impulse can be obtained for all systems (including those that are not subject to buckling under static conditions such as beams, shafts, etc.).

For multi-degree-of-freedom systems, it is possible to use the same concept of dynamic stability and procedure for estimating critical conditions, but with one exception. For these systems, critical conditions can be bracketed between lower and upper bounds (see Hsu, 1966, 1967; Simitses, 1974, 1980). One final comment for the case of ideal impulse: Note from Fig. 19.2, in the absence of damping (as assumed), the direction of the ideal impulse is immaterial. If the system is loaded in one direction (say that the resulting motion corresponds to positive θ), a critical condition exists when the system reaches position C with zero kinetic energy. If the system is loaded in the opposite direction, some negative θ position will be reached with zero kinetic energy; after that the direction of the motion will reverse, and finally the system will reach position C with zero kinetic energy. Both of these phenomena will occur for the same value of the ideal impulse.

Constant Load of Infinite Duration. Consider again a single-degree-of-freedom system. Total potential curves are plotted versus the generalized coordinate θ on Fig. 19.3. Note that the various curves correspond to different load values, P_i. The index i varies from 1 to 5 and the magnitude of the load increases with increasing index value. These curves are typical of systems that for each load value, contain at least two static equilibrium points, A_i and B_i. This is the case when the system is subject to limit point instability and/or bifurcational buckling with unstable branching under static application of the load (shallow arches and spherical caps, perfect or imperfect cylindrical and spherical shells, two-bar frames, etc.)

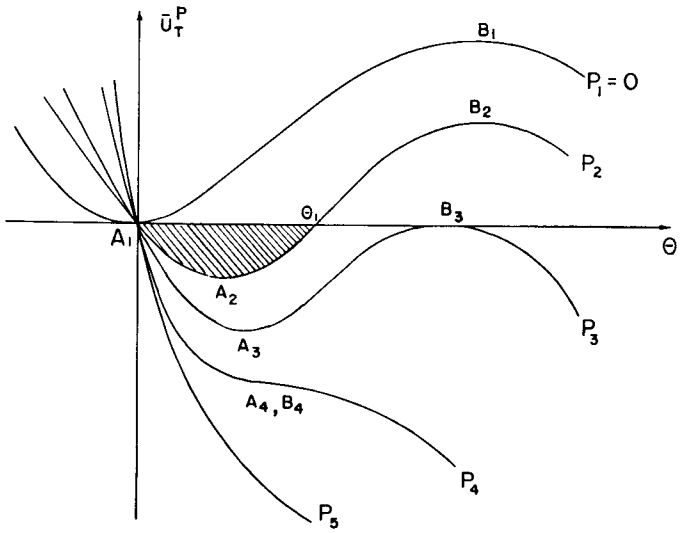

Fig. 19.3 Total potential curves for various loads.

Given such a system, one applies a given load suddenly with constant magnitude and infinite duration. For a conservative system,

$$\bar{U}_T^P + T^P = C \tag{19.28}$$

The potential may be defined in such a way that it is zero at the initial position ($\theta = 0$). In such case, the constant is zero, or

$$\bar{U}_T^P + T^P = 0 \tag{19.29}$$

Since the kinetic energy is a positive-definite function of the generalized velocity, motion is possible when the total potential is nonpositive (shaded area, on Fig. 19.3, for P_2). From this it is clear that for small values of the applied load, the system simply oscillates about the mean static equilibrium position. This is also an observed physical phenomenon. As the load increases, the total potential at the unstable point B_i decreases, it becomes zero (point B_3), and then it increases negatively until points A_i and B_i (A_4, B_4) coincide (the corresponding load, P_4, denotes the limit point under static loading). For loads higher than this (P_4), the stationary points (static equilibrium positions) disappear from the neighborhood. When the sudden load reaches the value corresponding to P_3, a critical condition exists because the system can reach position B_3 with zero kinetic energy and then move toward larger θ values ("buckled motion" can occur). Thus P_3 is a measure of the critical condition. Note that the value P_3 is smaller than the value of the limit point, P_4. This implies that the critical load under sudden application (infinite duration) is smaller than the corresponding static critical load.

In this case, also, one may wish to limit the dynamic response of the system to a value smaller than B_3 (see Fig. 19.3), say I. Then the maximum allowable (critical dynamic) load corresponds to P_2. Note that in multi-degree-of-freedom systems, one may easily establish upper and lower bounds for the critical dynamic load (see Hsu, 1966, 1967, 1968; Hsu et al, 1968; Simitses, 1965, 1980, 1982).

The foregoing concept has been extended to the case of suddenly loaded systems with constant load and finite duration (Simitses, 1965, 1980). Moreover, the effect of static preloading on the critical dynamic conditions has been investigated (Simitses, 1982).

REFERENCES

Abrahamson, G. R., and Goodier, J. N. (1966), "Dynamic Flexural Buckling of Rods, Within an Axial Plastic Compression Wave," *Trans. ASME J. Appl. Mech.*, Vol. 33, No. 2, pp. 241–247.

Alwar, R. S., and Reddy, B. S. (1979), "Dynamic Buckling of Isotropic and Orthotropic Shallow Spherical Cap with Circular Hole," *Int. J. Mech. Sci.*, Vol. 21, pp. 681–688.

Amiro, I. Y. (1979), "Critical Values of Compressive Forces Which Increase Rapidly with Time," *Sov. Appl. Mech.*, Vol. 15, No. 5, pp. 403–407 (translation).

Ariaratnam, S. T., and Sankar, T. S. (1968), "Dynamic Snap-Through of Shallow Arches Under Stochastic Loads," *AIAA J.*, Vol. 6, No. 5, pp. 798–802.

Ari-Gur, J., Weller, T., and Singer, J. (1980), "Experimental and Theoretical Studies of Columns Under Axial Impact," *15th Int. Congr. Theor. Appl. Mech.*, IUTAM, Toronto, Ontario, Canada.

Ball, R. E. (1975), "Dynamic Buckling of Structures," in *Shock and Vibration Computer Programs: Reviews and Summaries* (ed. W. Pilkey and B. Pilkey), Shock and Vibration Information Center, Washington, D.C., pp. 299–321.

Belytschko, T. (1976a), "A Survey of Numerical Methods and Computer Programs for Dynamic Structural Analysis," *Nucl. Eng. Des.*, Vol. 37, No. 1, pp. 23–34.

Belytschko, T. (1976b), "Computer Methods in Shock Wave Propagation Analysis," in *Computing in Applied Mechanics* (ed. R. F. Hartung), Applied Mechanics Symposia Series, AMD-18, American Society of Mechanical Engineers, New York, pp. 139–161.

Belytschko, T., Schwer, L., and Klein, M. J. (1977), "Large Displacement, Transient Analysis of Space Frames," *Int. J. Numer. Methods Eng.*, Vol. 11, pp. 65–84.

Benjamin, T. B. (1961), "Dynamics of a System of Articulated Pipes Conveying Fluid," *Proc. R. Soc.*, Vol. A261, pp. 457–499.

Blevins, R. D. (1974), "Fluid Elastic Whirling of a Tube Row," *Trans. ASME, J. Press. Vessel Tech.*, Vol. 96, No. 4, pp. 263–267.

Blevins, R. D. (1977), *Flow-Induced Vibration*, Van Nostrand Reinhold, New York.

Bolotin, V. V. (1963), *Nonconservative Problems of the Theory of Elastic Stability*, Moscow, 1961; English translation, Pergamon Press, Elmsford, N.Y.

Bolotin, V. V. (1964), *Dynamic Stability of Elastic Systems*, Holden-Day, San Francisco.

Bolotin, V. V. (1968), "Parametric Vibrations of Elastic Systems," *Prochost, 'Ustoichivost,' Kolebania*, Vol. 3 (ed. I. A. Birger and L. G. M. Panovko), Mashinostroenie, Moscow, Chap. 6.

Budiansky, B., and Roth, R. S. (1962), "Axisymmetric Dynamic Buckling of Clamped Shallow Spherical Shells," Collected Papers on Instability of Shell Structures, *NASA Techn. Note No. D-1510.*

Chawla, J. P. (1951), "Numerical Analysis of the Process of Buckling of Elastic and Inelastic Columns," *Proc. First U.S. Natl. Congr. Appl. Mech.*, June 11–16, pp. 435–441.

Chen, S. S. (1971), "Flow-Induced Instability of an Elastic Tube," *ASME Pap. 71-Vibr-39.*

Chen, S. S. (1974), "Parallel Flow-Induced Vibrations and Instabilities of Cylindrical Structures," *Shock Vib. Dig.*, Vol. 6, No. 10, pp. 1–11.

Chen S. S. (1975), "Vibration of Nuclear Fuel Bundles," *Nucl. Eng. Des.*, Vol. 35, No. 3, pp. 399–422.

Chen, S. S. (1977a), "A Mathematical Model for Cross-Flow-Induced Vibrations of Tube Rows," *3rd Int. Conf. Press. Vessel Tech.*, Part 1, pp. 415–426.

Chen, S. S. (1977b), "Flow-Induced Vibrations of Circular Cylindrical Structures," *Shock Vib. Dig.*, Vol. 9, No. 10, pp. 25–38; Vol. 9, No. 11, pp. 21–27.

Chen, S. S. (1980), "Cross-Flow-Induced Instabilities of Circular Cylinders," *Shock Vib. Dig.*, Vol. 12, No. 5, pp. 21–34.

Chen, S. S. (1981a), "Design Guide for Calculating the Instability Flow Velocity of Tube Arrays in Crossflow," *Tech. Memo. ANL-CT-81-40*, Argonne National Laboratory, Argonne, Ill., Dec.

Chen, S. S. (1981b), "Fluid Damping for Circular Cylindrical Structures," *Nucl. Eng. Des.*, Vol. 63, No. 1, pp. 81–100.

Chen, S. S., and Bernstein, M. D., eds. (1979), "Flow Induced Vibrations," *3d Natl. Congr. Press. Piping Technol.*, San Francisco, June.

Chen, S. S., and Chung, H. (1976), "Design Guide for Calculating Hydrodynamic-Mass: Part I. Circular Cylindrical Structures," *Tech. Memo. ANL-CT-76-45*, Argonne National Laboratory, Argonne, Ill.

Chen, S. S., and Jendrzejczyk, J. A. (1978), "Experiments on Fluidelastic Vibration of Cantilevered Tube Bundles," *Trans. ASME J. Mech. Des.*, Vol. 110, pp. 540–548.

Chenoweth, J. M., and Kistler, R. S. (1976), "Tube Vibrations in Shell-and-Tube Heat Exchanger," *Tech. Rep.*, Heat Transfer Research, Inc.

Connors, H. J. (1970), "Fluidelastic Vibration of Tube Arrays Excited by Cross-Flow," *Symp. Flow-Induced Vib. Heat Exch. ASME Winter Annu. Meet.*, pp. 42–56.

Davidson, J. F. (1953), "Buckling of Struts Under Dynamic Loading," *J. Mech. Phys. Solids*, Vol. 2, pp. 54–66.

Elishakoff, I. (1978a), "Axial Impact Buckling of a Column with Random Initial Imperfections," *Trans. ASME J. Appl. Mech.*, Vol. 45, No. 2, pp. 361–365.

Elishakoff, I. (1978b), "Impact Buckling of Thin Bar via Monte Carlo Method," *Trans. ASME, J. Appl. Mech.*, Vol. 45, No. 3, pp. 586–590.

Erickson, B., Nardo, S. V., Patel, S. A., and Hoff, N. J. (1956), "An Experimental Investigation of the Maximum Loads Supported by Elastic Columns in Rapid Compression Tests," *Proc. Soc. Exp. Stress Anal.*, Vol. 14, No. 1, pp. 13–20.

Gerard, G., and Becker, H. (1952), "Column Behavior Under Conditions of Impact," *J. Aeronaut. Sci.*, Vol. 19, No. 1, pp. 58–60.

Goldsmith, W. (1960), *Impact: The Theory and Physical Behavior of Colliding Solids*, Edward Arnold, London.

Goldstein, S. (1965), *Modern Developments in Fluid Dynamics*, Dover, New York.

Gregory, W. E., Jr., and Plaut, R. H. (1982), "Dynamic Stability Boundaries for Shallow Arches," *ASCE J. Eng. Mech. Div.*, Vol. 108, No. EM6, pp. 1036–1050.

Grybos, R. (1975), "Impact Stability of a Bar," *Int. J. Eng. Sci.*, Vol. 13, No. 5, pp. 463–477.

Hartz, B. J., and Clough, R. W. (1957), "Inelastic Response of Columns to Dynamic Loadings," *ASCE J. Eng. Mech. Div.*, Vol. 83, No. EM2, Pap. No. 1213.

Hayashi, T., and Sano, Y. (1972a), "Dynamic Buckling of Elastic Bars: First Report. The Case of Low Velocity Impact," *Bull. JSME*, Vol. 15, No. 88, pp. 1167–1175.

Hayashi, T., and Sano, Y. (1972b), "Dynamic Buckling of Elastic Bars: Second Report. The Case of High Velocity Impact," *Bull, JSME*, Vol. 15, No. 88, pp. 1176–1184.

Herrmann, G. (1967), "Stability of Equilibrium of Elastic Systems Subjected to Nonconservative Forces," *Appl. Mech. Rev.*, Vol. 20, pp. 103–108.

Hoff, N. J. (1951), "The Dynamics of the Buckling of Elastic Columns," *AMSE J. Appl. Mech.*, Vol. 18, No. 1, pp. 68–74.

Hoff, N. J., and Bruce, V. C. (1954), "Dynamic Analysis of the Buckling of Laterally Loaded Flat Arches," *J. Math. Phys.*, Vol. 32, pp. 276–388.

Hoff, N. J., Nardo, S. V., and Erickson, B. (1951), "The Maximum Load Supported by an Elastic Column in a Rapid Compression Test, *Proc. First U.S. Natl. Congr. Appl. Mech.*, June 11–16, pp. 419–423.

Holmes, P. J. (1978), "Pipes Supported at Both Ends Cannot Flutter," *Trans. ASME J. Appl. Mech.*, Vol. 45, No. 3, pp. 619–622.

Holzer, S. M. (1970), "Stability of Columns with Transient Loads," *ASCE J. Eng. Mech. Div.*, Vol. 96, No. EM6, pp. 913–930.

Holzer, S. M. (1971), "Response Bounds for Columns with Transient Loads," *Trans. ASME J. Appl. Mech.*, Vol. 38, No. 1, pp. 157–161.

Holzer, S. M. (1976), "Dynamic Stability of Elastic Imperfection-Sensitive Shells," *Shock Vib. Dig.*, Vol. 8, No. 4, pp. 3–10.

Holzer, S. M. (1979), "Dynamic Snap-Through of Shallow Arches and Spherical Caps," *Shock Vib. Dig.*, Vol. 11, No. 3, pp. 3–6.

Holzer, S. M., and Eubanks, R. A. (1969), "Stability of Columns Subject to Impulsive Loading," *ASCE J. Eng. Mech. Div.*, Vol. 95, No. EM4, pp. 897–920.

Housner, G. W. and Tsu, W. K. (1962), "Dynamic Behavior of supercritically Loaded Struts," *ASCE J. Eng. Mech. Div.*, Vol. 88, No. EM5, pp 41–65

Hsu, C. S. (1966), "On Dynamic Stability of Elastic Bodies with prescribed Initial Conditions," *Int. J. Eng. Sci.*, Vol. 4, pp. 1–21.

Hsu, C. S. (1967), "The Effects of Various Parameters on the Dynamic Stability of a Shallow Arch," *J. Appl. Mech.*, Vol. 34, No. 2, pp. 349–356.

Hsu, C. S. (1972), "Impulsive Parametric Excitation: Theory," *J. Appl. Mech.*, Vol. 39, pp. 551–558.

Hsu, C. S., Kuo, C. T., and Lee, S. S. (1968), "On the Final States of Shallow Arches on Elastic Foundations Subjected to Dynamic Loads," *J. Appl. Mech.*, Vol. 35, No. 4, pp. 713–723.

Huang, N. C. 91972), "Dynamic Buckling of Some Elastic Shallow Structures Subject to Periodic Loading with High Frequency," *Int. J. Solids Struct.*, Vol. 8, No. 3, pp. 315–326.

Huang, N. C., and Nachbar, W. (1968), "Dynamic Snap-Through of Imperfect Viscoelastic Shallow Arches," *J. Appl. Mech.*, Vol. 35, No. 2, pp. 289–296.

Huang, K.-Y, and Plaut, R. H. (1981), "Snap-through of a Shallow Arch Under Pulsating Load," in *Stability in the Mechanics of Continua* (ed. F. H. Schroeder), Proc. IUTAM Symp., Numbrecht, Germany, Aug. 30–Sept. 4, Springer-Verlag, Berlin.

Huffington, N. J., Jr. (1963), "Response of Elastic Columns to Axial Pulse Loading," *AIAA J.*, Vol. 1, No. 9, pp. 2099–2104.

Hughes, T. J. R. (1980), "Recent Developments of Computer Methods for Structural Analysis," *Nucl. Eng. Des.*, Vol. 57, No. 2, pp. 427–439.

IAEA (1977), "Summary Report: Specialists Meetings on LMFBR Flow Induced Vibrations," *IAEA IWGFR/21*, International Atomic Energy Agency, Argonne, Ill., September.

Ibrahim, R. A., Barr, A. D. S., Roberts, J. M. (1978), "Parametric Resonance Parts 1 to 5," *Shock Vib. Dig.*, Vol. 10, Nos. 1 to 5.

Johnson, E. R. (1980), "The Effect of Damping on Dynamic Snap-through," *J. Appl. Mech.*, Vol. 47, No. 3, pp. 601–606.

Junger, M., and Feit, D. (1972), *Sound, Structures and Their Interaction*, MIT Press, Cambridge, Mass.

Kao, R. (1980), "Nonlinear Dynamic Buckling of Spherical Caps with Initial Imperfections," *Comput. Struct.*, Vol. 12, No. 1, pp. 49–63.

Kao, R., and Perrone, N. (1978), "Dynamic Buckling of Axisymmetric Spherical Caps with Initial Imperfections," *Comput. Struct.*, Vol. 9, pp. 463–473.

King, R. (1977), "A Review of Vortex Shedding Research and Its Applications," *Ocean Eng.*, Vol. 4, pp. 141–171.

Kiryukhin, L. V., and Malyi, V. I. (1974), "Buckling of an Elastic Bar Under Longitudinal Impact," *Moscow Univ. Mech. Bull.*, Vol. 29, No. 3, pp. 24–28 (translation).

Koning, C., and Taub, J. (1934), "Impact Buckling of Thin Bars in the Elastic Range Hinged at Both Ends," NACA *Tech. Memo. No.* 748.

Kornev, V. M. (1968), "Modes of Stability Loss in an Elastic Rod Under Impact," *J. Appl. Mech. Tech. Phys.*, Vol. 9, No. 3, pp. 275–277.

Kornev, V. M. (1974), "Asymmetric Analysis of the Behavior of an Elastic Bar Under A Periodic Intensive Loading," *J. Appl. Mech. Tech. Phys.*, Vol. 13, No. 3, pp. 398–406 (translation).

Kornhauser, M. (1964), *Structural Effects of Impact*, Spartan Books, New York.

Krajcinovic, D., and Herrmann, G. (1968), "Parametric Resonance of Straight Bars Subjected to Repeated Impulsive Compression," *AIAA J.*, Vol. T, No. 10.

Lee, L. H. N. (1978), "Quasi-bifurcation of Rods within an Axial Plastic Compressive Wave," *Trans. ASME J. Appl. Mech.*, Vol. 45, No. 1, pp. 100–104.

Lee, L. H. N. (1981), "Dynamic Buckling of an Inelastic Column," *Int. J. Solids Struct.*, Vol. 17, No. 3, pp. 271–279.

Lindberg, H. E. (1965), "Impact Buckling of a Thin Bar," *Trans. ASME J. Appl. Mech.*, Vol. 32, No. 2, pp. 315–322.

Lubin, B. T., Haslinger, K. H., Puri, A., and Goldberg, J. E. (1977), "Experimental Data on Natural Frequency of a Tube Array," *Am. Soc. Mech. Eng. Pap. No. 77-FE-10.*

Malyi, V. I. (1972), "Long-Wave Approximation in Problems of Stability Loss Under Impact," *Mech. Solids*, Vol. 7, No. 4, pp. 120–125 (translation).

Malyi, V. I. (1973), "Buckling of a Rod Under Longitudinal Impact: Small Deflections," *Mech. Solids*, Vol. 8, No. 4, pp. 162–166 (translation).

Malyi, V. I., and Efimov, A. B. (1972), "Stability Loss of a Rod in Longitudinal Impact," *Sov. Phys. Dokl.*, Vol. 17, No. 2, pp. 176–177.

Malyshev, B. M. (1966), "Stability of Columns Under Impact Compression," *Mech. Solids*, Vol. 1, No. 4, pp. 86–89 (translation).

McIvor, I. K. (1964), "Dynamic Stability of Axially Vibrating Columns," *ASCE J. Eng. Mech. Div., ASCE*, Vol. 90, No. EM6, pp. 191–210.

McIvor, I. K., and Bernard, J. E. (1973), "The Dynamic Response of Columns Under Short Duration Axial Loads," *Trans. ASME J. Appl. Mech.*, Vol. 40, No. 3, pp. 688–692.

McLachlan, N. W. (1947), *Theory and Application of Mathieu Functions*, Oxford University Press, London.

Meier, J. H. (1945), "On the Dynamics of Elastic Buckling," *J. Aeronaut. Sci.*, Vol. 12, No. 4, pp. 433–440.

Mescall, J., and Tsui, T. (1971), "Influence of Damping on the Dynamic Stability of Spherical Caps Under Step Pressure Loading," *AIAA J.*, Vol. 9, No. 7, pp. 1244–1248.

Mettler, E. (1962), "Dynamic Buckling," *Handbook of Engineering Mechanics* (ed. W. Flugge), McGraw-Hill, New York, Chap. 62.

Mulcahy, T. M., and Chen, S. S. (1974), "Annotated Bibliography on Flow-Induced Vibrations," *Tech. Memo. ANL-CT-74-05*, Argonne National Laboratory, Argonne, Ill., Jan.

Mulcahy, T. M., and Wambsganss, M. W. (1976), "Flow-Induced Vibration of Nuclear Reactor System Components," *Shock Vib. Dig.*, Vol. 8, No. 7, pp. 33–45.

Naudascher, E., ed. (1972), "Flow-Induced Structural Vibrations," *IUTAM-IAHR Symp.*, Karlsruhe, Germany, Springer-Verlag, Berlin.

Naudascher, E., and Rockwell, D., eds. (1980), *Practical Experiences with Flow-Induced Vibrations*, Springer-Verlag, Berlin.

Nemat-Nasser, S. (1972), "On the Stability of Nonconservative Systems," in *Stability* (ed. H. H. E. Leipholz), Canada Study No. 6, University of Waterloo, Waterloo, Ontario, Canada.

Paidoussis, M. P. (1970), "Dynamics of Tubular Cantilevers Conveying Fluid," *J. Mech. Eng. Sci.*, Vol. 12, No. 2, pp. 85–103.

Paidoussis, M. P. (1975), "Flutter of Conservative System of Pipes Conveying Incompressible Fluid," *J. Mech. Eng. Sci.*, Vol. 17, No. 1, pp. 19–25.

Paidoussis, M. P., and Deksnis, E. B. (1970), "Articulated Models of Cantilevers Conveying Fluid: The Study of a Paradox," *J. Mech. Eng. Sci.*, Vol. 12, No. 4, pp. 288–300.

Pi, H. N., Ariaratnam, S. T., and Lennox, W. C. (1971), "First-Passage Time for the Snap-Through of a Shell-Type Structure," *J. Sound Vib.*, Vol. 14, No. 3, pp. 375–384.

Plaut, R. H. (1971), "Displacement Bounds for Beam-Columns with Initial Curvature Subjected to Transient Loads," *Int. J. Solids Struct.*, Vol. 7, No. 9, pp. 1229–1235.

Scanlan, R. H., and Simiu, E. (1978, 1996), *Wind Effects on Structures: An Introduction to Wind Engineering*, Wiley, New York.

Scanlan, R. H., and Wardlaw, R. L. (1973), "Reduction of Flow-Induced Structural Vibrations," *ASME Colloq. Isol. Mech. Vib. Impact Noise*, Cincinnati, Ohio, pp. 35–63.

Schmdit, G. (1975), *Parametererregte Schwingungen*, Deutscher Verlag der Wissenschaften, Berlin.

Schmitt, A. F. (1956), "A Method of Stepwise Integration in Problems of Impact Buckling," *ASME J. Appl. Mech*, Vol. 23, No. 2, pp. 291–294.

Sevin, E. (1960), "On the Elastic Bending of Columns Due to Dynamic Axial Forces Including Effects of Axial Inertia," *Trans. ASME J. Appl. Mech.*, Vol. 27, No. 1, pp. 125–131.

Shin, Y. S., and Wambsganss, M. W. (1975), "Flow-Induced Vibration in LMFBR Steam Generators: A State-of-the-Art Review," *Tech. Memo. ANL-75-16*, Argonne National Laboratory, Argonne, Ill.

Simitses, G. J. (1965), "Dynamic Snap-Through Buckling of Low Arches and Shallow Caps," Ph.D. dissertation, Department of Aeronautics and Astronautics, Stanford University, Stanford, Calif.

Simitses, G. J. (1974), "On the Dynamic Buckling of Shallow Spherical Caps," *J. Appl. Mech.*, Vol. 41, No. 1, pp. 299–300.

Simitses, G. J. (1980), "Dynamic Stability of Structural Elements Subjected to Step-Loads," *Proc. Army Symp. Solid Mech.*, Designing for Extremes: Environment, Loading, and Structural Behavior, South Yarmouth, Cape Cod, Mass., Sept. 30–Oct. 2, pp. 87–107.

Simitses, G. J. (1982), "Effect of Static Preloading on the Dynamic Stability of Structures," *Proc. AIAA/ASME/ASCE/AHS 23rd Struct., Struct. Dyn, Mater, Conf.*, New Orleans, La., Part 2, pp. 299–307.

Suzuki, S. I. (1969), "Effects of Solid Viscosities, Loading Velocities, and Initial Deflections to Dynamic Buckling Loads of a Column," *Aeronaut. J.*, Vol. 73, No. 706, pp. 890–894.

Taub, J. (1934), "Impact of Buckling of Thin Bars in the Elastic Range for Any End Condition," *NACA Tech. Memo. No. 749.*

Von Kármán, T., and Duwez, P. (1950), "The Propagation of Plastic Deformation in Solids," *J. Appl. Phys.*, Vol. 12, pp. 987–994.

Yamamoto, T., and Saito, A. (1970), "On the Vibrations of 'Summed and Differential Types' Under Parametric Excitation," *Mem. Fac. Eng. Nagoya Univ.*, Japan, pp. 54–123.

Zimcik, D. G., and Tennyson, R. C. (1979), "Stability of Circular Cylindrical Shells Under Transient Axial Impulsive Loading," *Proc. AIAA/ASME/ASCE/AHS 20th Struct. Struct. Dyn. Mater. Conf.*, St. Louis, Mo., Apr. A4–6, pp. 275–281.

CHAPTER TWENTY

STABILITY UNDER SEISMIC LOADING

20.1 INTRODUCTION

Earthquake ground motion at a given location can be characterized by three components of displacement, velocity or acceleration—two horizontal and one vertical—which are distributed in a more-or-less random manner in the time domain, albeit with certain dynamic characteristics. The vertical ground motion for most building structures does not seem to be too critical because of larger inherent reserve strengths in that direction. Therefore, for practical design purposes the horizontal components of ground motion are of most interest to determine the levels of inertia forces induced. A typical earthquake ground acceleration record is shown in Fig. 20.1.

It is well understood that seismic forces on a structure depend on the dynamic characteristics of the ground motion and of the structure. A *response spectrum* is a very useful practical tool in the seismic design of structures and the development of building codes. A response spectrum is a graph showing ordinates of maximum absolute value of a response parameter of a single-degree-of-freedom oscillator with the given damping plotted against its natural period or frequency. The response parameter that is of most design significance is the maximum absolute acceleration (spectral acceleration), which when multiplied by the mass gives the maximum inertia force. Shown in Fig. 20.2 are typical elastic acceleration response spectra due to a few strong ground motion records. In engineering terminology, an ordinate of the acceleration spectrum represents the elastic strength demand in terms of acceleration that needs to be multiplied by the seismically effective mass.

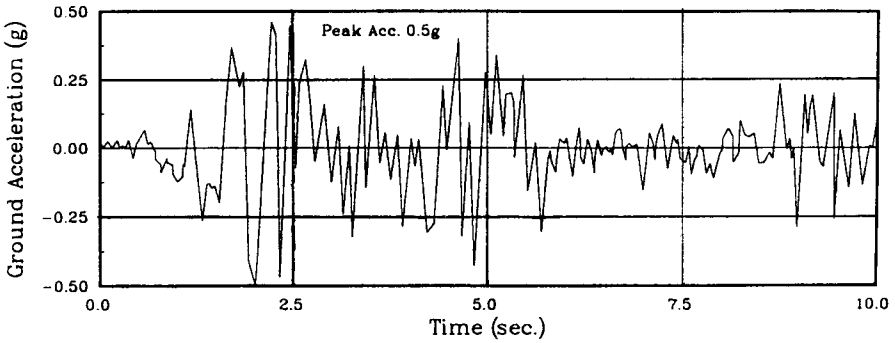

Fig. 20.1 Typical earthquake ground acceleration record.

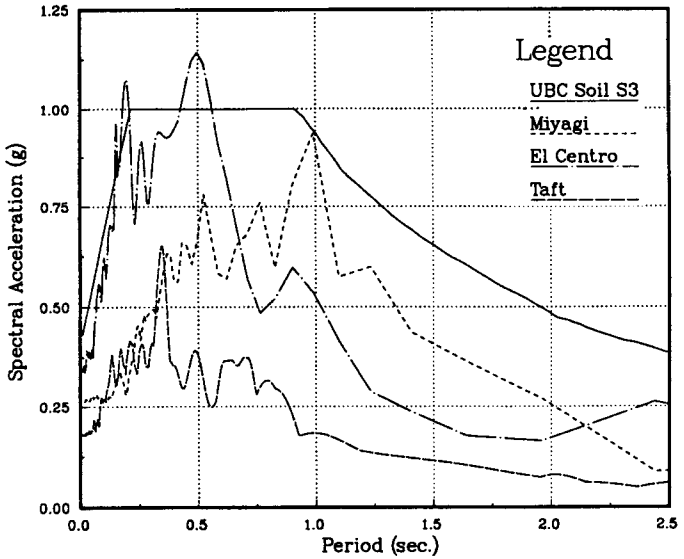

Fig. 20.2 Typical elastic acceleration response spectra.

When scaled to the expected ground motion peak values, acceleration spectra of the type shown in fig. 20.2 smoothed to account for variations in frequency content and modified by judgment to account for higher-mode effects, are used by codes to define the seismic strength demand presuming that the structure responds elastically, Fig. 20.3. The peak values of elastic acceleration response spectral ordinates due to strong earthquake ground motions typically range in the neighborhood of $1.0g$ and may be as high as 2 to $3g$. Clearly, designing common structures to remain elastic for such large lateral forces would be extremely uneconomical. Therefore, code-specified lateral design forces are reduced from these levels. This reduction is achieved by

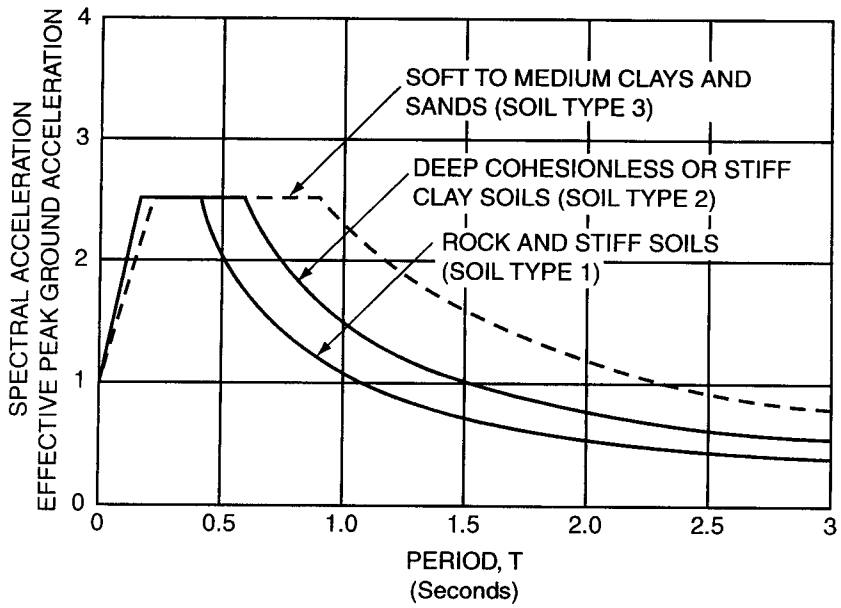

Fig. 20.3 Code-defined seismic strength demand.

dividing the required elastic force demands by response reduction factors such as R_w (typically ranging from 6 to 12; ICBO, 1994) or R (typically ranging from 5 to 8; NEHRP, 1994). Such reduced seismic design forces imply that a typical code-designed structure would remain serviceable (essentially elastic) during smaller frequent earthquakes, and safety and survival of the structure during a major earthquake will have to depend on the ability of the structure to deform inelastically. Thus, during a major earthquake, structures are typically expected to undergo large reversed cyclic deformations, thereby dissipating large amounts of earthquake input energy. This energy dissipation generally has a dampening effect on the response of the structure. The magnitude of the design forces, through factors such as R_w or R, is adjusted to reflect the inelastic performance of the structure. Systems with good inelastic behavior under large reversed cyclic deformations are assigned smaller design forces, and vice versa.

Ensuring the stability of structures in the context of current design practice is a rather complex issue. The structures must survive cyclic deformations involving large material as well as geometric nonlinearities, yet the design process is carried out at "fictitious" force levels, assuming elastic behavior without explicitly requiring inelastic response calculations under representative strong ground motions. In this chapter we discuss stability considerations from global (structural) to local (element) levels in current design practice in view of more realistic behavior characteristics of structures when subjected to major earthquakes.

The proceedings of a U.S.–Japan joint seminar on the stability and ductility of steel structures under cyclic loading held in Osaka, Japan, July 1–3, 1991 (Fukumoto and Lee, 1991) contain state-of-the-art discussions on various topics that affect the ductility and stability of steel structures and their components under seismic or other dynamic effects.

20.2 OVERALL SYSTEM STABILITY (*P*–Δ EFFECT)

Stability under seismic loading implies that the structural system must maintain a vertical load-carrying capacity in the presence of ground motions that create horizontal as well as vertical oscillations of the structure. Thus the issue is the superposition of time-varying "loads" on static loads, which brings dynamic considerations into the stability problem.

Figures 20.4 and 20.5 illustrate the issue. Figure 20.4 shows the lateral load-deflection relationship of a portal frame, which is loaded with constant vertical loads (P) and a monotonically increasing lateral load (H). Point A, which identifies the maximum lateral load that can be applied to the structure, is a critical quantity for static loading since its value cannot be maintained as displacements increase, and a sidesway collapse is imminent under static load application. For dynamic loading, point A identifies the strength of the structure in the presence of *P*–Δ effects, but incremental collapse is not imminent since dynamic loading implies energy input and stability is maintained as long

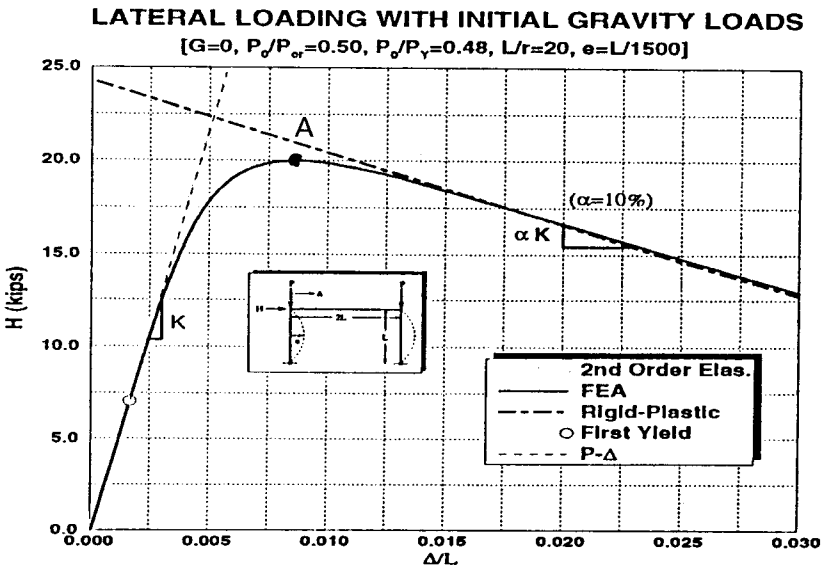

Fig. 20.4 Lateral load-deflection relationship for a portal frame.

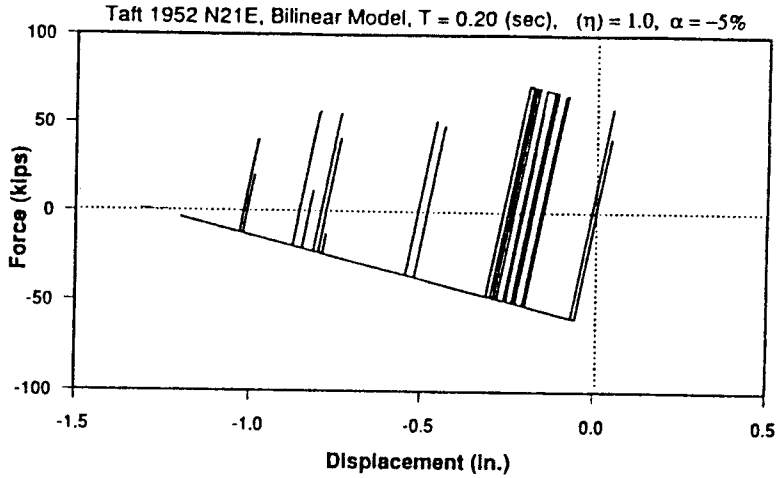

Fig. 20.5 Dynamic response of an idealized single-degree-of-freedom system (Rahnama and Krahwinkler, 1993)

as energy can be absorbed within the structural system. In concept, collapse will not occur unless the displacement associated with zero lateral resistance is reached.

Figure 20.5 shows the dynamic response of an idealized single-degree-of-freedom (SDOF) system whose hysteretic behavior is bilinear but includes *P*–Δ effects that lead to a negative post-elastic stiffness (Rahnama and Krawinkler, 1993). The presence of negative stiffness leads to drifting of the displacement response that brings the SDOF system close to collapse. In real structural systems a negative stiffness occurs when the P-Δ effect exceeds the hardening effect prior to or during mechanism motion. A negative stiffness may also be created by deterioration in the load-deformation response of individual elements, which may be caused by local instabilities, localized fractures, or member buckling. These three issues are discussed further in subsequent sections of this chapter.

Point A of Fig. 20.4 is a point of some importance in the characterization of dynamic response but of less importance in the context of stability. Point A defines the strength of the structure, a quantity that is needed to estimate inelastic deformation demands under severe ground motions. It also defines the strength and deformation level at which the structure *P*–Δ effect will lead to a negative stiffness of the dynamic response. In this respect point A affects the stability since a negative stiffness will lead to the aforementioned drifting of the displacement response.

Many investigators have studied the gravity load (*P*–Δ) effects on the inelastic seismic response of structural frames. Goel (1969) included the *P*–Δ effect to study the response of 10- and 25-storey single-bay unbraced moment frames.

The columns of the frames were assumed to behave elastically, while the girders followed curvilinear hysteretic behavior in bending. Two earthquake records representative of severe ground motions were used in the analysis. These were the north–south component of the El Centro 1940 earthquake and the S21°W component of the Taft earthquake of July 1952 with peak accelerations scaled to 0.5g. He concluded that the P–Δ effect had some influence on the periods of vibration but that the net effect on inelastic response was almost negligible. With the structure oscillating predominantly in the first mode, P–Δ shears acting in opposite directions from stories above and below a floor mass were cited as the probable reason. A study by Cheng and Tseng (1973) on a single-bay three-story frame arrived at a similar conclusion: that the change in natural period of oscillation of the frame due to the P–Δ effect may cause the lateral floor displacements and forces to increase or decrease, but not by substantial amounts.

During major earthquake shaking it is possible for plastic hinges to form in the columns, leading to formation of a story mechanism in an intermediate story or in the worst case, in the bottom story. In such a case, the structure above the story mechanism could behave as a single-degree-of-freedom (SDOF) inverted pendulum system with heavy mass above the "soft" story. P–Δ effects leading to the instability of SDOF systems under heavy gravity loads have been reported in the literature. Water towers or structures with a heavy mass, as sometimes encountered in industrial applications are among a few practical examples of such systems. Husid (1967) and Jennings and Husid (1968) carried out a pioneering study in this area. They studied the overturning effect of a gravity load on the collapse of simple yielding SDOF structures in which artificially generated strong ground motion records were used as excitation. Sun et al. (1973) and Wang (1975) followed the work of Husid and Jennings and made some valuable contributions. Wang (1975) developed a criterion to determine the likelihood of structural collapse by instability. The criterion can be used to measure the safety of simple yielding SDOF structural systems against collapse, and to examine the influence of structural and ground motion characteristics on stability.

More recently, Mazzolani and Piluso (1993) presented an excellent summary of the state of Italian research activity on this topic. They presented a simplified model for predicting P–Δ effects on the seismic response of steel structures. Equivalence between multiple-degree-of-freedom (MDOF) structures and the SDOF model was established through lateral load versus top-sway displacement behavior curves. Emphasis was placed on development and use for practical work of a reduction coefficient for ultimate strength as a function of the magnitude of vertical loads, target ductility, and amplification of response due to the P–Δ effect.

Despite the fact that the problem of the overall stability of steel structures under seismic loading has been studied by many investigators for a number of years, and the research work has produced a great amount of useful information, a very small part of the research results has found its way in the codes.

Generally, the current code treatment of the problem is much too simplistic. The main reason for this perhaps lies in the fact that current seismic design practice is based on elastic analysis at code-specified reduced design forces. Most codes do require consideration of overall structural stability (P–Δ effect) and spell out when the P–Δ effect need not be considered. For example, the Uniform Building Code (ICBO, 1994) treats the P–Δ effect in Section 1628.9 in the following manner:

> The resulting member forces and moments and the story drifts induced by P–Δ effects shall be considered in the evaluation of overall structural frame stability. P–Δ need not be considered when the ratio of secondary moment to primary moment does not exceed 0.10 . . . . In seismic zones 3 and 4, P–Δ need not be considered when the story drift ratio does not exceed $0.02/R_w$.

Including the P–Δ effect on the calculation of member forces and story drifts for design purposes does account to some extent for their amplification, which is a way of considering the reduction in strength and stiffness of the structure caused by the P–Δ effect. However, the procedure does not address in any way the real stability problem which may be caused during major earthquake shaking by possible negative stiffness beyond the point of maximum strength (point A in Fig. 20.4). Short of running second-order inelastic dynamic analyses for probable design ground motions, a second-order inelastic static analysis can determine the drift values that may lead to dynamic instability. Until such analyses become part of common design practice, it may be comforting to recognize that for most steel structures member or local instability issues may be more critical than the overall P–Δ effect. These issues are the subject of discussion in subsequent sections.

20.3 MEMBER INSTABILITY

Typical code-designed structures are expected to undergo large inelastic reversed cyclic deformations during strong earthquake motion. Therefore, systems with good inelastic behavior are "rewarded" with smaller seismic design forces. Good inelastic behavior of a structure is typified by full and stable hysteretic (force-deformation) loops, which provide the structure with its required ductility and energy dissipation capability to survive severe ground motion. The hysteretic behavior of a structure is, of course, made up of force-deformation response of its members and connections. Lateral-torsional buckling and local buckling have a significant impact on this behavior, since premature buckling may significantly reduce the ductility and energy dissipation of the system. Control of these forms of buckling is important if good seismic performance is to be achieved. It may not be practical to prevent buckling entirely; instead, the initiation and development of buckling is controlled so that adequate ductility and inelastic deformation are achieved before buckling adversely affects the performance of the structure.

20.3.1 Lateral-Torsional Buckling of Bending Members

In many design codes, lateral-torsional buckling strength is expressed by three lines or curves, which are functions of the equivalent slenderness parameter, λ_{eq}, as shown in Fig. 20.6. The slenderness parameter can be expressed as

$$\lambda_{eq} = \sqrt{\frac{M_p}{M_e}}$$

where M_p is the plastic moment capacity of the section and M_e is the elastic lateral-torsional buckling moment of the beam. M_p depends only on the yield stress and cross-sectional properties of the beam, and M_e depends on the cross-sectional properties and unsupported length. As a result, λ_{eq} is very dependent on the unsupported length of the beam. For the special case of a doubly symmetric H-section,

$$\lambda_{eq} = \frac{(kL_b/\pi r_y)\sqrt{F_y/C_bE}}{[1 + 0.05(t_f/h)k^4(L_b/r_y)^2]^{0.25}} \tag{20.1}$$

where

L_b = unsupported length
k = effective-length coefficient for lateral torsional buckling
r_y = radius of gyration about the minor axis
F_y = yield stress
E = Young's modulus
t_f = thickness of flange
h = depth of beam
C_b = equivalent moment coefficient to account for variation in bending moment over the length of the beam

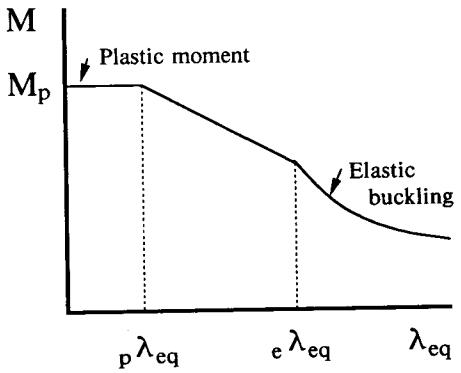

Fig. 20.6 Lateral-torsional buckling strength.

Further, the slenderness parameter can be approximated conservatively as

$$\lambda_{eq} = \frac{kL_b}{\pi r_y}\sqrt{\frac{F_y}{C_bE}}$$

for these doubly symmetric shapes. The curves shown in Fig. 20.6 are based on the concept that beams with very short unsupported lengths can develop the full plastic moment capacity, while beams with longer unsupported lengths will not be able to attain this capacity because of inelastic or elastic buckling (SSRC, 1988). Since seismic design of moment frames is usually based on the full plastic moment capacity of the beams, the first zone of Fig. 20.6 is of great importance in seismic design.

The design approach summarized in Eq. 20.1 and Fig. 20.6 was verified by experiments and has been widely accepted (Fukumoto and Itoh, 1983). The tests were conducted on laterally supported beams under static and monotonically increasing loads. The design concept may well apply to seismic loads, but seismic loads require cyclic inelastic deformation, and the lateral support requirements and the deterioration characteristics may be different under this loading. Further, seismic design requires a minimum rotational capacity under these cyclic loads without significant loss of resistance, and the combined effect of these demands may result in a more severe lateral support requirement.

Many experiments have been conducted to determine the rotation capacity of beams in the context of the plastic design. Figure 20.7 shows some typical results (AIJ, 1975). The rotation capacity, R_θ, is defined here as

$$R_\theta = \frac{\theta_f}{\theta_p}$$

where θ_f is the rotation angle at which the curve drops down in the moment–rotation relationship in experiments, and θ_p is the theoretical elastic value of the rotation angle when P_p is first reached.

Most experiments that examine the rotational capacity of beams are based on cyclic load tests. Stable hysteretic curves are possible with small cyclic rotations, but the stable behavior tends to deteriorate at larger cyclic rotations, as illustrated in Fig. 20.8 (Takanashi, 1973). The rate of deterioration depends on several factors, including the cyclic deformation history, amplitude of the deformation, and slenderness of the beam. However, research by Takanashi (1973) shows clearly that the rotational capacity for cyclic loading is less than the rotational capacity achieved in monotonic load tests. This is illustrated in Fig. 20.9, where the rotational capacities achieved during monotonic tests are plotted as circles, and the results of cyclic load tests with complete reversals are shown as triangles.

Unfortunately, the inelastic response developed during earthquakes is neither the same as that obtained during monotonic load tests nor as that

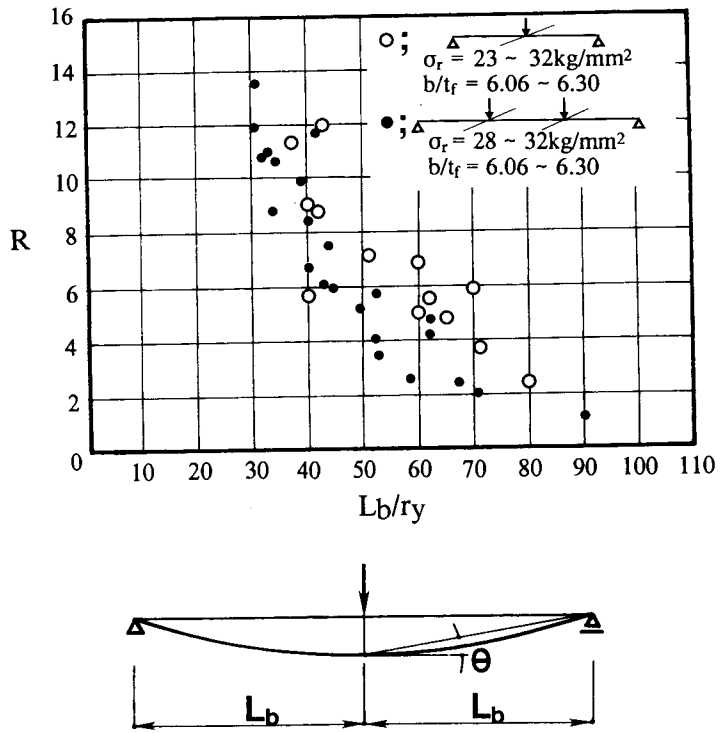

Fig. 20.7 Rotation capacity of beams (AIJ, 1975).

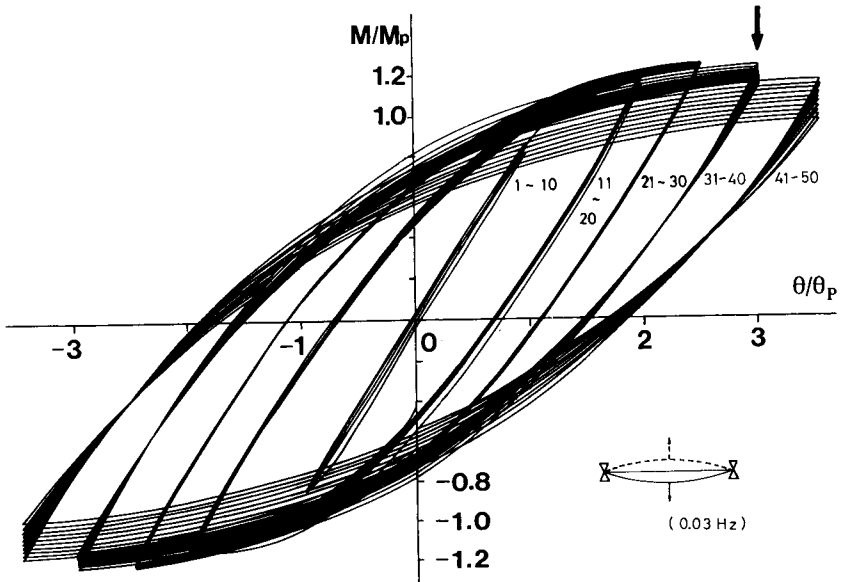

Fig. 20.8 Cyclic rotation behavior of beams (Takanashi, 1973).

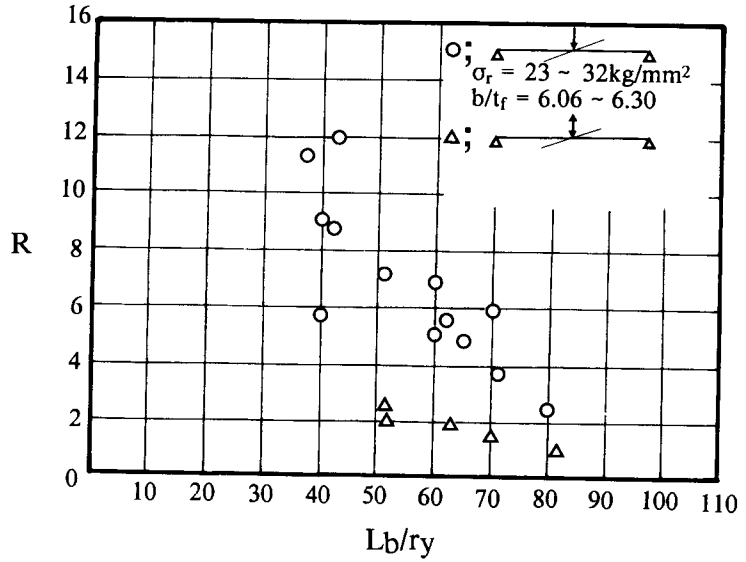

Fig. 20.9 Cyclic rotation capacity of beams (Takanashi, 1973).

obtained in most cyclic tests. Inelastic cyclic load tests often employ complete reversals of the deformation, which may lead to greater deterioration than is actually noted during an earthquake. Earthquake deformations, on the other hand, normally result in greater deterioration than that noted in monotonic tests. Pseudodynamic experiments by Takanashi et al. (1977) of a portal frame (with $L_b/r_y = 62.6$) illustrated in Fig. 20.10 were used to examine this difference, and the results are shown in Fig. 20.11. Figure 20.11 shows the maximum rotation achieved when the frame was subjected to the 1940 El Centro acceleration record, a sinusoidal base excitation with the same peak acceleration, and amplified versions (1.5 times El Centro and 1.2 times the sinsoidal) of these excitations. It can be seen that increased amplification results in substantial increases in rotational demand. Elements with a rotational demand greater than the monotonic rotation are likely to perform poorly during an earthquake. Elements with demand less than the rotation achieved in cyclic load tests are likely to perform well. Elements in the intermediate range have uncertain seismic behavior.

The preceding evaluation of rotational capacity and rotational demand depends on several factors, including the peak acceleration, acceleration record, and slenderness of the frame elements. Rigorous analyses are required to examine lateral–torsional stability for most practical conditions. As a result of these difficulties, most professional practice has evolved to using a limit on the unsupported length of the element as a simple controlling measure of the potential deterioration due to lateral–torsional buckling. In the UBC (ICBO,

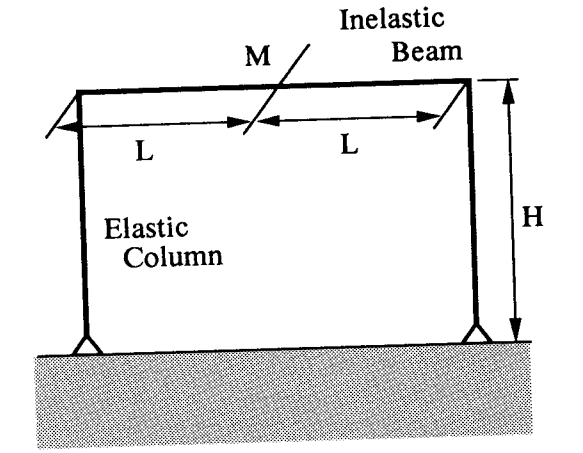

(a)

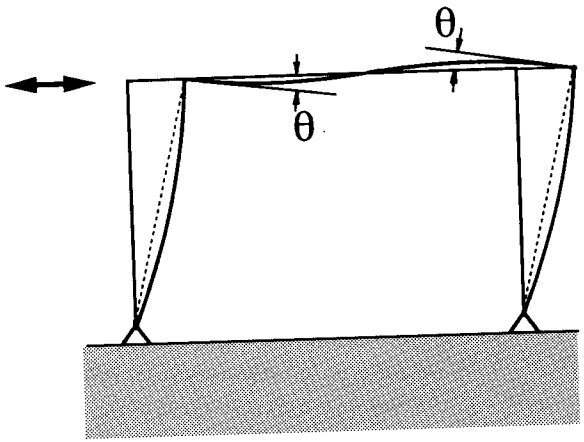

(b)

Fig. 20.10 (*a*) Schematic drawing of experimental portal frame. (*b*) Deflected shape of frame.

1994), a limit of $96r_y$ is employed for moment frames which require the greatest rotational capacity. In Japan, the maximum λ_{eq} for the greatest rotational capacity is 0.63. The maximum unsupported length is $89r_y$ for mild steel beams with symmetrical H-shaped sections subjected to equal end moments which cause reverse curvature.

Lateral-torsional buckling of beams takes on an even more important role in braced frames where floor beams are intersected by braces, such as in V or inverted-V (chevron) braced frames or eccentrically braced frames (EBFs).

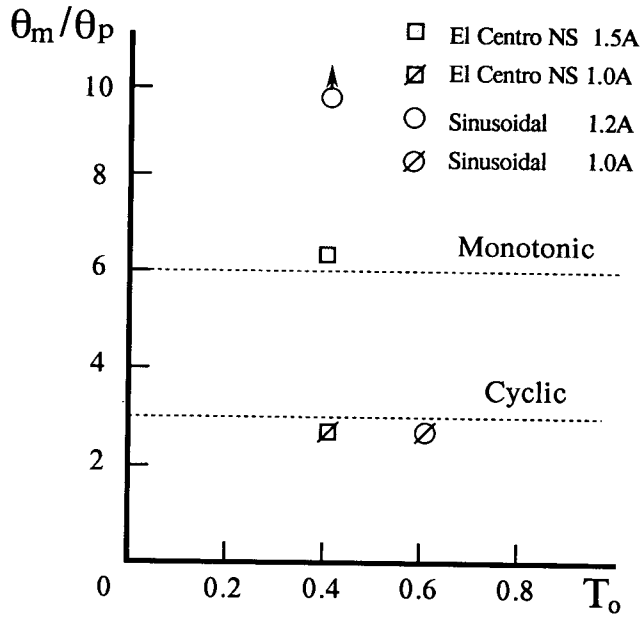

Fig. 20.11 Maximum rotations of frame under sinusoidal and seismic excitation (Takanashi et al. 1977).

This is because the braces apply large concentrated forces to the beams, with the system undergoing cyclic inelastic deformations. The UBC (ICBO, 1994) requires that both flanges of beams at the point of intersection of chevron braces be laterally supported directly or indirectly. Similarly, for EBFs the UBC (IBCO, 1994) requires that top and bottom flanges of beams intersected by eccentric bracing be laterally supported at the ends of the link beams (shear links) at intervals not to exceed $76/\sqrt{F_y}$ times the beam flange width. The latter requirement for spacing of lateral bracing is more stringent than that for beams in moment frames because the shear links in EBFs are expected to experience much greater plastic rotations than the beams in moment frames. Nevertheless, for the most part, these code requirements are based on rather limited test data tempered with much engineering judgment.

20.3.2 Buckling of Columns

Buckling of columns cannot be tolerated at all in any seismic event because these members are critical to the vertical load-carrying capability of the structural system. Large-ampitude cyclic displacements of the structure can induce rather large axial forces in the columns. This can be quite serious in columns of braced bays in concentric or eccentrically braced frames, where bracing members can cause a large accumulation of axial forces in the columns.

During their analytical study of a seven-story inverted V-braced steel structure subjected to severe earthquake ground motion, Jain and Goel (1979) found that one of the first-story columns in the braced bay underwent lateral-torsional buckling, resulting in excessively large permanent deformation of the structure. Later, Goel and Tan (1987) observed a similar phenomenon in their study of a six-story structure designed in accordance with the 1982 edition of UBC. The structure was designed as a pure braced structure with inverted V-bracing without any backup moment frame and analyzed for the north–south component of the 1978 Miyagi-ken-Oki earthquake record with the peak acceleration scaled to approximately $0.5g$. Large axial forces caused buckling of a few columns in the braced bay, which resulted in excessive deformation of the structure. The yield condition and deformed shape of the frame at several instants of time during the dynamic response are shown in Fig. 20.12. The horizontal displacement verus time history at the roof level is shown in Fig. 20.13. To eliminate the problem of column buckling, the design of the structure was modified. The columns in the braced bay were redesigned for a combination of factored gravity loads and the maximum force that could be transmitted from the braces. The dynamic response of the redesigned frame showed great improvement and no column buckling occurred under the same ground motion.

An eccentric braced frame with shear links is another example of structures in which heavy, nonbuckling bracing members are needed in order to utilize energy dissipation in the link beams. A six-story, two-bay by two-bay full-scale eccentrically braced structure was studied under the U.S.–Japan Cooperative Earthquake Research Program Utilizing Large Scale Testing Facilities in Tsukuba, Japan, in 1984. Goel and Hanson (1984) conducted an analytical study of that structure which indicated the possibility of column instability occurring under large lateral displacement.

The braced bay of the subject structure is shown in Fig. 20.14. Under gravity loads, W_D, and increasing horizontal forces (represented by H in the figure) the increasing shear forces in link beams would cause a maximum axial compressive force in column C3. Assuming bilinear shear force versus shear deformation behavior for the link beams, an approximate calculation of axial force in column C3 is shown in Fig. 20.14. V_p is the shear yield capacity of the link beam webs, and C_s represents the strain-hardening factor. Assuming that all the link beams yield simultaneously, it would only take $C_s = 1.1$ for column C3 (a W12 × 106 section with a yield strength of 254.0 N/mm^2) to reach its out-of-plane (weak-axis) buckling load $P_{cr} = 4814.7$ kN. The effective-length factor is assumed to be 0.8.

The results from a more precise computer analysis of the test structure under a total dead load $W_D = 514.8$ kN and monotonically increasing horizontal floor forces are shown in Figs. 20.15 and 20.16. The distribution of horizontal forces is assumed to represent the fundamental mode shape of the structure. A modified DRAIN-2D program was used in the analysis. A plot of horizontal force H versus the corresponding displacement at the roof level is shown in

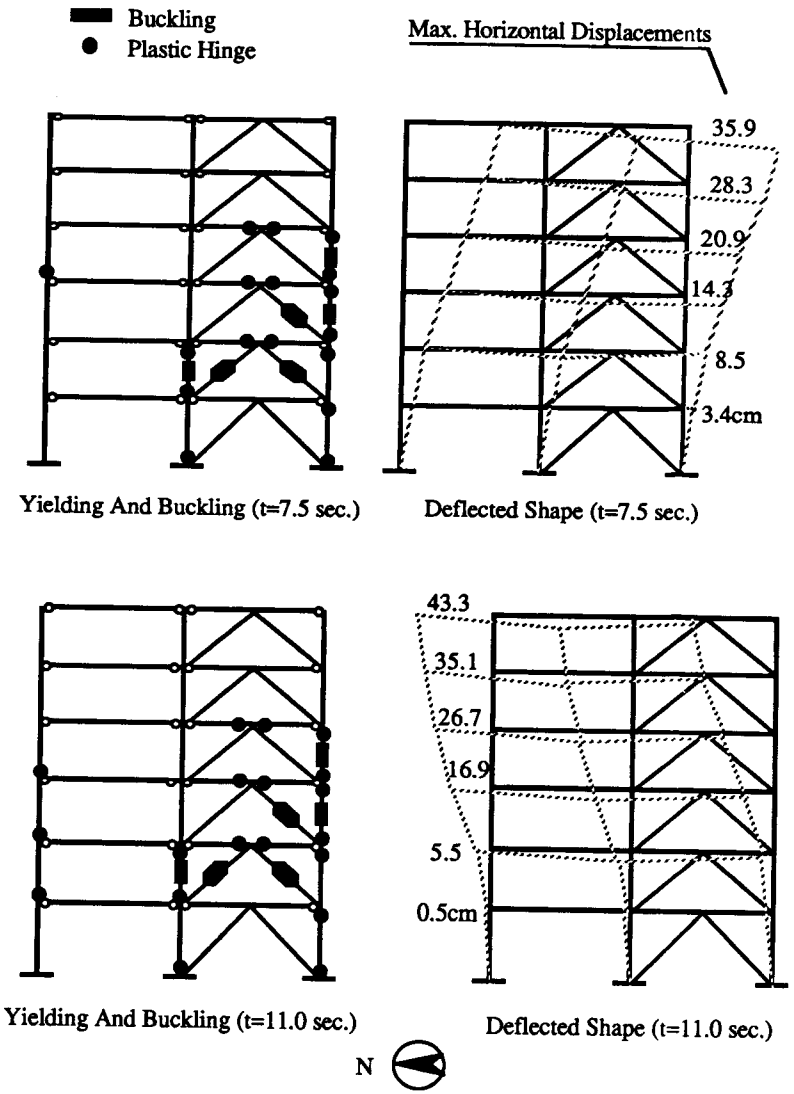

Fig. 20.12 Yield condition and deformed shape of six-story braced structure (Goel and Tang, 1987).

Fig. 20.16. Lateral–torsional buckling of column C3 occurred at a roof displacement of little over 12 cm, as indicated by the flatness of the force-displacement plot.

The final large-amplitude test of the subject structure was performed as a series of steady-state responses to three sinusoidal ground acceleration pulses of one cycle each. Maximum roof displacements of approximately 10, 15, and 20 cm were achieved in this test. At roof displacements of over 12 cm, quite

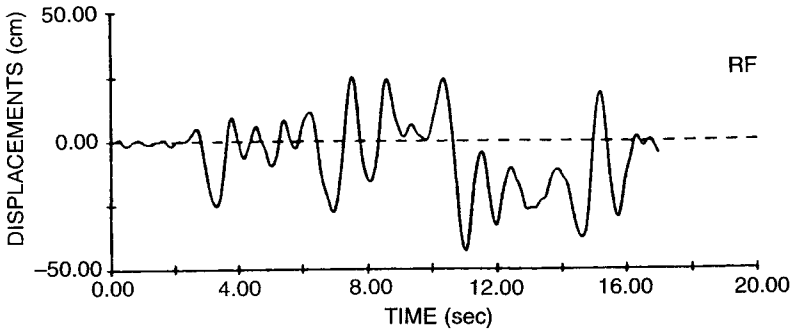

Fig. 20.13 Horizontal displacement-versus-time at roof level (Goel and Tang, 1987).

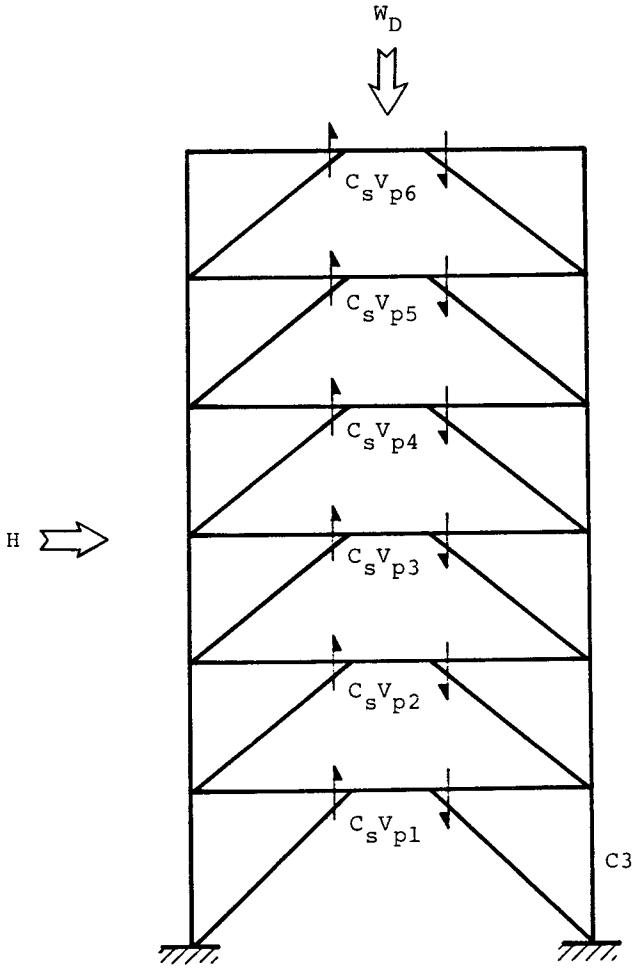

Fig. 20.14 Eccentrically braced structure studied in US-Japan study.

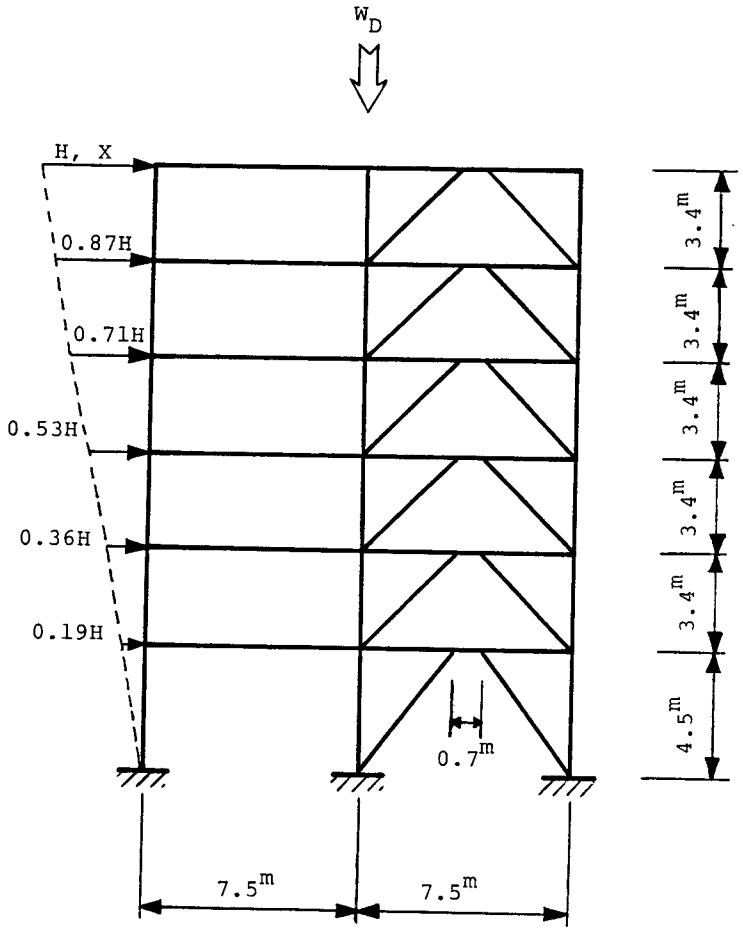

Fig. 20.15 Horizontal floor forces on test structure (Goel, 1984).

severe buckling of gusset plates connecting the braces to the link beams was observed in the first two stories (Fig. 20.17). Buckling of the gusset plates also led to severe lateral–torsional buckling of the bottom flange of the beams. It is quite possible that this localized buckling may have prevented severe distress in the column or bracing members in those stories during the test.

In current design practice, explicit checks against the possibility of column buckling at large seismic lateral displacements are not required. For example, according to the UBC (ICBO, 1994), the columns in steel structures are designed for load combinations, including specified lateral seismic structures at allowable stress limits. However, for structures in high seismic regions the columns are also required to have adequate compression strength to support a combination of full dead plus a fraction of live loads and a factor $\frac{3}{8}R_w$ times the lateral forces specified. This is a rather simplistic attempt to control column

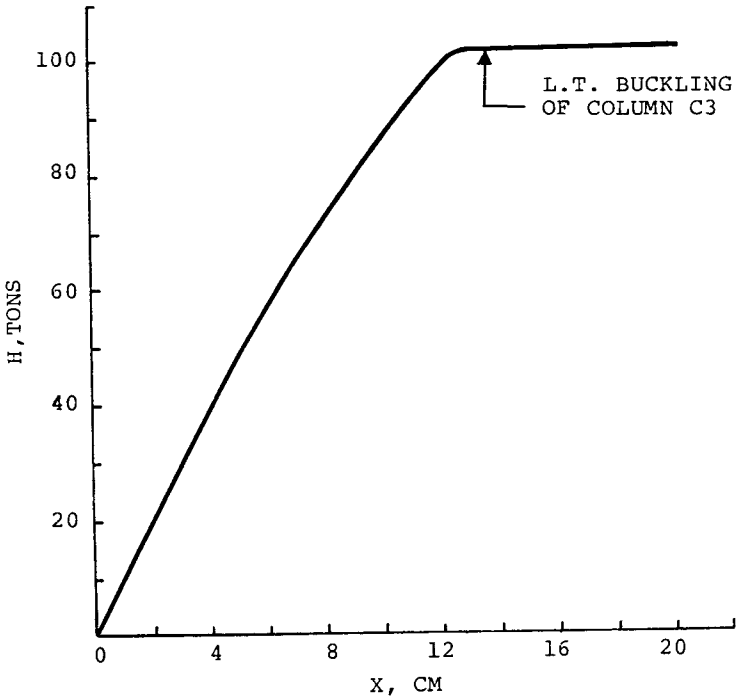

Fig. 20.16 Load-deflection plot at roof level (Goel, 1984).

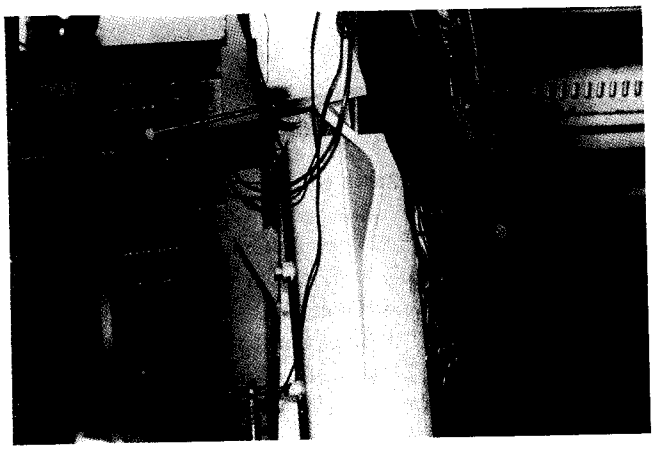

Fig. 20.17 Buckling of gusset plates connecting the braces to the link beams (Goel, 1984).

buckling under severe earthquake loading. Although the factor $\frac{3}{8}R_w$ may be adequate to represent severe earthquake loading in many structures, it may not be enough to prevent column overloads in some structures, especially when the members transferring axial forces in the columns may have significant overstrength above the nominal design values and undergo major strain hardening in regions of yielding, such as plastic hinging in beams of moment frames.

20.3.3 Buckling of Other Compression Members

Seismic overloads can also occur in other compression members as part of the lateral-force-resisting system. Sudden loss of strength and stiffness of the structure due to buckling of those members can sometimes lead to stability problems during a major seismic event. An example of such a structural system is moment frames in which truss girders are used as horizontal members. These truss girders carry gravity loads as well as function as horizontal members of the lateral-force-resisting moment frames. An experimental and analytical study of such frames was carried out by Goel and Itani (1994a). Truss girder–column subassemblage tests showed that under cyclic loading the system possesses rather poor hysteretic behavior, with large abrupt drops in strength and stiffness caused by buckling and early fractures of diagonal web members of the truss girders. A typical result is shown in fig. 20.18. Inelastic dynamic analysis of the longitudinal frame of a four-story study building, as shown in Fig. 20.19, showed that the degrading hysteretic behavior resulted in a drifting type of response which could lead to failure under heavier gravity loads in some cases (Fig. 20.20). Their study led to the development of a ductile truss–strong column framing system called a special truss moment frame (STMF), which possesses stable hysteretic behavior as shown in Fig. 20.21, with the yield mechanism shown in Fig. 20.22. Stable hysteretic force–deformation behavior results in improved seismic performance (Goel and Itani, 1994b).

20.4 LOCAL BUCKLING

Large cyclic deformations caused by severe ground shaking in a major earthquake can cause severe local buckling accompanied by yielding in compression plate elements of structural members. The resulting loss of strength and consequent early fractures can produce severely degrading hysteretic behavior with an associated poor structural response.

20.4.1 Open Sections

Two types of local buckling are important. Flange buckling is local buckling deformation of flanges under bending or combined bending and compression. Web buckling may be caused by compressive stress in the web due to bending

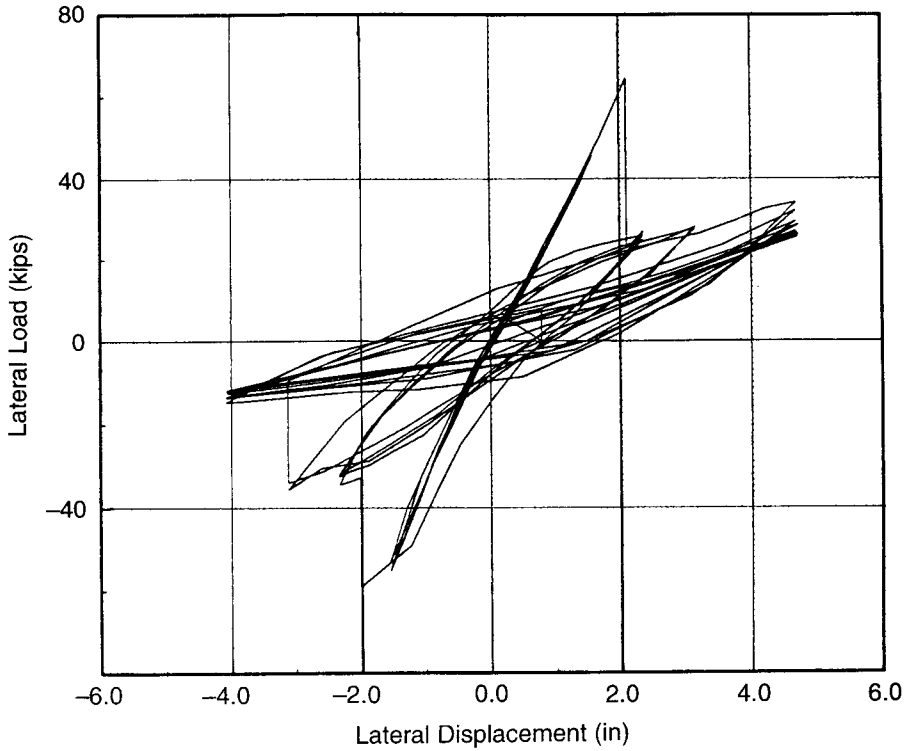

(*a*)

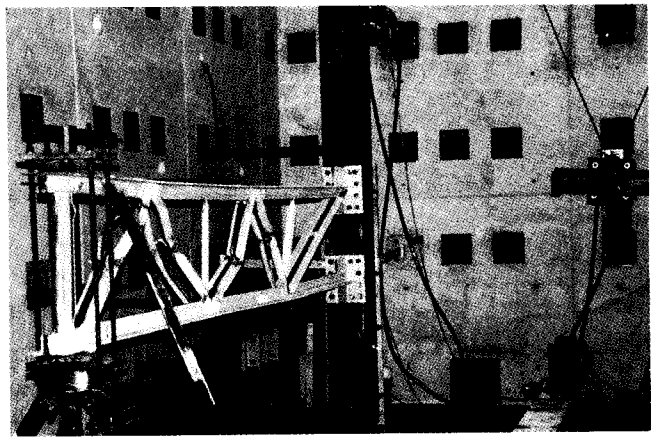

Fig. 20.18 (*a*) Experimental cyclic behavior of truss girder (Goel and Itani, 1994a). (*b*) Photo of truss girder with buckled webs (Goel and Itani, 1994a).

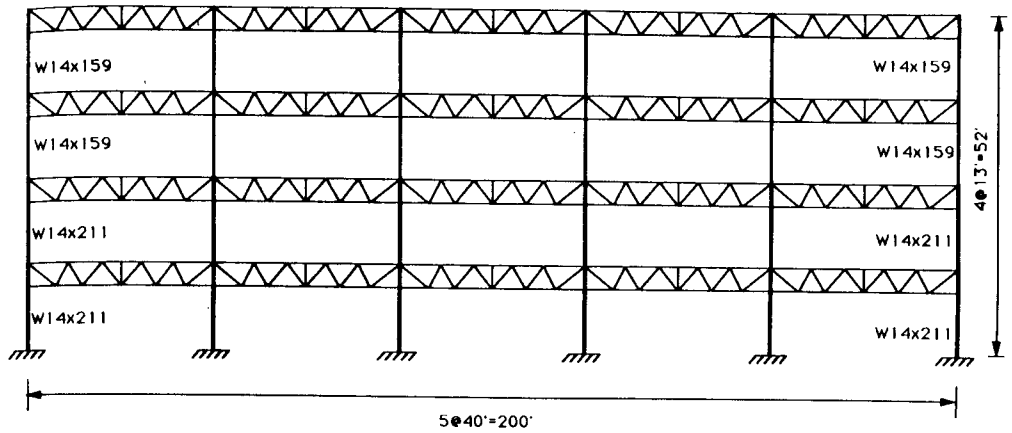

Fig. 20.19 Four-story building with truss frames (Goel and Itani, 1994).

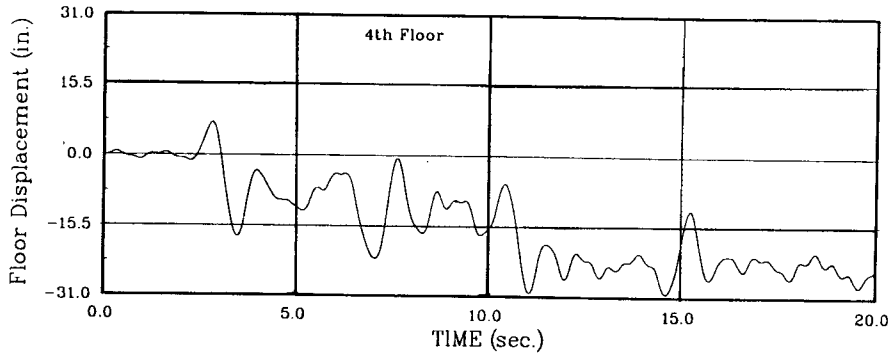

Fig. 20.20 Drifting-type displacement behavior of four-story building (Goel and Itani. 1994a).

or combined bending and axial load (bend buckling), or web buckling may be caused by high shear stresses in the web (shear buckling). Shear buckling is commonly considered in eccentrically braced frames and some other structural systems, but it is generally not expected in beams and columns of moment-resisting frames since bending moments rather than shear forces dominate frame behavior. However, recent changes in seismic design provisions for moment-resisting frames have encouraged the use of panel zone yielding during earthquakes (ICBO, 1994). This yield mechanism can be very stable and perhaps desirable for seismic behavior, but it is increasingly susceptible to shear buckling. Figure 20.23 shows a photograph of flange buckling combined with web bend buckling in a steel section subjected to cyclic inelastic deformation typical of those sustained during severe earthquake loading.

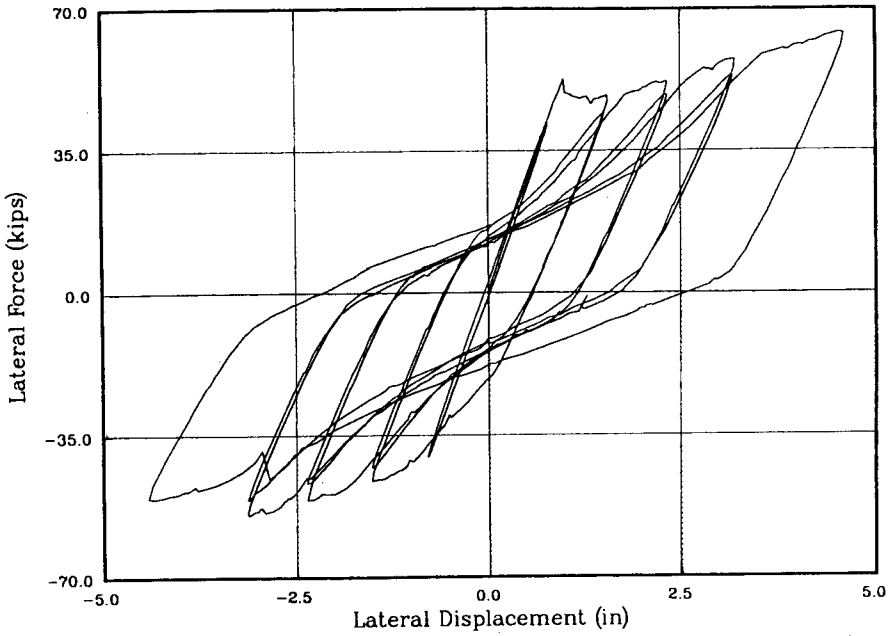

Fig. 20.21 Hysteritic behavior of special Truss Moment Frames (Goel and Itani, 1994b).

The importance of local buckling was clearly illustrated in a recent experimental program (Schneider et al., 1993) where subassemblages of nearly identical strength and stiffness were subjected to similar deformation histories. One of these elements had relatively slender web and flanges which were just at the present U.S. seismic design limits (ICBO, 1994), while the other had stockier flange and web sections. The force–deflection hysteretic curves of these two specimens are illustrated in Fig. 20.24*a* and *b*, respectively. Comparison of Fig. 20.24*a* and *b* shows much more rapid deterioration that occurs when local buckling dominates the inelastic behavior. It should be noted that the slenderness requirements are not intended to prevent local buckling completely, since it is nearly impossible when steel rolled shapes are subjected to severe inelastic deformation. Instead, the limits are intended to control the buckling and ensure good inelastic behavior. The ultimate issue becomes a question of how much ductility is needed for adequate seismic performance and how severe the buckling can be while still developing the desired ductility. Local buckling is a complex phenomenon depending on the interaction of bending moment, axial load, web and flange slenderness, yield stress of steel, and the required ductility, and as a result, seismic design for these criteria utilizes simplified approximations.

Flange buckling has long been recognized (Lay, 1965) as an important consideration in the design of steel beams for compactness or plastic design.

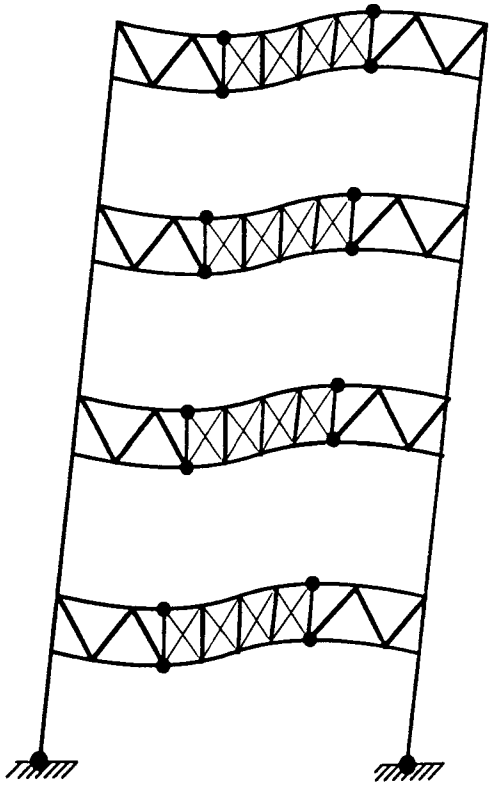

Fig. 20.22 Yield mechanism of four-story frame (Goel and Itani, 1994b).

These design limits result in yielding of the beam flange, and it is important that the beam maintain its bending capacity during plastic deformation. The design limits for flange buckling are related to elastic plate buckling where the elastic buckling stress is large enough to ensure that yielding can be achieved and the required plastic deformation can be attained without loss of bending capacity. These design limits have become slightly more generous (Yura et al., 1978) as the deformation requirements for ordinary steel design have become better understood. In current practice, flange buckling is controlled with the limit $b_f/2t_f < 65/\sqrt{F_y}$ in ordinary steel design. However, experiments (Krawinkler et al., 1971; Bertero et al., 1973; Suzuki et al., 1976) simulating inelastic cyclic deformations show that buckling can be a more severe problem during earthquakes. Large strain reversals lead to more rapid deterioration in the moment capacity, and a slightly more stringent limit is required for seismic design of steel frames designed for ductile behavior. Frames of this type have a flange slenderness limit of $b_f/2t_f < 52/\sqrt{F_y}$ in U.S. practice (ICBO, 1994); however, it should be noted that the member illustrated in Fig. 20.24*a* had a

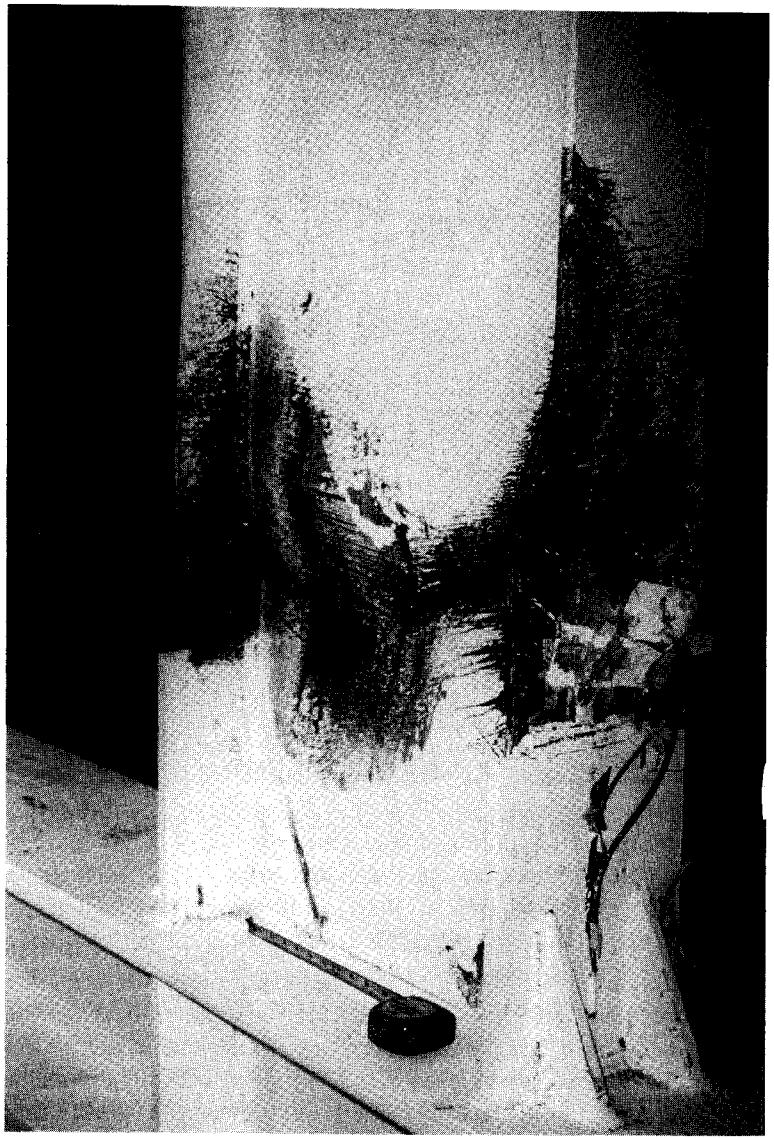

Fig. 20.23 Local buckling in steel section subjected to cyclic inelastic deformation.

flange slenderness very close to this design limit. It can be seen that the ductility is limited at this condition; however, this does not suggest that it is inadequate for safe seismic design. Research in Japan (Suzuki et al., 1976) has examined the rotational capacity of the flange and correlated it more directly to the flange slenderness. It is noted that the flange slenderness must decrease as the plastic rotation during seismic loading increases if ductile behavior is to be achieved.

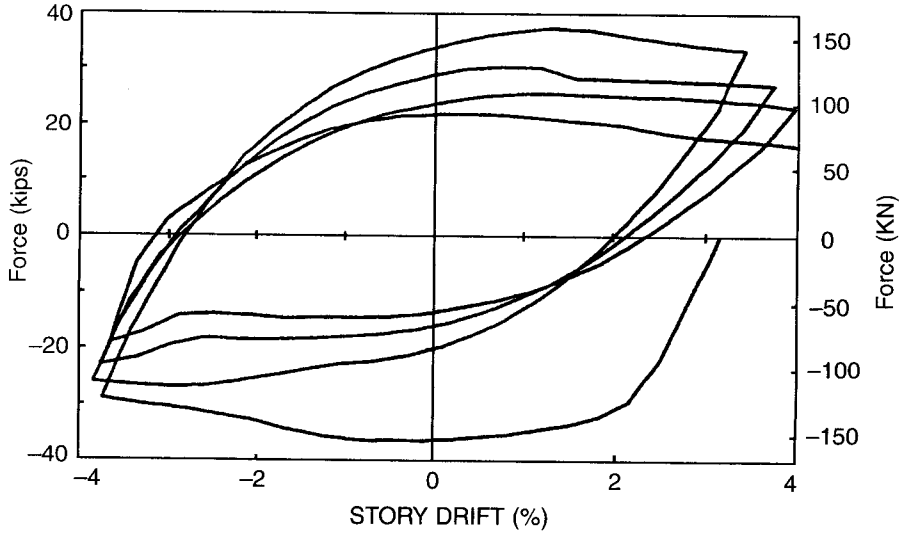

Fig. 20.24a Effect of plate slenderness on the cyclic force-deformation behavior; slenderness at code limit (Schneider et al., 1993).

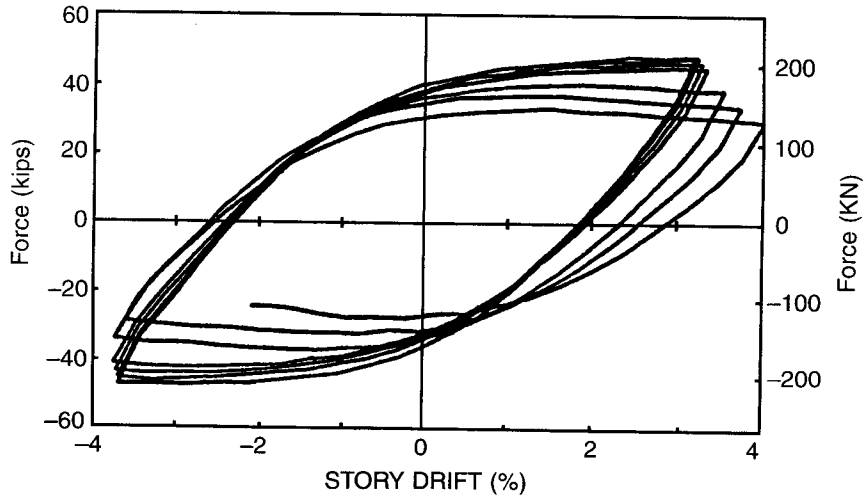

Fig. 20.24b Effect of plate slenderness on the cyclic force-deformation behavior; stockier plates (Schneider et al., 1993).

Japanese researchers (Suzuki et al., 1976, 1980) studied this reduction in rotational capacity under both monotonic and cyclic deformation as a function of flange slenderness. Rotational limits based on the bending moment yield stress and slenderness of the flange were proposed.

Web buckling is also known to affect the plastic deformation capacity of steel members. The primary mode of web buckling considered in seismic design is a form of bend buckling, and it is therefore dependent on the axial force, since the compressive stress in the web and the depth of the web in compression are increased with increasing compressive load. Again, limits on web slenderness have long been required for beams designed by compactness criteria or plastic design. The web of beams must satisfy

$$\frac{h}{t_w} \leq \lambda_p$$

where

$$\lambda_p = \begin{cases} \dfrac{640}{\sqrt{F_y}}\left(1 - \dfrac{2.75P}{\phi_b P_y}\right) & \text{for } \dfrac{P_u}{\phi_b P_y} \leq 0.125 \\ \dfrac{191}{\sqrt{F_y}}\left(2.33 - \dfrac{P_u}{\phi_b P_y}\right) & \text{for } \dfrac{P_u}{\phi_b P_y} > 0.125 \end{cases}$$

to control web bend buckling during plastic deformation in U.S. practice (AISC, 1993). These limits have been expressed in a number of different but similar equations but are also used for seismic design.

Recent research in the United States (Schneider et al., 1993) and Japan (Suzuki et al., 1976, 1980) have suggested that web buckling and flange buckling are interrelated. That is, web slenderness may affect flange buckling, and flange slenderness may have a similar effect on the web. The Japanese limit on flange slenderness (Kato, 1987) for seismic design of a beam-column designed for the greatest ductility is $d/t_w < 268/\sqrt{F_y}$ (F_y in ksi) except that

$$\frac{(b_f/2t_f)^2}{(75.4/\sqrt{F_{yf}})^2} + \frac{(d/t_w)^2}{(351/\sqrt{F_{yw}})^2} < 1.0$$

must also be satisfied. If the member is a a beam with no axial load, the limits are $\dfrac{d}{t_w} < \dfrac{377}{\sqrt{F_y}}$ (Fy is in ksi) except that

$$\frac{\left(\frac{b_f}{2t_f}\right)^2}{\left(\frac{75.4}{\sqrt{F_{yf}}}\right)^2} + \frac{\left(\frac{d}{t_w}\right)^2}{\left(\frac{479}{\sqrt{F_{yw}}}\right)^2} < 1.0$$

must also be satisfied. These limits are similar to those used for seismic design in the United States, except that they consider the more complex interaction of the web and flange slenderness.

20.4.2 Box Sections

Rectangular built-up box sections or tubular sections are often used for columns and bracing members. Damaging consequences of severe local buckling and early fractures in such members have been observed in some studies and in structure performance during major earthquakes in recent years. One of the most widely publicized and dramatic steel structure collapses in an earthquake was the collapse and severe damage to the Piño Suarez towers during the 1985 Mexico City earthquake (Astaneh, 1986). The Piño Suarez complex consisted of two 14-story and three 21-story steel structures which utilized columns of hollow box sections made of welded plates. The major failure mode observed in these structures was severe local buckling in the third story, caused by inelastic cyclic strains in the plate elements under combined bending and axial forces (Fig. 20.25). Built-up box and tubular sections are commonly used in Japan for columns in building and bridge structures. Many failures of steel structures during the January 17, 1995 earthquake in Kobe can be attributed to loss of strength and ductility due to severe local buckling similar to that experienced by the columns of the Piño Suarez towers in Mexico City in 1985.

When box or tubular sections are used for bracing members in concentrically braced frames (CBF), they share problems similar to or more severe than those encountered in columns. Bracing members in CBF are expected to buckle and yield at rather small story drifts on the order of 0.25 to 0.5%, which can easily be caused by moderate-intensity earthquake shaking. Studies by Jain et al. (1978), Tang and Goel (1987), and Hassan and Goel (1991) showed that in the event of a major earthquake, the bracing members in CBF could undergo

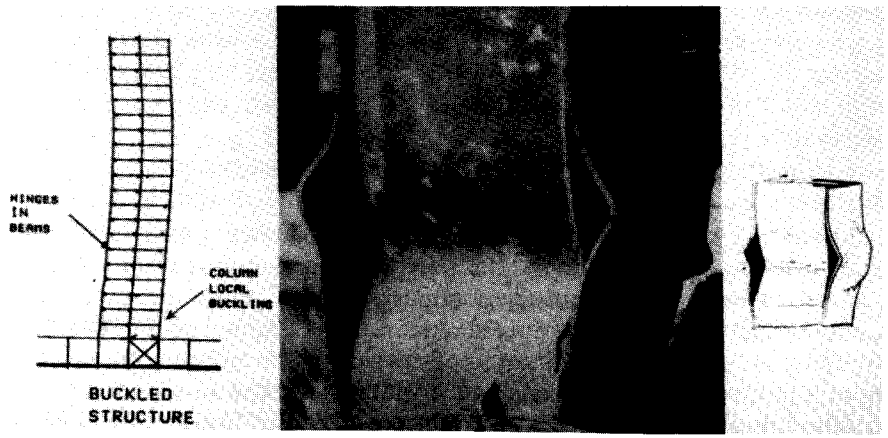

Fig. 20.25 Box column buckling in Mexico City earthquake of 1985 (Astaneh, 1986).

cyclic deformations in the postbuckling range that may be 10 to 20 times the axial yield deformation. Postbuckling deformation induces plastic hinges to form at midlength and at the ends of a bracing member which undergo cyclic rotations under large axial forces in compression and tension. Local buckling of compression flanges at the location of plastic hinges causes severe strain concentration at the corners of flanges with the webs resulting in initiation of very early cracking at those locations which spreads very quickly across the entire section. Testing work on full-size bracing members carried out by Gugerli and Goel (1982), Liu and Goel (1988), and Lee and Goel (1987) showed that even sections meeting the compactness criteria of plastic design did not have adequate ductility to survive deformations due to severe earthquake motions without premature fractures. Similar early fractures of square tubular bracing member sections were observed in the response of the full-size six-story two-bay steel structure tested by the pseudodynamic procedure under the U.S.–Japan Cooperative Earthquake Research Program. Complete fracture at midlength in one brace in the third story and 50 to 70% fracture in both braces in the second story occurred very early in the test, as shown in Fig. 20.26. More recently, early fractures of tubular bracing members were observed in at least one building during the Northridge earthquake of January 17, 1994. Early brace failures of this type can obviously result in excessive story drifts and unstable response under major earthquake ground motions, as shown in studies by Goel (1986), and Tang and Goel (1989).

For structural tubes made of A500 grade B steel, Goel and Tang (1987) and Tang and Goel (1989) proposed the following empirical criterion to compute the fracture life of a bracing member:

$$N_f = \frac{C(KL/r)(b/d)}{[(b-2t)/t]^2} \qquad \text{for } \frac{KL}{r} > 60$$

where

N_f = number of equivalent cycles to failure
$C = 262$, an empirical constant
KL/r = effective slenderness ratio of the member
b/d = width-to-depth ratio of the section
$(b-2t)/t$ = clear width-to-thickness ratio of the member

An equivalent standard cycle is defined as a displacement from zero to the tensile yield displacement and back to zero. The actual displacement history of a brace is converted to an equivalent number of cycles for fracture evaluation. Lee and Goel (1987) later proposed a more refined criterion. Nevertheless, according to both criteria the most important parameter affecting the fracture life of a rectangular tubular brace is the width-to-thickness ratio of the compression flange. Tang and Goel (1987) recommended that to prevent premature fracture of tubular braces in concentric braced frames during a severe earthquake, the limiting width-to-thickness ratio should be $95/\sqrt{F_y}$, which is half of that required by the current AISC–LRFD specification (AISC, 1993) for compact box sections.

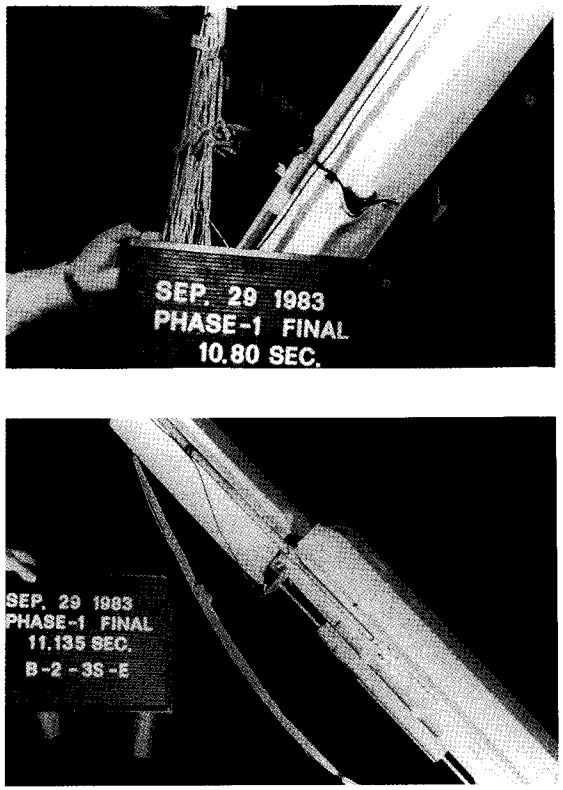

Fig. 20.26 Fracture of concentric brace in US-Japan test structure.

Liu and Goel (1988) and Lee and Goel (1987) studied the effect of concrete infill in square and rectangular tubular bracing members in an attempt to inhibit local buckling. They found that unlike hollow sections the compression flange at plastic hinges in concrete-filled specimens buckles outward rather than inward. Thus the severity of local buckling and consequent strain concentration at the corners are drastically reduced. Moreover, the section is able to retain its plastic moment capacity much better than is a hollow section. Thus the fracture life and overall hysteretic behavior are greatly improved. Lee and Goel (1987) proposed an empirical expression for equivalent width-to-thickness ratio of concrete-filled sections. Concrete infilling was able to reduce the effective width-to-thickness ratio by as much as 50%.

When codes specify reduced seismic design forces for structures based on stable and ductile behavior, it is reasonable that compactness requirements for

members are more stringent than those for plastic design under nonseismic conditions. This is because major earthquake motions impose cyclic deformations far into the inelastic range, whereas plastic design for nonseismic forces requires ductile behavior under essentially monotonically applied forces. The Uniform Building Code (ICBO, 1994) contains compactness requirements for bracing members in concentrically braced frames for which stable ductile behavior is expected. The limiting outside wall width-to-thickness ratio for rectangular tubular sections is specified as $110/\sqrt{F_y}$, which is based on the above-mentioned studies.

20.5 CONCLUDING REMARKS

An attempt has been made to present a brief overview of the current status of research work and related code requirements regarding stability under seismic loading. Clearly, the present-day code treatment of the subject is rather simplistic. This is mainly due to the fact that current common seismic design practice deals with reduced force and displacement levels translated into the elastic domain, making it rather difficult to incorporate stability issues more explicitly as they relate to inelastic response of structures and their components under design-level earthquake ground motions. Since 1981 the Japanese seismic codes have required determination, through analysis or testing, of force–displacement response of structures over 31 m high under monotonically increasing displacement up to levels expected during major earthquake motions. Practice elsewhere is gradually moving in the direction of using more advanced second-order inelastic static or dynamic analyses in seismic design work which would allow more direct incorporation of stability considerations at structure, member, and local levels.

REFERENCES

AIJ (1975), *Guide to the Plastic Design of Steel Structures*, Architectural Institute of Japan, Tokyo.

AISC (1993), *Load and Resistance Factor Design Specification for Structural Steel Buildings*, American Institute of Steel Construction, Chicago.

Astaneh, A. (1986), "A Report on the Behavior of Steel Structures During September 19, 1985, Earthquake of Mexico," *Proc. Ann. Tech. Session SSRC*, pp. 179–188.

Bertero, V. V., Krawinkler, H., and Popov, E. P. (1973), "Further Studies on Seismic Behavior of Steel Beam-Column Subassemblages," *EERC Rep. No. 73–27*, University of California, Berkeley, Calif.

Cheng, F. Y., and Tseng, W. H. (1973), "Dynamic Instability and Ultimate Capacity of Inelastic Systems Parametrically Excited by Earthquakes: Part I," *Tech. Rep.*, National Science Foundation, Aug. (available from U.S. Department of Commerce, National Technical Information Service, Springfield, Va, NTIS Access No. PB261096/AS).

Fukumoto, Y., and Itoh, Y. (1983), "Evaluation of Beam Strength from the Experimental Data-base Approach," *Proc. 3rd Int. Colloq. Stabil. Met. Struct.*, Structural Stability Research Council, Lehigh University, Bethlehem, Pa., pp. 133–149.

Fukumoto, Y., and Lee, G., (eds.) (1991), "Stability and Ductility of Steel Structures Under Cyclic Loading," *Proc. U.S.–Japan Joint Sem.*, Osaka, Japan, July 1–3, CRC Press, Boca Raton, Fla.

Goel, S. C. (1969), "P-Δ Effect and Column Axial Deformation in Aseismic Frames," *ASCE J. Struct. Div.*, Vol. 95, No. ST8, pp. 1693–1711.

Goel S. C. (1986), "Seismic Stability of Braced Steel Structures," *Proc. SSRC Ann. Techn. Session*, pp. 189–200.

Goel S. C., and Hanson, R. D. (1984), "Column Buckling in Braced Steel Frames Due to Lateral Loads," *Proc. SSRC Annu. Tech. Session*, pp. 243–249.

Goel, S. C., and Itani, A. (1994a), "Seismic Behavior of Open-Web Truss Moment Frames," *ASCE J. Struct. Eng.*, Vol. 120, No. 6, pp. 1763–1780.

Goel, S. C., and Itani, A. (1994b), "Seismic Resistant Special Truss Moment Frames," *ASCE J. Struct. Eng.*, Vol. 120, No. 6, pp. 1781–1797.

Goel, S. C., and Tang, X. (1987), "Brace Failures and Column Buckling in Steel Structures," *Proc. SSRC Annu. Tech. Session*, pp. 175–190.

Gugerli, H., and Goel, S. C. (1982), "Inelastic Cyclic Behavior of Steel Bracing Members," *Rep. No. UMEE 82R1*, Department of Civil Engineering, University of Michigan, Ann Arbor, Mich.

Hassan, O., and Goel, S. C. (1991), "Modeling of Bracing Members and Seismic Behavior of Concentrically Braced Steel Structures," *Rep. No. UMCE 91-1*, Department of Civil Engineering, University of Michigan, Ann Arbor, Mich.

Husid, R. (1967), "Gravity Effects on the Earthquake Response of Yielding Structures," Ph.D. thesis, California Institute of Technology, Pasadena, Calif., June.

ICBO (1994), "Structural Engineering Design Provisions," in *Uniform Building Code*, Vol. 2, International Conference of Building Officials, Whittier, Calif.

Jain, A. K., and Goel, S. C. (1979), "Seismic Response of Eccentric and Concentric Braced Steel Frames with Different Proportions," *Rep. No. UMEE 79R1*, Department of Civil Engineering, University of Michigan, Ann Arbor, Mich., July.

Jain, A. K., Goel, S. C., and Hanson, R. D. (1978), "Static and Dynamic Behavior of Bracing Members and Seismic Response of Braced Frames with Different Proportions," *Rep. No. UMEE 78R3*, Department of Civil Engineering, University of Michigan, Ann Arbor, Mich.

Jennings, P. C., and Husid, R. (1968), "Collapse of Yielding Structures During Earthquakes," *ASCE J. Eng. Mech. Div.*, Vol. 94, No. EM5.

Kato, B. (1987), "Deformation Capacity of Tubular Steel Members Governed by Local Buckling," *J. Struct. Constr. Eng.*, No. 378, Aug., pp. 27–36.

Krawinkler, H., Bertero, V. V., and Popov, E. P. (1971), "Inelastic Behavior of Beam-to-Column subassemblages," *EERC Rep. No. 71-7*, University of California, Berkeley, Calif.

Lay, M. G. (1965), "Flange Local Buckling in Wide-Flange Shapes," *ASCE J. Struct. Div.*, Vol. 91, No. ST6, pp. 95–116.

Lee, S., and Goel, S. C. (1987), "Seismic Behavior of Hollow and Concrete-Filled Square Tubular Bracing Members," *Rep. No. UMCEE 87-11*, Department of Civil Engineering, University of Michigan, Ann Arbor, Mich.

Liu, Z., and Goel, S. C. (1988), "Cyclic Load Behavior of Concrete-Filled Tubular Braces," *ASCE J. Struct. Eng.*, Vol. 114, No. 7, pp. 1488–1506.

Mazzolani, F. M., and Piluso, V. (1993), "P-Δ Effect on Seismic Resistant Steel Structures," *Proc. SSRC Annu. Tech. Session*, pp. 271–282.

NEHRP (1994), *NEHRP Recommended Provisions for the Development of Seismic Regulations for New Buildings*, Federal Emergency Management Agency, Washington, D.C., p. 222A.

Rahnama, M., and Krawinkler, H. (1993), "Effects of Soft Soils and Hysteresis Model on Seismic Demands," *John A. Blume Earthquake Eng. Center Rep. No. 108*, Department of Civil Engineering, Stanford University, Stanford, Calif.

Schneider, S. P., Roeder, C. W., and Carpenter, J. E. (1993), "Seismic Behavior of Moment Resisting Steel Frames: Experimental Studies," *ASCE J. Struct. Div.*, Vol. 119, No. ST6, pp. 1885–1902.

SSRC (1988), *Guide to Stability Criteria for Metal Structures*, 4th ed., Wiley-Interscience, New York.

Sun, C. K., Berg, G. V., and Hanson, R. D. (1973), "Gravity Effect on Single Degree Inelastic System," *ASCE J. Eng. Mech. Div.*, Vol. 99, No. EM1, pp. 183–200.

Suzuki, T., Tamamatu, K., Ono, T., and Kimura, I. (1976), "On the Effects of Flange Local Buckling on the Plastic Deformation Behavior of H-Shaped Beam-Columns" (in Japanese), *Proc. AIJ Annu. Meet.*, Oct., pp. 1071–1072.

Suzuki, T., Sakai, S., and Nukui, Y. (1980), "A Study on Deformation Capacity of H-shaped Beam-Columns with Flange Local Buckling" (in Japanese), *Proc. AIJ Annu. Meet.*, Sept., pp. 1151–1152.

Takanashi, K. (1973), "Inelastic Lateral Buckling of Steel Beams Subjected to Repeated and Reversed Loadings," *Proc. 6th World Conf. Earthquake Eng.*, Rome, pp. 795–798.

Takanashi, K., Udagawa, K., and Tanaka, H. (1977), "A Simulation of Earthquake Response of Steel Frames," *Proc. 6th World Conf. Earthquake Eng.*, New Delhi, India, Vol. III, pp. 3156–3162.

Tang, X., and Goel, S. C. (1987), "Seismic Analysis and Design Considerations of Concentrically Braced Steel Structures," *Rep. No. UMCE 87-4*, Department of Civil Engineering, University of Michigan, Ann Arbor, Mich.

Tang, X., and Goel, S. C. (1989), "Brace Fractures and Analysis of Phase I Structure," *ASCE J. Struct. Eng.*, Vol. 115, No. 8, pp. 1960–1976.

Wang, W. Y. L. (1975), "Structural Instability During Earthquakes and Accelerogram Simplification," *Rep. No. UMEE 75R2*, Department of Civil Engineering, University of Michigan, Ann Arbor, Mich., Apr.

Yura, J. A., Galambos, T. V., and Ravindra, M. K. (1978), "The Bending Resistance of Steel Beams," *ASCE J. Struct. Div.*, Vol. 104, No. ST9, pp. 1356–1370.

CHAPTER TWENTY-ONE

STABILITY ANALYSIS BY FINITE ELEMENT METHOD

21.1 INTRODUCTION

The mathematical model for stability analysis of structures can be expressed either in terms of partial differential equations or in terms of the appropriate equilibrium conditions applied to the potential energy functional. For instance, in the case of an axially loaded prismatic column, the governing differential equations for buckling in terms of the lateral displacement components v and w and torsional deformation ϕ, based on the treatment in Galambos (1968), with the exception that the x-coordinate is measured along the longitudinal axis of the member, are

$$EI_y \frac{d^4w}{dx^4} + P\left(\frac{d^2w}{dx^2} + y_0 \frac{d^2\phi}{dx^2}\right) = 0 \tag{21.1a}$$

$$EI_z \frac{d^4v}{dx^4} + P\left(\frac{d^2v}{dx^2} - z_0 \frac{d^2\phi}{dx^2}\right) = 0 \tag{21.1b}$$

$$EC_w \frac{d^4\phi}{dx^4} - \left[GJ - \left(y_0^2 + z_0^2 + \frac{I_y + I_z}{A}\right)P\right]\frac{d^2\phi}{dx^2} + P\left(y_0 \frac{d^2w}{dx^2} - z_0 \frac{d^2v}{dx^2}\right) = 0 \tag{21.1c}$$

whereas the change in total potential energy for a member of length l from straight to buckled configuration is given by

$$\Pi = \frac{1}{2}\int_0^{\lambda} \left\{ EI_y \left(\frac{d^2w}{dx^2}\right)^2 + EI_z \left(\frac{d^2v}{dx^2}\right)^2 + EC_w \left(\frac{d^2\phi}{dx^2}\right)^2 + GJ\left(\frac{d\phi}{dx}\right)^2 - P\left[\left(\frac{dw}{dx}\right)^2 + \left(\frac{dv}{dx}\right)^2 + \left(y_0^2 + z_0^2 + \frac{I_y + I_z}{A}\right)\left(\frac{d\phi}{dx}\right)^2 + 2y_0 \frac{d\phi}{dx}\frac{dw}{dx} - 2z_0 \frac{d\phi}{dx}\frac{dv}{dx}\right] \right\} dx \tag{21.2}$$

with the bifurcation condition $\delta\pi = 0$. These equations are for a one-dimensional domain and are based on the assumption that no cross-sectional distortion due to local buckling is possible. To model local or interactive buckling, the member is considered as a fabricated plate structure and treated accordingly (Timoshenko and Gere, 1961; Allen and Bulson, 1981).

The determination of the buckling load based on the models 21.1 and 21.2 is trivial if the column is isolated, straight, and prismatic; the material is elastic; residual stresses are absent; deformations are small, shear deformations are negligible; no local (or localized) instability is possible; and loading is conservative. Complexities arising out of departures from these idealizing conditions will not lead to a closed-form solution to the problem, and in most instances will cease to be a bifurcation buckling problem. Unfortunately, however, practical stability problems tend to deviate from the ideal condition, and in many situations the idealizing approximations may not be acceptable. Typical examples are those of a column that is part of a frame; a member in which axial and transverse loads are present; the problem of buckling of plate elements in beams, girders, and columns; and interactive (local–global) buckling, all in the presence of imperfections of different types. The main recourse to handling the effect of most of these deviations is the use of numerical methods such as Ritz's energy method, the finite difference method, the finite element method, and more recently, the boundary element method. The availability of low-cost digital computers of ever-increasing power, coupled with advances in discrete numerical algorithms such as the finite element method, has made the solution of such practical problems of increasing size and complexity a practicable reality. In the past, the finite difference method was widely used for buckling analysis (Galambos, 1968; Bushnell, 1974) but was replaced by the finite element method, which was found to be more versatile. Although the boundary element method, a close cousin of the finite element method, has recently been applied successfully to the stability analysis of beams and plates (Manolis et al., 1986) in the present stage of its development, its applicability to real-life problems of stability cannot yet be fully realized.

In the finite element method, a problem with infinite number of degrees of freedom is reduced to one with a finite number of degrees of freedom, leading

to a set of linear or nonlinear simultaneous equations in terms of the unknown degrees of freedom of the problem. In the simplest case, this is achieved by partitioning the problem domain into a number of subdomains (or finite elements) with connectivity between the elements provided through common nodal points. The values of the unknown parameters at such nodal points represent the degrees of freedom of the problem. This geometric discretization is followed by the choice of piecewise approximating functions for the unknown variables, namely, v, w, and ϕ in Eqs. 21.1 and 21.2, satisfying certain minimum continuity requirements at the interelement boundaries, depending on the choice of type of nodal variables, which in turn will depend on the assumptions made in the basic mathematical model. A typical example is whether the effect of transverse shear deformations is included or ignored in the formulation. The set of simultaneous equations is arrived at by using the weighted residual method if the differential equations are used or by applying the bifurcation (or neutral equilibrium) condition to the potential energy functional of the system.

The quality of the resulting approximate solution depends on the closeness of the finite element model to that represented by the mathematical model. The closenss is controlled by the attributes of the problem, the numerical algorithm used, the distribution and nature of degrees of freedom, the number of digits of accuracy used in computations, and the types of algorithms used to evaluate the integrals and to solve the simultaneous equations. In the case of elliptic problems the whole spatial domain needs refinement because the boundary conditions affect the whole region. Model refinement in the case of initial value problems requires different strategies than for elliptic problems in the sense that the initial value problems are open ended, the future does not affect the present, and the refinement can be varied from one stage to another depending on the local behavior of the solution. A typical example of an initial value problem is that of dynamic stability analysis satisfying Liapnunov's criterion of stability (Bazant and Cedolin, 1991). This problem is elliptic in space and hyperbolic in time, due to the inclusion of the inertia term with or without damping effects (Bathe et al., 1975). In the case of deterministic nonlinear dynamic stability analysis of some structures (with sensitivity to certain problem parameters), the response may show random aperiodic motions accompanied by a certain degree of order and is known as *chaotic response* (Moon and Holmes, 1983; Moon, 1986; Seydel, 1988). In this context one may consider the transition from regular to chaotic motion to represent branching of the equilibrium path.

In elliptic problems, the quality of a solution can be improved upon by refining the finite element model either by using more elements of smaller size (known as *h-extension*), or by increasing the order of the piecewise approximating functions over a fixed mesh (known as *p-extension*), or by a combination of the two (known as *hp-extension*). Yet another alternative is to redistribute the degrees of freedom by strategically changing the size of the elements, reducing the number of elements, and increasing the order of approx-

imating functions so that the total number of degrees of freedom remain unchanged (known as *r-extension*).

In bifurcation buckling analysis, the set of simultaneous equations leads to a linear eigenvalue problem (Gallagher and Padlog, 1963). The eigenvalues correspond to critical loads with different buckling mode shapes. The eigenvalue analysis is preceded by a linear static analysis to determine the prebuckling stress field which is used in the neutral equilibrium condition. If geometrical nonlinearity is included in the prebuckling stress analysis, it becomes a quadratic eigenvalue problem. The eigenvalue analysis usually gives unconservative results for practical structures. Therefore, for most real-world structures one needs to undertake nonlinear analysis requiring stepwise linear solutions and/or iterative corrections. In such an event, however, because of the absence of the bifurcation point in the equilibrium path, Eqs. 21.1 and 21.2 should be suitably modified to reflect the total effect. The sources of nonlinearity may be geometric, material, or nonlinear interfaces. The objective is to find the load level (limit load) at which the structure becomes unstable, causing it to collapse. If desired, it is possible to trace the load-deformation path as well as the stages of progressive failure up to collapse. It may be noted that such an analysis may sometimes be algorithmically complex and computationally challenging.

21.2 WEIGHTED RESIDUAL FORMULATION

The differential equation for structural stability as an elliptic boundary value problem can be expressed as

$$L_j(u_i) = F_j \quad \text{in} \quad \Omega \qquad \text{with } j = 1, 2, 3, \ldots, n_e \quad \text{and} \quad i = 1, 2, 3, \ldots, n_v \tag{21.3}$$

with the boundary conditions

$$u_i = u_{ig} \quad \text{on} \quad \Gamma_{ig} \tag{21.4}$$

$$A_k(u_1, u_2, \ldots) = q_{kg} \quad \text{on} \quad \Gamma_{kq} \tag{21.5}$$

in which L_j and A_k are differential operators, n_e is the number of equations, and n_v is the number of variables. In Eq. 21.1a

$$L_1 \equiv \left[\left(EI\frac{d^4}{dx^4} + P\frac{d^2}{dx^2}\right), Py_0\frac{d^2}{dx^2}\right]$$

and for a pin–pin column, $u_{ig} = 0$ and $q_{kg} = 0$ at the ends, with $A_k = d^2/dx^2$. These boundary conditions are essential and natural, respectively. The term on the right-hand side, F_j, is equal to zero. The region Ω is $0 < x < l$. Let u_i^a represent the approximation solution and ω_i the weight function. The weak form of the differential equations will then take the following symmetric bilinear form: Find u_i^a such that for all ω_i,

$$\int_\Omega D(\omega_i)\left[\int L_j(u_1, u_2, \ldots)\, d\Omega\right] d\Omega - \int_\Omega \omega_i F_j\, d\Omega - \int_{\Gamma_{kg}} \omega_i q_{kg}\, d\Gamma = 0 \tag{21.6}$$

Here D is a differential operator.

In the finite element model, the problem domain is partitioned into a number of elements Ω_j^e, $j = 1, 2, 3, \ldots, NE$, where NE denotes the number of elements. In the case of the column-buckling problem represented by Eq. 21.1, the elements will be one-dimensional. If, however, it is desired to analyze local or interactive buckling characteristics of a column, the operator L will refer to a two-dimensional space at the element level, and three- or four-sided flat (plate) or curved (shell) finite elements will be used to discretize the plate and/or shell components (Basu and Akhtar, 1991). Shell structures are often discretized by facete (i.e., flat plate) elements, and this introduces additional sources of error due to approximation of the shell geometry. Axisymmetric shells are sometimes discretized by a series of ring (or rotational) elements, and in order to introduce nonsymmetric buckling modes, the prebuckling symmetric deformation needs to be perturbed by nonsymmetric modes (Gould and Basu, 1977). In this case the number of governing partial differential equations will be equal to the number of displacement components. In some rare cases it may also be necessary to use three-dimensional elements with four to six faces (i.e., tetrahedral, pentahedral, and hexahedral elements).

In evaluating the elemental integrals, the unknown functions u_i^e and the weight functions ω_i need to be defined. A convenient choice for u_i^e is a polynomial in one-, two-, or three-dimensional space, depending on the element type. Such a choice needs to be made for all the displacement components in the problem. In the case of rolled-steel sections, the component rectangular plates are sometimes discretized by a series of rectangular strips of length equal to the length of the column, and the displacement fields in such elements are expressed by terms of Fourier series in the length direction and by polynomials along the width of an element (Graves-Smith and Sridharan, 1978). This is opposite to what is done in the case of axisymmetric shells, for which the meridional variation of deformations in a ring element are expressed in terms of polynomials, and in the circumferential direction the variation is expressed by Fourier series (Gould, 1985). Modeling with such finite elements is sometimes termed the finite strip method. In the context of the *p*-version, Akhtar and Basu (1991) and Basu and Akhtar (1991) modeled thin-walled members with each component plate of the member represented by a single

finite element. For instance, a member with a channel section was modeled with just three finite elements. In view of the large aspect ratio of these elements, higher-order polynomial variation of displacement is assumed along the length of the element and a lower-order approximation is taken in the shorter direction.

In the case of finite elements, a convenient choice for u_i for an element is

$$u_i = \sum_{j=1}^{n} u_{ij} N_j \tag{21.7}$$

in which N_j are shape functions in one-, two-, or three-dimensional space and u_{ij} are unknown coefficients (or nodal variables) of the element. The same shape functions can be used as the weight function and there will be an equation corresponding to each $\omega_i = N_i$, with $i = 1, 2, \ldots, n$. The substitution of u_i and ω_i into Eq. 21.6 will lead to the following matrix equation:

$$[K]\{d\} = \{R\} \tag{21.8}$$

in which $[K]$, $\{d\}$, and $\{R\}$ are obtained by accumulating the contributions of all the elements. For an element, however,

$$K_{ij} = \int_{\Omega_e} c_{ij} D(N_i) D(N_j)\, d\Omega \qquad R_i = \int_{\Omega_e} N_i F\, d\Omega \qquad \{d\} = \{u_1, u_2, \ldots\}$$

where c_{ij} is a function of geometric and material parameters of the problem.

The matrix $[K]$ in Eq. 21.8 will normally have two parts, one first order and the other second or higher order, which will be a function of $\{d\}$. In the bifurcation buckling analysis, $\{R\} = 0$ and the matrix equation takes the following standard form of the linear symmetric eigenvalue problem:

$$([K_0] - \lambda[K_g])\{d\} = 0 \tag{21.9}$$

Here $[K_0]$ represents the normal linear stiffness matrix of the structure, whereas λ is the critical load factor (or eigenvalue), and $[K_g]$, the geometric stiffness matrix, is a function of the prebuckling stresses (which are functions of $\{d\}$) for $\lambda = 1$. The load vector $\{R\}$ appearing in Eq. 21.8 will make sense in the case of nonlinear analysis.

21.3 VARIATIONAL FORMULATION

In this case, the substitution of the assumed expressions for u_i (Eq. 21.7) into the expression for potential energy (Eq. 21.2), the performance of indicated integrations, and application of the principle of stationary potential energy as shown below also leads to Eq. 21.8.

$$\delta\Pi = \frac{\partial \Pi}{\partial u_{11}}\, \partial u_{11} + \frac{\partial \Pi}{\partial u_{12}}\, \delta u_{12} + \frac{\partial \Pi}{\partial u_{13}} + \cdots = 0$$

or

$$\frac{\partial \Pi}{\partial u_{ij}} = 0 \qquad i = 1, 2, 3, \ldots, n_v \quad \text{and} \quad j = 1, 2, \ldots, n \tag{21.10}$$

21.4 EIGENVALUE ANALYSIS

The eigenvalue problem represented by Eq. 21.9 can be solved for eigenvalues and eigenvectors by using any of the scores of methods available. Some of the popular methods are direct, inverse iteration, Jacobi, Givens, Householder-QR, Ritz, subspace iteration, Sturm sequence, Lanczos, and so on. Numerous computer programs for eigenvalue and eigenvector determination can be found in the EISPACK program developed at Argonne National Laboratories, IMSL (International Mathematical and Statistics Library), and NAG Library. For computational efficiency, before assembly of the global system the elemental internal degrees of freedom, if any, can be condensed out by using, say, Guyan condensation (Guyan, 1965). It may be noted that although this reduction is not exact, the resulting error in eigenvalues and eigenvectors have been found to be small.

21.5 SECOND- AND HIGHER-ORDER ANALYSES

Equations 21.1 and 21.2 are based on small deformation theory and linear elastic behavior. If the right side of Eq. 21.8 is nonzero, signifying the absence of a primary deformation path, the stiffness matrix will reflect the effect of geometric and/or material nonlinearities so that $[K] = [K(d)]$. The effect of geometric nonlinearity can be incorporated with different levels of sophistication (Martin, 1965; Oden, 1972; Wood and Zienkiewicz, 1977; Wempner, 1979), which may range from small strain/medium displacement theory such as second-order theory to large strain/large displacement theory. For instance, in the case of the axial bar considered earlier with second-order theory, the total axial strain can be expressed as

$$\varepsilon_x = \frac{du}{dx} - z\frac{d^2w}{dx^2} - y\frac{d^2v}{dx^2} - \omega_n\frac{d^2\phi}{dx^2} + \frac{1}{2}\left[\left(\frac{dw}{dx} + y\frac{d\phi}{dx}\right)^2 + \left(\frac{dv}{dx} - z\frac{d\phi}{dx}\right)^2\right] \tag{21.11}$$

Here the terms in brackets represent the second-order contribution. The parameter ω_n represents normalized unit warping of the section.

In the case of problems modeled with two-dimensional elements, similar strain–displacement relationships can be written (Sanders, 1963; Martin, 1965; Washizu, 1982; Akhtar and Basu, 1991). The effect of geometric imperfections can be incorporated by using the actual geometry of the imperfect structure or by sensitivity analysis (Haug et al., 1986), and the effect of residual stresses can be incorporated as initial stresses (Akhtar and Basu, 1991; Basu and Akhtar, 1991; Dutta, 1992). The inclusion of the effect of nonlinear material behavior involves different levels of approximation, which may be rigid–plastic, elastic–plastic, elastic–plastic strain-hardening-softening materials. Assumption of rigid–plastic material lends to plastic analysis of frames and yield-line analysis of plates and shells. If elastic–plastic material is used, the common assumption in the case of framed structures is that of localized plasticity (Lee and Baus, 1989; Chen and Lui, 1991; Gross, 1993). Unless the axial forces are very small (say, less than $0.15AF_y$), the plastic-moment capacity of the section will be less than $M_p = ZF_y$. A more accurate approach is to consider the spread of plasticity (Chen, 1994), requiring extra computational effort in the generation of matrices of elements undergoing plastic deformations requiring discretization of cross sections by narrow strips (White et al., 1991). Although the finite element formulation is based mostly on an assumed displacement approach, Halder (1990) and Halder and McNee (1989) have shown that in the case of framed structures the use of an assumed stress approach can lead to a computationally efficient algorithm.

In the case of plates and shells, the effect of plasticity can be included by defining a suitable yield criterion (say, von Mises), flow rule (say, Prandtl–Reuss), and the type of hardening (isotropic or kinematic) (Stricklin et al., 1973; Chen and Han, 1988; Lubliner, 1990; Zienkiewicz and Taylor, 1991). If the structure is modeled by large higher-order elements (p-version), it may be more convenient to use Lobatto quadrature instead of the conventional Gauss quadrature in evaluating the integrals associated with the element matrices and vectors because the former scheme allows quadrature points at element boundaries which normally are seats of plastic flow initiation (Basu and Shang, 1991).

In the case of framed structures, the conventional approach is to assume the joints to be rigid or pinned. In reality, however, the joints are semirigid. Various schemes have been put forward for joint flexibilities in stability and nonlinear analysis of frames (Ackroyd, 1979; Chen, 1980; Kassimali, 1983; Lui and Chen, 1987; Lee, 1990; Lee and Basu, 1989; Chen and Lui, 1991; Deierlein, 1992). A conceptually simple but computationally expensive approach is to assign linear (or nonlinear) spring elements corresponding to the force components. In general, one can use three axial and three torsional springs to model each joint. A more convenient approach is to consider rotational flexibility only without introducing additional degrees of freedom (Lee and Basu, 1989; Allen and Bulson, 1980).

In the case of nonlinear analysis, the load-deformation path of a structure can be traced by a suitable incremental and/or iterative procedure. In the incremental method the load is applied in small incremental steps, whereas in the purely iterative method the equilibrium condition is satisfied through iterative corrections, the algorithmically simplest example of which is the direct substitution method. A large number of algorithms (Oden, 1972; Stricklin et al., 1973; Bathe et al., 1975; Bergan and Soreide, 1977; Wood and Zienkiewicz, 1977; Ziekiewicz and Taylor, 1991) have been put forward based on these approaches individually or in combination. The primary objective of these algorithms is to ensure that a given load level the residuum $(\{R\} - [K(d)]\{d\}$ is equal to zero. In the case of dynamic stability analysis, which involves inclusion of geometric nonlinearity, attempts have been to increase computational efficiency by using a modal superposition method (Kato and Matsuoka, 1975).

In the direct substitution method, the solution at the kth cycle of iteration can be expressed as

$$\{d^k\} = \{d^{k-1}\} + \kappa[K(d^{k-1})]^{-1}(\{R\} - [K(d^{k-1})]\{d^{k-1}\}) \tag{21.12}$$

In the recursive relationship above, the solution corresponding to $k = 1$, $\{d^1\}$, can be based on the linear part of the stiffness matrix only. The relaxation factor, κ, the value of which can be suitably assigned (say, between 1 and 1.75) to improve the convergence rate (i.e., to achieve a result within the desired tolerance limit with the fewest possible number of iterations).

The direct substitution method is computationally inefficient because it requires updating and inversion of the stiffness matrix in each iteration cycle. Popular iterative methods like the Newton–Raphson and the modified Newton–Raphson are more efficient. For instance, if the inverse of the stiffness matrix, $[K(d^{k-1})]^{-1}$, appearing in Eq. 21.12 is replaced by its linear counterpart, it will not be necessary to get the inverse in each cycle of iteration, and we get the modified Newton–Raphson method. However, this method will require more cycles of iteration to achieve a given level of accuracy.

In the incremental method, the load is incremented through a number of steps. When material nonlinearity is predominant, the first step will usually correspond to imminent satisfaction of the yield criterion at the most highly stressed point. If at the end of each step, the stiffness matrix is upgraded on the basis of the latest known $\{d\}$ = value, we have the *tangent-stiffness method.* If, on the other hand, the stiffness matrix is kept unchanged from step to step, we get the *initial-stiffness method.* But to prevent the results from diverging from the true equilibrium path, it is important that within each load step a number of

iterative cycles are used as a corrective measure. This is especially true in the case of the latter method and may also be necessary in the case of the tangent-stiffness method if relatively large load steps are used.

In nonlinear analysis, efforts to identify the limit point and to follow the unloading path often lead to numerical instability, which may sometimes correspond to snap-through buckling, such as in an arch or a spherical shell. These problems are specially characterized by the existence of multiple (say, two) displacement values at some load levels. Various algorithms (Ramm, 1981), such as those based on arc-length methods (Riks, 1979; Crisfield, 1981, 1983) and the ones involving change of independent variables (Batoz and Dhatt, 1979) have been put forward to accurately trace the load-deformation path beyond the limit point and for the identification of multiple displacement values.

21.6 UNCERTAINTIES IN STABILITY ANALYSIS

The geometric, material, and loading parameters of stability problems are random in nature. It is well known that the response of some structures is sensitive to these parameters (Galambos, 1983; Der Kiureghean, 1989). It is, thus recognized that there is a need for an efficient method to determine the reliability of bifurcation and limit estimates by applying stochastic methods in the stability analysis of structures. The normal procedure is to use the mean-based, second-order, second-moment method. The purpose of a stochastic analysis is to allow explicitly for uncertainties in any of the problem parameters (say, the random variation of sectional properties such as area and moment of inertia) by incorporating the statistical characteristics into the analysis such that the statistical characteristics of response quantities of interest (say, bifurcation load) can be obtained. Such an analysis undertaken in the context of the finite element method is known as the *stochastic finite element method* (SFEM). The basic idea of this method is to use Taylor's series expansion of all the vector and matrix stochastic field variables typical of deterministic finite element methods about the mean values of the random variables, retaining only up to second-order terms and to use in the analysis only the first two statistical moments. In this way equations for the expected values and autocovariances of the nodal displacements can be obtained in terms of the nodal displacement derivatives with respect to the random variables (Vanmarcke and Grigoriu, 1983; Benaroya and Rehark, 1988). The same results could be obtained by carrying out a series of deterministic analyses with each value of the random variables in the ensemble, and then the corresponding response quantities of interest can be subjected to a formal statistical analysis to obtain the desired statistical parameters. But the computational time required will be orders of magnitude more than that by SFEM. The formulation of SFEM for bifurcation buckling analysis is given in Kleiber and Hien (1992).

A disadvantage of the stochastic approach to stability analysis is the need for extensive information about the random variables and distibution functions of the model. In the event of a limited amount of information, an uncertain yet nonprobabilistic model known as a *convext model* can be used (Ben-Haim and Elishakoff, 1990). A convex model of uncertainty is a set of functions specified by global characteristics such as input load functions, spectral properties, or functions of bounded energy. This approach has been used for static and dynamic analysis of shells with fragmentary information about the initial imperfections. Finite element buckling analysis in the presence of uncertainties based on this relatively recent method is expected to be computationally more efficient than SFEM and interpretation of the results is expected to be simpler (Elishakoff, 1994).

21.7 COMPUTER SOFTWARE

A large number of commercial and public-domain finite element software for buckling and nonlinear analyses are available. Public-domain software are distributed at a nominal cost by such agencies as NISEE, COSMIC, USAWES, NTIS, and LLNL. The advantages of low cost and availability of the source code of public-domain software are more than offset by the disadvantages of lack of maintenance and user support, especially in a production environment. Some of the popular general-purpose software with capabilities to undertake buckling and nonlinear analyses with different degrees of sophistication are ABAQUS, ADINA, ANSYS, COSMOS, NIKE3D, DYNA2D, DYNA3D, MSC/NASTRAN, NISA, PATRAN, STARDYNE, and GT-STRUDL. A group of special-purpose software with capabilities to undertake both analysis and design of framed structures, including SAP90, STAADIII, SODA, and ROB06, can carry out elastic second-order analysis (P–Δ type), in some cases based on gross simplifications (Basu and Dey, 1992). Most of this general- and special-purpose software can be executed under an MS/Window and/or UNIX/X-Windows environment and include graphics pre- and post-processing capabilities. Essentially, this is h-version software with grafted limited p-version capability in some cases. The one-dimensional frame elements are based on hermitian polynomials.

The capability to generate the finite element mesh interactively is a highly desirable feature. This feature is present more or less in all the software. The source code of software for simple second-order or elastic–plastic analyses of plane rigid frames can be found in the published literature (Wang, 1986; Harrison, 1990). To compile the latest information about the aforementioned software, a questionnaire was sent to each developer. A summary of the responses received follows.

ABAQUS: Developed by Hibbitt, Karlsson, and Sorensen, Inc., 1020 Main Street, Pawtucket, RI 02860. *Minimum hardware*: workstation (preferably,

32-Mb RAM). General purpose. *Buckling analysis*: linear and nonlinear, lateral-torsional buckling of frame members, allows joint flexibility, fabricated plate and shell structures, incorporates geometric imperfections by perturbing the mesh by previously calculated eigenvectors. *Nonlinear analysis to collapse*: space frames, fabricated plate structures and shell structures, traces equilibrium path to collapse, elastic-plastic material behavior, geometric nonlinearity, residual stresses, nonlinear joint behavior, interaction of axial load with plastic moment capacity of a section, unloading at a plastic hinge, spread of plastic deformation in a member. *Number of validation problems*: over 5000. No database of AISC standard sections. Available for lease or purchase (price > $5000). Academic lease costs significantly less.

ANSYS: Developed by ANSYS, Inc., Johnson Road, Houston, PA 15342. General purpose. *Minimum hardware*: IBM-compatible PC (preferably, 32-MB RAM, 300-MB hard disk). *Buckling analysis*: linear and nonlinear, allows joint flexibility, fabricated plate and shell structures, explicitly input geometric imperfections. *Nonlinear analysis to collapse*: space frames, fabricated plate and shell structures, traces equilibrium path to collapse, elastic–plastic material behavior, geometric nonlinearity, residual stress effects as equivalent thermal strains, nonlinear joint behavior, interaction of axial load with plastic moment capacity of a section, unloading at a plastic hinge. Database of standard AISC sections consist of I-shaped sections only. Available for lease or purchase (price > $5000). Academic lease costs significantly less.

NISA/DISPLAY: Developed by E.M.R.C., P.O. Box 696, Troy, MI 48099. *Hardware requirements*: PCs to supercomputers. General purpose. *Buckling analysis*: linear and nonlinear, lateral-torsional buckling of frame members, allows joint flexibility, fabricated plate and shell structures, explicitly input geometric imperfections. *Nonlinear analysis to collapse*: space frames, fabricated plate and shell structures, traces equilibrium path to collapse, elastic–plastic material behavior, geometric nonlinearity, residual stresses, nonlinear joint behavior, interaction of axial load with plastic moment capacity of a section. *Number of validation problems*: over 100. Database of AISC standard sections. Available for lease or purchase (price: $1000 to $2000 on PCs; $2500 to $5000 on workstations). Academic purchase costs less.

STARDYNE: Developed by RSR Software, 3628 Madison Ave., No. 19, North Highlands, CA 95660. *Minimum hardware*: IBM-compatible PC running MS/Windows (12-MB RAM and 28-MB hard drive). General purpose. *Buckling analysis*: linear and nonlinear, lateral-torsional buckling of frame members, allows joint flexibility, fabricated plate and shell structures, explicitly input geometric imperfections. *Nonlinear analysis to collapse*: space frames, fabricated plate and shell structures, traces equilibrium path to collapse, elastic–plastic material behavior, geometric nonlinearity, residual stresses, nonlinear joint behavior, localized plastic hinge, unloading at a plastic hinge. *Validation problems*: some. Database of AISC standard sections. Available for lease or purchase (price: $4000 to $9000).

NIKE3D: Developed by Lawrence Livermore National Laboratory, University of California, P.O. Box 808, Livermore, CA 94551. *Minimum hardware*: workstation. Special purpose. *Nonlinear analysis to collapse*: beam (two-node), solid (eight-node), and shell (four-node) elements, large displacement/strain, huge library of nonlinear materials, traces equilibrium path up to collapse. Beam elements are of questionable utility. *Validation problems*: some. Public-domain software. A two-dimensional version of the software, NIKE2D, is available.

DYNA3D: Developed by Lawrence Livermore National Laboratory, University of California, P.O. Box 808, Livermore, CA 94551. *Minimum hardware*: workstation. Special purpose. This is the dynamic version of NIKE3D with expanded element and material libraries. Well suited for studying dynamic collapse of complex structures that can be modeled by solid or shell elements. *Validation problems*: some. Public-domain software. A suite of associated software for three-dimensional mesh generation (INGRID) and for interactive postprocessing (TAURUS). For the two-dimensional version of DYNA called DYNA2D, the mesh generator is called MAZE and the postprocessor is called ORION.

PAFELB: Developed by Center for Advanced Structural Engineering, School of Civil and Mining Engineering, University of Sydney, Sydney, NSW, Australia. *Hardware limitations*: none. Special purpose. *Buckling analysis*: linear and nonlinear, lateral-torsional buckling of frame members, fabricated plate structures. *Nonlinear analysis to collapse*: geometric nonlinearity. *Validation problems*: some, documented in a recent textbook by N. S. Trahair (1993). Available for purchase (price between $500 and $1000).

21.8 VALIDATION PROBLEMS

Validation problems are necessary to check the ability of a software to model the geometry of a structure, including required element types, cross-sectional shapes, joint types, and so on; allow for the effects of geometric imperfections and residual stresses, different load configurations, geometric nonlinearities, and material nonlinearities; and capabilities such as determination of the bifurcation load and tracing the equilibrium path up to collapse. All software mentioned in Section 21.7 comes with a set of a few to hundreds of test problems for validating the software and to demonstrate its use for different types of problems. Apart from input data files and sample output files, information on the problems can be gathered from the software manuals. Additional information about the capabilities of software can be obtained

from survey publications related to the software. But such publications soon become obsolete because software undergoes upgrading and improvement on a regular basis. If the available test problems are not representative enough, the user may identify his or her own test problem for which analytical results or well-defined measurements of experiments are available.

The National Agency for Finite Element Methods and Standards has prepared a number of generic benchmark problems for validating finite element analysis software (NAFEMS, 1989). Basu (1990) gave details of various aspects of validation of finite element analysis software for buckling and nonlinear analyses. He also discussed the issues related to the desirable attributes of software for such analyses and the selection of test problems. Moreover, Lui (1993) and Clarke et al. (1993) discussed different aspects of validation of second-order elastic and elastic–plastic frame analysis software and discussed a number of test problems on beams and two-dimensional frames. A majority of the test problems presented by Basu (1990) can be found in Lee and Basu (1989) and Basu and Akhtar (1991). These problems include beams, frames with rigid and semirigid connections, and thin-walled structural components. Another important source of test problems are such NAFEMS publications as Crisfield et al. (1987) for problems related to geometric nonlinearity.

REFERENCES

Ackroyd, M. H. (1979), "Nonlinear Inelastic Stability of Flexibly-Connected Plane Steel Frames," Ph.D. dissertation, University of Colorado, Boulder, Colo.

Akhtar, M. N., and Basu, P. K. (1991), "A New *p*-Version General Plate Finite Element," *Comput. Methods Appl. Mech. Eng.*, Vol. 85, pp. 219–236.

Allen, H. G., and Bulson, P. S. (1980), *Background to Buckling*, McGraw-Hill, New York.

Basu, P. K. (1990), "Draft Guidelines for Evaluating Existing Stability Analysis Software," *Report of Task Group 28: Computer Applications*, Structural Stability Research Council, Lehigh University, Bethlehem, Pa.

Basu, P. K., and Akhtar, M. N. (1991), "Interactive and Local Buckling of Thin-Walled Members," *Thin-Walled Struct.*, Vol. 12, pp. 335–352.

Basu, P. K., and Dey, A. (1992), "Computer Software for Stability Analysis of Frames," in *Lecture Notes of Task Group 29 Workshop on Plastic Hinge Based Method for Advanced Analysis and Design of Steel Frames*, Structural Stability Research Council, Lehigh University, Bethlehem, Pa.

Basu, P. K., and Shang, S. P. (1991), "*p*-Version Modeling of Material Nonlinearity in Thin-Walled Members," in *First U.S. Natl. Congr. Comput. Mech.*, Abstracts, Session W9A, U.S. Association of Computational Mechanics, Chicago, p. S6.

Bathe, K. J., Ramm, E., and Wilson, E. L. (1975), "Finite Element Formulation for Large Deformation Dynamic Analysis," *Int. J. Numer. Methods Eng.*, Vol. 9, pp. 353–386.

Batoz, J. L., and Dhatt, G. S. (1979), "Incremental Displacement Algorithms for Nonlinear Problems," *Int. J. Numer. Methods Eng.*, Vol. 14, No. 8, pp. 1262–1267.

Bazant, Z. P., and Cedolin, L. (1991), *Stability of Structures*, Oxford University Press, New York, pp. 144–198.

Benaroya, H., and Rehark, M. (1988), "Finite Element Methods in Probabilistic Structural Analysis: A Selective Review," *Appl. Mech. Rev.*, Vol. 41, pp. 201–213.

Ben-Haim, Y., and Elishakoff, I. (1990), *Convex Models of Uncertainty in Applied Mechanics*, Elsevier, New York.

Bushnell, D. (1974), "Stress, Stability and Vibration of Complex, Branched Shells of Revolution," *Comput. Struct.*, Vol. 4, pp. 399–435.

Chen, W. F. (1980), "End Restraint and Column Stabillity," *ASCE J. Struct. Div.*, Vol. 106, No. ST11, pp. 2279–2295.

Chen, W. F. (1994), "Second-Order Inelastic Analysis for Frame Design," in *Proc. 1994 SSRC 50th Anniv. Conf*, Structural Stability Research Council, Lehigh University, Bethlehem, Pa.

Chen, W. F., and Han, D. J. (1988), *Plasticity for Structural Engineers*, Springer-Verlag, New York.

Chen, W. F., and Lui, E. M. (1991), *Stability Design of Steel Frames*, CRC Press, Boca Raton, Fla.

Clarke, M. J., Bridge, R. O., Hancock, G. J., and Trahair, N. S. (1993), "Benchmarking and Verification of Second-Order Elastic and Inelastic Frame Analysis Programs," in *Plastic Hinge Based Methods for Advanced Analysis and Design of Steel Frames* (ed. D. W. White and W. F. Chen), Structural Stability Research Council, LeHigh University, Bethlehem, Pa., pp. 245–274.

Crisfield, M. A. (1981), "A Fast Incremental/Iterative Solution Procedure That Handles Snap-Through," *Comput. Struct.*, Vol. 13, pp. 55–62.

Crisfield, M. A. (1983), "An Arc-Length Method Including Line-Searches and Accelerations," *Int. J. Numer. Methods Eng.*, Vol. 19, pp. 1269–1289.

Crisfield, M. A., Hunt, G. W., and Duxbury, P. G. (1987), *Benchmark Tests for Geometric Nonlinearity*, NAFEMS, Glasgow, Scotland.

Deierlein, G. G. (1992), "An Inelastic Analysis and Design System for Steel Frames with Partially Restrained Connections," in *Connections in Steel Structures: Part II: Behavior, Strength, and Design* (ed. R. Bjorhovde, A. Colson, G. Haaijer, and J. W. B. Stark), American Institute of Steel Construction, Chicago, pp. 408–417.

Der Kiureghean, A. (1989), "Measures of Structural Safety Under Imperfect States of Knowledge," *J. Struct. Eng.*, Vol. 115, No. 5, pp. 1119–1140.

Dutta, A. (1992), "Finite Element Procedures for Inelastic Stability Analysis of Plate Structures," Ph.D. dissertation, Purdue University, West Lefayette, Ind.

Elishakoff, I. (1994), "Nonlinear Buckling of a Column with Initial Imperfections via Stochastic and Non-stochastic Convex Models," *Int. J. Non-linear Mech.*, Vol. 29, No. 1, pp. 71–82.

Galambos, T. V. (1968), *Structural Members and Frames*, Prentice Hall, Upper Saddle River, N.J.

Galambos, T. V. (1983), "Reliability of Axially Loaded Columns," *Eng. Struct.*, Vol. 5, pp. 73–78.

Gallagher, R. H., and Padlog, J. (1963), "Discrete Element Approach to Structural Stability Analysis," *AIAA J.*, Vol. 1, No. 6, pp. 1437–1439.

Gould, P. L. (1985), *Finite Element Analysis of Shells of Revolution*, Pitman Advanced Publishing Program, Boston.

Gould, P. L., and Basu, P. K. (1977), "Geometric Stiffness Matrices for the Finite Element Analysis of Rotational Shells," *J. Struct. Mech.*, Vol. 5, No. 1, pp. 87–105.

Graves-Smith, T. R., and Sridharan, S. (1978), "A Finite Strip Method for the Buckling of Plate Structures Under Arbitrary Loading," *Int. J. Mech. Sci.*, Vol. 20, pp. 685–693.

Gross, J. L. (1993), "Workgroup Summary Report: Plastic Hinge Based Techniques for Advanced Analysis," in *Plastic Hinge Based Methods for Advanced Analysis and Design of Steel Frames: An Assessment of the State-of-the-Art* (ed. D. W. White and W. F. Chen), Structural Stability Research Council, Lehigh University, Bethlehem, Pa.

Guyan, R. J. (1965), "Reduction of Stiffness and Mass Matrices," *J. AIAA.*, Vol. 3, p. 380.

Halder, A. (1990), "An Efficient Algorithm for Nonlinear Postbuckling Analysis of Structures," in *Proc. Annu. Tech. Session SSRC*, pp. 313–324.

Halder, A., and McNee, K. M. (1989), "Elasto-plastic Large Deformation Analysis of PR Steel Frames for LRFD," *Comput. Struct.*, Vol. 31, No. 5, pp. 811–823.

Harrison, H. B. (1990), *Structural Analysis and Design*, Part 1: pp. 125–134, Part 2: pp. 611–632, Pergamon Press, Elmsford, N.Y.

Haug, E. J., Choi, K. K., and Komkov, V. (1986), *Design Sensitivity Analysis of Structural Systems*, Academic Press, San Diego, Calif.

Kassimali, A. (1983), "Large Deformation Analysis of Elastic–Plastic Frames," *ASCE J. Struct. Eng.*, Vol. 109, No. 8, pp. 1869–1885.

Kato, S., and Matsuoka, O. (1975), "Dynamic Buckling Analysis of Spherical Shells by Combined Use of Finite Element Method and Mode Superposition Method," *J. Architect. Inst. Jpn.*, Vol. 50, No. 235–236 (Engl. transl.).

Klieber, M., and Hien, T. D. (1992), *The Stochastic Finite Element Method*, Wiley, New York.

Lee, S. L. (1990), "Limit Strength of Semi-rigid Frames," Ph.D. dissertation, Vanderbilt University, Nashville, Tenn.

Lee, S. L., and Basu, P. K. (1989), "Secant Method for Nonlinear Semi-rigid Frames," *J. Constr. Steel Res.*, Vol. 114, pp. 273–299.

Lubliner, J. (1990), *Plasticity Theory*, Macmillan, New York.

Lui, E. M. (1993), "Verification and Benchmark Problems: Work Group Summary Report," in *Plastic Hinge Based Methods for Advanced Analysis and Design of Steel Frames* (ed. D. W. White and W. F. Chen), Structural Stability Research Council, Lehigh University, Bethlehem, Pa., pp. 275–278.

Lui, E. M., and Chen, W. F. (1987), "Steel Frame Analysis with Flexible Joints," Special Issue on Joint Flexibility in Steel Frames (ed. W. F. Chen), *J. Constr. Steel Res.*, pp. 161–202.

Manolis, G. D., Beskos, D. E., and Pineros, M. F. (1986), "Beam and Plate Stability by Boundary Elements," *Comput. Struct.*, Vol. 22, No. 6, pp. 917–923.

Martin, H. C. (1965), "On the Derivation of Stiffness Matrices for the Analysis of Large Deflection and Stability Problems," in *Proc. Conf. Matrix Methods Struct. Mech.*, Wright Patterson Air Force Base, Ohio.

Moon, F. C. (1986), *Chaotic Vibrations*, Wiley, New York.

Moon, F. C., and Holmes, P. J. (1983), "Strange Attractors and Chaos in Nonlinear Mechanics," *ASME J. Appl. Mech.*, Vol. 50, pp. 1021–1032.

NAFEMS (1989), *The Standard NAFEMS Benchmarks*, Department of Trade and Industry, Glasgow, Scotland.

Oden, J. T. (1972), *Finite Elements of Nonlinear Continua*, McGraw-Hill, New York.

Ramm, E. (1981), "Strategies for Tracing Nonlinear Responses near Limit Points," in *Nonlinear Finite Element Analysis in Structural Mechanics*, Springer-Verlag, New York, pp. 63–89.

Riks, E. (1979), "An Incremental Approach to the Solution of Snapping and Buckling Problems," *Int. J. Solids Struct.*, Vol. 15, pp. 529–551.

Sanders, J. L., Jr. (1963), "Nonlinear Theories of Thin Shells," *Q. Appl. Math.*, Vol. 21, No. 1, pp. 21–36.

Seydel, R. (1988), *From Equilibrium to Chaos: Practical Bifurcation and Stability Analysis*, Elsevier, New York.

Stricklin, J. A., Heisler, W. E., and von Riesemann, W. A. (1973), "Evaluation of Solution Procedures for Material and/or Geometrically Nonlinear Structural Analysis," *J. AIAA*, Vol. 11, pp. 292–299.

Timoshenko, S. P., and Gere, J. M. (1961), *Theory of Elastic Stability*, McGraw-Hill, New York.

Trahair, N. S. (1993), *Flexural–Torsional Buckling of Structures*, E&FN Spon, London.

Vanmarcke, E. H., and Grigoriu, M. (1983), "Stochastic Finite Element Analysis of Simple Beams," *ASCE J. Eng. Mech.*, Vol. 109, No. 5, pp. 1203–1214.

Wang, Chu-Kia (1986), *Structural Analysis on Microcomputers*, Macmillan, New York, pp. 275–304.

Washizu, K. (1982), *Variational Methods in Elasticity and Plasticity*, 3rd ed., Pergamon Press, Elmsford, N.Y.

Wempner, G. A. (1979), "Discrete Approximations Related to Nonlinear Theories," *Int. J. Solids Struct.*, Vol. 7, pp. 1581–1599.

White, D. W., Liew, J. W. R., and Chen, W. F. (1991), "Second-Order Inelastic Analysis for Frame Design: A Report to SSRC Task Group 29 on Recent Research and the Perceived State-of-the-Art," *Res. Rep. No. CE-STR-91-12*, School of Civil Engineering, Purdue University, West Lafayette, Ind.

Wood, R. D., and Zienkiewicz, O. C. (1977), "Geometrically Nonlinear Analysis of Beams, Frames, Arches, and Axisymmetric Shells," *Comput. Struct.*, Vol. 17, pp. 725–735.

Zienkiewicz, O. C., and Taylor, R. L. (1991), *The Finite Element Method*, Vol. 2, 4th ed., McGraw-Hill, New York, pp. 211–311.

APPENDIX A

GENERAL REFERENCES ON STRUCTURAL STABILITY

Allen, H. G., and Bulson, P. S. (1980), *Background to Buckling*, McGraw-Hill, Maidenhead, Berkshire, England.

ASCE (1971), "Plastic Design in Steel: A Guide and a Commentary," *ASCE Man. Rep. Eng. Pract.*, American Society of Civil Engineers, New York.

ASTM (1967), "Test Methods for Compression Members," *ASTM Spec. Publ. No. 419*, American Society for Testing and Materials, Philadelphia, Pa.

Baker, J. F., Horne, M. R., and Heyman, J. (1956), *The Steel Skeleton*, Vol. II, *Plastic Behavior and Design*, Cambridge University Press, Cambridge.

Ballio, G., and Mazzolani, F. M. (1983), *Theory and Design of Steel Structures*, Chapman & Hall, London.

Bazant, Z. P., and Cedolin, L. (1991), *Stability of Structures*, Oxford University Press, New York.

Bleich, F. (1952), *Buckling Strength of Metal Structures*, Engineering Societies Monograph, McGraw-Hill, New York (prepared in collaboration with Column Research Council).

Brush, D. O., and Almroth, B. O. (1975), *Buckling of Bars, Plates, and Shells*, McGraw-Hill, New York.

Chajes, A. (1974), *Principles of Structural Stability Theory*, Prentice Hall, Upper Saddle River, N.J.

Chen, W. F., and Atsuta, T. (1977), *Theory of Beam-Columns*, Vols. 1 and 2, McGraw-Hill, New York.

Chen, W. F., and Han, D. J. (1985), *Tubular Members in Offshore Structures*, Pitman Advanced Publishing Program, Boston.

Chen, W. F., and Kim, S.-E. (1997), *LRFD Steel Design Using Advanced Analysis*, CRC Press, Boca Raton, Fla.

Chen, W. F., and Lui, E. M. (1987), *Structural Stability: Theory and Implementation*, Elsevier, New York.

Chen, W. F., and Lui, E. M. (1991), *Stability Design of Steel Frames*, CRC Press, Boca Raton, Fla.

Chen, W. F., and Sohal, I. (1995), *Plastic Design and Second-Order Analysis of Steel Frames*, Springer-Verlag, New York.

Chen, W. F., Goto, Y., and Liew, J. Y. R. (1996), *Stability Design of Semi-rigid Frames*, Wiley, New York.

Chilver, A. H., ed. (1967), *Thin-Walled Structures*, Wiley, New York.

Column Research Committee of Japan (1971), *Handbook of Structural Stability*, Corona Publishing Co., Tokyo (in English).

Column Research Council (1962), "Column Research Council Symposium on Metal Compression Members," *ASCE Trans.*, Vol. 127.

Eckhaus, W. (1965), *Studies in Nonlinear Stability Theory*, Springer-Verlag, New York.

Fukumoto, Y., and Lee, G. C. (1992), *Stability and Ductility of Steel Structures Under Cyclic Loading*, CRC Press, Boca Raton, Fla.

Galambos, T. V. (1968), *Structural Members and Frames*, Prentice-Hall, Upper Saddle River, N.J.

Gallagher, R. H. (1975), *Finite Element Analysis Fundamentals*, Prentice Hall, Upper Saddle River, N.J.

Gerard, G. (1962), *Introduction to Structural Stability Theory*, McGraw-Hill, New York.

Gjelswik, A. (1981), *Theory of Thin-Walled Bars*, Wiley, New York.

Hetenyi, M. (1946), *Beams on Elastic Foundations*, University of Michigan Press, Ann Arbor, Mich.

Hoff, N. J. (1956), *The Analysis of Structures*, Wiley, New York.

Johnston, B. G. (1981), "Selected Papers," FERS and SSRC, Bethlehem, Pa.

Johnston, B. G., ed. (1976), *Guide to Stability Design Criteria for Metal Structures*, 3rd ed., Wiley, New York.

Mazzolani, F. M. (1985), *Aluminum Alloy Structures*, Pitman Advanced Publishing Program, Boston.

McGuire, W. (1968), *Steel Structures*, Prentice Hall, Upper Saddle River, N.J.

Narayanan, R., ed. (1982), *Axially Compressed Structures*, Applied Science Publishers, Barking, Essex, England.

Narayanan, R., ed. (1983a), *Beams and Beam-Columns*, Applied Science Publishers, Barking Essex, England.

Narayanan, R., ed. (1983b), *Plated Structures*, Elsevier Applied Science Publishers, London.

Narayanan, R., ed. (1985a), *Steel Framed Structures*, Elsevier Applied Science Publishers, London.

Narayanan, R., ed. (1985b), *Shell Structures*, Elsevier Applied Science Publishers, Barking Essex, England.

Roorda, J. (1980), *Buckling of Elastic Structures*, University of Waterloo, Waterloo, Ontario, Canada.

Salmon C. G., and Johnson, J. E. (1995), *Steel Structures, Design and Behavior*, Harper & Collins, New York.

Sharp, M. L. (1992), *Behavior and Design of Aluminum Structures*, McGraw-Hill, New York.

Simitses, G. J. (1976), *An Introduction to the Elastic Stability of Structures*, Prentice Hall, Upper Saddle River, N.J.

SSRC (1991), *Stability of Metal Structures: A World View*, Structural Stability Research Council, Bethlehem, Pa.

SSRC (1993), *Is Your Structure Suitably Braced*, Structural Stability Research Council Bethlehem, Pa.

Supple, W. J. (1973), *Structural Instability: Fundamentals of Post-buckling Behavior of Structures*, IPC Science and Technology Press, Guildford, England.

Tall, L., ed. (1974), *Structural Steel Design*, Ronald Press, New York.

Thompson, J. M. T., and Hunt, G. W. (1984), *Elastic Instability Phenomena*, Wiley, New York.

Trahair, N. S. (1993), *Flexural-Torsional Buckling of Columns*, E&FN Spon, London.

Trahair, N. S., and Bradford, M. A. (1988), *The Behavior and Design of Steel Structures*, Chapman & Hall, London.

Vlasov, V. Z. (1961), *Thin-Walled Elastic Beams*, Israel Program for Scientific Translation, for NSF, Jerusalem (in English; original Russian edition, 1959).

Winter, G. (1975), *The Collected Papers of George Winter*, Cornell University Press, Ithaca, N.Y.

Yu, W.-W. (1991), *Cold-Formed Steel Design*, 2nd ed., Wiley, New York.

Ziegler, H. (1968), *Principles of Structural Stability*, Blaisdell, Waltham, Mass.

APPENDIX B

TECHNICAL MEMORANDUMS OF STRUCTURAL STABILITY RESEARCH COUNCIL

B.1 TECHNICAL MEMORANDUM NO. 1: THE BASIC COLUMN FORMULA*

The Column Research Council has brought out that it would be desirable to reach agreement among engineers as to the best method for predicting the ultimate load-capacity in compression of straight, prismatic, axially loaded, compact members of structural metals. It was proposed that Research Committee A of the Council be assigned the problem of reporting on the correctness and desirability of the tangent-modulus column formula. This formula involves simply the substitution of the tangent modulus, E_t, for E in the Euler formula. This formula may be written

$$\frac{P}{A} = \frac{\pi^2 E_t}{(KL/r)^2}$$

where

*Issued May 19, 1952. Technical Memorandum No. 5 reflects current position of SSRC and replaces Technical Memorandum No. 1.

P = the ultimate load (lb)
A = the cross-sectional area (in.^{2})
E_t = the compressive tangent modulus (slope of the compressive stress-strain curve) of the material in the column at the stress P/A (lb/in.^{2})
r = least radius-of-gyration of cross section (in.)
L = the length of the column (in.)
K = a constant depending on end conditions
$K = 2$ for one end fixed and the other end free
$K = 1$ for both ends simply supported
$K = 0.7$ for one end fixed and the other end simply supported
$K = 0.5$ for both ends fixed

For materials which exhibit upper and lower yield points in compression, the lower yield point is to be considered as the limiting value of P/A.

Information and reference to literature supporting the foregoing statement will be made available on request to the Secretary of the Column Research Council.

It is the considered opinion of the Column Research Council that the tangent-modulus formula for the buckling strength affords a proper basis for the establishment of working-load formulas.

The column formula presented here differs in form from the familiar Euler formula only in that the tangent modulus-of-elasticity is substituted for the ordinary modulus-of-elasticity. There is, however, a great practical difference between the two formulas, for whereas the Euler formula can be solved directly for the average stress corresponding to any given slenderness ratio, the tangent-modulus formula cannot. It is not the intention to advocate the use of the tangent-modulus formula in design, but rather to propose it as the basis for relating the compressive stress-strain properties of the material to the column strength of the material. The formula furnishes the information for approximating to the average stress in terms of the ratio of slenderness, for any type of centrally loaded column under consideration, by making suitable assumptions with respect to such items as accidental eccentricity, initial curvature of member, residual stresses, and variation in properties of the material.

Advisory Preface to Technical Memoranda Nos. 2, 3, and 4.

The reader is advised that Technical Memoranda Nos. 2, 3, and 4, although accurate, need care and interpretation when used in conjunction with modern testing and data acquisition equipment. Thus it may be inappropriate to adhere to a specific sensitivity of measured strain in Technical Memorandum No. 2 when the strain-measuring device referred to is no longer in general use. Similarly, for Technical Memoranda Nos. 3 and 4, it may not be appropriate to specify crosshead speeds in the testing machine when the testing machine has stroke or strain controlled by a servomechanism. In Technical memorandum

No. 4, the first alignment method of preparing the column for testing is no longer in general use—rather, most tests use the second alignment method, by which columns are tested "as is" with exact measurements of initial out-of-straightness which are used with analytical strength predictions. Although these Technical memoranda remain correct, it has not been possible to update them to reflect today's practice in this edition of the guide, since the methods in use today have not yet been standardized. These Technical Memoranda have been retained in this edition so as to provide a basis of comparison for the researcher.

B.2 TECHNICAL MEMORANDUM NO. 2: NOTES ON THE COMPRESSION TESTING OF METALS

For predicting column strength it is necessary to have compressive and tensile stress-strain curves of the column material. In order that the tension and compression specimens be as nearly as possible equally representative of the material, the thickness of compression specimens should approximate that of the tension specimens. Preferably each pair of tensile and compressive specimens should be cut from the same coupon (conveniently, the section or slice remaining from the residual strain measurements).

Specimens taken from a flange or web of a rolled shape, or from a plate, should be rectangular in cross section. They should be machined on all four sides with grinding as the final machining operation (on a magnetic grinder for steel). The ends of the specimens should be ground plane and normal to the longitudinal axis of the specimen. The ends should be parallel within close limits.

In general, compression specimens (Fig. B.1) should be no longer than necessary of accommodate a compressometer or resistance strain gages and

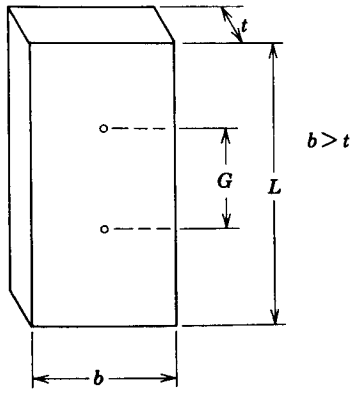

Fig. B.1 Compression test specimen.

have, between each end of the specimen and the adjacent end of the gage length, a distance, $\frac{1}{2}(L-G)$, at least equal to the greatest cross-sectional dimension, b. The compressometer should meet the specifications for Class A Extensometers (ASTM Standard E83–67, "Verification and Classification of Extensometers") which limit the error of indicated strain to 0.00001. The length should not be less than the greatest cross-sectional dimension; and in order to keep the specimen short, the gage length should not exceed twice this dimension. If the length of a rectangular specimen is more than about 4.5 times the length of the shorter side of the rectangle or, for a circular specimen, more than four times the diameter, difficulty may be expected in avoiding premature bending (column action), and special precautions must be taken to prevent excessive bending.*

Referring to Fig. B.1, the following relationships summarize the preceding requirements for a member of rectangular cross section:

$$G \geqslant b$$
$$G \geqslant t$$
$$4.5t \geqslant L \geqslant (G+2b)$$

in which G = gage length; b = specimen width; L = specimen length; and t = specimen thickness. Specimens should be measured with a micrometer reading to 0.001 in. (0.025 mm) and the dimensions recorded. Nominal dimensions should not be used in computations.

Both ends of a compressive specimen should bear on smoothly finished plane surfaces. The bearing blocks should be made of, or faced with, a suitably hard material so that the faces of the blocks will not suffer permanent deformation during the test. The blocks should be at least as thick as the smallest cross-sectional dimension of the specimen and should project beyond the contact area a distance at least half as great as the smallest cross-sectional dimension.

Precautions should be taken to ensure uniform distribution of strain over the cross section and to prevent relative rotation of upper and lower bearing surfaces during testing. The following are three suggested procedures for attaining these goals:

1. Use of a subpress loaded through a push rod acting at the lower end of the hollow plunger.
2. Use of bearing blocks that will permit initial adjustment for parallelism of bearing surfaces.†

*For rectangular specimens see ASTM Standard E9-70, "Methods of Compression Testing of Metallic materials."

† See Fig. 1 in ASTM Standard E9-70, "Methods of Compression Testing of Metallic materials."

3. Use of a thin capping layer of Hydrostone between the upper bearing block and the testing machine crosshead. While the hydrostone is setting, a small load should be maintained.

If tilting or lateral displacement of one testing machine crosshead relative to the other during loading is a suspected possibility, it is suggested that a subpress be used to load the compressive specimen so as to reduce the probability of bending during compression. The hollow plunger should fit closely within the annulus of the subpress frame (but vertical motion of the plunger should not be restricted).

Adjustable bearing blocks cannot be depended upon to compensate for tilting of the testing machine heads during loading and should be used only if appreciable relative tilting of the heads does not occur. If a spherical bearing block is used, it should be at the upper end of the specimen (for specimens tested with the longitudinal axis vertical). It is desirable that the center of the spherical surface lie within the flat surface on which the specimen bears. Also, it is essential that the longitudinal axis of the specimen pass, closely, the center of the spherical surface, so that the eccentricity of loading may not be great enough to overcome the friction necessary to rotate the block.

The compressive specimen should be aligned so that the deviation in strain indicated by any gage is less than 5% of the average of all gages when the specimen is subjected to a stress of about one-half the yield strength of the material. At least three strain gages need to be mounted on the specimen and monitored during the aligning operation to meet this requirement.

If the length of the specimen does not exceed the maximum recommended length (4 or 4.5 times a cross-section dimension for a circular or rectangular specimen, respectively), strains should be measured during the test with an averaging compressometer or with two strain gages mounted opposite each other. In the case of longer specimens tested without lateral support, reasonable certainty of uniform strain distribution can be obtained only with the use of not fewer than two strain gages on the wide sides of thin rectangular specimens, or three gages on thick rectangular or square specimens (one at the center of each of three sides), or three gages on circular specimens. Strain measurement with only one gage is unreliable. The stress-strain curve should extend from zero stress, and strain, to values for which the ratio of total stress to total strain is less than $0.7E$, or to a total strain of at least 0.01, whichever results in the larger strain.

Material properties will be a function of the loading rate and therefore the rate should be recorded. Dynamic loading should be interrupted in the yielding region so as to obtain at least three values of the static yield stress (yield stress at essentially zero strain rate) for metals with a yield plateau.

Compressive stress-strain curves should be plotted with stress as ordinate and strain as abscissa to as large a scale as the quality of the data justifies. The individual values of stress and strain should also be reported. When applying

the procedures above to material that is suspected of showing a considerable variation in properties, the specimens should be taken from a sufficient number of locations to define the extent of the variation in properties.

Determination of Typical Stress-Strain Curve from a Number of Stress-Strain Curves

It is assumed that the compressive stress-strain relationships of enough specimens will be determined so that all variations of the material likely to be submitted under a given specification will be represented. The yield strength values determined from the individual tests should be presented in the form of a distribution plot in which the percentage of the total number of tests for which the yield strength is within a certain range is plotted against the average of the range. The standard deviation should be indicated if the number of specimens is significant.

Several methods for constructing a typical stress-strain curve from a number of individual curves have been proposed. One simple method, which has had considerable use, is described as follows:

1. Record the strain departures from the modulus line for various fixed percentages of the particular individual yield strength value. These percentages should cover stresses from the proportional limit to above the yield strength.
2. Average all offset values for each of the fixed percentages. (For steel shapes it is recommended that the offsets be weighted in proportion to relative flange and web areas.) A curve may be plotted in which the ordinate is the percent of yield strength and the abscissa is the average strain offset from the initial modulus line.
3. For any appropriate yield strength value, a typical cuve can then be plotted by adding the offset values to the strain consistent with the elastic-modulus values.

Figure B.2 shows a typical compressive stress-strain curve of a high-strength aluminum alloy. Lines have been drawn tangent to this curve at different values of stress, P/A. The slopes of these lines define the corresponding tangent modulus, E_t, essential to the determination of the basic column strength.*†

*Convenient and accurate techniques are available for determining the tangent modulus; one such technique is described in *NACA TN*, No. 2640, "Interaction of Column and Local Buckling in compression members, " by P. P. Bijlaard and G. P. Fisher.

†See "The Basic Column formula," *Tech. Memo.*, No. 1, Column Research Council, May 19, 1952. (Presented previously in this Appendix.)

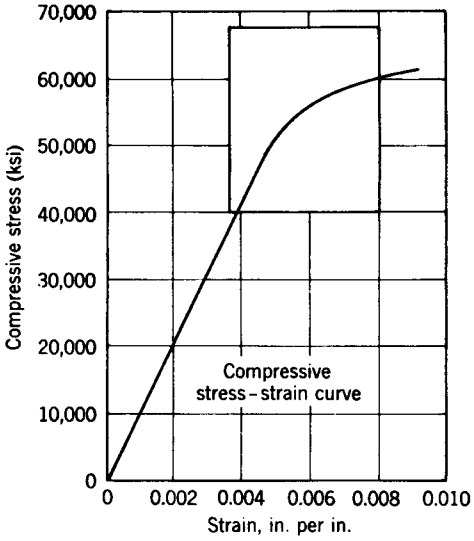

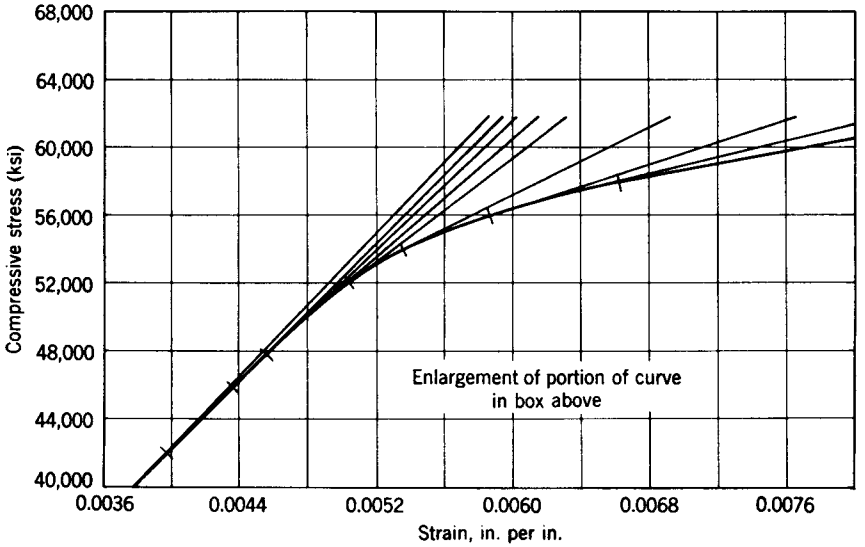

Fig. B.2 Typical compression stress-strain curve of a high-strength aluminum alloy. 1 ksi = 6.9 MPa.

B.3 TECHNICAL MEMORANDUM NO. 3: STUB-COLUMN TEST PROCEDURE‡§

A stub column is a member sufficiently short so as to preclude member buckling when compressed, but sufficiently long to contain the same initial residual stress patern as a much longer member cut from the same stock. For cold-formed steel sections, which generally have thin-walled plate elements, the stub-column test is aimed at determining the effect of local buckling as well as the effect of cold-forming on the column performance. For these sections the stub-column length should be sufficiently long to exhibit such behavior. Because column strength may be expressed as a function of the tangent modulus determined from the stress-strain relationship of the stub-column test,§§ this test is an important tool for investigating column strength.

The difference between Young's modulus and the tangent modulus at any load level, determined from a compression test on the complete cross section, essentially reflects the effect of residual stresses. This may be realized when one consideres that the cross section, hitherto completely elastic under load, becomes elastic-plastic at the proportional limit as the member is loaded further. The presence of residual stresses in the cross section implies that some fibers are in a state of residual compression. The fibers in a state of residual compression are the first to reach the yield point under load.

The difference between the behavior of a column free of residual stresses and one containing residual stresses lies in the fact that, beyond the proportional limit for the latter, both the tangent modulus and the effective moment-of-inertia are greater for the column free of residual stresses. (The behavior of a stub column, however, because of its shorter length, reflects only the effect of residual stresses on the tangent modulus; the reduction in the effective moment-of-inertia due to plastification has no effect on its behavior.) Under load, some parts of the column cross section will yield before others, leading to a decrease of the effective moment of inertia and hence in the strength of the column, as those proportions of the cross section which have yielded support

‡This document was originally prepared by L. Tall under the technical guidance of Task Group 1 of the Column Research Council as *Lehigh Univ. Fritz Eng. Lab. Rep.*, No. 220A.36 (February 1961), and was revised by an International Institute of Welding Working Group consisting of H. Louis (Belgium) Chairman, M. Marincek (Yugoslavia), and L. Tall (U.S.A.). It was approved by the IIW at the Annual Conference, Oslo, 1962, as Class C Document No. X-282-61. Task Group 6 of the Column Research Council further revised the document in 1974.

§See p. 808 for advisory preface.

§§Column strength is not always a direct function of the tangent modulus. for example, for an H-shape bent about the strong axis, irrespective of the stress-strain relationship and the pattern of residual stress, the function is direct. However, for an H-shape bent about the weak axis (only for rolled or welded built-up shapes with universal mill plates whose stress-strain curve can be considered as elastic perfectly plastic) the strength is approximately a function of the cube of the tangent modulus. Because there is no direct or simple relationship for other cases, care must be taken in applying the stub-column test results to the prediction of column strength.

no additional load if strain hardening is neglected. The residual stress distribution over the cross section, through its influence on the effective moment-of-inertia, is the connecting link between column strength and the tangent modulus of the stress-strain relationship of the stub column. That residual stresses are, indeed, a major factor affecting the strength of axially loaded, initially straight columns, and that a conservative value for this strength may be specified in terms of the tangent modulus determined from the results of a stub-column test, have been documented extensively.

Stub-Column Test Procedure

1. *Object.* To determine the average stress-strain relationship over the complete cross section by means of a compressive test of a stub column.

2. *Specimen*

a. The stub column should be cold-sawed from the stock at a distance at least equal to the shape depth away from a flame-cut end.

b. The length of hot-rolled stub columns should not be less than $2d + 10$ in. ($2d + 250$ mm) or $3d$, whichever is smaller, and not greater than $20r_y$ or $5d$, whichever is larger, in which d = depth of the shape and r_y = radius-of-gyration about the weak axis. For cold-formed shapes the length of the stub column should not be less than three times the largest dimension of the cross section and no more than 20 times the least radius-of-gyration.

c. The ends of the columns should be milled plane and perpendicular to the longitudinal axis of the column.* This operation may be omitted for light gage members which are difficult to mill, if their ends are welded to base plates.

d. The thickness of the flanges and webs and the length and cross-sectional area of the stub column should be measured and recorded.

3. *Instrumentation.* Mechanical dial indicator gages or electrical resistance gages may be used to determine the strains during testing. The use of dial gages over a comparatively large gage length is to be preferred as they provide a better average strain indication. The dial gages should read to 0.0001 in. (0.0025 mm) when read over a 10-in. (250 mm) gage length, or to 0.001 in. (0.025 mm) when installed between base plates over the whole length of the stub column. Where it can be demonstrated that electrical resistance gages give the same or better results, they may be used instead of dial gages.

*A tolerance across the milled surface of ±0.001 in. (±0.025 mm) is usually satisfactory.

The gage length should be placed symmetrically about the mid-height of the stub column. At least two gages in opposite positions should be used and the average of the readings taken. Corner gages over the complete column length are used for alignment; midheight gages are used for determining the stress-strain relationship. When four midheight gages are used instead of two, the corner gages may be omitted. (This is possible with the flange tips of an H-shape). Figure B.3 depicts typical gage arrangements for structural shapes.

For uniformity in stub-column testing, the following instrumentation is recommended for H-shapes:

a. Four 0.001-in. (0.025-mm) dial gages over the complete length of the stub column, at the four corners; to be used during alignment.
b. Two 0.0001-in. (0.0025-mm) dial gages on opposite flanges over a 10-in. (250-mm) gage length at mid-height; to be used to determine the stress-strain relationship. The points of attachment for the gage length are to be at the junction of the flange and web, to avoid the influence of local flange crippling on the readings. When early local flange crippling is unlikely, four 0.0001-in. (0.0025-in) dial gages ove ra 10-in. (250-mm) gage length may be clamped at mid-height to each flange tip. Corner alignment gages are then not needed.
c. As-rolled steel specimens should be whitewashed before testing. Flaking of the mill scale during testing gives a general area of the progress of yielding during the test.

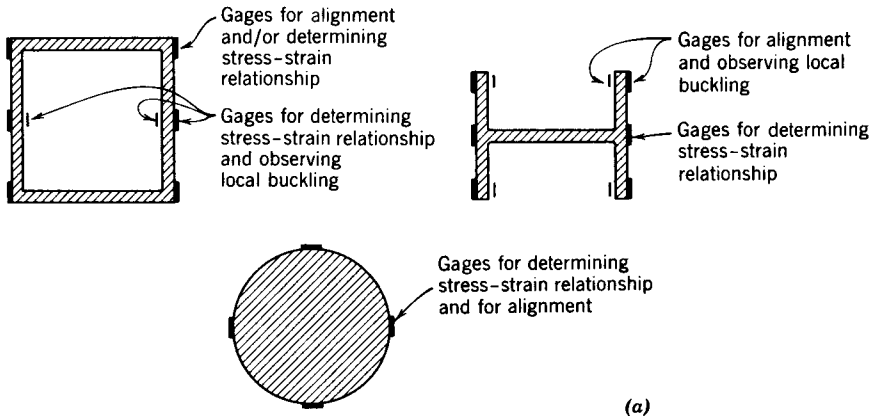

Fig. B.3 Position of gages for alignment and testing: (*a*) location of electrical resistance gages; (*b*), (*c*), (*d*) location of dial indicators;

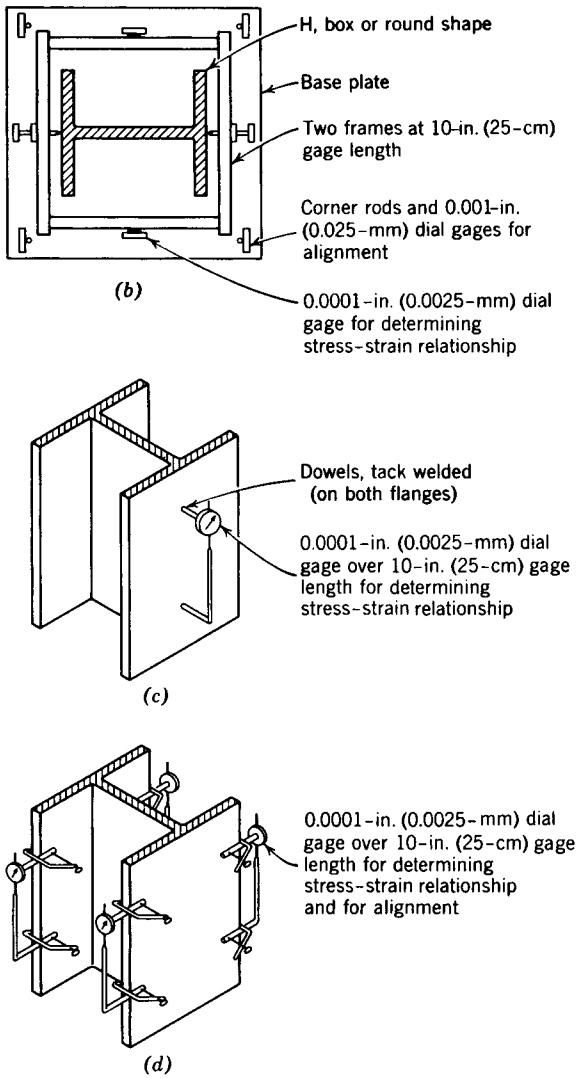

Fig. B.3 (*continued*)

4. *Test set-up.* The specimen should be set in the testing machine between flat bearing plates. These plates should be thick enough to ensure a uniform distribution of load through the specimen. The test set-up is shown in fig. B.4.

Alignment may be achieved with the use of special beveled bearing plates, or else by the use of spherical bearing blocks which are fixed by wedges after alignment to prevent rotation. Hydrostone bedding for the column ends has been used successfully as an aid to alignment, especially for light-gage members.

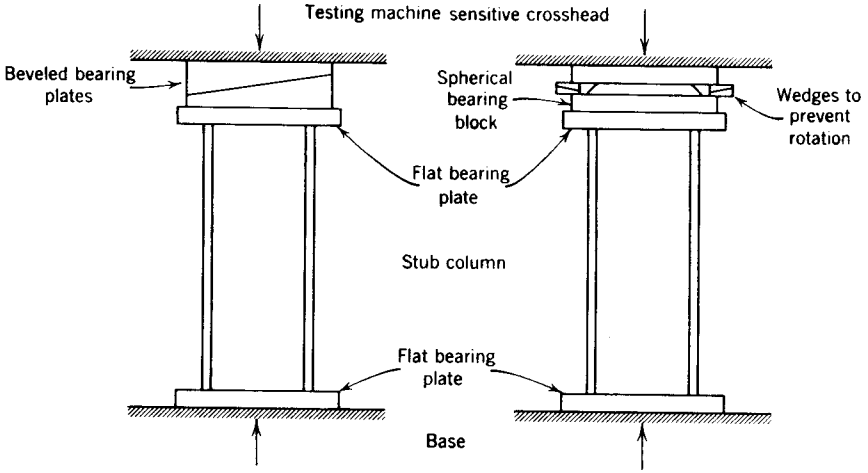

Fig. B4 Subcolumn set-up for testing.

5. *Alignment.* The specimen should be aligned at loads less than that corresponding to the proportional limit stress. For rolled H-shapes of mild structural steel this limit is about one-half of the predicted yield level load; for welded shapes the limit may be as low as one-quarter of the yield level load.

The alignment is performed by noting the variation of strain at the four corners of the specimen. The variation between the strains at any corner from the average strain should be less than 5% at the maximum alignment load. Alignment at low loads is unsatisfactory. The alignment loading should consist of several increments up to the maximum alignment load.

To check that the load is below the proportional limit, the stress-strain relationship may be plotted during the test and its linearity observed. It is inadvisable to exercise this control by observing the whitewash for flaking of the mill scale, because flaking begins at a load greater than that corresponding to the proportional limit stress as indicated by the plotted stress-strain relationship.

6. *Testing.* The stress-strain curve should be constructed from as many experimental data points as possible. To this end, the load increments in the elastic region should be less than 10% of the expected yield load. After the proportional limit has been reached, the load increments should be reduced so that there are sufficient data points to delineate the "knee" of the stress-strain curve. Strain increments may be more convenient than load increments to delineate the "knee" in the inelastic region. The proportional limit* will be

*It is assumed that the residual stresses are symmetrical with respect to the principal axes of the cross section and constant in the longitudinal direction, so that the proportional limit does not indicate localized yielding.

marked by the beginning of the deviation of the stress-strain relationship from linear behavior. Yield lines (made clearly visible by the whitewash as the mill scale flakes off) will indicate the progress of yielding. This matter is covered further in Item 10.

After the onset of yielding, readings should be recorded when both load and strain have stabilized. The criteria used to specify when data may be recorded depend on the type of machine used for testing. This is explained further in item 7.

To ensure correct evaluation of the yield level and other material properties, the test should be continued until one of the following conditions is satisfied:

a. After an immediate drop in load due to local plate buckling, the test should be continued until the load has dropped to about half the predicted yield level load.
b. For a specimen that exhibits a plastic region of considerable extent, the test should be continued until the load had dropped to about 80% the predicted yield level load.
c. For a specimen that strain hardens without apparent buckling, or which strain hardens without a plastic range, the test should be continued until the load is about 25% above that corresponding to the load computed from the yield strength based on the 0.2% strain offset criterion.

The load and strain at all initial load levels should be recorded. This is further outlined in Item 9. It may be necessary to remove some of the dial gages before the test is completed to avoid damage due to local buckling.

7. *Criteria for stabilization of load.* Standard criteria should be followed for recording of test data when the load is greater than that at the proportional limit. The criterion depends on the type of testing machine used, whether hydraulic or mechanical.

For mechanical testing machines (screw type) the criterion is as follows: no relative cross head movement with both the loading and bypass valves closed. For hydraulic systems that leak the criterion is a simulation of that for the screw-type machine. This is accomplished by balancing the load and bypass flows so that no relative motion of the crosshead occurs, and then by waiting for the load to stabilize.

These criteria are best applied by plotting the load change, or crosshead movement versus time, and noting the value corresponding to the asymptote (see Fig. B.5). The test data are recorded when:

a. The asymptotic load is approached, when using the load criterion.
b. The asymptotic crosshead movement is approached when using the crosshead movement criterion.

Readings should not be recorded until the asymptote is definite. Experience will indicate the time intervals required, but 3-min intervals are usually satis-

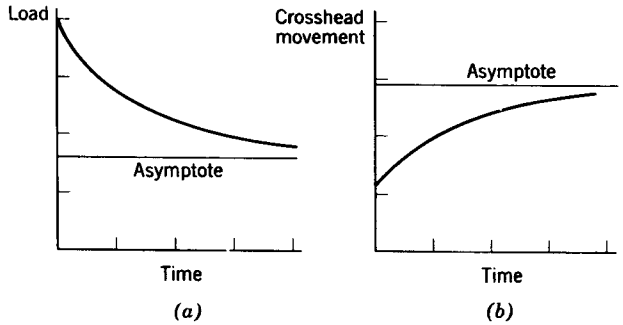

Fig. B.5 Criteria for load stabilization.

factory. The crosshead movement should be measured with a 0.001-in. (0.0025-mm) dial gage.

8. *Evaluation of data.* The test data should be evaluated in the following manner:

a. Plot the test data during the test to detect any inconsistencies.
b. Translate the test data to stress versus strain (based on the actual cross-sectional area) and plot the stress-strain relationship to a large scale. A typical stress-strain diagram is shown in Fig. B.6. A Ramberg Osgood type curve is often fitted to the test data.
c. Determine the tangent-modulus curve from the stress-strain relationship. this may be done by using a strip of mirror. The mirror is held normal to the curve, the normal being determined from the continuity of the stress-strain curve and its mirror image at the tangent point considered. Then a line is drawn along the mirror edge.

9. *Data to be reported.* In addition to presenting the stress-strain and stress-(tangent modulus) curves the following information, obtained from the stress-strain relationship given by the stub-column test, should be reported:

1. Young's modulus of elasticity
2. Proportional limit stress
3. Yield strength
4. Yield stress level
5. Elastic range
6. Elastic–plastic range
7. Plastic range
8. Onset of strain hardening
9. Strain-hardening range
10. Strain-hardening modulus

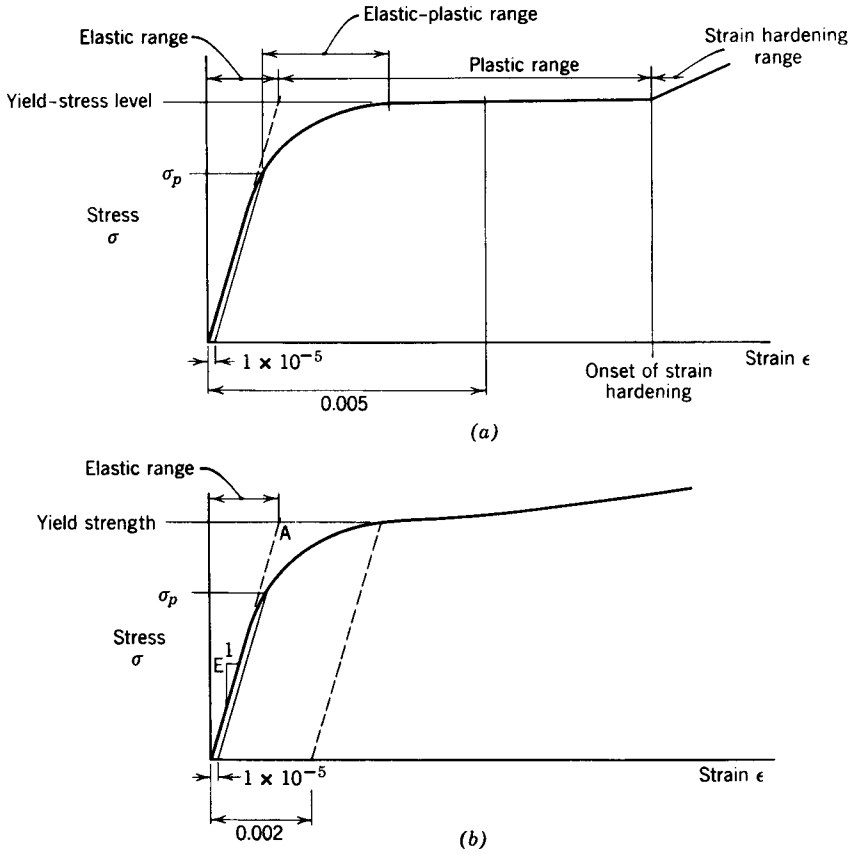

Fig. B.6 The stress-strain diagram.

The occurrence of local buckling and any unusual phenomena during the test should be recorded.

10. *Definition of terms.* The terms just listed in Item 9 should be defined and measured as follows:

1. *Young's modulus*, E, is the ratio of stress to strain in the elastic range. (The method of measuring is defined by ASTM Standard E 111-61, 1972, "Determination of Young's Modulus at Room Temperature.")
2. *Proportional limit stress*, σ_p, is the stress corresponding to the strain above which the stress is no longer proportional to strain. It is best determined by the use of a strain offset of 1×10^{-5}.
3. *Yield strength* is the "stress, corresponding to the load which produces in a material, under specific conditions of the test, a specified limiting plastic strain." This is the definition of ASTM Standard A370-72, and a

strain offset of 0.002 is suggested. (The yield-strength criterion is normally used when there is gradual yielding without a yield plateau. For stub-column stress-strain curves, the yield stress level is mainly used, and as it is an average value in the plastic range, it is more representative.)

4. *Yield stress level* is the stress corresponding to a strain of 0.005. This stress usually corresponds to the constant stress under yield when the stress-strain relationship is such as that shown in Fig. B.6*a*.
5. *Elastic range* is defined as the increment of strain between zero strain and the strain at the point A in Fig. B.6*b*.
6. *Elastic-plastic range* is the increment of strain between the strain at the proportional limit stress and the strain at which the stress first reaches the yield stress level.
7. *Plastic range* is defined as the increment of strain between the elastic range and the onset of strain hardening.
8. *Onset of strain hardening* may be defined as the strain corresponding to the intersection on the stress-strain curve of the yield stress level in the plastic range with the tangent to the curve in the strain-hardening range. This tangent is drawn as the average value in the strain increment of 0.002 after the apparent onset of strain hardening.
9. *Strain-hardening range* is the range of strain after the plastic range in which the material no longer strains at a constant or near-constant stress.
10. *Strain-hardening modulus* is the ratio of stress to strain in the initial strain-hardening range. It is taken as the average value in the strain increment of 0.005 after the onset of strain hardening.

B.4 TECHNICAL MEMORANDUM NO. 4: PROCEDURE FOR TESTING CENTRALLY LOADED COLUMNS*†

A column may be defined as a member whose length is considerably larger than any of its cross-sectional dimensions and which is subjected to compression in the longitudinal direction. If the resultant compressive force is approximately coincident with the longitudinal centroidal axis of the member, the column is said to be centrally loaded. Although columns have been extensively studied for more than two centuries, both analytically and experimentally, technological developments may necessitate further testing of centrally loaded columns.

*This document was prepared by Task Group 6 of the Column Research Council based on *Lehigh Univer. Fritz Eng. Lab. Rep.* No. 351.6, authored by N. Tebedge and L. Tall (1970).
†See page 808 for advisory preface.

The purpose of this memorandum is to set forth a suggested procedure for conducting such experiments.

The experimentally determined values of column strength form a wide scatter band when plotted versus the effective slenderness ratio, KL/r, in which KL denotes the effective column length and r the appropriate radius-of-gyration of the cross section. The scatter is due to geometrical imperfections of the column specimens, eccentric application of load, nonhomogeneity of the column material, residual stresses from the rolling and fabricating processes, variations in the action of loading machines, imperfections in the end fixtures, and other factors. The major sources of scatter are briefly discussed subsequently.

A geometrically perfect centrally loaded column would not deflect laterally at loads less than the critical load. However, all column specimens deflect from the beginning of loading because of bending that results from the initial curvature and twist of the specimen and the unavoidable eccentricity of load application. Nonhomogeneity of the column material results in bending of columns which are stressed above the proportional limit because the pattern of yielded zones of the cross section is not perfectly symmetrical with respect to the principal axes of the cross section.

Residual stresses from the rolling and fabricating processes, present in the column specimen prior to testing, cause scatter in the observed column strength because of patterns of the residual stresses among different specimens of the same size and shape cause variations in the load at the onset of yielding and, as residual stress patterns are generally not symmetric about the principal axes of the cross section, cause variations in the amount of column bending and twisting which, in turn, affects the column strength.

In column tests, as in stability tests of other structural elements, the response of the column is influenced by the action of the loading device. Loading devices may be categorized as gravity, deformation, and pressure types. The force-deflection characteristics of these types differ. The oldest form of testing device used for columns is the gravity-type. For such a system, the load-deflection characteristic is simple and can be graphically represented by a series of straight lines parallel to the deflection axis. Later, the screw-type testing machine became a common laboratory apparatus. These machines have the advantage of a well-defined load-deflection characteristic, the slope of which depends, essentially, on the elastic response of the loading system. As higher capacity loading machines were needed, the hydraulic testing machine was developed. This system, however, does not have an easily defined load-deflection characteirstic as it depends on the properties of the hydraulic system, temperature, and other factors. Loading of a column in a testing machine is always conducted under some finite loading rate and the experimental results are influenced by this.

Centrally loaded columns may have different end conditions, ranging, theoretically, from full restraint (fixed) to zero restraint (pinned), with respect to end rotation and warping. Most investigators have used the pinned-end condition for column testing for a number of reasons. Under the pinned-end

conditions the critical cross section is located near the mid-height of the column, thus making the cross section of interest remote from the boundary and, therefore, little influenced by end effects. For the same effectice slenderness ratio, the pinned-end condition requires the use of only half the column length used for the fixed-end condition. With the pinned-end condition, however, it is necessary to provide end fixtures that offer virtually no restraint to column-end rotation. Rotational restraint influences the effective slenderness ratio of the column and thereby contributes to scatter of experimental results.

Several schemes have been utilized to provide the pinned-end condition, some of which are shown in Fig. B.7, which is reproduced from Ref. B.1. The fixtures differ in that they are either "position-fixed" or "direction-fixed" (B.2).

Probably the best way to reduce end restraint is by means of a relatively large hardened cylindrical surface bearing on a hard flat surface. Rotation will be virtually frictionless, even with some indentation under load. Another interesting feature of cylindrical fixtures is that the effective column length can be made equal to the actual length of the column by designing the fixtures so that the center of the cylinder coincides with the centroidal axis of the cross section at the column end. With a cylindrical fixture, the column is essentially pin-ended about one axis (usually the minor principal axis) and is essentially fixed-ended about the other.

A schematic diagram of the end fixtures used at Fritz Engineering Laboratory is shown in Fig. B.8. A description of the fixtures, and their performance as "pins," is given in Ref. B.3.

In testing columns under the fixed-end condition, the full restraint may not be provided in the entire range of the test loads; thus the effective length of the column is not a constant but a function of the applied load. This may be due partly to the fact that the rigidity of the testing machine varies with the applied load and partly to the indeterminate nature of the stress distribution at the column end, particularly in the load range in which the material yields. These problems are eliminated by using pinned-end conditions because the critical conditions exists at about the mid-height cross section.

(1) Column Test Procedure

Preparation of Specimens. To minimize initial geometrical imperfections of the specimen, the column specimen is cut from a straight portion of the stock. Both ends of the specimen are milled. Columns may be tested with the ends bearing directly on the loading fixtures, provided the material of which the loading fixtures are made is sufficiently harder than that of the column to avoid damaging the fixtures. Otherwise, base plates should be welded to the specimen ends, matching the geometric center of the specimen to the center of the base plate. The welding procedure should be such that compressive residual stresses at the flange tips caused by the welding are minimized. For columns initially curved, the milled surfaces may not be par-

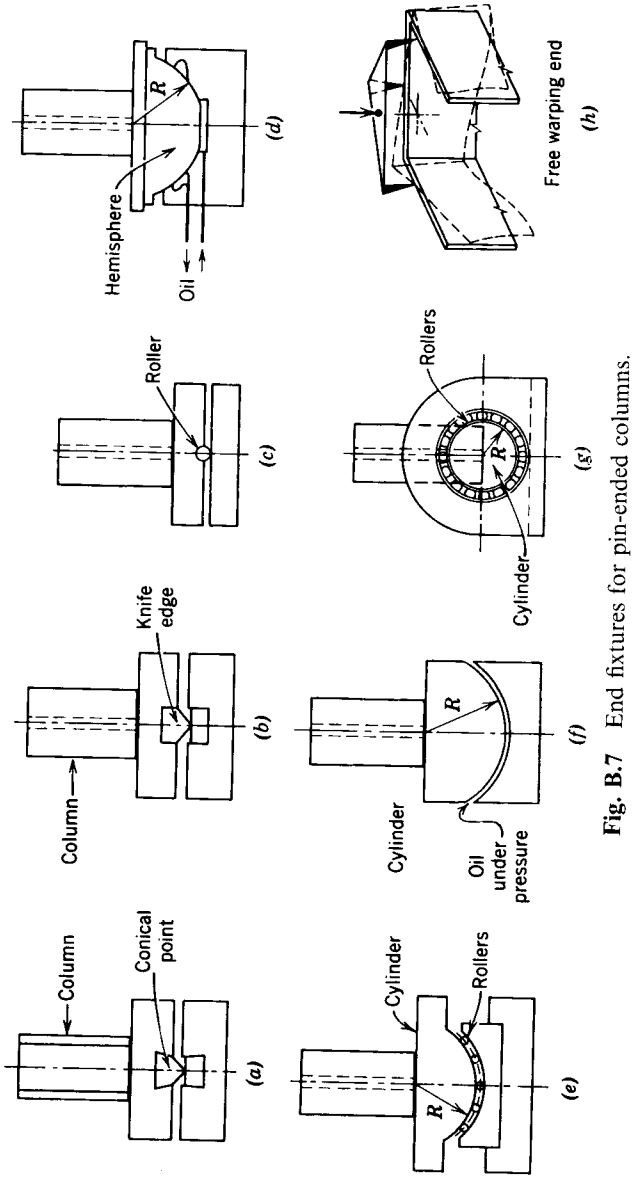

Fig. B.7 End fixtures for pin-ended columns.

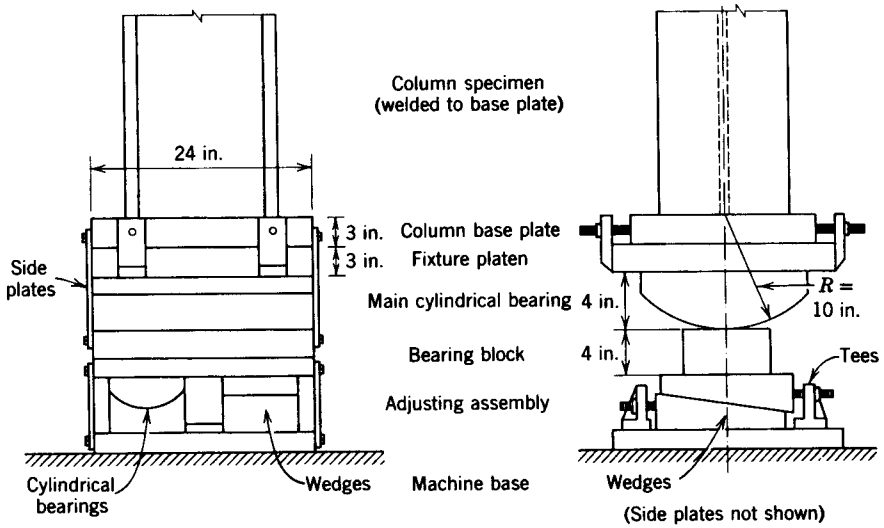

Fig. B.8 Standard column end fixture at Fritz Engineering Laboratory (capacity = 2.5 million pounds).

allel to each other, but will be perpendicular to the centerline at the ends because milling is usually performed with reference to the end portions of the columns. For relatively small column specimens, it is possible to machine the ends flat and parallel to each other by mounting the specimens on an arbor in a lathe. For small deviations in parallelism, the leveling plates at the sensitive crosshead of the testing machine may be adjusted to improve alignment. The tolerance in deviation must not exceed the range of adjustment of the leveling plates of the particular testing machine.

Initial Dimensions. The variation in cross-sectional area and shape, and the initial curvature and twist, will affect the column strength. Therefore, initial measurement of the specimen is an important step in column testing.

The cross section is measured to determine the variation between the actual dimensions of the section and the nominal catalog dimensions and to enable the computation of the required geometrical cross-sectional parameters. The dimensions shown in Fig. B.9 are measured at a number of stations along the column (the quarter points of the specimen are recommended, as a minimum).

The initial camber, sweep, and twist of the specimen are measured at intervals. Nine stations, spaced at one-eighth of the column lengths, are suggested. A method of determining the initial out-of-straightness and twist is shown in Fig. B.10. Readings are taken with a theodolite (stationed in line with the column and near one of the ends) on a strip scale mounted onto a movable carpenter's square. The sweep offset is determined from four readings—each

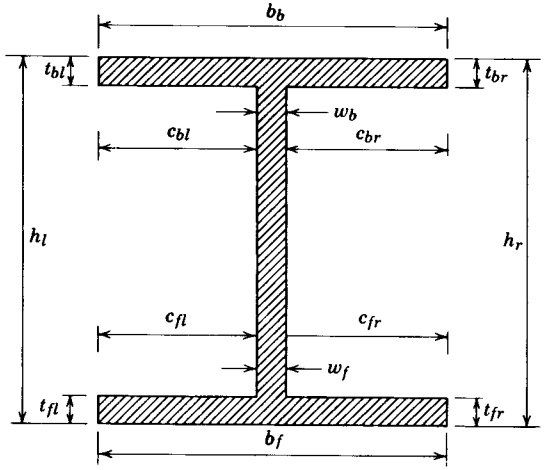

Fig. B.9 Measurements required to determine cross-secitonal properties of H-shaped column.

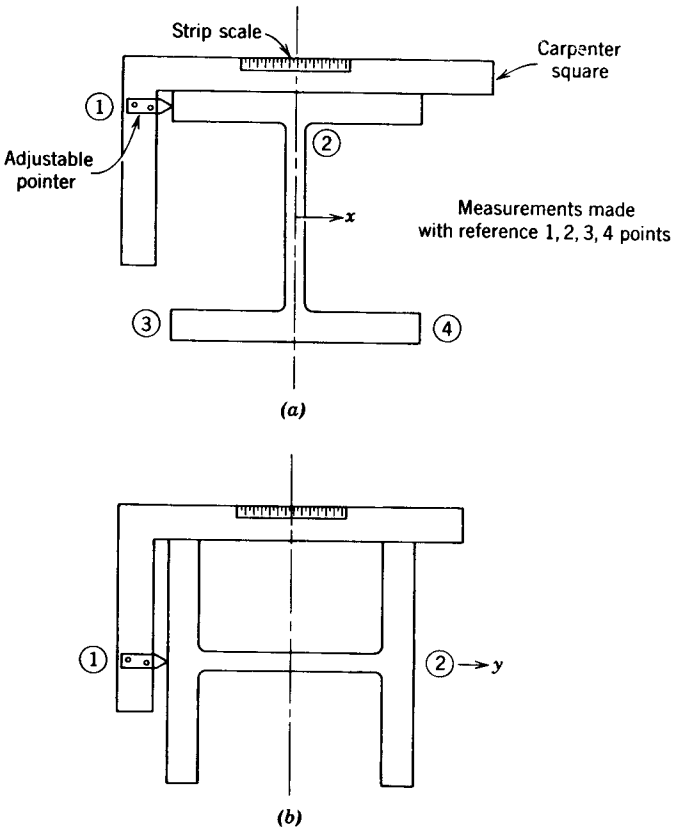

Fig. B.10 Method for measuring initial camber and sweep: (*a*) measurement normal to minor axis (sweep); (*b*) measurement normal to major axis (camber).

referenced to a flange tip. The average of the four readings is considered as the sweep offset. The camber offset is obtained from two readings, one referenced to each flange surface at the intersection of web and flange. The initial angle of twist is computed from the sweep offset readings and the cross-sectional dimensions. Values of initial out-of-straightness and twist are used in evaluating test results.

Aligning the Column Specimen. Aligning the specimen within the testing machine is the most important step in the column testing procedure, prior to loading. Two approaches have been used to align centrally loaded columns. In the first approach the column is aligned under load such that the axial stresses are essentially uniform over the mid-height and the quarter-point cross sections. The objective in this alignment method is to maximize the column load by minimizing the bending stresses caused by geometrical imperfections of the specimen.

In the second alignment method, the column is carefully aligned geometrically, but no special effort is made to secure a uniform stress distribution over the critical cross section. Geometric alignment is performed with respect to a specific reference point on the cross section (the specific reference point will be defined later). The method of geometric alignment is recommended as it is, generally, simpler and quicker. The end plates can easily be centered with reference to the centerline of the testing machine (B.4).

The specific reference point on the cross section utilized in geometrical alignment depends on the cross-sectional shape. For H-shaped cross sections the best centering point is the center of flanges because the web has little effect on buckling about the minor axis. This reference point may be located at the midpoint of the line connecting the two centers of the flanges (B.4).

Instrumentation. In some column investigations, only the ultimate load is measured during the test. However, it is usually desirable to measure the more important deflections and twists to compare the behavior of the column specimen under load with theoretical predictions of behavior. The instrumentation for column tests has changed markedly in the past few years due to progress made in measuring techniques and data acquisition systems, and it is now possible to obtain automatic recordings and plotting of the measurements. Such recordings have been found to be more convenient and more precise than manual readings.

The most important records needed in column testing are applied load and corresponding lateral displacements, twist, and overall column shortening. A typical column set-up and instrumentation are shown in Fig. B.11.

Lateral deflections normal to both principal cross-sectional axes may be automatically recorded by means of potentiometers attached at quarter points of the column (more points may be used for larger columns). Lateral deflections may also be measured from strip scales attached to the column and read with the aid of a theodolite.

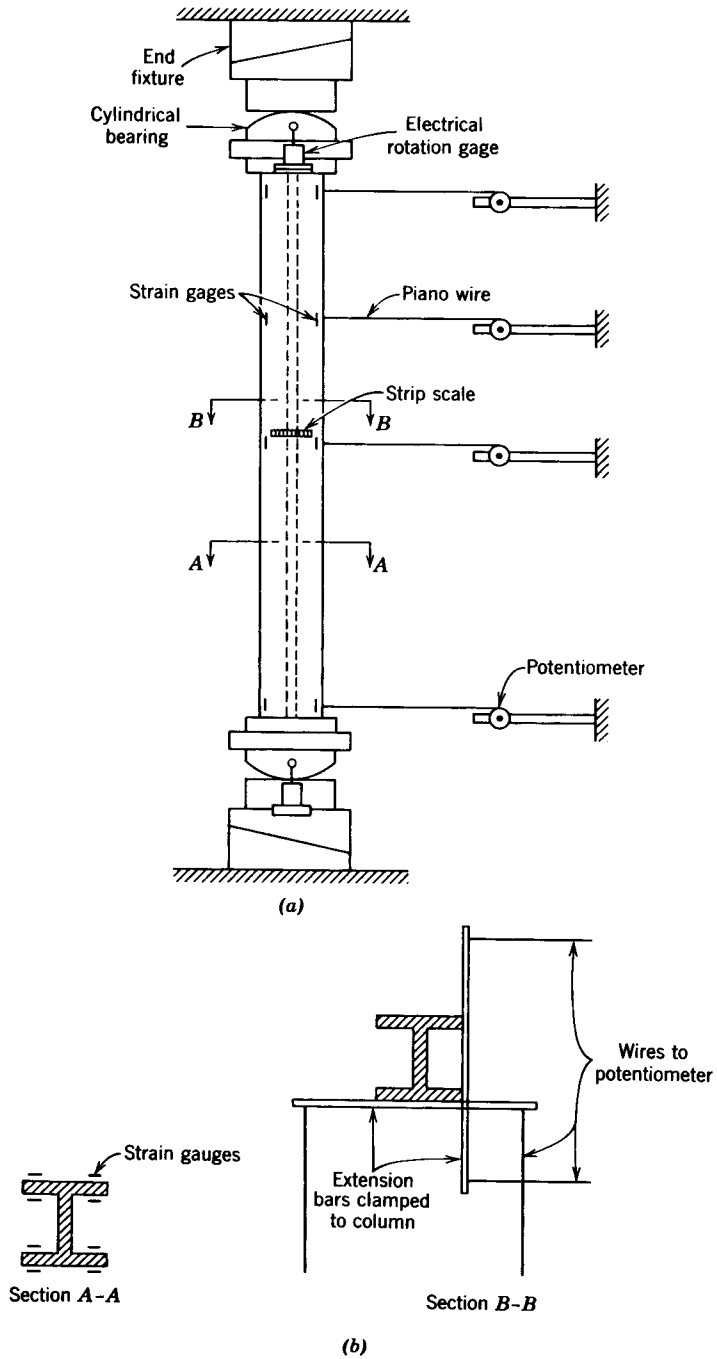

Fig. B.11 Column test set-up.

Strains are measured using electric-resistance strain gages. For ordinary pinned-end column tests, it is sufficient to mount eight strain gages at each end and at the midheight level. For long columns, it may be necessary to mount eight more strain gages at the quarter- and three-quarter points. As shown in section *A-A* of Fig. B.11, the gages should be mounted in pairs "back-to-back" to enable the local flange bending effects to be cancelled by averaging the readings of each pair of "back-to-back" gages.

In the fixed-end test condition more strain gages are mounted below and above the quarter- and three-quarter levels. This is done to determine the actual effective length of the column by locating the inflection points using the strain gage measurements.

End rotations are measured by mechanical or electrical rotation gages. Mechanical rotation gages (B.5) are assembled by mounting levels bars on support brackets welded to the base plate and the top plate of the column as shown in Fig. B.12*a*. Angle changes due to column-end rotation are measured by centering the level bubble with the micrometer screw adjustment. A dial gage attached to the end of the level bar gives an indication of the rotation of the bar over a gage length of 20 in. (508 mm). In the electrical rotation gage, rotations are determined from bending strains induced in a thin metallic strip from which a heavy pendulum is suspended as depicted in Fig. B.12*b*. It has been shown that the strain at any location of the strip is proportional to the end rotation (B.6).

The angles of twist are determined at mid-height and at the two ends by measuring at each level the differences in lateral deflections of the two flanges. For better accuracy, the measurements may be taken at points located at the ends of two rods attached transversely on the adjacent sides of the column, as shown in section *B-B* of Fig. B.11.

The overall shortening is determined by measuring the movement of the sensitive crosshead relative to the fixed crosshead using the dial gage or potentiometer.

Steel column specimens are whitewashed with hydrated lime. During testing, the whitewash cracking pattern indicates the progression of yielding in the column (the cracking reflects the flaking of the mill-scale at yielding zones).

Testing Procedure. After the specimen is aligned in the testing machine, the test is started with an initial load of $\frac{1}{20}$ to $\frac{1}{15}$ of the estimated ultimate load capacity of the column. This is done to preserve the alignment established at the beginning of the test. At this load all measuring devices are adjusted for initial readings.

Further load is applied at a rate of 1 ksi/min (6.9 MPa/min), and the corresponding deflections are recorded instantly. This rate is established when the column is still elastic. The dynamic curve is plotted until the ultimate load is reached, immediately after which the "maximum static" load is recorded. (The procedure for determining a "static" load is described subsequently.) After the maximum static load is recorded, compression of the specimen is resumed at

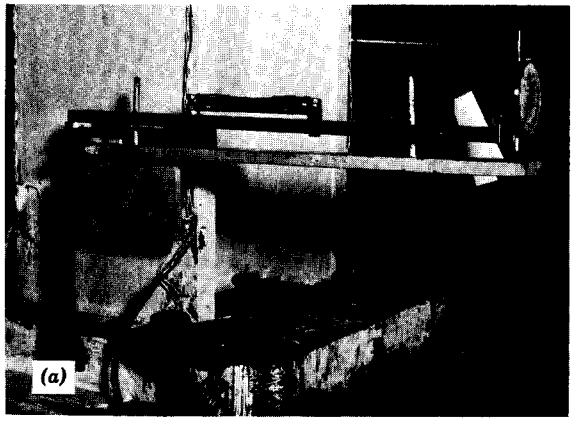

Fig. B.12 Rotation gages: (*a*) mechanical; (*b*) electrical.

the "strain rate" which was utilized for the elastic range. In hydraulic testing machines this may be accomplished, approximately, by using the same bypass valve and load valve settings as had been used in the elastic range. The specimen is compressed in the "unloading range" until the desired load-displacement curve is attained. An example of such a curve is shown in fig. B.13.

A static condition, as is needed to obtain the "maximum static" load, is when the column shape is unchanged under a constant load for a period of time. This means that the chord length of the column must remain constant, or practically, the distance between the crossheads must remain constant during the period. For screw-type testing machines the criteria can normally be satisfied by maintaining the crossheads in a stationary position. However, it is difficult to maintain the distance between cross-heads in hydraulic machines

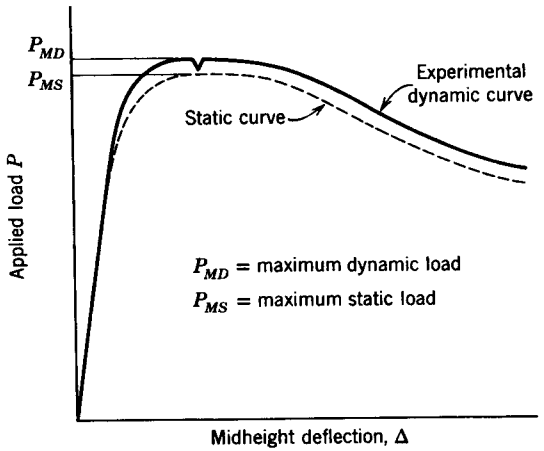

Fig. B.13 Typical load-deflection curve of column.

because of oil leakage and changes in oil properties due to the temperature changes that accompany pumping and throttling. To attain the static condition in the hydraulic machine, from the dynamic state, the bypass valve is further opened slowly until further lateral deflection of the column at mid-height ceases. The cessation of lateral deflection amounts to the condition of constant chord length. Alternatively, the relative crosshead displacements may be monitored, but this parameter is usually not as sensitive as lateral displacement.

(2) Test Results

Presentation of the Data. The behavior of the test specimen under load is determined with the assistance of measurements of lateral deflections at various levels along the two principal directions, rotations at the ends, strains at selected cross sections, angles of twist, and the column shortening. These measurements are compared to theoretical predictions. The results of the test are best presented in diagrammatic form. Such plots are shown in Figs. B.14 through B.19.

In Fig. B.14 typical plots of initial camber and sweep for a column are shown. They are used to determine the reduction in column strength due to initial out-of-straightness.

Figure B.15*a* shows the midheight load-deflection curve of the column along the minor axis, and Fig. B.15*b* along the major axis. The load-deflection curves give the most significant data of the column test.

Plots of the measured strains at mid-height of the column are shown in Fig. B.16. This plot may be compared with the stub column test result to detect any unusual behavior of the column.

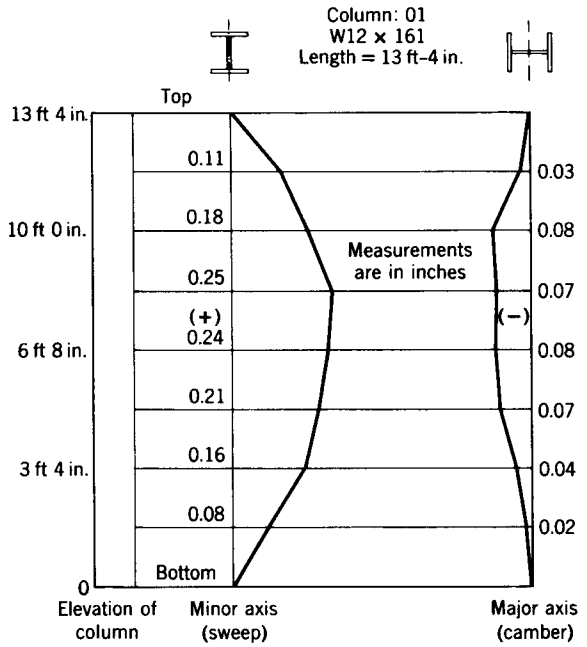

Fig. B.14 Initial camber and sweep of a column specimen.

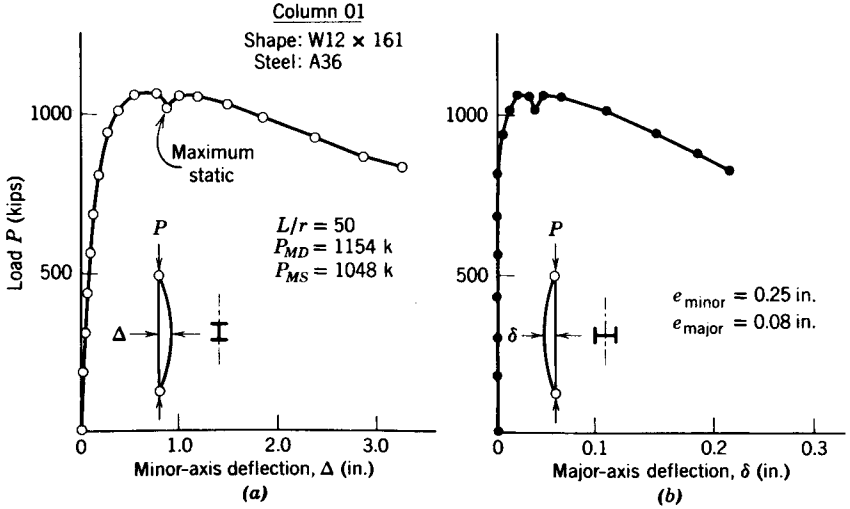

Fig. B.15 Load-deflection curves.

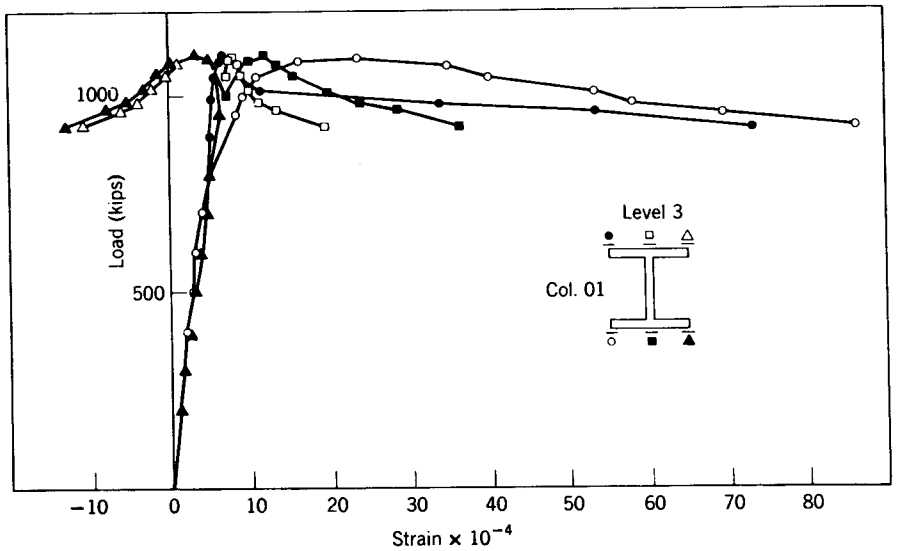

Fig. B.16 Strain measurements at mid-height section using strain gages.

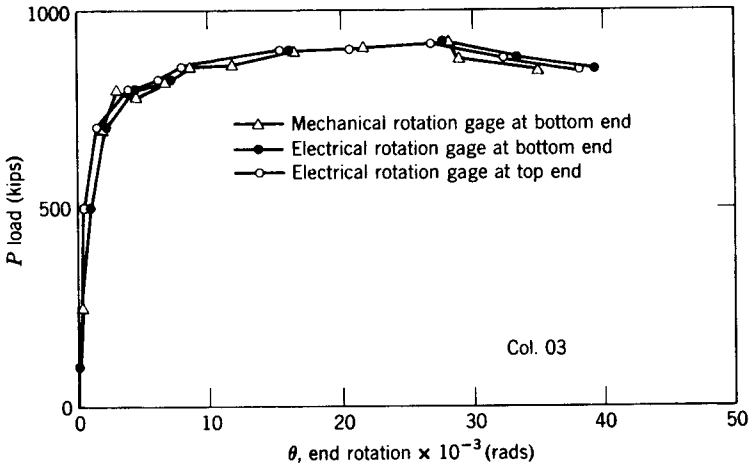

Fig. B.17 End rotations of column 03 determined from mechanical and electrical rotation gages.

End rotations of the column measured using both mechanical and electrical rotation gages are shown in Fig. B.17. The results may be checked by comparing them with the lateral displacements along the length of the column (see Fig. B.15).

The angles of twist at midheight and at the two ends are shown in Fig. B.18. The values are determined as discussed in the section on instrumentation.

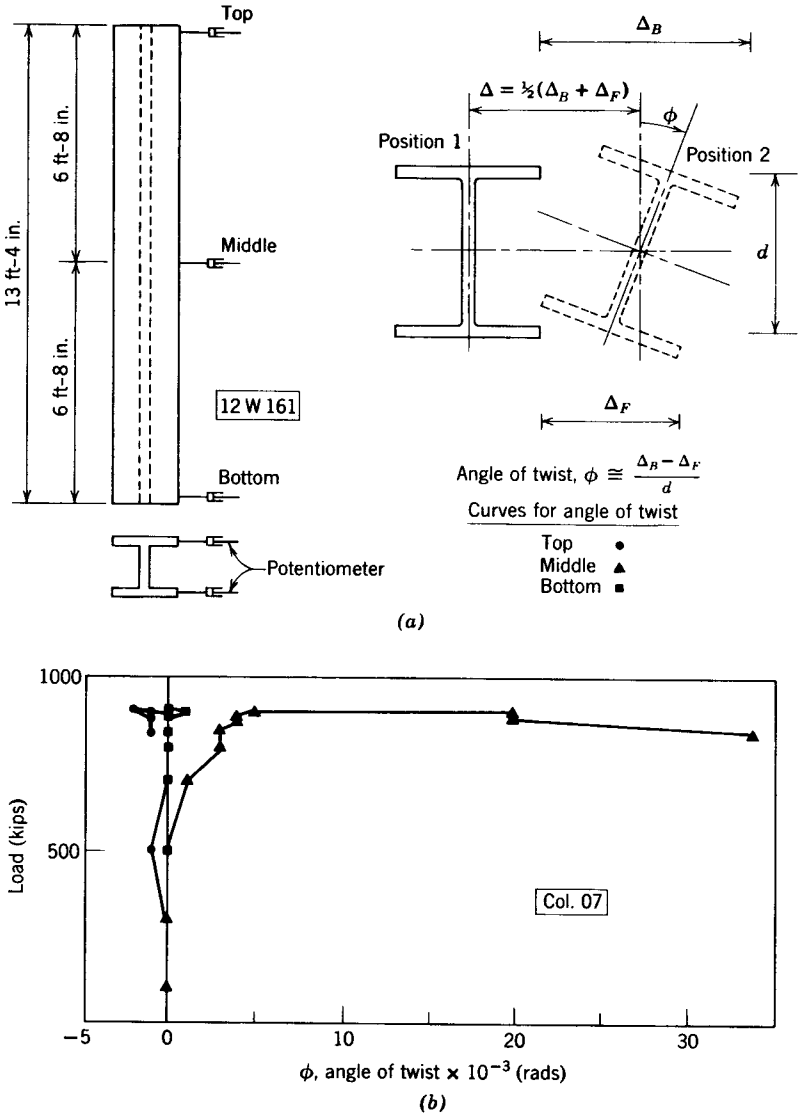

Fig. B.18 Angles of twist at three levels.

Figure B.19 shows a typical plot of the load versus the overall shortening of the column.

For hot-rolled steel columns the progression of yielding is detected from the cracking and flaking of the whitewash. The sequential development of the whitewash cracks may be recorded to indicate the yielding pattern during loading. Whenever local buckling or any other phenomena occur during the test they should be recorded.

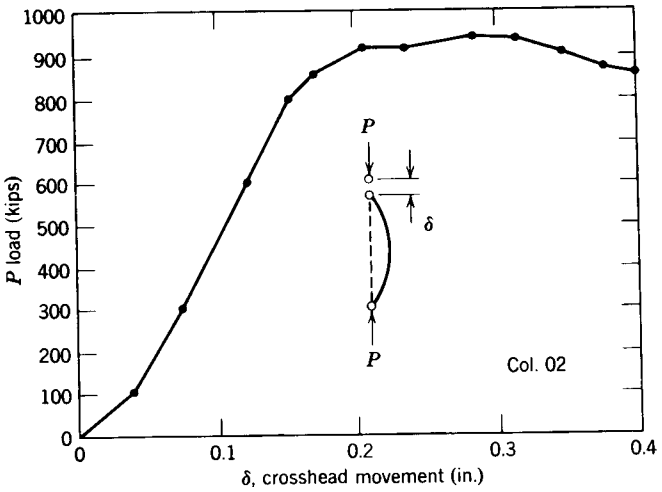

Fig. B.19 Load versus overall shortening curve.

Evaluation of Test Results. The test results may be evaluated by comparing the experimental load-deflection behavior and the theoretical prediction. A preliminary theoretical prediction can be made based on simplified assumptions of material properties, residual stresses, and measured initial out-of-straightness. The prediction may be improved if the actual residual stresses and the variations in material properties are used in the analysis. These properties should be determined from preliminary tests of specimens obtained from the original source stock. The preliminary test specimens should be cut immediately adjacent to that portion of the stock utilized for the column specimen.

B.5 TECHNICAL MEMORANDUM NO. 5: GENERAL PRINCIPLES FOR THE STABILITY DESIGN OF METAL STRUCTURES*

Research has shown that while the maximum strength of some types of centrally loaded columns is predicted by the tangent modulus buckling concept, this concept alone is not adequate for all types of structures and structural elements (for example, most hot-rolled and welded built-up columns, cylindrical shells and stiffened panels). To account for some of these inadequacies, the CRC Column Strength Formula, when adopted in 1960 as the basis for design by the American Institute of Steel Construction, included a variable

*Published in February 1981, *Civil Engineering* (ASCE).

factor of safety which, within the inelastic buckling range, increases as a function of column slenderness. In addition to the material non-linearities and residual stresses, which can be incorporated in the tangent modulus buckling concept, geometric imperfections (such as out-of-straightness), loading history, large deflections, post-buckling strength and behavior and connection response may affect significatly the limit of structural usefulness.

The maximum load resisting capacity of a member or frame determined inelastically by the inclusion of the effects mentioned above, has been termed its "maximum strength". Although the strength of an element may be thought of as a uniquely defined quantity, "maximum strength" is definitive in contrast with other concepts of strength such as tangent modulus, elastic modulus or first yield strength. For members, as distinct from frames, the dominant factor in the determination of the maximum strength, in addition to residual stress and material nonlinearity, is member out-of-straightness.

In elements for which the effect of imperfections must be assessed in the determintion of strength, end restraint may be significant, as it is in the tangent-modulus approach, and likewise, should be considered in formulation of design criteria.

In accordance with the foregoing discussion, the following principle represents the currently (1979) held position of Structural Stability Research Council with respect to stability in the design of metal structures:

> Maximum strength, determined by evaluation of those effects that influence significantly the maximum load-resisting capacity of a frame, member or element, is the proper basis for the establishment of strength design criteria.

This philosopy underlies the research effort and the *Guide* of SSRC. Also, it is the stated philosophy of the *Manual of Stability of Steel Structures* of the European Convention for Constructional Steelwork. It incorporates the tangent modulus buckling approach insofar as it provides the proper basis for defining the maximum strength of certain types of structures and elements, but is encompasses the members of frames in which initial geometric imperfections, large deflections, post-buckling strength and behavior, residual stresses, material non-linearities, load eccentricities and end restraint must be considered.

Implicit in the tangent modulus approach recomended in TM No. 1 was a procedure to establish the column buckling load/slenderness curve, determined theoretically from the tangent-modulus curve for the specific column section under consideration. Whenever possible, the procedure for the establishment of the load carrying capacity of frames, members or elements on the basis of maximum strength should be based on a mathematical model which incorporates:

1. Experimentally determined physical characteristics, such as residual stresses, material non-linearities, and cross-sectional variations in yield strength, rationalized as may be appropriate.

2. A statistically appropriate combination of acceptance characteristics that are specified in supply, fabrication and erection standards, such as out-of-straightness, underrun of cross-section, cross-section dimensional variations, material properties and erection tolerances.
3. Effect of boundary conditions, such as restraint applied to the end of members.

When it is not possible to determine maximum strength theoretically, experimentally determined values of maximum strength may be accepted provided that the tests have been controlled and the results adjusted to compensate for the inclusion of the most adverse combination of unfavorable factors, contributing to a reduction in strength below the experimentally determined values, which has an acceptable probability of occurrence.

Although the maximum strength of frames and the maximum strength of the component members are interdependent (but not necessarily coexistent), it is recognized that in many structures it is not practical to take this interdependent into account rigorously. At the same time, it is known that difficulties are encountered in complex frameworks when attempting to compensate automatically in column design for the instability of the entire frame (for example, by adjustment of column effective length). Therefore, SSRC recommends that, in design practice, the two aspects, stability of individual members and elements of the structure and stability of the structure as a whole, be considered independently. The proper basis for member design is the maximum strength of the restrained imperfect member. Where appropriate, second order effects (such as P–Δ effects in frames) determined with due regard for non-linear and non-coexistent response, should be included with the first order effects among the actions for which the member is to be designed.

B.6 TECHNICAL MEMORANDUM NO. 6: DETERMINATION OF RESIDUAL STRESSES*

Abstract: The paper explains the origin of residual stresses as well as the techniques and procedures for measurement. Residual stresses may be induced during manufacture as a result of non-uniform cooling of the metal and/or from cold working. The magnitude and pattern of residual stress can have a pronounced influence on the behavior of structural members. The most widely used technique of determining residual stresses is the method of sectioning and is fully described in detail in this paper.

*Prepared by an SSRC Task Group. Chairman: T. Peköz; Members: R. Bjorhovde, S. J. Errera, B. G. Johnston, D. R. Sherman, and L. Tall. Published in *Exp. Tech.*, Vol. 5, No. 3, September 1981.

List of Symbols

d = diameter of the contact edge in the gage hole
t = thickness of strip
L_g = gage length
N_i = initial middle ordinate
N_f = final middle ordinate
S_i = correction for initial middle ordinate
S_f = correction for final middle ordinate
α = internal angle of the extensometer gage point
δ = difference between initial and final middle ordinates
$\lambda_h, \lambda_n, \lambda_x, \lambda_t$ = correction factor

Introduction

Most metal products contain residual stresses induced during manufacture. One source of these stresses in hot-rolled steel shapes is the nonuniform cooling of the metal after it leaves the rolls. Steel shapes fabricated from hot-rolled products by means of welding have additional residual stresses due to nonuniform heating of the base metal as the weld metal is deposited, and the subsequent nonuniform cooling of the weldment.

In addition to these thermal residual stresses, steel products may possess residual stresses as a result of cold working. For example, rolled structural shapes and welded built-up shapes are often bent by gagging to remove camber or sweep, or to introduce camber or sweep. In some mills hot-rolled shapes are rotary straightened, a process in which the shape is successively bent in opposite curvature several times as it passes through rolls at ambient temperature, rendering the shape essentially straight. The metal undergoes plastic deformation during rotary straightening as evidenced by flaking of the mill scale on the product.

The magnitude of the residual thermal and cold-work stresses resulting from the processes described above is far greater in the longitudinal direction of the shape than in any transverse direction except for surface effects. Longitudinal residual stresses can have a pronounced influence on the behavior of structural members, especially in the case of columns and plate structures built up by welding, and it is with the determination of such stresses that this memorandum is primarily concerned. Longitudinal residual stresses vary with respect to the width and thickness of each plate-element comprising the shape. However, except for very thick elements, and for walls of cold-formed tubular members, the variation of residual stresses through the thickness is usually not important.

Residual stresses due to cold work are present in all products whose cross section is cold-formed from sheets, either by press-braking or roll-forming. The magnitude of residual stresses is greatest in the direction transverse to the bent

line, and the variation through the thickness is pronounced. However, because of Poisson's ratio, longitudinal stresses are created by the transverse stresses and these longitudinal stresses affect the behavior of members subjected to longitudinal compression, bending, and twist.

Aluminum structural shapes are usually extruded. Extruded shapes are straightened by stretching so that the finished product is virtually free of residual stresses. Aluminum sheets and plates may contain residual stresses from rolling, or from quenching if subjected to heat treatment after rolling. The flattening operation, which may consist of roller leveling or stretching, or both, does not always produce a stress-free product. These stresses may cause inconvenience in machining operations but are rarely of structural significance. Shapes built-up by welding contain residual stresses due to nonuniform heating and cooling during the welding process. The magnitude of the longitudinal stresses from this souce may reach the yield strength of the aluminum in its annealed state.

Techniques for Determining Residual Stress Magnitude

The techniques for determining the magnitude and distribution of residual stresses may be classified as nondestructive, semidestructive, and destructive. X-ray and ultrasonic methods are termed as nondestructive. Unfortunately, at the present time these methods are not practical for determining residual stresses in structural members. However, recent research such as that reported in Ref. B.7, shows significant potential benefits. The ultrasonic technique provides information on the difference between the principal (in the geometric sense) stresses only, and it is not practicable to interpret the residual stress in a specific direction.

In the semidestructive and destructive techniques the residual stresses are determined from distortions caused by the removal of material. Since the residual stresses in the body are in equilibrium, removal of stressed material by cutting, planing, drilling, grooving, or etching causes a relaxation in stress and a corresponding strain. The strain is measured, and the relaxation of stress is obtained by using Hooke's Law. The testing technique is said to be semidestructive if the amount of material removed is small compared to the initial volume of the specimen and if the specimen can be made whole again, as by welding. The technique is termed destructive if so much material is removed that the specimen is virtually destroyed.

Semidestructive techniques usually involve drilling holes in the specimen. The action of drilling alters the internal stress distribution resulting in deformation at the surface of the specimen. This deformation is interpreted as caused by residual stress. The hole-drilling method of residual stress determination as developed by Mathar, and that of Soete and Vancrombrugge were studied by Tebedge, Alpsten, and Tall (B.8, B.9). In Mathar's method two gage points are installed diametrically opposite and equidistant from the center of the hole to be drilled, to suit a sensitive mechanical extensometer. The axis of

the gage points and hole should be in the direction of the stress to be determined. The initial distance between the gage points is measured, the hole drilled, and the final spacing of the gage points measured. From the displacement of the gage points, caused by the deformation of the specimen during drilling, the relaxation in stress may be determined theoretically or by utilizing a calibration test.

In the semidestructive technique developed by Soete and Vancrombrugge (B.10, B.11) the strains induced in the specimen by drilling are measured with the aid of electrical strain gages. These strain gages are more convenient and reliable for one not experienced in the use of mechanical extensometers. They are available in rosette form and in small size. The advantage of small rosettes is that the drilled hole can be of correspondingly small diameter, thus minimizing damage to the specimen and allowing the work to be done with smaller tools. The direction of the principal strains can then be determined. Although Soete and Vancrombrugge's technique seems to possess many advantages compared with destructive techniques, it has not been utilized extensively in the United States. The foregoing semidestructive techniques are described in more detail in the papers by Tebedge, Alpsten, and Tall, which also includes an extensive bibliography.

Most studies of residual stresses in structural shapes have been performed using the destructive technique. A portion of the specimen (the test piece), located at a suitable distance from the ends of the specimen, is marked into strips as shown in Fig. B.20*a*. Gage holes are drilled near each end at the midwidth of each strip, and their longitudinal spacing is measured. The test pice is then cold-sawed from the specimen, appearing as in Figure B.20*b* after this operation, and the strips are cut from the test piece often by means of a thin milling cutter or band-saw. They have come to be termed *sections* and such a section is depicted in Figure B.20*c*. The distance between gage holes of each section is measured and the change in length of a section is interpreted with Hooke's Law as the average value of the residual stress present in that section prior to its removal from the specimen. It is believed the method of sectioning was first used in Fritz Laboratory in the late 1940's by Johnston and Luxion (B.12).

If it is desired to determine the variation of residual stress through the thickness of the section, the section is marked into strips as shown in Figure B.20*c*, gage holes are drilled at the ends of each strip, and the longitudinal distance between these is measured. The strips are then cut from the section to obtain what are termed *slices*. The distance between the gage holes of each slice is measured again, and the change in length of a slice is a measure of the average residual stress in the section from which it was cut. This destructive technique has been named *the method of sectioning* and will be described in more detail subsequently.

Electrical strain gages can be used to measure the strains in the method of sectioning. They have the distinct advantages that smaller sections may be used and fewer corrections are necessary. However, very careful and time-consum-

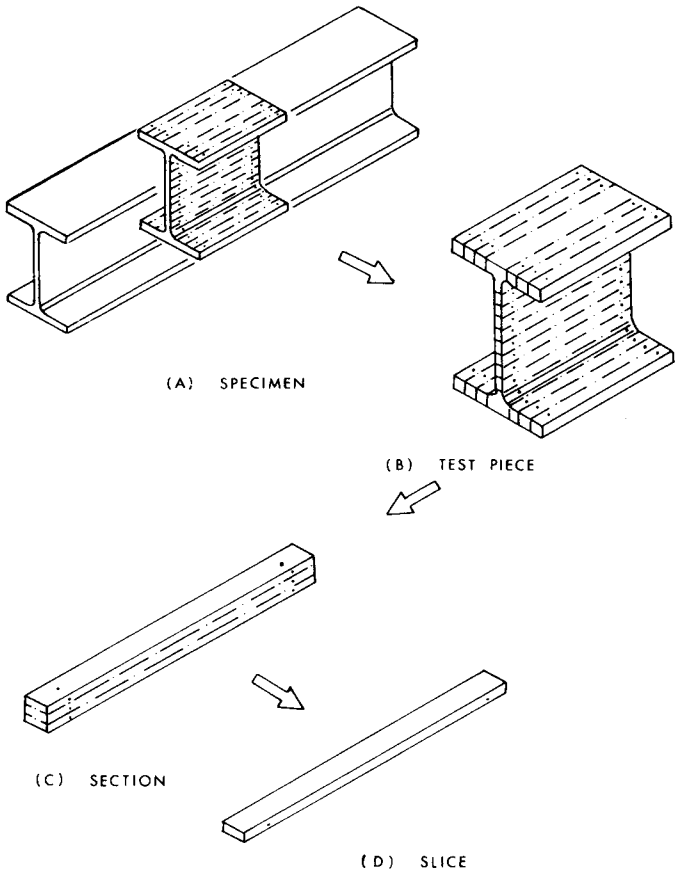

Fig. B.20 method of sectioning.

ing techniques are required to protect the gages from damage during the cutting operation and to ensure the same zero base if the gage wires have to be reattached to the instrumentation for the final readings.

Method of Sectioning

Preparation of Test Piece. The stock should be carefully examined for evidence of cold work prior to selecting the portion to be used as a specimen. If it is desired to determine the residual stresses due to thermal effects only, then the specimen should be cut from the portion of the stock that does not have transverse cracks in the mill scale if any are present. Such cracks are usually evidence that the member has been cold-straightened, either by gagging or rotary straightening. On the other hand, if it is desired to evaluate

the residual stresses caused by both cold work and thermal effects (the usual situation), then the specimen should have a representative pattern of mill scale cracks. In either case, the specimen should be cut to a minimum length equal to three times the largest transverse dimension, plus the gage length, plus 2 in. (50 mm), if it is to be cold-sawed from the stock. If the specimen is removed by flame cutting, it should be longer by an amount equal to the largest transverse dimension in order to minimize the possibility that this operation will disturb the residual stress pattern in the central portion of the specimen. The specimen should be wire brushed and washed with a solvent to remove traces of cutting oil and its ends should be deburred. The specimen is then ready for marking of the test piece.

The central portion of the specimen is usually coated with machinist's blueing or a similar compound for a distance equal to at least the gage length plus 2 in. (50 mm). Next, the lines defining the sections are scribed on both sides of all elements of the cross section, where possible. The width of the strips should be based on the expected residual stress gradient and the needs of the investigation.

When the sections have been scribed on the test piece, the gage holes for the extensometer are laid out. A gage length of 10 in. (254 mm) is recommended, partly because this is the length of one of the standard Whittmore Gages. The centers of the holes are punched on the centerline of each strip. These punch marks serve to guide the drill bit during drilling. It is convenient to use the punch fixture in the Whittemore kit, as the gage hole centers will then be located within the measuring range of the gage. If the relaxation of strain is to be measured on one side of the section only (either as a matter of convenience or because the second side is not accessible) the gage holes need be located only on the first side. If strains are to be measured on both sides, but only one side is accessible for drilling and the thickness of the section is less than about 1 in. (25 mm), gage holes centers need only be punched on the side accessible to the drill because those on the opposite side can be located by drilling through the section. In the case of thick sections the strains should be measured on both sides. It is preferable to punch the gage hole centers on both sides provided that drilling on both sides is possible.

The importance of careful preparation of the gage holes to receive the gage points of the Whittemore Gage cannot be overemphasized. The diameter of the gage holes should be as small as practicable. Where shallow holes are drilled into the sections, or through thin sections, drill bits of about 0.03 in. (0.75 mm) diameter are suitable. For holes through thick material it is advisable to double the drill bit diameter so as to avoid excessive "wander" as the bit advances. It is desirable to utilize a drill press or, for large shapes, a magnetic base drill stand, to ensure that the holes will be as close to normal to the surface as possible. The holes must be chamfered to remove burrs from the drilling operation and to bring the contact surfaces between the test piece and the gage points of the instrument below the surface of the test pice, in order to protect them from damage during subsequent handling and machining. The depth of chamfer

should be on the order of 0.02 in. (0.50 mm), and it is conventional practice to accomplish this with the reamer provided in the Whittemore kit. However, since the reamer is hand-held some researchers have found it desirable to use a guide block to aid in maintaining the reamer normal to the test piece. Such a guide block can be readily made by drilling an appropriately sized hole in a steel bar of about 1 in. (25 mm) thickness. Some investigators have reported success with a special bit with which the holes can be drilled and chamfered in a single operation (B.8, B.9).

Measuring Technique. For measuring the relaxation of strain resulting from removal of material the Whittemore Gage, or other comparable quality mechanical gage, with a nominal gage length of 10 in. (254 mm) is recommended. This is a portable mechanical extensometer with a dial gage graduated to 0.0001 in. (0.0025 mm) which is clamped to one of two steel coaxial tubes and bears on the other. To minimise temperature changes of the tubes due to handling, they are attached (internally) to a three-sided metal housing by means of flexible links. The observer holds the housing to operate the gage.

Measurements should be made with respect to the steel reference bar which is part of the Whiteemore kit so that, if the temperatures of the bar and the coaxial tubes are essentially equal, no correction need be made to account for instrument errors due to ambient temperature variations during the test. Furthermore, if the test piece is steel and precautions are taken to maintain the reference bar, Whittemore Gage, and test piece at the same temperature, then all the errors due to temperature change will be minimal and no temperature corrections are necessary.

In addition to measuring the longitudinal gage lengths it is also necessary to measure the curvature in planes normal and parallel to the strip surface for both the "initial" and "final" states when through the thickness residual stresses exist. Because the equilibrium of the strip is disturbed during the cutting operation, these curvatures change. This phenomenon is especially evident in strips cut from structural tubes (B.13). It is necessary to determine these curvature changes in order to correct for the following errors:

1. Error due to "final" gage length measurement along chord between gage holes, rather than along the arc lying in the surface plane. Correction denoted as λ_s.
2. Error due to "final" gage length measurement along chord, rather than along arc in plane normal to strip surface. Correction denoted as λ_n.
3. Error due to misalignment of instrument gage point and gage hole axes due to change of curvature in plane normal to strip surface. Correction denoted as λ_h.

In order to compute corrections for the first of these errors (due to the change in curvature in the surface planes), the middle ordinates in the "initial" and "final" states, respectively S_i and S_f, should be measured. Normally, $S_i = 0$. The corrections for the last two errors are functions of the change in curvature in a plane normal to the strip and can be computed from the middle ordinates N_i and N_f.

The suggested procedures for taking the "initial" and "final" measurements are essentially alike and may be outlined as follows:

1. Thoroughly clean all gage holes utilizing cotton swabs, solvent, and compressed air blasts. If the holes were covered with adhesive tape for protection during machining, they may be coated with a gummy residue because some adhesives are soluble in some cutting oils. Such deposits must be removed in order to secure repeatability of measurements.
2. Place the test piece, sections, or slices upon a sturdy table or other support so as to bring the work to a convenient height. The table should be located away from windows, radiators, and fans, and out of the path of drafts. The material should preferably not rest directly upon the table but rather on strips of wood, to reduce heat conduction. The parts should be arranged so that minimal handling is required after testing is commenced. Place the Whittemore gage and the reference bar directly upon the material to be measured, cover with a clean cloth, and wait (usually overnight) for the specimens, reference bar, and instrument to reach the same temperature.
3. When testing is to begin, remove the cloth cover and proceed with the measurements as expeditiously as possible. The data required are indicated on the suggested data sheet shown as Figure B.21. For each side of a strip take a reference bar reading before (columns 2 and 8) and after (columns 4 and 10) the three readings for the gage length (record average in columns 3 and 9). If the reference bar readings differ by more than one or two dial indicator units, discard the set of measurements. Such a difference indicates excessive temperature change, slipping of the dial indicator in its clamp, other instrument malfunction, or improper operation of the gages. If the largest difference between the three "initial" gage length readings exceeds three units, discard the set and redress the gage holes with the reamer. (After the "initial" readings have been completed, the gage holes must not be touched, except with a cotton swab.) The uncorrected gage lengths (columns 5 and 11) are determined by subtracting the average reference bar readings from the average gage-length readings.
4. The values of the middle ordinates, S (columns 6 and 12) and N (columns 7 and 13), are often measured with a dial indicator gage and fixture of the type described by Sherman (B.13). If the strips are cut from the test

DATA SHEET—RESIDUAL STRAIN MEASUREMENTS

Date _____ Test piece indent. _____

Time start _____ Temp. start _____ Initial/final measure. (indicate which).

Time finish _____ Temp. finish _____

Observer _____ Recorder _____

	Side A					
(1)	(2)	(3)	(4)	(5)	(6)	(7)
Section/Slice Identification	Ref. Bar Reading	Gage Length Avg. of 3	Ref. Bar Reading	Uncorrected Length with Respect to Ref. Bar	Middle Ordinates S	Middle Ordinates N

	Side B					
	(8)	(9)	(10)	(11)	(12)	(13)
	Ref. Bar Reading	Gage Length Avg. of 3	Ref. Bar Reading	Uncorrected Length with Respect to Ref. Bar	Middle Ordinates S	Middle Ordinates N

Fig. B.21 Heading for residual strain data sheet.

piece by a milling machine it is usually to take $S_i = 0$. When using the fixture, precautions should be taken to avoid contact with the gage holes.

Calculation of Curvature Corrections

The bending deformations accompanying removal of a section from the test piece, or a slice from a section, may have to be accounted for in determining the final gage distances. The three errors are listed previously. The first two errors, due to "final" measurement along the chord instead of the arc, may be corrrected adequately by adding the following quantity to the final measured values:

$$\lambda_n = \lambda_s = \frac{8\delta^2}{3L_g}$$

where L_g is the gage length, and $\delta = (S_f - S_i)$ or $(N_f - N_i)$ depending on the change of curvature under consideration. To account for misalignment of the conical extensometer point and gage hole axes, the correction to the observed final gage length is

$$\lambda_h = \frac{4d\delta}{L_g} \tan \frac{\alpha}{2}$$

where d is the diameter of the contact edge in the gage hole and α is the internal angle of the extensometer gage point.

If measurements are made on both surfaces of a section or slice, the middle thickness relaxation of strain is usually obtained from the average of the gage length changes on both surfaces, neglecting the corrections λ_n and λ_h. On the other hand if measurements are made only on one side, then all corrections λ_n, λ_s, and λ_h may be required. Furthermore, because curvature corrections λ_n, λ_s, and λ_h refer to the surface of the strip it may be necessary to apply a correction for curvature to obtain the final length at mid-thickness, if measurements are made on one surface only. This correction is

$$\lambda_t = \frac{5t\delta}{L_g}$$

where t is the thickness of the strip.

A further discussion of the above corrections is given in Ref. B.13.

Acknowledgments

The Council wishes to thank the former members of Task Group 6 who were active during the time of preparation of earlier drafts of the report. They were: L. S. Beedle, C. Birnstiel, J. W. Clark, E. W. Gradt, R. A. Hechtman, T. R. Higgins, and B. M. McNamee.

B.7 SSRC TECHNICAL MEMORANDUM NO. 7: TENSION TESTING*

Introduction

The tension yield strength is the key mechanical property required by most material specifications and design practice. Because of its standard usage, it is the most accepted value for analysing and comparing test data. Usually, the comparison is performed by "normalization," that is, the test resutls are non-dimensionalized with respect to the yield strength (stress). Thus, the tension

*Prepared by an SSRC Task Group; Chairman: L. Tall; Members: P. C. Birkemoe, R. Bjorhovde, S. J. Errera, K. H. Klippstein, R. A. LaBoube, T. Peköz, D. R. Sherman, and R. B. Testa. Approved by SSRC Executive Committee: October 23, 1986.

test becomes a most important aspect of a "test of stability" in which all or some portion of a structural shape is tested in compression. Since the tensile yield is sensitive to the rate of straining, normalized stability test data can easily be shifted by more than 20% if care is not exercised in conducting the tension test and in reporting the test method employed and its results.

Yield strength is not the only parameter that is important in evaluating tests of stability and theory, as it is often desirable to know other material properties such as the proportional limit and the strain hardening characteristics which can be obtained from a tension test. At the same time, the tension test method must conform as closely as possible to those of standard quality control tests so that the stability test results can be interpreted with respect to design standards.

Ideally, the strain rate in the tension test and the stability test should be the same. Due to the difficulty in conducting a stability test at a constant, known strain rate, the SSRC advocates the use of the static yield strength in stub column tests and the static load in tests of stability. Static values are obtained by loading the specimen with a load or deflection increment and then holding a constant distortion until the load is stabilized. This stable load is the static value. A static tensile yield strength is, therefore, the most appropriate value to be used in normalizing test data.

Purpose

This Technical Memorandum is intended to provide guidelines for obtaining the static yield strength level in a tension test so that consistent, uniform values are obtained and reported.

Equipment

Tension tests are performed on different types of testing machines in different laboratories. These machines can be grouped as screw-driven machines, manually controlled hydraulic machines and servo-controlled closed loop systems of the screw or hydraulic type. One common aspect of all these machines is that the specimen is loaded by the motion of a cross head, although a feedback mechanism can be used to relate the cross head motion to load or strain in the specimen. In manually operated machines, the feedback mechanism is the operator who watches a load dial and the output of a strain extensometer, whereas a closed loop machine uses a servo controller which provides the appropriate feedback to drive the cross head and thus maintain the desired rate of load, stroke, or strain. These systems control strain, load, or stroke more precisely and with faster response than a manually operated machine.

Another difference in testing machines is the manner of gripping the specimen. Threads, button heads, wedge grips or hydraulic grips are the most common methods. The characteristics of the grips have a distinct influence on the relationship between cross head motion and strain in the specimen.

Due to inelastic creep in the gripping, the strain in the specimen may change even though the cross head motion is completely stopped.

A Class 2B extensometer (strain error < 0.0002) will normally be satisfactory for monitoring strain. If accurate values of the modulus of elasticity are required in addition to the yield information, a more accurate extensometer or strain gage should be used.

Specimen

The tension test specimen should be prepared in accordance with ASTM E8 and any applicable product specification for the specimen in the test for stability. The end section for gripping and in some cases the size of the tension test specimen will be dictated by the testing machine. If the test for stability involves a rolled or standard shape, the tension test specimen should be taken from the piece as required by ASTM or other product specification. For fabricated test pieces, two tension test specimens are desirable. One should be taken from the plate or sheet material prior to fabrication. This provides a correlation with the material requirements. The other tension test specimen should be taken from the fabricated piece at a location that represents average properties resulting from strain hardening or work hardening and residual stresses. The tensile properties of this specimen are required for comparison with other data and for correlation with theory.

Procedure

Although it is desirable to operate the testing machine in a strain control mode, this may not always be practical. Even servo-controlled machines may go out of control if the extensometer slips, or it may be difficult to switch to a cross head or displacement control mode during loading. Consequently, operation of the testing machine in a cross head or stroke control mode is acceptable. In this event, it will be necessary to determine the rate of cross head motion that will produce the desired strain rate by loading the specimen to less than 50% of the anticipated yield and making adjustments in the rate of cross head motion as required. When yielding occurs, it is usually necessary to reduce the rate of cross head motion to obtain approximately the same rate of straining.

The rate of strain should be approximately the same as that obtained during loading in the stability test, but still within ASTM limits. A graphic plot of stress (or load) vs. strain is desirable but the data may be taken manually in sufficient increments to produce a well defined curve. When the strain reaches a value corresponding to approximately 0.2% offset ($0.002 + \sigma_y/E$),* the test should be interrupted by holding a constant strain or stopping the cross

*If the applicable material or product specification defines yield as 0.005 total strain, that value should be used in place of 0.2% offset throughout this technical memorandum.

head motion. This condition should be maintained for at most five minutes or until the load stabilizes. The lowest value of the load and the corresponding strain should be recorded. Straining is then resumed at the original strain rate. The test should be interrupted with static load values recorded at least two more times before strain hardening begins or at 0.005 increments of strain. Straining at the original rate should continue until the initial strain hardening characteristics of the material are evident, at which time the rate can be increased according to ASTM procedures until failure occurs.

Results

The stress-strain information should form one of the two curves shown in Fig. B.22. If the resulting curve is the flat yielding Type *A*, the static yield should be reported as the average of the three low values obtained. For rounded Type *B*

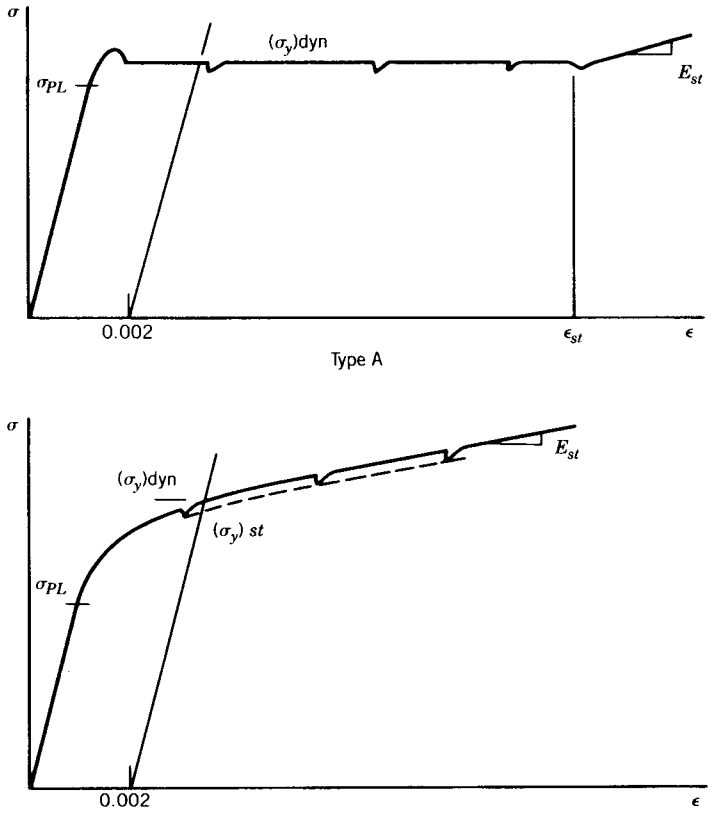

Fig. B.22 Typical tension test stress-strain curves.

stress-strain curves, a curve should be drawn through the low points of the three interruptions and the static yield determined by the 0.2% offset intercept.

Since the yield strength is not the only parameter important in stability theory, the following information obtained in the tension test should be reported:

1. Static yield strength (indicate if obtained by 0.2% offset).
2. Dynamic yield strength and strain rate.
3. Proportional limit.
4. Strain at initiation of strain hardening.
5. Strain hardening modulus.
6. Modulus of elasticity if other than the normally accepted value for the material has been obtained.

Three additional values that are normally part of a tension test should be reported for quality control purposes, although they are not a factor in stability.

7. Ultimate strength.
8. Percent elongation with statement of gage length.
9. Percent area reduction.

B.8 TECHNICAL MEMORANDUM NO. 8: STANDARD METHODS AND DEFINITIONS FOR TESTS FOR STATIC YIELD STRESS*

Introduction

Static yield stress is a reliable and consistent measure of the value at which steel yields and is independent of testing procedures and testing machine behavior. It is the yield stress corresponding to a strain rate of zero (or to a testing speed of zero). It is applicable to both tension and compression tests and to tests on both a coupon and the full cross section. Since the static yield stress is a conssitent and reliable measure, it serves as a valid basis of comparison between different steels compared to other measures of yield. For this reason it is also used to normalize† data from column tests or from other tests of stability so that comparisons with other data or with theory can be made without the influence of variation of yield. The Structural Stability Research

*Prepared by SSRC Task Group 6, *Test Methods*. Chairman: L. Tall, Members: P. C. Birkemoe, R. Bjorhovde, S. J. Errera, K. Klippstein, R. A. LaBoube, T. Pekoz, D. R. Sherman, R. B. Testa. (Adopted Nov. 1987).

†*Normalization* is the nondimensionalizing of test results with respect to the yield stress.

Council has advocated the use of static yield stress in normalizing data from tets of stability.

The yield point and yield strength of steel are affected directly by the rate of straining. Generally, the higher the rate, the higher the yield tends to become, until the ultimate load is reached without clearly defined yielding (B.14).

Since a particular type of steel could have many yield values depending on the strain rate, the speed of testing is of the utmost importance when defining yield stress. Actually, there are a number of definitions for the yield stress (B.15), and justification exists, to a greater or lesser degree, for using various values for design. Specifications do not take account of the size effect in the specimens and the differences in testing machines. Although *ASTM Methods and Definitions for Mechanical Testing of Steel Products (A 370-77)* limits the maximum testing speed for structural steel, some investigators use lower speeds than others with the result that discrepancies as high as 20% may exist in the measured value for yield stress (B.16). In addition, the testing speed and strain rate are two different quantities without a defined relationship. Hence, the use of the term "yield stress" has limited value, unless it is qualified by a strain rate. However, strain rate does not account for all the variation between tests; it cannot account for material differences or manufacturing methods. The difference due to chemistry and manufacturing procedures can be evaluated more clearly if the superimposed effects of strain rate are removed.

Definitions

Symbols used in this technical memorandum are σ, average stress, and ε, strain. Two of the terms used to define the strength of steel are yield point and yield strength as defined in *ASTM Definitions of Terms Relating to Methods of Mechanical Testing (E 6-81)*. Various methods to determine the quantities are described in Methods and Definitions, ASTM A370. In this technical memorandum, the following terms are used: upper yield point (σ_{uy}), lower yield point (σ_{ly}), dynamic yield stress (σ_{yd}), and static yield stress (σ_{ys}). These terms are shown in Fig. B.23, and they are defined as follows:

Upper Yield Point, σ_{uy}***:*** same as ASTM Definition E6 for yield point: "the first stress in a material, less than the maximum attainable stress, at which an increase in strain occurs without an increase in stress."*

Lower Yield Point, σ_{ly}***:*** lowest level of yield stress immediately following the upper yield point while maintaining a constant strain rate.

**ASTM Note*: It should be noted that only materials that exhibit the unique phenomenon of yielding have a "yield point".

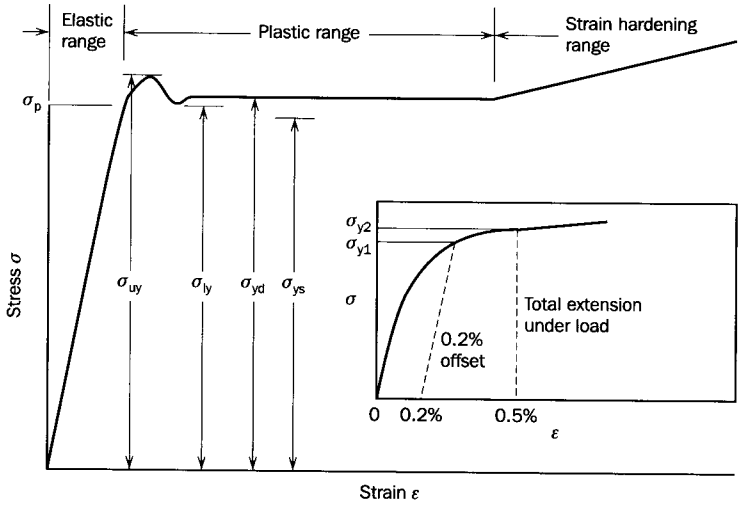

Fig. B.23 Stress-strain curve and definition of terms.

Dyname Yield Stress, σ_{yd}***:*** average stress during actual yielding in the plastic range. It remains fairly constant, provided that the strain rate remains constant, and is also referred to as the "dynamic yield stress level."

Static Yield Stress, σ_{ys}***:*** average stress during actual yielding in the plastic range at zero strain rate; this stress remains fairly constant, and is also referred to as the "static yield stress level." When the static yield stress is not a plateau (that is, constant with respect to strain), it is taken as the stress at zero strain rate corresponding to a total strain of 0.5% or to 0.2% offset, depending on the product specification.

Yield Stress, σ_y***:*** general term which includes all the definitions for the yield value.

Plastic Range of Strain, ε_y ***to*** ε_{st}***:*** range between the yield strain and the strain at the onset of strain-hardening.

Yield Strain, ε_y***:*** strain at which the yield stress first occurs. Its value depends on the definition of the yield stress.

Speed of Testing: rate of cross-head motion or rate of stress increase.

Maximum Speed: limiting speed in Methods and Definitions, ASTM A370.

It is impossible to test a specimen at zero strain rate and obtain a stress-strain diagram. However, a method for obtaining the stress corresponding to

zero strain rate is described below. Assuming that the strain rate is the only factor that influences the dynamic yield stress, a relationship between the strain rate and the ratio of dynamic yield stress to static yield stress has been established (B.17). For convenience, this ratio is termed the dynamic yield stress ratio, and it always will be greater than unity.

The term "yield strength" is defined in ASTM E6: "the stress at which a material exhibits a specified limiting deviation from the proportionality of stress to strain. The deviation is expressed in terms of strain."*

Method of Testing

The basic method of testing conforms to the usual standards, that is, to ASTM E8-81 and E9-91 for tension testing and compression testing, respectively (B.18), and to SSRC TM 2, TM 3, and TM 7, for the testing of tension and compression specimens and stub columns. The usual test procedure and testing speed is followed up to the yield point, or until the plot shows that the material is starting to strain in the plastic range. At this point, the cross head motion of the machine is stopped to record the static yield stress. At this stage the strain is between two to five times the yield strain—and the control mode is cross-head motion. (Although the modern servo-controlled testing machines enable control by strain, it is generally more convenient to control cross-head motion in order to avoid changing the control mode when the extensometer must be removed.) At this point, the plot of the load-strain curve drops from its original course indicating a decrease in load—this is accompanied by a slight increase in strain. About 5 minutes are needed to stabilize the load at zero cross-head motion. At the end of the 5 minutes, or when the load has stabilized, the magnitude of the load is recorded, either automatically on the running plot, or else visually. (Five minutes is suggested also as a maximum time limit since, in the case of hydraulic machines, strain reversal and a lower equilibrium load may be recorded due to leakage of oil in the system.)

The test is then continued by returning to the standard testing speed for a brief interval. This interval is approximately 5 seconds for a tension specimen being tested at the ASTM maximum speed of $\frac{1}{16}$ in./min per inch of gage length; the interval will be longer for slower test speeds. The foregoing is then repeated by stopping the cross-head motion of the machine again. The minimum value of load corresponding to the zero cross-head motion indicates the yield stress at a strain rate of zero (Fig. B.24). Depending on the extend of the plastic range of strain, two or three values of the static yield stress are recorded. Thus, a line is drawn between points 1, 2, and 3 on Fig. B.24. If the line is horizontal, the value indicates σ_{ys}. If the line is inclined to the horizontal, then the ordinate of the line at the 0.5% strain, or at the 0.2% offset, is taken as σ_{ys}.

ASTM Note: Whenever yield strength is specified, the method of test must be stated along with the percent offset or the total strain under load. The values obtained by the two methods may differ.

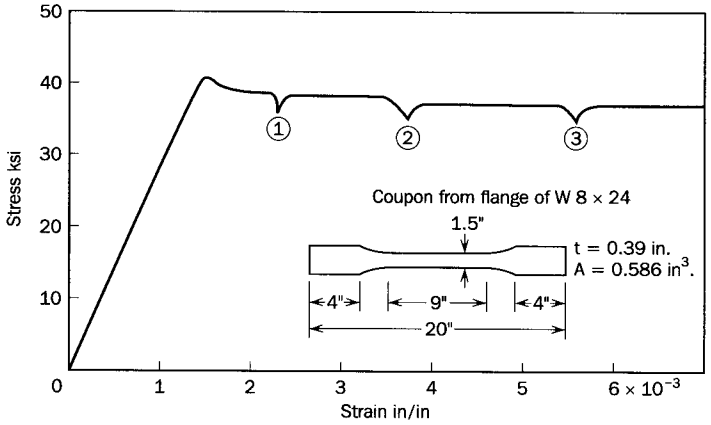

Fig. B24 Typical stress-strain diagram.

Commentary

Static Yield Stress. Normalization of test data is usually made with respect to the static yield stress. Ideally, the strain rate in tests used to obtain the yield stress for normalizing data and the strain rate in the stability test in question should be the same. Due to the difficulty of conducting stability tests at a constant known strain rate, the Structural Stability Research Council advocates the use of the "static yield stress" in the stub column test and in the tension test, and the use of the static load in a stability test. These static values are obtained by loading the specimen with a load or deflection increment and then holding a constant distortion until the load has stabilized. This stable load or stress is the static value.

Both the upper and lower yield points have been used in the past as the basis for designating the yield stress. It is common practice in the testing of tensile specimens to record the "yield" as the highest reading indicated by the free follower pointer on the load indicator dial, the actual load having dropped somewhat. In this Technical Memorandum, emphasis is given to the static yield stress and the dynamic yield stress. By its definition, the static yield stress is independent of the speed of testing. It is not affected by size of specimen or testing machine. Moreover, most loads on structures such as buildings are static. Therefore, the static yield stress level is a more uniform standard for comparison, and it is of direct application to the testing of structures and structural components and to research into their strength.

Relationship Between Static and Dynamic Yield Stress. The yield point and yield strength of steel are affected directly by the rate of straining. Generally, the higher the rate, the higher the yield stress tends to become until

the limit when the ultimate load is reached without yielding. The dynamic yield stress influenced by the speed of testing, size of specimen, and testing machine. Thus, for the same testing machine and size of specimen, the dynamic yield stress is a function of the speed of testing. The speed of testing may be defined by either the rate of separation of the cross-head, or by the strain rate—these have entirely different meanings.

The current method of designating testing speed introduces a problem. The ASTM specifies the rate of separation of cross-heads, since the specification of strain rate may not be a practicable method of controlling machines currently used in production testing. In Section 11.4.1 of Methods and Definitions, ASTM A 370, the rate of separation of cross-head is limited to $\frac{1}{16}$ inch (1.6 mm) per minutes per inch (25.4 mm) of gage length for tension specimens with reduced cross sections, hereafter called the maximum speed. In Section 11.4.3 of ASTM A 370, the speed of testing is limited by the rate of stressing of 100,000 psi (6.895 MPa) per minute.

Suppose the rate of separation of cross-heads of $\frac{1}{16}$ in./min per inch of gage length is used. For a 0.505-in.-diameter tension specimen of 2-in. gage length, the cross-head separation speed is $\frac{1}{8}$ in./min, and for a plate-type tension specimen of 8-in. gage length, the cross-head separation speed is $\frac{1}{2}$ in./min. The two specimens theoretically will have approximately the same strain rate of $\frac{1}{16}$ in./in./min or 1042 μin./in./sec, although the actual measured strain rates in the gage length will be significantly less. If the rate of stressing of 100,000 psi/min is used as the criterion, the corresponding calculated strain rate would be 55 μin./in./sec. (In this calculation, it is assumed that all of the deformation goes into the specimen in the indicated gage length.) Thus, the two criteria are too far apart for valid comparison of the results.

The strain induced in a specimen in the elastic range has been shown to be influenced by the response of the testing machine (B.17, B.19). It can be assumed that in the plastic range all the extension is absorbed by the specimen, and the testing machine does not undergo further deformation. This would indicate that the cross-head speed may not be linearly proportional to the strain rate. Thus, the same cross-head speed would produce a lower strain rate in the elastic range and a relatively higher strain rate in the plastic range.

The results of a study (B.17) into tension tests of 0.50 in. (13 mm) round specimens with 2 in. (51 mm) gage length and plate-type specimens with 8 in. (203 mm) gage length have shown that the dynamic yield stress, the static yield stress, and the strain rate are related by

$$\frac{\sigma_{yd}}{\sigma_{ys}} = 1 + k\dot{\epsilon}^n \tag{B.1}$$

where σ_{yd}/σ_{ys} = dynamic yield stress ratio
$\dot{\epsilon}$ = strain rate, μin./in./sec.
k = a constant, 0.021 for A36 steel
0.020 A441
0.023 A514
n = a constant, 0.26 for A36 steel
0.18 A441
0.08 A514

An alternative form of this relationship is

$$\sigma_{yd} - \sigma_{ys} = C\dot{\epsilon}^m \tag{B.2}$$

where C = a constant, 0.87 for A36
1.06 A441
2.57 A514
m = a constant, 0.24 for A36
0.18 A441
0.08 A415

Since the difference $(\sigma_{yd} - \sigma_{ys})$ is essentially the same for A36, A441, and A514 steel (Fig. B.25), an average curve was proposed (B.17):

$$\sigma_{yd} - \sigma_{ys} = 3.2 + 0.001\dot{\epsilon} \tag{B.3}$$

which is valid for the range of strain rate $200 < \dot{\epsilon} < 1600$. (Since the strain rate does not greatly affect the difference between static and dynamic yield stress for practical values of strain rate, the cross-head speed per inch of gage length per second may be used in place of strain rate in Eq. B.3.)

The relationship of B.1, B.2, and B.3 are shown in Fig. B.25 for the three grades of steel considered.

Tension tests of A36 and A633C steels using standard plate-type coupons with 2-in. (51-mm) and 8-in. (203-mm) gage lengths were also conducted (B.21). A low elastic strain rate of 10 μin./in./sec was obtained in a servo-controlled testing machine using the stroke-control mode. The comparison of dynamic and static yield stress levels is summarized below. The ratios and differences for the 8-in. (203-mm) specimens are similar to those in Fig. B.25 for A36 and A441 steels. The results are slightly higher for the 2-in. (51-mm) specimens.

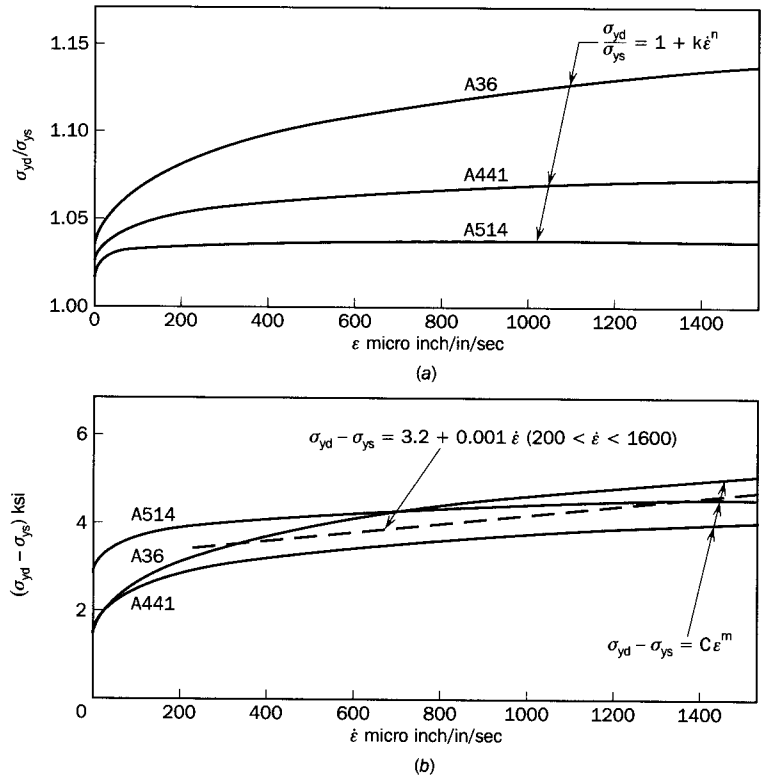

Fig. B.25 Estimated curves relating dynamic yield stress, static yield stress, and strain rate — A36, A441, and A514 steels.

	Number of tests	Average values [ksi (MPa)]			
		σ_{yd}	σ_{ys}	$\frac{\sigma_{yd}}{\sigma_{ys}}$	$\sigma_{yd} - \sigma_{ys}$
A36, 2 in.	16	42.4 (292)	39.2 (270)	1.08	3.2 (22)
A36, 8 in.	8	40.8 (281)	38.6 (266)	1.06	2.2 (15)
A633C, 2 in.	13	61.1 (421)	58.0 (400)	1.05	3.1 (21)
A633C, 8 in.	7	60.2 (415)	58.1 (401)	1.04	2.1 (14)

A strain rate of about 100 μin./in./sec corresponds to the testing rate normally used, and at such a strain rate (Fig. B.25*a*) the average dynamic yield stress ratios are 1.126, 1.070, and 1.040 for A36, A441, and A514 steels, respectively (B.17). Thus if no static yield stress has been recorded, as in the case of a mill test, the static yield stress may be inferred approximately from the recorded dynamic yield stress value by reducing it by 13, 7, and 4%, respectively, for those grades of steel—this approximation assumes that the mill test result, the upper yield stress σ_{uy}, is the same as the dynamic yield stress, σ_{yd}.

Further Considerations. There is a relationship between the yield stress obtained from a stub column test and from tension specimens from its cross section. One of the results of a stub column test is the static yield stress for the complete cross section (Technical Memorandum 3). It has been shown (B.20) that the σ_{ys} of the stub column corresponds to the weighted average of the σ_{ys} from tension specimens from the flange and web (weighted according to the respective areas).

B.9 TECHNICAL MEMORANDUM NO. 9: FLEXURAL TESTING

Introduction

The design of beams and beam-columns depends on knowledge of the flexural behavior of the member as established theoretically and confirmed by test. The modes of flexural behavior recognized in limit states design standards include attainment of cross-sectional strength, and elastic or inelastic lateral torsional buckling. The fundamental purpose of flexural tests is to develop or verify design equations, i.e., to establish how well proposed equations predict the behavior as given by the mean value of the ratios of the test/predicted moments and the associated coefficient of variation for a series of tests. In establishing these statistical parameters, both the material and geometric properties of the test beams must be determined in order that the test/predicted ratios reflect only the variability of the test strength relative to the design equation. Ancillary tests and measurements on representative samples are therefore conducted to determine the relevant geometric and material properties. See also Technical Memorandum No. 10 for statistical evaluation of test data.

Specimen

Provide a sufficient additional length of material from each different heat for the ancillary tests. The main flexural specimens vary in length from whatever length is required for lateral buckling tests to that for those tests with a constant moment region of length sufficient for all the instrumentation but not greater than $1.2r_y/\sqrt{F_Y/E}$, for example, for tests to determine M_p. For such strength tests, a length of two times the beam depth is recommended for the shear span.

Geometric Properties

Establish the width, depth, flange thickness, and web thickness from a sufficient number of measurements of each taken along the length of the beam to be statistically representative of the beam. Thirty measurements of each are

recommended. The contribution of fillets to the cross-sectional properties, A, S, Z, I, and J, should be included as it may be significant. For lateral–torsional buckling tests especially, establish the sweep, camber, out-of-parallel or flanges, and out-of-straightness of web and compare to the manufacturing or rolling tolerances. The latter two are especially important for welded three-plate shapes.

Material Properties

Conduct residual strain measurements and tension coupon tests on sections taken longitudinally from the entire cross-section in accordance with Technical Memorandum No. 6 and No. 7 respectively. A stub-column test curve, Technical Memorandum No. 3 can provide supplementary information on the overall behavior in compression, the maximum compressive residual stress, and the local buckling behavior.

Boundary Conditions

Because any and all unforeseen restraints increase both the stiffness and flexural strength of a beam, it is absolutely imperative that no restraints be introduced inadvertently. Boundary conditions must be known. Friction must be reduced to an absolute minimum. The devices shown her for attaining certain boundary and loading conditions are examples of what is considered to be good practice. They are in no way meant to preclude other designs that achieve comparable results. The objective is to have highly predictable conditions so that the loads and reactions, as vector quantities, are known both in magnitude and direction. It cannot be overemphasized that unwanted frictional forces leave the value of test results in serious doubt.

Figure B.26 shows the set-up for a typical flexural test, with two-point loading and simple boundary conditions at all load points and reactions, to determine the cross-sectional strength of a beam. For simple supports, when the coordinate axes are: x out-of-plane, y in the vertical direction, and z along the length of the member, translation in the z-direction and rotation about the x-axis must be allowed. The knife edge assemblies, placed adjacent to the specimen, allow the specimen to rotate about the x-axis as it deflects under load. The transverse rollers allow translation in the z-direction and, reacting against horizontal surfaces, ensure that the reactions and loads are vertical. The four sets of rollers are needed to keep the loading symmetric as the specimen deforms. Notice, that with no longitudinal restraint, the specimen is in neutral equilibrium. Adjustable stops should therefore be provided to keep the specimen centered but not restrained longitudinally. These are adjusted during the course of the test. As the specimen deflects, the load points move inward and the reactions outward changing the length of the shear span, which therefore must be measured.

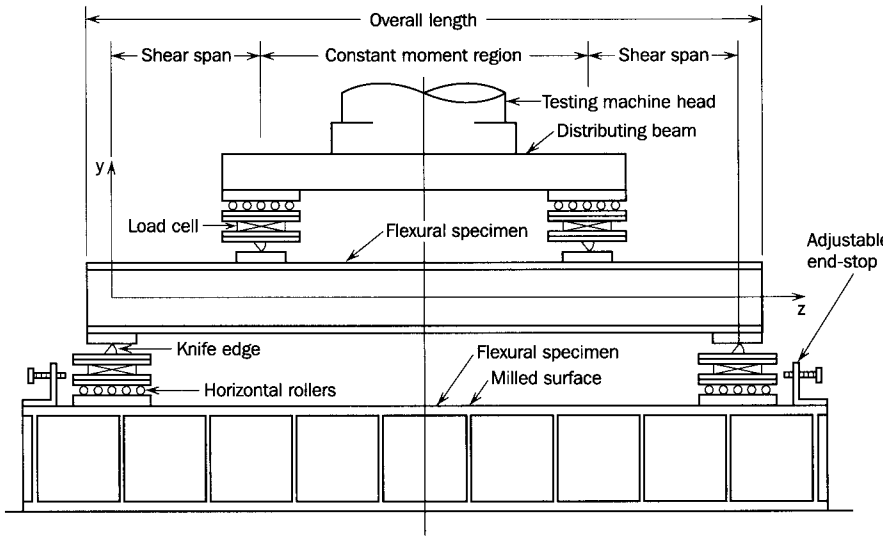

Fig. B.26 Flexural test set-up to determine cross-sectional strength.

Figure B.27 is a schematic diagram of a knife edge-roller assembly with a capacity of 3000 kN (675 kips) that is designed for large rotations. The design of knife edges and rollers depends on the magnitude of the contact stresses (B. 22). Air hardening chromoloy A2 steel is excellent for these because it distorts little on hardening and provides surface yield strengths in excess of 1800 MPa (260 ksi). Serrated knife edges and matching sloped serrated plates, as shown in Fig. B. 27 (B.23), acting like a rack and pinion system, can accommodate rotations of 30° or more. The slope is set at half the maximum anticipated rotation. For relatively small rotations, horizontal plate surfaces without serrations may be used, but, without serrations, the angle of rotation is limited by the frictional force that can be developed between the knife edge and the adjacent plate.

In lateral torsional buckling tests, the displacement in the vertical or y direction, the displacement of the load or reaction, is imposed. Any of the other 5 degrees of freedom, Δx, Δz, θx, θy, θz, may or may not be constrained as desired. In these tests, translations in the z and x directions are allowed by two perpendicular sets of rollers as illustrated subsequently as are the other devices. Rotations about x and z axes are provided for by two orthogonal knife edges or semi cylindrical rockers. A hemispherical rocker can be considered to provide three rotational degrees of freedom as the torsional restraint about a vertical axis due to friction is limited by the size of the contact area. The small bearing area however limits the loads that can be carried. Hence, when rotation about the vertical or y-axis is to be allowed, a thrust bearing should preferably be used. Thrust bearings are commerically available. Depending on their capa-

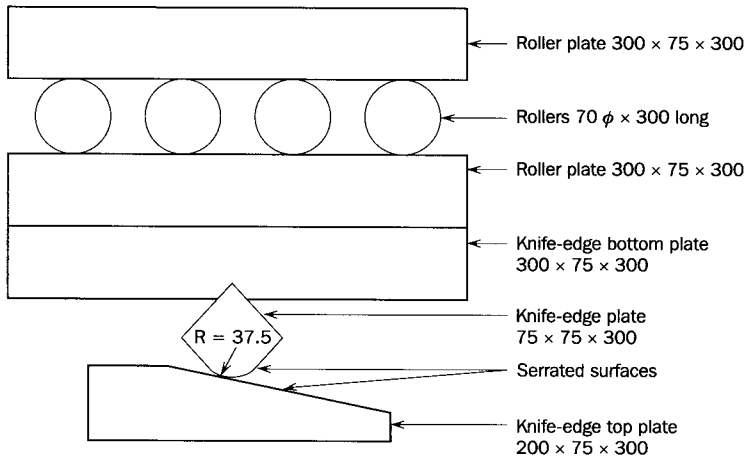

Notes: 1. Steel is air-hardening chromoloy A2. 2. Dimensions in millimeters

Fig. B.27 Knife-edge roller assembly.

city, they are about 9 to 60 mm high with a circular race of ball bearings at mid-height that can transfer compressive forces but allow rotation about the y-axis.

Figure B.28 shows an example of a test set-up for a lateral torsional buckling test of a beam with a single overhang and with loads applied at the cantilever tip and at five locations on the main or back span.

Figure B. 29 shows a loading frame which ensures that the load is applied vertically even though the beam specimen displaces laterally during the test. The inner frame is constrained to move vertically, even when it is loaded eccentrically by the displaced beam, by the rollers fastened to it at its corners and reacting against the outer frame. The horizontal forces of the rollers at opposite corners form a couple acting on the inner frame equal and opposite to that formed by the vertical load of the loading rods and the reaction of the displaced beam acting on the inner frame. Only vertical loads can be applied.

Figures B.30 shows different combinations of load devices and the corresponding cross-sectional displacements. The surfaces of roller and knife-edge assemblies must be kept clean as any dirt may introduce unwanted frictional forces. Typical reaction systems and the corresponding cross-sectional displacements or distortions are shown in Figures B.31. The four rounded noses in Fig. B.31 have a radius of about 20 mm and simply bear lightly against the web. They therefore prevent the web from moving laterally and provide a forked support. Any tangential frictional forces developed between the web and noses, should relative longitudinal movement be impending, are only a fraction of the bearing forces and are considered to be negligibly small. In Fig. B.31(b) the width of the bearing, load cells and roller plates must be sufficient to prevent uplift as the beam cross-section distorts.

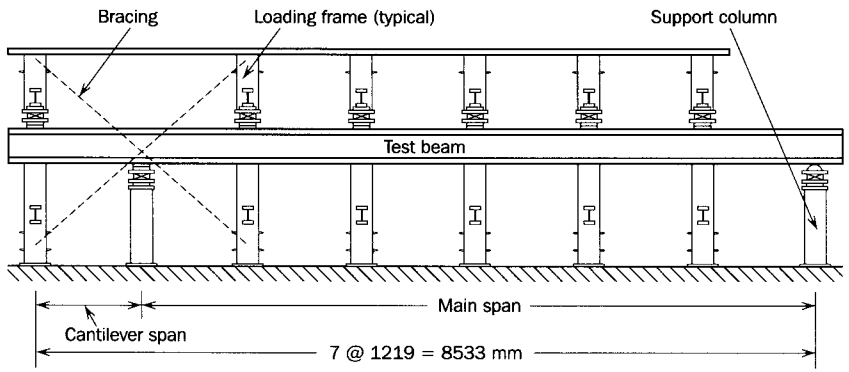

Fig. B.28 Set-up for lateral torsional buckling tests (section on longitudinal centerline) (B.25)

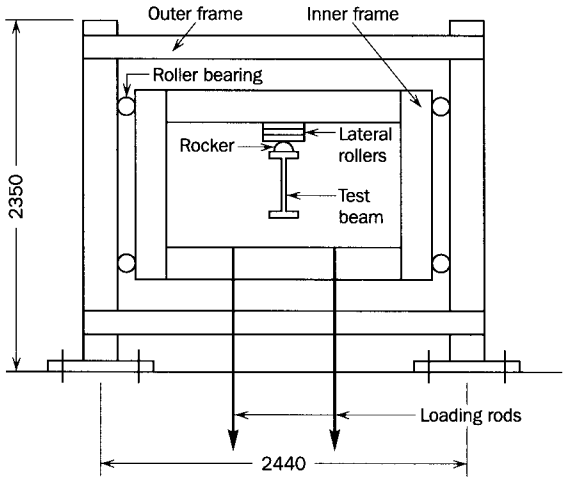

Fig. B.29 Loading frame to apply vertical loads to beams that displace laterally.

Test Measurements

Loads and Reactions. By measuring all loads and reactions using calibrated load cells, as shown in Fig. B.26, statics is then available to confirm the calibrations, to check the progress of the test, and to monitor any frictional losses. In no case should only the loads or the reactions be measured, as errors in calibration or frictional losses would then remain undetected, and increase the experimental error. In Fig. B.27 the load applied to the loading frame and hence to the test beam is measured by a load cell. By also measuring the two reactions (see Fig. B.28) any losses in the roller bearings can be deduced. Note as well, by statics, that the magnitudes of the reactions

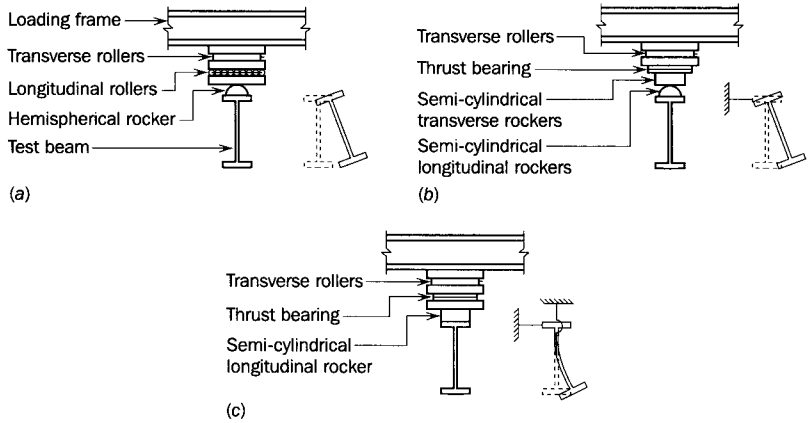

Fig. B.30 Loaded flange restraint conditions: (*a*) free to rotate and displace laterally; (*b*) free to rotate; (*c*) fixed against rotation about the longitudinal axis and lateral translation.

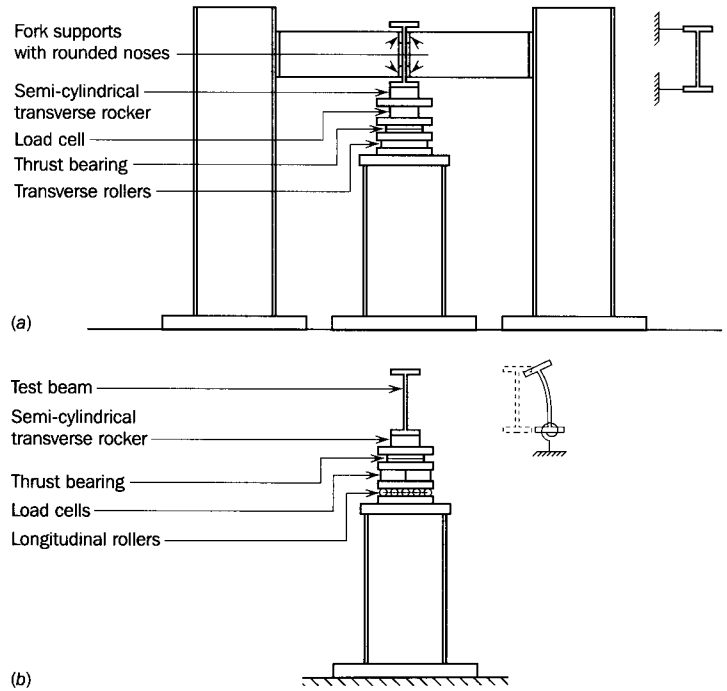

Fig. B.31 Reaction restraint conditions: (*a*) Beam fixed against lateral displacement and rotation; (*b*) bottom flange fixed against rotation, beam free to displace laterally.

can be checked against the loads during the course of the test and problems detected before it is too late.

Displacements and Distortions. Consideration should be given to making some redundant measurements. Cable LVDTs (linearly variable differential transformers) (B.24) or potentiometers are ideal for measuring displacements and can be used to measure large displacements with excellent sensitivity. Readings can be recorded electronically and very quickly. The number of LVDTs required depends on the displacements to be determined and whether the section distorts or not. For example, two LVDTs attached horizontally to the flange tips give the horizontal centroidal displacement provided the section does not distort. With six LVDTs at one cross-section, two attached horizontally and four attached vertically to the flange tips, web distortions can be calculated. Three dimensional displacement can also be measured by triangulation using two or more high precision electronic theodolites that sight on a mylar target mounted on the test specimen. A precision of 0.05 mm (0.002 in.) can be obtained regardless of the magnitude of the displacement. This sytem is particularly useful for tests with large displacements and rotations. Dial gauges are also useful for monitoring deflections during tests.

Strains. Electrical resistance strain gauges may be used to establish:

1. Strain distributions across the depth and hence the curvature
2. Strain distributions across the flange due to warping
3. Lateral bending strains in the web due to web distortion
4. Variations in strains along the beam

Test Procedure

Tests not taken to failure are of little or no value in establishing the behavior or strength of flexural members. A general procedure follows:

1. Set up reaction devices, load cells, and align the flexural specimen in the test frame.
2. Position loading devices with load cells.
3. Install and test instrumentation such as LVDTs, potentiometers, strain gauges, curvature meters, and monitoring instrumentation, take measurements to establish position of loads, reactions, and any restraining devices.
4. "Seat" the test specimen by applying about 20% of the anticipated maximum load while staying in the elastic range, perform statics checks, unload, and set instruments to zero.

5. Load monotonically to failure with increments determined from a load deflection curve plotted as the test progresses. Use displacement control for load increments as failure is approached when the stiffness of the system may be diminishing. Keep a test log book to record general observations in addition to the data recorded electronically. The book is invaluable later in establishing what happened and when. At each increment: (a) record measurements, (b) perform statics checks, (c) make visual observations, (d) take photographs as necessary, (e) record general behavior and any unusual occurrences. Make sketches in the log book.
6. Take residual measurements, notes and photographs as appropriate at the end of the test.

Test Report and Analyses

The test report should describe the test set-up, procedures and specimens in sufficient detail, so that other researchers can check the results independently. All relevant material properties, geometric properties, boundary conditions, loading, and deflections must therefore be presented. The analysis of the results should include a complete analysis of the geometric and material data to establish predicted moment resistances.

For tests to determine cross-sectionals strengths, as a minimum, the moment curvature relationship should be reported with an explanation of the effect of residual stresses, a description of overall behavior, the mode of failure, error analyses, and the ratio of test flexural strength to that predicted for the cross-section. After local buckling, curvatures are difficult to define and angle changes are considered to be a more appropriate measure.

For lateral torsional buckling tests, the analysis may be very extensive but should include a description of the overall behavior, test/predicted moment ratios, modes of failure, buckling shapes, cross-sectional distortions, error analyses, strain variations, and residual deformations.

The most important factor to establish in any test is the ratio of the test/predicted moment, the rationale, if it is the case, why it differs substantially from 1.0 and, for a series of tests, the coefficient of variation of the test/predicted moment ratio for the series.

B.10 TECHNICAL MEMORANDUM NO. 10: STATISTICAL EVALUATION OF TEST DATA FOR LIMIT STATES DESIGN

Introduction

The philosophy of limit states design (load and resistance factor design) is represented by the equation

$$\phi R \geq \Sigma \alpha_i S_i \tag{B.4}$$

which states that the factored resistance (design strength) shall be equal to or greater than the effect of the factored loads. Resistance factors, ϕ, and load factors, α_i, are chosen to provide selected small probabilities of failure. Although Eq. B.4 indicates that the resistance factors and the load factors are related to each other, Galambos and Ravindra (B.26–B.28) show that the resistance factor can be approximately expressed as

$$\phi = \rho_R \exp(-\beta \alpha_R V_R) \tag{B.5}$$

where

ρ_R = the bias coefficient for the resistance, i.e., the mean value of the ratio of the measured resistance to the nominal resistance
= the product of $\rho_G \rho_M \rho_P$, where in turn
ρ_G = the bias coefficient for the cross-sectional geometry, i.e., the mean value of the ratio of the relevant geometric property, such as A, b, d, t, I, S, Z, C_w, to the nominal value as given in steel design handbooks
ρ_M = the bias coefficient for the material property, i.e., the mean value of the ratio of the relevant material property, such as F_y, F_u, E to the nominal value as given in published steel material specifications
ρ_P = the bias coefficient for the design equation, i.e., the mean value of the ratio of the measured or test strength to that predicted by a design equation such as $M_p = F_y Z$
V_R = the coefficient of variation associated with ρ_R
$= \sqrt{V_G^2 + V_M^2 + V_P^2}$, when the quantities are not correlated, and V_G, V_M, and V_P are the coefficients of variation of the geometric properties, material properties, and test/predicted strength ratios
β = reliability index, currently taken to have a target value of about 3.0 for structural steel members in buildings and 4.5 for structural connections
α_R = the coefficient of separation taken as 0.55 (B.26) (not to be confused with the load factors α_i)

Because of the interdependence of the resistance factor, ϕ, and the load factors, α_i, when load factors are established for building structures as a whole based on a target value of 3.0 for β, an adjustment factor less than one must be applied to equation B.5 when calculating resistance factors for a target value for β of 4.5 for connections. Fisher et al. (B.29) show that this factor varied only from 0.86 to 0.90 for a broad range of live/dead load ratios; therefore a value of 0.88 is considered appropriate. Hence for members, from Eq. B.5 with $\beta = 3.0$ and $\alpha_R = 0.55$,

$$\phi = \rho_R \exp(-1.65 V_R) \tag{B.5a}$$

and for connections and their connectors from Eq. B.5 with $\beta = 4.5$, $\alpha_R = 0.55$ and the adjustment factor of 0.88,

$$\phi = 0.88 \rho_R \exp(-2.47 V_R) \tag{B.5b}$$

Therefore, for test data to be used statistically to determine resistance factors for limit states design, all the statistical parameters, ρ_G, ρ_M, and ρ_P must be determined or be available. It follows that, in tests, to determine how well an equation predicts the behavior of a component, i.e. the fit of the equation to the test results or the test/predicted ratio, the results must be based on measured geometric and material properties and not on nominal values. Thus the test/predicted ratio does not include any of the variation in the geometric and material properties. Test strengths predicted using nominal properties are of no value.

As well, incomplete reporting of the statistical parameters renders the test data virtually useless. Furthermore, as the sample size must be statistically significant, the work of several researchers will likely need to be combined. This emphasizes the importance of complete and accurate reporting of the test data. Raw data in the form of measurements of geometric and material properties and test strengths should be available so that statistical analyses can be carried out independently. The test must be described in detail so that, for example, the effects of boundary conditions on the behavior can be assessed.

Reporting Test Data

In addition to the general data reported such as the objectives and scope of the experimental program, the data should include:

1. Description of the test set-up and instrumentation (sensitivity and range).
2. Load-deflection curves and displaced shapes which illustrate the behavior.
3. Description of the failure and the failure criteria used.
4. Sufficient data so that calculations and statistical analyses can be reproduced. Thus the basic geometry, initial imperfections (if relevant), nominal and measured geometric and material properties and test/predicted ratios are required, and an error analysis.

For unique tests, possibly with elaborate specimens, boundary and load conditions, some simpler tests on specimens of known or readily predictable behavior need to be made to verify test procedures and the performance of the test equipment.

Geometric and Material Properties

Many data are available in the literature on the statistical variation of geometric and material properties of steel members, e.g., Galambos and Ravindra (B.28), Kennedy and Gad Aly (B.30), Baker and Kennedy (B.31), Kennedy and Baker (B.32), Kennedy et al. (B.33), and Rang et al. (B.34). Care must be taken that the data are appropriate to the circumstances at hand. Various national standards may have quite different requirements. Changes in manufacturing and rolling practices and in national standards may mean that some data are no longer applicable.

For both the geometric and material properties the bias coefficient, the coefficient of variation, and the type of distribution are required.

Chernenko and Kennedy (B.35) give procedures for calculating statistical data for cross-sectional properties such as for the area and moment of inertia when the variations in the plate width and thickness are known. Kennedy and Gad Aly (B.30) introduce participation factors to handle the case when, for example, in determining resistance factors for columns, the strength is governed by one material parameter (the yield strength) at low slenderness ratios and another (the modulus of elasticity) governs at high slenderness ratios.

Ratio of Test-to-Predicted Strengths

Physical Tests. To compute the test/predicted ratio for any test, the measured geometric and material properties of the test specimen are used in the design equation without a resistance factor to predict the strength. The measure of the fit of the design equation to the test results is given by the distribution of the test/predicted ratio as characterized by the bias coefficient, ρ_P, and the coefficient of variation, V_P.

Computer-Simulated Tests. Computer simulated tests, using finite element models that can model both material and geometric non-linearities, offer several advantages. They are quick, inexpensive and there are no physical limitations on the size of the model that can be "tested." They are, however, only as good as the assumptions inherent in the models and, therefore, they themselves must be verified by actual physical tests on real specimens. This comparison should demonstrate correspondence not only of maximum loads but also of the load deflection behavior. Computation of the test/predicted bias coefficient is a two-step multiplicative process. First physical tests are used to verify the computer model and then the computer model is used to verify the design equation. There is then one bias coefficient for the ratio of the physical test strength to the computer simulated strength which is multiplied by the ratio of the computer simulated strength to the strength predicted by the design equation. The coefficients of variation are combined as the square root of the sum of the squares. In some instances, when the com-

puter simulation itself is used to predict the design strength, as no relatively simple model exists, the ratio of the physical test strength to the computer simulated strength gives the test/predicted ratio directly.

When dealing with computer simulated tests, Chernenko and Kennedy (B.35) proposed a sequential method for considering the effects of out-of-straightness and residual stresses on column strengths that avoids the conservative approach of combining the worst residual stress effects with the maximum out-of-straightness effects. Test data are required on the distribution of out-of-straightness and some measure of residual stress effects. The bias coefficient of the test/predicted ratio is determined at the mean value of each of these two effects with a coefficient of variation for each effect in turn. The overall bias coefficient is then the product of all the contributing coefficients while the coefficients of variation are combined as the square root of the sum of the squares.

Other Factors

Discretization Factor, D. Steel shapes and plates are rolled in discrete sizes. The structural engineer tends to, or should, select sizes with a resistance equal to or greater than that required. (Not doing so encroaches upon the margin of safety.) Thus the value of the bias coefficient of the resistance supplied to that required, ρ_D, is greater than 1.0. The corresponding coefficient of variation for the data set, V_D, can also be calculated. This allows the effect of discretization to be included in the calculation of the resistance factor as another distribution.

Errors in Measurement, E_m. Errors in measurement may be random, systematic or blunders. Blunders are generally obvious and do not require statistical examination to be rejected. Systematic errors can be averted through proper calibration, redundant measurements, checks and due care in testing. For example, when the equations of statics are satisfied we are confident that the loads have been determined without systematic error. Chauvenet's criterion may be applied for the rejection of outliers of a data set which may have resulted from errors in measurement. The random errors that remain are as likely to be positive or negative resulting in a mean value of the bias coefficient, ρ_{Em}, of 1.00. The coefficient of variation of the errors in measurement, V_{Em}, will not be zero having typical values of about 0.02 to 0.04. This inflates the coefficient of variation of the measured quantity and may be accounted for in the calculations if an error anslysis is performed.

Monte Carlo Simulation. For cases when the probability distributions to be combined are of different types or for cases where the data are limited, provided that the general types of distribution and statistical parameters, ρ and V are known, a Monte Carlo simulation may be used to create the combined distribution for the resistance of the component. Then ρ_R and V_R can

be calculated. Care should be taken to ensure that the simulation process can be repeated. Note that the chi-square test or the Kolmogorov–Smirnov method can be used to verify the fit of a given distribution to the data set (B.36, B.39).

Example B.1 This example of the calculation of resistance factors is based on the experimental data given in Essa and Kennedy (B.37) for 31 tests to determine the distortional buckling strength of steel beams under a broad range of loading and restraint conditions. The results of two other tests have been excluded because unwanted frictional restraints caused higher energy buckling modes and therefore test strengths greater than expected. The relevant statistical data are given in Table B.1 where that for the modulus of elasticity is a re-evaluation of the data reported by Galambos and Ravindra (B.28).

Because the failure strengths for distortional buckling may range all the way from the fully plastic cross-sectional strength to an elastic buckling strength, material data are given for both the yield strength and the modulus of elasticity. As well statistical data for two different test/predicted ratios are given: (a) the data determined from an inelastic finite element analysis that considers the effect of residual stresses and the distortion of the web (B.38) and (b) as an extension of the finite element analysis, the data from design charts proposed by Essa and Kennedy (B.37). The coefficient of variation for the test/predicted ratio for the 31 tests has been adjusted using a coefficient of variation for errors in measurement, V_{em}, equal to the conservative value of 0.02. It is noted in

TABLE B.1 Statistical Data for Computing Resistance Factors

Parameter	Number of Tests or Simulations	Bias Coefficient, ρ	Coefficient of Variation, V	Ref.
Geometric factor				
Plastic section modulus	>352	0.99	0.038	(B.30)
Elastic section modulus	>352	0.99	0.021	
Material factor				
Elastic modulus	341	1.036	0.045	(B.28)
Yield strength	4796	1.060	0.051	(B.30)
Test/predicted ratio				
Finite element analysis	31	0.990	0.060	(B.38)
Design charts	257	1.016	0.013	(B.37)

passing that the statistical data for these tests reflect all the variations arising from the tests themselves as well as the simplifications in the finite element model. The resistance factors are calculated for the four combinations of failure modes and methods of predicting the strength. In the interests of simplicity the discretization factor has not been considered.

1. *Fully plastic strength and finite element analysis.* Equation B5.a is $\phi = \rho_R \exp(-1.65 V_R)$, where

$$\rho_R = \rho_G \rho_M \rho_P = \rho_Z \rho_{Fy} \rho_{FEM} = 0.99 \times 1.060 \times 0.99 = 1.039$$

and

$$V_R^2 = V_Z^2 + V_{Fy}^2 + V_{FEM}^2 = 0.038^2 + 0.051^2 + 0.060^2 = 0.088^2$$

Therefore,

$$\phi = 1.039 \exp(-1.65 \times 0.88) = 0.899 \quad \text{say, } 0.90$$

2. *Fully plastic strength and design charts.* Here there is an additional term for the test/predicted ratio as the procedure to get the test/predicted ratio has two steps. For the series of 31 physical tests the ratio of each test strength to that determined from the finite element analysis was found and hence the mean value and the coefficient of variation of this ratio. Next many finite element analysis results for situations that had not been physically tested were compared to the design charts. The latter, as derived, contain some approximations to make them generally applicable. This introduces a second set of variations. Thus

$$\rho_R = \rho_G \rho_M \rho_{P1} \rho_{P2} = \rho_Z \rho_{Fy} \rho_{FEM} \rho_{DC} = 0.99 \times 1.060 \times 0.99 \times 1.016 = 1.056$$

and

$$V_R^2 = V_Z^2 + V_{Fy}^2 + V_{FEM}^2 + V_{DC}^2 = 0.038^2 + 0.051^2 + 0.060^2 + 0.013^2 = 0.089^2$$

Therefore

$$\phi = 1.056 \exp(-1.65 \times 0.089) = 0.912 \quad \text{say, } 0.90$$

3. *Elastic buckling and finite element analysis.* The differences from the first calculation are that the geometric property is taken to be the elastic section modulus and the material factor is taken to be the modulus of elasticity. There are other geometric factors that are also relevant such as moments of inertia, but it is tacitly assumed that their statistical distributions are not dissimilar to that of the elastic section modulus. Thus

$$\rho_R = \rho_G \rho_M \rho_P = \rho_S \rho_E \rho_{FEM} = 0.99 \times 1.036 \times 0.99 = 1.015$$

and

$$V_R^2 = V_S^2 + V_E^2 + V_{FEM}^2 = 0.021^2 + 0.045^2 + 0.060^2 = 0.078^2$$

Therefore

$$\phi = 1.015 \exp(-1.65 \times 0.078) = 0.892 \quad \text{say, } 0.90$$

4. *Elastic buckling and design charts.* As in the second calculation there is an additional term for the test/predicted ratio. Thus

$$\rho_R = \rho_G \rho_M \rho_{P1} \rho_{P2} = \rho_S \rho_E \rho_{FEM} \rho_{DC} = 0.99 \times 1.036 \times 0.99 \times 1.016 = 1.031$$

and

$$V_R^2 = V_S^2 + V_E^2 + V_{FEM}^2 + V_{DC}^2 = 0.038^2 + 0.045^2 + 0.060^2 + 0.013^2 = 0.085^2$$

Therefore,

$$\phi = 1.013 \exp(-1.65 \times 0.085) = 0.895 \quad \text{say, } 0.90$$

A resistance factor of 0.90 for the four cases studied appears to be appropriate, if it was considered desirable in the interests of simplicity to have one value only. Using this value and by rearranging Eq. B.5, we have

$$\beta = \frac{-\log_e(\phi/\rho_R)}{\alpha_R V_R} = \frac{-\log_e(0.90/\rho_R)}{0.55 V_R} \tag{B.5}$$

The values of the reliability index, β, for the four cases are computed to be 2.97, 3.26, 2.80, and 2.91, respectively. These are grouped relatively closely to the target value of 3.0.

References

B.1 Estuar, F. R., and Tall, L. (1967), "Testing Pinned-End Steel Columns," in *Test Methods for Compression Members*, ASTM STP419, American Society for Testing and Materials, Philadelphia, Pa.

B.2 Salmon, E. H. (1931), *Materials and Structures*, Longmans, London.

B.3 Huber, A. W. (1958), "Fixtures for Testing Pin-Ended Columns," *ASTM Bull.*, No. 234, Dec.

B.4 Tebedge, N., Marek, P., and Tall, L. (1971), "On Testing Methods for Heavy Columns," *Fritz Eng. Lab. Rep. No. 351.4*, Lehigh University, Bethlehem, Pa., March.

B.5 Johnston, B. G., and Mount, E. H. (1939), "Designing Welded Frames for Continuity," *Weld. Res. J.*, Vol. 18.

B.6 Yarimci, E., Yura, J. A., and Lu, L. W. (1968). "Rotation Gages for Structural Research," *Exp. Mech.*, Vol. 8, No. 11.

B.7 Castex, L., and Maso, J. C. (1975), "Études des contraites résiduelles, diffractometriex, dans des profilés laminés d'acier doux," *Constr. Met.* (CTICM, France), No. 2.

B.8 Tebedge, N., Alpsten, G., and Tall, L. (1972), "Measurement of Residual Stresses: A Comparative Study of Methods," *Proc. Conf. Rec. Interpret. Eng. Meas.*, Institute of Marine Engineers, London, April 5 (also available as *Fritz Eng. Lab. Rep. No. 337.8*, Lehigh University, Bethlehem, Pa., Feb. 1971).

B.9 Tebedge, N., Alpsten, G., and Tall, L. (1973), "Residual-Stress Measurement by the Sectioning Method," *Exp. Mech.*, Vol. 13, pp. 88–96.

B.10 Soete, W., and Vancrombrugge, A. (1955), "An Industrial Method for the Determination of Residual Stresses," *Proc. Soc. Exp. Stress Anal.*, Vol. 8, No. 1.

B.11 Randle, N. J., and Vigness, F. (1966), "Hole-Drilling Strain Gage Method of Measuring Residual Stresses," *Exp. Mech.*, Vol. 6.

B.12 Luxion, W., and Johnson, B. G. (1948), "Plastic Behavior of Wide Flange Beams," *Weld. J.*, Vol. 27, p. 538s.

B.13 Sherman, D. R. (1969), "Residual Stress Measurement in Tubular Members," *ASCE J. Struct. Div.*, Vol. 95, No. ST4, pp. 635–648.

B.14 Nadai, A. (1950), *Theory of Flow and Fracture of Solids*, McGraw-Hill, New York.

B.15 Tall, L. (ed.) (1974), *Structural Steel Design*, Ronald Press, New York.

B.16 Beedle, L. S., and Tall, L. (1960), "Basic Column Strength," *ASCE J. Struct. Div.*, Vol. 86, No. ST7, pp. 138–178.

B.17 Nagaraja Rao, N. R., Lohrmann, M., and Tall, L. (1966), "Effects of Strain Rate on the Yield Stress of Structural Steels," *ASTM J. Mater.*, Vol. 1, No. 1.

B.18 ASTM (1982), *Annual Book of ASTM Standards: Part 10: Metals*, American Society for Testing and Materials, Philadelphia, Pa.

B.19 Gozum, A. T., and Huber, A. W. (1955), "Material Properties, Residual Stresses and Column Strength," *Fritz Eng. Lab. Rep. No. 220.14*, Lehigh University, Bethlehem, Pa.

B.20 Tall, L., and Alpsten, G. A. (1969), "On the Scatter in Yield Strength and Residual Stresses in Steel Members," *Proc. IABSE Symp. Concepts Safety Struct. Methods Des.*, London.

B.21 Roloff, S. J. (1984), "Stress-Strain Properties of Fabricated Steel Pipe," *Proc. Annu. Techn. Session SSRC*, Bethlehem, Pa.

B.22 Boresi, A. P., and Sidebottom, O. M. (1985), *Advanced Mechanics of Materials*, 4th ed., Wiley, New York.

B.23 Brattland, A., and Kennedy, D. J. L. (1992), "Flexural Tests of Two Full-Scale Composite Trusses," *Can. J. Civ. Eng.*, Vol. 19, pp. 279–295.

B.24 Sabnis, G., Harris, H. G., White, R. N., and Mirza, M. S. (1985), *Structural Modeling and Experimental Techniques*, Prentice Hall, Upper Saddle River, N.J.

B.25 Albert, C., Essa, H. S., and Kennedy, D. J. L. (1992), "Distortional Buckling of Steel Beams in Cantilever Suspended Span Construction," *Can. J. Civ. Eng.*, Vol. 19, pp. 767–780.

B.26 Galambos, T. V., and Ravindra, M. K. (1973), "Tentative Load and Resistance Factor Design Criteria for Steel Buildings," *Res. Rep. 18*, Civil Engineering Department, Washington University, St. Louis, Mo.

B.27 Galambos, T. V., and Ravindra, M. K. (1977), "The Basis for Load and Resistance Factor Design Criteria for Steel Building Structures," *Can. J. Civ. Eng.*, Vol. 4, pp. 178–189.

B.28 Galambos, T. V., and Ravindra, M. K. (1978), "Properties of Steel for Use in LRFD," *ASCE J. Struct. Eng.*, Vol. 104, No. ST9, pp. 1459–1468.

B.29 Fisher, J. W., Galambos, T. V., Kulak, G. L., and Ravindra, M. K. (1978), "Load and Resistance Factor Design Criteria for Connectors," *ASCE J. Struct. Eng.*, Vol. 104, No. ST9, pp. 1427–1441.

B.30 Kennedy, D. J. L., and Gad Aly, M. M. (1980), "Limit States Design of Steel Structures: Performance Factors," *Can. J. Civ. Eng.*, Vol. 7, pp. 45–77.

B.31 Baker, K. A., and Kennedy, D. J. L. (1984), "Resistance Factors for Laterally Unsupported Steel Beams and Biaxially Loaded Steel Beam-Columns," *Can. J. Civ. Eng.*, Vol. 11, pp. 1008–1019.

B.32 Kennedy, D. J. L., and Baker, K. A. (1984), "Resistance Factors for Steel Highway Bridges," *Can. J. Civ. Eng.*, Vol. 11, pp. 324–334.

B.33 Kennedy, D. J. L., Gagnon, D. P., Allen, D. E., and MacGregor, J. G. (1992), "Canadian Highway Bridge Evaluation: Load and Resistance Factors," *Can. J. Civ. Eng.*, Vol. 19, pp. 992–1006.

B. 34 Rang, T. N., Galambos, T. V., Yu, W.-W., and Ravindra, M. K. (1978), "Load and Resistance Factor Design of Cold-formed Steel Structural Members," *Proc. 4th Int. Spec. Conf. Cold-formed Steel Struct.*, University of Missouri–Rolla, Rolla, Mo., June.

B.35 Chernenko, D. E., and Kennedy, D. J. L. (1991), "An Analysis of the Performance of Welded Wide Flange Columns," *Can. J. Civ. Eng.*, Vol. 18, pp. 537–555.

B.36 Kennedy, J. B., and Neville, A. M. (1986), *Basic Statistical Methods for Engineers and Scientists*, 3rd ed., Harper & Row, New York.

B.37 Essa, H. E., and Kennedy, D. J. L. (1995), "Design of Steel Beams in Cantilever-Suspended Span Construction," *ASCE J. Struct. Eng.*, Vol. 121, No. 11, pp. 1667–1673.

B.38 Albert, C., Essa, H. S., and Kennedy, D. J. L. (1992), "Distortional Buckling of Steel Beams in Cantilever Suspended Span Construction," *Can. J. Civ. Eng.*, Vol. 19, pp. 767–780.

B.39 Ang, A., and Tang, W. H. (1975), *Probability Concepts of Engineering Planning and Design*, Vol. I: *Basic Principles*, Wiley, New York.

APPENDIX C

STRUCTURAL STABILITY RESEARCH COUNCIL

The following is a summary of pertinent information about the SSRC.

Purposes

The general purposes of the Structural Stability Research Council shall be:

1. To maintain a forum where the structural stability aspects of metal and composite metal-and-concrete structures and their components can be presented for evaluation, and pertinent structural research problems proposed for investigation.
2. To review the world's literature on structural stability of metal and composite metal-and-concrete structures and study the properties of materials available for their construction, and to make the results widely available to the engineering profession.
3. To organize, administer and guide cooperative research projects in the field of structural stability, and to solicit financial support for such projects.
4. To promote publication and dissemination of research information in the field of structural stability.
5. To study the application of the results of research to stability design of metal and composite metal-and-concrete structures, and to develop comprehensive and consistent strength and performance criteria and encourage consideration thereof by specification-writing bodies.

Membership

Organizations or Firms concerned with investigation and design of metal and composite structures may be invited by the Council to become Sponsors, Participating Organizations or Participating Firms.

Sponsors: minimum fee of $1500 per year. May appoint up to 5 representatives.

Participating organization: minimum fee of $300 per year; may appoint up to 3 representatives.

Participating firm: fee of $500 (sustaining) or $175 (contributing) per year; may appoint up to 2 representatives.

Participating company: fee of $700 (sustaining) or $500 (contributing) per year; may appoint up to 3 representatives.

The voting membership of the Council consists of Representatives of Sponsors, Participating Organizations and Participating Firms; Members-at-Large; Corresponding Members; and Life Members.

Representatives: individuals appointed by Organizations or Firms subjects to the approval of the Executive Committee.

Members-at-Large: individuals who have expressed interest in the work of the Council, and who have done or are doing work germane to its interest, may be elected by the Council, following nomination by the Executive Committee. Fee—$40 per year.

Corresponding members: individuals appointed by the Executive Committee to maintain contact with organizations in other countries that are active in areas of interest to the Council. Fee—voluntary.

Life members: active Council members of appropriate age and service to SSRC may be elected to the Council, following nomination by the Executive Committee. Fee—voluntary.

Sponsors (1997)

American Institute of Steel Construction
American Iron and Steel Institute
American Petroleum Institute
Exxon Production Research Company
Howard, Needles, Tammen and Bergendoff
Kawada Industries
NUCOR Research and Development
Sumitomo Metal Industries, Ltd.

UNOCAL Science and Technology Division
Yokogama Construction Company

Participating Organizations (1997)

Aluminum Association
American Bureau of Shipping
American Society of Civil Engineers
American Society of Mechanical Engineers
Australian Institute of Steel Construction
Canadian Institute of Steel Construction
Canadian Society for Civil Engineering
Federal Highway Administration
Institute of The Ironworking Industry
International Conference of Building Officials
Metal Buildings Manufacturers Association
Naval Surface Warfare Center
New Zealand H.E.R.A.
South African Institute of Steel Construction
Steel Deck Institute
Steel Joist Institute
Structural Engineers Association of California
The Steel Construction Institute
The Steel Institute of New York
U.S. Department of Labor—OSHA

Participating Companies (1997)

Sustaining

CBI Technical Services Company

Contributing

Butler Manufacturing Company
Fluor Daniel, Inc.
Mobil Research and Development Corporation
Sargent & Lundy

Participating Firms (1997)

Sustaining

Iffland Kavanagh and Waterbury, P. C.
Stanley D. Lindsey & Associates
Loomis & Loomis
Walter P. Moore and Associates, Inc.
Leslie E. Robertson and Associates
Weiskopf & Pickworth

Contributing

AMN Engineers
Amoco Production Company
Bettigole Andrews and Clark
Black & Veatch
Boyd Brown Stude & Chambers
Carruthers & Wallace, Ltd.
Computerized Structural Design, Inc.
Degenkolb Engineers
DRC Consultants, Inc.
Edwards and Kelcey Engineers, Inc.
Fay, Spofford & Thorndike, Inc.
Gannett Fleming, Inc.
Graef, Anhalt, Schloemer & Associates, Inc.
Hardesty & Hanover
HDR Engineering, Inc.
LeMessurier Consultants, Inc.
Leonhardt, Andra und Partner
Modjeski and Masters
Morrison Hershfield Limited
Parsons Brinkerhoff Quade & Douglas, Inc.
Skimore Owings and Merrill
Steiman Boynton Gronquist & Birdsall
TAMS Consultants, Inc.
The Cantor Seinuk Group, P. C.
The Sear-Brown Group, Inc.
Thornton-Tomasetti Engineers
Vollmer Associates

Whitney, Bailey, Cox & Magnani
Wiss, Janney, Elstner Associates, Inc.

Activities (1997)

No.	*Task Group*	*Chairman*
1	Centrally Loaded Columns	D. J. L. Kennedy
4	Frame Stability and Columns as Frame Members	G. G. Deierlein
6	Test Methods	L. Tall
11	International Cooperation on Stability Studies	M. Ivanyi
13	Thin-Walled Metal Construction	W. S. Easterling
14	Horizontally Curved Girders	J. M. Yadlosky
15	Beams	S. Vinnakota
17	Doubly Curved Shells and Shell-Like Structures	N. F. Morris
18	Tubular Members	P. C. Birkemoe
20	Composite Members and Systems	R. Leon
24	Stability Under Seismic Loading	S. C. Goel
25	Connection Restraint Characteristics	A. V. Goverdhan
26	Stability of Angle Members	L. A. Lutz
27	Plate and Box Girders	M. Elgaaly
28	Computer Applications	P. K. Basu
29	2nd Order Inelastic Analysis for Frame Design	D. W. White
30	Bracing Members	T. Hellwig

No.	*Subject*	*Task Reporter*
11	Stability of Aluminum Structural Members	C. C. Menzemer
14	Fire Effects on Structural Stability	D. F. Boring
15	Curved Compression Members	S. Kuranishi
16	Stiffened Plate Structures	A. Mansour
20	Large Deflection Buckling	A. Chajes
21	Tapered Members	J. M. Fisher
22	Aerospace Structures	M. Schneider
23	Beam-Columns	H. J. Hjelmstad
24	Stability of Advanced Composite Materials	C. K. Shield

Officers (1997)

Chairman: Clarence D. Miller
Vice Chairman: Reidar Bjorhovde
Director: James M. Ricles
Director Emeritus: Lynn S. Beedle
Treasurer: Jackson L. Durkee

Executive Committee (1997)

Lynn S. Beedle—Lehigh University
Peter C. Birkemoe—University of Toronto
Reidar Bjorhovde—University of Pittsburgh
Wai-Fah Chen—Purdue University
Jackson L. Durkee—Consulting Structural Engineer
Mohamed Elgaaly—Drexel University
Gerard F. Fox—Consultant
Yuzuru Fujita—Japan Welding Engineering Society
Theodore V. Galambos—University of Minnesota
Dann H. Hall—BSDI
Nestor R. Iwankiw—American Institute of Steel Construction
Peter W. Marshall—Consultant
Clarence D. Miller—Consultant
James M. Ricles—Lehigh University
Donald R. Sherman—University of Wisconsin–Milwaukee

Headquarters Staff (1997)

(215) 758-3522

James M. Ricles—Director
Perry Green—Technical Secretary
Diana Walsh—Administrative Secretary

NAME INDEX

SUBJECT INDEX